

Selectivity Control in 3d Transition Metal-Catalyzed C–H Activation

Dissertation

for the award of the degree

“Doctor rerum naturalium”

of the Georg-August-Universität Göttingen



within the doctoral program of chemistry

of the Georg-August-University School of Science (GAUSS)

submitted by

Joachim Loup

from Vully-les-Lacs (Montmagny) VD, Switzerland

Göttingen, 2019

Thesis Committee

Prof. Dr. Lutz Ackermann, Institute of Organic and Biomolecular Chemistry,
Göttingen

Prof. Dr. Alexander Breder, Institut für Organische Chemie, Regensburg/Institute of
Organic and Biomolecular Chemistry, Göttingen

Members of the Examination Board

Reviewer: Prof. Dr. Lutz Ackermann, Institute of Organic and Biomolecular
Chemistry, Göttingen

Second Reviewer: Prof. Dr. Alexander Breder, Institut für Organische Chemie,
Regensburg/Institute of Organic and Biomolecular Chemistry, Göttingen

Further Members of the Examination Board

Prof. Dr. Manuel Alcarazo, Institute of Organic and Biomolecular Chemistry,
Göttingen

Dr. Shoubhik Das, Institute of Organic and Biomolecular Chemistry, Göttingen

Prof. Dr. Dietmar Stalke, Institute of Inorganic Chemistry, Göttingen

Prof. Dr. Dr. h.c.mult. Lutz F. Tietze, Institute of Organic and Biomolecular
Chemistry, Göttingen

Date of the Oral Examination: 16.08.2019

Table of Contents

| | |
|--|----|
| 1. Introduction | 1 |
| 1.1. Transition Metal-Catalyzed C–H Activation | 1 |
| 1.2. Cobalt-Catalyzed C–H Activation..... | 8 |
| 1.2.1. Early Contributions | 8 |
| 1.2.2. Cobalt(III)-Catalyzed C–H Activation | 10 |
| 1.2.3. Enantioselective Cobalt-Catalyzed C–H Functionalizations under Reductive Conditions | 19 |
| 1.3. Iron-Catalyzed C–H Activation..... | 23 |
| 1.4. Nickel-Catalyzed C–H Activation | 32 |
| 1.4.1. General Information..... | 32 |
| 1.4.2. Nickel-Catalyzed C–H Activation by Alkene Hydroarylation | 35 |
| 1.4.3. Enantioselective Nickel-Catalyzed C–H Activation | 39 |
| 2. Objectives | 47 |
| 3. Results and Discussion..... | 50 |
| 3.1. Cobalt(III)-Catalyzed C–H Amidation by Oxazoline Assistance | 50 |
| 3.1.1. Optimization Studies | 51 |
| 3.1.2. Substrate Scope..... | 54 |
| 3.1.3. Mechanistic Studies | 62 |
| 3.2. Asymmetric Iron-Catalyzed Hydroarylations by C–H Activation | 66 |
| 3.2.1. Optimization Studies | 67 |
| 3.2.2. Substrate Scope and Limitations..... | 83 |
| 3.2.3. Determination of the Absolute Configuration | 94 |
| 3.2.4. Product Diversification..... | 96 |

| | |
|--|-----|
| 3.2.5. Mechanistic Studies | 98 |
| 3.2.6. Proposed Mechanism | 117 |
| 3.2.7. Iron-Catalyzed Alkyne Hydroarylations | 119 |
| 3.3. Asymmetric Nickel-Catalyzed Hydroarylations by C–H Activation | 122 |
| 3.3.1. Preliminary Studies towards Asymmetric Intermolecular Hydroarylations by C–H Activation | 123 |
| 3.3.2. Optimization Studies of Enantioselective Intramolecular Nickel-Catalyzed Hydroarylations <i>via</i> C–H Activation..... | 127 |
| 3.3.3. Substrate Scope and Limitations | 134 |
| 3.3.4. Mechanistic Studies..... | 141 |
| 3.3.5. Proposed Mechanism | 144 |
| 3.3.6. Product Diversification | 147 |
| 4. Summary and Outlook..... | 149 |
| 5. Experimental Part..... | 154 |
| 5.1. General Remarks..... | 154 |
| 5.2. General Procedures..... | 160 |
| 5.3. Cobalt(III)-Catalyzed Directed C–H Amidation..... | 167 |
| 5.3.1. Experimental Procedures and Analytical Data..... | 167 |
| 5.3.2. Mechanistic Studies..... | 183 |
| 5.4. Synthesis of Novel Chiral Ligands | 185 |
| 5.4.1. Experimental Procedures and Analytical Data of Novel Chiral NHC Precursors | 185 |
| 5.4.2. Experimental Procedures and Analytical Data of Novel Chiral HASPOs | 201 |
| 5.5. Iron-Catalyzed Enantioselective C–H Alkylation with Alkenes | 204 |

| | |
|---|-----|
| 5.5.1. Experimental Procedures and Analytical Data | 204 |
| 5.5.2. Product Diversification..... | 236 |
| 5.5.3. Mechanistic Studies | 246 |
| 5.6. Asymmetric Nickel-Catalyzed Hydroarylations by C–H Activation..... | 262 |
| 5.6.1. Experimental Procedures and Analytical Data for the Intermolecular Nickel-Catalyzed Hydroarylation of Alkenes..... | 262 |
| 5.6.2. Mechanistic Studies for the Intermolecular Nickel-Catalyzed Hydroarylation of Alkenes | 262 |
| 5.6.3 Experimental Procedures and Analytical Data for the Asymmetric Intramolecular Nickel-Catalyzed Hydroarylation of Alkenes | 264 |
| 5.6.4. Mechanistic Studies for the Asymmetric Intramolecular Nickel- Catalyzed Hydroarylation of Alkenes..... | 276 |
| 5.6.5. Product Diversification..... | 278 |
| 5.7. Crystallographic Data | 281 |
| 6. References | 293 |
| Acknowledgements..... | 325 |
| Annexes..... | 328 |

List of Abbreviations

| | |
|--------------|---|
| Å | ångström |
| Ac | acetyl |
| acac | acetyl acetonate |
| $[\alpha]_D$ | specific rotation at 589 nm |
| Ad | adamantyl |
| Alk | alkyl |
| Am | amyl |
| AMLA | ambiphilic metal ligand activation |
| app | apparent |
| aq. | aqueous |
| Ar | aryl |
| atm | atmospheric pressure |
| ATR | attenuated total reflection |
| <i>b</i> | branched |
| BDE | bond dissociation energy (at 298 K) |
| BDMAEE | bis-(2-dimethylaminoethyl)ether |
| BDPP | bis-(diphenylphosphino)pentane |
| BHT | 2,6-di- <i>tert</i> -butyl-4-methylphenol |
| BIES | base-assisted internal electrophilic substitution |
| BINAP | 2,2'-bis(diphenylphosphino)-1,1'-binaphthyl |
| BINOL | [1,1'-binaphthalene]-2,2'-diol |
| Bn | benzyl |
| Boc | <i>tert</i> -butyloxycarbonyl |
| BOX | bis(oxazoline) |

| | |
|-----------------|---|
| bpy | 2,2'-bipyridine |
| Bu | butyl |
| br | broad |
| Bz | benzoyl |
| C | Celsius |
| c | concentration (in g / 100 mL) |
| CAAC | cyclic alkyl amino carbene |
| calc. | calculated |
| <i>cat.</i> | catalytic |
| CMD | concerted metalation deprotonation |
| cod | 1,5-cyclooctadiene |
| Cp | cyclopentadienyl |
| Cp* | pentamethylcyclopentadienyl |
| CPME | cyclopentyl methyl ether |
| Cp ^t | 1,3-di- <i>tert</i> -butylcyclopentadienyl |
| C _q | quaternary carbon |
| Cy | cyclohexyl |
| Cyp | cyclopentyl |
| δ | chemical shift (NMR) or isomer shift (<i>Mössbauer</i> spectroscopy) |
| d | doublet |
| DACH | 1,2-diaminocyclohexane |
| dba | dibenzylideneacetone |
| 2,3-DCB | 2,3-dichlorobutane |
| DCE | 1,2-dichloroethane |
| DCIB | 1,2-dichloroisobutane |

| | |
|--------------|--------------------------------------|
| ΔE_Q | quadrupole splitting |
| DFT | density functional theory |
| DG | directing group |
| Dipp | 2,6-diisopropylphenyl |
| DMF | <i>N,N</i> -dimethylformamide |
| DMPU | 1,3-dimethyl-1,3-diazinan-2-one |
| DMSO | dimethyl sulfoxide |
| DoM | directed <i>ortho</i> -metalation |
| DPEN | 1,2-diphenylethane-1,2-diamine |
| dppb | 1,3-bis(diphenylphosphino)butane |
| dppbz | 1,2-bis(diphenylphosphino)benzene |
| dppe | 1,3-bis(diphenylphosphino)ethane |
| dppf | 1,1'-bis(diphenylphosphino)ferrocene |
| dppm | 1,3-bis(diphenylphosphino)methane |
| dppp | 1,3-bis(diphenylphosphino)propane |
| d.r. | diastereomeric ratio |
| ee | enantiomeric excess |
| EI | electron ionization |
| equiv | equivalents |
| e.r. | enantiomeric ratio |
| ESI | electrospray ionization |
| Et | ethyl |
| EWG | electron-withdrawing group |
| Fc | ferrocenyl |
| FGI | functional group interconversion |

| | |
|------------|--|
| g | gram |
| GC | gas chromatography |
| <i>gem</i> | geminal |
| h | hour or hexet |
| HASPO | heteroatom-substituted secondary phosphine oxide |
| Hept | heptyl |
| hept | heptet |
| Het | heteroaryl or heteroatom |
| HFIP | 1,1,1,3,3,3-hexafluoro-2-propanol |
| HPLC | high-performance liquid chromatography |
| HR-MS | high resolution mass spectrometry |
| Hz | hertz |
| <i>i</i> | <i>iso</i> |
| ICy·HCl | 1,3-dicyclohexyl-1 <i>H</i> -imidazol-3-ium chloride |
| Ile | isoleucine |
| IMes·HCl | 1,3-dimesityl-1 <i>H</i> -imidazol-3-ium chloride |
| IPr·HCl | 1,3-bis(2,6-diisopropylphenyl)-1 <i>H</i> -imidazol-3-ium chloride |
| IXyl·HCl | 1,3-bis(2,6-dimethylphenyl)-1 <i>H</i> -imidazol-3-ium chloride |
| IR | infrared |
| <i>J</i> | coupling constant |
| K | Kelvin |
| <i>k</i> | reaction rate constant |
| kcal | kilocalorie |
| KIE | kinetic isotope effect |

| | |
|------------|---|
| L | liter or (pre-)ligand |
| / | linear |
| LED | light-emitting diode |
| LiHMDS | lithium bis(trimethylsilyl)amide |
| LLHT | ligand-to-ligand hydrogen transfer |
| M | metal or molar |
| <i>m</i> | <i>meta</i> |
| m | multiplet |
| M. p. | melting point |
| <i>m/z</i> | mass-to-charge ratio |
| MAD | methylaluminium bis(2,6-di- <i>tert</i> -butyl-4-methylphenoxide) |
| Mc | metallocenyl |
| Me | methyl |
| Mes | mesityl |
| mg | milligram |
| MHz | megahertz |
| min | minutes |
| mm | millimeter |
| mmol | millimole |
| MOM | methoxymethyl |
| MPAA | mono- <i>N</i> -protected amino acid |
| MS | mass spectrometry or molecular sieves |
| Ms | methanesulfonyl (mesyl) |
| Np | naphthyl |
| NBS | <i>N</i> -bromosuccinimide |

| | |
|----------|---|
| NHC | N-heterocyclic carbene |
| NHO | N-heterocyclic olefin |
| NLE | non-linear effect |
| NMP | <i>N</i> -methylpyrrolidinone |
| NMR | nuclear magnetic resonance |
| n.r. | no reaction |
| <i>o</i> | <i>ortho</i> |
| ∅ | diameter |
| ODCB | 1,2-dichlorobenzene |
| p | pentet |
| <i>p</i> | <i>para</i> |
| Pent | pentyl |
| Ph | phenyl |
| Ph-BPE | 1,2-bis-(2,5-diphenylphospholano)ethane |
| phen | 1,10-phenanthroline |
| Piv | pivaloyl (trimethylacetyl) |
| PMB | <i>para</i> -methoxybenzyl |
| PMDETA | <i>N,N,N',N'',N'''</i> -pentamethyldiethylenetriamine |
| PMP | <i>para</i> -methoxyphenyl |
| ppm | parts-per-million |
| Pr | propyl |
| py | pyridyl |
| PyBOX | 2,6-bis(oxazoliny)pyridine |
| pym | pyrimidyl |
| Q | 8-quinolyl |

| | |
|----------------|---|
| q | quartet |
| R | (organic) rest |
| R _L | large substituent |
| <i>rac</i> | racemic |
| R _c | ruthenocenyl |
| rDG | removable directing group |
| rel. int. | relative intensity |
| rt | room temperature |
| s | singlet or second |
| sat. | saturated |
| SET | single electron transfer |
| <i>Si</i> | R ₃ Si |
| sIMes·HCl | 1,3-dimesitylimidazolium chloride |
| sIXyl·HCl | 1,3-bis(2,6-dimethylphenyl)-imidazolium chloride |
| SN | nucleophilic substitution |
| SPO | secondary phosphine oxide |
| SPS | solvent purification system |
| <i>T</i> | temperature |
| t | triplet or time |
| <i>t</i> | <i>tert</i> |
| TADDOL | $\alpha,\alpha,\alpha',\alpha'$ -tetraaryl-2,2-disubstituted 1,3-dioxolane-4,5-dimethanol |
| TAM | triazolyldimethylmethyl |
| TBS | <i>tert</i> -butyldimethylsilyl |
| TEMPO | 2,2,6,6-tetramethylpiperidine- <i>N</i> -oxide |
| Tf | trifluoromethanesulfonyl (triflyl) |

X

| | |
|----------|---|
| TFA | trifluoroacetic acid |
| TFE | 2,2,2-trifluoroethanol |
| THF | tetrahydrofuran |
| TLC | thin layer chromatography |
| TM | transition metal |
| TMEDA | <i>N,N,N',N'</i> -tetramethylethane-1,2-diamine |
| TMS | trimethylsilyl |
| Ts | <i>para</i> -toluenesulfonyl (tosyl) |
| TPP | tetraphenylporphyrin dianion |
| t_r | retention time |
| UV | ultraviolet |
| X | (pseudo)halide |
| Xantphos | 4,5-bis(diphenylphosphino)-9,9-dimethylxanthene |

1. Introduction

The tremendous development of organic synthesis within the last century has allowed for the preparation of life-saving pharmaceuticals, crop-protection agents, functional materials such as polymers, and dyes, among others, affecting the life of billions of people. Despite its transformative nature, which has resulted in diverse applications with countless benefits for the society, chemistry continues to be perceived as a polluting science due to resource and energy consumption, waste generation, and the use of toxic chemicals.

In order to obviate or at least reduce these drawbacks, the development of more environment-friendly, resource-,^[1] step- and atom-economical^[2] synthetic methodologies is highly desirable. In this perspective, *Anastas* and *Warner* proposed the “12 Principles of Green Chemistry”,^[3] which are meant to guide the synthetic chemist towards environmentally-benign chemical processes. Among those, catalysis, that is the use of catalytic rather than stoichiometric amounts of reagents, and the direct use of readily available chemicals without the need of pre-functionalization are particularly attractive approaches to reduce the formation of byproducts and thereby chemical waste. Furthermore, the use of less-toxic compounds and mild reaction conditions is also expected to enable safer chemical processes.

1.1. Transition Metal-Catalyzed C–H Activation

“A dream of organic chemists has been the discovery of coupling reactions with no prefunctionalization of the coupling partners.” (V. Snieckus)^[4]

Organic synthesis, including catalytic reactions, has long been dominated by the transformation of functional groups, hence requiring pre-functionalized starting materials. In this context, a major achievement of catalysis in the past five decades

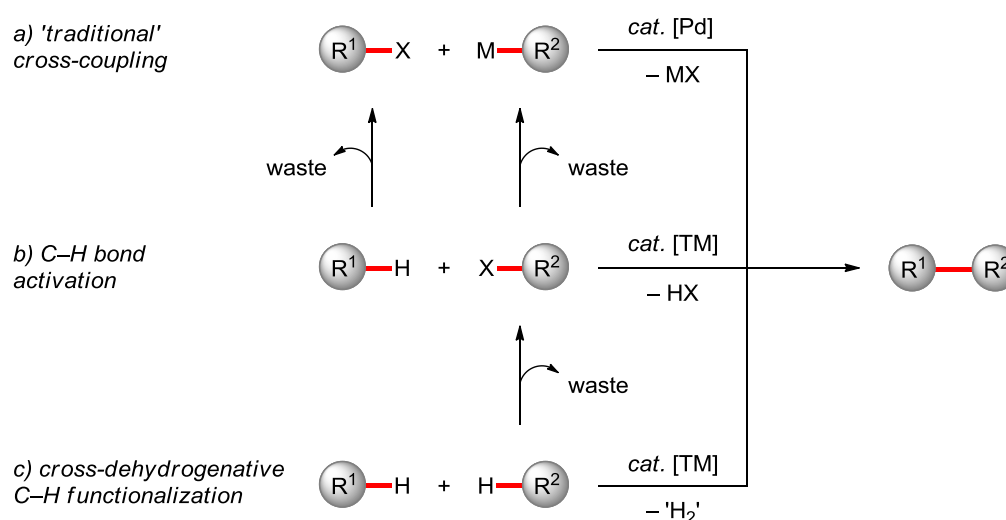
has been the development of transition metal-catalyzed cross-couplings, forming carbon–carbon (C–C) and carbon–heteroatom (C–Het) bonds.^[4] Interestingly, pioneering results were obtained as early as in the late 19th century by, *inter alia*, *Glaser*^[5] and *Ullmann*^[6] using stoichiometric or catalytic amounts of copper. Nevertheless, transition metal-mediated coupling reactions have only found broad applications since the development of palladium-catalyzed cross-couplings between organometallic reagents with organic electrophiles.^[4]

Major successes in this field have been realized for the formation of C–C bonds using diverse coupling partners, resulting in the development of numerous name reactions, such as the *Suzuki–Miyaura*,^[7] *Negishi*,^[8] *Mizoroki–Heck*,^[9] *Kumada–Corriu*,^[10] *Hiyama*,^[11] *Stille*^[12] and *Sonogashira–Hagihara*^[13] cross-coupling reactions. Additionally, while not always C–C bond forming processes, the *Tsuji–Trost* reaction^[14] as well as the *Buchwald–Hartwig* amination^[15] should be mentioned as other significant milestones in palladium coupling catalysis. Palladium-catalyzed cross-couplings are nowadays a routine tool in organic synthesis, with applications ranging from material sciences to the late-stage diversification of biologically active compounds,^[16] and their importance was recognized by the Nobel Prize in Chemistry awarded collectively to *Heck*, *Negishi* and *Suzuki* in 2010.^[4,17]

However, those processes still suffer from various drawbacks which significantly affect their ecological footprint. Indeed, the need for rare noble transition metal catalysts, pre-functionalized substrates and sensitive organometallic reagents, as well as the generation of stoichiometric amounts of harmful waste, render those processes hazardous and harmful to the environment.

Significant achievements have been made to address those limitations, which include the use of sustainable non-noble metal catalysts such as nickel^[18] and iron,^[19] the use of biomass-derived solvents,^[20] and the development of reusable^[21] or highly active catalysts operating at low loadings.^[22] However, those approaches do not tackle the main issues of cross-coupling chemistry, namely the need for pre-functionalized starting materials and the generation of stoichiometric waste byproducts.

Therefore, the direct functionalization of omnipresent C–H bonds would appear as a highly desirable alternative to conventional cross-couplings due to the improved step- and atom-economy (Scheme 1.1). In this context, catalytic C–H activation has experienced a tremendous development in recent years,^[23] and has now surfaced as a transformative tool for molecular syntheses, with notable applications in pharmaceutical industries,^[24] as well as the synthesis of complex bioactive natural products^[25] and material sciences,^[26] among others. Nevertheless, the direct functionalization of C–H bonds with organic electrophiles still requires the prefunctionalization of one of the coupling partners, generating a stoichiometric amount of (pseudo)halogenated byproducts (Scheme 1.1b). In contrast, hydroarylations^[27] would be perfectly atom-economical, redox-neutral, and more step-economical as well since no pre-functionalization is required. Cross-dehydrogenative C–H activation would also, in theory, be a fully atom-economical approach, as only molecular hydrogen is formally generated as a byproduct (Scheme 1.1c). However, those reactions usually require a stoichiometric oxidant, which results in stoichiometric waste generation, and typically suffer from a rather narrow substrate scope.

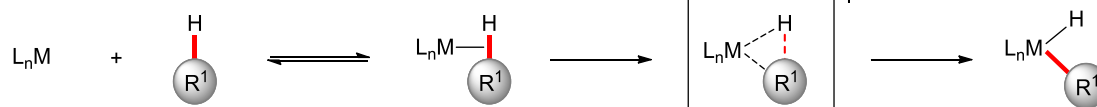


Scheme 1.1. Comparison of traditional cross-coupling vs. C–H activation.

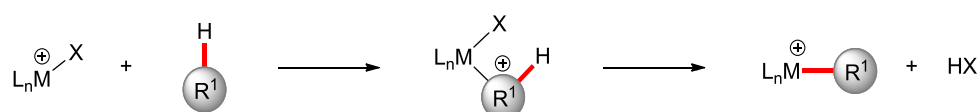
Nevertheless, several challenges which need to be overcome are associated with synthetically useful C–H activation. First, the C–H bond is typically significantly more stable than the C–X bond of common cross-coupling partners (e.g. $\text{BDE}(\text{Ph-H}) \approx 113 \text{ kcal mol}^{-1}$ vs. $\text{BDE}(\text{Ph-Cl}) \approx 97 \text{ kcal mol}^{-1}$, $\text{BDE}(\text{Ph-Br}) \approx 84 \text{ kcal mol}^{-1}$, $\text{BDE}(\text{Ph-I}) \approx 67 \text{ kcal mol}^{-1}$).^[28] While early examples of C–H activations required harsh reaction conditions which strongly limited their applications to the synthesis of complex and sensitive molecules, recent progress has focused on the development of milder^[29] and more selective processes. The mechanism of the key C–H cleavage step has been studied extensively as its understanding is particularly important for the design of efficient catalytic processes. Excluding outer-sphere mechanisms (e.g. carbene/nitrene insertions^[30] or radical reactions^[31]), five general modes of action have been proposed for the C–H metalation step depending on the nature of the substrate, the metal catalyst, its ligands and oxidation state (Scheme 1.2).^[32] These pathways consist of oxidative addition, electrophilic substitution, σ -bond metathesis, 1,2-addition and base-assisted metalation. The oxidative addition pathway is typical for electron-rich, low-valent complexes of late transition metals, such as rhenium, ruthenium, osmium, iridium, platinum and even iron,^[32b] from which higher oxidation states are readily accessible (Scheme 1.2a). While this mechanism has also been proposed for early transition metals, later findings provided support for σ -bond metathesis, typically involving an alkyl- or hydride-metal complex (*vide infra*). Late transition metals in high oxidation states, such as Pd(II), Pt(II), Pt(IV), or Hg(II), tend to undergo C–H activation by an electrophilic substitution in which the metal acts as a Lewis acid. In those processes, the putative intermediate is formed by electrophilic attack of the metal, usually in a strongly polar medium (Scheme 1.2b). For early transition metals, as well as lanthanides and actinides, σ -bond metathesis tends to be the preferred pathway. A key feature of this mechanism is the concerted formation and breaking of C–H and C–M bonds in the transition state (Scheme 1.2c).^[32b] The 1,2-addition route is observed for metals with an unsaturated M=Y bond, typically imido, oxo and alkylidene complexes. Those transformations occur *via* a $[2_{\sigma}+2_{\pi}]$ -type reaction where the Y group serves as the formal hydrogen acceptor (Scheme 1.2d). Finally,

another category of C–H cleavage processes is the base-assisted C–H activation. Here, the base, most commonly a carboxylate,^[32a] facilitates the proton abstraction during the C–H scission step.

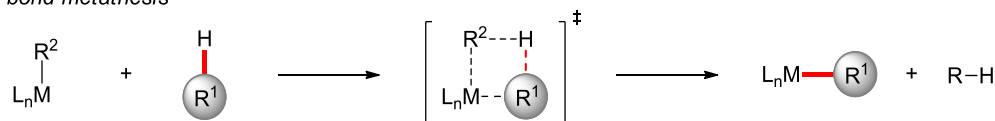
a) oxidative addition



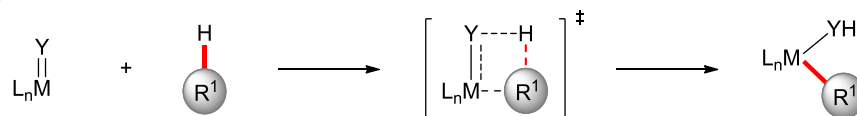
b) electrophilic substitution



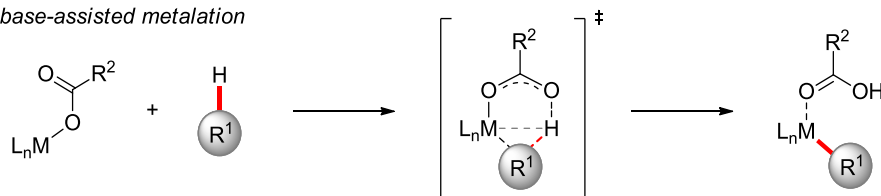
c) σ -bond metathesis



d) 1,2-addition



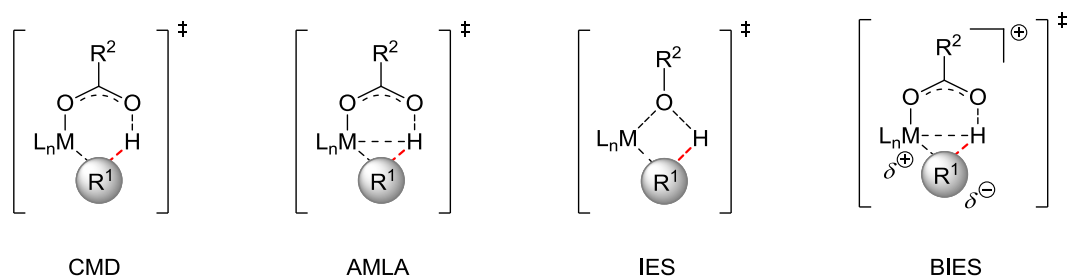
e) base-assisted metalation



Scheme 1.2. Different pathways for organometallic C–H activation.

Further investigations on base-assisted C–H activations unravelled several different possible pathways (Scheme 1.3). Following the pioneering theoretical studies of *Sakaki*,^[33] the synergistic interaction between the metal center, carboxylate-ligand and C–H bond was rationalized by *Gorelsky* and the late *Fagnou*, leading to the

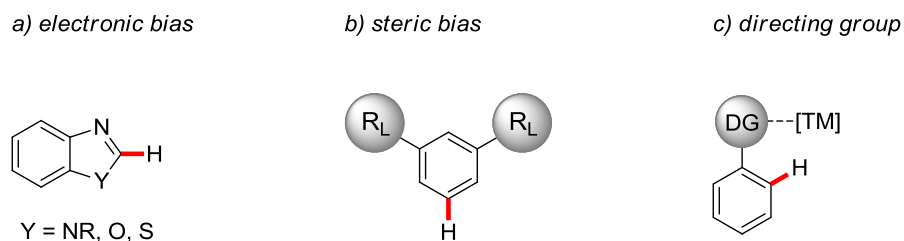
concept of *concerted metalation-deprotonation* (CMD) occurring *via* a six-membered transition state.^[34] Subsequent computational studies by *Macgregor* suggested the relevance of an agostic metal-hydrogen interaction in a mechanism named *ambiphilic metal-ligand activation* (AMLA).^[32c,35] Those processes are typically characterized by a considerable kinetic isotope effect (KIE) and a preference for electron-deficient substrates. In contrast, the term *internal electrophilic substitution* (IES)^[36] describes a mechanism occurring through a highly strained four-membered ring transition state. This process has been proposed for reactions involving alkoxide bases. Recently, the concept of *base-assisted internal electrophilic substitution* (BIES)^[37] has emerged in order to explain the preference for electron-rich substrates in several catalytic transformations.



Scheme 1.3. Proposed transition states for base-assisted C–H metalations.

Another challenge of C–H activation chemistry is the fact that C–H bonds are omnipresent in organic compounds and have almost identical bond dissociation energies. The control of selectivity in those transformations is therefore a task of key importance. Various approaches have been developed to tackle this issue, namely the use of substrate's electronic bias, steric control, or a Lewis-basic group that coordinates to the transition metal catalyst and directs the C–H activation at the desired position (Scheme 1.4). Since electronic and steric biases depend on the substrate itself, those approaches usually result in a rather narrow substrate scope. In contrast, the introduction of a directing group^[38] (DG) allows for a broad variety of substrates to be selectively functionalized. Nevertheless, a major limitation of this approach is the need to incorporate the directing group in the substrate. However,

the use of weakly coordinating,^[39] removable^[40] or transient^[41] directing groups has considerably expanded the possibilities of this approach.



Scheme 1.4. Methods to achieve positional selectivity in C–H activation.

Major progress in the field of C–H activation has been achieved with late transition metal catalysts. However, due to their high cost,^[42] low abundance^[43] and high toxicity,^[44] this approach is rather not sustainable. Therefore, the development of catalytic methods for the functionalization of otherwise inert C–H bonds employing non-noble 3d metals has attracted considerable interest in the last decade.^[45] *Inter alia*, the development of cobalt-,^[46] iron-,^[47] nickel-,^[48] manganese-^[49] and copper-catalyzed^[50] C–H activations has been particularly successful.

Despite those major advances, full selectivity control in enantioselective C–H functionalizations continues to heavily rely on precious 4d and 5d transition metals, prominently featuring toxic and expensive palladium, rhodium, and iridium complexes.^[51] Indeed, only a few extremely rare examples of enantioselective C–H functionalizations utilizing first-row transition metal catalysts had been published at the outset of this thesis. However, several additional contributions to this burgeoning field of research would later be disclosed in the course of the present work, by *Ackermann* and *Cramer*, among others (*vide infra*).^[52] In this context, it should be noted that the development of catalytic enantioselective methodologies in organic synthesis is a topic of extremely high interest, as best exemplified by the Nobel Prize in Chemistry awarded in 2001 to *Noyori*, *Knowles* and *Sharpless* for their seminal contributions to asymmetric catalysis.^[53] Therefore, given the sustainable nature and transformative power of 3d metal-catalyzed C–H activations, further exciting

developments are expected in the near future in this rapidly-evolving research area.^[52]

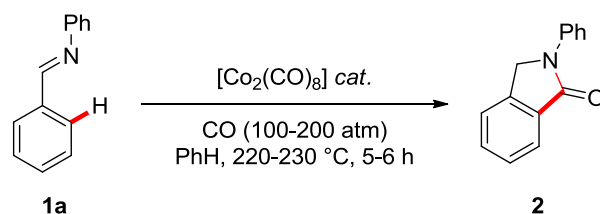
1.2. Cobalt-Catalyzed C–H Activation

The potential of cobalt complexes in catalysis has long been recognized. Indeed, during the course of World War II, *Roelen* discovered, while studying the *Fischer–Tropsch* process, that cobalt was able to promote the hydrocarbonylation of ethylene.^[54] The reaction was found to occur in solution and, consequently, is sometimes considered as the birth of homogeneous catalysis.^[54]

Thereafter, *Kharasch* reported on the cobalt-catalyzed homo-coupling of aryl Grignard reagents.^[55] Later notable developments of cobalt chemistry in organic synthesis include the well-known *Pauson–Khand*^[56] and *Nicholas*^[57] reactions, cross-couplings,^[58] hydrogenations,^[59] cycloadditions, annulations, and many more.^[60]

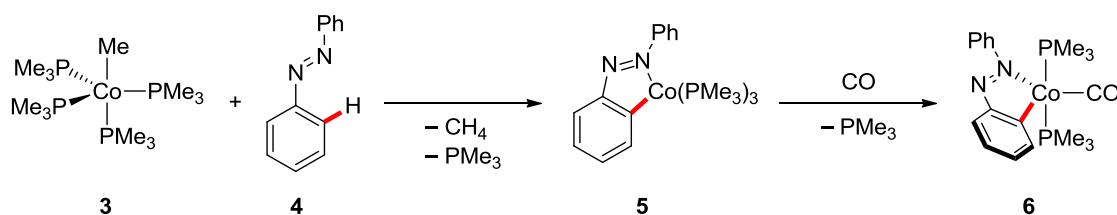
1.2.1. Early Contributions

In the 1950s, *Murahashi* disclosed the synthesis of 2-phenylphthalimidine **2** from imine **1a** and carbon monoxide in the presence of catalytic dicobalt octacarbonyl (Scheme 1.5).^[61] The scope of the transformation was soon extended to include azobenzenes.^[62] This work is absolutely remarkable as it not only represents the first cobalt-catalyzed organometallic C–H activation, but also one of the first examples of directing group assisted C–H activation, if not the first.



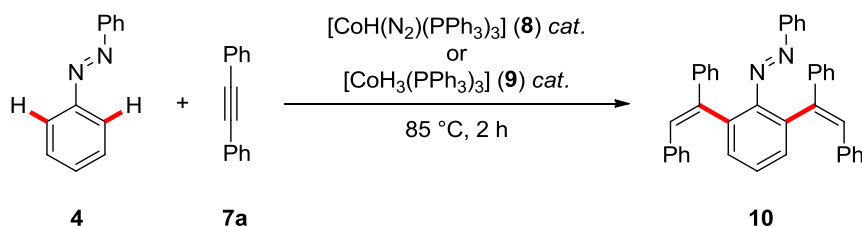
Scheme 1.5. Cobalt-catalyzed carbonylative cyclization of imines.^[61]

This work remained largely neglected until the early 1990s with *Klein's* studies on the preparation of cyclometalated cobalt complexes from $[\text{Co}(\text{CH}_3)(\text{PMe}_3)_4]$ (**3**) and various chelating substrates (Scheme 1.6).^[63] Experimental evidence suggested the reaction to be initiated by the dissociation of a PMe_3 ligand, which is replaced by azobenzene **4**, followed by *ortho*-metalation with elimination of methane to deliver **5**.^[63f] Interestingly, unlike in *Murahashi's* work, no cyclized product was obtained upon exposure to carbon monoxide. Remarkably, due to the high reactivity of complex **3**, even 4-membered metallacycles could be obtained.^[63e]



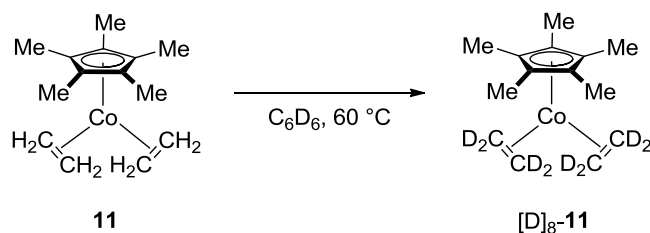
Scheme 1.6. Stoichiometric cyclocobaltation of azobenzene **4**.^[63f]

A major contribution in cobalt catalysis was achieved in 1994 by *Kisch*, who reported on the hydroarylation of tolane **7a** with azobenzene **4** using a catalytic amount of cobalt-hydride complexes **8** or **9** (Scheme 1.7).^[64] This work represents the first cobalt-catalyzed C–H hydroarylation of alkynes, where the authors proposed the active catalyst to be generated *in situ* after the loss of N_2 or H_2 , respectively. Following the seminal work of *Kisch*, *Petit* used a related well-defined, low-valent phosphine-cobalt complex $\text{Co}(\text{PMe}_3)_4$ as catalyst for various hydroarylations of alkynes and alkenes.^[65]



Scheme 1.7. Cobalt-catalyzed hydroarylation of toluene **7a** with azobenzene **4**.^[64]

Another key finding which would pave the way to future developments was subsequently disclosed by *Brookhart*,^[66] who observed H/D scrambling in Cp*Co(I) complex **11** upon heating in deuterated benzene (Scheme 1.8). Interestingly, the authors proposed the C(sp²)–H bonds to be activated through oxidative addition of a 16-electron cobalt species.



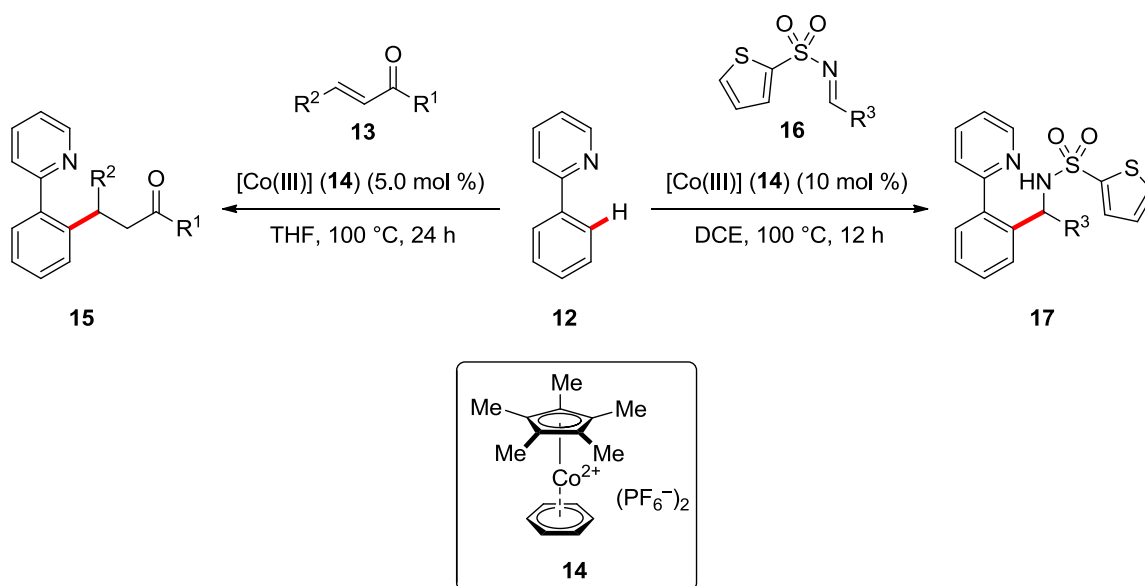
Scheme 1.8. H/D scrambling of complex **11** in C₆D₆.^[66]

Based on the contributions discussed above, cobalt-catalyzed C–H activation was for years dominated by the use of “low-valent” cobalt complexes or reductive conditions, with key contributions to the field by *Nakamura*,^[67] *Yoshikai*,^[46a,46d,68] and *Ackermann*,^[69] among others.^[45,46c] It is noteworthy that, in most of these studies, the active catalyst is ill-defined, being generated *in situ* from a cobalt salt, a (pre-)ligand and an organometallic species.

1.2.2. Cobalt(III)-Catalyzed C–H Activation

The use of cyclopentadienyl-rhodium(III) catalysts allowed for remarkable advancements in the field of transition metal-catalyzed C–H activation.^[70] However,

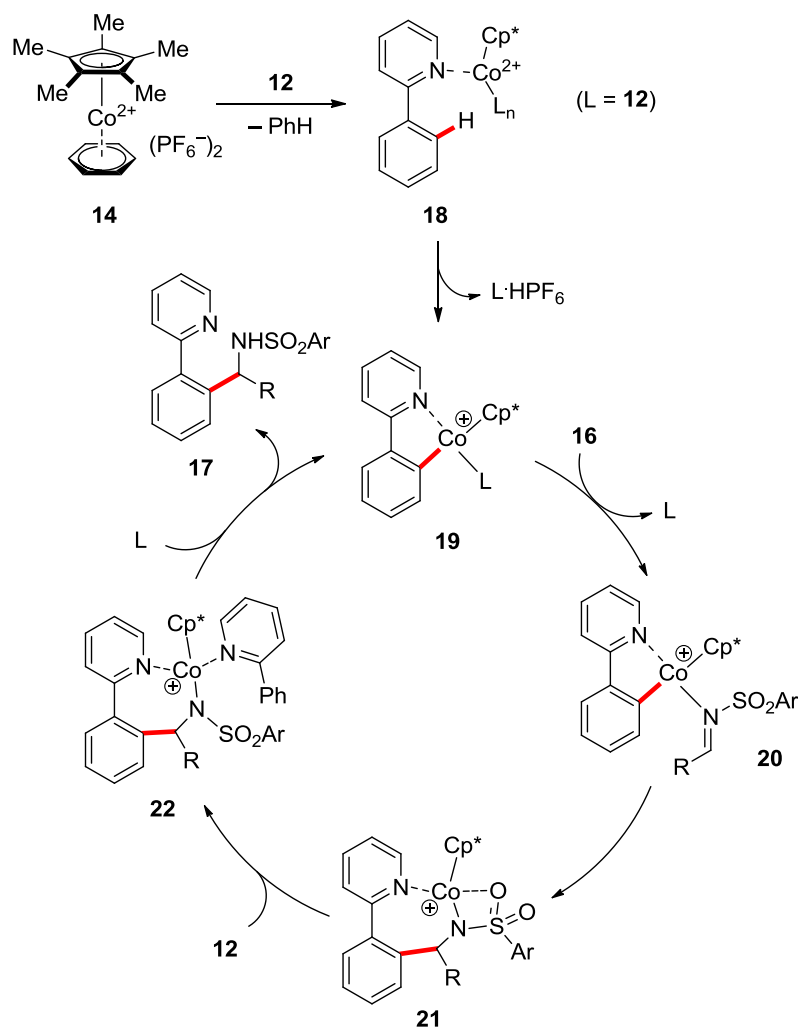
due to the low natural abundance and high cost of rhodium, the development of alternatives employing earth-abundant metals is highly desirable. In this context, a major progress was achieved in 2013 by *Yoshino, Matsunaga and Kanai*, who discovered the previously known cationic Cp*Co(III) complex **14**^[71] to be a potent catalyst for C–H activation (Scheme 1.9).^[72] It is noteworthy that, while various cyclopentadienyl-cobalt(III) complexes had been described previously,^[71,73] their use in C–H activation had remained unprecedented until then. Among the various cyclopentadienyl derivatives that were investigated, Cp* was identified as the best ligand, while other derivatives fell short in the envisioned transformation.^[72] Furthermore, no conversion was obtained with simple cobalt salts.



Scheme 1.9. Cobalt(III)-catalyzed hydroarylation of α,β -unsaturated ketones **13** and *N*-sulfonyl imines **16**.^[72]

Based on related rhodium(III)-catalyzed transformations,^[74] the mechanism of the cobalt(III)-catalyzed hydroarylation was proposed to be initiated by the displacement of the labile benzene ligand by the phenylpyridine substrate **12** to form **18** (Scheme 1.10).^[72] The authors suggested the subsequent C–H activation step to occur *via* an electrophilic aromatic substitution or a concerted metalation-deprotonation mechanism to form the cyclometalated intermediate **19**, which is

assumed to be the active catalyst. After ligand exchange with imine **16** to give **20**, insertion of the latter to give intermediate **21**, and proto-demetalation, the product **17** is released while the active catalyst is regenerated. In a subsequent report, this chemistry was extended to indole substrates by *Kanai* and *Matsunaga* using carboxylate additives which allowed for high catalytic efficacy.^[75]

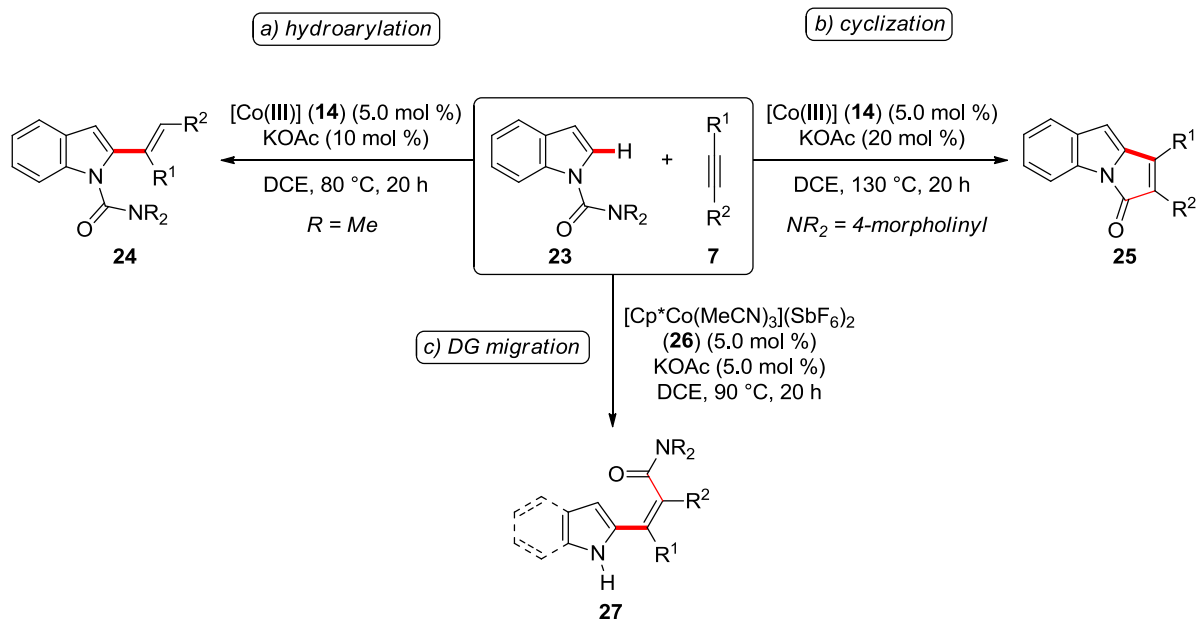


Scheme 1.10. Proposed mechanism of the Cp*Co(III)-catalyzed hydroarylation of imines **16**.^[72]

Taking inspiration from this elegant work, numerous reports on Cp*Co(III)-catalyzed C–H activation were disclosed in the following years.^[45,46,76] Only selected relevant

examples are discussed in this thesis, with a focus on enantioselective transformations.

The insertion reactions were not limited to activated C–C and C–N double bonds. Indeed, *Matsunaga, Kanai* and coworkers developed procedures for the selective cobalt-catalyzed hydroarylation of alkynes **7** with *N*-carbamoyl indoles and pyrroles **23** (Scheme 1.11).^[77] Remarkably, small changes of the directing group or the reaction conditions had a profound impact on the selectivity of the reaction. Indeed, while a judicious choice of the carbamate directing group and reaction temperature allowed for either the formation of the hydroarylated product **24** or the thermodynamically more stable cyclized product **25** (Scheme 1.11a–b),^[77d] the use of the cationic complexes $[\text{Cp}^*\text{Co}(\text{MeCN})_3]^{2+}$ provided access to tetrasubstituted alkenes **27** (Scheme 1.11c).^[77a] DFT calculations suggested the C–H cleavage step to occur through an acetate-enabled CMD manifold. Interestingly, $\text{Cp}^*\text{Rh}(\text{III})$ catalysts were found to be inefficient in the envisioned transformations, giving only small amounts of the alkenylated product **24**. The findings highlighted the different reactivity and complementarity of cobalt as compared to rhodium. Thus, the high nucleophilicity of the C–Co bond allowed for a unique reactivity.^[46a,46b,77a,77d] This difference may, partly, be explained by the higher electronegativity of cobalt compared to rhodium.^[78] The unique reactivity of cobalt(III) catalysts was also exploited by *Ackermann* in an allylation by C–H/C–C activation, where the less stable *Z*-isomer was selectively obtained, using $\text{Cp}^*\text{Co}(\text{III})$ catalysts, while the corresponding rhodium(III) complex gave unselective mixtures of diastereomers.^[79]

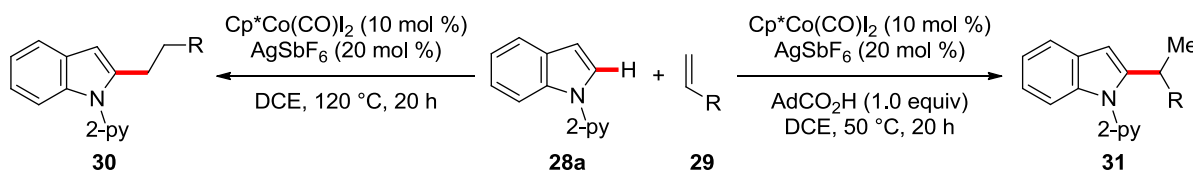


Scheme 1.11. Selectivity control in Cp*Co(III)-catalyzed C–H activation of indoles **23** with alkynes **7**.^[77a,77d]

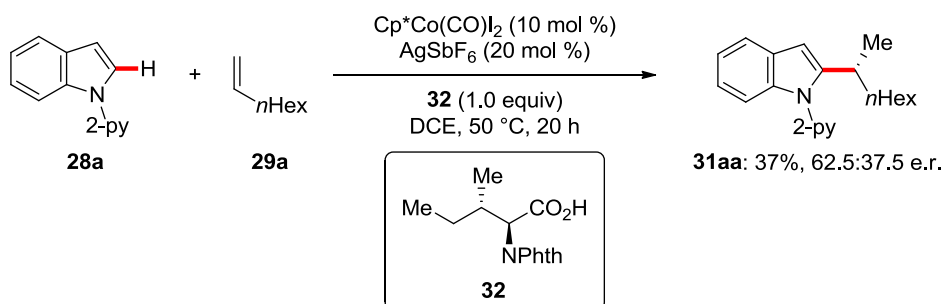
The scope of Cp*Co(III)-catalyzed C–H activations by hydroarylation is not limited to alkynes. Indeed, unactivated alkenes, and even allenes,^[80] have been employed as coupling partners in C–H activations. However, in the case of alkenes **29**, the control of linear vs. branched selectivities represents a challenging issue. Ackermann and coworkers disclosed in 2017 a procedure for the selective hydroarylation of unactivated alkenes (Scheme 1.12a).^[37b] Remarkably, while the *anti-Markovnikov* isomer **30** was obtained in the absence of additives, the introduction of 1.0 equivalent of 1-AdCO₂H was found to promote the selective formation of the branched product **31**. Detailed experimental and computational mechanistic studies revealed the switch of selectivity to be caused by a change of mechanism. Indeed, in the absence of the carboxylic acid additive, the C–H cleavage step was found to proceed *via* a ligand-to-ligand hydrogen transfer (LLHT)^[32a,37b,81] manifold involving two substrates **28** and delivering the linear product **30**. In contrast, 1-AdCO₂H was found to enable a base-assisted internal electrophilic type substitution (BIES) delivering the branched product **31**. This work also provided a proof-of-concept for an asymmetric version of this reaction. Thus, various chiral carboxylic acids were

tested in the transformation, with *N*-phthaloyl protected isoleucine (**32**) providing product **31aa** with 62.5:37.5 e.r. (Scheme 1.12b).

a) selectivity control in cobalt-catalyzed hydroarylations

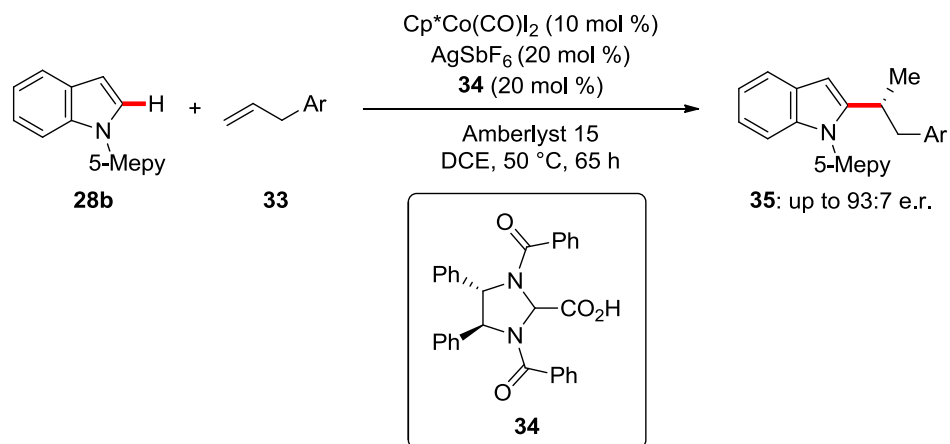


b) preliminary results towards an asymmetric transformation



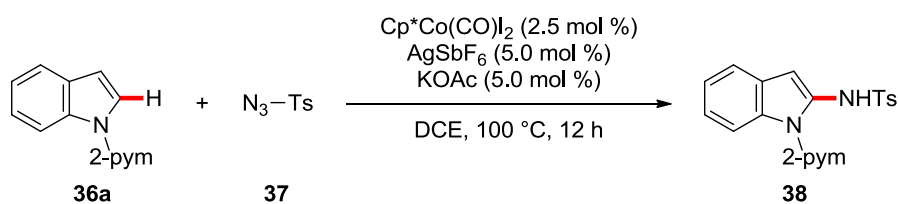
Scheme 1.12. Selectivity control in cobalt-catalyzed C–H alkylations.^[37b]

Triggered by this seminal report, the *Ackermann* group disclosed in 2018 the first highly enantioselective cyclopentadienyl-cobalt(III)-catalyzed C–H activation (Scheme 1.13).^[82] Essential to success was the design of the new chiral carboxylic acid **34**. Under the reaction conditions, various indoles **28b** and allylbenzene derivatives **33** were smoothly converted to the alkylated products **35** with excellent enantioselectivity. Computational studies and H/D-exchange experiments suggested the enantio-determining step to be an irreversible proto-demetalation promoted by the chiral acid **34**.



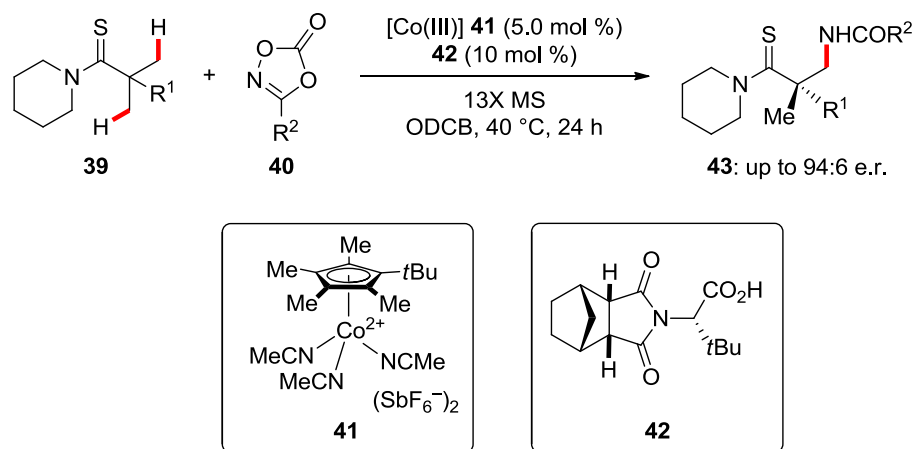
Scheme 1.13. Enantioselective cobalt(III)-catalyzed alkylation of indoles **28b**.^[82]

Furthermore, $\text{Cp}^*\text{Co}(\text{III})$ catalysis is not restricted to hydroarylations. Other C–C bond forming reactions include *inter alia* alkynylations,^[83] allylations,^[84] aminocarbonylations^[85] and various annulations.^[45] Besides C–C bond forming processes, the formation of C–X and C–N bonds has proven quite successful as well. In this context, *Matsunaga* and *Kanai* established a protocol for the C–H amination of indoles **36** with azides **37** using $\text{Cp}^*\text{Co}(\text{CO})\text{I}_2$ as an air-stable pre-catalyst (Scheme 1.14).^[86] Using $\text{Cp}^*\text{Co}(\text{CO})\text{I}_2$ and a silver salt to generate the cationic catalyst *in situ*, rather than using the highly sensitive sandwich complex **14**, has since been a widely applied approach due to its user-friendly nature. However, due to the inherently unsafe handling of usually explosive and toxic^[87] azides, protocols employing safer aminating reagents would be highly desirable. Other $\text{Cp}^*\text{Co}(\text{III})$ -catalyzed C–(pseudo)Het bond-forming reactions include halogenations,^[84d,88] cyanations^[84d,89] and thiolations,^[90] among others.^[45,46,76]



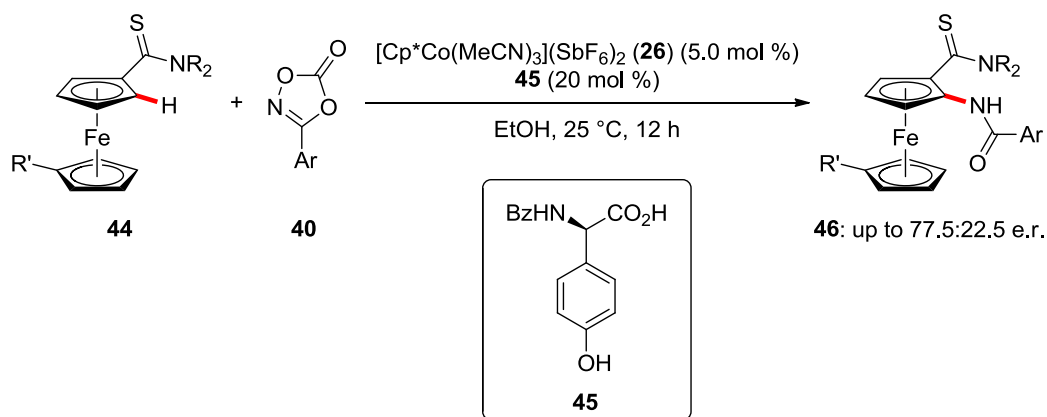
Scheme 1.14. Cobalt-catalyzed C–H amination of indoles **36** with azides **37**.^[86]

Inspired by this report and the topical interest for C–H aminations,^[23e] several research groups developed additional cobalt-catalyzed transformations to forge C–N bonds. Among other findings, the research groups of *Chang*,^[91] *Jiao*^[92] and *Ackermann*^[37e] independently pioneered the use of dioxazolones **40** as safer but potent amidating reagents in cobalt catalysis (see Chapter 3.1). Two years later, *Dixon* and *Seayad* reported a thioamide-assisted amidation of C(sp³)–H bonds.^[93] This work remains one of the rare examples of C(sp³)–H activation with a cobalt catalyst. DFT calculations provided support for the C–H activation step to proceed *via* an external carboxylate-assisted concerted metalation/deprotonation mechanism. Subsequently, *Matsunaga* and coworkers developed an asymmetric version of this protocol (Scheme 1.15).^[94] Here, the highly enantioselective C(sp³)–H amidation of thioamides **39** was achieved by the combination of the chiral carboxylic acid **42** with an achiral cobalt(III) complex. A remarkable feature of this work was the identification of the novel (*tert*-butyl-tetramethylcyclopentadienyl)Co(III) complex **41**, which promoted the reaction with higher enantioselectivity than the standard Cp*Co(III) complexes. Interestingly, while the tuning of the cyclopentadienyl ligand has been intensively investigated in rhodium catalysis,^[70a] variations of the Cp* ligand remain underdeveloped in Co(III)-catalyzed C–H activation. It is noteworthy that this approach represents the first example of enantioselective inner-sphere C(sp³)–H activation with a 3d transition metal catalyst.



Scheme 1.15. Enantioselective cobalt(III)-catalyzed C(sp³)–H amidation of thioamides **39**.^[94]

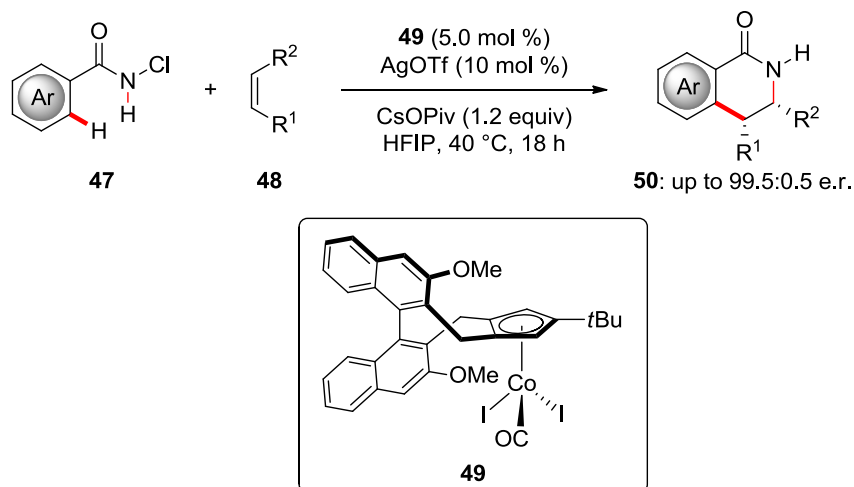
The concept of cooperation between an achiral cobalt(III) catalyst and a chiral carboxylic acid was further exploited by *Shi* and coworkers, who, taking inspiration from previous works on the cobalt-catalyzed amidation of ferrocenes by the same research group^[95] and *Ackermann*,^[96] achieved the enantioselective amidation of ferrocenes **44** with dioxazolones **40** (Scheme 1.16).^[97] Here, the design of the novel chiral monoprotected amino acid (MPAA) ligand **45** allowed for the synthesis of amidated ferrocene thioamides **46** with high yield but moderate enantioselectivity. Interestingly, the modest optical purity could be improved by a single crystallization to afford the amidated products in >99% ee.



Scheme 1.16. Enantioselective cobalt(III)-catalyzed C–H amidation of ferrocenes **44**.^[97]

As discussed above, the pioneering examples of enantioselective cyclopentadienyl-cobalt(III)-catalyzed C–H transformations relied on the use of a simple achiral $\text{Cp}^*\text{Co}(\text{III})$ -catalyst in combination with an external chiral carboxylic acid. Very recently, *Cramer* reported a complementary approach based on the use of the finely designed trisubstituted^[98] chiral cyclopentadienyl-cobalt complex **49**.^[99] This catalyst proved highly efficient for the asymmetric synthesis of dihydroisoquinolones **50** from *N*-chlorobenzamides **47** and a diverse set of alkenes **48**^[100] (Scheme 1.17).^[99] The introduction of a bulky *tert*-butyl group on the chiral Cp ligand was essential to achieve high enantioselectivities, and was found to affect the dihedral angle of the binaphthyl backbone. A remarkably diverse set of alkenes was fully tolerated in the transformation, including styrenes, unactivated alkenes, acrylates and

N-vinylphthalimide, providing the cyclized product as a single regioisomer. In contrast, rhodium(III) complexes provided the products **50** with both lower regio- and enantioselectivities.^[101]



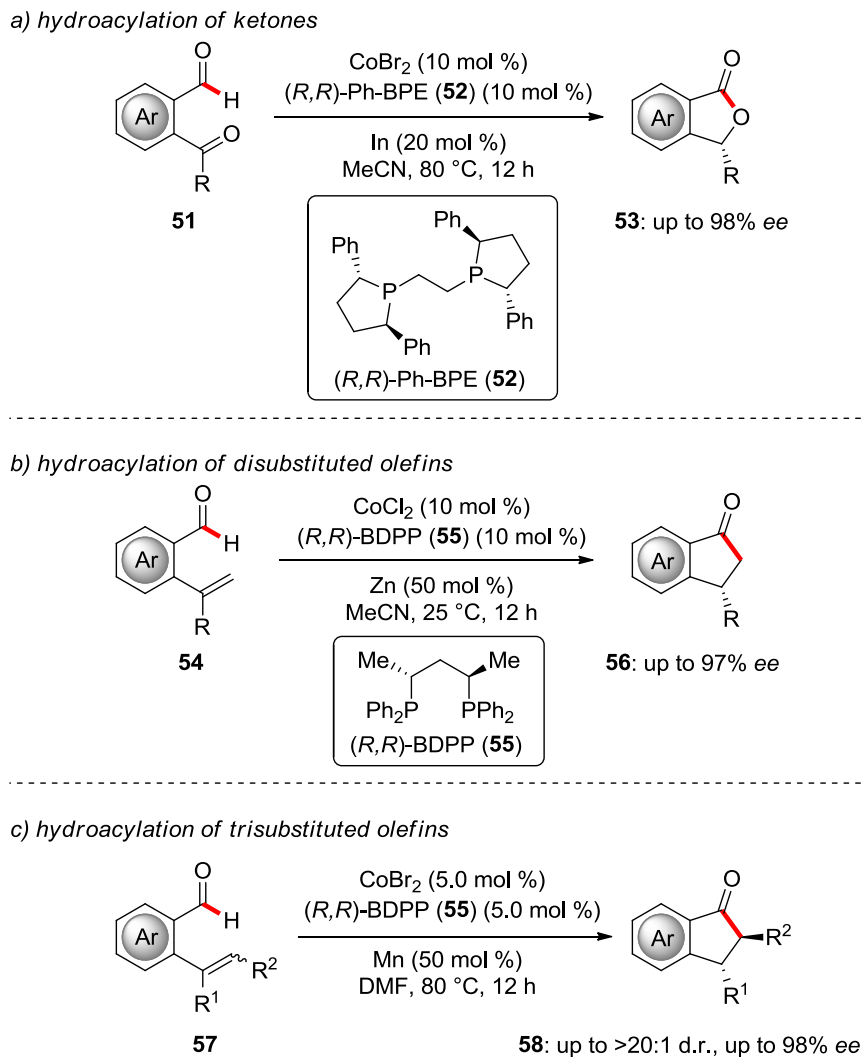
Scheme 1.17. Chiral cyclopentadienyl cobalt(III)-catalyzed C–H functionalizations with alkenes.^[99]

1.2.3. Enantioselective Cobalt-Catalyzed C–H Functionalizations under Reductive Conditions

In addition to the reports discussed above employing high-valent Cp*Co(III) complexes (Schemes 1.12–13, 1.15–17), several protocols employing cobalt catalysts for asymmetric C–H functionalizations under reductive conditions have been recently disclosed as well, but remain rare. Those reports highlight the current interest for enantioselective C–H activation with earth-abundant 3d metals,^[52] and the need to conduct further research in this burgeoning field of research.

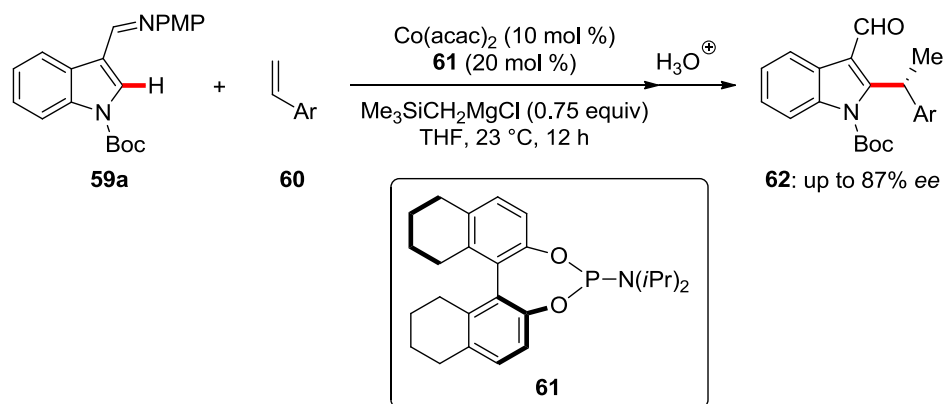
In 2014, the *Yoshikai* group disclosed an elegant enantioselective intramolecular hydroacylation of 2-acylbenzaldehydes **51** and 2-alkenylbenzaldehydes **54** for the synthesis of synthetically meaningful chiral phthalide **53** and indanone **56** building blocks (Scheme 1.18a–b).^[102] Previously, this type of asymmetric transformations had only been achieved with costly rhodium catalysts.^[103] The combination of CoBr₂

with (*R,R*)-Ph-BPE (**52**) was found to provide optimal results for the intramolecular hydroacylation of 2-acylbenzaldehydes **51** (Scheme 1.18a). The protocol could be extended to 2-alkenylbenzaldehydes **54** when using CoCl_2 and (*R,R*)-BDPP (**55**) as the optimal catalytic system to deliver indanones **56** (Scheme 1.18b). Mechanistic studies provided evidence for a relatively facile C–H activation step and a subsequent rate-limiting reductive elimination step. In a later report, *Yoshikai* and *Gosmini* expanded this approach from disubstituted alkenes **54** to more challenging trisubstituted alkenes **57**, allowing for the expedient synthesis of highly functionalized chiral cyclic ketones **58** (Scheme 1.18c).^[104] Here, the combination of CoBr_2 and (*R,R*)-BDPP (**55**) provided optimal results. Interestingly, the authors noted that the *E/Z* ratio of the starting materials **57** only had a minor effect on the enantiomeric excess of the products **58**.



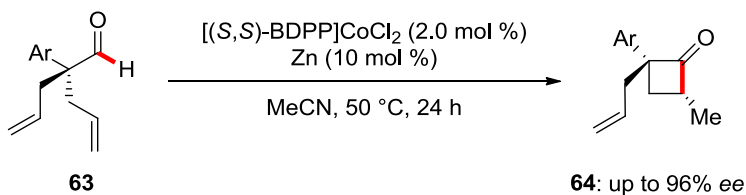
Scheme 1.18. Enantioselective cobalt-catalyzed intramolecular hydroacylations.^[102,104]

Yoshikai had previously disclosed a cobalt-catalyzed C–H alkylation of indoles with alkenes.^[105] In 2015, the same research group developed an enantioselective variation of this reaction (Scheme 1.19).^[106] Remarkably, this work represents the first asymmetric *intermolecular* transformation by cobalt-catalyzed C–H activation. While simple BINOL-derived phosphoramidites provided the desired alkylated product **62** in low yield and enantiomeric excess, variations of the chiral diol backbone significantly increased the enantioselectivity of the transformation. Thereby, diversely substituted indoles **59a** and styrene derivatives **60** furnished the alkylated products **62** in good yields and high enantioselectivities in the presence of TMSCH₂MgCl.



Scheme 1.19. Enantioselective cobalt-catalyzed hydroarylation of styrenes **60** with indoles **59a**.^[106]

In 2017, the *Dong* group disclosed a unique desymmetrization strategy for the intramolecular enantioselective hydroacylation of alkenes **63** to construct chiral cyclobutanone derivatives **64** (Scheme 1.20).^[107] A cobalt catalyst with (*S,S*)-BDPP (*ent*-**55**) as the chiral ligand enabled the highly selective synthesis of unusual strained four-membered rings **64** rather than their five-membered regioisomers. The authors tested diversely α -substituted dienyl aldehydes **63** which underwent the cyclization with high regio- and enantio-selectivities, with sensitive functionalities such as TMS or chloro being fully tolerated in the transformation. Mechanistic studies provided support for a cobalt(0)/cobalt(II) catalytic cycle.



Scheme 1.20. Enantioselective hydroacylation for the synthesis of cyclobutanones **64**.^[107]

1.3. Iron-Catalyzed C–H Activation

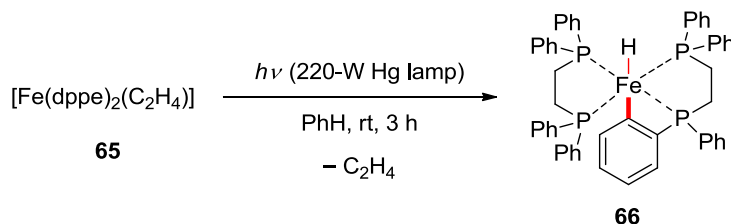
Iron is by far the most abundant metal on Earth.^[43] Applications of iron catalysts in molecular syntheses benefit from comparatively low costs and toxicities, as well as a broad array of available oxidation states.^[108] Furthermore, the considerable increase of prices of many late transition metals in recent years created a demand for less expensive alternatives.^[108b]

The independent synthesis of pentacarbonyliron in 1891 by *Mond*^[109] and *Berthelot*^[110] is usually considered as the birth of organoiron chemistry.^[108c] A subsequent milestone of iron chemistry was the identification of iron salts as potent catalysts in reactions with Grignard reagents, including homocouplings, by *Kharasch* in 1941.^[55,111] The serendipitous discovery of ferrocene, reported by *Pauson* and *Kealy* in 1951^[112] and whose transformative applications would change the face of chemistry,^[113] was another major contribution in organometallic iron chemistry. The 1950s also marked the first use of well-defined organoiron species in organic synthesis with the preparation of hydroquinone by *Reppe* from acetylene and iron carbonyl complexes.^[114]

A breakthrough in organoiron catalysis was the identification of iron salts as catalysts in cross-couplings between Grignard reagents and vinyl bromides by *Kochi* in 1971,^[115] which, remarkably, predated subsequent works with palladium and nickel catalysts.^[4] Interestingly, the authors probed various metal halides and identified iron as “one of the most effective metal catalysts for the promotion of the reactions between Grignard reagents and organic halides.”^[115a] Although the use of iron catalysts in cross-couplings was first overlooked due to the development of palladium catalysis,^[4] it has since experienced a renaissance. However, despite major progress,^[19] good mechanistic understanding^[19] is lacking and the design of novel ligands is required for further advancements.^[47b]

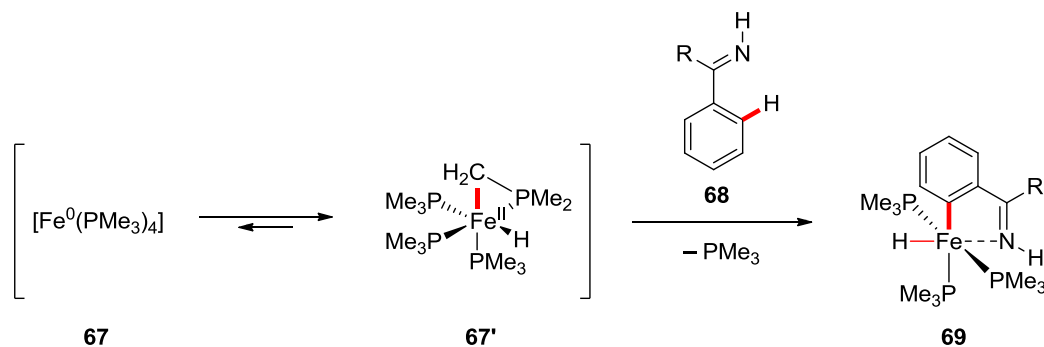
From a historical point of view, it should be noted that stoichiometric C–H activation with iron complexes were reported as early as 1968 by *Hata*.^[116] Irradiation of the

iron(0) complex **65** resulted in the loss of ethylene and oxidative addition into a C(sp²)–H bond of the phosphine ligand (Scheme 1.21).



Scheme 1.21. Synthesis of cyclometalated complex **66** by photoinduced C(sp²)–H activation.^[116]

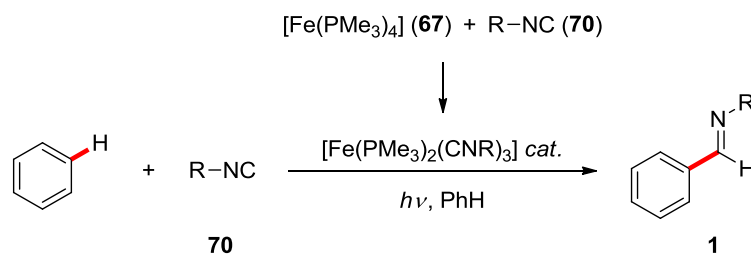
Later works further demonstrated the feasibility of stoichiometric C–H activation with highly reactive low-valent iron complexes.^[117] Among others, Fe(PMe₃)₄ (**67**), first independently prepared by *Muetterties*^[117b] and *Schmidbaur*^[118] in 1975, has been particularly effective in directing group-assisted cyclometalations (Scheme 1.22).^[119] Interestingly, Fe(PMe₃)₄ was found to predominantly exist as an iron(II) species due to C–H activation of the phosphine ligand.^[117b,118]



Scheme 1.22. Stoichiometric *ortho*-C–H metalation of ketimines with Fe(PMe₃)₄.^[119]

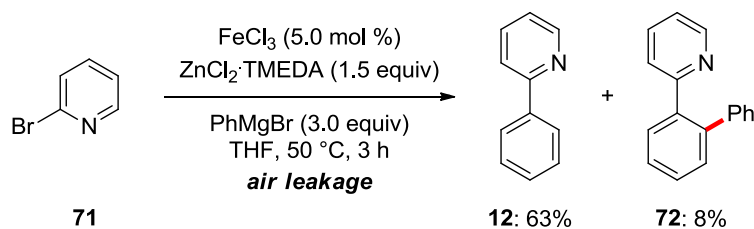
Fe(PMe₃)₄ would later prove instrumental to the development of *catalytic* C–H activations. Indeed, the first efforts towards a catalytic C–H activation employing an iron complex were reported by *Jones* in 1987.^[120] Here, the use of a catalyst generated from Fe(PMe₃)₄ (**67**) and isocyanide ligands (**70**) allowed for the synthesis of imines **1** from benzene under UV irradiation (Scheme 1.23). A reaction conducted

in C_6D_6 showed the solvent – and not the PMe_3 ligand – to be the source of the aldimine's hydrogen. Low concentrations were required due to substrate inhibition, and the authors suggested that light was needed to induce the dissociation of an isocyanide ligand to generate a reactive species able to insert into a C–H bond. Furthermore, in a later report over four decades after its original discovery, $Fe(PMe_3)_4$ was finally found to be effective in iron-catalyzed C–H activations without the need of additional ligands, as elegantly demonstrated by *Kakiuchi* for the carbonyl-assisted hydroarylation of alkenes.^[121] On the same line, a carbonyl-directed C–H methylation had been reported by *E. Nakamura* shortly before.^[122]



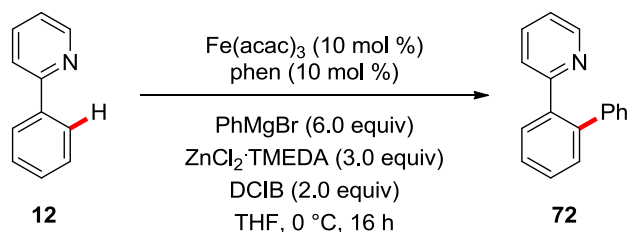
Scheme 1.23. Aldimine synthesis by iron-catalyzed C–H activation.^[120]

In 2008, a breakthrough in the field of iron-catalyzed inner-sphere C–H activation was made by *E. Nakamura*, who disclosed an iron-catalyzed oxidative C–H arylation.^[123] Interestingly, this discovery was made by serendipity by an undergraduate student working on an iron-catalyzed cross-coupling reaction.^[124] In addition to the expected product **12**, a small amount of the *ortho*-arylated phenylpyridine **72** was obtained as well (Scheme 1.24). Oxygen traces, as well as 2,2'-bipyridine (bpy) – another byproduct of the reaction – were later identified as essential to the formation of the C–H arylated product.



Scheme 1.24. Discovery of iron-catalyzed C–H arylation as a byproduct of cross-coupling.^[123]

After extensive optimization of this iron-catalyzed C–H arylation, 1,2-dichloro-2-methylpropane (DCIB) was identified as the optimal oxidant and phenanthroline as the best ligand (Scheme 1.25).^[123] Interestingly, the zinc additive was essential for the reaction to occur. While its role has been proposed to be the *in situ* generation of arylzinc species, Mg-free Ph₂Zn and PhZnBr fell short in delivering any arylated product **72**, either in the absence or in the presence of TMEDA.

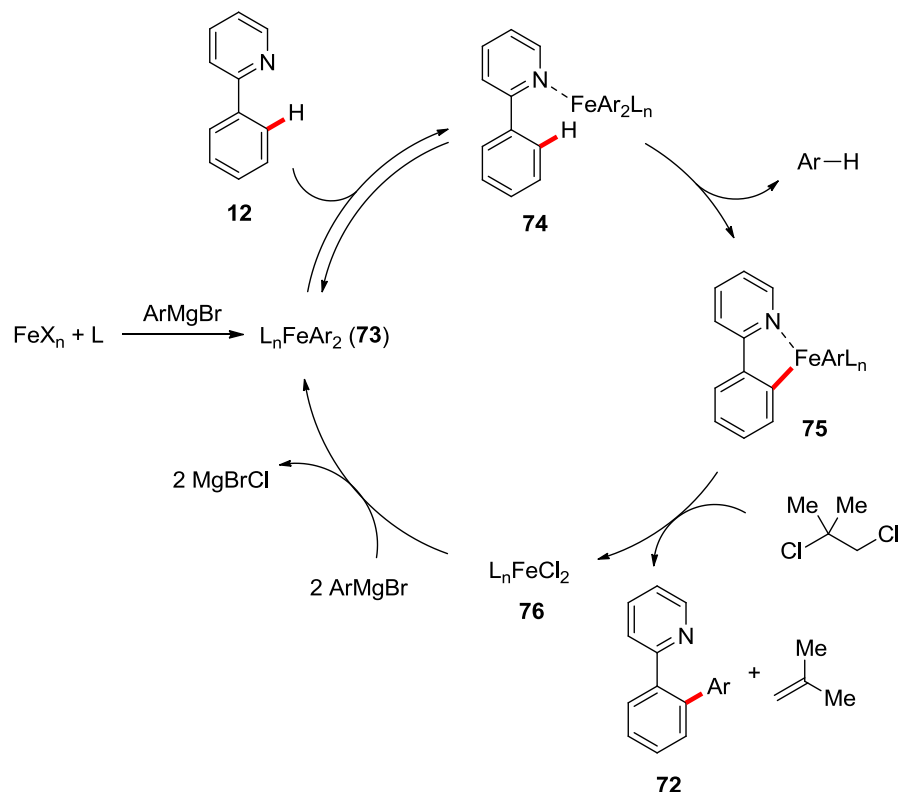


Scheme 1.25. First example of iron-catalyzed C–H arylation.^[123]

Subsequent achievements by *Nakamura* and others in the research area of iron-catalyzed C(sp²)–H arylation include, *inter alia*, the use of more synthetically useful imines^[125] and amides^[126] as the directing groups, the use of environmentally benign oxygen as oxidant,^[127] the arylation of non-aromatic C(sp²)–H bonds,^[128] the direct use of Grignard reagents in the absence of zinc additives,^[129] and the use of metallic magnesium to prevent the handling of sensitive and dangerous organometallic reagents.^[130]

While the authors did not propose a mechanism in their original reports, a plausible catalytic cycle was later suggested by *Nakamura* and coworkers based on KIE

studies and stoichiometric reactions (Scheme 1.26).^[129] A possible cycle is initiated by the formation of an aryliron species (**73**) by transmetalation of the aryl Grignard reagent to the iron center. Then, after a reversible coordination of the iron center to the pyridyl group of **12**, an irreversible C–H metalation with concomitant elimination of an arene can happen. Subsequently, the cyclometalated intermediate **75** can undergo a C–C bond forming reductive elimination upon reaction with DCIB to generate the desired arylated product **72**, isobutene, and dichloroiron species **76**. Finally, a transmetalation of **76** with the Grignard reagent regenerates the active species and closes the catalytic cycle.

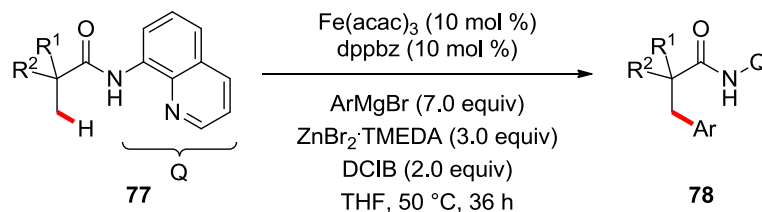
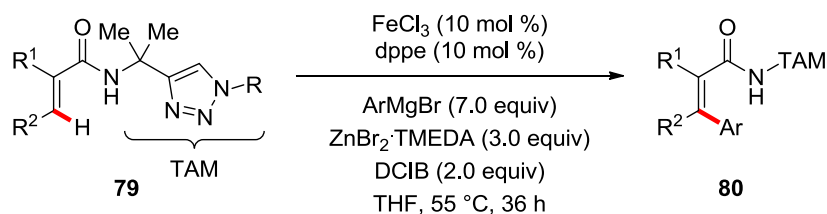
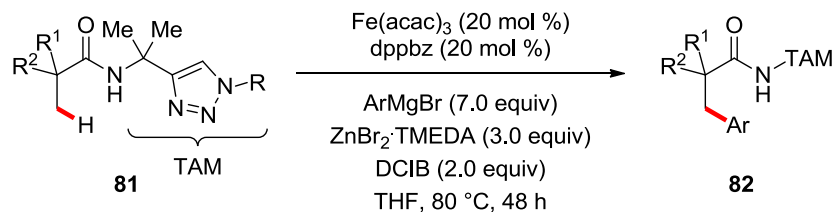


Scheme 1.26. Proposed mechanism of the oxidative iron-catalyzed C–H arylation.^[129]

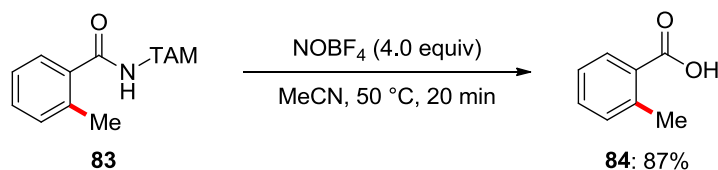
Thereafter, theoretical calculations on the mechanism of this reaction were reported by *Shaik* and *Chen*.^[131] Their findings suggest that both Fe(II) and Fe(III) can promote the C–H activation by means of an uncommon two-state reactivity^[132] (TSR) scenario. In this way, the initially excited low-spin singlet and doublet states

crossover through the high-spin ground states to promote the C–H scission. Furthermore, the authors suggested the C–H cleavage step to occur through a type of σ -bond metathesis. The key C–C bond forming step was proposed to occur *via* reductive elimination from an iron(III) species, after which the iron catalyst is re-oxidized by DCIB *via* a single electron transfer (SET) mechanism.

A breakthrough in the field was the introduction of bidentate^[133] directing groups, which not only allowed for unprecedented iron-catalyzed C(sp³)–H activations, but also significantly expanded the scope of possible transformations beyond oxidative arylations with organometallic reagents. In this context, *E. Nakamura* reported on an iron-catalyzed C(sp³)–H arylation of carboxamides **77** under the assistance of the 8-aminoquinoline directing group initially introduced by *Daugulis*^[134] for palladium catalysis (Scheme 1.27a).^[135] The important KIE and preference for terminal methyl groups over internal alkyl substituents provided support for an inner-sphere C–H activation process rather than a radical pathway. Shortly afterwards, *Ackermann* designed a modular triazole directing group which proved effective for the iron-catalyzed arylation of both C(sp²)–H and C(sp³)–H positions (Scheme 1.27b).^[136] It should be noted that all those transformations require bidentate phosphines as the ligands.

a) *E. Nakamura*b) *Ackermann*i. $\text{C}(\text{sp}^2)\text{-H}$ arylationii. $\text{C}(\text{sp}^3)\text{-H}$ arylation

iii. traceless removal of the TAM directing group



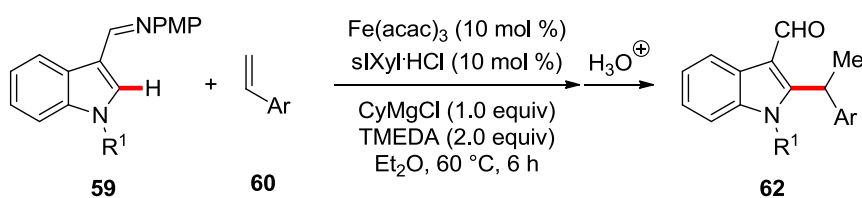
Scheme 1.27. Iron-catalyzed C–H arylation under bidentate directing group assistance.^[135-137]

Other significant advances were subsequently achieved under the assistance of bidentate directing groups by the research groups of *E. Nakamura*, *Ackermann* and *Cook*, among others. Major progresses include, but are not limited to, C–H alkylations with Grignard reagents or alkyl halides,^[138] $\text{C}(\text{sp}^2)\text{-H}$ allylations,^[137,139] $\text{C}(\text{sp}^2)\text{-H}$ benzylations,^[137,138d] $\text{C}(\text{sp}^2)\text{-H}$ alkynylations with alkynyl bromides,^[140]

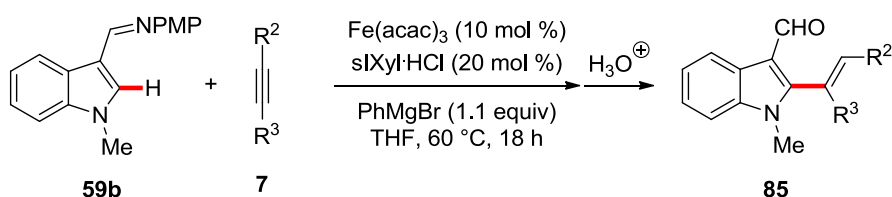
C(sp²)-H aminations with *N*-chloroamines,^[141] C-H alkenylations and arylations with organoboron reagents,^[142] C(sp²)-H and C(sp³)-H methylations with AlMe₃,^[143] various annulation reactions with alkynes^[144] and allenes,^[145] the C(sp²)-H alkylation of benzylamine derivatives^[146] and the two-fold C-H activation/cross-coupling of heteroarenes.^[147]

A rare iron-catalyzed C-H activation by hydroarylation was disclosed by *Yoshikai* in 2015.^[148] Taking inspiration from their previous work on cobalt catalysis^[105,106] (Scheme 1.19) and from the similar reactivity of iron and cobalt complexes in stoichiometric C-H activations,^[63c] the authors devised an iron-NHC catalyst for the addition of 3-iminoindoles **59** to styrenes **60** (Scheme 1.28a).^[148] Slight modifications of the reaction conditions allowed for the use of alkynes **7** as well (Scheme 1.28b).

a) iron-catalyzed hydroarylation of styrenes



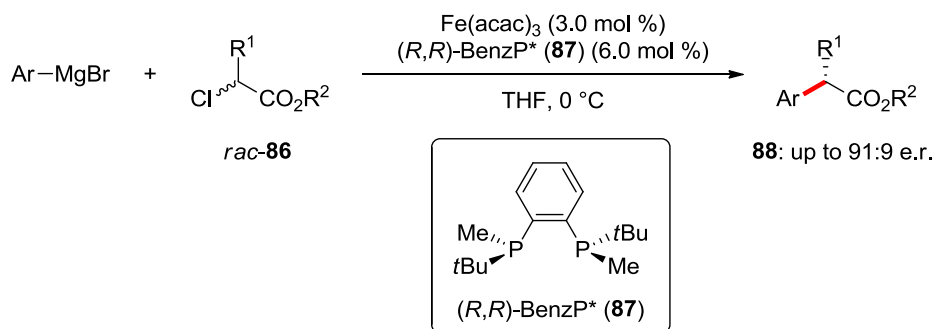
b) iron-catalyzed hydroarylation of internal alkynes



Scheme 1.28. Iron-catalyzed hydroarylations of styrenes and alkynes with indoles **59**.^[148]

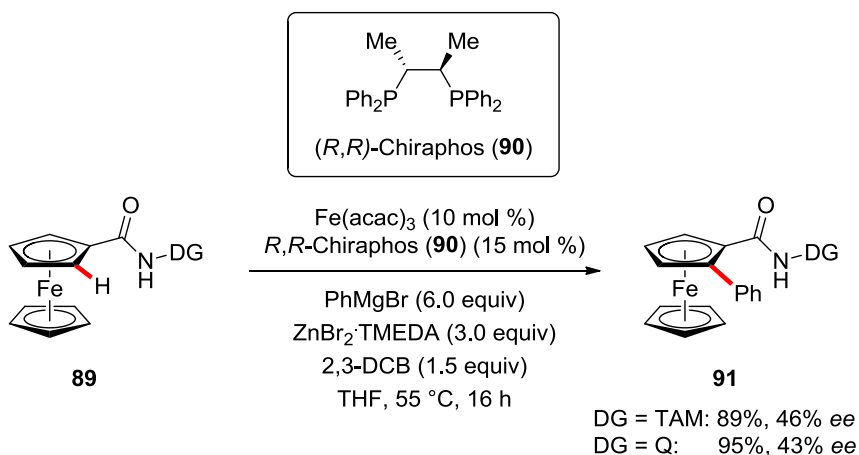
Despite major progress, iron-catalyzed C-H activation is still a recent field of research. Among other expected advances, the development of enantioselective C-H functionalizations is highly desirable. In this context, it should be noted that examples of asymmetric transformations by organometallic iron catalysts remain extremely rare. Indeed, only a single example had been reported at the outset of the

present work, namely an iron-catalyzed cross-coupling of α -chloroesters **86** with aryl Grignard reagents by *M. Nakamura* (Scheme 1.29).^[149] This approach would later be extended to arylborates.^[150]



Scheme 1.29. Iron-catalyzed enantioselective cross-coupling of α -chloroesters **86** with Grignard reagents.^[149]

While our work^[151] represents the very first enantioselective functionalization by iron-catalyzed inner-sphere C–H activation (see Chapter 3.2), it is noteworthy that *Butenschön* reported shortly afterwards an asymmetric arylation of ferrocene derivatives **89**, providing the planar-chiral product **91** in moderate enantiomeric excess (Scheme 1.30).^[152] It should be noted that *Ackermann* had previously identified ferrocene amides **89** as viable substrates in iron-catalyzed C–H activation.^[137]



Scheme 1.30. Enantioselective iron-catalyzed C–H arylation of ferrocenes **89**.^[152]

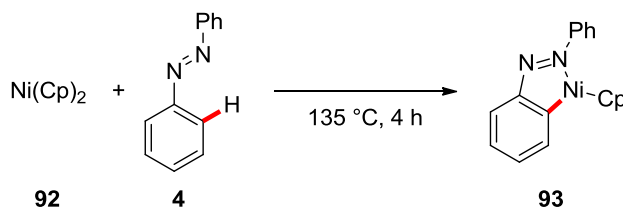
1.4. Nickel-Catalyzed C–H Activation

1.4.1. General Information

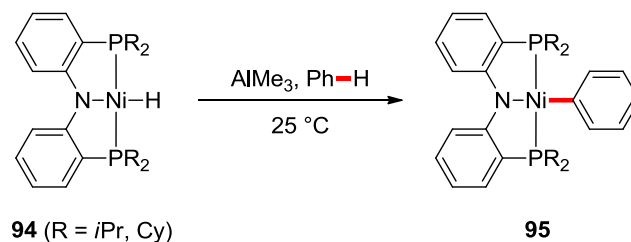
Nickel catalysts have been recognized as powerful tools in molecular syntheses, with numerous applications in C–C bond forming processes.^[153] Among others, applications to cross-coupling chemistry,^[18a,18b,18d,154] and the functionalization of otherwise inert C–O,^[18c,18e,155] C–F,^[156] and C–H bonds^[45,48] have gained significant momentum in recent years. While nickel has been considered as the “*impoverished younger sibling of palladium*”,^[153d] its high reactivity and unique properties, such as facile oxidative addition and a number of readily available oxidation states, render it particularly attractive in catalysis.^[153c,153d] Furthermore, it should be noted that the use of nickel in catalysis, notably in cross-couplings, actually pre-dates many noble metals.^[4]

The potential of nickel for C–H activation was first demonstrated by *Dubeck* and *Kleiman* in 1963,^[157] who prepared the cyclometalated complex **93** by the reaction of nickelocene **92** with azobenzene **4** (Scheme 1.31a). Thereafter, no other stoichiometric nickelation of non-activated^[158] C–H bonds was reported for several decades, until *Liang* discovered in 2006 that the pincer nickel complex **94** could react with benzene to deliver **95** without the need of a directing group (Scheme 1.31b).^[159]

a) cyclometalation of azobenzene **4** with nickelocene **92**



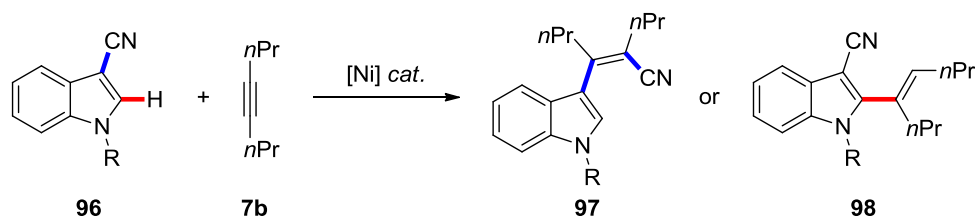
b) undirected C–H nickelation of benzene



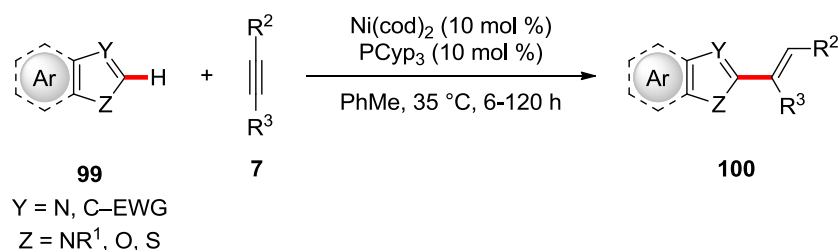
Scheme 1.31. Stoichiometric nickel-mediated C–H activations.^[157,159]

In the same year, *Nakao* and *Hiyama* discovered by serendipity that nickel(0) species could catalyze the functionalization of activated, that is somewhat acidic, C–H bond with alkynes **7** (Scheme 1.32).^[160] *Tsuda* and *Saegusa* had previously demonstrated the potential of nickel catalysts in related hydroacylation reactions.^[158f] The selective activation of a C–H bond over a C–CN bond of *N*-protected 3-cyanoindoles **96** could be controlled by the proper choice of the ligand and *N*-protecting group of the indole.^[160] Under the optimized reaction conditions, diverse azoles **99**, including benzimidazoles, electron-poor indoles, caffeine, benzofuran, benzothiophene, benzoxazole and thiazole, could be alkenylated selectively at the C2 position. Based on preliminary experimental mechanistic studies, the authors proposed the C–H cleavage step to occur *via* oxidative addition. However, a later study by *Zimmerman* and *Montgomery* suggested the possibility of a ligand-to-ligand hydrogen transfer (LLHT) manifold.^[161]

a) serendipitous discovery of nickel-catalyzed C–H alkenylation



b) nickel-catalyzed C–H alkenylation under optimized conditions

**Scheme 1.32.** Nickel-catalyzed hydroheteroarylation of alkynes with azoles.^[160]

Afterwards, the scope of the hydroheteroarylation of alkynes was expanded to other heterocycles, with major contributions of *Nakao/Hiyama*, *Ong/Yap* and *Miura*. Among others, oxadiazoles,^[162] pyrazoles,^[163] simple imidazoles,^[164] pyridine oxides,^[165] pyridines,^[166] pyridones^[167] and pentafluorobenzene^[168] were identified as viable substrates in the nickel-catalyzed hydro(hetero)arylation of alkynes. For substrates bearing less acidic C–H bonds, the addition of co-catalytic Lewis acidic organoaluminium additives was needed for the reaction to occur. In addition to azoles **99**, formamides proved to be suitable substrates as well.^[169] Taking inspiration of the success of nickel catalysts in the hydroarylation of alkynes, this chemistry was later expanded to alkenes (*vide infra*) and even allenes.^[170]

While not directly relevant to the topic of this thesis, it should be mentioned that other non-hydroarylation-type nickel-catalyzed C–H activations have been reported as well. Among other transformations, the arylation,^[171] alkylation with alkyl (pseudo)halides,^[172] alkynylation with alkynyl bromides^[173] or terminal alkynes^[174] and alkenylation^[171a,171d,175] of C–H acidic azoles are nowadays well established processes. Furthermore, nickel-catalyzed C–H activations are not limited to C–H

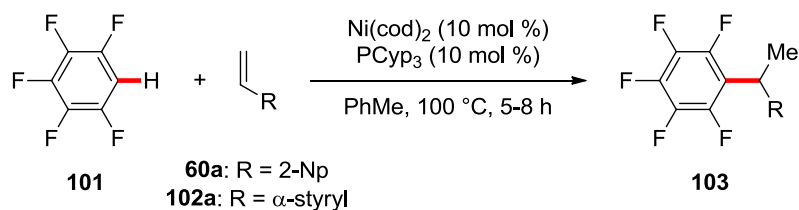
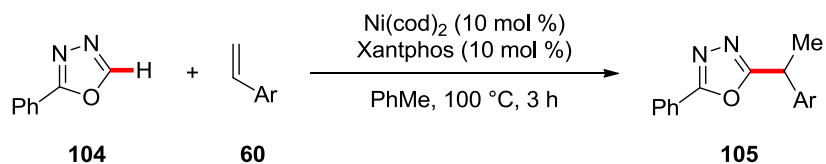
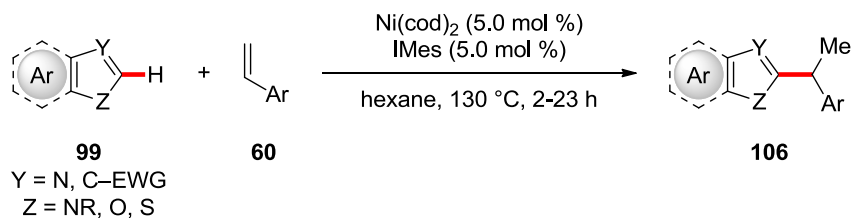
acidic heteroarenes. Indeed, truly unactivated C–H bonds have been functionalized as well, but this chemistry remains so far mostly restricted to the use of bidentate directing groups.^[176] In this context, the C(sp²)–H arylation,^[177] alkylation,^[178] alkynylation with alkynyl bromides^[179] or terminal alkynes,^[180] alkyne annulation,^[181] allylation,^[178d,182] carbonylation^[183] and thiolation^[184] of benzamide derivatives have *inter alia* been achieved with nickel catalysts. The use of bidentate directing groups also allowed the functionalization of C(sp³)–H positions.^[45,48c,176] While C–H transformations of unactivated arenes were long restricted to the use of bidentate directing groups, major progress in the field was reported by *Ackermann* who recently introduced the simple and easily removable 2-pyrimidyl directing group for the *ortho*-functionalization of aniline derivatives.^[185] Similarly, *Punji* disclosed several nickel-catalyzed C–H functionalizations of indoles bearing monodentate directing groups.^[186]

1.4.2. Nickel-Catalyzed C–H Activation by Alkene Hydroarylation

The use of alkenes has gained considerable attention in transition metal-catalyzed C–H activation.^[187] Indeed, due to their low cost, availability and sustainability (no need for pre-functionalization), alkenes are attractive coupling partners for the formation of C–C bonds. In this context, nickel catalysts have proven particularly powerful for the hydrofunctionalization of C–C multiple bonds.^[48a,188] Furthermore, the hydroarylation of alkenes generates C(sp³) positions, offering opportunities for the development of asymmetric transformations employing chiral nickel catalysts.

Taking inspiration from their pioneering works on the hydroarylation of alkynes,^[188a] *Nakao* and *Hiyama* reported in 2008 the unprecedented hydroarylation of conjugated alkenes with pentafluorobenzene (**101**) using reaction conditions nearly identical to those used for alkynes (Scheme 1.33a).^[168] Interestingly, the branched product was selectively obtained. *Miura* disclosed in 2009 the hydroarylation of styrenes **60** with oxadiazoles **104** using Ni(cod)₂ and the bidentate phosphine ligand Xantphos as the catalytic system (Scheme 1.33b).^[162] Similar findings were reported

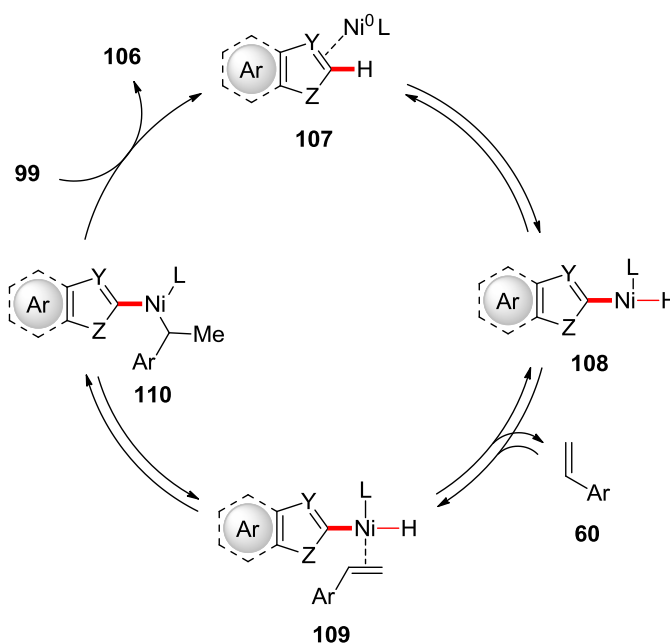
shortly afterwards by *Nakao* and *Hiyama* who identified the NHC ligand IMes as optimal for the envisioned transformation (Scheme 1.33c).^[189] Remarkably, the authors were also able to use simple alkyl-substituted alkenes for the first time under more forcing conditions. In sharp contrast to conjugated alkenes, the linear product was obtained in this case. The nickel/NHC manifold would later prove broadly applicable in the hydroarylation of alkenes with (hetero)arenes.^[45,48a]

a) *Nakao/Hiyama*b) *Miura*c) *Nakao/Hiyama*

Scheme 1.33. Early examples of nickel-catalyzed hydroarylations of alkenes with (hetero)arenes.^[162,168,189]

Based on deuterium-labeling experiments, the C–H cleavage step was proposed to occur *via* a reversible oxidative addition of a nickel(0) complex into the C–H bond (Scheme 1.34).^[162,168,189] Then, coordination of the alkene followed by hydronicelation of the latter produces intermediate **110**. Those steps are proposed to be reversible, thus explaining the observed H/D scrambling. Thereafter, an

irreversible and rate-determining reductive elimination delivers product **106** and regenerates intermediate **107**. Furthermore, *Nakao/Hiyama* and *Miura* proposed the formation of the *Markovnikov* product to be favored because of the formation of π -benzyl or π -allyl nickel intermediates, which would also explain the poor performance of alkyl-substituted alkenes and acrylates in these reactions.^[162,168,189]



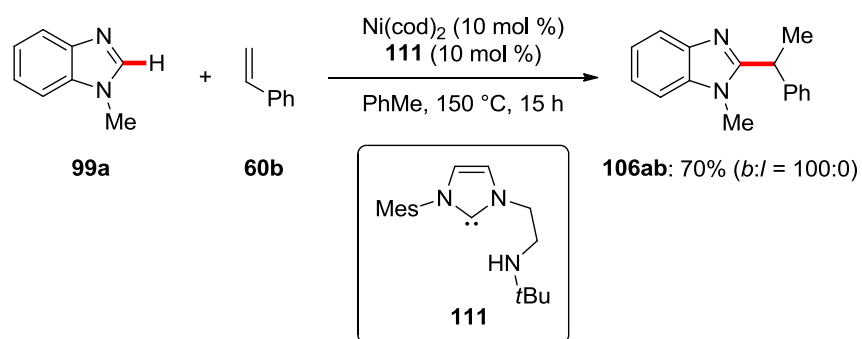
Scheme 1.34. Proposed catalytic cycle of the nickel-catalyzed hydroarylation of vinylarenes **60** with azoles **99**.^[189]

Subsequently, the origin of the regioselectivity of the reaction was investigated in detail by DFT by *Shi*.^[190] This study provided support to the mechanism proposed by *Nakao*, *Hiyama* and *Miura*, and revealed a secondary orbital overlap between the styrene's aryl group and the nickel center. This interaction was found to accelerate the rate-limiting C–C bond forming reductive elimination and favor the formation of the *Markovnikov* product from conjugated alkenes. In case of simple alkyl-substituted olefins, this interaction is absent and the sterically less hindered linear product is thus formed favorably.

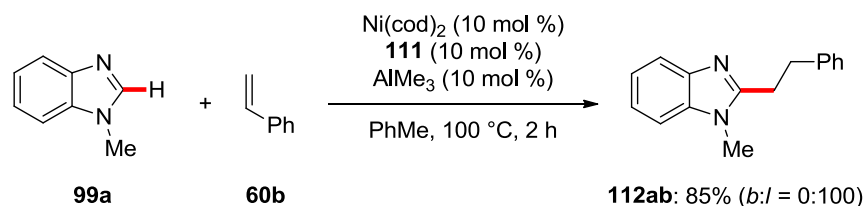
A major breakthrough in the nickel-catalyzed hydroarylation of alkenes was the introduction of Lewis acidic organoaluminium additives, which not only allowed

transformations of unactivated heteroarenes and alkenes, but also proved critical to control the selectivity of the reaction. Among other substrates, pyridones^[167,191] and pyridines^[192] could be coupled with alkenes in the presence of AlMe_3 or MAD as additive, as observed previously for the hydroarylation of alkynes. While non-conjugated alkenes otherwise remain very challenging in nickel-catalyzed hydroarylations, organoaluminium additives were found to facilitate their use in either inter- or intramolecular reactions with various heteroarenes.^[167,191–193] The regioselectivity of those transformations is of particular interest. While the branched product **106** is normally obtained from conjugated alkenes, aliphatic olefins usually provide the linear product.^[190] In this context, *Ong* was able to reverse the usual selectivity of the hydroarylation of styrene **60** with benzimidazoles **99** by the addition of co-catalytic AlMe_3 (Scheme 1.35).^[194] Unselective mixtures were obtained with other Lewis acids.

a) branched-selectivity under Al-free conditions

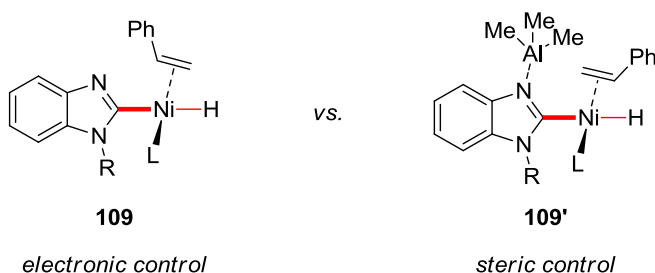


b) linear-selectivity with AlMe_3



Scheme 1.35. Regioselectivity control in nickel-catalyzed hydroarylations of styrenes **60** with benzimidazoles **99**.^[194]

Detailed mechanistic studies were conducted by *Ong* and coworkers to delineate the mechanism of this process and the role of AlMe_3 .^[194a] Their findings revealed that AlMe_3 not only controlled the regioselectivity of the transformation, but also significantly increased the rate of product formation. In contrast, the aluminium-free reaction was found to be much slower, still being in its induction period after 3 h. The authors were also able to observe a Ni–H species, which may indicate an oxidative addition pathway to be involved in the transformation. Furthermore, the adduct of the benzimidazole substrate and AlMe_3 was isolated. Based on those findings, the linear selectivity was proposed to result from steric control during the insertion of the styrene into the Ni–H bond (Scheme 1.36). In contrast, in the absence of the organoaluminium additive, hydride insertion at the β -carbon of styrene is electronically favored, giving the branched product.



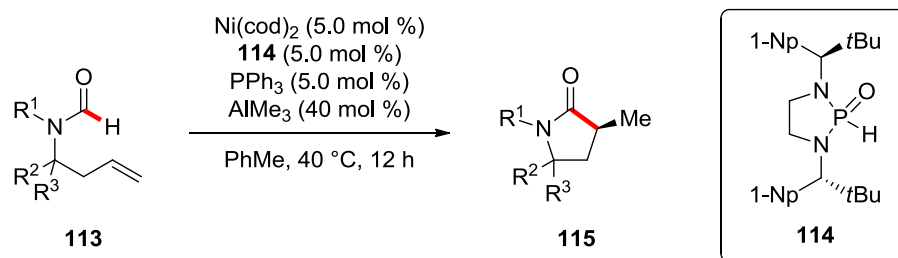
Scheme 1.36. Model for selectivity switch in the nickel-catalyzed hydroarylation of styrenes.^[194]

1.4.3. Enantioselective Nickel-Catalyzed C–H Activation

While nickel-catalyzed inner-sphere C–H activations, especially hydroarylations, are nowadays well established, asymmetric transformations remain scarce. Thus far, all known examples involve the asymmetric functionalization of alkenes.^[52]

Taking inspiration from previous works by *Nakao* and *Hiyama*,^[169] *Cramer* reported an enantioselective nickel-catalyzed intramolecular hydrocarbamoylation of homoallylic formamides **113** (Scheme 1.37).^[195] In this context, it should be mentioned that (C=O)–H activations have been accomplished with a broad range of

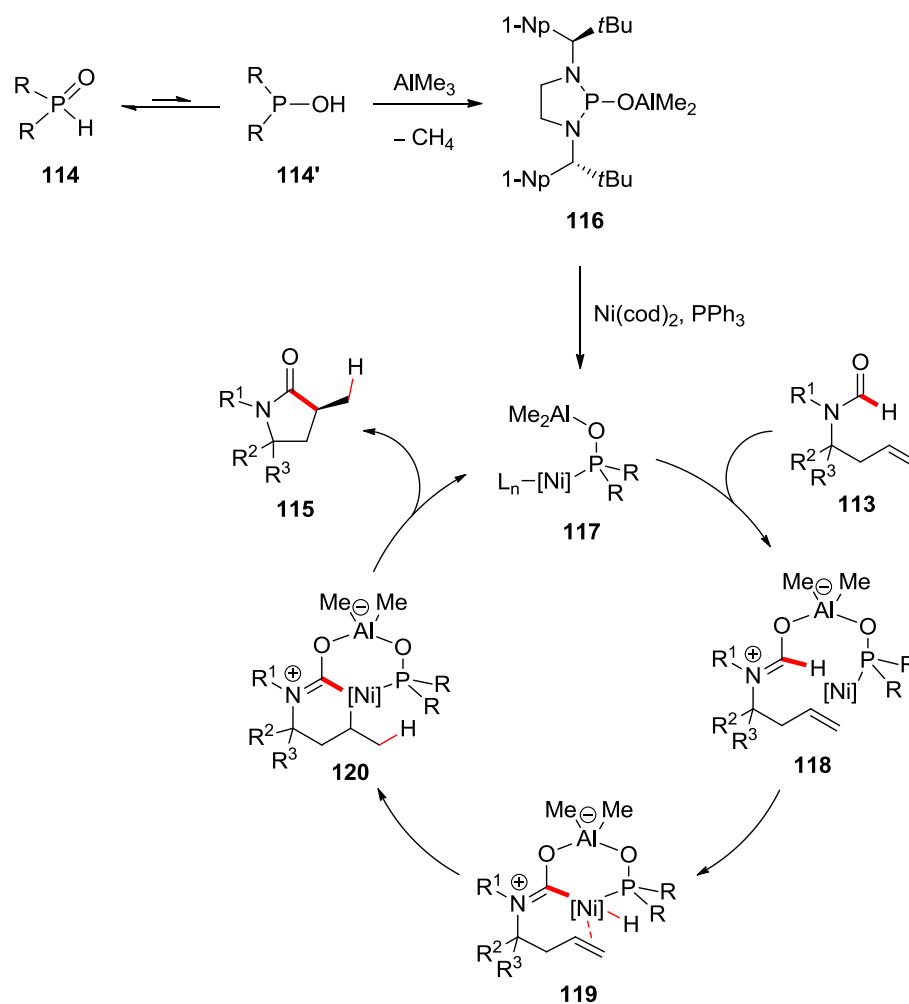
catalysts, with the hydroacylations of alkenes and alkynes being extensively documented.^[196] A significant fraction of formyl C–H activations has been proposed to occur through radical mechanisms,^[31a] taking advantage of the low bond dissociation energy (BDE) of the formyl C–H bond.^[28] The chiral heteroatom-substituted secondary phosphine oxide^[197] (HASPO) **114** preligand developed by *Cramer* enabled the asymmetric synthesis of pyrrolidinones **115**, featuring a Ni/Al^[198] heterobimetallic^[23b] activation mode. While a nickel catalyst solely prepared from the chiral SPO performed poorly, the addition of a co-catalytic amount of phosphine led to an increased efficacy, presumably by assisting the displacement of the cod ligand from the precatalyst. This work is truly remarkable as it represents the first enantioselective transformation by inner-sphere C–H activation with a 3d transition metal catalyst.^[52]



Scheme 1.37. Enantioselective intramolecular nickel-catalyzed hydrocarbonylations of alkenes.^[195]

A reasonable catalytic cycle was proposed to begin with the formation of the Al/SPO adduct **116**, a bifunctional ligand whose aluminium center retains its Lewis acidity while the Lewis basic phosphorous atom can coordinate to the nickel center (Scheme 1.38). The aluminium center then activates the carbonyl group of **113**, providing intermediate **118**. Thereafter, oxidative of the C–H bond on nickel generates the six-membered hetero-bimetallic cycle **119**. Migratory insertion then leads to complex **120**, and reductive elimination releases lactam **115** and regenerates the heterobimetallic catalyst **117**. This mechanism was further supported by the independent synthesis of the Lewis acid/SPO adduct **116**, which

was found to promote the cyclization with excellent yield and enantioselectivity without additional AlMe_3 or PPh_3 .

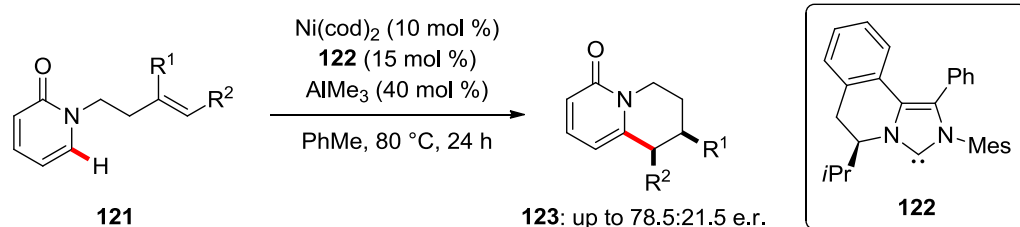


Scheme 1.38. Plausible mechanism of the nickel-catalyzed hydrocarbomoylation.^[195]

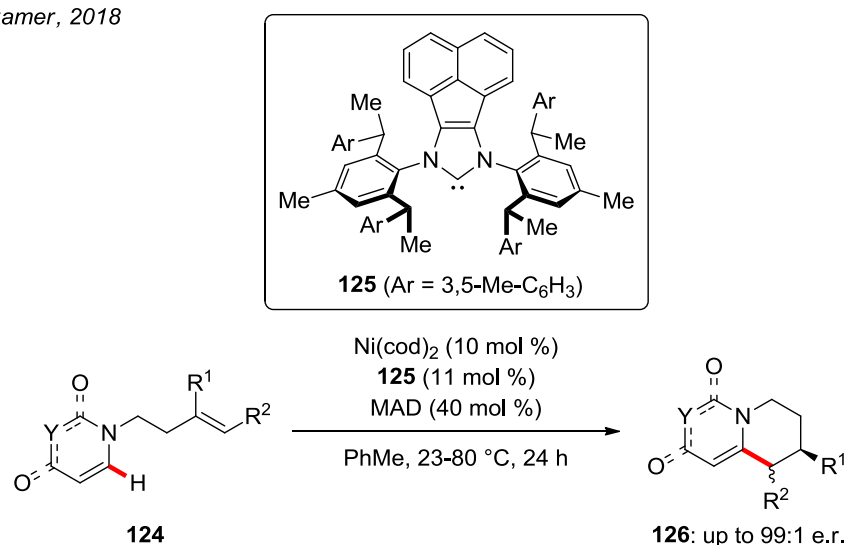
As previously mentioned, *Nakao* and *Hiyama* developed an intramolecular C–H alkylation of pyridones with unactivated tethered alkenes using a nickel- $\text{P}(\text{iPr})_3$ catalytic system in the presence of AlMe_3 .^[167] Inspired by these results, *Cramer* subsequently developed a ligand-controlled regiodivergent annulation of pyridones **121**, with *IPr* giving selectively the *endo*-cyclized product, while the *exo*-product was obtained with *cod* as the ligand.^[193] Preliminary efforts towards an asymmetric version of this reaction were also disclosed (Scheme 1.39a). The chiral NHC ligand

122, based on the design of *Hong* and coworkers,^[199] provided the *endo*-cyclized products **123** in 78.5:21.5 e.r.

a) *Cramer, 2015*



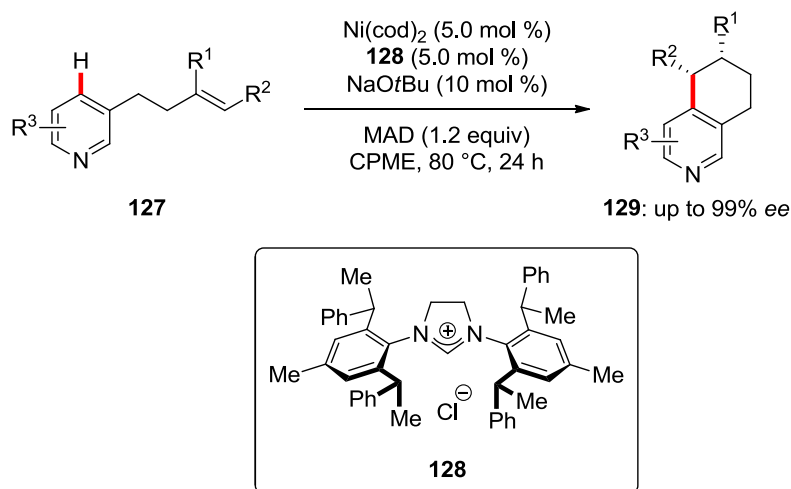
b) *Cramer, 2018*



Scheme 1.39. Enantioselective nickel-catalyzed hydroarylation with pyridones.^[193,200]

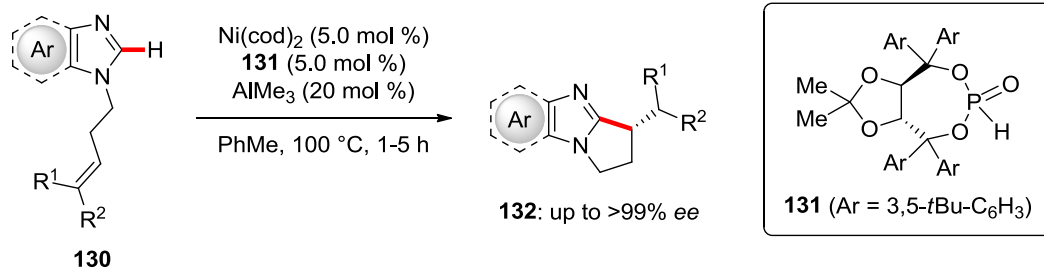
Further investigations by *Cramer* on the asymmetric cyclization of pyridones with tethered olefins led to the discovery of the novel chiral NHC **125**, inspired from a previous ligand design by *Gawley*^[201] with a modified acenaphthene backbone (Scheme 1.39b).^[200] Under the optimized reaction conditions, the *endo*-cyclized annulated pyridones and uracils **126** were obtained from diversely decorated alkenes **124** in excellent yields and enantiomeric excesses at mild reaction temperatures in the presence of MAD. Based on literature precedents,^[202] the authors proposed the C–H cleavage step to occur through a LLHT manifold. This approach was later extended to pyridines **127** by *Shi* under similar reaction

conditions (Scheme 1.40).^[203] Thus, the corresponding tetrahydro(iso)quinolines **129** were obtained with excellent diastereo- and regio-selectivities.



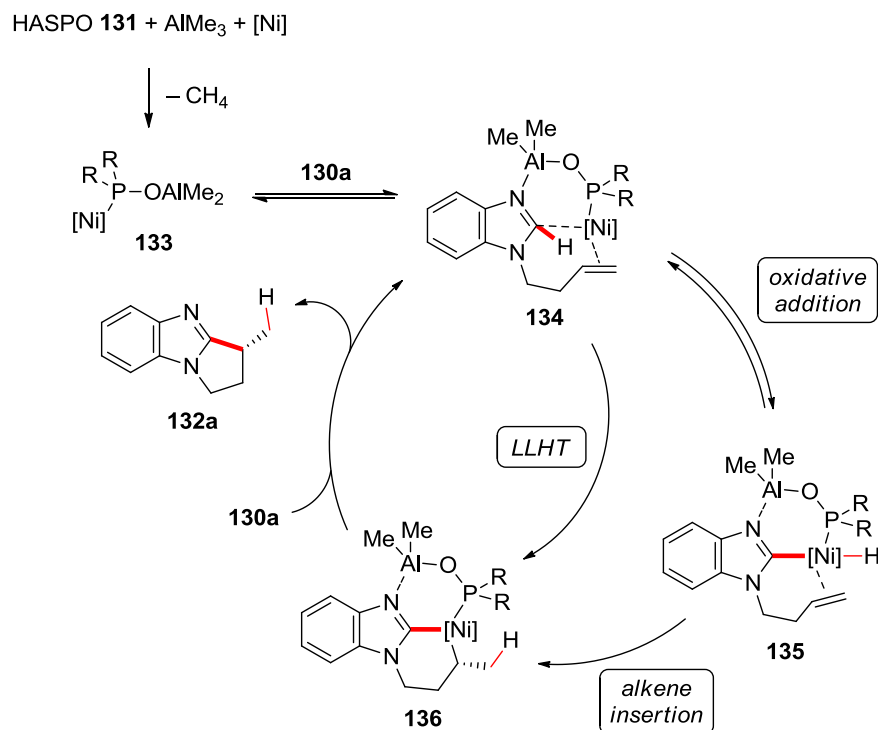
Scheme 1.40. Enantioselective nickel-catalyzed hydroarylation with pyridines **127**.^[203]

Following the elegant studies of *Bergman* and *Ellman*,^[204] the undirected cyclization of azoles with tethered alkenes has long been dominated by rhodium(I) catalysts, with a notable exception by *Cavell* for the nickel-catalyzed cyclization of highly activated (benz)imidazolium salts.^[205] In this context, *Ye* reported on the unprecedented nickel-catalyzed enantio- and *exo*-selective hydroarylation of olefins **130** with tethered imidazoles (Scheme 1.41).^[206] The TADDOL-derived HASPO preligand **131** enabled a nickel-aluminum bimetallic catalysis. Such TADDOL-HASPOs had previously been exploited in asymmetric organocatalysis,^[207] but their use in enantioselective transition-metal catalysis had remained rare.^[208] Thus, diverse polycyclic azoles **132** with β -stereocenters were obtained in outstanding yields and enantioselectivities. Interestingly, sensitive functional groups, including bromo-substituents, as well as diversely substituted alkenes, proved viable in the nickel catalysis.



Scheme 1.41. Asymmetric nickel-catalyzed exo-selective hydroarylation of alkenes **130**.^[206]

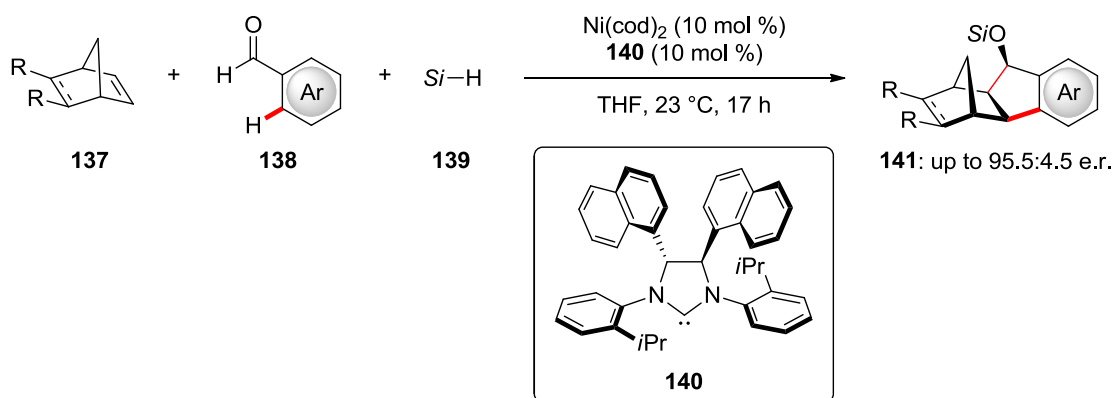
In analogy to the hydrocarbamoylation presented above (Schemes 1.37–1.38), a plausible catalytic cycle begins with the formation of an Al/SPO adduct, which can coordinate the nickel precursor to deliver complex **133** (Scheme 1.42). Then, through a heterobimetallic mode of activation, the aluminium center can be coordinated by the imidazole's nitrogen, while the nickel center binds the alkene to give intermediate **134**. The authors suggested the C–H cleavage step to occur through a direct LLHT from the imidazole to the olefin, but an oxidative addition pathway could not be entirely ruled out.



Scheme 1.42. Proposed mechanism of the asymmetric nickel-catalyzed exo-selective hydroarylation.^[206]

While nickel-catalyzed intramolecular asymmetric hydroarylations have been recognized as a powerful tool for the synthesis of important polycyclic bioactive scaffolds, enantioselective intermolecular versions remain hitherto largely unknown.

In 2011, *Fukuzawa* disclosed an elegant nickel/NHC-catalyzed three-component reaction between benzaldehydes **138**, norbornenes **137**, and silanes **139** leading to polycyclic indanols **141**.^[209] Thereafter, *Cramer* designed the chiral NHC ligand **140** to achieve this transformation in an enantioselective fashion (Scheme 1.43).^[210] Interestingly, while the flanking *N*-aryl substituents of *Grubbs*-type chiral NHCs^[211] have been extensively investigated, modifications of the chiral backbone remain underexplored. This transformation allowed for the expedient diastereoselective synthesis of annulated indanols **141** bearing five contiguous stereocenters.



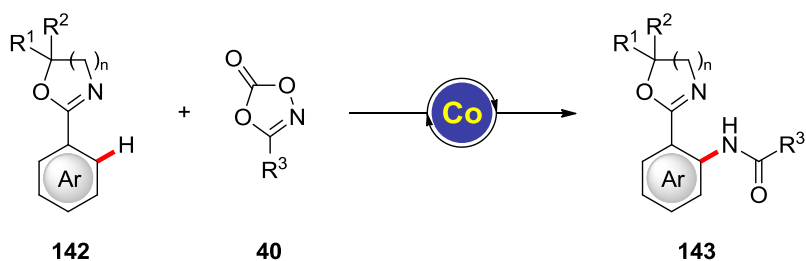
Scheme 1.43. Nickel-catalyzed asymmetric reductive three-component coupling.^[210]

Despite significant progress in very recent years with non-noble metals,^[52] such as nickel^[193,200,203,206] and cobalt^[106] (Schemes 1.13, 1.19, 1.39–1.41), enantioselective hydroarylation-type C–H activations^[23] remain vastly dominated by costly noble 4d and 5d transition metals, such as iridium^[212], rhodium,^[213] and others,^[214] or rare-earth complexes.^[215] Therefore, the development of new chiral catalysts based on earth-abundant, inexpensive and less-toxic 3d transition metals is highly desirable.

2. Objectives

Methods for the selective functionalization of otherwise inert C–H bonds have been recognized as a transformative tool in synthetic organic chemistry, with applications ranging from the synthesis of complex bioactive compounds to material sciences.^[23k,23n,23p,40a,216] In particular, 3d metal catalysts have emerged in recent years as inexpensive, earth-abundant and less toxic alternatives to their heavier counterparts.^[45] However, full selectivity control in base metal-catalyzed C–H activation continues to be challenging.^[52] In this context, the development of novel 3d transition metal catalysts enabling chemo- and stereo-selective C–H functionalizations should be investigated.

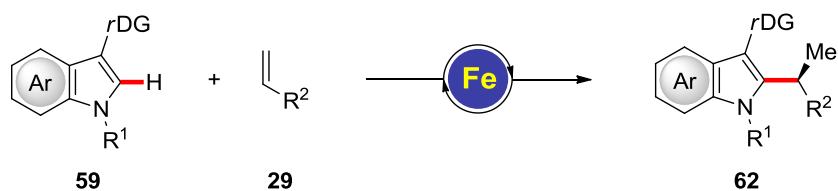
As catalytic C–H aminations typically rely on noble metal catalysts or require harsh reaction conditions,^[23e,217] we became interested in the development of a user-friendly and broadly applicable protocol for the cobalt-catalyzed C–H amidation of synthetically useful 2-aryloxazolines **142** employing dioxazolones **40** as versatile amidating reagents (Scheme 2.1).^[37e] Mechanistic studies were performed to delineate the mode of action of the C–H activation.



Scheme 2.1. Cobalt-catalyzed C–H amidation.

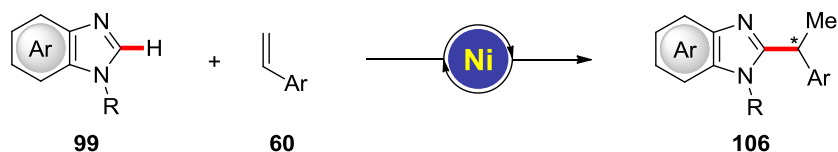
The enantioselective functionalization of C–H bonds remains largely dominated by noble transition metal catalysts such as palladium, rhodium and iridium.^[51] While significant progress has been very recently achieved by employing earth-abundant non-precious 3d metals,^[52] iron-catalyzed asymmetric functionalizations by inner-sphere C–H activation remained completely unprecedented at the outset of this

work,^[47] and represent an exceptional challenge in asymmetric catalysis. In this context, we initiated the development of the first enantioselective iron-catalyzed C–H alkylation by alkene hydroarylation (Scheme 2.2).^[151] The design of novel chiral NHC ligands proved to be crucial to achieve high enantioselectivities. Furthermore, detailed studies by ⁵⁷Fe Mössbauer spectroscopy and electrospray-ionization mass spectrometry were conducted to unravel the nature of the *in situ* generated catalyst.^[218]



Scheme 2.2. Iron-catalyzed enantioselective C–H secondary alkylation.

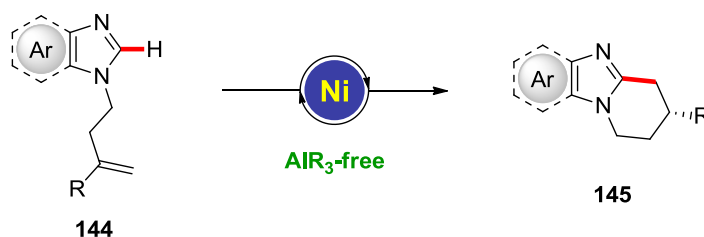
Inspired by the success of nickel/NHC complexes as catalysts for alkene hydroarylations *via* undirected heteroaromatic C–H activation,^[27,188a] we decided to probe the newly designed chiral NHC ligands in the nickel-catalyzed secondary alkylation of benzimidazoles **99** with styrenes **60**. While nickel-catalyzed intermolecular hydroarylations are well-documented, the development of an asymmetric protocol remains unprecedented. Promising enantioselectivities were observed for the first time in this preliminary work.



Scheme 2.3. Nickel-catalyzed enantioselective intermolecular C–H alkylation.

The cyclization of heteroarenes with tethered alkenes has long been dominated by rhodium(I) catalysts, following the elegant pioneering studies by *Bergman* and *Ellman*.^[204,213d,219] Recently, nickel-catalyzed hydroarylation-type C–H activation has

emerged as a cost-efficient alternative.^[27,48a] However, the intramolecular hydroarylations of unactivated alkenes remain strongly limited by the requirement of pyrophoric organoaluminium additives, significantly compromising their functional group tolerance and synthetic utility.^[200,203,206] This observation prompted us to investigate the asymmetric cyclization of *N*-homoallylimidazoles **144** under aluminium-free conditions (Scheme 2.4).^[220] Interestingly, the *endo* product **145** was selectively obtained, which in sharp contrast to previously reported methods.^[206] Mechanistic studies were then conducted in order to delineate the unique reactivity of the developed catalytic system.

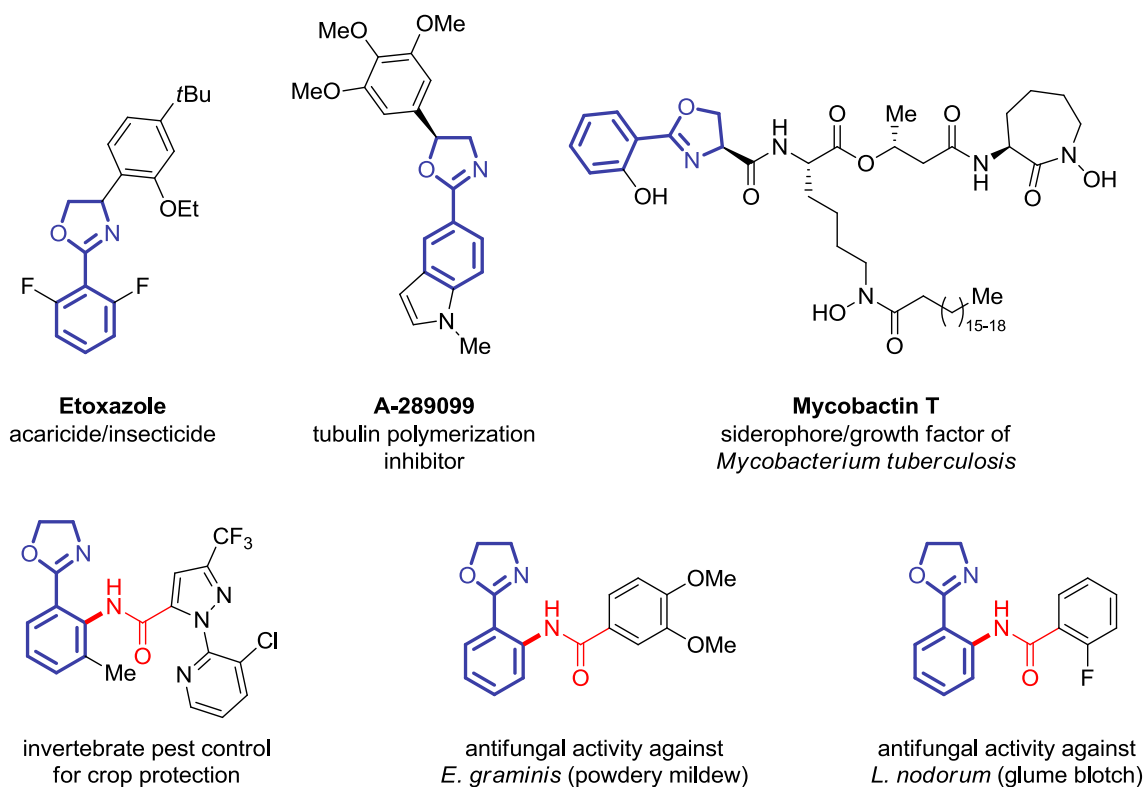


Scheme 2.4. Nickel-catalyzed enantioselective intramolecular C–H alkylation.

3. Results and Discussion

3.1. Cobalt(III)-Catalyzed C–H Amidation by Oxazoline Assistance

Diversely decorated 2-aryloxazolines are key structural motifs in bioactive natural products and compounds relevant to the pharmaceutical and agrochemical industries, among others (Scheme 3.1).^[221] In the context of this work, it is noteworthy that several *ortho*-amidated 2-phenyloxazolines have been patented or even commercialized as pesticides or fungicides, with applications to crop protection.^[222] Furthermore, oxazolines are versatile and readily accessible synthetic intermediates which can easily be transformed into a wealth of diverse functional groups.^[223] Additionally, oxazolines are powerful ligands in transition metal-catalyzed transformations.^[224]



Scheme 3.1. Selected examples of bioactive 2-aryloxazolines.

Hence, methods to access highly functionalized oxazoline derivatives are highly sought after by the synthetic community. The *ortho*-functionalization of 2-aryloxazolines through directed *ortho*-metalation (DoM) is well documented.^[225] However, such methods require relatively harsh reaction conditions, such as an excess of organolithium bases, which strongly limit their functional group tolerance. Therefore, catalytic processes operating under mild conditions and avoiding cryogenic conditions are highly desirable.

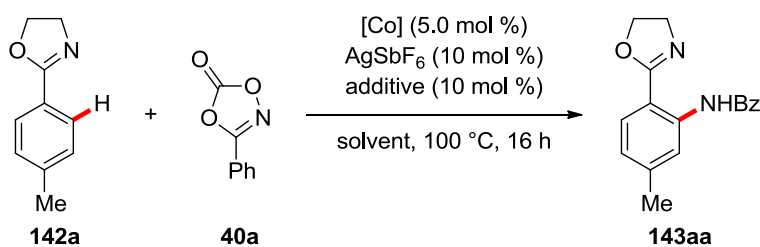
Thereby, we became interested in the development of an atom- and step-economical method for the diversification of oxazolines. Despite the significant progress of oxidative C–H amination reactions in recent years, most pre-existing methodologies either required harsh reaction conditions or are restricted to noble transition metal catalysts, such as iridium, rhodium, palladium and ruthenium.^[23e,217] Also, many of these processes typically employed azides as aminating reagents, bearing major safety concerns. We hence decided to explore the feasibility of cobalt(III)-catalyzed amidations of 2-aryloxazolines **142** using dioxazolones **40** as user-friendly and safer^[226] amination reagents.

3.1.1. Optimization Studies

After initial results were obtained by *Dr. Ruhuai Mei* for the Cp*Co(III)-catalyzed amidation of various substrates bearing Lewis-basic directing groups,^[227] it was decided to focus on 2-aryloxazolines due to their importance as synthetic intermediates and key motifs in bioactive compounds. 2-Tolyloxazoline **142a** and dioxazolone **40a** were selected as model substrates for optimization studies towards the envisioned C–H transformation (Table 3.1). A preliminary solvent optimization performed by *Dr. R. Mei* identified DCE as the optimal reaction medium (entries 1–2). Increasing the amount of silver salts and carboxylate additives to 20 mol % proved beneficial (entry 3). Additional solvents were probed in the transformation, giving the desired amidated arene **143aa** in low to moderate yields (entries 4–9). The effect of additives on the C–H amidation was then extensively

studied (entries 10–22). Interestingly, several carboxylic acids, carboxylates, carbonates, phosphates, and mono-protected amino acids were found to promote the desired transformation, albeit with lower efficacy than NaOAc. However, sodium mesitylcarboxylate and trichloroacetate gave remarkably poor results, presumably due to excessive steric hindrance and lower basicity, respectively. Lower reaction temperatures were detrimental to the reaction outcome (entry 23). Other cobalt precursors were tested in the oxazoline-assisted C–H amidation (entries 24–27), revealing $\text{Cp}^*\text{Co}(\text{CO})\text{I}_2$ to be the most potent catalyst. While cationic $[\text{Cp}^*\text{Co}(\text{MeCN})_3](\text{SbF}_6)_2$ or dimeric $[\text{Cp}^*\text{CoI}_2]_2$ were only slightly less efficient than $\text{Cp}^*\text{Co}(\text{CO})\text{I}_2$, simple cobalt salts such as CoCl_2 or unsubstituted $\text{CpCo}(\text{III})$ complexes in contrast fell short in the desired catalytic transformation. Finally, control experiments confirmed the importance of the $\text{Cp}^*\text{Co}(\text{III})$ -catalyst and the NaOAc additive (entries 28–29).

Table 3.1. Optimization of the oxazoline-assisted cobalt(III)-catalyzed amidation.^[a]



| Entry | [Co] | Solvent | Additive | Yield [%] ^[b] |
|--------------------|---|----------------------------|----------|--------------------------|
| 1 ^[c] | $\text{Cp}^*\text{Co}(\text{CO})\text{I}_2$ | TFE | NaOAc | n.r. |
| 2 ^[c] | $\text{Cp}^*\text{Co}(\text{CO})\text{I}_2$ | DCE | NaOAc | 65 |
| 3 ^[c,d] | $\text{Cp}^*\text{Co}(\text{CO})\text{I}_2$ | DCE | NaOAc | 68 |
| 4 ^[d] | $\text{Cp}^*\text{Co}(\text{CO})\text{I}_2$ | PhCF ₃ | NaOAc | 53 |
| 5 ^[d] | $\text{Cp}^*\text{Co}(\text{CO})\text{I}_2$ | 1,4-dioxane | NaOAc | 24 |
| 6 ^[d] | $\text{Cp}^*\text{Co}(\text{CO})\text{I}_2$ | EtOAc | NaOAc | <10 |
| 7 ^[d] | $\text{Cp}^*\text{Co}(\text{CO})\text{I}_2$ | <i>n</i> Bu ₂ O | NaOAc | 21 |

| | | | | |
|---------------------|---|---------------|------------------------------------|--------|
| 8 ^[d] | Cp*Co(CO)I ₂ | <i>t</i> AmOH | NaOAc | 6 |
| 9 ^[d] | Cp*Co(CO)I ₂ | PhMe | NaOAc | 31 |
| 10 ^[c] | Cp*Co(CO)I ₂ | DCE | KOAc | 47 |
| 11 ^[c] | Cp*Co(CO)I ₂ | DCE | PivOH | 58 |
| 12 ^[c] | Cp*Co(CO)I ₂ | DCE | NaOPiv | 63 |
| 13 ^[d] | Cp*Co(CO)I ₂ | DCE | NaO ₂ CMes | 3 |
| 14 ^[d] | Cp*Co(CO)I ₂ | DCE | NaO ₂ CAd | 44 |
| 15 ^[d] | Cp*Co(CO)I ₂ | DCE | Ac-Ile-CO ₂ Na | 17 |
| 16 ^[d] | Cp*Co(CO)I ₂ | DCE | NaO ₂ CCCl ₃ | 4 |
| 17 ^[e] | Cp*Co(CO)I ₂ | DCE | Zn(OAc) ₂ | 29 |
| 18 ^[d] | Cp*Co(CO)I ₂ | DCE | NaHCO ₃ | 40 |
| 19 ^[d] | Cp*Co(CO)I ₂ | DCE | NaOBz | 51 |
| 20 ^[d] | Cp*Co(CO)I ₂ | DCE | Na ₂ HPO ₄ | 40 |
| 21 ^[d] | Cp*Co(CO)I ₂ | DCE | LiOAc | 49 |
| 22 ^[d] | Cp*Co(CO)I ₂ | DCE | HCO ₂ Na | 47 |
| 23 ^[d,f] | Cp*Co(CO)I ₂ | DCE | NaOAc | 39 |
| 24 ^[c,d] | [Cp*CoI ₂] ₂ | DCE | NaOAc | 61 |
| 25 ^[d] | CpCo(CO)I ₂ | DCE | NaOAc | traces |
| 26 ^[c] | CoCl ₂ | DCE | NaOAc | n.r. |
| 27 ^[c] | [Cp*Co(MeCN) ₃](SbF ₆) ₂ | DCE | - | 54 |
| 28 ^[c] | Cp*Co(CO)I ₂ | DCE | - | 35 |
| 29 ^[c] | - | DCE | NaOAc | n.r. |

| | | | | |
|-------------------|---|-----|-------|---|
| 30 ^[g] | [Cp*Co(MeCN) ₃](SbF ₆) ₂ | DCE | NaOAc | 3 |
|-------------------|---|-----|-------|---|

^[a] Reaction conditions: **142a** (0.50 mmol), **40a** (1.2 equiv), [Co] (5.0 mol %), AgSbF₆ (10 mol %), additive (10 mol %), solvent (2.0 mL), 100 °C, 16 h. ^[b] Isolated yield. ^[c] Performed by *Dr. R. Mei*. ^[d] Additive (20 mol %) and AgSbF₆ (20 mol %). ^[e] Additive (10 mol %) and AgSbF₆ (20 mol %). ^[f] At 85 °C. ^[g] Under blue LED irradiation at 23 °C in the presence of RuTPP(CO) (1.0 mol %) as co-catalyst. AgSbF₆ was omitted.

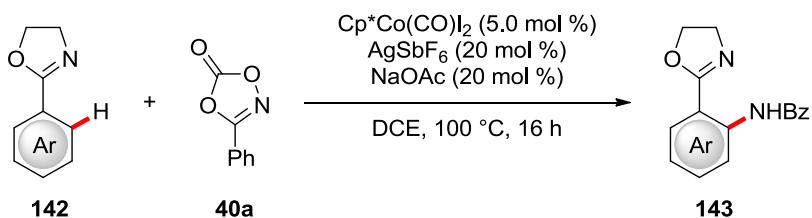
It should be noted that no 2,6-diamidated product was detected, presumably due to intramolecular hydrogen bonds between the directing group's nitrogen and the amide's N–H group, preventing the functionalization of the second *ortho*-position. Furthermore, it is noteworthy that no aminocarbonylation product was observed in any of those reactions either, despite dioxazolones being reported to decompose to the corresponding isocyanates *via* heat- or light-induced *Lossen* rearrangements.^[228] These findings are complementary to a previous report by *Ackermann* on the use of acylazides in cobalt(III)-catalyzed C–H aminocarbonylations, where the authors proposed isocyanates to be formed *in situ* *via* a *Curtius* rearrangement,^[85] and highlight the unique reactivity of dioxazolones **40** as aminating reagents. Along the same lines, dioxazolones are documented to undergo light-induced N–O cleavage with CO₂ loss in the presence of ruthenium(II) porphyrin catalysts to form rutheno *N*-acyl nitrene intermediates.^[229] We hence decided to investigate whether the desired C–H amidation would be feasible at ambient temperature under light irradiation in the presence of catalytic [Ru(TPP)CO] (Table 3.1, entry 30). Unfortunately, a significant conversion of the starting material was not detected under those conditions.

3.1.2. Substrate Scope

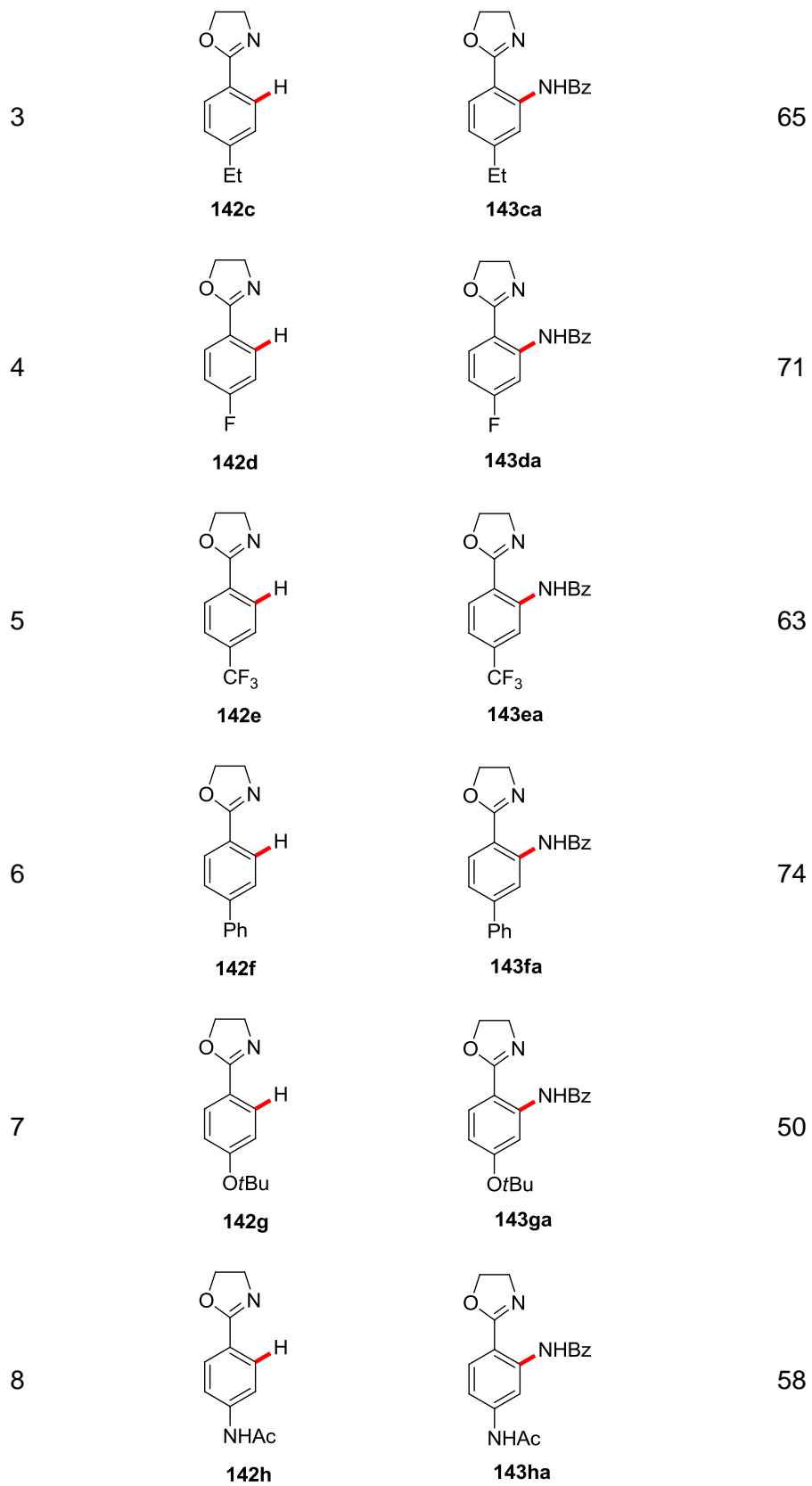
With the optimized catalytic system in hand, the versatility and robustness of the Cp*Co(III)-catalyzed oxazolonyl-directed C–H amination was then investigated. Various 2-phenyloxazolines **142** were efficiently converted to the amide products **143** with high efficacy (Table 3.2). Among others, a wealth of alkyl, aryl, ether and

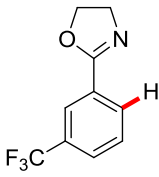
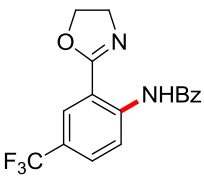
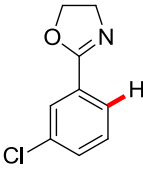
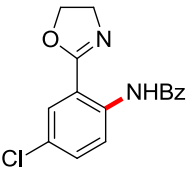
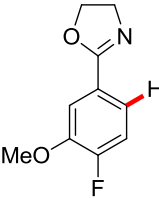
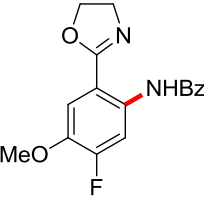
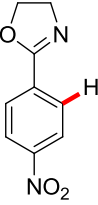
halogenated substituents were fully tolerated in the transformation, affording products **143** in moderate to good yield (entries 1–7). Remarkably, even the secondary amide **142h** bearing free N–H groups was successfully transformed into the desired product **143ha** with complete site-selectivity (entry 8). *meta*-Substituted 2-phenyloxazolines **142i-k** were also viable substrates for the cobalt-catalyzed C–H nitrogenation, and were functionalized on the less sterically hindered *ortho*-position with complete positional selectivity (entries 9–11). Moreover, the C–H amidation was found to be scalable. Indeed, a gram-scale reaction was carried and provided product **143aa** without any loss of efficacy.

Table 3.2. Substrate scope of 2-aryloxazolines **142** in the cobalt-catalyzed C–H amidation.^[a]



| Entry | Oxazoline | Product | Yield [%] ^[b] |
|-------|-----------------|------------------|--|
| 1 | 142a | 143aa | 56 ^[c] 58 ^[d] |
| 2 | 142b | 143ba | 71 |



| | | | |
|----|---|--|--|
| 9 |  <p>142i</p> |  <p>143ia</p> | 65 |
| 10 |  <p>142j</p> |  <p>143ja</p> | 67 ^[e] 74 ^[f] |
| 11 |  <p>142k</p> |  <p>143ka</p> | 74 |
| 12 |  <p>142l</p> | --- | n.r. |

^[a] Reaction conditions: **142** (0.50 mmol), **40** (1.2 equiv), Cp*Co(CO)I₂ (5.0 mol %), AgSbF₆ (20 mol %), NaOAc (20 mol %), DCE (2.0 mL), 100 °C, 16 h. ^[b] Isolated yields. ^[c] Reaction carried on 5.6 mmol scale. ^[d] Reaction carried on 0.25 mmol scale. ^[e] Performed by *Dr. R. Mei*. ^[f] Using [Cp*RhCl₂]₂ (2.5 mol %) instead of Cp*Co(CO)I₂.

The versatile Cp*Co(III)-catalyst however encountered also limitations. 2-Phenyloxazolines bearing *ortho*-substituents could only be converted to the desired amides in low to moderate yield. Also, no conversion of the starting material was detected when using nitro-substituted oxazoline **142l** (Table 3.2, entry 12).

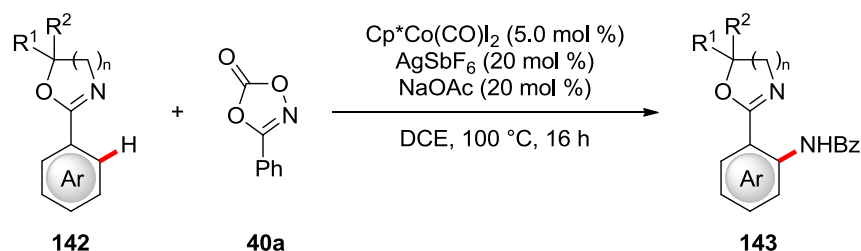
Furthermore, [Cp*RhCl₂]₂ was also tested as catalyst in the transformation of 2-(*meta*-chlorophenyl)-oxazoline **142j**. No significant difference of chemo- or site-

selectivity compared to $\text{Cp}^*\text{Co}(\text{CO})\text{I}_2$ was observed, providing product **143ja** in a similar yield (Table 3.2, entry 10).

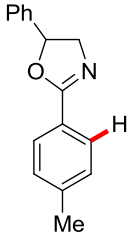
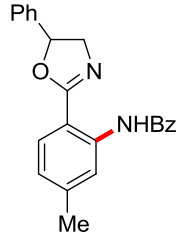
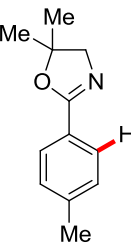
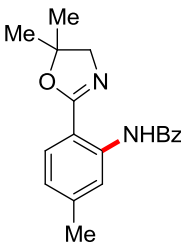
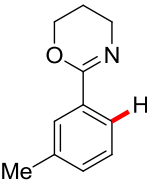
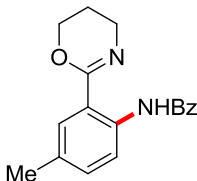
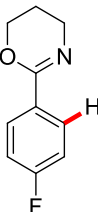
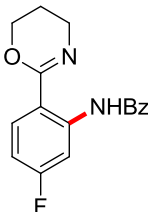
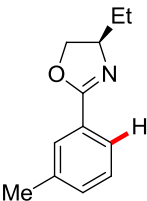
Additional substrates **142**, including 2-phenyloxazolines bearing sensitive halogen, ester and cyano substituents, as well as differently substituted dioxazolones **40**, were also investigated by *Dr. R. Mei* in the transformation, and thus were found to give the desired amidated products.^[37e,227a]

Thereafter, the effect of the substitution pattern of the oxazoline moiety was studied (Table 3.3). Diversely functionalized oxazolines as well as six-membered dihydrooxazines were efficiently converted to amides **143** in good to excellent yield (entries 1–5). However, additional substituents adjacent to the nitrogen atom of the oxazoliny group were not tolerated, with 4-ethyloxazoline **142r** remaining untouched when submitted to the reaction conditions (entry 6). This outcome is likely explained by an excessive steric hindrance near the catalyst-coordinating nitrogen atom of the oxazoline directing group. Indeed, the reactivity of cobalt(III) is greatly affected by steric factors due to its small ionic radius.^[46a,46b]

Table 3.3. Substrate scope of substituted oxazolines and oxazines **142** in the cobalt-catalyzed C–H amidation.^[a]

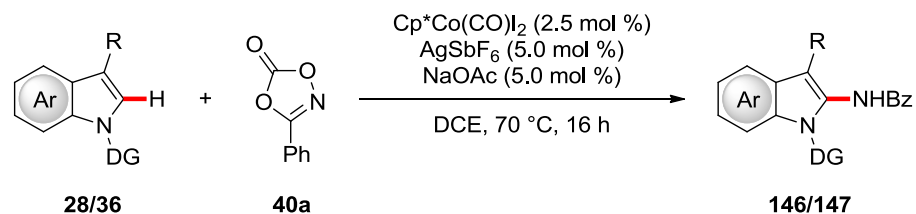


| Entry | Oxazoline | Product | Yield [%] ^[b] |
|-------|-----------------|------------------|--------------------------|
| 1 | 142m | 143ma | 85 |

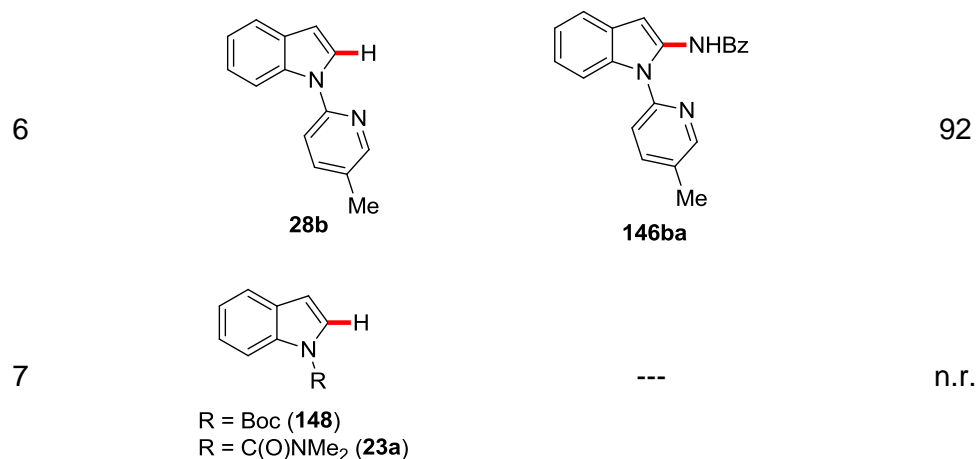
| | | | |
|---|--|--|--------|
| 2 |  142n |  143na | 74 |
| 3 |  142o |  143oa | 86 |
| 4 |  142p |  143pa | 66 |
| 5 |  142q |  143qa | 71 |
| 6 |  142r | --- | traces |

^[a] Reaction conditions: **142** (0.50 mmol), **40** (1.2 equiv), Cp*Co(CO)I₂ (5.0 mol %), AgSbF₆ (20 mol %), NaOAc (20 mol %), DCE (2.0 mL), 100 °C, 16 h. ^[b] Isolated yields.

Gratifyingly, the scope of the Cp*Co(III)-catalyzed C–H amidation was not limited to 2-phenyloxazolines **142**. Indeed, various indoles **28/36** were efficiently and selectively functionalized at the C2-position under the assistance of removable pyridyl (py) and pyrimidyl (pym) directing groups in the presence of diverse alkyl, alkoxy and ester substituents, highlighting the versatility and the robustness of the developed methodology (Table 3.4). Remarkably, due to the higher inherent reactivity of indoles **28/36** compared to 2-aryloxazolines **142**, the synthesis of amidated products **146/147** was found to be viable at a low catalyst loading of 2.5 mol % and a rather mild reaction temperature of 70 °C, after further optimization by *Dr. R. Mei*.^[227b] Cp^tCo(CO)I₂ (Cp^t = 1,3-di-*tert*-butylcyclopentadienyl) was also tested as the catalyst in the cobalt-catalyzed C–H amidation of indoles due to recent reports indicating the superiority of Cp^t over Cp* in rhodium(III)-catalyzed transformations.^[230] However, in the present case, the desired product **147aa** was only formed in a moderate yield of 27% when using the Cp^t catalyst, compared to the 86% obtained when the Cp* complex was employed (entry 1). For more challenging substrates, such as sterically hindered C3-alkylated indole **36b**, increasing the reaction temperature as well as the catalyst loading improved the reaction outcome to afford the desired product **147ba** in synthetically useful yields (entry 2). Furthermore, it is noteworthy that, while 2-aryloxazolines **142** absolutely required carboxylate additives for the transformation to occur with high catalytic efficacy, the more reactive indole substrates **28/36** could be amidated in high yield even in the absence of the base additive (entry 2). However, weakly coordinating directing groups such as carbamates and ureas fell short in the envisioned cobalt-catalyzed amidation (entry 10).

Table 3.4. Substrate scope of substituted indoles **28/36** in the cobalt-catalyzed C–H amidation.^[a]

| Entry | Indole | Product | Yield [%] ^[b] |
|-------|----------------|------------------|--|
| 1 | 36a | 147aa | 86 27 ^[c] |
| 2 | 36b | 147ba | 39 65 ^[d] 61 ^[d,e] |
| 3 | 28c | 146ca | 91 |
| 4 | 28d | 146da | 96 |
| 5 | 28e | 146ea | 97 |



^[a] Reaction conditions: **28/36** (0.50 mmol), **40** (1.2 equiv), Cp*Co(CO)I₂ (2.5 mol %), AgSbF₆ (5.0 mol %), NaOAc (5.0 mol %), DCE (2.0 mL), 70 °C, 16 h. ^[b] Isolated yields. ^[c] Using Cp*Co(CO)I₂ instead of Cp*Co(CO)I₂. ^[d] Using Cp*Co(CO)I₂ (5.0 mol %), AgSbF₆ (10 mol %) and NaOAc (10 mol %) at 100 °C. ^[e] NaOAc was omitted.

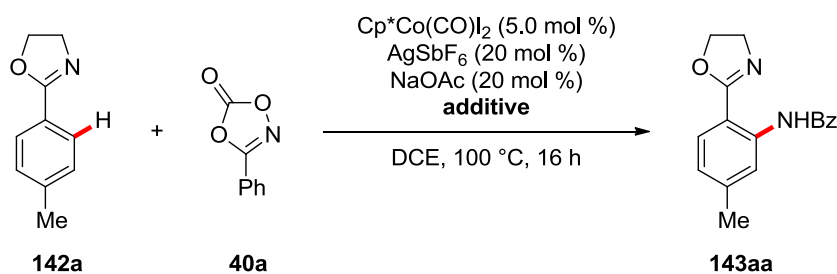
Moreover, the reactions of additional indole substrates **28** bearing sensitive electrophilic functional groups, such as bromo and iodo, as well as differently substituted dioxazolones **40**, including thiophene moieties, were studied in detail by *Dr. R. Mei*, and showcased the chemo-selectivity and robustness of the developed C–H functionalization methodology.^[37e,227a] In addition to 2-aryloxazonlines **142** and *N*-pyri(mi)dyliindoles **28/36**, other substrate classes were smoothly amidated employing the developed methodology. Indeed, 2-phenylpyridines, *N*-phenylpyrazoles, *N*-phenylindazoles and 2-phenylpyrimidines were among other efficiently converted to the corresponding amides by the Cp*Co(CO)I₂ catalyst, as reported by *Dr. R. Mei*.^[227a]

3.1.3. Mechanistic Studies

Given the unique features of the versatile cobalt-catalyzed C–H amidation, we became interested in delineating its mode of action. Towards this objective, experimental mechanistic studies were conducted.

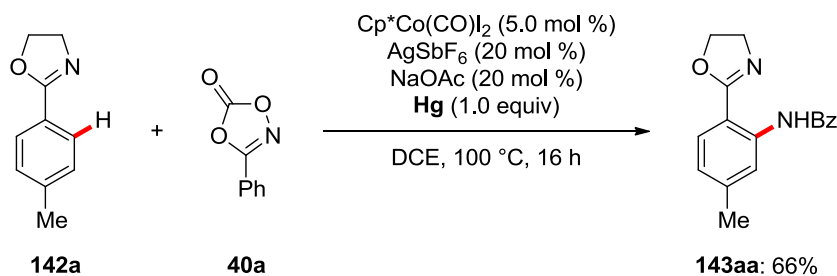
First, the effect on the reaction of various radical scavengers, such as TEMPO and BHT, was probed (Scheme 3.2a). Here, only a mild reduction of the yield was observed, supporting the catalytic transformation not to occur *via* a radical-based mechanism. This observation contrasts with mechanistic studies performed for cobalt-catalyzed C–H alkoxylation, where a SET process has been proposed.^[231] A mercury poisoning test was conducted to probe the homogeneity of the reaction (Scheme 3.2b). Here, no significant reduction of the catalytic activity was observed in the presence of a stoichiometric amount of metallic mercury, which supports the homogenous nature of the catalytic process.

a) radical scavengers



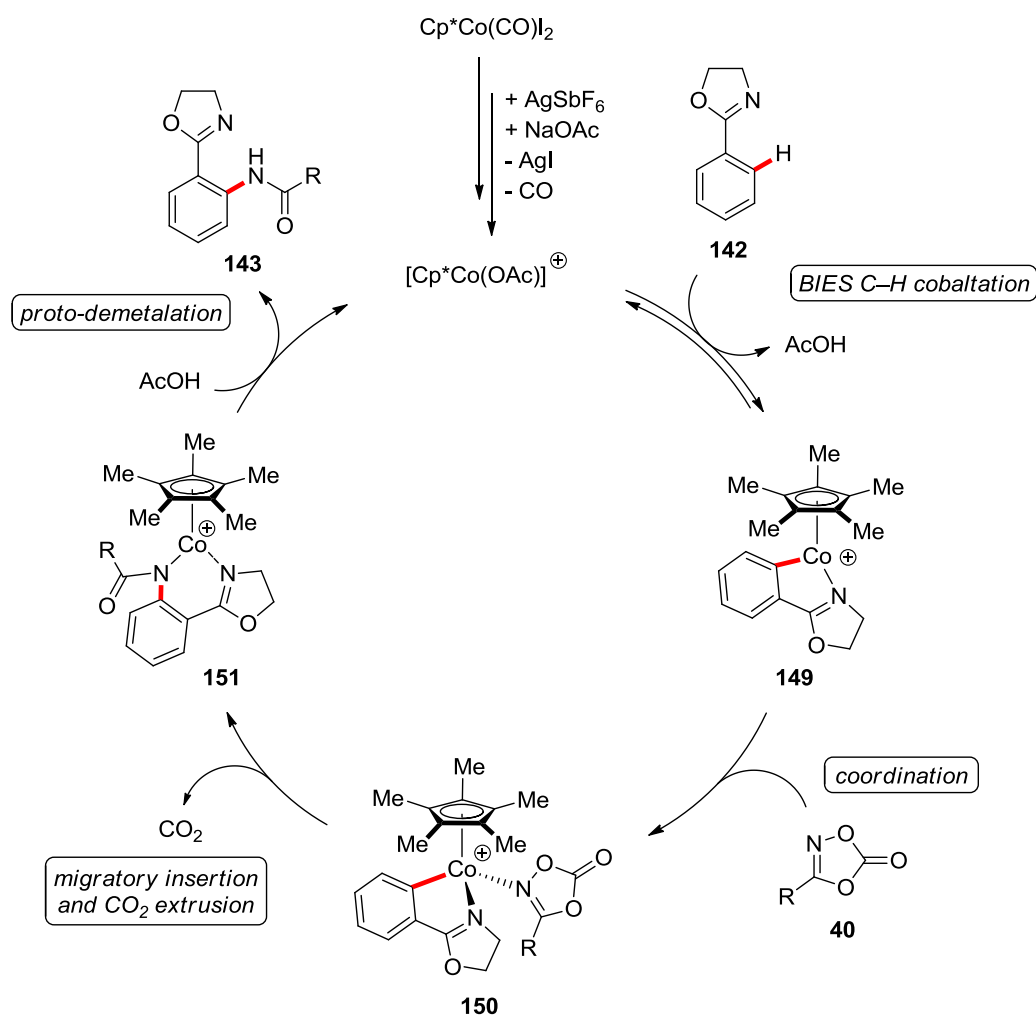
| Additive | Yield |
|--|-------|
| none: | 68% |
| TEMPO (1.0 equiv): | 46% |
| TEMPO (2.0 equiv): | 49% |
| BHT (1.0 equiv): | 48% |
| (<i>E</i>)-stilbene (1.0 equiv): | 63% |
| $\text{Ph}_2\text{C}=\text{CH}_2$ (1.0 equiv): | 67% |
| galvinoxyl (1.0 equiv): | 14% |

b) mercury drop test



Scheme 3.2. Effect of radical scavengers on the cobalt(III)-catalyzed C–H amidation and mercury drop test.

Reactions with an isotopically labeled protic co-solvent were performed by *Dr. R. Mei*.^[227a] A considerable H/D scrambling was observed in the absence of dioxazolones **40**. Yet, no deuterium incorporation was detected in the presence of the amidation reagent **40**. Furthermore, kinetic studies were conducted by *Dr. R. Mei*.^[227a] A kinetic isotope effect (KIE) of $k_H/k_D \approx 2.3$ revealed the C–H cleavage step to be kinetically relevant. Additionally, competition experiments between differently substituted substrates indicated more electron-rich 2-aryloxazolines **142** to react preferentially, which supports the C–H activation event to occur through a base-assisted, intermolecular electrophilic substitution-type (BIES) C–H metalation manifold.^[37]



Scheme 3.3. Plausible catalytic cycle of the $\text{Cp}^*\text{Co}(\text{III})$ -catalyzed C–H amidation.

Based on the conducted mechanistic studies and previous reports, the transformation is believed to be initiated by the formation of the catalytically active cationic complex $\text{Cp}^*\text{Co}(\text{OAc})^+$ through halogen abstraction by the silver salt and coordination by the carboxylate additive (Scheme 3.3). Then, a plausible catalytic cycle begins with a kinetically relevant, acetate-assisted C–H metalation to generate cobaltacycle **149**, which is believed to occur *via* a BIES mechanism.^[37] Thereafter, coordination of the dioxazolone **40** provides intermediate **150**. Finally, CO_2 extrusion and protodemetalation by the formed acetic acid provide the desired amidated product **143** and regenerate the active cobalt(III)-carboxylate catalyst.

3.2. Asymmetric Iron-Catalyzed Hydroarylations by C–H Activation

While major achievements in the research area of C–H activation have been realized with the aid of precious, rather toxic noble transition metals, recent focus has shifted to earth-abundant and inexpensive 3d metals.^[45] However, despite substantial advances, full selectivity control in enantioselective C–H transformations continues to heavily rely on noble 4d and 5d transition metals, mostly palladium, rhodium and iridium complexes.^[51] In sharp contrast, enantioselective C–H functionalizations with sustainable 3d metals remain underdeveloped, but have gained significant momentum during the course of this doctoral thesis.^[52]

In this context, enantioselective transformations by inner-sphere iron-catalyzed C–H activation remained unprecedented at the outset of this work. Drawing inspiration from the work of *Yoshikai* on the racemic iron-catalyzed hydroarylation of styrenes **60** and alkynes **7** with indoles **59** (Scheme 1.28),^[148] the possibility to develop an asymmetric iron-catalyzed C–H alkylation was investigated. The envisioned transformation is highly desirable due to its perfect atom-economy^[2] and the use of readily available, non-prefunctionalized alkenes, making the process environmentally benign.

While our work represents the first enantioselective iron-catalyzed transformation *via* organometallic C–H activation, it should be noted that a few examples of iron-catalyzed enantioselective C–H functionalizations *via* outer-sphere mechanisms have been previously reported.^[232] Atroposelective oxidative couplings of 2-naphthols^[233] and biomimetic C(sp³)–H hydroxylations^[234] have indeed been achieved with chiral iron catalysts in moderate to excellent enantioselectivities. Furthermore, it should be duly noted that, to the best of our knowledge,^[232,235] chiral NHC ligands had never been used in asymmetric iron catalysis prior to this work.

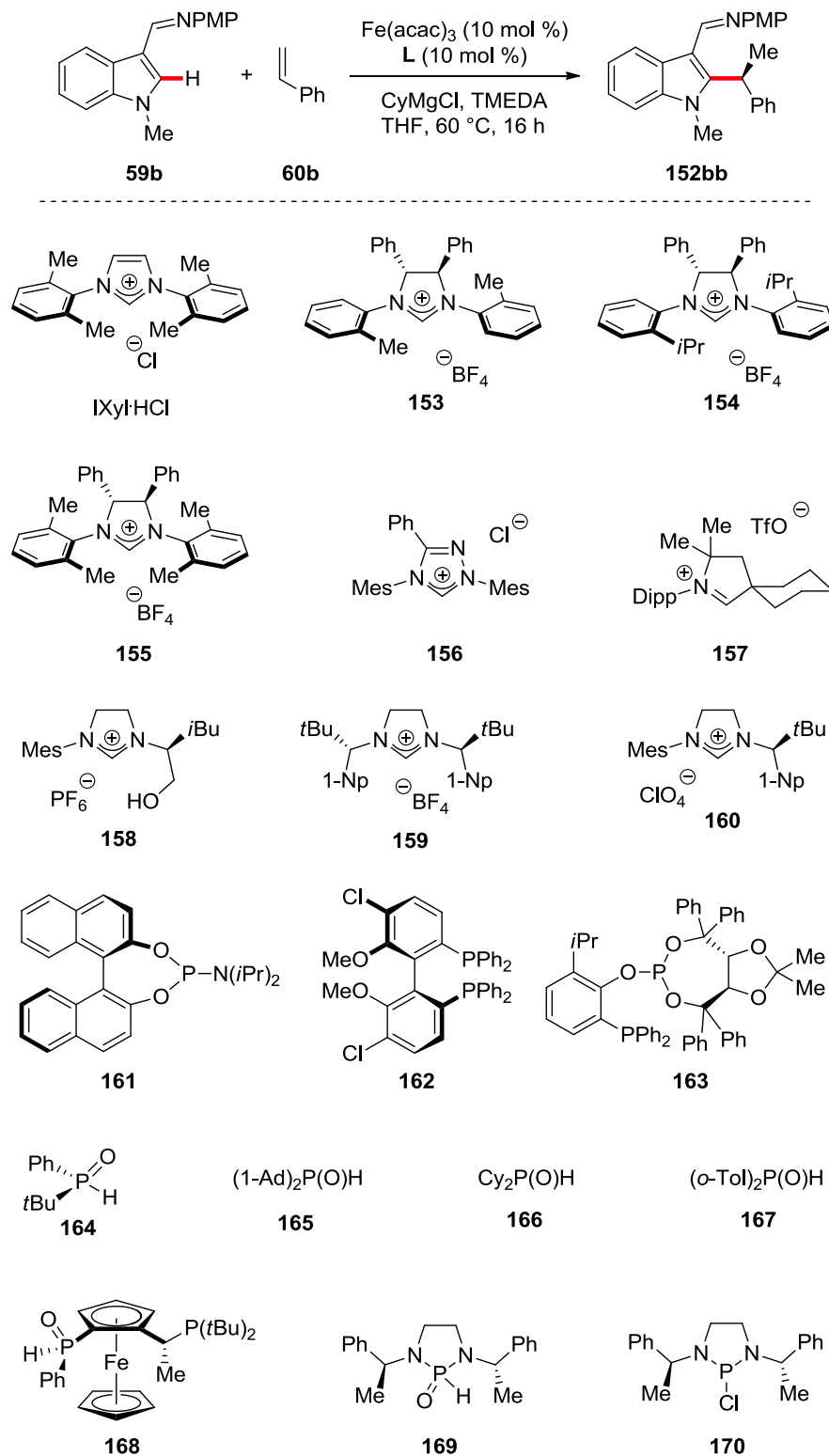
3.2.1. Optimization Studies

The optimization studies began by probing the effect of various (pre-)ligands on the envisioned enantioselective C2-alkylation of indole **59b** with styrene **60b** (Table 3.5). It should be emphasized that, in addition to chiral NHC^[235d,236] precursors, different ligand classes, including achiral ligands, were tested in order to understand the requirements of the transformation. Indeed, only a very limited number of ligands were reportedly tested by *Yoshikai* in the racemic transformation,^[148] which remains the sole example of this kind of reaction under iron catalysis. *Yoshikai* and coworkers investigated a narrow class of bis-aryl substituted NHC precursors, with the best reaction outcome being obtained with sIXyl·HCl while more sterically hindered NHC ligands gave poor results. A few simple phosphine and bipyridyl ligands were also tested, but fell short in providing the C–H alkylated indole in synthetically useful yields. We hence became interested in the performance of different ligands or differently substituted NHC precursors in this transformation.

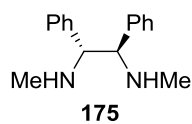
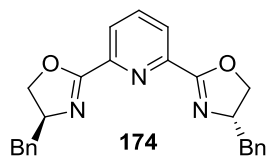
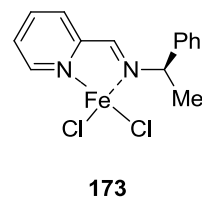
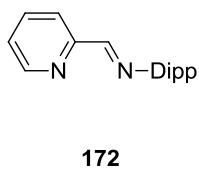
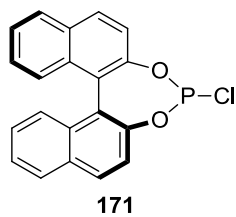
The desired C–H alkylated product **152bb** could be obtained in excellent yield using a slight modification of the reported conditions,^[148] and a control experiment demonstrated the importance of the ligand (entries 1–2). No significant enantio-induction was observed when TMEDA was replaced with (–)-sparteine (entry 3). The simple chiral NHC precursor **153**, originally introduced by *Grubbs* as a chiral sIMes analogue for enantioselective alkene metathesis,^[211] provided product **152bb** in low yield but promising enantioselectivity (entry 4). Various additives were tested in combination with **153**, but did not improve the reaction outcome (entries 5–8). Interestingly, the bulkier ligand **154** gave even poorer results, with the opposite enantiomer being obtained as the “major” product (entry 9). Intrigued by whether the poor results of **153**, which closely resembles the capable IXyl·HCl pre-ligand, were due to the chiral diphenyl backbone or to the lacking *ortho*-methyl substituent, **155** was tested in the transformation (entry 10). While the alkylated product **152bb** was formed in good yield, no significant enantioselectivity was observed. Different carbene classes, such as *Berkessel's* triazolium-based NHC pre-ligand **156**^[237] and CAAC^[238] precursor **157**, were also tested in the reaction (entries 11–12). While

moderate to good conversions were observed, their performance was not superior to the common IXyl-HCl or IMes-HCl NHC precursors. Then, chiral alkyl-substituted NHC precursors **158–160** were investigated in the enantioselective alkylation, but unfortunately gave extremely poor results (entries 13–15).

To further uncover the required ligand properties, different types of (pre-)ligands were tested in the transformation. No significant conversion or enantio-induction was observed with phosphine or phosphoramidite ligands (entries 16–18). A rather promising enantioselectivity was observed with the prototypical chiral secondary phosphine oxide (SPO) **164**, despite the poor conversion (entry 19). Other simple, non-chiral SPOs were hence investigated, but only provided the alkylated product **152bb** in low yields (entries 20–22). Additional (HA)SPOs were then probed, without major success (entries 23–24). Phosphine chlorides^[239] **170–171** were tested as well, but failed to deliver any desired product (entries 25–26). It should be noted that phosphine chloride pre-ligands may react with the Grignard reagent to generate the corresponding phosphine *in situ*, although findings by *Ackermann* in the context of palladium-catalyzed *Kumada–Corriu* couplings provide support for the formation of tertiary phosphines not to occur under similar conditions.^[239a] The performance of nitrogen-based ligands in the envisioned iron-catalyzed asymmetric hydroarylation was then explored. As promising results were obtained with the bidentate ligand **172**, its chiral analogue **173**, which had been previously successfully employed in iron-catalyzed hydrofunctionalizations of alkenes,^[240] was probed in the C–H alkylation, but no significant enantio-induction was observed (entries 27–28). Furthermore, PyBOX^[224g] **174** and diamine **175** were tested, but failed to deliver any promising results (entries 29–30).

Table 3.5. Preliminary ligand optimization for the iron-catalyzed hydroarylation of styrene **60b** with indole **59b**.^[a]

3. Results and Discussion



| Entry | L | Yield [%] ^[b] | e.r. ^[c] |
|--------------------|------------|--------------------------|---------------------|
| 1 | IXyl·HCl | 92 | 50:50 |
| 2 | --- | <2% | - |
| 3 ^[d] | IXyl·HCl | 53 | <5% ee |
| 4 | 153 | 11 | 60:40 |
| 5 ^[e] | 153 | traces | - |
| 6 ^[f] | 153 | n.r. | - |
| 7 ^[f.g] | 153 | n.r. | - |
| 8 ^[h] | 153 | traces | - |
| 9 | 154 | 6 | 45:55 |
| 10 | 155 | 61 | 54:46 |
| 11 | 156 | 66 | - |
| 12 | 157 | 23 | - |
| 13 | 158 | 4 | <5% ee |
| 14 | 159 | 5 | <5% ee |
| 15 | 160 | 8 | <5% ee |

| | | | |
|-------------------|------------|--------|--------|
| 16 | 161 | 12 | <5% ee |
| 17 | 162 | 15 | <5% ee |
| 18 | 163 | 2 | <5% ee |
| 19 | 164 | 8 | 59:41 |
| 20 | 165 | 20 | - |
| 21 | 166 | 18 | - |
| 22 | 167 | 20 | - |
| 23 | 168 | 22 | <5% ee |
| 24 | 169 | 5 | <5% ee |
| 25 | 170 | traces | - |
| 26 | 171 | traces | - |
| 27 | 172 | 32 | - |
| 28 ^[i] | 173 | 17 | <5% ee |
| 29 | 174 | 12 | 55:45 |
| 30 | 175 | 10 | <5% ee |

^[a] Reaction conditions: **59b** (0.25 mmol), **60b** (1.5 equiv), Fe(acac)₃ (10 mol %), **L** (10 mol %), CyMgCl (1.0 equiv), TMEDA (2.0 equiv), THF (0.50 mL), 60 °C, 16 h.

^[b] Yield of the isolated product. ^[c] Determined by chiral HPLC analysis.

^[d] (-)-Sparteine (2.0 equiv) instead of TMEDA. ^[e] THF/NMP (5/1) as solvent.

^[f] [ZnBr₂·TMEDA] (2.0 equiv) was added. ^[g] TMEDA was omitted. ^[h] LiCl (1.0 equiv) was added. ^[i] Fe(acac)₃ was omitted.

Based on the results discussed above (Table 3.5), it became apparent that only bis-aryl NHCs seem to be suitable ligands in this transformation, as no significant enantio-induction and/or conversion was observed with other ligand classes or differently decorated NHC precursors. Hence, we attempted to rationalize the effect of the substituents of the flanking phenyl groups of the NHC core in order to design

more selective and effective ligands for this transformation (Scheme 3.4a). It should be noted that the development of chiral analogues of the common monodentate NHC ligands IMes and IPr has been described as an extremely challenging task. Indeed, the differences of steric and electronic properties of chiral NHC ligands compared to IMes or IPr often render them incompetent for the envisioned transformations.^[241]

First, the comparison of xylyl-substituted pre-ligands (IXyl-HCl and **155**) to NHC precursor **153** lacking an *ortho*-methyl group clearly indicated that both substituents in 2- and 6-positions of the *N*-aryl groups are essential for the reaction to provide the desired alkylated product in good yield (Table 3.5, entries 1, 4, 10). However, no significant enantioselectivity was ever observed with this design. The introduction of bulkier *ortho*-substituents on the aryl groups of *Grubbs*-type^[211] NHC ligands would seem highly desirable, as it has been a successful approach in many previous reports.^[242] However, additional steric bulk on the *ortho*-position is not tolerated in the present case, as exemplified by the extremely poor performances of **154** (Table 3.5, entry 9) or IPr in *Yoshikai's* racemic C–H alkylation.^[148]

Therefore, it appeared clearly that a novel ligand design was required here. Based on the results discussed above, it emerged that two small (i.e. primary) *ortho*-substituents at the 2- and 6-positions of the flanking aryl groups are necessary in order to achieve high conversions, although no significant enantio-induction was observed with this substitution pattern. Hence, the design of a NHC ligand able to provide the alkylated product with both high yield and enantioselectivity seemed to be an unsolvable problem at first. However, we reasoned that replacing the second methyl substituent at the 6-position of the *N*-aryl group with a bulky substituent at the adjacent *meta* 5-position might just do the trick, providing enough steric bulk on both sides of the aryl group, but not too close to the metal center. Interestingly, the envisioned design would create a wide and rather flexible (due to free rotation about the C–N bond) C₂-symmetric chiral pocket (Fig. 3.4b). Indeed, it is expected, based on the original design by *Grubbs*,^[211] that the chiral DPEN backbone will repel the *ortho*-methyl substituent of the *N*-aryl groups. The flanking aryl groups then act as

chiral relays to position the large *meta*-substituents on opposite sides of the NHC core, transferring the stereo-information of the chiral backbone to the substrates bound to the metal center during the reaction. This assumption was subsequently supported by a recent publication by *Michon* and coworkers in which the X-ray crystal structure of a rhodium(I) complex with a NHC ligand following the same design was reported.^[243] While the introduction of bulky *meta*-substituents had been described previously, it should be noted that the reported 2,5-disubstituted *N*-aryl groups always bore large *ortho*-substituents.^[236,244]

a) inspiration for *meta*-substituted NHC ligands

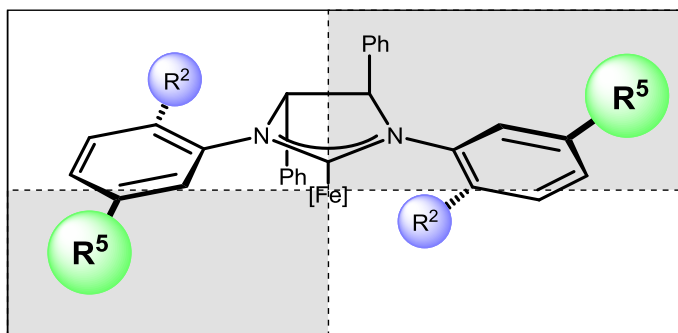


The problem with R^6 :

- $R^6 = H$ (**153**): moderate enantio-induction, poor conversion
- $R^6 = Me$ (**155**): poor enantio-induction, high conversion
- Bulkier (i.e. 2° alkyl) *ortho*-substituents: poor enantio-induction and conversion

What about bulky *meta*-substituents?

b) stereochemical model

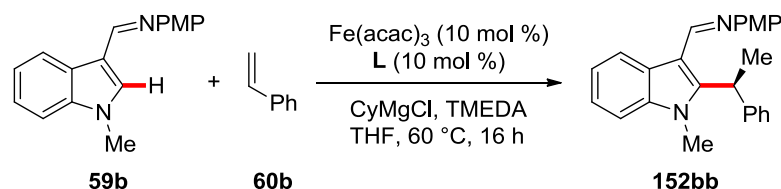


Scheme 3.4. Rationale for remote *meta*-substituted NHC ligands.

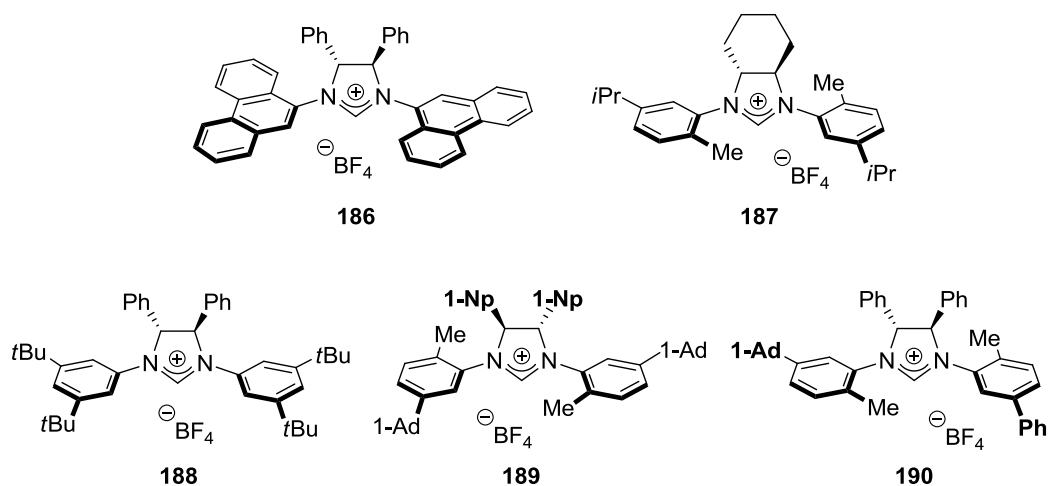
Thereby, various NHC precursors bearing *N*-aryl groups with *meta*-substituents were prepared and probed in the envisioned transformation (Table 3.6). While the prototypical chiral NHC precursor **153** only provided poor results (Table 3.5, entry 1 and Table 3.6, entry 4), the introduction of a simple *meta*-methyl substituent exhibited a huge beneficial effect on the reaction outcome (Table 3.6, entry 2).

Extensive variations of the *meta*-substituent (entries 3–9) revealed an isopropyl group to be optimal (entry 3). Variations of the *ortho*-substituent were probed as well, but a methoxy substituent provided inferior results compared to a simple methyl group (entry 5). *N*-9-phenanthryl-NHC precursor **186** was tested as well. Despite the promising conversion, no significant enantio-induction was observed (entry 10). Variations of the chiral DPEN backbone were then investigated. Remarkably, a NHC precursor derived from DACH (**187**, entry 11) promoted the hydroarylation with an isolated yield similar to its DPEN-derived analogue (**177**, entry 3), but no significant enantioselectivity was observed. Changing the ligand-to-metal ratio from 1:1 to 2:1 improved the reaction outcome considerably, increasing the enantiomeric ratio to 75:25 (entry 12). Finally, replacing TMEDA with other amine additives had a rather limited effect on the outcome of the transformation (entries 13–14).

Table 3.6. Optimization of chiral NHC pre-ligands for the enantioselective hydroarylation of styrene.^[a]



| L | R ² | R ⁵ |
|------------|----------------|---|
| 153 | Me | H |
| 176 | Me | Me |
| 177 | Me | <i>i</i> Pr |
| 178 | Me | <i>t</i> Bu |
| 179 | OMe | <i>t</i> Bu |
| 180 | Me | 1-Ad |
| 181 | Et | 1-Ad |
| 182 | Me | Ph |
| 183 | Me | 4- <i>t</i> Bu-C ₆ H ₄ |
| 184 | Me | CH(4-F-C ₆ H ₄) ₂ |
| 185 | Me | 4-Hept |



| Entry | L | Yield [%] ^[b] | e.r. ^[c] |
|-------------------|-----|--------------------------|---------------------|
| 1 | 153 | 11 | 60:40 |
| 2 | 176 | 48 | 67:33 |
| 3 | 177 | 67 | 71:29 |
| 4 | 178 | 53 | 70:30 |
| 5 | 179 | 21 | 58:42 |
| 6 | 180 | 58 | 69:31 |
| 7 | 182 | 23 | 64:36 |
| 8 | 184 | 33 | 66:34 |
| 9 | 185 | 36 | 66:34 |
| 10 | 186 | 62 | 55:45 |
| 11 | 187 | 57 | <5% ee |
| 12 ^[d] | 177 | 65 | 75:25 |

| | | | |
|---------------------|-----|----|-------|
| 13 ^[d,e] | 177 | 68 | 72:28 |
| 14 ^[d,f] | 177 | 58 | 68:32 |

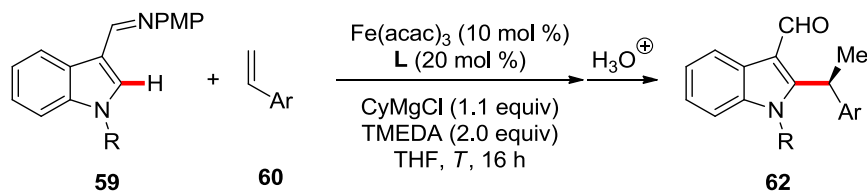
^[a] Reaction conditions: **59b** (0.25 mmol), **60b** (1.5 equiv), Fe(acac)₃ (10 mol %), **L** (10 mol %), CyMgCl (1.0 equiv), TMEDA (2.0 equiv), THF (0.50 mL), 60 °C, 16 h.

^[b] Yield of the isolated product. ^[c] Determined by chiral HPLC analysis. ^[d] **L** (20 mol %) and CyMgCl (1.1 equiv). ^[e] PMDETA instead of TMEDA. ^[f] BDMAEE instead of TMEDA.

As asymmetric catalysis can sometimes be very substrate-specific, differently decorated indoles and styrenes were probed in the transformation (Table 3.7). First, the impact of the indole's *N*-protecting group was investigated (entries 1–5). Whereas different *N*-alkyl substituents proved viable in the reaction, Boc and *p*-tosyl protecting groups fell short in delivering any C–H alkylated product, in complete agreement with the previous report of *Yoshikai*.^[148] Interestingly, those findings are in stark contrast to the cobalt-catalyzed hydroarylation of styrenes with indoles developed by the same research group, where electron-withdrawing groups such as Boc were not only tolerated, but superior to alkyl or benzyl moieties.^[106] MOM-protected indole **59g** provided nearly identical results compared to *N*-methylindole **59b**, while the introduction of a bulkier benzyl group had a critical effect. Indeed, both the yield and the enantioselectivity were significantly improved (entry 5). Further optimization studies were conducted using this substrate (entries 6–9). Different Grignard reagents or lower catalyst loadings did not afford satisfactory results. Remarkably, in sharp contrast to the work of *Yoshikai*,^[148] the transformation was found to occur even in the absence of TMEDA, albeit in lower efficiency and selectivity. With the optimal indole substrate **59c** in hand, various styrene derivatives **60** were tested in the iron-catalyzed asymmetric hydroarylation. 2-Vinylnaphthalene **60a** showed poor performance in the transformation, while *para*-fluorostyrene **60g** did not give better results than simple styrene **60b** (entries 10–11). Gratifyingly, the use of electron-rich 4-methoxystyrene **60c** provided a far better yield and enantioselectivity compared to other styrene analogues (entry 12). The excellent conversion allowed us to lower the reaction temperature to 45 °C, improving the

enantioselectivity to 89:11 e.r., while maintaining a synthetically useful yield (entry 13). While these conditions were initially used to study the substrate scope and limitations of the transformation (*vide infra*), a subsequent ligand screening revealed the superiority of *meta*-adamantyl ligand **180**, which provided the hydroarylation product **62cc** with an enantiomeric ratio of 92:8 (entries 14–19). Interestingly, the importance of the small *ortho*-methyl group was confirmed, as poor results were obtained with either a bulkier or no substituent (entries 15–16). Additionally, the introduction of a bulkier substituents in the chiral backbone did not improve the enantioselectivity (entry 17), in contrast to a previous work of *Cramer* and coworkers (Scheme 1.43).^[210] Outstanding conversions were obtained with C_2 - and C_1 -symmetrical^[241] precursors bearing *meta*-aryl substituents, but lower enantiomeric excesses were observed (entries 18–19). Finally, FeF_3 fell short in delivering any hydroarylation product (entry 20), despite its documented superiority over other iron precursors in iron/NHC-catalyzed *Kumada–Corriu*-type cross-couplings.^[245]

Table 3.7. Substrate engineering and final optimization for the enantioselective hydroarylation of styrenes.^[a] (Ligand structures are given in Table 3.6.)



| Entry | R | Ar | L | T [°C] | Yield [%] ^[b] | e.r. ^[c] |
|------------------|-----|----|------------|--------|--------------------------|---------------------|
| 1 ^[d] | Me | Ph | 177 | 60 | 65 | 75:25 |
| 2 ^[d] | Boc | Ph | 177 | 60 | n.r. | - |
| 3 ^[d] | Ts | Ph | 177 | 60 | n.r. | - |
| 4 | MOM | Ph | 177 | 60 | 64 | 75:25 |
| 5 ^[d] | Bn | Ph | 177 | 60 | 73 | 80:20 |

3. Results and Discussion

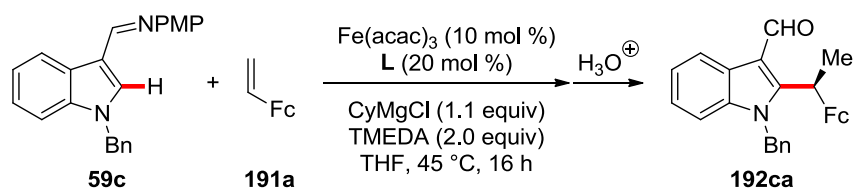
| | | | | | | |
|--------------------|----|-----------------------------------|------------|----|--------|-------|
| 6 ^[d,e] | Bn | Ph | 177 | 60 | 43 | 78:22 |
| 7 ^[d,f] | Bn | Ph | 177 | 60 | n.r. | - |
| 8 ^[d,g] | Bn | Ph | 177 | 60 | 42 | 68:32 |
| 9 ^[d,h] | Bn | Ph | 177 | 60 | 52 | 76:24 |
| 10 | Bn | 2-Np | 177 | 60 | 46 | 56:44 |
| 11 | Bn | 4-F-C ₆ H ₄ | 177 | 60 | 72 | 81:19 |
| 12 | Bn | PMP | 177 | 60 | 93 | 85:15 |
| 13 | Bn | PMP | 177 | 45 | 76 | 89:11 |
| 14 | Bn | PMP | 180 | 45 | 95 | 92:8 |
| 15 | Bn | PMP | 181 | 45 | 78 | 90:10 |
| 16 | Bn | PMP | 188 | 45 | 10 | 58:42 |
| 17 | Bn | PMP | 189 | 45 | 87 | 11:89 |
| 18 | Bn | PMP | 183 | 45 | 98 | 75:25 |
| 19 | Bn | PMP | 190 | 45 | 98 | 87:13 |
| 20 ^[i] | Bn | PMP | 180 | 45 | traces | - |

^[a] Reaction conditions: **59** (0.25 mmol), **60** (1.5 equiv), Fe(acac)₃ (10 mol %), **L** (20 mol %), CyMgCl (1.1 equiv), TMEDA (2.0 equiv), THF (0.50 mL), 60 °C, 16 h. ^[b] Yield of the isolated product. ^[c] Determined by chiral HPLC analysis. ^[d] No hydrolysis, the product was isolated as the imine. ^[e] PhMgCl instead of CyMgCl. ^[f] TMSCH₂MgCl instead of CyMgCl. ^[g] Fe(acac)₃ (3.0 mol %) and **177** (6.0 mol %). ^[h] TMEDA was omitted. ^[i] FeF₃ instead of Fe(acac)₃.

While studying the substrate scope of the reaction (*vide infra*), vinylferrocene **191a** was identified as a suitable coupling partner in this transformation, providing the hydroarylation product with unprecedented enantioselectivities. Those findings prompted us to re-optimize the reaction for this unique class of substrates. Ferrocene derivatives are particularly important in asymmetric catalysis,^[246] material

sciences,^[247] and bioinorganic chemistry,^[248] among others.^[113] First, a representative set of chiral NHC precursors was probed in the asymmetric alkylation of *N*-benzylindole **59c** with vinylferrocene **191a** (Table 3.8). The simple *Grubbs'* carbenes **153** and **154** performed poorly in the envisioned reaction, but confirmed the importance of the *ortho*-methyl groups (entries 1–2). An excellent conversion but only a moderate enantio-induction were observed with xylyl-substituted NHC precursor **155** (entry 3). Once more, the introduction of *meta*-substituents on the flanking aryl group of the NHC had a dramatic effect and allowed for high enantioselectivities (entries 4–8). Remarkably, a clear trend was observed depending on the size of the *meta*-alkyl substituent, with 1-adamantyl groups giving optimal results (entry 7). Interestingly, *meta*-phenyl substituents gave the highest conversion despite the moderate enantio-induction (entry 8). *Kündig's* *N,N'*-alkyl-substituted NHCs^[249] were probed as well, but performed extremely poorly (entries 9–10), in agreement with previous work for the hydroarylation of styrenes (Table 3.5).

Table 3.8. Ligand optimization of the enantioselective hydroarylation of vinylferrocene **191a**.^[a]



| L | R ² | R ⁵ | R ⁶ |
|------------|----------------|----------------|----------------|
| 153 | Me | H | H |
| 154 | <i>i</i> Pr | H | H |
| 155 | Me | H | Me |
| 176 | Me | Me | H |
| 177 | Me | <i>i</i> Pr | H |
| 178 | Me | <i>t</i> Bu | H |
| 180 | Me | 1-Ad | H |
| 182 | Me | Ph | H |

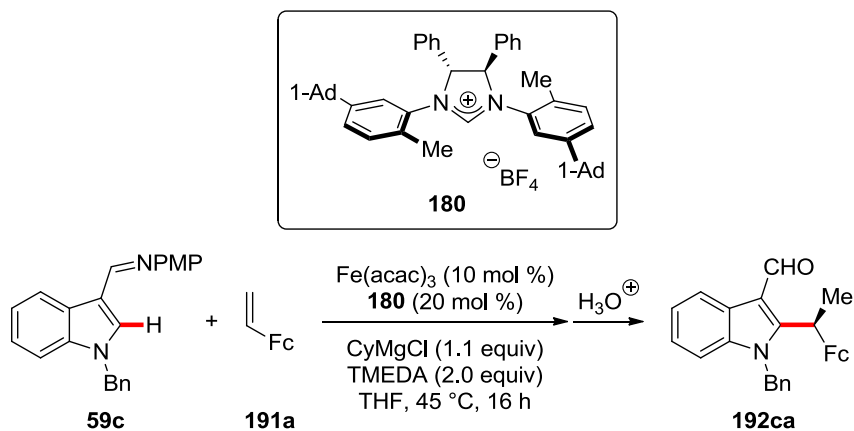
| Entry | L | Yield [%] ^[b] | e.r. ^[c] |
|------------------|-------------|--------------------------|---------------------|
| 1 ^[d] | 153 | 5.5 | 25:75 |
| 2 ^[d] | 154 | 3.3 | 54:46 |
| 3 | 155 | 81 | 41:59 |
| 4 | 176 | 69 | 11:89 |
| 5 | 177 | 69 | 7:93 |
| 6 | 178 | 53 | 5:95 |
| 7 | 180 | 69 | 4:96 |
| 8 | 182 | 76 | 12:88 |
| 9 | 159' | n.r. | - |
| 10 | 193 | n.r. | - |

^[a] Reaction conditions: **59c** (0.25 mmol), **191a** (1.5 equiv), Fe(acac)₃ (10 mol %), **L** (20 mol %), CyMgCl (1.1 equiv), TMEDA (2.0 equiv), THF (0.50 mL), 45 °C, 16 h. ^[b] Yield of the isolated product. ^[c] Determined by HPLC analysis. ^[d] At 60 °C.

Additional optimization studies and control experiments were then conducted (Table 3.9). A *Job* plot^[250] of the ligand-to-metal ratio confirmed a 2:1 ratio to be optimal (entries 1–4). However, the only slightly lower conversion obtained using a 1:1 ligand-to-metal ratio, along with the previous work of *Yoshikai*,^[148] would rather indicate a mono-ligated iron/NHC catalyst to be operative in the transformation. Moreover, detailed mechanistic studies provided further support for a mono-NHC ligated iron species to be catalytically active (*vide infra*). Sub-stoichiometric amounts of CyMgCl only provided the desired alkylated product **192ca** in low yields, supporting the Grignard reagent to play a bigger role than just serving as a base to generate the free NHC *in situ* (entries 5–7). Other organomagnesium reagents were tested in the transformation, but proved to be inferior to CyMgCl (entries 8–11). Interestingly, while the highest conversions were obtained with organometallic

species prone to β -hydride elimination after transmetalation to iron^[240b,251] (entries 1 and 9), significant conversion was observed with PhMgCl as well (entry 8). In contrast, no conversion was observed using NaOtBu as the base (entry 12), which supports an *in situ* generated organoiron species to be involved in the catalysis. Despite the different oxidation states and counter-ions, FeCl₂ provided results comparable to Fe(acac)₃ (entry 13). A reaction conducted at ambient temperature furnished the alkylated product **192ca** with a slightly higher enantiomeric ratio of 97:3, but significantly lower yield (entry 14). In contrast, increasing the temperature to 60 °C improved the yield but lowered the enantioselectivity (entry 15). Once again, in stark contrast to the work of *Yoshikai*,^[148] the transformation was found to occur even in the absence of TMEDA, albeit in lower efficiency (entry 16). Finally, control experiments confirmed the key role of the iron catalyst, as no product formation was detected in the absence of Fe(acac)₃ or using other first-row transition metal salts (entries 17–20).

Table 3.9. Further optimization studies and control experiments for the enantioselective hydroarylation of vinylferrocene **191a**.^[a]



| Entry | Deviation from the standard conditions | Yield [%] ^[b] | e.r. ^[c] |
|------------------|--|--------------------------|---------------------|
| 1 | none | 69 | 4:96 |
| 2 ^[d] | 180 (5.0 mol %) | 36 | 8:92 |
| 3 ^[d] | 180 (10 mol %) | 53 | 5:95 |

3. Results and Discussion

| | | | |
|------------------|--|------|------|
| 4 ^[e] | 180 (30 mol %) | 65 | 4:96 |
| 5 | CyMgCl was omitted | n.r. | - |
| 6 | CyMgCl (0.50 equiv) | 18 | 4:96 |
| 7 | CyMgCl (0.60 equiv) | 26 | 4:96 |
| 8 | PhMgCl instead of CyMgCl | 33 | 4:96 |
| 9 | <i>i</i> PrMgCl instead of CyMgCl | 55 | 5:95 |
| 11 | TMSCH ₂ MgCl instead of CyMgCl | n.r. | - |
| 12 | NaOtBu instead of CyMgCl | n.r. | - |
| 13 | FeCl ₂ instead of Fe(acac) ₃ | 50 | 5:95 |
| 14 | at 23 °C | 40 | 3:97 |
| 15 | at 60 °C | 72 | 6:94 |
| 16 | TMEDA was omitted | 39 | 5:95 |
| 17 | Fe(acac) ₃ was omitted | - | - |
| 18 | Co(acac) ₂ instead of Fe(acac) ₃ | - | - |
| 19 | Mn(acac) ₂ instead of Fe(acac) ₃ | - | - |
| 20 | Ni(acac) ₂ instead of Fe(acac) ₃ | - | - |

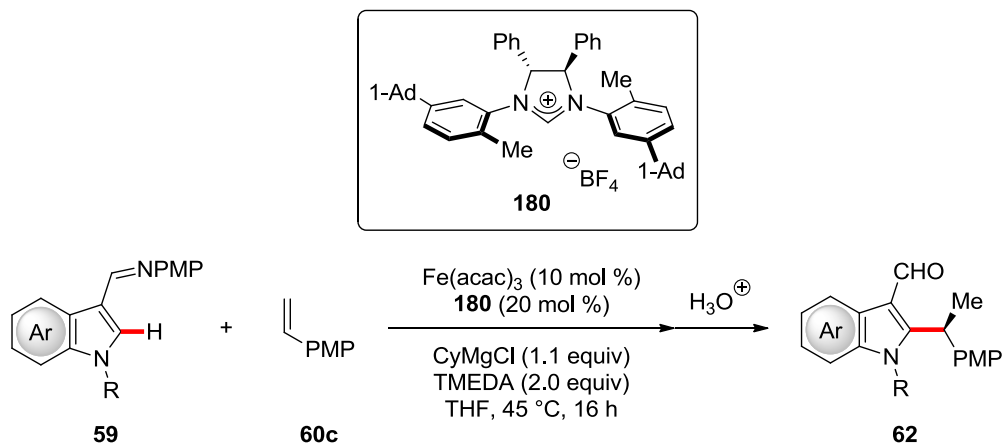
^[a] Reaction conditions: **59c** (0.25 mmol), **191a** (1.5 equiv), Fe(acac)₃ (10 mol %), **180** (20 mol %), CyMgCl (1.1 equiv), TMEDA (2.0 equiv), THF (0.50 mL), 45 °C, 16 h. ^[b] Yield of the isolated product. ^[c] Determined by chiral HPLC analysis. ^[d] CyMgCl (1.0 equiv). ^[e] CyMgCl (1.2 equiv).

It should be highlighted that such high enantioselectivities are remarkable in organometallic iron catalysis and remain unmatched as of today. Indeed, at the outset of this work, the only previous example of such an asymmetric transformation was an iron-catalyzed *Kumada–Corriu* cross-coupling employing a complex chiral bidentate phosphine, which provided the coupled products in up to 91:9 e.r.

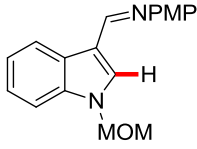
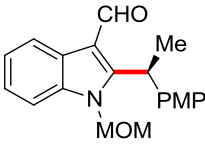
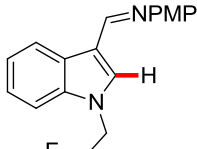
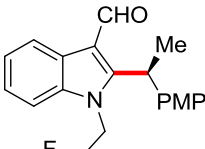
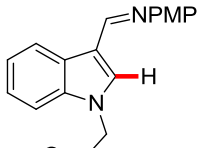
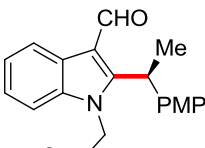
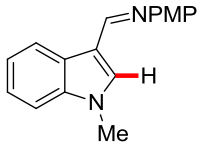
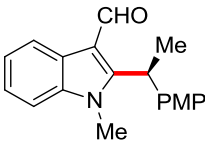
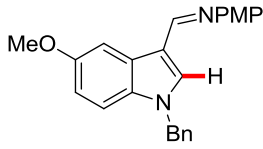
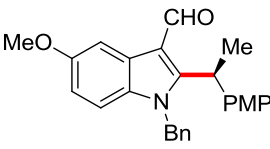
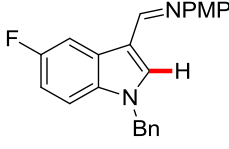
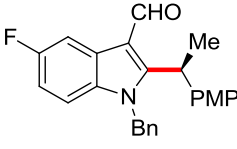
(Scheme 1.29).^[149] Later works on cross-couplings^[150] and C–H activation^[152] provided the corresponding products with even lower enantioselectivities. Thus, enantiomeric excesses over 90%, furthermore obtained with a monodentate chiral ligand, are absolutely outstanding in this burgeoning field of catalysis. Indeed, the present work not only represents the first enantioselective transformation by inner-sphere iron-catalyzed C–H activation, but also the first use of chiral NHC ligands in asymmetric iron catalysis.

3.2.2. Substrate Scope and Limitations

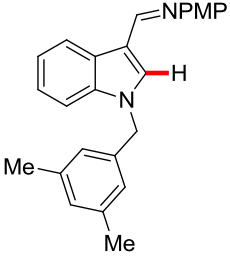
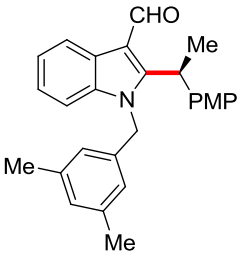
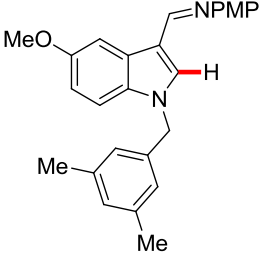
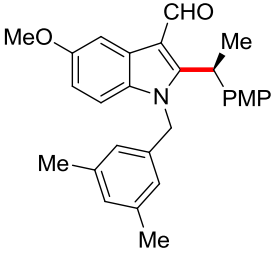
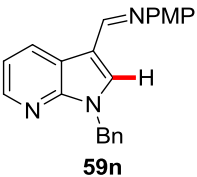
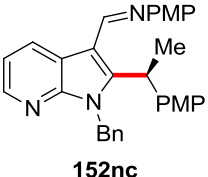
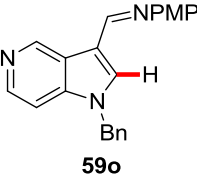
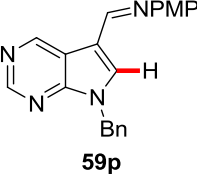
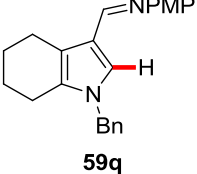
With the optimized iron catalyst in hands, its performance in the intermolecular asymmetric C–H alkylation of indole derivatives **59** with the electron-rich 4-methoxystyrene (**60c**) was explored (Table 3.10). The desired carbaldehydes **62** were obtained with excellent yields and high levels of enantiocontrol from diversely substituted indoles **59** (entries 1–12). Indeed, electron-rich as well as electron-poor indoles **59** were amenable to the present reaction. Furthermore, the transformation was fully compatible with numerous functionalities on the indole nitrogen, including alkyl and benzyl substituents bearing synthetically useful functional groups. It is noteworthy that NHC precursor **177**, bearing *meta*-*i*Pr substituents, was found to furnish products **62fc**, **62gc** and **62bc** with a slightly improved enantioselectivity compared to pre-ligand **180** (entries 4, 5, 8). Remarkably, the pharmacologically relevant 7-azaindole **59n** was also identified as a viable substrate for the first time in iron-catalyzed C–H activations, although the alkylated product **62nc** was only obtained with a moderate enantiomeric ratio of 76:24 (entry 13). A single recrystallization however improved the enantiomeric ratio to 90:10. Yet, other azaindoles gave unsatisfactory results so far (entries 14–15). Furthermore, no significant conversion was observed using pyrrole **59q** or benzothiophene **194** (entries 16–17).

Table 3.10. Substrate scope of substituted (aza)indoles **59** in the iron-catalyzed enantioselective C–H alkylation with styrene **60c**.^[a]

| Entry | (Aza)indole | Product | Yield [%] ^[b] | e.r. ^[c] |
|-------|-------------|---------|--------------------------|-------------------------------|
| 1 | | | 95 76 ^[d] | 92:8 89:11 ^[d] |
| 2 | | | 80 72 ^[d] | 92:8 88:12 ^[d] |
| 3 | | | 94 96 ^[d] | 92:8 90:10 ^[d] |
| 4 | | | 87 70 ^[d] | 86:14 89:11 ^[d] |

| | | | | |
|----|---|---|-------------------------|-------------------------------|
| 5 |  59g |  62gc | 80 84 ^[d] | 86:14 87:13 ^[d] |
| 6 |  59h |  62hc | 96 81 ^[d] | 94:6 91:9 ^[d] |
| 7 |  59i |  62ic | 82 76 ^[d] | 94:6 91:9 ^[d] |
| 8 |  59b |  62bc | 93 76 ^[d] | 84:16 85:15 ^[d] |
| 9 |  59j |  62jc | 98 85 ^[d] | 93:7 90:10 ^[d] |
| 10 |  59k |  62kc | 95 76 ^[d] | 93:7 91:9 ^[d] |

3. Results and Discussion

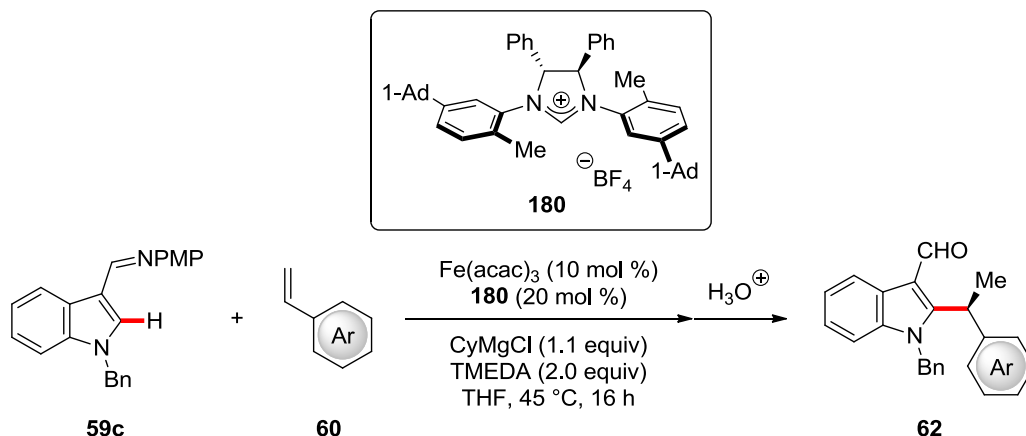
| | | | | |
|-------------------|---|--|-------------------------|-------------------------------|
| 11 |  <p>59l</p> |  <p>62lc</p> | 90 85 ^[d] | 91:9 90:10 ^[d] |
| 12 |  <p>59m</p> |  <p>62mc</p> | 96 72 ^[d] | 91:9 89:11 ^[d] |
| 13 ^[e] |  <p>59n</p> |  <p>152nc</p> | 84 51 ^[f] | 76:24 90:10 ^[f] |
| 14 ^[e] |  <p>59o</p> | --- | traces | - |
| 15 ^[e] |  <p>59p</p> | --- | <10% ^[g] | - |
| 16 |  <p>59q</p> | --- | <5% ^[g] | - |



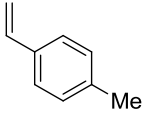
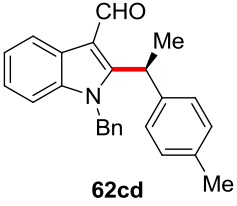
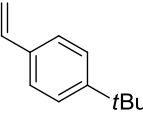
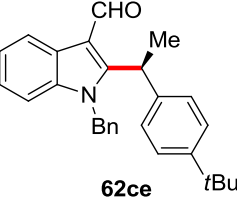
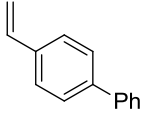
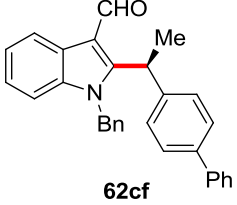
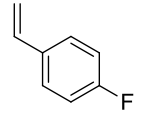
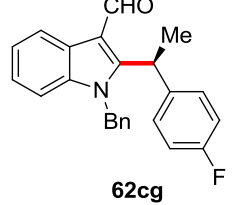
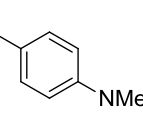
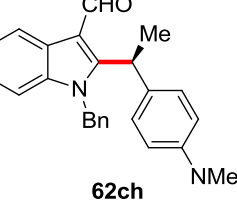
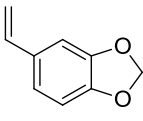
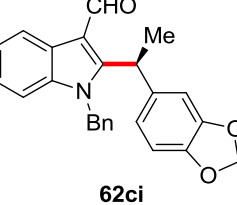
^[a] Reaction conditions: **59** (0.25 mmol), **60c** (1.5 equiv), Fe(acac)₃ (10 mol %), **180** (20 mol %), CyMgCl (1.1 equiv), TMEDA (2.0 equiv), THF (0.50 mL), 45 °C, 16 h. ^[b] Yield of the isolated product. ^[c] Determined by chiral HPLC analysis. ^[d] Using **177** instead of **180**. ^[e] No hydrolysis, product isolated as the imine. ^[f] After recrystallization from *i*PrOH. ^[g] Determined by ¹H NMR.

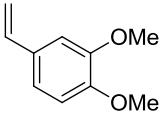
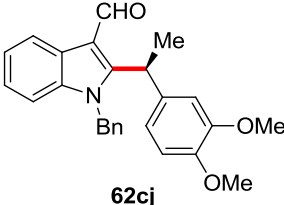
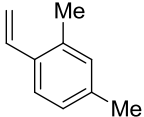
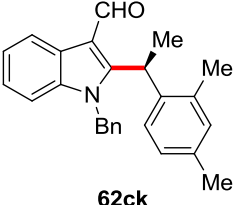
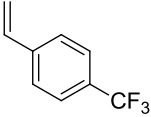
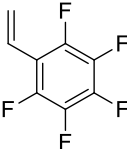
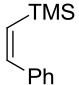
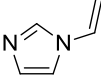
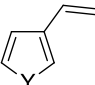
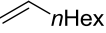
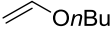
Thereafter, a variety of styrenes **60** were tested in the C–H transformation (Table 3.11). Diverse vinylarenes **60** with electron-rich and electron-poor substituents smoothly underwent the iron-catalyzed hydroarylation with good to excellent levels of enantioselectivity, providing exclusively the branched products **62** (entries 1–8). The high chemoselectivity and broad substrate scope of the transformation were however met with some limitations. No significant conversion was observed with styrenes bearing perfluorinated groups or additional substituents on the alkene (entries 9–11). Additionally, several vinylheteroarenes **60** were probed in the intermolecular hydroarylation, but no desired alkylated product could be obtained (entries 12–13). Unactivated alkenes such as 1-octene **29a** also failed to provide any C–H alkylated indole (entry 14). Vinyl ethers, vinyl silanes and dienes **102** also fell short in the reaction (entries 15–17).

Table 3.11. Substrate scope of vinylarenes **60** in the iron-catalyzed enantioselective C–H alkylation.^[a]



3. Results and Discussion

| Entry | Alkene | Product | Yield [%] ^[b] | e.r. ^[c] |
|-------|---|--|--------------------------|-------------------------------|
| 1 |  <p>60d</p> |  <p>62cd</p> | 82 | 90:10 |
| 2 |  <p>60e</p> |  <p>62ce</p> | 73 69 ^[d] | 86:14 85:15 ^[d] |
| 3 |  <p>60f</p> |  <p>62cf</p> | 64 39 ^[d] | 84:16 82:18 ^[d] |
| 4 |  <p>60g</p> |  <p>62cg</p> | 61 61 ^[d] | 88:12 85:15 ^[d] |
| 5 |  <p>60h</p> |  <p>62ch</p> | 76 46 ^[d] | 93:7 90:10 ^[d] |
| 6 |  <p>60i</p> |  <p>62ci</p> | 79 85 ^[d] | 85:15 84:16 ^[d] |

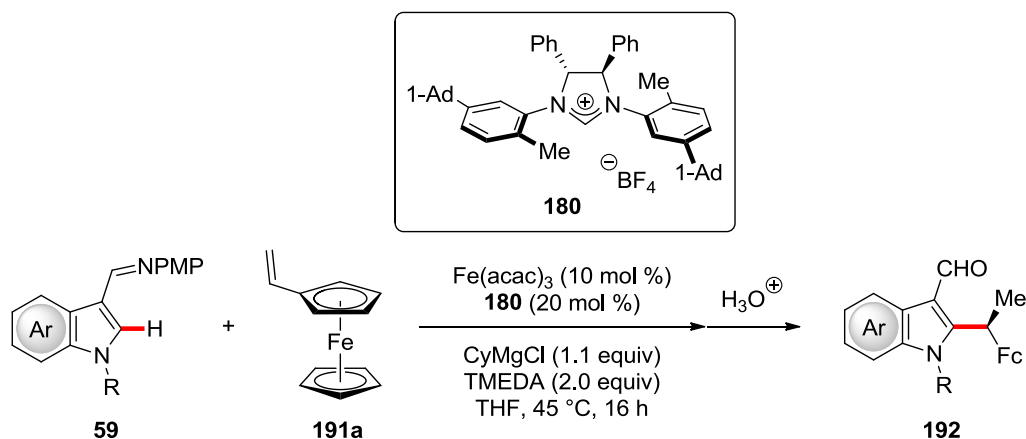
| | | | | |
|----|--|---|-------------------------|-------------------------------|
| 7 |  <p>60j</p> |  <p>62cj</p> | 56 81 ^[d] | 90:10 87:13 ^[d] |
| 8 |  <p>60k</p> |  <p>62ck</p> | 41 62 ^[d] | 90:10 86:14 ^[d] |
| 9 |  <p>60l</p> | --- | <10% ^[d] | - |
| 10 |  <p>60m</p> | --- | n.r. ^[d] | - |
| 11 |  <p>60n</p> | --- | <10% ^[d] | - |
| 12 |  <p>60o</p> | --- | n.r. ^[d] | - |
| 13 |  <p>Y = S (60p) Y = NBn (60q)</p> | --- | <10% ^[d] | - |
| 14 |  <p>29a</p> | --- | n.r. ^[d] | - |
| 15 |  <p>195</p> | --- | n.r. ^[d] | - |

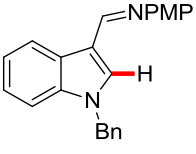
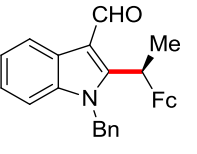
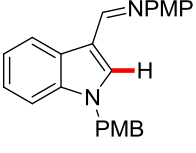
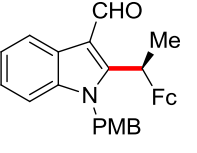
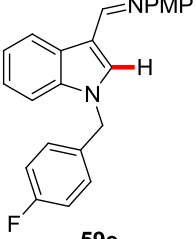
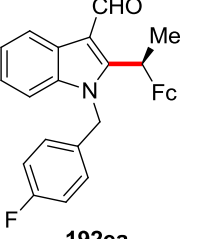
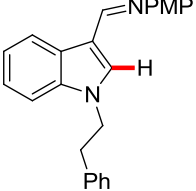
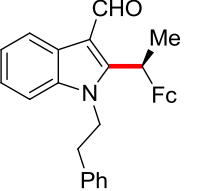
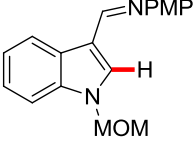
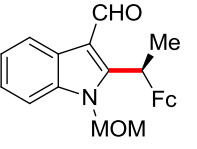
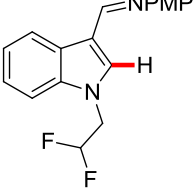
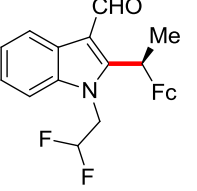
| | | | | |
|----|--|-----|---------------------|---|
| 16 |  | --- | n.r. ^[d] | - |
| 17 |  R = H (102a) R = Ph (102b) | --- | n.r. ^[d] | - |

^[a] Reaction conditions: **59c** (0.25 mmol), **60** (1.5 equiv), Fe(acac)₃ (10 mol %), **180** (20 mol %), CyMgCl (1.1 equiv), TMEDA (2.0 equiv), THF (0.50 mL), 45 °C, 16 h. ^[b] Yield of the isolated product. ^[c] Determined by chiral HPLC analysis. ^[d] Using **177** instead of **180**.

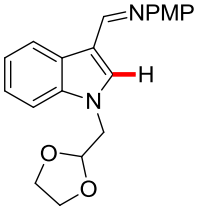
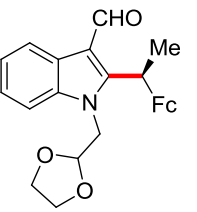
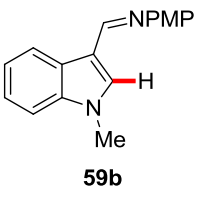
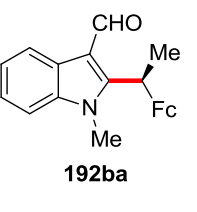
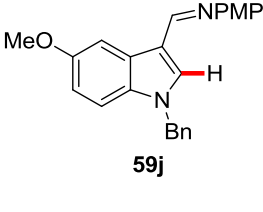
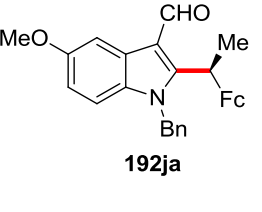
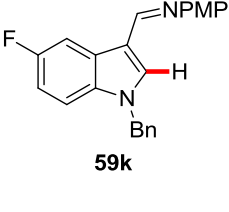
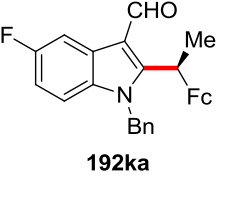
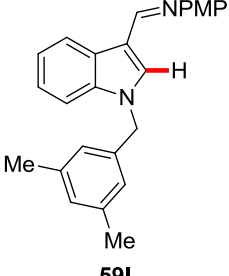
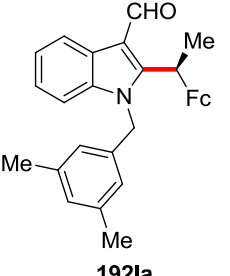
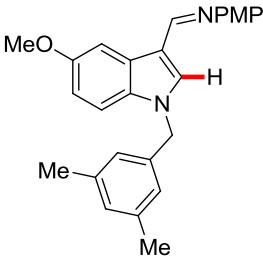
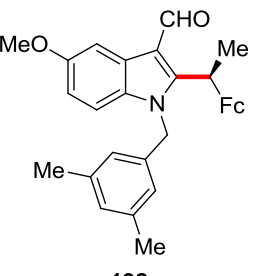
While various vinylheteroarenes failed to deliver any C–H alkylated product in the envisioned iron-catalyzed enantioselective hydroarylation (*vide supra*), vinylferrocene **191a** was in contrast identified as a viable substrate in this transformation. To our delight, differently substituted indoles **59** bearing electron-rich, electron-poor and various *N*-substituents were functionalized in moderate to good yields and outstanding levels of enantioselectivity, usually over 90% ee (Table 3.12, entries 1–12). Pharmacologically meaningful azaindole **59n** participated in the reaction as well, providing the alkylated product **192** in moderate yield, but excellent positional selectivity (entry 13).

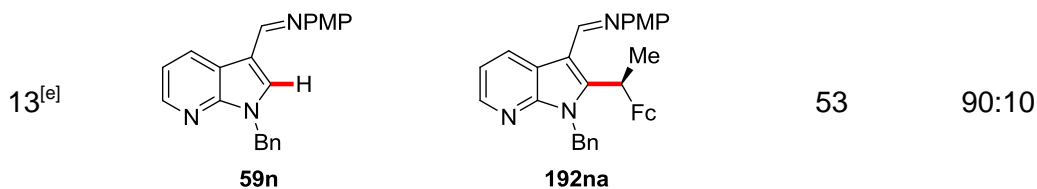
Table 3.12. Substrate scope of substituted (aza)indoles **59** in the iron-catalyzed enantioselective C–H alkylation with vinylferrocene **191a**.^[a]



| Entry | (Aza)indole | Product | Yield [%] ^[b] | e.r. ^[c] |
|-------|---|---|--------------------------|-----------------------------|
| 1 |  59c |  192ca | 69 69 ^[d] | 96:4 93:7 ^[d] |
| 2 |  59d |  192da | 64 43 ^[d] | 95:5 93:7 ^[d] |
| 3 |  59e |  192ea | 72 71 ^[d] | 95:5 93:7 ^[d] |
| 4 |  59f |  192fa | 56 57 ^[d] | 92:8 93:7 ^[d] |
| 5 |  59g |  192ga | 52 41 ^[d] | 96:4 94:6 ^[d] |
| 6 |  59h |  192ha | 51 64 ^[d] | 96:4 93:7 ^[d] |

3. Results and Discussion

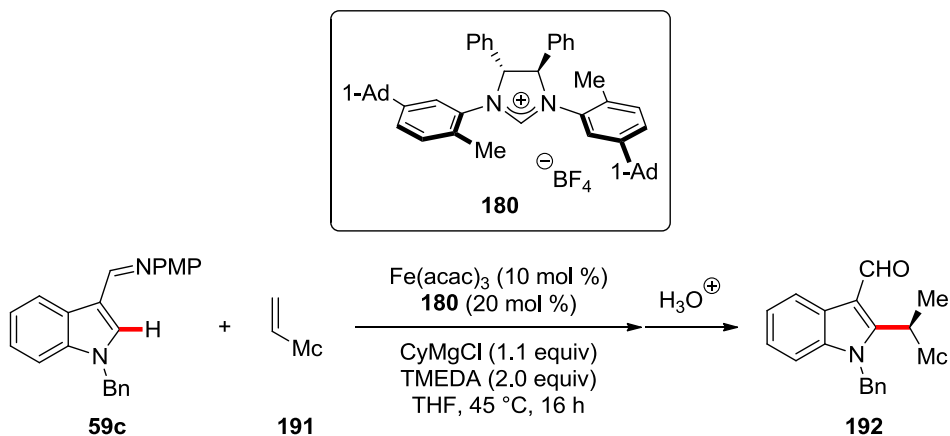
| | | | | |
|----|---|---|-------------------------|-----------------------------|
| 7 |  <p>59i</p> |  <p>192ia</p> | 39 54 ^[d] | 95:5 93:7 ^[d] |
| 8 |  <p>59b</p> |  <p>192ba</p> | 53 55 ^[d] | 94:6 93:7 ^[d] |
| 9 |  <p>59j</p> |  <p>192ja</p> | 77 79 ^[d] | 96:4 94:6 ^[d] |
| 10 |  <p>59k</p> |  <p>192ka</p> | 42 62 ^[d] | 95:5 92:8 ^[d] |
| 11 |  <p>59l</p> |  <p>192la</p> | 49 43 ^[d] | 95:5 93:7 ^[d] |
| 12 |  <p>59m</p> |  <p>192ma</p> | 69 | 96:4 |

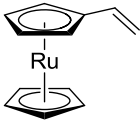
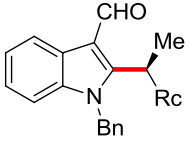
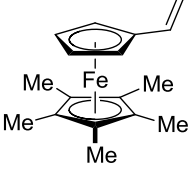
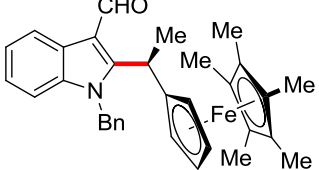


^[a] Reaction conditions: **59** (0.25 mmol), **191a** (1.5 equiv), Fe(acac)₃ (10 mol %), **180** (20 mol %), CyMgCl (1.1 equiv), TMEDA (2.0 equiv), THF (0.50 mL), 45 °C, 16 h. ^[b] Yield of the isolated product. ^[c] Determined by chiral HPLC analysis. ^[d] Using **177** instead of **180**. ^[e] Product isolated as the imine.

Differently substituted vinylmetallocenes **191** were then tested in the iron-catalyzed C2-alkylation of indoles (Table 3.13). In addition to ferrocenylalkenes, the isoelectronic but larger ruthenocenyl-substituted olefin **191b** smoothly underwent the asymmetric hydroarylation (entry 1). Furthermore, the sterically hindered pentamethylferrocene-derived olefin **191c** proved to be a viable substrate in the transformation as well, providing the highly congested *Markovnikov* product **192** in good yield and excellent enantioselectivity (entry 2). The preparation of highly enantiomerically-enriched ferrocenyl- and ruthenocenyl-indoles once more showcased the remarkable selectivity and versatility and of the developed catalytic system.

Table 3.13. Substrate scope of vinylmetallocenes **191** in the iron-catalyzed enantioselective C–H alkylation.^[a]

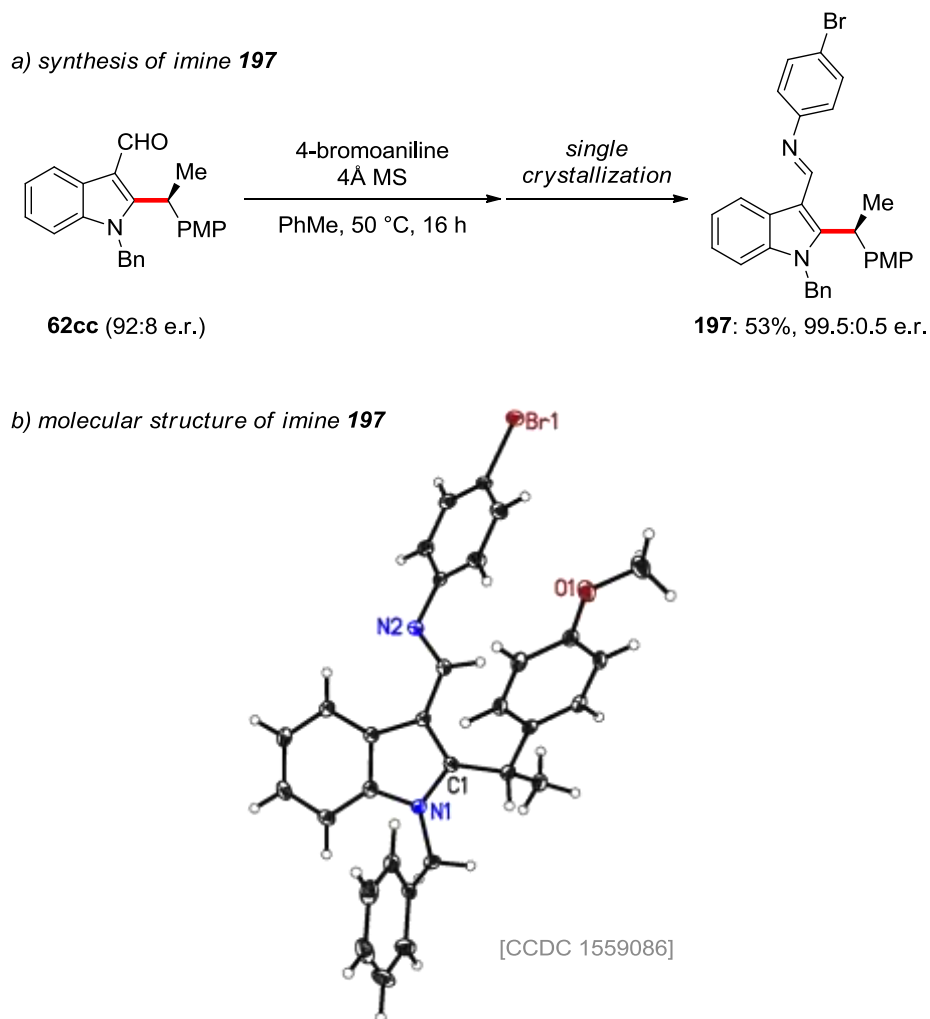


| Entry | Vinylmetallocene | Product | Yield [%] ^[b] | e.r. ^[c] |
|-------|--|--|--------------------------|-----------------------------|
| 1 |  191b |  192cb | 48 62 ^[d] | 96:4 93:7 ^[d] |
| 2 |  191c |  192cc | 58 67 ^[d] | 95:5 93:7 ^[d] |

^[a] Reaction conditions: **59c** (0.25 mmol), **191** (1.5 equiv), Fe(acac)₃ (10 mol %), **180** (20 mol %), CyMgCl (1.1 equiv), TMEDA (2.0 equiv), THF (0.50 mL), 45 °C, 16 h. ^[b] Yield of the isolated product. ^[c] Determined by chiral HPLC analysis. ^[d] Using **177** instead of **180**.

3.2.3. Determination of the Absolute Configuration

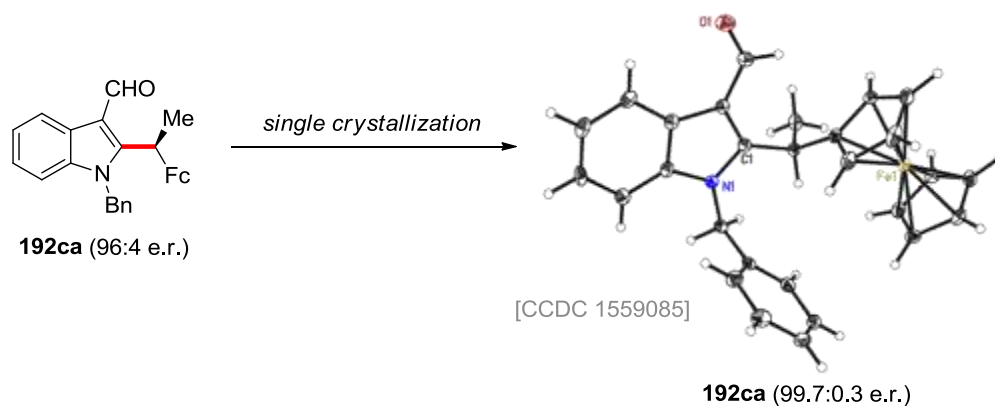
The determination of the absolute configuration is of primordial importance in asymmetric catalysis. Since styrene derivatives **60** are amorphous solids and lack heavy atoms, the highly crystalline bromo-substituted imine **197** was prepared in one step and obtained in 99% ee after a single crystallization (Scheme 3.5). Crystals suitable for X-ray diffraction were then grown by slow evaporation, allowing for the assignment of the absolute configuration. The product was found to be the *S*-enantiomer.



Scheme 3.5. a) Synthesis and b) ORTEP plot of imine **197**. Anisotropic displacement parameters are depicted at the 50% probability level. The crystal structure was measured and solved by *H. Keil* and approved by *Prof. D. Stalke*.

Likewise, ferrocene derivative **192ca** could be crystallized directly, providing the product in >99% ee (Scheme 3.6). Due to the iron atom of the ferrocene moiety, no additional heavy atom had to be installed in the compound, and crystals suitable for X-ray diffraction analysis could be grown directly by slow evaporation from benzene. The *R*-enantiomer was found to be selectively formed in the transformation. The different *R/S* configuration observed with vinylmetallocenes compared to styrenes is only due to different relative priorities of aryl and metallocenyl groups compared to the indole core according to the *Cahn–Ingold–Prelog* sequence rules.^[252] Interestingly, C–H⋯ π interactions can be observed between the *N*-benzyl

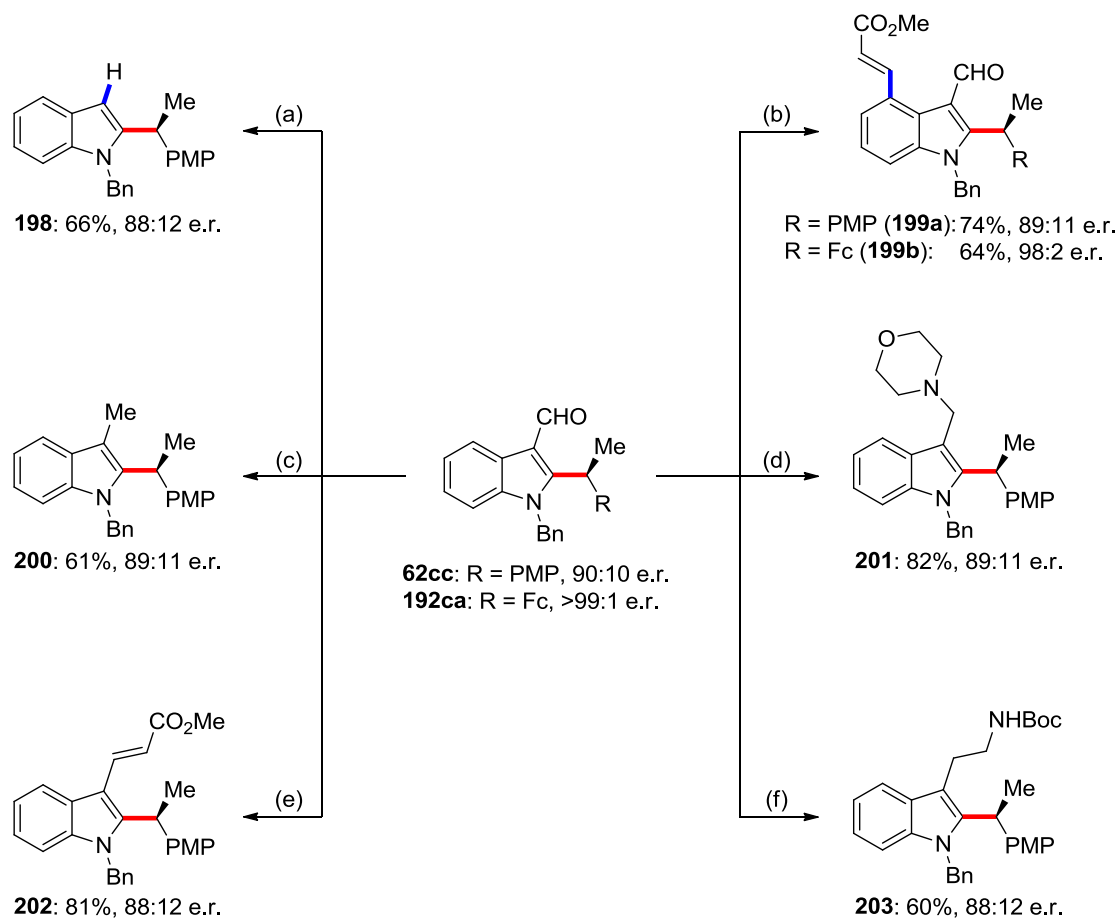
substituent of the indole and the ferrocenyl group, which might explain the importance of the benzyl group in order to obtain high enantioselectivities.



Scheme 3.6. Preparation and ORTEP plot of **192ca**. Anisotropic displacement parameters are depicted at the 50% probability level. The crystal structure was measured and solved by *H. Keil* and approved by *Prof. D. Stalke*.

3.2.4. Product Diversification

The synthetic utility of the iron-catalyzed C–H alkylation was further illustrated by late-stage diversification of the thus-obtained products (Scheme 3.7). The formyl group could be removed in a traceless fashion under palladium catalysis without significant loss of the enantiomeric excess (Scheme 3.7a). It is noteworthy that higher catalyst loadings or reaction temperatures provided the deformylated product in higher yields, but substantial racemization was then observed. The weakly coordinating^[39,253] formyl motif could also be used as directing group to promote C–H functionalization at the indole's C4-position. Using the methodology reported by *Ramaiah Prabhu*,^[254] the benzene core could be alkenylated with methyl acrylate using a ruthenium catalyst,^[255] giving access to highly functionalized indoles through position-selective twofold C–H activation (Scheme 3.7b).



Scheme 3.7. Product diversification. a) Pd(OAc)₂ (8.0 mol %), cyclohexane, 4 Å MS, 140 °C. b) [RuCl₂(*p*-cymene)]₂ (5.0 mol %), AgSbF₆ (20 mol %), Cu(OAc)₂·H₂O, methyl acrylate, DCE, 120 °C. c) H₂, Pd/C, EtOH, 23 °C. d) Morpholine, NaBH(OAc)₃, AcOH, DCE, 23 °C. e) Ph₃PCHCO₂Me, PhMe, 130 °C. f) i. NH₄OAc, MeNO₂, 90 °C; ii. LiAlH₄, THF, 85 °C; iii. Boc₂O, Et₃N, 1,4-dioxane, 23 °C.

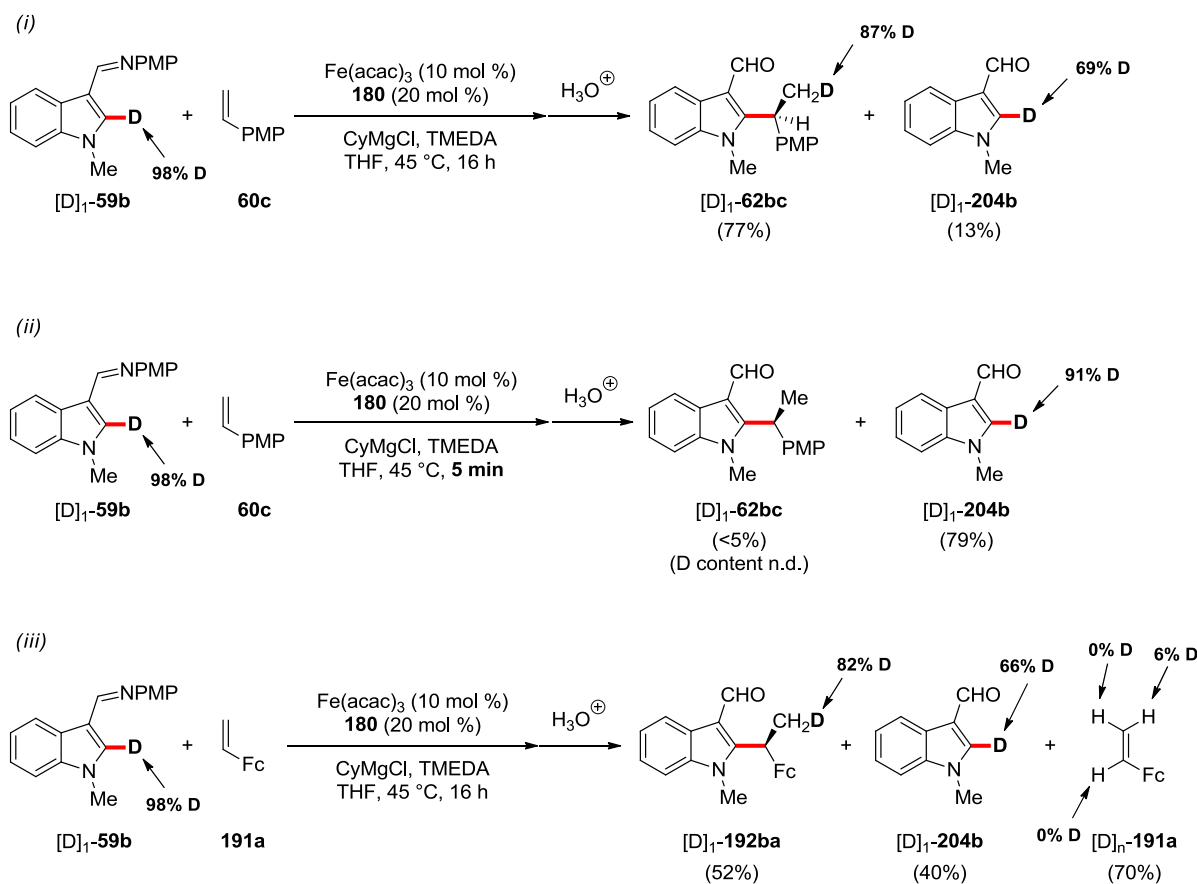
Various transformations of the synthetically useful formyl group were also conducted (Scheme 3.7c–f). The formyl group could be reduced to a methyl group, or converted to other functional groups *via* reductive amination or *Wittig* reaction. Additionally, the pharmacologically relevant protected tryptamine **203** could also be obtained in 3 steps without significant racemization.

3.2.5. Mechanistic Studies

Given the unique features of the developed asymmetric iron-catalyzed C–H alkylation, we became interested in delineating its mode of action. Hence, experimental and computational^[256] mechanistic studies were performed in order to gain insights into the reaction's mechanism.

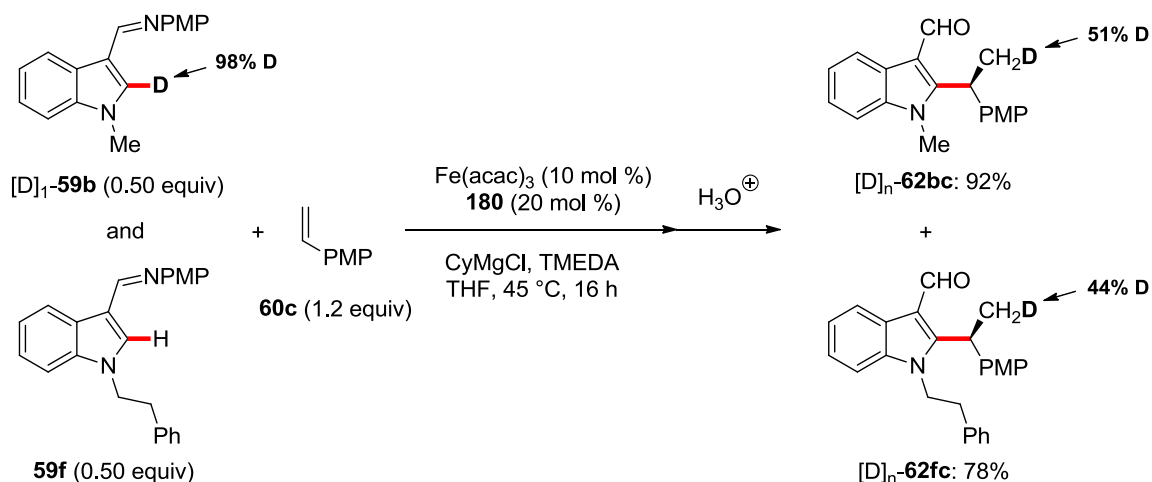
3.2.5.1. Deuterium Labeling Experiments

First, experiments with isotopically labelled indole substrate [D]₁-**59b** were conducted (Scheme 3.8). The deuterium atom was found to be selectively transferred to the terminal position of the alkene, which provides support for an inner-sphere C–H activation. This observation can be rationalized with the C–H scission occurring by ligand-to-ligand hydrogen-transfer (LLHT) or C–H oxidative addition to a low-valent iron species. Interestingly, no deuterium incorporation was observed at the methine position as it was the case in the related work of *Yoshikai*.^[148]



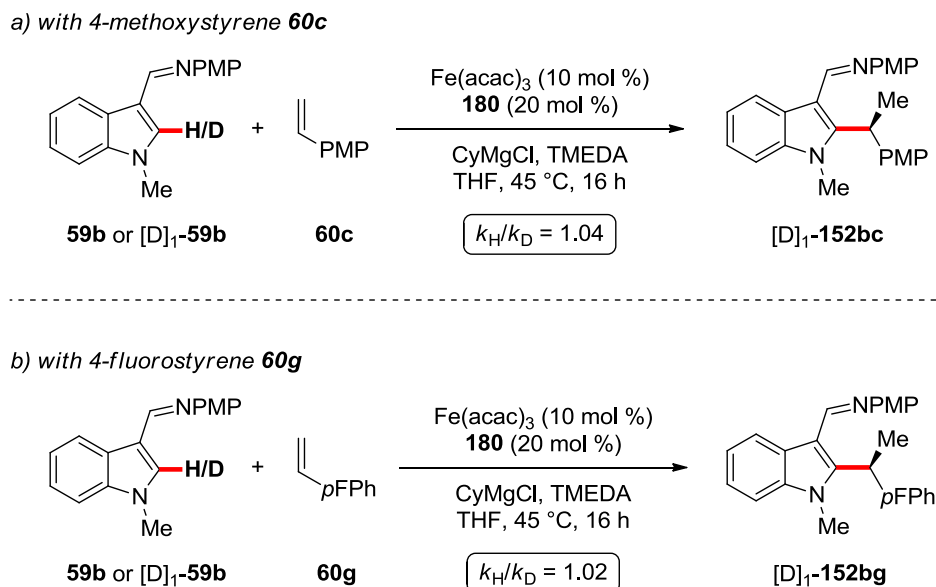
Scheme 3.8. Reactions with isotopically labeled substrate $[D]_1\text{-59b}$.

Thereafter, a crossover experiment was conducted between deuterated and non-deuterated substrates (Scheme 3.9). $[D]_1\text{-59b}$ and **59f** were selected due to their similar efficacy in the transformation and the easy separation of their corresponding products by silica gel chromatography. Remarkably, a nearly identical deuterium incorporation was observed in both products $[D]_n\text{-62bc}$ and $[D]_n\text{-62fc}$. This finding seemingly rules out the oxidative addition/reductive elimination pathway initially proposed by *Yoshikai* for the racemic reaction^[148] and provides support for a LLHT-manifold.^[32a,37b,81]



Scheme 3.9. Crossover experiment between deuterated and non-deuterated substrates **59**.

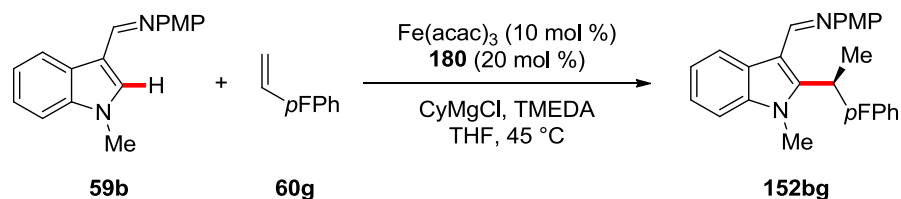
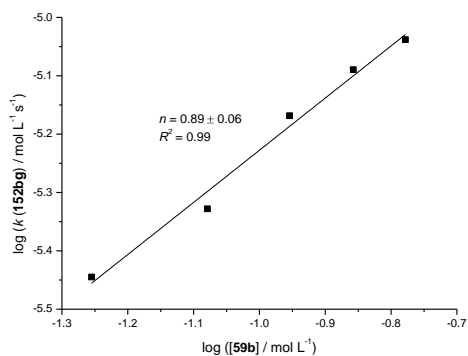
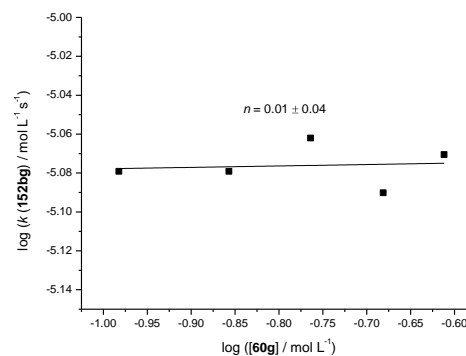
Furthermore, additional experiments with deuterated substrate **[D]₁-59b** revealed a kinetic isotope effect (KIE) of $k_{\text{H}}/k_{\text{D}} \approx 1.0$ (Scheme 3.10). A KIE of this magnitude suggests that the C–H cleavage step is not turnover-limiting,^[257] and provides evidence for a facile and reversible C–H activation event.



Scheme 3.10. KIE studies. Experiment *b* was conducted by Dr. D. Zell.

3.2.5.2. Kinetics

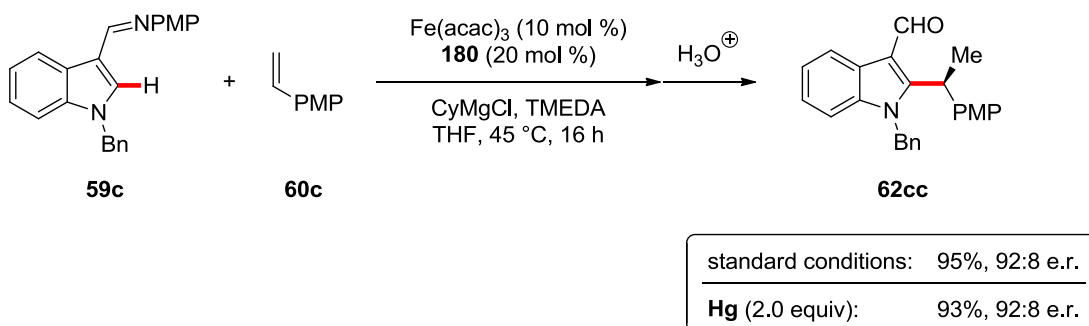
Subsequently, detailed kinetic studies of the enantioselective C–H alkylation were conducted by *Dr. D. Zell*.^[151] A first-order dependence on the concentration of the indole substrate **59b** was observed, along with a saturation kinetics behavior for the styrene **60g** (Scheme 3.11).

a) 1st order in indole **59b**b) 0th order in styrene **60g**

Scheme 3.11. Kinetic analysis. The experiments were conducted by *Dr. D. Zell*.

3.2.5.3. Mercury Drop Test

A mercury poisoning test was conducted to probe the homogeneity of the catalytic process (Scheme 3.12). No significant reduction of the catalytic activity was observed in the presence of an excess of metallic mercury, which confirms the homogenous nature of the transformation.

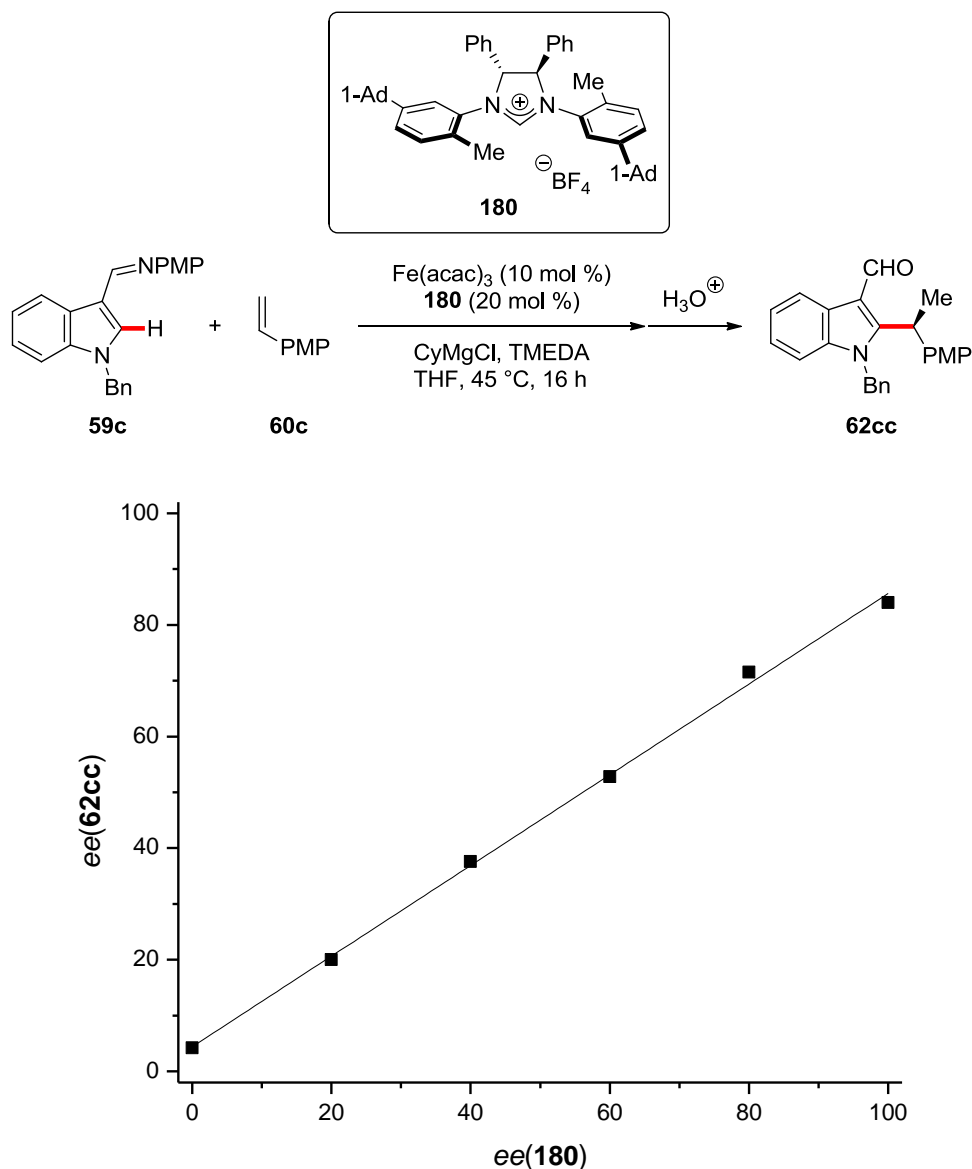


Scheme 3.12. Mercury drop test for the iron-catalyzed C–H alkylation.

This finding is especially important since iron(0) nanoparticles are known to form upon exposure of iron salts to Grignard reagents,^[258] and their presence in the reaction mixture has been indirectly supported by ^{57}Fe Mössbauer spectroscopic studies (*vide infra*). Nevertheless, iron(0) nanoparticles do not appear to play a role in the catalyzed transformation.

3.2.5.4. Non-Linear Effect Studies

The effect of the enantiomeric excess of ligand **180** over the enantiomeric induction of the transformation was investigated (Scheme 3.13). The absence of a non-linear effect (NLE) renders a multi-ligand containing catalyst or catalytically competent oligomers unlikely to be operative in the asymmetric C–H secondary alkylation.^[259] Hence, the beneficial effect of a ligand-to-metal ratio of 2:1 is apparently not due to the formation of bis-NHC-ligated iron species.



Scheme 3.13. Non-linear effect studies.

3.2.5.5. *In situ* Analysis by Mass Spectrometry and Mössbauer Spectroscopy

While detailed kinetic studies, deuterium labelling experiments and non-linear effect studies were performed to delineate the *modus operandi* of the unique iron-catalyzed enantioselective C–H alkylation (*vide supra*), the oxidation state and coordination sphere of the active catalyst have remained thus far speculative. Indeed, in iron/NHC-catalyzed C–H activations,^[148,151,260] as well as in related

“low-valent” cobalt/NHC-catalyzed C–H activations,^[46c,46d,69a,69c] the active catalyst is usually generated *in situ* from a metal salt and an imidazol(in)ium NHC precursor in the presence of a Grignard reagent. The use of well-defined iron/NHC complexes as catalysts is well documented in molecular syntheses in different contexts.^[235a–c] In contrast, no well-defined iron catalysts or intermediates have so far been isolated or characterized in the context of C–H activation, with the notable exception of *Tatsumi* and *Ohki* employing a half sandwich iron(II)/NHC complex for undirected C–H borylations of heteroarenes.^[261] In the reactions employing *in situ* generated iron catalysts, the organometallic reagent has been proposed to play a dual role, serving both as the base and a potential reductant. The mechanism of the generation of the catalytically active species, as well as possible side-reactions occurring during this process, have thus far been overlooked.^[262] Furthermore, iron species with formal oxidation states ranging from -2 ^[263] to $+4$ ^[264] have been observed in reactions of iron precursors with Grignard reagents.^[108a,265] It is noteworthy that some of these species have been postulated as intermediates in iron-catalyzed *Kumada–Corriu*-type cross-couplings^[19] operating under reaction conditions similar to iron-catalyzed C–H activations. So far, all information on the oxidation state of the *in situ* generated iron catalysts enabling the C–H activation has been gained through DFT calculations regarding iron-catalyzed oxidative C–H functionalizations with alkyl halides.^[131] Hence, the nature of the catalytically active species in the asymmetric iron-catalyzed hydroarylation has remained unknown until now.

Interestingly, *Yoshikai* originally proposed a “low-valent”^[266] Fe/NHC complex generated *in situ* through the reduction of the iron(III) pre-catalyst by the Grignard reagent to be operative in the racemic hydroarylation of vinylarenes and alkynes with indoles, and the C–H activation step to occur *via* oxidative addition into the C–H bond.^[148] *Yoshikai* attributed the requirement of an excess of the Grignard reagent to the possible formation of ferrate species. In the course of the optimization studies for the enantioselective secondary alkylation of indoles **59**, it was observed that Fe(acac)₃ and FeCl₂ pre-catalysts, despite their different oxidation states and counterions, gave comparable conversions and enantioselectivities (Table 3.9). This observation suggested that the iron precursors were transformed by the Grignard

reagent to the same catalytically competent iron species. Another possibility is the *in situ* formation of organoferrates. Indeed, *Koszinowski* recently reported that the nature of the iron precursor has very little effect on the transmetalation reactions with organometallic species to form such complexes.^[267] These observations raised the question as to the nature of the active iron catalyst and its mode of action, and highlight the need for detailed, comprehensive mechanistic studies to unravel fundamental aspects of iron-catalyzed C–H activations. Such mechanistic insights have recently been gained for iron-catalyzed *Kumada–Corriu*-type cross-coupling reactions *via Mössbauer* spectroscopy and mass spectrometry, among other analytical methods.^[265,267,268] These reports highlighted the dynamic nature and remarkable complexity of organometallic iron chemistry.

Therefore, we became interested in the application of electrospray-ionization (ESI) mass spectrometry and ⁵⁷Fe *Mössbauer* spectroscopy to unravel the key intermediates formed *in situ* in the enantioselective iron-catalyzed C–H alkylation.^[218] In contrast to ESI-MS, ⁵⁷Fe *Mössbauer* spectroscopy has the advantage of probing the entire population of iron species, regardless of their individual charge. This research work was conducted in collaboration with the research groups of *Prof. Dr. K. Koszinowski* (ESI-MS) and *Prof. Dr. F. Meyer* (*Mössbauer* spectroscopy).

We decided to follow a step-by-step approach and therefore initiated our investigations by probing the species formed in a stoichiometric reaction between the iron precatalyst, the Grignard reagent and TMEDA in THF, without the NHC precursor **180** or the indole substrate **59**. Negative-ion mode ESI-MS of a solution of Fe(acac)₃ treated with 8.0 equiv of CyMgCl in the presence of TMEDA (4.0 equiv) showed a mixture of various organoferrate species, among which Cy₃Fe(II)[−] and Cy₄Fe(III)[−] were dominant (Fig. 3.1a). Previous reports had already demonstrated the formation of abundant organoferrates upon transmetalation of iron precursors with Grignard reagents under similar reaction conditions.^[267] Although ESI-MS cannot directly detect any neutral species, the observation of small amounts of Cy₅Fe₂[−] and Cy₄Fe₂Cl[−], both with iron in an average oxidation state of +2, may indicate the presence of neutral organoiron complexes, such as Cy₂Fe or CyFeCl,

which supposedly reacted with $\text{Cy}_3\text{Fe}(\text{II})^-$ to afford the dinuclear aggregates. The low abundance of the dinuclear anions can be attributed to TMEDA, which has previously been shown to prevent the formation of polynuclear organoferrates.^[267,269] All the observed organoferrates were found to be highly unstable, presumably due to β -hydride elimination, and completely vanished within 2 minutes. Experiments conducted with the better-behaved PhMgCl were therefore performed as well. PhMgCl has previously been shown to promote the desired C–H alkylation as well, albeit with a slightly diminished performance (*vide supra*, Tables 3.7, 3.9). It should also be noted that phenyl Grignard reagents have proven instrumental in other iron/NHC-catalyzed C–H activations.^[148,260] Likewise, iron(II) and iron(III) phenylferrates were detected by ESI-MS in the reaction of $\text{Fe}(\text{acac})_3$ with PhMgCl in the presence of TMEDA (Fig. 3.1b), being in full agreement with previous findings.^[267,269b,270]

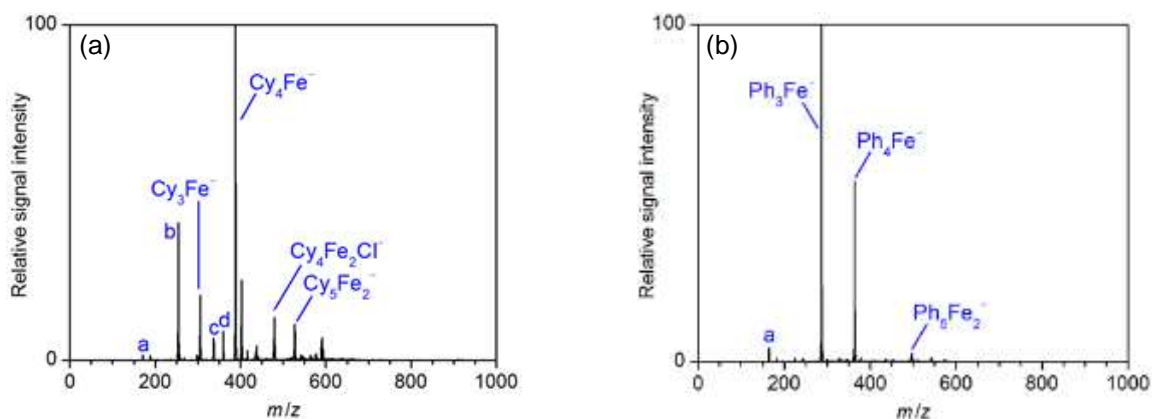


Figure 3.1. (a) Negative-ion mode ESI mass spectrum of a solution of the products formed in the reaction of $\text{Fe}(\text{acac})_3$ (10 mM) with TMEDA (4.0 equiv) and CyMgCl (8.0 equiv) in THF; $a = [\text{Cy}, \text{Fe}, \text{O}_2]^-$, $b = [\text{Cy}_2, \text{Fe}, \text{O}_2]^-$, $c = [\text{Cy}_3, \text{Fe}, \text{O}_2]^-$, $d = \text{Cy}_4\text{Al}^-$. Ions a – c resulted from reactions with residual traces of oxygen, d from an aluminum contamination. (b) Negative-ion mode ESI mass spectrum of a solution of the products formed in the reaction of $\text{Fe}(\text{acac})_3$ (10 mM) with TMEDA (4.0 equiv) and PhMgCl (8.0 equiv) in THF; $a = [\text{Ph}, \text{Fe}, \text{O}_2]^-$. Ions a resulted from reactions with residual traces of oxygen. The experiments were conducted by Dr. T. Parchomyk.

A frozen solution of $^{57}\text{FeCl}_2/\text{CyMgCl}/\text{TMEDA}$ in THF was next analyzed by ^{57}Fe Mössbauer spectroscopy at 80 K (Fig. 3.2a). The obtained spectrum featured the

signatures of two iron species, which were assigned to a major high-spin iron(III) species and a minor low-coordinate iron(II) species, in line with the formation of $\text{Cy}_4\text{Fe(III)}^-$ and $\text{Cy}_3\text{Fe(II)}^-$ observed by ESI-MS. Interestingly, we did not detect any $\text{Cy}_4\text{Fe(IV)}$, which has been observed by *Fürstner* in a related setting.^[264] The remarkable formation of a dominating iron(III) species from the iron(II) precursor in the presence of Grignard reagents and the absence of any external oxidant can be attributed to disproportionation with concomitant formation of low-valent iron species, as previously reported.^[267] Yet, no low-valent iron species could be detected in our experiments. Therefore, a *Mössbauer* spectrum was recorded at 7 K (Fig. 3.2b), but was essentially identical to the spectrum recorded at 80 K. No signal for iron(0) nanoparticles^[258] or other low-valent iron species could be observed by ^{57}Fe *Mössbauer* spectroscopy. However, unfavorable relaxation dynamics^[271] may lead to pronounced line broadening, which prevents detection of iron nanoparticles.

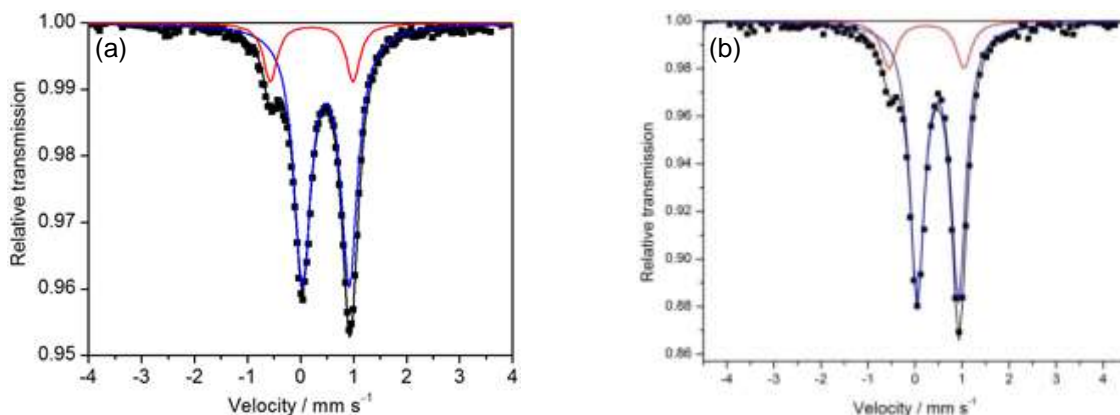


Figure 3.2. (a) *Mössbauer* spectrum of a frozen solution ($T = 80$ K) of the products formed in the reaction of $^{57}\text{FeCl}_2$ (5.0 mM), TMEDA (4.0 equiv) and CyMgCl (8.0 equiv) in THF; components of the fit: $\delta(\text{blue}) = 0.48 \text{ mm s}^{-1}$, $\Delta E_{\text{Q}}(\text{blue}) = 0.89 \text{ mm s}^{-1}$, rel. int. = 84%; $\delta(\text{red}) = 0.21 \text{ mm s}^{-1}$, $\Delta E_{\text{Q}}(\text{red}) = 1.56 \text{ mm s}^{-1}$, rel. int. = 16%. (b) *Mössbauer* spectrum and components of the fit of a frozen solution ($T = 7$ K) of the products formed in the reaction of $^{57}\text{FeCl}_2$ (5.0 mM), TMEDA (4.0 equiv) and CyMgCl (8.0 equiv) in THF; components of the fit: $\delta(\text{blue}) = 0.48 \text{ mm s}^{-1}$, $\Delta E_{\text{Q}}(\text{blue}) = 0.88 \text{ mm s}^{-1}$, rel. int. = 85%; $\delta(\text{red}) = 0.24 \text{ mm s}^{-1}$, $\Delta E_{\text{Q}}(\text{red}) = 1.59 \text{ mm s}^{-1}$, rel. int. = 15%. The spectra were recorded and interpreted by Dr. S. Demeshko.

The instability of the cyclohexylferrates was further highlighted by ^{57}Fe Mössbauer spectroscopic analysis of the same reaction after it was allowed to warm to 23 °C (Fig. 3.3). The spectrum showed the complete disappearance of the iron(II) ate complex, a reduced amount of $\text{Cy}_4\text{Fe(III)}^-$ and the emergence of a new dominant species, whose unspecific doublet unfortunately does not allow for assignment.

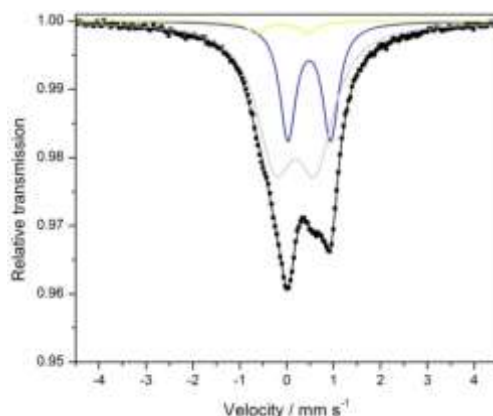


Figure 3.3. Mössbauer spectrum and components of the fit of a frozen solution ($T = 80$ K) of the products formed in the reaction of $^{57}\text{FeCl}_2$ (5.0 mM), TMEDA (4.0 equiv) and CyMgCl (8.0 equiv) in THF at 23 °C; components of the fit: $\delta(\text{gray}) = 0.19 \text{ mm s}^{-1}$, $\Delta E_Q(\text{gray}) = 0.86 \text{ mm s}^{-1}$, rel. int. = 68%; $\delta(\text{blue}) = 0.48 \text{ mm s}^{-1}$, $\Delta E_Q(\text{blue}) = 0.91 \text{ mm s}^{-1}$, rel. int. = 28%; $\delta(\text{yellow}) = -0.10 \text{ mm s}^{-1}$, $\Delta E_Q(\text{yellow}) = 1.10 \text{ mm s}^{-1}$, rel. int. = 3%. The spectrum was recorded and interpreted by *Dr. S. Demeshko*.

A similar spectrum was obtained from the reaction of $^{57}\text{FeCl}_2$ with PhMgCl in the presence of TMEDA (Fig. 3.4), indicating the formation of the phenylferrates $\text{Ph}_3\text{Fe(II)}^-$ and $\text{Ph}_4\text{Fe(III)}^-$, being in line with the ESI-MS results (Fig. 3.1b) and previous reports.^[267,269b] As the catalyzed C–H activation was found to completely shut down in the absence of the NHC ligand (*vide supra*, Table 3.5), the observed NHC ligand-free organoferrates are assumed to be catalytically inactive, but are plausible intermediates of the generation of the catalytically competent species.

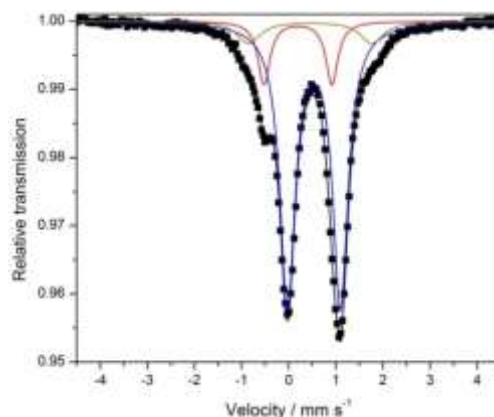


Figure 3.4. Mössbauer spectrum of a frozen solution ($T = 80$ K) of the products formed in the reaction of $^{57}\text{FeCl}_2$ (5.0 mM), TMEDA (4.0 equiv) and PhMgCl (8.0 equiv) in THF; components of the fit: $\delta(\text{blue}) = 0.54 \text{ mm s}^{-1}$, $\Delta E_Q(\text{blue}) = 1.12 \text{ mm s}^{-1}$, rel. int. = 78%; $\delta(\text{red}) = 0.20 \text{ mm s}^{-1}$, $\Delta E_Q(\text{red}) = 1.44 \text{ mm s}^{-1}$, rel. int. = 13%; $\delta(\text{dark yellow}) = 0.46 \text{ mm s}^{-1}$, $\Delta E_Q(\text{dark yellow}) = 2.61 \text{ mm s}^{-1}$, rel. int. = 9%. The spectrum was recorded and interpreted by Dr. S. Demeshko.

Subsequently, similar experiments were performed in the presence of the chiral NHC precursor **180**. While the homoleptic ferrates remained present in the solution, two newly formed iron(II) species could also be detected by ESI-MS, namely $\text{Cy}_3\text{Fe}(\text{NHC})^-$ and $\text{Cy}_2\text{FeH}(\text{NHC})^-$ (Fig. 3.5). The latter, with a significantly higher intensity, is believed to result from β -hydride elimination of the former. Interestingly, no NHC complexes of iron(III) or low-valent iron were detected, suggesting the selective formation of Fe(II)/NHC species in the reaction. It should be noted that the peak corresponding to the Cy_4Al^- contamination only appears so intense because of the relative low intensity of the anionic iron species.

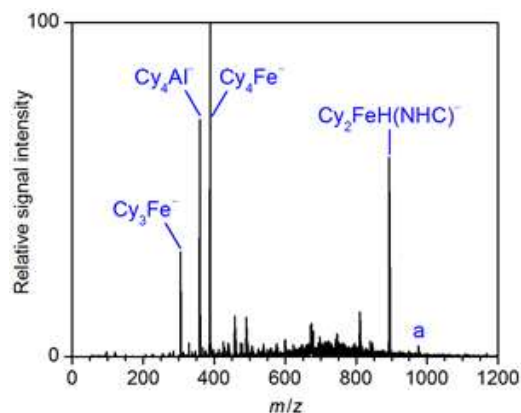


Figure 3.5. Negative-ion mode ESI mass spectrum of a solution of the products formed in the reaction of $\text{Fe}(\text{acac})_3$ (10 mM) with TMEDA (4.0 equiv), CyMgCl (8.0 equiv) and **180** (1.0 equiv) in THF; $a = [\text{Fe}(\text{NHC})\text{Cy}_3]^-$. NHC = $\text{C}_{49}\text{H}_{54}\text{N}_2$. The experiment was conducted by S. Lüf.

When a similar experiment was performed using PhMgCl , Fe/NHC species could not be observed (Fig. 3.6a). Yet, the relative intensity of the iron(II) ate complex was noticeably reduced, which indicates its consumption for the formation of neutral species not detectable by ESI mass spectrometry. Besides, no magnesium-NHC complexes or residual imidazolium salt could be observed by positive-mode ESI-MS in any of the experiments (Fig. 3.6b). In this context, it should be mentioned that organomagnesium(II)/NHC complexes are known^[272] and relevant in asymmetric catalysis.^[273] Also, a recent study by *Bedford* on iron-catalyzed *Negishi*-type reactions suggests that the phosphine ligand binds to the zinc rather than the iron atom.^[274] In contrast, the present findings provide evidence for the NHC to coordinate to the iron catalyst, and not to magnesium(II).

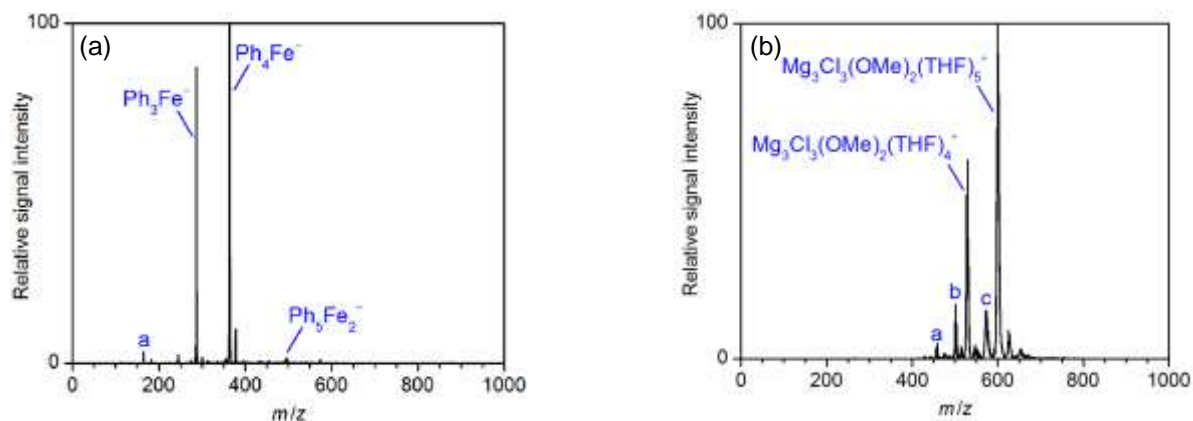


Figure 3.6. (a) Negative-ion mode ESI spectrum of a solution of the products formed in the reaction of $\text{Fe}(\text{acac})_3$ (10 mM) with TMEDA (4.0 equiv), PhMgCl (8.0 equiv) and **180** (1.0 equiv) in THF; $a = [\text{Ph}_3\text{FeO}_2]^-$. (b) Positive-ion mode ESI spectrum representative of all experiments; $a = \text{Mg}_3\text{Cl}_3(\text{OMe})(\text{OH})(\text{TMEDA})^{2+}$, $b = \text{Mg}_3\text{Cl}_3(\text{OMe})_2(\text{THF})_2(\text{TMEDA})^+$, $c = \text{Mg}_3\text{Cl}_3(\text{OMe})_2(\text{THF})_3(\text{TMEDA})^+$. The incorporated methoxides originate from traces of methanol as reported previously.^[267,268c,275] The experiments were conducted by *Dr. T. Parchomyk*.

When a frozen solution of $^{57}\text{FeCl}_2/\mathbf{180}/\text{CyMgCl}/\text{TMEDA}$ was analyzed by ^{57}Fe Mössbauer spectroscopy, a rather intricate spectrum could be observed, which has been simulated well assuming five subspectra (Fig. 3.7a).^[276] Two subspectra (Fig. 3.7a, blue and red) are almost identical to the previously detected ferrates (Fig. 3.2a). The most pronounced new signal (Fig. 3.7a, green) can be attributed to a low-coordinate iron(II) high-spin complex, most likely trigonal-planar $\text{Cy}_2\text{Fe}(\text{NHC})$,^[277] in good agreement with ESI-MS (Fig. 3.5). Another newly formed species (Fig. 3.7a, magenta), with a higher isomer shift of 0.54 mm s^{-1} together with a lower quadrupole splitting of 2.04 mm s^{-1} , may indicate a more symmetric iron(II) high-spin species with a higher coordination number such as $\text{Cy}_3\text{Fe}(\text{NHC})^-$, as detected by ESI-MS (Fig. 3.5). An additional minor species (Fig. 3.7a, cyan) was also observed in the ^{57}Fe Mössbauer spectrum of the reaction with CyMgCl , but its non-characteristic doublet does not allow for further assignment.

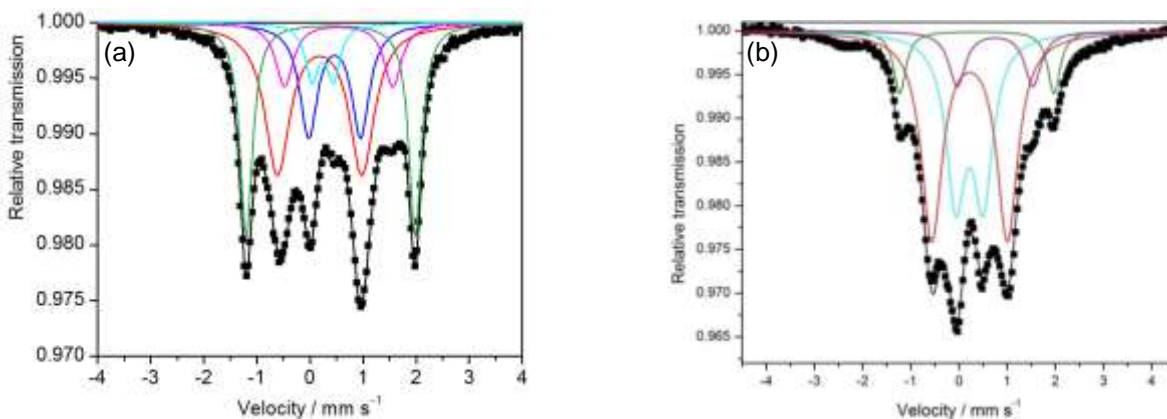


Figure 3.7. (a) *Mössbauer* spectrum of a frozen solution ($T = 80$ K) of the products formed in the reaction of $^{57}\text{FeCl}_2$ (5.0 mM), TMEDA (4.0 equiv), **180** (1.0 equiv) and CyMgCl (8.0 equiv) in THF; components of the fit: $\delta(\text{red}) = 0.18 \text{ mm s}^{-1}$, $\Delta E_Q(\text{red}) = 1.59 \text{ mm s}^{-1}$, rel. int. = 36%; $\delta(\text{green}) = 0.39 \text{ mm s}^{-1}$, $\Delta E_Q(\text{green}) = 3.19 \text{ mm s}^{-1}$, rel. int. = 27%; $\delta(\text{blue}) = 0.46 \text{ mm s}^{-1}$, $\Delta E_Q(\text{blue}) = 0.98 \text{ mm s}^{-1}$, rel. int. = 19%; $\delta(\text{magenta}) = 0.54 \text{ mm s}^{-1}$, $\Delta E_Q(\text{magenta}) = 2.04 \text{ mm s}^{-1}$, rel. int. = 11%; $\delta(\text{cyan}) = 0.24 \text{ mm s}^{-1}$, $\Delta E_Q(\text{cyan}) = 0.40 \text{ mm s}^{-1}$, rel. int. = 7%.^[276] (b) *Mössbauer* spectrum and components of the fit of a frozen solution ($T = 80$ K) of the products formed in the reaction of $^{57}\text{FeCl}_2$ (5.0 mM), TMEDA (4.0 equiv), CyMgCl (8.0 equiv) and **180** (1.0 equiv) in THF at 23 °C; components of the fit: $\delta(\text{red}) = 0.22 \text{ mm s}^{-1}$, $\Delta E_Q(\text{red}) = 1.57 \text{ mm s}^{-1}$, rel. int. = 47%; $\delta(\text{cyan}) = 0.22 \text{ mm s}^{-1}$, $\Delta E_Q(\text{cyan}) = 0.57 \text{ mm s}^{-1}$, rel. int. = 34%; $\delta(\text{purple}) = 0.75 \text{ mm s}^{-1}$, $\Delta E_Q(\text{purple}) = 1.57 \text{ mm s}^{-1}$, rel. int. = 10%; $\delta(\text{green}) = 0.37 \text{ mm s}^{-1}$, $\Delta E_Q(\text{green}) = 3.20 \text{ mm s}^{-1}$, rel. int. = 9%. The spectra were recorded and interpreted by *Dr. S. Demeshko*.

Two related iron(II) species were also observed in the corresponding reaction with PhMgCl (Fig. 3.8). However, no species related to the minor uncharacteristic signal observed before (Fig. 3.7a, cyan) was detected in this experiment. It is hence believed that this species was formed *via* β -hydride elimination from the $\text{Cy}_2\text{Fe}(\text{NHC})$ complex. This hypothesis is further corroborated by the observation that, when the sample was prepared at higher temperatures (Fig. 3.7b), this species (Fig. 3.7a, cyan) became more pronounced, while the intensity of the $\text{Cy}_2\text{Fe}(\text{NHC})$ signal was reduced (Fig. 3.7b, green).

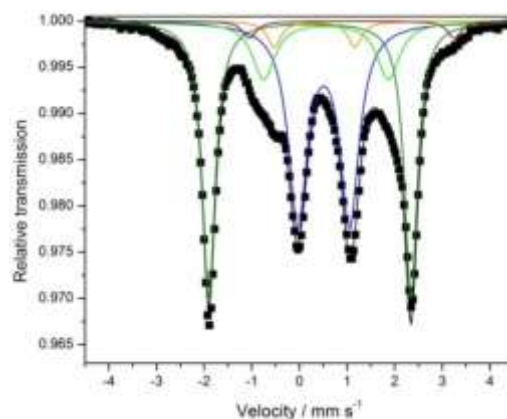


Figure 3.8. Mössbauer spectrum and components of the fit of a frozen solution ($T = 80$ K) of the products formed in the reaction of $^{57}\text{FeCl}_2$ (5.0 mM), TMEDA (4.0 equiv), PhMgCl (8.0 equiv) and **180** (1.0 equiv) in THF; components of the fit: δ (blue) = 0.51 mm s^{-1} , ΔE_Q (blue) = 1.09 mm s^{-1} , rel. int. = 40%; δ (green) = 0.22 mm s^{-1} , ΔE_Q (green) = 4.25 mm s^{-1} , rel. int. = 39%; δ (light green) = 0.56 mm s^{-1} , ΔE_Q (light green) = 2.62 mm s^{-1} , rel. int. = 14%; δ (orange) = 0.32 mm s^{-1} , ΔE_Q (orange) = 1.70 mm s^{-1} , rel. int. = 4%; δ (wine) = 1.10 mm s^{-1} , ΔE_Q (wine) = 4.30 mm s^{-1} , rel. int. = 3%. The spectrum was recorded and interpreted by Dr. S. Demeshko.

Thereafter, additional experiments in the presence of the indole substrate **59b** were performed. In addition to the previously observed species, $[\text{Cy}_4\text{Fe}(\text{indole})]^-$ was observed by ESI-MS analysis of the reaction of $^{57}\text{FeCl}_2/\text{CyMgCl}/\text{TMEDA}/\mathbf{180}/\mathbf{59b}$ (Fig. 3.9a). Yet, this species is believed to be catalytically irrelevant in the C–H activation due to the absence of the NHC ligand. Again, the apparent high intensity of the Cy_4Al^- peak is due to the relative low intensity of the anionic iron species. ESI-MS analysis of the reaction of $^{57}\text{FeCl}_2/\text{PhMgCl}/\text{TMEDA}/\mathbf{180}/\mathbf{59b}$ did not reveal any new species, but showed the almost complete disappearance of the $\text{Ph}_3\text{Fe}(\text{II})^-$ ferrate (Fig. 3.9b). Its consumption may suggest a reaction between the iron(II) ate complex, or a species in equilibrium with it, and the substrate **59** to form a neutral species. Therefore, this observation is suggestive of an organometallic iron(II) species to be involved in the catalysis as an intermediate or in the generation of the active catalyst.

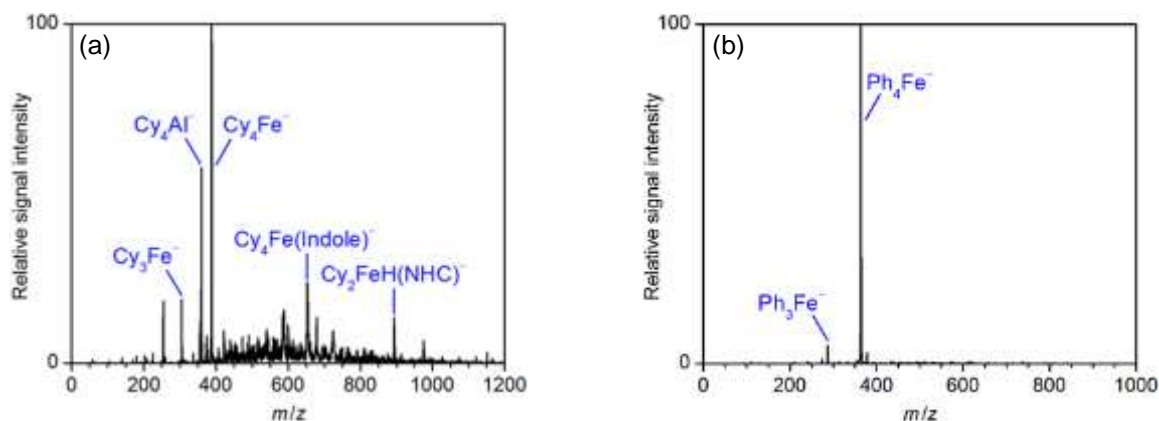


Figure 3.9. (a) Negative-ion mode ESI spectrum of a solution of the products formed in the reaction of $Fe(acac)_3$ (10 mM) with TMEDA (4.0 equiv), $CyMgCl$ (8.0 equiv), **180** (1.0 equiv) and **59b** (1.0 equiv) in THF. (b) Negative-ion mode ESI spectrum of a solution of the products formed in the reaction of $Fe(acac)_3$ (10 mM) with TMEDA (4.0 equiv), $PhMgCl$ (8.0 equiv), **180** (1.0 equiv) and **59b** (1.0 equiv) in THF. The experiments were conducted by S. Lülff and Dr. T. Parchomyk, respectively.

Further, no new species or significant changes upon the addition of substrate **59b** were observed by ^{57}Fe Mössbauer spectroscopy analysis of the analogous reactions with either $CyMgCl$ or $PhMgCl$ (Fig. 3.10). Yet, a slight reduction of the intensity of the species believed to be $R_2Fe(NHC)$ was observed (Fig. 3.10a–b, green), possibly indicating its consumption in a reaction with **59b**.

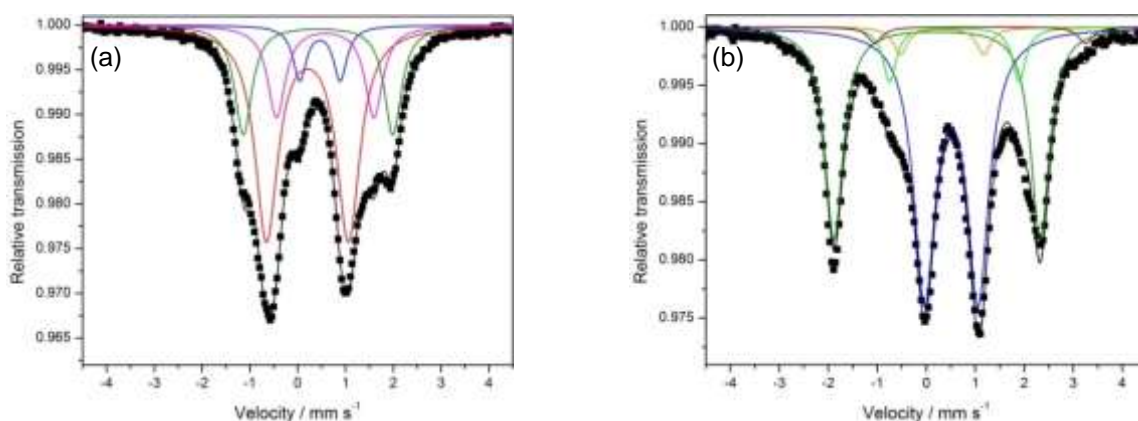


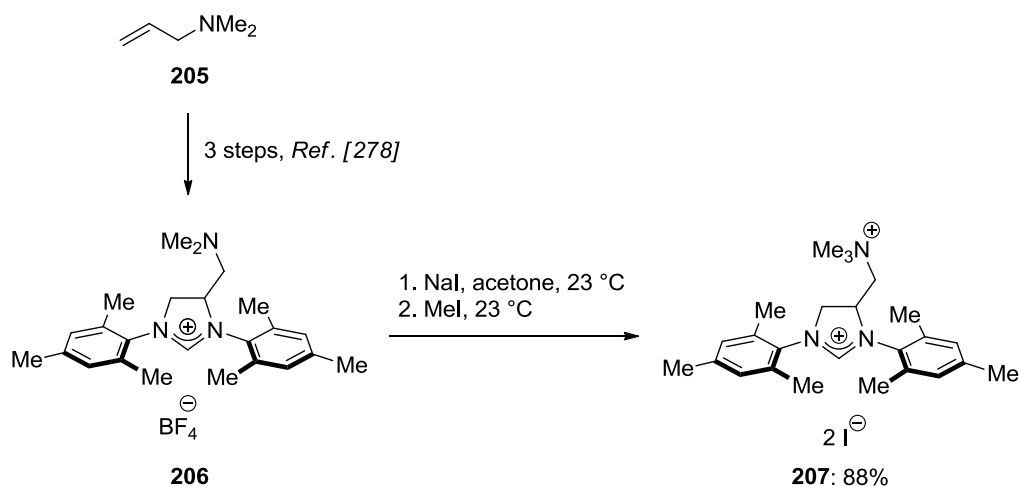
Figure 3.10. (a) Mössbauer spectrum and components of the fit of a frozen solution ($T = 80\ K$) of the products formed in the reaction of $^{57}FeCl_2$ (5.0 mM), TMEDA (4.0 equiv), $CyMgCl$ (8.0 equiv), **180** (1.0 equiv) and **59b** (1.0 equiv) in THF; components of the fit: $\delta(\text{red}) = 0.20\ mm\ s^{-1}$, $\Delta E_Q(\text{red}) = 1.71\ mm\ s^{-1}$, rel. int. = 53%; $\delta(\text{green}) = 0.43\ mm\ s^{-1}$,

$\Delta E_Q(\text{green}) = 3.13 \text{ mm s}^{-1}$, rel. int. = 21%; $\delta(\text{magenta}) = 0.58 \text{ mm s}^{-1}$,
 $\Delta E_Q(\text{magenta}) = 2.04 \text{ mm s}^{-1}$, rel. int. = 18%; $\delta(\text{blue}) = 0.47 \text{ mm s}^{-1}$, $\Delta E_Q(\text{blue}) =$
 0.84 mm s^{-1} , rel. int. = 8%. (b) *Mössbauer* spectrum and components of the fit of a frozen
 solution ($T = 80 \text{ K}$) of the products formed in the reaction of $^{57}\text{FeCl}_2$ (5.0 mM), TMEDA
 (4.0 equiv), PhMgCl (8.0 equiv), **180** (1.0 equiv) and **59b** (1.0 equiv) in THF; components of
 the fit: $\delta(\text{blue}) = 0.51 \text{ mm s}^{-1}$, $\Delta E_Q(\text{blue}) = 1.09 \text{ mm s}^{-1}$, rel. int. = 52%;
 $\delta(\text{green}) = 0.22 \text{ mm s}^{-1}$, $\Delta E_Q(\text{green}) = 4.21 \text{ mm s}^{-1}$, rel. int. = 36%;
 $\delta(\text{light green}) = 0.57 \text{ mm s}^{-1}$, $\Delta E_Q(\text{light green}) = 2.64 \text{ mm s}^{-1}$, rel. int. = 7%;
 $\delta(\text{orange}) = 0.32 \text{ mm s}^{-1}$, $\Delta E_Q(\text{orange}) = 1.70 \text{ mm s}^{-1}$, rel. int. = 4%; $\delta(\text{wine}) = 1.10 \text{ mm s}^{-1}$,
 $\Delta E_Q(\text{wine}) = 4.30 \text{ mm s}^{-1}$, rel. int. = 2%. The spectra were recorded and interpreted by *Dr. S.*
Demeshko.

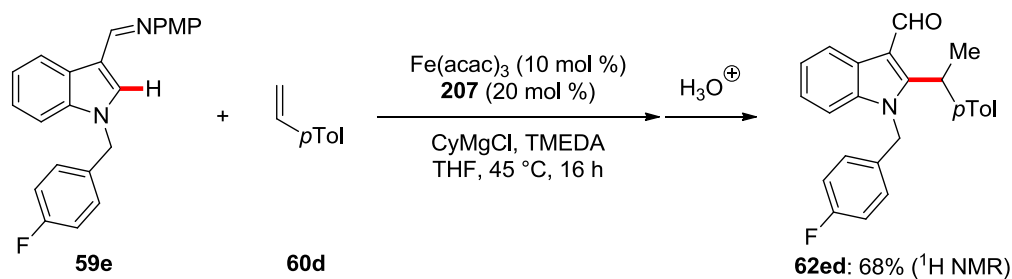
In summary, our experimental findings suggest the formation of organometallic
 iron(II)/NHC complexes as intermediates in the iron-catalyzed enantioselective C–H
 alkylation of indoles **59** with vinylarenes **60/191**. No interaction between iron and
 TMEDA was observed in any of the experiments, which suggests that TMEDA
 coordinates to the magnesium(II) ions and does not interact with the iron catalyst.
 Additionally, our observations provide support to the long-proposed role of Grignard
 reagents to serve as both reductant and base in iron-catalyzed C–H activations.

The major limitation of mass spectrometry is, obviously, the difficulty to observe
 neutral species. As a consequence, we reasoned that the use of a charge-tagged
 NHC ligand would allow for the detection of otherwise neutral $\text{R}_2\text{Fe(II)NHC}$ species.
 For example, phosphonium-tags have previously been employed by *Koszinowski* to
 detect species formed in iron-catalyzed cross-couplings.^[269a] We hence became
 interested in the synthesis of a positively charged NHC precursor resembling
 pre-ligand **180**. Starting from the amino-tagged NHC precursor **206** reported by
Grela and coworkers,^[278] the ammonium-tagged imidazolium **207** was prepared
 readily in two steps *via* salt metathesis and a *Menshutkin* reaction with methyl iodide
 (Scheme 3.14). A test reaction revealed **207** to be a potent pre-ligand for the iron-
 catalyzed hydroarylation, giving the alkylated product with an efficacy comparable to
 IMe \cdot HCl (Scheme 3.15).^[148] However, ESI-MS measurements performed by *Dr. T.*
Parchomyk and *F. Kraft* of the *Koszinowski* research group have so far remained
 unsuccessful. Indeed, problems of very poor solubility and loss of MeI in solution

have so far prevented us from observing the expected NHC-ligated iron species by ESI-MS.^[279] Interestingly, *Grela* and coworkers prepared the ammonium-tagged NHC/ruthenium complex by a late-stage methylation of the corresponding neutral amino-NHC/ruthenium complex.^[278] In a later work, it was revealed that the direct complexation of the ammonium-tagged NHC precursor with ruthenium had also been unsuccessful.^[280]



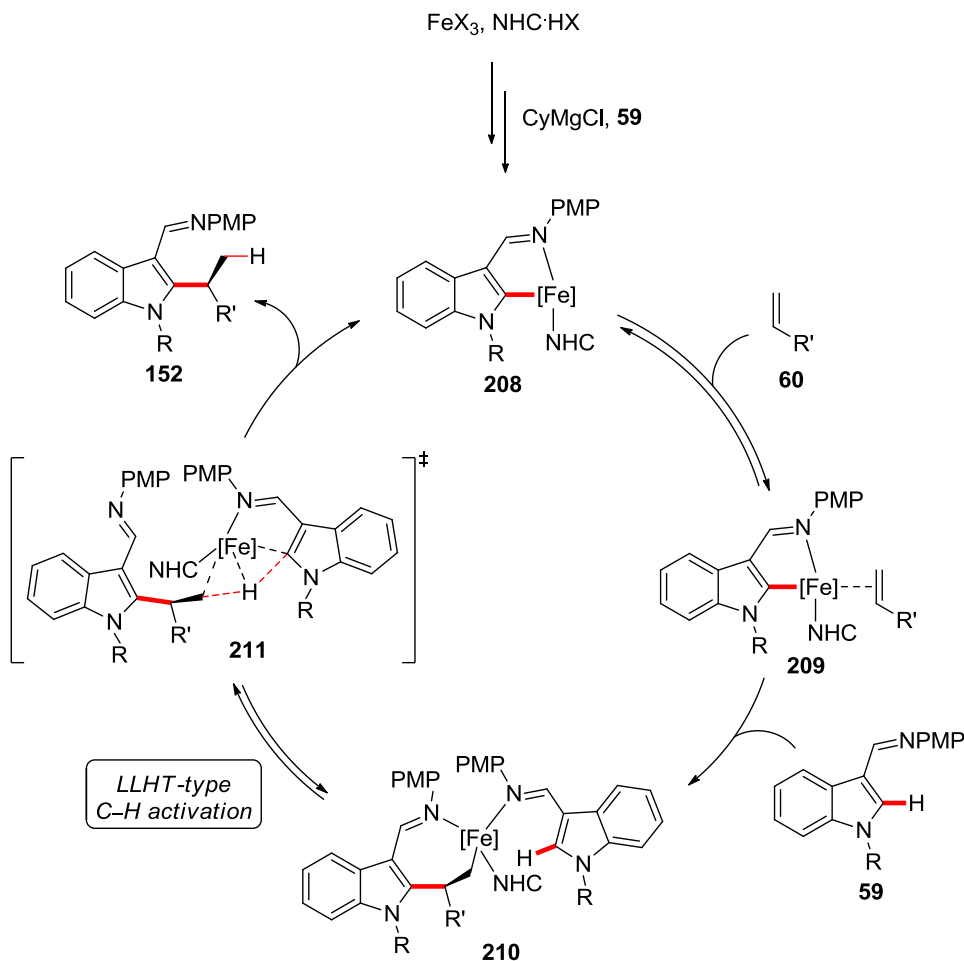
Scheme 3.14. Synthesis of charge-tagged NHC precursor **207**.



Scheme 3.15. Reaction with charge-tagged NHC precursor **207** as the pre-ligand.

3.2.6. Proposed Mechanism

Based on the conducted mechanistic studies and literature precedents, the catalytic cycle is proposed to begin with the formation of an active organometallic iron catalyst through the reduction of the iron(III) precursor by the action of the Grignard reagent (Scheme 3.16). While β -hydride elimination certainly plays a role in the reduction of the iron precursor when CyMgCl is employed, this process does not seem to be essential since significant conversions were observed when using PhMgCl (Tables 3.7, 3.9). In the latter case, the reduction process likely occurs *via* reductive elimination from a Ph₂[Fe] species, as alternative processes through radical expulsion are disfavored.^[267] Nevertheless, ⁵⁷Fe Mössbauer spectroscopy strongly supports a facile β -hydride elimination to occur even at ambient temperature (Fig. 3.8b). Additionally, iron(II)–hydride species were detected by ESI-MS as well (Fig. 3.5, 3.9a). Hence, the Cy₂Fe(NHC) species observed by ⁵⁷Fe Mössbauer spectroscopy (Fig. 3.7) is most likely only an intermediate of the catalyst generation process. Furthermore, in consideration of our mechanistic studies and previous reports,^[267,269b,281] the TMEDA additive is believed to induce deaggregation and coordinate to the organomagnesium reagent rather than the active NHC-ligated iron catalyst.



Scheme 3.16. Proposed mechanism of the asymmetric iron-catalyzed alkylation.

After the *in situ* formation of an organometallic mono-NHC-iron catalyst, the latter can be coordinated by the alkene **60** in a reversible fashion leading to its zeroth-order dependence (Scheme 3.11). The subsequent kinetically relevant migratory insertion is assisted by coordination of the substrate **59**,^[282] explaining its first-order rate law. Given the facile inner-sphere C–H cleavage, the selective deuterium transfer to the methyl group in product $[\text{D}]_1\text{-62}$ (Schemes 3.8) and the crossover experiment (Scheme 3.9), the C–H metalation step is proposed to occur *via* a ligand-to-ligand hydrogen transfer (LLHT) manifold, by the action of the coordinated substrate **59**. It should be noted that a turnover-limiting initial coordination of substrate **59**, followed by C–H activation by oxidative addition, would also be in

agreement with our kinetic findings. However, the crossover experiment, along with preliminary computational studies by DFT,^[256] seem to favor a LLHT regime.

3.2.7. Iron-Catalyzed Alkyne Hydroarylations

In the original report by *Yoshikai* and coworkers, the substrate scope of the racemic iron-catalyzed hydroarylations was not limited to vinylarenes. Indeed, internal alkynes proved viable as well.^[148] While the alkenylated products do not possess any chiral center, we speculated that axial chirality might exist across the C–C bond generated in the transformation. This hypothesis was confirmed by the synthesis of compound **85ca** and the separation of its atropisomers by chiral HPLC (Figure 3.11). Methods for the synthesis of axially chiral compounds are of high interest for synthetic chemists due to the importance of axially chiral natural products^[283] and chiral ligands,^[70c,284] among others. Interestingly, while several examples of atroposelective C–H activations employing noble transition metal catalysts are reported in the literature,^[213h,285] the selective synthesis of axially chiral compounds *via* 3d transition metal-catalyzed C–H activation remains thus far unprecedented.^[52]

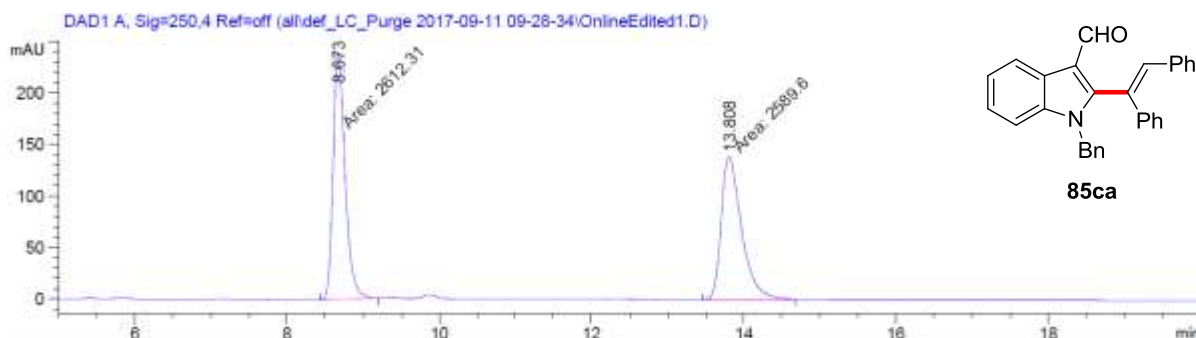
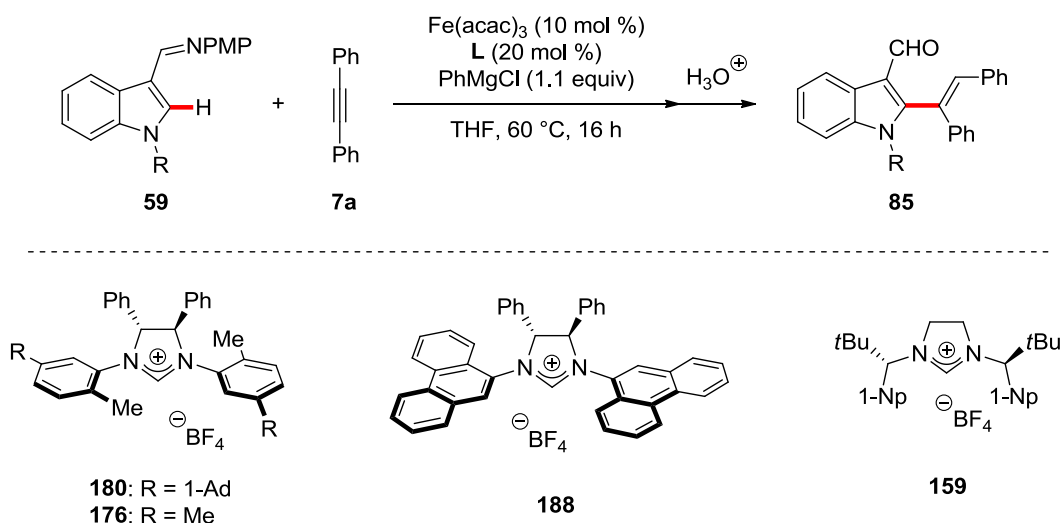


Figure 3.11. Chiral HPLC chromatogram of **85ca** (Daicel CHIRALPAK® IB-3, *n*-hexane/*i*PrOH = 80/20, flow rate 1.0 mL/min).

Hence, intrigued by the possibility to develop an enantioselective version, a representative set of chiral NHC ligands were tested in the envisioned asymmetric transformation employing *N*-benzylindole **59c** and tolane **7a** (Table 3.14). Sadly,

while low conversion was obtained under a slight modification of *Yoshika's* conditions (entry 1), no product was detected with any of the tested chiral pre-ligands (entries 2–4). Since the racemic reaction is only reported on *N*-methylindole **59b**, we reasoned that the extra steric bulk of the benzyl substituent might hinder the catalysis. Therefore, various NHC precursors were tested for the alkenylation of *N*-methylindole **59b**. While the expected product **85ba** was obtained in moderate yield using IXyl (entry 5), no conversion was obtained when employing chiral ligands (entries 6–8). Furthermore, the analysis by chiral HPLC of product **85ba** revealed the existence of a plateau between the peaks of the two atropisomers, which clearly indicates their interconversion at ambient temperature (Figure 3.12).^[286] The observed lack of reactivity, as well as the conformational instability of the formed atropisomers, prompted us to discontinue this project.

Table 3.14. Iron-catalyzed hydroarylation of alkyne **7a** with indoles **59**.^[a]



| Entry | R | L | Yield [%] ^[b] | e.r. |
|-------|----|------------|--------------------------|------|
| 1 | Bn | IXyl·HCl | 13 | - |
| 2 | Bn | 180 | n.r. | - |
| 3 | Bn | 176 | n.r. | - |
| 4 | Bn | 186 | n.r. | - |

| | | | | |
|---|----|------------|--------|---|
| 5 | Me | IXyl·HCl | 49 | - |
| 6 | Me | 180 | traces | - |
| 7 | Me | 176 | n.r. | - |
| 8 | Me | 159 | n.r. | - |

^[a] Reaction conditions: **59** (0.25 mmol), **7a** (2.0 equiv), Fe(acac)₃ (10 mol %), **L** (20 mol %), PhMgCl (1.1 equiv), THF (0.50 mL), 60 °C, 16 h. ^[b] Yield of the isolated product.

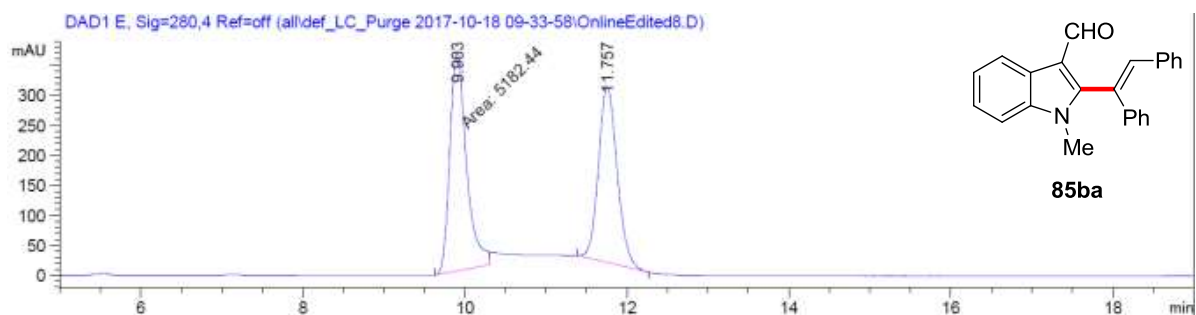


Figure 3.12. Chiral HPLC chromatogram of **85ba**. The plateau between the two peaks indicates on-column interconversion of the two atropisomers^[286] (Daicel CHIRALPAK[®] IC-3, *n*-hexane/*i*PrOH = 70/30, flow rate 1.0 mL/min).

3.3. Asymmetric Nickel-Catalyzed Hydroarylations by C–H Activation

Nickel complexes have been recognized as powerful tools in molecular syntheses, with numerous applications to C–C bond forming processes.^[153d,153e] Due to its high abundance in the Earth's crust, broad range of accessible oxidation states, and comparatively low cost,^[287] nickel catalysis has experienced a considerable development in recent years. Among others, applications to cross-coupling chemistry^[18] and the functionalization of otherwise inert C–H bonds^[45,48b,48c] have attracted significant interest. In particular, nickel catalysts have emerged as an especially powerful tool for hydroarylation-type C–H activations.^[27,188a]

However, asymmetric nickel-catalyzed hydroarylations remain rare. While major progress has been recently achieved for *intramolecular* hydroarylations employing nickel/aluminium^[288] heterobimetallic^[23b] catalysis,^[193,200,203,206] enantioselective *intermolecular* processes are unprecedented. In a broader context, asymmetric intermolecular nickel-catalyzed C–H functionalizations remain unknown, with only one single exception by *Cramer* for the reductive three-component coupling of benzaldehydes, norbornenes and silanes (Scheme 1.43).^[210]

In this context, the association of N-heterocyclic carbene (NHC) ligands with nickel is remarkably versatile and has been intensively exploited for, *inter alia*, C–C forming processes *via* hydroarylation reactions or cross-couplings.^[289] These literature precedents prompted us to investigate the performance of the novel chiral NHC precursors that were developed for asymmetric iron-catalyzed hydroarylations (Chapter 3.2) in the unprecedented nickel-catalyzed asymmetric secondary alkylation of benzimidazoles **99** with styrenes **60**.

3.3.1. Preliminary Studies towards Asymmetric Intermolecular Hydroarylations by C–H Activation

Initially, we selected the well-documented branched-selective hydroarylation of styrenes **60** with azoles **99**^[162,189,194b,290] as a model system to probe our novel chiral NHC precursors. NaOtBu was used as a base to generate the free NHC *in situ*, as was previously reported.^[170,203] A preliminary ligand optimization^[291] identified *N,N*-diaryl NHCs, similar to those used in the enantioselective iron-catalyzed hydroarylation (Chapter 3.2), as optimal ligands for the transformation in terms of conversion. Other ligand classes, including *N,N*-dialkyl NHCs, phosphines, phosphine oxides, diamines, BOX ligands, dienes and phosphoramidites, gave all conversions lower than 25%. However, enantiomeric excesses were found to be highly irreproducible. Intrigued by those issues, we decided to investigate their cause. A base-induced racemization was immediately suspected to occur since the chiral center, a bis-benzylic position substituted with an electron-withdrawing benzimidazole moiety, is rather activated. Furthermore, 2-allylbenzimidazoles are reported to isomerize in a similar setting, even at a lower temperature of 100 °C.^[170] Therefore, the effect of the amount of base and various additives on the transformation was studied in order to prevent the suspected racemization (Table 3.15). First, an increase of the amount of base led to a decreased enantiomeric ratio (entries 1–2). Lowering the amount of base was found to improve the enantioselectivity of the transformation, but resulted in low conversions (entries 3–4). These findings provide strong support for the suspected base-induced racemization. Thereafter, the effect of various additives was probed in the asymmetric hydroarylation. As inconsistent enantioselectivities were obtained when using toluene from different sources (SPS, distilled over Na, etc.), the trace water content was suspected to play a key role in the irreproducibility of the reaction. Hence, co-catalytic amounts of water were added into the reaction. Remarkably, traces of water were found to strongly improve the enantiomeric excess of product **106bc** (entries 5–8). Other protic or Lewis acidic additives were then tested in the reaction (entries 9–12), the best results being obtained in the presence of a

co-catalytic amount of BHT (entry 12). While the beneficial effect of protic additives is not fully understood yet, it is suspected that they might “neutralize” the excess of NaOtBu, thus preventing the racemization of product **106bc**. Meanwhile, the linear product was obtained selectively in the presence of a co-catalytic amount of AlMe₃, as expected from literature precedents (entry 13).^[194]

Table 3.15. Effect of the base and other additives of the enantioselective nickel-catalyzed intermolecular hydroarylation of styrene **60c** with benzimidazole **99b**.^[a]

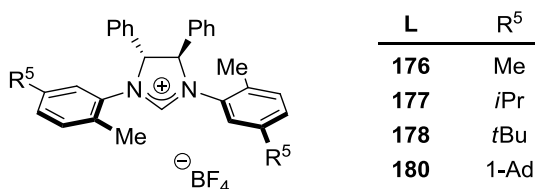
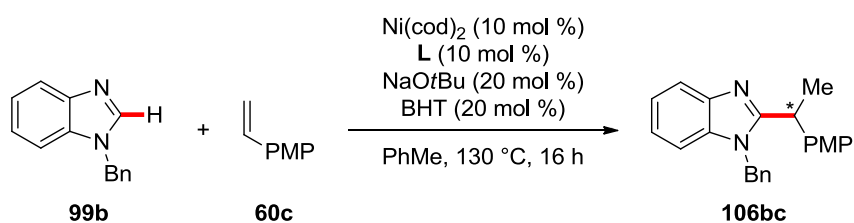
| Entry | Additive | Yield [%] ^[b] | e.r. ^[c] |
|------------------|---|--------------------------|---------------------|
| 1 | - | 49–67 | 58:42–79:21 |
| 2 ^[d] | - | 62 | 55:45 |
| 3 ^[e] | - | 22 | 78:22 |
| 4 ^[f] | - | traces | - |
| 5 ^[d] | H ₂ O ^[g] (2.0 equiv) | 30 | 80:20 |
| 6 ^[d] | H ₂ O ^[g] (1.0 equiv) | 30 | 80:20 |
| 7 ^[d] | H ₂ O ^[g] (50 mol %) | 57 | 79:21 |
| 8 ^[d] | H ₂ O ^[g] (20 mol %) | 50 | 68:32 |
| 9 ^[d] | BPh ₃ (50 mol %) | 26 | 73:27 |

| | | | |
|----|------------------------------|------------------|-------|
| 10 | <i>t</i> AmOH ^[h] | 60 | 61:39 |
| 11 | BHT (50 mol %) | 53 | 80:20 |
| 12 | BHT (20 mol %) | 57 | 80:20 |
| 13 | AlMe ₃ (40 mol %) | 0 ^[i] | - |

^[a] Reaction conditions: **99b** (0.50 mmol), **60c** (2.0 equiv), Ni(cod)₂ (10 mol %), **L** (10 mol %), NaOtBu (20 mol %), additive, PhMe (2.0 mL), 130 °C, 16 h. ^[b] Isolated yields. ^[c] Determined by chiral HPLC. ^[d] Using NaOtBu (40 mol %). ^[e] Using NaOtBu (15 mol %). ^[f] Using NaOtBu (10 mol %). ^[g] Degassed H₂O. ^[h] PhMe/*t*AmOH = 15/1 was used as the reaction medium. ^[i] The linear product **112** was obtained in 91% yield.

With the issues of racemization and irreproducibility being solved, a representative set of chiral NHC precursors was then tested in the envisioned asymmetric hydroarylation (Table 3.16). Somewhat surprisingly, all the pre-ligands probed in the reaction provided the alkylated product **106bc** with almost identical enantioselectivities and similar yields.

Table 3.16. Further ligand optimization in the presence of BHT as additive.^[a]

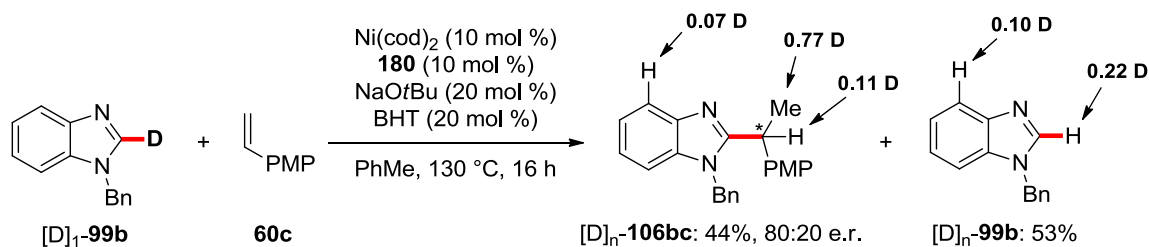


| Entry | L | Yield [%] ^[b] | e.r. ^[c] |
|-------|------------|--------------------------|---------------------|
| 1 | 176 | 37 | 82:18 |

| | | | |
|---|------------|----|-----------|
| 2 | 177 | 52 | 79.5:20.5 |
| 3 | 178 | 56 | 80.5:19.5 |
| 4 | 180 | 57 | 80:20 |

^[a] Reaction conditions: **99b** (0.50 mmol), **60c** (2.0 equiv), Ni(cod)₂ (10 mol %), **L** (10 mol %), NaOtBu (20 mol %), BHT (20 mol %), PhMe (2.0 mL), 130 °C, 16 h. ^[b] Isolated yields. ^[c] Determined by chiral HPLC.

Preliminary mechanistic studies were conducted to delineate the mode of action of the C–H activation. A reaction with the deuterated substrate [D]₁-**99b** was performed. Interestingly, while most of the deuterium was selectively transferred to the methyl group, indicating an organometallic C–H bond cleavage, significant scrambling was observed. This observation can be rationalized with a facile and reversible C–H scission step.



Scheme 3.17. Reaction with deuterium-labeled substrate [D]₁-**99b**.

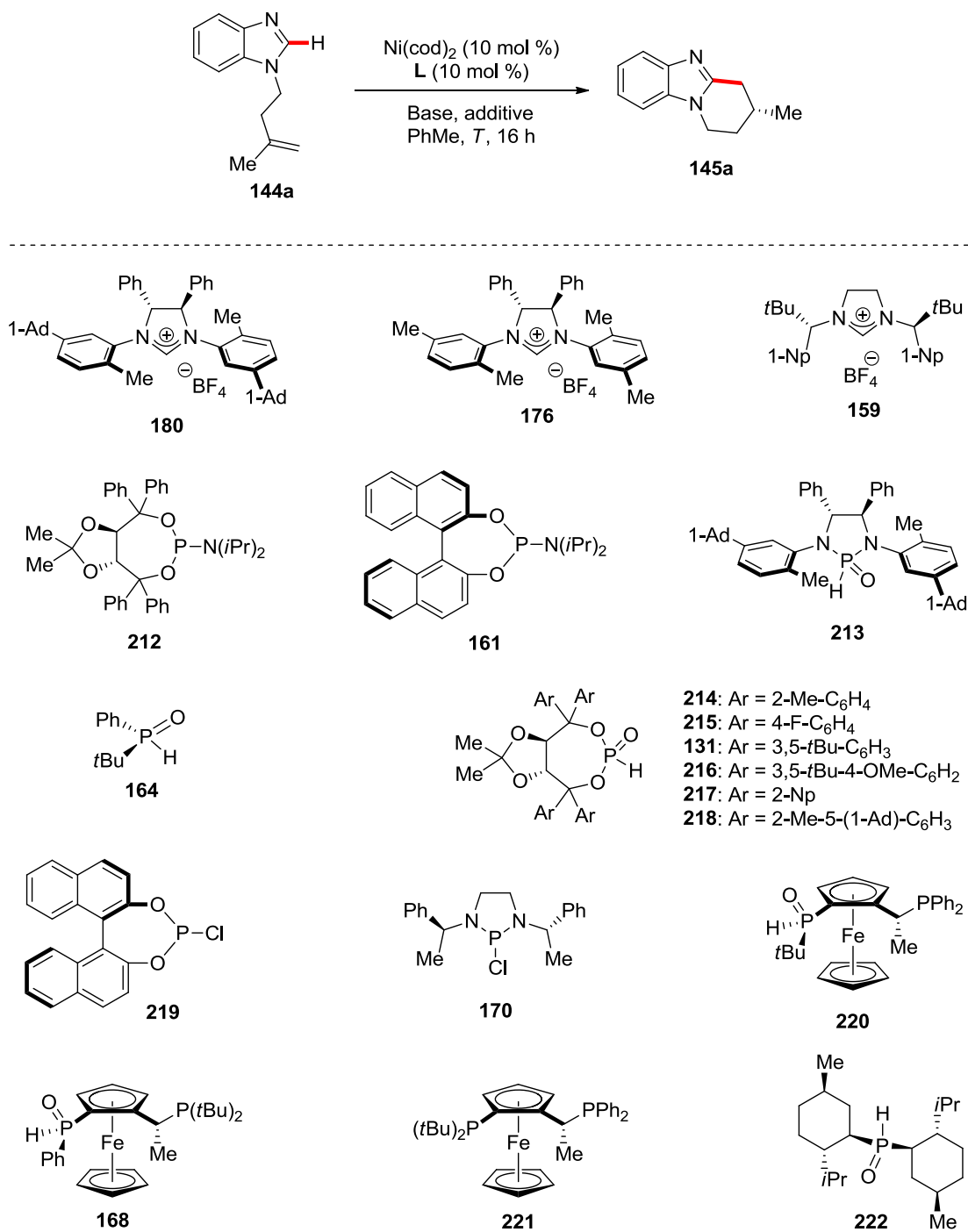
Meanwhile, as asymmetric catalysis is known to be substrate-specific, different types of heteroarenes and alkenes were probed in the envisioned asymmetric hydroarylation. Notably, promising results were obtained for intramolecular transformations. Those findings motivated us to investigate enantioselective nickel-catalyzed cyclizations by C–H activation (*vide infra*).

3.3.2. Optimization Studies of Enantioselective Intramolecular Nickel-Catalyzed Hydroarylations *via* C–H Activation

Chemo-, regio- and enantio-selective cyclizations are of key importance in synthetic chemistry, with applications to, *inter alia*, the synthesis of pharmaceuticals and bioactive natural products.^[56a,193,292]

In this context, intramolecular hydroarylations^[27] represent a particularly attractive cyclization strategy due to its perfect atom economy.^[2] While nickel catalysts have emerged as powerful tools for the hydroarylations of C–C multiple bonds,^[48a,188a] intramolecular processes have long been restricted to the functionalization of highly activated azolium salts.^[205] In recent years, the development of heterobimetallic nickel/aluminium catalysis^[198] has allowed for the use of unactivated alkenes and substrates bearing less acidic C–H bonds. Despite being highly desirable, enantioselective methodologies remained extremely scarce at the outset of this work.^[193,195] However, this research area has attracted significant attention during the course of this thesis, as several examples were independently reported by other research groups.^[200,203,206] It is noteworthy that all those works absolutely require pyrophoric Lewis acidic organoaluminium additives, such as AlMe₃ or MAD,^[293] for the reaction to occur.

Therefore, we decided to investigate the asymmetric cyclization of *N*-homoallylimidazoles **144** by nickel-catalyzed hydroarylation (Table 3.17). This model substrate was selected due to literature precedents with rhodium(I) catalysts^[219b] and the importance of the benzimidazole scaffold in bioactive compounds.^[294] Our optimization studies began by testing a wealth of chiral ligands for the envisioned asymmetric alkene hydroarylation. First, various representative NHC precursors and phosphoramidites were tested in the transformation, but fell short in delivering any product (entries 1–5). In agreement with literature precedents (*vide supra*), the addition of AlMe₃ was found to enable the desired cyclization (entry 6). Interestingly, the *endo* product was selectively obtained, in sharp contrast to another methodology independently reported by Ye around the same time.^[206]

Table 3.17. Optimization of the ligand for the enantioselective Ni-catalyzed cyclization.^[a]

| Entry | Ligand | Base | Additive | T [°C] | Yield [%] ^[b] | e.r. ^[c] |
|------------------|------------|-------------------|---|--------|--------------------------|---------------------|
| 1 | 180 | NaOtBu (20 mol %) | - | 130 | n.r. | - |
| 2 | 176 | NaOtBu (20 mol %) | - | 130 | n.r. | - |
| 3 | 159 | NaOtBu (20 mol %) | - | 130 | n.r. | - |
| 4 | 212 | - | - | 130 | n.r. | - |
| 5 | 161 | - | - | 130 | n.r. | - |
| 6 | 180 | NaOtBu (20 mol %) | AlMe ₃ (40 mol %) | 130 | 53 | 67:33 |
| 7 | 180 | NaOtBu (20 mol %) | AlMe ₃ (40 mol %) | 100 | n.r. | - |
| 8 | 180 | NaOtBu (20 mol %) | AlMe ₃ (1.0 equiv) | 130 | 43 | 67:33 |
| 9 ^[d] | 180 | NaOtBu (20 mol %) | AlMe ₃ (40 mol %) | 130 | n.r. | - |
| 10 | 213 | - | AlMe ₃ (40 mol %) | 130 | 88 | 32:68 |
| 11 | 213 | - | AlMe ₃ (40 mol %) + PPh ₃ (10 mol %) | 130 | n.r. | - |
| 12 | 213 | - | MAD (40 mol %) | 130 | n.r. | - |
| 13 | 213 | - | BPh ₃ (40 mol %) | 130 | n.r. | - |
| 14 | 213 | - | AlMe ₃ (40 mol %) | 110 | n.r. | - |
| 15 | 213 | - | AlMe ₃ (40 mol %) | 95 | n.r. | - |
| 16 | 161 | - | AlMe ₃ (40 mol %) | 130 | 22 | 50:50 |
| 17 | 164 | - | AlMe ₃ (40 mol %) | 130 | 67 | 53:47 |
| 18 | - | - | AlMe ₃ (40 mol %) | 130 | traces | - |
| 19 | 214 | - | AlMe ₃ (40 mol %) | 130 | 70 | 32:68 |
| 20 | 214 | - | AlMe ₃ (40 mol %) | 110 | 65 | 33:67 |
| 21 | 214 | - | AlMe ₃ (40 mol %) | 95 | 66 | 32:68 |
| 22 | 214 | - | AlMe ₃ (40 mol %) | 80 | traces | - |
| 23 | 214 | - | AlMe ₃ (20 mol %) | 95 | 50 | 33:67 |
| 24 | 214 | - | AlMe ₃ (60 mol %) | 95 | 47 | 33:67 |

3. Results and Discussion

| | | | | | | |
|-------------------|------------|-------------------|-------------------------------|-----|--------|-------|
| 25 | 214 | - | - | 95 | n.r. | - |
| 26 ^[d] | 214 | - | AlMe ₃ (40 mol %) | 95 | n.r. | - |
| 27 ^[e] | 214 | - | AlMe ₃ (40 mol %) | 95 | 60 | 39:61 |
| 28 ^[f] | 214 | - | AlMe ₃ (40 mol %) | 95 | traces | - |
| 29 | 215 | - | AlMe ₃ (40 mol %) | 130 | 12 | 50:50 |
| 30 | 131 | - | AlMe ₃ (40 mol %) | 95 | 89 | 48:52 |
| 31 | 216 | - | AlMe ₃ (40 mol %) | 95 | 56 | 53:47 |
| 32 | 217 | - | AlMe ₃ (40 mol %) | 95 | n.r. | - |
| 33 | 218 | - | AlMe ₃ (40 mol %) | 95 | traces | - |
| 34 | 218 | - | AlMe ₃ (40 mol %) | 110 | 55 | 54:46 |
| 35 | 219 | - | AlMe ₃ (40 mol %) | 130 | n.r. | - |
| 36 | 170 | - | AlMe ₃ (40 mol %) | 130 | n.r. | - |
| 37 | 170 | NaOtBu (10 mol %) | AlMe ₃ (40 mol %) | 130 | 16 | 56:44 |
| 38 | 220 | - | AlMe ₃ (40 mol %) | 95 | 88 | >99:1 |
| 39 ^[d] | 220 | - | AlMe ₃ (40 mol %) | 95 | n.r. | - |
| 40 | 168 | - | AlMe ₃ (40 mol %) | 95 | 86 | 23:77 |
| 41 ^[g] | 220 | - | AlMe ₃ (10 mol %) | 95 | 95 | >99:1 |
| 42 ^[g] | 221 | - | AlMe ₃ (10 mol %) | 95 | 13 | 55:45 |
| 43 | 221 | - | - | 95 | n.r. | - |
| 44 | 222 | - | AlMe ₃ (40 mol %) | 95 | 85 | 80:20 |
| 45 ^[h] | 220 | - | AlMe ₃ (4.0 mol %) | 95 | 97 | >99:1 |
| 46 | 220 | - | AlMe ₃ (10 mol %) | 85 | 95 | >99:1 |
| 47 | 220 | - | AlMe ₃ (10 mol %) | 75 | 94 | >99:1 |
| 48 | 220 | - | - | 95 | 91 | 96:4 |

^[a] Reaction conditions: **144a** (0.50 mmol), Ni(cod)₂ (10 mol %), **L** (10 mol %), additive (40 mol %), base (20 mol %), PhMe (2.0 mL), 16 h. ^[b] Yield of the isolated product. ^[c] Determined by chiral HPLC analysis. ^[d] Ni(cod)₂ was omitted. ^[e] **214** (15 mol %). ^[f] **214** (5.0 mol %). ^[g] Using Ni(cod)₂ (2.5 mol %) and **L** (2.5 mol %) in PhMe (1.0 mL). ^[h] Using Ni(cod)₂ (1.0 mol %) and **220** (1.0 mol %) in PhMe (1.0 mL).

The desired product was obtained in moderate yield and enantiomeric excess when using the previously developed NHC precursor **180** (entry 6). Lowering the temperature or increasing the amount of AlMe₃ did not improve the outcome of the reaction (entries 7–8). A control experiment proved the importance of the nickel catalyst (entry 9).

Inspired by the success of (HA)SPO pre-ligands in nickel catalysis,^[155a,195,206,208,239b] this ligand class was investigated in the envisioned transformation. The novel chiral HASPO **213**, derived from the same diamine intermediate as **180**, gave promising results (entry 10). The introduction of additional co-catalytic PPh₃ completely suppressed the reactivity (entry 11), despite being reported as beneficial in other transformations occurring under a Ni/Al/SPO regime (see Scheme 1.37).^[195,206,208] Interestingly, MAD or BPh₃ fell short in delivering any cyclized product (entries 12–13). Again, lower reaction temperatures proved detrimental to the transformation (entries 14–15). Other ligand types were tested as well. Monodentate phosphoramidites, such as ligands **161**, provided product **145a** in poor yield without significant enantio-induction (entry 16). Then, the prototypical *P*-chiral secondary phosphine oxide (SPO) **164** provided the product in good yield, but only poor enantioselectivity (entry 17). Furthermore, a control experiment confirmed the importance of the ligand (entry 18). As (HA)SPOs seemed to be the most promising ligand class at this point, we probed next other HASPO pre-ligands, including TADDOL-derived **214** (entry 19). Interestingly, while TADDOL-based phosphine oxides had previously been employed in asymmetric organocatalysis,^[207] their use in transition metal catalysis remains rare.^[206,208] Remarkably, **214** proved to be superior to previously investigated ligands, as the reaction temperature could be lowered to 95 °C (entries 20–22). A *Job* plot of the amount of AlMe₃ confirmed 40 mol % to be optimal (entries 23–25), and a control experiment confirmed the key role of the

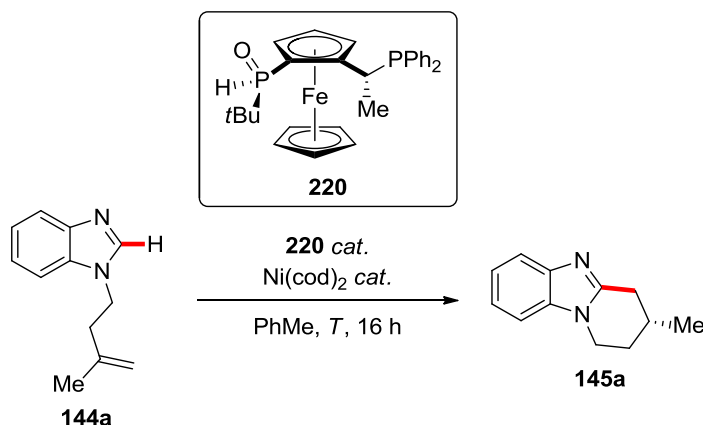
nickel catalyst (entry 26). Variations of the ligand-to-metal ratio suggested a 1:1 ratio to be optimal under those conditions (entries 27–28). While the *ortho*-tolyl derivative **214** gave promising results even at lower temperatures, HASPO derived from differently substituted TADDOLs performed poorly in the desired transformation (entries 29–34). As phosphine chlorides are reported to exhibit a reactivity similar to (HA)SPOs,^[239a] **219** and **170** were probed in the desired asymmetric cyclization, but no conversion of the alkene **144a** was observed (entries 35–36). However, some product formation could be observed after the addition of co-catalytic NaOtBu (entry 37), presumably due to the *in situ* formation of the corresponding diaminoxophosphine.^[239b]

Thereafter, JoSPOphos-type ligands were tested due to their well-documented efficacy in rhodium(I)-catalyzed enantioselective hydrofunctionalization reactions.^[295] Applications of the JoSPOphos ligand family besides rhodium(I) catalysis remain scarce, with notable exceptions in ruthenium-^[296] and cobalt-catalyzed^[297] asymmetric hydrogenations. To our delight, JoSPOphos **220** afforded the desired product **145a** in excellent yield and perfect enantioselectivity (entry 38). In this context, it is noteworthy that this transformation represents the first use of JoSPOphos pre-ligand **220** with a transition metal other than rhodium(I). Once again, a control experiment confirmed the importance of the nickel catalyst (entry 39). The related ligand **168** provided the cyclized product in similar yield but only moderate enantioselectivity (entry 40). The catalyst loading could be lowered to 2.5 mol % without losing any activity (entry 41). Meanwhile, poor results were obtained with the corresponding JosiPhos ligand **221**, highlighting the superiority of the secondary phosphine oxide moiety (entries 42–43). The dimethyl-substituted SPO **222** recently disclosed by *Hintermann*^[298] was probed as well in the asymmetric C–H alkylation (entry 44). Remarkably, the obtained enantiomeric excess of 60% is the highest observed with a monodentate chiral ligand. Thereafter, **220** was found to promote the reaction with catalyst loadings as low as 1.0 mol % (entry 45). Moreover, the excellent performance of the JoSPOphos-derived catalyst at lower temperature once again showcased its remarkable activity (entries 46–47). Extraordinarily, control experiments revealed the JoSPOphos-enabled alkene

hydroarylation to occur smoothly even in the absence of pyrophoric AlMe_3 as additive (entry 48). It should be noted that nickel-catalyzed hydroarylations of non-activated alkenes in the absence of organoaluminium reagents are extremely rare,^[189,299] and had never been achieved in an enantioselective fashion previously.

Given the unique opportunity for improved functional group tolerance, we decided to further optimize the AlMe_3 -free conditions (Table 3.18). Control experiments confirmed the importance of the nickel catalyst and of pre-ligand **220** (entry 1–3). Lower catalyst loadings did not significantly affect the conversion, but lower enantioselectivities were observed here (entries 4–7). Lower temperatures did not prove beneficial to the reaction outcome (entries 8–9). Thereafter, variations of the ligand-to-metal ratio provided informative results (entries 10–15). A ligand-to-nickel ratio of 2:1 was found to significantly reduce the enantioselectivity of the reaction, as well as the yield at lower catalyst loadings. Somewhat surprisingly, the use of an excess of nickel provided the highest enantioselectivities, the best results being obtained with a **220**/Ni ratio of 1:2 (entry 13). A larger excess of nickel did not considerably alter the enantioselectivity of the reaction, but lower conversions were observed. Possibly, an excess of nickel may be required in order to prevent the formation of less selective bis-ligated nickel species.^[300]

Table 3.18. Optimization of the additive-free hydroarylation.^[a]



| Entry | Ni(cod) ₂ [mol %] | 220 [mol %] | T [°C] | Yield [%] ^[b] | e.r. ^[c] |
|------------------|------------------------------|--------------------|--------|--------------------------|---------------------|
| 1 | 10 | 10 | 95 | 91 | 97:3 |
| 2 | 0 | 10 | 95 | n.r. | - |
| 3 | 10 | 0 | 95 | traces | - |
| 4 | 5.0 | 5.0 | 95 | 98 | 89:11 |
| 5 | 2.5 | 2.5 | 95 | 88 | 90:10 |
| 6 ^[d] | 2.5 | 2.5 | 95 | n.r. | - |
| 7 | 1.0 | 1.0 | 95 | 82 | 91:9 |
| 8 | 2.5 | 2.5 | 85 | 73 | 87:13 |
| 9 | 2.5 | 2.5 | 75 | 16 | 80:20 |
| 10 | 10 | 20 | 95 | 59 | 76:24 |
| 11 | 10 | 5.0 | 95 | 89 | 97:3 |
| 12 | 5.0 | 10 | 95 | 38 | 77:23 |
| 13 | 5.0 | 2.5 | 95 | 96 | 96:4 |
| 14 | 5.0 | 1.25 | 95 | 31 | 94:6 |
| 15 | 2.5 | 1.0 | 95 | 78 | 96:4 |

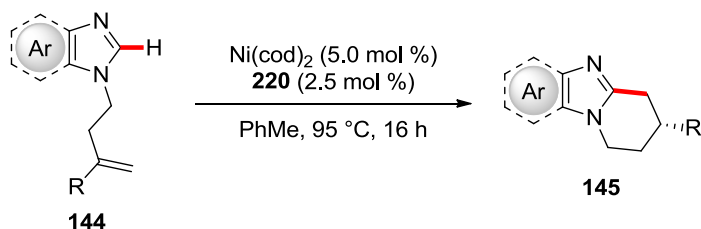
^[a] Reaction conditions: **144a** (0.50 mmol), Ni(cod)₂, **220**, PhMe (1.0 mL), 16 h. ^[b] Yield of the isolated product. ^[c] Determined by chiral HPLC analysis of the isolated product. ^[d] Using Ni(acac)₂ instead of Ni(cod)₂.

3.3.3. Substrate Scope and Limitations

With the optimized conditions in hand, we next decided to explore the versatility and robustness of the nickel-catalyzed asymmetric hydroarylation. The remarkably simple catalytic system proved able to cyclize various alkene-tethered heteroarenes

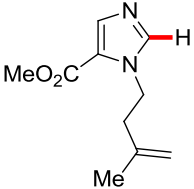

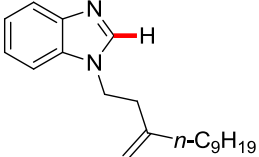
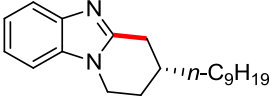
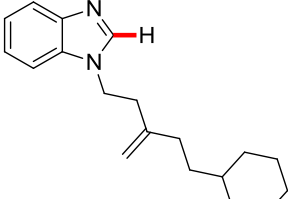
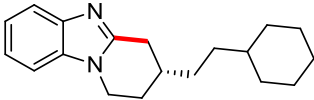
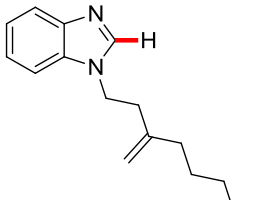
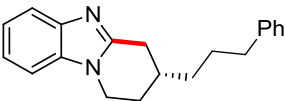
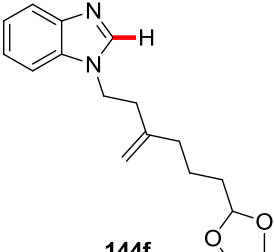
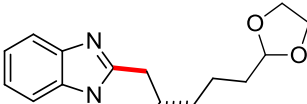
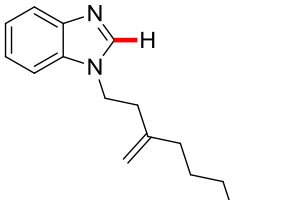
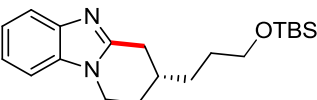
144 in outstanding yields and levels of enantioselectivity (Table 3.19). The substrate scope of the transformation was not limited to benzannulated azoles. Indeed, even the simple ester-substituted imidazole **144b** was efficiently converted in a highly enantioselective fashion (entry 2). Moreover, a variety of highly functionalized tethered prochiral alkenes **144** were fully tolerated in the transformation, providing the desired cyclized products **145** in high yields and excellent levels of enantiocontrol (entries 3–10). Extended alkyl chains, bulky cycloalkyl and benzyl groups, cyclic acetals and silyl ethers were smoothly converted, proving the C–H alkylated products **145** with high selectivity control. Remarkably, additional double bonds in the tethered alkene were compatible with the transformation, with the distal olefins left completely untouched. Indeed, *N*- γ -geranyl- **144h** and *N*- γ -farnesyl-benzimidazole **144i** were selectively cyclized to the desired products **145**, with only the proximal *exo*-double bond reacting. Additionally, even unhindered terminal alkenes, such as **144j**, proved to be viable substrates for the C–H alkylation, without significant formation of polycyclic byproducts.

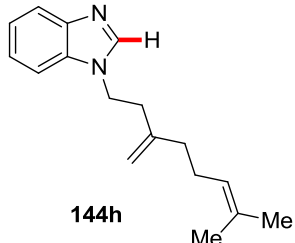
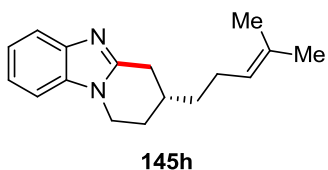
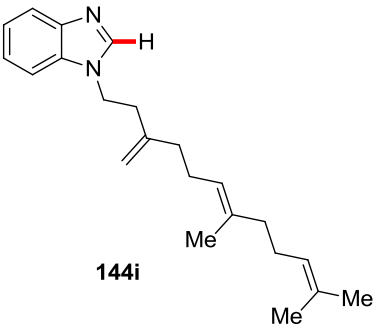
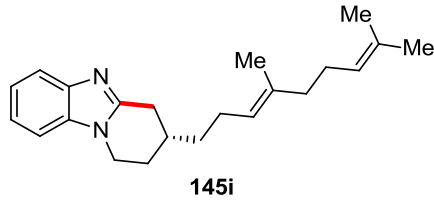
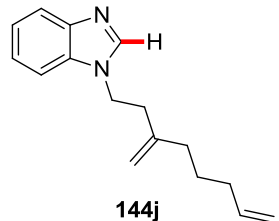
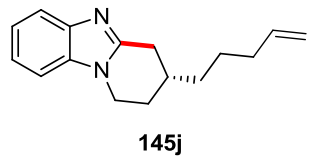
Table 3.19. Substrate scope of *gem*-substituted olefins **144** and heterocycles in the nickel-catalyzed intramolecular hydroarylation.^[a]



| Entry | Substrate | Product | Yield [%] ^[b] | e.r. ^[c] |
|-------|-----------------|-----------------|--------------------------|---------------------|
| 1 | 144a | 145a | 96 | 96:4 |

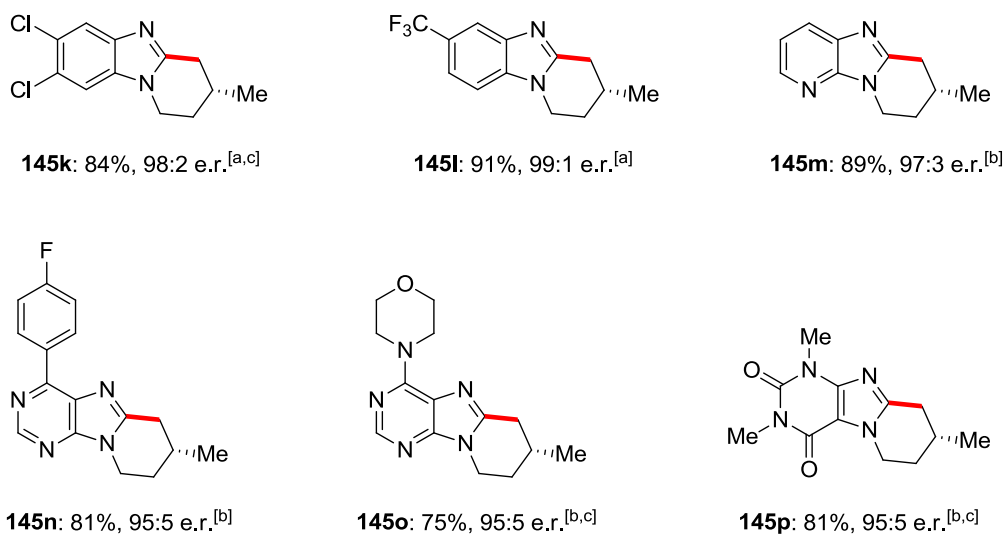
3. Results and Discussion

| | | | | |
|---|--|---|-------------------------|-----------------------------|
| 2 |  <p>144b</p> |  <p>145b</p> | 39 66 ^[d] | 99:1 99:1 ^[d] |
| 3 |  <p>144c</p> |  <p>145c</p> | 88 | 96:4 |
| 4 |  <p>144d</p> |  <p>145d</p> | 85 | 98:2 |
| 5 |  <p>144e</p> |  <p>145e</p> | 81 | 97:3 |
| 6 |  <p>144f</p> |  <p>145f</p> | 83 | 95:5 |
| 7 |  <p>144g</p> |  <p>145g</p> | 87 ^[d] | 98:2 ^[d] |

| | | | | |
|----|---|--|-------------------------|-----------------------------|
| 8 |  <p>144h</p> |  <p>145h</p> | 84 | 97:3 |
| 9 |  <p>144i</p> |  <p>145i</p> | 84 | 99:1 |
| 10 |  <p>144j</p> |  <p>145j</p> | 29 54 ^[d] | 97:3 97:3 ^[d] |

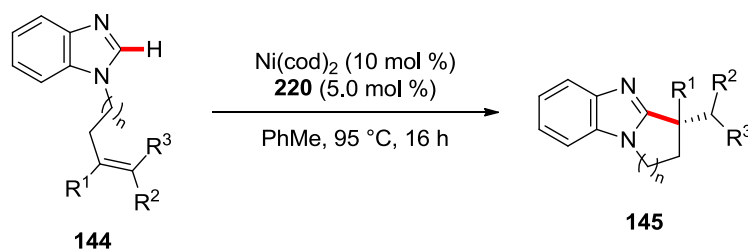
^[a] Reaction conditions: **144** (0.50 mmol), Ni(cod)₂ (5.0 mol %), **220** (2.5 mol %), PhMe (1.0 mL), 95 °C, 16 h. ^[b] Isolated yields. ^[c] Determined by chiral HPLC analysis. ^[d] With Ni(cod)₂ (10 mol %) and **220** (5.0 mol %).

Moreover, numerous additional substrates **144** were tested by *V. Müller* and *Dr. D. Ghori* in the nickel-catalyzed intramolecular hydroarylation, with a focus on the heteroarene moiety. Various substituted benzimidazoles, including electron-rich, electron-poor and polychlorinated derivatives performed well in the reaction, once again showcasing the chemo-selectivity and versatility of the developed organoaluminium-free C–H functionalization methodology (Scheme 3.18). Beside diversely decorated benzimidazoles, a variety of pharmaceutically relevant motifs, including aza-benzimidazoles, highly functionalized purines and theophylline derivatives, were efficiently converted to the cyclized products **145** with high selectivity control.



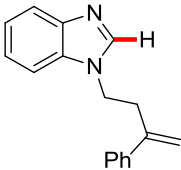
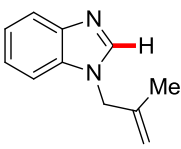
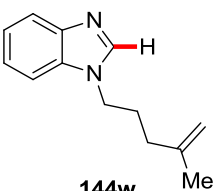
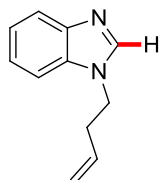
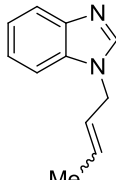
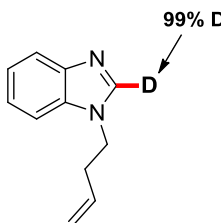
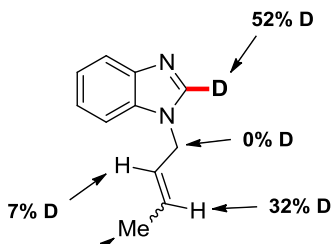
Scheme 3.18. Selected additional examples of the substrate scope. ^[a] Performed by Dr. D. Ghorai. ^[b] Performed by V. Müller. ^[c] With Ni(cod)₂ (10 mol %) and **220** (5.0 mol %).

Further studies were conducted to understand the effect of the substitution pattern of the tethered alkene **144** (Table 3.20). The findings revealed that 1,1-disubstituted alkenes were essential to achieve high conversion and stereo-selectivity, as substrates lacking the *gem*-disubstitution pattern, despite high enantioselectivities, were found to give the 5-membered *exo*-cyclized product **145** in low to moderate yields (entries 1–2). More sterically encumbered substrates, such as **144s** and **144t**, fell short in delivering any cyclized product (entries 3–4). Aryl-substituted alkenes, or alkenes with shorter or longer tethers, gave unsatisfactory results too (entries 5–7). Interestingly, in the case of the unsubstituted substrate **144x**, the isomerized alkene **223** was obtained as the major product of the transformation, which could be supportive of the formation of a nickel-hydride and/or a π -allyl-nickel intermediate (entry 8).^[299b,301] This hypothesis was further substantiated by performing the same reaction with the deuterated analog [D]₁-**144x**, as H/D scrambling was observed along the double bond and the allylic methyl group (entry 9).

Table 3.10. Effect of the substitution pattern of the olefin.^[a]

| Entry | Substrate | Product | Yield [%] ^[b] | e.r. ^[c] |
|-------|--|--|--------------------------|---------------------|
| 1 | <p style="text-align: center;">144q</p> | <p style="text-align: center;">145q</p> | 41 | 97:3 |
| 2 | <p style="text-align: center;">144r</p> | <p style="text-align: center;">145r</p> | 16 | 96:4 |
| 3 | <p style="text-align: center;">144s</p> | --- | n.r. | - |
| 4 | <p style="text-align: center;">144t</p> | --- | n.r. | - |

3. Results and Discussion

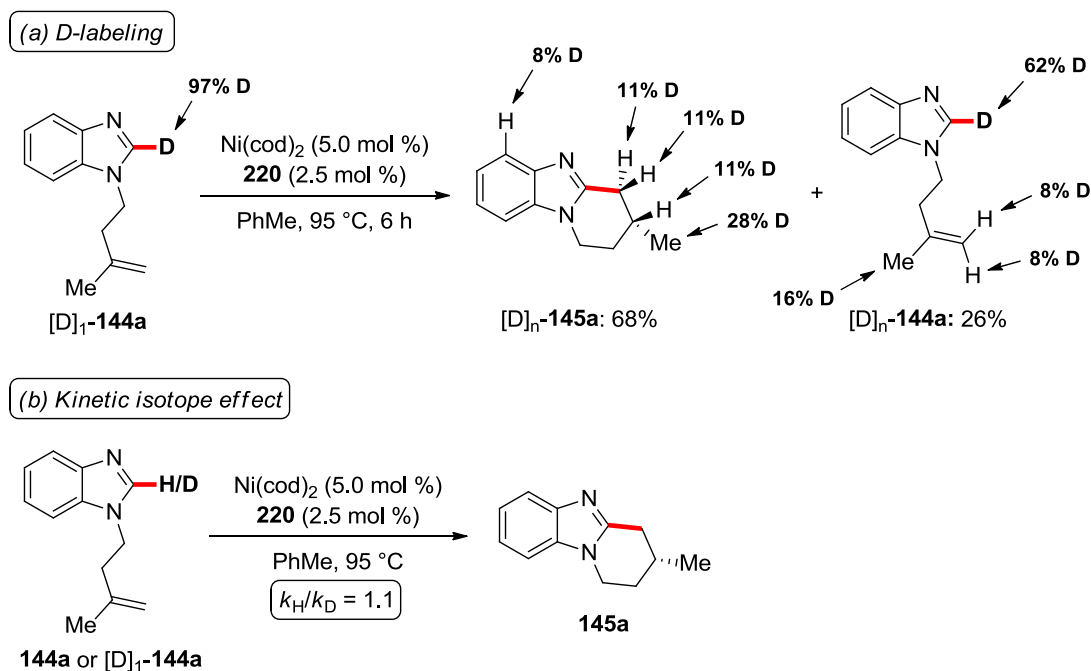
| | | | | |
|------------------|--|---|--------|---|
| 5 |  <p>144u</p> | --- | traces | - |
| 6 |  <p>144v</p> | --- | n.r. | - |
| 7 ^[d] |  <p>144w</p> | --- | n.r. | - |
| 8 |  <p>144x</p> |  <p>223 (E/Z = 4:1)</p> | 74 | - |
| 9 |  <p>[D]₁-144x</p> |  <p>[D]_n-223 (E/Z = 4:1)</p> | 76 | - |

^[a] Reaction conditions: **144** (0.50 mmol), Ni(cod)₂ (10 mol %), **220** (5.0 mol %), PhMe (1.0 mL), 95 °C, 16 h. ^[b] Yield of the isolated product. ^[c] Determined by chiral HPLC analysis. ^[d] Experiment conducted by V. Müller.

3.3.4. Mechanistic Studies

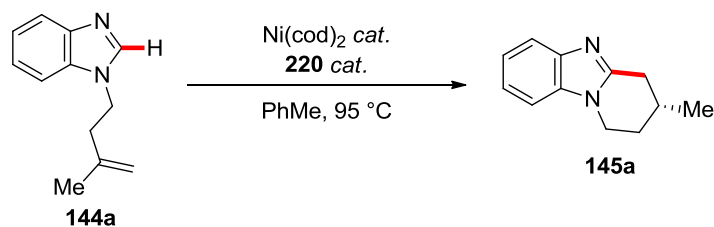
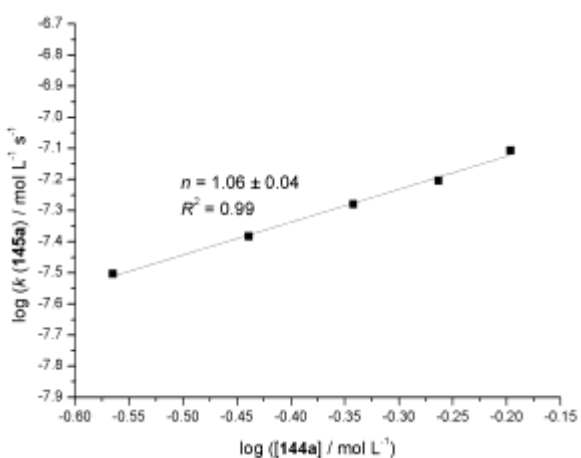
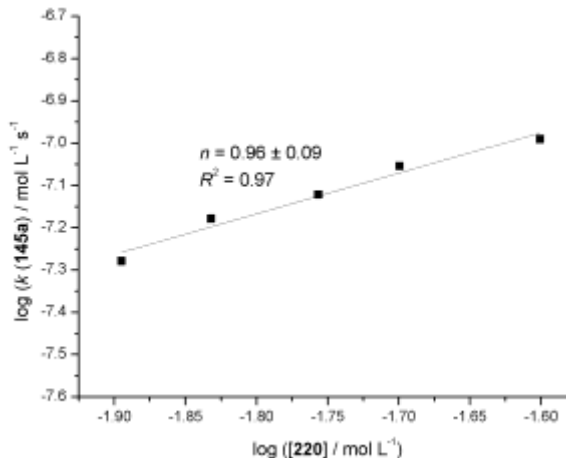
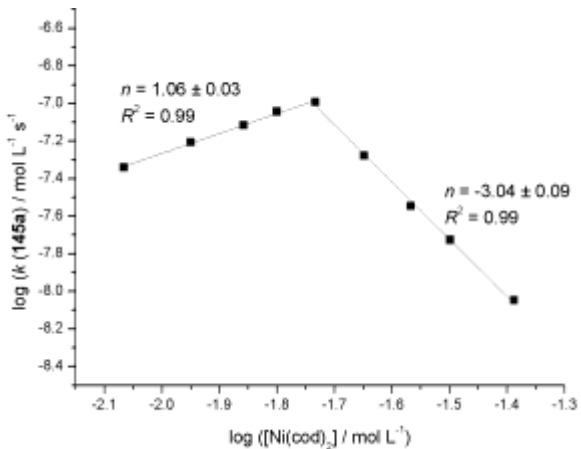
3.3.4.1. Deuterium Labeling Experiments and Kinetic Studies

Given the unique features of the asymmetric aluminium-free nickel-catalyzed C–H alkylation, we became attracted to unravel its mode of action. To this end, experiments with deuterated compounds and detailed kinetic studies were conducted by *V. Müller*.^[220] First, a reaction performed with deuterated substrate $[D]_1\text{-144a}$ revealed H/D scrambling at the methyl group and positions of the former olefin (Scheme 3.20a). This observation can be rationalized with a facile and reversible C–H cleavage step, and is strikingly different from *Ye's* nickel-catalyzed *exo*-selective cyclization in which no scrambling was observed.^[206] Then, C–H activation performed with isotopically labeled compound $[D]_1\text{-144a}$ showed a kinetic isotope effect (KIE) of $k_H/k_D \approx 1.1$ (Scheme 3.20b), suggesting the C–H scission step not to be turnover limiting.^[257]

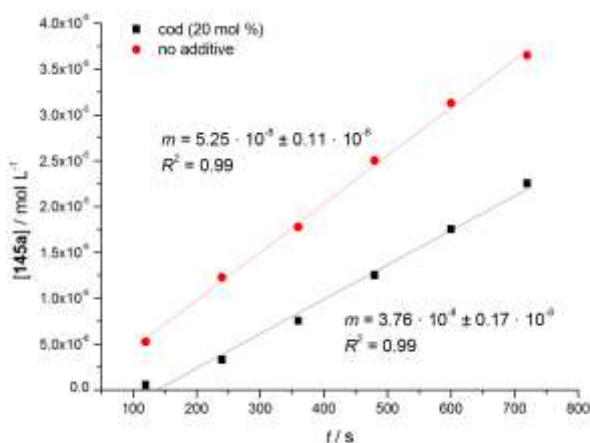


Scheme 3.20. Deuterium labeling experiments. Experiments conducted by *V. Müller*.

Furthermore, detailed kinetic studies conducted by *V. Müller* revealed a first-order rate dependence in the substrate **144**, the pre-ligand **220** and the nickel precursor, in the latter case with an inhibition at higher nickel concentrations (Scheme 3.21a–c). A possible interpretation to this rather unusual finding could be the existence of a critical nickel concentration beyond which an autocatalytic deactivation of the catalyst occurs, possibly *via* aggregation of nickel, as was previously proposed for palladium catalysis.^[302] Another explanation to the detrimental effect of higher concentrations of Ni(cod)₂ could be the competitive coordination of free cod to the nickel center, resulting in off-cycle intermediates decelerating the catalysis, as previously reported by *Zimmerman/Montgomery*.^[161,202b] This hypothesis is further substantiated by the observation that, in the presence of additional free cod, the transformation was found to indeed proceed at a lower rate. This finding provides additional support to the hypothesis that inhibition of the active nickel catalyst is caused by free cod originating from the consumption/degradation of the added Ni(cod)₂ (Scheme 3.21d).^[220]

a) order in substrate **144a**b) order in pre-ligand **220**c) order in Ni(cod)_2 

d) effect of cod on the reaction rate

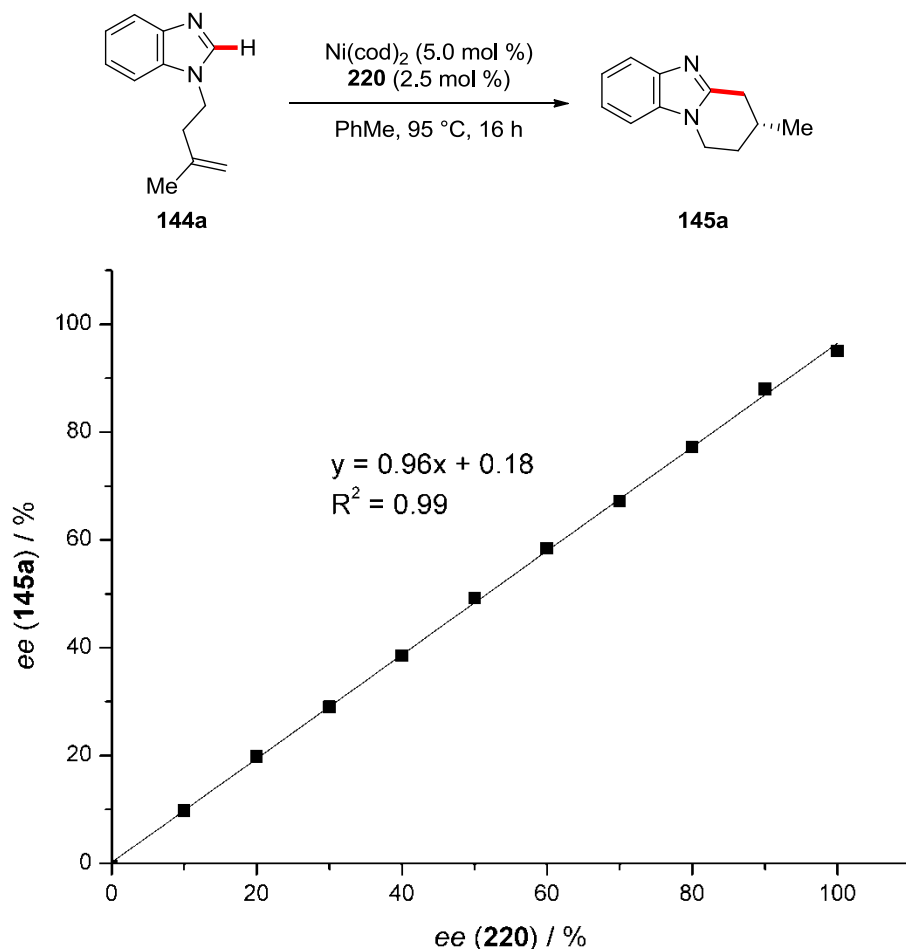


Scheme 3.21. Kinetic analysis nickel-catalyzed hydroarylation. Experiments conducted by V. Müller.

3.3.4.2. Non-Linear Effect Studies

In order to get some insights into the unusual ligand-to-metal ratio of 1:2, the effect of the enantiomeric excess of JoSPoPhos pre-ligand **220** over the enantiomeric induction of the transformation was investigated (Scheme 3.22). Here, the absence

of a non-linear effect (NLE) apparently excludes a multi-ligand containing catalyst or catalytically competent oligomers to be operative in the asymmetric nickel-catalyzed intramolecular hydroarylation.^[259]



Scheme 3.22. Non-linear effect studies.

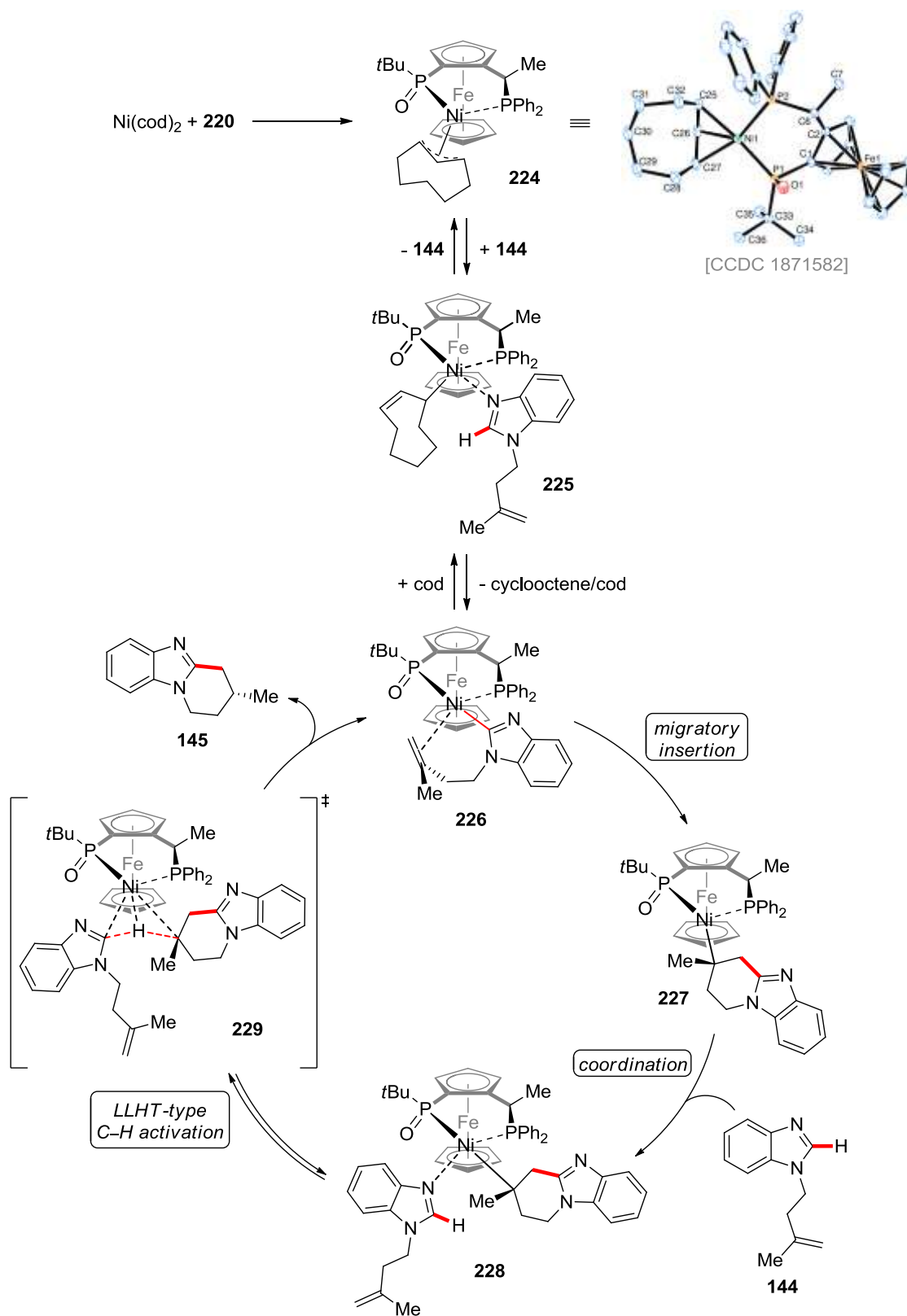
3.3.5. Proposed Mechanism

Based on our detailed mechanistic studies and previous literature reports,^[81,190,202a,303] the catalytic reaction is proposed to be initiated by the formation of the organometallic nickel(II) complex **224** (Scheme 3.23). Complex **224** was prepared by *Dr. D. Ghorai* from a stoichiometric reaction of $\text{Ni}(\text{cod})_2$ with pre-ligand

220, and found to be active in both stoichiometric and catalytic reactions with **144a**.^[220] A plausible pathway for the generation of complex **224** could be the oxidative addition of nickel(0) into the P(O)–H bond, as it has been previously reported in the literature,^[304] followed by hydride migration to the bound cod and chain walking.^[161] It should also be noted that this coordination mode of bidentate ligands containing a phosphine oxide moiety has previously been reported for iridium(I) complexes.^[305] Interestingly, *Pfaltz* and coworkers described the ligand as a *P*-coordinating, *O*-anionic phosphinite rather than a *P*-anionic deprotonated phosphine oxide.^[305]

Complex **224** is then coordinated by substrate **144** to form intermediate **225**, which after loss of a cyclooctene molecule yields intermediate **226**, the proposed active catalyst. Intermediate **226** then undergoes the stereo-determining and C–C bond forming migratory insertion to deliver the cyclized intermediate **227**. After a kinetically relevant coordination of a second substrate **144**, explaining its first-order kinetic dependence, the key C–H activation event occurs. In view of our mechanistic studies, we propose the facile C–H cleavage to occur *via* a ligand-to-ligand hydrogen transfer (LLHT) manifold.^[81,156a,202c,299b,306] The observed H/D scrambling and olefin isomerization are believed to be caused by side-reactions of the catalyst, presumably involving a nickel- π -allyl or a nickel-hydride species which may possibly result from oxidative addition into the P(O)–H bond during the catalyst generation process.

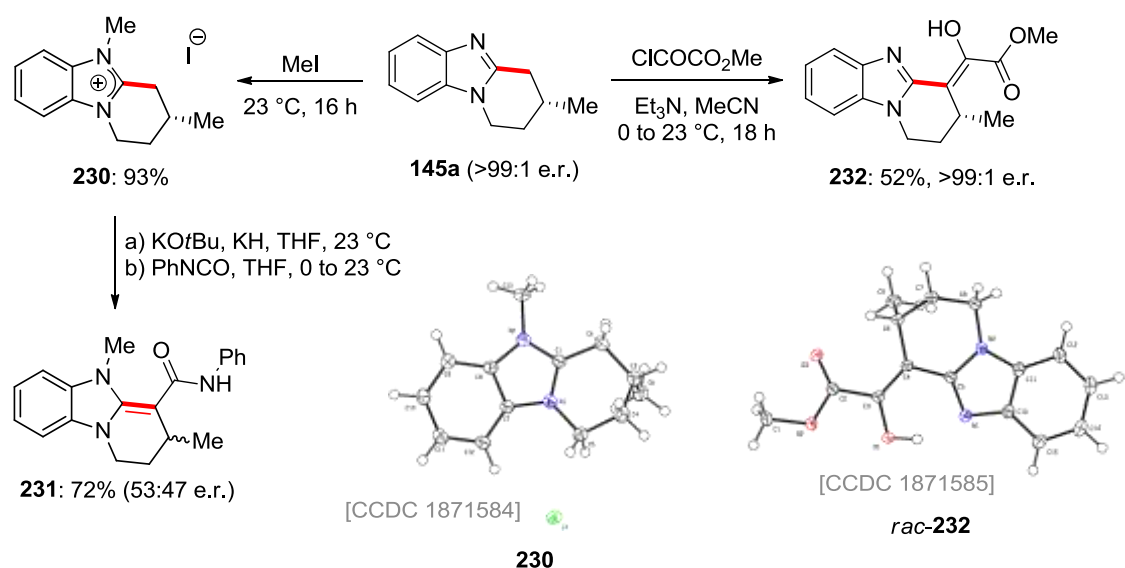
According to the proposed catalytic cycle, complex **224** is a plausible off-cycle intermediate, or a resting state, whose reversible formation is favored by higher concentrations of cod, explaining the negative order in Ni(cod)₂ above a certain concentration (Scheme 3.21c) and rationalizing the detrimental effect of adding an excess of free cod to the catalytic reaction (Schemes 3.21d). Indeed, such cod-incorporating π -allyl complexes are documented to be stable off-cycle intermediates whose formation diminishes the catalytic efficiency.^[161,202b]



Scheme 3.23. Proposed catalytic cycle. Complex **224** was prepared and crystallized by *Dr. D. Ghorai*. The crystal structure was measured and solved by *Dr. C. Golz*.

3.3.6. Product Diversification

The synthetic value of the nickel-catalyzed C–H alkylation was further demonstrated by late-stage diversification of the thus-obtained products (Scheme 3.24). In an attempt to introduce a heavy atom in order to determine the absolute configuration *via* X-ray diffraction crystallography, benzimidazolium iodide **230** was prepared by treating the standard product **145a** with methyl iodide. The *R*-configuration of the cyclized product was confirmed by X-ray diffraction analysis.



Scheme 3.24. Diversification of **145a** and molecular structure of products **230** and **232** with thermal ellipsoids at 50% probability level. The crystal structures were measured and solved by *Dr. C. Golz*.

Thereafter, further transformations of the activated 2-substituent of the benzimidazolium moiety were attempted. The formation of reactive N-heterocyclic olefins (NHO) upon treatment of 2-alkylimidazolium with a base is indeed well documented.^[307] The resulting electron-rich NHO intermediate was successfully trapped using phenyl isocyanate as the electrophile to provide amide **231** in good yield. Unfortunately, the product was obtained as a racemic mixture, presumably due to base-induced racemization of the activated allylic position during the process.

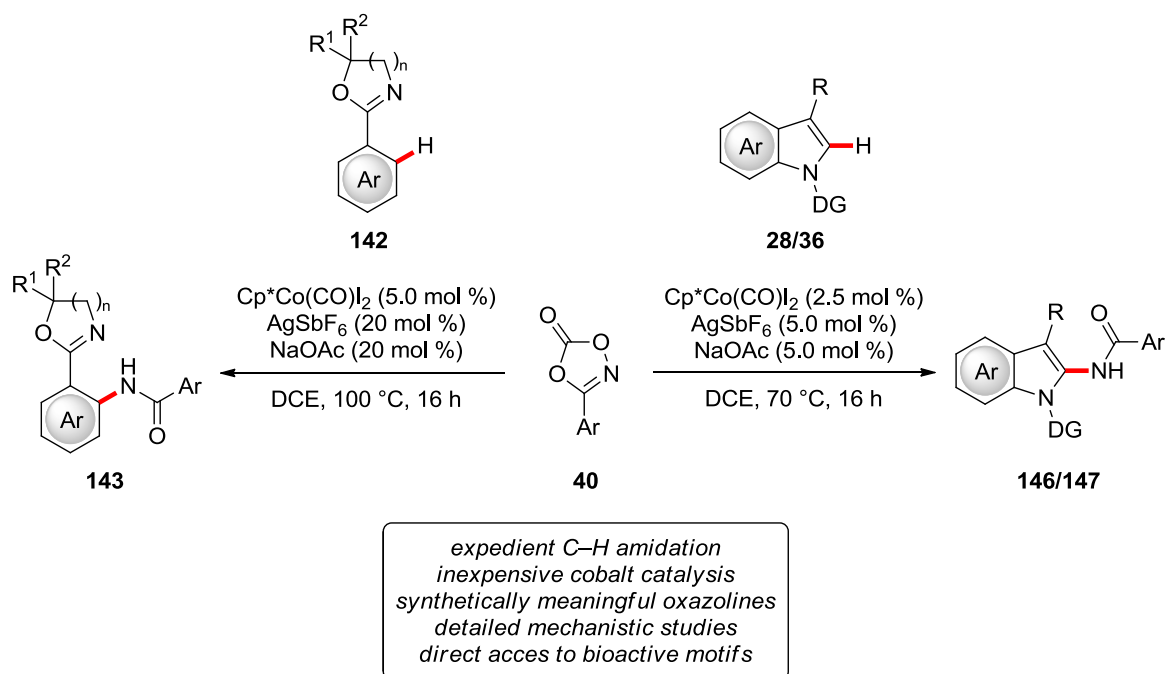
Therefore, we aimed to functionalize the same position under milder conditions. To our delight, the cyclized product **145a** could be directly functionalized under racemization-free conditions using a procedure reported by *Roush*^[308] to provide α -keto-ester **232**, whose structure was unambiguously confirmed by X-ray diffraction analysis. Interestingly, such polycyclic α -keto esters are regarded as valuable synthetic intermediates for the synthesis of antiviral agents.^[308]

Overall, the synthetic utility of the developed enantioselective nickel-catalyzed hydroarylation was further showcased by late-stage diversification of the obtained products, as pharmaceutically relevant motifs could be obtained under racemization-free conditions.

4. Summary and Outlook

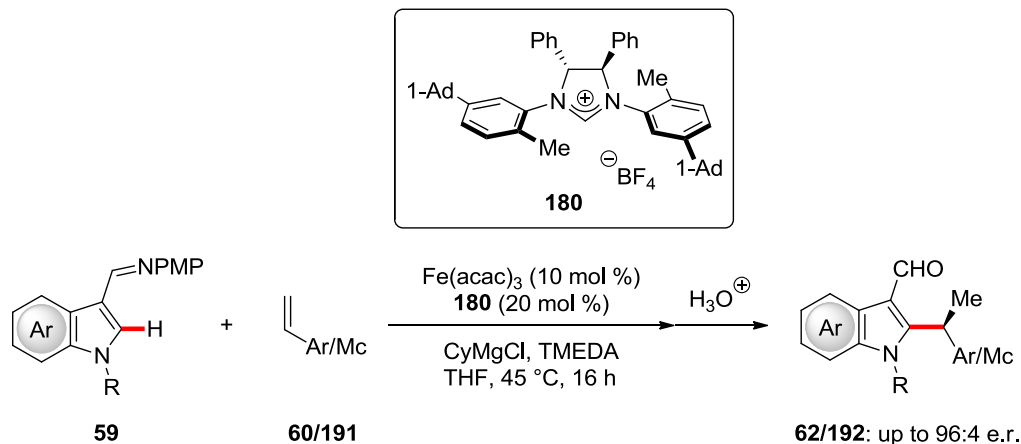
Organic synthesis has long relied on time- and energy-consuming prefunctionalization strategies which generate stoichiometric amounts of waste. Recently, the direct functionalization of C–H bonds has emerged as an environmentally benign alternative that avoids lengthy syntheses, and has attracted substantial interest from both academia and the chemical industries. However, the selective functionalization of omnipresent C–H bonds remains challenging and hence a research topic of high interest. While major progress was initially achieved with noble transition metal catalysts, the use of inexpensive and earth-abundant 3d metals has gained significant momentum within the last decade.

In the first project, the first cobalt-catalyzed C–H functionalization by the assistance of synthetically useful oxazolines was developed (Scheme 4.1).^[37e,227a] Previous work on catalytic C–H aminations had relied on noble transition metal catalysts or harsh reaction conditions.^[23e,217] The versatile, robust and user-friendly Cp*Co(III) catalyst allowed for the direct C–H amidation of arenes and indoles using dioxazolones **40** as amidating reagents under the assistance of, *inter alia*, oxazolinylyl, pyridyl and pyrimidyl directing groups. Mechanistic studies provided strong support for a kinetically relevant C–H cobaltation *via* an acetate-enabled BIES manifold, and revealed the transformation to be homogenous in nature. Radical intermediates were excluded by reactions conducted in the presence of radical scavengers.



Scheme 4.1. Cobalt(III)-catalyzed C–H amidation.

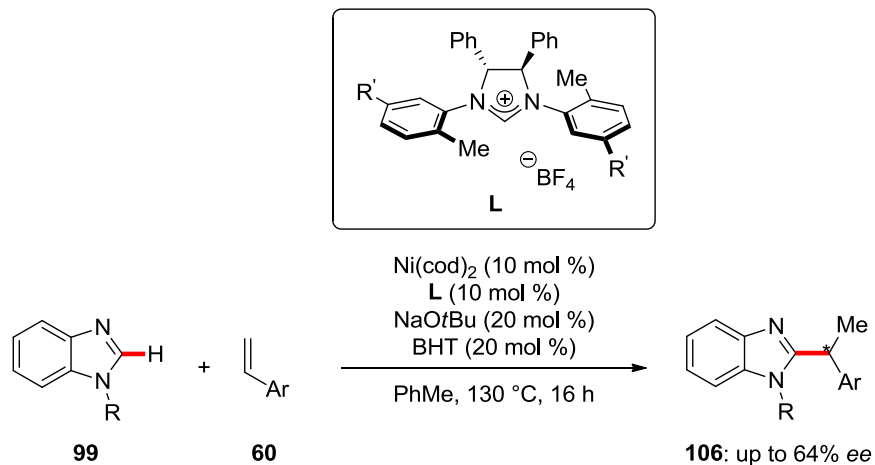
While significant progress in the field of first-row transition metal-catalyzed C–H activation was achieved within the last decade,^[45] enantioselective transformations continue to heavily rely on noble 4d and 5d metals.^[51] However, the last few years have witnessed the emergence of 3d-metal catalyzed asymmetric C–H activations, but examples remain scarce as this research area is still in its infancy.^[52] In this context, the first enantioselective iron-catalyzed C–H functionalization by inner-sphere C–H activation was developed (Scheme 4.2).^[151] In the course of extensive optimization studies, the design of the novel *meta*-substituted NHC precursor **180** was found to be critical to success. A broad range of indoles and azaindoles **59** proved viable substrates in the hydroarylation of diversely substituted styrenes **60** and vinylmetallocenes **191**, providing the products **62/192** in up to 96:4 e.r. and complete branched-selectivity. Remarkably, this work constitutes the first and, so far, only highly enantioselective transformation *via* inner-sphere iron-catalyzed C–H activation. Moreover, this work also represents the unprecedented use of a chiral NHC ligand in enantioselective iron catalysis.



Scheme 4.2. Enantioselective iron-catalyzed C–H alkylation.

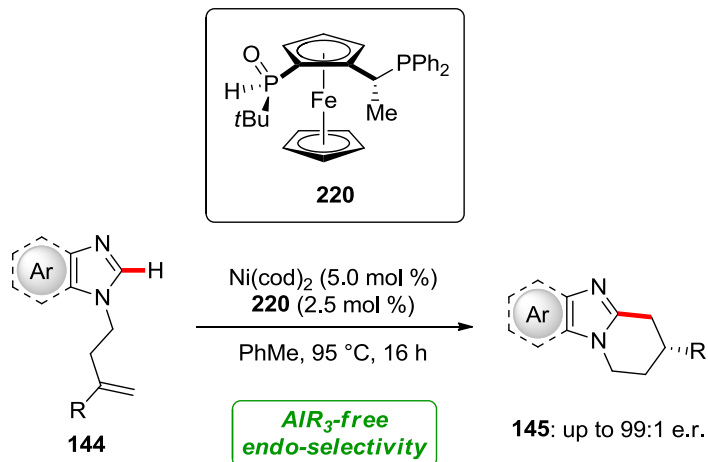
Detailed mechanistic studies were conducted to delineate the mechanism of the transformation. Our findings support a facile C–H cleavage occurring through a ligand-to-ligand hydrogen transfer manifold, and revealed the reaction to be homogenous in nature. Furthermore, kinetic studies unravelled a first-order dependence in the indole substrate **59** and a rather uncommon zeroth order in the alkene **60**. Additionally, an *in situ* analysis of the transformation by electrospray-ionization mass spectrometry and ^{57}Fe Mössbauer spectroscopy was performed and supports an organometallic mono-NHC-ligated iron(II) species to be involved in the catalysis.^[218] Remarkably, while “low-valent” iron species have initially been proposed to be active in iron-catalyzed C–H activations in the presence of Grignard reagents, this work provides the first direct evidence of an iron(II) species in such processes.

Thereafter, we then became interested in the development of new enantioselective transformations employing our novel chiral NHC pre-ligands. Among the attempted reactions, asymmetric nickel-catalyzed hydroarylations appeared most promising. Significant enantioselectivities were observed in preliminary studies on intermolecular undirected C–H alkylations of benzimidazoles **99** with styrenes **60** (Scheme 4.3). While the observed enantioselectivities are only moderate, this transformation represents the first example of enantioselective undirected intermolecular nickel-catalyzed C–H activations.



Scheme 4.3. Enantioselective nickel-catalyzed intermolecular hydroarylations.

Finally, drawing inspiration from those preliminary results, we devised the first asymmetric *endo*-selective cyclization of azoles with alkenes (Scheme 4.4).^[220] Remarkably, in sharp contrast to other nickel-catalyzed intramolecular hydroarylations with unactivated alkenes,^[193,195,200,203,206] the developed methodology obviates the need for pyrophoric organoaluminium reagents.^[309] Various substituted benzimidazoles **144**, including electron-rich, electron-poor and polychlorinated derivatives performed well in the transformation. Moreover, the reaction was not limited to benzimidazoles since a broad variety of bioactive heterocyclic motifs, including highly functionalized purines and theophylline derivatives, were smoothly converted to the cyclized products **145** under the optimized reaction conditions. Furthermore, the transformation was found to be highly chemoselective, as for substrates bearing several olefinic motifs solely reacted at the proximal alkene, with the distal olefins remaining untouched. The detailed mechanistic studies provide support to the formation of an organometallic nickel(II) species as the active catalyst and a facile C–H cleavage step occurring through a LLHT manifold. Finally, the absence of a non-linear effect is indicative of a mono-ligated nickel catalyst to be operative in the asymmetric hydroarylation.



Scheme 4.4. Enantioselective nickel-catalyzed intramolecular hydroarylations.

Given the topical interest for 3d metal-catalyzed C–H activation, further exciting developments in this rapidly-evolving research area are anticipated in the near future.

5. Experimental Part

5.1. General Remarks

All reactions involving air- and/or moisture-sensitive compounds were conducted under a dry nitrogen atmosphere using pre-dried glassware and standard Schlenk techniques. If not otherwise noted, yields refer to isolated compounds which were estimated to be >95% pure based on ^1H NMR and/or GC analysis.

Vacuum

The following average pressure was measured on the used rotary vane pump RD4 from Vacuubrand[®]: $0.8 \cdot 10^{-1}$ mbar (uncorrected value).

Melting Points

Melting points were measured on a Stuart[®] Melting Point Apparatus SMP3 from Barloworld Scientific. Values are uncorrected.

Chromatography

Analytical thin layer chromatography (TLC) was performed on silica gel 60 F254 aluminium sheets from Merck. Plates were either visualized under irradiation at 254 nm or 365 nm or developed by treatment with a potassium permanganate solution followed by careful warming. Chromatographic purifications were accomplished by column chromatography on Merck Geduran[®] silica gel, grade 60 (40–63 μm , 70–230 mesh ASTM).

Infrared Spectroscopy

IR spectra were recorded using a Bruker[®] Alpha-P ATR spectrometer. Liquid samples were measured as film and solid samples neat. Spectra were recorded in the range from 4000 to 400 cm^{-1} . Analysis of the spectral data was carried out using Opus 6. Absorption is given in wave numbers (cm^{-1}).

Nuclear Magnetic Resonance Spectroscopy

NMR spectra were recorded on Mercury Plus 300, VNMRS 300, Inova 500 and 600 from Varian[®], or Avance 300, Avance III 300 and 400, Avance III HD 400 and 500 from Bruker[®]. Chemical shifts are reported in δ -values in ppm relative to the residual proton peak or carbon peak of the deuterated solvent.

| | ¹ H NMR | ¹³ C NMR |
|------------------------|--------------------|---------------------|
| CDCl ₃ | 7.26 | 77.16 |
| DMSO-d ₆ | 2.50 | 39.52 |
| Benzene-d ₆ | 7.16 | 128.06 |
| MeOH-d ₄ | 3.31 | 49.00 |

The coupling constants J are reported in hertz (Hz). Analysis of the recorded spectra was carried out using MestReNova 10.0 software.

Gas Chromatography

Monitoring of reaction process *via* gas chromatography or coupled gas chromatography-mass spectrometry was performed using a 7890 GC-system with/without mass detector 5975C (Triple-Axis-Detector) or a 7890B GC-system coupled with a 5977A mass detector, both from Agilent Technologies[®].

Mass Spectrometry

Electron ionization (EI) and EI high resolution mass spectra (HR-MS) were measured on a time-of-flight mass spectrometer AccuTOF from JEOL. Electrospray ionization (ESI) mass spectra were recorded on an Io-Trap mass spectrometer LCQ from Finnigan, a quadrupole time-of-flight maXis from Bruker Daltonic or on a time-of-flight mass spectrometer microTOF from Bruker Daltonic. ESI-HR-MS spectra were recorded on a Bruker Apex IV or Bruker Daltonic 7T, Fourier transform ion cyclotron resonance (FTICR) mass spectrometer. The ratios of mass to charge (m/z) are indicated, intensities relative to the base peak ($I = 100$) are written in parentheses.

Chiral HPLC

Chiral HPLC chromatograms were recorded on an Agilent 1290 Infinity using CHIRALPAK[®] IA-3, IB-3, IC-3, ID-3, IE-3 and IF-3 columns (3.0 μm particle size; \varnothing : 4.6 mm and 250 mm length) at ambient temperature.

Specific Rotations

Optical rotations were measured on a Jasco P-2000 or an Anton Paar MCP 150 polarimeter using a 10 cm cell with a Na 589 nm filter. Concentrations are indicated in g / 100 mL.

Mössbauer Spectroscopy

Mössbauer spectra were recorded with a ⁵⁷Co source in a Rh matrix using an alternating constant acceleration *Wissel* Mössbauer spectrometer operated in the transmission mode and equipped with a *Janis* closed-cycle helium cryostat. Isomer shifts are given relative to iron metal at ambient temperature. Simulation of the

experimental data was performed with the *Mfit* program using *Lorentzian* line doublets.^[310]

Solvents

All solvents for reactions involving air- and/or moisture-sensitive reagents were dried, distilled and stored under an inert atmosphere (dry nitrogen) according to the following standard procedures.

1,2-Dichloroethane (DCE), *N*-methyl-2-pyrrolidone (NMP) and 1,3-dimethyl-3,4,5,6-tetrahydro-2(1*H*)-pyrimidinone (DMPU) were dried over CaH₂ for 8 h, degassed and distilled under reduced pressure. 1,4-Dioxane, di-*n*-butylether (*n*Bu₂O) and *tert*-amyl alcohol (*t*AmOH) were dried over Na for 8 h, degassed and distilled under reduced pressure.

CH₂Cl₂, DMF, THF, Et₂O and PhMe were obtained from a MBRAUN MB SPS-800 solvent purification system.

Chemicals

Chemicals obtained from commercial sources with a purity >95% were used as received without further purification. CyMgCl was prepared from chlorocyclohexane and magnesium turnings in anhydrous THF under nitrogen atmosphere, and titrated before use with I₂/LiCl.^[311] Pre-ligands **220** (commercial name: SL-J681-1), *ent*-**220** (SL-J681-2), and **168** (SL-J688-1) were obtained from Solvias AG.

The following compounds were known from the literature and synthesized according to previously known methods:

Dioxazolone **40a**,^[229b] 2-aryl oxazines **142**,^[312] (pyridin-2-yl)-1*H*-indoles **28** and (pyrimidin-2-yl)-1*H*-indoles **36**,^[313] Cp*Co(CO)I₂,^[86] RuTPP(CO),^[314] indoles **59c**, **59b** and [D]₁-**59b**,^[105] indole **59a**,^[106] chiral NHC precursors **153** and **154**,^[211] **158**,^[315]

159,^[316] **160**^[241] and **179**,^[243] phosphoramidites **161**^[106] and **212**,^[317] SchmalzPhos **163**,^[318] HASPO **169** and phosphine chloride **170**,^[195] iron complex **173**,^[319] diamine **175**,^[320] styrenes **60f**, **60h**, **60i** and **60j**,^[321] (*Z*)-trimethyl(styryl)silane **60n**,^[322] vinylthiophene **60p**,^[323] vinylferrocene **191a**,^[324] vinylruthenocene **191b**,^[325] 1-vinyl-1',2',3',4',5'-pentamethylferrocene **191c**,^[326] benzimidazole **144a**,^[219b] benzimidazoles **144r**, **144s**, **144x**, and [D]₁-**144x**,^[206] and TADDOL-SPOs **131**, **216** and **217**.^[206,207]

The following compounds were kindly synthesized and provided by the persons listed below:

Karsten Rauch: IMes·HCl, IPr·HCl, (HA)SPOs **164–167**, **214** and **215**, [RuCl₂(*p*-cymene)]₂, [Cp*RhCl₂]₂, dry and/or degassed solvents (DCE, *t*AmOH, 1,4-dioxane, NMP, H₂O).

Dr. Ruhuai Mei: oxazolines **142j**, **142p** and **142r**, indole **36a**, [Cp*Co(CO)]₂.

Sven C. Richter: IXyl·HCl.

Dr. Sebastian Lackner: PyBOX ligand **174**.

Dr. Marc Moselage: CAAC precursor **157**, dry DMPU.

Dr. Gianpiero Cera: ligand **172**.

Dr. Tobias Parchomyk (Koszinowski research group): ⁵⁷FeCl₂.

Dr. Nicolas Sauermann: [Cp*CoI₂]₂, dry DMPU.

Dr. Thomas Müller: *N*-Bn-benzimidazole **99b**.

Dr. Hui Wang: [Cp*Co(MeCN)₃](SbF₆)₂ (**26**) and NaO₂C-Ile-Ac.

Dr. Alexander Bechtoldt: dienes **112a** and **112b**.

Prof. Dr. E. Peter Kündig and coworkers (Université de Genève): chiral NHC precursors **159'** and **193**.

Prof. Dr. Hintermann and coworkers (Technische Universität München): SPO **222**.

Prof. Dr. Albrecht Berkessel and coworkers (Universität zu Köln): NHC precursor **156**.

5.2. General Procedures

General Procedure for the Cobalt-Catalyzed C–H Amidation of 2-Aryloxazolines **142** (GP1)

2-Aryloxazoline **142** (0.50 mmol, 1.0 equiv), dioxazolone **40** (0.60 mmol, 1.2 equiv), Cp*Co(CO)I₂ (11.9 mg, 0.025 mmol, 5.0 mol %), AgSbF₆ (34 mg, 0.10 mmol, 20 mol %) and NaOAc (8.2 mg, 0.10 mmol, 20 mol %) were placed into an oven-dried 25 mL Schlenk tube equipped with a septum under N₂ atmosphere. DCE (2.0 mL) was introduced *via* cannula. The reaction mixture was stirred at 100 °C for 16 h. After cooling to ambient temperature, the reaction mixture was dry loaded onto silica gel and purified by flash column chromatography (*n*-hexane/EtOAc) to afford the desired product **143**.

General Procedure for the Cobalt-Catalyzed C–H Amidation of Indoles **28/36** (GP2)

Indole **28/36** (0.50 mmol, 1.0 equiv), dioxazolone **40** (0.60 mmol, 1.2 equiv), Cp*Co(CO)I₂ (5.9 mg, 0.0125 mmol, 2.5 mol %), AgSbF₆ (8.6 mg, 0.025 mmol, 5.0 mol %) and NaOAc (2.1 mg, 0.025 mmol, 5.0 mol %) were placed into an oven-dried 25 mL Schlenk tube equipped with a septum under N₂ atmosphere. DCE (2.0 mL) was introduced *via* cannula. The reaction mixture was stirred at 70 °C for 16 h. After cooling to ambient temperature, the reaction mixture was dry loaded onto silica gel and purified by flash column chromatography (*n*-hexane/EtOAc) to afford the desired product **146/147**.

General Procedure for the Synthesis of Indoles **59** (GP3)

A solution of 3-formylindole (3.44 mmol, 1.0 equiv) in anhydrous DMF (35 mL) was cooled to 0 °C. NaH (165 mg, 4.13 mmol, 1.2 equiv, 60% in mineral oil) was then added portionwise under ice-cooling. The resulting suspension was stirred at 0 °C

for 15 min, then allowed to warm up to ambient temperature and stirred for 1 h. The reaction mixture was then cooled to 0 °C, and the corresponding alkyl halide (4.13 mmol, 1.2 equiv) was added slowly under ice cooling. The resulting suspension was stirred at 0 °C for 15 min, then stirred overnight at the indicated temperature (23 °C for benzyl bromides, methoxymethyl chloride and 2-bromo-1,1-difluoroethane, 60 °C for other alkyl halides). The reaction mixture was cooled to 0 °C, poured into sat. aqueous NH₄Cl (100 mL), and extracted with EtOAc (3 × 100 mL). The combined organic phases were washed with H₂O (3 × 100 mL) and brine (50 mL), dried over Na₂SO₄, and concentrated under reduced pressure. The residue was triturated with *n*-hexane to provide the product **204**, which was used in the next step without further purification.

The crude product **204** was suspended in PhMe (15 mL) at ambient temperature. *p*-Anisidine (467 mg, 3.79 mmol, 1.1 equiv) and activated 4 Å MS (5.0 g) were then added in one portion. The resulting suspension was stirred at 60 °C for 16 h. The suspension was allowed to cool to ambient temperature and filtered. The filtrate was concentrated under reduced pressure. The residue was recrystallized from *n*-hexane/CH₂Cl₂/isopropanol. The crystals were collected by filtration, washed with cold pentane and dried under vacuum to provide the pure imine **59**.

The analytical data of (aza)indoles **59** have been reported elsewhere^[151] and are not included in this thesis.

General Procedure for the Synthesis of Chiral Imidazolinium Salts (GP4)

Following a modified procedure,^[211] Pd(OAc)₂ (16.0 mg, 71 μmol, 5.0 mol %), (+/-)-BINAP (88.0 mg, 0.14 mmol, 10 mol %), and NaOtBu (410 mg, 4.26 mmol, 3.0 equiv) were added under nitrogen atmosphere to anhydrous PhMe (25 mL) and stirred for 30 min at ambient temperature. (*R,R*)-Diphenylethylenediamine (300 mg, 1.42 mmol, 1.0 equiv) and the corresponding aryl bromide (2.98 mmol, 2.1 equiv) were then added and the solution was stirred at 100 °C for 16 h. The solution was cooled to ambient temperature, diluted with *n*-hexane (75 mL), and filtered through a

plug of silica. The silica was washed with *n*-hexane/CH₂Cl₂ = 1/1 to elute the product. The volatiles were removed *in vacuo*. The residue was purified by rapid flash chromatography (*n*-hexane/CH₂Cl₂) to provide the crude *N,N'*-diarylated diamine. The crude *N,N'*-diarylated diamine (1.0 equiv), ammonium tetrafluoroborate (1.2 equiv) were stirred in triethyl orthoformate at 120 °C for 5 h. The solution was then allowed to cool to ambient temperature. The reaction mixture was dry loaded onto silica gel and purified by column chromatography (CH₂Cl₂/acetone or *n*-hexane/acetone).

General Procedures for the Iron-catalyzed Enantioselective C–H Alkylation with Solid Alkenes (GP5)

In an oven-dried 25 mL Schlenk tube were placed the indole substrate **59** (0.25 mmol, 1.0 equiv), Fe(acac)₃ (8.8 mg, 0.025 mmol, 10 mol %), **180** (38 mg, 0.050 mmol, 20 mol %) and vinylarene **60** or **191** (0.38 mmol, 1.5 equiv). The Schlenk tube was closed with a rubber septum, then evacuated and backfilled with nitrogen 3 times. THF (0.50 mL) and TMEDA (58 mg, 0.50 mmol, 2.0 equiv) were added *via* syringe. CyMgCl (0.28 mmol, 1.1 equiv, typically 1M) was then added dropwise at ambient temperature. The resulting mixture was stirred at 45 °C for 16 h. The reaction mixture was allowed to cool to ambient temperature and diluted with THF (1.5 mL). HCl (3.0 M, 2.0 mL) was added in a single portion, and the resulting mixture was stirred at ambient temperature for 2 h. The mixture was poured into sat. aqueous NH₄Cl (10 mL) and extracted with EtOAc (3 × 10 mL). The combined organic layers were washed with brine (10 mL), dried over Na₂SO₄, and concentrated under reduced pressure. The residue was purified by silica gel chromatography (*n*-hexane/EtOAc) to afford the desired product **62/192**.

General Procedures for the Iron-catalyzed Enantioselective C–H Alkylation with Liquid Alkenes (GP6)

In an oven-dried 25 mL Schlenk tube were placed the indole substrate **59** (0.25 mmol, 1.0 equiv), Fe(acac)₃ (8.8 mg, 0.025 mmol, 10 mol %) and **180** (38 mg, 0.050 mmol, 20 mol %). The Schlenk tube was closed with a rubber septum, then evacuated and backfilled with nitrogen 3 times. THF (0.50 mL), TMEDA (58 mg, 0.50 mmol, 2.0 equiv) and vinylarene **60** (0.38 mmol, 1.5 equiv) were added *via* syringe. CyMgCl (0.28 mmol, 1.1 equiv, typically 1M) was then added dropwise at ambient temperature. The resulting mixture was stirred at 45 °C for 16 h. The reaction mixture was allowed to cool to ambient temperature and diluted with THF (1.5 mL). HCl (3.0 M, 2.0 mL) was added in a single portion, and the resulting mixture was stirred at ambient temperature for 2 h. The mixture was poured into sat. aqueous NH₄Cl (10 mL) and extracted with EtOAc (3 × 10 mL). The combined organic layers were washed with brine (10 mL), dried over Na₂SO₄, and concentrated under reduced pressure. The residue was purified by silica gel chromatography (*n*-hexane/EtOAc) to afford the desired product **62**.

General Procedure for the Synthesis of Racemic Alkylated Indoles 62/192 (GP7)

General procedures **GP5** or **GP6** were followed using 1,3-bis(2,6-dimethylphenyl)-1*H*-imidazol-3-ium chloride (IXyl-HCl) (7.8 mg, 25 μmol, 10 mol %) instead of **180**.

General Procedure for the Iron-Catalyzed Hydroarylation of Alkynes 7 (GP8)

In an oven-dried 25 mL Schlenk tube were placed the indole substrate **59** (0.25 mmol, 1.0 equiv), Fe(acac)₃ (8.8 mg, 0.025 mmol, 10 mol %), **L** (0.050 mmol, 20 mol %) and tolane **7** (0.50 mmol, 2.0 equiv). The Schlenk tube was closed with a rubber septum, then evacuated and backfilled with nitrogen 3 times. THF (0.50 mL) was added *via* syringe. PhMgCl (0.14 mL, 0.28 mmol, 1.1 equiv, 1.9 M) was then

added dropwise at ambient temperature. The resulting mixture was stirred at 60 °C for 16 h. The reaction mixture was allowed to cool to ambient temperature and diluted with THF (1.5 mL). HCl (3.0 M, 2.0 mL) was added in a single portion, and the resulting mixture was stirred at ambient temperature for 2 h. The mixture was poured into sat. aqueous NH₄Cl (10 mL) and extracted with EtOAc (3 × 10 mL). The combined organic layers were washed with brine (10 mL), dried over Na₂SO₄, and concentrated under reduced pressure. The residue was purified by silica gel chromatography (*n*-hexane/EtOAc) to afford the desired product.

The analytical data are in accordance with those previously reported in the literature.^[148]

General Procedure for the Enantioselective Nickel-Catalyzed Intermolecular Hydroarylation (GP9)

An oven-dried 25 mL Schlenk tube was charged with *N*-benzylbenzimidazole **99b** (104 mg, 0.50 mmol, 1.0 equiv) and **L** (10 mol %, 50 μmol), and introduced into a nitrogen-filled glovebox. Ni(cod)₂ (13.8 mg, 50 μmol, 10 mol %), NaOtBu (9.6 mg, 0.10 mmol, 20 mol %) and PhMe (2.0 mL) were then added. The resulting mixture was stirred at ambient temperature for 3 min. BHT (22.0 mg, 0.10 mmol, 20 mol %) was then added, followed by 4-methoxystyrene **60c** (134 mg, 1.0 mmol, 2.0 equiv). The Schlenk tube was closed, taken out of the glovebox, placed in a pre-heated oil bath at 130 °C and stirred for 16 h. The reaction mixture was allowed to cool to ambient temperature, diluted with EtOAc (5.0 mL), filtered through a short plug of SiO₂, rinsed with EtOAc (3 × 10 mL) and concentrated under reduced pressure. The residue was purified by column chromatography on silica gel (*n*-hexane/EtOAc = 4.5/1→3/1) to yield **106bc** as a colorless oil.

General Procedure for the Synthesis of Alkene-Tethered Azoles 144 (GP10)

Following a modified procedure,^[193] MsCl (1.2 equiv) was added dropwise to a solution of the unsaturated alcohol (1.0 equiv), Et₃N (1.5 equiv) and DMAP (5.0 mol %) in dry CH₂Cl₂ (0.10 M) at 0 °C. The reaction mixture was allowed to warm to 23 °C, stirred for 16 h, and diluted with CH₂Cl₂ to 4 × the initial volume. The obtained solution was washed successively with 2M HCl (twice), sat. aqueous NaHCO₃, brine and dried (Na₂SO₄). Concentration under reduced pressure afforded the crude mesylate which was used in the next step without further purification.

A solution of benzimidazole (500 mg, 4.23 mmol, 1.00 equiv) in anhydrous DMF (40 mL) was cooled to 0 °C. NaH (203 mg, 5.08 mmol, 1.20 equiv, 60% in mineral oil) was then added portionwise under ice-cooling. The resulting suspension was stirred at 0 °C for 15 min, then allowed to warm up to ambient temperature and stirred for 1 h. The reaction mixture was then cooled to 0 °C, and the corresponding mesylate (5.08 mmol, 1.2 equiv) was added slowly under ice cooling. The resulting suspension was stirred at 0 °C for 15 min, then stirred at 23 °C for 16 h. The reaction mixture was cooled to 0 °C, poured into sat. aqueous NH₄Cl (100 mL), and extracted with EtOAc (3 × 100 mL). The combined organic phases were washed with H₂O (4 × 100 mL) and brine (50 mL), dried over Na₂SO₄, and concentrated under reduced pressure. The residue was purified by column chromatography on silica gel (*n*-hexane/EtOAc).

The analytical data of alkene-tethered azoles **144** have been reported elsewhere^[220] and are not included in this thesis.

General Procedure for the Nickel-Catalyzed Enantioselective Intramolecular Hydroarylation (GP11)

An oven-dried 25 mL Schlenk tube was charged with substrate **144** (0.50 mmol, 1.0 equiv), Ni(cod)₂ (6.9 mg, 25 μmol, 5.0 mol %), **220** (6.3 mg, 12.5 μmol, 2.5 mol %) and PhMe (1.0 mL) under N₂. The Schlenk tube was closed with a rubber

septum and placed in a pre-heated oil bath at 95 °C. The reaction mixture was stirred at 95 °C for 16 h, then cooled to ambient temperature and diluted with EtOAc (5 mL). The mixture was filtered through a short plug of silica gel, rinsed with EtOAc (4 × 10 mL) and concentrated under reduced pressure. The residue was purified by column chromatography on silica gel (*n*-hexane/EtOAc) to provide the product **145**.

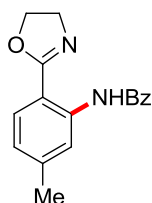
General Procedure for the Nickel-Catalyzed Racemic Intramolecular Hydroarylation (GP12)

The general procedure **GP11** was followed using Ni(cod)₂ (13.8 mg, 50 μmol, 10 mol %), AlMe₃ (0.10 mL, 0.20 mmol, 0.40 equiv, 2M in PhMe) and *rac*-Ph(*t*Bu)P(O)H (9.1 mg, 50 μmol, 10 mol %) instead of **220**.

5.3. Cobalt(III)-Catalyzed Directed C–H Amidation

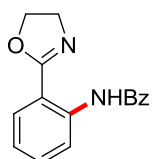
5.3.1. Experimental Procedures and Analytical Data

***N*-[2-(4,5-Dihydrooxazol-2-yl)-5-methylphenyl]benzamide (143aa)**



The general procedure **GP1** was followed using oxazoline **142a** (81 mg, 0.25 mmol, 1.0 equiv), dioxazolone **40a** (49 mg, 0.30 mmol, 1.2 equiv), Cp*Co(CO)I₂ (6.0 mg, 0.013 mmol, 5.0 mol %), AgSbF₆ (17 mg, 0.050 mmol, 20 mol %) and NaOAc (4.1 mg, 0.050 mmol, 20 mol %) in DCE (1.0 mL). Purification by column chromatography on silica gel (*n*-hexane/EtOAc = 5/1) yielded **143aa** (39 mg, 56%) as a white solid. Reaction carried on 5.6 mmol: 905 mg, 58%. Reaction performed by Dr. R. Mei on 0.50 mmol: 95 mg, 68%. **M. p.** = 149–150 °C. **¹H NMR** (400 MHz, CDCl₃): δ = 13.00 (s, 1H), 8.82 (s, 1H), 8.10 (d, *J* = 8.1 Hz, 2H), 7.77 (d, *J* = 8.0 Hz, 1H), 7.58–7.45 (m, 3H), 6.92 (dd, *J* = 8.0, 1.4 Hz, 1H), 4.41–4.33 (m, 2H), 4.19–4.14 (m, 2H), 2.43 (s, 3H). **¹³C NMR** (100 MHz, CDCl₃): δ = 166.0 (C_q), 164.9 (C_q), 143.4 (C_q), 140.0 (C_q), 135.3 (C_q), 131.5 (CH), 129.1 (CH), 128.5 (CH), 127.7 (CH), 123.3 (CH), 120.3 (CH), 111.0 (C_q), 66.1 (CH₂), 54.6 (CH₂), 22.1 (CH₃). **IR** (ATR): 3055, 2982, 2915, 1677, 1363, 1155, 1103, 1055, 817, 754, cm⁻¹. **MS (EI)** *m/z* (relative intensity) 281 (20) [M+H⁺], 280 (55), 263 (25), 203 (100), 160 (50). HR-MS (EI) *m/z* calcd for C₁₇H₁₆N₂O₂ [M⁺] 280.1212, found 280.1212.

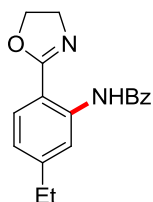
***N*-[2-(4,5-Dihydrooxazol-2-yl)phenyl]benzamide (143ba)**



The general procedure **GP1** was followed using oxazoline **142b** (74 mg, 0.50 mmol, 1.0 equiv) and dioxazolone **40a** (98 mg, 0.60 mmol, 1.2 equiv). Purification by column chromatography on silica gel (*n*-hexane/EtOAc = 11/2) yielded **143ba** (95 mg, 71%) as a white solid. **M. p.** = 143–145 °C. **¹H NMR** (400 MHz, CDCl₃): δ = 13.03 (s, 1H), 8.97 (dd, *J* = 8.5, 1.2 Hz, 1H), 8.10 (d, *J* = 8.1 Hz, 2H), 7.91 (dd, *J* = 7.9, 1.7 Hz, 1H), 7.59–7.45 (m, 4H), 7.12 (ddd, *J* = 7.9, 7.3, 1.2 Hz, 1H), 4.42 (td, *J* = 9.4, 1.1 Hz, 2H), 4.21 (td, *J* = 9.4, 1.1 Hz, 2H). **¹³C NMR** (100 MHz, CDCl₃): δ = 166.2 (C_q), 165.1 (C_q), 140.4 (C_q), 135.5 (C_q), 132.8 (CH), 131.8 (CH), 129.4 (CH), 128.7 (CH), 127.9 (CH), 122.5 (CH), 120.1 (CH), 113.7 (C_q), 66.4 (CH₂), 54.9 (CH₂). **IR** (ATR): 3026, 1614, 1446, 1303, 1058, 943, 748, 703, 674 cm⁻¹. **MS (EI)** *m/z* (relative intensity) 266 (56) [M⁺], 189 (96), 146 (42), 105 (100), 77 (75), 51 (12). **HR-MS** (ESI) *m/z* calcd for C₁₆H₁₃N₂O₂ [M–H]⁻: 265.0983, found: 265.0991.

The analytical data are in accordance with those previously reported in the literature.^[327]

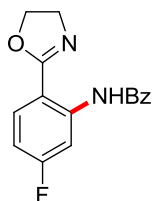
N[2-(4,5-Dihydrooxazol-2-yl)-5-ethylphenyl]benzamide (**143ca**)



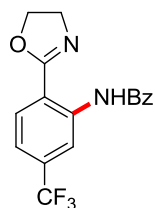
The general procedure **GP1** was followed using oxazoline **142c** (88 mg, 0.50 mmol, 1.0 equiv) and dioxazolone **40a** (98 mg, 0.60 mmol, 1.2 equiv). Purification by column chromatography on silica gel (*n*-hexane/EtOAc = 7/1) yielded **143ca** (95 mg, 65%) as a white solid. **M. p.** = 122–124 °C. **¹H NMR** (300 MHz, CDCl₃): δ = 13.02 (s, 1H), 8.87 (dq, *J* = 1.8, 0.6 Hz, 1H), 8.17–8.05 (m, 2H), 7.81 (d, *J* = 8.1 Hz, 1H), 7.61–7.43 (m, 3H), 6.96 (ddt, *J* = 8.1, 1.7, 0.6 Hz, 1H), 4.40 (td, *J* = 9.1, 1.0 Hz, 2H), 4.19 (td, *J* = 9.1, 1.0 Hz, 2H), 2.74 (q, *J* = 7.6 Hz, 2H), 1.30 (t, *J* = 7.6 Hz, 3H). **¹³C NMR** (125 MHz, CDCl₃): δ = 166.1 (C_q), 165.0 (C_q), 149.8 (C_q), 140.3 (C_q), 135.5 (C_q), 131.6 (CH), 129.3 (CH), 128.6 (CH), 127.8 (CH), 122.2 (CH), 119.4 (CH), 111.3

(C_q), 66.3 (CH₂), 54.8 (CH₂), 29.6 (CH₂), 15.5 (CH₃). **IR** (ATR): 3065, 2962, 1620, 1580, 1296, 1242, 1052, 698, 678 cm⁻¹. **MS (EI)** *m/z* (relative intensity) 294 (49) [M⁺], 277 (14), 217 (100), 174 (36), 105 (47), 77 (49). **HR-MS** (EI) *m/z* calcd for C₁₈H₁₈N₂O₂ [M⁺]: 294.1368, found: 294.1376.

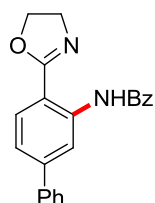
***N*-[2-(4,5-Dihydrooxazol-2-yl)-5-fluorophenyl]benzamide (143da)**



The general procedure **GP1** was followed using oxazoline **142d** (83 mg, 0.50 mmol, 1.0 equiv) and dioxazolone **40a** (98 mg, 0.60 mmol, 1.2 equiv). Purification by column chromatography on silica gel (*n*-hexane/EtOAc = 85/15) yielded **143da** (101 mg, 71%) as a white solid. **M. p.** = 163–165 °C. **¹H NMR** (300 MHz, CDCl₃): δ = 13.16 (s, 1H), 8.79 (dd, *J* = 12.2, 2.6 Hz, 1H), 8.08 (d, *J* = 8.0 Hz, 2H), 7.88 (dd, *J* = 8.9, 6.5 Hz, 1H), 7.62–7.43 (m, 3H), 6.80 (ddd, *J* = 8.9, 7.6, 2.6 Hz, 1H), 4.41 (td, *J* = 9.2, 1.3 Hz, 2H), 4.19 (td, *J* = 9.2, 1.3 Hz, 2H). **¹³C NMR** (100 MHz, CDCl₃): δ = 166.2 (C_q), 165.0 (d, ¹*J*_{C-F} = 249.0 Hz, C_q), 164.4 (C_q), 142.1 (d, ³*J*_{C-F} = 12.8 Hz, C_q), 134.9 (C_q), 131.9 (CH), 131.1 (d, ³*J*_{C-F} = 10.4 Hz, CH), 128.6 (CH), 127.8 (CH), 109.8 (d, ⁴*J*_{C-F} = 2.9 Hz, C_q), 109.5 (d, ²*J*_{C-F} = 22.5 Hz, CH), 107.3 (d, ²*J*_{C-F} = 28.8 Hz, CH), 66.3 (CH₂), 54.6 (CH₂). **¹⁹F NMR** (282 MHz, CDCl₃): δ = -104.2 (m). **IR** (ATR): 3111, 2975, 1614, 1599, 1544, 1430, 1255, 705 cm⁻¹. **MS (EI)** *m/z* (relative intensity) 284 (33) [M⁺], 207 (84), 164 (30), 105 (100), 77 (45), 44 (10). **HR-MS** (ESI) *m/z* calcd for C₁₆H₁₄N₂O₂F [M+H⁺]: 285.1034, found: 285.1038.

***N*-[2-(4,5-Dihydrooxazol-2-yl)-5-(trifluoromethyl)phenyl]benzamide (143ea)**

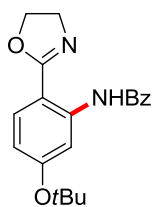
The general procedure **GP1** was followed using oxazoline **142e** (108 mg, 0.50 mmol, 1.0 equiv) and dioxazolone **40a** (98 mg, 0.60 mmol, 1.2 equiv). Purification by column chromatography on silica gel (*n*-hexane/EtOAc = 85/15) yielded **143ea** (106 mg, 63%) as a white solid. **M. p.** = 191–193 °C. **¹H NMR** (300 MHz, CDCl₃): δ = 13.10 (s, 1H), 9.34 (d, *J* = 1.8 Hz, 1H), 8.08 (d, *J* = 8.0 Hz, 2H), 8.02–7.93 (m, 1H), 7.63–7.44 (m, 3H), 7.33 (ddd, *J* = 8.3, 1.8, 0.7 Hz, 1H), 4.46 (td, *J* = 9.3, 1.3 Hz, 2H), 4.24 (td, *J* = 9.3, 1.3 Hz, 2H). **¹³C NMR** (100 MHz, CDCl₃): δ = 166.2 (C_q), 164.2 (C_q), 140.6 (C_q), 134.7 (C_q), 134.1 (q, ²*J*_{C-F} = 32.7 Hz, C_q), 132.0 (CH), 129.8 (CH), 128.7 (CH), 127.7 (CH), 123.6 (q, ¹*J*_{C-F} = 273.1 Hz, C_q), 118.7 (q, ³*J*_{C-F} = 3.8 Hz, CH), 116.9 (q, ³*J*_{C-F} = 4.2 Hz, CH), 116.0 (C_q), 66.5 (CH₂), 54.8 (CH₂). **¹⁹F NMR** (282 MHz, CDCl₃): δ = -63.2 (s). **IR** (ATR): 3016, 1622, 1588, 1426, 1333, 1118, 1081, 1055, 922, 899, 701 cm⁻¹. **MS (EI)** *m/z* (relative intensity) 334 (28) [M⁺], 257 (36), 214 (14), 158 (7), 105 (100), 77 (44), 51 (6). **HR-MS** (ESI) *m/z* calcd for C₁₇H₁₄N₂O₂F₃ [M+H⁺]: 335.1002, found: 335.1005.

***N*-[4-(4,5-Dihydrooxazol-2-yl)-[1,1'-biphenyl]-3-yl]benzamide (143fa)**

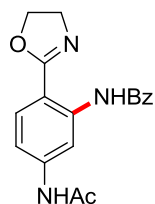
The general procedure **GP1** was followed using oxazoline **142f** (112 mg, 0.50 mmol, 1.0 equiv) and dioxazolone **40a** (98 mg, 0.60 mmol, 1.2 equiv). Purification by column chromatography on silica gel (*n*-hexane/EtOAc = 6/1) yielded **143fa** (127 mg, 74%) as a white solid. **M. p.** = 170–171 °C. **¹H NMR** (300 MHz, CDCl₃):

δ = 13.08 (s, 1H), 9.34 (d, J = 1.8 Hz, 1H), 8.12 (d, J = 8.1 Hz, 2H), 7.95 (d, J = 8.2 Hz, 1H), 7.80–7.69 (m, 2H), 7.62–7.32 (m, 7H), 4.41 (td, J = 9.2, 0.9 Hz, 2H), 4.21 (td, J = 9.2, 0.9 Hz, 2H). $^{13}\text{C NMR}$ (100 MHz, CDCl_3): δ = 166.3 (C_q), 165.0 (C_q), 145.3 (C_q), 140.7 (C_q), 140.2 (C_q), 135.4 (C_q), 131.8 (CH), 129.8 (CH), 128.9 (CH), 128.7 (CH), 128.2 (CH), 127.9 (CH), 127.5 (CH), 121.1 (CH), 118.5 (CH), 112.5 (C_q), 66.4 (CH_2), 54.9 (CH_2). IR (ATR): 3056, 1618, 1569, 1409, 1249, 1064, 697, 678 cm^{-1} . MS (EI) m/z (relative intensity) 342 (64) [M^+], 265 (100), 222 (35), 166 (15), 105 (55), 77 (57). HR-MS (EI) m/z calcd for $\text{C}_{22}\text{H}_{18}\text{N}_2\text{O}_2$ [M^+]: 342.1368, found: 342.1364.

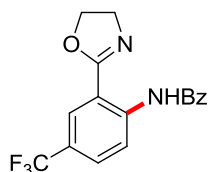
N[5-(*tert*-Butoxy)-2-(4,5-dihydrooxazol-2-yl)phenyl]benzamide (**143ga**)



The general procedure **GP1** was followed using oxazoline **142g** (110 mg, 0.50 mmol, 1.0 equiv) and dioxazolone **40a** (98 mg, 0.60 mmol, 1.2 equiv). Purification by column chromatography on silica gel (*n*-hexane/EtOAc = 7.5/1) yielded **143ga** (84 mg, 50%) as a white solid. **M. p.** = 120–122 °C. $^1\text{H NMR}$ (500 MHz, CDCl_3): δ = 13.05 (s, 1H), 8.76 (d, J = 2.4 Hz, 1H), 8.13–8.07 (d, J = 8.1 Hz, 2H), 7.77 (d, J = 8.7 Hz, 1H), 7.57–7.45 (m, 3H), 6.70 (dd, J = 8.7, 2.4 Hz, 1H), 4.36 (td, J = 9.3, 0.9 Hz, 2H), 4.15 (td, J = 9.3, 0.9 Hz, 2H), 1.49 (s, 9H). $^{13}\text{C NMR}$ (125 MHz, CDCl_3): δ = 166.3 (C_q), 164.9 (C_q), 159.8 (C_q), 141.2 (C_q), 135.4 (C_q), 131.7 (CH), 130.0 (CH), 127.8 (CH), 127.8 (CH), 116.8 (CH), 113.1 (CH), 108.0 (C_q), 79.6 (C_q), 66.2 (CH_2), 54.6 (CH_2), 29.1 (CH_3). IR (ATR): 2978, 2935, 2877, 1630, 1578, 1362, 1257, 1239, 707 cm^{-1} . MS (EI) m/z (relative intensity) 338 (7) [M^+], 282 (67), 205 (100), 162 (19), 105 (83), 77 (53), 57 (24). HR-MS (EI) m/z calcd for $\text{C}_{20}\text{H}_{22}\text{N}_2\text{O}_3$ [M^+]: 338.1630, found: 338.1627.

***N*-[5-Acetamido-2-(4,5-dihydrooxazol-2-yl)phenyl]benzamide (143ha)**

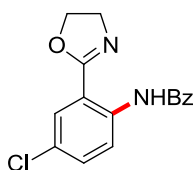
The general procedure **GP1** was followed using oxazoline **142h** (102 mg, 0.50 mmol, 1.0 equiv) and dioxazolone **40a** (98 mg, 0.60 mmol, 1.2 equiv). Purification by column chromatography on silica gel (*n*-hexane/EtOAc = 2/1) yielded **143ha** (94 mg, 58%) as a white solid. **M. p.** = 189–191 °C. **¹H NMR** (300 MHz, DMSO-*d*₆): δ = 13.07 (s, 1H), 10.28 (s, 1H), 8.96 (d, *J* = 2.1 Hz, 1H), 8.02 (d, *J* = 7.8 Hz, 2H), 7.80 (d, *J* = 8.7 Hz, 1H), 7.72–7.53 (m, 4H), 4.42 (td, *J* = 9.1, 1.1 Hz, 2H), 4.16 (td, *J* = 9.1, 1.1 Hz, 2H), 2.09 (s, 3H). **¹³C NMR** (100 MHz, CDCl₃): δ = 168.8 (C_q), 166.6 (C_q), 164.9 (C_q), 142.0 (CH), 140.7 (C_q), 135.2 (CH), 132.0 (CH), 130.8 (CH), 128.8 (CH), 127.9 (CH), 113.8 (C_q), 109.8 (C_q), 109.6 (C_q), 66.4 (CH₂), 54.7 (CH₂), 24.9 (CH₃). **IR** (ATR): 3312, 3278, 1621, 1518, 1402, 1360, 1286, 1240, 1061, 704 cm⁻¹. **MS (EI)** *m/z* (relative intensity) 323 (23) [M⁺], 246 (38), 204 (11), 161 (10), 105 (44), 77 (39), 58 (15), 43 (100). **HR-MS** (EI) *m/z* calcd for C₁₈H₁₇N₃O₃ [M⁺]: 323.1270, found: 323.1266.

***N*-[2-(4,5-Dihydrooxazol-2-yl)-4-(trifluoromethyl)phenyl]benzamide (143ia)**

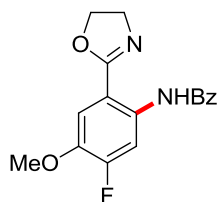
The general procedure **GP1** was followed using oxazoline **142i** (108 mg, 0.50 mmol, 1.0 equiv) and dioxazolone **40a** (98 mg, 0.60 mmol, 1.2 equiv). Purification by column chromatography on silica gel (*n*-hexane/EtOAc = 7/1) yielded **143ia** (108 mg, 65%) as a white solid. **M. p.** = 184–187 °C. **¹H NMR** (300 MHz, CDCl₃): δ = 13.17 (s, 1H), 9.11 (dt, *J* = 8.9, 0.7 Hz, 1H), 8.19 (dt, *J* = 2.3, 0.6 Hz, 1H), 8.09 (d, *J* = 8.1 Hz,

2H), 7.75 (ddt, $J = 8.9, 2.3, 0.6$ Hz, 1H), 7.64–7.45 (m, 3H), 4.48 (td, $J = 9.1, 1.6$ Hz, 2H), 4.26 (td, $J = 9.1, 1.6$ Hz, 2H). $^{13}\text{C NMR}$ (125 MHz, CDCl_3): $\delta = 166.2$ (C_q), 164.0 (C_q), 142.8 (C_q), 134.7 (C_q), 132.0 (CH), 129.2 (q, $^3J_{\text{C-F}} = 3.4$ Hz, CH), 128.6 (CH), 127.7 (CH), 126.5 (q, $^3J_{\text{C-F}} = 4.0$ Hz, CH), 124.9 (q, $^1J_{\text{C-F}} = 271.3$ Hz, C_q), 124.2 (q, $^2J_{\text{C-F}} = 33.4$ Hz, C_q), 119.9 (CH), 113.4 (C_q), 66.6 (CH_2), 54.8 (CH_2). $^{19}\text{F NMR}$ (282 MHz, CDCl_3): $\delta = -62.2$ (s). **IR** (ATR): 3013, 1627, 1308, 1237, 1107, 1082, 1058, 952, 695 cm^{-1} . **MS (EI)** m/z (relative intensity) 334 (38) [M^+], 257 (57), 214 (21), 158 (10), 105 (100), 77 (64). **HR-MS** (EI) m/z calcd for $\text{C}_{17}\text{H}_{13}\text{N}_2\text{O}_2\text{F}_3$ [M^+]: 334.0929, found: 334.0923.

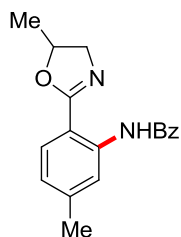
N-[4-Chloro-2-(4,5-dihydrooxazol-2-yl)phenyl]benzamide (**143ja**)



The general procedure **GP1** was followed using oxazoline **142j** (91 mg, 0.50 mmol, 1.0 equiv), dioxazolone **40a** (98 mg, 0.60 mmol, 1.2 equiv), $[\text{Cp}^*\text{RhCl}_2]_2$ (7.7 mg, 0.013 mmol, 2.5 mol %), AgSbF_6 (34 mg, 0.10 mmol, 20 mol %) and NaOAc (8.2 mg, 0.10 mmol, 20 mol %). Purification by column chromatography on silica gel (n -hexane/EtOAc = 5/1) yielded **143ja** (111 mg, 74%) as a white solid. (Reaction performed by *Dr. R. Mei* using $\text{Cp}^*\text{Co}(\text{CO})\text{I}_2$: 101 mg, 67%.) **M. p.** = 140–141 °C. $^1\text{H NMR}$ (400 MHz, CDCl_3): $\delta = 12.88$ (s, 1H), 8.90 (d, $J = 9.0$ Hz, 1H), 8.01 (d, $J = 8.2$ Hz, 2H), 7.77 (d, $J = 2.6$ Hz, 1H), 7.54–7.45 (m, 1H), 7.49–7.40 (m, 2H), 7.39 (dd, $J = 9.0, 2.6$ Hz, 1H), 4.34 (td, $J = 9.4, 1.0$ Hz, 2H), 4.12 (td, $J = 9.4, 1.0$ Hz, 2H). $^{13}\text{C NMR}$ (100 MHz, CDCl_3): $\delta = 165.8$ (C_q), 163.8 (C_q), 138.6 (C_q), 134.8 (C_q), 132.2 (CH), 131.7 (CH), 128.8 (CH), 128.5 (CH), 127.6 (CH), 127.2 (C_q), 121.0 (CH), 114.7 (C_q), 66.3 (CH_2), 54.6 (CH_2). **IR** (ATR): 3048, 2969, 1666, 1615, 1579, 1474, 1230, 1057, 950, 693 cm^{-1} . **MS (EI)** m/z (relative intensity) 300 (30) [M^+] (^{35}Cl), 307 (5), 223 (30), 180 (15), 124 (15), 105 (100). **HR-MS** (EI) m/z calcd for $\text{C}_{16}\text{H}_{13}^{35}\text{ClN}_2\text{O}_2$ [M^+] 300.0666, found 300.0655.

***N*-[2-(4,5-Dihydrooxazol-2-yl)-5-fluoro-4-methoxyphenyl]benzamide (143ka)**

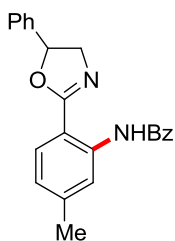
The general procedure **GP1** was followed using oxazoline **142k** (98 mg, 0.50 mmol, 1.0 equiv) and dioxazolone **40a** (98 mg, 0.60 mmol, 1.2 equiv). Purification by column chromatography on silica gel (*n*-hexane/EtOAc = 4.5/1) yielded **143ka** (116 mg, 74%) as a white solid. **M. p.** = 161–163 °C. **¹H NMR** (300 MHz, CDCl₃): δ = 12.93 (s, 1H), 8.86 (d, *J* = 14.3 Hz, 1H), 8.06 (d, *J* = 8.0 Hz, 2H), 7.61–7.43 (m, 4H), 4.43 (td, *J* = 9.3, 1.4 Hz, 2H), 4.21 (td, *J* = 9.3, 1.4 Hz, 2H), 3.91 (s, 3H). **¹³C NMR** (125 MHz, CDCl₃): δ = 165.6 (C_q), 164.1 (C_q), 154.3 (d, ¹*J*_{C-F} = 250.9 Hz, C_q), 142.5 (d, ²*J*_{C-F} = 11.6 Hz, C_q), 135.0 (d, ⁴*J*_{C-F} = 10.9 Hz, C_q), 135.0 (C_q), 131.6 (CH), 128.5 (CH), 127.6 (CH), 113.9 (d, ³*J*_{C-F} = 3.8 Hz, CH), 109.4 (d, ³*J*_{C-F} = 3.4 Hz, C_q), 108.8 (d, ²*J*_{C-F} = 25.5 Hz, CH), 66.3 (CH₂), 56.6 (CH₃), 54.7 (CH₂). **¹⁹F NMR** (282 MHz, CDCl₃): δ = -125.8 (ddd, *J* = 14.3, 9.2, 1.5 Hz). **IR** (ATR): 2968, 1614, 1544, 1271, 1206, 1020, 944, 877, 702 cm⁻¹. **MS (EI)** *m/z* (relative intensity) 314 (26) [M⁺], 297 (5), 237 (18), 194 (6), 105 (100), 77 (21). **HR-MS** (EI) *m/z* calcd for C₁₇H₁₅N₂O₃F [M⁺]: 314.1067, found: 314.1071.

***N*-[5-Methyl-2-(5-methyl-4,5-dihydrooxazol-2-yl)phenyl]benzamide (143ma)**

The general procedure **GP1** was followed using oxazoline **142m** (88 mg, 0.50 mmol, 1.0 equiv) and dioxazolone **40a** (98 mg, 0.60 mmol, 1.2 equiv). Purification by column chromatography on silica gel (*n*-hexane/EtOAc = 8/1) yielded **143ma**

(125 mg, 85%) as a white solid. **M. p.** = 126–128 °C. **¹H NMR** (400 MHz, CDCl₃): δ = 13.06 (s, 1H), 8.83 (dq, J = 1.1, 0.6 Hz, 1H), 8.16–8.06 (m, 2H), 7.78 (d, J = 8.0 Hz, 1H), 7.59–7.45 (m, 3H), 6.97–6.88 (m, 1H), 4.81 (ddq, J = 9.4, 7.4, 6.2 Hz, 1H), 4.26 (dd, J = 14.2, 9.4 Hz, 1H), 3.73 (dd, J = 14.2, 7.4 Hz, 1H), 2.44 (s, 3H), 1.44 (d, J = 6.2 Hz, 3H). **¹³C NMR** (100 MHz, CDCl₃): δ = 166.2 (C_q), 164.5 (C_q), 143.5 (C_q), 140.2 (C_q), 135.6 (C_q), 131.7 (CH), 129.3 (CH), 128.7 (CH), 127.9 (CH), 123.4 (CH), 120.5 (CH), 111.4 (C_q), 75.0 (CH), 61.3 (CH₂), 22.2 (CH₃), 21.1 (CH₃). **IR** (ATR): 3063, 2974, 1622, 1585, 1295, 1243, 1062, 1049, 696, 677 cm⁻¹. **MS (EI)** m/z (relative intensity) 294 (22) [M⁺], 217 (100), 160 (29), 105 (34), 77 (44). **HR-MS** (EI) m/z calcd for C₁₈H₁₈N₂O₂ [M⁺]: 294.1368, found: 294.1370.

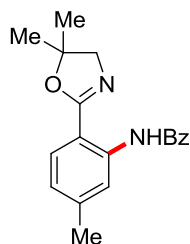
***N*-[5-Methyl-2-(5-phenyl-4,5-dihydrooxazol-2-yl)phenyl]benzamide (143na)**



The general procedure **GP1** was followed using oxazoline **142n** (119 mg, 0.50 mmol, 1.0 equiv) and dioxazolone **40a** (98 mg, 0.60 mmol, 1.2 equiv). Purification by column chromatography on silica gel (*n*-hexane/EtOAc = 8/1) yielded **143na** (131 mg, 74%) as a white solid. **M. p.** = 131–133 °C. **¹H NMR** (400 MHz, CDCl₃): δ = 12.99 (s, 1H), 8.88 (t, J = 1.1 Hz, 1H), 8.16–8.06 (m, 2H), 7.90 (d, J = 8.0 Hz, 1H), 7.61–7.45 (m, 3H), 7.45–7.30 (m, 5H), 6.96 (ddd, J = 8.0, 1.7, 0.8 Hz, 1H), 5.64 (dd, J = 10.1, 7.7 Hz, 1H), 4.60 (dd, J = 14.5, 10.1 Hz, 1H), 4.13 (dd, J = 14.5, 7.7 Hz, 1H), 2.46 (s, 3H). **¹³C NMR** (100 MHz, CDCl₃): δ = 166.2 (C_q), 164.6 (C_q), 143.8 (C_q), 140.7 (C_q), 140.4 (C_q), 135.5 (C_q), 131.7 (CH), 129.5 (CH), 129.0 (CH), 128.7 (CH), 128.6 (CH), 127.9 (CH), 125.8 (CH), 123.6 (CH), 120.6 (CH), 111.0 (C_q), 79.6 (CH), 62.9 (CH₂), 22.3 (CH₃). **IR** (ATR): 3066, 2965, 1618, 1294, 1055, 759, 707, 694, 677 cm⁻¹. **MS (EI)** m/z (relative intensity) 356 (40) [M⁺],

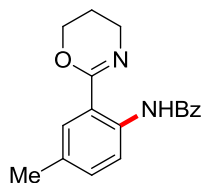
279 (45), 238 (25), 160 (61), 119 (27), 105 (99), 77 (100). **HR-MS** (EI) m/z calcd for $C_{23}H_{20}N_2O_2$ [M^+]: 356.1525, found: 356.1533.

***N*-[2-(5,5-Dimethyl-4,5-dihydrooxazol-2-yl)-5-methylphenyl]benzamide (143oa)**



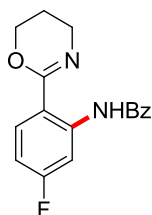
The general procedure **GP1** was followed using oxazoline **142o** (95 mg, 0.50 mmol, 1.0 equiv) and dioxazolone **40a** (98 mg, 0.60 mmol, 1.2 equiv). Purification by column chromatography on silica gel (*n*-hexane/EtOAc = 8/1) yielded **143oa** (132 mg, 86%) as a white solid. **M. p.** = 103–105 °C. **¹H NMR** (400 MHz, $CDCl_3$): δ = 13.13 (s, 1H), 8.87–8.81 (m, 1H), 8.16–8.07 (m, 2H), 7.78 (d, J = 8.0 Hz, 1H), 7.58–7.45 (m, 3H), 6.93 (ddd, J = 8.0, 1.7, 0.8 Hz, 1H), 3.89 (s, 2H), 2.44 (s, 3H), 1.50 (s, 6H). **¹³C NMR** (100 MHz, $CDCl_3$): δ = 166.1 (C_q), 163.9 (C_q), 143.3 (C_q), 140.2 (C_q), 135.6 (C_q), 131.6 (CH), 129.2 (CH), 128.6 (CH), 127.9 (CH), 123.3 (CH), 120.4 (CH), 111.7 (C_q), 82.9 (C_q), 66.6 (CH_2), 27.4 (CH_3), 22.2 (CH_3). **IR** (ATR): 3065, 2974, 2873, 1620, 1583, 1298, 1059, 695, 677 cm^{-1} . **MS** (EI) m/z (relative intensity) 308 (53) [M^+], 275 (21), 231 (100), 160 (93), 134 (14), 105 (72), 77 (69), 51 (9). **HR-MS** (ESI) m/z calcd for $C_{19}H_{21}N_2O_2$ [$M+H^+$]: 309.1598, found: 309.1598.

***N*-[2-(5,6-Dihydro-4*H*-1,3-oxazin-2-yl)-5-fluorophenyl]benzamide (143pa)**



The general procedure **GP1** was followed using oxazine **142p** (88 mg, 0.50 mmol, 1.0 equiv) and dioxazolone **40a** (98 mg, 0.60 mmol, 1.2 equiv). Purification by column chromatography on silica gel (*n*-hexane/EtOAc = 8/1) yielded **143pa** (97 mg, 66%) as a white solid. **M. p.** = 127–129 °C. **¹H NMR** (300 MHz, CDCl₃): δ = 13.87 (s, 1H), 8.81 (d, *J* = 8.5 Hz, 1H), 8.07–7.97 (m, 2H), 7.72 (d, *J* = 2.1 Hz, 1H), 7.58–7.41 (m, 3H), 7.27 (dd, *J* = 8.5, 2.1 Hz, 1H), 4.42 (t, *J* = 5.4 Hz, 2H), 3.73 (t, *J* = 5.9 Hz, 2H), 2.34 (s, 3H), 2.04 (tt, *J* = 5.9, 5.4 Hz, 2H). **¹³C NMR** (125 MHz, CDCl₃): δ = 165.7 (C_q), 157.1 (C_q), 137.9 (C_q), 136.1 (C_q), 132.3 (CH), 131.5 (C_q), 131.4 (CH), 128.6 (CH), 128.4 (CH), 127.6 (CH), 120.1 (CH), 118.3 (C_q), 65.5 (CH₂), 42.1 (CH₂), 21.7 (CH₂), 21.0 (CH₃). **IR** (ATR): 2853, 1641, 1595, 1525, 1349, 1237, 822, 701, 543 cm⁻¹. **MS (EI)** *m/z* (relative intensity) 294 (54) [M⁺], 217 (100), 189 (11), 160 (61), 105 (52), 77 (61). **HR-MS** (ESI) *m/z* calcd for C₁₈H₁₉N₂O₂ [M+H⁺]: 295.1441, found: 295.1444.

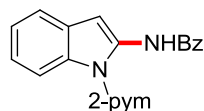
***N*-[2-(5,6-Dihydro-4*H*-1,3-oxazin-2-yl)-4-methylphenyl]benzamide (143qa)**



The general procedure **GP1** was followed using oxazine **142q** (90 mg, 0.50 mmol, 1.0 equiv) and dioxazolone **40a** (98 mg, 0.60 mmol, 1.2 equiv). Purification by column chromatography on silica gel (*n*-hexane/EtOAc = 85/15) yielded **143qa** (106 mg, 71%) as a white solid. **M. p.** = 144–147 °C. **¹H NMR** (400 MHz, CDCl₃): δ = 14.19 (s, 1H), 8.75 (dd, *J* = 12.1, 2.7 Hz, 1H), 8.06–7.96 (m, 2H), 7.89 (dd, *J* = 8.9, 6.6 Hz, 1H), 7.58–7.43 (m, 3H), 6.74 (ddd, *J* = 8.9, 7.5, 2.7 Hz, 1H), 4.41 (tt, *J* = 5.2, 0.8 Hz, 2H), 3.72 (t, *J* = 5.9 Hz, 2H), 2.04 (tt, *J* = 5.9, 5.2 Hz, 2H). **¹³C NMR** (100 MHz, CDCl₃): δ = 166.0 (C_q), 164.3 (d, ¹*J*_{C-F} = 249.0 Hz, C_q), 156.6 (C_q), 142.2 (d, ³*J*_{C-F} = 12.5 Hz, C_q), 135.5 (C_q), 131.6 (CH), 129.8 (d, ³*J*_{C-F} = 10.2 Hz, CH), 128.5 (CH), 127.6 (CH), 114.4 (d, ⁴*J*_{C-F} = 2.9 Hz, C_q), 108.9 (d, ²*J*_{C-F} = 22.1 Hz, CH),

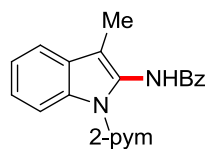
107.2 (d, $^2J_{C-F} = 28.2$ Hz, CH), 65.5 (CH₂), 41.9 (CH₂), 21.6 (CH₂). **¹⁹F NMR** (282 MHz, CDCl₃): $\delta = -(106.36-106.53)$ (m). **IR** (ATR): 2894, 2859, 1642, 1533, 1261, 1134, 703, 676 cm⁻¹. **MS (EI)** *m/z* (relative intensity) 298 (34) [M⁺], 221 (100), 193 (9), 164 (62), 105 (55), 77 (49), 51 (7). **HR-MS** (ESI) *m/z* calcd for C₁₇H₁₆N₂O₂F [M+H⁺]: 299.1190, found: 299.1192.

***N*-[1-(Pyrimidin-2-yl)-1*H*-indol-2-yl]benzamide (147aa)**



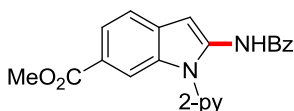
The general procedure **GP2** was followed using indole substrate **36a** (98 mg, 0.50 mmol, 1.0 equiv) and dioxazolone **40a** (98 mg, 0.60 mmol, 1.2 equiv). Purification by column chromatography on silica gel (*n*-hexane/EtOAc = 2/1) yielded **147aa** (148 mg, 94%) as a pale yellow solid. **M. p.** = 137–138 °C. **¹H NMR** (300 MHz, CDCl₃): $\delta = 12.99$ (s, 1H), 8.63–8.59 (m, 1H), 8.57–8.55 (m, 2H), 7.94–7.87 (m, 2H), 7.55–7.41 (m, 4H), 7.37 (s, 1H), 7.17 (pd, $J = 7.2, 1.5$ Hz, 2H), 6.95 (t, $J = 4.8$ Hz, 1H). **¹³C NMR** (75 MHz, CDCl₃): $\delta = 163.5$ (C_q), 158.6 (C_q), 157.3 (CH), 135.5 (C_q), 134.4 (C_q), 132.5 (C_q), 131.7 (CH), 129.9 (C_q), 128.7 (CH), 126.9 (CH), 123.0 (CH), 122.4 (CH), 119.7 (CH), 116.5 (CH), 115.9 (CH), 95.6 (CH). **IR** (ATR): 3015, 1667, 1587, 1492, 1348, 1253, 791, 703, 588, 444 cm⁻¹. **MS (EI)** *m/z* (relative intensity), 315 (5) [M+H⁺], 314 (40) [M⁺], 231 (10), 210 (20), 105 (100). **HR-MS** (EI) *m/z* calcd for C₁₉H₁₄N₄O [M⁺] 314.1168, found 314.1165.

***N*-[3-Methyl-1-(pyrimidin-2-yl)-1*H*-indol-2-yl]benzamide (147ba)**



The general procedure **GP2** was followed using indole **36b** (105 mg, 0.50 mmol, 1.0 equiv), dioxazolone **40a** (98 mg, 0.60 mmol, 1.2 equiv), [Cp*Co(CO)I₂] (11.9 mg, 0.025 mmol, 5.0 mol %), AgSbF₆ (17 mg, 0.050 mmol, 10 mol %) and NaOAc (4.1 mg, 0.050 mmol, 10 mol %) at 100 °C. Purification by column chromatography on silica gel (*n*-hexane/EtOAc = 8:2→6:4) yielded **147ba** (106 mg, 65%) as a white solid. (Without NaOAc: 101 mg, 61%.) **M. p.** = 159–160 °C. **¹H NMR** (300 MHz, CDCl₃): δ = 10.88 (s, 1H), 8.70 (d, *J* = 4.8 Hz, 2H), 8.56–8.46 (m, 1H), 7.99 (d, *J* = 6.9 Hz, 2H), 7.61–7.43 (m, 4H), 7.34–7.20 (m, 2H), 7.04 (t, *J* = 4.8 Hz, 1H), 2.31 (s, 3H). **¹³C NMR** (125 MHz, CDCl₃): δ = 158.1 (C_q), 157.9 (CH), 157.9 (C_q), 134.5 (C_q), 134.2 (C_q), 132.0 (CH), 130.0 (C_q), 129.1 (C_q), 128.8 (CH), 127.5 (CH), 123.6 (CH), 122.5 (CH), 118.5 (CH), 116.1 (CH), 114.9 (CH), 110.3 (C_q), 10.2 (CH₃). **IR** (ATR): 1673, 1562, 1503, 1429, 1272, 740, 710, 624 cm⁻¹. **MS (EI)** *m/z* (relative intensity) 328 (58) [M⁺], 223 (95), 207 (26), 153 (12) 105 (100), 77 (51), 44 (55). **HR-MS** (ESI) *m/z* calcd for C₂₀H₁₇N₄O [M+H⁺]: 329.1397, found: 329.1396.

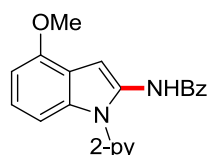
Methyl 2-Benzamido-1-(pyridin-2-yl)-1*H*-indole-6-carboxylate (**146ca**)



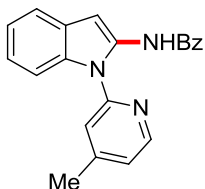
The general procedure **GP2** was followed using indole **28c** (126 mg, 0.50 mmol, 1.0 equiv) and dioxazolone **2a** (98 mg, 0.60 mmol, 1.2 equiv). Purification by column chromatography on silica gel (*n*-hexane/EtOAc = 3:1→3:2) yielded **146ca** (169 mg, 91%) as an off-white solid. **M. p.** = 180–183 °C. **¹H NMR** (500 MHz, CDCl₃): δ = 11.95 (s, 1H), 8.67 (ddd, *J* = 5.0, 2.0, 0.9 Hz, 1H), 8.32 (dt, *J* = 1.5, 0.8 Hz, 1H), 8.02 (ddd, *J* = 8.3, 7.5, 1.9 Hz, 1H), 7.97–7.87 (m, 3H), 7.82 (dt, *J* = 8.2, 0.9 Hz, 1H), 7.63 (dd, *J* = 8.2, 0.6 Hz, 1H), 7.57 (ddt, *J* = 8.2, 6.4, 1.3 Hz, 1H), 7.52 (ddt, *J* = 8.2, 6.6, 1.4 Hz, 2H), 7.39–7.32 (m, 2H), 3.93 (s, 3H). **¹³C NMR** (125 MHz, CDCl₃): δ = 168.0 (C_q), 163.9 (C_q), 151.7 (C_q), 148.4 (CH), 140.1 (CH), 137.9 (C_q), 134.1 (C_q), 133.9 (C_q), 132.3 (CH), 131.5 (C_q), 129.0 (CH), 127.3 (CH), 123.6 (CH), 123.4 (C_q), 121.5 (CH), 120.1 (CH), 118.5 (CH), 112.6 (CH), 93.9 (CH), 52.1 (CH₃).

IR (ATR): 3059, 2952, 1703, 1673, 1530, 1436, 1262, 1219, 998, 786 cm^{-1} . **MS (EI)** m/z (relative intensity) 371 (34) [M^+], 281 (17), 253 (8), 207 (54), 105 (100), 77 (30), 44 (18). **HR-MS** (ESI) m/z calcd for $\text{C}_{22}\text{H}_{18}\text{N}_3\text{O}_3$ [$\text{M}+\text{H}^+$]: 372.1343, found: 372.1332.

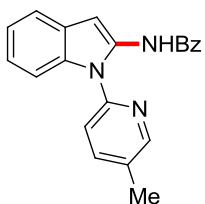
N[4-Methoxy-1-(pyridin-2-yl)-1*H*-indol-2-yl]benzamide (**146da**)



The general procedure **GP2** was followed using indole **28d** (112 mg, 0.50 mmol, 1.0 equiv) and dioxazolone **40a** (98 mg, 0.60 mmol, 1.2 equiv). Purification by column chromatography on silica gel (*n*-hexane/EtOAc = 3/1) yielded **146da** (165 mg, 96%) as a pale yellow solid. **M. p.** = 152–154 °C. **¹H NMR** (500 MHz, CDCl_3): δ = 11.75 (s, 1H), 8.61 (ddd, J = 4.9, 2.0, 0.9 Hz, 1H), 7.97–7.86 (m, 3H), 7.75 (dt, J = 8.3, 1.0 Hz, 1H), 7.58–7.45 (m, 3H), 7.41 (s, 1H), 7.30–7.18 (m, 2H), 7.11 (t, J = 8.1 Hz, 1H), 6.66 (dd, J = 7.9, 0.6 Hz, 1H), 3.98 (s, 3H). **¹³C NMR** (125 MHz, CDCl_3): δ = 163.5 (C_q), 153.4 (C_q), 152.2 (C_q), 148.2 (CH), 139.5 (CH), 134.5 (C_q), 133.5 (C_q), 133.2 (C_q), 131.9 (CH), 128.8 (CH), 127.1 (CH), 122.7 (CH), 120.9 (CH), 119.9 (C_q), 118.2 (CH), 104.0 (CH), 102.7 (CH), 91.2 (CH), 55.7 (CH_3). **IR** (ATR): 3057, 2954, 1666, 1538, 1470, 1437, 1250, 1090, 764, 686 cm^{-1} . **MS (EI)** m/z (relative intensity) 343 (69) [M^+], 281 (6), 238 (27), 207 (20), 169 (7), 105 (100), 77 (40), 44 (11). **HR-MS** (ESI) m/z calcd for $\text{C}_{21}\text{H}_{18}\text{N}_3\text{O}_2$ [$\text{M}+\text{H}^+$]: 344.1394, found: 344.1394.

***N*-[1-(4-Methylpyridin-2-yl)-1*H*-indol-2-yl]benzamide (146ea)**

The general procedure **GP2** was followed using indole **28e** (104 mg, 0.50 mmol, 1.0 equiv) and dioxazolone **40a** (98 mg, 0.60 mmol, 1.2 equiv). Purification by column chromatography on silica gel (*n*-hexane/EtOAc = 5/1) yielded **146ea** (159 mg, 97%) as an off-white solid. **M. p.** = 166–169 °C. **¹H NMR** (500 MHz, CDCl₃): δ = 11.92 (s, 1H), 8.52–8.46 (m, 1H), 7.97–7.91 (m, 2H), 7.66–7.58 (m, 3H), 7.58–7.50 (m, 2H), 7.50–7.46 (m, 1H), 7.29 (s, 1H), 7.28–7.16 (m, 2H), 7.11 (ddd, *J* = 5.2, 1.5, 0.8 Hz, 1H), 2.49 (s, 3H). **¹³C NMR** (125 MHz, CDCl₃): δ = 163.8 (C_q), 152.2 (C_q), 151.4 (C_q), 147.9 (CH), 135.1 (C_q), 134.4 (C_q), 132.0 (CH), 132.0 (C_q), 129.8 (C_q), 128.9 (CH), 127.2 (CH), 122.2 (CH), 122.1 (CH), 121.7 (CH), 120.8 (CH), 118.6 (CH), 110.7 (CH), 93.6 (CH), 21.6 (CH₃). **IR** (ATR): 3228, 3044, 1672, 1523, 1459, 1259, 805, 685, 636, 447 cm⁻¹. **MS (EI)** *m/z* (relative intensity) 327 (60) [M⁺], 222 (26), 195 (26), 105 (100), 77 (41), 44 (33). **HR-MS** (ESI) *m/z* calcd for C₂₁H₁₈N₃O [M+H⁺]: 328.1444, found: 328.1447.

***N*-[1-(5-Methylpyridin-2-yl)-1*H*-indol-2-yl]benzamide (146ba)**

The general procedure **GP2** was followed using indole **28b** (104 mg, 0.50 mmol, 1.0 equiv) and dioxazolone **40a** (98 mg, 0.60 mmol, 1.2 equiv). Purification by column chromatography on silica gel (*n*-hexane/EtOAc = 5/1) yielded **146ba** (151 mg, 92%) as a pale yellow solid. **M. p.** = 171–173 °C. **¹H NMR** (300 MHz, CDCl₃): δ = 11.80 (s, 1H), 8.45 (dp, *J* = 2.3, 0.8 Hz, 1H), 8.00–7.86 (m, 2H), 7.75

(ddd, $J = 8.4, 2.4, 0.7$ Hz, 1H), 7.67 (dd, $J = 8.4, 0.8$ Hz, 1H), 7.65–7.61 (m, 1H), 7.60–7.47 (m, 4H), 7.28 (t, $J = 0.5$ Hz, 1H), 7.24–7.13 (m, 2H), 2.44 (s, 3H). **^{13}C NMR** (125 MHz, CDCl_3): $\delta = 163.6$ (C_q), 149.9 (C_q), 148.2 (CH), 140.1 (CH), 134.9 (C_q), 134.4 (C_q), 132.0 (C_q), 131.9 (CH), 130.7 (C_q), 129.6 (C_q), 128.8 (CH), 127.2 (CH), 121.9 (CH), 121.7 (CH), 120.7 (CH), 117.6 (CH), 110.5 (CH), 93.5 (CH), 18.2 (CH_3). **IR** (ATR): 3183, 3049, 1683, 1539, 1477, 1455, 783, 690, 650, 637 cm^{-1} . **MS (EI)** m/z (relative intensity) 327 (60) [M^+], 281 (24), 253 (13), 207 (76), 105 (100), 77 (35), 44 (22). **HR-MS** (ESI) m/z calcd for $\text{C}_{21}\text{H}_{18}\text{N}_3\text{O}$ [$\text{M}+\text{H}^+$]: 328.1444, found: 328.1444.

5.3.2. Mechanistic Studies

Reactions with Radical Scavengers

142a (81 mg, 0.50 mmol, 1.0 equiv), **40a** (98 mg, 0.60 mmol, 1.2 equiv), Cp*Co(CO)I₂ (11.9 mg, 0.025 mmol, 5.0 mol %), AgSbF₆ (34 mg, 0.10 mmol, 20 mol %), NaOAc (8.2 mg, 0.10 mmol, 20 mol %) and the radical scavenger were placed into an oven-dried 25 mL Schlenk tube equipped with a septum under N₂ atmosphere. DCE (2.0 mL) was introduced *via* cannula. The reaction mixture was stirred at 100 °C for 16 h. After cooling to ambient temperature, the reaction mixture was dry loaded onto silica gel and purified by flash column chromatography (*n*-hexane/EtOAc = 7/1) to yield the product **143aa** as an off-white solid.

Table 5.1. Effect of radical scavengers on the cobalt-catalyzed C–H amidation.

| Entry | Radical scavenger | Yield [%] ^[a] |
|-------|---|--------------------------|
| 1 | <i>none</i> | 68 |
| 2 | TEMPO (1.0 equiv) | 46 |
| 3 | TEMPO (2.0 equiv) | 49 |
| 4 | BHT (1.0 equiv) | 48 |
| 5 | (<i>E</i>)-stilbene (1.0 equiv) | 63 |
| 6 | Ph ₂ C=CH ₂ (1.0 equiv) | 67 |
| 7 | galvinoxyl (1.0 equiv) | 14 |

^[a] Isolated yield.

Mercury Poisoning Test

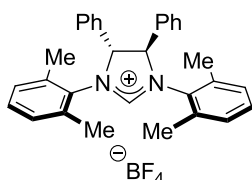
142a (81 mg, 0.50 mmol, 1.0 equiv), **40a** (98 mg, 0.60 mmol, 1.2 equiv), Cp*Co(CO)I₂ (12 mg, 0.025 mmol, 5.0 mol %), AgSbF₆ (34 mg, 0.10 mmol,

20 mol %), and NaOAc (8.2 mg, 0.10 mmol, 20 mol %) were placed into a 25 mL Schlenk tube equipped with a septum under N₂ atmosphere. DCE (2.0 mL) was introduced *via* cannula. The reaction mixture was stirred at 100 °C for 2.5 min and mercury (100 mg, 0.50 mmol, 1.0 equiv) was added *via* syringe. At this point, no detectable formation of **143aa** was observed by GC-MS analysis of an aliquot of the reaction mixture. The reaction mixture was stirred at 100 °C for 16 h. After cooling to ambient temperature, the reaction mixture was dry loaded onto silica gel and purified by flash column chromatography (*n*-hexane/EtOAc = 7/1) to yield the product **143aa** (92 mg, 66%) as a white solid.

5.4. Synthesis of Novel Chiral Ligands

5.4.1. Experimental Procedures and Analytical Data of Novel Chiral NHC Precursors

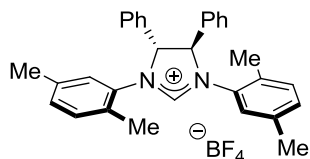
(4*R*,5*R*)-1,3-Bis(2,6-dimethylphenyl)-4,5-diphenyl-4,5-dihydro-1*H*-imidazol-3-ium Tetrafluoroborate (**155**)



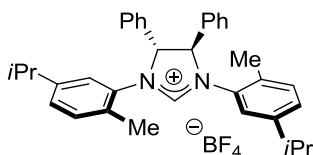
The general procedure **GP4** was followed using (*R,R*)-diphenylethylenediamine (200 mg, 0.94 mmol, 1.0 equiv), Pd(OAc)₂ (21.1 mg, 94 μmol, 10 mol %), (+/-)-BINAP (117 mg, 188 μmol, 20 mol %), NaOtBu (271 mg, 2.82 mmol, 3.0 equiv) and 2-bromo-1,3-dimethylbenzene (366 mg, 1.98 mmol, 2.1 equiv) in PhMe (20 mL). Short column chromatography (*n*-hexane/CH₂Cl₂ = 3/2→1/1) yielded the crude diarylated diamine (285 mg, 72%). The crude *N,N'*-diarylated diamine (280 mg, 0.67 mmol, 1.0 equiv) was treated with ammonium tetrafluoroborate (84 mg, 0.80 mmol, 1.2 equiv) and triethyl orthoformate (1.0 mL). Purification by column chromatography (CH₂Cl₂/acetone = 9/1→4/1) yielded **155** (277 mg, 80%) as a white solid. **M. p.** = 149–151 °C. **¹H NMR** (300 MHz, CDCl₃): δ = 8.78 (s, 1H), 7.44–7.32 (m, 10H), 7.18 (d, *J* = 3.9 Hz, 4H), 6.94 (dd, *J* = 6.7, 2.7 Hz, 2H), 6.04 (d, *J* = 0.7 Hz, 2H), 2.72 (s, 6H), 2.00 (s, 6H). **¹³C NMR** (125 MHz, CDCl₃): δ = 158.2 (CH), 136.6 (C_q), 134.5 (C_q), 131.2 (C_q), 131.1 (CH), 130.8 (CH), 130.3 (CH), 129.5 (CH), 129.5 (CH), 129.4 (CH), 128.8 (CH), 72.9 (CH), 19.1 (CH₃), 18.4 (CH₃). **¹⁹F NMR** (282 MHz, CDCl₃): δ = -152.84 (s), -152.90 (dd, *J* = 2.5, 0.8 Hz). **IR** (ATR): 3059, 1613, 1222, 1050, 1031, 699 cm⁻¹. **MS (ESI)** *m/z* (relative intensity): 431 (100) [M-BF₄]⁺. **HR-MS** (ESI) *m/z* calcd for C₃₁H₃₁N₂ [M-BF₄]⁺ 431.2482, found 431.2479. **[α]_D²⁰**: +303.1 (*c* = 1.05, CHCl₃).

The analytical data are in accordance with those previously reported in the literature.^[328]

(4*R*,5*R*)-1,3-Bis(2,5-dimethylphenyl)-4,5-diphenyl-4,5-dihydro-1*H*-imidazol-3-ium Tetrafluoroborate (176)



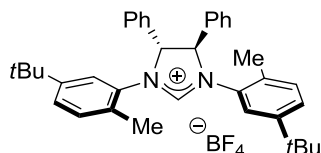
The general procedure **GP4** was followed using (*R,R*)-diphenylethylenediamine (150 mg, 0.71 mmol, 1.0 equiv), Pd(OAc)₂ (7.9 mg, 35 μmol, 5.0 mol %), (+/-)-BINAP (44 mg, 71 μmol, 10 mol %), NaOtBu (204 mg, 2.12 mmol, 3.0 equiv) and 2-bromo-1,4-dimethylbenzene (275 mg, 1.48 mmol, 2.1 equiv) in PhMe (15 mL). Short column chromatography (*n*-hexane/CH₂Cl₂ = 2/1) yielded the crude diarylated diamine (300 mg, quantitative). The crude *N,N'*-diarylated diamine (300 mg, 0.71 mmol, 1.0 equiv) was treated with ammonium tetrafluoroborate (90 mg, 0.86 mmol, 1.2 equiv) and triethyl orthoformate (1.5 mL). Purification by column chromatography (CH₂Cl₂/acetone = 7/1) yielded **176** (313 mg, 85%) as a white solid. **M. p.** = 125–127 °C. **¹H NMR** (400 MHz, CDCl₃): δ = 8.45 (*d*, *J* = 0.7 Hz, 1H), 7.44–7.32 (*m*, 10H), 7.28 (*t*, *J* = 1.1 Hz, 2H), 7.09–6.98 (*m*, 4H), 5.78 (*d*, *J* = 0.7 Hz, 2H), 2.39 (*s*, 6H), 2.24 (*s*, 6H). **¹³C NMR** (100 MHz, CDCl₃): δ = 157.4 (CH), 138.0 (C_q), 133.7 (C_q), 132.4 (C_q), 131.4 (CH), 130.9 (CH), 130.3 (CH), 129.8 (C_q), 129.7 (CH), 128.1 (CH), 127.9 (CH), 76.1 (CH), 20.6 (CH₃), 17.9 (CH₃). **¹⁹F NMR** (282 MHz, CDCl₃): δ = -151.31 (*s*), -151.36 (*d*, *J* = 2.5 Hz). **IR** (ATR): 3066, 1613, 1049, 1035, 756, 700 cm⁻¹. **MS (ESI)** *m/z* (relative intensity): 431 (100) [M-BF₄]⁺. **HR-MS** (ESI) *m/z* calcd for C₃₁H₃₁N₂ [M-BF₄]⁺ 431.2482, found 431.2481. **[α]_D²⁰**: +412.1 (*c* = 1.01, CHCl₃).

(4*R*,5*R*)-1,3-Bis(5-isopropyl-2-methylphenyl)-4,5-diphenyl-4,5-dihydro-1*H*-imidazol-3-ium Tetrafluoroborate (177)

Under inert atmosphere, an oven-dried 100 mL Schlenk flask was charged with (*R,R*)-diphenylethylenediamine (350 mg, 1.65 mmol, 1.0 equiv), Pd(dba)₂ (95 mg, 0.16 mmol, 10 mol %), dppf (183 mg, 0.33 mmol, 20 mol %) and NaOtBu (475 mg, 4.94 mmol, 3.0 equiv). The flask was evacuated and backfilled with nitrogen 3 times. PhMe (20 mL) and freshly prepared 5-isopropyl-2-methylphenyl trifluoromethanesulfonate^[329] (980 mg, 3.46 mmol, 2.1 equiv) were then added *via* syringe. The flask was then placed in a pre-heated oil bath at 100 °C, and stirred for 16 h. The solution was then cooled to ambient temperature, diluted with *n*-hexane (60 mL), filtered through a plug of silica and washed with *n*-hexane/CH₂Cl₂ = 1/1. The filtrate was concentrated under reduced pressure. Short column chromatography (*n*-hexane/CH₂Cl₂ = 4/1) yielded the crude *N,N'*-diarylated diamine as a pale yellow foam (605 mg, 78%). The crude *N,N'*-diarylated diamine (600 mg, 1.28 mmol, 1.0 equiv), ammonium tetrafluoroborate (161 mg, 1.54 mmol, 1.2 equiv), and triethyl orthoformate (5.0 mL) were stirred at 120 °C for 5 h. The solution was then allowed to cool to ambient temperature. The reaction mixture was dry loaded onto silica gel and purified by column chromatography (CH₂Cl₂/acetone = 15/1→10/1). The obtained product was washed with Et₂O until colorless to yield **177** (529 mg, 72%) as a colorless powder. **M. p.** = 133–135 °C. **¹H NMR** (500 MHz, CDCl₃): δ = 8.52 (s, 1H), 7.45–7.35 (m, 10H), 7.25 (d, *J* = 1.7 Hz, 2H), 7.10 (qd, *J* = 8.0, 1.4 Hz, 4H), 5.81 (s, 2H), 2.82 (hept, *J* = 6.9 Hz, 2H), 2.44 (s, 6H), 1.11 (dd, *J* = 6.9, 6.2 Hz, 12H). **¹³C NMR** (125 MHz, CDCl₃): δ = 157.1 (CH), 149.0 (C_q), 133.6 (C_q), 132.4 (C_q), 131.4 (CH), 130.3 (CH), 130.0 (C_q), 129.6 (CH), 128.3 (CH), 128.2 (CH), 125.9 (CH), 76.0 (CH), 33.3 (CH), 23.6 (CH₃), 23.4 (CH₃), 17.9 (CH₃). **¹⁹F NMR** (282 MHz, CDCl₃): δ = -151.20 (s), -151.25 (dd, *J* = 2.1, 0.9 Hz). **IR** (ATR): 2962, 1624, 1613, 1212, 1049, 701 cm⁻¹. **MS (ESI)** *m/z* (relative intensity):

487 (100) $[M-BF_4]^+$. **HR-MS** (ESI) m/z calcd for $C_{35}H_{39}N_2 [M-BF_4]^+$ 487.3108, found 487.3106. $[\alpha]_D^{20}$: +379.9 ($c = 1.03$, $CHCl_3$).

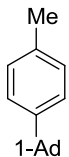
(4*R*,5*R*)-1,3-Bis[5-(*tert*-butyl)-2-methylphenyl]-4,5-diphenyl-4,5-dihydro-1*H*-imidazol-3-ium Tetrafluoroborate (178)



The general procedure **GP4** was followed using (*R,R*)-diphenylethylenediamine (100 mg, 0.47 mmol, 1.0 equiv), $Pd(OAc)_2$ (5.3 mg, 24 μ mol, 5.0 mol %), (+/-)-BINAP (29 mg, 47 μ mol, 10 mol %), $NaOtBu$ (136 mg, 1.42 mmol, 3.0 equiv) and 2-bromo-4-(*tert*-butyl)-1-methylbenzene^[330] (225 mg, 0.99 mmol, 2.1 equiv) in PhMe (10 mL). Short column chromatography (*n*-hexane/ $CH_2Cl_2 = 4/1$) yielded the crude diarylated diamine (240 mg, quantitative). The crude *N,N*-diarylated diamine (240 mg, 0.47 mmol, 1.0 equiv) was treated with ammonium tetrafluoroborate (60 mg, 0.56 mmol, 1.2 equiv) and triethyl orthoformate (4.0 mL). Purification by column chromatography (CH_2Cl_2 /acetone = 15/1 \rightarrow 5/1) yielded **178** (210 mg, 74%) as a white solid. **M. p.** = 125–128 °C. **1H NMR** (300 MHz, $CDCl_3$): δ = 8.52 (s, 1H), 7.47–7.32 (m, 12H), 7.24 (dd, $J = 8.0, 2.0$ Hz, 2H), 7.13 (dd, $J = 8.0, 0.7$ Hz, 2H), 5.81 (s, 2H), 2.46 (s, 6H), 1.18 (s, 18H). **^{13}C NMR** (125 MHz, $CDCl_3$): δ = 157.0 (CH), 151.2 (C_q), 133.5 (C_q), 132.2 (C_q), 131.1 (CH), 130.2 (CH), 129.7 (C_q), 129.5 (CH), 128.3 (CH), 126.8 (CH), 125.1 (CH), 76.1 (CH), 34.6 (C_q), 31.0 (CH_3), 17.8 (CH_3). **^{19}F NMR** (282 MHz, $CDCl_3$): δ = -151.14 (s), -151.19 (d, $J = 2.2$ Hz). **IR** (ATR): 2962, 1604, 1214, 1050, 1031, 700 cm^{-1} . **MS (ESI)** m/z (relative intensity): 515 (100) $[M-BF_4]^+$. **HR-MS** (ESI) m/z calcd for $C_{37}H_{43}N_2 [M-BF_4]^+$ 515.3421, found 515.3420. $[\alpha]_D^{20}$: +326.0 ($c = 1.00$, $CHCl_3$).

Synthesis of 180

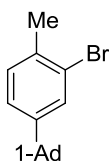
1-(*p*-Tolyl)adamantane (233)



Following a modified procedure,^[331] a suspension of 1-bromoadamantane (15.0 g, 69.7 mmol, 1.00 equiv), Pd/C 10 wt. % (3.70 g, 3.50 mmol, 5.00 mol %), K₂CO₃ (11.6 g, 83.6 mmol, 1.20 equiv) and PhMe (200 mL) was refluxed for 16 h under a slow stream of N₂. The mixture was allowed to cool to ambient temperature, diluted with *n*-hexane (200 mL), filtered through a plug of Celite[®] and concentrated under reduced pressure. The residue was recrystallized from *n*-hexane at -30 °C, collected by filtration, washed with cold *n*-pentane and dried under high vacuum to provide 1-(*p*-tolyl)adamantane **233** (13.8 g, 87%) as a colorless crystalline solid.

The analytical data are in agreement with those previously reported in the literature.^[331]

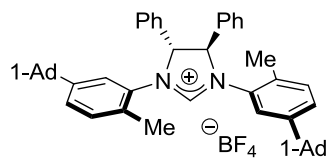
1-(3-Bromo-4-methylphenyl)adamantane (234)



Following a modified procedure,^[330] 1-(*p*-tolyl)adamantane **233** (5.57 g, 24.6 mmol, 1.0 equiv) was dissolved in chloroform (12.2 mL). The flask was wrapped with aluminum foil and placed in an ice bath. Under stirring, bromine (1.27 mL, 24.6 mmol, 1.0 equiv) was added dropwise *via* syringe. The mixture was stirred at ambient temperature for 16 h. Then, the solution was poured into NaHSO₃ (0.1 M, 100 mL) and extracted with *n*-hexane (3 × 100 mL). The combined organic layer was washed with brine (50 mL), dried over Na₂SO₄, and concentrated under reduced

pressure. The residue was taken into *n*-hexane and filtered through a short plug of silica gel. The silica was washed with *n*-hexane. The combined filtrate was concentrated under reduced pressure and the residue recrystallized from *n*-hexane at $-30\text{ }^{\circ}\text{C}$ to yield the product **234** as a white crystalline solid (5.82 g, 77%). **M. p.** = 115–117 $^{\circ}\text{C}$. **$^1\text{H NMR}$** (400 MHz, CDCl_3): δ = 7.50 (d, J = 1.8 Hz, 1H), 7.20 (dd, J = 8.0, 1.8 Hz, 1H), 7.17 (dt, J = 8.0, 0.6 Hz, 1H), 2.36 (s, 3H), 2.09 (h, J = 2.7 Hz, 3H), 1.94–1.85 (m, 6H), 1.84–1.68 (m, 6H). **$^{13}\text{C NMR}$** (100 MHz, CDCl_3): δ = 151.1 (C_q), 134.7 (C_q), 130.4 (CH), 129.0 (CH), 124.9 (C_q), 123.8 (CH), 43.1 (CH_2), 36.7 (CH_2), 36.0 (C_q), 28.9 (CH), 22.3 (CH_3). **IR** (ATR): 2902, 2845, 1493, 1447, 1031, 801, 675 cm^{-1} . **MS (EI)** m/z (relative intensity): 306 (65) $[\text{M}]^+$ (^{81}Br), 304 (65) $[\text{M}]^+$ (^{79}Br), 249 (34) (^{81}Br), 247 (33) (^{79}Br), 168 (100), 94 (24). **HR-MS** (EI) m/z calcd for $\text{C}_{17}\text{H}_{21}^{79}\text{Br} [\text{M}]^+$ 304.0827, found 304.0834.

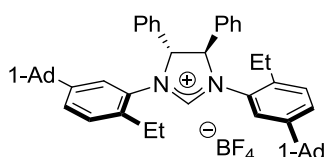
(4*R*,5*R*)-1,3-Bis[5-(adamantan-1-yl)-2-methylphenyl]-4,5-diphenyl-4,5-dihydro-1*H*-imidazol-3-ium Tetrafluoroborate (180)



The general procedure **GP4** was followed using (*R,R*)-diphenylethylenediamine (200 mg, 0.94 mmol, 1.0 equiv), $\text{Pd}(\text{OAc})_2$ (10.6 mg, 47 μmol , 5.0 mol %), (+/–)-BINAP (59 mg, 94 μmol , 10 mol %), NaOtBu (272 mg, 2.83 mmol, 3.0 equiv) and 1-(3-bromo-4-methylphenyl)adamantane **234** (604 mg, 1.98 mmol, 2.1 equiv) in PhMe (15 mL). Short column chromatography (*n*-hexane/ CH_2Cl_2 = 6/1) yielded the crude diarylated diamine (602 mg, 91%). The crude *N,N*-diarylated diamine (565 mg, 0.85 mmol, 1.0 equiv) was treated with ammonium tetrafluoroborate (108 mg, 1.03 mmol, 1.2 equiv) and triethyl orthoformate (4.0 mL). Purification by column chromatography (*n*-hexane/acetone = 3/1→1/1) yielded **180** (522 mg, 81%) as an off-white solid. **M. p.** = 196–198 $^{\circ}\text{C}$. **$^1\text{H NMR}$** (300 MHz, CDCl_3): δ = 8.59 (s, 1H), 7.49–7.34 (m, 10H), 7.28 (d, J = 1.9 Hz, 2H), 7.22 (dd, J = 8.0, 2.0 Hz, 2H),

7.15 (d, $J = 8.1$ Hz, 2H), 5.81 (d, $J = 0.6$ Hz, 2H), 2.47 (s, 6H), 2.10–2.00 (m, 6H), 1.80–1.68 (m, 24H). $^{13}\text{C NMR}$ (125 MHz, CDCl_3): $\delta = 157.0$ (CH), 151.3 (C_q), 133.7 (C_q), 132.3 (C_q), 131.2 (CH), 130.1 (CH), 129.8 (C_q), 129.5 (CH), 128.3 (CH), 126.5 (CH), 124.5 (CH), 76.1 (CH), 42.7 (CH_2), 36.6 (CH_2), 36.1 (C_q), 28.9 (CH), 17.9 (CH_3). $^{19}\text{F NMR}$ (282 MHz, CDCl_3): $\delta = -151.11$ (s), -151.17 (d, $J = 2.2$ Hz). **IR** (ATR): 2899, 2846, 1604, 1213, 1052, 755, 699 cm^{-1} . **MS (ESI)** m/z (relative intensity): 671 (100) $[\text{M}-\text{BF}_4]^+$. **HR-MS** (ESI) m/z calcd for $\text{C}_{49}\text{H}_{55}\text{N}_2$ $[\text{M}-\text{BF}_4]^+$ 671.4360, found 671.4360. $[\alpha]_{\text{D}}^{20}$: +278.6 ($c = 1.02$, CHCl_3).

(4*R*,5*R*)-1,3-Bis[5-(adamantan-1-yl)-2-ethylphenyl]-4,5-diphenyl-4,5-dihydro-1*H*-imidazol-3-ium Tetrafluoroborate (181)

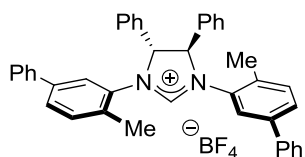


1-(3-Bromo-4-ethylphenyl)adamantane was prepared in 2 steps from ethylbenzene following the same procedure as for the synthesis of **234**.^[330,331] The crude product was used without purification.

The general procedure **GP4** was followed using (*R,R*)-diphenylethylenediamine (202 mg, 0.95 mmol, 1.0 equiv), $\text{Pd}(\text{OAc})_2$ (21.4 mg, 95 μmol , 10 mol %), (+/–)-BINAP (119 mg, 191 μmol , 20 mol %), NaOtBu (275 mg, 2.86 mmol, 3.0 equiv) and crude 1-(3-bromo-4-ethylphenyl)adamantane (638 mg, 2.0 mmol, 2.1 equiv) in PhMe (20 mL). Short column chromatography (*n*-hexane/ $\text{CH}_2\text{Cl}_2 = 7/1 \rightarrow 3/1$) yielded the crude diarylated diamine (470 mg, 72%) as a yellow foam. The crude *N,N*-diarylated diamine (470 mg, 0.68 mmol, 1.0 equiv) was treated with ammonium tetrafluoroborate (86 mg, 0.82 mmol, 1.2 equiv) and triethyl orthoformate (3.0 mL). Purification by column chromatography ($\text{CH}_2\text{Cl}_2/\text{acetone} = 35/1 \rightarrow 20/1$) yielded **181** (364 mg, 68%) as a pale yellow solid. **M. p.** = 167–169 °C. $^1\text{H NMR}$ (500 MHz, CDCl_3): $\delta = 8.41$ (s, 1H), 7.46–7.37 (m, 10H), 7.36 (d, $J = 2.0$ Hz, 2H), 7.27 (dd, $J = 8.1, 1.8$ Hz, 2H), 7.19 (d, $J = 8.2$ Hz, 2H), 5.81 (s, 2H), 2.81–2.71 (m, 4H), 2.09–

2.00 (m, 6H), 1.76–1.71 (m, 24H), 1.32 (t, $J = 7.4$ Hz, 6H). $^{13}\text{C NMR}$ (125 MHz, CDCl_3): $\delta = 157.3$ (CH), 151.4 (C_q), 136.0 (C_q), 133.6 (C_q), 131.8 (C_q), 130.4 (CH), 129.7 (CH), 129.1 (CH), 128.7 (CH), 126.9 (CH), 125.3 (CH), 76.6 (CH), 42.7 (CH_2), 36.7 (CH_2), 36.2 (C_q), 28.9 (CH), 23.7 (CH_2), 15.2 (CH_3). $^{19}\text{F NMR}$ (471 MHz, CDCl_3): $\delta = -150.93, -150.99$ (d, $J = 2.3$ Hz). **IR** (ATR): 2900, 2847, 1603, 1454, 1268, 1211, 1052, 699 cm^{-1} . **MS (ESI)** m/z (relative intensity): 699 (100) $[\text{M}-\text{BF}_4]^+$. **HR-MS** (ESI) m/z calcd for $\text{C}_{51}\text{H}_{59}\text{N}_2$ $[\text{M}-\text{BF}_4]^+$ 699.4673, found 699.4674. $[\alpha]_{\text{D}}^{20}$: -237.7 ($c = 0.97, \text{CHCl}_3$).

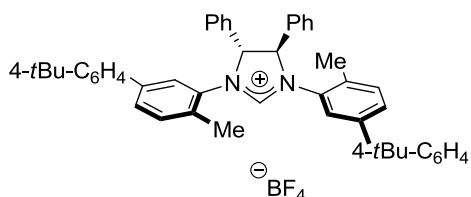
(4*R*,5*R*)-1,3-Bis(4-methyl-[1,1'-biphenyl]-3-yl)-4,5-diphenyl-4,5-dihydro-1*H*-imidazol-3-ium Tetrafluoroborate (182)



The general procedure **GP4** was followed using (*R,R*)-diphenylethylenediamine (180 mg, 0.85 mmol, 1.0 equiv), $\text{Pd}(\text{OAc})_2$ (9.5 mg, 42 μmol , 5.0 mol %), (+/–)-BINAP (53 mg, 85 μmol , 10 mol %), NaOtBu (244 mg, 2.54 mmol, 3.0 equiv) and 3-bromo-4-methyl-1,1'-biphenyl^[332] (440 mg, 1.78 mmol, 2.1 equiv) in PhMe (15 mL). Short column chromatography (*n*-hexane/ $\text{CH}_2\text{Cl}_2 = 4/1 \rightarrow 2.5/1$) yielded the crude diarylated diamine (395 mg, 85%). The crude *N,N*-diarylated diamine (375 mg, 0.69 mmol, 1.0 equiv) was treated with ammonium tetrafluoroborate (87 mg, 0.83 mmol, 1.2 equiv) and triethyl orthoformate (2.5 mL). Purification by column chromatography ($\text{CH}_2\text{Cl}_2/\text{acetone} = 15/1 \rightarrow 5/1$) yielded **182** (379 mg, 85%) as an off-white solid. **M. p.** = 162–164 °C. $^1\text{H NMR}$ (300 MHz, CDCl_3): $\delta = 8.58$ (s, 1H), 7.64 (d, $J = 1.8$ Hz, 2H), 7.55–7.48 (m, 4H), 7.47–7.27 (m, 18H), 7.23 (d, $J = 8.0$ Hz, 2H), 5.85 (s, 2H), 2.50 (s, 6H). $^{13}\text{C NMR}$ (125 MHz, CDCl_3): $\delta = 157.7$ (CH), 140.8 (C_q), 138.7 (C_q), 133.3 (C_q), 133.0 (C_q), 132.0 (CH), 131.9 (C_q), 130.3 (CH), 129.7 (CH), 128.8 (CH), 128.5 (CH), 128.2 (CH), 127.7 (CH), 127.0 (CH), 125.8 (CH), 76.3 (CH), 18.2 (CH_3). $^{19}\text{F NMR}$ (282 MHz, CDCl_3): $\delta = -150.45$ (s),

–150.50 (d, $J = 2.2$ Hz). **IR** (ATR): 3060, 1600, 1212, 1052, 759, 697 cm^{-1} . **MS (ESI)** m/z (relative intensity): 555 (100) $[\text{M}-\text{BF}_4]^+$. **HR-MS** (ESI) m/z calcd for $\text{C}_{41}\text{H}_{35}\text{N}_2$ $[\text{M}-\text{BF}_4]^+$ 555.2795, found 555.2796. $[\alpha]_{\text{D}}^{20}$: +383.6 ($c = 1.10$, CHCl_3).

(4*R*,5*R*)-1,3-Bis(4'-(*tert*-butyl)-4-methyl-[1,1'-biphenyl]-3-yl)-4,5-diphenyl-4,5-dihydro-1*H*-imidazol-3-ium Tetrafluoroborate (183)



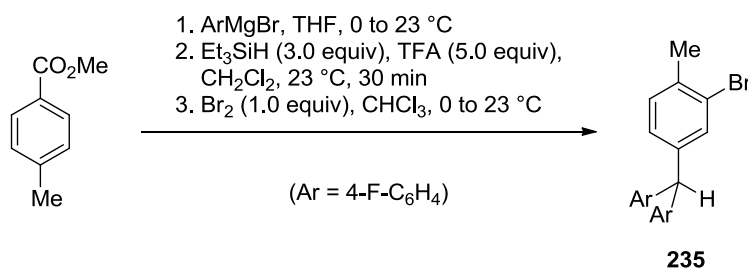
3-Bromo-4'-(*tert*-butyl)-4-methyl-1,1'-biphenyl was prepared following reported procedures.^[332]

The general procedure **GP4** was followed using (*R,R*)-diphenylethylenediamine (300 mg, 1.41 mmol, 1.0 equiv), $\text{Pd}(\text{OAc})_2$ (15.9 mg, 71 μmol , 5.0 mol %), (+/–)-BINAP (88 mg, 14.1 μmol , 10 mol %), NaOtBu (407 mg, 4.24 mmol, 3.0 equiv) and 3-bromo-4'-(*tert*-butyl)-4-methyl-1,1'-biphenyl (900 mg, 2.97 mmol, 2.1 equiv, 70% purity) in PhMe (12.0 mL). Short column chromatography (*n*-hexane/ $\text{CH}_2\text{Cl}_2 = 10/1 \rightarrow 2.5/1$) yielded the crude diarylated diamine (853 mg, 92%) as an off-white foam. The crude *N,N*-diarylated diamine (853 mg, 1.30 mmol, 1.0 equiv) was treated with ammonium tetrafluoroborate (170 mg, 1.62 mmol, 1.25 equiv) and triethyl orthoformate (5.0 mL). Purification by column chromatography ($\text{CH}_2\text{Cl}_2/\text{acetone} = 30/1 \rightarrow 7/1$) followed by recrystallization from *i*PrOH (8.0 mL) yielded **183** (911 mg, 93%) as an off-white solid. **M. p.** = 325–326 °C. **$^1\text{H NMR}$** (400 MHz, CDCl_3): $\delta = 8.60$ (s, 1H), 7.67 (d, $J = 1.9$ Hz, 2H), 7.51–7.46 (m, 4H), 7.46–7.42 (m, 10H), 7.42–7.34 (m, 6H), 7.22 (d, $J = 8.0$ Hz, 2H), 5.86 (s, 2H), 2.49 (s, 6H), 1.34 (s, 18H). **$^{13}\text{C NMR}$** (100 MHz, CDCl_3): $\delta = 157.9$ (CH), 151.0 (C_q), 140.9 (C_q), 136.0 (C_q), 133.6 (C_q), 133.2 (C_q), 132.2 (CH), 131.7 (C_q), 130.5 (CH), 129.9 (CH), 128.5 (CH), 128.4 (CH), 126.8 (CH), 126.0 (CH), 125.8 (CH), 76.5 (CH), 34.7 (C_q), 31.5 (CH_3), 18.2 (CH_3). **$^{19}\text{F NMR}$** (376 MHz, CDCl_3): $\delta = -150.61, -150.66$ (d, $J = 2.2$ Hz). **IR** (ATR): 2962,

1607, 1495, 1213, 1053, 818, 699, 567 cm^{-1} . **MS (ESI)** m/z (relative intensity): 667 (100) $[\text{M}-\text{BF}_4]^+$. **HR-MS** (ESI) m/z calcd for $\text{C}_{49}\text{H}_{51}\text{N}_2$ $[\text{M}-\text{BF}_4]^+$ 667.4047, found 667.4047. $[\alpha]_{\text{D}}^{20}$: +333.5 ($c = 1.0$, acetone).

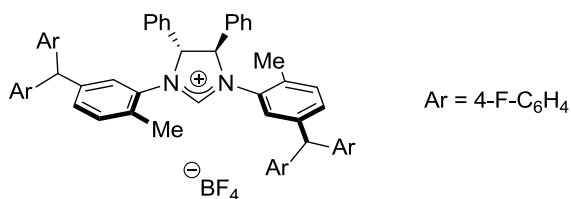
Synthesis of 184

4,4'-[(3-Bromo-4-methylphenyl)methylene]bis(fluorobenzene) (235)



235 was prepared from methyl *p*-toluate following reported procedures.^[330,333] The crude product **235** was used in the next step without further purification.

(4*R*,5*R*)-1,3-Bis{5-[bis(4-fluorophenyl)methyl]-2-methylphenyl}-4,5-diphenyl-4,5-dihydro-1*H*-imidazol-3-ium Tetrafluoroborate (184)

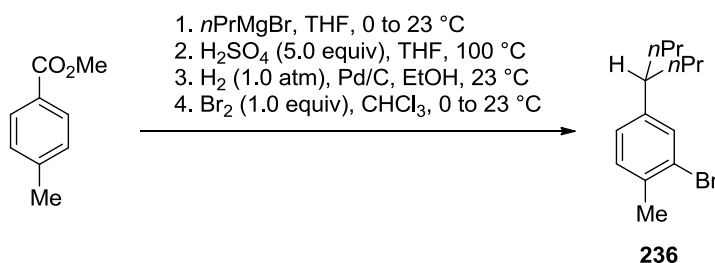


The general procedure **GP4** was followed using (*R,R*)-diphenylethylenediamine (120 mg, 0.57 mmol, 1.0 equiv), $\text{Pd}(\text{dba})_2$ (36 mg, 63 μmol , 11 mol %), *dppf* (63 mg, 114 μmol , 20 mol %), NaOtBu (163 mg, 1.70 mmol, 3.0 equiv) and crude 4,4'-[(3-bromo-4-methylphenyl)methylene]bis(fluorobenzene) (**235**) (591 mg, 1.20 mmol, 2.1 equiv, 70% purity) in PhMe (8.0 mL). Short column chromatography (*n*-hexane/ $\text{CH}_2\text{Cl}_2 = 9/1 \rightarrow 4/1$) yielded the crude diarylated diamine (402 mg, 90%) as an off-white foam. The crude *N,N*-diarylated diamine (380 mg, 0.48 mmol,

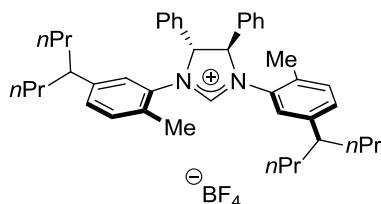
1.0 equiv) was treated with ammonium tetrafluoroborate (60 mg, 0.57 mmol, 1.2 equiv) and triethyl orthoformate (4.0 mL). Purification by column chromatography (CH₂Cl₂/acetone = 13/1) yielded **184** (394 mg, 92%) as an off-white solid. **M. p.** = 132–133 °C. **¹H NMR** (500 MHz, CDCl₃): δ = 8.78 (s, 1H), 7.38–7.31 (m, 2H), 7.30–7.25 (m, 4H), 7.20–7.15 (m, 4H), 7.14 (d, *J* = 7.9 Hz, 2H), 6.91 (m, 20H), 5.56 (s, 2H), 5.44 (s, 2H), 2.43 (s, 6H). **¹³C NMR** (125 MHz, CDCl₃): δ = 161.6 (d, ¹*J*_{C-F} = 245.2 Hz, C_q), 161.6 (d, ¹*J*_{C-F} = 245.2 Hz, C_q), 157.8 (CH), 143.9 (C_q), 138.6 (d, ⁴*J*_{C-F} = 3.2 Hz, C_q), 138.5 (d, ⁴*J*_{C-F} = 3.2 Hz, C_q), 133.6 (C_q), 132.6 (C_q), 132.0 (CH), 131.4 (C_q), 130.9 (CH), 130.9 (d, ³*J*_{C-F} = 8.1 Hz, CH), 130.9 (d, ³*J*_{C-F} = 8.1 Hz, CH), 130.5 (CH), 129.8 (CH), 128.6 (CH), 128.0 (CH), 115.4 (d, ²*J*_{C-F} = 21.3 Hz, CH), 115.4 (d, ²*J*_{C-F} = 21.3 Hz, CH), 76.1 (CH), 54.2 (CH), 18.1 (CH₃). **¹⁹F NMR** (282 MHz, CDCl₃): δ = -116.48 (tdd, *J* = 13.8, 8.2, 5.6 Hz), -151.03 (d, *J* = 1.5 Hz), -151.08 (d, *J* = 2.7 Hz). **IR** (ATR): 1602, 1504, 1219, 1158, 1050, 822, 755, 699, 565 cm⁻¹. **MS (ESI)** *m/z* (relative intensity): 807 (100) [M-BF₄]⁺. **HR-MS** (ESI) *m/z* calcd for C₅₅H₄₃N₂F₄ [M-BF₄]⁺ 807.3357, found 807.3364. **[α]_D²⁰**: +238.0 (*c* = 1.08, CHCl₃).

Synthesis of 185

2-Bromo-4-(heptan-4-yl)-1-methylbenzene (236)

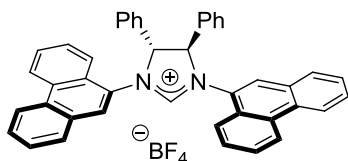


236 was prepared from methyl *p*-toluate following reported procedures.^[330,334] The crude product **236** was used in the next step without further purification.

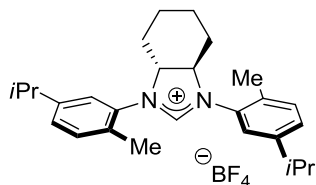
(4*R*,5*R*)-1,3-Bis[5-(heptan-4-yl)-2-methylphenyl]-4,5-diphenyl-4,5-dihydro-1*H*-imidazol-3-ium Tetrafluoroborate (185)

The general procedure **GP4** was followed using (*R,R*)-diphenylethylenediamine (150 mg, 0.71 mmol, 1.0 equiv), Pd(OAc)₂ (7.9 mg, 35 μmol, 5.0 mol %), (+/–)-BINAP (44 mg, 71 μmol, 10 mol %), NaOtBu (204 mg, 2.12 mmol, 3.0 equiv) and crude 2-bromo-4-(heptan-4-yl)-1-methylbenzene (**236**) (615 mg, 1.49 mmol, 2.1 equiv, 65% purity) in PhMe (12 mL). Short column chromatography (*n*-hexane/CH₂Cl₂ = 12/1) yielded the crude diarylated diamine (379 mg, 90%). The crude *N,N*-diarylated diamine (378 mg, 0.64 mmol, 1.0 equiv) was treated with ammonium tetrafluoroborate (81 mg, 0.77 mmol, 1.2 equiv) and triethyl orthoformate (4.0 mL). Purification by column chromatography (CH₂Cl₂/acetone = 19/1→10/1) yielded **185** (190 mg, 43%) as an off-white foam. **M. p.** = 88–90 °C. **¹H NMR** (500 MHz, CDCl₃): δ = 8.51 (s, 1H), 7.44–7.29 (m, 10H), 7.13 (d, *J* = 1.7 Hz, 2H), 7.09 (d, *J* = 7.8 Hz, 2H), 6.97 (dd, *J* = 7.8, 1.8 Hz, 2H), 5.82 (s, 2H), 2.46 (s, 6H), 2.45–2.36 (m, 2H), 1.50–1.39 (m, 4H), 1.39–1.29 (m, 4H), 1.00–0.87 (m, 4H), 0.87–0.75 (m, 4H), 0.73 (t, *J* = 7.2 Hz, 6H), 0.72 (t, *J* = 7.2 Hz, 6H). **¹³C NMR** (100 MHz, CDCl₃): δ = 156.9 (CH), 146.6 (C_q), 133.6 (C_q), 132.5 (C_q), 131.5 (CH), 130.3 (CH), 130.2 (C_q), 129.7 (CH), 129.5 (CH), 128.5 (CH), 127.2 (CH), 76.1 (CH), 45.0 (CH), 39.1 (CH₂), 38.8 (CH₂), 20.6 (CH₂), 20.6 (CH₂), 18.1 (CH₃), 14.2 (CH₃), 14.2 (CH₃). **¹⁹F NMR** (377 MHz, CDCl₃): δ = –151.15, –151.20 (d, *J* = 2.1 Hz). **IR** (ATR): 2955, 2928, 1606, 1456, 1214, 1051, 700 cm^{–1}. **MS (ESI)** *m/z* (relative intensity): 599 (100) [M–BF₄]⁺. **HR-MS** (ESI) *m/z* calcd for C₄₃H₅₅N₂ [M–BF₄]⁺ 599.4360, found 599.4359. **[α]_D²⁰**: +331.2 (c = 0.51, CHCl₃).

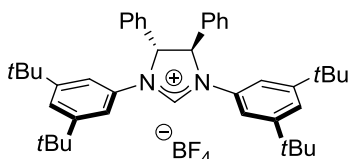
**(4*R*,5*R*)-1,3-Di(phenanthren-9-yl)-4,5-diphenyl-4,5-dihydro-1*H*-imidazol-3-ium
Tetrafluoroborate (186)**



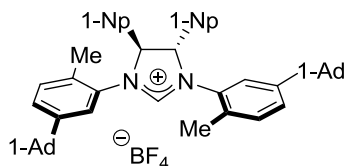
The general procedure **GP4** was followed using (*R,R*)-diphenylethylenediamine (100 mg, 0.47 mmol, 1.0 equiv), Pd(OAc)₂ (5.3 mg, 24 μmol, 5.0 mol %), (+/-)-BINAP (29 mg, 47 μmol, 10 mol %), NaOtBu (136 mg, 1.42 mmol, 3.0 equiv) and 9-bromophenanthrene (254 mg, 0.99 mmol, 2.1 equiv) in PhMe (8.0 mL). Short column chromatography (*n*-hexane/CH₂Cl₂ = 16/1→3/1) yielded the crude diarylated diamine (284 mg, quantitative) as a yellow foam. The crude *N,N'*-diarylated diamine (280 mg, 0.50 mmol, 1.0 equiv) was treated with ammonium tetrafluoroborate (62 mg, 0.59 mmol, 1.2 equiv) and triethyl orthoformate (8.0 mL). Purification by column chromatography (CH₂Cl₂/acetone = 15/1→3/1) yielded **186** (275 mg, 83%) as a yellow solid. **M. p.** = 221–223 °C. **¹H NMR** (300 MHz, CDCl₃): δ = 8.59 (dd, *J* = 8.5, 1.1 Hz, 2H), 8.50 (d, *J* = 8.3 Hz, 2H), 8.31 (s, 2H), 8.13–8.01 (m, 3H), 7.97 (dd, *J* = 8.1, 1.3 Hz, 2H), 7.76 (ddd, *J* = 8.1, 7.0, 1.1 Hz, 2H), 7.61 (ddd, *J* = 8.4, 7.0, 1.3 Hz, 4H), 7.57–7.50 (m, 4H), 7.48–7.38 (m, 2H), 7.32–7.18 (m, 6H), 6.26 (s, 2H). **¹³C NMR** (125 MHz, CDCl₃): δ = 158.8 (CH), 132.5 (C_q), 131.3 (C_q), 130.5 (C_q), 130.4 (CH), 130.3 (C_q), 130.2 (CH), 129.6 (CH), 129.6 (CH), 128.7 (CH), 128.7 (CH), 128.1 (C_q), 128.0 (CH), 127.8 (CH), 127.7 (CH), 127.1 (C_q), 123.8 (CH), 122.4 (CH), 121.6 (CH), 77.3 (CH). **¹⁹F NMR** (282 MHz, CDCl₃): δ = -149.68 (m). **IR** (ATR): 3065, 1605, 1028, 749, 726, 698 cm⁻¹. **MS (ESI)** *m/z* (relative intensity): 575 (100) [M-BF₄]⁺. **HR-MS** (ESI) *m/z* calcd for C₄₃H₃₁N₂ [M-BF₄]⁺ 575.2482, found 575.2475. **[α]_D²⁰**: +427.1 (*c* = 0.99, CHCl₃).

(3*aR*,7*aR*)-1,3-Bis(5-isopropyl-2-methylphenyl)-3*a*,4,5,6,7,7*a*-hexahydro-1*H*-benzo[*d*]imidazol-3-ium Tetrafluoroborate (187)

The general procedure **GP4** was followed using (1*R*,2*R*)-cyclohexane-1,2-diamine (116 mg, 1.02 mmol, 1.0 equiv), Pd(dba)₂ (64 mg, 0.11 mmol, 11 mol %), dppf (112 mg, 0.20 mmol, 20 mol %), NaOtBu (292 mg, 3.04 mmol, 3.0 equiv) and 5-isopropyl-2-methylphenyl trifluoromethanesulfonate^[329] (600 mg, 2.13 mmol, 2.1 equiv) in PhMe (10.0 mL). Short column chromatography (*n*-hexane/CH₂Cl₂ = 8/1→4/1) yielded the crude diarylated diamine (90 mg, 23%) as a yellow foam. The crude *N,N*-diarylated diamine (90 mg, 0.24 mmol, 1.0 equiv) was treated with ammonium tetrafluoroborate (30 mg, 0.29 mmol, 1.2 equiv) and triethyl orthoformate (1.5 mL). Purification by column chromatography (CH₂Cl₂/acetone = 9/1→5/1) yielded **187** (65.8 mg, 73%) as a pale yellow foam. **M. p.** = 90–92 °C. **¹H NMR** (500 MHz, CDCl₃): δ = 7.97 (s, 1H), 7.49 (s, 2H), 7.24 (app s, 4H), 4.31 (s, 2H), 2.96 (p, *J* = 6.8 Hz, 2H), 2.35 (s, 6H), 2.09 (d, *J* = 10.6 Hz, 2H), 1.96 (d, *J* = 8.5 Hz, 2H), 1.86 (app s, 2H), 1.51–1.39 (m, 2H), 1.26 (d, *J* = 6.7 Hz, 12H). **¹³C NMR** (125 MHz, CDCl₃): δ = 159.0 (CH), 149.7 (C_q), 132.9 (C_q), 131.6 (CH), 131.0 (C_q), 128.5 (CH), 125.9 (CH), 71.4 (CH), 33.7 (CH), 27.6 (CH₂), 24.0 (CH₃), 23.9 (CH₃), 23.9 (CH₂), 17.6 (CH₃). **¹⁹F NMR** (471 MHz, CDCl₃): δ = -151.33, -151.39 (d, *J* = 2.2 Hz). **IR** (ATR): 2900, 2847, 1591, 1449, 1256, 1038, 942, 755 cm⁻¹. **MS (ESI) *m/z*** (relative intensity): 389 (100) [M-BF₄]⁺. **HR-MS** (ESI) *m/z* calcd for C₂₇H₃₇N₂ [M-BF₄]⁺ 389.2951, found 389.2952. **[α]_D²⁰**: +33.9 (c = 0.81, CHCl₃).

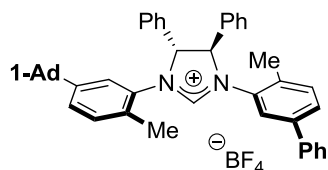
(4*R*,5*R*)-1,3-Bis(3,5-di-*tert*-butylphenyl)-4,5-diphenyl-4,5-dihydro-1*H*-imidazol-3-ium Tetrafluoroborate (188)

The general procedure **GP4** was followed using (*R,R*)-diphenylethylenediamine (200 mg, 0.94 mmol, 1.0 equiv), Pd(OAc)₂ (11.0 mg, 49 μmol, 5.0 mol %), (+/-)-BINAP (59 mg, 95 μmol, 10 mol %), NaOtBu (272 mg, 2.83 mmol, 3.0 equiv) and 1-bromo-3,5-di-*tert*-butylbenzene (533 mg, 1.98 mmol, 2.1 equiv) in PhMe (15 mL). Short column chromatography (*n*-hexane/CH₂Cl₂ = 8/1→4/1) yielded the crude diarylated diamine (557 mg, quantitative). The crude *N,N'*-diarylated diamine (557 mg, 0.95 mmol, 1.0 equiv) was treated with ammonium tetrafluoroborate (119 mg, 1.14 mmol, 1.2 equiv) and triethyl orthoformate (3.0 mL). Purification by column chromatography (CH₂Cl₂/acetone = 20/1→15/1) yielded **188** (545 mg, 87%) as a white solid. **M. p.** = 275–277 °C. ¹H NMR (500 MHz, CDCl₃): δ = 9.37 (s, 1H), 7.46–7.37 (m, 10H), 7.31 (t, *J* = 1.6 Hz, 2H), 7.17 (s, 2H), 7.16 (s, 2H), 5.71 (d, *J* = 0.5 Hz, 2H), 1.22 (s, 36H). ¹³C NMR (125 MHz, CDCl₃): δ = 153.4 (CH), 153.2 (C_q), 135.0 (C_q), 134.1 (C_q), 130.2 (CH), 130.1 (CH), 127.5 (CH), 122.8 (CH), 116.1 (CH), 75.4 (CH), 35.3 (C_q), 31.2 (CH₃). ¹⁹F NMR (471 MHz, CDCl₃): δ = -150.31, -150.37 (d, *J* = 2.2 Hz). IR (ATR): 2902, 1619, 1583, 1054, 756, 700 cm⁻¹. **MS (ESI)** *m/z* (relative intensity): 599 (100) [M-BF₄]⁺. **HR-MS** (ESI) *m/z* calcd for C₄₃H₅₅N₂ [M-BF₄]⁺ 599.4360, found 599.4352. [α]_D²⁰: +190.5 (c = 1.02, CHCl₃).

(4*S*,5*S*)-1,3-Bis[5-(adamantan-1-yl)-2-methylphenyl]-4,5-di(naphthalen-1-yl)-4,5-dihydro-1*H*-imidazol-3-ium Tetrafluoroborate (189)

The general procedure **GP4** was followed using (1*S*,2*S*)-1,2-di(naphthalen-1-yl)ethane-1,2-diamine^[335] (480 mg, 1.54 mmol, 1.0 equiv), Pd(OAc)₂ (34.5 mg, 0.15 mmol, 10 mol %), (+/-)-BINAP (191 mg, 0.31 mmol, 20 mol %), NaOtBu (443 mg, 4.61 mmol, 3.0 equiv) and 1-(3-bromo-4-methylphenyl)adamantane **234** (985 mg, 3.23 mmol, 2.1 equiv) in PhMe (20 mL). Short column chromatography (*n*-hexane/CH₂Cl₂ = 7/1→1/1) yielded the crude diarylated diamine (737 mg, 63%) as an off-white foam. The crude *N,N'*-diarylated diamine (737 mg, 0.97 mmol, 1.0 equiv) was treated with ammonium tetrafluoroborate (122 mg, 1.16 mmol, 1.2 equiv) and triethyl orthoformate (3.0 mL). Purification by column chromatography (CH₂Cl₂/acetone = 25/1→10/1), followed by recrystallization from *i*PrOH (5.0 mL), yielded **189** (656 mg, 79%) as a white solid. **M. p.** = 292–293 °C. **¹H NMR** (600 MHz, CDCl₃): δ = 9.59–8.25 (brm, 2H), 8.24–7.27 (brm, 11H), 7.23–7.03 (brm, 8H), 7.04–6.08 (brm, 2H), 2.69–2.41 (m, 6H), 2.14–1.84 (m, 6H), 1.83–1.34 (m, 24H). As previously reported in a similar situation,^[210] peaks were noticeably broadened and difficult to integrate, likely due to slow rotation. **¹³C NMR** (125 MHz, CDCl₃): δ = 157.7 (CH), 151.4 (C_q), 133.7 (C_q), 132.8 (C_q), 132.0 (CH), 131.6 (CH), 131.3 (C_q), 130.6 (CH), 130.1 (C_q), 129.5 (C_q), 129.1 (CH), 128.2 (CH), 127.3 (CH), 126.3 (CH), 126.0 (CH), 123.9 (CH), 121.1 (CH), 71.0 (CH), 42.6 (CH₂), 36.7 (CH₂), 36.1 (C_q), 28.9 (CH), 18.4 (CH₃). **¹⁹F NMR** (376 MHz, CDCl₃): δ = -151.19, -151.24 (d, *J* = 2.5 Hz). **IR** (ATR): 2900, 1592, 1260, 1052, 800, 773, 477 cm⁻¹. **MS (ESI)** *m/z* (relative intensity): 771 (100) [M-BF₄]⁺. **HR-MS** (ESI) *m/z* calcd for C₅₇H₅₉N₂ [M-BF₄]⁺ 771.4673, found 771.4668. **[α]_D²⁰**: -352.7 (c = 1.0, CHCl₃).

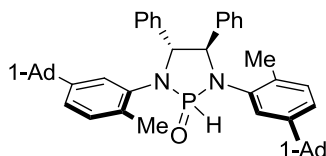
(4*R*,5*R*)-1-[5-(Adamantan-1-yl)-2-methylphenyl]-3-(4-methyl-[1,1'-biphenyl]-3-yl)-4,5-diphenyl-4,5-dihydro-1*H*-imidazol-3-ium Tetrafluoroborate (190)



190 was prepared following a procedure reported in the literature^[242c] from (*R,R*)-diphenylethylenediamine (368 mg, 1.73 mmol, 1.0 equiv), 3-bromo-4-methyl-1,1'-biphenyl^[330] (450 mg, 1.82 mmol, 1.05 equiv) and 1-(3-bromo-4-methylphenyl)adamantane **234** (1.2 equiv in the 2nd step). After purification by column chromatography (CH₂Cl₂/acetone = 16/1→6/1) and recrystallization from *i*PrOH (3.0 mL) at -30 °C, **190** (556 mg, 46% over 3 steps) was obtained as a white solid. **M. p.** = 154–156 °C. **¹H NMR** (400 MHz, CDCl₃): δ = 8.54 (s, 1H), 7.62 (d, *J* = 1.8 Hz, 1H), 7.54–7.45 (m, 4H), 7.45–7.34 (m, 11H), 7.33–7.27 (m, 2H), 7.24 (d, *J* = 4.0 Hz, 1H), 7.22 (dd, *J* = 8.1, 2.0 Hz, 1H), 7.14 (d, *J* = 8.1 Hz, 1H), 5.93 (d, *J* = 10.4 Hz, 1H), 5.74 (d, *J* = 10.4 Hz, 1H), 2.49 (s, 3H), 2.46 (s, 3H), 2.09–2.00 (m, 3H), 1.78–1.66 (m, 12H). **¹³C NMR** (100 MHz, CDCl₃): δ = 157.5 (CH), 151.6 (C_q), 141.0 (C_q), 139.0 (C_q), 133.7 (C_q), 133.6 (C_q), 133.3 (C_q), 132.4 (C_q), 132.3 (CH), 132.1 (C_q), 131.4 (CH), 130.5 (CH), 130.4 (CH), 130.0 (C_q), 129.9 (CH), 129.8 (CH), 129.0 (CH), 128.7 (CH), 128.6 (CH), 128.3 (CH), 127.9 (CH), 127.2 (CH), 126.8 (CH), 125.6 (CH), 125.2 (CH), 76.4 (CH), 76.1 (CH), 42.7 (CH₂), 36.7 (CH₂), 36.2 (C_q), 28.9 (CH), 18.2 (CH₃), 18.0 (CH₃). **¹⁹F NMR** (376 MHz, CDCl₃): δ = -150.81, -150.86 (d, *J* = 2.4 Hz). **IR** (ATR): 2901, 2847, 1604, 1213, 1052, 760, 698 cm⁻¹. **MS (ESI)** *m/z* (relative intensity): 613 (100) [M-BF₄]⁺. **HR-MS** (ESI) *m/z* calcd for C₄₅H₄₅N₂ [M-BF₄]⁺ 613.3578, found 613.3571. **[α]_D²⁰**: +340.4 (c = 1.0, CHCl₃).

5.4.2. Experimental Procedures and Analytical Data of Novel Chiral HASPOs

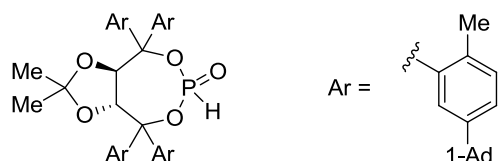
(4*R*,5*R*)-1,3-Bis[5-(adamantan-1-yl)-2-methylphenyl]-4,5-diphenyl-1,3,2-diazaphospholidine 2-Oxide (**213**)



Following a modified procedure,^[239b] PCl₃ (45 μL, 0.51 mmol, 1.0 equiv) was added dropwise at 0 °C to a solution of the *N,N*-diarylated diamine (see the synthesis of

pre-ligand **180** (340 mg, 0.51 mmol, 1.0 equiv) and Et₃N (0.54 mL, 3.85 mmol, 7.5 equiv) in CH₂Cl₂ (2.1 mL). After stirring at ambient temperature for 1 h, H₂O (9.3 μL, 0.51 mmol, 1.0 equiv) was added at 0 °C. The resulting mixture was stirred for 20 h at 23 °C, filtered through Celite[®] and concentrated under reduced pressure. The residue was purified by column chromatography on silica gel (*n*-hexane/EtOAc = 19/1→9/1) to yield **213** (211 mg, 58%) as a yellow foam. **M. p.** = 147–149 °C. **¹H NMR** (300 MHz, CDCl₃): δ = 8.07 (d, *J*_{H-P} = 603.3 Hz, 1H), 7.44 (dd, *J* = 7.9, 1.7 Hz, 2H), 7.34–7.17 (m, 9H), 7.05–6.94 (m, 5H), 5.12 (ddd, *J* = 6.1, 3.1, 1.0 Hz, 1H), 4.90 (t, *J* = 6.0 Hz, 1H), 2.46 (s, 3H), 2.41 (s, 3H), 2.12–1.93 (m, 6H), 1.84–1.62 (m, 24H). **¹³C NMR** (125 MHz, CDCl₃): δ = 150.1 (C_q), 149.8 (C_q), 139.4 (C_q), 139.4 (C_q), 138.6 (C_q), 138.5 (C_q), 136.7 (C_q), 136.6 (C_q), 136.0 (C_q), 135.9 (C_q), 134.3 (C_q), 134.2 (C_q), 132.4 (C_q), 132.4 (C_q), 130.9 (CH), 128.6 (CH), 128.5 (CH), 128.3 (CH), 128.2 (CH), 128.1 (CH), 127.7 (CH), 126.2 (CH), 124.5 (CH), 123.7 (CH), 123.0 (CH), 72.6 (d, *J* = 9.0 Hz, CH), 72.5 (d, *J* = 10.2 Hz, CH), 43.2 (CH₂), 43.2 (CH₂), 37.0 (CH₂), 37.0 (CH₂), 36.0 (C_q), 36.0 (C_q), 29.1 (CH), 19.1 (CH₃), 18.7 (CH₃). **³¹P NMR** (162 MHz, CDCl₃): δ = 9.94. **IR** (ATR): 2899, 2846, 1450, 1240, 1137, 1005, 751, 698 cm⁻¹. **MS (ESI)** *m/z* (relative intensity): 2143 (100) [3M+Na]⁺, 1437 (37) [2M+Na]⁺, 729 (35) [M+Na]⁺. **HR-MS** (ESI) *m/z* calcd for C₄₈H₅₅N₂OPNa [M+Na]⁺ 729.3944, found 729.3943. [α]_D²⁰: +82.3 (c = 0.74, CHCl₃).

(3*aR*,8*aR*)-2,2-Dimethyl-4,4,8,8-tetra(2-methyl-5-adamant-1-ylphenyl)tetrahydro-[1,3]dioxolo[4,5-*e*][1,3,2]dioxaphosphepine 6-Oxide (218**)**



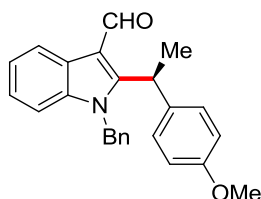
The corresponding (*R,R*)-TADDOL was prepared in 2 steps from L-(+)-diethyl tartrate and **234** following reported procedures.^[336]

Following a modified procedure,^[207] PCl₃ (158 μL, 1.81 mmol, 1.2 equiv) was added dropwise at 0 °C to a solution of the diol (1.60 g, 1.51 mmol, 1.0 equiv) and Et₃N

(0.63 mL, 4.53 mmol, 3.0 equiv) in THF (9.0 mL). After stirring at ambient temperature for 16 h, Et₃N (0.21 mL, 1.51 mmol, 1.0 equiv) and H₂O (27 μL, 1.51 mmol, 1.0 equiv) were added at 0 °C. The resulting mixture was stirred for 8 h at 23 °C, filtered through Celite[®] and concentrated under reduced pressure. The residue was purified by column chromatography on silica gel (*n*-hexane/EtOAc = 25/1→6/1) to yield **218** (835 mg, 50%) as a colorless solid. **M. p.** = 229–231 °C. **¹H NMR** (400 MHz, CDCl₃): δ = 8.54–7.35 (brm, 4H), 7.26–6.78 (brm, 9H), 6.39–5.48 (brm, 2H), 2.31–1.32 (m, 72H), 1.18–0.17 (m, 6H). As previously reported in a similar situation,^[207] peaks were noticeably broadened and difficult to integrate, likely due to slow rotation. **¹³C NMR** (100 MHz, CDCl₃): δ = 148.9 (C_q), 147.9 (C_q), 147.5 (C_q), 140.1 (C_q), 136.4 (C_q), 136.1 (C_q), 135.8 (C_q), 134.8 (C_q), 132.9 (CH), 132.5 (CH), 132.5 (CH), 132.3 (CH), 126.1 (CH), 125.1 (CH), 124.6 (CH), 124.4 (CH), 113.4 (C_q), 91.3 (C_q), 90.5 (C_q), 81.3 (CH), 80.7 (CH), 77.4 (CH), 43.3 (CH₂), 43.3 (CH₂), 37.0 (CH₂), 36.9 (CH₂), 36.8 (CH₂), 36.8 (CH₂), 36.3 (CH), 36.1 (C_q), 36.0 (C_q), 29.1 (CH), 29.1 (CH), 29.0 (CH), 29.0 (CH), 27.1 (CH₃), 25.9 (CH₃), 23.0 (CH₃), 22.5 (CH₃), 21.2 (CH₃), 21.0 (CH₃). **³¹P NMR** (162 MHz, CDCl₃): δ = -7.14. **IR** (ATR): 2900, 2847, 1449, 1084, 975, 941, 806, 755 cm⁻¹. **MS (ESI)** *m/z* (relative intensity): 1128 (100) [M+Na]⁺. **HR-MS** (ESI) *m/z* calcd for C₇₅H₉₃O₅PNa [M+Na]⁺ 1127.6653, found 1127.6659. **[α]_D²⁰**: -123.9 (c = 1.10, CHCl₃).

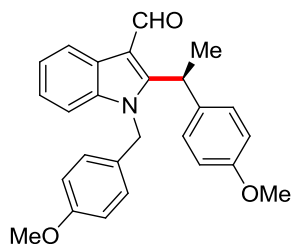
5.5. Iron-Catalyzed Enantioselective C–H Alkylation with Alkenes

5.5.1. Experimental Procedures and Analytical Data

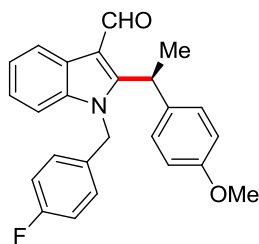
(S)-1-Benzyl-2-[1-(4-methoxyphenyl)ethyl]-1*H*-indole-3-carbaldehyde (62cc)

The general procedure **GP6** was followed using indole **59c** (85 mg, 0.25 mmol, 1.0 equiv) and styrene **60c** (50 mg, 0.38 mmol, 1.5 equiv). Purification by column chromatography on silica gel (*n*-hexane/EtOAc = 8/1→6/1) yielded **62cc** (88.0 mg, 95%) as a yellow solid. **M. p.** = 58–59 °C. **¹H NMR** (400 MHz, CDCl₃): δ = 10.22 (s, 1H), 8.43 (ddd, *J* = 7.9, 1.3, 0.7 Hz, 1H), 7.31 (ddd, *J* = 8.0, 7.1, 1.1 Hz, 1H), 7.29–7.20 (m, 4H), 7.14 (dt, *J* = 8.1, 0.9 Hz, 1H), 7.11 (dd, *J* = 8.9, 0.9 Hz, 2H), 6.90 (dddd, *J* = 6.7, 2.7, 2.0, 1.1 Hz, 2H), 6.80 (d, *J* = 8.8 Hz, 2H), 5.25 (d, *J* = 17.1 Hz, 1H), 5.21 (d, *J* = 17.1 Hz, 1H), 4.99 (q, *J* = 7.4 Hz, 1H), 3.77 (s, 3H), 1.72 (d, *J* = 7.4 Hz, 3H). **¹³C NMR** (100 MHz, CDCl₃): δ = 185.4 (CH), 158.5 (C_q), 154.2 (C_q), 137.0 (C_q), 136.0 (C_q), 133.2 (C_q), 128.9 (CH), 128.0 (CH), 127.6 (CH), 126.0 (C_q), 125.8 (CH), 123.7 (CH), 123.1 (CH), 121.7 (CH), 114.8 (C_q), 114.2 (CH), 110.1 (CH), 55.3 (CH₃), 47.5 (CH₂), 34.3 (CH), 20.0 (CH₃). **IR** (ATR): 2929, 1643, 1510, 1246, 1179, 1029, 744 cm⁻¹. **MS (EI)** *m/z* (relative intensity): 369 (79) [M]⁺, 261 (30), 197 (84), 91 (100). **HR-MS** (EI) *m/z* calcd for C₂₅H₂₃NO₂ [M]⁺ 369.1729, found 369.1735. **[α]_D²³**: –54.9 (*c* = 1.74, CHCl₃). **HPLC separation** (Chiralpak[®] IA-3, *n*-hexane/*i*PrOH 80:20, 1.0 mL/min, detection at 273 nm): *t_r*(major) = 8.3 min, *t_r*(minor) = 9.5 min, 92:8 e.r.

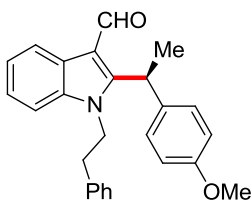
(S)-1-(4-Methoxybenzyl)-2-[1-(4-methoxyphenyl)ethyl]-1*H*-indole-3-carbaldehyde (62dc)



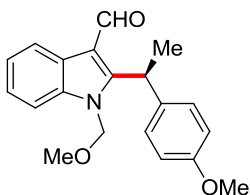
The general procedure **GP6** was followed using indole **59d** (93 mg, 0.25 mmol, 1.0 equiv) and styrene **60c** (50 mg, 0.38 mmol, 1.5 equiv). Purification by column chromatography on silica gel (*n*-hexane/EtOAc = 8/1→5.5/1) yielded **62dc** (79.4 mg, 80%) as a yellow solid. **M. p.** = 56–57 °C. **¹H NMR** (500 MHz, CDCl₃): δ = 10.20 (s, 1H), 8.42 (dt, *J* = 7.9, 1.0 Hz, 1H), 7.30 (ddd, *J* = 8.1, 7.1, 1.1 Hz, 1H), 7.23 (ddd, *J* = 8.3, 7.1, 1.3 Hz, 1H), 7.16 (dt, *J* = 8.2, 1.0 Hz, 1H), 7.11 (d, *J* = 8.4 Hz, 2H), 6.86–6.74 (m, 6H), 5.19 (d, *J* = 17.1 Hz, 1H), 5.15 (d, *J* = 17.1 Hz, 1H), 4.99 (q, *J* = 7.4 Hz, 1H), 3.77 (s, 3H), 3.76 (s, 3H), 1.72 (d, *J* = 7.4 Hz, 3H). **¹³C NMR** (125 MHz, CDCl₃): δ = 185.2 (CH), 158.9 (C_q), 158.3 (C_q), 154.1 (C_q), 137.0 (C_q), 133.3 (C_q), 128.0 (CH), 127.9 (C_q), 127.0 (CH), 126.0 (C_q), 123.5 (CH), 123.0 (CH), 121.7 (CH), 114.7 (C_q), 114.2 (CH), 114.1 (CH), 110.2 (CH), 55.3 (CH₃), 55.3 (CH₃), 47.1 (CH₂), 34.5 (CH), 20.2 (CH₃). **IR** (ATR): 2929, 1643, 1509, 1244, 1175, 1030, 739 cm⁻¹. **MS (EI)** *m/z* (relative intensity): 399 (31) [M]⁺, 278 (40), 263 (10), 250 (13), 227 (24), 121 (100). **HR-MS** (EI) *m/z* calcd for C₂₆H₂₅NO₃ [M]⁺ 399.1834, found 399.1826. **[α]_D²³**: –52.4 (*c* = 1.17, CHCl₃). **HPLC separation** (Chiralpak[®] IA-3, *n*-hexane/*i*PrOH 80:20, 1.0 mL/min, detection at 250 nm): *t_r* (major) = 10.4 min, *t_r* (minor) = 11.7 min, 92:8 e.r.

(S)-1-(4-Fluorobenzyl)-2-[1-(4-methoxyphenyl)ethyl]-1*H*-indole-3-carbaldehyde (62ec)

The general procedure **GP6** was followed using indole **59e** (90 mg, 0.25 mmol, 1.0 equiv) and styrene **60c** (50 mg, 0.38 mmol, 1.5 equiv). Purification by column chromatography on silica gel (*n*-hexane/EtOAc = 8/1→5.5/1) yielded **62ec** (90.9 mg, 94%) as a yellow solid. **M. p.** = 60–61 °C. **¹H NMR** (500 MHz, CDCl₃): δ = 10.24 (s, 1H), 8.43 (ddd, *J* = 7.8, 1.2, 0.7 Hz, 1H), 7.32 (ddd, *J* = 8.0, 7.1, 1.0 Hz, 1H), 7.23 (ddd, *J* = 8.3, 7.2, 1.2 Hz, 1H), 7.14–7.08 (m, 3H), 6.94 (t, *J* = 8.6 Hz, 2H), 6.84 (dd, *J* = 8.9, 5.1 Hz, 2H), 6.80 (d, *J* = 8.8 Hz, 2H), 5.19 (s, 2H), 5.02 (q, *J* = 7.4 Hz, 1H), 3.77 (s, 3H), 1.72 (d, *J* = 7.4 Hz, 3H). **¹³C NMR** (125 MHz, CDCl₃): δ = 185.3 (CH), 162.0 (d, ¹*J*_{C-F} = 246.5 Hz, C_q), 158.4 (C_q), 154.0 (C_q), 136.9 (C_q), 132.9 (C_q), 131.6 (d, ⁴*J*_{C-F} = 3.1 Hz, C_q), 128.0 (CH), 127.4 (d, ³*J*_{C-F} = 8.2 Hz, CH), 125.9 (C_q), 123.7 (CH), 123.2 (CH), 121.7 (CH), 115.7 (d, ²*J*_{C-F} = 21.7 Hz, CH), 114.8 (C_q), 114.1 (CH), 110.0 (CH), 55.2 (CH₃), 46.9 (CH₂), 34.2 (CH), 19.9 (CH₃). **¹⁹F NMR** (471 MHz, CDCl₃): δ = -114.54 (tt, *J* = 8.5, 5.2 Hz). **IR** (ATR): 2932, 1644, 1508, 1247, 823, 743 cm⁻¹. **MS (ESI)** *m/z* (relative intensity): 797 (28) [2M+Na]⁺, 410 (42) [M+Na]⁺, 388 (100) [M+H]⁺, 280 (9). **HR-MS** (ESI) *m/z* calcd for C₂₅H₂₃NO₂F [M+H]⁺ 388.1707, found 388.1696. **[α]_D²³**: -58.1 (c = 1.47, CHCl₃). **HPLC separation** (Chiralpak[®] IA-3, *n*-hexane/*i*PrOH 80:20, 1.0 mL/min, detection at 250 nm): *t_r* (major) = 8.6 min, *t_r* (minor) = 10.0 min, 92:8 e.r.

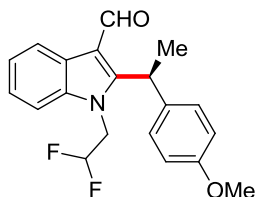
(S)-2-[1-(4-Methoxyphenyl)ethyl]-1-phenethyl-1H-indole-3-carbaldehyde (62fc)

The general procedure **GP6** was followed using indole **59f** (89 mg, 0.25 mmol, 1.0 equiv) and styrene **60c** (50 mg, 0.38 mmol, 1.5 equiv). Purification by column chromatography on silica gel (*n*-hexane/EtOAc = 9/1→7/1) yielded **62fc** (83.4 mg, 87%) as a yellow solid. Using **177**: 67.5 mg (70%), 89:11 e.r. **M. p.** = 48–49 °C. **¹H NMR** (300 MHz, CDCl₃): δ = 10.22 (s, 1H), 8.49–8.37 (m, 1H), 7.44–7.22 (m, 6H), 7.18 (dd, *J* = 8.9, 0.9 Hz, 2H), 7.02 (dd, *J* = 7.9, 1.6 Hz, 2H), 6.89 (d, *J* = 8.8 Hz, 2H), 4.95 (q, *J* = 7.4 Hz, 1H), 4.22 (ddd, *J* = 8.9, 6.9, 1.4 Hz, 2H), 3.80 (s, 3H), 2.94 (ddd, *J* = 13.3, 8.8, 6.7 Hz, 1H), 2.64–2.51 (m, 1H), 1.79 (d, *J* = 7.4 Hz, 3H). **¹³C NMR** (125 MHz, CDCl₃): δ = 185.0 (CH), 158.4 (C_q), 153.4 (C_q), 137.4 (C_q), 136.1 (C_q), 133.4 (C_q), 128.7 (CH), 128.5 (CH), 128.1 (CH), 126.9 (CH), 126.2 (C_q), 123.4 (CH), 122.9 (CH), 121.8 (CH), 114.4 (C_q), 114.2 (CH), 109.7 (CH), 55.3 (CH₃), 46.1 (CH₂), 35.3 (CH₂), 34.4 (CH), 20.0 (CH₃). **IR** (ATR): 2931, 1643, 1510, 1246, 745, 699 cm⁻¹. **MS (ESI)** *m/z* (relative intensity): 789 (16) [2M+Na]⁺, 767 (5) [2M+H]⁺, 398 (22), 384 (100) [M+H]⁺, 117 (12). **HR-MS** (ESI) *m/z* calcd for C₂₆H₂₆NO₂ [M+H]⁺ 384.1958, found 384.1969. **[α]_D²⁰**: –19.6 (*c* = 1.20, CHCl₃). **HPLC separation** (Chiralpak[®] IA-3, *n*-hexane/*i*PrOH 80:20, 1.0 mL/min, detection at 250 nm): *t_r* (major) = 7.6 min, *t_r* (minor) = 8.6 min, 86:14 e.r.

(S)-1-(Methoxymethyl)-2-[1-(4-methoxyphenyl)ethyl]-1H-indole-3-carbaldehyde (62gc)

The general procedure **GP6** was followed using indole **59g** (74 mg, 0.25 mmol, 1.0 equiv) and styrene **60c** (50 mg, 0.38 mmol, 1.5 equiv). Purification by column chromatography on silica gel (*n*-hexane/EtOAc = 8/1→6/1) yielded **62gc** (64.9 mg, 80%) as a yellow oil. Using **177**: 68.0 mg (84%), 87:13 e.r. **¹H NMR** (500 MHz, CDCl₃): δ = 10.20 (s, 1H), 8.41–8.34 (m, 1H), 7.48–7.42 (m, 1H), 7.31 (ddd, *J* = 8.0, 7.2, 0.9 Hz, 2H), 7.21 (d, *J* = 8.0 Hz, 2H), 6.86 (d, *J* = 8.8 Hz, 2H), 5.35 (d, *J* = 11.0 Hz, 1H), 5.31 (d, *J* = 11.0 Hz, 1H), 5.07 (q, *J* = 7.3 Hz, 1H), 3.79 (s, 3H), 3.21 (s, 3H), 1.89 (d, *J* = 7.4 Hz, 3H). **¹³C NMR** (125 MHz, CDCl₃): δ = 185.8 (CH), 158.5 (C_q), 154.6 (C_q), 137.1 (C_q), 133.5 (C_q), 128.1 (CH), 125.8 (C_q), 123.8 (CH), 123.3 (CH), 121.8 (CH), 115.3 (C_q), 114.1 (CH), 109.9 (CH), 74.4 (CH₂), 56.1 (CH₃), 55.3 (CH₃), 34.2 (CH), 20.5 (CH₃). **IR** (ATR): 2932, 2836, 1647, 1510, 1247, 1029, 748 cm⁻¹. **MS (EI)** *m/z* (relative intensity): 323 (100) [M]⁺, 276 (40), 263 (27), 215 (29), 151 (44), 121 (50). **HR-MS** (EI) *m/z* calcd for C₂₀H₂₁NO₃ [M]⁺ 323.1521, found 323.1530. **[α]_D²⁰**: -51.0 (*c* = 1.01, CHCl₃). **HPLC separation** (Chiralpak[®] IB-3, *n*-hexane/*i*PrOH 80:20, 1.0 mL/min, detection at 273 nm): *t_r* (major) = 9.6 min, *t_r* (minor) = 10.4 min, 86:14 e.r.

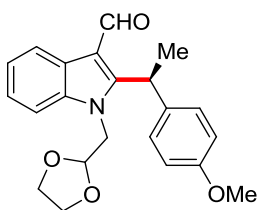
(S)-1-(2,2-Difluoroethyl)-2-[1-(4-methoxyphenyl)ethyl]-1*H*-indole-3-carbaldehyde (62hc)



The general procedure **GP6** was followed using indole **59h** (79 mg, 0.25 mmol, 1.0 equiv) and styrene **60c** (50 mg, 0.38 mmol, 1.5 equiv). Purification by column chromatography on silica gel (*n*-hexane/EtOAc = 8/1→6/1) yielded **62hc** (82.4 mg, 96%) as a yellow solid. **M. p.** = 49–50 °C. **¹H NMR** (500 MHz, CDCl₃): δ = 10.22 (s, 1H), 8.39 (dt, *J* = 5.4, 2.1 Hz, 1H), 7.38–7.29 (m, 3H), 7.20 (dd, *J* = 8.9, 0.9 Hz, 2H), 6.88 (d, *J* = 8.8 Hz, 2H), 5.44 (tt, *J* = 55.2, 4.2 Hz, 1H), 5.05 (q, *J* = 7.4 Hz, 1H), 4.47–4.33 (m, 2H), 3.80 (s, 3H), 1.88 (d, *J* = 7.5 Hz, 3H). **¹³C NMR** (125 MHz,

CDCl₃): δ = 185.5 (CH), 158.7 (C_q), 153.9 (C_q), 136.9 (C_q), 133.0 (C_q), 128.1 (CH), 125.9 (C_q), 124.0 (CH), 123.5 (CH), 121.8 (CH), 115.3 (C_q), 114.4 (CH), 113.2 (t, ¹J_{C-F} = 245.3 Hz, CH), 109.7 (CH), 55.3 (CH₃), 46.4 (t, ²J_{C-F} = 28.9 Hz, CH₂), 34.2 (CH), 20.2 (CH₃). **¹⁹F NMR** (471 MHz, CDCl₃): δ = -119.04 (dt, *J* = 55.3, 13.2 Hz). **IR** (ATR): 2960, 2838, 1644, 1511, 1248, 1057, 747 cm⁻¹. **MS (EI)** *m/z* (relative intensity): 343 (100) [M]⁺, 328 (44), 326 (33), 311 (25), 235 (56), 121 (30). **HR-MS** (EI) *m/z* calcd for C₂₀H₁₉F₂NO₂ [M]⁺ 343.1384, found 343.1386. **[α]_D²³**: -77.5 (c = 1.50, CHCl₃). **HPLC separation** (Chiralpak[®] IA-3, *n*-hexane/*i*PrOH 80:20, 1.0 mL/min, detection at 250 nm): *t_r* (major) = 8.4 min, *t_r* (minor) = 9.1 min, 94:6 e.r.

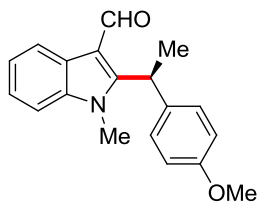
(S)-1-[(1,3-Dioxolan-2-yl)methyl]-2-[1-(4-methoxyphenyl)ethyl]-1*H*-indole-3-carbaldehyde (62ic)



The general procedure **GP6** was followed using indole **59i** (84 mg, 0.25 mmol, 1.0 equiv) and styrene **60c** (50 mg, 0.38 mmol, 1.5 equiv). Purification by column chromatography on silica gel (*n*-hexane/EtOAc = 6/1→3/1) yielded **62ic** (75.2 mg, 82%) as a yellow solid. **M. p.** = 129–132 °C. **¹H NMR** (300 MHz, CDCl₃): δ = 10.01 (s, 1H), 8.40–8.33 (m, 1H), 7.50–7.43 (m, 1H), 7.33–7.26 (m, 2H), 7.20 (dd, *J* = 8.9, 0.9 Hz, 2H), 6.84 (d, *J* = 8.8 Hz, 2H), 5.13 (t, *J* = 3.4 Hz, 1H), 4.93 (q, *J* = 7.3 Hz, 1H), 4.34 (dd, *J* = 3.4, 1.0 Hz, 2H), 3.86–3.81 (m, 4H), 3.79 (s, 3H), 1.88 (d, *J* = 7.3 Hz, 3H). **¹³C NMR** (125 MHz, CDCl₃): δ = 185.9 (CH), 158.3 (C_q), 155.2 (C_q), 137.0 (C_q), 134.2 (C_q), 128.1 (CH), 125.9 (C_q), 123.3 (CH), 123.0 (CH), 121.8 (CH), 114.6 (C_q), 114.1 (CH), 110.5 (CH), 101.9 (CH), 65.3 (CH₂), 65.3 (CH₂), 55.3 (CH₃), 46.7 (CH₂), 34.9 (CH), 21.3 (CH₃). **IR** (ATR): 2925, 1633, 1511, 1247, 1030, 745 cm⁻¹. **MS (ESI)** *m/z* (relative intensity): 753 (16) [2M+Na]⁺, 471 (36), 388 (16) [M+Na]⁺, 366 (100) [M+H]⁺, 216 (22), 124 (16). **HR-MS** (ESI) *m/z* calcd for

$C_{22}H_{24}NO_4$ $[M+H]^+$ 366.1700, found 366.1708. $[\alpha]_D^{23}$: -36.4 ($c = 1.33$, $CHCl_3$). **HPLC separation** (Chiralpak[®] IF-3, *n*-hexane/*i*PrOH 80:20, 0.75 mL/min, detection at 250 nm): t_r (minor) = 18.3 min, t_r (major) = 21.1 min, 6:94 e.r.

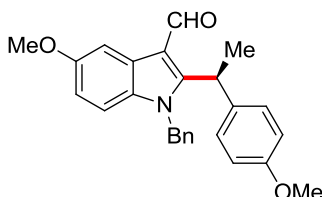
(S)-2-[1-(4-Methoxyphenyl)ethyl]-1-methyl-1H-indole-3-carbaldehyde (62bc)



The general procedure **GP6** was followed using indole **59b** (66 mg, 0.25 mmol, 1.0 equiv) and styrene **60c** (50 mg, 0.38 mmol, 1.5 equiv). Purification by column chromatography on silica gel (*n*-hexane/EtOAc = 8/1→5/1) yielded **62bc** (68.2 mg, 93%) as a yellow oil. Using **177**: 55.7 mg (76%), 85:15 e.r. **¹H NMR** (500 MHz, $CDCl_3$): $\delta = 10.26$ (s, 1H), 8.38 (ddd, $J = 7.6, 3.1, 1.5$ Hz, 1H), 7.34–7.26 (m, 3H), 7.17 (dd, $J = 8.9, 1.0$ Hz, 2H), 6.87 (d, $J = 8.8$ Hz, 2H), 5.16 (q, $J = 7.4$ Hz, 1H), 3.80 (s, 3H), 3.47 (s, 3H), 1.86 (d, $J = 7.4$ Hz, 3H). **¹³C NMR** (125 MHz, $CDCl_3$): $\delta = 184.8$ (CH), 158.4 (C_q), 153.8 (C_q), 137.3 (C_q), 132.9 (C_q), 128.0 (CH), 125.7 (C_q), 123.4 (CH), 123.0 (CH), 121.4 (CH), 114.4 (C_q), 114.2 (CH), 109.2 (CH), 55.3 (CH_3), 33.7 (CH), 31.1 (CH_3), 18.8 (CH_3). **IR** (ATR): 2933, 1643, 1510, 1468, 1246, 750 cm^{-1} . **MS (ESI)** m/z (relative intensity): 609 (20) $[2M+Na]^+$, 316 (26) $[M+Na]^+$, 294 (100) $[M+H]^+$, 186 (22). **HR-MS** (ESI) m/z calcd for $C_{19}H_{20}NO_2$ $[M+H]^+$ 294.1489, found 294.1489. $[\alpha]_D^{20}$: -70.6 ($c = 0.94$, $CHCl_3$). **HPLC separation** (Chiralpak[®] IA-3, *n*-hexane/*i*PrOH 80:20, 1.0 mL/min, detection at 250 nm): t_r (major) = 10.6 min, t_r (minor) = 11.5 min, 84:16 e.r.

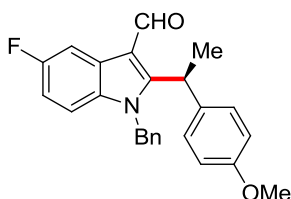
The analytical data are in accordance with those previously reported in the literature for the racemic compound.^[148]

(S)-1-Benzyl-5-methoxy-2-[1-(4-methoxyphenyl)ethyl]-1*H*-indole-3-carbaldehyde (62jc)



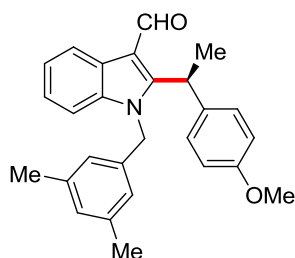
The general procedure **GP6** was followed using indole **59j** (93 mg, 0.25 mmol, 1.0 equiv) and styrene **60c** (50 mg, 0.38 mmol, 1.5 equiv). Purification by column chromatography on silica gel (*n*-hexane/EtOAc = 7/1→5/1) yielded **62jc** (97.9 mg, 98%) as a yellow solid. **M. p.** = 59–60 °C. **¹H NMR** (300 MHz, CDCl₃): δ = 10.16 (s, 1H), 7.94 (d, *J* = 2.5 Hz, 1H), 7.33–7.17 (m, 3H), 7.11 (dd, *J* = 9.0, 0.9 Hz, 2H), 7.02 (dd, *J* = 8.9, 0.5 Hz, 1H), 6.94–6.87 (m, 2H), 6.85 (dd, *J* = 8.9, 2.6 Hz, 1H), 6.80 (d, *J* = 8.8 Hz, 2H), 5.26–5.13 (m, 2H), 4.91 (q, *J* = 7.3 Hz, 1H), 3.90 (s, 3H), 3.77 (s, 3H), 1.71 (d, *J* = 7.4 Hz, 3H). **¹³C NMR** (125 MHz, CDCl₃): δ = 185.2 (CH), 158.3 (C_q), 156.8 (C_q), 154.2 (C_q), 135.9 (C_q), 133.2 (C_q), 131.7 (C_q), 128.8 (CH), 127.9 (CH), 127.6 (CH), 126.6 (C_q), 125.7 (CH), 114.7 (C_q), 114.1 (CH), 113.8 (CH), 110.9 (CH), 103.4 (CH), 55.9 (CH₃), 55.3 (CH₃), 47.7 (CH₂), 34.5 (CH), 20.2 (CH₃). **IR** (ATR): 2933, 1642, 1510, 1453, 1246, 1031, 696 cm⁻¹. **MS (EI)** *m/z* (relative intensity): 399 (76) [M]⁺, 308 (42), 291 (26), 278 (23), 200 (22), 197 (74), 91 (100). **HR-MS** (EI) *m/z* calcd for C₂₆H₂₅NO₃ [M]⁺ 399.1834, found 399.1826. [α]_D²³: –60.0 (c = 1.68, CHCl₃). **HPLC separation** (Chiralpak[®] IA-3, *n*-hexane/*i*PrOH 80:20, 1.0 mL/min, detection at 273 nm): *t_r* (major) = 9.4 min, *t_r* (minor) = 11.1 min, 93:7 e.r.

(S)-1-Benzyl-5-fluoro-2-[1-(4-methoxyphenyl)ethyl]-1*H*-indole-3-carbaldehyde (62kc)



The general procedure **GP6** was followed using indole **59k** (90 mg, 0.25 mmol, 1.0 equiv) and styrene **60c** (50 mg, 0.38 mmol, 1.5 equiv). Purification by column chromatography on silica gel (*n*-hexane/EtOAc = 8/1→6/1) yielded **62kc** (92.0 mg, 95%) as a yellow solid. **M. p.** = 54–56 °C. **¹H NMR** (400 MHz, CDCl₃): δ = 10.16 (s, 1H), 8.11 (dd, *J* = 9.4, 2.6 Hz, 1H), 7.33–7.21 (m, 3H), 7.11 (d, *J* = 8.1 Hz, 2H), 7.05 (dd, *J* = 8.9, 4.2 Hz, 1H), 6.94 (ddd, *J* = 8.9, 2.6, 2.6 Hz, 1H), 6.92–6.85 (m, 2H), 6.81 (d, *J* = 8.8 Hz, 2H), 5.25 (d, *J* = 17.3 Hz, 1H), 5.19 (d, *J* = 17.2 Hz, 1H), 4.94 (q, *J* = 7.3 Hz, 1H), 3.77 (s, 3H), 1.72 (d, *J* = 7.4 Hz, 3H). **¹³C NMR** (100 MHz, CDCl₃): δ = 185.1 (CH), 160.0 (d, ¹*J*_{C-F} = 238.8 Hz, C_q), 158.5 (C_q), 155.3 (C_q), 135.7 (C_q), 133.4 (C_q), 132.9 (C_q), 128.9 (CH), 128.0 (CH), 127.8 (CH), 126.6 (d, ³*J*_{C-F} = 11.0 Hz, C_q), 125.7 (CH), 114.8 (d, ⁴*J*_{C-F} = 4.3 Hz, C_q), 114.2 (CH), 111.8 (d, ²*J*_{C-F} = 26.2 Hz, CH), 111.0 (d, ³*J*_{C-F} = 9.6 Hz, CH), 107.4 (d, ²*J*_{C-F} = 24.9 Hz, CH), 55.3 (CH₃), 47.7 (CH₂), 34.5 (CH), 20.0 (CH₃). **¹⁹F NMR** (376 MHz, CDCl₃): δ = -120.24 (ddd, *J* = 9.3, 4.3, 4.3 Hz). **IR** (ATR): 2928, 1646, 1510, 1454, 1247, 1026 cm⁻¹. **MS (ESI)** *m/z* (relative intensity): 410 (24) [M+Na]⁺, 388 (100) [M+H]⁺, 372 (30), 289 (27), 280 (9). **HR-MS** (ESI) *m/z* calcd for C₂₅H₂₃NO₂F [M+H]⁺ 388.1707, found 388.1701. **[α]_D²³**: -54.9 (c = 1.53, CHCl₃). **HPLC separation** (Chiralpak[®] IA-3, *n*-hexane/*i*PrOH 80:20, 1.0 mL/min, detection at 250 nm): *t_r* (major) = 8.1 min, *t_r* (minor) = 9.4 min, 93:7 e.r.

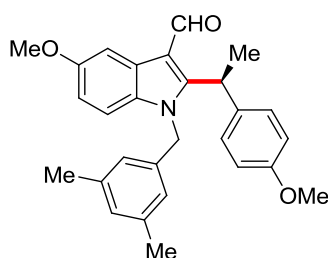
(S)-1-(3,5-Dimethylbenzyl)-2-[1-(4-methoxyphenyl)ethyl]-1*H*-indole-3-carbaldehyde (62lc)



The general procedure **GP6** was followed using indole **59l** (92 mg, 0.25 mmol, 1.0 equiv) and styrene **60c** (50 mg, 0.38 mmol, 1.5 equiv). Purification by column chromatography on silica gel (*n*-hexane/EtOAc = 9/1→7/1) yielded **62lc** (89.5 mg,

90%) as a yellow solid. **M. p.** = 56–58 °C. **¹H NMR** (300 MHz, CDCl₃): δ = 10.22 (s, 1H), 8.43 (ddd, *J* = 7.8, 1.3, 0.8 Hz, 1H), 7.31 (ddd, *J* = 7.9, 6.9, 1.3 Hz, 1H), 7.23 (ddd, *J* = 8.2, 6.9, 1.4 Hz, 1H), 7.17 (ddd, *J* = 8.1, 1.4, 0.8 Hz, 1H), 7.13 (dd, *J* = 9.0, 0.9 Hz, 2H), 6.87 (ddd, *J* = 1.6, 0.9, 0.9 Hz, 1H), 6.81 (d, *J* = 8.8 Hz, 2H), 6.55–6.47 (m, 2H), 5.18 (s, 2H), 4.97 (q, *J* = 7.4 Hz, 1H), 3.78 (s, 3H), 2.21 (s, 3H), 2.21 (s, 3H), 1.75 (d, *J* = 7.4 Hz, 3H). **¹³C NMR** (125 MHz, CDCl₃): δ = 185.3 (CH), 158.3 (C_q), 154.2 (C_q), 138.4 (C_q), 137.0 (C_q), 135.8 (C_q), 133.3 (C_q), 129.2 (CH), 128.0 (CH), 125.9 (C_q), 123.5 (CH), 123.5 (CH), 123.0 (CH), 121.6 (CH), 114.7 (C_q), 114.0 (CH), 110.2 (CH), 55.3 (CH₃), 47.6 (CH₂), 34.5 (CH), 21.3 (CH₃), 20.3 (CH₃). **IR** (ATR): 2922, 1644, 1510, 1458, 1247, 1179, 745 cm⁻¹. **MS (EI)** *m/z* (relative intensity): 397 (77) [M]⁺, 289 (26), 278 (30), 263 (22), 225 (100), 119 (77), 91 (24). **HR-MS** (EI) *m/z* calcd for C₂₇H₂₇NO₂ [M]⁺ 397.2042, found 397.2042. **[α]_D²³**: -43.4 (*c* = 1.62, CHCl₃). **HPLC separation** (Chiralpak[®] IA-3, *n*-hexane/*i*PrOH 80:20, 1.0 mL/min, detection at 273 nm): *t_r* (major) = 6.6 min, *t_r* (minor) = 7.6 min, 91:9 e.r.

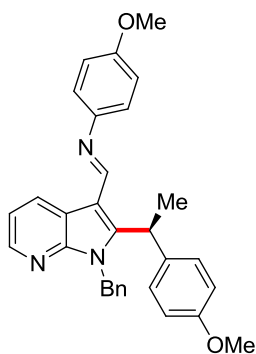
(S)-1-(3,5-Dimethylbenzyl)-5-methoxy-2-[1-(4-methoxyphenyl)ethyl]-1*H*-indole-3-carbaldehyde (62mc)



The general procedure **GP6** was followed using indole **59m** (100 mg, 0.25 mmol, 1.0 equiv) and styrene **60c** (50 mg, 0.38 mmol, 1.5 equiv). Purification by column chromatography on silica gel (*n*-hexane/EtOAc = 10/1→6/1) yielded **62mc** (102.6 mg, 96%) as a yellow solid. **M. p.** = 57–58 °C. **¹H NMR** (300 MHz, CDCl₃): δ = 10.16 (s, 1H), 7.95 (d, *J* = 2.5 Hz, 1H), 7.11 (d, *J* = 8.8 Hz, 2H), 7.04 (d, *J* = 8.9 Hz, 1H), 6.87 (s, 1H), 6.85 (dd, *J* = 8.9, 2.5 Hz, 1H), 6.80 (d, *J* = 8.8 Hz, 2H), 6.54–6.46 (m, 2H), 5.14 (s, 2H), 4.88 (q, *J* = 7.3 Hz, 1H), 3.91 (s, 3H), 3.77 (s, 3H), 2.21 (s, 6H), 1.74 (d, *J* = 7.4 Hz, 3H). **¹³C NMR** (125 MHz, CDCl₃): δ = 185.2 (CH),

158.3 (C_q), 156.7 (C_q), 154.2 (C_q), 138.4 (C_q), 135.8 (C_q), 133.4 (C_q), 131.8 (C_q), 129.2 (CH), 128.0 (CH), 126.6 (C_q), 123.5 (CH), 114.5 (C_q), 114.0 (CH), 113.7 (CH), 111.0 (CH), 103.3 (CH), 55.9 (CH₃), 55.3 (CH₃), 47.7 (CH₂), 34.6 (CH), 21.3 (CH₃), 20.4 (CH₃). **IR** (ATR): 2932, 1643, 1510, 1457, 1246, 1034, 831 cm⁻¹. **MS (ESI)** *m/z* (relative intensity): 855 (39) [2M+H]⁺, 428 (100) [M+H]⁺. **HR-MS** (ESI) *m/z* calcd for C₂₈H₃₀NO₃ [M+H]⁺ 428.2220, found 428.2220. **[α]_D²³**: -46.4 (c = 1.96, CHCl₃). **HPLC separation** (Chiralpak[®] IA-3, *n*-hexane/*i*PrOH 80:20, 1.0 mL/min, detection at 250 nm): *t_r* (major) = 7.5 min, *t_r* (minor) = 8.9 min, 91:9 e.r.

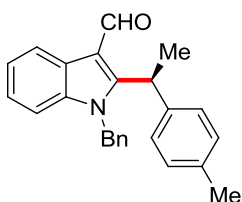
(S)-N-([1-Benzyl-2-(1-(4-methoxyphenyl)ethyl)-1H-pyrrolo[2,3-b]pyridin-3-yl]methylene)-4-methoxyaniline (152nc)



The general procedure **GP6** was followed using azaindole **59n** (85 mg, 0.25 mmol, 1.0 equiv) and styrene **60c** (50 mg, 0.38 mmol, 1.5 equiv). The reaction mixture was diluted with sat. aqueous NaHCO₃ (10 mL) and extracted with EtOAc (3 × 10 mL). The combined organic layers were washed with brine (10 mL), dried over Na₂SO₄, and concentrated under reduced pressure. The residue was purified by silica gel chromatography (*n*-hexane/EtOAc = 8/1→6/1) to yield **152nc** (100.2 mg, 84%, 24:76 e.r.) as an off-white solid. The product was recrystallized from *i*PrOH (5 mL) to provide further enantioenriched **152nc** (60.6 mg, 51%, 10:90 e.r.) as a colorless crystalline solid. **M. p.** = 170–171 °C. **¹H NMR** (600 MHz, CDCl₃): δ = 8.91 (dd, *J* = 7.8, 1.7 Hz, 1H), 8.50 (s, 1H), 8.37 (dd, *J* = 4.7, 1.6 Hz, 1H), 7.28–7.19 (m, 4H), 7.07 (dd, *J* = 8.9, 0.8 Hz, 2H), 7.02–6.98 (m, 4H), 6.86 (d, *J* = 8.9 Hz, 2H), 6.81 (d, *J* = 8.8 Hz, 2H), 5.62 (d, *J* = 16.5 Hz, 1H), 5.50 (d, *J* = 16.5 Hz, 1H), 4.70 (q,

$J = 7.3$ Hz, 1H), 3.80 (s, 3H), 3.77 (s, 3H), 1.60 (d, $J = 7.4$ Hz, 3H). $^{13}\text{C NMR}$ (125 MHz, CDCl_3): $\delta = 158.3$ (C_q), 157.4 (C_q), 153.0 (CH), 149.5 (C_q), 148.5 (C_q), 146.4 (C_q), 143.9 (CH), 137.5 (C_q), 134.0 (C_q), 131.1 (CH), 128.7 (CH), 128.2 (CH), 127.4 (CH), 126.3 (CH), 121.8 (CH), 118.8 (C_q), 118.1 (CH), 114.2 (CH), 114.0 (CH), 110.4 (C_q), 55.5 (CH_3), 55.3 (CH_3), 45.3 (CH_2), 35.0 (CH), 20.4 (CH_3). **IR** (ATR): 2934, 2834, 1497, 1427, 1242, 1031, 826, 728 cm^{-1} . **MS (ESI)** m/z (relative intensity): 476 (100) $[\text{M}+\text{H}]^+$. **HR-MS** (ESI) m/z calcd for $\text{C}_{31}\text{H}_{30}\text{N}_3\text{O}_2$ $[\text{M}+\text{H}]^+$ 476.2333, found 476.2332. $[\alpha]_{\text{D}}^{23}$: +192.7 ($c = 1.11$, CHCl_3). **HPLC separation** (Chiralpak[®] IF-3, n -hexane/ i PrOH 90:10, 1.0 mL/min, detection at 273 nm): t_r (minor) = 9.4 min, t_r (major) = 10.8 min, 24:76 e.r., 10:90 e.r. after recrystallization.

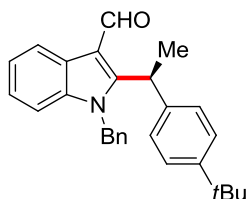
(S)-1-Benzyl-2-[1-(*p*-tolyl)ethyl]-1*H*-indole-3-carbaldehyde (62cd)



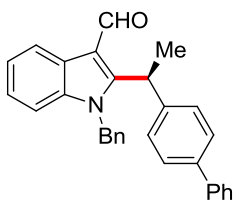
The general procedure **GP6** was followed using indole **59c** (85 mg, 0.25 mmol, 1.0 equiv) and styrene **60d** (44 mg, 0.38 mmol, 1.5 equiv). Purification by column chromatography on silica gel (n -hexane/EtOAc = 11/1) yielded **62cd** (72.7 mg, 82%) as a yellow solid. **M. p.** = 69–71 °C. $^1\text{H NMR}$ (400 MHz, CDCl_3): $\delta = 10.23$ (s, 1H), 8.44 (ddd, $J = 7.9, 1.3, 0.8$ Hz, 1H), 7.31 (ddd, $J = 8.0, 7.1, 1.0$ Hz, 1H), 7.29–7.23 (m, 3H), 7.22 (dd, $J = 7.1, 1.2$ Hz, 1H), 7.15 (dt, $J = 8.2, 1.0$ Hz, 1H), 7.09 (app s, 4H), 6.91 (dd, $J = 7.1, 2.6$ Hz, 2H), 5.26 (d, $J = 17.2$ Hz, 1H), 5.21 (d, $J = 17.2$ Hz, 1H), 5.00 (q, $J = 7.4$ Hz, 1H), 2.31 (s, 3H), 1.73 (d, $J = 7.4$ Hz, 3H). $^{13}\text{C NMR}$ (100 MHz, CDCl_3): $\delta = 185.4$ (CH), 154.2 (C_q), 138.2 (C_q), 137.0 (C_q), 136.6 (C_q), 136.0 (C_q), 129.4 (CH), 128.8 (CH), 127.6 (CH), 126.9 (CH), 126.0 (C_q), 125.8 (CH), 123.6 (CH), 123.1 (CH), 121.7 (CH), 114.8 (C_q), 110.1 (CH), 47.5 (CH_2), 34.7 (CH), 20.9 (CH_3), 19.9 (CH_3). **IR** (ATR): 2912, 1644, 1421, 1395, 1039, 806, 729 cm^{-1} . **MS (EI)** m/z (relative intensity): 353 (75) $[\text{M}]^+$, 261 (22), 218 (35), 181 (75), 91 (100). **HR-MS** (EI) m/z calcd for $\text{C}_{25}\text{H}_{23}\text{NO}$ $[\text{M}]^+$ 353.1780, found 353.1775. $[\alpha]_{\text{D}}^{23}$: –51.3

($c = 1.33$, CHCl_3). **HPLC separation** (Chiralpak[®] IA-3, n -hexane/ i PrOH 80:20, 1.0 mL/min, detection at 250 nm): t_r (major) = 6.5 min, t_r (minor) = 7.2 min, 90:10 e.r.

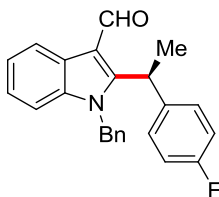
(S)-1-Benzyl-2-{1-[4-(*tert*-butyl)phenyl]ethyl}-1*H*-indole-3-carbaldehyde (62ce)



The general procedure **GP6** was followed using indole **59c** (85 mg, 0.25 mmol, 1.0 equiv) and styrene **60e** (60 mg, 0.38 mmol, 1.5 equiv). Purification by column chromatography on silica gel (n -hexane/EtOAc = 15/1→11/1) yielded **62ce** (72.2 mg, 73%) as a yellow oil. **¹H NMR** (300 MHz, CDCl_3): $\delta = 10.24$ (s, 1H), 8.44 (ddd, $J = 7.9, 1.4, 0.8$ Hz, 1H), 7.35–7.19 (m, 7H), 7.18–7.09 (m, 3H), 6.96–6.83 (m, 2H), 5.27 (s, 2H), 5.00 (q, $J = 7.4$ Hz, 1H), 1.75 (d, $J = 7.4$ Hz, 3H), 1.28 (s, 9H). **¹³C NMR** (125 MHz, CDCl_3): $\delta = 185.3$ (CH), 154.1 (C_q), 149.8 (C_q), 138.0 (C_q), 136.9 (C_q), 135.8 (C_q), 128.7 (CH), 127.5 (CH), 126.6 (CH), 125.9 (C_q), 125.7 (CH), 125.6 (CH), 123.6 (CH), 123.1 (CH), 121.7 (CH), 114.8 (C_q), 110.1 (CH), 47.6 (CH_2), 34.8 (CH), 34.4 (C_q), 31.3 (CH_3), 20.0 (CH_3). **IR** (ATR): 2961, 1645, 1454, 1421, 1395, 745 cm^{-1} . **MS (EI)** m/z (relative intensity): 395 (57) [M]⁺, 338 (25), 261 (19), 248 (23), 223 (67), 91 (100). **HR-MS** (EI) m/z calcd for $\text{C}_{28}\text{H}_{29}\text{NO}$ [M]⁺ 395.2249, found 395.2239. **$[\alpha]_D^{23}$** : -34.8 ($c = 1.34$, CHCl_3). **HPLC separation** (Chiralpak[®] IA-3, n -hexane/ i PrOH 80:20, 1.0 mL/min, detection at 250 nm): t_r (minor) = 5.6 min, t_r (major) = 6.1 min, 14:86 e.r.

(S)-2-{1-([1,1'-Biphenyl]-4-yl)ethyl}-1-benzyl-1H-indole-3-carbaldehyde (62cf)

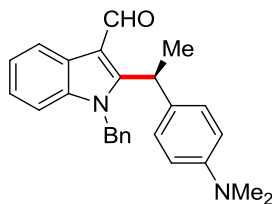
The general procedure **GP5** was followed using indole **59c** (85 mg, 0.25 mmol, 1.0 equiv) and styrene **60f** (68 mg, 0.38 mmol, 1.5 equiv). Purification by column chromatography on silica gel (*n*-hexane/EtOAc = 15/1→10/1) yielded **62cf** (66.9 mg, 64%) as a yellow solid. **M. p.** = 84–85 °C. **¹H NMR** (300 MHz, CDCl₃): δ = 10.29 (s, 1H), 8.44 (ddd, *J* = 7.8, 1.3, 0.7 Hz, 1H), 7.58–7.39 (m, 6H), 7.38–7.20 (m, 8H), 7.17 (dt, *J* = 8.1, 1.1 Hz, 1H), 6.97–6.86 (m, 2H), 5.27 (s, 2H), 5.10 (q, *J* = 7.4 Hz, 1H), 1.79 (d, *J* = 7.4 Hz, 3H). **¹³C NMR** (125 MHz, CDCl₃): δ = 185.1 (CH), 153.6 (C_q), 140.3 (C_q), 140.2 (C_q), 139.8 (C_q), 137.0 (C_q), 135.8 (C_q), 128.8 (CH), 128.7 (CH), 127.6 (CH), 127.4 (CH), 127.4 (CH), 127.3 (CH), 126.9 (CH), 126.0 (C_q), 125.7 (CH), 123.7 (CH), 123.2 (CH), 121.6 (CH), 114.8 (C_q), 110.2 (CH), 47.7 (CH₂), 34.9 (CH), 20.0 (CH₃). **IR** (ATR): 2927, 1644, 1453, 1395, 1039, 746, 694 cm⁻¹. **MS (EI)** *m/z* (relative intensity): 415 (92) [M]⁺, 280 (42), 261 (39), 243 (96), 91 (100). **HR-MS** (EI) *m/z* calcd for C₃₀H₂₅NO [M]⁺ 415.1936, found 415.1934. **[α]_D²³**: -49.0 (c = 1.18, CHCl₃). **HPLC separation** (Chiralpak[®] IB-3, *n*-hexane/*i*PrOH 70:30, 1.0 mL/min, detection at 250 nm): *t_r* (major) = 10.1 min, *t_r* (minor) = 14.3 min, 84:16 e.r.

(S)-1-Benzyl-2-[1-(4-fluorophenyl)ethyl]-1H-indole-3-carbaldehyde (62cg)

The general procedure **GP6** was followed using indole **59c** (85 mg, 0.25 mmol, 1.0 equiv) and styrene **60g** (46 mg, 0.38 mmol, 1.5 equiv). Purification by column chromatography on silica gel (*n*-hexane/EtOAc = 12/1→9/1) yielded **62cg** (54.2 mg,

61%) as a yellow solid. **M. p.** = 56–57 °C. $^1\text{H NMR}$ (500 MHz, CDCl_3): δ = 10.22 (s, 1H), 8.41 (dt, J = 7.9, 1.0 Hz, 1H), 7.32 (ddd, J = 8.0, 7.1, 1.1 Hz, 1H), 7.30–7.21 (m, 4H), 7.17 (ddd, J = 6.6, 1.6, 0.9 Hz, 2H), 7.15 (dd, J = 5.3, 1.0 Hz, 1H), 6.95 (t, J = 8.6 Hz, 2H), 6.89 (ddt, J = 6.2, 1.8, 0.8 Hz, 2H), 5.23 (s, 2H), 5.03 (q, J = 7.4 Hz, 1H), 1.74 (d, J = 7.4 Hz, 3H). $^{13}\text{C NMR}$ (125 MHz, CDCl_3): δ = 185.2 (CH), 161.6 (d, $^1J_{\text{C-F}}$ = 246.4 Hz, C_q), 153.3 (C_q), 137.0 (C_q), 137.0 (d, $^4J_{\text{C-F}}$ = 3.2 Hz, C_q), 135.7 (C_q), 128.9 (CH), 128.5 (d, $^3J_{\text{C-F}}$ = 7.8 Hz, CH), 127.7 (CH), 126.0 (C_q), 125.7 (CH), 123.8 (CH), 123.2 (CH), 121.6 (CH), 115.6 (d, $^2J_{\text{C-F}}$ = 21.3 Hz, CH), 114.7 (C_q), 110.2 (CH), 47.5 (CH_2), 34.4 (CH), 20.0 (CH_3). $^{19}\text{F NMR}$ (471 MHz, CDCl_3): δ = -115.64 (ttt, J = 8.5, 5.3, 1.5 Hz). **IR** (ATR): 2926, 1644, 1507, 1396, 743, 695 cm^{-1} . **MS (ESI)** m/z (relative intensity): 1092 (26), 913 (16), 737 (67) $[2\text{M}+\text{Na}]^+$, 380 (38) $[\text{M}+\text{Na}]^+$, 358 (100) $[\text{M}+\text{H}]^+$, 214 (9). **HR-MS** (ESI) m/z calcd for $\text{C}_{24}\text{H}_{21}\text{NOF}$ $[\text{M}+\text{H}]^+$ 358.1602, found 358.1608. $[\alpha]_{\text{D}}^{23}$: -61.9 (c = 0.99, CHCl_3). **HPLC separation** (Chiralpak[®] IA-3, *n*-hexane/*i*PrOH 80:20, 1.0 mL/min, detection at 250 nm): t_r (major) = 7.0 min, t_r (minor) = 7.6 min, 88:12 e.r.

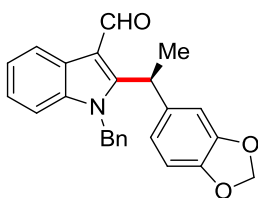
(S)-1-Benzyl-2-{1-[4-(dimethylamino)phenyl]ethyl}-1H-indole-3-carbaldehyde (62ch)



The general procedure **GP6** was followed using indole **59c** (85 mg, 0.25 mmol, 1.0 equiv) and styrene **60h** (55 mg, 0.38 mmol, 1.5 equiv). Purification by column chromatography on silica gel (*n*-hexane/EtOAc = 9/1→6/1) yielded **62ch** (72.4 mg, 76%) as a yellow solid. **M. p.** = 55–57 °C. $^1\text{H NMR}$ (300 MHz, CDCl_3): δ = 10.23 (s, 1H), 8.44 (ddd, J = 7.8, 1.3, 0.7 Hz, 1H), 7.35–7.17 (m, 5H), 7.13 (dt, J = 8.1, 1.0 Hz, 1H), 7.06 (dd, J = 9.0, 0.9 Hz, 2H), 6.98–6.85 (m, 2H), 6.64 (d, J = 8.8 Hz, 2H), 5.27 (d, J = 17.3 Hz, 1H), 5.21 (d, J = 17.3 Hz, 1H), 4.95 (q, J = 7.4 Hz, 1H), 2.92 (s, 6H), 1.70 (d, J = 7.4 Hz, 3H). $^{13}\text{C NMR}$ (100 MHz, CDCl_3): δ = 185.6 (CH), 155.0 (C_q),

149.4 (C_q), 137.1 (C_q), 136.2 (C_q), 128.8 (CH), 128.7 (C_q), 127.6 (CH), 127.5 (CH), 126.0 (C_q), 125.8 (CH), 123.5 (CH), 123.0 (CH), 121.8 (CH), 114.8 (C_q), 112.8 (CH), 110.1 (CH), 47.5 (CH₂), 40.5 (CH₃), 34.2 (CH), 20.0 (CH₃). **IR** (ATR): 2924, 1643, 1519, 1453, 1395, 746 cm⁻¹. **MS (EI)** *m/z* (relative intensity): 382 (100) [M]⁺, 365 (48), 291 (34), 261 (73), 247 (36), 210 (48), 91 (69). **HR-MS** (EI) *m/z* calcd for C₂₆H₂₆N₂O [M]⁺ 382.2045, found 382.2041. [α]_D²³: -55.2 (c = 1.31, CHCl₃). **HPLC separation** (Chiralpak[®] IA-3, *n*-hexane/*i*PrOH 80:20, 1.0 mL/min, detection at 273 nm): *t_r* (major) = 7.9 min, *t_r* (minor) = 9.1 min, 93:7 e.r.

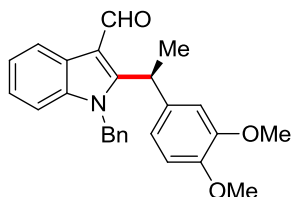
(S)-2-{1-(Benzo[d][1,3]dioxol-5-yl)ethyl}-1-benzyl-1*H*-indole-3-carbaldehyde (62ci)



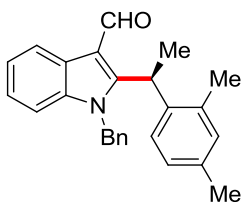
The general procedure **GP6** was followed using indole **59c** (85 mg, 0.25 mmol, 1.0 equiv) and styrene **60i** (56 mg, 0.38 mmol, 1.5 equiv). Purification by column chromatography on silica gel (*n*-hexane/EtOAc = 8/1→5/1) yielded **62ci** (75.4 mg, 79%) as a yellow solid. **M. p.** = 62–63 °C. **¹H NMR** (300 MHz, CDCl₃): δ = 10.24 (s, 1H), 8.42 (ddd, *J* = 7.8, 1.4, 0.7 Hz, 1H), 7.35–7.29 (m, 1H), 7.29–7.19 (m, 4H), 7.15 (dt, *J* = 7.6, 0.7 Hz, 1H), 6.94–6.85 (m, 2H), 6.74–6.60 (m, 3H), 5.90 (ddd, *J* = 7.2, 1.4, 0.5 Hz, 2H), 5.26 (s, 2H), 4.97 (q, *J* = 7.4 Hz, 1H), 1.70 (d, *J* = 7.4 Hz, 3H). **¹³C NMR** (125 MHz, CDCl₃): δ = 185.1 (CH), 153.6 (C_q), 148.0 (C_q), 146.4 (C_q), 137.0 (C_q), 135.8 (C_q), 135.0 (C_q), 128.8 (CH), 127.5 (CH), 125.9 (C_q), 125.7 (CH), 123.7 (CH), 123.1 (CH), 121.6 (CH), 119.8 (CH), 114.7 (C_q), 110.1 (CH), 108.2 (CH), 107.9 (CH), 101.1 (CH₂), 47.6 (CH₂), 34.8 (CH), 20.1 (CH₃). **IR** (ATR): 2926, 1644, 1486, 1233, 1035, 745 cm⁻¹. **MS (ESI)** *m/z* (relative intensity): 767 (11) [2M+H]⁺, 489 (9), 384 (100) [M+H]⁺, 269 (6). **HR-MS** (ESI) *m/z* calcd for C₂₅H₂₂NO₃ [M+H]⁺ 384.1594, found 384.1593. [α]_D²³: -45.7 (c = 1.49, CHCl₃). **HPLC separation**

(Chiralpak® IA-3, *n*-hexane/*i*PrOH 80:20, 1.0 mL/min, detection at 250 nm):
 t_r (major) = 9.7 min, t_r (minor) = 10.5 min, 85:15 e.r.

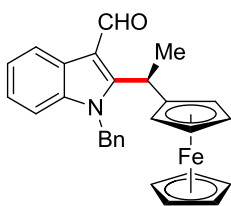
(S)-1-Benzyl-2-[1-(3,4-dimethoxyphenyl)ethyl]-1*H*-indole-3-carbaldehyde (62cj)



The general procedure **GP6** was followed using indole **59c** (85 mg, 0.25 mmol, 1.0 equiv) and styrene **60j** (62 mg, 0.38 mmol, 1.5 equiv). Purification by column chromatography on silica gel (*n*-hexane/EtOAc = 8/1→5/1) yielded **62cj** (55.9 mg, 56%) as a yellow solid. **M. p.** = 57–58 °C. **¹H NMR** (300 MHz, CDCl₃): δ = 10.23 (s, 1H), 8.43 (ddd, *J* = 7.8, 1.4, 0.8 Hz, 1H), 7.32 (ddd, *J* = 7.8, 7.0, 1.3 Hz, 1H), 7.28–7.20 (m, 4H), 7.16 (d, *J* = 7.9 Hz, 1H), 6.90 (ddt, *J* = 5.9, 2.5, 0.8 Hz, 2H), 6.80 (ddd, *J* = 8.3, 1.9, 0.8 Hz, 1H), 6.76 (d, *J* = 8.3 Hz, 1H), 6.60 (d, *J* = 1.8 Hz, 1H), 5.26 (s, 2H), 5.00 (q, *J* = 7.3 Hz, 1H), 3.84 (s, 3H), 3.70 (s, 3H), 1.73 (d, *J* = 7.4 Hz, 3H). **¹³C NMR** (125 MHz, CDCl₃): δ = 185.2 (CH), 153.9 (C_q), 149.1 (C_q), 148.0 (C_q), 137.0 (C_q), 135.9 (C_q), 133.6 (C_q), 128.7 (CH), 127.6 (CH), 125.9 (C_q), 125.7 (CH), 123.6 (CH), 123.1 (CH), 121.7 (CH), 118.8 (CH), 114.7 (C_q), 111.2 (CH), 110.8 (CH), 110.1 (CH), 55.9 (CH₃), 55.9 (CH₃), 47.5 (CH₂), 34.8 (CH), 20.2 (CH₃). **IR** (ATR): 2930, 1644, 1513, 1453, 1237, 1144, 1024, 745 cm⁻¹. **MS (ESI)** *m/z* (relative intensity): 1220 (8) [3M+Na]⁺, 821 (20) [2M+Na]⁺, 799 (16) [2M+H]⁺, 422 (20) [M+Na]⁺, 400 (100) [M+H]⁺, 293 (10). **HR-MS** (ESI) *m/z* calcd for C₂₆H₂₆NO₃ [M+H]⁺ 400.1907, found 400.1903. **[α]_D²³**: –63.5 (*c* = 0.94, CHCl₃). **HPLC separation** (Chiralpak® IA-3, *n*-hexane/*i*PrOH 80:20, 1.0 mL/min, detection at 250 nm):
 t_r (major) = 10.4 min, t_r (minor) = 12.3 min, 90:10 e.r.

(S)-1-Benzyl-2-[1-(2,4-dimethylphenyl)ethyl]-1H-indole-3-carbaldehyde (62ck)

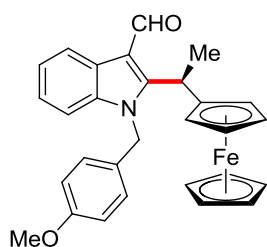
The general procedure **GP6** was followed using indole **59c** (85 mg, 0.25 mmol, 1.0 equiv) and styrene **60k** (50 mg, 0.38 mmol, 1.5 equiv). Purification by column chromatography on silica gel (*n*-hexane/EtOAc = 17/1→12/1) yielded **62ck** (37.7 mg, 41%) as a light yellow oil. $^1\text{H NMR}$ (500 MHz, CDCl_3): δ = 10.20 (s, 1H), 8.41 (dt, J = 7.9, 1.0 Hz, 1H), 7.31 (ddd, J = 8.0, 7.0, 1.1 Hz, 1H), 7.25 (d, J = 7.9 Hz, 1H), 7.24–7.20 (m, 4H), 7.18 (dt, J = 8.2, 1.0 Hz, 1H), 6.99 (dd, J = 7.9, 1.9 Hz, 1H), 6.88–6.76 (m, 3H), 5.25 (s, 2H), 4.94 (q, J = 7.3 Hz, 1H), 2.25 (s, 3H), 1.95 (s, 3H), 1.70 (d, J = 7.3 Hz, 3H). $^{13}\text{C NMR}$ (125 MHz, CDCl_3): δ = 185.7 (CH), 153.3 (C_q), 137.0 (C_q), 136.9 (C_q), 136.4 (C_q), 136.2 (C_q), 135.7 (C_q), 131.9 (CH), 128.7 (CH), 127.5 (CH), 127.0 (CH), 126.3 (CH), 126.1 (C_q), 125.8 (CH), 123.6 (CH), 123.1 (CH), 121.6 (CH), 114.8 (C_q), 110.0 (CH), 47.2 (CH_2), 34.2 (CH), 20.9 (CH_3), 20.8 (CH_3), 19.7 (CH_3). IR (ATR): 2921, 1643, 1453, 1395, 1039, 743 cm^{-1} . MS (ESI) m/z (relative intensity): 757 (31) $[2\text{M}+\text{Na}]^+$, 473 (19), 390 (24) $[\text{M}+\text{Na}]^+$, 368 (100) $[\text{M}+\text{H}]^+$. HR-MS (ESI) m/z calcd for $\text{C}_{26}\text{H}_{26}\text{NO}$ $[\text{M}+\text{H}]^+$ 368.2009, found 368.2006. $[\alpha]_D^{23}$: -66.8 (c = 0.52, CHCl_3). HPLC separation (Chiralpak[®] IA-3, *n*-hexane/*i*PrOH 80:20, 1.0 mL/min, detection at 250 nm): t_r (major) = 5.9 min, t_r (minor) = 6.5 min, 91:9 e.r.

(R)-1-Benzyl-2-(1-ferrocenylethyl)-1H-indole-3-carbaldehyde (192ca)

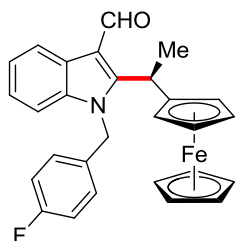
The general procedure **GP5** was followed using indole **59c** (85 mg, 0.25 mmol, 1.0 equiv) and vinylferrocene (**191a**) (80 mg, 0.38 mmol, 1.5 equiv). Purification by column chromatography on silica gel (*n*-hexane/EtOAc = 12/1→9/1) yielded **192ca** (76.9 mg, 69%) as an orange solid. **M. p.** = 61–63 °C. **¹H NMR** (300 MHz, CDCl₃): δ = 10.17 (s, 1H), 8.37 (d, *J* = 7.6 Hz, 1H), 7.38–7.27 (m, 4H), 7.26–7.18 (m, 1H), 7.16 (d, *J* = 8.0 Hz, 1H), 7.02–6.92 (m, 2H), 5.39 (d, *J* = 17.3 Hz, 1H), 5.29 (d, *J* = 17.1 Hz, 1H), 4.93 (brs, 1H), 4.36 (dt, *J* = 2.7, 1.4, Hz, 1H), 4.27–4.10 (m, 1H), 4.09–4.04 (m, 6H), 3.84 (s, 1H), 1.68 (d, *J* = 7.4 Hz, 3H). **¹³C NMR** (125 MHz, CDCl₃): δ = 185.3 (CH), 154.8 (C_q), 136.8 (C_q), 136.3 (C_q), 128.9 (CH), 127.8 (CH), 125.9 (CH), 125.9 (C_q), 123.5 (CH), 123.1 (CH), 121.7 (CH), 113.7 (C_q), 109.9 (CH), 90.0 (C_q), 69.0 (CH), 68.7 (CH), 68.7 (CH), 67.0 (CH), 66.6 (CH), 47.4 (CH₂), 31.5 (CH), 20.1 (CH₃). **IR** (ATR): 2926, 1643, 1422, 1398, 813, 744, 480 cm⁻¹. **MS (EI)** *m/z* (relative intensity): 447 (100) [M]⁺, 382 (64), 381 (75), 290 (50), 262 (45). **HR-MS** (EI) *m/z* calcd for C₂₈H₂₅FeNO [M]⁺ 447.1286, found 447.1263. **[α]_D²³**: +220.0 (*c* = 1.19, CHCl₃). **HPLC separation** (Chiralpak[®] IF-3, *n*-hexane/*i*PrOH 80:20, 0.75 mL/min, detection at 250 nm): *t_r* (minor) = 18.3 min, *t_r* (major) = 21.6 min, 4:96 e.r.

192ca (190 mg, 0.42 mmol, 96:4 e.r.) was recrystallized from *n*-hexane/CH₂Cl₂ to furnish the optically pure product (116 mg, 0.26 mmol, 61%) as a dark yellow solid. **[α]_D²³**: +347.8 (*c* = 1.17, CHCl₃). **HPLC separation** (Chiralpak[®] IF-3, *n*-hexane/*i*PrOH 80:20, 0.75 mL/min, detection at 273 nm): *t_r* (minor) = 18.7 min, *t_r* (major) = 22.1 min, 0.3:99.7 e.r. Crystals suitable for X-ray crystallography were grown by slow evaporation from a solution of **192ca** in benzene.

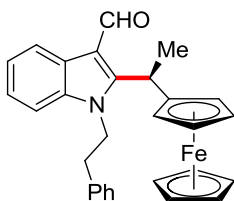
**(R)-2-(1-Ferrocenylethyl)-1-(4-methoxybenzyl)-1H-indole-3-carbaldehyde
(192da)**



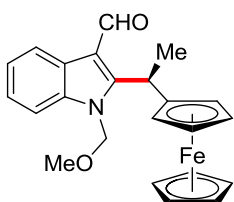
The general procedure **GP5** was followed using indole **59d** (93 mg, 0.25 mmol, 1.0 equiv) and vinylferrocene (**191a**) (80 mg, 0.38 mmol, 1.5 equiv). Purification by column chromatography on silica gel (*n*-hexane/EtOAc = 10/1→7.5/1) yielded **192da** (75.8 mg, 64%) as an orange solid. **M. p.** = 67–69 °C. **¹H NMR** (400 MHz, CDCl₃): δ = 10.17 (s, 1H), 8.36 (dt, *J* = 7.9, 1.1 Hz, 1H), 7.32–7.21 (m, 1H), 7.24–7.18 (m, 1H), 7.16 (d, *J* = 8.2 Hz, 1H), 6.89 (d, *J* = 8.4 Hz, 2H), 6.83 (d, *J* = 8.8 Hz, 2H), 5.32 (d, *J* = 16.8 Hz, 1H), 5.24 (d, *J* = 16.8 Hz, 1H), 4.94 (brs, 1H), 4.36 (dt, *J* = 2.6, 1.3 Hz, 1H), 4.11–4.04 (m, 7H), 3.86 (s, 1H), 3.79 (s, 3H), 1.67 (d, *J* = 7.4 Hz, 3H). **¹³C NMR** (100 MHz, CDCl₃): δ = 185.2 (CH), 159.1 (C_q), 154.8 (C_q), 136.8 (C_q), 128.2 (C_q), 127.1 (CH), 125.9 (C_q), 123.4 (CH), 123.0 (CH), 121.7 (CH), 114.3 (CH), 113.6 (C_q), 110.0 (CH), 90.2 (C_q), 69.0 (CH), 68.7 (CH), 68.7 (CH), 67.1 (CH), 66.7 (CH), 55.3 (CH₃), 47.0 (CH₂), 31.5 (CH), 20.1 (CH₃). **IR** (ATR): 2961, 2929, 1642, 1510, 1245, 1026, 814, 742 cm⁻¹. **MS (ESI)** *m/z* (relative intensity): 577 (60), 572 (62), 535 (45), 500 (94) [M+Na]⁺, 478 (100) [M+H]⁺, 460 (32). **HR-MS** (ESI) *m/z* calcd for C₂₉H₂₈FeNO₂ [M+H]⁺ 478.1464, found 478.1444. **[α]_D²³**: +152.1 (c = 1.33, CHCl₃). **HPLC separation** (Chiralpak[®] IF-3, *n*-hexane/*i*PrOH 80:20, 0.75 mL/min, detection at 250 nm): *t_r* (minor) = 23.3 min, *t_r* (major) = 28.9 min, 5:95 e.r.

(R)-2-(1-Ferrocenylethyl)-1-(4-fluorobenzyl)-1H-indole-3-carbaldehyde (192ea)

The general procedure **GP5** was followed using indole **59e** (90 mg, 0.25 mmol, 1.0 equiv) and vinylferrocene (**191a**) (80 mg, 0.38 mmol, 1.5 equiv). Purification by column chromatography on silica gel (*n*-hexane/EtOAc = 13/1→7.5/1) yielded **192ea** (83.2 mg, 72%) as an orange solid. **M. p.** = 64–66 °C. **¹H NMR** (500 MHz, CDCl₃): δ = 10.22 (s, 1H), 8.36 (dt, *J* = 7.9, 1.0 Hz, 1H), 7.28 (ddd, *J* = 8.0, 7.1, 1.0 Hz, 1H), 7.21 (ddd, *J* = 8.3, 7.2, 1.3 Hz, 1H), 7.10 (d, *J* = 8.3 Hz, 1H), 6.98 (t, *J* = 8.6 Hz, 2H), 6.91–6.86 (m, 2H), 5.33 (d, *J* = 17.2 Hz, 1H), 5.25 (d, *J* = 16.9 Hz, 1H), 4.99 (brs, 1H), 4.35 (dt, *J* = 2.6, 1.4 Hz, 1H), 4.09 (s, 5H), 4.08 (ddd, *J* = 2.5, 1.3, 1.3 Hz, 1H), 4.06 (ddd, *J* = 2.5, 1.3, 1.3 Hz, 1H), 3.87 (s, 1H), 1.66 (d, *J* = 7.4 Hz, 3H). **¹³C NMR** (125 MHz, CDCl₃): δ = 185.1 (CH), 162.1 (d, ¹*J*_{C-F} = 246.8 Hz, C_q), 154.4 (C_q), 136.7 (C_q), 131.9 (d, ⁴*J*_{C-F} = 3.1 Hz, C_q), 127.5 (d, ³*J*_{C-F} = 8.2 Hz, CH), 125.9 (C_q), 123.6 (CH), 123.1 (CH), 121.7 (CH), 115.8 (d, ²*J*_{C-F} = 21.6 Hz, CH), 113.7 (C_q), 109.9 (CH), 89.8 (C_q), 69.0 (CH), 68.8 (CH), 68.7 (CH), 67.1 (CH), 66.6 (CH), 46.9 (CH₂), 31.4 (CH), 19.9 (CH₃). **¹⁹F NMR** (471 MHz, CDCl₃): δ = -114.36 (s). **IR** (ATR): 2904, 1643, 1509, 1222, 1039, 819, 743 cm⁻¹. **MS (EI)** *m/z* (relative intensity): 465 (100) [M]⁺, 400 (61), 399 (86), 290 (38), 109 (50). **HR-MS** (ESI) *m/z* calcd for C₂₈H₂₅FFeNO [M+H]⁺ 466.1264, found 466.1257. **[α]_D²³**: +175.8 (*c* = 1.45, CHCl₃). **HPLC separation** (Chiralpak[®] IF-3, *n*-hexane/*i*PrOH 80:20, 0.75 mL/min, detection at 250 nm): *t_r* (minor) = 19.2 min, *t_r* (major) = 22.4 min, 5:95 e.r.

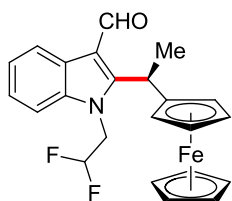
(R)-2-(1-Ferrocenylethyl)-1-phenethyl-1H-indole-3-carbaldehyde (192fa)

The general procedure **GP5** was followed using indole **59f** (89 mg, 0.25 mmol, 1.0 equiv) and vinylferrocene (**191a**) (80 mg, 0.38 mmol, 1.5 equiv). Purification by column chromatography on silica gel (*n*-hexane/EtOAc = 15/1→10/1) yielded **192fa** (64.6 mg, 56%) as an orange solid. Using **177**: 65.4 mg (57%), 7:93 e.r. **M. p.** = 62–63 °C. **¹H NMR** (300 MHz, CDCl₃): δ = 10.20 (s, 1H), 8.40–8.32 (m, 1H), 7.38–7.27 (m, 6H), 7.13 (d, *J* = 6.3 Hz, 2H), 5.03 (brs, 1H), 4.46 (dt, *J* = 2.6, 1.3 Hz, 1H), 4.41–4.18 (m, 8H), 4.17 (ddd, *J* = 2.4, 1.2, 1.2 Hz, 1H), 4.10–4.05 (m, 1H), 2.95 (td, *J* = 12.0, 10.3, 5.3 Hz, 1H), 2.58 (brs, 1H), 1.73 (d, *J* = 7.4 Hz, 3H). **¹³C NMR** (125 MHz, CDCl₃): δ = 184.6 (CH), 153.6 (C_q), 137.6 (C_q), 136.0 (C_q), 128.7 (CH), 128.6 (CH), 126.9 (CH), 126.1 (C_q), 123.3 (CH), 122.9 (CH), 121.6 (CH), 113.2 (C_q), 109.7 (CH), 90.0 (C_q), 69.1 (CH), 69.1 (CH), 68.9 (CH), 67.3 (CH), 66.9 (CH), 46.1 (CH₂), 35.3 (CH₂), 31.2 (CH), 19.5 (CH₃). **IR** (ATR): 2932, 1636, 1423, 1038, 809, 740, 695 cm⁻¹. **MS (ESI)** *m/z* (relative intensity): 484 (94) [M+Na]⁺, 462 (100) [M+H]⁺, 444 (72). **HR-MS** (ESI) *m/z* calcd for C₂₉H₂₈FeNO [M+H]⁺ 462.1515, found 462.1507. **[α]_D²³**: +185.3 (*c* = 1.16, CHCl₃). **HPLC separation** (Chiralpak[®] IA-3, *n*-hexane/*i*PrOH 80:20, 1.0 mL/min, detection at 250 nm): *t_r* (minor) = 8.0 min, *t_r* (major) = 10.6 min, 8:92 e.r.

(R)-2-(1-Ferrocenylethyl)-1-(methoxymethyl)-1H-indole-3-carbaldehyde (192ga)

The general procedure **GP5** was followed using indole **59g** (74 mg, 0.25 mmol, 1.0 equiv) and vinylferrocene (**191a**) (80 mg, 0.38 mmol, 1.5 equiv). Purification by column chromatography on silica gel (*n*-hexane/EtOAc = 9/1→7/1) yielded **192ga** (52.2 mg, 52%) as an orange oil. **¹H NMR** (300 MHz, CDCl₃): δ = 10.25 (s, 1H), 8.37–8.27 (m, 1H), 7.48–7.36 (m, 1H), 7.34–7.23 (m, 2H), 5.40 (s, 2H), 5.06 (q, *J* = 7.3 Hz, 1H), 4.47 (dt, *J* = 2.7, 1.3 Hz, 1H), 4.25–4.17 (m, 5H), 4.16 (td, *J* = 2.4, 1.2 Hz, 1H), 4.13 (td, *J* = 2.4, 1.3 Hz, 1H), 4.07 (dt, *J* = 2.6, 1.3 Hz, 1H), 3.23 (s, 3H), 1.82 (d, *J* = 7.4 Hz, 3H). **¹³C NMR** (125 MHz, CDCl₃): δ = 185.3 (CH), 154.7 (C_q), 136.8 (C_q), 125.7 (C_q), 123.6 (CH), 123.1 (CH), 121.6 (CH), 114.3 (C_q), 109.8 (CH), 90.2 (C_q), 74.3 (CH₂), 69.1 (CH), 68.8 (CH), 68.8 (CH), 67.1 (CH), 66.8 (CH), 56.1 (CH₃), 31.4 (CH), 20.5 (CH₃). **IR** (ATR): 2902, 1647, 1386, 1038, 817, 749 cm⁻¹. **MS (ESI)** *m/z* (relative intensity): 825 (44) [2M+Na]⁺, 424 (75) [M+Na]⁺, 402 (24) [M+H]⁺, 384 (14), 213 (100). **HR-MS** (ESI) *m/z* calcd for C₂₃H₂₄FeNO₂ [M+H]⁺ 402.1151, found 402.1162. [α]_D²³: +206.3 (c = 0.79, CHCl₃). **HPLC separation** (Chiralpak[®] ID-3, *n*-hexane/*i*PrOH 70:30, 1.0 mL/min, detection at 273 nm): *t*_r (minor) = 12.2 min, *t*_r (major) = 12.8 min, 4:96 e.r.

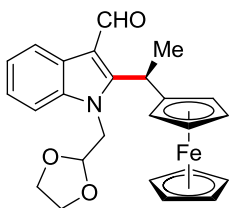
(*R*)-1-(2,2-Difluoroethyl)-2-(1-ferrocenylethyl)-1*H*-indole-3-carbaldehyde (192ha)



The general procedure **GP5** was followed using indole **59h** (79 mg, 0.25 mmol, 1.0 equiv) and vinylferrocene (**191a**) (80 mg, 0.38 mmol, 1.5 equiv). Purification by column chromatography on silica gel (*n*-hexane/EtOAc = 10/1) yielded **192ha** (53.7 mg, 51%) as an orange solid. **M. p.** = 62–64 °C. **¹H NMR** (500 MHz, CDCl₃): δ = 10.26 (s, 1H), 8.34–8.29 (m, 1H), 7.35–7.27 (m, 3H), 5.40 (t, *J* = 53.2 Hz, 1H), 5.13 (s, 1H), 4.53–4.35 (m, 3H), 4.25–4.19 (m, 6H), 4.18 (td, *J* = 2.5, 1.3 Hz, 1H), 4.11 (dt, *J* = 2.6, 1.4 Hz, 1H), 1.80 (d, *J* = 7.5 Hz, 3H). **¹³C NMR** (125 MHz, CDCl₃):

δ = 185.1 (CH), 154.0 (C_q), 136.8 (C_q), 125.8 (C_q), 123.8 (CH), 123.4 (CH), 121.4 (CH), 114.1 (C_q), 113.5 (t, $^1J_{C-F}$ = 245.2 Hz, CH), 109.8 (CH), 89.7 (C_q), 69.2 (CH), 69.2 (CH), 68.9 (CH), 67.5 (CH), 66.8 (CH), 46.4 (t, $^2J_{C-F}$ = 29.0 Hz, CH₂), 31.0 (CH), 19.7 (CH₃). **^{19}F NMR** (471 MHz, CDCl₃): δ = -119.18 (d, J = 55.3 Hz). **IR** (ATR): 2903, 1653, 1396, 1042, 1019, 812, 747 cm⁻¹. **MS (EI)** m/z (relative intensity): 421 (100) [M]⁺, 356 (42), 355 (93), 230 (31), 138 (30), 121 (45). **HR-MS** (ESI) m/z calcd for C₂₃H₂₂F₂FeNO [M+H]⁺ 422.1014, found 422.1011. **$[\alpha]_D^{23}$** : +230.1 (c = 0.63, CHCl₃). **HPLC separation** (Chiralpak[®] IA-3, *n*-hexane/*i*PrOH 80:20, 1.0 mL/min, detection at 273 nm): t_r (minor) = 8.3 min, t_r (major) = 10.0 min, 4:96 e.r.

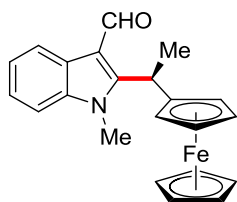
(*R*)-1-[(1,3-Dioxolan-2-yl)methyl]-2-(1-ferrocenylethyl)-1*H*-indole-3-carbaldehyde (192ia)



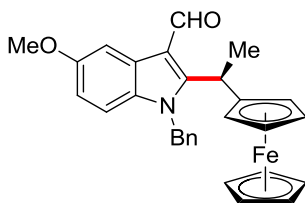
The general procedure **GP5** was followed using indole **59i** (84 mg, 0.25 mmol, 1.0 equiv) and vinylferrocene (**191a**) (80 mg, 0.38 mmol, 1.5 equiv). Purification by column chromatography on silica gel (*n*-hexane/EtOAc = 6/1→4/1) yielded **192ia** (43.2 mg, 39%) as an orange solid. **M. p.** = 75–77 °C. **^1H NMR** (500 MHz, CDCl₃): δ = 10.08 (s, 1H), 8.33–8.28 (m, 1H), 7.47–7.39 (m, 1H), 7.29–7.23 (m, 2H), 5.13 (s, 1H), 4.92 (brs, 1H), 4.44 (dt, J = 2.5, 1.4 Hz, 1H), 4.40 (dd, J = 15.3, 2.9 Hz, 1H), 4.35 (dd, J = 15.3, 3.9 Hz, 1H), 4.17 (s, 5H), 4.15 (td, J = 2.5, 1.3 Hz, 1H), 4.12 (td, J = 2.5, 1.2 Hz, 1H), 4.09 (dt, J = 2.5, 1.3 Hz, 1H), 3.93–3.84 (m, 4H), 1.80 (d, J = 7.3 Hz, 3H). **^{13}C NMR** (125 MHz, CDCl₃): δ = 185.9 (CH), 155.8 (C_q), 136.8 (C_q), 125.8 (C_q), 123.2 (CH), 123.0 (CH), 121.7 (CH), 113.7 (C_q), 110.5 (CH), 102.1 (CH), 91.0 (C_q), 68.9 (CH), 68.8 (CH), 68.8 (CH), 67.1 (CH), 66.9 (CH), 65.3 (CH₂), 65.2 (CH₂), 46.6 (CH₂), 31.6 (CH), 20.8 (CH₃). **IR** (ATR): 2917, 1642, 1460, 1041, 817, 745 cm⁻¹. **MS (ESI)** m/z (relative intensity): 909 (47) [2M+Na]⁺, 466 (100) [M+Na]⁺,

444 (39) $[M+H]^+$. **HR-MS** (ESI) m/z calcd for $C_{25}H_{26}FeNO_3$ $[M+H]^+$ 444.1257, found 444.1255. $[\alpha]_D^{23}$: +176.1 ($c = 0.67$, $CHCl_3$). **HPLC separation** (Chiralpak[®] IF-3, n -hexane/ i PrOH 70:30, 1.0 mL/min, detection at 250 nm): t_r (minor) = 10.5 min, t_r (major) = 13.1 min, 5:95 e.r.

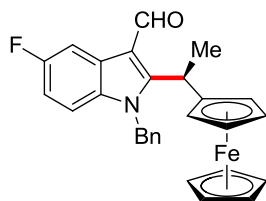
(R)-2-(1-Ferrocenylethyl)-1-methyl-1H-indole-3-carbaldehyde (192ba)



The general procedure **GP5** was followed using indole **59b** (66 mg, 0.25 mmol, 1.0 equiv) and vinylferrocene (**191a**) (80 mg, 0.38 mmol, 1.5 equiv). Purification by column chromatography on silica gel (n -hexane/EtOAc = 11/1 \rightarrow 8.5/1) yielded **192ba** (49.3 mg, 53%) as an orange oil. **¹H NMR** (300 MHz, $CDCl_3$): $\delta = 10.25$ (s, 1H), 8.39–8.26 (m, 1H), 7.36–7.18 (m, 3H), 5.17 (q, $J = 7.3$ Hz, 1H), 4.44 (dtd, $J = 2.7, 1.3, 0.7$ Hz, 1H), 4.25–4.17 (m, 5H), 4.18–4.14 (m, 1H), 4.13 (ddd, $J = 2.5, 1.3, 1.3$ Hz, 1H), 4.03 (dtd, $J = 2.6, 1.4, 0.3$ Hz, 1H), 3.56 (s, 3H), 1.77 (d, $J = 7.4$ Hz, 3H). **¹³C NMR** (125 MHz, $CDCl_3$): $\delta = 184.3$ (CH), 153.8 (C_q), 137.1 (C_q), 125.7 (C_q), 123.2 (CH), 122.8 (CH), 121.1 (CH), 113.2 (C_q), 109.1 (CH), 89.6 (C_q), 69.1 (CH), 68.7 (CH), 68.6 (CH), 67.1 (CH), 66.8 (CH), 31.2 (CH), 31.0 (CH_3), 19.0 (CH_3). **IR** (ATR): 2903, 1642, 1391, 1039, 815, 746, 479 cm^{-1} . **MS (EI)** m/z (relative intensity): 371 (100) $[M]^+$, 306 (53), 305 (94), 278 (73). **HR-MS** (EI) m/z calcd for $C_{22}H_{21}FeNO$ $[M]^+$ 371.0973, found 371.0962. $[\alpha]_D^{23}$: +217.3 ($c = 0.85$, $CHCl_3$). **HPLC separation** (Chiralpak[®] IF-3, n -hexane/ i PrOH 80:20, 0.75 mL/min, detection at 250 nm): t_r (minor) = 19.0 min, t_r (major) = 21.7 min, 6:94 e.r.

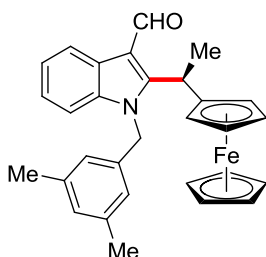
(R)-1-Benzyl-2-(1-ferrocenylethyl)-5-methoxy-1H-indole-3-carbaldehyde (192ja)

The general procedure **GP5** was followed using indole **59j** (93 mg, 0.25mmol, 1.0 equiv) and vinylferrocene (**191a**) (80 mg, 0.38 mmol, 1.5 equiv). Purification by column chromatography on silica gel (*n*-hexane/EtOAc = 10/1→7/1) yielded **192ja** (91.9 mg, 77%) as an orange solid. **M. p.** = 77–79 °C. **¹H NMR** (400 MHz, CDCl₃): δ = 10.13 (s, 1H), 7.89 (d, *J* = 2.5 Hz, 1H), 7.37–7.26 (m, 3H), 7.04 (d, *J* = 8.8 Hz, 1H), 6.97 (d, *J* = 6.5 Hz, 2H), 6.84 (dd, *J* = 8.9, 2.5 Hz, 1H), 5.35 (d, *J* = 17.2 Hz, 1H), 5.26 (d, *J* = 17.1 Hz, 1H), 4.85 (brs, 1H), 4.35 (dt, *J* = 2.6, 1.3 Hz, 1H), 4.08 (td, *J* = 2.5, 1.3 Hz, 1H), 4.07–4.02 (m, 6H), 3.88 (s, 3H), 3.83 (s, 1H), 1.66 (d, *J* = 7.4 Hz, 3H). **¹³C NMR** (100 MHz, CDCl₃): δ = 185.2 (CH), 156.8 (C_q), 154.8 (C_q), 136.3 (C_q), 131.6 (C_q), 128.9 (CH), 127.8 (CH), 126.5 (C_q), 125.9 (CH), 113.7 (CH), 113.6 (C_q), 110.8 (CH), 103.3 (CH), 90.1 (C_q), 68.9 (CH), 68.7 (CH), 68.7 (CH), 67.0 (CH), 66.6 (CH), 55.8 (CH₃), 47.6 (CH₂), 31.6 (CH), 20.2 (CH₃). **IR** (ATR): 2930, 1640, 1453, 1041, 799, 750, 697 cm⁻¹. **MS (ESI)** *m/z* (relative intensity): 1932 (17) [4M+Na]⁺, 1454 (51) [3M+Na]⁺, 977 (100) [2M+Na]⁺, 500 (97) [M+Na]⁺, 478 (57) [M+H]⁺. **HR-MS** (ESI) *m/z* calcd for C₂₉H₂₈FeNO₂ [M+H]⁺ 478.1464, found 478.1452. **[α]_D²³**: +259.9 (c = 1.75, CHCl₃). **HPLC separation** (Chiralpak[®] ID-3, *n*-hexane/*i*PrOH 70:30, 1.0 mL/min, detection at 273 nm): *t_r* (major) = 19.1 min, *t_r* (minor) = 22.9 min, 96:4 e.r.

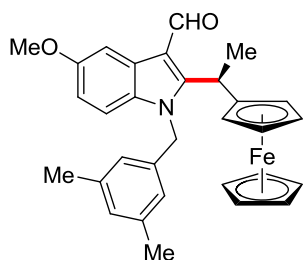
(R)-1-Benzyl-2-(1-ferrocenylethyl)-5-fluoro-1H-indole-3-carbaldehyde (192ka)

The general procedure **GP5** was followed using indole **59k** (90 mg, 0.25 mmol, 1.0 equiv) and vinylferrocene (**191a**) (80 mg, 0.38 mmol, 1.5 equiv). Purification by column chromatography on silica gel (*n*-hexane/EtOAc = 12/1→9.5/1) yielded **192ka** (48.9 mg, 42%) as an orange solid. **M. p.** = 62–64 °C. **¹H NMR** (500 MHz, CDCl₃): δ = 10.11 (s, 1H), 8.04 (dd, *J* = 9.4, 2.6 Hz, 1H), 7.38–7.27 (m, 3H), 7.09–7.03 (m, 1H), 6.98–6.89 (m, 3H), 5.36 (d, *J* = 17.3 Hz, 1H), 5.29 (d, *J* = 17.0 Hz, 1H), 4.87 (brs, 1H), 4.35 (dt, *J* = 2.7, 1.3 Hz, 1H), 4.16–4.02 (m, 7H), 3.85–3.81 (m, 1H), 1.67 (d, *J* = 7.4 Hz, 3H). **¹³C NMR** (125 MHz, CDCl₃): δ = 185.0 (CH), 160.0 (d, ¹*J*_{C-F} = 238.6 Hz, C_q), 155.8 (C_q), 136.0 (C_q), 133.2 (C_q), 129.0 (CH), 127.9 (CH), 126.5 (d, ³*J*_{C-F} = 11.0 Hz, C_q), 125.8 (CH), 113.7 (d, ⁴*J*_{C-F} = 4.4 Hz, C_q), 111.7 (d, ²*J*_{C-F} = 26.2 Hz, CH), 110.8 (d, ³*J*_{C-F} = 9.5 Hz, CH), 107.4 (d, ²*J*_{C-F} = 25.2 Hz, CH), 89.8 (C_q), 69.0 (CH), 68.8 (CH), 68.7 (CH), 67.1 (CH), 66.6 (CH), 47.7 (CH₂), 31.7 (CH), 20.1 (CH₃). **¹⁹F NMR** (471 MHz, CDCl₃): δ = -120.36 (td, *J* = 9.2, 4.2 Hz). **IR** (ATR): 2903, 1645, 1104, 1024, 1001, 797 cm⁻¹. **MS (ESI)** *m/z* (relative intensity): 953 (10) [2M+Na]⁺, 488 (47) [M+Na]⁺, 466 (8) [M+H]⁺, 253 (18), 213 (100). **HR-MS** (ESI) *m/z* calcd for C₂₈H₂₅FFeNO [M+H]⁺ 466.1264, found 466.1257. **[α]_D²³**: +159.4 (c = 0.45, CHCl₃). **HPLC separation** (Chiralpak[®] ID-3, *n*-hexane/*i*PrOH 70:30, 1.0 mL/min, detection at 250 nm): *t_r*(major) = 15.7 min, *t_r*(minor) = 17.2 min, 95:5 e.r.

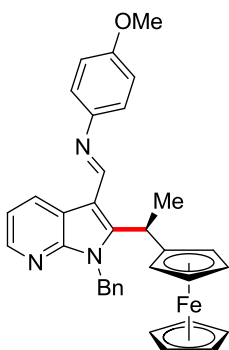
**(R)-1-(3,5-Dimethylbenzyl)-2-(1-ferrocenylethyl)-1H-indole-3-carbaldehyde
(192la)**



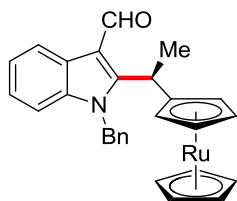
The general procedure **GP5** was followed using indole **59I** (92 mg, 0.25 mmol, 1.0 equiv) and vinylferrocene (**191a**) (80 mg, 0.38 mmol, 1.5 equiv). Purification by column chromatography on silica gel (*n*-hexane/EtOAc = 12.5/1) yielded **192la** (57.9 mg, 49%) as an orange solid. **M. p.** = 54–56 °C. **¹H NMR** (500 MHz, CDCl₃): δ = 10.14 (s, 1H), 8.36 (dt, *J* = 7.9, 1.0 Hz, 1H), 7.28 (ddd, *J* = 7.9, 6.6, 1.5 Hz, 1H), 7.22 (td, *J* = 7.4, 6.6, 1.3 Hz, 1H), 7.19 (d, *J* = 8.5 Hz, 1H), 6.93 (s, 1H), 6.60 (s, 2H), 5.34 (d, *J* = 17.2 Hz, 1H), 5.21 (d, *J* = 16.9 Hz, 1H), 4.88 (brs, 1H), 4.36 (dt, *J* = 2.6, 1.4 Hz, 1H), 4.08 (td, *J* = 2.5, 1.3 Hz, 1H), 4.07–4.01 (m, 6H), 3.84 (s, 1H), 2.26 (s, 6H), 1.69 (d, *J* = 7.4 Hz, 3H). **¹³C NMR** (125 MHz, CDCl₃): δ = 185.4 (CH), 155.0 (C_q), 138.6 (C_q), 136.9 (C_q), 136.3 (C_q), 129.4 (CH), 125.9 (C_q), 123.7 (CH), 123.5 (CH), 123.0 (CH), 121.7 (CH), 113.6 (C_q), 110.0 (CH), 90.3 (C_q), 68.9 (CH), 68.7 (CH), 68.7 (CH), 67.0 (CH), 66.7 (CH), 47.4 (CH₂), 31.5 (CH), 21.3 (CH₃), 20.3 (CH₃). **IR** (ATR): 2920, 1643, 1459, 1040, 815, 746, 479 cm⁻¹. **MS (ESI)** *m/z* (relative intensity): 973 (51) [2M+Na]⁺, 498 (100) [M+Na]⁺, 476 (67) [M+H]⁺, 335 (25), 213 (80). **HR-MS** (ESI) *m/z* calcd for C₃₀H₃₀FeNO [M+H]⁺ 476.1672, found 476.1666. **[α]_D²³**: +180.7 (c = 1.06, CHCl₃). **HPLC separation** (Chiralpak[®] IF-3, *n*-hexane/*i*PrOH 80:20, 0.75 mL/min, detection at 250 nm): *t_r* (minor) = 17.5 min, *t_r* (major) = 22.2 min, 5:95 e.r.

(R)-1-(3,5-Dimethylbenzyl)-2-(1-ferrocenylethyl)-5-methoxy-1H-indole-3-carbaldehyde (192ma)

The general procedure **GP5** was followed using indole **59m** (100 mg, 0.25 mmol, 1.0 equiv) and vinylferrocene (**191a**) (80 mg, 0.38 mmol, 1.5 equiv). Purification by column chromatography on silica gel (*n*-hexane/EtOAc = 12/1→7/1) yielded **192ma** (87.2 mg, 69%) as an orange solid. **M. p.** = 79–81 °C. **¹H NMR** (300 MHz, CDCl₃): δ = 10.10 (s, 1H), 7.89 (d, *J* = 2.5 Hz, 1H), 7.07 (d, *J* = 8.9 Hz, 1H), 6.93 (s, 1H), 6.84 (dd, *J* = 8.9, 2.6 Hz, 1H), 6.59 (s, 2H), 5.30 (d, *J* = 17.0 Hz, 1H), 5.18 (d, *J* = 17.0 Hz, 1H), 4.81 (brs, 1H), 4.37–4.34 (m, 1H), 4.08 (td, *J* = 2.5, 1.3 Hz, 1H), 4.24–3.91 (m, 6H), 3.89 (s, 3H), 3.86–3.83 (m, 1H), 2.26 (s, 6H), 1.68 (d, *J* = 7.4 Hz, 3H). **¹³C NMR** (125 MHz, CDCl₃): δ = 185.1 (CH), 156.7 (C_q), 154.9 (C_q), 138.5 (C_q), 136.2 (C_q), 131.6 (C_q), 129.3 (CH), 126.5 (C_q), 123.6 (CH), 113.6 (CH), 113.5 (C_q), 110.8 (CH), 103.3 (CH), 90.3 (C_q), 68.9 (CH), 68.7 (CH), 68.7 (CH), 67.0 (CH), 66.7 (CH), 55.9 (CH₃), 47.6 (CH₂), 31.7 (CH), 21.4 (CH₃), 20.3 (CH₃). **IR** (ATR): 2914, 1641, 1457, 1424, 1042, 798, 751 cm⁻¹. **MS (ESI)** *m/z* (relative intensity): 661 (13), 528 (100) [M+Na]⁺, 506 (58) [M+H]⁺, 289 (15), 213 (59). **HR-MS** (ESI) *m/z* calcd for C₃₁H₃₂FeNO₂ [M+H]⁺ 506.1777, found 506.1775. **[α]_D²³**: +238.9 (*c* = 1.48, CHCl₃). **HPLC separation** (Chiralpak[®] ID-3, *n*-hexane/*i*PrOH 70:30, 1.0 mL/min, detection at 273 nm): *t_r* (major) = 18.6 min, *t_r* (minor) = 22.6 min, 96:4 e.r.

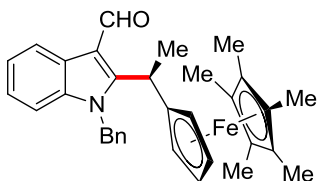
(R)-N-[[1-Benzyl-2-(1-ferrocenylethyl)-1H-pyrrolo[2,3-b]pyridin-3-yl]methylene]-4-methoxyaniline (192na)

The general procedure **GP5** was followed using azaindole **59n** (85 mg, 0.25 mmol, 1.0 equiv) and vinylferrocene (**191a**) (50 mg, 0.38 mmol, 1.5 equiv). The reaction mixture was diluted with sat. aqueous NaHCO₃ (10 mL) and extracted with EtOAc (3 × 10 mL). The combined organic layers were washed with brine (10 mL), dried over Na₂SO₄, and concentrated under reduced pressure. The residue was purified by silica gel chromatography (*n*-hexane/EtOAc = 10/1 + 0.5% Et₃N) to yield **192na** (72.7 mg, 53%) as an orange solid. **M. p.** = 63–64 °C. **¹H NMR** (600 MHz, CDCl₃): δ = 8.85 (dd, *J* = 7.8, 1.6 Hz, 1H), 8.48 (s, 1H), 8.35 (dd, *J* = 4.7, 1.7 Hz, 1H), 7.40–7.30 (m, 3H), 7.21 (dd, *J* = 7.8, 4.7 Hz, 1H), 7.11 (d, *J* = 7.2 Hz, 2H), 6.98 (d, *J* = 8.8 Hz, 2H), 6.85 (d, *J* = 8.9 Hz, 2H), 6.07 (d, *J* = 16.3 Hz, 1H), 5.28 (d, *J* = 16.3 Hz, 1H), 4.58 (q, *J* = 7.3 Hz, 1H), 4.38 (dt, *J* = 2.6, 1.3 Hz, 1H), 4.12 (td, *J* = 2.5, 1.3 Hz, 1H), 4.06 (td, *J* = 2.5, 1.3 Hz, 1H), 3.98 (s, 5H), 3.81 (s, 3H), 3.64 (dd, *J* = 2.5, 1.3 Hz, 1H), 1.60 (d, *J* = 7.3 Hz, 3H). **¹³C NMR** (125 MHz, CDCl₃): δ = 157.2 (C_q), 153.0 (CH), 150.1 (C_q), 148.2 (C_q), 146.4 (C_q), 143.6 (CH), 137.9 (C_q), 131.1 (CH), 128.8 (CH), 127.6 (CH), 126.4 (CH), 121.9 (CH), 118.8 (C_q), 118.0 (CH), 114.1 (CH), 109.5 (C_q), 90.8 (C_q), 68.9 (CH), 68.9 (CH), 68.9 (CH), 66.8 (CH), 66.7 (CH), 55.5 (CH₃), 45.2 (CH₂), 32.2 (CH), 20.3 (CH₃). **IR** (ATR): 2934, 1613, 1498, 1428, 1242, 728 cm⁻¹. **MS (ESI)** *m/z* (relative intensity): 554 (100) [M+H]⁺. **HR-MS** (ESI) *m/z* calcd for C₃₄H₃₂N₃OFe [M+H]⁺ 554.1890, found 554.1884. **[α]_D²³**: +309.1 (*c* = 1.16, CHCl₃). **HPLC separation** (Chiralpak[®] IF-3, *n*-hexane/*i*PrOH 90:10, 1.0 mL/min, detection at 273 nm): *t_r* (minor) = 11.3 min, *t_r* (major) = 11.8 min, 10:90 e.r.

(R)-1-Benzyl-2-(1-ruthenocenylethyl)-1H-indole-3-carbaldehyde (192cb)

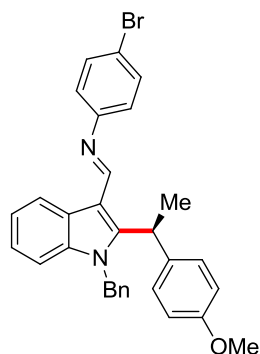
The general procedure **GP5** was followed using indole **59c** (93 mg, 0.25 mmol, 1.0 equiv) and vinylruthenocene (**191b**) (96 mg, 0.38 mmol, 1.5 equiv). Purification by column chromatography on silica gel (*n*-hexane/EtOAc = 13/1→7.5/1) yielded **192cb** (59.1 mg, 48%) as a dark yellow solid. **M. p.** = 52–54 °C. **¹H NMR** (500 MHz, CDCl₃): δ = 10.28 (s, 1H), 8.39 (dt, *J* = 7.9, 1.0 Hz, 1H), 7.34–7.25 (m, 4H), 7.22 (td, *J* = 7.6, 1.3 Hz, 1H), 7.18 (d, *J* = 8.1 Hz, 1H), 6.97 (dd, *J* = 7.9, 1.7 Hz, 2H), 5.43 (d, *J* = 17.2 Hz, 1H), 5.39 (d, *J* = 17.1 Hz, 1H), 4.74 (dt, *J* = 2.4, 1.1 Hz, 1H), 4.61 (brs, 1H), 4.48 (s, 5H), 4.44 (td, *J* = 2.3, 1.1 Hz, 1H), 4.42 (td, *J* = 2.3, 1.1 Hz, 1H), 4.33 (brs, 1H), 1.56 (d, *J* = 7.5 Hz, 3H). **¹³C NMR** (125 MHz, CDCl₃): δ = 185.3 (CH), 154.6 (C_q), 136.8 (C_q), 136.2 (C_q), 128.9 (CH), 127.8 (CH), 125.9 (C_q), 125.8 (CH), 123.6 (CH), 123.1 (CH), 121.9 (CH), 113.9 (C_q), 110.0 (CH), 94.0 (C_q), 71.2 (CH), 71.0 (CH), 70.7 (CH), 69.6 (CH), 69.5 (CH), 47.5 (CH₂), 31.5 (CH), 20.9 (CH₃). **IR** (ATR): 2904, 1643, 1453, 1022, 805, 744 cm⁻¹. **MS (EI)** *m/z* (relative intensity): 493 (39) [M]⁺ (¹⁰²Ru), 384 (28), 317 (40), 300 (28), 259 (24), 91 (100). **HR-MS** (ESI) *m/z* calcd for C₂₈H₂₆NO¹⁰²Ru [M+H]⁺ 494.1060, found 494.1038. **[α]_D²³**: +103.2 (*c* = 0.95, CHCl₃). **HPLC separation** (Chiralpak[®] IF-3, *n*-hexane/*i*PrOH 80:20, 0.75 mL/min, detection at 273 nm): *t_r* (minor) = 20.8 min, *t_r* (major) = 21.9 min, 4:96 e.r.

(R)-1-Benzyl-2-[1-(1',2',3',4',5'-pentamethylferrocenyl)ethyl]-1H-indole-3-carbaldehyde (192cc)



The general procedure **GP6** was followed using indole **59c** (93 mg, 0.25 mmol, 1.0 equiv) and vinylferrocene **191c** (106 mg, 0.38 mmol, 1.5 equiv). Purification by column chromatography on silica gel (*n*-hexane/EtOAc = 20/1) yielded **192cc** (75.0 mg, 58%) as an orange solid. **M. p.** = 91–94 °C. **¹H NMR** (500 MHz, CDCl₃): δ = 10.25 (brs, 1H), 8.37 (d, *J* = 7.9 Hz, 1H), 7.34–7.21 (m, 4H), 7.18 (t, *J* = 7.6 Hz, 1H), 7.14–6.99 (m, 1H), 6.99–6.70 (m, 2H), 5.25 (brs, 3H), 3.81 (s, 1H), 3.63 (td, *J* = 2.4, 1.1 Hz, 1H), 3.59 (td, *J* = 2.4, 1.1 Hz, 1H), 3.36 (s, 1H), 1.83 (s, 15H), 1.55 (d, *J* = 7.4 Hz, 3H). **¹³C NMR** (125 MHz, CDCl₃): δ = 185.1 (CH), 155.5 (C_q), 136.9 (C_q), 136.2 (C_q), 128.8 (CH), 127.5 (CH), 125.8 (C_q), 125.6 (CH), 123.4 (CH), 123.0 (CH), 121.6 (CH), 113.7 (C_q), 110.0 (CH), 88.9 (C_q), 80.0 (C_q), 73.4 (CH), 71.4 (CH), 71.3 (CH), 68.6 (CH), 47.2 (CH₂), 28.8 (CH), 19.4 (CH₃), 11.0 (CH₃). **IR** (ATR): 2898, 1638, 1423, 1028, 819, 729 cm⁻¹. **MS (EI)** *m/z* (relative intensity): 517 (100) [M]⁺, 382 (32), 381 (39), 290 (23), 262 (19). **HR-MS** (EI) *m/z* calcd for C₃₃H₃₅FeNO [M]⁺ 517.2069, found 517.2051. **[α]_D²³**: +287.0 (*c* = 1.20, CHCl₃). **HPLC separation** (Chiralpak[®] IF-3, *n*-hexane/*i*PrOH 90:10, 1.0 mL/min, detection at 250 nm): *t_r* (major) = 12.7 min, *t_r* (minor) = 13.5 min, 95:5 e.r.

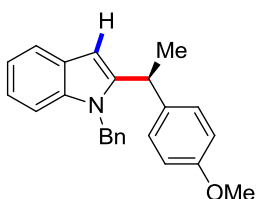
5.5.2. Product Diversification

(S)-N-[[1-Benzyl-2-(1-(4-methoxyphenyl)ethyl)-1H-indol-3-yl]methylene]-4-bromoaniline (197)

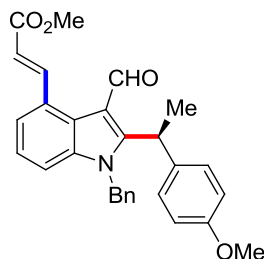
62cc (90 mg, 0.24 mmol, 1.0 equiv, 92:8 e.r.), 4-bromoaniline (46 mg, 0.27 mmol, 1.1 equiv) and activated 4Å molecular sieves (1.0 g) were suspended in PhMe (5.0 mL) and stirred at 50 °C for 16 h. The suspension was allowed to cool to ambient temperature, filtered and concentrated under reduced pressure. The residue was recrystallized from *n*-hexane/isopropanol to provide the optically pure imine **197** as a white crystalline solid (67 mg, 53%). **M. p.** = 179–181 °C. **¹H NMR** (300 MHz, CDCl₃): δ = 8.66 (ddd, *J* = 7.8, 1.4, 0.7 Hz, 1H), 8.61 (s, 1H), 7.43 (d, *J* = 8.7 Hz, 2H), 7.29 (ddd, *J* = 7.8, 6.8, 1.5 Hz, 1H), 7.26–7.19 (m, 4H), 7.17 (ddd, *J* = 8.0, 1.5, 0.8 Hz, 1H), 7.12 (d, *J* = 8.2 Hz, 2H), 6.96 (d, *J* = 8.7 Hz, 2H), 6.94–6.88 (m, 2H), 6.81 (d, *J* = 8.8 Hz, 2H), 5.27 (s, 2H), 4.85 (q, *J* = 7.3 Hz, 1H), 3.78 (s, 3H), 1.67 (d, *J* = 7.4 Hz, 3H). **¹³C NMR** (125 MHz, CDCl₃): δ = 158.3 (C_q), 155.0 (CH), 152.8 (C_q), 149.8 (C_q), 137.3 (C_q), 136.6 (C_q), 133.9 (C_q), 131.8 (CH), 128.7 (CH), 128.1 (CH), 127.4 (CH), 126.0 (C_q), 125.8 (CH), 123.2 (CH), 122.6 (CH), 122.5 (CH), 122.1 (CH), 117.7 (C_q), 114.0 (CH), 111.9 (C_q), 109.8 (CH), 55.4 (CH₃), 47.4 (CH₂), 34.5 (CH), 20.0 (CH₃). **IR** (ATR): 2923, 2827, 1604, 1570, 1421, 752, 725 cm⁻¹. **MS (ESI)** *m/z* (relative intensity): 525 (100) [M+H]⁺ (⁸¹Br), 523 (100) [M+H]⁺ (⁷⁹Br), 475 (8). **HR-MS** (ESI) *m/z* calcd for C₃₁H₂₈N₂O⁸¹Br [M+H]⁺ 525.1361, found 525.1360. **[α]_D²³**: +60.1 (c = 0.84, CHCl₃). **HPLC separation** (Chiralpak[®] IA-3, *n*-hexane/*i*PrOH 80:20, 1.0 mL/min, detection at 273 nm): *t_r* (major) = 5.9 min, *t_r* (minor) = 6.7 min, 99.5:0.5 e.r.

Crystals suitable for X-ray crystallography were grown by slow evaporation of a solution of **197** in a mixture of *n*-hexane/EtOAc/CH₂Cl₂.

(S)-1-Benzyl-2-[1-(4-methoxyphenyl)ethyl]-1*H*-indole (198)



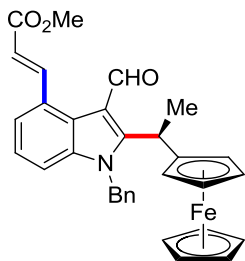
Following a modified procedure,^[337] a 20 mL oven-dried screw cap reaction tube was charged with 4Å molecular sieves (60 mg), **62cc** (50 mg, 0.135 mmol, 1.0 equiv, 90:10 e.r.), Pd(OAc)₂ (2.5 mg, 11 μmol, 8.0 mol %) and cyclohexane (0.75 mL). The tube was tightly closed by screw cap and placed in a pre-heated oil bath at 140 °C. The reaction mixture was vigorously stirred for 24 h. The reaction mixture was allowed to cool to ambient temperature and filtered through a short plug of Celite[®]. The Celite[®] was washed with EtOAc. The filtrate was concentrated under reduced pressure. Purification of the residue by column chromatography on silica gel (*n*-hexane/EtOAc = 25/1) yielded deformylated product **198** (30.5 mg, 66%) as a colorless oil. ¹H NMR (500 MHz, CDCl₃): δ = 7.68 (ddd, *J* = 5.9, 3.1, 0.8 Hz, 1H), 7.26–7.20 (m, 3H), 7.20–7.15 (m, 1H), 7.13 (dd, *J* = 6.1, 3.1 Hz, 2H), 7.04 (d, *J* = 8.6 Hz, 2H), 6.85 (ddd, *J* = 6.9, 1.8, 0.8 Hz, 2H), 6.79 (d, *J* = 8.7 Hz, 2H), 6.62 (t, *J* = 0.9 Hz, 1H), 5.20 (d, *J* = 17.2 Hz, 1H), 4.96 (d, *J* = 17.2 Hz, 1H), 4.04 (q, *J* = 7.3 Hz, 1H), 3.78 (s, 3H), 1.64 (d, *J* = 7.1 Hz, 3H). ¹³C NMR (125 MHz, CDCl₃): δ = 158.1 (C_q), 144.1 (C_q), 138.0 (C_q), 137.6 (C_q), 136.9 (C_q), 128.6 (CH), 128.2 (CH), 127.8 (C_q), 127.0 (CH), 125.8 (CH), 121.2 (CH), 120.1 (CH), 119.5 (CH), 114.0 (CH), 109.3 (CH), 99.8 (CH), 55.2 (CH₃), 46.3 (CH₂), 37.1 (CH), 22.9 (CH₃). IR (ATR): 2928, 1509, 1452, 1241, 1031, 830, 727 cm⁻¹. MS (EI) *m/z* (relative intensity): 341 (94) [M]⁺, 326 (100), 91 (70). HR-MS (ESI) *m/z* calcd for C₂₄H₂₄NO [M+H]⁺ 342.1852, found 342.1851. [α]_D²³: +58.3 (c = 0.62, CHCl₃). HPLC separation (Chiralpak[®] IA-3, *n*-hexane/*i*PrOH 80:20, 1.0 mL/min, detection at 273 nm): *t_r* (major) = 4.2 min, *t_r* (minor) = 4.8 min, 88:12 e.r.

(S,E)-Methyl 3-{1-Benzyl-3-formyl-2-[1-(4-methoxyphenyl)ethyl]-1H-indol-4-yl}acrylate (199a)

Following a modified procedure,^[254] a 5 mL round-bottom flask was charged under air with **62cc** (74 mg, 0.20 mmol, 1.0 equiv, 90:10 e.r.), $[\text{RuCl}_2(p\text{-cymene})]_2$ (6.1 mg, 10 μmol , 5.0 mol %), AgSbF_6 (13.7 mg, 40 μmol , 20 mol %), $\text{Cu}(\text{OAc})_2 \cdot \text{H}_2\text{O}$ (20.0 mg, 0.10 mmol, 0.50 equiv) and 1,2-dichloroethane (2.0 mL). Methyl acrylate (0.15 mL, 1.60 mmol, 8.0 equiv) was then added in a single portion. The flask was equipped with a condenser and placed in a pre-heated oil bath at 120 °C. The reaction mixture was stirred at 120 °C for 16 h. The suspension was allowed to cool down to ambient temperature, diluted with *n*-hexane/EtOAc 1/1 (5 mL), filtered through a short plug of silica gel, and eluted with *n*-hexane/EtOAc 1/1 (3 \times 20 mL). The filtrate was concentrated under reduced pressure and purified by column chromatography on silica gel (*n*-hexane/EtOAc = 7/1 \rightarrow 3/1) to yield **199a** (67.3 mg, 74%) as a yellow foam. **M. p.** = 65–67 °C. **¹H NMR** (400 MHz, CDCl_3): δ = 10.37 (s, 1H), 8.99 (d, J = 15.8 Hz, 1H), 7.49 (dt, J = 7.5, 0.9 Hz, 1H), 7.28–7.20 (m, 3H), 7.20 (ddd, J = 8.1, 7.4, 0.6 Hz, 1H), 7.12 (dd, J = 8.2, 1.0 Hz, 1H), 7.09 (dd, J = 9.0, 1.0 Hz, 2H), 6.86–6.81 (m, 2H), 6.79 (d, J = 8.8 Hz, 2H), 6.40 (d, J = 15.8 Hz, 1H), 5.45 (q, J = 7.4 Hz, 1H), 5.24 (d, J = 17.3 Hz, 1H), 5.17 (d, J = 17.3 Hz, 1H), 3.86 (s, 3H), 3.76 (s, 3H), 1.67 (d, J = 7.4 Hz, 3H). **¹³C NMR** (100 MHz, CDCl_3): δ = 185.3 (CH), 167.4 (C_q), 158.4 (C_q), 155.5 (C_q), 145.6 (CH), 137.9 (C_q), 135.6 (C_q), 132.8 (C_q), 129.3 (C_q), 128.8 (CH), 127.9 (CH), 127.6 (CH), 125.6 (CH), 124.7 (C_q), 123.5 (CH), 122.0 (CH), 119.3 (CH), 115.5 (C_q), 114.1 (CH), 112.0 (CH), 55.3 (CH_3), 51.7 (CH_3), 47.7 (CH_2), 33.7 (CH), 18.7 (CH_3). **IR** (ATR): 2948, 1712, 1654, 1510, 1247, 1163, 1031, 725 cm^{-1} . **MS (EI)** m/z (relative intensity): 453 (44) $[\text{M}]^+$, 394 (35), 393 (57), 392 (44), 302 (42), 197 (88), 91 (100). **HR-MS** (EI) m/z calcd for $\text{C}_{29}\text{H}_{27}\text{NO}_4$ $[\text{M}]^+$ 453.1940, found 453.1931. **$[\alpha]_D^{23}$** : -93.8 (c = 0.53, CHCl_3). **HPLC separation**

(Chiralpak® IA-3, *n*-hexane/*i*PrOH 80:20, 1.0 mL/min, detection at 273 nm):
 t_r (major) = 11.1 min, t_r (minor) = 15.4 min, 89:11 e.r.

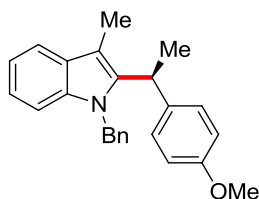
(*R,E*)-Methyl 3-[1-Benzyl-3-formyl-2-(1-ferrocenylethyl)-1*H*-indol-4-yl]acrylate (199b)



Following a modified procedure,^[254] a 5 mL round-bottom flask was charged under air with recrystallized **192ca** (89 mg, 0.20 mmol, 1.0 equiv, 99.7:0.3 e.r.), [RuCl₂(*p*-cymene)]₂ (6.1 mg, 10 μmol, 5.0 mol %), AgSbF₆ (13.7 mg, 40 μmol, 20 mol %), Cu(OAc)₂·H₂O (20 mg, 0.10 mmol, 0.50 equiv) and 1,2-dichloroethane (2.0 mL). Methyl acrylate (0.15 mL, 1.60 mmol, 8.0 equiv) was then added in a single portion. The flask was equipped with a condenser and placed in a pre-heated oil bath at 120 °C. The reaction mixture was stirred at 120 °C for 16 h. The suspension was allowed to cool down to ambient temperature, diluted with *n*-hexane/EtOAc 1/1 (5 mL), filtered through a short plug of silica gel, and eluted with *n*-hexane/EtOAc 1/1 (3 × 20 mL). The filtrate was concentrated under reduced pressure and purified by column chromatography on silica gel (*n*-hexane/EtOAc = 7/1→4.5/1) to yield **199b** (67.9 mg, 64%) as an orange solid. **M. p.** = 79–80 °C. **¹H NMR** (300 MHz, CDCl₃): δ = 10.36 (s, 1H), 8.98 (d, *J* = 15.8 Hz, 1H), 7.47 (d, *J* = 7.1 Hz, 1H), 7.36–7.03 (m, 5H), 6.95–6.79 (m, 2H), 6.38 (d, *J* = 15.8 Hz, 1H), 5.52–5.19 (m, 3H), 4.33 (dt, *J* = 2.6, 1.3 Hz, 1H), 4.10 (brs, 5H), 4.06 (td, *J* = 2.4, 1.3 Hz, 1H), 4.04 (td, *J* = 2.4, 1.2 Hz, 1H), 3.93–3.86 (m, 1H), 3.86 (s, 3H), 1.63 (d, *J* = 7.4 Hz, 3H). **¹³C NMR** (125 MHz, CDCl₃): δ = 184.9 (CH), 167.3 (C_q), 145.6 (CH), 137.7 (C_q), 135.8 (C_q), 129.2 (C_q), 128.8 (CH), 127.6 (CH), 125.7 (CH), 124.6 (C_q), 123.4 (CH), 121.8 (CH), 119.1 (CH), 114.6 (C_q), 111.8 (CH), 89.8 (C_q), 69.1 (CH), 68.8 (CH), 68.7 (CH), 67.0 (CH), 66.6 (CH), 51.7 (CH₃), 47.7 (CH₂), 31.3 (CH), 19.1

(CH₃). One C_q could not be observed. **IR** (ATR): 2925, 1712, 1655, 1259, 1164, 1018, 794, 727 cm⁻¹. **MS (ESI)** *m/z* (relative intensity): 1085 (33) [2M+Na]⁺, 554 (100) [M+Na]⁺, 532 (20) [M+H]⁺, 281 (23), 213 (22). **HR-MS** (ESI) *m/z* calcd for C₃₂H₃₀FeNO₃ [M+H]⁺ 532.1570, found 532.1565. [α]_D²³: +292.9 (c = 0.59, CHCl₃). **HPLC separation** (Chiralpak[®] IF-3, *n*-hexane/*i*PrOH 70:30, 1.0 mL/min, detection at 273 nm): *t_r* (major) = 12.8 min, *t_r* (minor) = 14.1 min, 98:2 e.r.

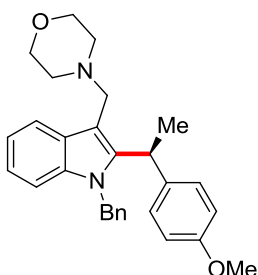
(S)-1-Benzyl-2-[1-(4-methoxyphenyl)ethyl]-3-methyl-1*H*-indole (200)



A 100 mL two-necked flask was charged with **62cc** (50 mg, 0.135 mmol, 1.0 equiv, 90:10 e.r.), Pd/C 10 wt. % (15 mg, 0.014 mmol, 10 mol %) and EtOH (15 mL). The flask was rapidly evacuated and backfilled with H₂ 3 times. The suspension was then vigorously stirred under H₂ atmosphere for 16 h at ambient temperature. The suspension was diluted with *n*-hexane (50 mL) and filtered through a short plug of Celite[®]. The Celite[®] was washed with *n*-hexane/EtOAc (1/1). The filtrate was concentrated under reduced pressure, and the residue purified by column chromatography on silica gel (*n*-hexane/EtOAc = 15/1) to yield **200** (29.3 mg, 61%) as a colorless solid. **M. p.** = 91–93 °C. **¹H NMR** (300 MHz, CDCl₃): δ = 7.66–7.53 (m, 1H), 7.27–7.16 (m, 3H), 7.15–7.10 (m, 3H), 7.07 (dd, *J* = 8.9, 0.8 Hz, 2H), 6.90 (ddd, *J* = 6.8, 1.9, 0.9 Hz, 2H), 6.78 (d, *J* = 8.8 Hz, 2H), 5.20 (d, *J* = 17.5 Hz, 1H), 5.12 (d, *J* = 17.5 Hz, 1H), 4.44 (q, *J* = 7.3 Hz, 1H), 3.78 (s, 3H), 2.30 (s, 3H), 1.62 (d, *J* = 7.4 Hz, 3H). **¹³C NMR** (125 MHz, CDCl₃): δ = 157.8 (C_q), 139.2 (C_q), 138.3 (C_q), 136.5 (C_q), 135.5 (C_q), 128.9 (C_q), 128.5 (CH), 128.0 (CH), 126.9 (CH), 125.8 (CH), 121.2 (CH), 118.9 (CH), 118.1 (CH), 113.7 (CH), 109.2 (CH), 107.6 (C_q), 55.3 (CH₃), 46.9 (CH₂), 34.9 (CH), 19.9 (CH₃), 9.5 (CH₃). **IR** (ATR): 2924, 1508, 1466, 1241, 1173, 1034, 736 cm⁻¹. **MS (EI)** *m/z* (relative intensity): 355 (100) [M]⁺, 340 (75), 234 (22), 91 (55). **HR-MS** (EI) *m/z* calcd for C₂₅H₂₅NO [M]⁺ 355.1936, found 355.1940.

$[\alpha]_D^{23}$: -22.8 ($c = 0.532$, CHCl_3). **HPLC separation** (Chiralpak[®] IA-3, *n*-hexane/*i*PrOH 99:1, 1.0 mL/min, detection at 273 nm): t_r (major) = 6.3 min, t_r (minor) = 7.0 min, 89:11 e.r.

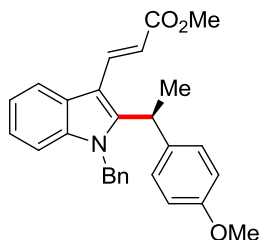
(S)-4-[[1-Benzyl-2-(1-(4-methoxyphenyl)ethyl)-1*H*-indol-3-yl]methyl]morpholine (201)



A solution of **62cc** (75 mg, 0.20 mmol, 1.0 equiv, 90:10 e.r.), morpholine (35 mg, 0.41 mmol, 2.0 equiv), $\text{NaBH}(\text{OAc})_3$ (172 mg, 0.81 mmol, 4.0 equiv) and AcOH (1 drop) in DCE (2.0 mL) was stirred at ambient temperature for 18 h. The reaction mixture was diluted with CH_2Cl_2 (10 mL), washed with sat. aqueous NaHCO_3 (10 mL), and dried over Na_2SO_4 . After removal of volatiles under reduced pressure, the residue was purified by column chromatography on silica gel (*n*-hexane/EtOAc = 7.5/1→5.5/1) to yield **201** (73.3 mg, 82%) as a colorless oil. **¹H NMR** (300 MHz, CDCl_3): $\delta = 7.79\text{--}7.72$ (m, 1H), 7.25–7.17 (m, 3H), 7.17–7.02 (m, 5H), 6.84 (ddt, $J = 6.2, 2.5, 0.9$ Hz, 2H), 6.76 (d, $J = 8.8$ Hz, 2H), 5.13 (s, 2H), 4.63 (q, $J = 7.3$ Hz, 1H), 3.77 (s, 3H), 3.72–3.50 (m, 6H), 2.52–2.40 (m, 4H), 1.63 (d, $J = 7.4$ Hz, 3H). **¹³C NMR** (125 MHz, CDCl_3): $\delta = 157.9$ (C_q), 142.1 (C_q), 137.9 (C_q), 136.4 (C_q), 134.9 (C_q), 128.9 (C_q), 128.5 (CH), 128.2 (CH), 126.9 (CH), 125.7 (CH), 121.2 (CH), 119.3 (CH), 118.7 (CH), 113.6 (CH), 109.4 (CH), 108.5 (C_q), 67.3 (CH_2), 55.3 (CH_3), 53.6 (CH_2), 52.8 (CH_2), 47.1 (CH_2), 34.6 (CH), 19.1 (CH_3). **IR** (ATR): 2928, 1510, 1453, 1246, 1114, 1031, 736 cm^{-1} . **MS (ESI)** m/z (relative intensity): 441 (6) $[\text{M}+\text{H}]^+$, 392 (6), 354 (100). **HR-MS** (ESI) m/z calcd for $\text{C}_{29}\text{H}_{33}\text{N}_2\text{O}_2$ $[\text{M}+\text{H}]^+$ 441.2537, found 441.2538. $[\alpha]_D^{23}$: -41.1 ($c = 0.50$, CHCl_3). **HPLC separation** (Chiralpak[®] IF-3,

n-hexane/*i*PrOH 90:10, 1.0 mL/min, detection at 273 nm): t_r (minor) = 6.8 min, t_r (major) = 7.2 min, 11:89 e.r.

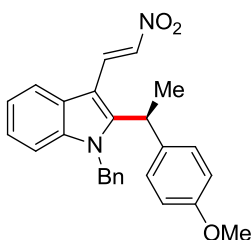
**(*S,E*)-Methyl 3-{1-Benzyl-2-[1-(4-methoxyphenyl)ethyl]-1*H*-indol-3-yl}acrylate
(202)**



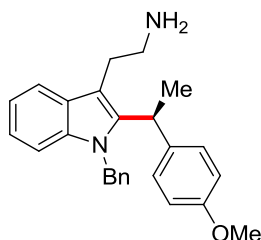
Following a modified procedure,^[338] **62cc** (75 mg, 0.20 mmol, 1.0 equiv, 90:10 e.r.) and methyl (triphenylphosphoranylidene)acetate (204 mg, 0.61 mmol, 3.0 equiv) were suspended in PhMe (5.0 mL). The resulting mixture was stirred under reflux (130 °C) for 16 h. The reaction mixture was allowed to cool down to ambient temperature, and diluted with EtOAc (15 mL). The solution was washed with H₂O (15 mL) and brine (15 mL), dried over Na₂SO₄, and concentrated under reduced pressure. The residue was purified by column chromatography on silica gel (*n*-hexane/EtOAc = 12/1) to provide **202** (70.0 mg, 81%) as an off-white solid. **M. p.** = 63–64 °C. **¹H NMR** (400 MHz, CDCl₃): δ = 8.09 (d, J = 15.8 Hz, 1H), 7.99 (ddd, J = 7.7, 1.3, 0.7 Hz, 1H), 7.30–7.17 (m, 5H), 7.17 (ddd, J = 8.2, 7.1, 1.2 Hz, 1H), 7.13–7.04 (m, 3H), 6.88–6.81 (m, 2H), 6.79 (d, J = 8.8 Hz, 2H), 6.54 (d, J = 15.8 Hz, 1H), 5.16 (d, J = 17.4 Hz, 1H), 5.10 (d, J = 17.4 Hz, 1H), 4.82 (q, J = 7.4 Hz, 1H), 3.80 (s, 3H), 3.77 (s, 3H), 1.64 (d, J = 7.4 Hz, 3H). **¹³C NMR** (100 MHz, CDCl₃): δ = 168.8 (C_q), 158.2 (C_q), 147.9 (C_q), 137.9 (CH), 137.8 (C_q), 136.7 (C_q), 133.5 (C_q), 128.7 (CH), 128.0 (CH), 127.3 (CH), 125.9 (C_q), 125.7 (CH), 122.8 (CH), 121.6 (CH), 120.5 (CH), 114.0 (CH), 113.0 (CH), 110.4 (CH), 109.8 (C_q), 55.3 (CH₃), 51.3 (CH₃), 47.5 (CH₂), 34.0 (CH), 19.2 (CH₃). **IR** (ATR): 2963, 1705, 1611, 1245, 1163, 1028, 726 cm⁻¹. **MS (ESI)** m/z (relative intensity): 873 (60) [2M+Na]⁺, 448 (100) [M+Na]⁺, 426 (74) [M+H]⁺, 117 (91). **HR-MS** (ESI) m/z calcd for C₂₈H₂₈NO₃ [M+H]⁺ 426.2064, found 426.2077. **[α]_D²³**: -65.5 (c = 0.67, CHCl₃). **HPLC**

separation (Chiralpak[®] IA-3, *n*-hexane/*i*PrOH 80:20, 1.0 mL/min, detection at 273 nm): t_r (major) = 5.9 min, t_r (minor) = 6.6 min, 88:12 e.r.

(*S,E*)-1-Benzyl-2-[1-(4-methoxyphenyl)ethyl]-3-(2-nitrovinyl)-1*H*-indole (237)



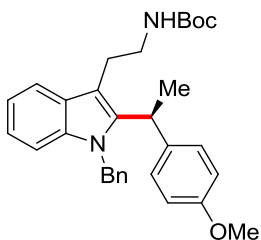
A 5 mL round-bottom flask was loaded with **62cc** (80 mg, 0.22 mmol, 1.0 equiv, 90:10 e.r.), ammonium acetate (33 mg, 0.43 mmol, 2.0 equiv) and nitromethane (1.5 mL). The resulting solution was stirred at 90 °C for 16 h. The reaction mixture was concentrated under reduced pressure, and the residue was purified by column chromatography on silica gel (*n*-hexane/EtOAc = 12/1) to provide **237** (74.8 mg, 84%) as a bright yellow solid. **M. p.** = 45–47 °C. **¹H NMR** (400 MHz, CDCl₃): δ = 8.43 (d, J = 13.3 Hz, 1H), 7.85 (d, J = 13.2 Hz, 1H), 7.81 (dt, J = 8.0, 1.1 Hz, 1H), 7.33 (ddd, J = 8.1, 7.1, 1.2 Hz, 1H), 7.29–7.22 (m, 4H), 7.18 (dt, J = 8.0, 1.0 Hz, 1H), 7.07 (dd, J = 9.0, 0.9 Hz, 2H), 6.91–6.86 (m, 2H), 6.82 (d, J = 8.8 Hz, 2H), 5.25 (d, J = 17.4 Hz, 1H), 5.20 (d, J = 17.4 Hz, 1H), 4.80 (q, J = 7.4 Hz, 1H), 3.78 (s, 3H), 1.68 (d, J = 7.4 Hz, 3H). **¹³C NMR** (100 MHz, CDCl₃): δ = 158.5 (C_q), 152.2 (C_q), 138.0 (C_q), 135.9 (C_q), 132.8 (CH), 132.6 (C_q), 132.2 (CH), 128.9 (CH), 128.0 (CH), 127.7 (CH), 125.7 (CH), 125.3 (C_q), 123.7 (CH), 122.8 (CH), 120.6 (CH), 114.3 (CH), 111.0 (CH), 106.2 (C_q), 55.3 (CH₃), 47.8 (CH₂), 34.3 (CH), 19.4 (CH₃). **IR** (ATR): 2965, 1606, 1510, 1245, 1176, 961, 733 cm⁻¹. **MS (ESI)** m/z (relative intensity): 847 (31) [2M+Na]⁺, 435 (88) [M+Na]⁺, 413 (53) [M+H]⁺, 177 (32), 117 (100). **HR-MS** (ESI) m/z calcd for C₂₆H₂₅N₂O₃ [M+H]⁺ 413.1860, found 413.1873. **[α]_D²³**: -77.6 (c = 0.63, CHCl₃). **HPLC separation** (Chiralpak[®] IF-3, *n*-hexane/*i*PrOH 90:10, 1.0 mL/min, detection at 273 nm): t_r (minor) = 12.4 min, t_r (major) = 13.2 min, 11:89 e.r.

(S)-2-{1-Benzyl-2-[1-(4-methoxyphenyl)ethyl]-1H-indol-3-yl}ethanamine (238)

A 5 mL round-bottom flask was charged with **237** (40 mg, 0.097 mmol, 1.0 equiv, 89:11 e.r.). THF (3.0 mL) was then added, followed by LiAlH₄ (11 mg, 0.29 mmol, 3.0 equiv). The resulting suspension was refluxed at 85 °C for 2.5 h. The reaction mixture was cooled to 0 °C with an ice bath, and methanol was carefully added dropwise. The mixture was then poured into sat. aqueous NaHCO₃ (10 mL) and extracted with EtOAc (3 × 10 mL). The combined organic layer was washed with brine (15 mL), dried over Na₂SO₄, and concentrated under reduced pressure. The residue was purified by column chromatography on silica gel (CH₂Cl₂/MeOH = 10/1 + 0.5% Et₃N) to yield tryptamine **238** (28.3 mg, 76%) as a colorless solid. **M. p.** = 71–72 °C. **¹H NMR** (400 MHz, CDCl₃): δ = 7.72–7.65 (m, 1H), 7.25–7.15 (m, 3H), 7.11–7.06 (m, 3H), 7.03 (d, *J* = 8.6 Hz, 2H), 6.87 (dd, *J* = 7.8, 1.5 Hz, 2H), 6.76 (d, *J* = 8.7 Hz, 2H), 6.02 (brs, 2H), 5.13 (s, 2H), 4.51 (q, *J* = 7.3 Hz, 1H), 3.71 (s, 3H), 3.18–3.09 (m, 2H), 3.08–3.00 (m, 1H), 2.90 (dt, *J* = 12.2, 7.7 Hz, 1H), 1.59 (d, *J* = 7.4 Hz, 3H). **¹³C NMR** (100 MHz, CDCl₃): δ = 158.0 (C_q), 140.9 (C_q), 137.9 (C_q), 136.8 (C_q), 134.7 (C_q), 128.6 (CH), 128.1 (CH), 128.0 (C_q), 127.0 (CH), 125.8 (CH), 121.6 (CH), 119.6 (CH), 118.3 (CH), 113.9 (CH), 109.6 (CH), 107.7 (C_q), 55.2 (CH₃), 47.2 (CH₂), 41.4 (CH₂), 34.2 (CH), 25.3 (CH₂), 19.6 (CH₃). **IR** (ATR): 2927, 1510, 1466, 1244, 1177, 1030, 736 cm⁻¹. **MS (ESI)** *m/z* (relative intensity): 769 (6) [2M+H]⁺, 385 (100) [M+H]⁺, 368 (20), 251 (16), 135 (37). **HR-MS** (ESI) *m/z* calcd for C₂₆H₂₉N₂O [M+H]⁺ 385.2274, found 385.2288.

The two enantiomers could at this stage not be separated by chiral HPLC (*vide infra*).

(S)-tert-Butyl (2-[1-Benzyl-2-(1-(4-methoxyphenyl)ethyl)-1H-indol-3-yl]ethyl)carbamate (203)



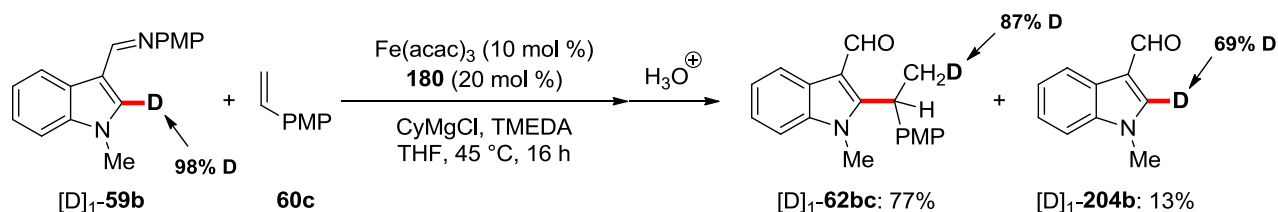
To a solution of tryptamine **238** (21.0 mg, 0.055 mmol, 1.0 equiv) in 1,4-dioxane (1.0 mL) were added Et₃N (17 mg, 0.16 mmol, 3.0 equiv) and Boc₂O (18 mg, 0.080 mmol, 1.5 equiv). The resulting solution was stirred at ambient temperature for 16 h. The reaction mixture was then concentrated under reduced pressure and the residue purified by column chromatography on silica gel (*n*-hexane/EtOAc = 8/1) to provide **203** (24.9 mg, 94%) as a colorless solid. **M. p.** = 57–59 °C. **¹H NMR** (500 MHz, CDCl₃): δ = 7.63 (dd, *J* = 6.2, 2.8 Hz, 1H), 7.25–7.15 (m, 3H), 7.15–7.05 (m, 3H), 7.05 (dd, *J* = 8.9, 0.8 Hz, 2H), 6.85 (dd, *J* = 7.7, 1.5 Hz, 2H), 6.77 (d, *J* = 8.7 Hz, 2H), 5.11 (s, 2H), 4.61–4.54 (m, 1H), 4.51 (q, *J* = 7.3 Hz, 1H), 3.77 (s, 3H), 3.41–3.23 (m, 2H), 2.95 (t, *J* = 7.0 Hz, 2H), 1.59 (d, *J* = 7.4 Hz, 3H), 1.41 (s, 9H). **¹³C NMR** (125 MHz, CDCl₃): δ = 158.0 (C_q), 155.8 (C_q), 140.6 (C_q), 138.0 (C_q), 136.8 (C_q), 134.9 (C_q), 128.5 (CH), 128.2 (C_q), 128.0 (CH), 127.0 (CH), 125.8 (CH), 121.4 (CH), 119.3 (CH), 118.5 (CH), 113.8 (CH), 109.6 (CH), 109.3 (C_q), 78.9 (C_q), 55.2 (CH₃), 47.2 (CH₂), 41.3 (CH₂), 34.1 (CH), 28.4 (CH₃), 25.3 (CH₂), 19.6 (CH₃). **IR** (ATR): 2927, 1698, 1509, 1466, 1245, 1172, 734 cm⁻¹. **MS (EI)** *m/z* (relative intensity): 354 (100) [M]⁺, 248 (19), 91 (89). **HR-MS** (EI) *m/z* calcd for C₃₁H₃₆N₂O₃ [M]⁺ 484.2726, found 484.2730. **[α]_D²³**: –53.5 (*c* = 0.23, CHCl₃). **HPLC separation** (Chiralpak[®] IB-3, *n*-hexane/*i*PrOH 80:20, 1.0 mL/min, detection at 273 nm): *t_r* (minor) = 6.2 min, *t_r* (major) = 6.7 min, 12:88 e.r.

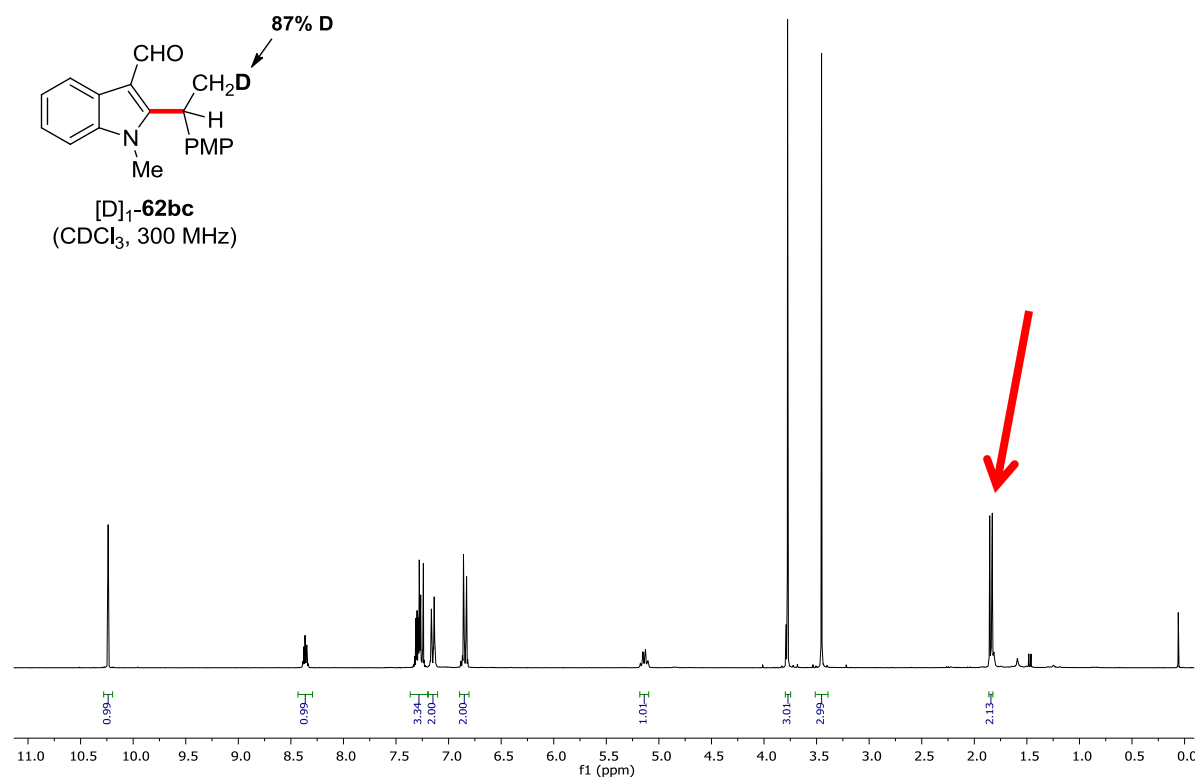
5.5.3. Mechanistic Studies

Deuterium-Labeling Experiments

With 4-methoxystyrene (**60c**):

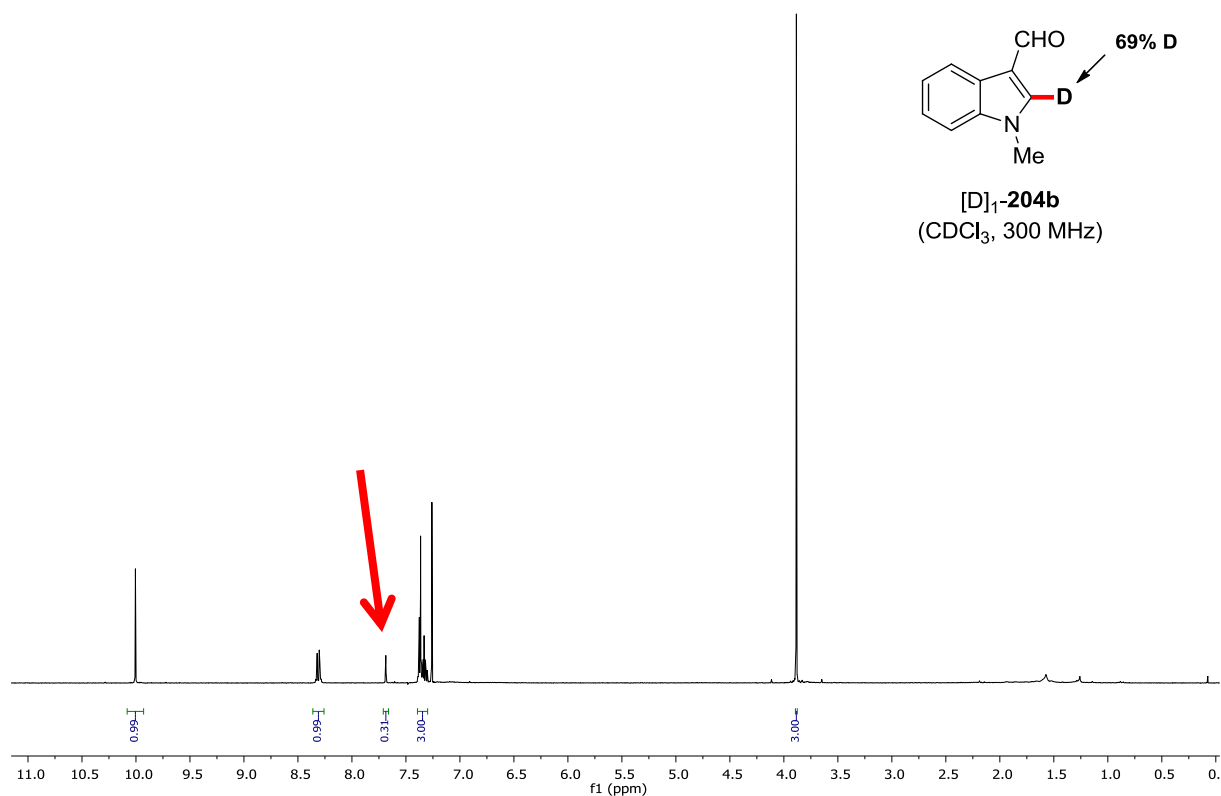
In an oven-dried 25 mL Schlenk tube were placed the indole substrate $[D]_1$ -**59b** (66 mg, 0.25 mmol, 1.0 equiv), $[Fe(acac)_3]$ (8.8 mg, 0.025 mmol, 10 mol %) and **180** (38 mg, 0.050 mmol, 20 mol %). The Schlenk tube was closed with a rubber septum, then evacuated and backfilled with N_2 3 times. THF (0.50 mL), TMEDA (58 mg, 0.50 mmol, 2.0 equiv) and 4-methoxystyrene (**60c**) (50 mg, 0.38 mmol, 1.5 equiv) were added *via* syringe. $CyMgCl$ (0.22 mL, 0.275 mmol, 1.1 equiv, 1.23 M in THF) was then added dropwise at ambient temperature. The resulting mixture was stirred at 45 °C for 16 h. The reaction mixture was allowed to cool to ambient temperature and diluted with THF (1.5 mL). HCl (3.0 M, 2.0 mL) was added in a single portion, and the resulting mixture was stirred at ambient temperature for 2 h. The mixture was poured into sat. aqueous NH_4Cl (10 mL) and extracted with $EtOAc$ (3×10 mL). The combined organic layers were washed with brine (10 mL), dried over Na_2SO_4 , and concentrated under reduced pressure. The yields of recovered starting materials and hydroarylation product were determined by 1H NMR analysis of the crude mixture using 1,1,2,2-tetrachloroethane as an internal standard. The crude mixture was purified by silica gel chromatography (*n*-hexane/ $EtOAc$ 10/1→2/1) to afford the product and hydrolyzed starting material. Deuterium contents were determined by 1H NMR spectroscopic analysis.



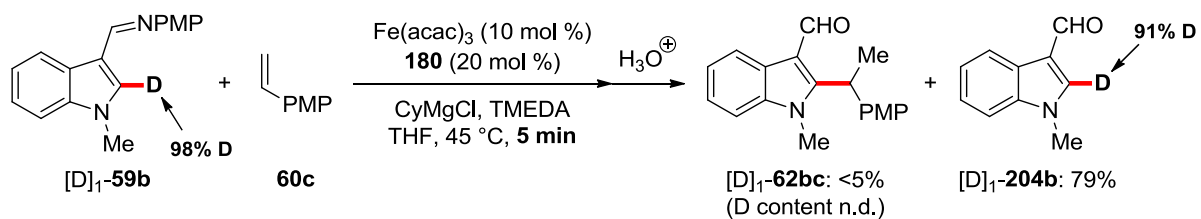


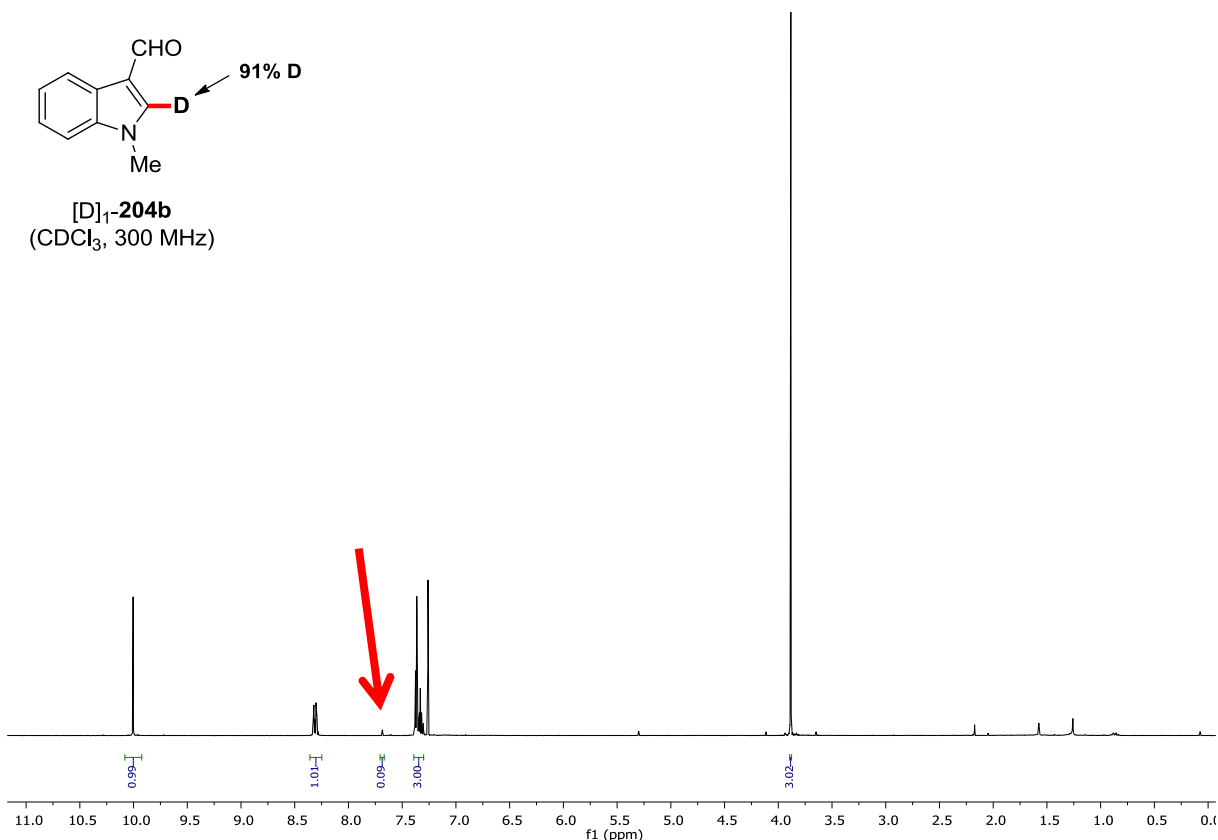
In contrast to the work of Yoshikai,^[148] no deuterium incorporation was observed at the methine position.

5. Experimental Part



The same procedure as described above was followed, conducting the reaction for 5.0 min.



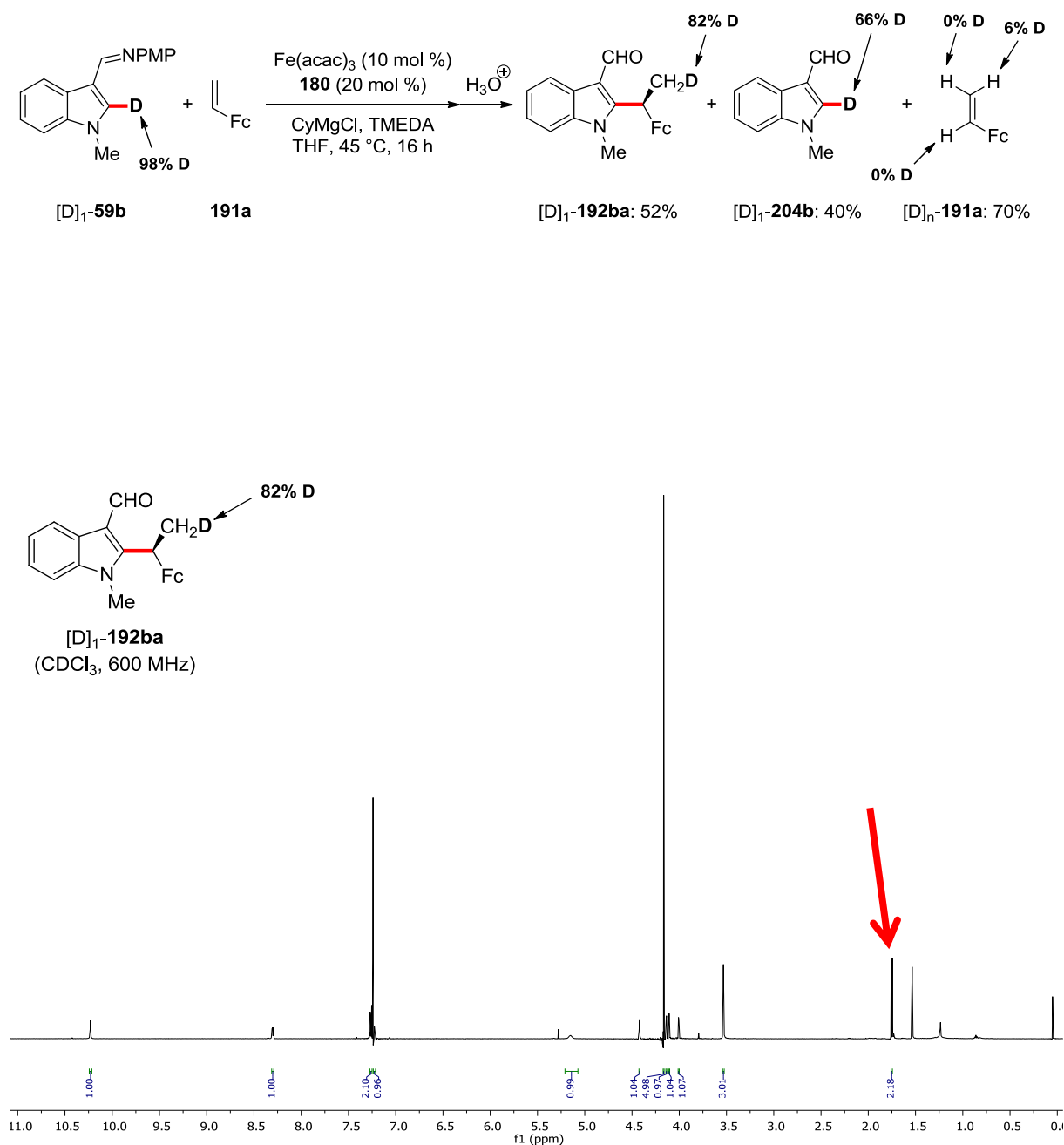


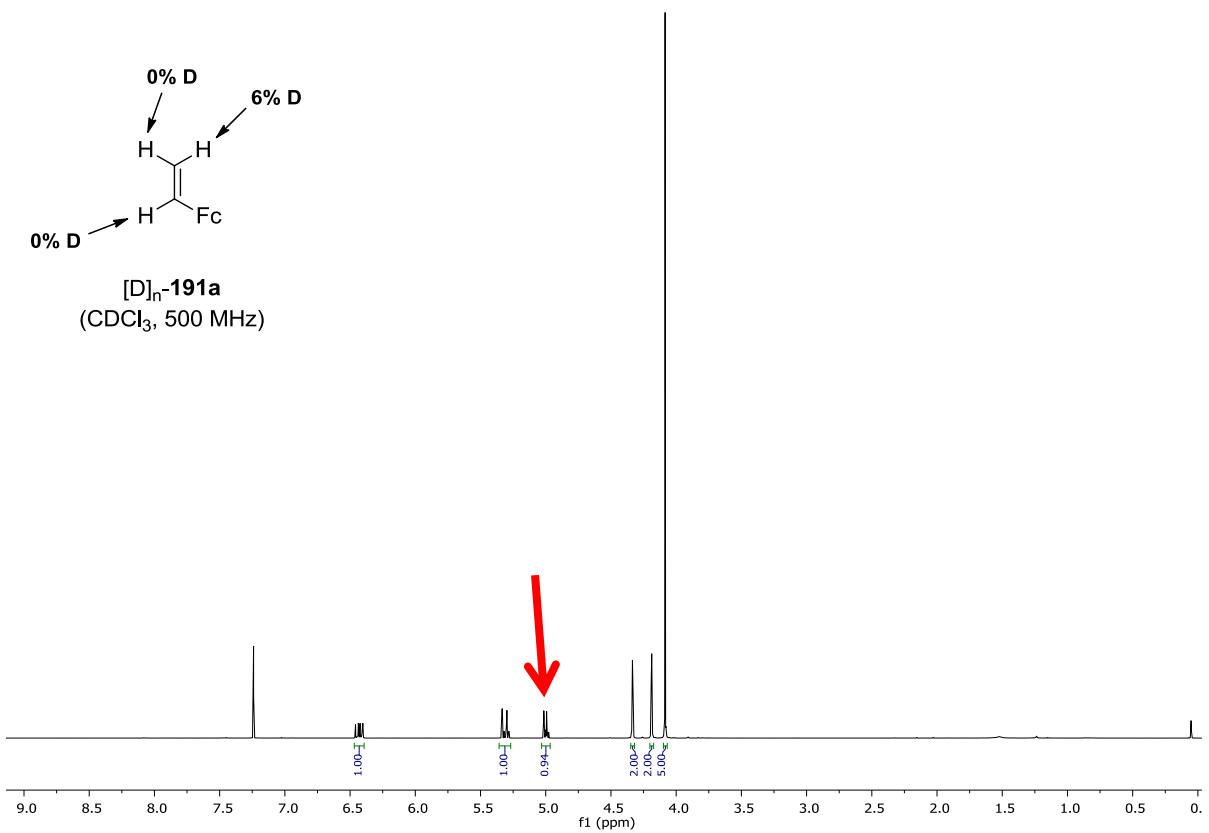
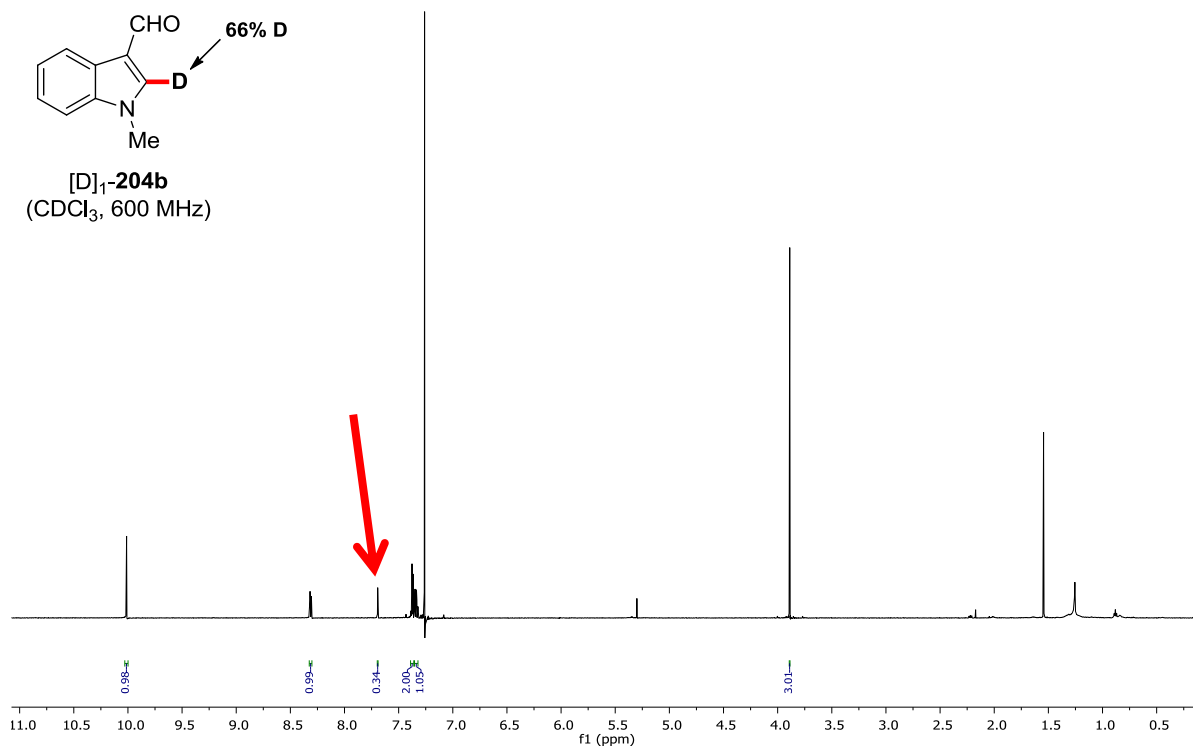
With Vinylferrocene (**191a**):

In an oven-dried 25 mL Schlenk tube were placed the indole substrate **[D]₁-59b** (66 mg, 0.25 mmol, 1.0 equiv), $[\text{Fe}(\text{acac})_3]$ (8.8 mg, 0.025 mmol, 10 mol %), **180** (38 mg, 0.050 mmol, 20 mol %) and vinylferrocene (**191a**) (80 mg, 0.38 mmol, 1.5 equiv). The Schlenk tube was closed with a rubber septum, then evacuated and backfilled with N_2 3 times. THF (0.50 mL) and TMEDA (58 mg, 0.50 mmol, 2.0 equiv) were added *via* syringe. CyMgCl (0.28 mL, 0.275 mmol, 1.1 equiv, 1.0 M in THF) was then added dropwise at ambient temperature. The resulting mixture was stirred at 45 °C for 16 h. The reaction mixture was allowed to cool to ambient temperature and diluted with THF (1.5 mL). HCl (3.0 M, 2.0 mL) was added in a single portion, and the resulting mixture was stirred at ambient temperature for 2 h. The mixture was poured into sat. aqueous NH_4Cl (10 mL) and extracted with EtOAc (3 × 10 mL). The combined organic layers were washed with brine (10 mL), dried over Na_2SO_4 , and concentrated under reduced pressure. The yields of recovered starting materials

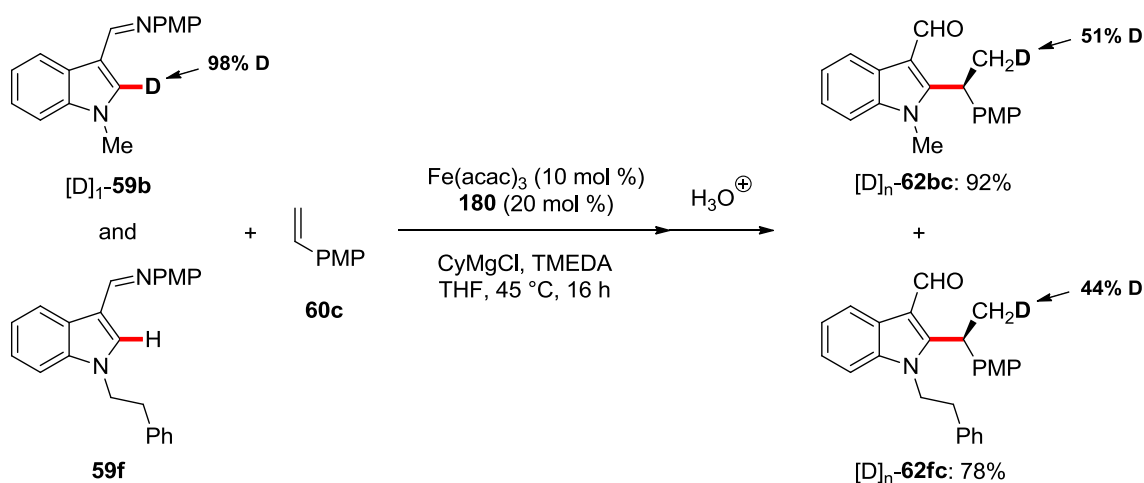
5. Experimental Part

and hydroarylation product were determined by ^1H NMR analysis of the crude mixture using 1,1,2,2-tetrachloroethane as an internal standard. The crude mixture was purified by silica gel chromatography (*n*-hexane/EtOAc 25/1 \rightarrow 2/1) to afford the product and hydrolyzed starting material. Deuterium contents were determined by ^1H NMR spectroscopic analysis.

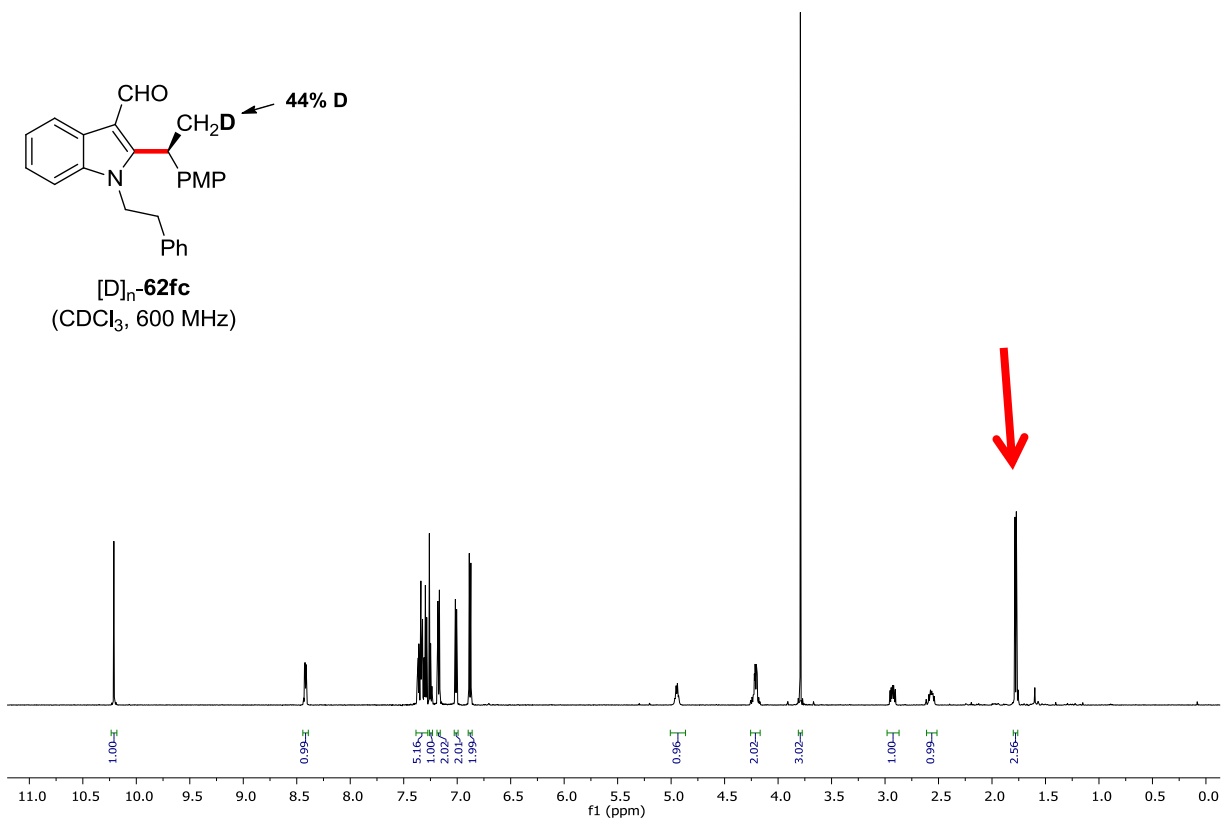
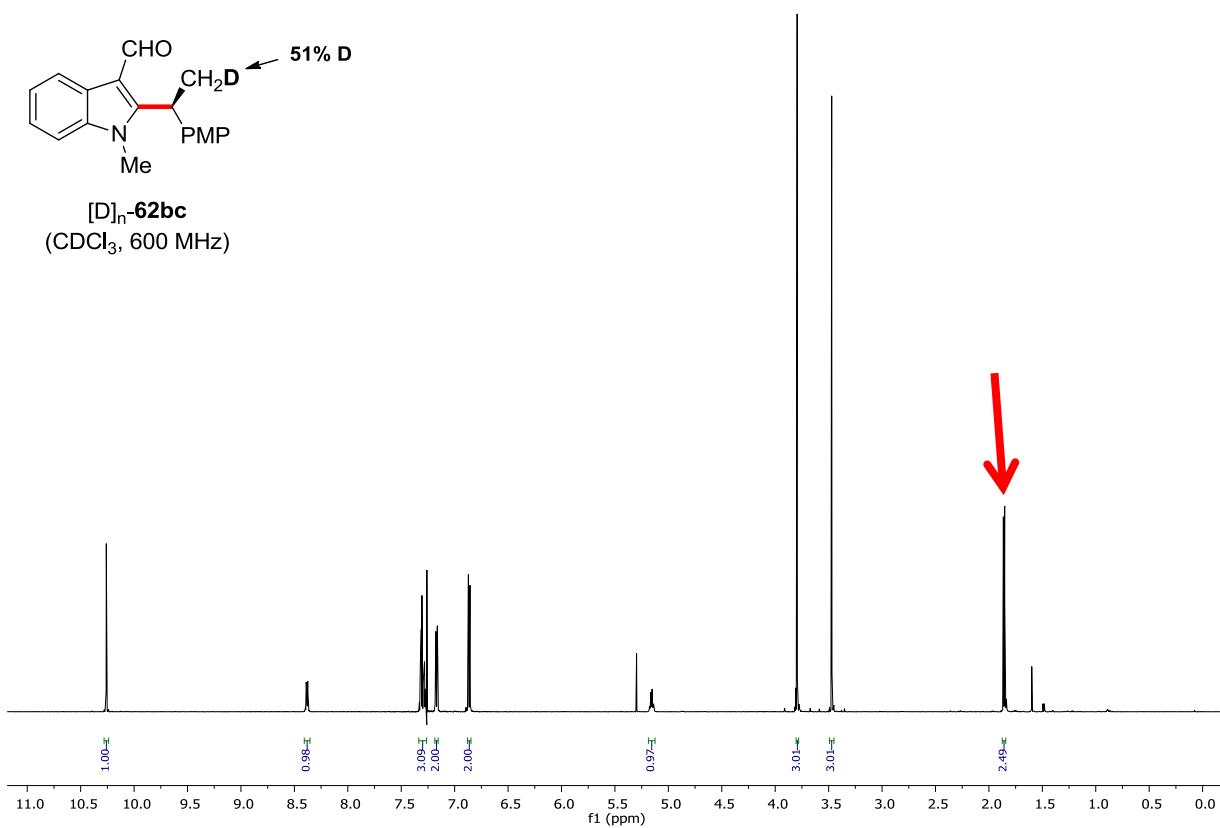




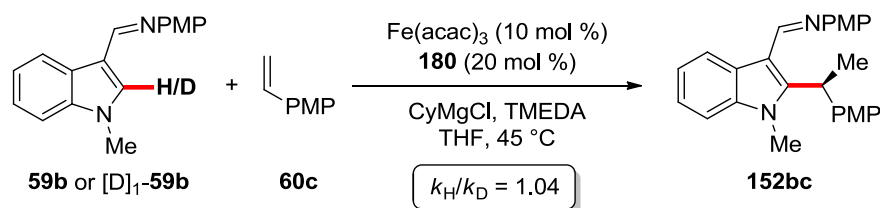
Crossover Experiment



In an oven-dried 25 mL Schlenk tube were placed indole substrates $[D]_1\text{-59b}$ (66 mg, 0.25 mmol, 0.50 equiv) and $\mathbf{59f}$ (89 mg, 0.25 mmol, 0.50 equiv), $\text{Fe}(\text{acac})_3$ (17.6 mg, 0.050 mmol, 10 mol %) and $\mathbf{180}$ (76 mg, 0.10 mmol, 20 mol %). The Schlenk tube was closed with a rubber septum, then evacuated and backfilled with nitrogen 3 times. THF (1.0 mL), TMEDA (116 mg, 1.0 mmol, 2.0 equiv) and styrene $\mathbf{60c}$ (100 mg, 0.75 mmol, 1.5 equiv) were added *via* syringe. CyMgCl (0.59 mL, 0.55 mmol, 1.1 equiv, 0.93 M in THF) was then added dropwise at ambient temperature. The resulting mixture was stirred at 45 °C for 16 h. The reaction mixture was allowed to cool to ambient temperature and diluted with THF (3.0 mL). HCl (3.0 M, 4.0 mL) was added in a single portion, and the resulting mixture was stirred at ambient temperature for 2 h. The mixture was poured into sat. aqueous NH_4Cl (20 mL) and extracted with EtOAc (3 × 20 mL). The combined organic layers were washed with brine (20 mL), dried over Na_2SO_4 , and concentrated under reduced pressure. The residue was purified by silica gel chromatography (*n*-hexane/ EtOAc = 9/1 5/1) to afford $[D]_n\text{-62bc}$ (67.5 mg, 92%) and $[D]_n\text{-62fc}$ (75.2 mg, 78%). Deuterium contents were determined by ^1H NMR spectroscopic analysis.



KIE Studies



The kinetic isotope effect (KIE) was examined by applying the initial rate method. In an oven-dried 25 mL Schlenk tube were placed the indole substrates **59b** or **[D]₁-59b** (198 or 199 mg, 0.75 mmol, 1.0 equiv), $\text{Fe}(\text{acac})_3$ (26.4 mg, 0.075 mmol, 10 mol %) and **180** (114 mg, 0.15 mmol, 20 mol %). The Schlenk tubes were closed with a rubber septum, then evacuated and backfilled with nitrogen 3 times. THF (1.50 mL), TMEDA (174 mg, 1.50 mmol, 2.0 equiv) and 4-methoxystyrene **60c** (150 mg, 1.125 mmol, 1.5 equiv) were added *via* syringe. CyMgCl (0.67 mL, 0.825 mmol, 1.1 equiv, 1.23 M in THF) was then added dropwise at ambient temperature. The Schlenk tubes were placed in a pre-heated oil bath at 45 °C ($t = 0$ min). Aliquots (100 μL) were removed periodically every 5 min *via* syringe, diluted with EtOH (0.50 mL), then with CH_2Cl_2 (2.5 mL) and filtered through a short plug of silica gel. The plug was washed with EtOAc. The combined filtrates were concentrated *in vacuo*. Conversion was determined by ^1H NMR using 1,1,2,2-tetrachloroethane as an internal standard.

Table 5.2. Kinetic Isotope Effect.

| t/min | 152bc / % | [D]₁-152bc / % |
|----------------|------------------|----------------------------------|
| 5 | 4 | 6 |
| 10 | 7 | 8 |
| 15 | 9 | 8 |
| 20 | 12 | 10 |
| 25 | 15 | 15 |
| 30 | 17 | 19 |

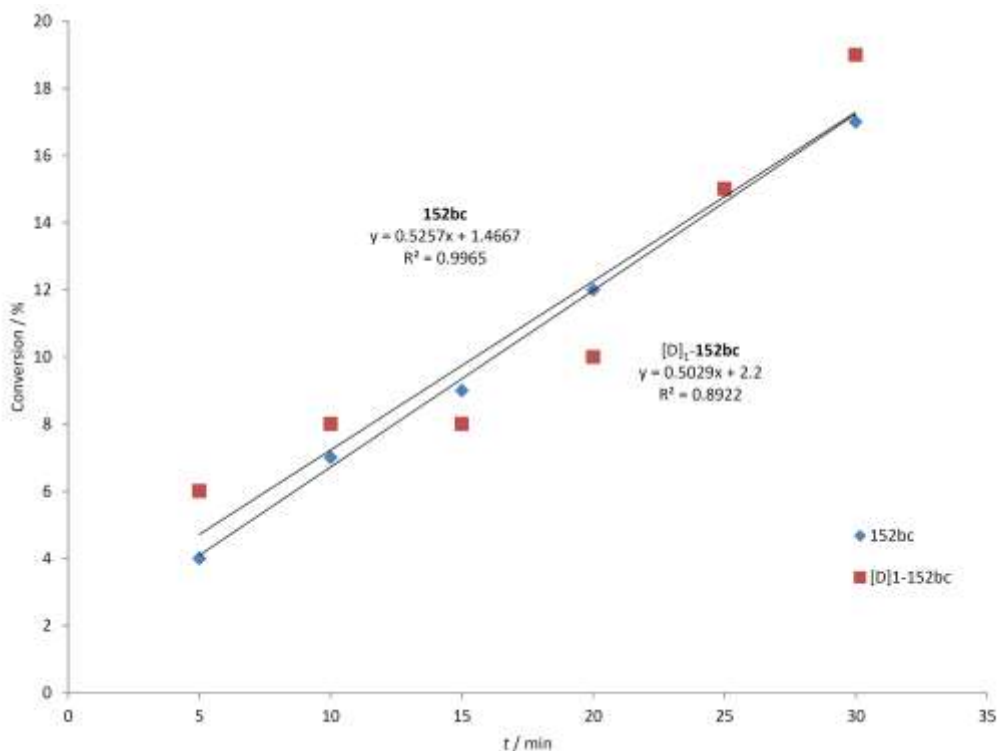


Figure 5.1. Kinetic Isotope Effect.

Additionally, KIE studies of the reaction with 4-fluorostyrene (**60g**) were conducted by *Dr. D. Zell*.^[151]

Mercury Drop Test

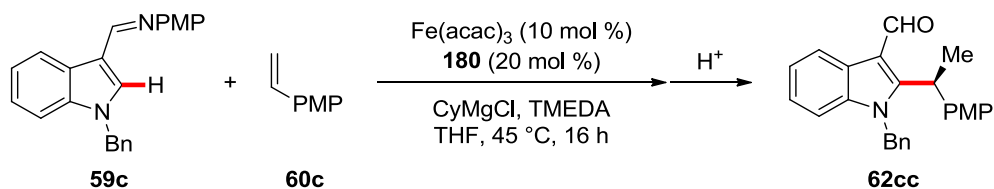
In an oven-dried 25 mL Schlenk tube were placed indole **59c** (85 mg, 0.25 mmol, 1.0 equiv), Fe(acac)₃ (8.8 mg, 0.025 mmol, 10 mol %) and **180** (38 mg, 0.050 mmol, 20 mol %). The Schlenk tube was closed with a rubber septum, then evacuated and backfilled with nitrogen 3 times. THF (0.50 mL), TMEDA (58 mg, 0.50 mmol, 2.0 equiv) and vinylarene **60c** (0.38 mmol, 1.5 equiv) were added *via* syringe. CyMgCl (0.27 mL, 0.28 mmol, 1.1 equiv, 1.03 M) was then added dropwise at ambient temperature. The resulting mixture was stirred at ambient temperature for 1.0 min. Hg (100 mg, 0.50 mmol, 2.0 equiv) was added *via* syringe. The reaction mixture was then stirred at 45 °C for 16 h. The reaction mixture was allowed to cool to ambient temperature and diluted with THF (1.5 mL). HCl (3.0 M, 2.0 mL) was

added in a single portion, and the resulting mixture was stirred at ambient temperature for 2 h. The mixture was poured into sat. aqueous NH_4Cl (10 mL) and extracted with EtOAc (3 \times 10 mL). The combined organic layers were washed with brine (10 mL), dried over Na_2SO_4 , and concentrated under reduced pressure. The residue was purified by silica gel chromatography (*n*-hexane/EtOAc = 8/1 \rightarrow 6/1) to afford **62cc** (85.7 mg, 93%, 93:7 e.r.).

Non-Linear Effect Studies

In an oven-dried 25 mL Schlenk tube were placed the indole substrate **59c** (0.25 mmol, 1.0 equiv), $\text{Fe}(\text{acac})_3$ (8.8 mg, 0.025 mmol, 10 mol %) and a mixture of **180** and *ent*-**180** (total amount: 38 mg, 0.050 mmol, 20 mol %). The Schlenk tube was closed with a rubber septum, then evacuated and backfilled with nitrogen 3 times. THF (0.50 mL), TMEDA (58 mg, 0.50 mmol, 2.0 equiv) and vinylarene **60c** (0.38 mmol, 1.5 equiv) were added *via* syringe. CyMgCl (0.28 mmol, 1.1 equiv, typically 1.0 M) was then added dropwise at ambient temperature. The resulting mixture was stirred at 45 °C for 16 h. The reaction mixture was allowed to cool to ambient temperature and diluted with THF (1.5 mL). HCl (3.0 M, 2.0 mL) was added in a single portion, and the resulting mixture was stirred at ambient temperature for 2 h. The mixture was poured into sat. aqueous NH_4Cl (10 mL) and extracted with EtOAc (3 \times 10 mL). The combined organic layers were washed with brine (10 mL), dried over Na_2SO_4 , and concentrated under reduced pressure. The conversion was determined by ^1H NMR using 1,1,2,2-tetrachloroethane as an internal standard. Enantiomeric excesses were measured by chiral HPLC analysis of the crude product (Chiralpak[®] IA-3, *n*-hexane/*i*PrOH 80:20, 1.0 mL/min).

Table 5.3. NLE studies.



| Entry | ee(180) | ee(62cc) ^[a] | Yield ^[b] |
|-------|---------|-------------------------|----------------------|
| 1 | 0% | 4.2% | 88% |
| 2 | 20% | 20.0% | 90% |
| 3 | 40% | 37.6% | 91% |
| 4 | 60% | 52.8% | 88% |
| 5 | 80% | 71.5% | 89% |
| 6 | 100% | 84.0% | 90% |

^[a] Determined by chiral HPLC analysis of the crude reaction mixture.

^[b] Determined by crude ¹H NMR using 1,1,2,2-tetrachloroethane as internal standard.

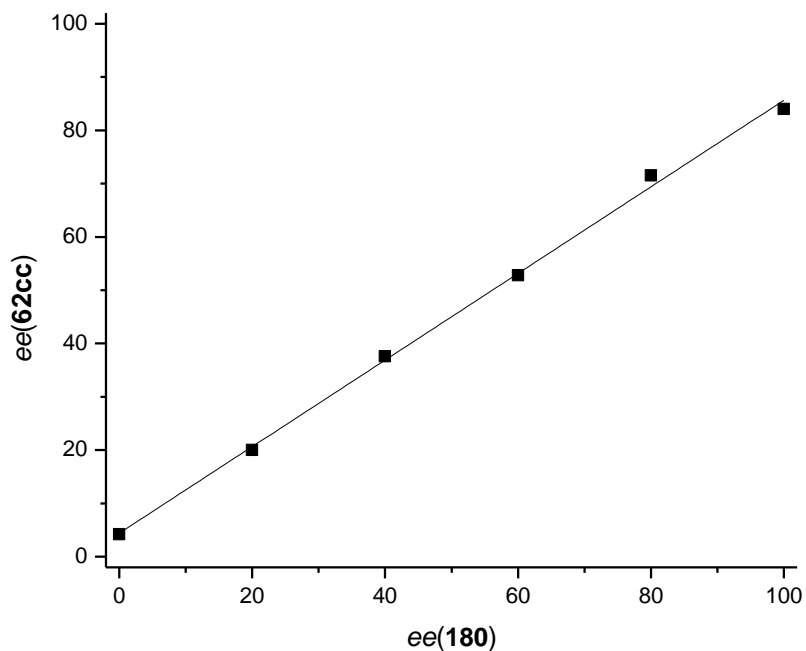


Figure 5.2. Absence of a non-linear effect.

Mössbauer Spectroscopy

Mössbauer sample solutions were prepared by the addition of the Grignard reagent (8.0 equiv) to solutions of $^{57}\text{FeCl}_2$ (5.0 mM, 1.0 equiv) and TMEDA (4.0 equiv) in THF in a N_2 -filled glovebox (unless specified otherwise: at $-20\text{ }^\circ\text{C}$ for CyMgCl , and at $23\text{ }^\circ\text{C}$ for PhMgCl) and directly transferred into the *Mössbauer* sample cell before immediately freezing in liquid nitrogen (outside of the glovebox). **180** and **59b** were added before the Grignard reagent.

After preparation, the spectra were recorded and interpreted by *Dr. S. Demeshko* (*Meyer* research group). All *Mössbauer* parameters are summarized in Tables 5.4–5.5.

Table 5.4. Mössbauer parameters of reactions with CyMgCl.

| Reaction | Figure | δ [mm s ⁻¹] | ΔE_Q [mm s ⁻¹] | Rel. int. [%] | Color | Assignment |
|---|------------|--------------------------------|------------------------------------|---------------|---------|--|
| ⁵⁷ FeCl ₂ (5.0 mM) + TMEDA (4.0 equiv) + CyMgCl (8.0 equiv) | Fig. 3.2a | 0.48 | 0.89 | 84 | blue | Cy ₄ Fe(III) ⁻ |
| | | 0.21 | 1.56 | 16 | red | Cy ₃ Fe(II) ⁻ |
| ⁵⁷ FeCl ₂ (5.0 mM) + TMEDA (4.0 equiv) + CyMgCl (8.0 equiv) ^[a] | Fig. 3.2b | 0.48 | 0.88 | 85 | blue | Cy ₄ Fe(III) ⁻ |
| | | 0.24 | 1.59 | 15 | red | Cy ₃ Fe(II) ⁻ |
| ⁵⁷ FeCl ₂ (5.0 mM) + TMEDA (4.0 equiv) + CyMgCl (8.0 equiv) ^[b] | Fig. 3.3 | 0.19 | 0.86 | 68 | gray | --- |
| | | 0.48 | 0.91 | 28 | blue | Cy ₄ Fe(III) ⁻ |
| | | -0.10 | 1.10 | 3 | yellow | --- |
| ⁵⁷ FeCl ₂ (5.0 mM) + TMEDA (4.0 equiv) + 180 (1.0 equiv) + CyMgCl (8.0 equiv) | Fig. 3.7a | 0.18 | 1.59 | 36 | red | Cy ₃ Fe(II) ⁻ |
| | | 0.39 | 3.19 | 27 | green | Cy ₂ Fe(II)(NHC) |
| | | 0.46 | 0.98 | 19 | blue | Cy ₄ Fe(III) ⁻ |
| | | 0.54 | 2.04 | 11 | magenta | Cy ₃ Fe(II)(NHC) ⁻ |
| | | 0.24 | 0.40 | 7 | cyan | --- |
| ⁵⁷ FeCl ₂ (5.0 mM) + TMEDA (4.0 equiv) + 180 (1.0 equiv) + CyMgCl (8.0 equiv) ^[b] | Fig. 3.7b | 0.22 | 1.57 | 47 | red | Cy ₃ Fe(II) ⁻ |
| | | 0.22 | 0.57 | 34 | cyan | --- |
| | | 0.75 | 1.57 | 10 | purple | --- |
| | | 0.37 | 3.20 | 9 | green | Cy ₂ Fe(II)(NHC) |
| ⁵⁷ FeCl ₂ (5.0 mM) + TMEDA (4.0 equiv) + 180 (1.0 equiv) + 59b (1.0 equiv) + CyMgCl (8.0 equiv) | Fig. 3.10a | 0.20 | 1.71 | 53 | red | Cy ₃ Fe(II) ⁻ |
| | | 0.43 | 3.13 | 21 | green | Cy ₂ Fe(II)(NHC) |
| | | 0.58 | 2.04 | 18 | magenta | Cy ₃ Fe(II)(NHC) ⁻ |
| | | 0.47 | 0.84 | 8 | blue | Cy ₄ Fe(III) ⁻ |

^[a] Recorded at 7 K. ^[b] Prepared at 23 °C. NHC = C₄₉H₅₄N₂.

Table 5.5. Mössbauer parameters of reactions with PhMgCl.

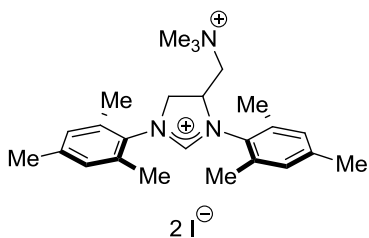
| Reaction | Figure | δ [mm s ⁻¹] | ΔE_Q [mm s ⁻¹] | Rel. int. [%] | Color | Assignment |
|---|------------|--------------------------------|------------------------------------|---------------|-------------|--------------------------------------|
| ⁵⁷ FeCl ₂ (5.0 mM) + TMEDA (4.0 equiv) + PhMgCl (8.0 equiv) | Fig. 3.4 | 0.54 | 1.12 | 78 | blue | Ph ₄ Fe(III) ⁻ |
| | | 0.20 | 1.44 | 13 | red | Ph ₃ Fe(II) ⁻ |
| | | 0.46 | 2.61 | 9 | dark yellow | --- |
| ⁵⁷ FeCl ₂ (5.0 mM) + TMEDA (4.0 equiv) + 180 (1.0 equiv) + PhMgCl (8.0 equiv) | Fig. 3.8 | 0.51 | 1.09 | 40 | blue | Ph ₄ Fe(III) ⁻ |
| | | 0.22 | 4.25 | 39 | green | Ph ₂ Fe(II)(NHC) |
| | | 0.56 | 2.62 | 14 | light green | --- |
| | | 0.32 | 1.70 | 4 | orange | --- |
| | | 1.10 | 4.30 | 3 | wine | --- |
| ⁵⁷ FeCl ₂ (5.0 mM) + TMEDA (4.0 equiv) + 180 (1.0 equiv) + 59b (1.0 equiv) + PhMgCl (8.0 equiv) | Fig. 3.10b | 0.51 | 1.09 | 52 | blue | Ph ₄ Fe(III) ⁻ |
| | | 0.22 | 4.21 | 36 | green | Ph ₂ Fe(II)(NHC) |
| | | 0.57 | 2.64 | 7 | light green | --- |
| | | 0.32 | 1.70 | 4 | orange | --- |
| | | 1.10 | 4.30 | 2 | wine | --- |

ESI-MS

Standard sample solutions were prepared by the addition of the Grignard reagent (8.0 equiv) to a solution of Fe(acac)₃ (1.0 equiv), TMEDA (4.0 equiv) in THF at -78 °C, and dilution to 10 mM. **180** and **59b** were added before the Grignard reagent.

Samples were prepared and analyzed by *Dr. T. Parchomyk* and *S. Lülfi* (Koszinowski research group).

1,3-Dimesityl-4-[(trimethylammonio)methyl]-4,5-dihydro-1H-imidazol-3-ium Iodide (207)



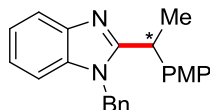
The amino-tagged NHC precursor **206**^[278] (3.0 g, 6.65 mmol, 1.0 equiv) was dissolved in acetone (25 mL) and NaI (6.0 g, 40 mmol, 6.0 equiv) was added. The reaction mixture was stirred at 23 °C for 14 h and then evaporated under reduced pressure. The residue was suspended in CH₂Cl₂, filtered through a short plug of Celite[®] and concentrated to yield the crude imidazolium iodide quantitatively.

The imidazolium iodide (400 mg, 0.81 mmol, 1.0 equiv) was suspended in MeI (5.1 mL, 81 mmol, 100 equiv) and stirred at 23 °C for 14 h. Et₂O (5.0 mL) was added to the reaction mixture. The precipitate was collected by filtration, washed with Et₂O (10 mL) and dried *in vacuo* to provide **207** (452 mg, 88%) as a colorless solid. **M. p.** = 308 °C (decomposition). **¹H NMR** (300 MHz, DMSO-d₆): δ = 9.13 (s, 1H), 7.20–7.13 (m, 2H), 7.12 (app s, 2H), 5.60 (q, *J* = 10.5 Hz, 1H), 4.92 (t, *J* = 11.7 Hz, 1H), 4.56 (t, *J* = 11.1 Hz, 1H), 4.41 (dd, *J* = 13.1, 10.1 Hz, 1H), 3.39 (d, *J* = 13.1 Hz, 1H), 3.11 (s, 9H), 2.40 (app s, 9H), 2.35–2.24 (m, 9H). **¹³C NMR** (125 MHz, DMSO-d₆): δ = 161.0 (CH), 140.2 (C_q), 140.2 (C_q), 136.6 (C_q), 135.8 (C_q), 135.7 (C_q), 135.0 (C_q), 130.3 (CH), 130.2 (C_q), 130.1 (CH), 129.6 (CH), 129.5 (CH), 127.9 (C_q), 63.7 (CH₂), 57.8 (CH), 56.7 (CH₂), 52.8 (CH₃), 20.7 (CH₃), 20.6 (CH₃), 18.3 (CH₃), 18.0 (CH₃), 17.5 (CH₃), 17.4 (CH₃). **IR** (ATR): 2995, 1628, 1482, 1461, 1262, 1021, 871, 815 cm⁻¹. **MS (ESI)** *m/z* (relative intensity): 190 (100) [2M-2I]²⁺. **HR-MS** (ESI) *m/z* calcd for C₂₅H₃₇N₃ [2M-2I]²⁺ 189.6488, found 189.6491.

5.6. Asymmetric Nickel-Catalyzed Hydroarylations by C–H Activation

5.6.1. Experimental Procedures and Analytical Data for the Intermolecular Nickel-Catalyzed Hydroarylation of Alkenes

1-Benzyl-2-[1-(4-methoxyphenyl)ethyl]-1*H*-benzo[*d*]imidazole (106bc)

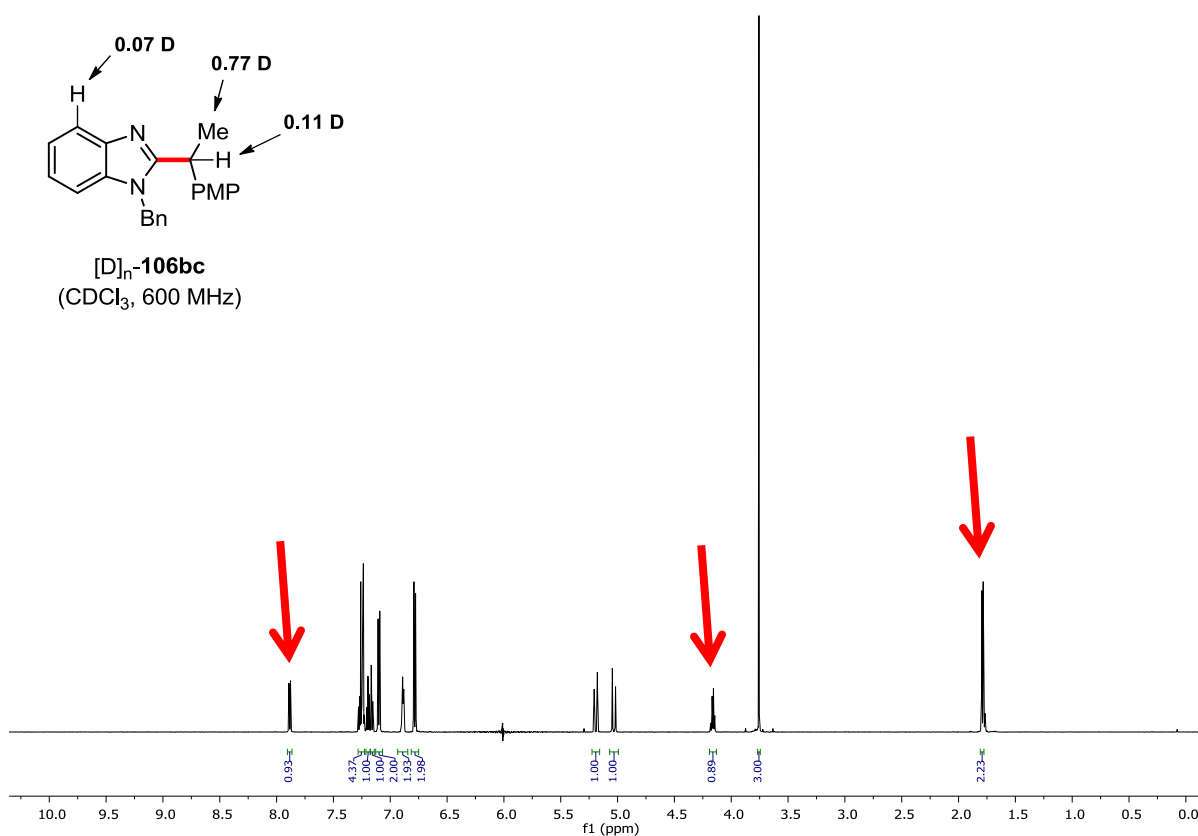


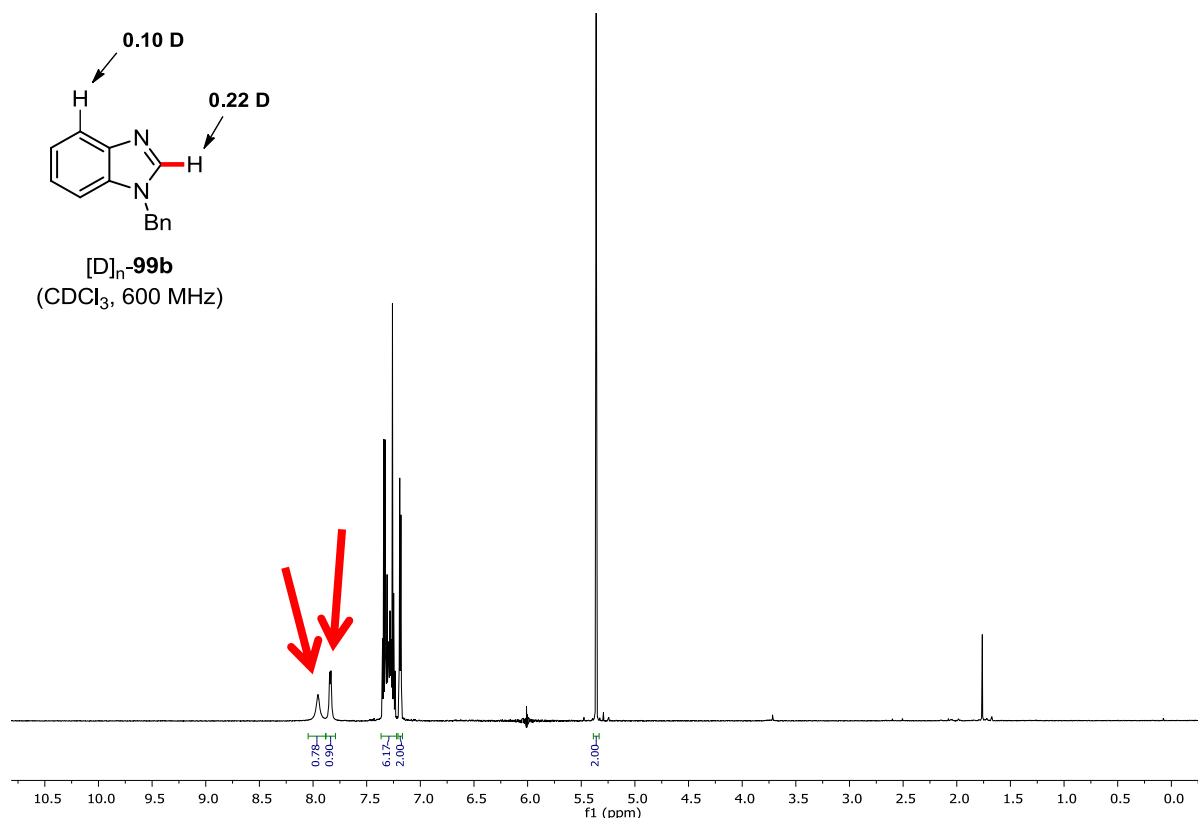
The general procedure **GP9** was followed using **180** (38 mg, 50 μmol , 10 mol %). Purification by column chromatography on silica gel (*n*-hexane/EtOAc = 4.5/1 \rightarrow 3/1) yielded **106bc** (91.5 mg, 53%) as a thick colorless oil. **$^1\text{H NMR}$** (400 MHz, CDCl_3): δ = 7.89 (dt, J = 8.1, 0.9 Hz, 1H), 7.29–7.22 (m, 4H), 7.20 (td, J = 8.0, 1.2 Hz, 1H), 7.17–7.14 (m, 1H), 7.10 (d, J = 8.7 Hz, 2H), 6.93–6.85 (m, 2H), 6.78 (d, J = 8.7 Hz, 2H), 5.19 (d, J = 16.8 Hz, 1H), 5.03 (d, J = 16.9 Hz, 1H), 4.16 (q, J = 7.0 Hz, 1H), 3.76 (s, 3H), 1.79 (d, J = 7.1 Hz, 3H). **$^{13}\text{C NMR}$** (125 MHz, CDCl_3): δ = 158.5 (C_q), 157.2 (C_q), 142.6 (C_q), 136.1 (C_q), 135.9 (C_q), 135.1 (C_q), 128.9 (CH), 128.4 (CH), 127.7 (CH), 126.2 (CH), 122.6 (CH), 122.0 (CH), 119.8 (CH), 114.4 (CH), 109.6 (CH), 55.4 (CH_3), 46.9 (CH_2), 38.3 (CH), 22.3 (CH_3). **IR** (ATR): 2929, 1509, 1453, 1241, 1176, 1030, 831, 727 cm^{-1} . **MS (ESI)** m/z (relative intensity): 365 (33) $[\text{M}+\text{Na}]^+$, 343 (100) $[\text{M}+\text{H}]^+$. **HR-MS** (ESI) m/z calcd for $\text{C}_{23}\text{H}_{23}\text{N}_2\text{O}$ $[\text{M}+\text{H}]^+$ 343.1805, found 343.1798. **$[\alpha]_D^{20}$** : -60.9 (c = 1.0, CHCl_3). **HPLC separation** (Chiralpak[®] IB-3, *n*-hexane/*i*PrOH 80:20, 1.0 mL/min, detection at 250 nm): t_r (major) = 6.6 min, t_r (minor) = 9.2 min, 20:80 e.r.

5.6.2. Mechanistic Studies for the Intermolecular Nickel-Catalyzed Hydroarylation of Alkenes

$[\text{D}]_1$ -**99b** was prepared by treating **99b** with oxalyl chloride/ D_2O , following a procedure previously reported in the literature.^[339]

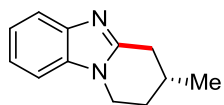
The general procedure **GP9** was followed using [D]₁-**99b** (105 mg, 0.50 mmol, 1.0 equiv) and **180** (38 mg, 50 μmol, 10 mol %). Purification by column chromatography on silica gel (*n*-hexane/EtOAc = 4.5/1→0/1) yielded [D]_n-**106bc** (74.8 mg, 44%) as a thick colorless oil and re-isolated [D]_n-**99b** (55.7 mg, 53%) as a colorless solid. Deuterium contents were determined by ¹H NMR spectroscopic analysis.





5.6.3 Experimental Procedures and Analytical Data for the Asymmetric Intramolecular Nickel-Catalyzed Hydroarylation of Alkenes

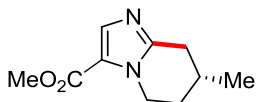
(*R*)-3-Methyl-1,2,3,4-tetrahydrobenzo[4,5]imidazo[1,2-*a*]pyridine (145a)



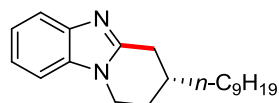
The general procedure **GP11** was followed using **144a** (93 mg, 0.50 mmol, 1.0 equiv). Purification by column chromatography on silica gel (*n*-hexane/EtOAc = 1/2→0/1) yielded **145a** (89.5 mg, 96%) as a white solid. **M. p.** = 135–136 °C. **¹H NMR** (300 MHz, CDCl₃): δ = 7.80–7.70 (m, 1H), 7.38–7.21 (m, 3H), 4.24 (ddd, *J* = 12.1, 5.9, 3.0 Hz, 1H), 3.98 (td, *J* = 11.7, 11.3, 4.9 Hz, 1H), 3.25 (ddd, *J* = 17.1, 4.8, 1.9 Hz, 1H), 2.67 (dd, *J* = 17.1, 10.7 Hz, 1H), 2.29–2.07 (m, 2H), 1.82 (dtd, *J* = 14.0, 10.7, 5.7 Hz, 1H), 1.24 (d, *J* = 6.5 Hz, 3H). **¹³C NMR** (75 MHz, CDCl₃):

δ = 151.8 (C_q), 143.1 (C_q), 134.6 (C_q), 122.0 (CH), 121.7 (CH), 118.9 (CH), 108.8 (CH), 41.6 (CH₂), 33.5 (CH₂), 30.5 (CH₂), 27.7 (CH), 21.1 (CH₃). **IR** (ATR): 3050, 2948, 2921, 2864, 1458, 1417, 1285, 739, 437 cm⁻¹. **MS (ESI)** *m/z* (relative intensity): 187 (100) [M+H]⁺. **HR-MS** (ESI) *m/z* calcd for C₁₂H₁₅N₂ [M+H]⁺ 187.1230, found 187.1230. **[α]_D²⁰**: +63.6 (*c* = 1.00, CHCl₃). **HPLC separation** (Chiralpak[®] IC-3, *n*-hexane/*i*PrOH 80:20, 1.0 mL/min, detection at 273 nm): *t_r* (major) = 16.8 min, *t_r* (minor) = 18.6 min, 96:4 e.r.

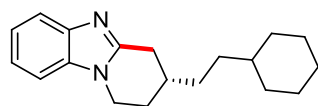
(*R*)-Methyl 7-Methyl-5,6,7,8-tetrahydroimidazo[1,2-*a*]pyridine-2-carboxylate (145b)



The general procedure **GP11** was followed using **144b** (97 mg, 0.50 mmol, 1.0 equiv), Ni(cod)₂ (13.8 mg, 50.0 μmol, 10.0 mol %) and **220** (12.6 mg, 25.0 μmol, 5.00 mol %) in PhMe (1.0 mL). Purification by column chromatography on silica gel (*n*-hexane/EtOAc = 1.5/1→1/2) yielded **145b** (64.1 mg, 66%) as a white solid. **M. p.** = 74–76 °C. **¹H NMR** (300 MHz, CDCl₃): δ = 7.66 (s, 1H), 4.54 (ddd, *J* = 13.9, 5.8, 3.0 Hz, 1H), 4.01 (ddd, *J* = 14.4, 11.0, 4.9 Hz, 1H), 3.81 (s, 3H), 3.04 (ddd, *J* = 17.2, 4.9, 1.8 Hz, 1H), 2.44 (dd, *J* = 17.2, 10.3 Hz, 1H), 2.13–1.91 (m, 2H), 1.63 (dtd, *J* = 14.1, 11.2, 5.6 Hz, 1H), 1.12 (d, *J* = 6.5 Hz, 3H). **¹³C NMR** (75 MHz, CDCl₃): δ = 161.1 (C_q), 150.3 (C_q), 137.0 (CH), 121.9 (C_q), 51.3 (CH₃), 44.6 (CH₂), 33.3 (CH₂), 30.7 (CH₂), 26.8 (CH), 21.1 (CH₃). **IR** (ATR): 2957, 1704, 1443, 1224, 1176, 1141, 1072, 766 cm⁻¹. **MS (ESI)** *m/z* (relative intensity): 209 (21), 195 (100) [M+H]⁺, 127 (25). **HR-MS** (ESI) *m/z* calcd for C₁₀H₁₅N₂O₂ [M+H]⁺ 195.1128, found 195.1123. **[α]_D²⁰**: +72.8 (*c* = 0.29, CHCl₃). **HPLC separation** (Chiralpak[®] ID-3, *n*-hexane/*i*PrOH 60:40, 1.0 mL/min, detection at 250 nm): *t_r* (major) = 7.6 min, *t_r* (minor) = 8.2 min, 99:1 e.r.

(R)-3-Nonyl-1,2,3,4-tetrahydrobenzo[4,5]imidazo[1,2-a]pyridine (145c)

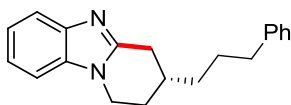
The general procedure **GP11** was followed using **144c** (149 mg, 0.50 mmol, 1.0 equiv). Purification by column chromatography on silica gel (*n*-hexane/EtOAc = 3/1→1.5/1) yielded **145c** (131.0 mg, 88%) as a white solid. **M. p.** = 85–86 °C. **¹H NMR** (300 MHz, CDCl₃): δ = 7.72–7.64 (m, 1H), 7.33–7.16 (m, 3H), 4.22 (ddd, *J* = 12.0, 5.7, 3.2 Hz, 1H), 3.95 (ddd, *J* = 12.0, 10.7, 5.0 Hz, 1H), 3.24 (ddd, *J* = 17.1, 4.8, 1.7 Hz, 1H), 2.64 (dd, *J* = 17.1, 10.4 Hz, 1H), 2.27–2.17 (m, 1H), 2.07–1.93 (m, 1H), 1.78 (dtd, *J* = 13.4, 10.8, 5.7 Hz, 1H), 1.57–1.15 (m, 16H), 0.89 (t, *J* = 6.8 Hz, 3H). **¹³C NMR** (125 MHz, CDCl₃): δ = 152.0 (C_q), 143.2 (C_q), 134.6 (C_q), 122.1 (CH), 121.7 (CH), 119.0 (CH), 108.8 (CH), 41.8 (CH₂), 35.7 (CH₂), 32.8 (CH), 32.1 (CH₂), 32.0 (CH₂), 29.9 (CH₂), 29.8 (CH₂), 29.8 (CH₂), 29.5 (CH₂), 29.0 (CH₂), 27.0 (CH₂), 22.9 (CH₂), 14.3 (CH₃). **IR** (ATR): 2920, 2851, 1513, 1459, 1421, 1287, 740 cm⁻¹. **MS (ESI)** *m/z* (relative intensity): 299 (100) [M+H]⁺. **HR-MS** (ESI) *m/z* calcd for C₂₀H₃₁N₂ [M+H]⁺ 299.2482, found 299.2480. **[α]_D²⁰**: +37.2 (*c* = 1.01, CHCl₃). **HPLC separation** (Chiralpak[®] IC-3, *n*-hexane/*i*PrOH 80:20, 1.0 mL/min, detection at 273 nm): *t_r* (major) = 11.3 min, *t_r* (minor) = 12.4 min, 96:4 e.r.

(R)-3-(2-Cyclohexylethyl)-1,2,3,4-tetrahydrobenzo[4,5]imidazo[1,2-a]pyridine (145d)

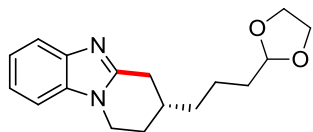
The general procedure **GP11** was followed using **144d** (141 mg, 0.50 mmol, 1.0 equiv). Purification by column chromatography on silica gel (*n*-hexane/EtOAc = 4/1→2/1) yielded **145d** (119.3 mg, 85%) as a white solid. **M. p.** = 134–135 °C. **¹H NMR** (300 MHz, CDCl₃): δ = 7.72–7.64 (m, 1H), 7.34–7.15 (m, 3H), 4.22 (ddd, *J* = 11.9, 5.7, 3.2 Hz, 1H), 3.94 (ddd, *J* = 11.9, 10.6, 5.0 Hz, 1H), 3.24 (ddd, *J* = 17.1,

4.8, 1.7 Hz, 1H), 2.64 (dd, $J = 17.1, 10.3$ Hz, 1H), 2.28–2.15 (m, 1H), 2.04–1.86 (m, 1H), 1.86–1.58 (m, 6H), 1.54–1.42 (m, 2H), 1.37–1.07 (m, 6H), 1.01–0.79 (m, 2H). $^{13}\text{C NMR}$ (125 MHz, CDCl_3): $\delta = 152.0$ (C_q), 143.2 (C_q), 134.6 (C_q), 122.1 (CH), 121.7 (CH), 119.0 (CH), 108.8 (CH), 41.8 (CH_2), 37.9 (CH), 34.7 (CH_2), 33.6 (CH_2), 33.6 (CH_2), 33.1 (CH), 32.9 (CH_2), 32.0 (CH_2), 28.9 (CH_2), 26.6 (CH_2). **IR** (ATR): 2916, 2847, 1514, 1455, 1417, 1284, 737 cm^{-1} . **MS (ESI)** m/z (relative intensity): 283 (100) $[\text{M}+\text{H}]^+$. **HR-MS** (ESI) m/z calcd for $\text{C}_{19}\text{H}_{27}\text{N}_2$ $[\text{M}+\text{H}]^+$ 283.2169, found 283.2161. $[\alpha]_{\text{D}}^{20}$: +45.0 ($c = 1.03$, CHCl_3). **HPLC separation** (Chiralpak[®] IC-3, *n*-hexane/*i*PrOH 80:20, 1.0 mL/min, detection at 250 nm): t_r (major) = 14.5 min, t_r (minor) = 16.3 min, 98:2 e.r.

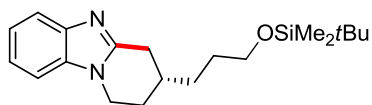
(*R*)-3-(3-Phenylpropyl)-1,2,3,4-tetrahydrobenzo[4,5]imidazo[1,2-*a*]pyridine (145e)



The general procedure **GP11** was followed using **144e** (145 mg, 0.50 mmol, 1.0 equiv). Purification by column chromatography on silica gel (*n*-hexane/EtOAc = 3/1→1/1) yielded **145e** (116.9 mg, 81%) as a white solid. **M. p.** = 80–83 °C. $^1\text{H NMR}$ (300 MHz, CDCl_3): $\delta = 7.77$ – 7.66 (m, 1H), 7.40–7.13 (m, 8H), 4.22 (ddd, $J = 12.1, 5.7, 3.2$ Hz, 1H), 3.93 (td, $J = 11.4, 5.0$ Hz, 1H), 3.27 (ddd, $J = 17.0, 4.8, 1.7$ Hz, 1H), 2.76–2.57 (m, 3H), 2.29–2.15 (m, 1H), 2.11–1.94 (m, 1H), 1.88–1.68 (m, 3H), 1.61–1.47 (m, 2H). $^{13}\text{C NMR}$ (125 MHz, CDCl_3): $\delta = 151.7$ (C_q), 143.1 (C_q), 142.1 (C_q), 134.5 (C_q), 128.4 (CH), 128.4 (CH), 125.9 (CH), 122.1 (CH), 121.7 (CH), 119.0 (CH), 108.8 (CH), 41.7 (CH_2), 36.0 (CH_2), 35.1 (CH_2), 32.7 (CH), 31.9 (CH_2), 28.8 (CH_2), 28.8 (CH_2). **IR** (ATR): 3026, 2919, 2856, 1510, 1483, 1455, 1284, 742, 691 cm^{-1} . **MS (ESI)** m/z (relative intensity): 291 (100) $[\text{M}+\text{H}]^+$. **HR-MS** (ESI) m/z calcd for $\text{C}_{20}\text{H}_{23}\text{N}_2$ $[\text{M}+\text{H}]^+$ 291.1856, found 291.1855. $[\alpha]_{\text{D}}^{20}$: +39.3 ($c = 1.01$, CHCl_3). **HPLC separation** (Chiralpak[®] IC-3, *n*-hexane/*i*PrOH 80:20, 1.0 mL/min, detection at 273 nm): t_r (major) = 20.6 min, t_r (minor) = 25.5 min, 97:3 e.r.

(R)-3-[3-(1,3-Dioxolan-2-yl)propyl]-1,2,3,4-tetrahydrobenzo[4,5]imidazo[1,2-a]pyridine (145f)

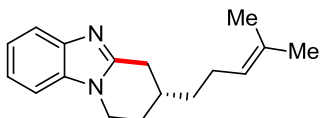
The general procedure **GP11** was followed using **144f** (143 mg, 0.50 mmol, 1.0 equiv). Purification by column chromatography on silica gel (*n*-hexane/EtOAc = 1/1→0/1) yielded **145f** (118.5 mg, 83%) as a white solid. **M. p.** = 99–100 °C. **¹H NMR** (300 MHz, CDCl₃): δ = 7.75–7.61 (m, 1H), 7.35–7.15 (m, 3H), 4.89 (t, *J* = 4.6 Hz, 1H), 4.23 (ddd, *J* = 12.0, 5.7, 3.2 Hz, 1H), 4.04–3.81 (m, 5H), 3.25 (ddd, *J* = 17.1, 4.8, 1.7 Hz, 1H), 2.66 (dd, *J* = 17.1, 10.4 Hz, 1H), 2.32–2.17 (m, 1H), 2.12–1.91 (m, 1H), 1.87–1.65 (m, 3H), 1.65–1.47 (m, 4H). **¹³C NMR** (125 MHz, CDCl₃): δ = 151.8 (C_q), 143.2 (C_q), 134.6 (C_q), 122.1 (CH), 121.7 (CH), 119.0 (CH), 108.8 (CH), 104.4 (CH), 65.1 (CH₂), 41.8 (CH₂), 35.5 (CH₂), 34.0 (CH₂), 32.9 (CH), 32.0 (CH₂), 28.8 (CH₂), 21.5 (CH₂). **IR** (ATR): 2922, 2893, 1457, 1415, 1106, 1053, 1021, 741 cm⁻¹. **MS (ESI)** *m/z* (relative intensity): 287 (100) [M+H]⁺. **HR-MS** (ESI) *m/z* calcd for C₁₇H₂₃N₂O₂ [M+H]⁺ 287.1754, found 287.1753. **[α]_D²⁰**: +39.1 (c = 0.42, CHCl₃). **HPLC separation** (Chiralpak[®] IC-3, *n*-hexane/*i*PrOH 30:70, 1.0 mL/min, detection at 273 nm): *t_r* (major) = 12.8 min, *t_r* (minor) = 15.6 min, 95:5 e.r.

(R)-3-[3-[(*tert*-Butyldimethylsilyl)oxy]propyl]-1,2,3,4-tetrahydrobenzo[4,5]imidazo[1,2-a]pyridine (145g)

The general procedure **GP11** was followed using **144g** (172 mg, 0.50 mmol, 1.0 equiv), Ni(cod)₂ (13.8 mg, 50.0 μmol, 10.0 mol %) and **220** (12.6 mg, 25.0 μmol, 5.00 mol %) in PhMe (1.0 mL). Purification by column chromatography on silica gel (*n*-hexane/EtOAc = 3/1→1/1.5) yielded **145g** (149.3 mg, 87%) as a white solid. **M. p.** = 134–135 °C. **¹H NMR** (500 MHz, CDCl₃): δ = 7.73–7.64 (m, 1H), 7.33–7.26

(m, 1H), 7.26–7.18 (m, 2H), 4.24 (ddd, $J = 12.0, 5.7, 3.1$ Hz, 1H), 3.95 (td, $J = 11.4, 5.0$ Hz, 1H), 3.66 (td, $J = 6.3, 2.3$ Hz, 2H), 3.25 (ddd, $J = 17.1, 4.8, 1.7$ Hz, 1H), 2.65 (dd, $J = 17.1, 10.6$ Hz, 1H), 2.23 (dtd, $J = 12.9, 4.9, 2.6$ Hz, 1H), 2.08–1.95 (m, 1H), 1.84–1.75 (m, 1H), 1.72–1.61 (m, 2H), 1.61–1.46 (m, 2H), 0.90 (s, 9H), 0.06 (s, 6H). $^{13}\text{C NMR}$ (125 MHz, CDCl_3): $\delta = 151.9$ (C_q), 143.2 (C_q), 134.6 (C_q), 122.2 (CH), 121.8 (CH), 119.1 (CH), 108.9 (CH), 63.1 (CH_2), 41.8 (CH_2), 32.6 (CH), 31.9 (CH_2), 31.9 (CH_2), 30.1 (CH_2), 28.9 (CH_2), 26.1 (CH_3), 18.5 (C_q), -5.1 (CH_3). **IR** (ATR): 2933, 2854, 1457, 1251, 1094, 832, 771, 739 cm^{-1} . **MS (ESI)** m/z (relative intensity): 345 (100) $[\text{M}+\text{H}]^+$. **HR-MS** (ESI) m/z calcd for $\text{C}_{20}\text{H}_{33}\text{N}_2\text{OSi}$ $[\text{M}+\text{H}]^+$ 345.2357, found 345.2358. $[\alpha]_D^{20}$: +37.6 ($c = 0.59, \text{CHCl}_3$). **HPLC separation** (Chiralpak[®] IB-3, *n*-hexane/THF 80:20, 1.5 mL/min, detection at 280 nm): t_r (major) = 8.4 min, t_r (minor) = 10.6 min, 98:2 e.r.

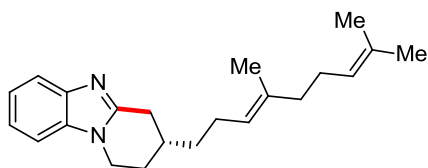
(R)-3-(4-Methylpent-3-en-1-yl)-1,2,3,4-tetrahydrobenzo[4,5]imidazo[1,2-a]pyridine (145h)



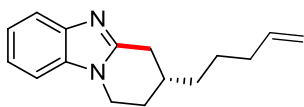
The general procedure **GP11** was followed using **144h** (127 mg, 0.50 mmol, 1.0 equiv). Purification by column chromatography on silica gel (*n*-hexane/EtOAc = 3/1→1.5/1) yielded **145h** (106.4 mg, 84%) as a white solid. **M. p.** = 98–99 °C. $^1\text{H NMR}$ (300 MHz, CDCl_3): $\delta = 7.73$ –7.64 (m, 1H), 7.33–7.18 (m, 3H), 5.17–5.08 (m, 1H), 4.24 (ddd, $J = 12.1, 5.7, 3.2$ Hz, 1H), 3.96 (td, $J = 11.4, 5.0$ Hz, 1H), 3.26 (ddd, $J = 17.1, 4.8, 1.7$ Hz, 1H), 2.66 (dd, $J = 17.1, 10.4$ Hz, 1H), 2.28–2.18 (m, 1H), 2.20–2.07 (m, 2H), 2.08–1.93 (m, 1H), 1.80 (dtd, $J = 13.4, 10.9, 5.8$ Hz, 1H), 1.70 (s, 3H), 1.64 (s, 3H), 1.57–1.48 (m, 2H). $^{13}\text{C NMR}$ (100 MHz, CDCl_3): $\delta = 151.9$ (C_q), 143.2 (C_q), 134.6 (C_q), 132.3 (C_q), 123.8 (CH), 122.1 (CH), 121.7 (CH), 119.0 (CH), 108.8 (CH), 41.7 (CH_2), 35.6 (CH_2), 32.1 (CH), 31.7 (CH_2), 28.8 (CH_2), 25.8 (CH_3), 25.2 (CH_2), 17.9 (CH_3). **IR** (ATR): 2957, 2924, 2852, 1486, 1450, 1286, 1228, 742 cm^{-1} . **MS (ESI)** m/z (relative intensity): 255 (100) $[\text{M}+\text{H}]^+$. **HR-MS** (ESI) m/z

calcd for $C_{17}H_{23}N_2$ $[M+H]^+$ 255.1856, found 255.1853. $[\alpha]_D^{20}$: +45.4 ($c = 1.01$, $CHCl_3$). **HPLC separation** (Chiralpak[®] IC-3, *n*-hexane/*i*PrOH 80:20, 1.0 mL/min, detection at 273 nm): t_r (major) = 13.6 min, t_r (minor) = 15.3 min, 97:3 e.r.

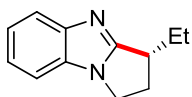
(*R,E*)-3-(4,8-Dimethylnona-3,7-dien-1-yl)-1,2,3,4-tetrahydrobenzo[4,5]imidazo[1,2-*a*]pyridine (145i)



The general procedure **GP11** was followed using **144i** (161 mg, 0.50 mmol, 1.0 equiv). Purification by column chromatography on silica gel (*n*-hexane/EtOAc = 3.5/1→2/1) yielded **145i** (134.6 mg, 84%) as a white solid. **M. p.** = 79–80 °C. **¹H NMR** (300 MHz, $CDCl_3$): $\delta = 7.73$ – 7.64 (m, 1H), 7.33 – 7.17 (m, 3H), 5.18 – 5.04 (m, 2H), 4.23 (ddd, $J = 11.9, 5.7, 3.2$ Hz, 1H), 3.95 (ddd, $J = 11.9, 10.7, 5.0$ Hz, 1H), 3.25 (ddd, $J = 17.1, 4.8, 1.7$ Hz, 1H), 2.66 (dd, $J = 17.1, 10.4$ Hz, 1H), 2.28 – 2.19 (m, 1H), 2.21 – 2.09 (m, 2H), 2.10 – 1.94 (m, 5H), 1.87 – 1.67 (m, 1H), 1.65 (s, 3H), 1.63 (s, 3H), 1.59 (s, 3H), 1.58 – 1.49 (m, 2H). **¹³C NMR** (125 MHz, $CDCl_3$): $\delta = 151.9$ (C_q), 143.2 (C_q), 135.9 (C_q), 134.6 (C_q), 131.5 (C_q), 124.3 (CH), 123.6 (CH), 122.1 (CH), 121.7 (CH), 119.0 (CH), 108.8 (CH), 41.8 (CH_2), 39.9 (CH_2), 35.7 (CH_2), 32.3 (CH), 31.9 (CH_2), 29.0 (CH_2), 26.9 (CH_2), 25.9 (CH_3), 25.3 (CH_2), 17.9 (CH_3), 16.3 (CH_3). **IR** (ATR): 2962, 2911, 2851, 1510, 1451, 1322, 1107, 742 cm^{-1} . **MS (ESI)** m/z (relative intensity): 323 (100) $[M+H]^+$. **HR-MS** (ESI) m/z calcd for $C_{22}H_{31}N_2$ $[M+H]^+$ 323.2482, found 323.2478. $[\alpha]_D^{20}$: +34.2 ($c = 1.22$, $CHCl_3$). **HPLC separation** (Chiralpak[®] IC-3, *n*-hexane/*i*PrOH 80:20, 1.0 mL/min, detection at 273 nm): t_r (major) = 10.8 min, t_r (minor) = 11.9 min, 99:1 e.r.

(R)-3-(Pent-4-en-1-yl)-1,2,3,4-tetrahydrobenzo[4,5]imidazo[1,2-a]pyridine (145j)

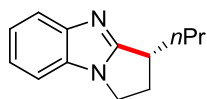
The general procedure **GP11** was followed using **144j** (120 mg, 0.50 mmol, 1.0 equiv), Ni(cod)₂ (13.8 mg, 50.0 μmol, 10.0 mol %) and **220** (12.6 mg, 25.0 μmol, 5.00 mol %) in PhMe (1.0 mL). Purification by column chromatography on silica gel (*n*-hexane/EtOAc = 3/1→1.5/1) yielded **145j** (64.3 mg, 54%) as a white solid. **M. p.** = 110–111 °C. **¹H NMR** (600 MHz, CDCl₃): δ = 7.71–7.65 (m, 1H), 7.31–7.27 (m, 1H), 7.26–7.20 (m, 2H), 5.82 (ddt, *J* = 17.1, 10.2, 6.7 Hz, 1H), 5.03 (ddt, *J* = 17.1, 1.8, 1.6 Hz, 1H), 4.98 (ddt, *J* = 10.2, 2.3, 1.3 Hz, 1H), 4.23 (ddd, *J* = 11.9, 5.7, 3.2 Hz, 1H), 3.95 (ddd, *J* = 11.7, 10.9, 5.0 Hz, 1H), 3.25 (ddd, *J* = 17.0, 4.8, 1.7 Hz, 1H), 2.65 (dd, *J* = 17.0, 10.5 Hz, 1H), 2.26–2.19 (m, 1H), 2.11 (q, *J* = 6.9 Hz, 2H), 2.05–1.96 (m, 1H), 1.79 (dtd, *J* = 13.5, 10.9, 5.8 Hz, 1H), 1.59–1.45 (m, 4H). **¹³C NMR** (125 MHz, CDCl₃): δ = 151.8 (C_q), 143.2 (C_q), 138.5 (CH), 134.6 (C_q), 122.1 (CH), 121.7 (CH), 119.0 (CH), 114.9 (CH₂), 108.8 (CH), 41.8 (CH₂), 35.1 (CH₂), 33.9 (CH₂), 32.8 (CH), 32.0 (CH₂), 28.9 (CH₂), 26.3 (CH₂). **IR** (ATR): 2927, 2856, 1511, 1456, 1414, 1284, 907, 742 cm⁻¹. **MS (ESI)** *m/z* (relative intensity): 259 (35), 241 (100) [M+H]⁺. **HR-MS** (ESI) *m/z* calcd for C₁₆H₂₁N₂ [M+H]⁺ 241.1699, found 241.1697. **[α]_D²⁰**: +54.9 (c = 0.42, CHCl₃). **HPLC separation** (Chiralpak[®] IC-3, *n*-hexane/*i*PrOH 80:20, 1.0 mL/min, detection at 250 nm): *t_r* (major) = 15.4 min, *t_r* (minor) = 18.1 min, 97:3 e.r.

(R)-3-Ethyl-2,3-dihydro-1H-benzo[*d*]pyrrolo[1,2-*a*]imidazole (145q)

The general procedure **GP11** was followed using **144q** (93 mg, 0.50 mmol, 1.0 equiv), Ni(cod)₂ (13.8 mg, 50.0 μmol, 10.0 mol %) and **220** (12.6 mg, 25.0 μmol, 5.00 mol %) in PhMe (1.0 mL). Purification by column chromatography on silica gel

(*n*-hexane/EtOAc = 1/1→1/3) yielded **145q** (37.9 mg, 41%) as a pale yellow oil. **¹H NMR** (300 MHz, CDCl₃): δ = 7.78–7.69 (m, 1H), 7.33–7.17 (m, 3H), 4.12 (ddd, *J* = 10.2, 8.7, 4.2 Hz, 1H), 4.00 (ddd, *J* = 10.2, 8.1, 7.0 Hz, 1H), 3.28–3.16 (m, 1H), 2.86 (dtd, *J* = 12.6, 8.3, 4.2 Hz, 1H), 2.35 (ddt, *J* = 13.0, 8.8, 7.0 Hz, 1H), 2.16–1.92 (m, 1H), 1.72 (dp, *J* = 13.6, 7.5 Hz, 1H), 1.12 (t, *J* = 7.4 Hz, 3H). **¹³C NMR** (125 MHz, CDCl₃): δ = 163.6 (C_q), 148.6 (C_q), 132.2 (C_q), 121.8 (CH), 121.6 (CH), 119.7 (CH), 109.5 (CH), 42.1 (CH₂), 37.7 (CH), 32.9 (CH₂), 26.3 (CH₂), 11.9 (CH₃). **IR** (ATR): 2962, 2931, 1524, 1451, 1415, 1277, 908, 730 cm⁻¹. **MS (ESI)** *m/z* (relative intensity): 187 (100) [M+H]⁺. **HR-MS** (ESI) *m/z* calcd for C₁₂H₁₅N₂ [M+H]⁺ 187.1230, found 187.1231. **[α]_D²⁰**: -1.1 (*c* = 0.60, CHCl₃). **HPLC separation** (Chiralpak[®] IC-3, *n*-hexane/*i*PrOH 80:20, 1.0 mL/min, detection at 250 nm): *t_r* (major) = 10.7 min, *t_r* (minor) = 15.0 min, 97:3 e.r.

(*R*)-3-Propyl-2,3-dihydro-1*H*-benzo[*d*]pyrrolo[1,2-*a*]imidazole (**145r**)

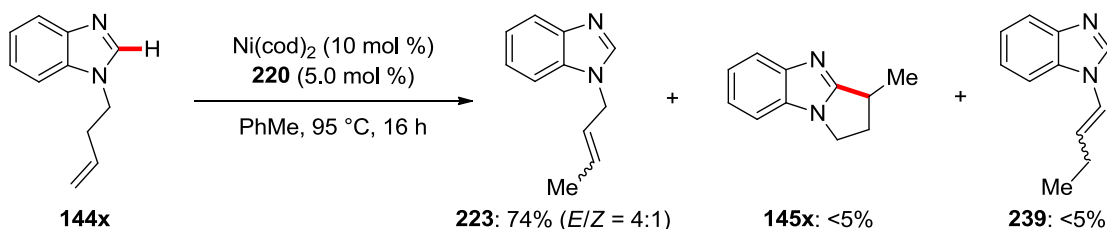


The general procedure **GP11** was followed using **144r** (100 mg, 0.50 mmol, 1.0 equiv), Ni(cod)₂ (13.8 mg, 50.0 μmol, 10.0 mol %) and **220** (12.6 mg, 25.0 μmol, 5.00 mol %) in PhMe (1.0 mL). Purification by column chromatography on silica gel (*n*-hexane/EtOAc = 2/1→1/1.5) yielded **145r** (16.4 mg, 16%) as a white solid. **M. p.** = 63–65 °C. **¹H NMR** (300 MHz, CDCl₃): δ = 7.77–7.67 (m, 1H), 7.34–7.24 (m, 1H), 7.24–7.16 (m, 2H), 4.13 (ddd, *J* = 10.2, 8.7, 4.2 Hz, 1H), 4.00 (ddd, *J* = 10.1, 8.0, 7.0 Hz, 1H), 3.27 (tdd, *J* = 8.1, 7.1, 5.8 Hz, 1H), 2.86 (dtd, *J* = 12.6, 8.2, 4.2 Hz, 1H), 2.34 (ddt, *J* = 12.9, 8.7, 7.0 Hz, 1H), 2.10–1.91 (m, 1H), 1.71–1.42 (m, 3H), 0.99 (t, *J* = 7.2 Hz, 3H). **¹³C NMR** (100 MHz, CDCl₃): δ = 164.0 (C_q), 148.8 (C_q), 132.3 (C_q), 121.8 (CH), 121.7 (CH), 119.8 (CH), 109.5 (CH), 42.1 (CH₂), 36.1 (CH), 35.5 (CH₂), 33.3 (CH₂), 20.7 (CH₂), 14.1 (CH₃). **IR** (ATR): 2955, 2929, 1522, 1451, 1411, 1275, 1217, 740 cm⁻¹. **MS (ESI)** *m/z* (relative intensity): 201 (100) [M+H]⁺. **HR-MS** (ESI) *m/z* calcd for C₁₃H₁₇N₂ [M+H]⁺ 201.1386, found 201.1386. **[α]_D²⁰**: -0.4

($c = 0.38$, CHCl_3). **HPLC separation** (Chiralpak[®] IC-3, *n*-hexane/*i*PrOH 80:20, 1.0 mL/min, detection at 250 nm): t_r (major) = 9.7 min, t_r (minor) = 13.1 min, 96:4 e.r.

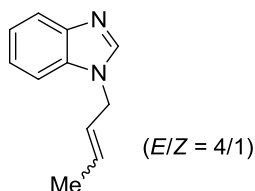
The analytical data are in accordance with those previously reported in the literature.^[206]

Alkene Isomerization



The general procedure **GP11** was followed using **144x** (86 mg, 0.50 mmol, 1.0 equiv), $\text{Ni}(\text{cod})_2$ (13.8 mg, 50.0 μmol , 10.0 mol %) and **220** (12.6 mg, 25.0 μmol , 5.00 mol %) in PhMe (1.0 mL). Purification by column chromatography on silica gel (*n*-hexane/EtOAc = 1.5/1 \rightarrow 1/3) yielded **223** (63.8 mg, 74%) as a pale yellow oil. The E/Z ratio was determined by ^1H NMR analysis of the crude product.

1-(But-2-en-1-yl)-1*H*-benzo[*d*]imidazole (**223**)



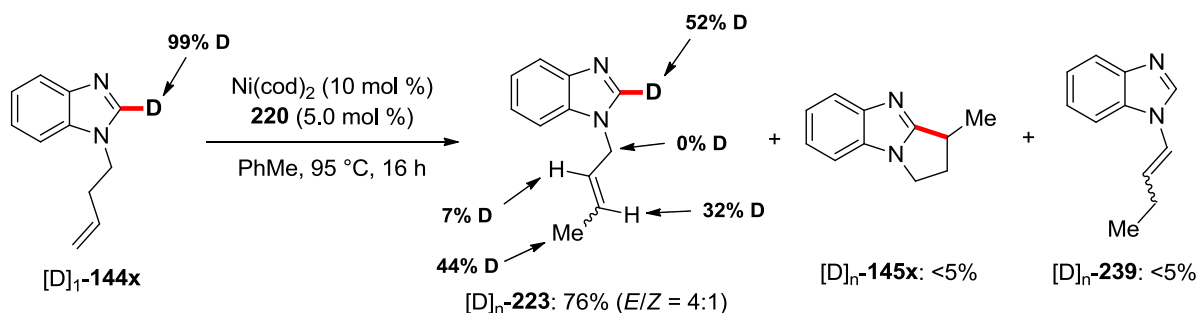
^1H NMR (600 MHz, CDCl_3): $\delta = 7.88$ (s, 1H), 7.82–7.78 (m, 1H), 7.39–7.35 (m, 1H), 7.31–7.24 (m, 2H), 5.86–5.79 (m, 0.16H, *Z*-isomer), 5.77–5.69 (m, 0.84H, *E*-isomer), 5.67–5.57 (m, 1H), 4.78 (ddd, $J = 6.8, 1.7, 0.9$ Hz, 0.34H, *Z*-isomer), 4.70–4.66 (m, 1.70H, *E*-isomer), 1.84 (ddt, $J = 7.0, 1.9, 0.9$ Hz, 0.50H, *Z*-isomer), 1.72 (dq, $J = 6.2, 1.3$ Hz, 2.51H, *E*-isomer). ^{13}C NMR (75 MHz, CDCl_3): $\delta = 144.1$ (C_q , both isomers), 142.9 (CH, both isomers), 142.7 (C_q , both isomers), 134.0 (CH, *Z*-isomer), 130.7

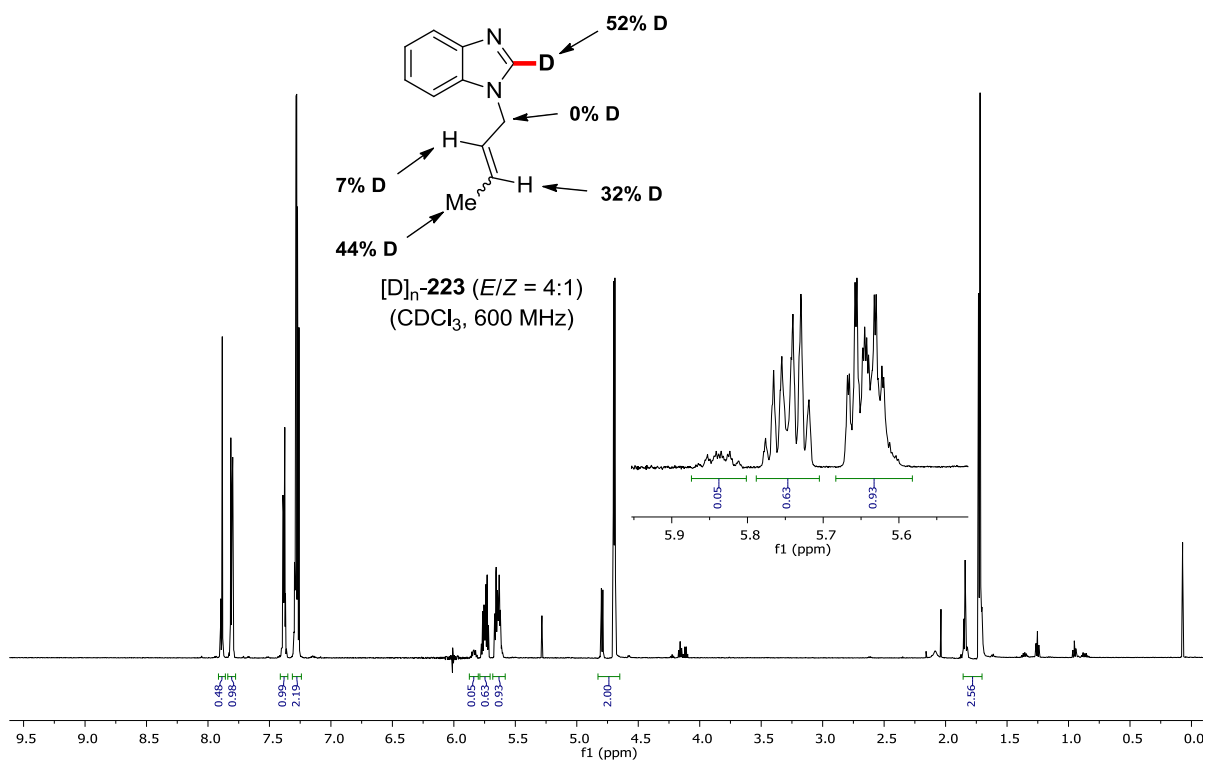
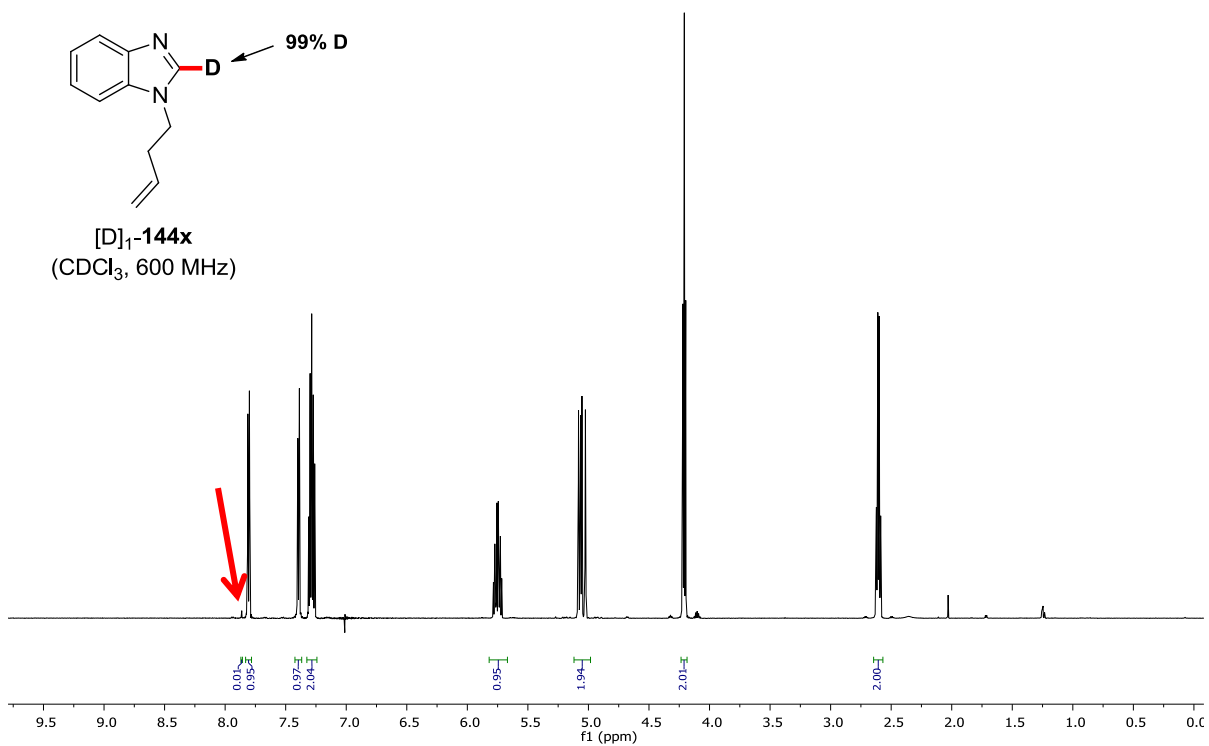
(CH, *E*-isomer), 129.7 (CH, *Z*-isomer), 124.9 (CH, *E*-isomer), 124.0 (CH, *Z*-isomer), 122.9 (CH, *E*-isomer), 122.2 (CH, *Z*-isomer), 122.1 (CH, *E*-isomer), 120.5 (CH, *Z*-isomer), 120.5 (CH, *E*-isomer), 110.0 (CH, *E*-isomer), 109.8 (CH, *Z*-isomer), 47.0 (CH₂, *E*-isomer), 41.8 (CH₂, *Z*-isomer), 17.7 (CH₃, *E*-isomer), 13.3 (CH₃, *Z*-isomer). **IR** (ATR): 2917, 1493, 1458, 1285, 1260, 1198, 963, 743 cm⁻¹. **MS (ESI)** *m/z* (relative intensity): 195 (3) [M+Na]⁺, 173 (100) [M+H]⁺, 119 (18). **HR-MS** (ESI) *m/z* calcd for C₁₁H₁₃N₂ [M+H]⁺ 173.1073, found 173.1072.

The analytical data for the major *E*-isomer are in accordance with those previously reported in the literature.^[340]

Alkene Isomerization with D-Labeling

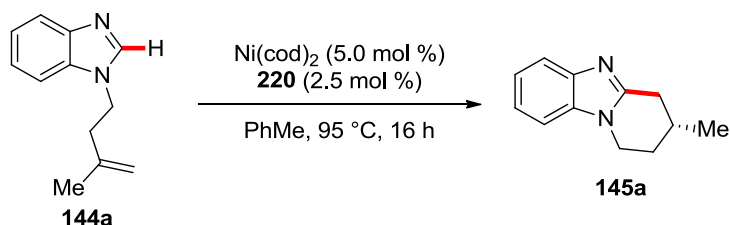
The general procedure **GP11** was followed using [D]₁-**144x** (86 mg, 0.50 mmol, 1.0 equiv), Ni(cod)₂ (13.8 mg, 50.0 μmol, 10.0 mol %) and **220** (12.6 mg, 25.0 μmol, 5.00 mol %) in PhMe (1.0 mL). Purification by column chromatography on silica gel (*n*-hexane/EtOAc = 1.5/1→1/3) yielded [D]_n-**223** (66.1 mg, 76%) as a pale yellow oil. The *E/Z* ratio was determined by ¹H NMR analysis of the crude product. Deuterium incorporation was determined by ¹H NMR spectroscopic analysis of the isolated product.





5.6.4. Mechanistic Studies for the Asymmetric Intramolecular Nickel-Catalyzed Hydroarylation of Alkenes

Non-Linear Effect Studies



Inside a nitrogen-filled glovebox, an oven-dried 25 mL Schlenk tube was charged with a mixture of stock solutions of **220** and *ent*-**220** in PhMe (both $c = 6.90$ mg/mL) for a total volume of 1.0 mL. $\text{Ni}(\text{cod})_2$ (6.9 mg, 25 μmol , 5.0 mol %), and substrate **144a** (93 mg, 0.50 mmol, 1.0 equiv) were then added. The Schlenk tube was closed with a rubber septum, taken out of the glovebox, and placed in a pre-heated oil bath at 95 °C. The reaction mixture was stirred at 95 °C for 16 h, then cooled to 23 °C and diluted with EtOAc (5.0 mL). The mixture was filtered through a short plug of silica gel, rinsed with EtOAc (4 \times 10 mL) and concentrated *in vacuo*. The conversion was determined by ^1H NMR using 1,1,2,2-tetrachloroethane as an internal standard. Enantiomeric excesses were measured by chiral HPLC analysis of the crude product (Chiralpak[®] IC-3, *n*-hexane/*i*PrOH 80:20, 1.0 mL/min).

Table 5.6. Non-Linear Effect Studies.

| Entry | ee(220) ^[a] | ee(144a) ^[b] | Yield ^[c] |
|-------|---------------------------------|----------------------------------|----------------------|
| 1 | 0% | -0.6 | >98% |
| 2 | 10% | 9.8 | >98% |
| 3 | 20% | 19.8 | >98% |
| 4 | 30% | 29.0 | >98% |
| 5 | 40% | 38.6 | >98% |

| | | | |
|----|------|------|------|
| 6 | 50% | 49.2 | >98% |
| 7 | 60% | 58.4 | >98% |
| 8 | 70% | 67.2 | >98% |
| 9 | 80% | 77.2 | >98% |
| 10 | 90% | 88.0 | >98% |
| 11 | 100% | 95.0 | >98% |

^[a] Prepared by mixing two stock solutions of each enantiomer of pre-ligand **220**.

^[b] Determined by chiral HPLC analysis of the crude reaction mixture.

^[c] Determined by crude ¹H NMR using 1,1,2,2-tetrachloroethane (1.0 equiv) as internal standard.

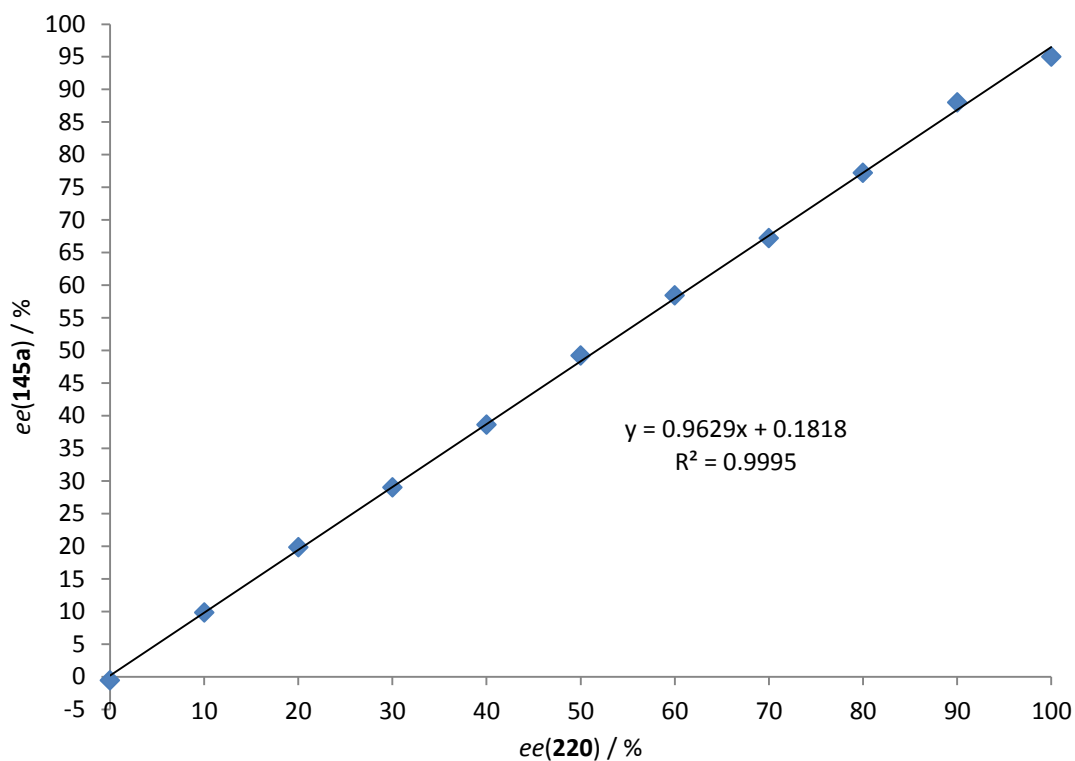
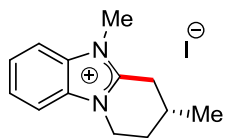


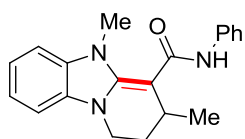
Figure 5.3. Absence of a non-linear effect.

5.6.5. Product Diversification

(R)-3,5-Dimethyl-1,2,3,4-tetrahydrobenzo[4,5]imidazo[1,2-a]pyridin-5-ium iodide (230)

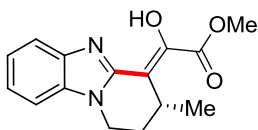
Following a modified procedure,^[341] **145a** (75 mg, 0.40 mmol, 1.0 equiv, >99:1 e.r.) was dissolved in methyl iodide (1.5 mL) and the resulting mixture was stirred for 16 h. The resulting suspension was diluted with Et₂O (15 mL). The precipitate was collected by filtration, washed with Et₂O (3 × 5 mL) and dried *in vacuo* to provide benzimidazolium iodide **230** (123.5 mg, 93%) as a white powder. **M. p.** = 151 °C (decomposition). **¹H NMR** (300 MHz, CDCl₃): δ = 7.72–7.61 (m, 2H), 7.62–7.48 (m, 2H), 4.47 (ddd, *J* = 12.7, 5.7, 2.5 Hz, 1H), 4.28 (td, *J* = 11.9, 4.8 Hz, 1H), 4.02 (s, 3H), 3.73 (ddd, *J* = 18.1, 5.4, 1.0 Hz, 1H), 3.04 (dd, *J* = 18.2, 10.3 Hz, 1H), 2.67–2.49 (m, 1H), 2.36–2.25 (m, 1H), 2.02 (dtd, *J* = 14.0, 11.4, 5.6 Hz, 1H), 1.27 (d, *J* = 6.7 Hz, 3H). **¹³C NMR** (125 MHz, CDCl₃): δ = 151.0 (C_q), 131.9 (C_q), 131.0 (C_q), 126.8 (CH), 126.4 (CH), 112.5 (CH), 112.3 (CH), 43.8 (CH₂), 32.7 (CH), 30.8 (CH₂), 28.9 (CH₂), 25.7 (CH₃), 21.0 (CH₃). **IR** (ATR): 3017, 2955, 2909, 1537, 1470, 760, 427 cm⁻¹. **MS (ESI)** *m/z* (relative intensity): 201 (100) [M-I]⁺. **HR-MS** (ESI) *m/z* calcd for C₁₃H₁₇N₂ [M-I]⁺ 201.1386, found 201.1386. **[α]_D²⁰**: +50.7 (*c* = 0.60, CHCl₃).

Crystals suitable for X-ray crystallography were grown by vapor diffusion from Et₂O into a saturated solution of **230** in EtOH.

3,5-Dimethyl-N-phenyl-1,2,3,5-tetrahydrobenzo[4,5]imidazo[1,2-a]pyridine-4-carboxamide (231)

Following a modified procedure,^[307a] benzimidazolium iodide **230** (200 mg, 0.61 mmol, 1.0 equiv, >99:1 e.r.), potassium hydride (29.3 mg, 0.73 mmol, 1.2 equiv), and potassium *tert*-butoxide (1.4 mg, 12 μ mol, 2.0 mol %) were combined with THF (3.5 mL) inside a nitrogen-filled glovebox. The suspension was stirred at 23 °C for 20 h, and then filtered through a short plug of Celite[®]. The filter cake was washed with THF (3 \times 5.0 mL). The filtrate was cooled to 0 °C, and phenyl isocyanate (109 mg, 0.91 mmol, 1.5 equiv) was added dropwise under inert atmosphere. The resulting solution was stirred for 1 h at 0 °C; then at 23 °C for 16 h. The reaction mixture was concentrated under reduced pressure, and the residue was recrystallized from Et₂O/MeOH = 25/1 at -30 °C to provide **231** (140 mg, 72%) as a pale yellow solid. **M. p.** = 168 °C (decomposition). **¹H NMR** (300 MHz, C₆D₆): δ = 7.81 (d, *J* = 7.9 Hz, 2H), 7.24 (dd, *J* = 8.5, 7.3 Hz, 2H), 6.97–6.81 (m, 3H), 6.74 (brs, 1H), 6.52–6.40 (m, 2H), 3.18 (s, 3H), 3.15–3.05 (m, 1H), 2.95–2.78 (m, 2H), 1.43 (tt, *J* = 12.7, 5.1 Hz, 1H), 1.30–1.18 (m, 1H), 1.01 (d, *J* = 6.8 Hz, 3H). **¹³C NMR** (75 MHz, CDCl₃): δ = 165.7 (C_q), 150.7 (C_q), 140.2 (C_q), 135.9 (C_q), 133.0 (C_q), 129.1 (CH), 122.2 (CH), 121.5 (CH), 121.1 (CH), 119.1 (CH), 108.0 (CH), 105.9 (CH), 79.2 (C_q), 37.6 (CH₂), 35.9 (CH₃), 28.7 (CH), 28.5 (CH₂), 21.8 (CH₃). **IR** (ATR): 3341, 2953, 1539, 1495, 1428, 1307, 1188, 1147, 731 cm⁻¹. **MS (ESI)** *m/z* (relative intensity): 320 (100) [M+H]⁺. **HR-MS** (ESI) *m/z* calcd for C₂₀H₂₂N₃O [M+H]⁺ 320.1757, found 320.1758. **HPLC separation** (Chiralpak[®] IA-3, *n*-hexane/*i*PrOH 70:30, 1.0 mL/min, detection at 273 nm): *t_r* (major) = 9.4 min, *t_r* (minor) = 11.2 min, 53:47 e.r.

(*R*)-Methyl 2-(3-Methyl-1,2,3,5-tetrahydrobenzo[4,5]imidazo[1,2-*a*]pyridin-4-yl)-2-oxoacetate (232)



Following a modified procedure,^[308] methyl 2-chloro-2-oxoacetate (122 μ L, 1.34 mmol, 1.50 equiv) was added dropwise to an ice-cold solution of **145a** (166 mg,

0.89 mmol, 1.0 equiv, >99:1 e.r.) and Et₃N (621 μL, 4.46 mmol, 5.00 equiv) in acetonitrile (9.0 mL). The resulting suspension was stirred at 0 °C for 2 h, then at 23 °C for 18 h. The mixture was diluted with EtOAc (20 mL) and filtered through a short plug of Celite[®], which was rinsed with EtOAc (3 × 20 mL). The volatiles were removed under reduced pressure, and the residue was purified by column chromatography (*n*-hexane/EtOAc = 5/1→2/1) to provide **232** (126 mg, 52%) as a yellow solid. **M. p.** = 137–139 °C. **¹H NMR** (500 MHz, CDCl₃): δ = 13.93 (brs, 1H), 7.66–7.60 (m, 1H), 7.36–7.32 (m, 1H), 7.32–7.28 (m, 2H), 4.21 (ddd, *J* = 12.3, 5.6, 1.7 Hz, 1H), 4.09 (td, *J* = 12.6, 4.2 Hz, 1H), 3.90 (s, 3H), 3.86 (tdd, *J* = 7.1, 5.2, 3.3 Hz, 1H), 2.14 (tdd, *J* = 13.0, 5.6, 4.1 Hz, 1H), 2.05 (dddd, *J* = 13.7, 4.5, 2.9, 1.7 Hz, 1H), 1.27 (d, *J* = 7.0 Hz, 3H). **¹³C NMR** (125 MHz, CDCl₃): δ = 164.7 (C_q), 152.6 (C_q), 150.3 (C_q), 137.9 (C_q), 132.9 (C_q), 123.4 (CH), 123.3 (CH), 117.0 (CH), 109.1 (CH), 106.4 (C_q), 52.3 (CH₃), 37.9 (CH₂), 28.5 (CH₂), 26.0 (CH), 19.8 (CH₃). **IR** (ATR): 2951, 1720, 1536, 1292, 1253, 1211, 1153, 748 cm⁻¹. **MS (ESI)** *m/z* (relative intensity): 567 (17) [2M+Na]⁺, 295 (48) [M+Na]⁺, 273 (100) [M+H]⁺, 213 (7) [M-CO₂Me]⁺. **HR-MS** (ESI) *m/z* calcd for C₁₅H₁₇N₂O₃ [M+H]⁺ 273.1234, found 273.1236. **[α]_D²⁰**: -0.76 (c = 1.00, CHCl₃). **HPLC separation** (Chiralpak[®] IC-3, *n*-hexane/*i*PrOH 25:75, 0.50 mL/min, detection at 290 nm): *t_r* (major) = 31.2 min, *t_r* (minor) = 41.5 min, >99:1 e.r.

Crystals suitable for X-ray crystallography were grown by slow evaporation from a solution of *rac*-**232** in *i*PrOH/CH₂Cl₂ = 25/1.

5.7. Crystallographic Data

The crystal structures of **192ca** and **197** were measured and solved by *H. Keil* (*Stalke* research group).

The data were collected from a shock-cooled crystal at 100(2) K on a 'BRUKER D8' three circle diffractometer equipped with an INCOATEC Mo Microsource with mirror optics (MoK α radiation, $\lambda = 0.71073$ Å). The data were integrated with SAINT.^[342] A multi-scan absorption correction and a 3λ correction^[343] was applied using SADABS.^[344] The structures were solved by SHELXT^[345] and refined on F^2 using SHELXL^[346] in the graphical user interface SHELXLX.^[347]

Table 5.7. Crystal data and structure refinement of **192ca** and **197**.

| Compound | 192ca | 197 |
|--|---|--|
| CCDC number | 1559085 | 1559086 |
| Empirical formula | C ₂₈ H ₂₅ FeNO | C ₃₁ H ₂₇ BrN ₂ O |
| Formula weight | 447.34 | 523.45 |
| Temperature [K] | 100(2) | 100(2) |
| Wavelength [Å] | 0.71073 | 0.71073 |
| Crystal system | Orthorhombic | Orthorhombic |
| Space group | P2 ₁ 2 ₁ 2 ₁ | P2 ₁ 2 ₁ 2 ₁ |
| a[Å] | 11.061(2) | 9.643(2) |
| b[Å] | 11.652(2) | 10.147(2) |
| c[Å] | 16.748(3) | 25.036(3) |
| a[°] | 90 | 90 |
| b[°] | 90 | 90 |
| g[°] | 90 | 90 |
| Volume [Å ³] | 2158.5(7) | 2449.7(8) |
| Z | 4 | 4 |
| Absorption coefficient [mm ⁻¹] | 0.719 | 1.706 |

| | | |
|--|-----------------------------|-----------------------------|
| F(000) | 936 | 1080 |
| Crystal size [mm ³] | 0.3 x 0.2 x 0.2 | 0.2 x 0.2 x 0.1 |
| Theta range for data collection | 2.129 to 26.382° | 1.627 to 26.376° |
| Reflections collected | 25569 | 54351 |
| Independent reflections | 4407 | 5006 |
| R _{int} | 0.0366 | 0.0419 |
| Max. and min. transmission | 0.7454 and 0.6670 | 0.7454 and 0.6485 |
| Data / restraints / parameters | 4407 / 0 / 281 | 5006 / 0 / 318 |
| Goodness-of-fit on F ² | 1.032 | 1.051 |
| Final R indices [$I > 2\sigma(I)$] | R1 = 0.0237 wR2 = 0.0552 | R1 = 0.0195 wR2 = 0.0452 |
| R indices (all data) | R1 = 0.0272 wR2 = 0.0567 | R1 = 0.0213 wR2 = 0.0457 |
| Absolute structure parameter | 0.013(6) | 0.010(3) |
| Largest diff. peak and hole [e Å ⁻³] | 0.242 and -0.212 | 0.222 and -0.152 |

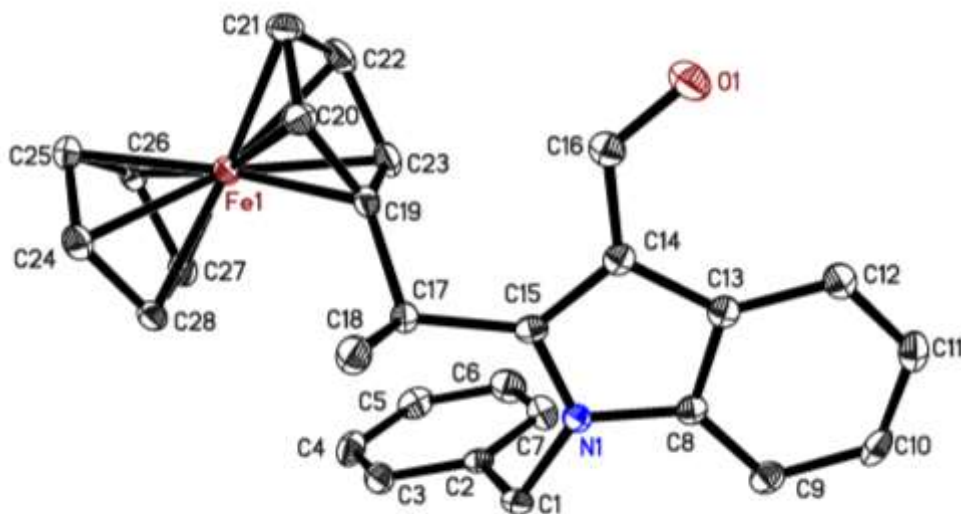


Figure 5.4. Molecular structure of **192ca** with thermal ellipsoids at 50% probability level. The hydrogen atoms are omitted for clarity.

Table 5.8. Bond lengths [Å] and angles [°] for **192ca**.

| | | | |
|-------------|----------|-------------------|------------|
| Fe(1)-C(23) | 2.032(2) | C(24)-Fe(1)-C(25) | 40.67(9) |
| Fe(1)-C(27) | 2.038(2) | C(26)-Fe(1)-C(25) | 40.44(9) |
| Fe(1)-C(19) | 2.042(2) | C(20)-Fe(1)-C(25) | 124.86(9) |
| Fe(1)-C(28) | 2.043(2) | C(23)-Fe(1)-C(21) | 68.57(11) |
| Fe(1)-C(22) | 2.047(3) | C(27)-Fe(1)-C(21) | 159.15(10) |
| Fe(1)-C(24) | 2.047(2) | C(19)-Fe(1)-C(21) | 68.67(10) |
| Fe(1)-C(26) | 2.048(2) | C(28)-Fe(1)-C(21) | 159.60(10) |
| Fe(1)-C(20) | 2.048(2) | C(22)-Fe(1)-C(21) | 40.39(11) |
| Fe(1)-C(25) | 2.051(2) | C(24)-Fe(1)-C(21) | 124.72(11) |
| Fe(1)-C(21) | 2.052(2) | C(26)-Fe(1)-C(21) | 124.34(10) |
| C(1)-N(1) | 1.365(3) | C(20)-Fe(1)-C(21) | 40.71(10) |
| C(1)-C(2) | 1.392(3) | C(25)-Fe(1)-C(21) | 110.06(10) |
| C(1)-C(17) | 1.513(3) | N(1)-C(1)-C(2) | 108.9(2) |
| O(1)-C(9) | 1.227(3) | N(1)-C(1)-C(17) | 120.4(2) |
| N(1)-C(8) | 1.396(3) | C(2)-C(1)-C(17) | 130.7(2) |
| N(1)-C(10) | 1.464(3) | C(1)-N(1)-C(8) | 109.54(19) |
| C(10)-C(11) | 1.514(3) | C(1)-N(1)-C(10) | 126.35(19) |
| C(11)-C(16) | 1.389(3) | C(8)-N(1)-C(10) | 123.99(19) |
| C(11)-C(12) | 1.395(3) | N(1)-C(10)-C(11) | 113.09(19) |
| C(2)-C(9) | 1.431(3) | C(16)-C(11)-C(12) | 118.9(2) |
| C(2)-C(3) | 1.444(3) | C(16)-C(11)-C(10) | 119.5(2) |
| C(16)-C(15) | 1.388(3) | C(12)-C(11)-C(10) | 121.5(2) |
| C(3)-C(8) | 1.404(3) | C(1)-C(2)-C(9) | 126.2(2) |
| C(3)-C(4) | 1.407(3) | C(1)-C(2)-C(3) | 107.2(2) |
| C(15)-C(14) | 1.387(4) | C(9)-C(2)-C(3) | 126.7(2) |
| C(4)-C(5) | 1.383(3) | C(15)-C(16)-C(11) | 120.6(2) |
| C(14)-C(13) | 1.384(4) | C(8)-C(3)-C(4) | 119.2(2) |
| C(5)-C(6) | 1.391(4) | C(8)-C(3)-C(2) | 106.6(2) |
| C(13)-C(12) | 1.383(3) | C(4)-C(3)-C(2) | 134.2(2) |
| C(6)-C(7) | 1.384(3) | C(14)-C(15)-C(16) | 120.1(2) |
| C(7)-C(8) | 1.397(3) | C(5)-C(4)-C(3) | 118.0(2) |
| C(17)-C(19) | 1.520(3) | C(13)-C(14)-C(15) | 119.5(2) |
| C(17)-C(18) | 1.533(3) | C(4)-C(5)-C(6) | 121.9(2) |
| C(19)-C(23) | 1.426(3) | C(12)-C(13)-C(14) | 120.5(2) |
| C(19)-C(20) | 1.429(3) | C(7)-C(6)-C(5) | 121.5(2) |

5. Experimental Part

| | | | |
|-------------------|------------|-------------------|------------|
| C(20)-C(21) | 1.426(4) | C(13)-C(12)-C(11) | 120.4(2) |
| C(21)-C(22) | 1.415(4) | C(6)-C(7)-C(8) | 116.8(2) |
| C(22)-C(23) | 1.424(3) | N(1)-C(8)-C(7) | 129.6(2) |
| C(24)-C(28) | 1.423(3) | N(1)-C(8)-C(3) | 107.76(19) |
| C(24)-C(25) | 1.424(3) | C(7)-C(8)-C(3) | 122.6(2) |
| C(25)-C(26) | 1.416(3) | O(1)-C(9)-C(2) | 125.3(2) |
| C(26)-C(27) | 1.420(4) | C(1)-C(17)-C(19) | 112.25(19) |
| C(27)-C(28) | 1.422(3) | C(1)-C(17)-C(18) | 110.90(19) |
| | | C(19)-C(17)-C(18) | 112.49(19) |
| C(23)-Fe(1)-C(27) | 105.29(10) | C(23)-C(19)-C(20) | 107.6(2) |
| C(23)-Fe(1)-C(19) | 40.98(9) | C(23)-C(19)-C(17) | 125.3(2) |
| C(27)-Fe(1)-C(19) | 120.57(10) | C(20)-C(19)-C(17) | 127.1(2) |
| C(23)-Fe(1)-C(28) | 120.57(10) | C(23)-C(19)-Fe(1) | 69.15(12) |
| C(27)-Fe(1)-C(28) | 40.76(10) | C(20)-C(19)-Fe(1) | 69.79(12) |
| C(19)-Fe(1)-C(28) | 105.42(10) | C(17)-C(19)-Fe(1) | 125.29(16) |
| C(23)-Fe(1)-C(22) | 40.87(10) | C(21)-C(20)-C(19) | 108.0(2) |
| C(27)-Fe(1)-C(22) | 122.15(11) | C(21)-C(20)-Fe(1) | 69.79(13) |
| C(19)-Fe(1)-C(22) | 68.68(10) | C(19)-C(20)-Fe(1) | 69.32(13) |
| C(28)-Fe(1)-C(22) | 157.51(10) | C(22)-C(21)-C(20) | 108.1(2) |
| C(23)-Fe(1)-C(24) | 157.52(10) | C(22)-C(21)-Fe(1) | 69.60(15) |
| C(27)-Fe(1)-C(24) | 68.42(10) | C(20)-C(21)-Fe(1) | 69.50(14) |
| C(19)-Fe(1)-C(24) | 122.21(10) | C(21)-C(22)-C(23) | 108.3(2) |
| C(28)-Fe(1)-C(24) | 40.71(10) | C(21)-C(22)-Fe(1) | 70.02(15) |
| C(22)-Fe(1)-C(24) | 160.61(11) | C(23)-C(22)-Fe(1) | 69.03(14) |
| C(23)-Fe(1)-C(26) | 121.69(10) | C(22)-C(23)-C(19) | 108.0(2) |
| C(27)-Fe(1)-C(26) | 40.68(10) | C(22)-C(23)-Fe(1) | 70.10(14) |
| C(19)-Fe(1)-C(26) | 157.19(9) | C(19)-C(23)-Fe(1) | 69.87(13) |
| C(28)-Fe(1)-C(26) | 68.59(10) | C(28)-C(24)-C(25) | 107.8(2) |
| C(22)-Fe(1)-C(26) | 107.98(10) | C(28)-C(24)-Fe(1) | 69.51(14) |
| C(24)-Fe(1)-C(26) | 68.45(10) | C(25)-C(24)-Fe(1) | 69.80(14) |
| C(23)-Fe(1)-C(20) | 68.77(10) | C(26)-C(25)-C(24) | 108.4(2) |
| C(27)-Fe(1)-C(20) | 157.54(10) | C(26)-C(25)-Fe(1) | 69.69(14) |
| C(19)-Fe(1)-C(20) | 40.89(9) | C(24)-C(25)-Fe(1) | 69.53(13) |
| C(28)-Fe(1)-C(20) | 122.24(10) | C(25)-C(26)-C(27) | 107.7(2) |
| C(22)-Fe(1)-C(20) | 68.35(11) | C(25)-C(26)-Fe(1) | 69.87(14) |
| C(24)-Fe(1)-C(20) | 108.35(10) | C(27)-C(26)-Fe(1) | 69.29(13) |
| C(26)-Fe(1)-C(20) | 160.74(10) | C(26)-C(27)-C(28) | 108.4(2) |

| | | | |
|-------------------|------------|-------------------|-----------|
| C(23)-Fe(1)-C(25) | 158.92(9) | C(26)-C(27)-Fe(1) | 70.04(14) |
| C(27)-Fe(1)-C(25) | 68.14(10) | C(28)-C(27)-Fe(1) | 69.81(13) |
| C(19)-Fe(1)-C(25) | 159.72(9) | C(27)-C(28)-C(24) | 107.7(2) |
| C(28)-Fe(1)-C(25) | 68.37(9) | C(27)-C(28)-Fe(1) | 69.42(14) |
| C(22)-Fe(1)-C(25) | 124.36(10) | C(24)-C(28)-Fe(1) | 69.78(14) |

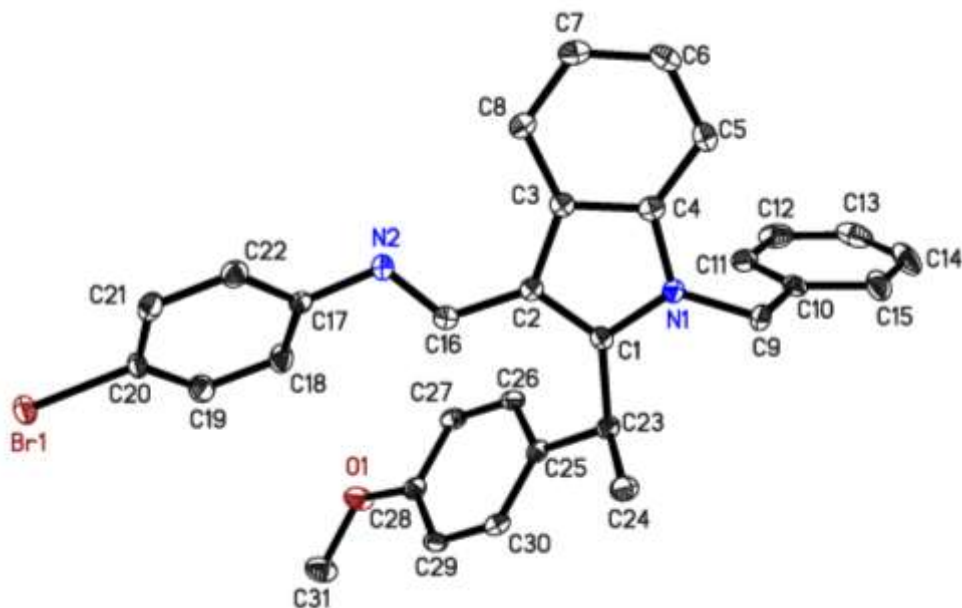


Figure 5.5. Molecular structure of **197** with thermal ellipsoids at 50% probability level. The hydrogen atoms are omitted for clarity.

Table 5.9. Bond lengths [Å] and angles [°] for **197**.

| | | | |
|-------------|----------|-------------------|------------|
| Br(1)-C(20) | 1.906(2) | C(16)-N(2)-C(17) | 117.49(19) |
| O(1)-C(28) | 1.368(3) | C(1)-C(2)-C(16) | 126.0(2) |
| O(1)-C(31) | 1.428(3) | C(1)-C(2)-C(3) | 106.85(18) |
| N(1)-C(1) | 1.375(3) | C(16)-C(2)-C(3) | 127.10(19) |
| N(1)-C(4) | 1.388(3) | C(1)-C(23)-C(25) | 112.90(17) |
| N(1)-C(9) | 1.456(3) | C(1)-C(23)-C(24) | 109.38(18) |
| C(1)-C(2) | 1.391(3) | C(25)-C(23)-C(24) | 114.02(19) |
| C(1)-C(23) | 1.517(3) | C(30)-C(25)-C(26) | 117.4(2) |
| N(2)-C(16) | 1.287(3) | C(30)-C(25)-C(23) | 122.16(18) |
| N(2)-C(17) | 1.417(3) | C(26)-C(25)-C(23) | 120.44(19) |

5. Experimental Part

| | | | |
|------------------|------------|-------------------|------------|
| C(2)-C(16) | 1.439(3) | C(27)-C(26)-C(25) | 121.6(2) |
| C(2)-C(3) | 1.447(3) | C(26)-C(27)-C(28) | 119.81(19) |
| C(23)-C(25) | 1.528(3) | O(1)-C(28)-C(29) | 125.1(2) |
| C(23)-C(24) | 1.534(3) | O(1)-C(28)-C(27) | 115.38(18) |
| C(25)-C(30) | 1.386(3) | C(29)-C(28)-C(27) | 119.5(2) |
| C(25)-C(26) | 1.403(3) | C(28)-C(29)-C(30) | 119.9(2) |
| C(26)-C(27) | 1.378(3) | C(25)-C(30)-C(29) | 121.8(2) |
| C(27)-C(28) | 1.401(3) | C(8)-C(3)-C(4) | 119.0(2) |
| C(28)-C(29) | 1.381(3) | C(8)-C(3)-C(2) | 134.4(2) |
| C(29)-C(30) | 1.391(3) | C(4)-C(3)-C(2) | 106.66(18) |
| C(3)-C(8) | 1.403(3) | N(1)-C(4)-C(5) | 129.2(2) |
| C(3)-C(4) | 1.406(3) | N(1)-C(4)-C(3) | 108.12(19) |
| C(4)-C(5) | 1.393(3) | C(5)-C(4)-C(3) | 122.7(2) |
| C(5)-C(6) | 1.384(3) | C(6)-C(5)-C(4) | 117.1(2) |
| C(7)-C(8) | 1.382(3) | N(2)-C(16)-C(2) | 122.3(2) |
| C(7)-C(6) | 1.398(3) | C(8)-C(7)-C(6) | 121.6(2) |
| C(17)-C(22) | 1.396(3) | C(5)-C(6)-C(7) | 121.2(2) |
| C(17)-C(18) | 1.398(3) | C(22)-C(17)-C(18) | 119.1(2) |
| C(18)-C(19) | 1.391(3) | C(22)-C(17)-N(2) | 117.7(2) |
| C(9)-C(10) | 1.520(3) | C(18)-C(17)-N(2) | 123.2(2) |
| C(22)-C(21) | 1.386(3) | C(7)-C(8)-C(3) | 118.5(2) |
| C(10)-C(11) | 1.389(3) | C(19)-C(18)-C(17) | 119.9(2) |
| C(10)-C(15) | 1.390(3) | N(1)-C(9)-C(10) | 113.54(18) |
| C(19)-C(20) | 1.381(3) | C(21)-C(22)-C(17) | 121.0(2) |
| C(11)-C(12) | 1.392(3) | C(11)-C(10)-C(15) | 119.3(2) |
| C(20)-C(21) | 1.381(3) | C(11)-C(10)-C(9) | 121.7(2) |
| C(12)-C(13) | 1.379(4) | C(15)-C(10)-C(9) | 119.1(2) |
| C(13)-C(14) | 1.377(4) | C(20)-C(19)-C(18) | 119.6(2) |
| C(15)-C(14) | 1.401(4) | C(10)-C(11)-C(12) | 120.4(2) |
| | | C(19)-C(20)-C(21) | 121.6(2) |
| C(28)-O(1)-C(31) | 117.47(17) | C(19)-C(20)-Br(1) | 119.98(18) |
| C(1)-N(1)-C(4) | 109.28(18) | C(21)-C(20)-Br(1) | 118.46(17) |
| C(1)-N(1)-C(9) | 128.11(18) | C(13)-C(12)-C(11) | 120.1(2) |
| C(4)-N(1)-C(9) | 122.61(18) | C(20)-C(21)-C(22) | 118.8(2) |
| N(1)-C(1)-C(2) | 109.07(18) | C(14)-C(13)-C(12) | 120.0(2) |
| N(1)-C(1)-C(23) | 120.08(18) | C(10)-C(15)-C(14) | 119.9(2) |
| C(2)-C(1)-C(23) | 130.85(19) | C(13)-C(14)-C(15) | 120.3(2) |

The crystal structures of **230** and *rac*-**232** were measured and solved by *Dr. C. Golz*.

A suitable crystal was selected and mounted on a 'Bruker APEX-II CCD' diffractometer. The crystal was kept at 100 K during data collection. Using Olex2,^[348] the structure was solved with the XT^[345] structure solution program using intrinsic phasing and refined with the XL^[349] refinement package using least squares minimization.

X-Ray Crystallographic Data of **230**

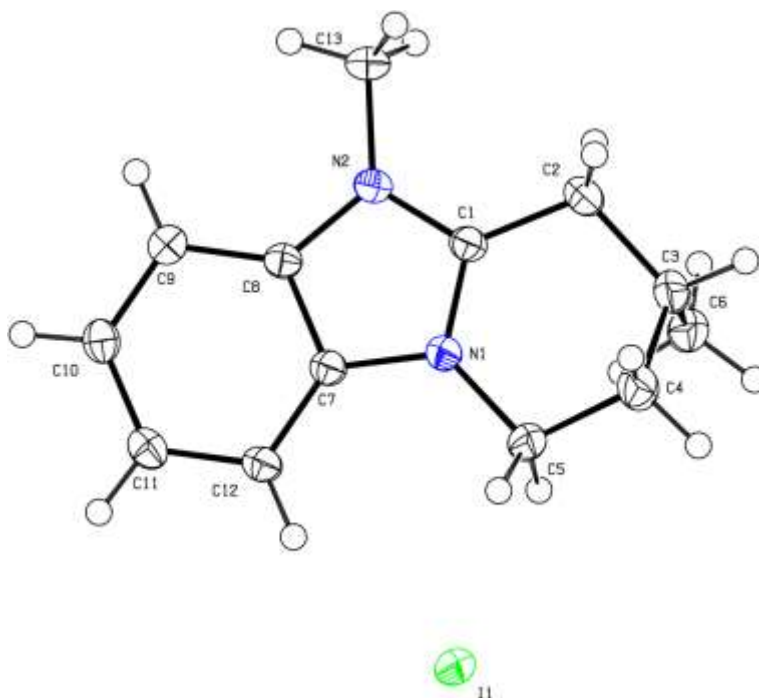


Figure 5.6. Molecular structure of **230** with thermal ellipsoids at 50% probability level.

Table 5.10. Crystal data and structure refinement for **230**.

| | |
|-------------------|---|
| Compound | 230 |
| CCDC number | 1871584 |
| Empirical formula | C ₁₃ H ₁₇ IN ₂ |

5. Experimental Part

| | |
|--|--|
| Formula weight | 328.18 |
| Temperature/K | 100.0 |
| Crystal system | orthorhombic |
| Space group | P2 ₁ 2 ₁ 2 ₁ |
| a/Å | 6.4848(3) |
| b/Å | 12.6132(6) |
| c/Å | 15.9161(8) |
| α /° | 90 |
| β /° | 90 |
| γ /° | 90 |
| Volume/Å ³ | 1301.84(11) |
| Z | 4 |
| $\rho_{\text{calc}}/\text{g}\cdot\text{cm}^{-3}$ | 1.674 |
| μ/mm^{-1} | 2.436 |
| F(000) | 648.0 |
| Crystal size/mm ³ | 0.237 × 0.166 × 0.138 |
| Radiation | MoK α (λ = 0.71073) |
| 2 θ range for data collection/° | 5.118 to 65.194 |
| Index ranges | -9 ≤ h ≤ 9, -19 ≤ k ≤ 15, -24 ≤ l ≤ 23 |
| Reflections collected | 19301 |
| Independent reflections | 4738 [R_{int} = 0.0180, R_{sigma} = 0.0153] |
| Data/restraints/parameters | 4738/0/147 |
| Goodness-of-fit on F ² | 1.104 |
| Final R indexes [$l \geq 2\sigma(l)$] | R_1 = 0.0144, wR_2 = 0.0389 |
| Final R indexes [all data] | R_1 = 0.0146, wR_2 = 0.0391 |
| Largest diff. peak/hole / e Å ⁻³ | 0.46/-0.46 |
| Flack parameter | -0.009(6) |

Table 5.11. Bond lengths for **230**.

| Atom | Atom | Length/Å | Atom | Atom | Length/Å |
|------|------|------------|------|------|------------|
| N1 | C1 | 1.3398(17) | C3 | C6 | 1.525(3) |
| N1 | C5 | 1.4742(19) | C4 | C5 | 1.526(3) |
| N1 | C7 | 1.3886(18) | C7 | C8 | 1.3973(19) |
| N2 | C1 | 1.3389(18) | C7 | C12 | 1.3887(19) |
| N2 | C8 | 1.3897(17) | C8 | C9 | 1.394(2) |
| N2 | C13 | 1.4643(18) | C9 | C10 | 1.386(2) |
| C1 | C2 | 1.484(2) | C10 | C11 | 1.404(2) |
| C2 | C3 | 1.541(3) | C11 | C12 | 1.385(2) |
| C3 | C4 | 1.523(3) | | | |

Table 5.12. Bond angles for **230**.

| Atom | Atom | Atom | Angle/° | Atom | Atom | Atom | Angle/° |
|------|------|------|------------|------|------|------|------------|
| C1 | N1 | C5 | 125.02(12) | C3 | C4 | C5 | 112.16(16) |
| C1 | N1 | C7 | 108.58(12) | N1 | C5 | C4 | 109.25(13) |
| C7 | N1 | C5 | 126.39(12) | N1 | C7 | C8 | 106.56(11) |
| C1 | N2 | C8 | 108.52(11) | N1 | C7 | C12 | 131.02(13) |
| C1 | N2 | C13 | 124.57(12) | C12 | C7 | C8 | 122.41(13) |
| C8 | N2 | C13 | 126.92(12) | N2 | C8 | C7 | 106.61(12) |
| N1 | C1 | C2 | 124.23(13) | N2 | C8 | C9 | 131.80(13) |
| N2 | C1 | N1 | 109.72(12) | C9 | C8 | C7 | 121.58(12) |
| N2 | C1 | C2 | 126.06(13) | C10 | C9 | C8 | 116.04(13) |
| C1 | C2 | C3 | 110.14(13) | C9 | C10 | C11 | 122.10(13) |
| C4 | C3 | C2 | 109.30(16) | C12 | C11 | C10 | 121.86(13) |
| C4 | C3 | C6 | 112.71(17) | C11 | C12 | C7 | 116.00(13) |
| C6 | C3 | C2 | 111.66(16) | | | | |

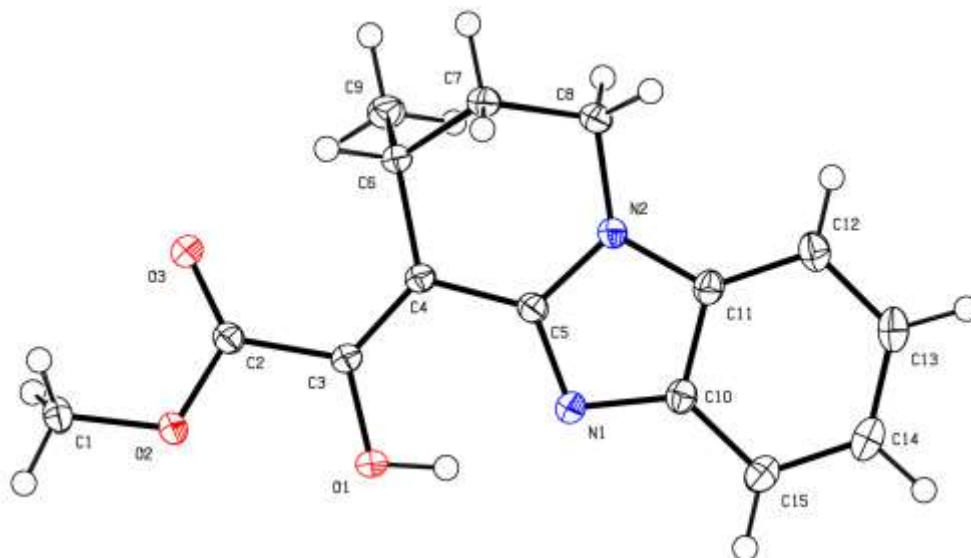
X-Ray Crystallographic Data of *rac*-232

Figure 5.7. Molecular structure of *rac*-232 with thermal ellipsoids at 50% probability level.

Table 5.13. Crystal data and structure refinement for *rac*-232.

| | |
|-----------------------|---|
| Compound | <i>rac</i> -232 |
| CCDC number | 1871585 |
| Empirical formula | C ₁₅ H ₁₆ N ₂ O ₃ |
| Formula weight | 272.30 |
| Temperature/K | 99.98 |
| Crystal system | monoclinic |
| Space group | P2 ₁ /c |
| <i>a</i> /Å | 7.3560(4) |
| <i>b</i> /Å | 15.9260(7) |
| <i>c</i> /Å | 11.3561(5) |
| α /° | 90 |
| β /° | 107.168(2) |
| γ /° | 90 |
| Volume/Å ³ | 1271.11(11) |

| | |
|--|--|
| Z | 4 |
| $\rho_{\text{calc}}/\text{g}\cdot\text{cm}^{-3}$ | 1.423 |
| μ/mm^{-1} | 0.100 |
| F(000) | 576.0 |
| Crystal size/ mm^3 | 0.273 × 0.2 × 0.11 |
| Radiation | MoK α ($\lambda = 0.71073$) |
| 2 θ range for data collection/ $^\circ$ | 5.116 to 59.474 |
| Index ranges | -10 ≤ h ≤ 10, -22 ≤ k ≤ 22, -15 ≤ l ≤ 15 |
| Reflections collected | 20336 |
| Independent reflections | 3597 [$R_{\text{int}} = 0.0287$, $R_{\text{sigma}} = 0.0209$] |
| Data/restraints/parameters | 3597/0/187 |
| Goodness-of-fit on F^2 | 1.072 |
| Final R indexes [$I \geq 2\sigma(I)$] | $R_1 = 0.0418$, $wR_2 = 0.1038$ |
| Final R indexes [all data] | $R_1 = 0.0484$, $wR_2 = 0.1084$ |
| Largest diff. peak/hole / $e \text{ \AA}^{-3}$ | 0.38/-0.25 |

Table 5.14. Bond Lengths for *rac*-232.

| Atom | Atom | Length/ \AA | Atom | Atom | Length/ \AA |
|------|------|----------------------|------|------|----------------------|
| O1 | C3 | 1.3502(13) | C4 | C5 | 1.4492(16) |
| O2 | C1 | 1.4460(14) | C4 | C6 | 1.5200(15) |
| O2 | C2 | 1.3393(13) | C6 | C7 | 1.5367(16) |
| O3 | C2 | 1.2086(14) | C6 | C9 | 1.5277(17) |
| N1 | C5 | 1.3367(14) | C7 | C8 | 1.5259(17) |
| N1 | C10 | 1.3886(15) | C10 | C11 | 1.4081(16) |
| N2 | C5 | 1.3676(14) | C10 | C15 | 1.3967(16) |
| N2 | C8 | 1.4674(14) | C11 | C12 | 1.3938(16) |
| N2 | C11 | 1.3806(14) | C12 | C13 | 1.3857(18) |
| C2 | C3 | 1.4936(16) | C13 | C14 | 1.4055(19) |
| C3 | C4 | 1.3608(15) | C14 | C15 | 1.3896(18) |

Table 5.15. Bond Angles for *rac*-232.

| Atom | Atom | Atom | Angle/° | Atom | Atom | Atom | Angle/° |
|------|------|------|------------|------|------|------|------------|
| C2 | O2 | C1 | 114.79(9) | N2 | C5 | C4 | 121.96(10) |
| C5 | N1 | C10 | 105.11(9) | C4 | C6 | C7 | 109.72(9) |
| C5 | N2 | C8 | 124.93(10) | C4 | C6 | C9 | 110.71(10) |
| C5 | N2 | C11 | 107.07(9) | C9 | C6 | C7 | 112.00(10) |
| C11 | N2 | C8 | 127.88(10) | C8 | C7 | C6 | 112.45(10) |
| O2 | C2 | C3 | 111.44(9) | N2 | C8 | C7 | 108.96(9) |
| O3 | C2 | O2 | 123.31(11) | N1 | C10 | C11 | 109.62(10) |
| O3 | C2 | C3 | 125.24(10) | N1 | C10 | C15 | 130.27(11) |
| O1 | C3 | C2 | 113.33(9) | C15 | C10 | C11 | 120.10(11) |
| O1 | C3 | C4 | 123.98(10) | N2 | C11 | C10 | 105.71(10) |
| C4 | C3 | C2 | 122.69(10) | N2 | C11 | C12 | 131.55(11) |
| C3 | C4 | C5 | 117.81(10) | C12 | C11 | C10 | 122.72(11) |
| C3 | C4 | C6 | 126.20(10) | C13 | C12 | C11 | 116.38(11) |
| C5 | C4 | C6 | 115.97(9) | C12 | C13 | C14 | 121.70(12) |
| N1 | C5 | N2 | 112.48(10) | C15 | C14 | C13 | 121.61(11) |
| N1 | C5 | C4 | 125.56(10) | C14 | C15 | C10 | 117.48(11) |

6. References

- [1] T. H. Meyer, L. H. Finger, P. Gandeepan, L. Ackermann, *Trends Chem.* **2019**, *1*, 63–76.
- [2] a) B. M. Trost, *Angew. Chem. Int. Ed.* **1995**, *34*, 259–281; b) B. M. Trost, *Science* **1991**, *254*, 1471–1477.
- [3] a) P. T. Anastas, M. M. Kirchhoff, *Acc. Chem. Res.* **2002**, *35*, 686–694; b) P. T. Anastas, J. C. Warner, *Green chemistry: theory and practice*, Oxford University Press, Oxford, **1998**.
- [4] C. C. C. Johansson Seechurn, M. O. Kitching, T. J. Colacot, V. Snieckus, *Angew. Chem. Int. Ed.* **2012**, *51*, 5062–5085.
- [5] C. Glaser, *Ber. Dtsch. Chem. Ges.* **1869**, *2*, 422–424.
- [6] a) P. E. Fanta, *Synthesis* **1974**, 9–21; b) F. Ullmann, J. Bielecki, *Ber. Dtsch. Chem. Ges.* **1901**, *34*, 2174–2185.
- [7] a) N. Miyaura, A. Suzuki, *Chem. Rev.* **1995**, *95*, 2457–2483; b) N. Miyaura, A. Suzuki, *J. Chem. Soc., Chem. Commun.* **1979**, 866–867; c) N. Miyaura, K. Yamada, A. Suzuki, *Tetrahedron Lett.* **1979**, *20*, 3437–3440.
- [8] a) A. O. King, N. Okukado, E.-i. Negishi, *J. Chem. Soc., Chem. Commun.* **1977**, 683–684; b) E. Negishi, A. O. King, N. Okukado, *J. Org. Chem.* **1977**, *42*, 1821–1823.
- [9] a) R. F. Heck, J. P. Nolley, *J. Org. Chem.* **1972**, *37*, 2320–2322; b) T. Mizoroki, K. Mori, A. Ozaki, *Bull. Chem. Soc. Jpn.* **1971**, *44*, 581.
- [10] a) K. Tamao, K. Sumitani, M. Kumada, *J. Am. Chem. Soc.* **1972**, *94*, 4374–4376; b) R. J. P. Corriu, J. P. Masse, *J. Chem. Soc., Chem. Commun.* **1972**, 144.
- [11] a) T. Hiyama, *J. Organomet. Chem.* **2002**, *653*, 58–61; b) Y. Hatanaka, T. Hiyama, *J. Org. Chem.* **1988**, *53*, 918–920.
- [12] a) J. K. Stille, *Angew. Chem. Int. Ed.* **1986**, *25*, 508–524; b) D. Milstein, J. K. Stille, *J. Am. Chem. Soc.* **1979**, *101*, 4992–4998; c) D. Milstein, J. K. Stille, *J. Am. Chem. Soc.* **1978**, *100*, 3636–3638.

- [13] a) R. Chinchilla, C. Nájera, *Chem. Soc. Rev.* **2011**, *40*, 5084–5121; b) R. Chinchilla, C. Nájera, *Chem. Rev.* **2007**, *107*, 874–922; c) K. Sonogashira, *J. Organomet. Chem.* **2002**, *653*, 46–49; d) K. Sonogashira, Y. Tohda, N. Hagihara, *Tetrahedron Lett.* **1975**, *16*, 4467–4470.
- [14] a) B. M. Trost, D. L. Van Vranken, *Chem. Rev.* **1996**, *96*, 395–422; b) B. M. Trost, P. E. Strege, *J. Am. Chem. Soc.* **1977**, *99*, 1649–1651; c) B. M. Trost, T. J. Fullerton, *J. Am. Chem. Soc.* **1973**, *95*, 292–294; d) J. Tsuji, H. Takahashi, M. Morikawa, *Tetrahedron Lett.* **1965**, *6*, 4387–4388.
- [15] a) F. Paul, J. Patt, J. F. Hartwig, *J. Am. Chem. Soc.* **1994**, *116*, 5969–5970; b) A. S. Guram, S. L. Buchwald, *J. Am. Chem. Soc.* **1994**, *116*, 7901–7902.
- [16] a) A. de Meijere, S. Bräse, M. Oestreich, *Metal-Catalyzed Cross-Coupling Reactions and More*, Wiley-VCH, Weinheim, **2014**; b) G. A. Molander, J. P. Wolfe, M. Larhed, *Cross Coupling and Heck-Type Reactions*, Georg Thieme, Stuttgart, **2013**.
- [17] The Nobel Prize in Chemistry 2010 - Press Release: https://www.nobelprize.org/nobel_prizes/chemistry/laureates/2010/press.html (accessed on 10.04.2019).
- [18] a) L. N. Cavalcanti, G. A. Molander, *Top. Curr. Chem.* **2016**, *374*, 39; b) T. Iwasaki, N. Kambe, *Top. Curr. Chem.* **2016**, *374*, 66; c) M. Tobisu, N. Chatani, *Top. Curr. Chem.* **2016**, *374*, 41; d) X. Hu, *Chem. Sci.* **2011**, *2*, 1867–1886; e) B. M. Rosen, K. W. Quasdorf, D. A. Wilson, N. Zhang, A.-M. Resmerita, N. K. Garg, V. Percec, *Chem. Rev.* **2011**, *111*, 1346–1416.
- [19] a) A. Piontek, E. Bisz, M. Szostak, *Angew. Chem. Int. Ed.* **2018**, *57*, 11116–11128; b) T. L. Mako, J. A. Byers, *Inorg. Chem. Front.* **2016**, *3*, 766–790; c) C. Cassani, G. Bergonzini, C.-J. Wallentin, *ACS Catal.* **2016**, *6*, 1640–1648; d) E. Nakamura, T. Hatakeyama, S. Ito, K. Ishizuka, L. Ilies, M. Nakamura, *Org. React.* **2014**, *83*, 1–210; e) R. Jana, T. P. Pathak, M. S. Sigman, *Chem. Rev.* **2011**, *111*, 1417–1492; f) E. Nakamura, N. Yoshikai, *J. Org. Chem.* **2010**, *75*, 6061–6067; g) W. M. Czaplik, M. Mayer, J. Cvengroš, A. J. von Wangelin, *ChemSusChem* **2009**, *2*, 396–417; h) B. D. Sherry, A. Fürstner, *Acc. Chem. Res.* **2008**, *41*, 1500–1511.

- [20] a) P. Gandeepan, N. Kaplaneris, S. Santoro, L. Vaccaro, L. Ackermann, *ACS Sustain. Chem. Eng.* **2019**, *7*, 8023–8040; b) E. Bisz, M. Szostak, *ChemSusChem* **2018**, *11*, 1290–1294; c) S. Santoro, F. Ferlin, L. Luciani, L. Ackermann, L. Vaccaro, *Green Chem.* **2017**, *19*, 1601–1612; d) V. Pace, P. Hoyos, L. Castoldi, P. Domínguez de María, A. R. Alcántara, *ChemSusChem* **2012**, *5*, 1369–1379.
- [21] a) S. Santoro, S. I. Kozhushkov, L. Ackermann, L. Vaccaro, *Green Chem.* **2016**, *18*, 3471–3493; b) Á. Molnár, *Chem. Rev.* **2011**, *111*, 2251–2320; c) M. Benaglia, *Recoverable and Recyclable Catalysts*, John Wiley & Sons, Chichester, **2009**.
- [22] a) T. Gensch, M. J. James, T. Dalton, F. Glorius, *Angew. Chem. Int. Ed.* **2018**, *57*, 2296–2306; b) J.-C. Hierso, M. Beaupérin, P. Meunier, *Eur. J. Inorg. Chem.* **2007**, 3767–3780.
- [23] Selected reviews: a) J. C. K. Chu, T. Rovis, *Angew. Chem. Int. Ed.* **2018**, *57*, 62–101; b) M. M. Lorion, K. Maindan, A. R. Kapdi, L. Ackermann, *Chem. Soc. Rev.* **2017**, *46*, 7399–7420; c) Y. Wei, P. Hu, M. Zhang, W. Su, *Chem. Rev.* **2017**, *117*, 8864–8907; d) J. A. Leitch, C. G. Frost, *Chem. Soc. Rev.* **2017**, *46*, 7145–7153; e) Y. Park, Y. Kim, S. Chang, *Chem. Rev.* **2017**, *117*, 9247–9301; f) J. He, M. Wasa, K. S. L. Chan, Q. Shao, J.-Q. Yu, *Chem. Rev.* **2017**, *117*, 8754–8786; g) Q.-Z. Zheng, N. Jiao, *Chem. Soc. Rev.* **2016**, *45*, 4590–4627; h) A. Dey, S. Maity, D. Maiti, *Chem. Commun.* **2016**, *52*, 12398–12414; i) G. E. M. Crisenza, J. F. Bower, *Chem. Lett.* **2016**, *45*, 2–9; j) O. Daugulis, J. Roane, L. D. Tran, *Acc. Chem. Res.* **2015**, *48*, 1053–1064; k) J. Wencel-Delord, F. Glorius, *Nat. Chem.* **2013**, *5*, 369–375; l) G. Rouquet, N. Chatani, *Angew. Chem. Int. Ed.* **2013**, *52*, 11726–11743; m) L. Ackermann, R. Vicente, A. R. Kapdi, *Angew. Chem. Int. Ed.* **2009**, *48*, 9792–9826; n) L. Ackermann, *Modern Arylation Methods*, Wiley-VCH, Weinheim, **2009**; o) X. Chen, K. M. Engle, D.-H. Wang, J.-Q. Yu, *Angew. Chem. Int. Ed.* **2009**, *48*, 5094–5115; p) R. G. Bergman, *Nature* **2007**, *446*, 391–393.
- [24] a) M. Seki, *Org. Process Res. Dev.* **2016**, *20*, 867–877; b) L. Ackermann, *Org. Process Res. Dev.* **2015**, *19*, 260–269.

- [25] a) S. K. Sinha, G. Zanoni, D. Maiti, *Asian J. Org. Chem.* **2018**, *7*, 1178–1192; b) J. Yamaguchi, A. D. Yamaguchi, K. Itami, *Angew. Chem. Int. Ed.* **2012**, *51*, 8960–9009.
- [26] a) J. Zhang, L. J. Kang, T. C. Parker, S. B. Blakey, C. K. Luscombe, S. R. Marder, *Molecules* **2018**, *23*, 922; b) J.-R. Pouliot, F. Grenier, J. T. Blaskovits, S. Beaupré, M. Leclerc, *Chem. Rev.* **2016**, *116*, 14225–14274.
- [27] L. Ackermann, L. G. Habgood, T. B. Gunnoe, *Catalytic Hydroarylation of Carbon-Carbon Multiple Bonds*, Wiley-VCH, Weinheim, **2018**.
- [28] S. J. Blanksby, G. B. Ellison, *Acc. Chem. Res.* **2003**, *36*, 255–263.
- [29] T. Gensch, M. N. Hopkinson, F. Glorius, J. Wencel-Delord, *Chem. Soc. Rev.* **2016**, *45*, 2900–2936.
- [30] a) H. M. L. Davies, K. Liao, *Nat. Rev. Chem.* **2019**, *3*, 347–360; b) M. P. Doyle, R. Duffy, M. Ratnikov, L. Zhou, *Chem. Rev.* **2010**, *110*, 704–724; c) H. M. L. Davies, J. R. Manning, *Nature* **2008**, *451*, 417–424; d) H. M. L. Davies, X. Dai, in *Comprehensive Organometallic Chemistry III* (Eds.: D. M. P. Mingos, R. H. Crabtree), Elsevier, Oxford, **2007**, pp. 167–212; e) H. M. L. Davies, R. E. J. Beckwith, *Chem. Rev.* **2003**, *103*, 2861–2904.
- [31] a) H. Yi, G. Zhang, H. Wang, Z. Huang, J. Wang, A. K. Singh, A. Lei, *Chem. Rev.* **2017**, *117*, 9016–9085; b) J.-T. Yu, C. Pan, *Chem. Commun.* **2016**, *52*, 2220–2236.
- [32] a) L. Ackermann, *Chem. Rev.* **2011**, *111*, 1315–1345; b) D. Balcells, E. Clot, O. Eisenstein, *Chem. Rev.* **2010**, *110*, 749–823; c) Y. Boutadla, D. L. Davies, S. A. Macgregor, A. I. Poblador-Bahamonde, *Dalton Trans.* **2009**, 5820–5831.
- [33] B. Biswas, M. Sugimoto, S. Sakaki, *Organometallics* **2000**, *19*, 3895–3908.
- [34] a) D. Lapointe, K. Fagnou, *Chem. Lett.* **2010**, *39*, 1118–1126; b) S. I. Gorelsky, D. Lapointe, K. Fagnou, *J. Am. Chem. Soc.* **2008**, *130*, 10848–10849; c) L.-C. Campeau, M. Parisien, A. Jean, K. Fagnou, *J. Am. Chem. Soc.* **2006**, *128*, 581–590; d) D. García-Cuadrado, A. A. C. Braga, F. Maseras, A. M. Echavarren, *J. Am. Chem. Soc.* **2006**, *128*, 1066–1067.

- [35] a) R. A. Alharis, C. L. McMullin, D. L. Davies, K. Singh, S. A. Macgregor, *J. Am. Chem. Soc.* **2019**, *141*, 8896–8906; b) Y. Boutadla, D. L. Davies, S. A. Macgregor, A. I. Poblador-Bahamonde, *Dalton Trans.* **2009**, 5887–5893.
- [36] J. Oxgaard, W. J. Tenn, R. J. Nielsen, R. A. Periana, W. A. Goddard, *Organometallics* **2007**, *26*, 1565–1567.
- [37] a) E. Tan, O. Quinonero, M. Elena de Orbe, A. M. Echavarren, *ACS Catal.* **2018**, *8*, 2166–2172; b) D. Zell, M. Bursch, V. Müller, S. Grimme, L. Ackermann, *Angew. Chem. Int. Ed.* **2017**, *56*, 10378–10382; c) D. Santrač, S. Cella, W. Wang, L. Ackermann, *Eur. J. Org. Chem.* **2016**, 5429–5436; d) H. Wang, M. Moselage, M. J. González, L. Ackermann, *ACS Catal.* **2016**, *6*, 2705–2709; e) R. Mei, J. Loup, L. Ackermann, *ACS Catal.* **2016**, *6*, 793–797; f) C. Tirler, L. Ackermann, *Tetrahedron* **2015**, *71*, 4543–4551; g) W. Ma, R. Mei, G. Tenti, L. Ackermann, *Chem. Eur. J.* **2014**, *20*, 15248–15251.
- [38] a) C. Sambigioglio, D. Schönbauer, R. Blicek, T. Dao-Huy, G. Pototschnig, P. Schaaf, T. Wiesinger, M. F. Zia, J. Wencel-Delord, T. Besset, B. U. W. Maes, M. Schnürch, *Chem. Soc. Rev.* **2018**, *47*, 6603–6743; b) Z. Chen, B. Wang, J. Zhang, W. Yu, Z. Liu, Y. Zhang, *Org. Chem. Front.* **2015**, *2*, 1107–1295.
- [39] S. De Sarkar, W. Liu, S. I. Kozhushkov, L. Ackermann, *Adv. Synth. Catal.* **2014**, *356*, 1461–1479.
- [40] a) W. Ma, P. Gandeepan, J. Li, L. Ackermann, *Org. Chem. Front.* **2017**, *4*, 1435–1467; b) F. Zhang, D. R. Spring, *Chem. Soc. Rev.* **2014**, *43*, 6906–6919.
- [41] P. Gandeepan, L. Ackermann, *Chem* **2018**, *4*, 199–222.
- [42] a) <http://www.infomine.com/investment/metal-prices/> (consulted on 11.04.2019); b) <https://mineralprices.com/> (consulted on 11.04.2019).
- [43] J. W. Morgan, E. Anders, *Proc. Natl. Acad. Sci. USA* **1980**, *77*, 6973–6977.
- [44] a) P. B. Tchounwou, C. G. Yedjou, A. K. Patlolla, D. J. Sutton, in *Molecular, clinical, and environmental toxicology* (Ed.: A. Luch), Springer, Basel, **2009**, pp. 133–164; b) S. H. Gilani, Y. Alibhai, *J. Toxicol. Environ. Health* **1990**, *30*, 23–31.

- [45] P. Gandeepan, T. Müller, D. Zell, G. Cera, S. Warratz, L. Ackermann, *Chem. Rev.* **2019**, *119*, 2192–2452.
- [46] a) T. Yoshino, S. Matsunaga, *Synlett* **2019**, DOI:10.1055/s-0037-1611814; b) T. Yoshino, S. Matsunaga, *Adv. Synth. Catal.* **2017**, *359*, 1245–1262; c) M. Moselage, J. Li, L. Ackermann, *ACS Catal.* **2016**, *6*, 498–525; d) K. Gao, N. Yoshikai, *Acc. Chem. Res.* **2014**, *47*, 1208–1219.
- [47] a) N. Yoshikai, *Isr. J. Chem.* **2017**, *57*, 1117–1130; b) R. Shang, L. Ilies, E. Nakamura, *Chem. Rev.* **2017**, *117*, 9086–9139; c) G. Cera, L. Ackermann, *Top. Curr. Chem.* **2016**, *374*, 57.
- [48] a) Y. Nakao, in *Catalytic Hydroarylation of Carbon-Carbon Multiple Bonds* (Eds.: L. Ackermann, T. B. Gunnoe, L. G. Habgood), Wiley-VCH, Weinheim, **2017**, pp. 175–192; b) J. Yamaguchi, K. Muto, K. Itami, *Top. Curr. Chem.* **2016**, *374*, 55; c) L. C. M. Castro, N. Chatani, *Chem. Lett.* **2015**, *44*, 410–421.
- [49] a) Y. Hu, B. Zhou, C. Wang, *Acc. Chem. Res.* **2018**, *51*, 816–827; b) W. Liu, L. Ackermann, *ACS Catal.* **2016**, *6*, 3743–3752.
- [50] a) X. Zhu, S. Chiba, *Chem. Soc. Rev.* **2016**, *45*, 4504–4523; b) S. D. McCann, S. S. Stahl, *Acc. Chem. Res.* **2015**, *48*, 1756–1766; c) S. E. Allen, R. R. Walvoord, R. Padilla-Salinas, M. C. Kozlowski, *Chem. Rev.* **2013**, *113*, 6234–6458.
- [51] a) T. G. Saint-Denis, R.-Y. Zhu, G. Chen, Q.-F. Wu, J.-Q. Yu, *Science* **2018**, *359*, eaao4798; b) C. G. Newton, S.-G. Wang, C. C. Oliveira, N. Cramer, *Chem. Rev.* **2017**, *117*, 8908–8976.
- [52] a) J. Loup, U. Dhawa, F. Pesciaioli, J. Wencel-Delord, L. Ackermann, *Angew. Chem. Int. Ed.* **2019**, DOI:10.1002/anie.201904214; b) Ł. Woźniak, N. Cramer, *Trends Chem.* **2019**, DOI:10.1016/j.trechm.2019.03.013.
- [53] The Nobel Prize in Chemistry 2001 - Press Release: <https://www.nobelprize.org/prizes/chemistry/2001/press-release/> (accessed on 11.04.2019).
- [54] F. Hebrard, P. Kalck, *Chem. Rev.* **2009**, *109*, 4272–4282.
- [55] M. S. Kharasch, E. K. Fields, *J. Am. Chem. Soc.* **1941**, *63*, 2316–2320.

- [56] a) H.-W. Lee, F.-Y. Kwong, *Eur. J. Org. Chem.* **2010**, 789–811; b) I. U. Khand, G. R. Knox, P. L. Pauson, W. E. Watts, *J. Chem. Soc., Perkin Trans. 1* **1973**, 975–977; c) I. U. Khand, G. R. Knox, P. L. Pauson, W. E. Watts, *J. Chem. Soc. D* **1971**, 36a.
- [57] a) R. F. Lockwood, K. M. Nicholas, *Tetrahedron Lett.* **1977**, 18, 4163–4165; b) K. M. Nicholas, R. Pettit, *J. Organomet. Chem.* **1972**, 44, C21–C24.
- [58] G. Cahiez, A. Moyeux, *Chem. Rev.* **2010**, 110, 1435–1462.
- [59] a) W. Liu, B. Sahoo, K. Junge, M. Beller, *Acc. Chem. Res.* **2018**, 51, 1858–1869; b) P. J. Chirik, *Acc. Chem. Res.* **2015**, 48, 1687–1695.
- [60] P. Gandeepan, C.-H. Cheng, *Acc. Chem. Res.* **2015**, 48, 1194–1206.
- [61] S. Murahashi, *J. Am. Chem. Soc.* **1955**, 77, 6403–6404.
- [62] S. Murahashi, S. Horie, *J. Am. Chem. Soc.* **1956**, 78, 4816–4817.
- [63] a) S. Camadanli, R. Beck, U. Flörke, H.-F. Klein, *Dalton Trans.* **2008**, 5701–5704; b) R. Beck, H. Sun, X. Li, S. Camadanli, H.-F. Klein, *Eur. J. Inorg. Chem.* **2008**, 3253–3257; c) H.-F. Klein, S. Camadanli, R. Beck, D. Leukel, U. Flörke, *Angew. Chem. Int. Ed.* **2005**, 44, 975–977; d) H.-F. Klein, R. Beck, U. Flörke, H.-J. Haupt, *Eur. J. Inorg. Chem.* **2003**, 1380–1387; e) H.-F. Klein, S. Schneider, M. He, U. Floerke, H.-J. Haupt, *Eur. J. Inorg. Chem.* **2000**, 2295–2301; f) H.-F. Klein, M. Helwig, U. Koch, U. Flörke, H.-J. Haupt, *Z. Naturforsch. B.* **1993**, 48, 778–784.
- [64] G. Halbritter, F. Knoch, A. Wolski, H. Kisch, *Angew. Chem. Int. Ed.* **1994**, 33, 1603–1605.
- [65] a) B. J. Fallon, E. Derat, M. Amatore, C. Aubert, F. Chemla, F. Ferreira, A. Perez-Luna, M. Petit, *Org. Lett.* **2016**, 18, 2292–2295; b) B. J. Fallon, J.-B. Garsi, E. Derat, M. Amatore, C. Aubert, M. Petit, *ACS Catal.* **2015**, 5, 7493–7497; c) B. J. Fallon, E. Derat, M. Amatore, C. Aubert, F. Chemla, F. Ferreira, A. Perez-Luna, M. Petit, *J. Am. Chem. Soc.* **2015**, 137, 2448–2451.
- [66] C. P. Lenges, M. Brookhart, B. E. Grant, *J. Organomet. Chem.* **1997**, 528, 199–203.

- [67] a) Q. Chen, L. Ilies, N. Yoshikai, E. Nakamura, *Org. Lett.* **2011**, *13*, 3232–3234; b) L. Ilies, Q. Chen, X. Zeng, E. Nakamura, *J. Am. Chem. Soc.* **2011**, *133*, 5221–5223.
- [68] N. Yoshikai, *Bull. Chem. Soc. Jpn.* **2014**, *87*, 843–857.
- [69] a) N. Sauermann, J. Loup, D. Kootz, V. R. Yatham, A. Berkessel, L. Ackermann, *Synthesis* **2017**, *49*, 3476–3484; b) J. Li, L. Ackermann, *Chem. Eur. J.* **2015**, *21*, 5718–5722; c) L. Ackermann, *J. Org. Chem.* **2014**, *79*, 8948–8954; d) B. Punji, W. Song, G. A. Shevchenko, L. Ackermann, *Chem. Eur. J.* **2013**, *19*, 10605–10610; e) W. Song, L. Ackermann, *Angew. Chem. Int. Ed.* **2012**, *51*, 8251–8254.
- [70] Selected reviews: a) T. Piou, T. Rovis, *Acc. Chem. Res.* **2018**, *51*, 170–180; b) X. Qi, Y. Li, R. Bai, Y. Lan, *Acc. Chem. Res.* **2017**, *50*, 2799–2808; c) B. Ye, N. Cramer, *Acc. Chem. Res.* **2015**, *48*, 1308–1318; d) G. Song, X. Li, *Acc. Chem. Res.* **2015**, *48*, 1007–1020.
- [71] U. Koelle, B. Fuss, M. V. Rajasekharan, B. L. Ramakrishna, J. H. Ammeter, M. C. Boehm, *J. Am. Chem. Soc.* **1984**, *106*, 4152–4160.
- [72] T. Yoshino, H. Ikemoto, S. Matsunaga, M. Kanai, *Angew. Chem. Int. Ed.* **2013**, *52*, 2207–2211.
- [73] Selected examples: a) W. Li, L.-H. Weng, G.-X. Jin, *Inorg. Chem. Commun.* **2004**, *7*, 1174–1177; b) C. D. Ontiveros, J. A. Morrison, *Organometallics* **1986**, *5*, 1446–1448; c) R. F. Heck, *Inorg. Chem.* **1965**, *4*, 855–857.
- [74] a) M. E. Tauchert, C. D. Incarvito, A. L. Rheingold, R. G. Bergman, J. A. Ellman, *J. Am. Chem. Soc.* **2012**, *134*, 1482–1485; b) Y. Li, X.-S. Zhang, H. Li, W.-H. Wang, K. Chen, B.-J. Li, Z.-J. Shi, *Chem. Sci.* **2012**, *3*, 1634–1639.
- [75] T. Yoshino, H. Ikemoto, S. Matsunaga, M. Kanai, *Chem. Eur. J.* **2013**, *19*, 9142–9146.
- [76] a) P. G. Chirila, C. J. Whiteoak, *Dalton Trans.* **2017**, *46*, 9721–9739; b) S. Wang, S.-Y. Chen, X.-Q. Yu, *Chem. Comm.* **2017**, *53*, 3165–3180.
- [77] a) H. Ikemoto, R. Tanaka, K. Sakata, M. Kanai, T. Yoshino, S. Matsunaga, *Angew. Chem. Int. Ed.* **2017**, *56*, 7156–7160; b) K. Sakata, M. Eda, Y.

- Kitaoka, T. Yoshino, S. Matsunaga, *J. Org. Chem.* **2017**, *82*, 7379–7387; c) R. Tanaka, H. Ikemoto, M. Kanai, T. Yoshino, S. Matsunaga, *Org. Lett.* **2016**, *18*, 5732–5735; d) H. Ikemoto, T. Yoshino, K. Sakata, S. Matsunaga, M. Kanai, *J. Am. Chem. Soc.* **2014**, *136*, 5424–5431.
- [78] A. L. Allred, *J. Inorg. Nucl. Chem.* **1961**, *17*, 215–221.
- [79] D. Zell, Q. Bu, M. Feldt, L. Ackermann, *Angew. Chem. Int. Ed.* **2016**, *55*, 7408–7412.
- [80] S. Nakanowatari, R. Mei, M. Feldt, L. Ackermann, *ACS Catal.* **2017**, *7*, 2511–2515.
- [81] S. Tang, O. Eisenstein, Y. Nakao, S. Sakaki, *Organometallics* **2017**, *36*, 2761–2771.
- [82] F. Pesciaioli, U. Dhawa, J. C. A. Oliveira, R. Yin, M. John, L. Ackermann, *Angew. Chem. Int. Ed.* **2018**, *57*, 15425–15429.
- [83] a) N. Sauermann, M. J. González, L. Ackermann, *Org. Lett.* **2015**, *17*, 5316–5319; b) Z.-Z. Zhang, B. Liu, C.-Y. Wang, B.-F. Shi, *Org. Lett.* **2015**, *17*, 4094–4097.
- [84] a) M. Moselage, N. Sauermann, J. Koeller, W. Liu, D. Gelman, L. Ackermann, *Synlett* **2015**, *26*, 1596–1600; b) T. Gensch, S. Vásquez-Céspedes, D.-G. Yu, F. Glorius, *Org. Lett.* **2015**, *17*, 3714–3717; c) Y. Suzuki, B. Sun, K. Sakata, T. Yoshino, S. Matsunaga, M. Kanai, *Angew. Chem. Int. Ed.* **2015**, *54*, 9944–9947; d) D.-G. Yu, T. Gensch, F. de Azambuja, S. Vásquez-Céspedes, F. Glorius, *J. Am. Chem. Soc.* **2014**, *136*, 17722–17725.
- [85] J. Li, L. Ackermann, *Angew. Chem. Int. Ed.* **2015**, *54*, 8551–8554.
- [86] B. Sun, T. Yoshino, S. Matsunaga, M. Kanai, *Adv. Synth. Catal.* **2014**, *356*, 1491–1495.
- [87] https://pubchem.ncbi.nlm.nih.gov/compound/Tosyl_azide (consulted on 15.04.2019).
- [88] A. B. Pawar, D. M. Lade, *Org. Biomol. Chem.* **2016**, *14*, 3275–3283.
- [89] a) J. Li, L. Ackermann, *Angew. Chem. Int. Ed.* **2015**, *54*, 3635–3638; b) A. B. Pawar, S. Chang, *Org. Lett.* **2015**, *17*, 660–663.

- [90] T. Gensch, F. J. R. Klauck, F. Glorius, *Angew. Chem. Int. Ed.* **2016**, *55*, 11287–11291.
- [91] J. Park, S. Chang, *Angew. Chem. Int. Ed.* **2015**, *54*, 14103–14107.
- [92] Y. Liang, Y.-F. Liang, C. Tang, Y. Yuan, N. Jiao, *Chem. Eur. J.* **2015**, *21*, 16395–16399.
- [93] P. W. Tan, A. M. Mak, M. B. Sullivan, D. J. Dixon, J. Seayad, *Angew. Chem. Int. Ed.* **2017**, *56*, 16550–16554.
- [94] S. Fukagawa, Y. Kato, R. Tanaka, M. Kojima, T. Yoshino, S. Matsunaga, *Angew. Chem. Int. Ed.* **2019**, *58*, 1153–1157.
- [95] D.-Y. Huang, Q.-J. Yao, S. Zhang, X.-T. Xu, K. Zhang, B.-F. Shi, *Org. Lett.* **2019**, *21*, 951–954.
- [96] S. R. Yetra, Z. Shen, H. Wang, L. Ackermann, *Beilstein J. Org. Chem.* **2018**, *14*, 1546–1553.
- [97] Y.-H. Liu, P.-X. Li, Q.-J. Yao, Z.-Z. Zhang, D.-Y. Huang, M. D. Le, H. Song, L. Liu, B.-F. Shi, *Org. Lett.* **2019**, *21*, 1895–1899.
- [98] Y. Sun, N. Cramer, *Chem. Sci.* **2018**, *9*, 2981–2985.
- [99] K. Ozols, Y.-S. Jang, N. Cramer, *J. Am. Chem. Soc.* **2019**, *141*, 5675–5680.
- [100] X. Yu, K. Chen, Q. Wang, W. Zhang, J. Zhu, *Org. Chem. Front.* **2018**, *5*, 994–997.
- [101] B. Audic, M. D. Wodrich, N. Cramer, *Chem. Sci.* **2019**, *10*, 781–787.
- [102] J. Yang, N. Yoshikai, *J. Am. Chem. Soc.* **2014**, *136*, 16748–16751.
- [103] a) D. H. T. Phan, B. Kim, V. M. Dong, *J. Am. Chem. Soc.* **2009**, *131*, 15608–15609; b) K. Kundu, J. V. McCullagh, A. T. Morehead, *J. Am. Chem. Soc.* **2005**, *127*, 16042–16043.
- [104] J. Yang, A. Rérat, Y. J. Lim, C. Gosmini, N. Yoshikai, *Angew. Chem. Int. Ed.* **2017**, *56*, 2449–2453.
- [105] T. Yamakawa, N. Yoshikai, *Chem. Asian J.* **2014**, *9*, 1242–1246.
- [106] P.-S. Lee, N. Yoshikai, *Org. Lett.* **2015**, *17*, 22–25.

- [107] D. K. Kim, J. Riedel, R. S. Kim, V. M. Dong, *J. Am. Chem. Soc.* **2017**, *139*, 10208–10211.
- [108] a) A. Fürstner, *ACS Cent. Sci.* **2016**, *2*, 778–789; b) I. Bauer, H.-J. Knölker, *Chem. Rev.* **2015**, *115*, 3170–3387; c) B. Plietker, *Iron Catalysis in Organic Chemistry*, Wiley-VCH, Weinheim, **2008**; d) S. Enthaler, K. Junge, M. Beller, *Angew. Chem. Int. Ed.* **2008**, *47*, 3317–3321; e) C. Bolm, J. Legros, J. Le Paih, L. Zani, *Chem. Rev.* **2004**, *104*, 6217–6254.
- [109] L. Mond, F. Quincke, *J. Chem. Soc., Trans.* **1891**, *59*, 604–607.
- [110] M. Berthelot, *Hebd. Séances Acad. Sci.* **1891**, *112*, 1343–1349.
- [111] M. S. Kharasch, P. O. Tawney, *J. Am. Chem. Soc.* **1941**, *63*, 2308–2316.
- [112] T. J. Kealy, P. L. Pauson, *Nature* **1951**, *168*, 1039–1040.
- [113] A. Togni, T. Hayashi, *Ferrocenes: Homogeneous Catalysis, Organic Synthesis, Materials Science*, Wiley-VCH, Weinheim, **1995**.
- [114] W. Reppe, H. Vetter, *Liebigs Ann. Chem.* **1953**, *582*, 133–161.
- [115] a) M. Tamura, J. K. Kochi, *J. Am. Chem. Soc.* **1971**, *93*, 1487–1489; b) M. Tamura, J. Kochi, *Synthesis* **1971**, 303–305.
- [116] G. Hata, H. Kondo, A. Miyake, *J. Am. Chem. Soc.* **1968**, *90*, 2278–2281.
- [117] a) M. V. Baker, L. D. Field, *J. Am. Chem. Soc.* **1987**, *109*, 2825–2826; b) J. W. Rathke, E. L. Muetterties, *J. Am. Chem. Soc.* **1975**, *97*, 3272–3273.
- [118] H. H. Karsch, H.-F. Klein, H. Schmidbaur, *Angew. Chem. Int. Ed.* **1975**, *14*, 637–638.
- [119] S. Camadanli, R. Beck, U. Flörke, H.-F. Klein, *Organometallics* **2009**, *28*, 2300–2310.
- [120] W. D. Jones, G. P. Foster, J. M. Putinas, *J. Am. Chem. Soc.* **1987**, *109*, 5047–5048.
- [121] N. Kimura, T. Kochi, F. Kakiuchi, *J. Am. Chem. Soc.* **2017**, *139*, 14849–14852.
- [122] R. Shang, L. Ilies, E. Nakamura, *J. Am. Chem. Soc.* **2016**, *138*, 10132–10135.

- [123] J. Norinder, A. Matsumoto, N. Yoshikai, E. Nakamura, *J. Am. Chem. Soc.* **2008**, *130*, 5858–5859.
- [124] E. Nakamura, Two stories of iron - <https://chemistrycommunity.nature.com/users/209773-eiichi-nakamura/posts/246018-two-stories-of-iron> (consulted on 17.04.2019).
- [125] a) J. J. Sirois, R. Davis, B. DeBoef, *Org. Lett.* **2014**, *16*, 868–871; b) N. Yoshikai, A. Matsumoto, J. Norinder, E. Nakamura, *Angew. Chem. Int. Ed.* **2009**, *48*, 2925–2928.
- [126] L. Ilies, E. Konno, Q. Chen, E. Nakamura, *Asian J. Org. Chem.* **2012**, *1*, 142–145.
- [127] N. Yoshikai, A. Matsumoto, J. Norinder, E. Nakamura, *Synlett* **2010**, 313–316.
- [128] L. Ilies, S. Asako, E. Nakamura, *J. Am. Chem. Soc.* **2011**, *133*, 7672–7675.
- [129] N. Yoshikai, S. Asako, T. Yamakawa, L. Ilies, E. Nakamura, *Chem. Asian J.* **2011**, *6*, 3059–3065.
- [130] L. Ilies, M. Kobayashi, A. Matsumoto, N. Yoshikai, E. Nakamura, *Adv. Synth. Catal.* **2012**, *354*, 593–596.
- [131] Y. Sun, H. Tang, K. Chen, L. Hu, J. Yao, S. Shaik, H. Chen, *J. Am. Chem. Soc.* **2016**, *138*, 3715–3730.
- [132] a) P. Ma, H. Chen, *ACS Catal.* **2019**, *9*, 1962–1972; b) J. N. Harvey, R. Poli, K. M. Smith, *Coord. Chem. Rev.* **2003**, *238–239*, 347–361; c) D. Schröder, S. Shaik, H. Schwarz, *Acc. Chem. Res.* **2000**, *33*, 139–145.
- [133] H. Tang, X.-R. Huang, J. Yao, H. Chen, *J. Org. Chem.* **2015**, *80*, 4672–4682.
- [134] V. G. Zaitsev, D. Shabashov, O. Daugulis, *J. Am. Chem. Soc.* **2005**, *127*, 13154–13155.
- [135] R. Shang, L. Ilies, A. Matsumoto, E. Nakamura, *J. Am. Chem. Soc.* **2013**, *135*, 6030–6032.
- [136] Q. Gu, H. H. Al Mamari, K. Graczyk, E. Diers, L. Ackermann, *Angew. Chem. Int. Ed.* **2014**, *53*, 3868–3871.

- [137] G. Cera, T. Haven, L. Ackermann, *Angew. Chem. Int. Ed.* **2016**, *55*, 1484–1488.
- [138] a) L. Ilies, S. Ichikawa, S. Asako, T. Matsubara, E. Nakamura, *Adv. Synth. Catal.* **2015**, *357*, 2175–2179; b) K. Graczyk, T. Haven, L. Ackermann, *Chem. Eur. J.* **2015**, *21*, 8812–8815; c) L. Ilies, T. Matsubara, S. Ichikawa, S. Asako, E. Nakamura, *J. Am. Chem. Soc.* **2014**, *136*, 13126–13129; d) E. R. Fruchey, B. M. Monks, S. P. Cook, *J. Am. Chem. Soc.* **2014**, *136*, 13130–13133; e) B. M. Monks, E. R. Fruchey, S. P. Cook, *Angew. Chem. Int. Ed.* **2014**, *53*, 11065–11069.
- [139] S. Asako, L. Ilies, E. Nakamura, *J. Am. Chem. Soc.* **2013**, *135*, 17755–17757.
- [140] G. Cera, T. Haven, L. Ackermann, *Chem. Eur. J.* **2017**, *23*, 3577–3582.
- [141] T. Matsubara, S. Asako, L. Ilies, E. Nakamura, *J. Am. Chem. Soc.* **2014**, *136*, 646–649.
- [142] a) L. Ilies, Y. Itabashi, R. Shang, E. Nakamura, *ACS Catal.* **2017**, *7*, 89–92; b) R. Shang, L. Ilies, S. Asako, E. Nakamura, *J. Am. Chem. Soc.* **2014**, *136*, 14349–14352.
- [143] R. Shang, L. Ilies, E. Nakamura, *J. Am. Chem. Soc.* **2015**, *137*, 7660–7663.
- [144] a) L. Ilies, Y. Arslanoglu, T. Matsubara, E. Nakamura, *Asian J. Org. Chem.* **2018**, *7*, 1327–1329; b) G. Cera, T. Haven, L. Ackermann, *Chem. Commun.* **2017**, *53*, 6460–6463; c) T. Matsubara, L. Ilies, E. Nakamura, *Chem. Asian J.* **2016**, *11*, 380–384.
- [145] J. Mo, T. Müller, J. C. A. Oliveira, L. Ackermann, *Angew. Chem. Int. Ed.* **2018**, *57*, 7719–7723.
- [146] Z. Shen, G. Cera, T. Haven, L. Ackermann, *Org. Lett.* **2017**, *19*, 3795–3798.
- [147] T. Doba, T. Matsubara, L. Ilies, R. Shang, E. Nakamura, *Nat. Catal.* **2019**, *2*, 400–406.
- [148] M. Y. Wong, T. Yamakawa, N. Yoshikai, *Org. Lett.* **2015**, *17*, 442–445.
- [149] M. Jin, L. Adak, M. Nakamura, *J. Am. Chem. Soc.* **2015**, *137*, 7128–7134.

- [150] T. Iwamoto, C. Okuzono, L. Adak, M. Jin, M. Nakamura, *Chem. Commun.* **2019**, 55, 1128–1131.
- [151] J. Loup, D. Zell, J. C. A. Oliveira, H. Keil, D. Stalke, L. Ackermann, *Angew. Chem. Int. Ed.* **2017**, 56, 14197–14201.
- [152] D. Schmiel, H. Butenschön, *Organometallics* **2017**, 36, 4979–4989.
- [153] a) R. Shi, Z. Zhang, X. Hu, *Acc. Chem. Res.* **2019**, 52, 1471–1483; b) E. A. Standley, S. Z. Tasker, K. L. Jensen, T. F. Jamison, *Acc. Chem. Res.* **2015**, 48, 1503–1514; c) V. P. Ananikov, *ACS Catal.* **2015**, 5, 1964–1971; d) S. Z. Tasker, E. A. Standley, T. F. Jamison, *Nature* **2014**, 509, 299–309; e) Y. Tamaru, *Modern organonickel chemistry*, Wiley-VCH, Weinheim, **2005**.
- [154] E. Richmond, J. Moran, *Synthesis* **2018**, 50, 499–513.
- [155] a) D. Ghorai, J. Loup, G. Zanoni, L. Ackermann, *Synlett* **2019**, 30, 429–432; b) C. Zarate, M. van Gemmeren, R. J. Somerville, R. Martin, *Adv. Organomet. Chem.* **2016**, 66, 143–222; c) M. Tobisu, N. Chatani, *Acc. Chem. Res.* **2015**, 48, 1717–1726; d) E. J. Tollefson, L. E. Hanna, E. R. Jarvo, *Acc. Chem. Res.* **2015**, 48, 2344–2353; e) J. Cornella, C. Zarate, R. Martin, *Chem. Soc. Rev.* **2014**, 43, 8081–8097.
- [156] a) O. Eisenstein, J. Milani, R. N. Perutz, *Chem. Rev.* **2017**, 117, 8710–8753; b) T. Ahrens, J. Kohlmann, M. Ahrens, T. Braun, *Chem. Rev.* **2015**, 115, 931–972; c) L. Ackermann, R. Born, J. H. Spatz, D. Meyer, *Angew. Chem. Int. Ed.* **2005**, 44, 7216–7219.
- [157] J. P. Kleiman, M. Dubeck, *J. Am. Chem. Soc.* **1963**, 85, 1544–1545.
- [158] For examples of C–H nickelation of activated positions, see: a) A. L. Keen, S. A. Johnson, *J. Am. Chem. Soc.* **2006**, 128, 1806–1807; b) N. M. Brunkan, D. M. Brestensky, W. D. Jones, *J. Am. Chem. Soc.* **2004**, 126, 3627–3641; c) N. D. Clement, K. J. Cavell, C. Jones, C. J. Elsevier, *Angew. Chem. Int. Ed.* **2004**, 43, 1277–1279; d) N. D. Clement, K. J. Cavell, *Angew. Chem. Int. Ed.* **2004**, 43, 3845–3847; e) S. Ogoshi, M. Ueta, M.-a. Oka, H. Kurosawa, *Chem. Commun.* **2004**, 2732–2733; f) T. Tsuda, T. Kiyoi, T. Saegusa, *J. Org. Chem.* **1990**, 55, 2554–2558.

- [159] L.-C. Liang, P.-S. Chien, Y.-L. Huang, *J. Am. Chem. Soc.* **2006**, *128*, 15562–15563.
- [160] Y. Nakao, K. S. Kanyiva, S. Oda, T. Hiyama, *J. Am. Chem. Soc.* **2006**, *128*, 8146–8147.
- [161] A. J. Nett, W. Zhao, P. M. Zimmerman, J. Montgomery, *J. Am. Chem. Soc.* **2015**, *137*, 7636–7639.
- [162] T. Mukai, K. Hirano, T. Satoh, M. Miura, *J. Org. Chem.* **2009**, *74*, 6410–6413.
- [163] K. S. Kanyiva, Y. Nakao, T. Hiyama, *Heterocycles* **2007**, *72*, 677–680.
- [164] K. S. Kanyiva, F. Löbermann, Y. Nakao, T. Hiyama, *Tetrahedron Lett.* **2009**, *50*, 3463–3466.
- [165] K. S. Kanyiva, Y. Nakao, T. Hiyama, *Angew. Chem. Int. Ed.* **2007**, *46*, 8872–8874.
- [166] a) C.-C. Tsai, W.-C. Shih, C.-H. Fang, C.-Y. Li, T.-G. Ong, G. P. A. Yap, *J. Am. Chem. Soc.* **2010**, *132*, 11887–11889; b) Y. Nakao, K. S. Kanyiva, T. Hiyama, *J. Am. Chem. Soc.* **2008**, *130*, 2448–2449.
- [167] Y. Nakao, H. Idei, K. S. Kanyiva, T. Hiyama, *J. Am. Chem. Soc.* **2009**, *131*, 15996–15997.
- [168] Y. Nakao, N. Kashihara, K. S. Kanyiva, T. Hiyama, *J. Am. Chem. Soc.* **2008**, *130*, 16170–16171.
- [169] Y. Nakao, H. Idei, K. S. Kanyiva, T. Hiyama, *J. Am. Chem. Soc.* **2009**, *131*, 5070–5071.
- [170] S. Nakanowatari, T. Müller, J. C. A. Oliveira, L. Ackermann, *Angew. Chem. Int. Ed.* **2017**, *56*, 15891–15895.
- [171] a) K. Muto, T. Hatakeyama, J. Yamaguchi, K. Itami, *Chem. Sci.* **2015**, *6*, 6792–6798; b) K. Muto, J. Yamaguchi, K. Itami, *J. Am. Chem. Soc.* **2012**, *134*, 169–172; c) K. Amaike, K. Muto, J. Yamaguchi, K. Itami, *J. Am. Chem. Soc.* **2012**, *134*, 13573–13576; d) H. Hitoshi, H. Koji, S. Tetsuya, M. Masahiro, *ChemCatChem* **2010**, *2*, 1403–1406; e) J. Canivet, J. Yamaguchi, I. Ban, K. Itami, *Org. Lett.* **2009**, *11*, 1733–1736; f) H. Hachiya, K. Hirano, T. Satoh, M. Miura, *Org. Lett.* **2009**, *11*, 1737–1740.

- [172] a) T. Yao, K. Hirano, T. Satoh, M. Miura, *Angew. Chem. Int. Ed.* **2012**, *51*, 775–779; b) L. Ackermann, B. Punji, W. Song, *Adv. Synth. Catal.* **2011**, *353*, 3325–3329; c) O. Vechorkin, V. Proust, X. Hu, *Angew. Chem. Int. Ed.* **2010**, *49*, 3061–3064; d) T. Yao, K. Hirano, T. Satoh, M. Miura, *Chem. Eur. J.* **2010**, *16*, 12307–12311.
- [173] N. Matsuyama, K. Hirano, T. Satoh, M. Miura, *Org. Lett.* **2009**, *11*, 4156–4159.
- [174] N. Matsuyama, M. Kitahara, K. Hirano, T. Satoh, M. Miura, *Org. Lett.* **2010**, *12*, 2358–2361.
- [175] H. Hachiya, K. Hirano, T. Satoh, M. Miura, *Angew. Chem. Int. Ed.* **2010**, *49*, 2202–2205.
- [176] N. Chatani, *Top. Organomet. Chem.* **2016**, *56*, 19–46.
- [177] A. Yokota, Y. Aihara, N. Chatani, *J. Org. Chem.* **2014**, *79*, 11922–11932.
- [178] a) T. Uemura, M. Yamaguchi, N. Chatani, *Angew. Chem. Int. Ed.* **2016**, *55*, 3162–3165; b) Y. Aihara, J. Wuelbern, N. Chatani, *Bull. Chem. Soc. Jpn.* **2015**, *88*, 438–446; c) W. Song, S. Lackner, L. Ackermann, *Angew. Chem. Int. Ed.* **2014**, *53*, 2477–2480; d) Y. Aihara, N. Chatani, *J. Am. Chem. Soc.* **2013**, *135*, 5308–5311.
- [179] a) V. G. Landge, C. H. Shewale, G. Jaiswal, M. K. Sahoo, S. P. Midya, E. Balaraman, *Catal. Sci. Technol.* **2016**, *6*, 1946–1951; b) Y.-J. Liu, Y.-H. Liu, S.-Y. Yan, B.-F. Shi, *Chem. Commun.* **2015**, *51*, 6388–6391; c) J. Yi, L. Yang, C. Xia, F. Li, *J. Org. Chem.* **2015**, *80*, 6213–6221.
- [180] Y.-H. Liu, Y.-J. Liu, S.-Y. Yan, B.-F. Shi, *Chem. Commun.* **2015**, *51*, 11650–11653.
- [181] H. Shiota, Y. Ano, Y. Aihara, Y. Fukumoto, N. Chatani, *J. Am. Chem. Soc.* **2011**, *133*, 14952–14955.
- [182] a) N. Barsu, D. Kalsi, B. Sundararaju, *Chem. Eur. J.* **2015**, *21*, 9364–9368; b) X. Cong, Y. Li, Y. Wei, X. Zeng, *Org. Lett.* **2014**, *16*, 3926–3929.
- [183] X. Wu, Y. Zhao, H. Ge, *J. Am. Chem. Soc.* **2015**, *137*, 4924–4927.

- [184] a) V. P. Reddy, R. Qiu, T. Iwasaki, N. Kambe, *Org. Biomol. Chem.* **2015**, *13*, 6803–6813; b) S.-Y. Yan, Y.-J. Liu, B. Liu, Y.-H. Liu, B.-F. Shi, *Chem. Commun.* **2015**, *51*, 4069–4072; c) K. Yang, Y. Wang, X. Chen, A. A. Kadi, H.-K. Fun, H. Sun, Y. Zhang, H. Lu, *Chem. Commun.* **2015**, *51*, 3582–3585.
- [185] a) D. Ghorai, L. H. Finger, G. Zanoni, L. Ackermann, *ACS Catal.* **2018**, *8*, 11657–11662; b) Z. Ruan, D. Ghorai, G. Zanoni, L. Ackermann, *Chem. Commun.* **2017**, *53*, 9113–9116; c) Z. Ruan, S. Lackner, L. Ackermann, *Angew. Chem. Int. Ed.* **2016**, *55*, 3153–3157; d) Z. Ruan, S. Lackner, L. Ackermann, *ACS Catal.* **2016**, *6*, 4690–4693; e) T. Müller, L. Ackermann, *Chem. Eur. J.* **2016**, *22*, 14151–14154.
- [186] a) R. A. Jagtap, C. P. Vinod, B. Punji, *ACS Catal.* **2019**, *9*, 431–441; b) S. M. Khake, S. Jain, U. N. Patel, R. G. Gonnade, K. Vanka, B. Punji, *Organometallics* **2018**, *37*, 2037–2045; c) S. M. Khake, V. Soni, R. G. Gonnade, B. Punji, *Chem. Eur. J.* **2017**, *23*, 2907–2914; d) V. Soni, R. A. Jagtap, R. G. Gonnade, B. Punji, *ACS Catal.* **2016**, *6*, 5666–5672.
- [187] Z. Dong, Z. Ren, S. J. Thompson, Y. Xu, G. Dong, *Chem. Rev.* **2017**, *117*, 9333–9403.
- [188] a) Y. Nakao, *Chem. Rec.* **2011**, *11*, 242–251; b) P. W. N. M. van Leeuwen, in *Stereoselective Synthesis 1, Vol. 1* (Ed.: J. G. de Vries), Georg Thieme Verlag, Stuttgart, **2011**, pp. 409–475.
- [189] Y. Nakao, N. Kashihara, K. S. Kanyiva, T. Hiyama, *Angew. Chem. Int. Ed.* **2010**, *49*, 4451–4454.
- [190] Y.-Y. Jiang, Z. Li, J. Shi, *Organometallics* **2012**, *31*, 4356–4366.
- [191] R. Tamura, Y. Yamada, Y. Nakao, T. Hiyama, *Angew. Chem. Int. Ed.* **2012**, *51*, 5679–5682.
- [192] Y. Nakao, Y. Yamada, N. Kashihara, T. Hiyama, *J. Am. Chem. Soc.* **2010**, *132*, 13666–13668.
- [193] P. A. Donets, N. Cramer, *Angew. Chem. Int. Ed.* **2015**, *54*, 633–637.

- [194] a) W.-C. Chen, Y.-C. Lai, W.-C. Shih, M.-S. Yu, G. P. A. Yap, T.-G. Ong, *Chem. Eur. J.* **2014**, *20*, 8099–8105; b) W.-C. Shih, W.-C. Chen, Y.-C. Lai, M.-S. Yu, J.-J. Ho, G. P. A. Yap, T.-G. Ong, *Org. Lett.* **2012**, *14*, 2046–2049.
- [195] P. A. Donets, N. Cramer, *J. Am. Chem. Soc.* **2013**, *135*, 11772–11775.
- [196] a) S. K. Murphy, V. M. Dong, *Chem. Comm.* **2014**, *50*, 13645–13649; b) J. C. Leung, M. J. Krische, *Chem. Sci.* **2012**, *3*, 2202–2209; c) M. C. Willis, *Chem. Rev.* **2010**, *110*, 725–748.
- [197] a) T. M. Shaikh, C.-M. Weng, F.-E. Hong, *Coord. Chem. Rev.* **2012**, *256*, 771–803; b) L. Ackermann, *Isr. J. Chem.* **2010**, *50*, 652–663; c) L. Ackermann, in *Trivalent Phosphorus Compounds in Asymmetric Catalysis, Synthesis and Applications* (Ed.: A. Börner), Wiley-VCH, Weinheim, **2008**, pp. 831–847; d) L. Ackermann, *Synthesis* **2006**, 1557–1571.
- [198] Y.-X. Wang, M. Ye, *Sci. China Chem.* **2018**, *61*, 1004–1013.
- [199] D. Hirsch-Weil, K. A. Abboud, S. Hong, *Chem. Commun.* **2010**, *46*, 7525–7527.
- [200] J. Diesel, A. M. Finogenova, N. Cramer, *J. Am. Chem. Soc.* **2018**, *140*, 4489–4493.
- [201] a) A. Albright, D. Eddings, R. Black, C. J. Welch, N. N. Gerasimchuk, R. E. Gawley, *J. Org. Chem.* **2011**, *76*, 7341–7351; b) A. Albright, R. E. Gawley, *J. Am. Chem. Soc.* **2011**, *133*, 19680–19683.
- [202] a) V. Singh, Y. Nakao, S. Sakaki, M. M. Deshmukh, *J. Org. Chem.* **2017**, *82*, 289–301; b) A. J. Nett, J. Montgomery, P. M. Zimmerman, *ACS Catal.* **2017**, *7*, 7352–7362; c) J. Guihaumé, S. Halbert, O. Eisenstein, R. N. Perutz, *Organometallics* **2012**, *31*, 1300–1314.
- [203] W.-B. Zhang, X.-T. Yang, J.-B. Ma, Z.-M. Su, S.-L. Shi, *J. Am. Chem. Soc.* **2019**, *141*, 5628–5634.
- [204] a) D. A. Colby, R. G. Bergman, J. A. Ellman, *Chem. Rev.* **2010**, *110*, 624–655; b) J. C. Lewis, R. G. Bergman, J. A. Ellman, *Acc. Chem. Res.* **2008**, *41*, 1013–1025.

- [205] A. T. Normand, S. K. Yen, H. V. Huynh, T. S. A. Hor, K. J. Cavell, *Organometallics* **2008**, *27*, 3153–3160.
- [206] Y.-X. Wang, S.-L. Qi, Y.-X. Luan, X.-W. Han, S. Wang, H. Chen, M. Ye, *J. Am. Chem. Soc.* **2018**, *140*, 5360–5364.
- [207] X. Linghu, J. R. Potnick, J. S. Johnson, *J. Am. Chem. Soc.* **2004**, *126*, 3070–3071.
- [208] Q.-S. Liu, D.-Y. Wang, Z.-J. Yang, Y.-X. Luan, J.-F. Yang, J.-F. Li, Y.-G. Pu, M. Ye, *J. Am. Chem. Soc.* **2017**, *139*, 18150–18153.
- [209] K. Ogata, Y. Atsuumi, D. Shimada, S.-i. Fukuzawa, *Angew. Chem. Int. Ed.* **2011**, *50*, 5896–5899.
- [210] J. S. E. Ahlin, N. Cramer, *Org. Lett.* **2016**, *18*, 3242–3245.
- [211] T. J. Seiders, D. W. Ward, R. H. Grubbs, *Org. Lett.* **2001**, *3*, 3225–3228.
- [212] a) S. Grélaud, P. Cooper, L. J. Feron, J. F. Bower, *J. Am. Chem. Soc.* **2018**, *140*, 9351–9356; b) T. Shibata, M. Michino, H. Kurita, Y.-k. Tahara, K. S. Kanyiva, *Chem. Eur. J.* **2017**, *23*, 88–91; c) M. Hatano, Y. Ebe, T. Nishimura, H. Yorimitsu, *J. Am. Chem. Soc.* **2016**, *138*, 4010–4013; d) T. Shibata, N. Ryu, H. Takano, *Adv. Synth. Catal.* **2015**, *357*, 1131–1135; e) Y. Ebe, T. Nishimura, *J. Am. Chem. Soc.* **2015**, *137*, 5899–5902; f) C. S. Sevov, J. F. Hartwig, *J. Am. Chem. Soc.* **2013**, *135*, 2116–2119; g) S. Pan, N. Ryu, T. Shibata, *J. Am. Chem. Soc.* **2012**, *134*, 17474–17477; h) R. Dorta, A. Togni, *Chem. Commun.* **2003**, 760–761.
- [213] a) C. M. Filloux, T. Rovis, *J. Am. Chem. Soc.* **2015**, *137*, 508–517; b) B. Ye, P. A. Donets, N. Cramer, *Angew. Chem. Int. Ed.* **2014**, *53*, 507–511; c) B. Ye, N. Cramer, *J. Am. Chem. Soc.* **2013**, *135*, 636–639; d) A. S. Tsai, R. M. Wilson, H. Harada, R. G. Bergman, J. A. Ellman, *Chem. Commun.* **2009**, 3910–3912; e) H. Harada, R. K. Thalji, R. G. Bergman, J. A. Ellman, *J. Org. Chem.* **2008**, *73*, 6772–6779; f) R. M. Wilson, R. K. Thalji, R. G. Bergman, J. A. Ellman, *Org. Lett.* **2006**, *8*, 1745–1747; g) R. K. Thalji, J. A. Ellman, R. G. Bergman, *J. Am. Chem. Soc.* **2004**, *126*, 7192–7193; h) F. Kakiuchi, P. Le Gendre, A. Yamada, H. Ohtaki, S. Murai, *Tetrahedron: Asymmetry* **2000**, *11*,

- 2647–2651; i) N. Fujii, F. Kakiuchi, A. Yamada, N. Chatani, S. Murai, *Chem. Lett.* **1997**, 26, 425–426.
- [214] S. Rodewald, R. F. Jordan, *J. Am. Chem. Soc.* **1994**, 116, 4491–4492.
- [215] G. Song, W. W. N. O, Z. Hou, *J. Am. Chem. Soc.* **2014**, 136, 12209–12212.
- [216] a) Y. Segawa, T. Maekawa, K. Itami, *Angew. Chem. Int. Ed.* **2015**, 54, 66–81; b) L. McMurray, F. O'Hara, M. J. Gaunt, *Chem. Soc. Rev.* **2011**, 40, 1885–1898; c) O. Baudoin, *Chem. Soc. Rev.* **2011**, 40, 4902–4911.
- [217] a) D. Hazelard, P.-A. Nocquet, P. Compain, *Org. Chem. Front.* **2017**, 4, 2500–2521; b) P. Subramanian, G. C. Rudolf, K. P. Kaliappan, *Chem. Asian J.* **2016**, 11, 168–192; c) M.-L. Louillat, F. W. Patureau, *Chem. Soc. Rev.* **2014**, 43, 901–910; d) F. Collet, C. Lescot, P. Dauban, *Chem. Soc. Rev.* **2011**, 40, 1926–1936.
- [218] J. Loup, T. Parchomyk, S. Lülfi, S. Demeshko, F. Meyer, K. Koszinowski, L. Ackermann, *Dalton Trans.* **2019**, 48, 5135–5139.
- [219] a) J. C. Rech, M. Yato, D. Duckett, B. Ember, P. V. LoGrasso, R. G. Bergman, J. A. Ellman, *J. Am. Chem. Soc.* **2007**, 129, 490–491; b) K. L. Tan, A. Vasudevan, R. G. Bergman, J. A. Ellman, A. J. Souers, *Org. Lett.* **2003**, 5, 2131–2134; c) K. L. Tan, R. G. Bergman, J. A. Ellman, *J. Am. Chem. Soc.* **2002**, 124, 3202–3203; d) K. L. Tan, R. G. Bergman, J. A. Ellman, *J. Am. Chem. Soc.* **2001**, 123, 2685–2686.
- [220] J. Loup, V. Müller, D. Ghorai, L. Ackermann, *Angew. Chem. Int. Ed.* **2019**, 58, 1749–1753.
- [221] a) K. M. Nelson, C. E. Salomon, C. C. Aldrich, *J. Nat. Prod.* **2012**, 75, 1037–1043; b) Q. Li, K. W. Woods, A. Claiborne, I. I. S. L. Gwaltney, K. J. Barr, G. Liu, L. Gehrke, R. B. Credo, Y. H. Hui, J. Lee, R. B. Warner, P. Kovar, M. A. Nukkala, N. A. Zielinski, S. K. Tahir, M. Fitzgerald, K. H. Kim, K. Marsh, D. Frost, S.-C. Ng, S. Rosenberg, H. L. Sham, *Bioorg. Med. Chem. Lett.* **2002**, 12, 465–469; c) G. A. Snow, *Biochem J.* **1965**, 97, 166–175.
- [222] a) D. Clark, B. Finkelstein, G. Lahm, T. Selby, T. Stevenson, WO 2003016304 A1, 2003; b) J. Suzuki, T. Ishida, I. Shibuya, K. Toda, *J. Pestic. Sci.* **2001**, 26, 215–223.

- [223] a) T. G. Gant, A. I. Meyers, *Tetrahedron* **1994**, *50*, 2297–2360; b) A. I. Meyers, E. D. Mihelich, *Angew. Chem. Int. Ed.* **1976**, *15*, 270–281; c) J. A. Frump, *Chem. Rev.* **1971**, *71*, 483–505.
- [224] a) G. Yang, W. Zhang, *Chem. Soc. Rev.* **2018**, *47*, 1783–1810; b) G. Desimoni, G. Faita, K. A. Jørgensen, *Chem. Rev.* **2011**, *111*, PR284–PR437; c) C. C. Bausch, A. Pfaltz, in *Privileged Chiral Ligands and Catalysts* (Ed.: Q. L. Zhou), Wiley-VCH, Weinheim, **2011**, pp. 221–256; d) G. C. Hargaden, P. J. Guiry, *Chem. Rev.* **2009**, *109*, 2505–2550; e) G. Desimoni, G. Faita, K. A. Jørgensen, *Chem. Rev.* **2006**, *106*, 3561–3651; f) H. A. McManus, P. J. Guiry, *Chem. Rev.* **2004**, *104*, 4151–4202; g) G. Desimoni, G. Faita, P. Quadrelli, *Chem. Rev.* **2003**, *103*, 3119–3154.
- [225] a) L. Gupta, A. C. Hoepker, K. J. Singh, D. B. Collum, *J. Org. Chem.* **2009**, *74*, 2231–2233; b) C. G. Hartung, V. Snieckus, in *Modern Arene Chemistry* (Ed.: D. Astruc), Wiley-VCH, Weinheim, **2002**, pp. 330–367; c) E. Wehman, G. Van Koten, J. T. B. H. Jastrzebski, M. A. Rotteveel, C. H. Stam, *Organometallics* **1988**, *7*, 1477–1485.
- [226] Y. Park, S. Jee, J. G. Kim, S. Chang, *Org. Process Res. Dev.* **2015**, *19*, 1024–1029.
- [227] a) R. Mei, Doctoral thesis, Georg-August-Universität Göttingen, **2017**; b) R. Mei, L. Ackermann, *unpublished results*.
- [228] a) P. Dubé, N. F. F. Nathel, M. Vetelino, M. Couturier, C. L. Aboussafy, S. Pichette, M. L. Jorgensen, M. Hardink, *Org. Lett.* **2009**, *11*, 5622–5625; b) E. Eibler, J. Käsbauer, H. Pohl, J. Sauer, *Tetrahedron Lett.* **1987**, *28*, 1097–1100; c) J. Sauer, K. K. Mayer, *Tetrahedron Lett.* **1968**, *9*, 319–324.
- [229] a) V. Bizet, C. Bolm, *Eur. J. Org. Chem.* **2015**, 2854–2860; b) V. Bizet, L. Buglioni, C. Bolm, *Angew. Chem. Int. Ed.* **2014**, *53*, 5639–5642.
- [230] T. K. Hyster, D. M. Dalton, T. Rovis, *Chem. Sci.* **2015**, *6*, 254–258.
- [231] X.-K. Guo, L.-B. Zhang, D. Wei, J.-L. Niu, *Chem. Sci.* **2015**, *6*, 7059–7071.
- [232] a) H. Pellissier, *Coord. Chem. Rev.* **2019**, *386*, 1–31; b) K. Gopalaiah, *Chem. Rev.* **2013**, *113*, 3248–3296.

- [233] a) N. V. Tkachenko, O. Y. Lyakin, D. G. Samsonenko, E. P. Talsi, K. P. Bryliakov, *Catal. Commun.* **2018**, *104*, 112–117; b) S. Narute, D. Pappo, *Org. Lett.* **2017**, *19*, 2917–2920; c) S. Narute, R. Parnes, F. D. Toste, D. Pappo, *J. Am. Chem. Soc.* **2016**, *138*, 16553–16560; d) H. Egami, K. Matsumoto, T. Oguma, T. Kunisu, T. Katsuki, *J. Am. Chem. Soc.* **2010**, *132*, 13633–13635.
- [234] J. T. Groves, P. Viski, *J. Am. Chem. Soc.* **1989**, *111*, 8537–8538.
- [235] a) C. Johnson, M. Albrecht, *Coord. Chem. Rev.* **2017**, *352*, 1–14; b) K. Riener, S. Haslinger, A. Raba, M. P. Högerl, M. Cokoja, W. A. Herrmann, F. E. Kühn, *Chem. Rev.* **2014**, *114*, 5215–5272; c) D. Bézier, J.-B. Sortais, C. Darcel, *Adv. Synth. Catal.* **2013**, *355*, 19–33; d) F. Wang, L.-j. Liu, W. Wang, S. Li, M. Shi, *Coord. Chem. Rev.* **2012**, *256*, 804–853.
- [236] D. Janssen-Müller, C. Schleppehorst, F. Glorius, *Chem. Soc. Rev.* **2017**, *46*, 4845–4854.
- [237] V. R. Yatham, W. Harnying, D. Kootz, J.-M. Neudörfl, N. E. Schlörer, A. Berkessel, *J. Am. Chem. Soc.* **2016**, *138*, 2670–2677.
- [238] V. Lavallo, Y. Canac, C. Präsang, B. Donnadiou, G. Bertrand, *Angew. Chem. Int. Ed.* **2005**, *44*, 5705–5709.
- [239] a) L. Ackermann, A. R. Kapdi, C. Schulzke, *Org. Lett.* **2010**, *12*, 2298–2301; b) L. Ackermann, R. Born, *Angew. Chem. Int. Ed.* **2005**, *44*, 2444–2447; c) L. Ackermann, *Org. Lett.* **2005**, *7*, 3123–3125.
- [240] a) E. McNeill, T. Ritter, *Acc. Chem. Res.* **2015**, *48*, 2330–2343; b) M. D. Greenhalgh, A. S. Jones, S. P. Thomas, *ChemCatChem* **2015**, *7*, 190–222.
- [241] J. S. E. Ahlin, P. A. Donets, N. Cramer, *Angew. Chem. Int. Ed.* **2014**, *53*, 13229–13233.
- [242] Selected examples: a) H. Wang, G. Lu, G. J. Sormunen, H. A. Malik, P. Liu, J. Montgomery, *J. Am. Chem. Soc.* **2017**, *139*, 9317–9324; b) R. Savka, M. Bergmann, Y. Kanai, S. Foro, H. Plenio, *Chem. Eur. J.* **2016**, *22*, 9667–9675; c) C.-Y. Ho, C.-W. Chan, L. He, *Angew. Chem. Int. Ed.* **2015**, *54*, 4512–4516; d) L. Wu, L. Falivene, E. Drinkel, S. Grant, A. Linden, L. Cavallo, R. Dorta, *Angew. Chem. Int. Ed.* **2012**, *51*, 2870–2873; e) T. W. Funk, J. M. Berlin, R.

- H. Grubbs, *J. Am. Chem. Soc.* **2006**, *128*, 1840–1846; f) J. M. Berlin, S. D. Goldberg, R. H. Grubbs, *Angew. Chem. Int. Ed.* **2006**, *45*, 7591–7595.
- [243] M.-A. Abadie, K. MacIntyre, C. Boulho, P. Hoggan, F. Capet, F. Agbossou-Niedercorn, C. Michon, *Organometallics* **2019**, *38*, 536–543.
- [244] Selected references: a) Y. Zhou, Y. Shi, S. Torker, A. H. Hoveyda, *J. Am. Chem. Soc.* **2018**, *140*, 16842–16854; b) V. Pace, J. P. Rae, H. Y. Harb, D. J. Procter, *Chem. Commun.* **2013**, *49*, 5150–5152; c) K.-s. Lee, A. H. Hoveyda, *J. Org. Chem.* **2009**, *74*, 4455–4462.
- [245] a) R. Agata, T. Iwamoto, N. Nakagawa, K. Isozaki, T. Hatakeyama, H. Takaya, M. Nakamura, *Synthesis* **2015**, *47*, 1733–1740; b) T. Hatakeyama, S. Hashimoto, K. Ishizuka, M. Nakamura, *J. Am. Chem. Soc.* **2009**, *131*, 11949–11963; c) T. Hatakeyama, M. Nakamura, *J. Am. Chem. Soc.* **2007**, *129*, 9844–9845.
- [246] a) H. Blaser, B. Pugin, F. Spindler, E. Mejía, A. Togni, in *Privileged Chiral Ligands and Catalysts* (Ed.: Q. L. Zhou), Wiley-VCH, Weinheim, **2011**, pp. 93–136; b) L.-X. Dai, X.-L. Hou, *Chiral Ferrocenes in Asymmetric Catalysis: Synthesis and Applications*, Wiley-VCH, Weinheim, **2010**.
- [247] a) R. Pietschnig, *Chem. Soc. Rev.* **2016**, *45*, 5216–5231; b) S. Barlow, S. R. Marder, in *Functional Organic Materials* (Eds.: T. J. J. Müller, U. H. F. Bunz), Wiley-VCH, Weinheim, **2007**, pp. 393–437.
- [248] a) M. Patra, G. Gasser, *Nat. Rev. Chem.* **2017**, *1*, 0066; b) K. Kowalski, *Coord. Chem. Rev.* **2016**, *317*, 132–156; c) G. Jaouen, A. Vessières, S. Top, *Chem. Soc. Rev.* **2015**, *44*, 8802–8817; d) D. R. van Staveren, N. Metzler-Nolte, *Chem. Rev.* **2004**, *104*, 5931–5986.
- [249] a) D. Katayev, E. Larionov, M. Nakanishi, C. Besnard, E. P. Kündig, *Chem. Eur. J.* **2014**, *20*, 15021–15030; b) E. P. Kündig, T. M. Seidel, Y.-x. Jia, G. Bernardinelli, *Angew. Chem. Int. Ed.* **2007**, *46*, 8484–8487.
- [250] J. S. Renny, L. L. Tomasevich, E. H. Tallmadge, D. B. Collum, *Angew. Chem. Int. Ed.* **2013**, *52*, 11998–12013.
- [251] a) M. D. Greenhalgh, S. P. Thomas, *J. Am. Chem. Soc.* **2012**, *134*, 11900–11903; b) E. Shirakawa, D. Ikeda, S. Masui, M. Yoshida, T. Hayashi, *J. Am.*

- Chem. Soc.* **2012**, *134*, 272–279; c) E. Shirakawa, D. Ikeda, S. Yamaguchi, T. Hayashi, *Chem. Commun.* **2008**, 1214–1216; d) J. Vela, S. Vaddadi, T. R. Cundari, J. M. Smith, E. A. Gregory, R. J. Lachicotte, C. J. Flaschenriem, P. L. Holland, *Organometallics* **2004**, *23*, 5226–5239; e) J. Vela, J. M. Smith, R. J. Lachicotte, P. L. Holland, *Chem. Commun.* **2002**, 2886–2887; f) D. L. Reger, E. C. Culbertson, *Inorg. Chem.* **1977**, *16*, 3104–3107.
- [252] V. Prelog, G. Helmchen, *Angew. Chem. Int. Ed.* **1982**, *21*, 567–583.
- [253] K. M. Engle, T.-S. Mei, M. Wasa, J.-Q. Yu, *Acc. Chem. Res.* **2012**, *45*, 788–802.
- [254] V. Lanke, K. Ramaiah Prabhu, *Org. Lett.* **2013**, *15*, 6262–6265.
- [255] R. Manikandan, M. Jeganmohan, *Chem. Commun.* **2017**, *53*, 8931–8947.
- [256] J. C. A. Oliveira, L. Ackermann, *unpublished results*.
- [257] E. M. Simmons, J. F. Hartwig, *Angew. Chem. Int. Ed.* **2012**, *51*, 3066–3072.
- [258] R. B. Bedford, M. Betham, D. W. Bruce, S. A. Davis, R. M. Frost, M. Hird, *Chem. Commun.* **2006**, 1398–1400.
- [259] T. Satyanarayana, S. Abraham, H. B. Kagan, *Angew. Chem. Int. Ed.* **2009**, *48*, 456–494.
- [260] B. Zhou, H. Sato, L. Ilies, E. Nakamura, *ACS Catal.* **2018**, *8*, 8–11.
- [261] T. Hatanaka, Y. Ohki, K. Tatsumi, *Chem. Asian J.* **2010**, *5*, 1657–1666.
- [262] A. A. Danopoulos, A. Massard, G. Frison, P. Braunstein, *Angew. Chem. Int. Ed.* **2018**, *57*, 14550–14554.
- [263] a) R. Martin, A. Fürstner, *Angew. Chem. Int. Ed.* **2004**, *43*, 3955–3957; b) A. Fürstner, A. Leitner, *Angew. Chem. Int. Ed.* **2002**, *41*, 609–612; c) A. Fürstner, A. Leitner, M. Méndez, H. Krause, *J. Am. Chem. Soc.* **2002**, *124*, 13856–13863.
- [264] A. Casitas, J. A. Rees, R. Goddard, E. Bill, S. DeBeer, A. Fürstner, *Angew. Chem. Int. Ed.* **2017**, *56*, 10108–10113.
- [265] R. B. Bedford, *Acc. Chem. Res.* **2015**, *48*, 1485–1493.

- [266] In this context, low-valent iron species have been defined as having an oxidation state below 2+ (See Ref. [268b]).
- [267] T. Parchomyk, S. Demeshko, F. Meyer, K. Koszinowski, *J. Am. Chem. Soc.* **2018**, *140*, 9709–9720.
- [268] a) M. L. Neidig, S. H. Carpenter, D. J. Curran, J. C. DeMuth, V. E. Fleischauer, T. E. Iannuzzi, P. G. N. Neate, J. D. Sears, N. J. Wolford, *Acc. Chem. Res.* **2019**, *52*, 140–150; b) J. D. Sears, P. G. N. Neate, M. L. Neidig, *J. Am. Chem. Soc.* **2018**, *140*, 11872–11883; c) S. B. Muñoz III, S. L. Daifuku, J. D. Sears, T. M. Baker, S. H. Carpenter, W. W. Brennessel, M. L. Neidig, *Angew. Chem. Int. Ed.* **2018**, *57*, 6496–6500; d) S. H. Carpenter, T. M. Baker, S. B. Muñoz III, W. W. Brennessel, M. L. Neidig, *Chem. Sci.* **2018**, *9*, 7931–7939; e) T. Parchomyk, K. Koszinowski, *Synthesis* **2017**, *49*, 3269–3280; f) S. H. Carpenter, M. L. Neidig, *Isr. J. Chem.* **2017**, *57*, 1106–1116; g) J. L. Kneebone, W. W. Brennessel, M. L. Neidig, *J. Am. Chem. Soc.* **2017**, *139*, 6988–7003; h) S. B. Muñoz III, S. L. Daifuku, W. W. Brennessel, M. L. Neidig, *J. Am. Chem. Soc.* **2016**, *138*, 7492–7495; i) S. L. Daifuku, M. H. Al-Afyouni, B. E. R. Snyder, J. L. Kneebone, M. L. Neidig, *J. Am. Chem. Soc.* **2014**, *136*, 9132–9143; j) M. H. Al-Afyouni, K. L. Fillman, W. W. Brennessel, M. L. Neidig, *J. Am. Chem. Soc.* **2014**, *136*, 15457–15460.
- [269] a) T. Parchomyk, K. Koszinowski, *Chem. Eur. J.* **2017**, *23*, 3213–3219; b) T. Parchomyk, K. Koszinowski, *Chem. Eur. J.* **2016**, *22*, 15609–15613.
- [270] T. Parchomyk, K. Koszinowski, *Chem. Eur. J.* **2018**, *24*, 16342–16347.
- [271] P. Gütllich, E. Bill, A. X. Trautwein, *Mössbauer Spectroscopy and Transition Metal Chemistry*, Springer, Heidelberg, **2011**.
- [272] a) Y. O. Wong, L. A. Freeman, A. D. Agakidou, D. A. Dickie, C. E. Webster, R. J. Gilliard, *Organometallics* **2019**, *38*, 688–696; b) A. R. Kennedy, R. E. Mulvey, S. D. Robertson, *Dalton Trans.* **2010**, *39*, 9091–9099; and references therein.
- [273] a) D. Grassi, A. Alexakis, *Adv. Synth. Catal.* **2015**, *357*, 3171–3186; b) O. Jackowski, A. Alexakis, *Angew. Chem. Int. Ed.* **2010**, *49*, 3346–3350; and references therein.

- [274] A. M. Messinis, S. L. J. Luckham, P. P. Wells, D. Gianolio, E. K. Gibson, H. M. O'Brien, H. A. Sparkes, S. A. Davis, J. Callison, D. Elorriaga, O. Hernandez-Fajardo, R. B. Bedford, *Nat. Catal.* **2019**, *2*, 123–133.
- [275] C. Schnegelsberg, T. D. Blümke, K. Koszinowski, *J. Mass Spectrom.* **2015**, *50*, 1393–1395.
- [276] Different fits with five subspectra are possible.
- [277] a) S. B. Muñoz III, V. E. Fleischauer, W. W. Brennessel, M. L. Neidig, *Organometallics* **2018**, *37*, 3093–3101; b) V. E. Fleischauer, S. B. Muñoz III, P. G. N. Neate, W. W. Brennessel, M. L. Neidig, *Chem. Sci.* **2018**, *9*, 1878–1891; c) K. L. Fillman, J. A. Przyojski, M. H. Al-Afyouni, Z. J. Tonzetich, M. L. Neidig, *Chem. Sci.* **2015**, *6*, 1178–1188; d) Y. Liu, L. Wang, L. Deng, *Organometallics* **2015**, *34*, 4401–4407.
- [278] K. Skowerski, C. Wierzbicka, G. Szczepaniak, Ł. Gułajski, M. Bieniek, K. Grela, *Green Chem.* **2012**, *14*, 3264–3268.
- [279] F. Kraft, T. Parchomyk, K. Koszinowski, *unpublished results*.
- [280] A. Jana, K. Grela, *Chem. Commun.* **2018**, *54*, 122–139.
- [281] a) R. B. Bedford, P. B. Brenner, D. Elorriaga, J. N. Harvey, J. Nunn, *Dalton Trans.* **2016**, *45*, 15811–15817; b) R. B. Bedford, P. B. Brenner, E. Carter, P. M. Cogswell, M. F. Haddow, J. N. Harvey, D. M. Murphy, J. Nunn, C. H. Woodall, *Angew. Chem. Int. Ed.* **2014**, *53*, 1804–1808.
- [282] a) J. Zhao, S. Zhang, W.-X. Zhang, Z. Xi, *Coord. Chem. Rev.* **2014**, *270–271*, 2–13; b) M. J. Wax, R. G. Bergman, *J. Am. Chem. Soc.* **1981**, *103*, 7028–7030.
- [283] a) G. Bringmann, T. Gulder, T. A. M. Gulder, M. Breuning, *Chem. Rev.* **2011**, *111*, 563–639; b) M. C. Kozłowski, B. J. Morgan, E. C. Linton, *Chem. Soc. Rev.* **2009**, *38*, 3193–3207.
- [284] M. Berthod, G. Mignani, G. Woodward, M. Lemaire, *Chem. Rev.* **2005**, *105*, 1801–1836.
- [285] Selected examples: a) H. Li, X. Yan, J. Zhang, W. Guo, J. Jiang, J. Wang, *Angew. Chem. Int. Ed.* **2019**, *58*, 6732–6736; b) J. Luo, T. Zhang, L. Wang,

- G. Liao, Q.-J. Yao, Y.-J. Wu, B.-B. Zhan, Y. Lan, X.-F. Lin, B.-F. Shi, *Angew. Chem. Int. Ed.* **2019**, *58*, 6708–6712; c) C. G. Newton, E. Braconi, J. Kuziola, M. D. Wodrich, N. Cramer, *Angew. Chem. Int. Ed.* **2018**, *57*, 11040–11044; d) Y.-S. Jang, Ł. Woźniak, J. Pedroni, N. Cramer, *Angew. Chem. Int. Ed.* **2018**, *57*, 12901–12905; e) Z.-J. Jia, C. Merten, R. Gontla, C. G. Daniliuc, A. P. Antonchick, H. Waldmann, *Angew. Chem. Int. Ed.* **2017**, *56*, 2429–2434; f) Q.-J. Yao, S. Zhang, B.-B. Zhan, B.-F. Shi, *Angew. Chem. Int. Ed.* **2017**, *56*, 6617–6621; g) J. Zheng, W.-J. Cui, C. Zheng, S.-L. You, *J. Am. Chem. Soc.* **2016**, *138*, 5242–5245; h) Y. Kuninobu, K. Yamauchi, N. Tamura, T. Seiki, K. Takai, *Angew. Chem. Int. Ed.* **2013**, *52*, 1520–1522; i) K. Yamaguchi, J. Yamaguchi, A. Studer, K. Itami, *Chem. Sci.* **2012**, *3*, 2165–2169; for a recent review, see: j) G. Liao, T. Zhou, Q.-J. Yao, B.-F. Shi, *Chem. Commun.* **2019**, DOI:10.1039/C9CC03967H.
- [286] X. Bu, P. J. Skrdla, P. G. Dormer, Y. Bereznitski, *J. Chromatogr. A* **2010**, *1217*, 7255–7264.
- [287] K. S. Egorova, V. P. Ananikov, *Angew. Chem. Int. Ed.* **2016**, *55*, 12150–12162.
- [288] Y.-X. Wang, M. Ye, *Sci. China Chem.* **2018**, *61*, 1004–1013.
- [289] a) V. Ritleng, M. Henrion, M. J. Chetcuti, *ACS Catal.* **2016**, *6*, 890–906; b) A. P. Prakasham, P. Ghosh, *Inorg. Chim. Acta* **2015**, *431*, 61–100.
- [290] G. Vijaykumar, A. Jose, P. K. Vardhanapu, S. P, S. K. Mandal, *Organometallics* **2017**, *36*, 4753–4758.
- [291] Results not discussed in this thesis due to issues of reproducibility.
- [292] a) F. De Simone, J. Waser, *Chimia* **2012**, *66*, 233–236; b) A. Whiting, in *Advanced asymmetric synthesis* (Ed.: G. R. Stephenson), Chapman & Hall, London, **1996**, pp. 126–145.
- [293] K. Maruoka, T. Itoh, H. Yamamoto, *J. Am. Chem. Soc.* **1985**, *107*, 4573–4576.
- [294] a) D. Song, S. Ma, *ChemMedChem* **2016**, *11*, 646–659; b) P. Singla, V. Luxami, K. Paul, *RSC Adv.* **2014**, *4*, 12422–12440; c) M. Gaba, S. Singh, C.

- Mohan, *Eur. J. Med. Chem.* **2014**, *76*, 494–505; d) Y. Bansal, O. Silakari, *Biorg. Med. Chem.* **2012**, *20*, 6208–6236.
- [295] a) T.-T. Gao, W.-W. Zhang, X. Sun, H.-X. Lu, B.-J. Li, *J. Am. Chem. Soc.* **2019**, *141*, 4670–4677; b) D. Berthold, B. Breit, *Org. Lett.* **2018**, *20*, 598–601; c) X.-H. Yang, V. M. Dong, *J. Am. Chem. Soc.* **2017**, *139*, 1774–1777; d) A. M. Haydl, L. J. Hilpert, B. Breit, *Chem. Eur. J.* **2016**, *22*, 6547–6551; e) X. Wu, Z. Chen, Y.-B. Bai, V. M. Dong, *J. Am. Chem. Soc.* **2016**, *138*, 12013–12016; f) A. M. Haydl, K. Xu, B. Breit, *Angew. Chem. Int. Ed.* **2015**, *54*, 7149–7153; g) K. Xu, W. Raimondi, T. Bury, B. Breit, *Chem. Commun.* **2015**, *51*, 10861–10863; h) K. Xu, N. Thieme, B. Breit, *Angew. Chem. Int. Ed.* **2014**, *53*, 7268–7271; i) H. Landert, F. Spindler, A. Wyss, H.-U. Blaser, B. Pugin, Y. Ribourduille, B. Gschwend, B. Ramalingam, A. Pfaltz, *Angew. Chem. Int. Ed.* **2010**, *49*, 6873–6876.
- [296] M. Christensen, A. Nolting, M. Shevlin, M. Weisel, P. E. Maligres, J. Lee, R. K. Orr, C. W. Plummer, M. T. Tudge, L.-C. Campeau, R. T. Ruck, *J. Org. Chem.* **2016**, *81*, 824–830.
- [297] M. R. Friedfeld, H. Zhong, R. T. Ruck, M. Shevlin, P. J. Chirik, *Science* **2018**, *360*, 888–893.
- [298] S. Koller, J. Gatzka, K. M. Wong, P. J. Altmann, A. Pöthig, L. Hintermann, *J. Org. Chem.* **2018**, *83*, 15009–15028.
- [299] a) Y. Schramm, M. Takeuchi, K. Semba, Y. Nakao, J. F. Hartwig, *J. Am. Chem. Soc.* **2015**, *137*, 12215–12218; b) J. S. Bair, Y. Schramm, A. G. Sergeev, E. Clot, O. Eisenstein, J. F. Hartwig, *J. Am. Chem. Soc.* **2014**, *136*, 13098–13101.
- [300] For examples of detrimental effects or changes of enantioselectivity with higher ligand-to-metal ratios, see: a) A. Schätz, R. Rasappan, M. Hager, A. Gissibl, O. Reiser, *Chem. Eur. J.* **2008**, *14*, 7259–7265; b) Z. Shao, J. Wang, K. Ding, A. S. C. Chan, *Adv. Synth. Catal.* **2007**, *349*, 2375–2379; c) M. I. Burguete, M. Collado, J. Escorihuela, S. V. Luis, *Angew. Chem. Int. Ed.* **2007**, *46*, 9002–9005; d) H. Danjo, M. Higuchi, M. Yada, T. Imamoto, *Tetrahedron Lett.* **2004**, *45*, 603–606.

- [301] For examples of nickel-catalyzed alkene isomerization, see: a) Y. He, Y. Cai, S. Zhu, *J. Am. Chem. Soc.* **2017**, *139*, 1061–1064; b) M. Gaydou, T. Moragas, F. Juliá-Hernández, R. Martin, *J. Am. Chem. Soc.* **2017**, *139*, 12161–12164; c) I. Buslov, J. Becouse, S. Mazza, M. Montandon-Clerc, X. Hu, *Angew. Chem. Int. Ed.* **2015**, *54*, 14523–14526; d) W.-C. Lee, C.-H. Wang, Y.-H. Lin, W.-C. Shih, T.-G. Ong, *Org. Lett.* **2013**, *15*, 5358–5361.
- [302] A. F. Schmidt, V. V. Smirnov, A. Al-Halaiga, *Kinet. Catal.* **2007**, *48*, 390–397.
- [303] a) Y. Gao, K. N. Houk, C.-Y. Ho, X. Hong, *Org. Biomol. Chem.* **2017**, *15*, 7131–7139; b) X. Hong, J. Wang, Y.-F. Yang, L. He, C.-Y. Ho, K. N. Houk, *ACS Catal.* **2015**, *5*, 5545–5555.
- [304] a) L.-B. Han, Y. Ono, H. Yazawa, *Org. Lett.* **2005**, *7*, 2909–2911; b) L.-B. Han, C. Zhang, H. Yazawa, S. Shimada, *J. Am. Chem. Soc.* **2004**, *126*, 5080–5081.
- [305] M. Liniger, B. Gschwend, M. Neuburger, S. Schaffner, A. Pfaltz, *Organometallics* **2010**, *29*, 5953–5958.
- [306] L.-J. Xiao, X.-N. Fu, M.-J. Zhou, J.-H. Xie, L.-X. Wang, X.-F. Xu, Q.-L. Zhou, *J. Am. Chem. Soc.* **2016**, *138*, 2957–2960.
- [307] a) L. H. Finger, J. Guschlbauer, K. Harms, J. Sundermeyer, *Chem. Eur. J.* **2016**, *22*, 16292–16303; b) R. D. Crocker, T. V. Nguyen, *Chem. Eur. J.* **2016**, *22*, 2208–2213.
- [308] W. Roush, N. A. N. Zheng, V. St Georgiev, US 87833904 A1, 2005.
- [309] For another example of aluminium-free nickel-catalyzed C–H alkylation by hydroarylation published after our work, see: J. Diesel, D. Grosheva, S. Kodama, N. Cramer, *Angew. Chem. Int. Ed.* **2019**, DOI:10.1002/anie.201904774.
- [310] E. Bill, *Mfit Program*; Max-Planck Institute for Chemical Energy Conversion: Mülheim/Ruhr, Germany, **2008**.
- [311] A. Krasovskiy, P. Knochel, *Synthesis* **2006**, 890–891.
- [312] M. Ishihara, H. Togo, *Tetrahedron* **2007**, *63*, 1474–1480.
- [313] L. Ackermann, A. V. Lygin, *Org. Lett.* **2011**, *13*, 3332–3335.

- [314] D. P. Rillema, J. K. Nagle, L. F. Barringer, T. J. Meyer, *J. Am. Chem. Soc.* **1981**, *103*, 56–62.
- [315] a) C. Jahier-Diallo, M. S. T. Morin, P. Queval, M. Rouen, I. Artur, P. Querard, L. Toupet, C. Crévisy, O. Baslé, M. Mauduit, *Chem. Eur. J.* **2015**, *21*, 993–997; b) H. Clavier, L. Coutable, L. Toupet, J.-C. Guillemin, M. Mauduit, *J. Organomet. Chem.* **2005**, *690*, 5237–5254.
- [316] D. Katayev, Y.-X. Jia, A. K. Sharma, D. Banerjee, C. Besnard, R. B. Sunoj, E. P. Kündig, *Chem. Eur. J.* **2013**, *19*, 11916–11927.
- [317] A. Alexakis, J. Burton, J. Vastra, C. Benhaim, X. Fournioux, A. van den Heuvel, J.-M. Levêque, F. Mazé, S. Rosset, *Eur. J. Org. Chem.* **2000**, 4011–4027.
- [318] M. Dindaroğlu, A. Falk, H.-G. Schmalz, *Synthesis* **2013**, *45*, 527–535.
- [319] B. Moreau, J. Y. Wu, T. Ritter, *Org. Lett.* **2009**, *11*, 337–339.
- [320] V. F. Kuznetsov, G. R. Jefferson, G. P. A. Yap, H. Alper, *Organometallics* **2002**, *21*, 4241–4248.
- [321] a) I. Colomer, R. Coura Barcelos, T. J. Donohoe, *Angew. Chem. Int. Ed.* **2016**, *55*, 4748–4752; b) Z. Segaula, J. Leclercq, V. Verones, N. Flouquet, M. Lecoeur, L. Ach, N. Renault, A. Barczyk, P. Melnyk, P. Berthelot, X. Thuru, N. Lebegue, *J. Med. Chem.* **2016**, *59*, 8422–8440; c) W. Liu, L. Li, Z. Chen, C.-J. Li, *Org. Biomol. Chem.* **2015**, *13*, 6170–6174; d) C. Bao, G. Fan, Q. Lin, B. Li, S. Cheng, Q. Huang, L. Zhu, *Org. Lett.* **2012**, *14*, 572–575.
- [322] A. E. Sheshenev, M. S. Baird, I. G. Bolesov, A. S. Shashkov, *Tetrahedron* **2009**, *65*, 10552–10564.
- [323] S. Nakamura, D. Hayama, *Angew. Chem. Int. Ed.* **2017**, *56*, 8785–8789.
- [324] a) S. Movahhed, J. Westphal, M. Dindaroğlu, A. Falk, H.-G. Schmalz, *Chem. Eur. J.* **2016**, *22*, 7381–7384; b) R. Sanders, U. T. Mueller-Westerhoff, *J. Organomet. Chem.* **1996**, *512*, 219–224.
- [325] a) A. R. Kenaree, T. J. Cuthbert, S. M. Barbon, P. D. Boyle, E. R. Gillies, P. J. Ragogna, J. B. Gilroy, *Organometallics* **2015**, *34*, 4272–4280; b) M. R.

- Malachowski, M. F. Grau, J. M. Thomas, A. L. Rheingold, C. E. Moore, *Inorg. Chim. Acta* **2010**, *364*, 132–137.
- [326] a) F. M. Geisler, G. Helmchen, *Synthesis* **2006**, 2201–2205; b) B. Bildstein, A. Hradsky, H. Kopacka, R. Malleier, K.-H. Ongania, *J. Organomet. Chem.* **1997**, *540*, 127–145.
- [327] M. Shang, S.-Z. Sun, H.-X. Dai, J.-Q. Yu, *J. Am. Chem. Soc.* **2014**, *136*, 3354–3357.
- [328] M. R. Chaulagain, G. J. Sormunen, J. Montgomery, *J. Am. Chem. Soc.* **2007**, *129*, 9568–9569.
- [329] R. S. Shaikh, S. J. S. Düsel, B. König, *ACS Catal.* **2016**, *6*, 8410–8414.
- [330] A. Podgoršek, S. Stavber, M. Zupan, J. Iskra, *Eur. J. Org. Chem.* **2006**, 483–488.
- [331] S. Bräse, B. Waegell, A. de Meijere, *Synthesis* **1998**, 148–152.
- [332] R. D. Grigg, R. Van Hovel, J. M. Schomaker, *J. Am. Chem. Soc.* **2012**, *134*, 16131–16134.
- [333] a) H. Yang, X. Zhang, L. Zhou, P. Wang, *J. Org. Chem.* **2011**, *76*, 2040–2048; b) E. Alvarez-Manzaneda, R. Chahboun, E. Cabrera, E. Alvarez, R. Alvarez-Manzaneda, M. Hmamouchi, H. Es-Samti, *Tetrahedron Lett.* **2007**, *48*, 8930–8934.
- [334] S. Meiries, G. Le Duc, A. Chartoire, A. Collado, K. Speck, K. S. A. Arachchige, A. M. Z. Slawin, S. P. Nolan, *Chem. Eur. J.* **2013**, *19*, 17358–17368.
- [335] H. Kim, Y. Nguyen, C. P.-H. Yen, L. Chagal, A. J. Lough, B. M. Kim, J. Chin, *J. Am. Chem. Soc.* **2008**, *130*, 12184–12191.
- [336] a) D. Seebach, A. K. Beck, A. Heckel, *Angew. Chem. Int. Ed.* **2001**, *40*, 92–138; b) A. Hafner, R. O. Duthaler, R. Marti, G. Rihs, P. Rothe-Streit, F. Schwarzenbach, *J. Am. Chem. Soc.* **1992**, *114*, 2321–2336.
- [337] A. Modak, A. Deb, T. Patra, S. Rana, S. Maity, D. Maiti, *Chem. Commun.* **2012**, *48*, 4253–4255.

- [338] K. D. Schleicher, Y. Sasaki, A. Tam, D. Kato, K. K. Duncan, D. L. Boger, *J. Med. Chem.* **2013**, *56*, 483–495.
- [339] J. Moran, P. Dornan, A. M. Beauchemin, *Org. Lett.* **2007**, *9*, 3893–3896.
- [340] C. Seipelt, P. López, T. Kirschgen, A. Dölle, M. D. Zeidler, I. Fonseca, F. H. Cano, B. Paloma, *Tetrahedron Lett.* **1999**, *40*, 1739–1742.
- [341] A. Purkait, S. K. Roy, H. K. Srivastava, C. K. Jana, *Org. Lett.* **2017**, *19*, 2540–2543.
- [342] Bruker AXS Inc., in *Bruker Apex CCD, SAINT v8.30C* (Ed.: Bruker AXS Inst. Inc.), WI, USA, Madison, **2013**.
- [343] L. Krause, R. Herbst-Irmer, D. Stalke, *J. Appl. Crystallogr.* **2015**, *48*, 1907–1913.
- [344] L. Krause, R. Herbst-Irmer, G. M. Sheldrick, D. Stalke, *J. Appl. Crystallogr.* **2015**, *48*, 3–10.
- [345] G. M. Sheldrick, *Acta Crystallogr.* **2015**, *A71*, 3–8.
- [346] G. M. Sheldrick, *Acta Crystallogr.* **2015**, *C71*, 3–8.
- [347] C. B. Hübschle, G. M. Sheldrick, B. Dittrich, *J. Appl. Crystallogr.* **2011**, *44*, 1281–1284.
- [348] O. V. Dolomanov, L. J. Bourhis, R. J. Gildea, J. A. K. Howard, H. Puschmann, *J. Appl. Crystallogr.* **2009**, *42*, 339–341.
- [349] G. M. Sheldrick, *Acta Crystallogr.* **2008**, *A64*, 112–122.

Acknowledgements

First, I would like to express my deepest gratitude to Prof. Dr. Lutz Ackermann for giving me the opportunity to conduct my PhD in his research group. Thank you for your support, your guidance and your interest in my projects.

I am grateful to Prof. Dr. Alexander Breder for accepting to be my second supervisor. I also would like to thank Prof. Dr. Manuel Alcarazo, Dr. Shoubhik Das, Prof. Dr. Dietmar Stalke and Prof. Dr. Dr. h.c.mult. Lutz F. Tietze for agreeing to take part in my defense.

I would like to thank the people from our research group with whom I had the opportunity to collaborate: Dr. Ruhuai Mei, Valentin Müller, Dr. João C. A. de Oliveira, Dr. Daniel Zell, Dr. Debasish Ghorai, Dr. Nicolas Sauermann, Uttam Dhawa and Dr. Fabio Pescioli. My deepest thanks also go to Dr. Tobias Parchomyk, Stefan Lülff, Prof. Dr. Konrad Koszinowski, Dr. Serhiy Demeshko and Prof. Dr. Franc Meyer for their invaluable contributions in the context of our collaboration on iron chemistry. Thank you all!

I would also like to extend my gratitude to Dr. Christopher Golz, Helena Keil and Prof. Dr. Dietmar Stalke for their assistance with X-ray diffraction analysis, as well as to all the members of the analytical departments (NMR and mass spectrometry) at the IOBC for their continuous support to our research work. I would also like to thank Felix Krätzschar and Prof. Dr. Alexander Breder for their assistance and advice on the measurement of specific rotations.

I would like to thank Stefan Beußhausen for taking care of the instruments of our research group, especially the chiral HPLC, the glovebox and the SPS, which I used almost on a daily basis in the last four years. Thank you for your invaluable help!

My gratitude also goes to Karsten Rauch for his continuous support to our lab work, and especially for the preparation of various (HA)SPOs and carbene precursors.

I would like to thank Mrs. Gabriele Keil-Knepel for her continuous assistance with administrative tasks.

I also would like to express my gratitude to all past and present members of the Ackermann research group, especially to members of Lab 308 (a.k.a. “the Best Lab”): Dr. Gianpiero Cera, Dr. Lars Finger, Dr. Thomas Müller, Torben Rogge, Sachiyo Nakanowatari, Zhigao Shen, Dr. Wei-Jun Kong, Dr. Zhixiong “Jenson” Ruan, Dr. Nicolas Sauermann, Dr. Ramesh Chandra Samanta, Jiayu Mo, Dr. Huawen Huang, Renato Lucio De Carvalho, Talita Barbara Gontijo, Dr. Antonis Messinis, Antoine Bigot and Karsten Rauch. It has been an honor working with you guys! In this context, I would like to particularly thank Dr. Gianpiero Cera for his precious advices and suggestions on iron catalysis, Dr. Thomas Müller and Sachiyo Nakanowatari for their advices on nickel catalysis, and Torben Rogge for his help with various instruments.

I also would like to thank Prof. Dr. Albrecht Berkessel, Prof. Dr. Lukas Hintermann, and Prof. Dr. E. Peter Kündig for the generous donation of various NHC precursors and SPOs. I would also like to express my gratitude to my coworkers and students from whom I obtained chemicals.

I would like to sincerely thank all the people who proofread this thesis: Dr. Thomas Müller, Nikolaos Kaplaneris, Torben Rogge, Valentin Müller, Dr. João C. A. de Oliveira, Dr. Elżbieta Gońka, Isaac Choi, Maximilian Stangier, Dr. Lars Finger, Dr. Jongwoo Son, Julia Struwe, Wei Wang, Cuiju Zhu, Tjark Meyer and Leonardo Massignan. I also would like to thank all the people who previously corrected manuscripts, supporting information, posters, abstracts and proposals for me: Dr. Thomas Müller, Torben Rogge, Dr. Fabio Pescioli, Dr. Lars Finger, Dr. Yu-Feng Liang, Valentin Müller, Dr. Hui Wang, Dr. Weiping Liu, Ralf Steinbock, Dr. João C. A. de Oliveira, Dr. Parthasarathi Subramanian, Dr. Nicolas Sauermann, Dr. Marc Moselage, Dr. Vladislav Kotek, and Cuiju Zhu. Thank you all for your time and your patience!

I also would like to express my gratitude to my former supervisors for teaching me so much about chemistry and giving me the opportunity to conduct research within their laboratories, particularly Prof. Dr. Jérôme Waser, Dr. Florian de Nanteuil, Prof. Dr. Sandrine Gerber, Dr. Holger Sellner and Dr. Kenji Namoto.

Last but not least, I would like to thank my family for their continuous support and their love throughout my life.

Curriculum Vitae

Personal Information

Name: Joachim Loup
Date of Birth: 11.04.1990
Place of Birth: Lausanne VD, Switzerland
Place of Origin: Vully-les-Lacs (Montmagny) VD, Switzerland
Nationality: Switzerland
ORCID: 0000-0002-0033-5033

Academic Education

05.2015–08.2019 **PhD Thesis** (Supervisor: Prof. Dr. Lutz Ackermann) at the Georg-August-University Göttingen, Germany.
Title: *“Selectivity Control in 3d Transition Metal-Catalyzed C–H Activation”*

09.2011–04.2013 **Master of Science MSc** in Molecular and Biological Chemistry at the École Polytechnique Fédérale de Lausanne (EPFL), Switzerland. Final grade: 5.51/6.
Master Thesis: *“Catalytic Friedel-Crafts Reaction of Aminocyclopropanes”* (Supervisor: Prof. Dr. Jérôme Waser).

09.2008–07.2011 **Bachelor of Science BSc** in Chemistry and Chemical Engineering at the École Polytechnique Fédérale de Lausanne (EPFL), Switzerland. Final grade: 5.78/6; final ranking: 1/50.

08.2010–05.2011 **Academic exchange** (2 semesters) at the National University of Singapore (NUS), Singapore.

School Education

- 08.2005–07.2008 **Maturity certificate** at the *Gymnase intercantonal de la Broye* in Payerne VD, Switzerland.
- 08.1995–07.2005 **Kindergarten, primary and secondary schools** in Payerne VD, Switzerland.

Industrial Experience

- 02.2014–11.2014 Internship at Novartis Institutes for BioMedical Research (NIBR), Novartis AG, Basel, Switzerland.
Topic: Synthesis of protease inhibitors.
- 04.2013–09.2013 Internship at Pharma Research and Early Development (pRED), F. Hoffmann-La Roche Ltd, Basel, Switzerland.
Topic: Synthesis of transcription factor enhancers and serine protease inhibitors.

Teaching Experience

- 2017–2018 Assistant of the course "*Methoden der Modernen Organischen und Biomolekularen Chemie*" (2 semesters).
- 2016–2018 Assistant of the practical course "*Chemisches Praktikum für Studierende der Human- und Zahnmedizin*" (3 semesters).
- 2017–2018 Assistant of the practical course "*Organisch-Chemisches-Fortgeschrittenenpraktikum*" (1 semester).

Publications

- 9) J. Loup,[‡] U. Dhawa,[‡] F. Pesciaioli, J. Wencel-Delord, L. Ackermann, “*Enantioselective C–H Activation with Earth-Abundant 3d Transition Metals*”, *Angew. Chem. Int. Ed.* **2019**, DOI:10.1002/anie.201904214. (‡ Both authors contributed equally.)
- 8) J. Loup, T. Parchomyk, S. Lülfi, S. Demeshko, F. Meyer, K. Koszinowski, L. Ackermann, “*Mössbauer and mass spectrometry support for iron(II) catalysts in enantioselective C–H activation*”, *Dalton Trans.* **2019**, 48, 5135–5139.
- 7) D. Ghorai, J. Loup, G. Zanoni, L. Ackermann, “*Air-Stable Secondary Phosphine Oxides (SPOs) for Nickel-Catalyzed Cross-Couplings of Aryl Ethers by C–O Activation*” *Synlett* **2019**, 30, 429–432.
- 6) J. Loup,[‡] V. Müller,[‡] D. Ghorai, L. Ackermann, “*Enantioselective Aluminum-Free Alkene Hydroarylations through C–H Activation by a Chiral Nickel/JoSPOphos Manifold*” *Angew. Chem. Int. Ed.* **2019**, 58, 1749–1753. (‡ Both authors contributed equally.)
- 5) K. Namoto, F. Sirockin, H. Sellner, C. Wiesmann, F. Villard, R. J. Moreau, E. Valeur, Stephanie C. Paulding, S. Schleege, K. Schipp, J. Loup, L. Andrews, R. Swale, M. Robinson, C. J. Farady, “*Structure-based design and synthesis of macrocyclic human rhinovirus 3C protease inhibitors*” *Bioorg. Med. Chem. Lett.* **2018**, 28, 906–909.
- 4) J. Loup, D. Zell, J. C. A. Oliveira, H. Keil, D. Stalke, L. Ackermann, “*Asymmetric Iron-Catalyzed C–H Alkylation Enabled by Remote Ligand meta-Substitution*” *Angew. Chem. Int. Ed.* **2017**, 56, 14197–14201. (Highlighted in *Synfacts*, *ChemistryViews*, *Sigma-Aldrich* and *Nachrichten aus der Chemie, Trendbericht Organische Chemie*)
- 3) N. Sauermann, J. Loup, D. Kootz, A. Berkessel, L. Ackermann, “*Triazolylidene Ligands Allow Cobalt-Catalyzed C–H/C–O Alkenylations at Ambient Temperature*” *Synthesis* **2017**, 49, 3476–3484.
- 2) R. Mei,[‡] J. Loup,[‡] L. Ackermann, “*Oxazolonyl-Assisted C–H Amidation by Cobalt(III) Catalysis*” *ACS Catal.* **2016**, 6, 793–797. (‡ Both authors contributed equally.) (Cited >130 times as of 07.2019)

1) F. de Nanteuil, J. Loup, J. Waser, “Catalytic Friedel–Crafts Reaction of Aminocyclopropanes” *Org. Lett.* **2013**, *15*, 3738–3741.

Conferences

- 02.2019 *3rd Workshop of the SPP 1807*, Erlangen, Germany (Poster presentation)
- 02.2019 *12th CaRLa Winter School*, Heidelberg, Germany (Poster presentation and flash talk)
- 09.2018 *ORCHEM 2018*, Berlin, Germany (Poster presentation)
- 07.2018 *3rd Summer School of the SPP 1807*, DESY Hamburg, Germany (Oral presentation)
- 11.2017 *Evaluation of the SPP 1807*, Gießen, Germany (Poster presentation)
- 07.2017 *2nd Summer School of the SPP 1807*, Rostock, Germany (Oral presentation)
- 10.2016 *2nd Workshop of the SPP 1807*, Cologne, Germany (Poster presentation)
- 05.2016 *1st Summer School of the SPP 1807*, Bremen, Germany (Oral presentation)
- 10.2015 *1st Workshop of the SPP 1807*, Göttingen, Germany (Poster presentation)

Erklärung

Ich versichere, dass ich die vorliegende Dissertation in dem Zeitraum von Mai 2015 bis Juli 2019 am Institut für Organische und Biomolekulare Chemie der Georg-August-Universität Göttingen

auf Anregung und unter Anleitung von

Herrn Prof. Dr. Lutz Ackermann

selbstständig durchgeführt und keine anderen als die angegebenen Hilfsmittel und Quellen verwendet habe.

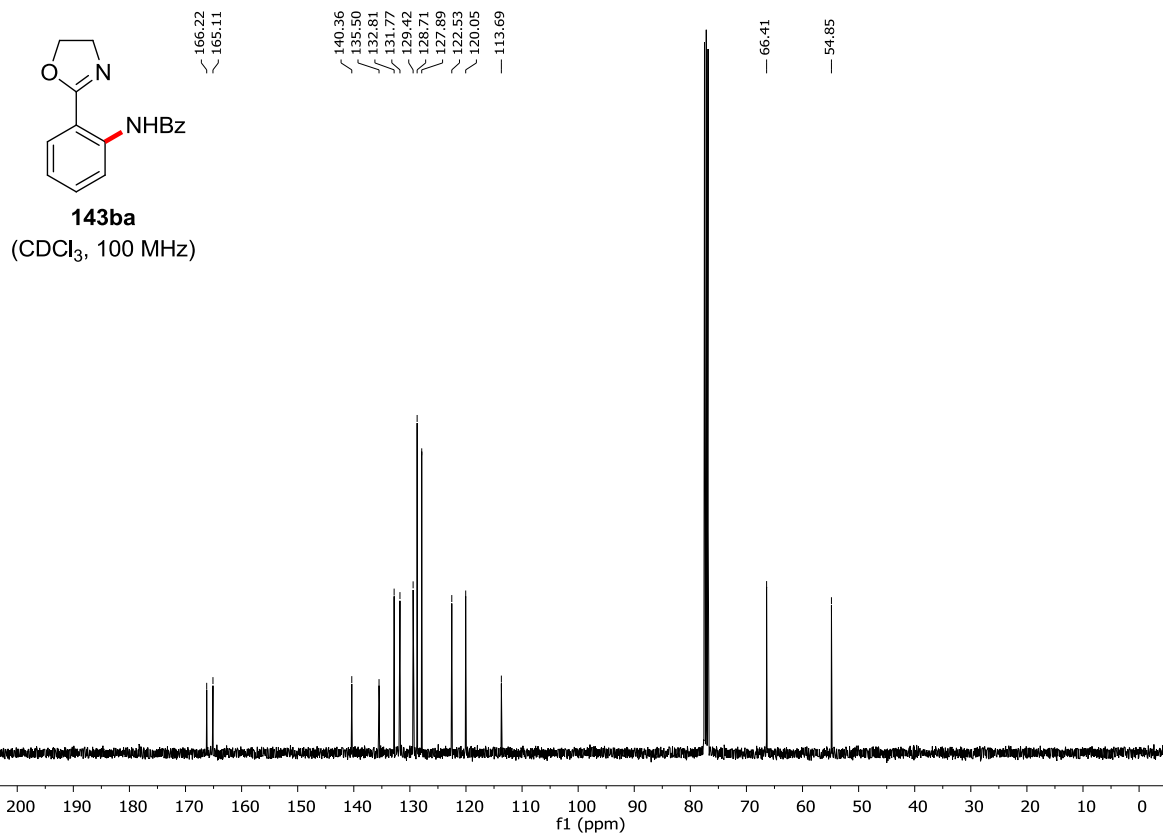
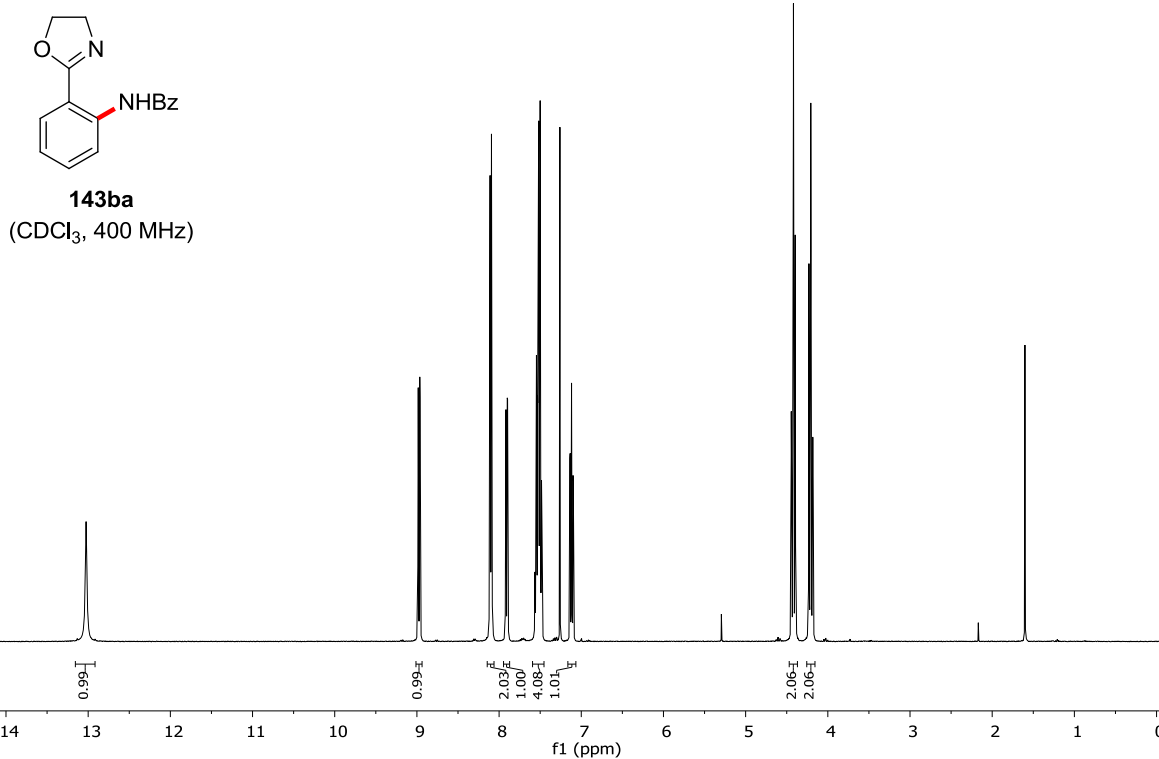
Göttingen, den 08.07.2019

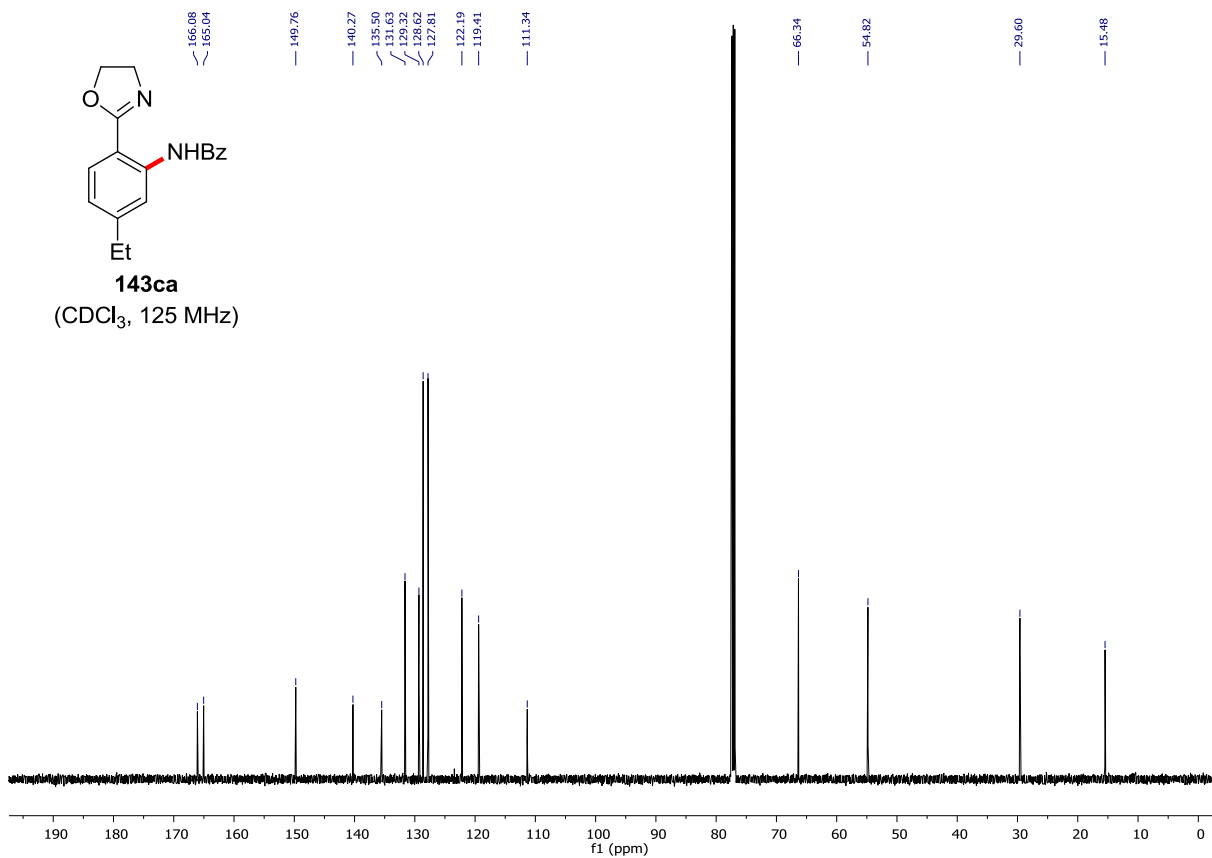
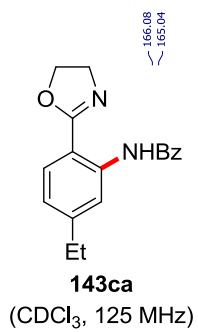
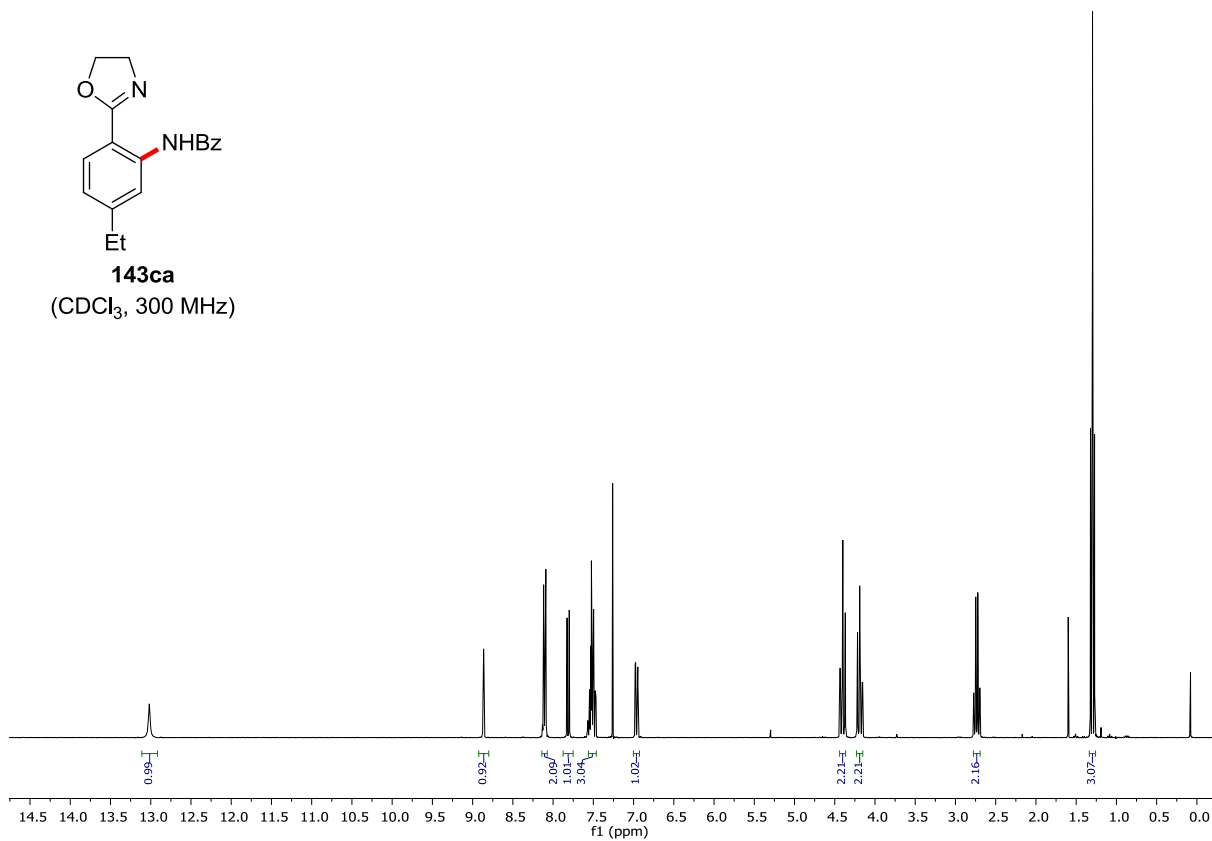
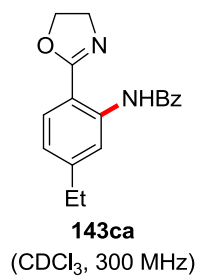
Disclaimer

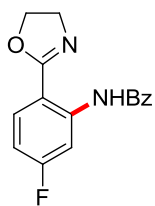
Elements of the following publications are reproduced for non-commercial purposes with permission of the editors:

- Ref. [37e]: Reprinted with permission from R. Mei, J. Loup, L. Ackermann, *ACS Catal.* **2016**, *6*, 793–797. Copyright 2015 American Chemical Society.
- Ref. [151]: J. Loup, D. Zell, J. C. A. Oliveira, H. Keil, D. Stalke, L. Ackermann, *Angew. Chem. Int. Ed.* **2017**, *56*, 14197–14201. Copyright Clearance Center's RightsLink® order: 4560300036116.
- Ref. [218]: J. Loup, T. Parchomyk, S. Lülff, S. Demeshko, F. Meyer, K. Koszinowski, L. Ackermann, *Dalton Trans.* **2019**, *48*, 5135–5139 – Published by The Royal Society of Chemistry.
- Ref. [220]: J. Loup, V. Müller, D. Ghorai, L. Ackermann, *Angew. Chem. Int. Ed.* **2019**, *58*, 1749–1753. Copyright Clearance Center's RightsLink® order: 4560300144210.

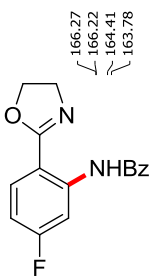
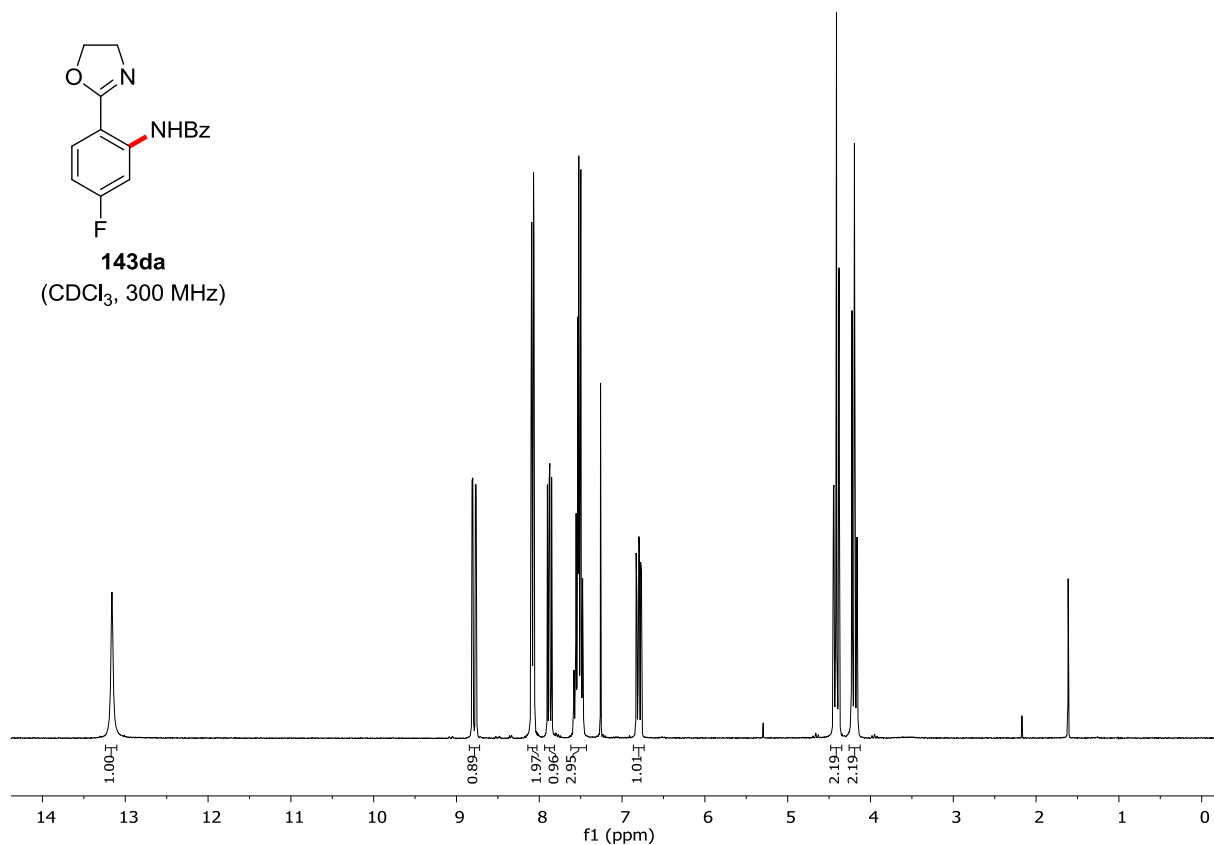
NMR Spectra and HPLC Chromatograms



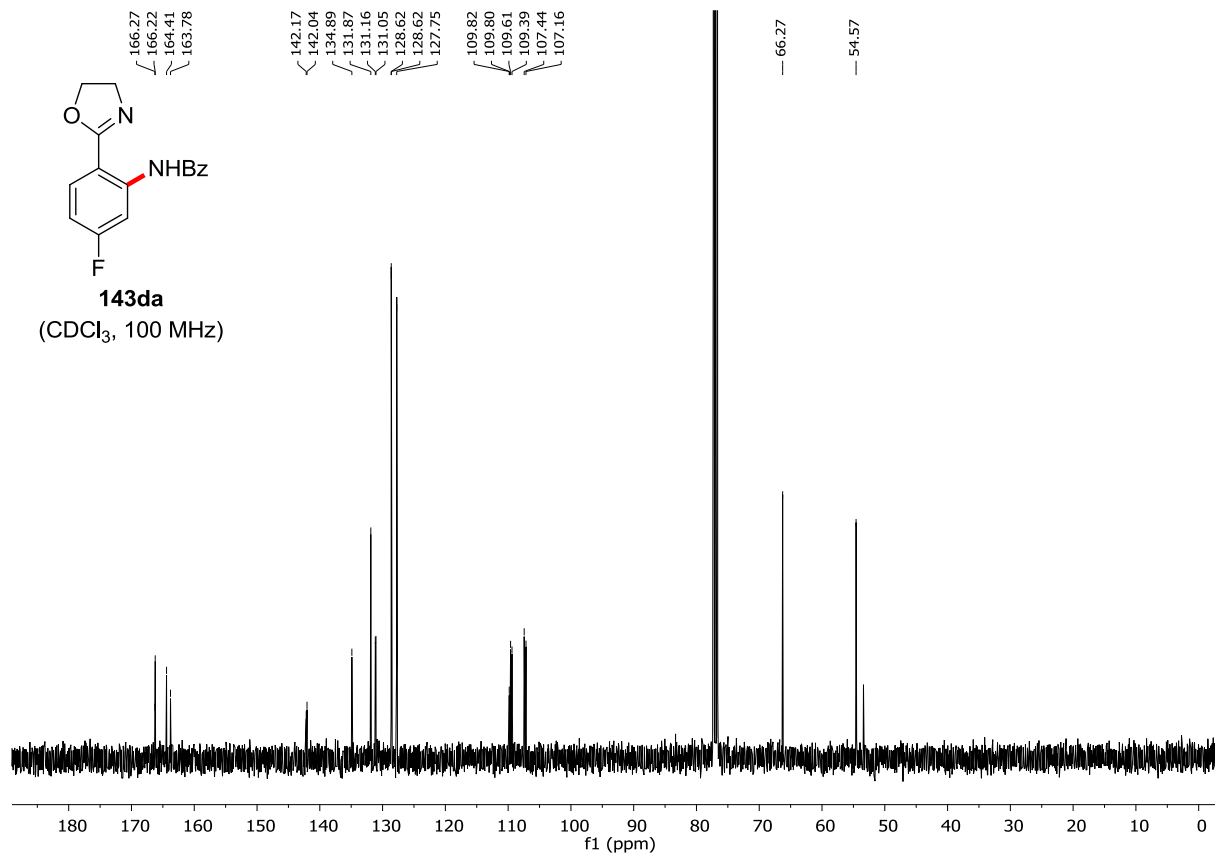


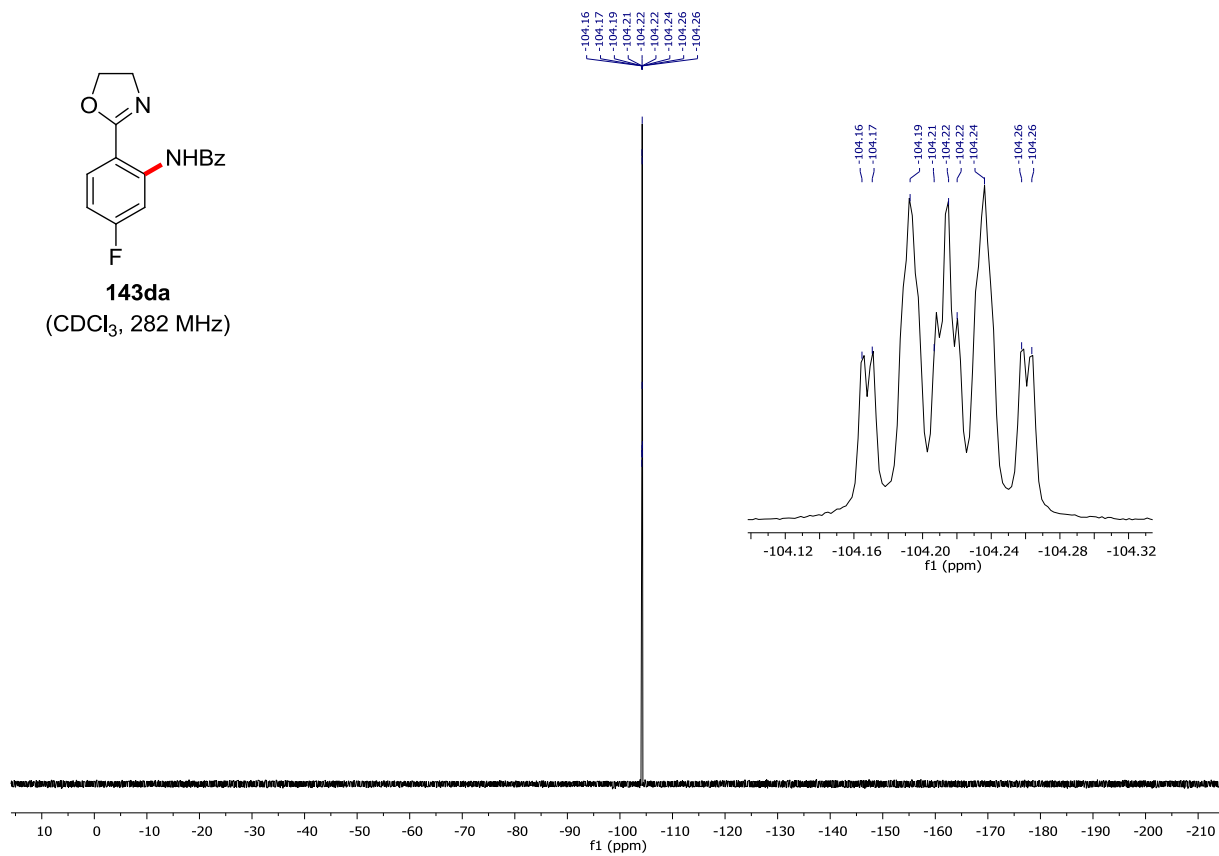
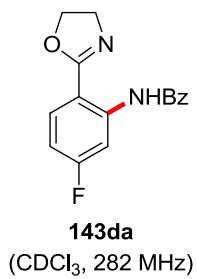


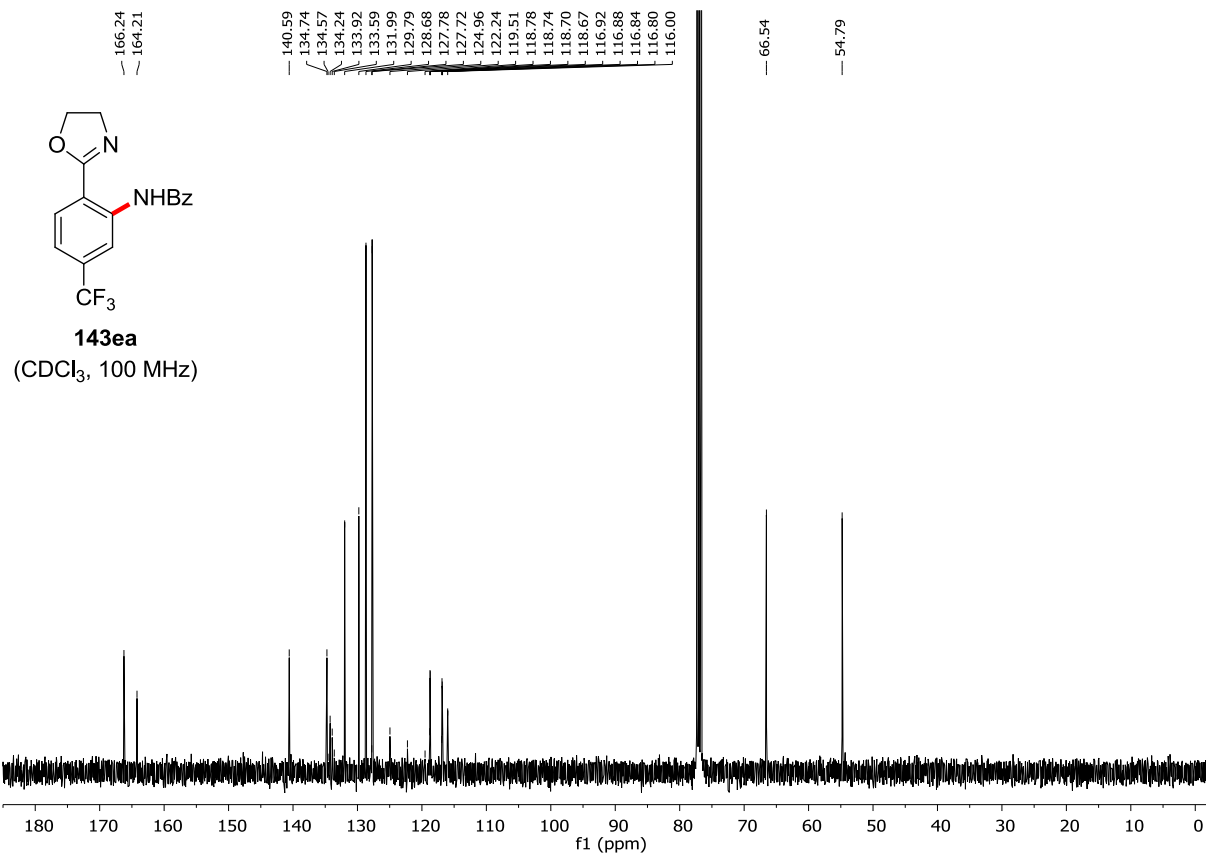
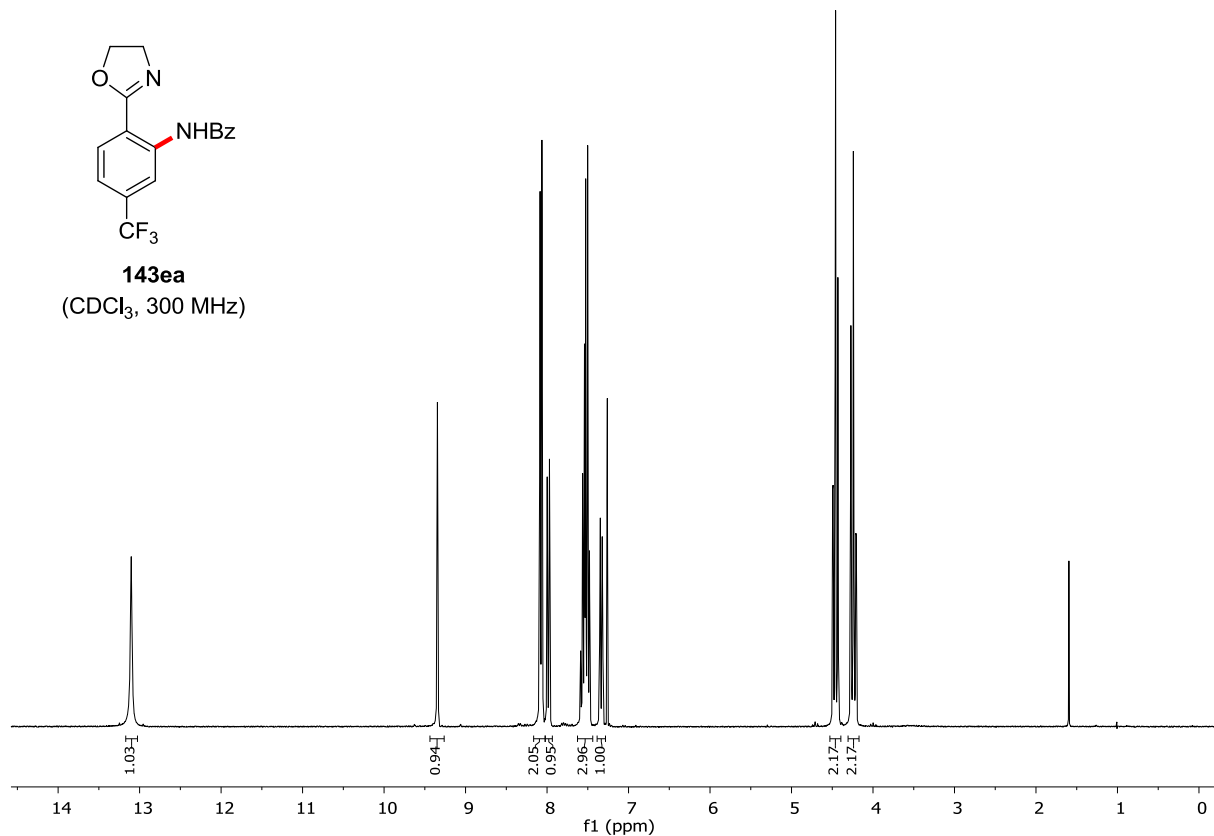
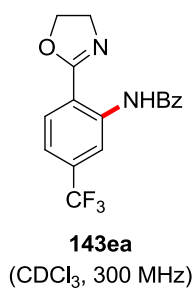
143da
(CDCl₃, 300 MHz)

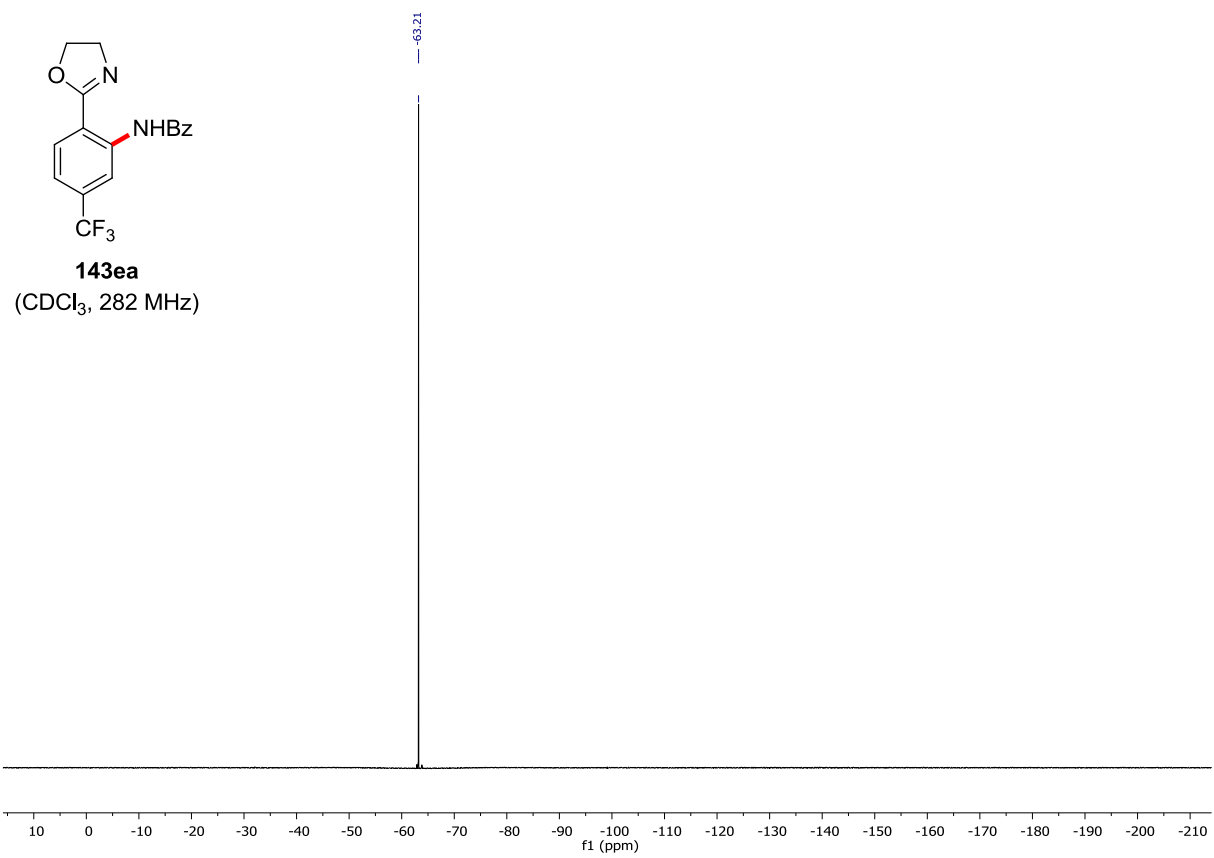


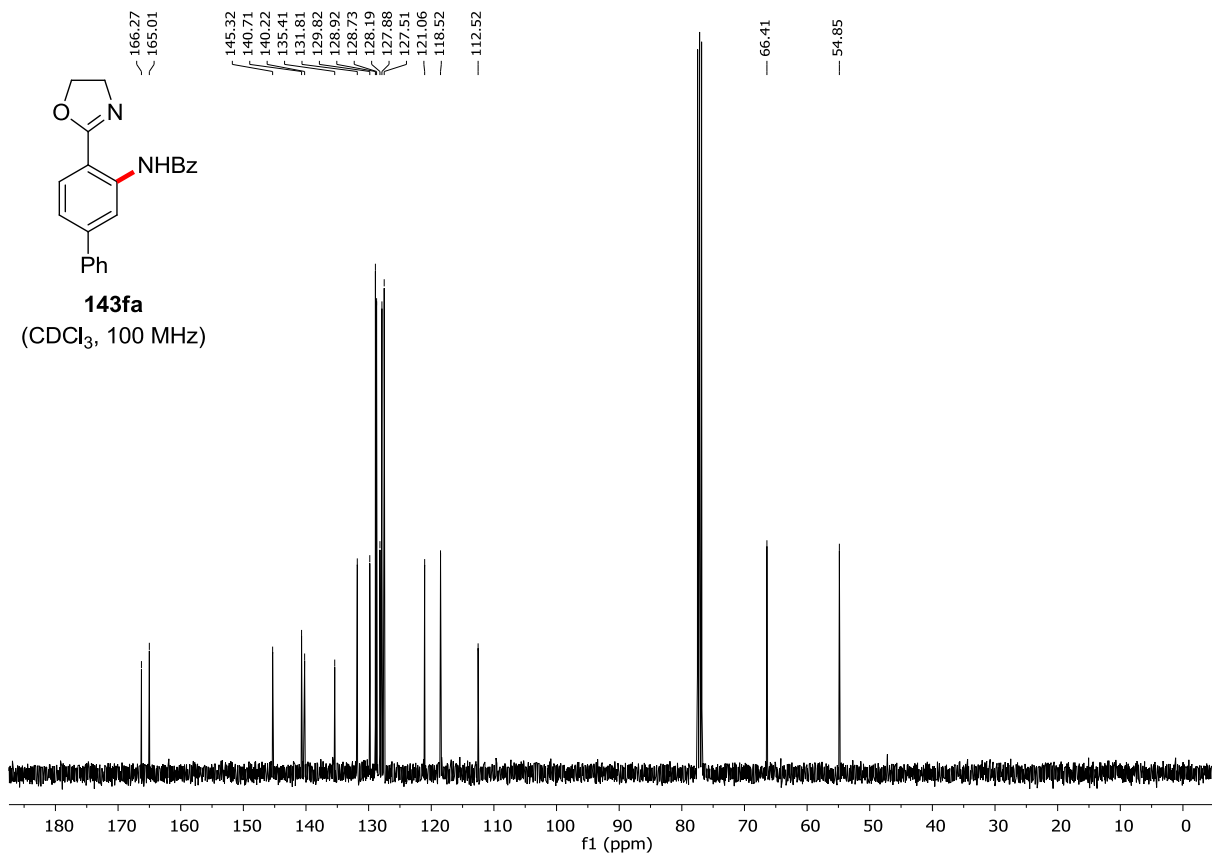
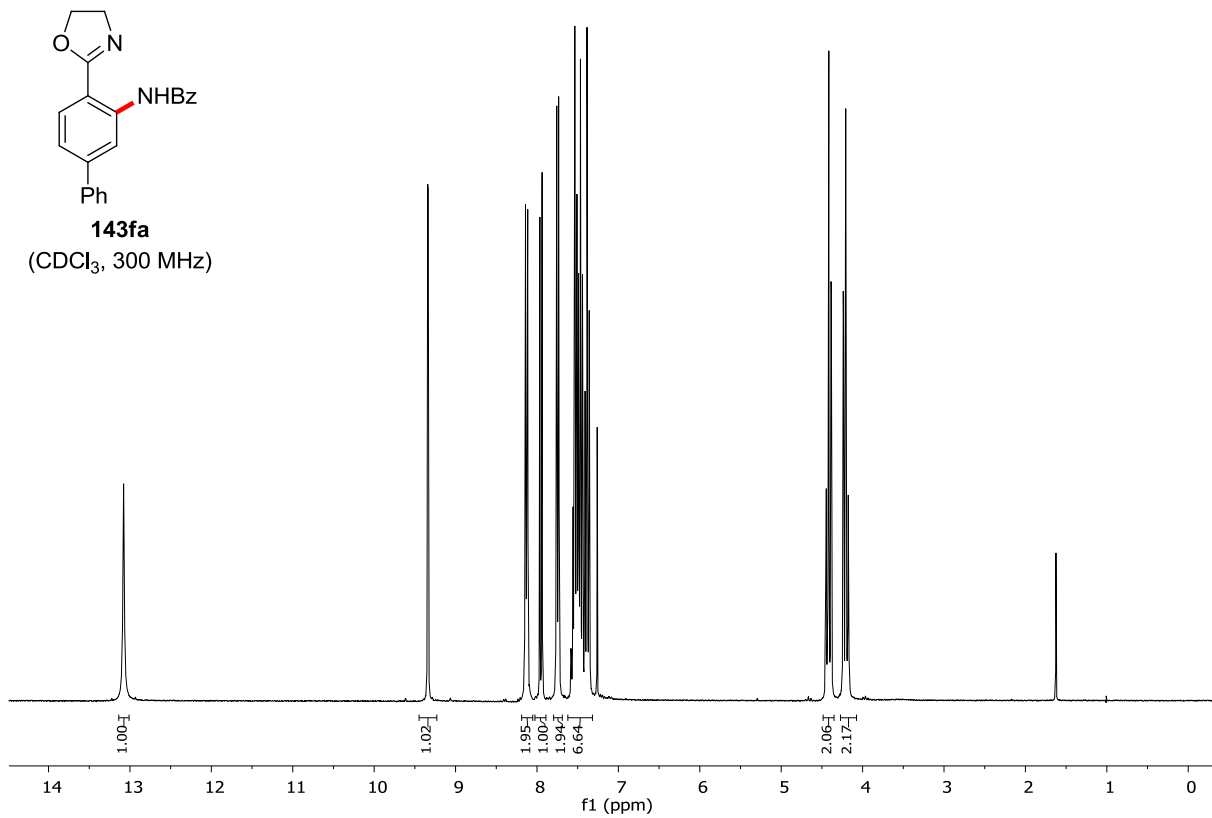
143da
(CDCl₃, 100 MHz)

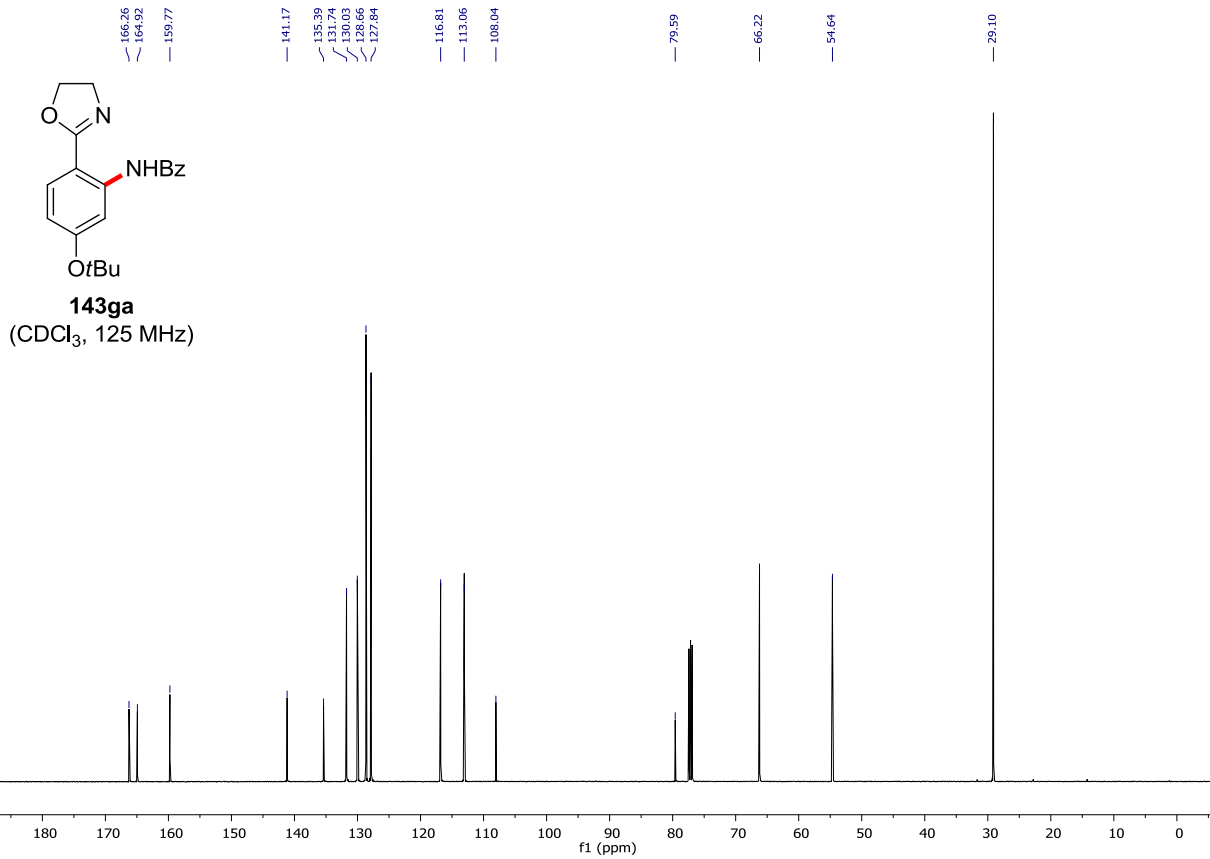
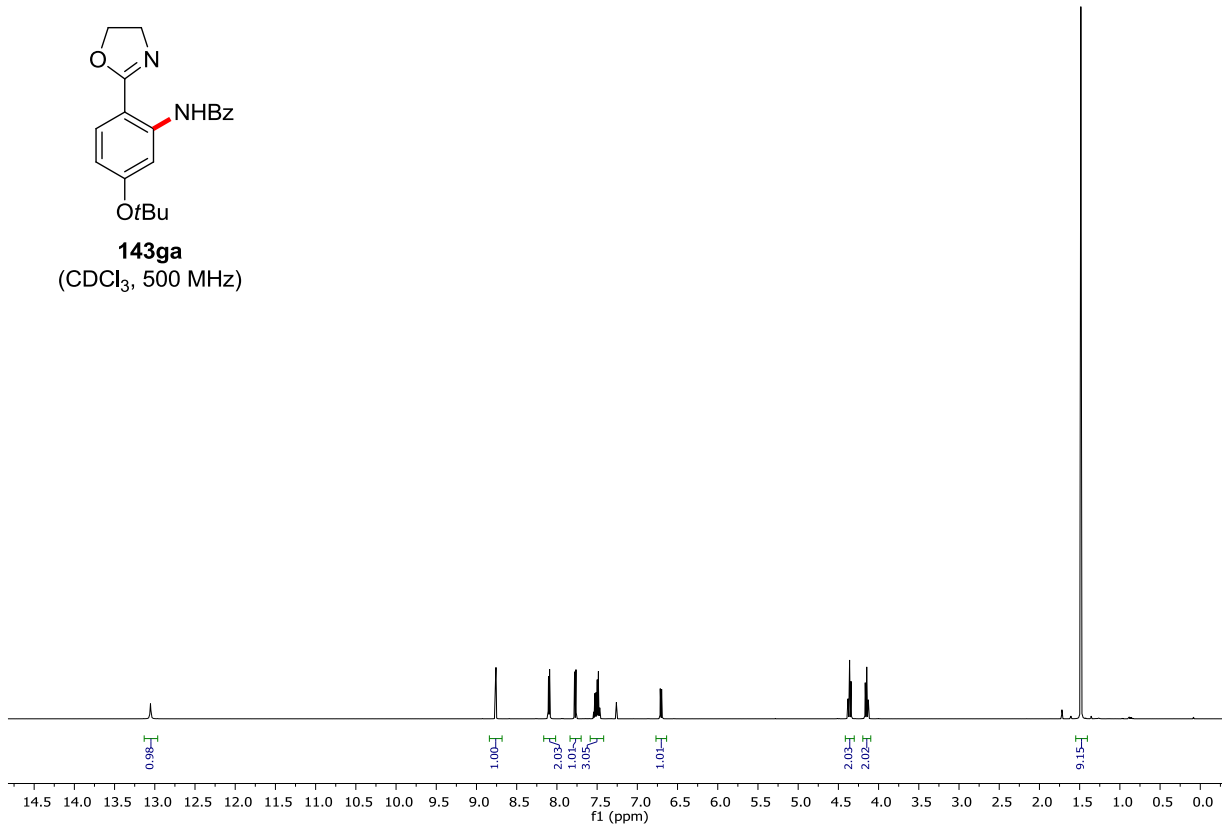
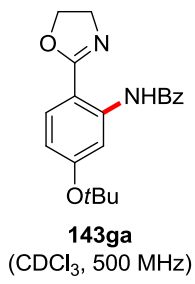


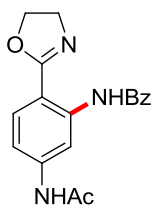




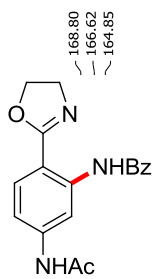
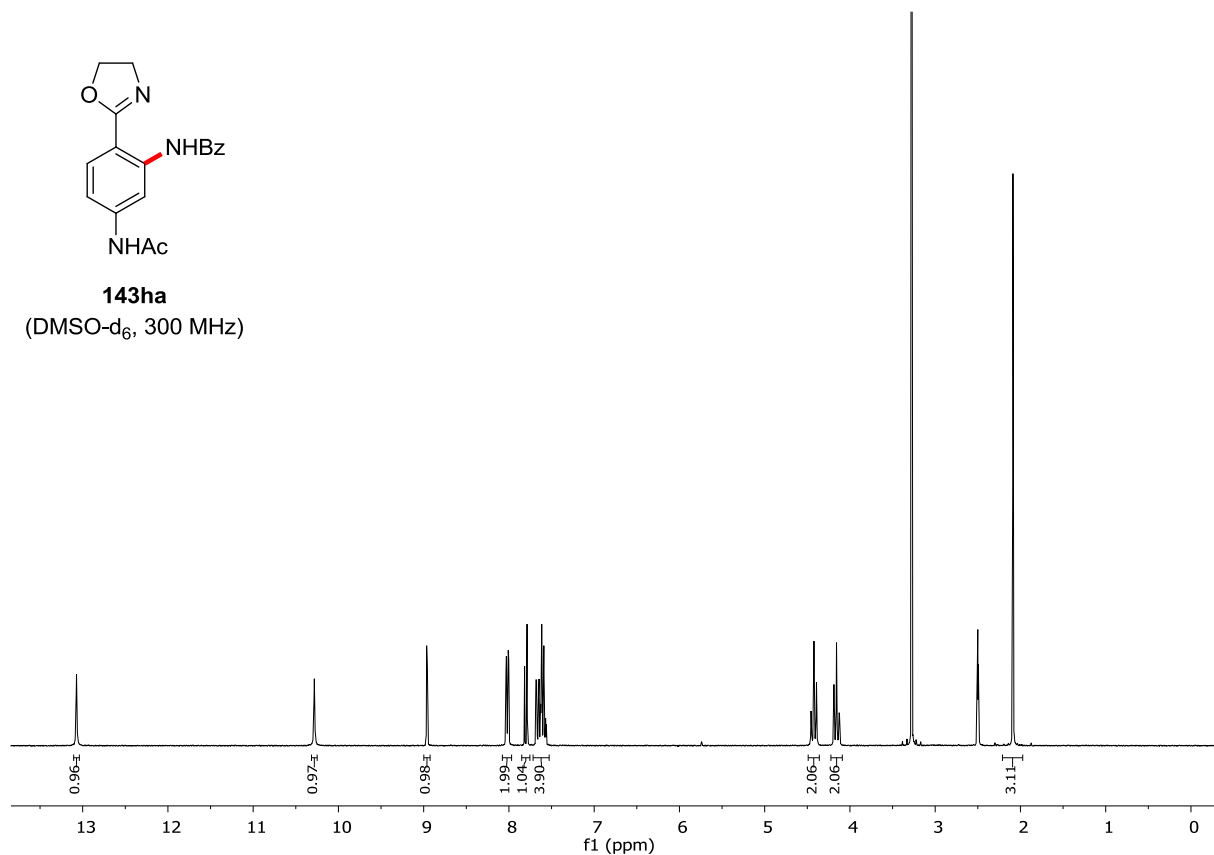




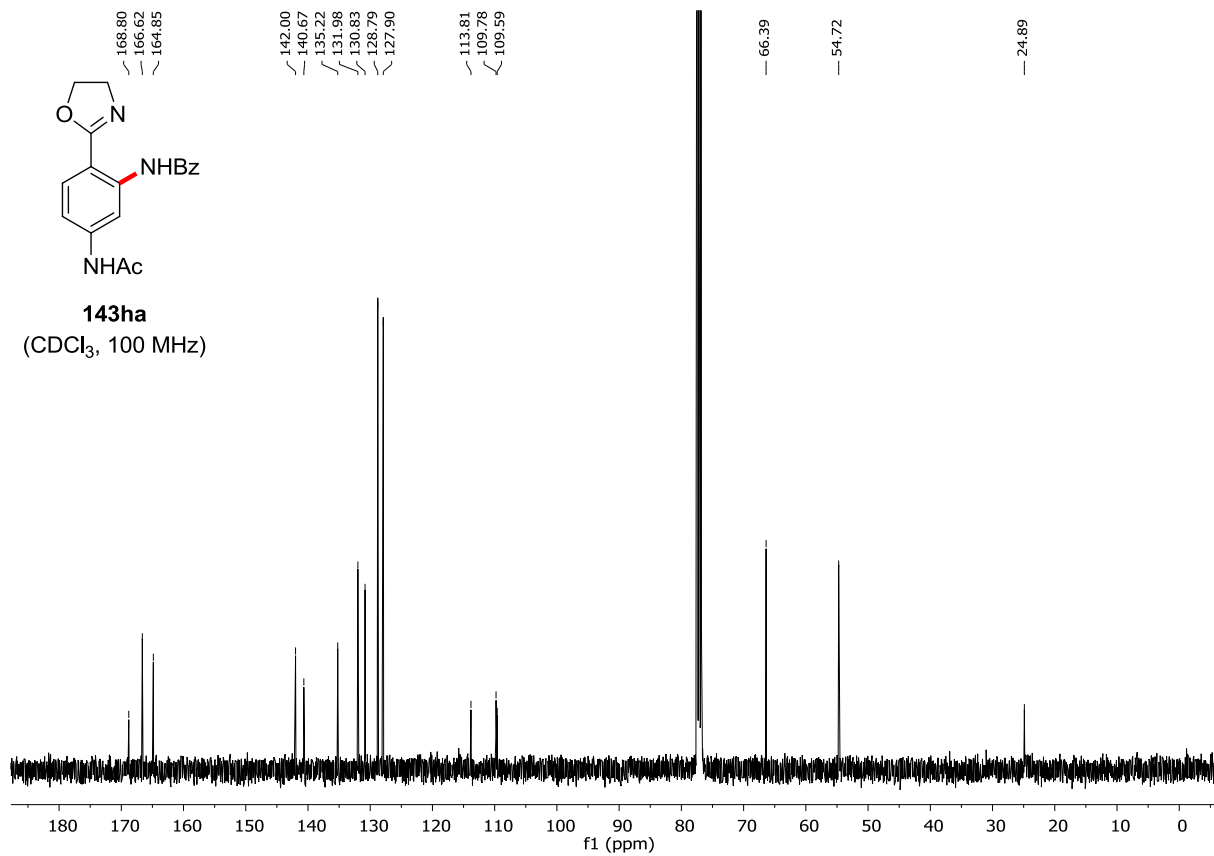


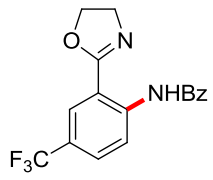


143ha
(DMSO-d₆, 300 MHz)

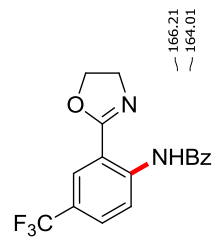
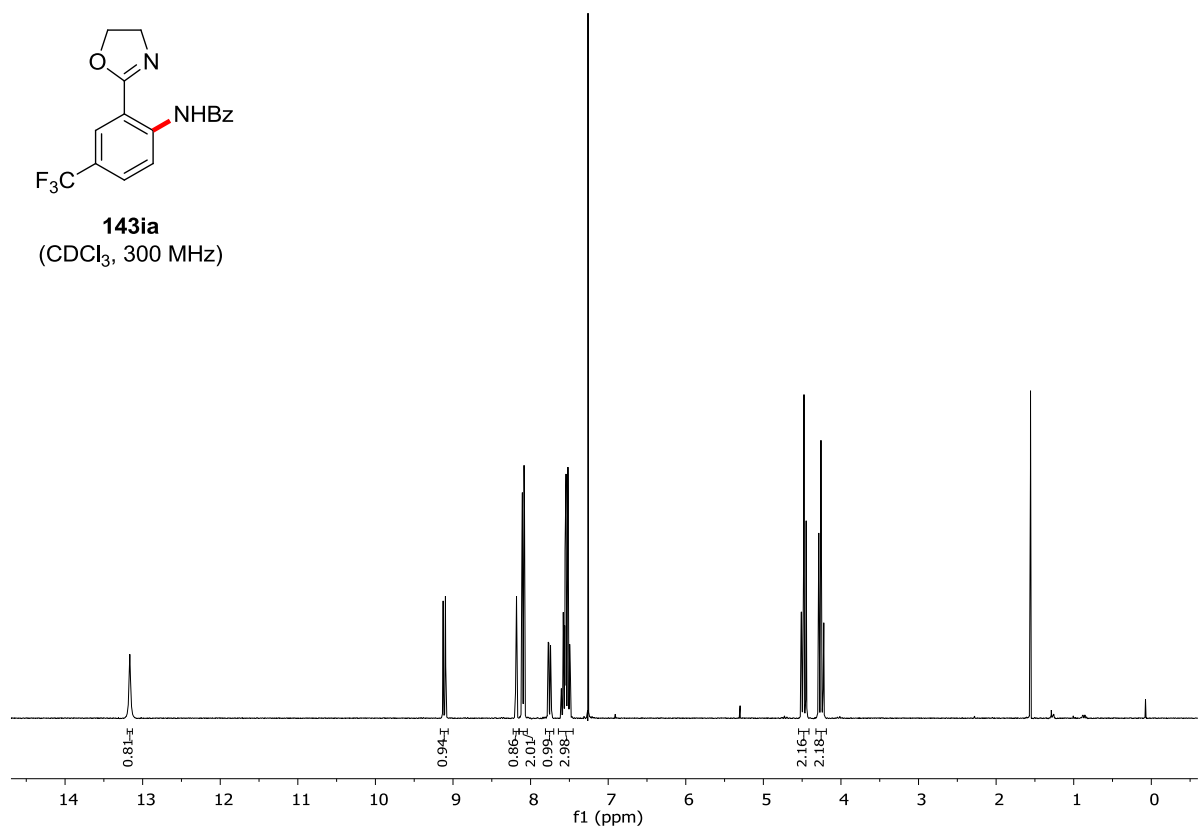


143ha
(CDCl₃, 100 MHz)

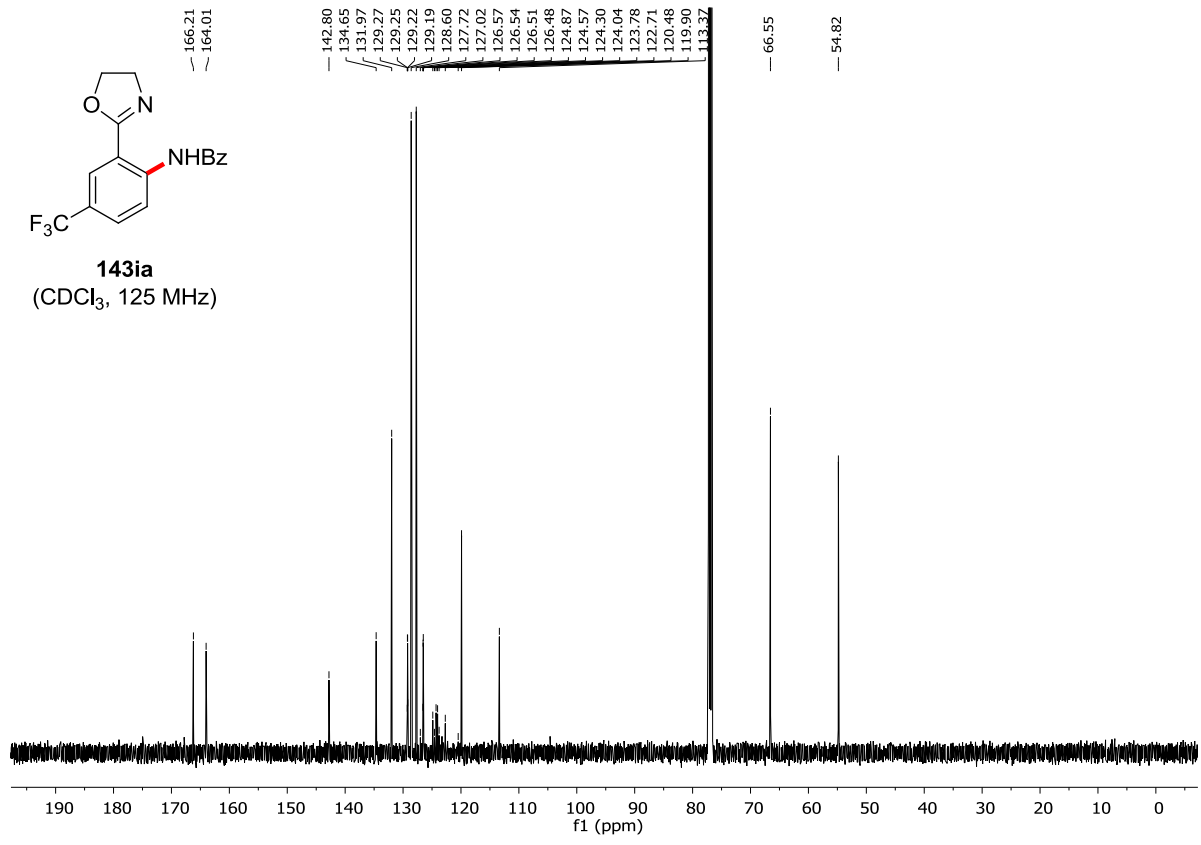


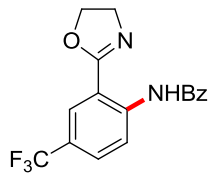


143ia
(CDCl₃, 300 MHz)

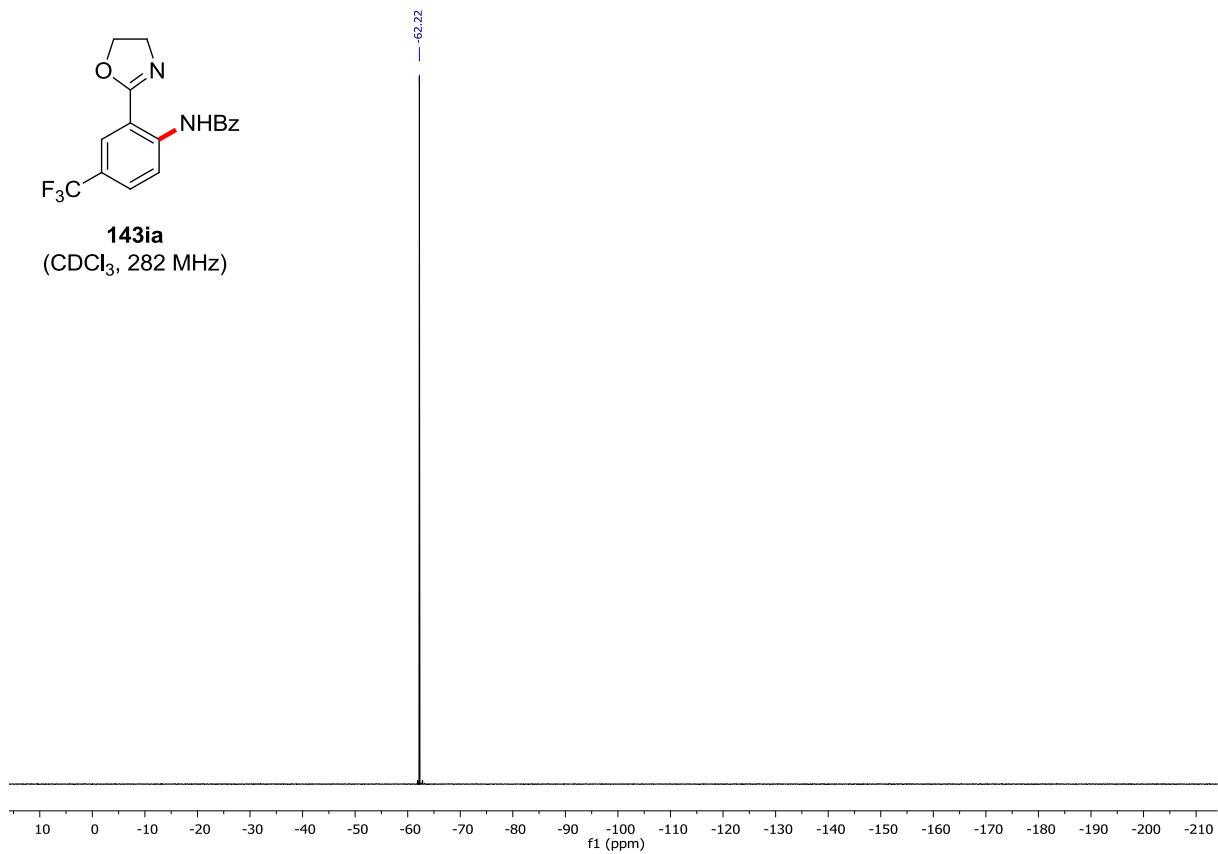


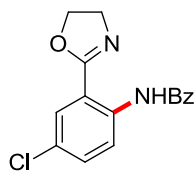
143ia
(CDCl₃, 125 MHz)



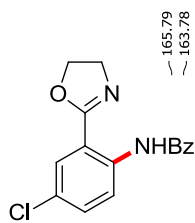
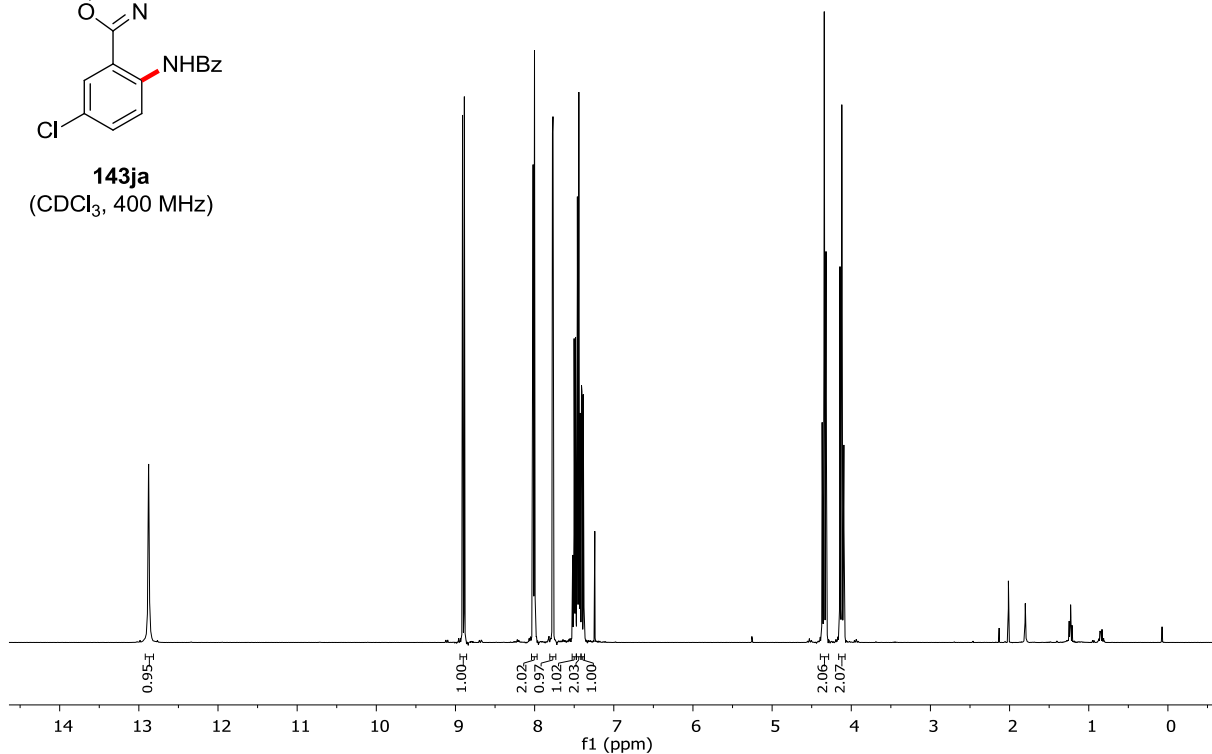


143ia
(CDCl₃, 282 MHz)

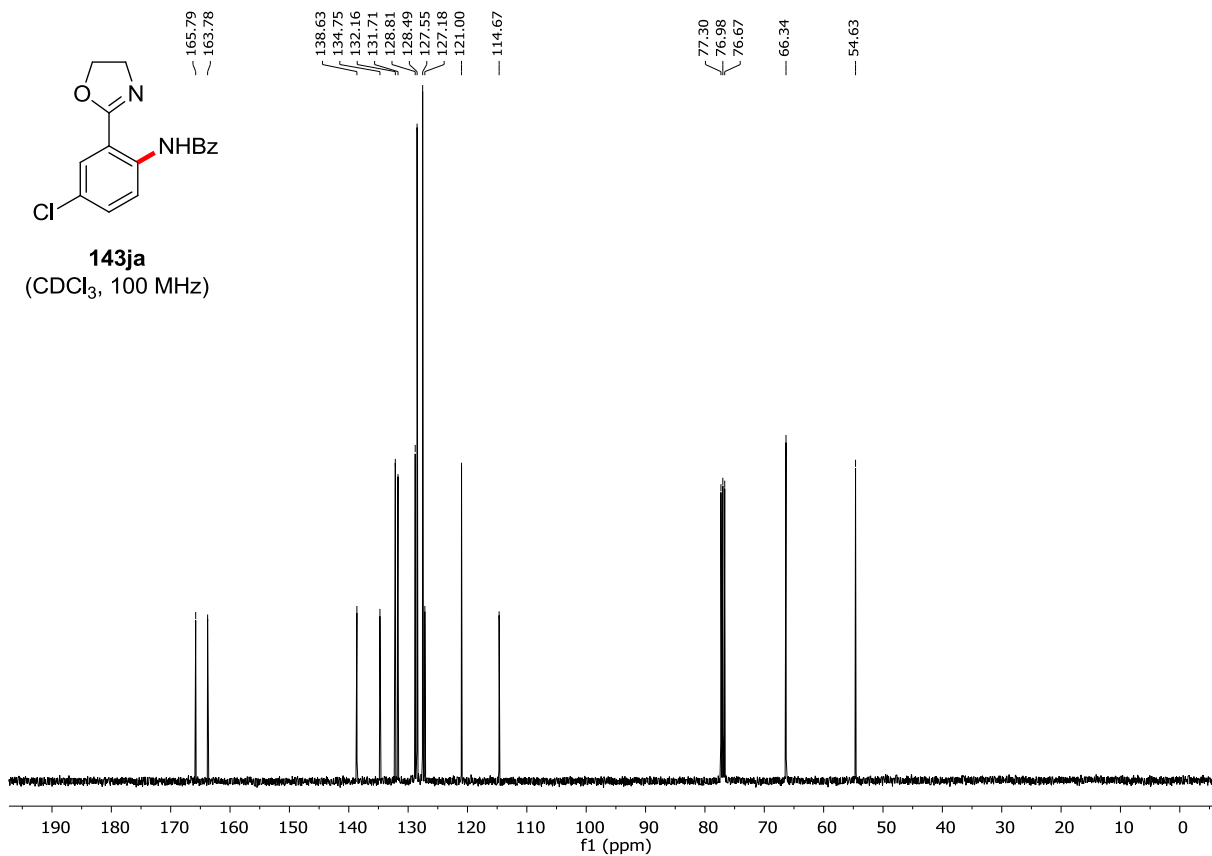


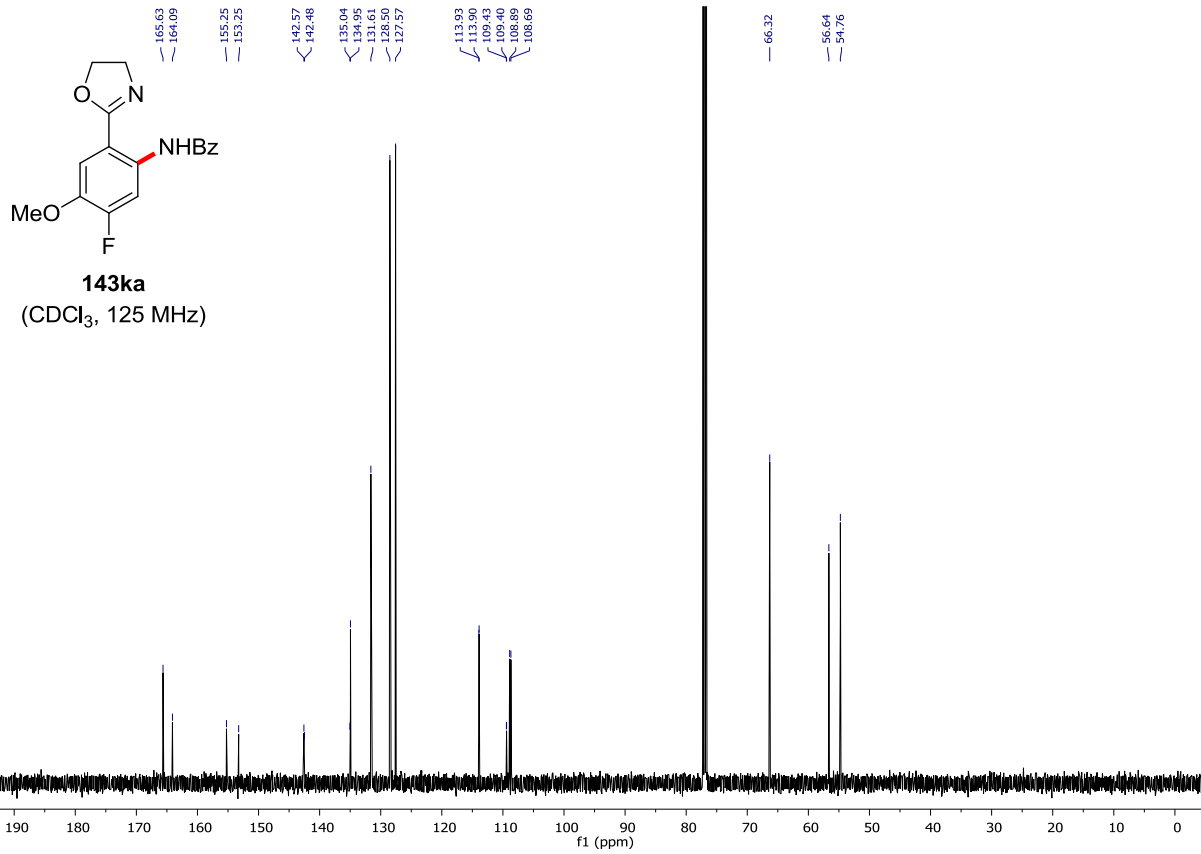
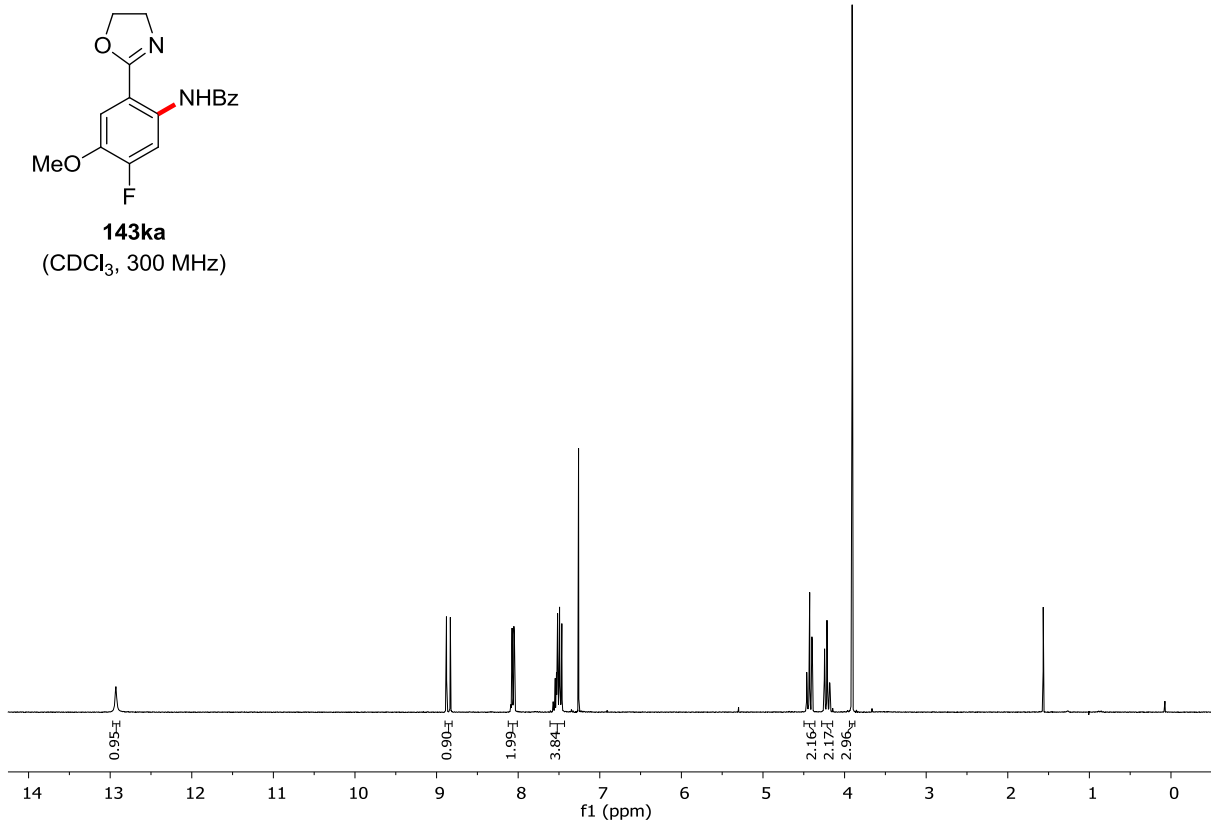
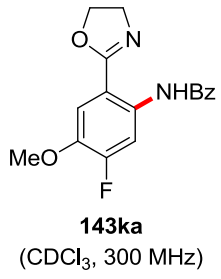


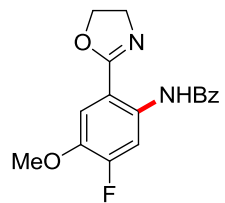
143ja
(CDCl₃, 400 MHz)



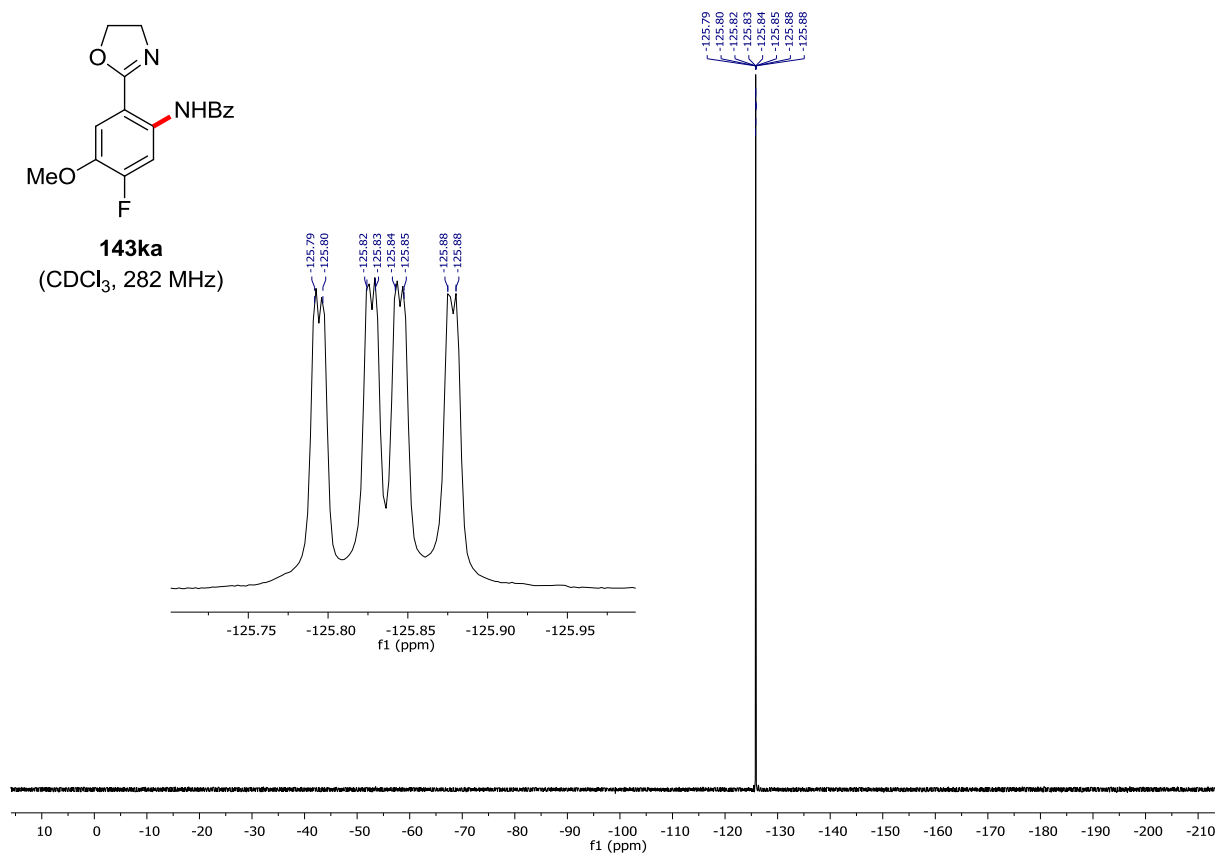
143ja
(CDCl₃, 100 MHz)

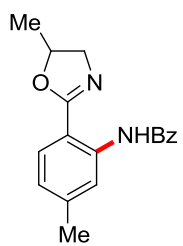




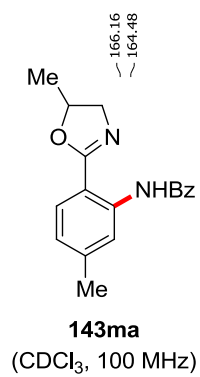
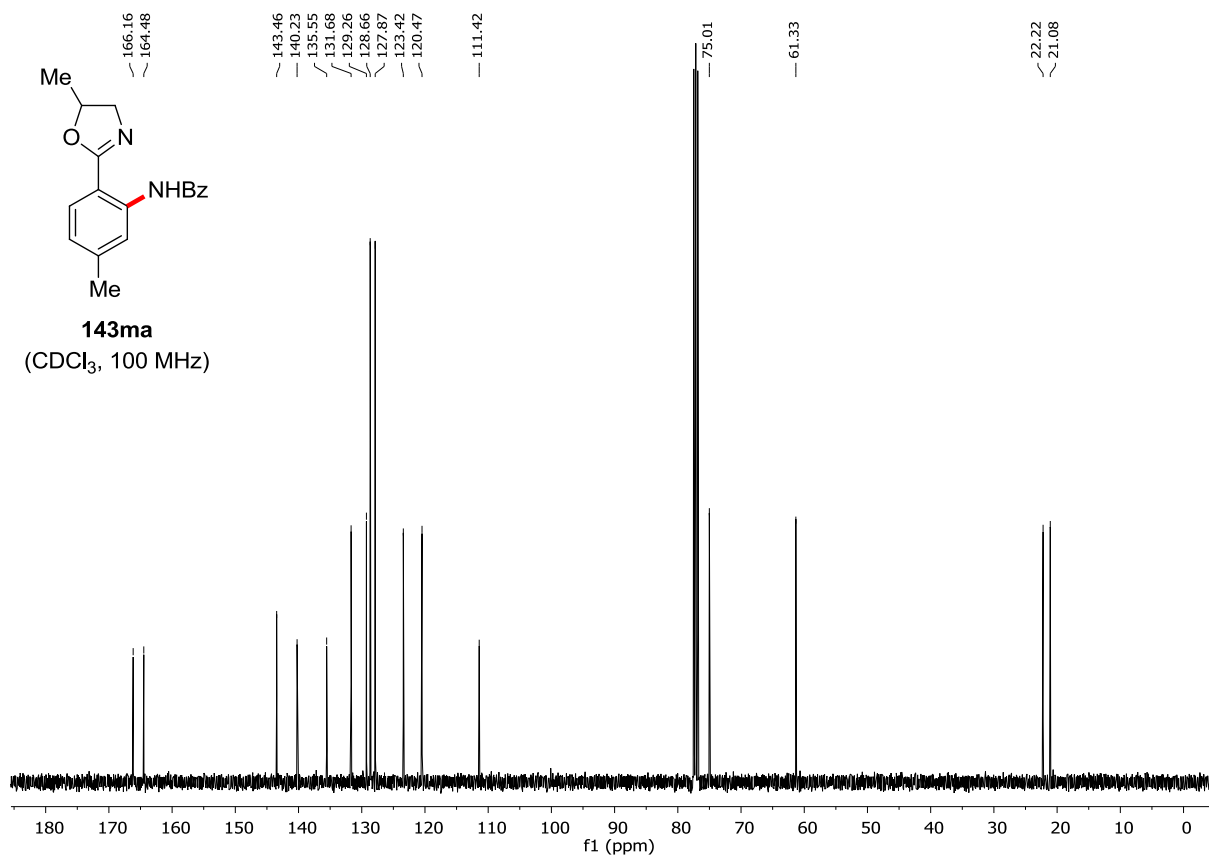
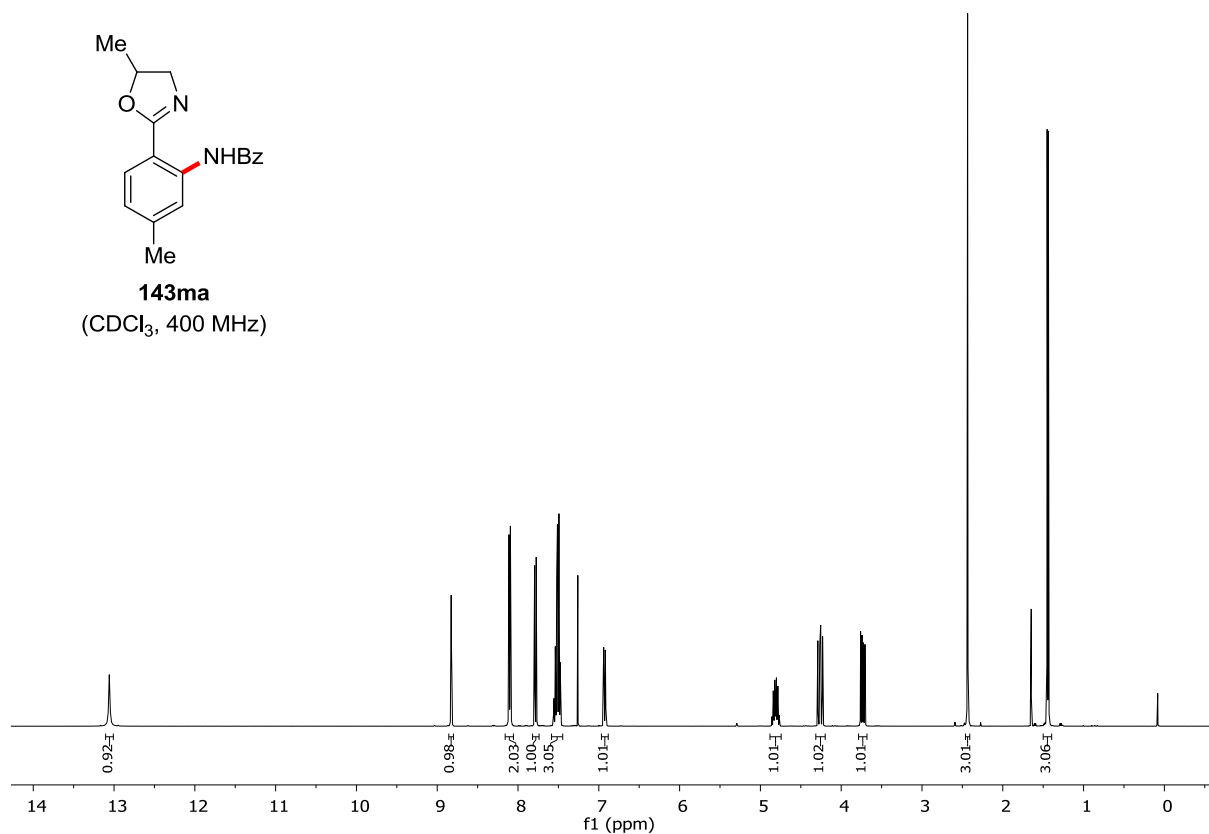


143ka
(CDCl₃, 282 MHz)

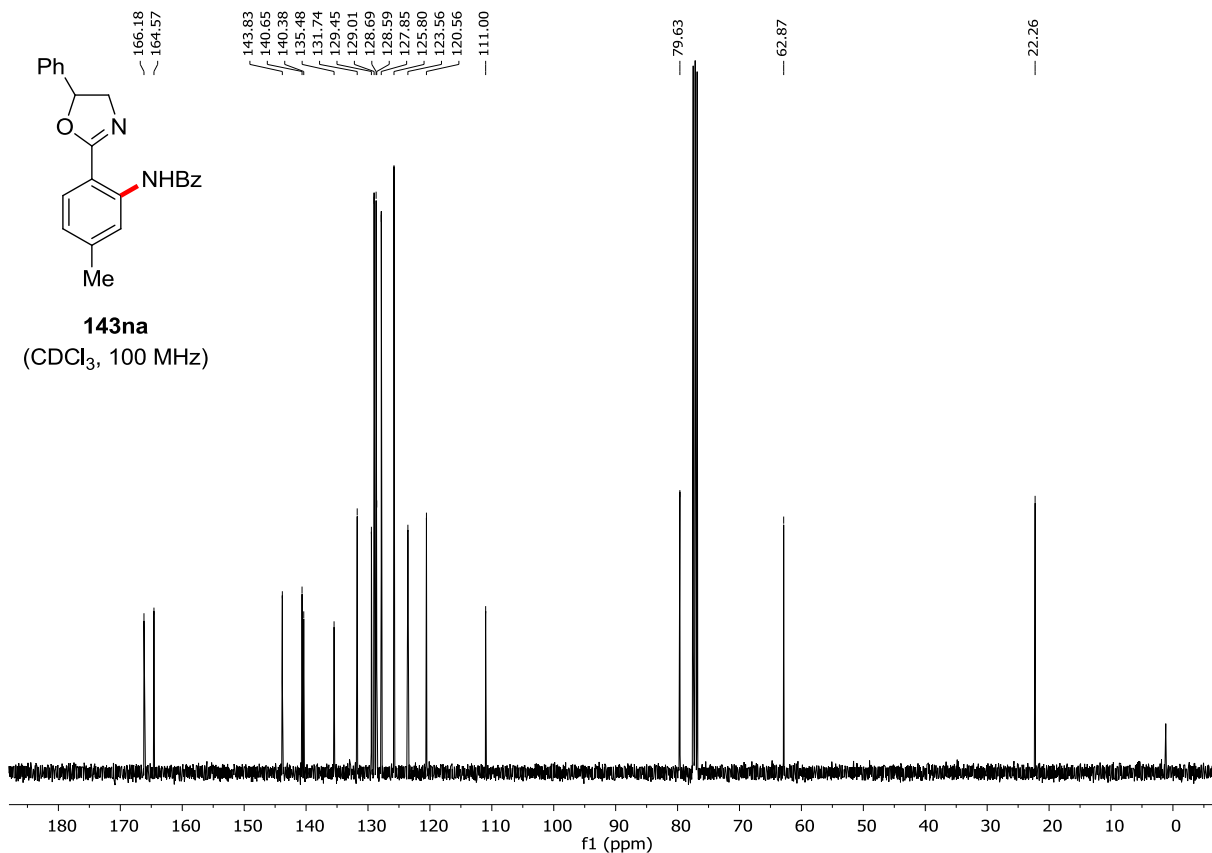
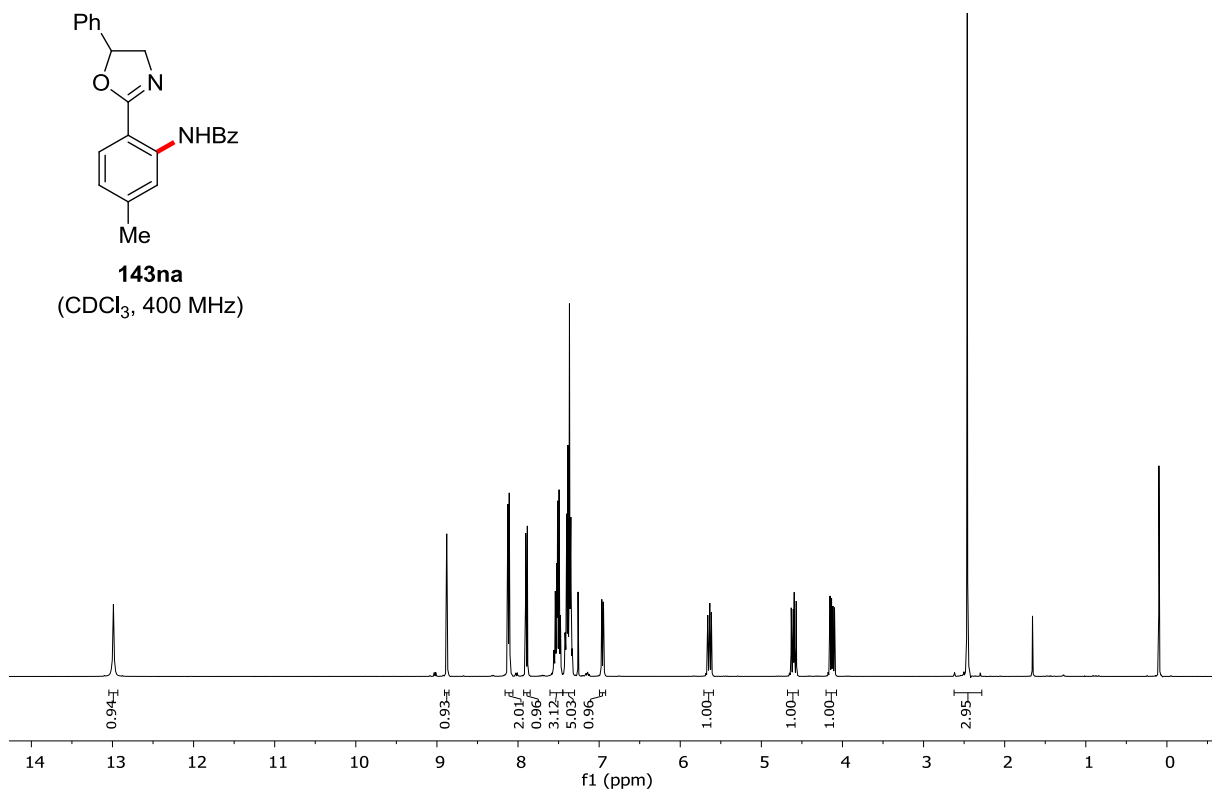
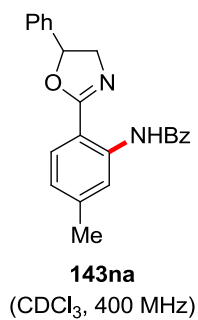


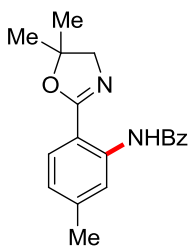


143ma
(CDCl₃, 400 MHz)

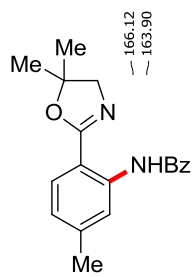
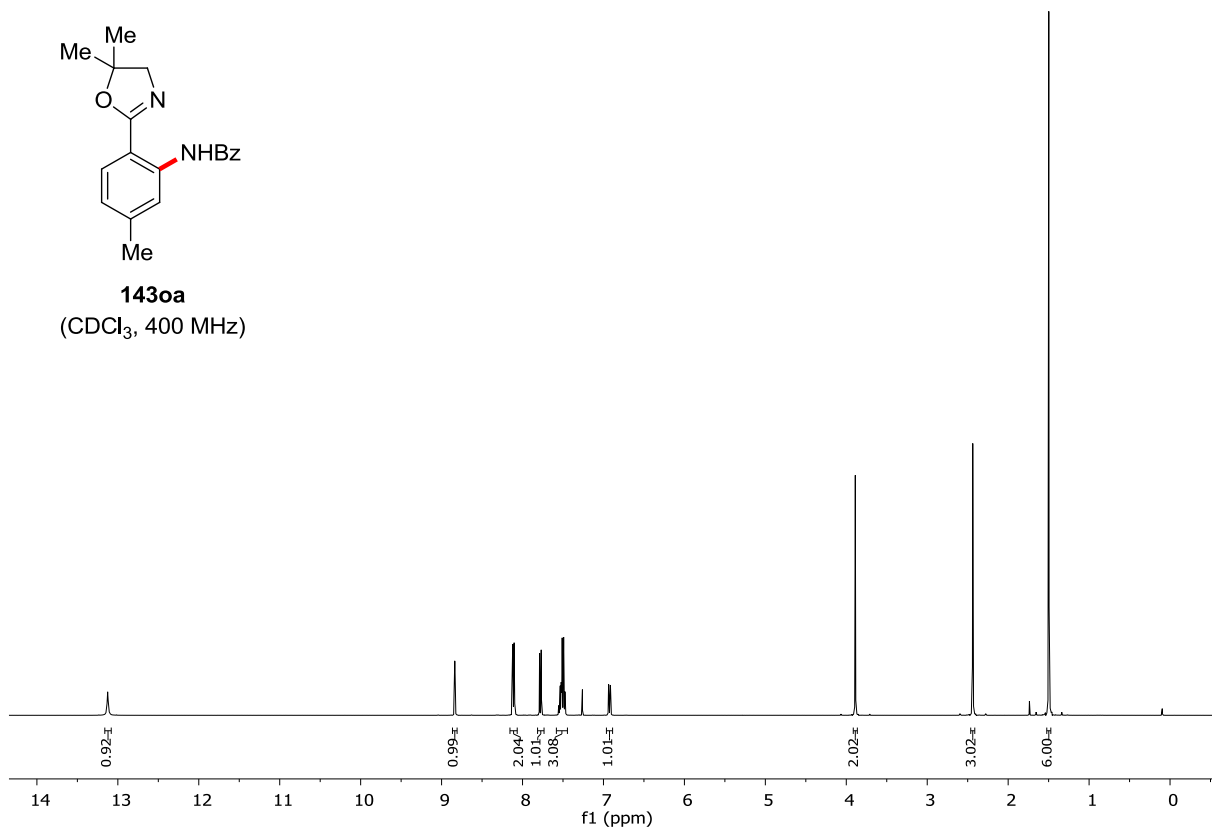


143ma
(CDCl₃, 100 MHz)

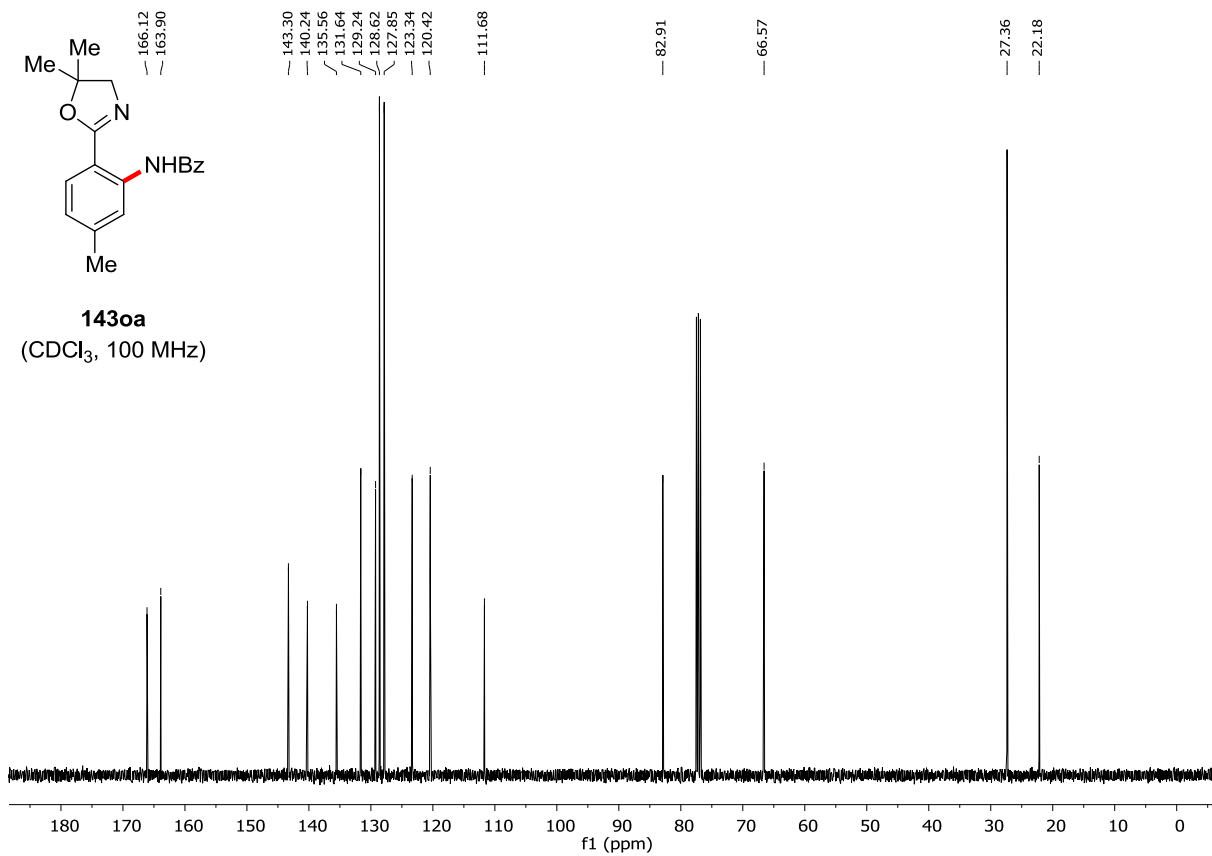


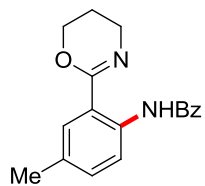


143oa
(CDCl₃, 400 MHz)

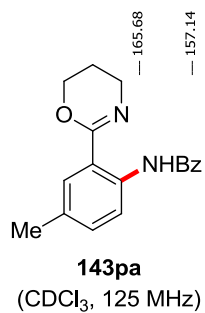
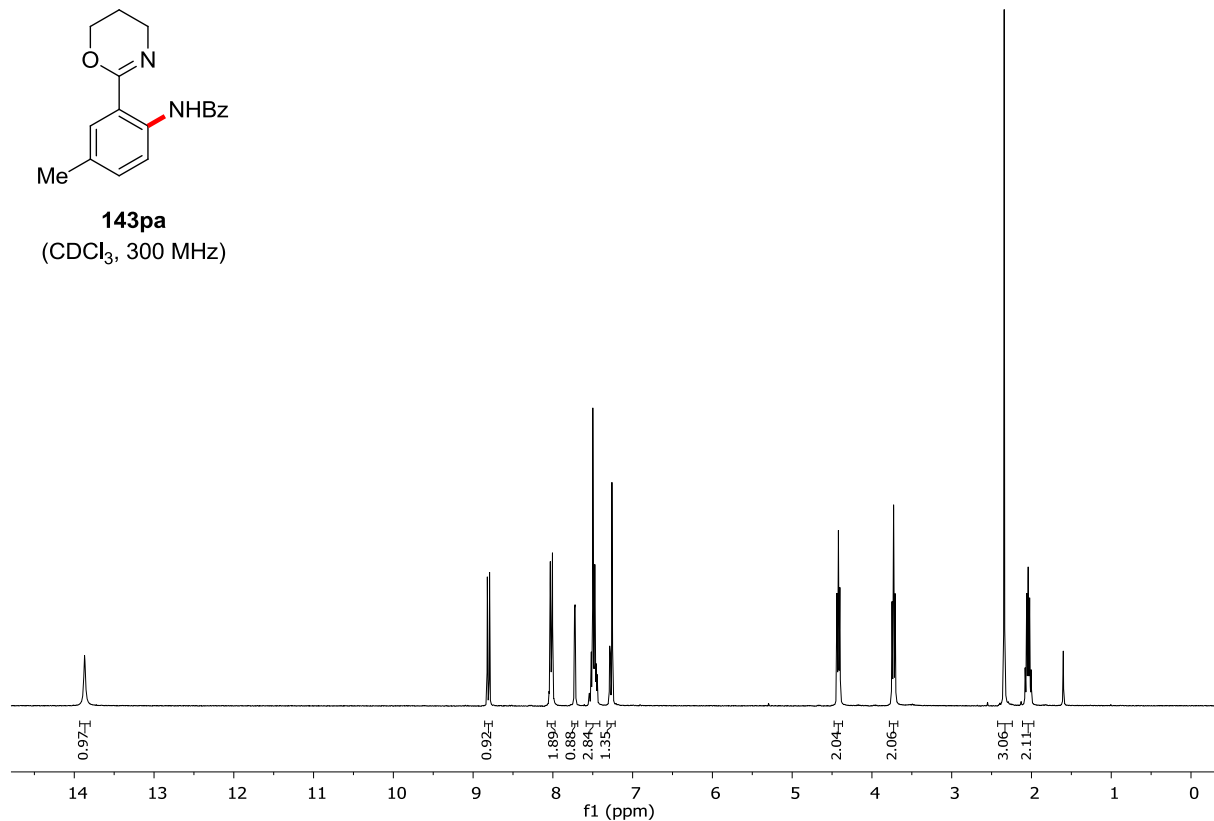


143oa
(CDCl₃, 100 MHz)

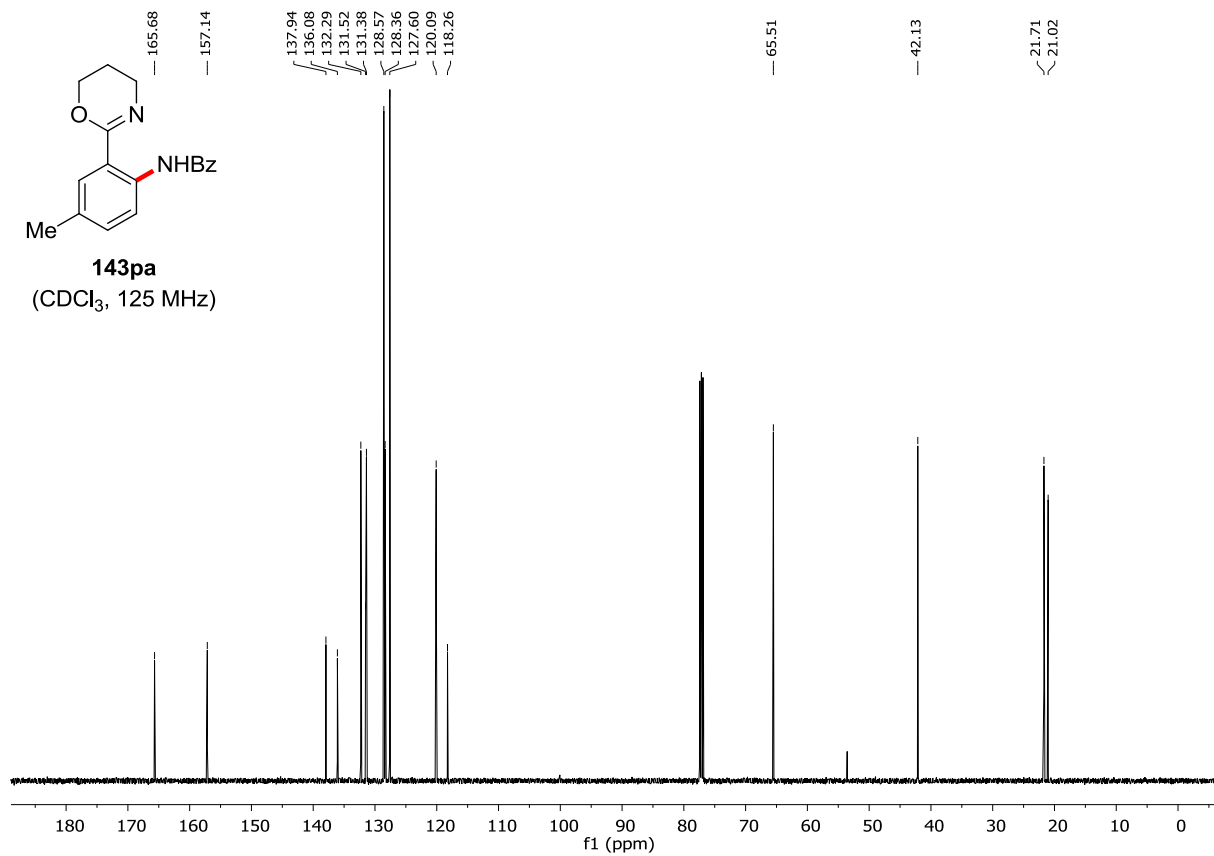


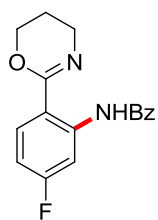


143pa
(CDCl₃, 300 MHz)

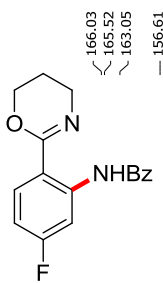
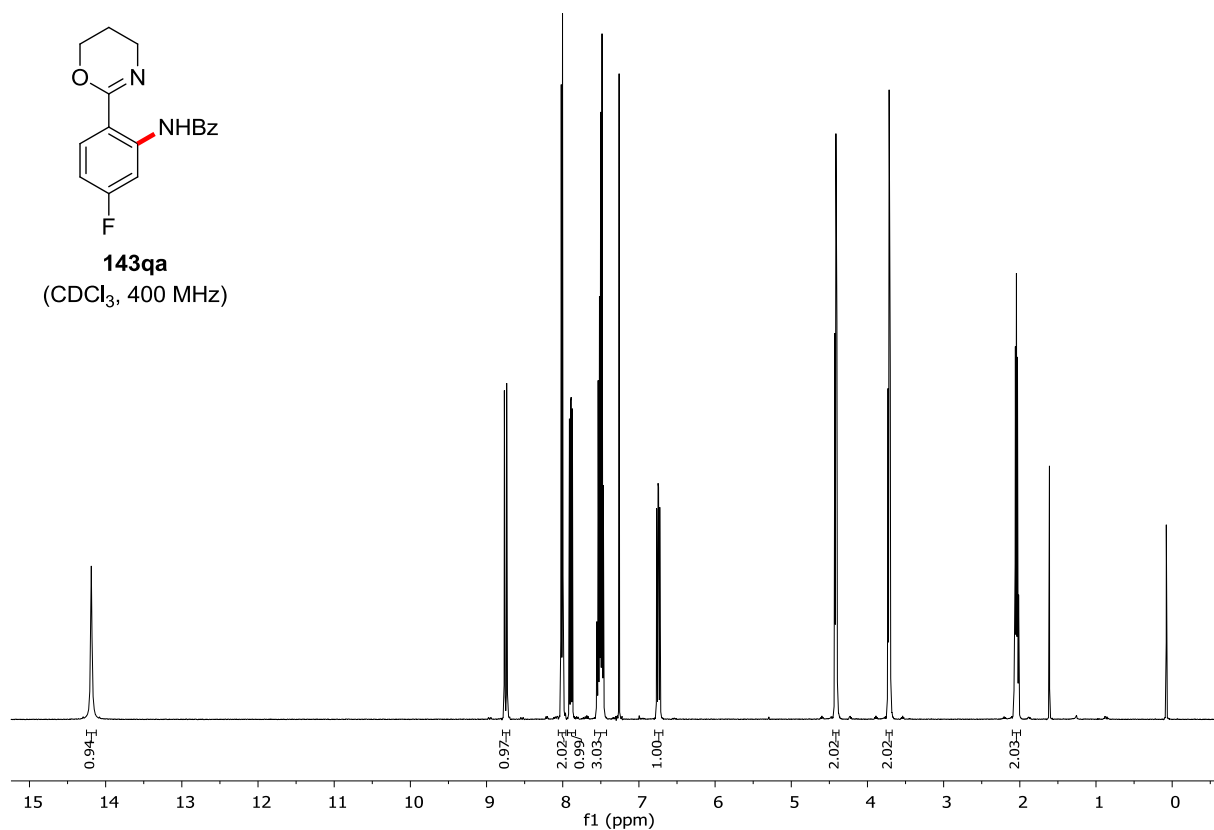


143pa
(CDCl₃, 125 MHz)

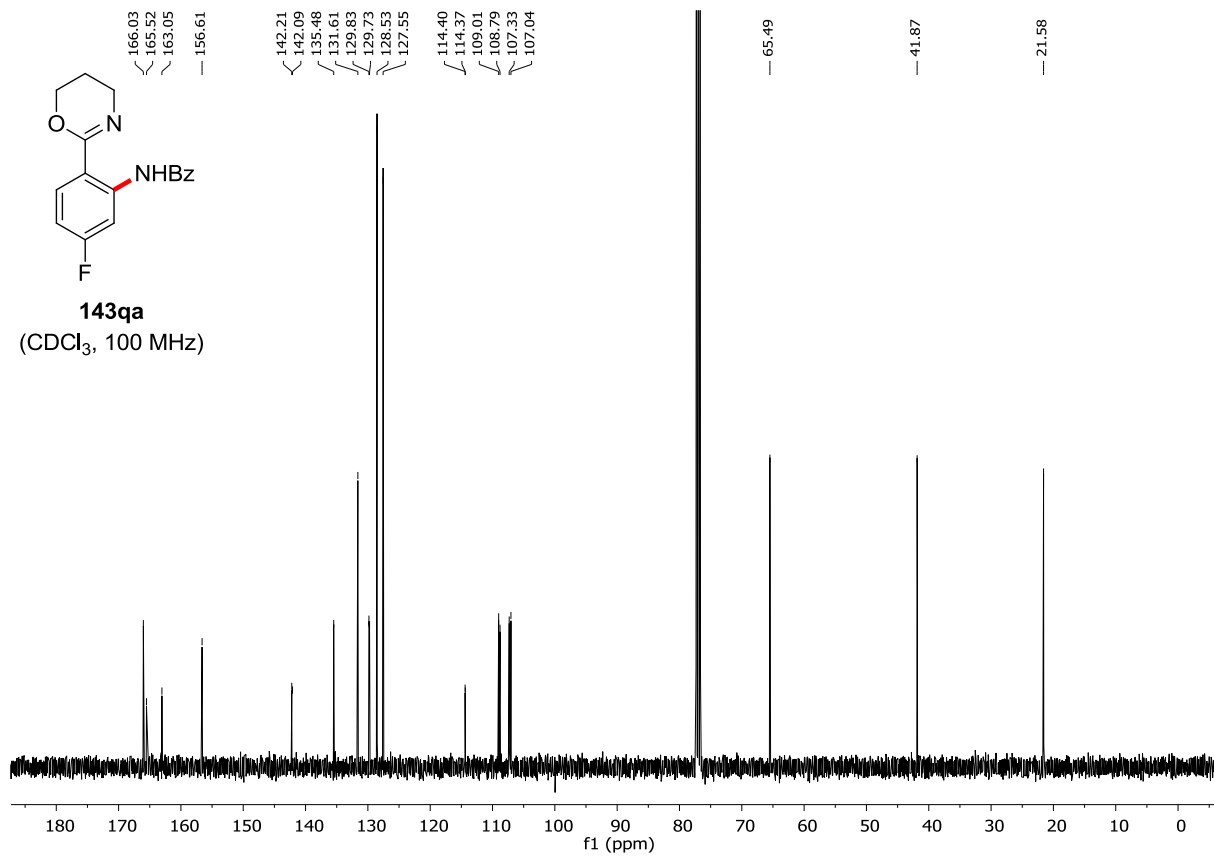


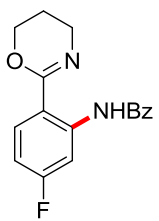


143qa
(CDCl₃, 400 MHz)

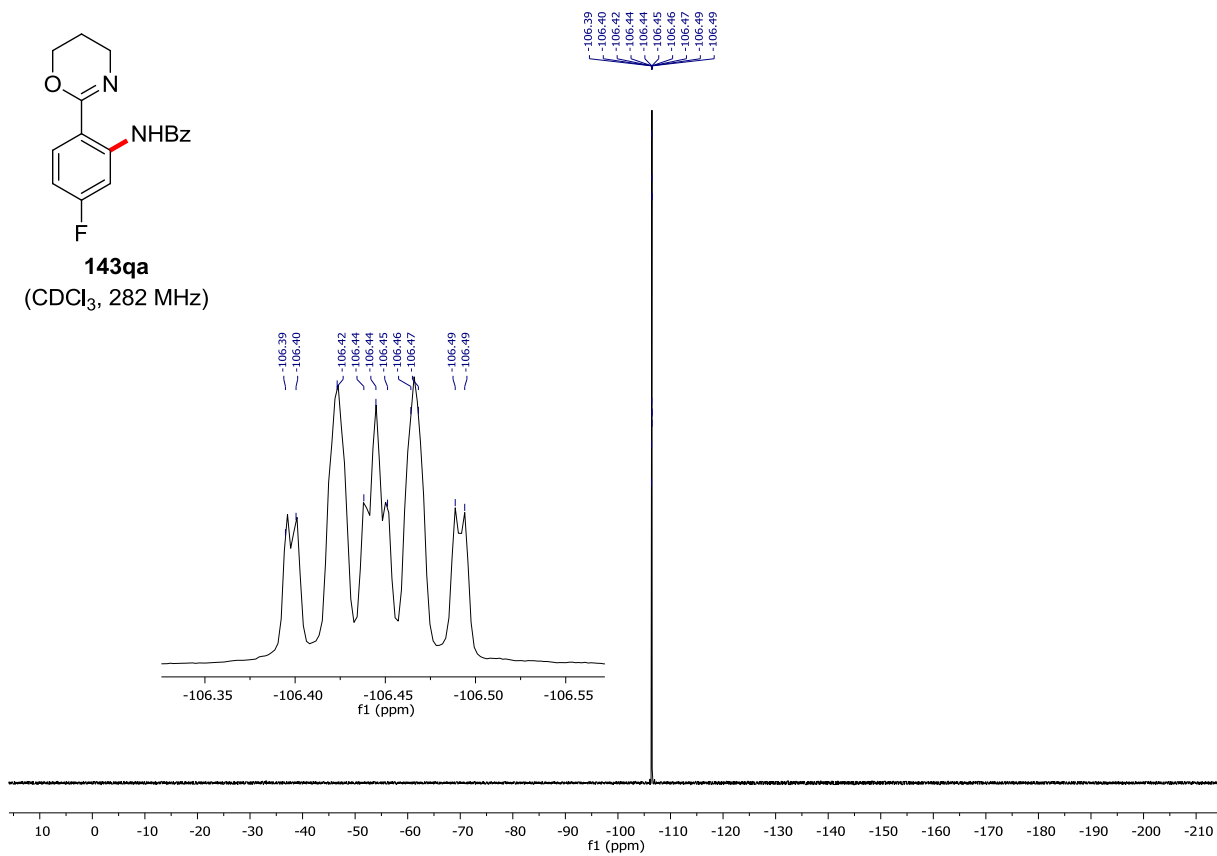


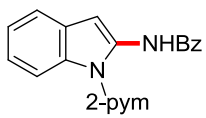
143qa
(CDCl₃, 100 MHz)



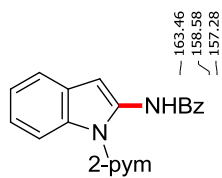
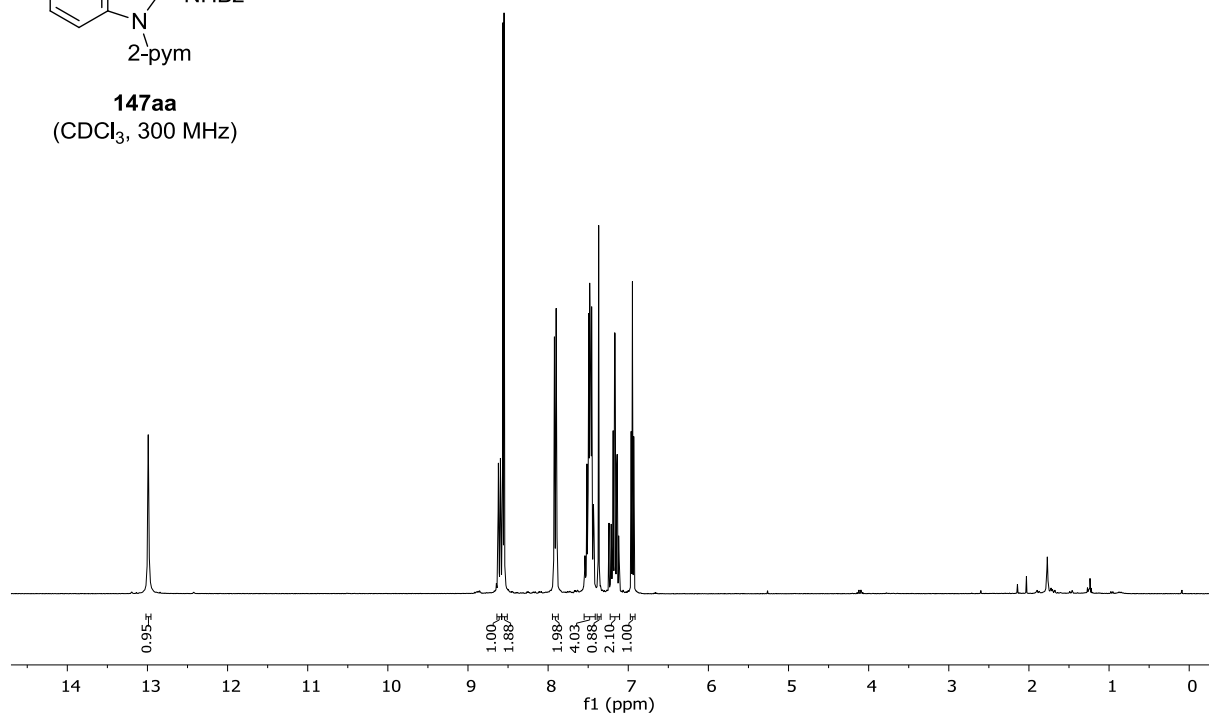


143qa
(CDCl₃, 282 MHz)

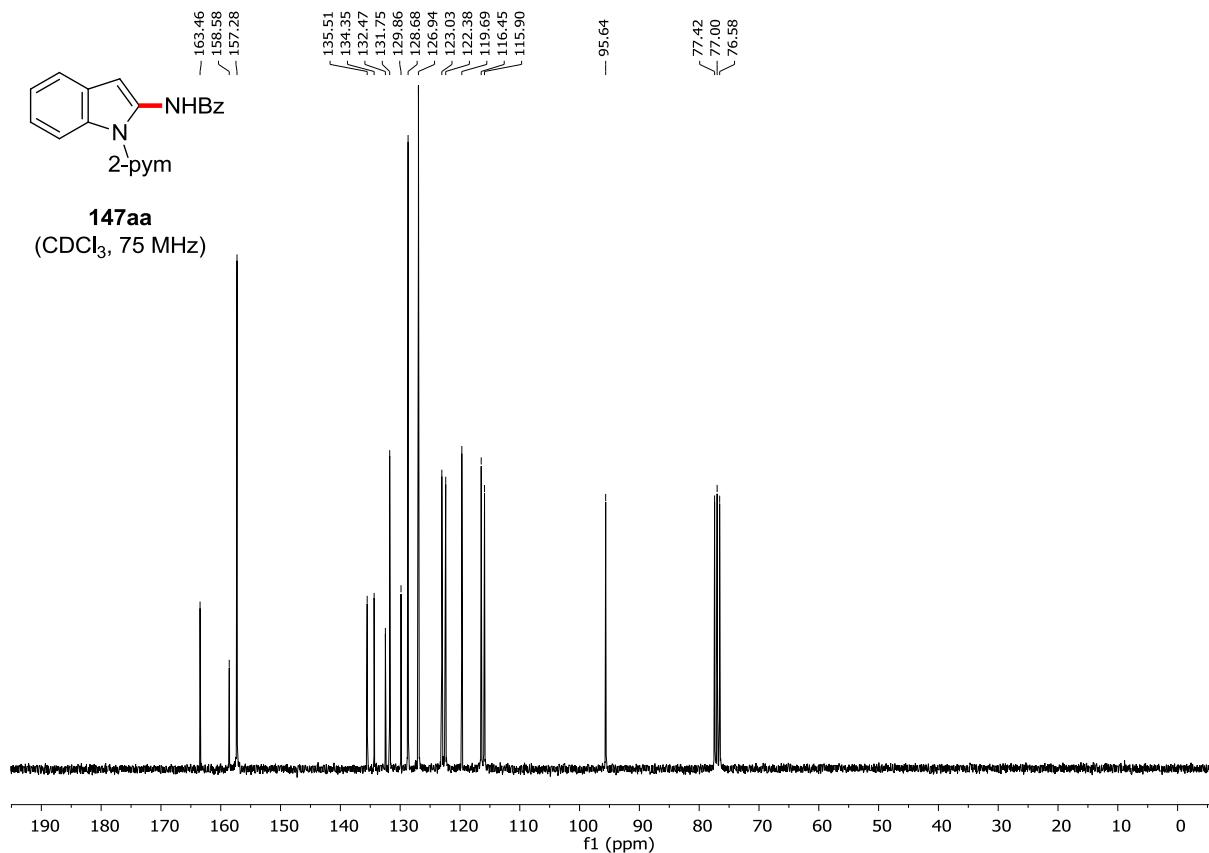


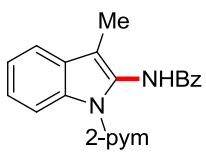


147aa
(CDCl₃, 300 MHz)

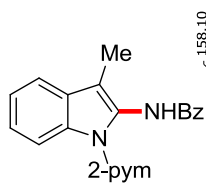
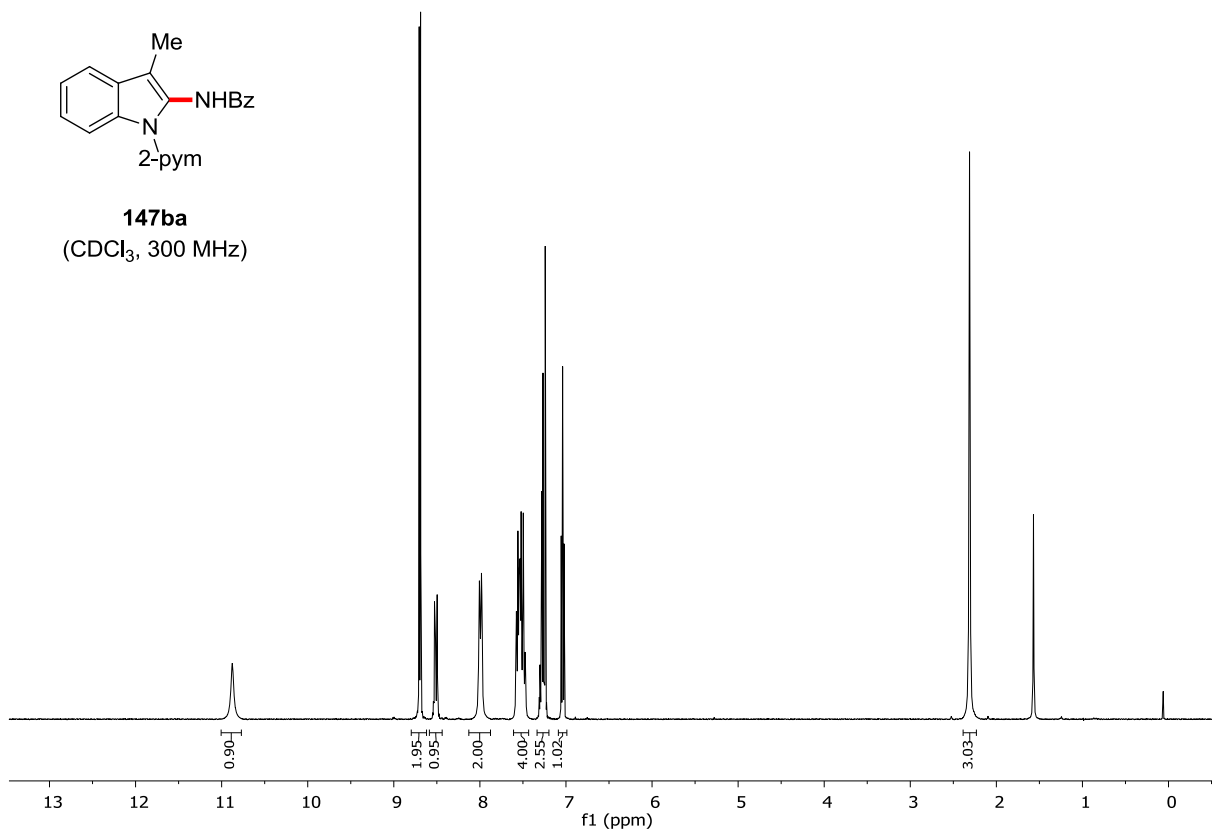


147aa
(CDCl₃, 75 MHz)

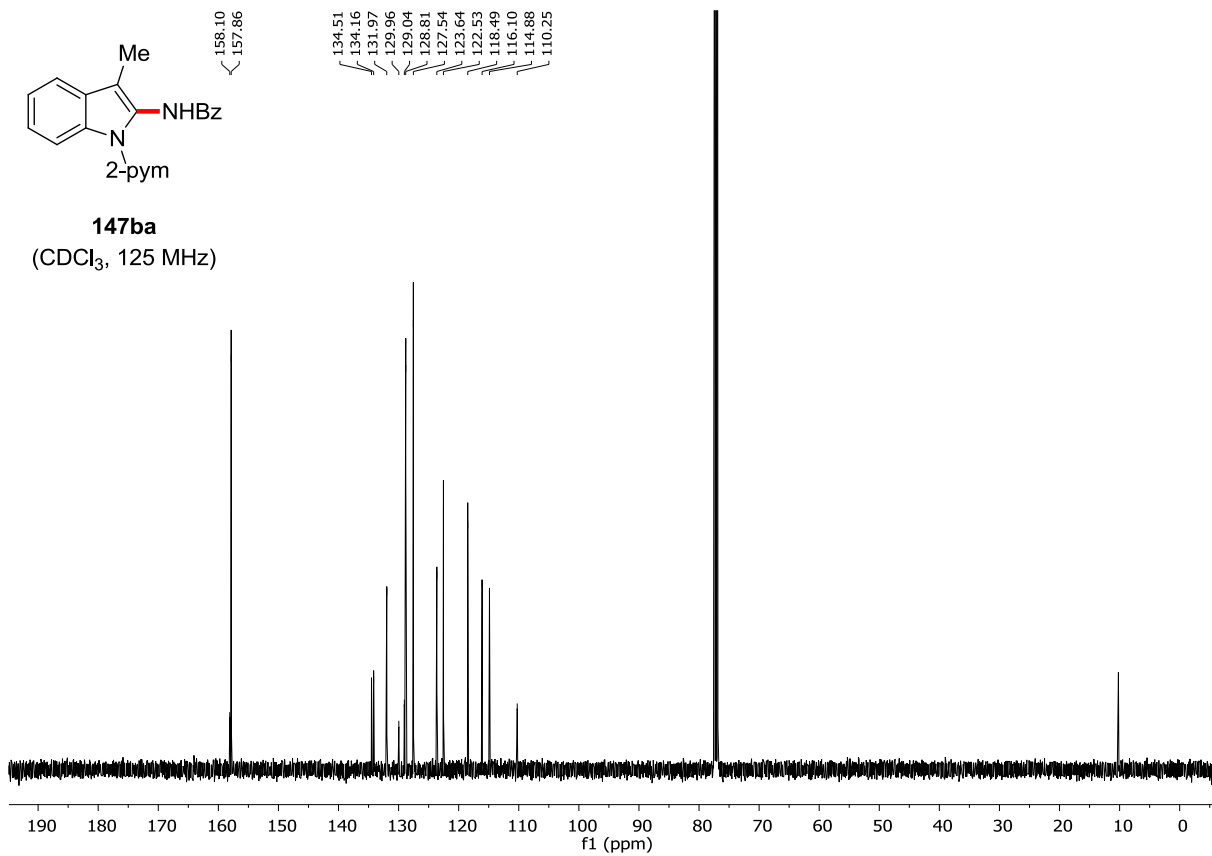




147ba
(CDCl₃, 300 MHz)

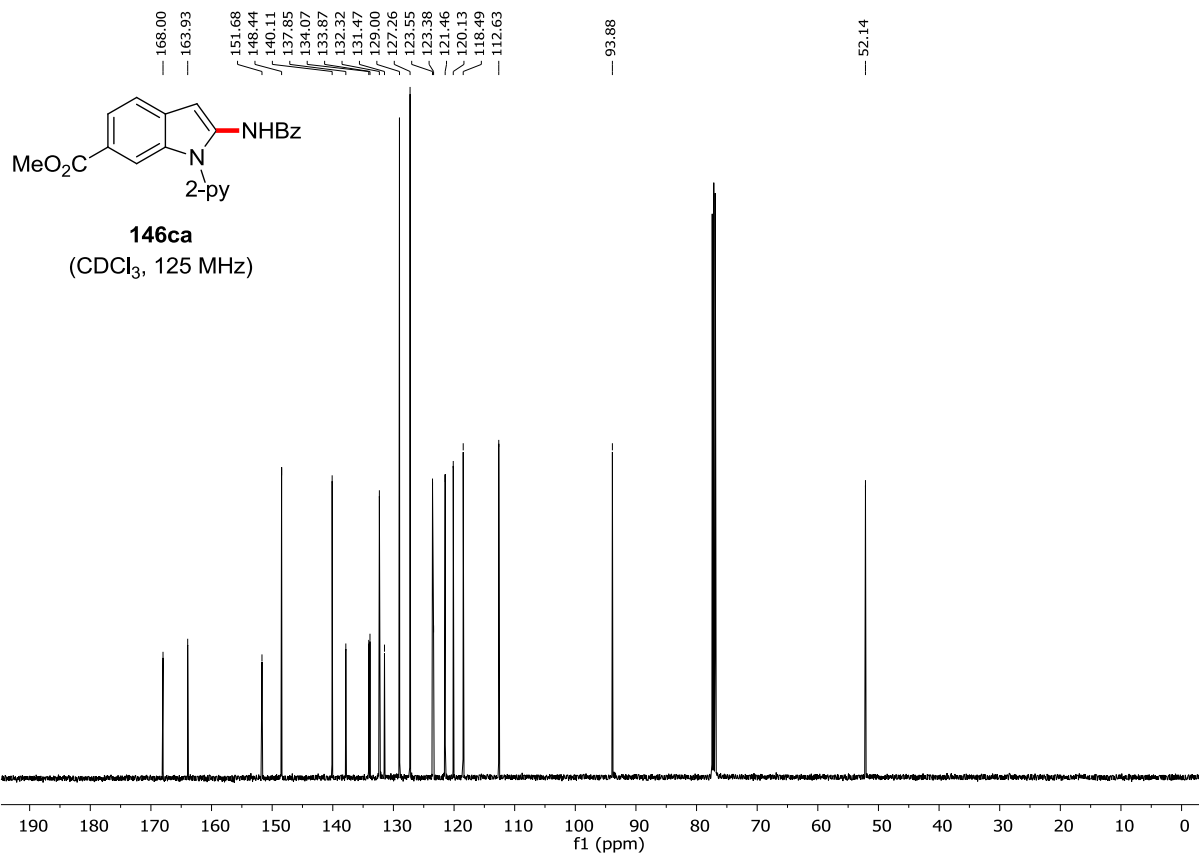
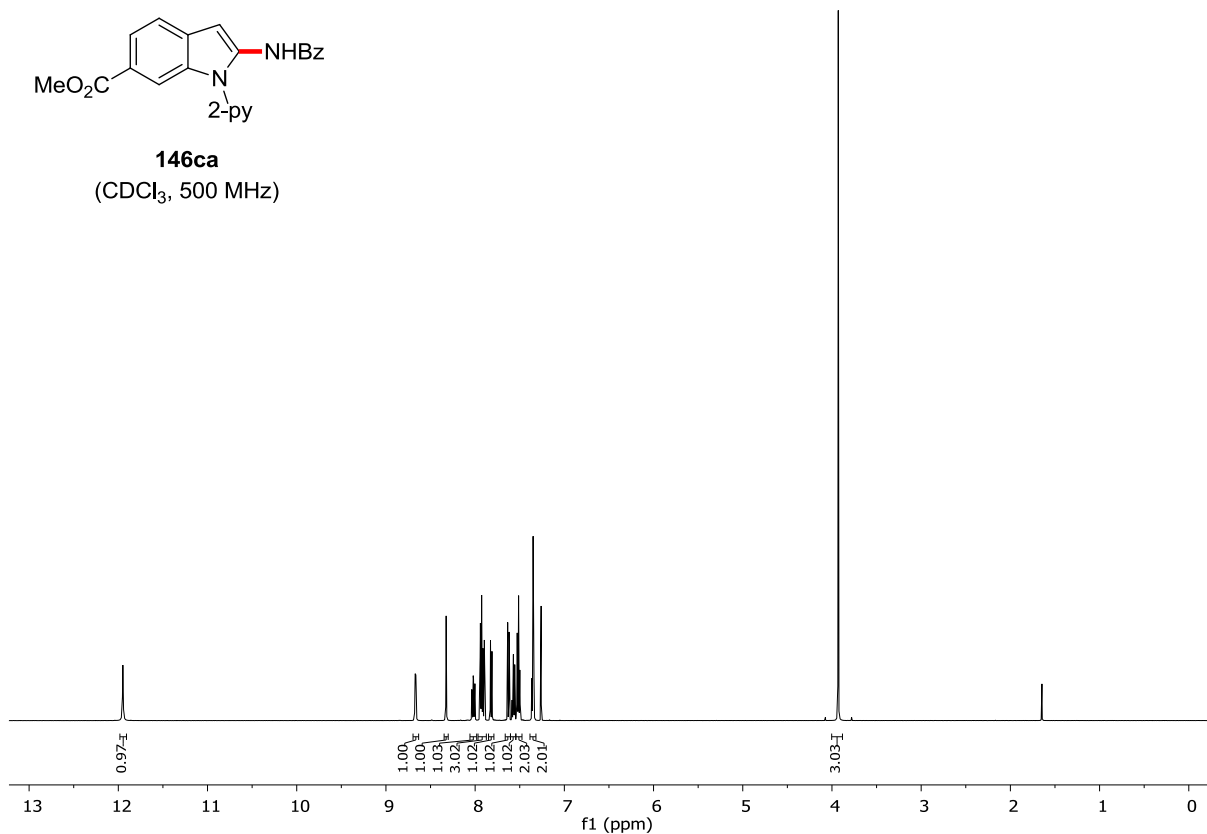


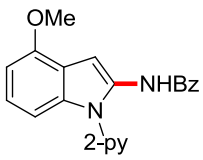
147ba
(CDCl₃, 125 MHz)



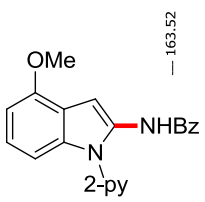
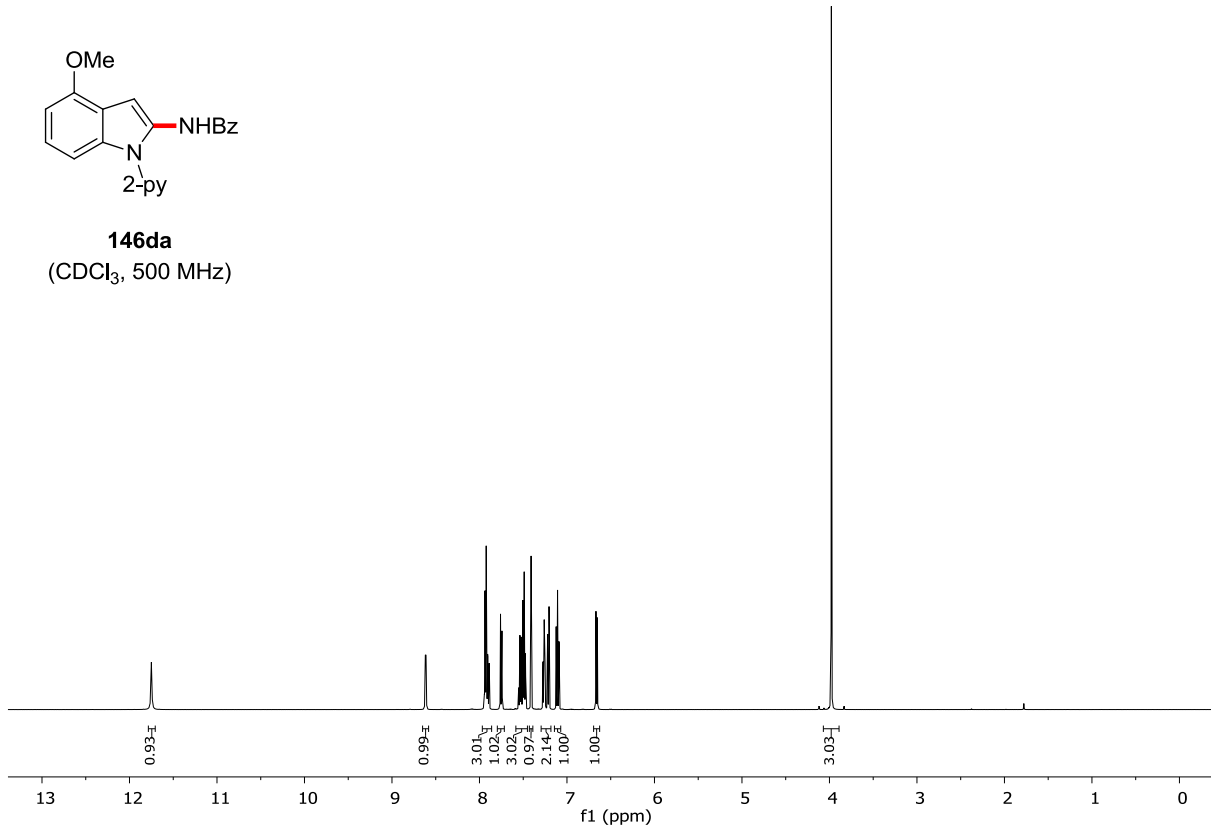


146ca
(CDCl₃, 500 MHz)

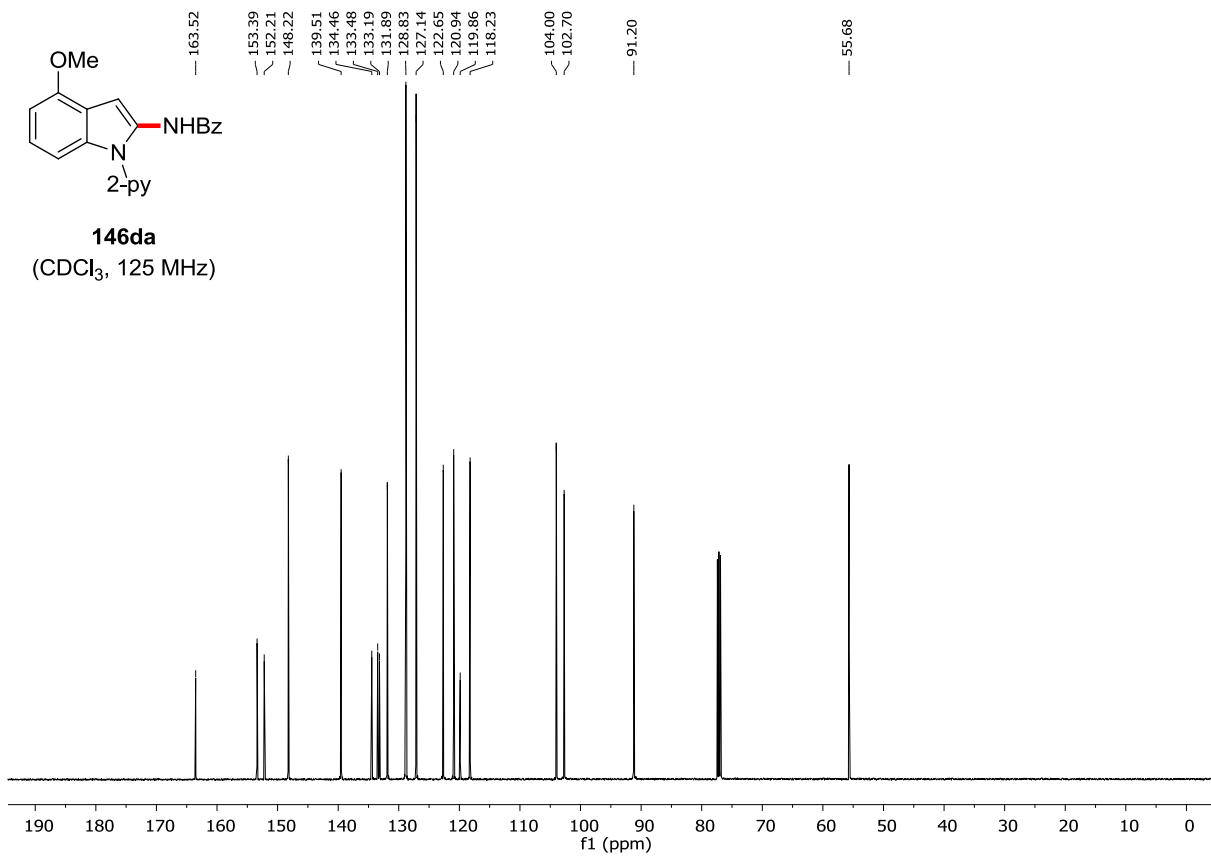


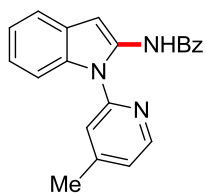


146da
(CDCl₃, 500 MHz)

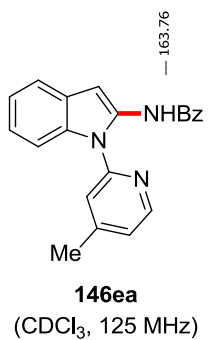
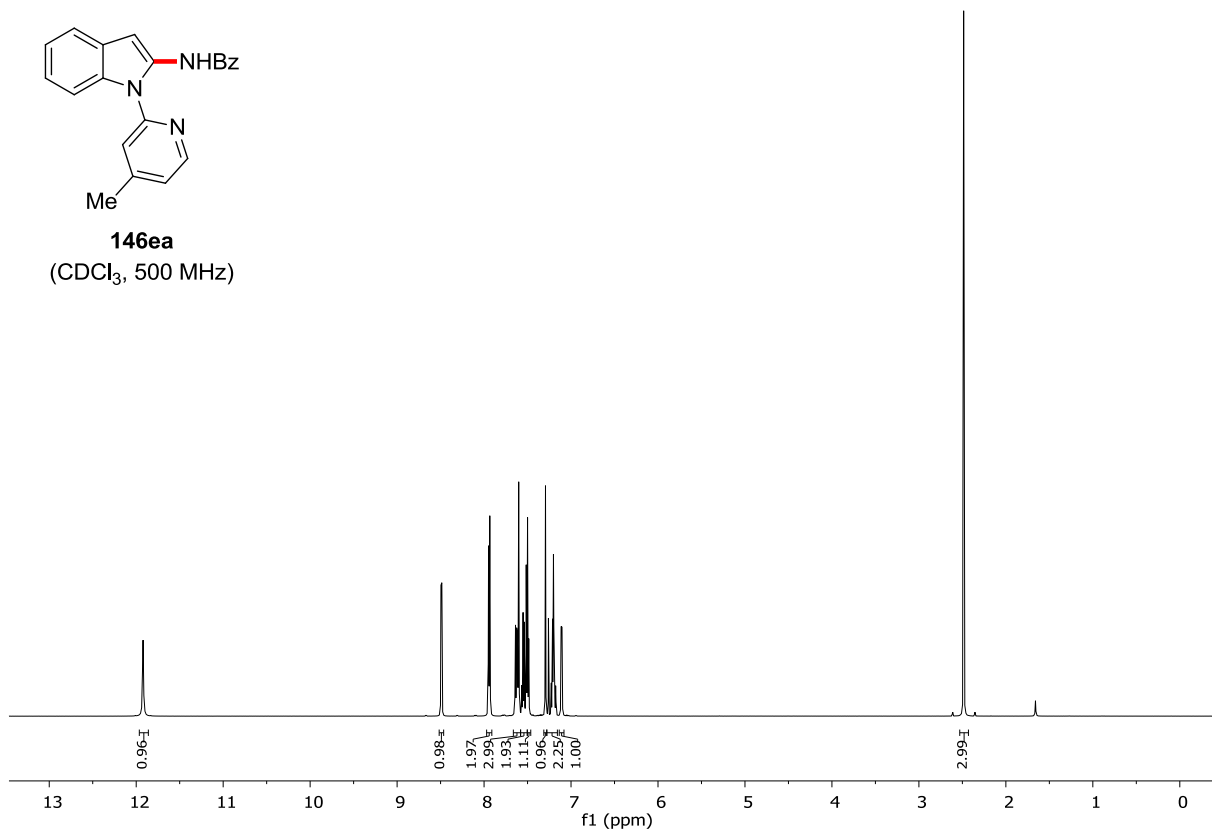


146da
(CDCl₃, 125 MHz)

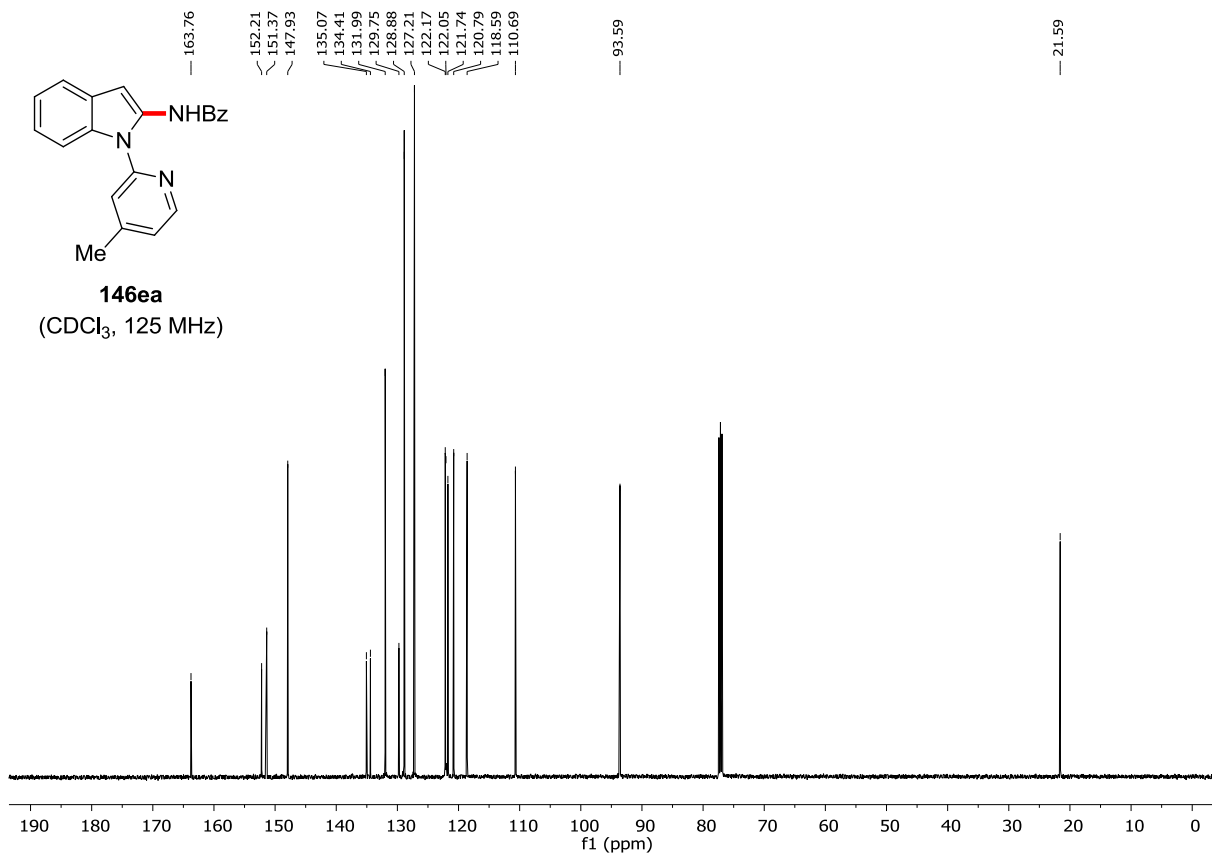


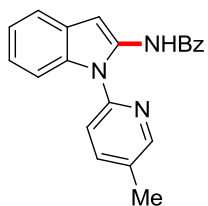


146ea
(CDCl₃, 500 MHz)

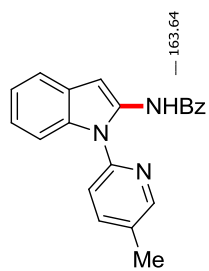
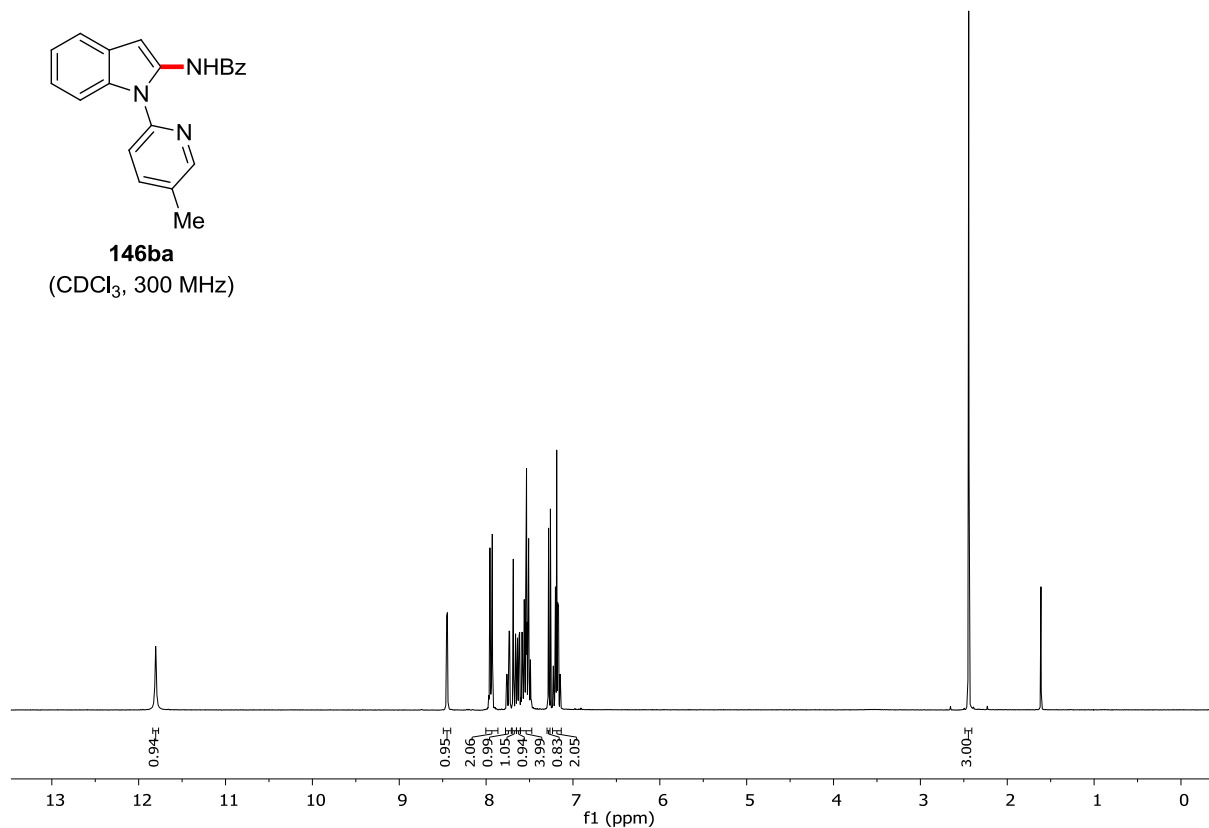


146ea
(CDCl₃, 125 MHz)

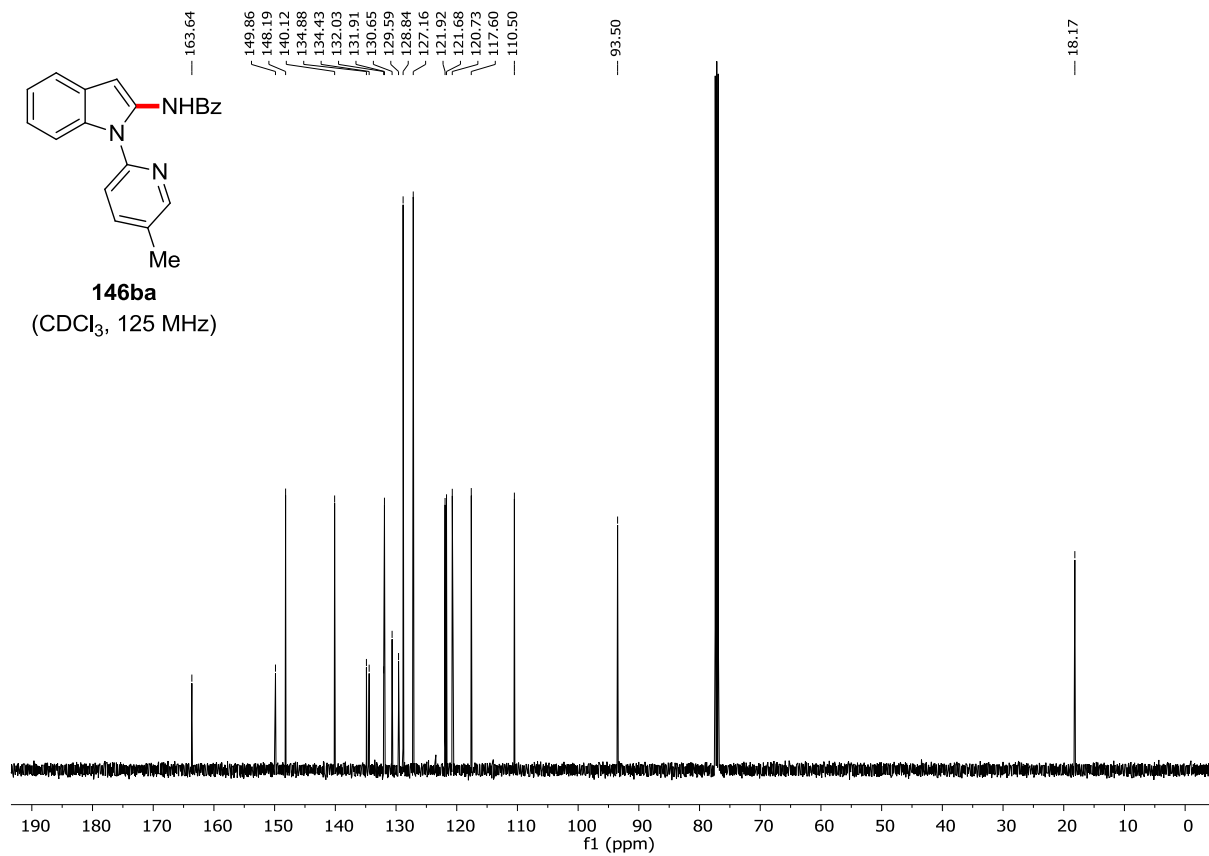


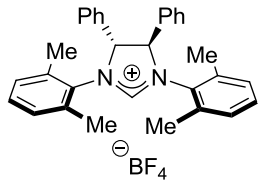


146ba
(CDCl₃, 300 MHz)

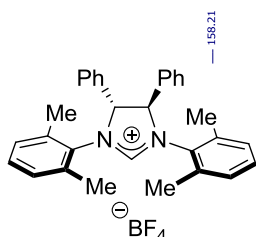
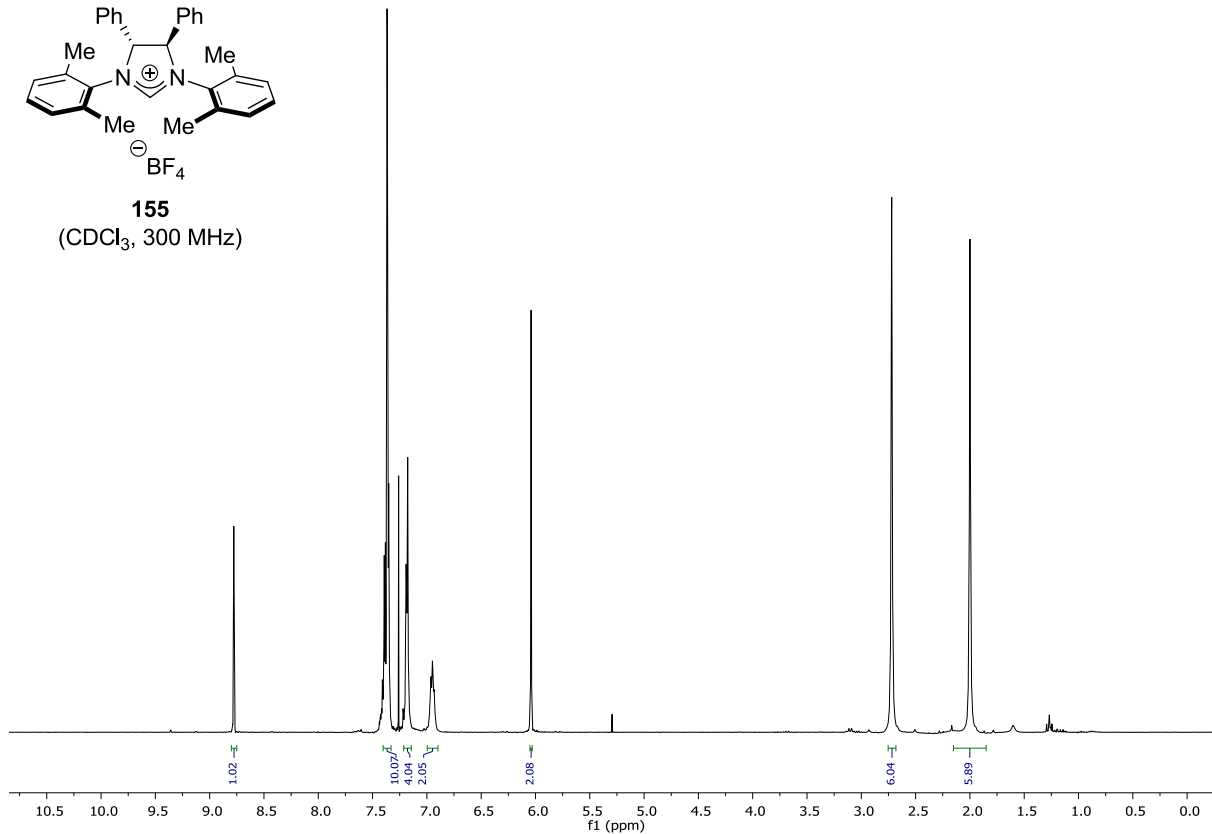


146ba
(CDCl₃, 125 MHz)

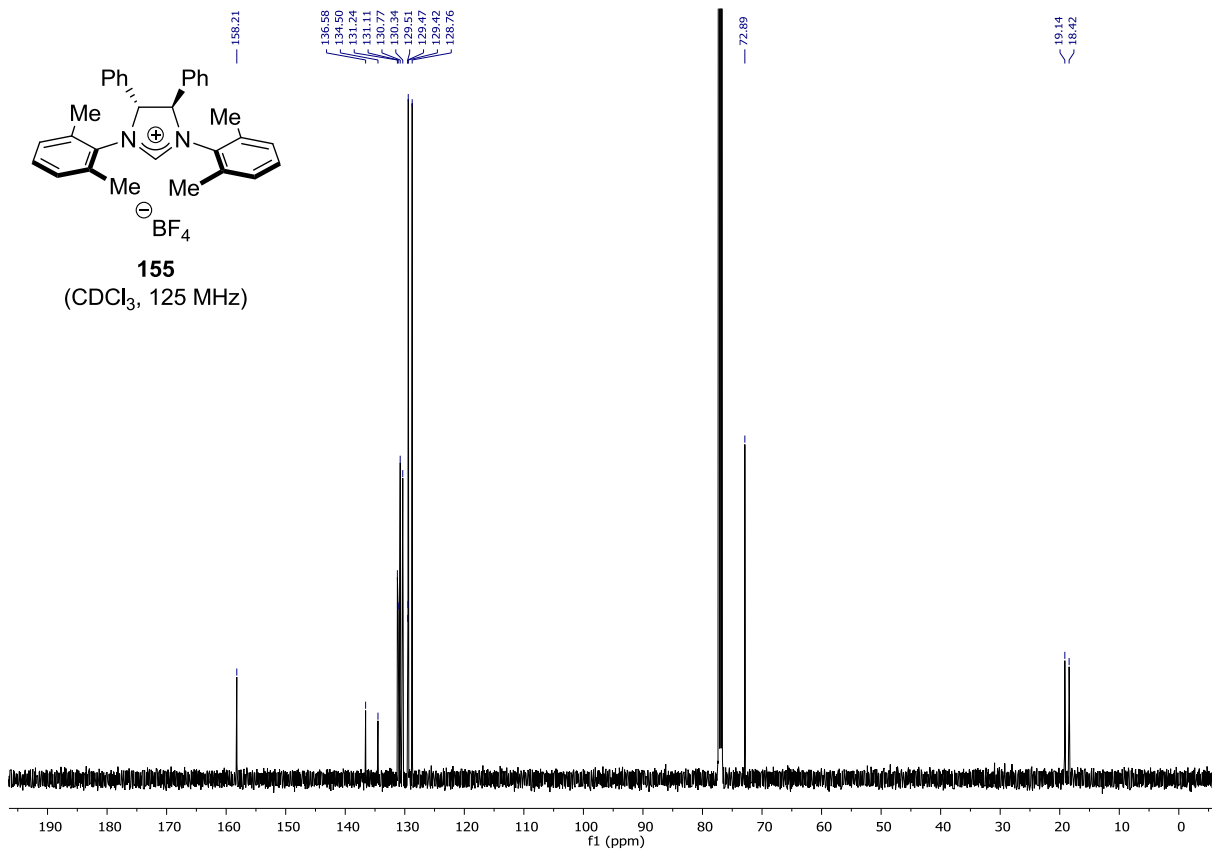


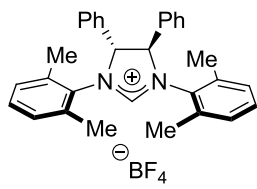


155
(CDCl_3 , 300 MHz)

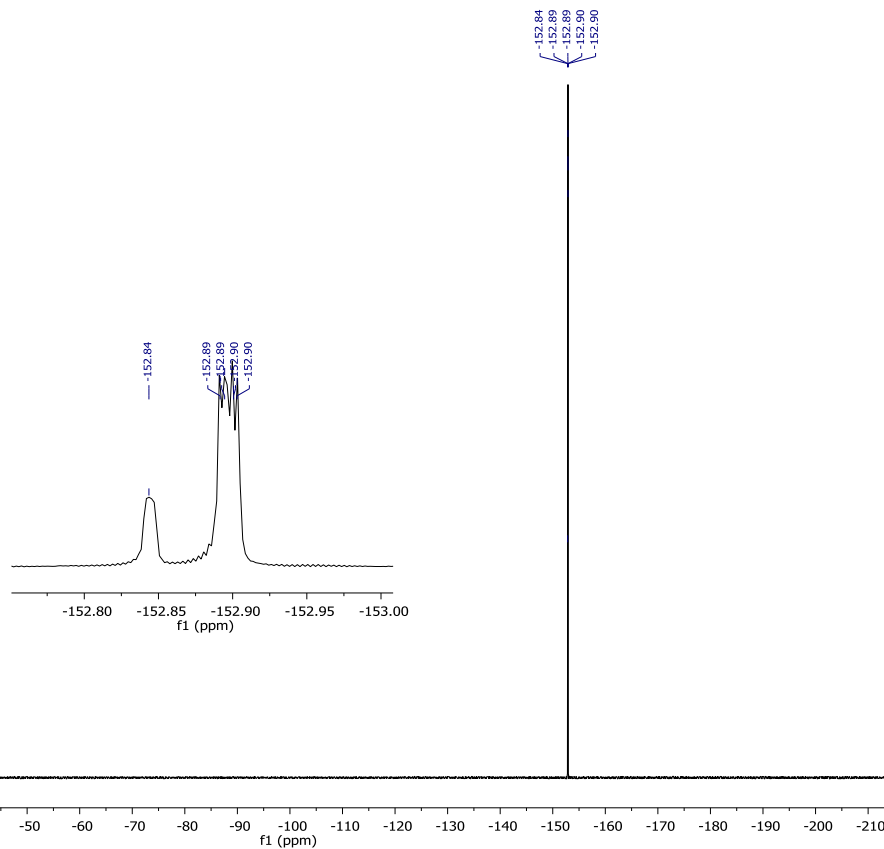


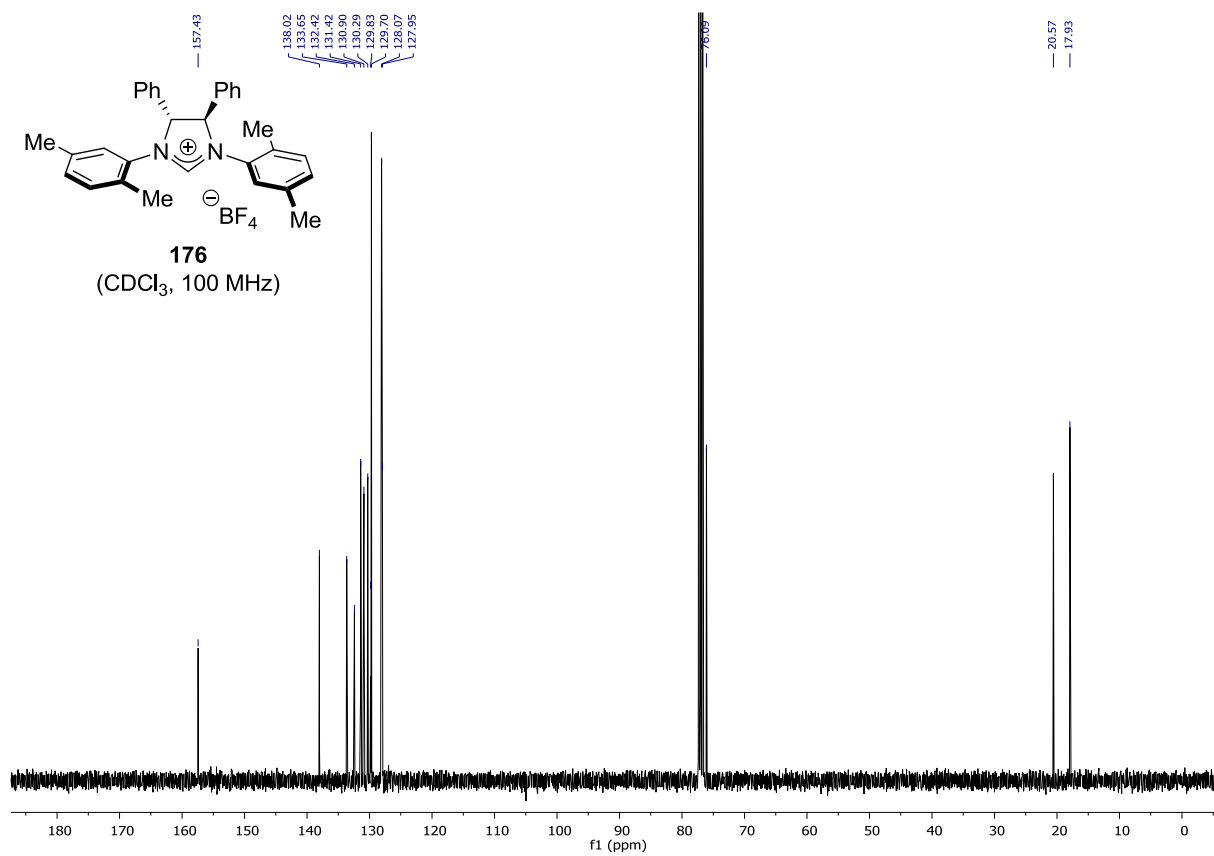
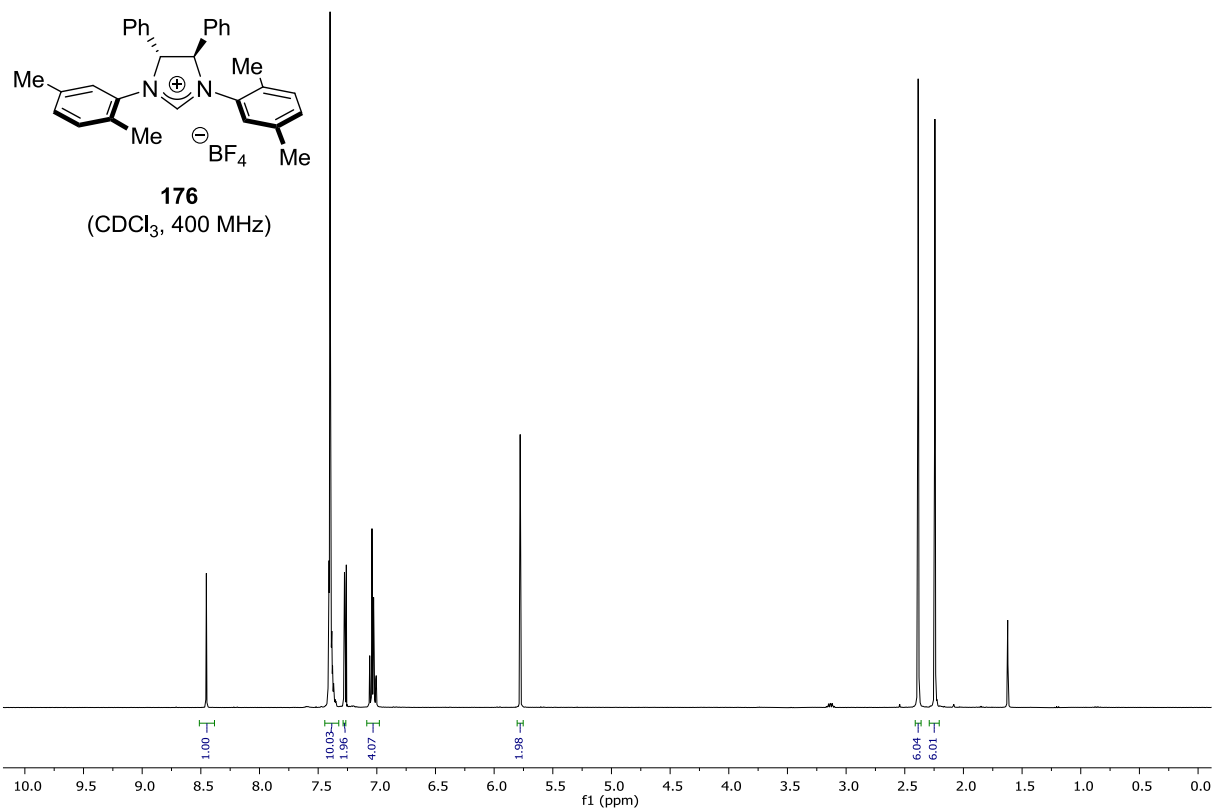
155
(CDCl_3 , 125 MHz)

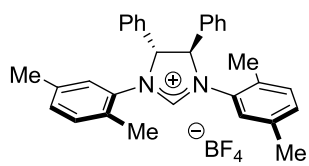




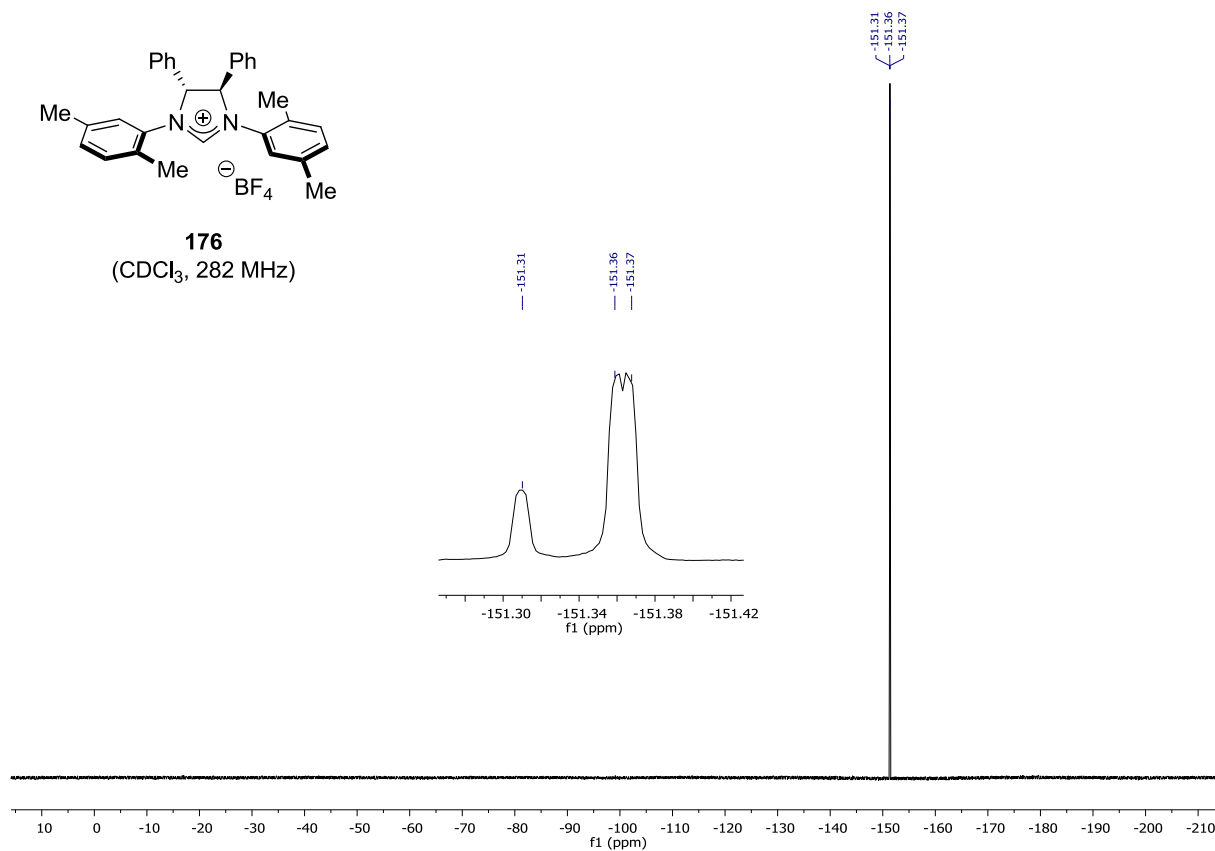
155
(CDCl_3 , 282 MHz)

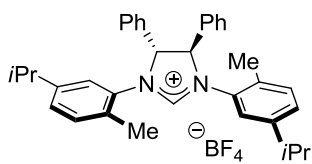




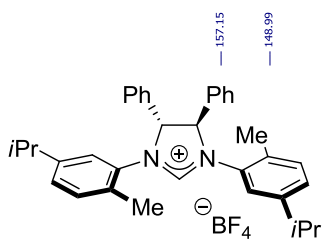
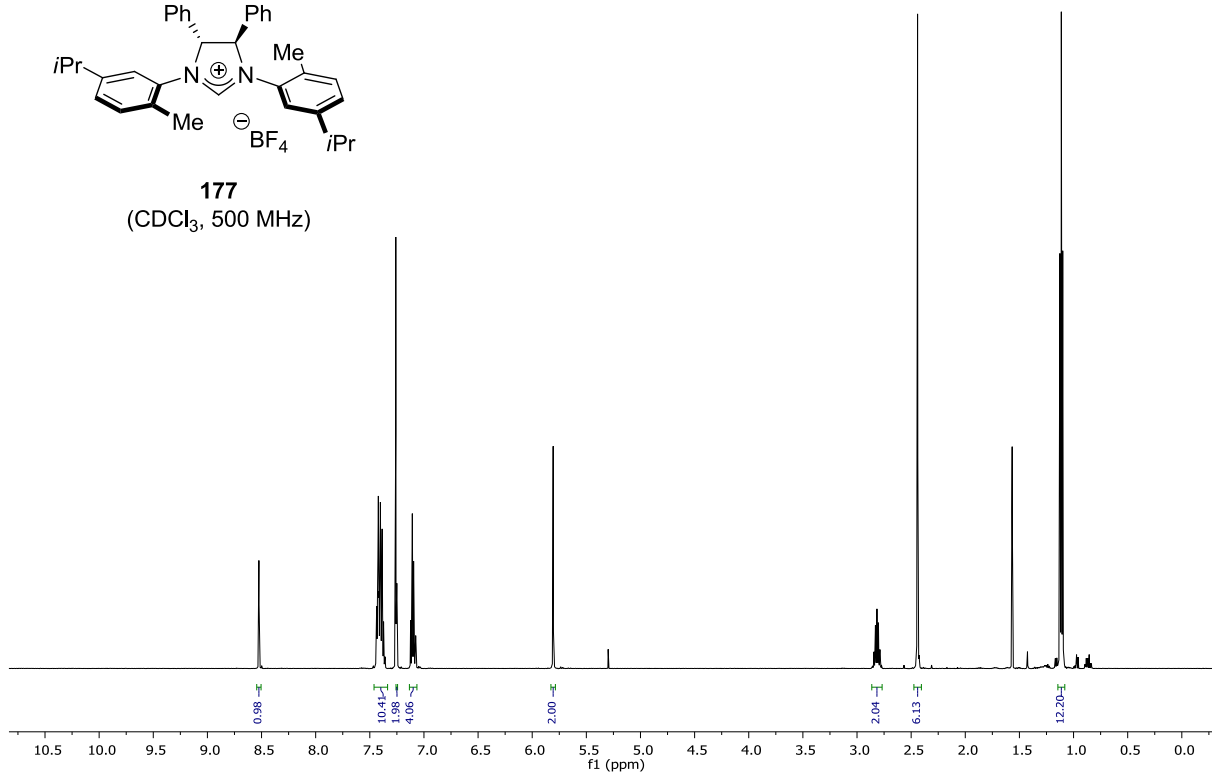


176
(CDCl₃, 282 MHz)

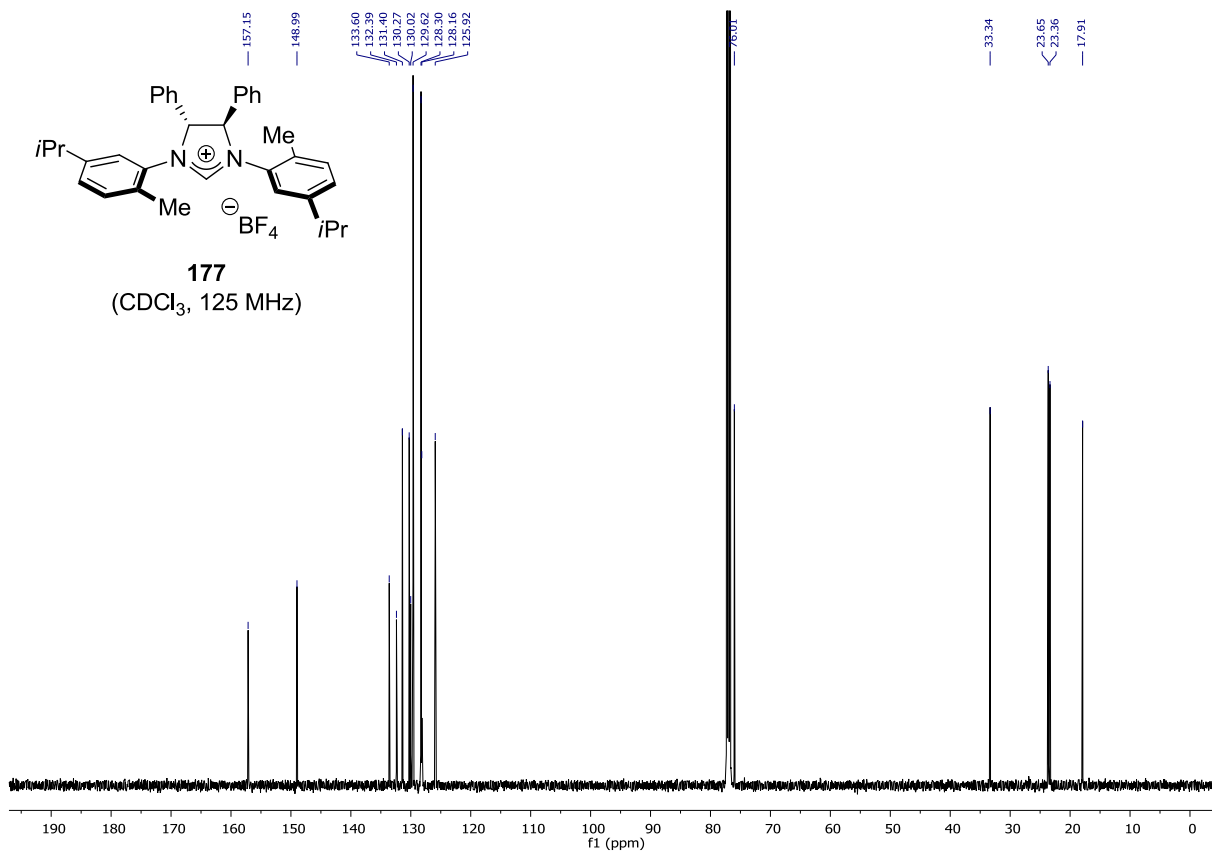


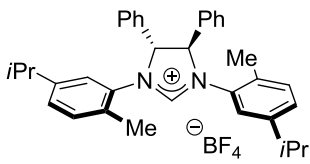


177
(CDCl₃, 500 MHz)

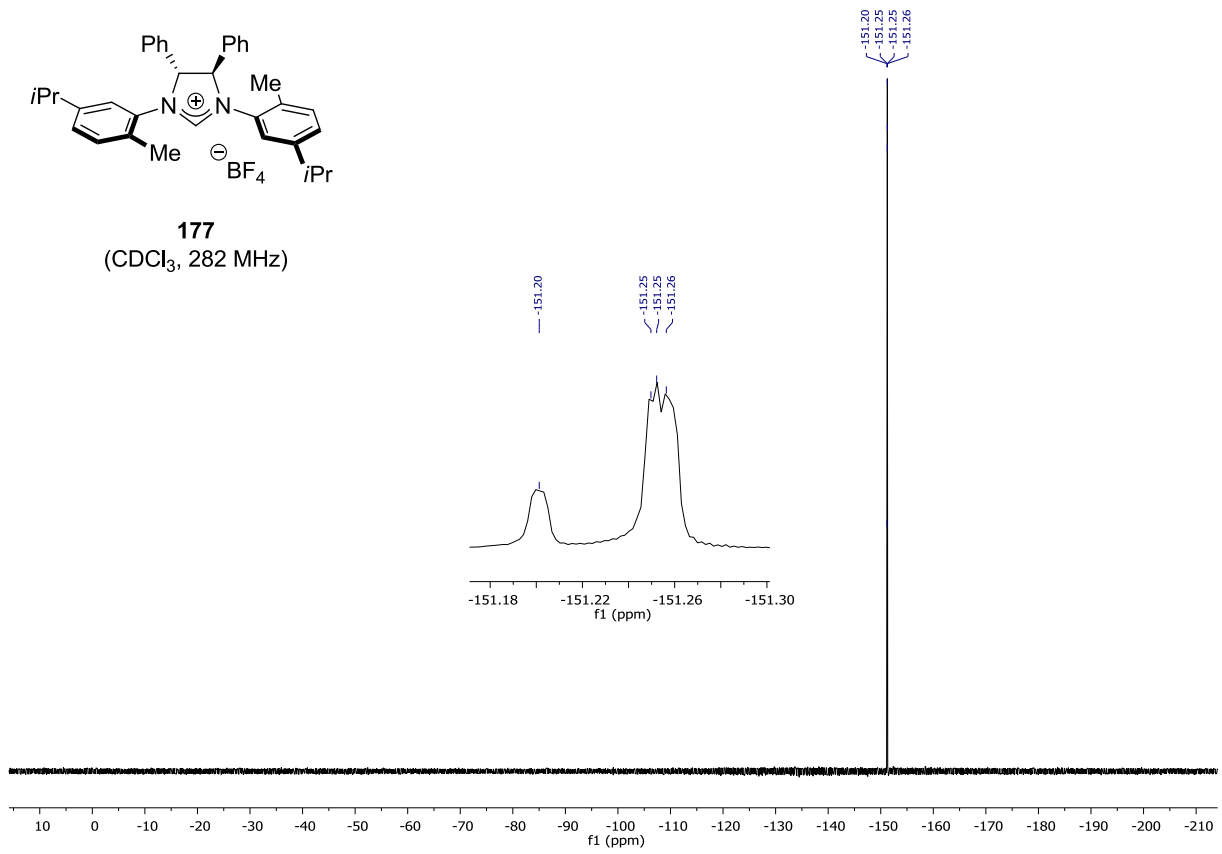


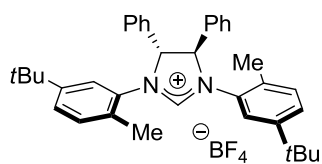
177
(CDCl₃, 125 MHz)



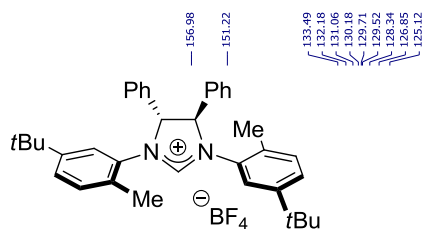
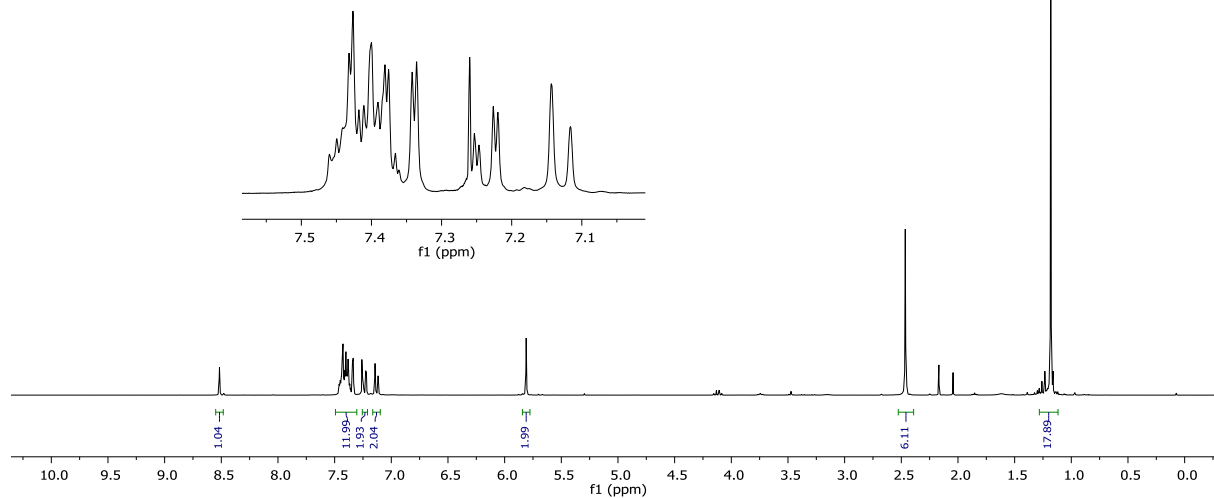


177
(CDCl₃, 282 MHz)

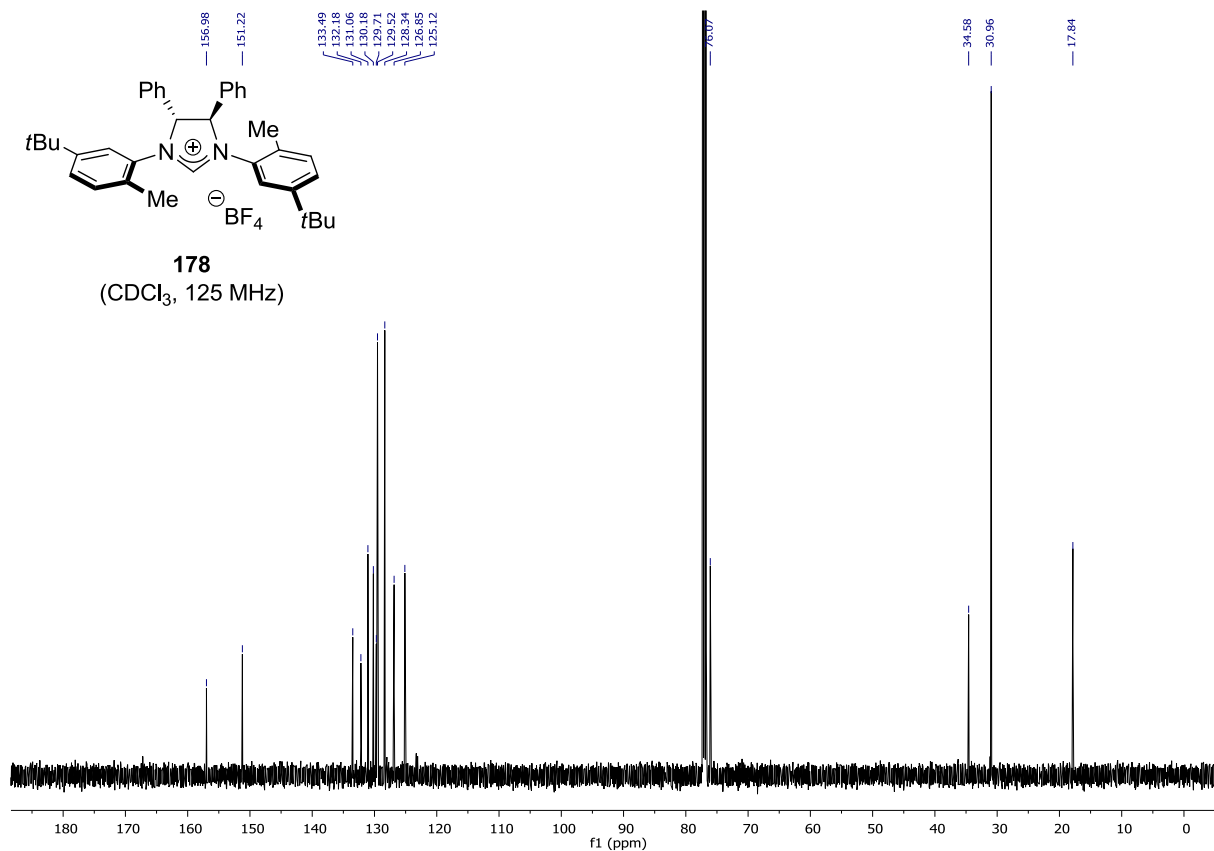


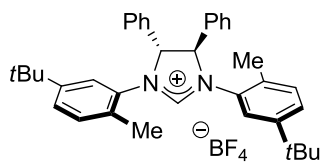


178
(CDCl₃, 300 MHz)

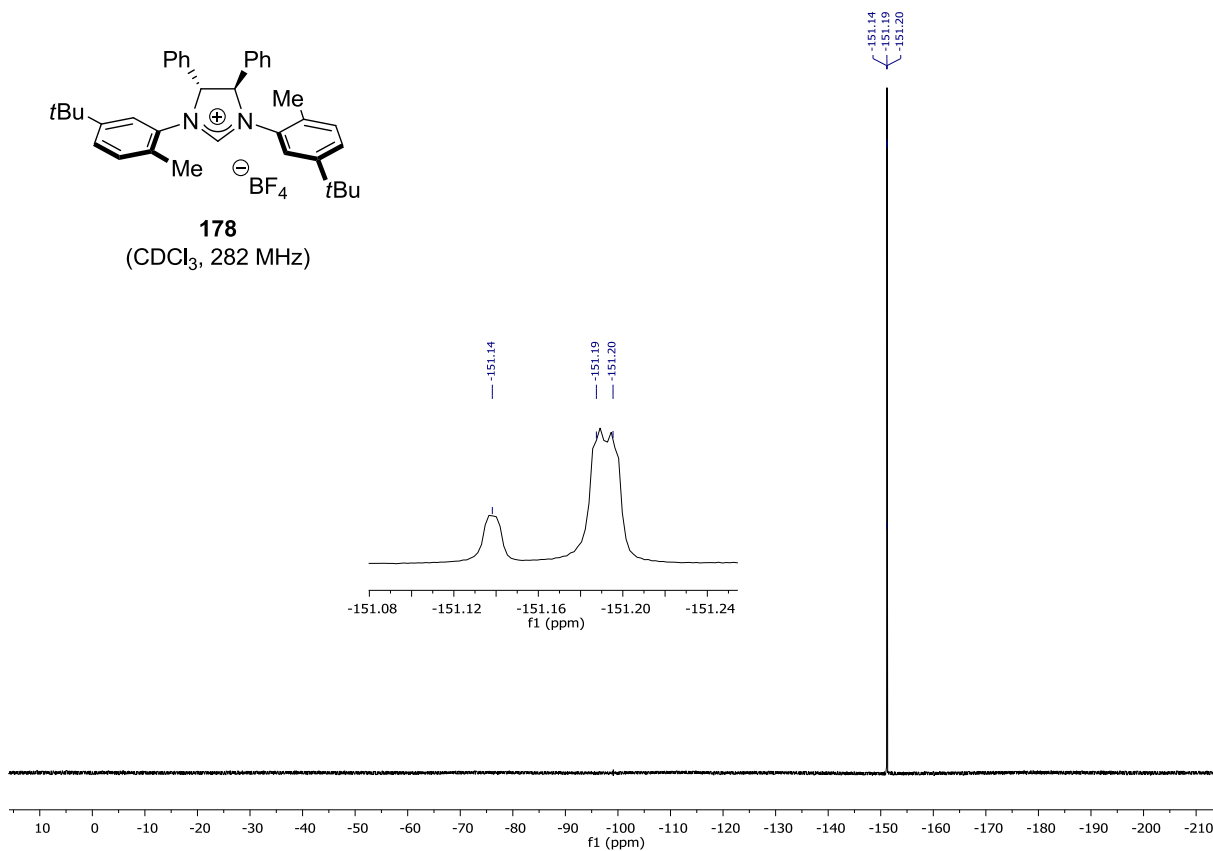


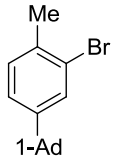
178
(CDCl₃, 125 MHz)



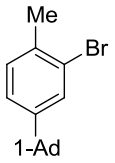
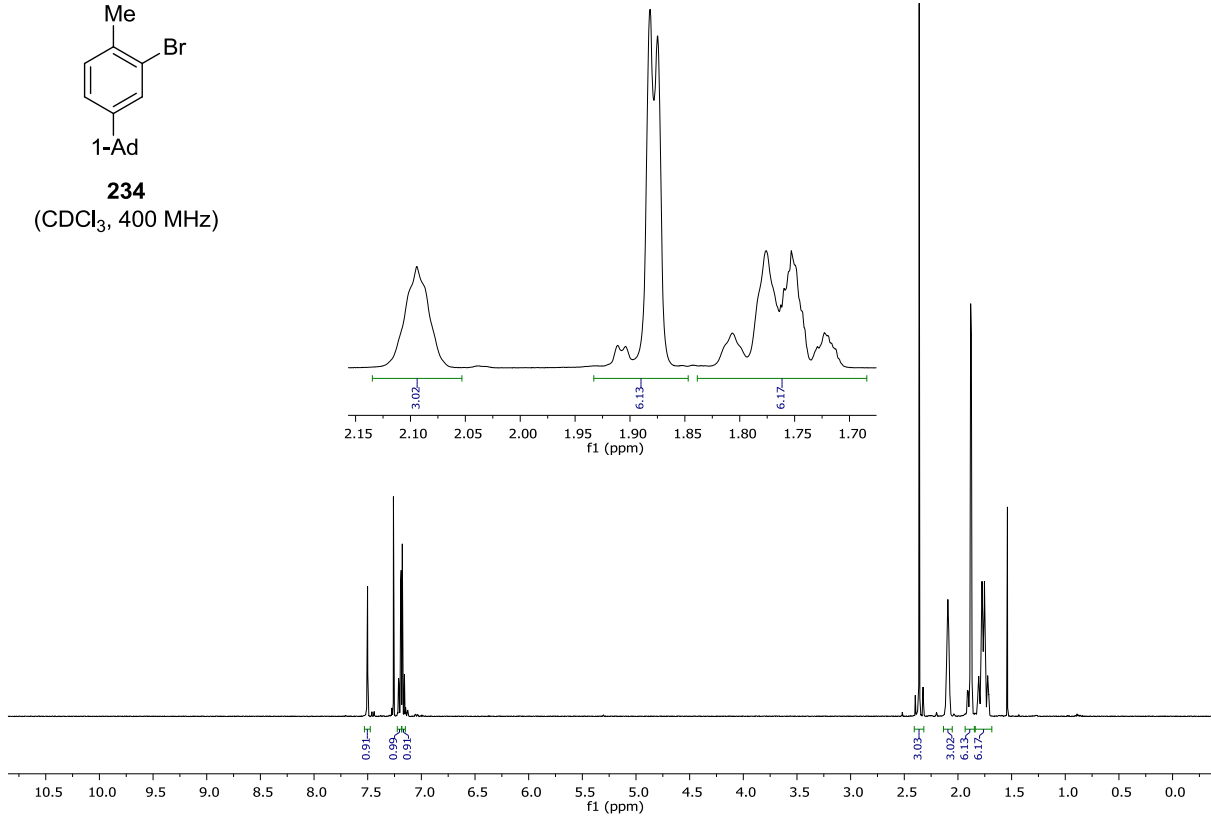


178
(CDCl₃, 282 MHz)

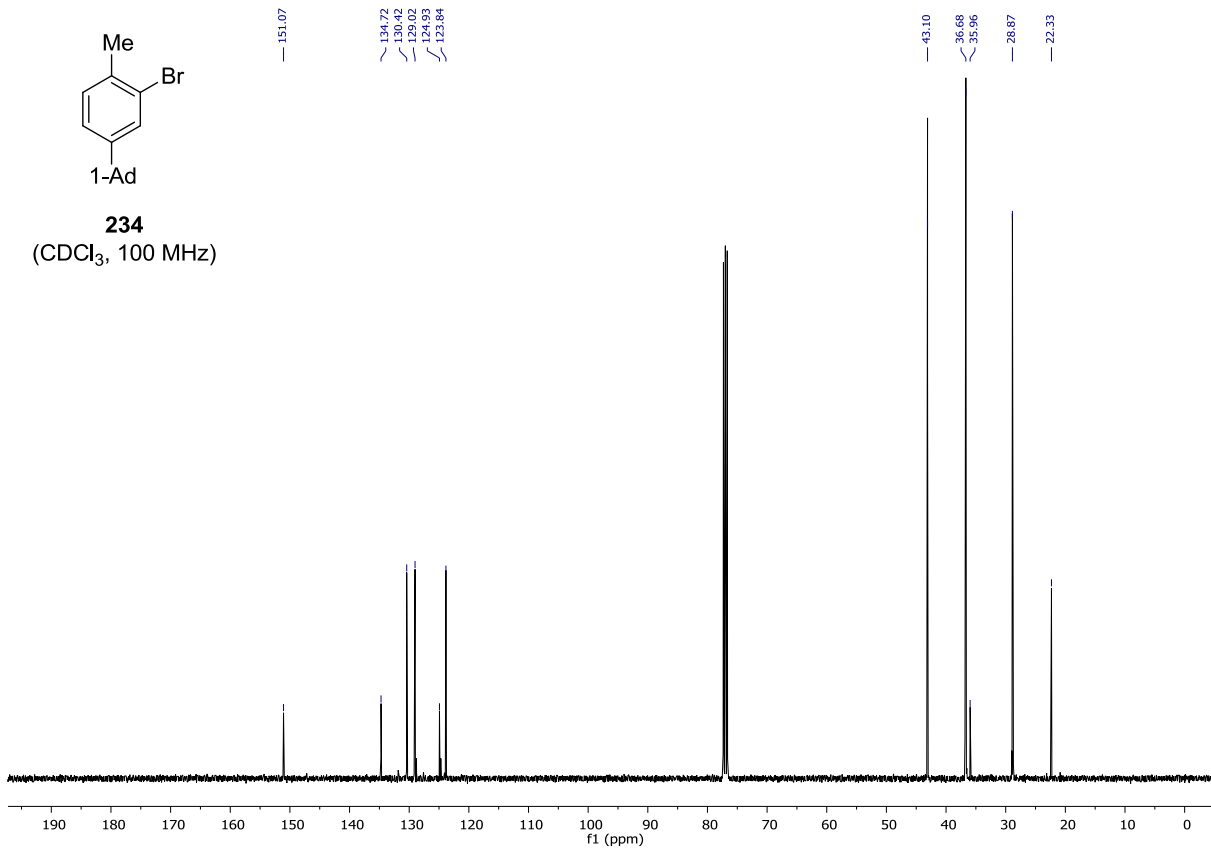


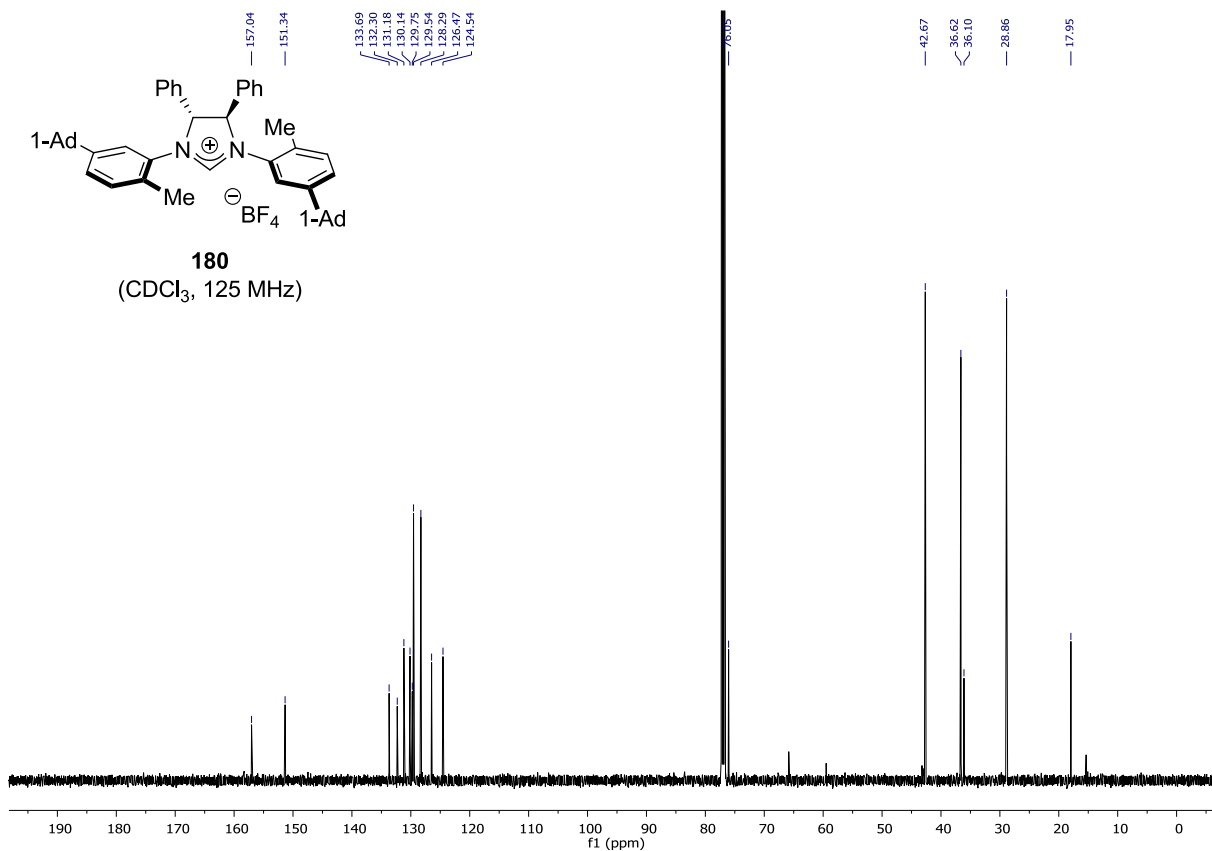
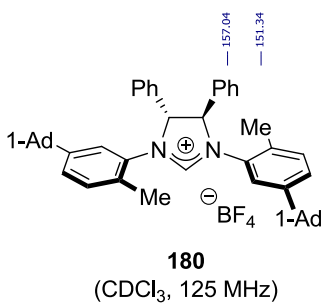
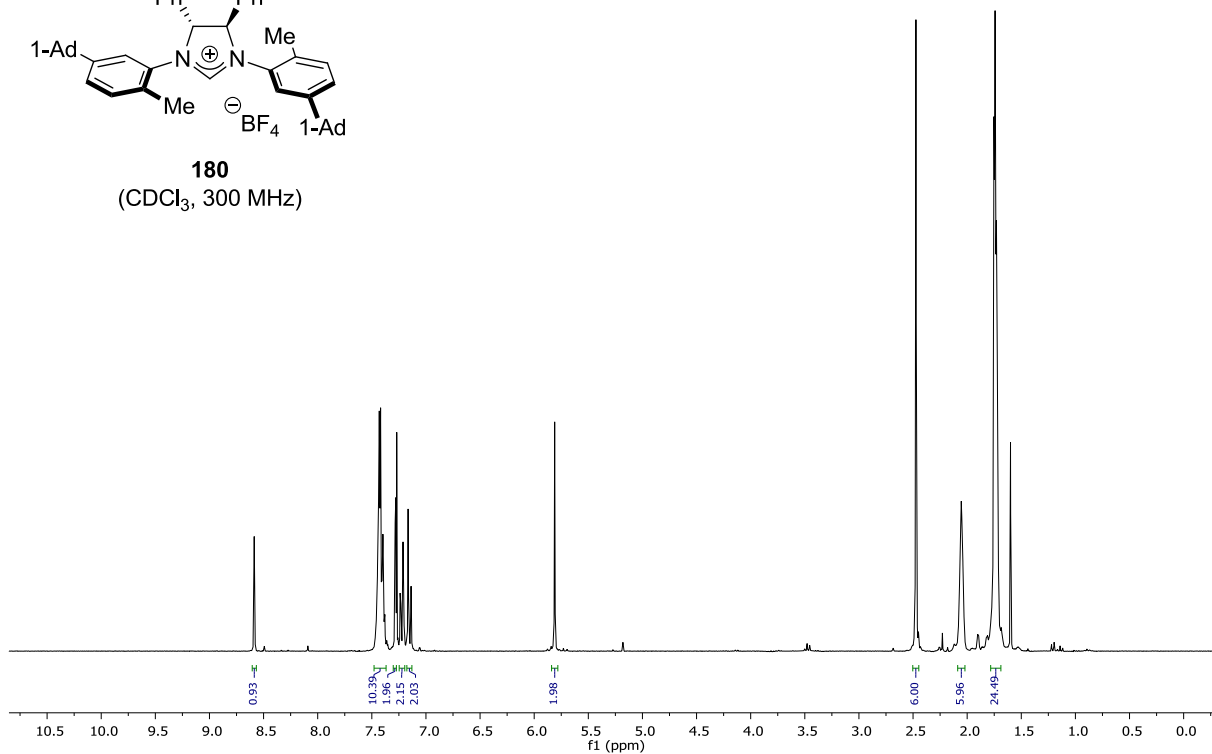
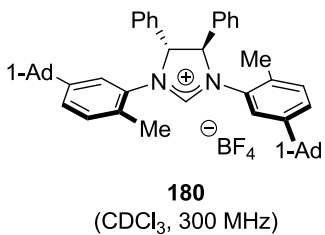


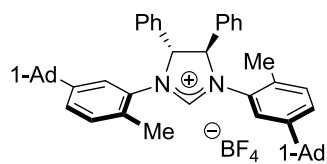
234
(CDCl₃, 400 MHz)



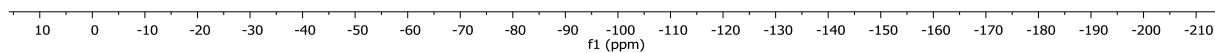
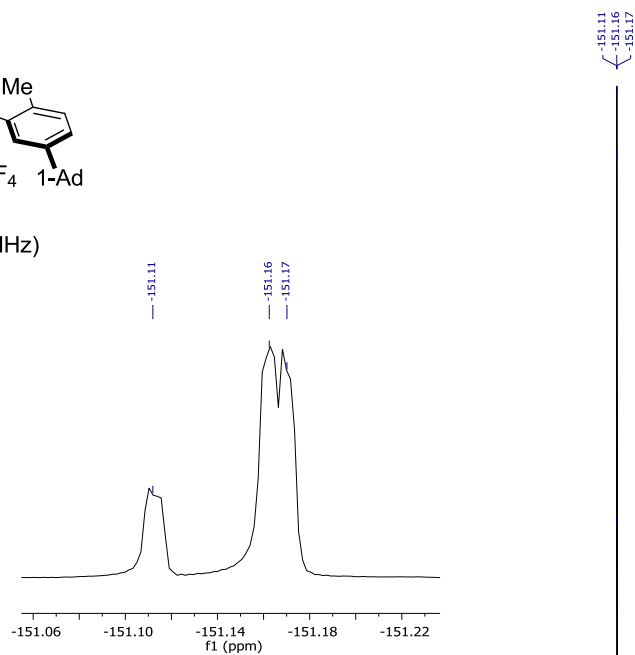
234
(CDCl₃, 100 MHz)

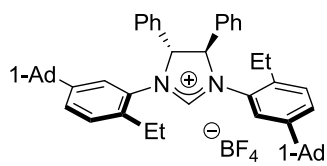




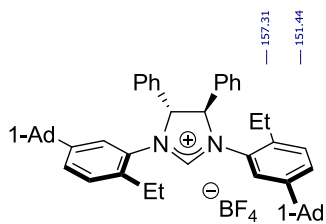
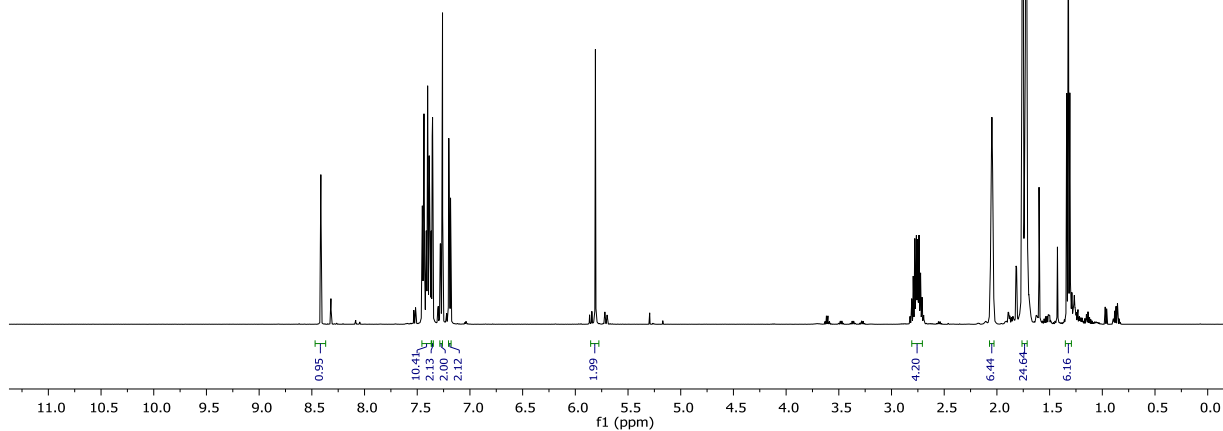


180
(CDCl₃, 282 MHz)

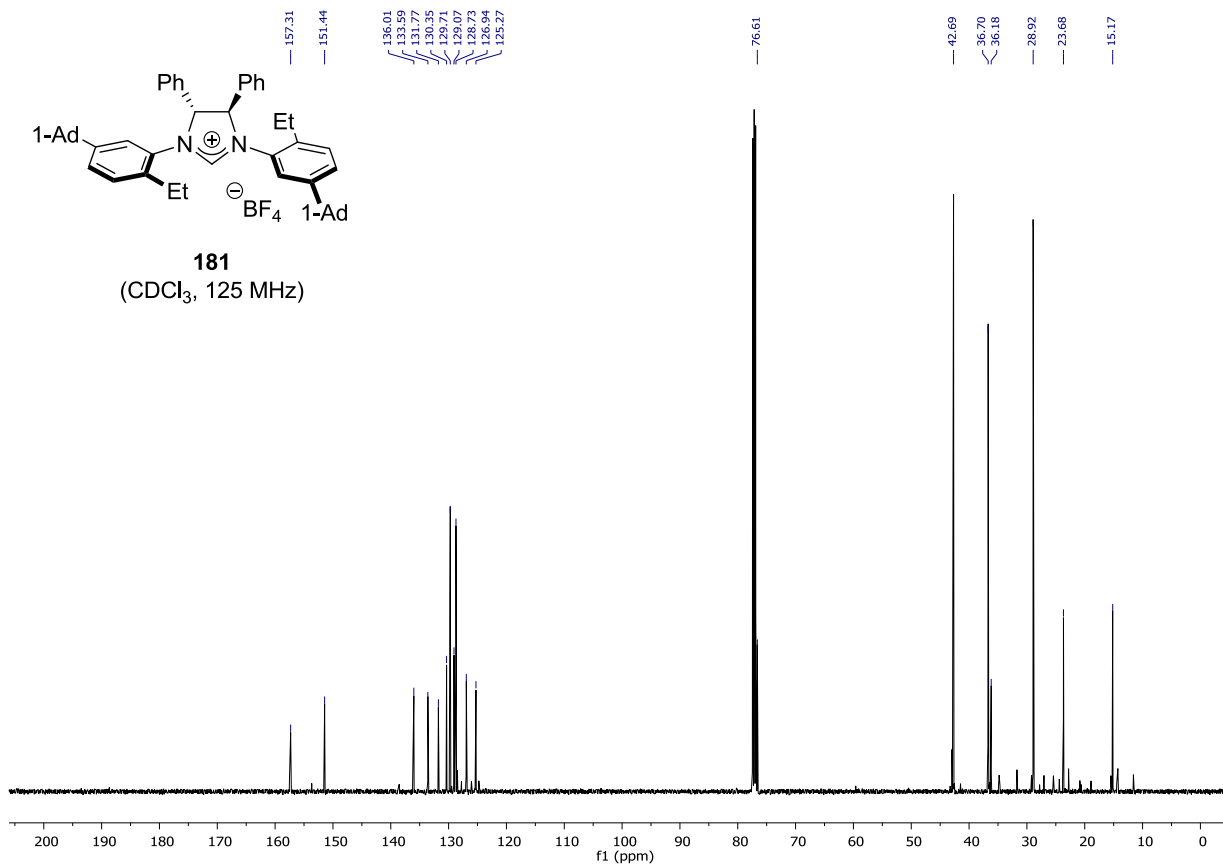


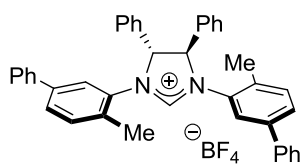


181
(CDCl₃, 500 MHz)

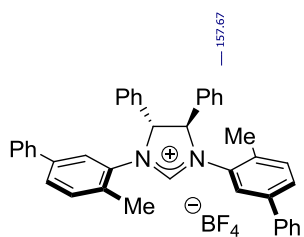
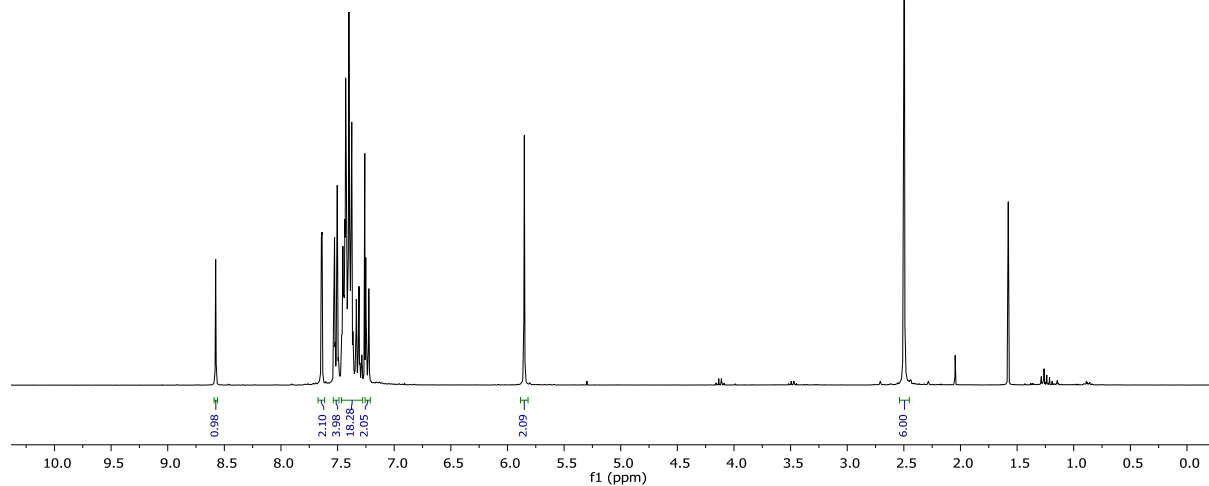


181
(CDCl₃, 125 MHz)

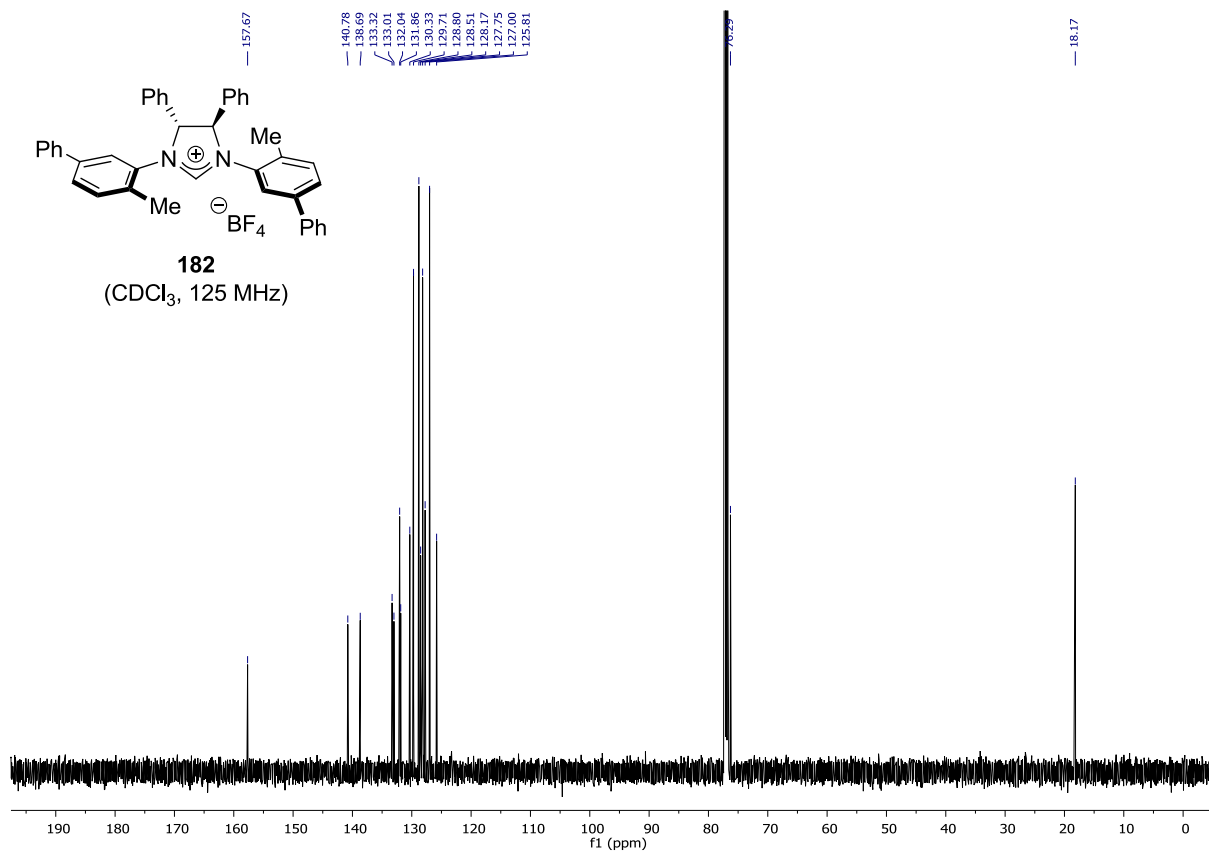


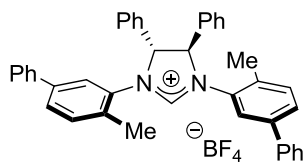


182
(CDCl₃, 300 MHz)

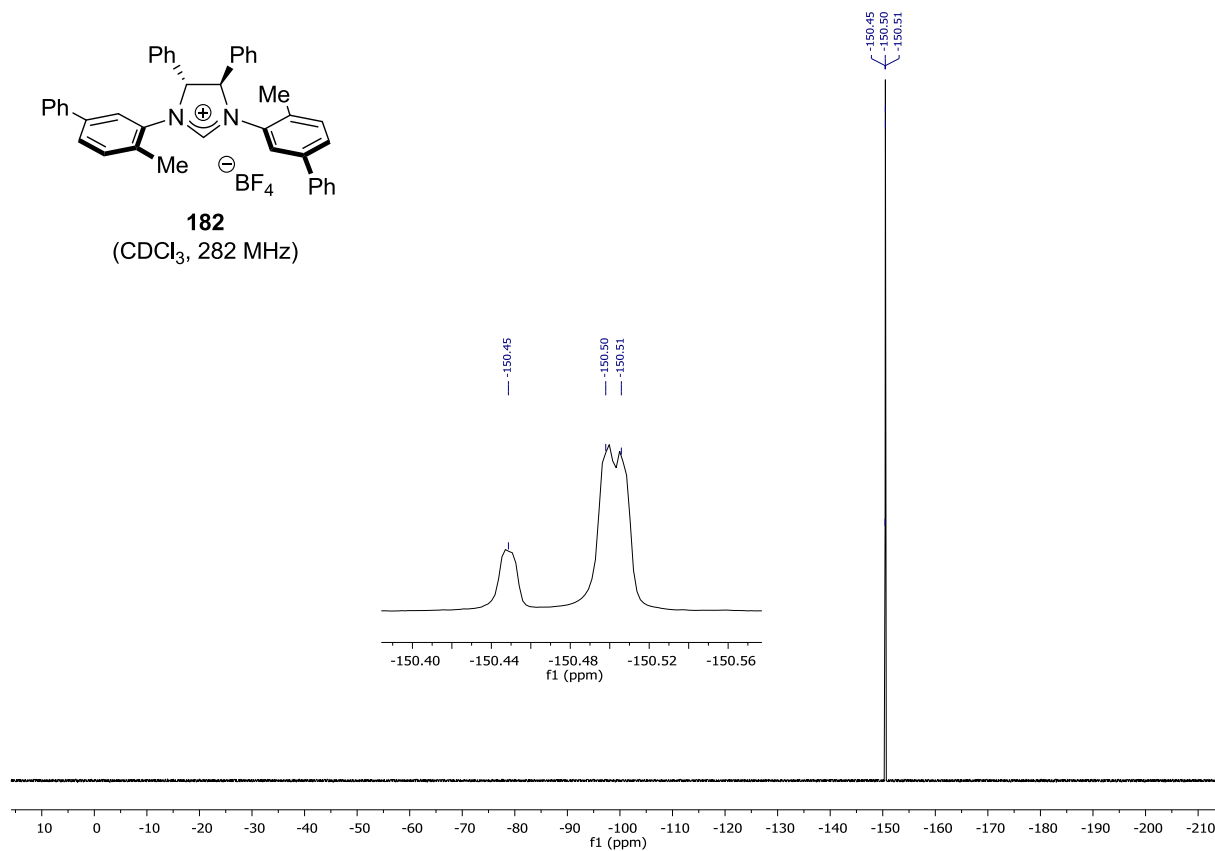


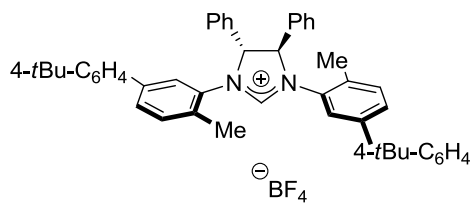
182
(CDCl₃, 125 MHz)



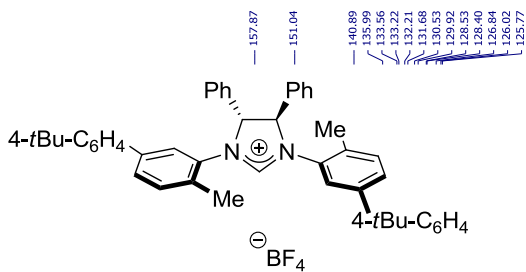
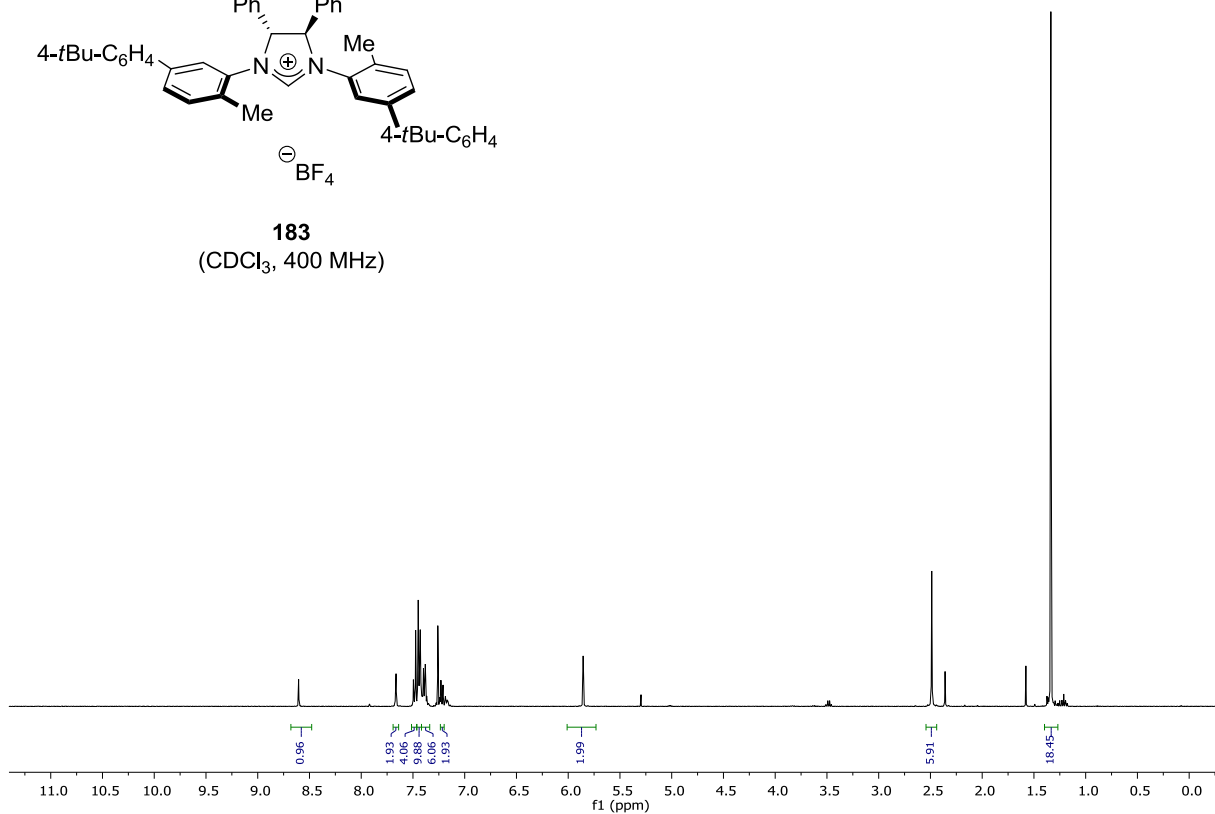


182
(CDCl₃, 282 MHz)

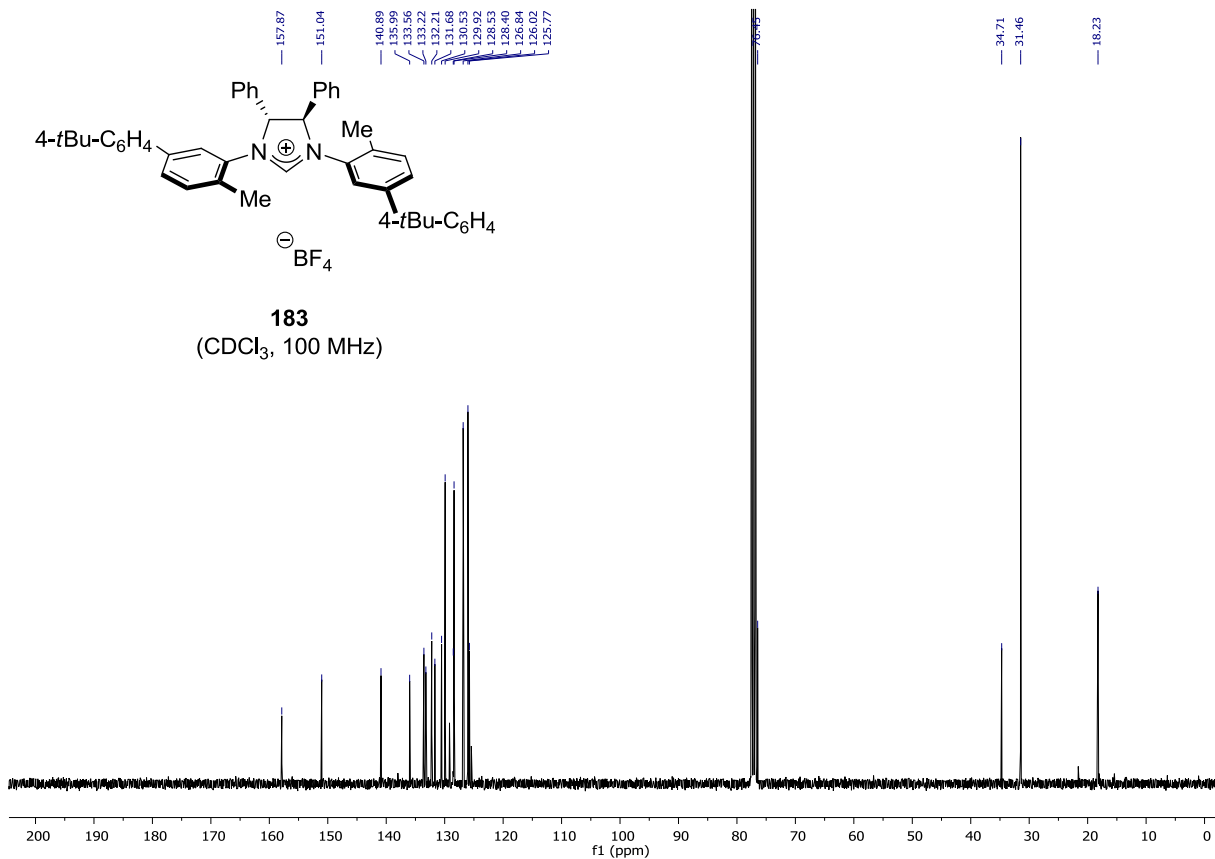


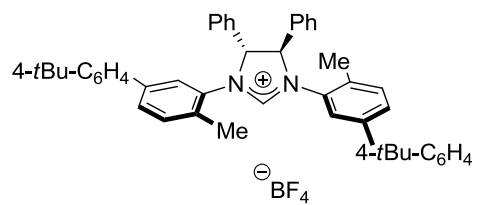


183
(CDCl₃, 400 MHz)

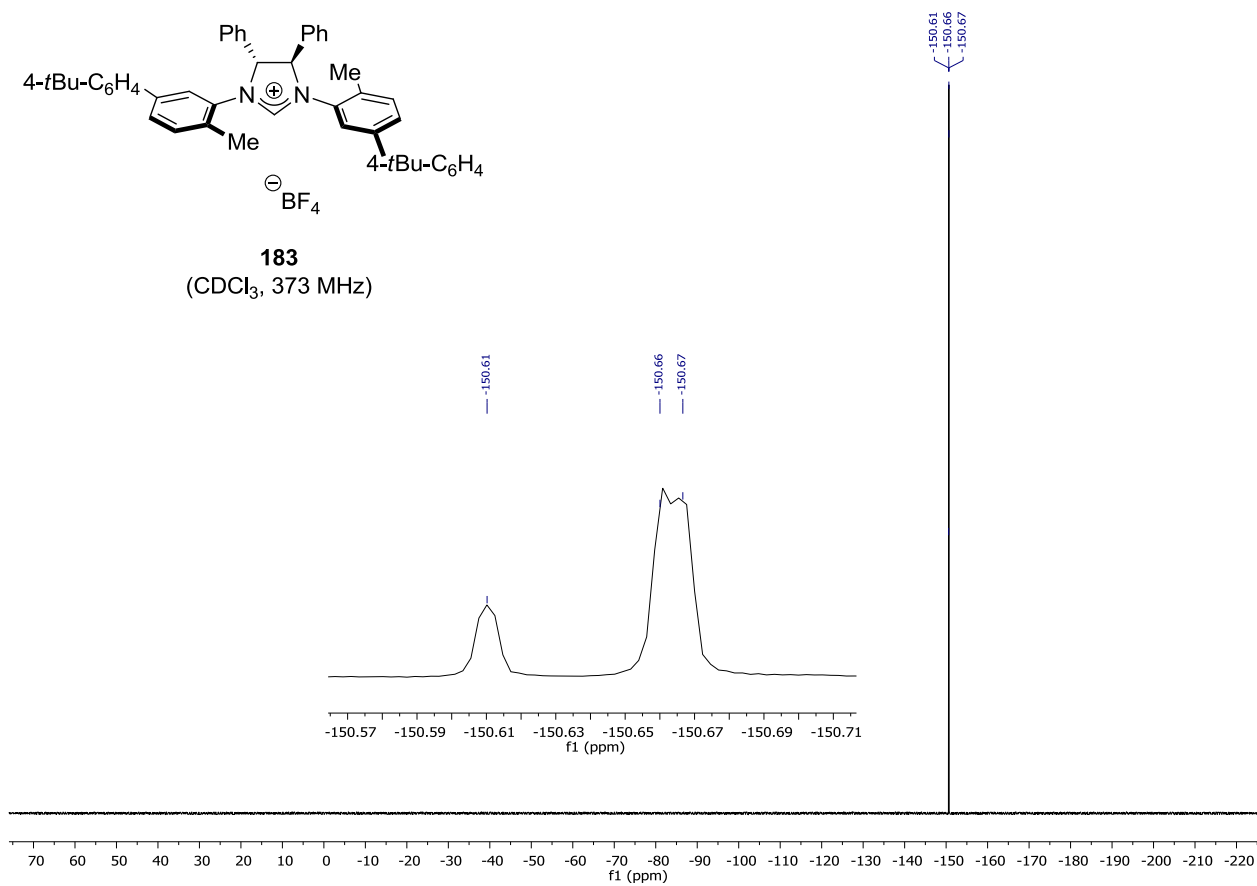


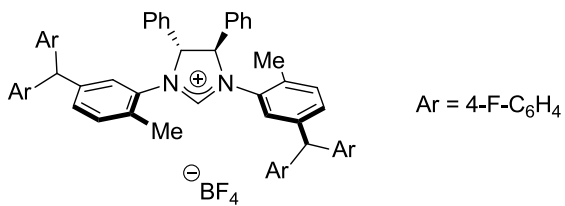
183
(CDCl₃, 100 MHz)



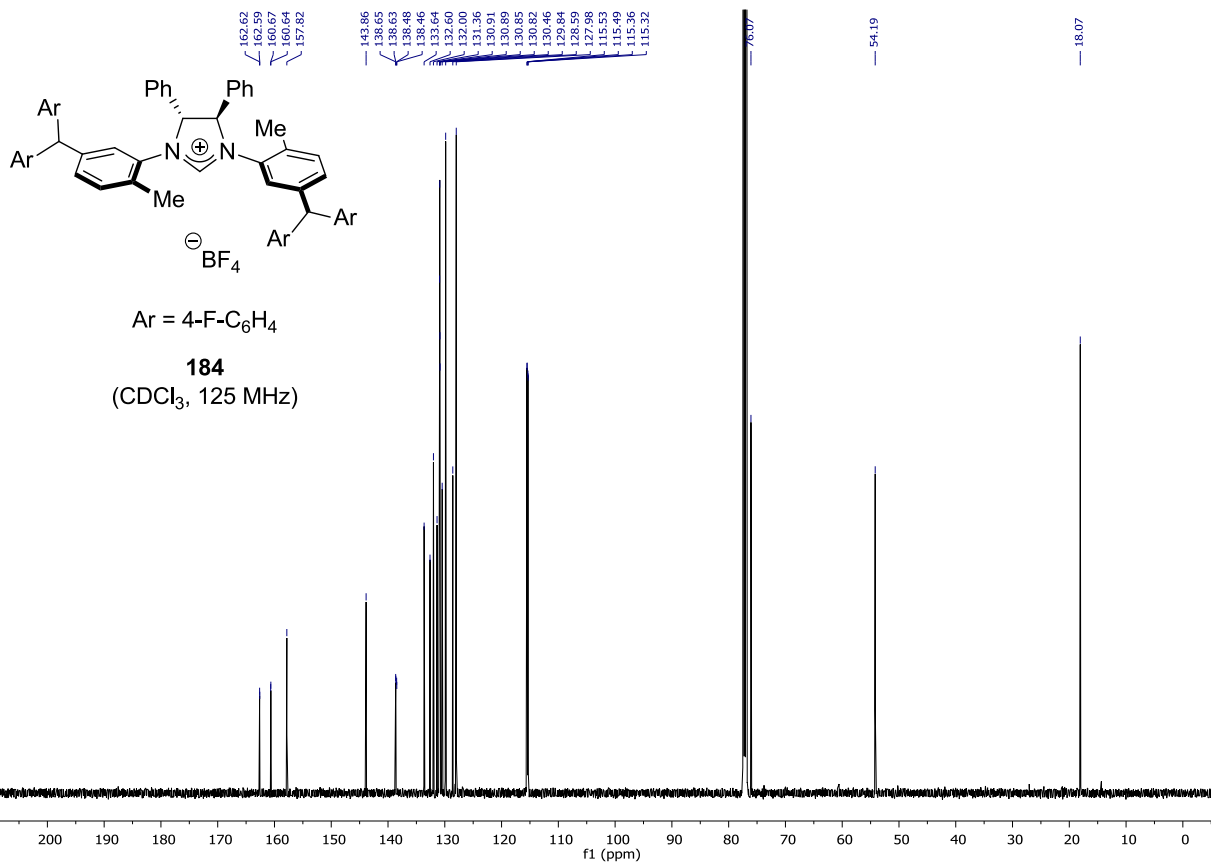
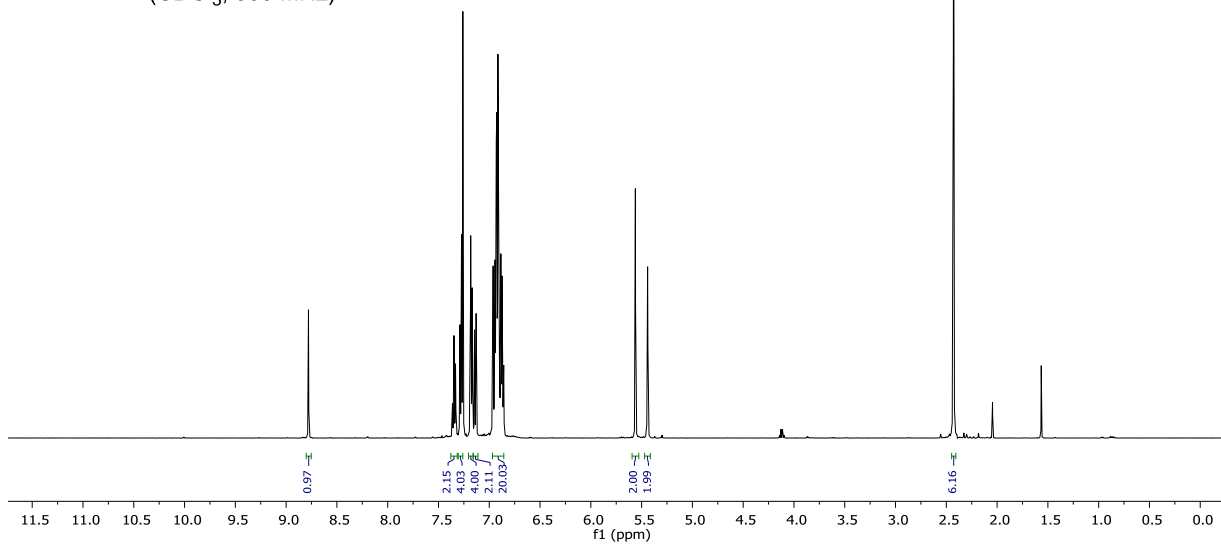


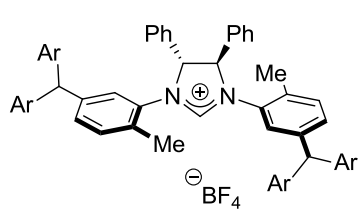
183
(CDCl₃, 373 MHz)



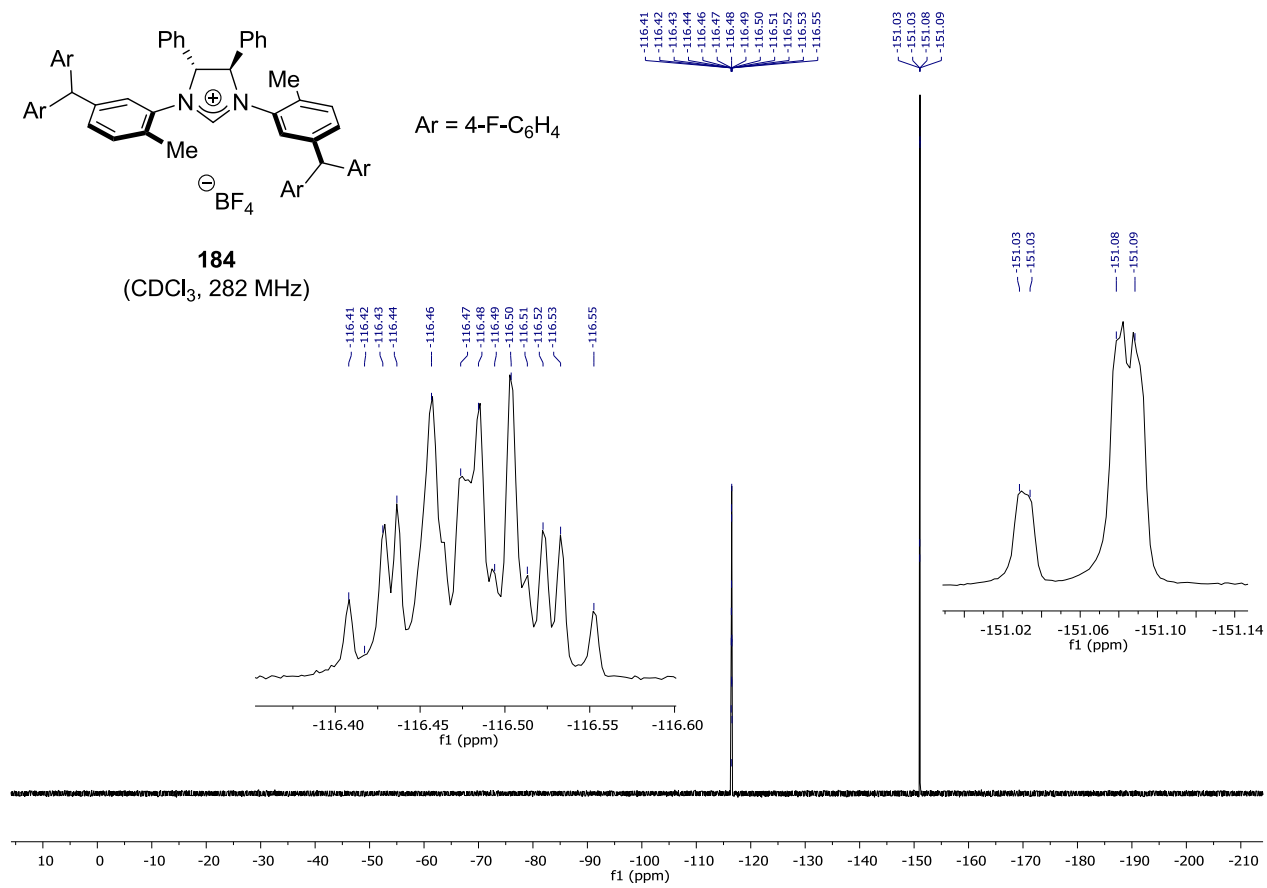


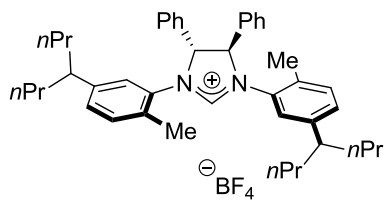
184
(CDCl₃, 500 MHz)



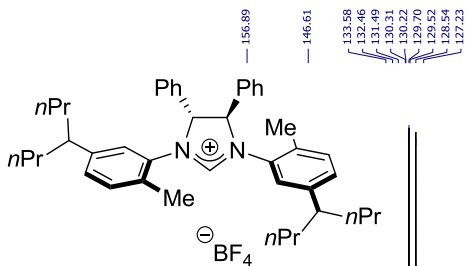
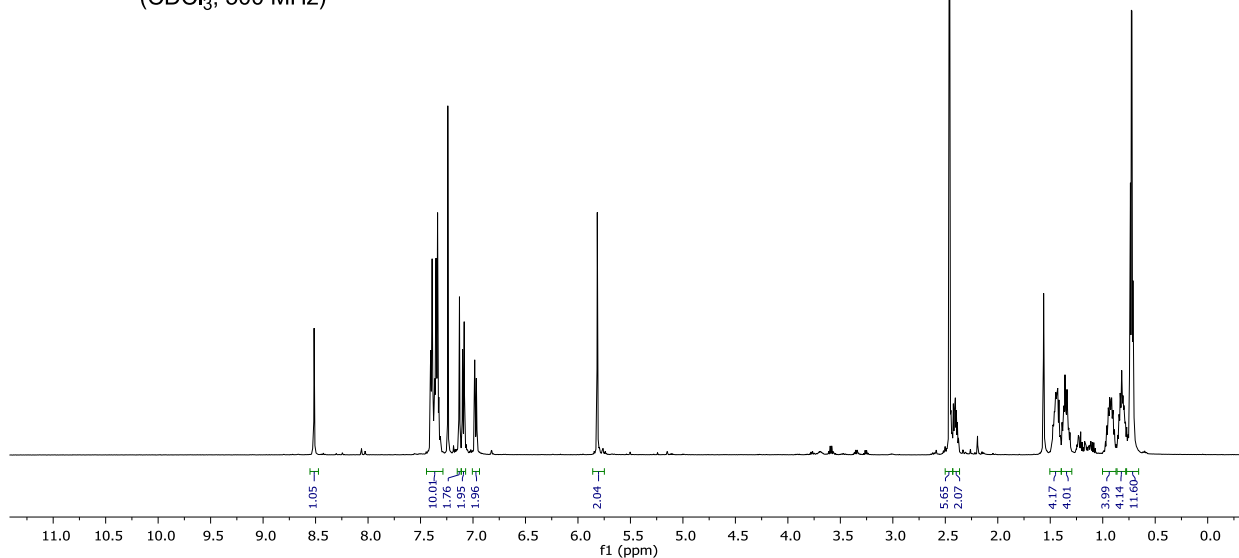


184
(CDCl₃, 282 MHz)

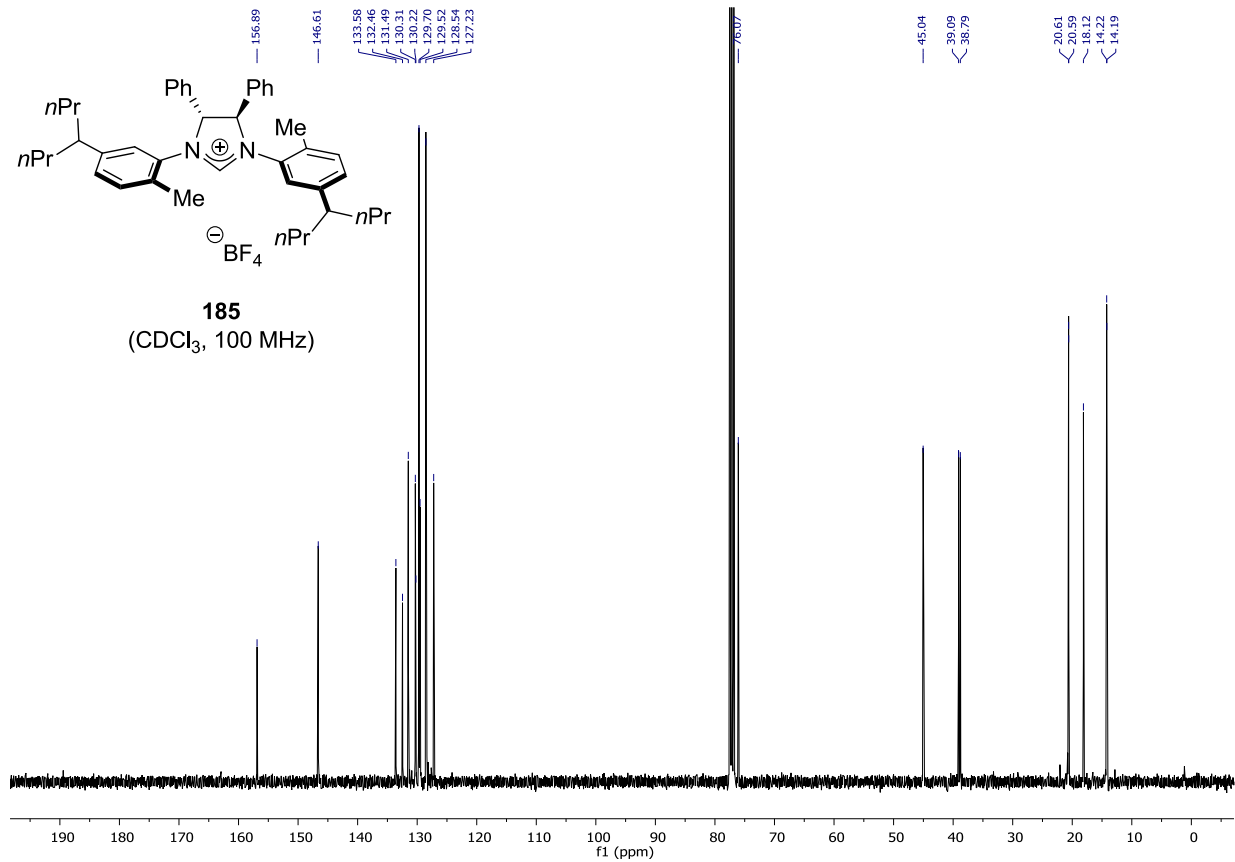


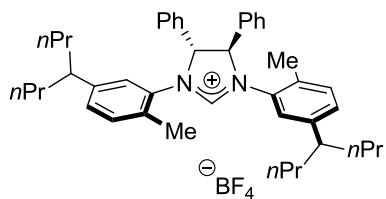


185
(CDCl₃, 500 MHz)

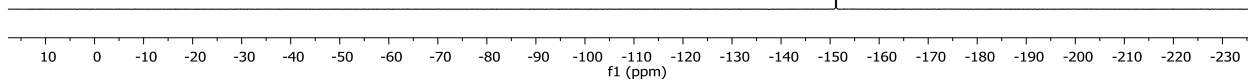
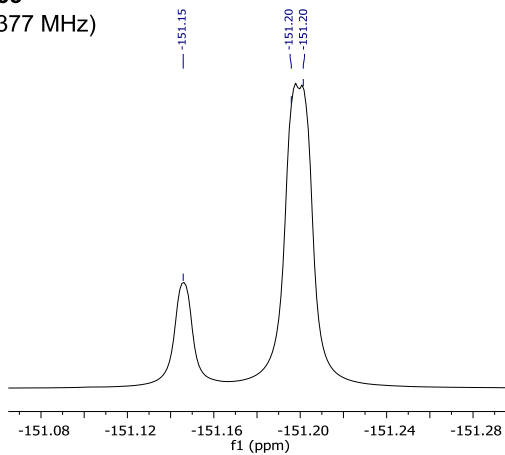


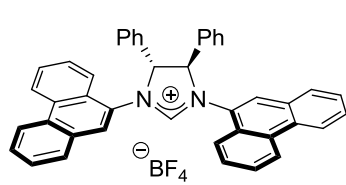
185
(CDCl₃, 100 MHz)



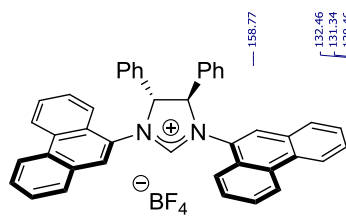
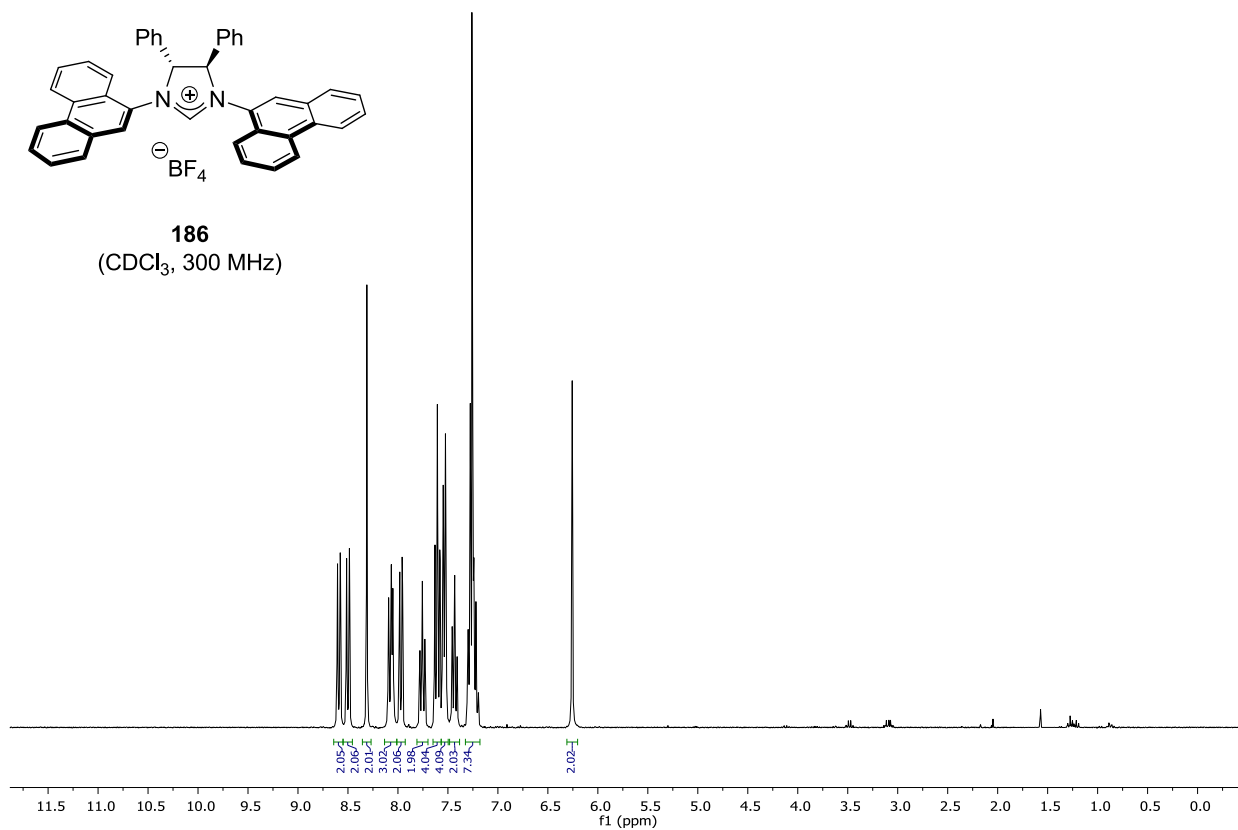


185
(CDCl_3 , 377 MHz)

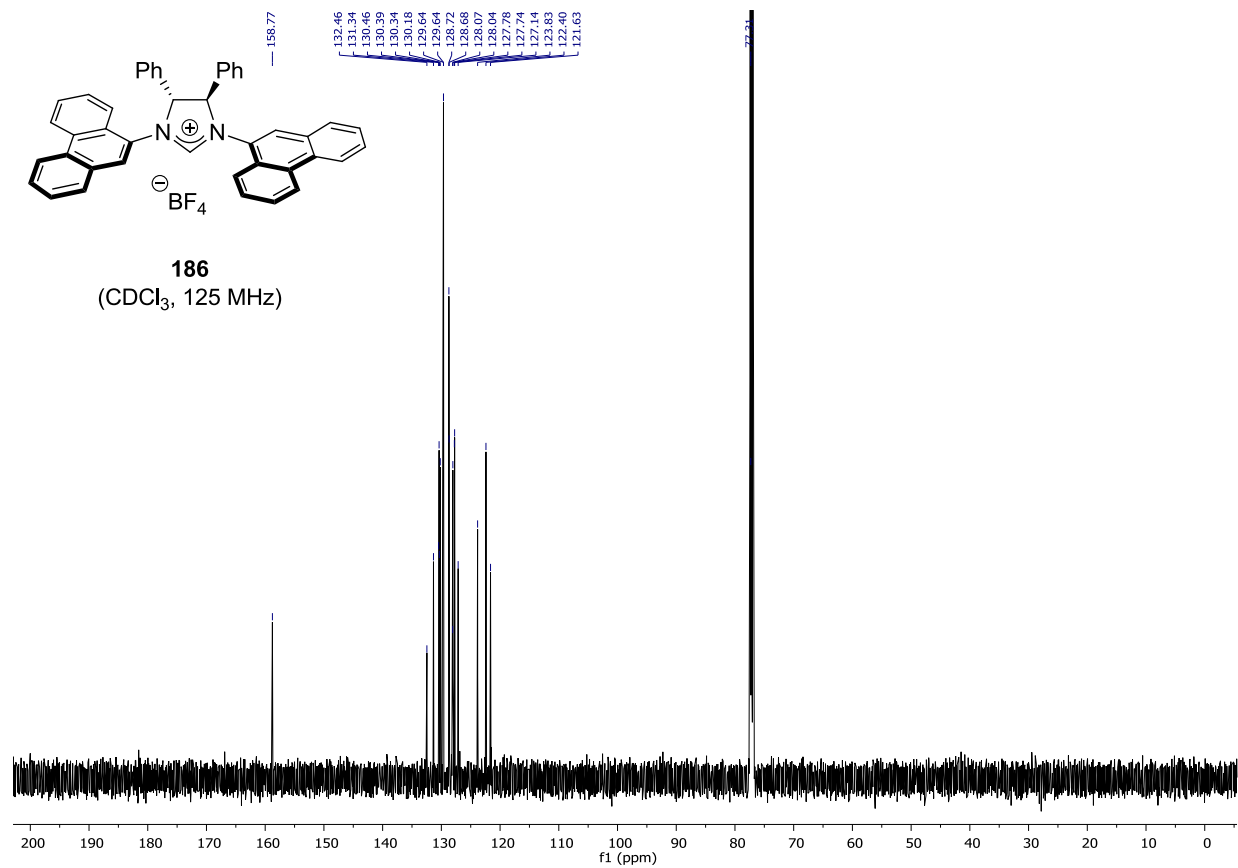


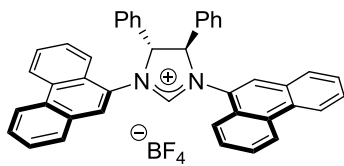


186
(CDCl₃, 300 MHz)

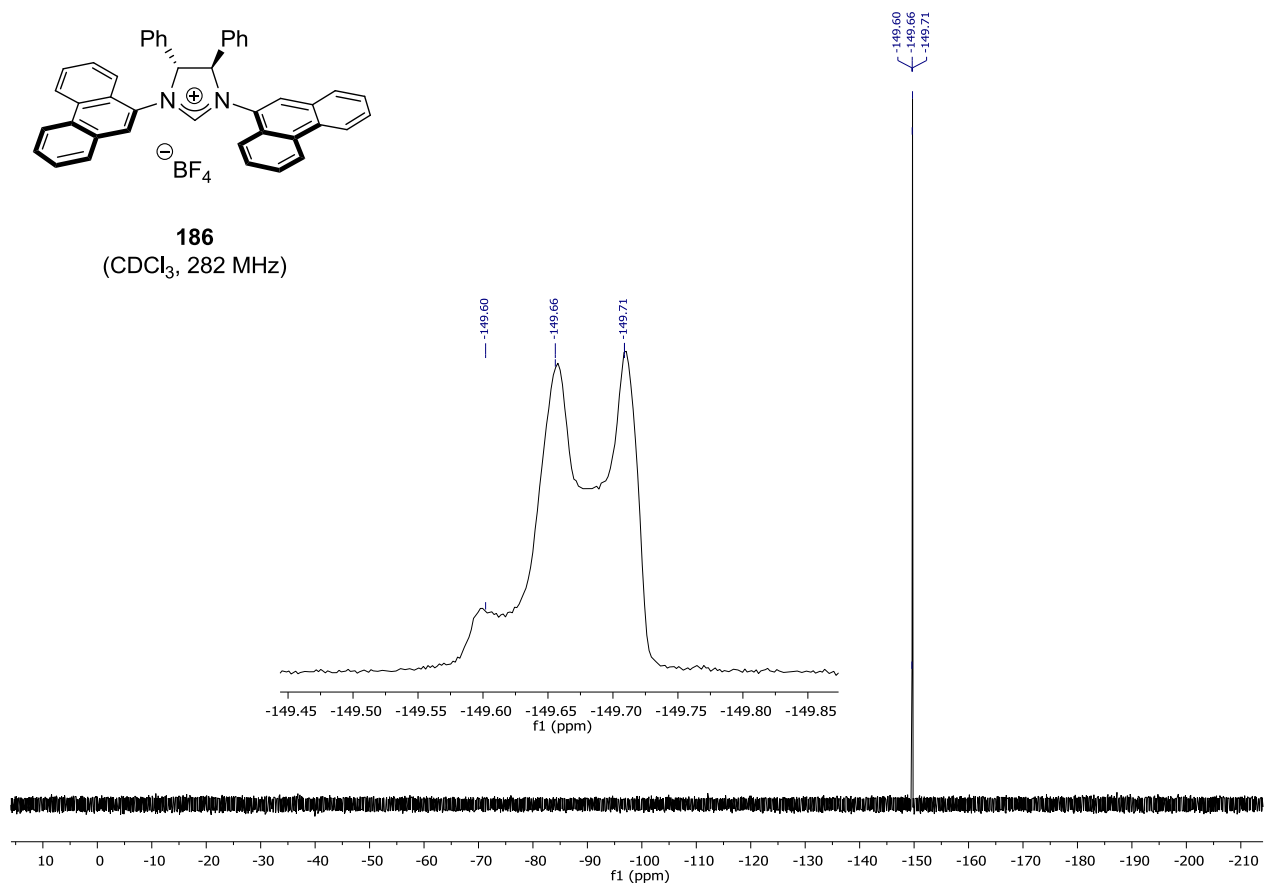


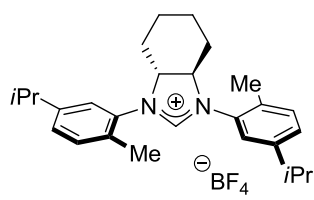
186
(CDCl₃, 125 MHz)



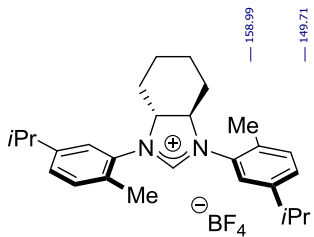
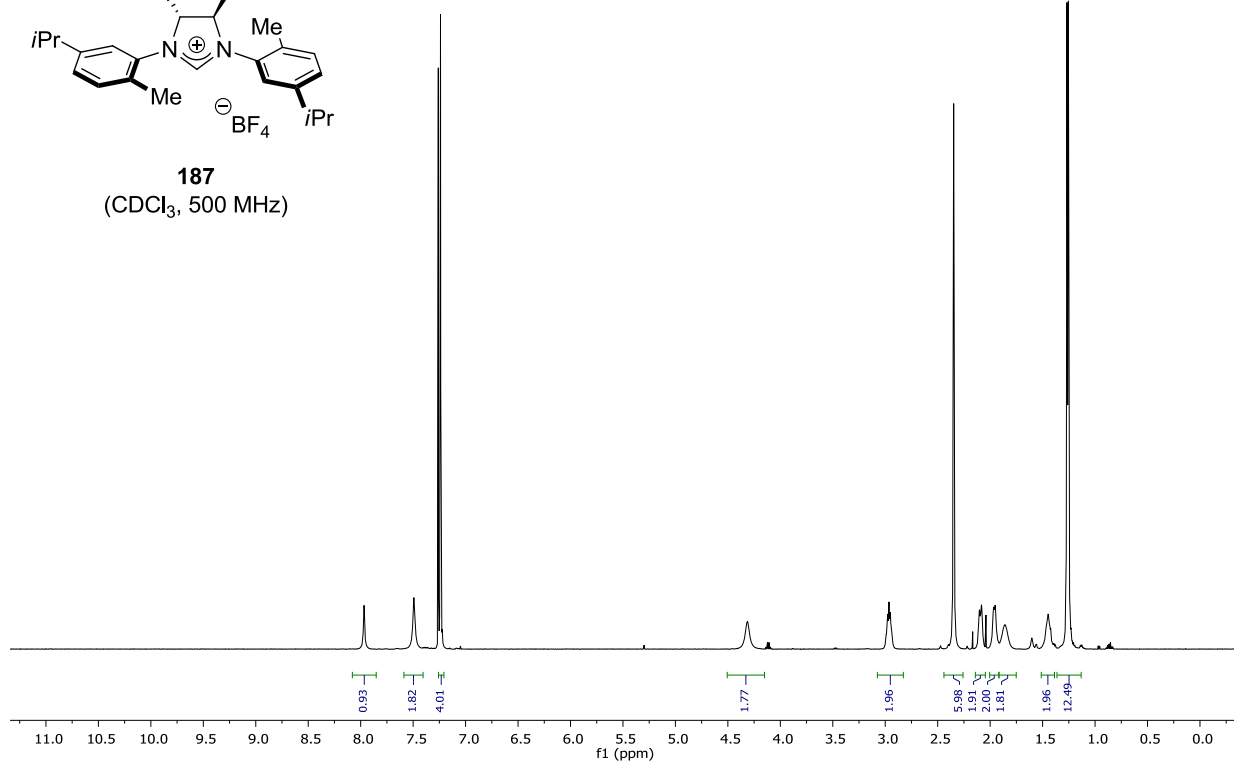


186
(CDCl₃, 282 MHz)

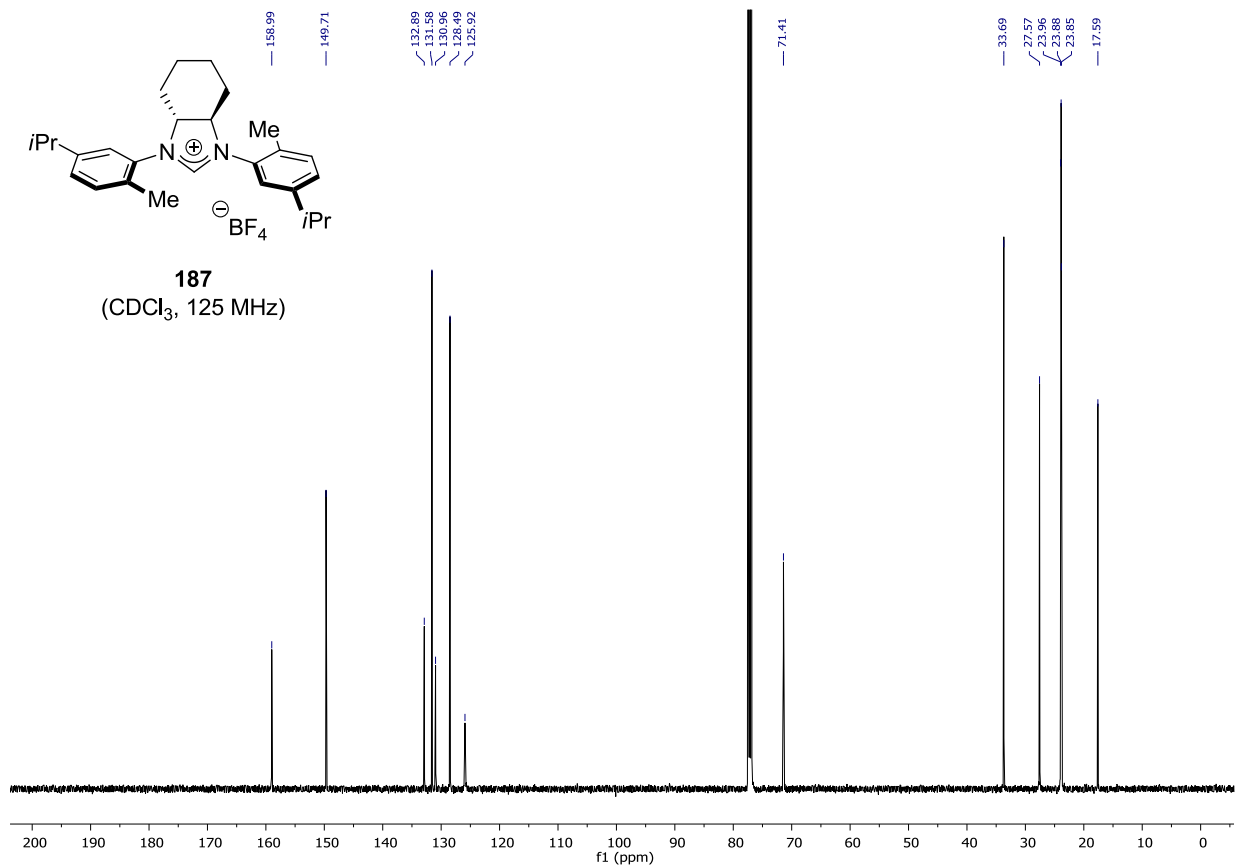


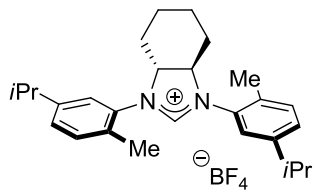


187
(CDCl₃, 500 MHz)

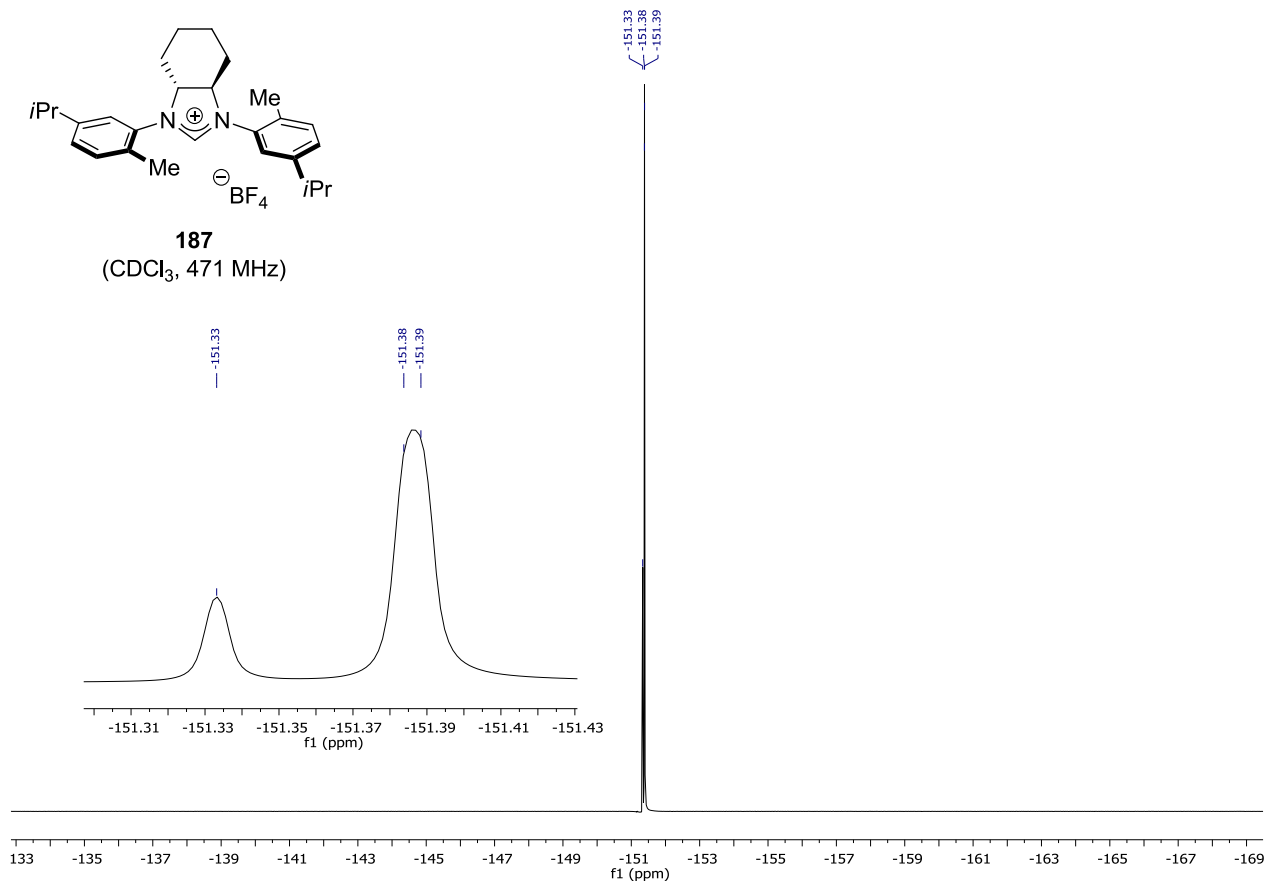


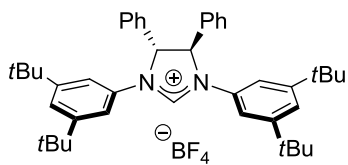
187
(CDCl₃, 125 MHz)



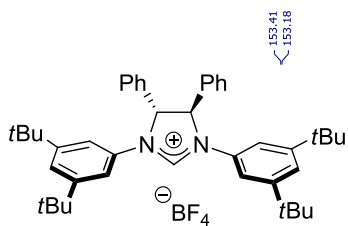
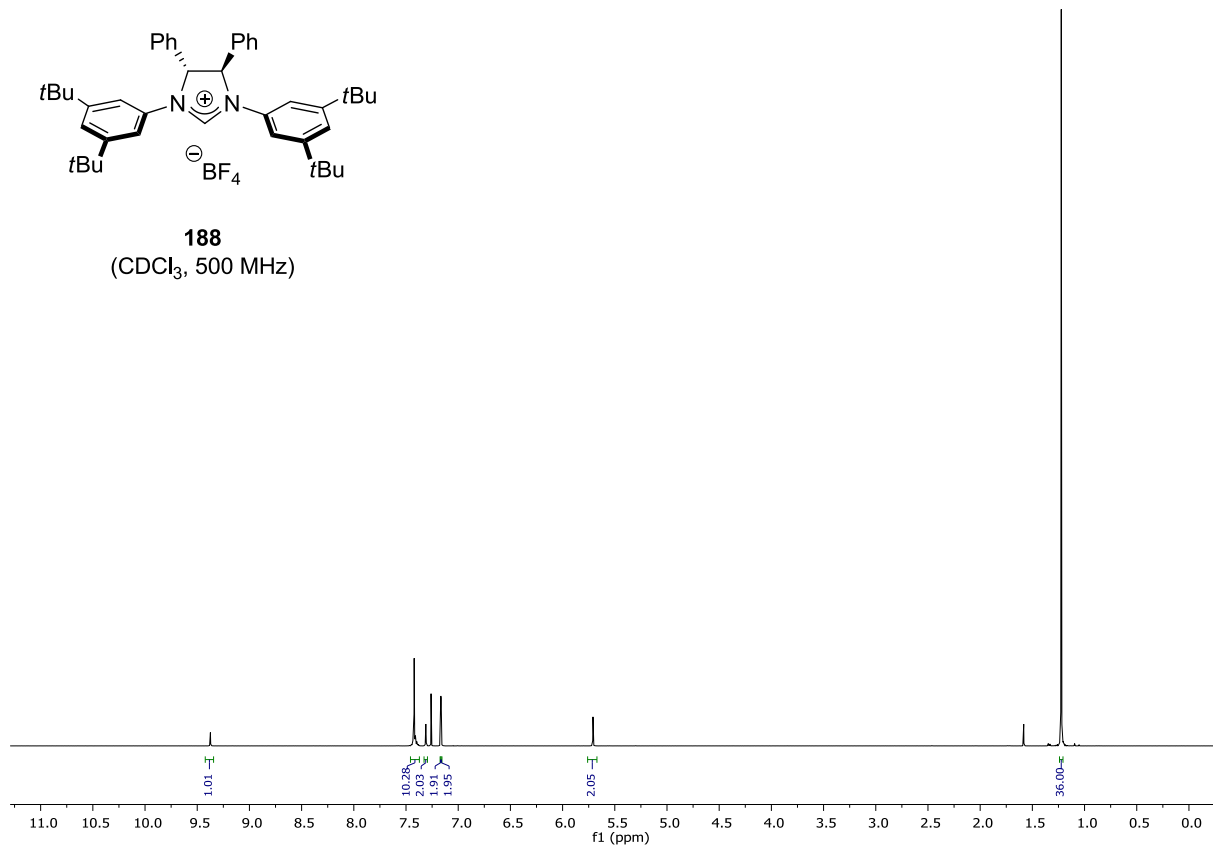


187
(CDCl_3 , 471 MHz)

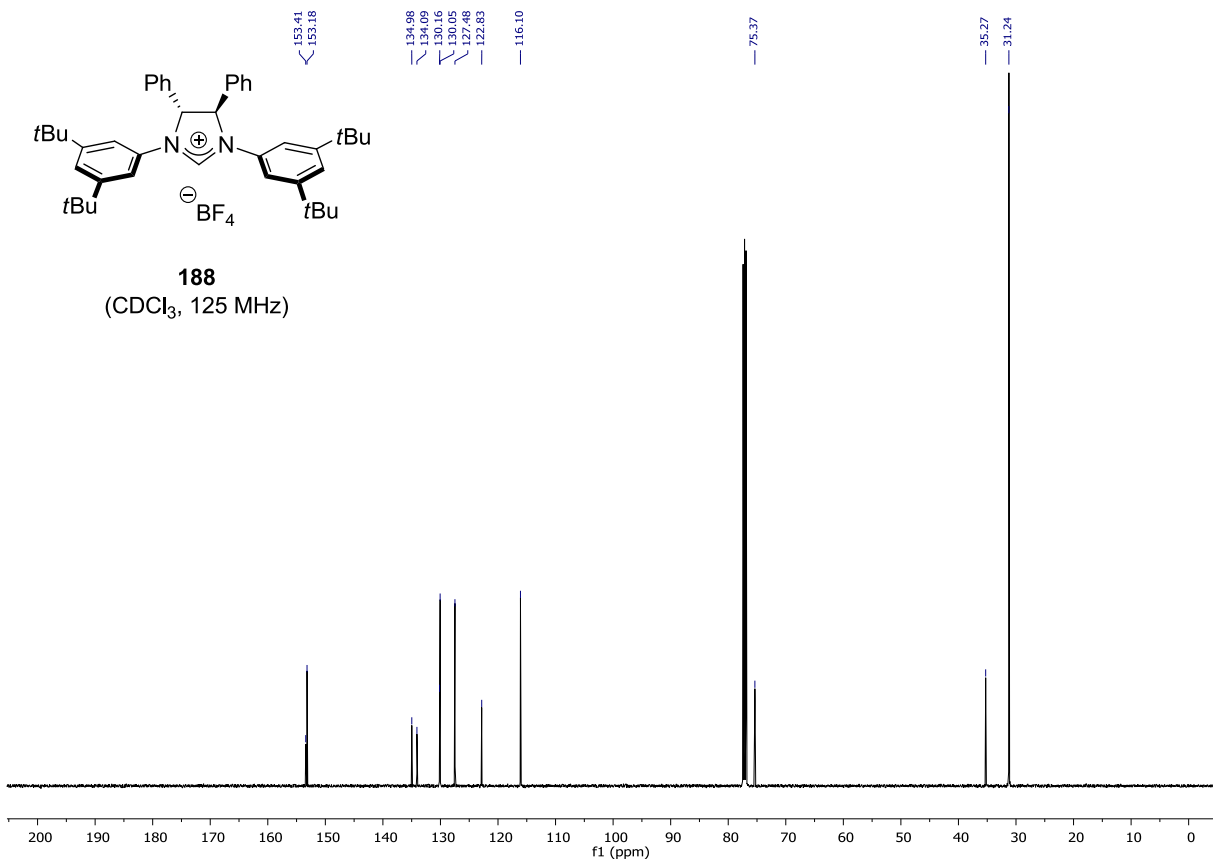


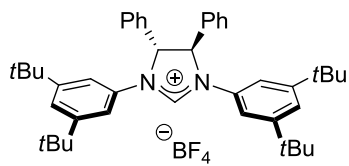


188
(CDCl₃, 500 MHz)

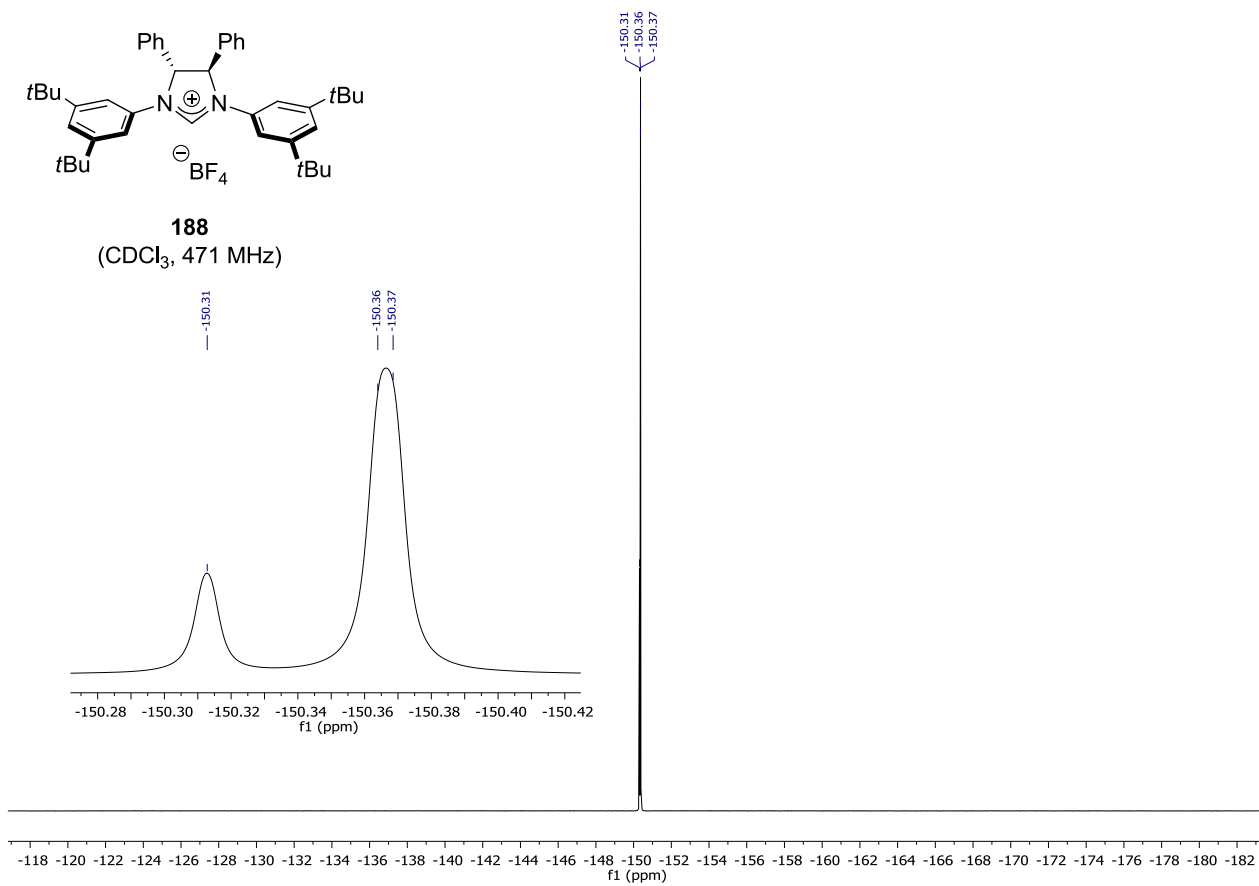


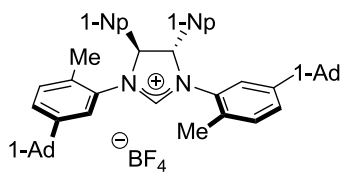
188
(CDCl₃, 125 MHz)



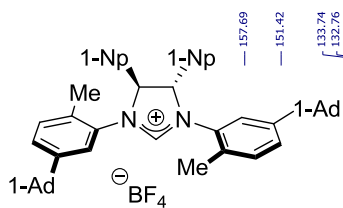
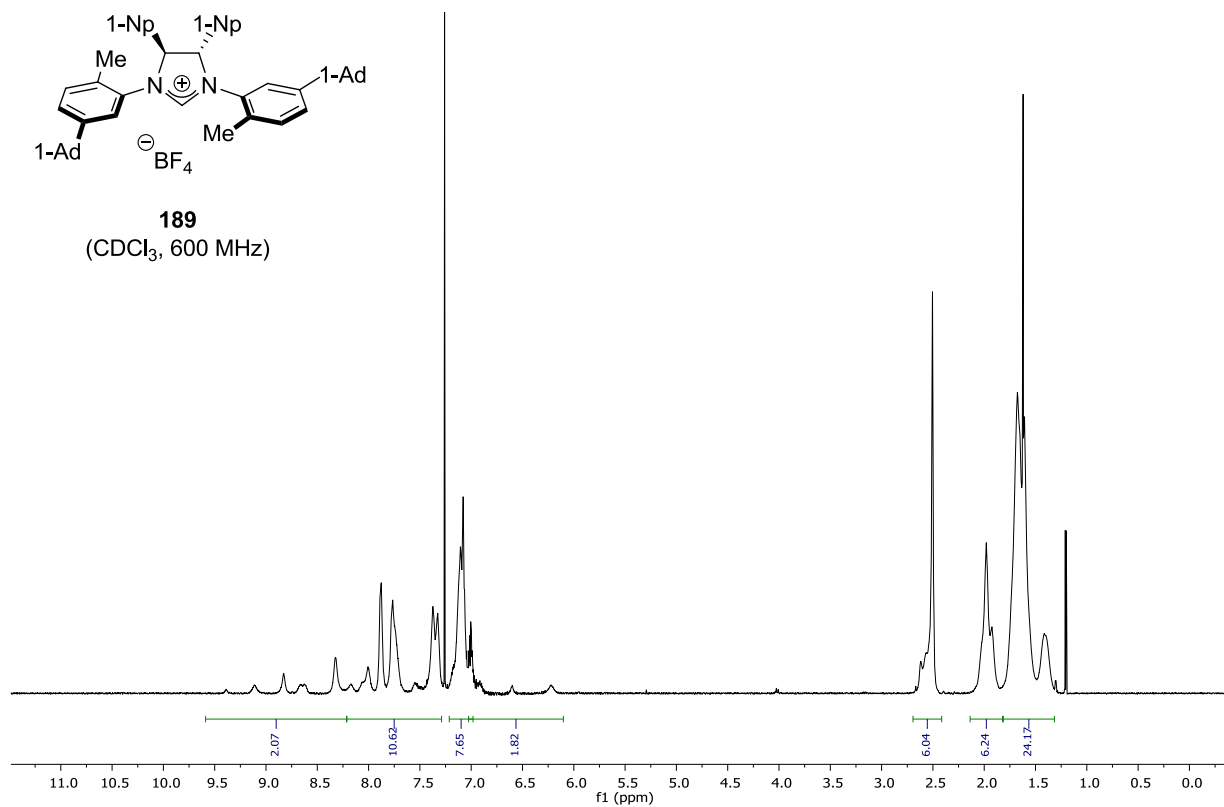


188
(CDCl₃, 471 MHz)

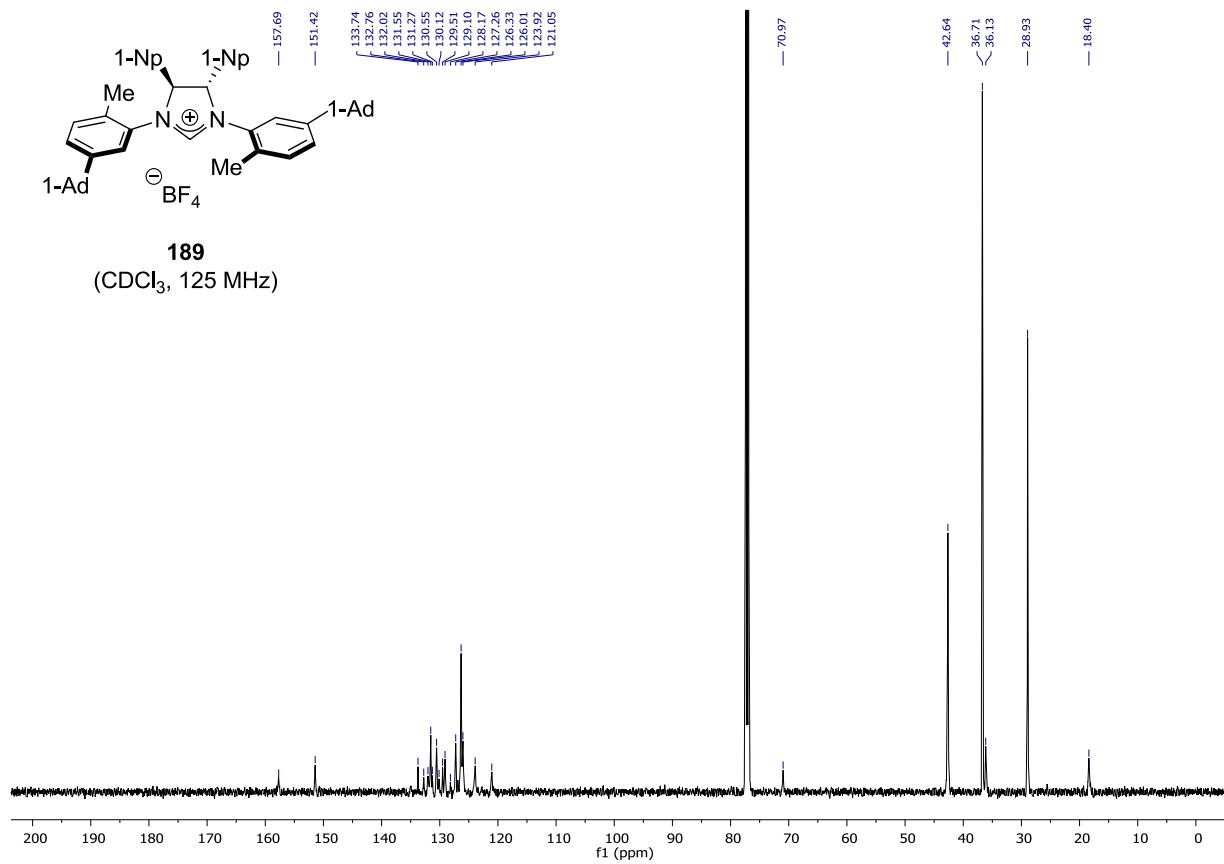


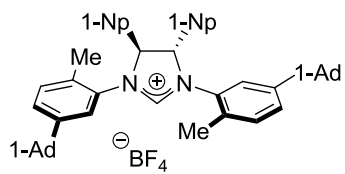


189
(CDCl₃, 600 MHz)

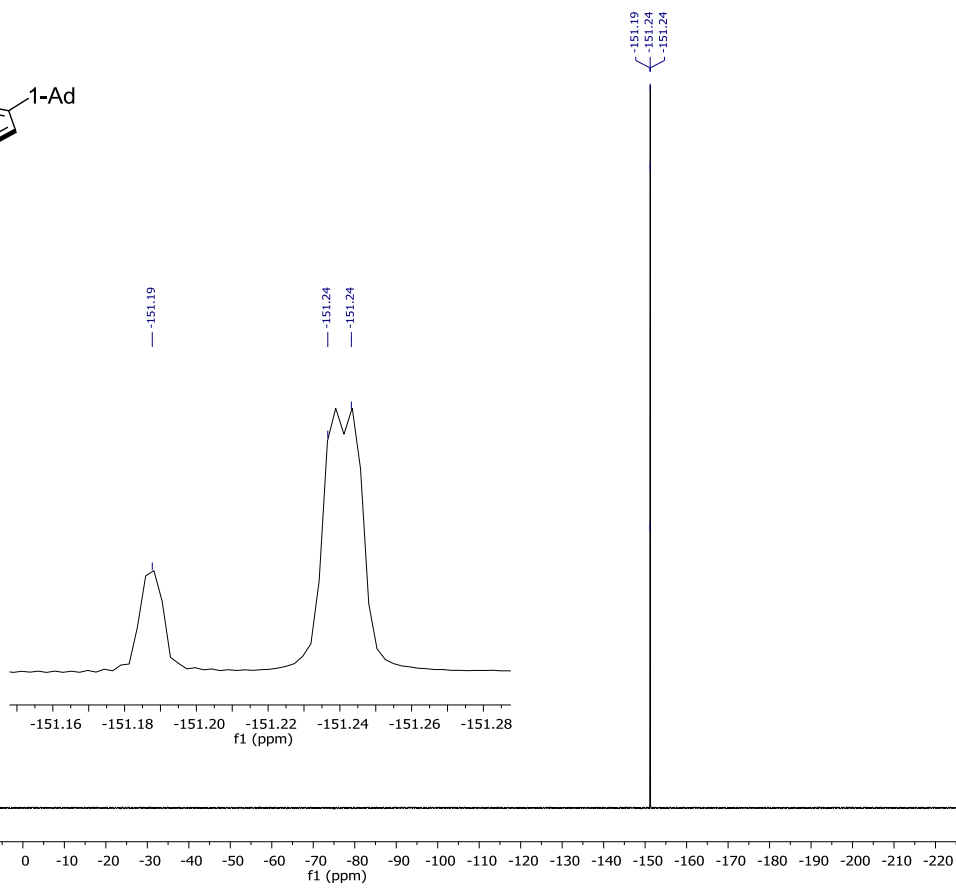


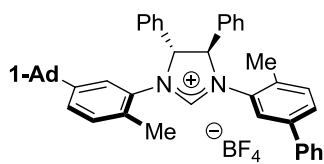
189
(CDCl₃, 125 MHz)



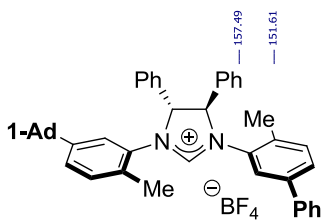
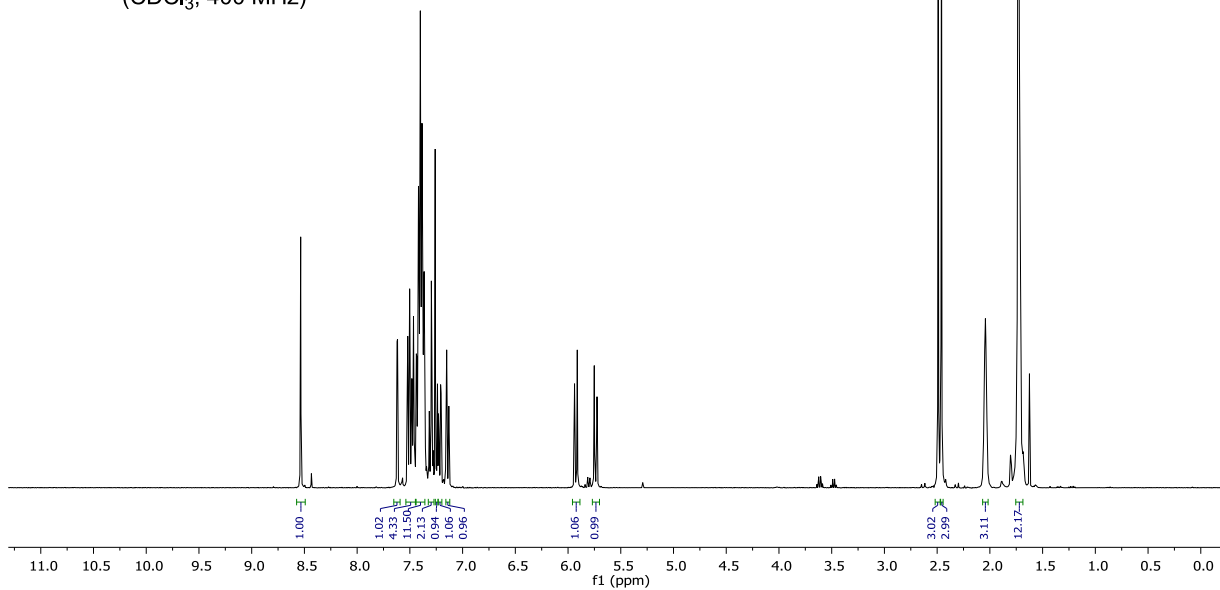


189
(CDCl₃, 376 MHz)

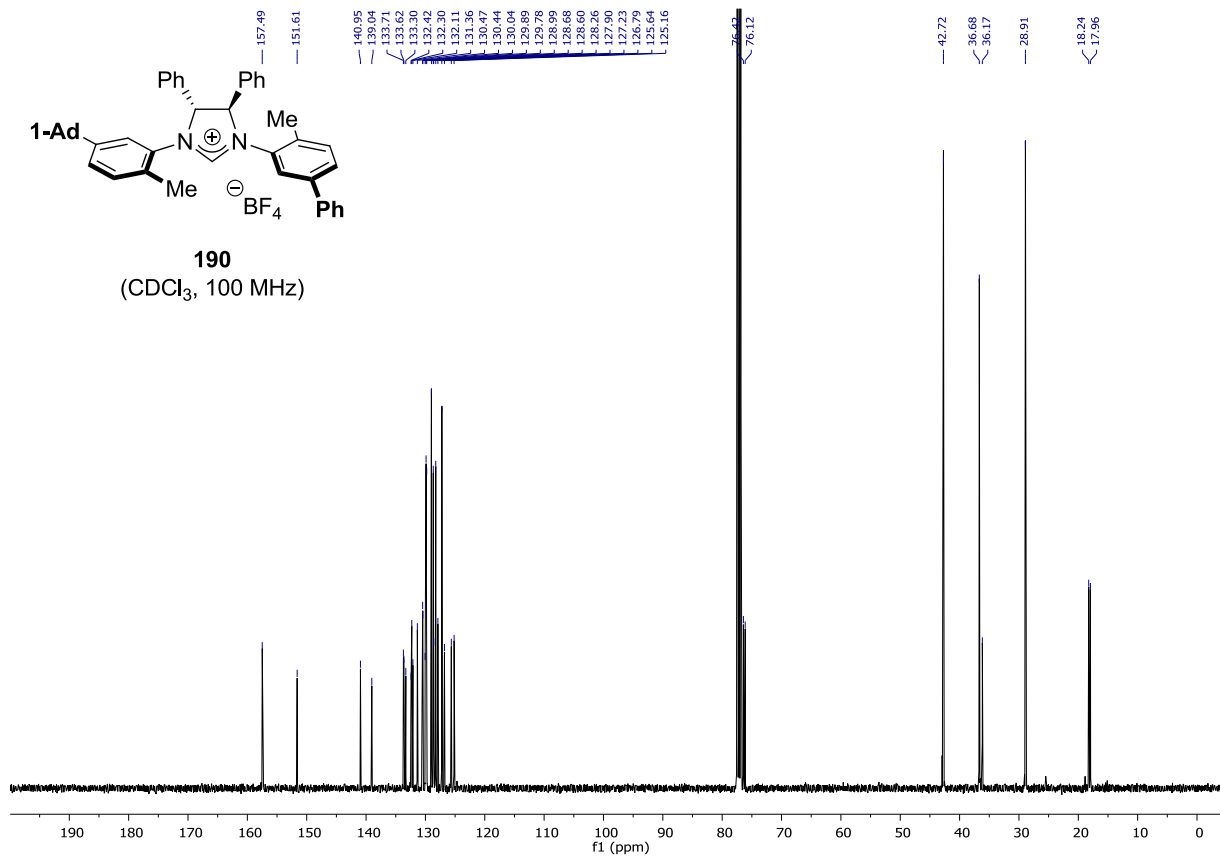


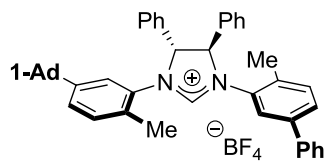


190
(CDCl₃, 400 MHz)

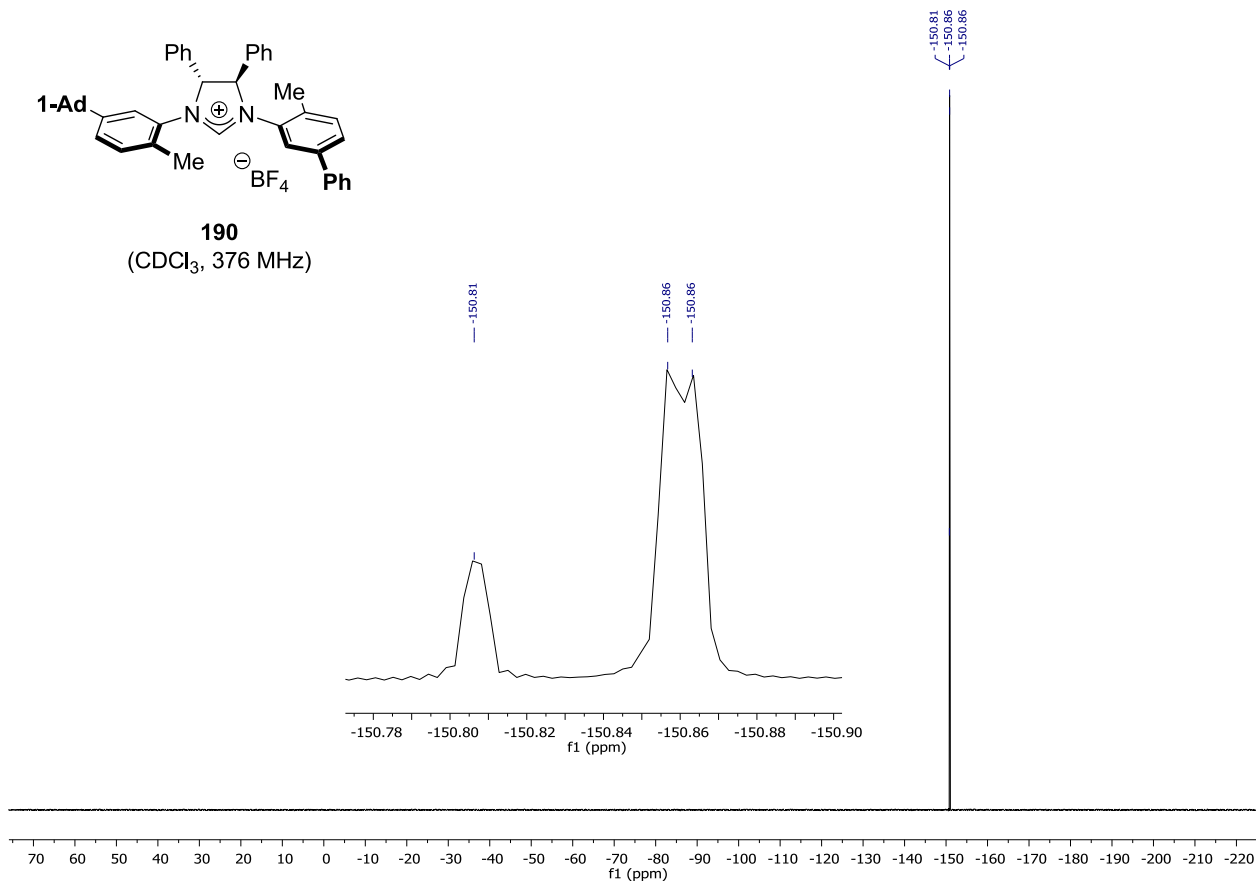


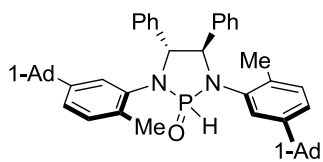
190
(CDCl₃, 100 MHz)



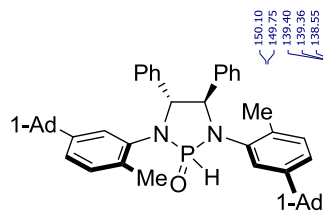
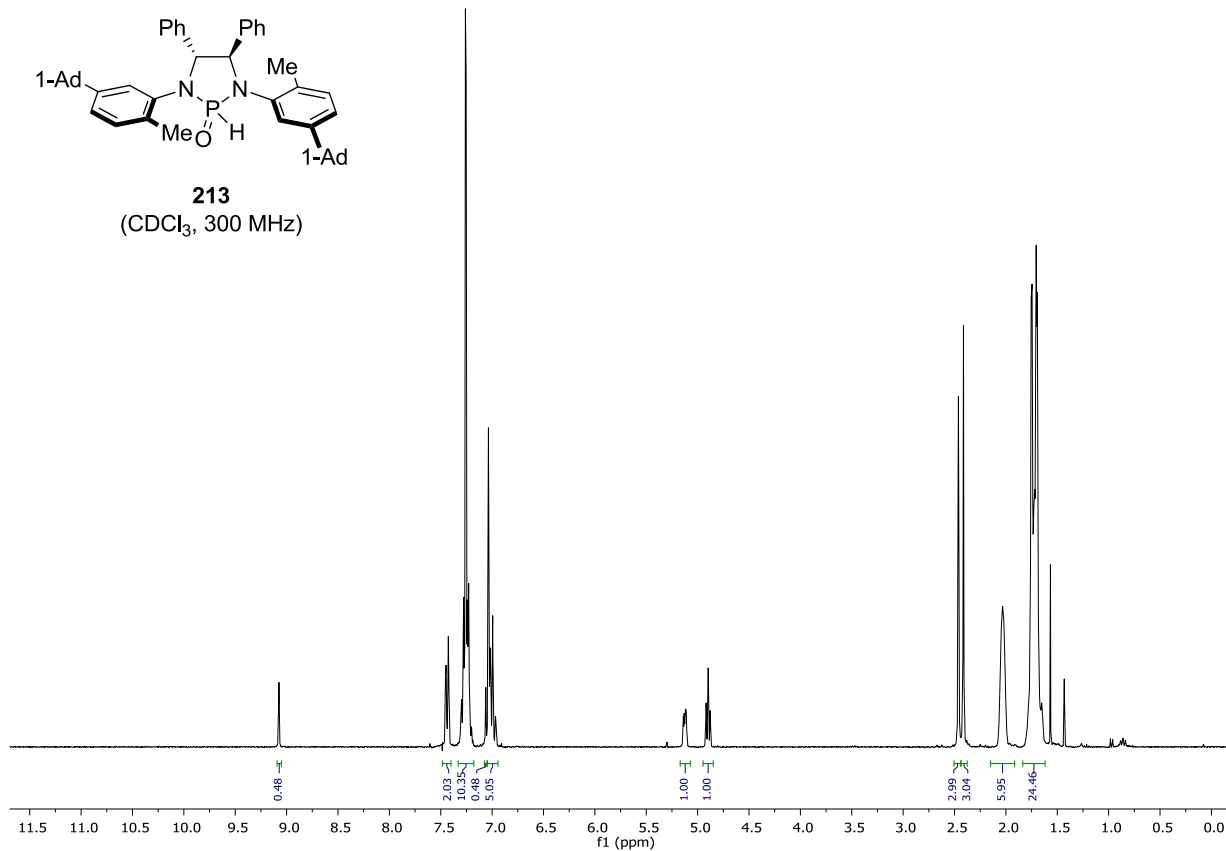


190
(CDCl₃, 376 MHz)

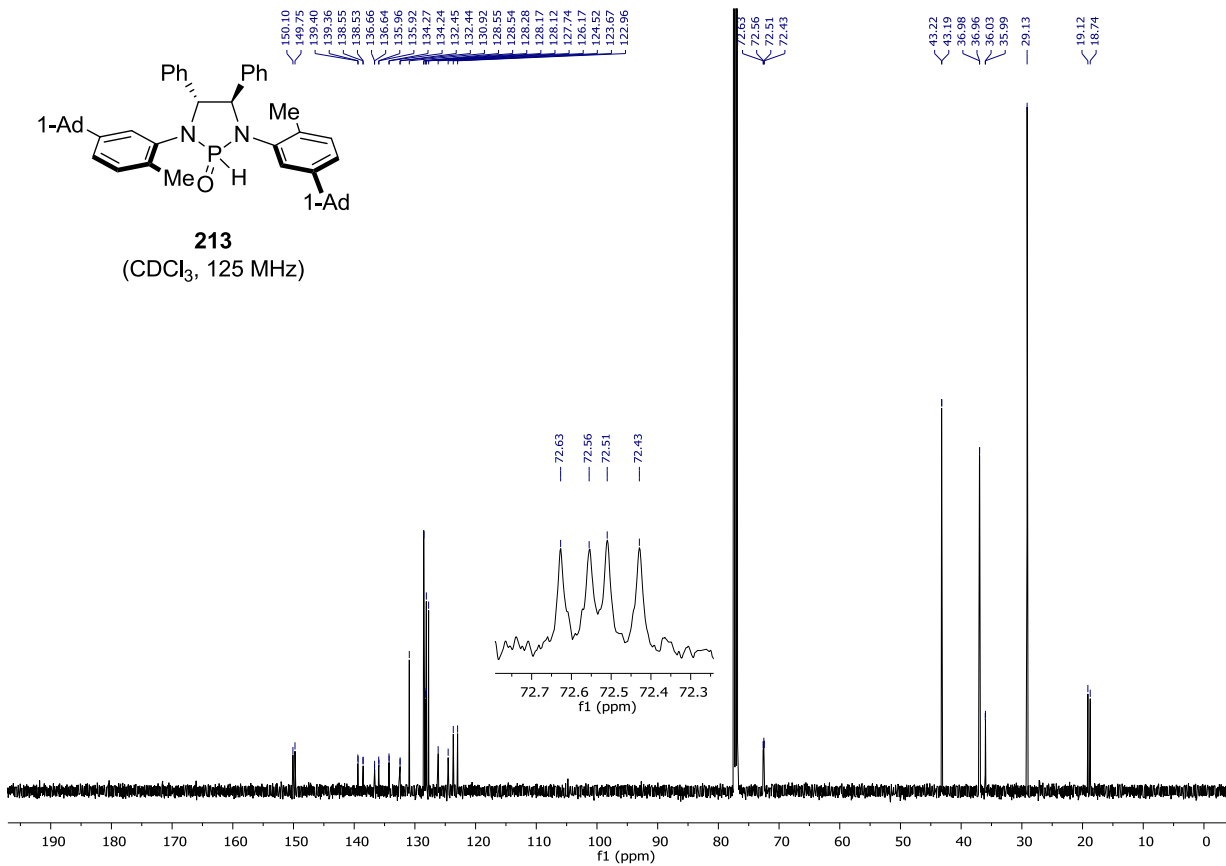


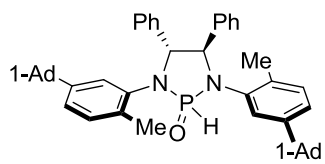


213
(CDCl₃, 300 MHz)

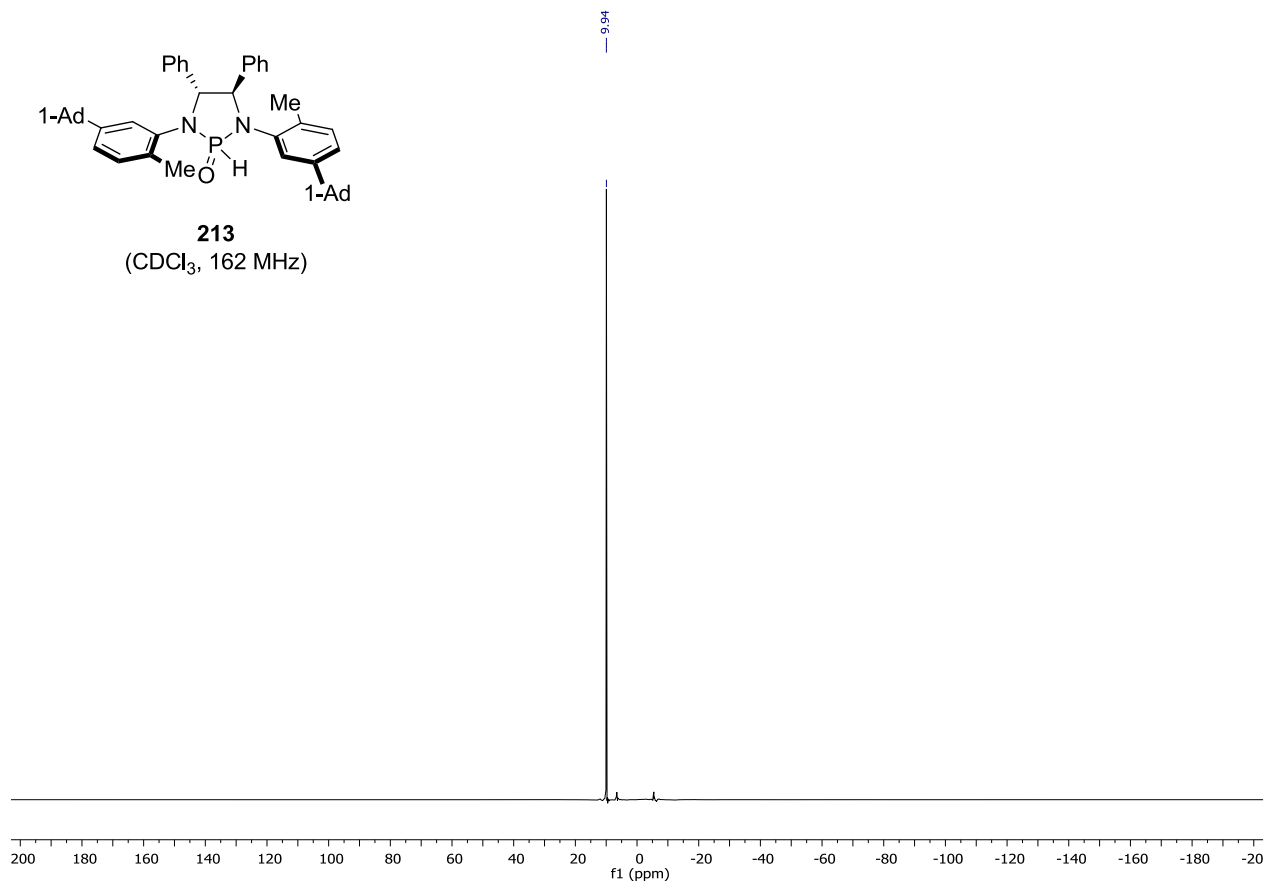


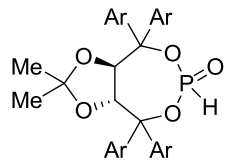
213
(CDCl₃, 125 MHz)



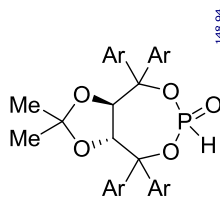
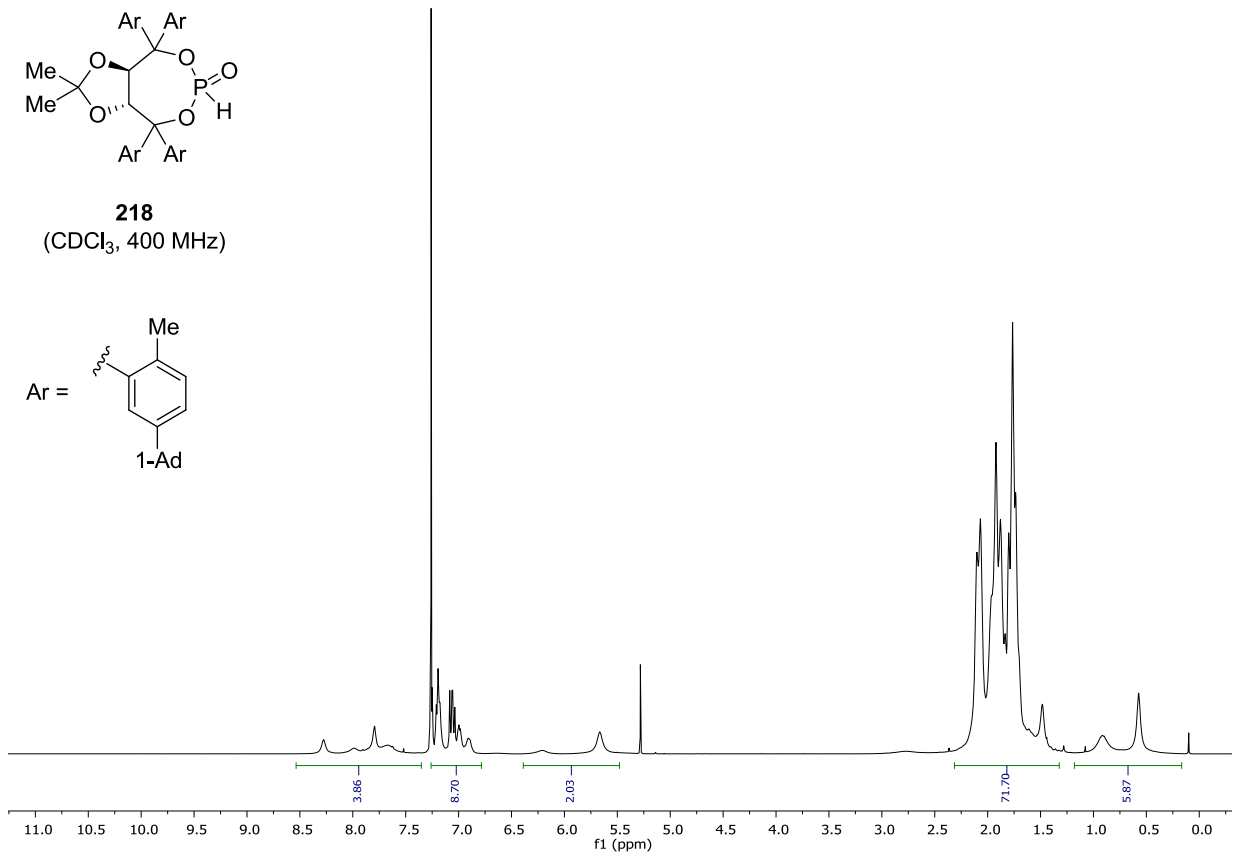
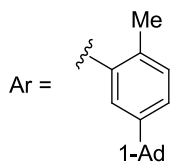


213
(CDCl₃, 162 MHz)

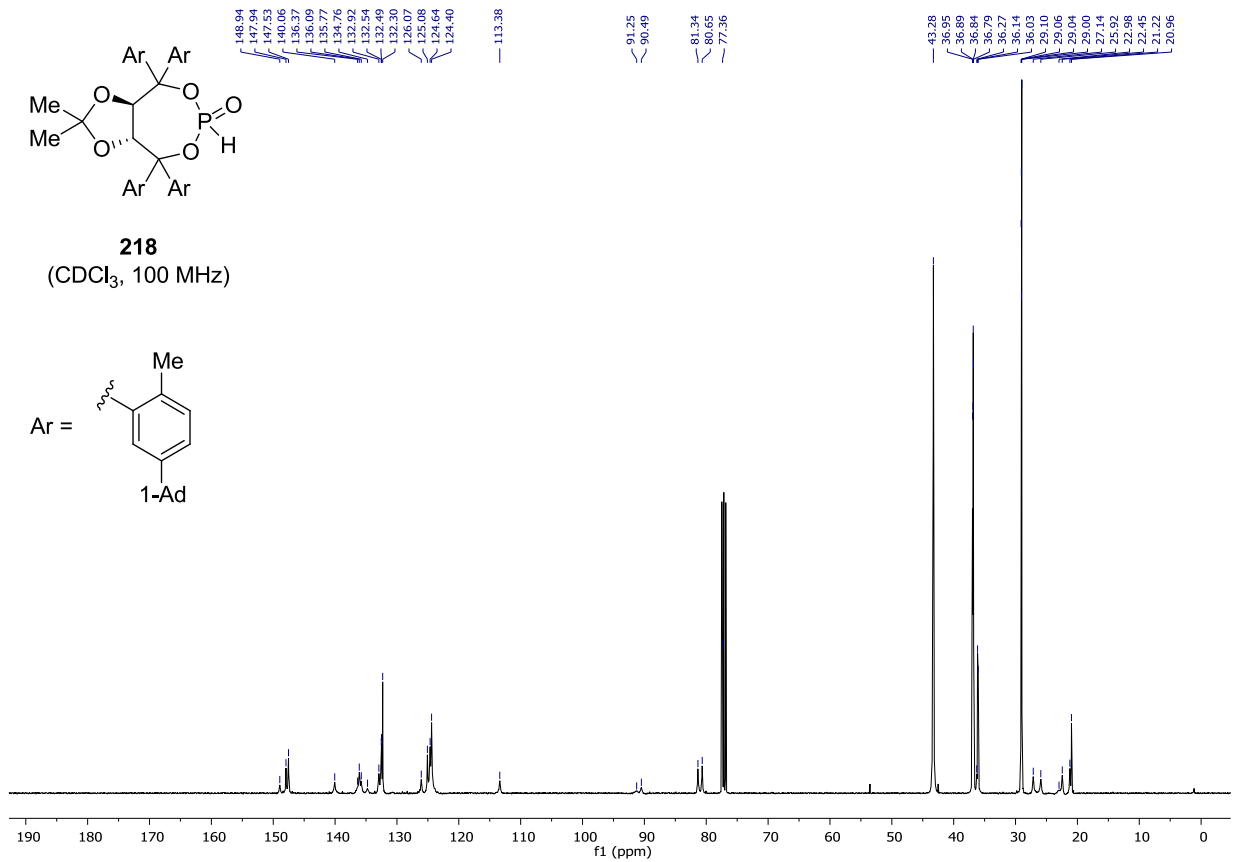
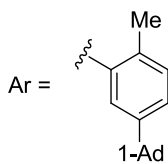


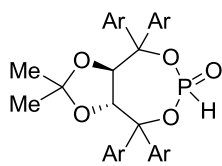


218
(CDCl₃, 400 MHz)

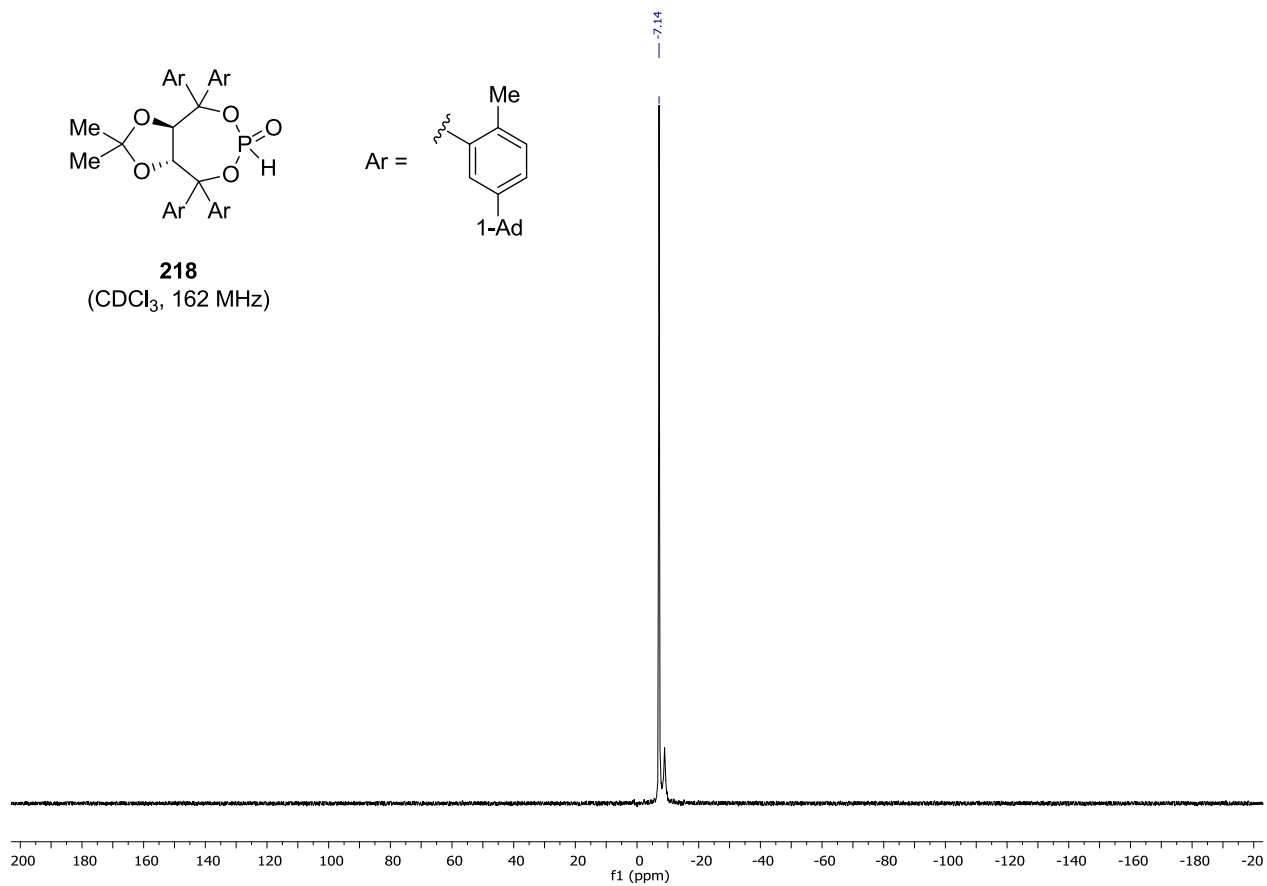
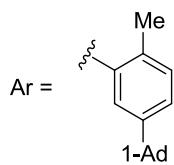


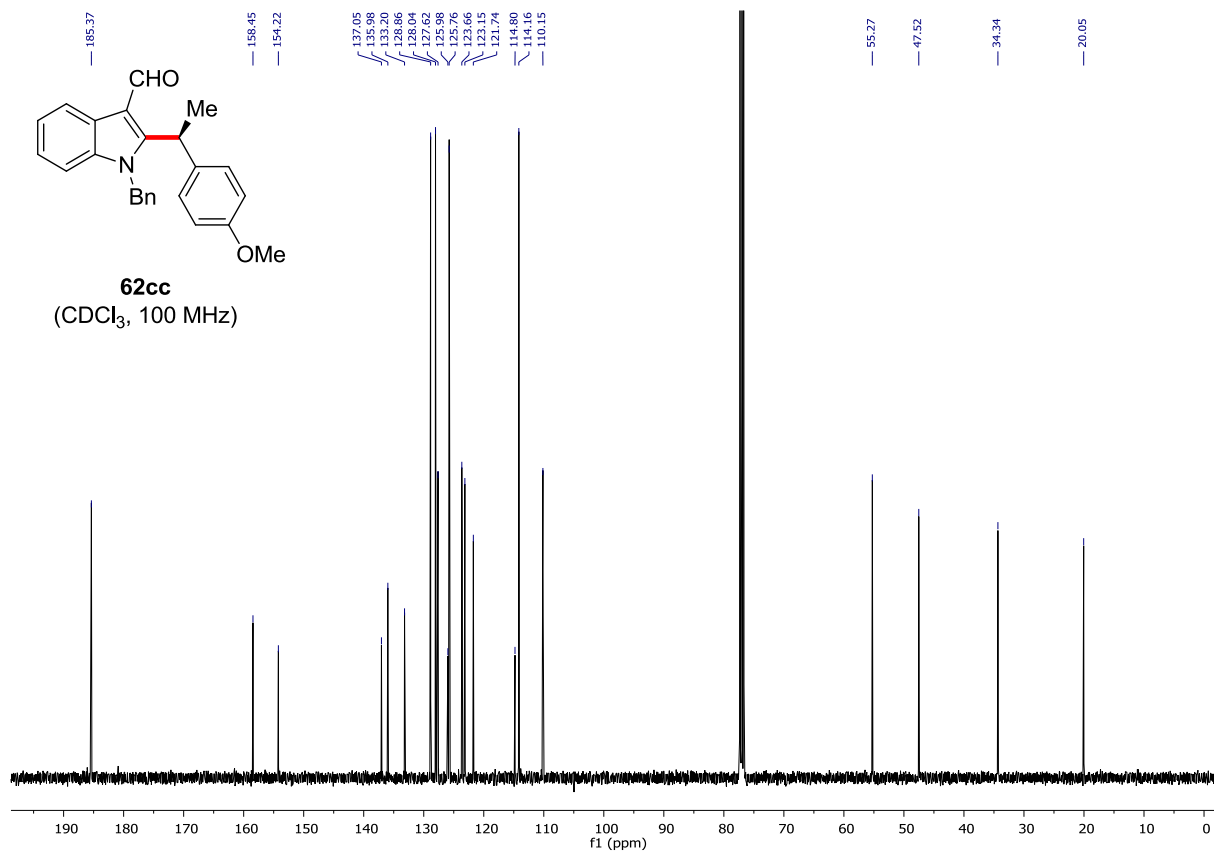
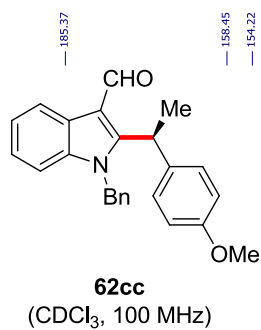
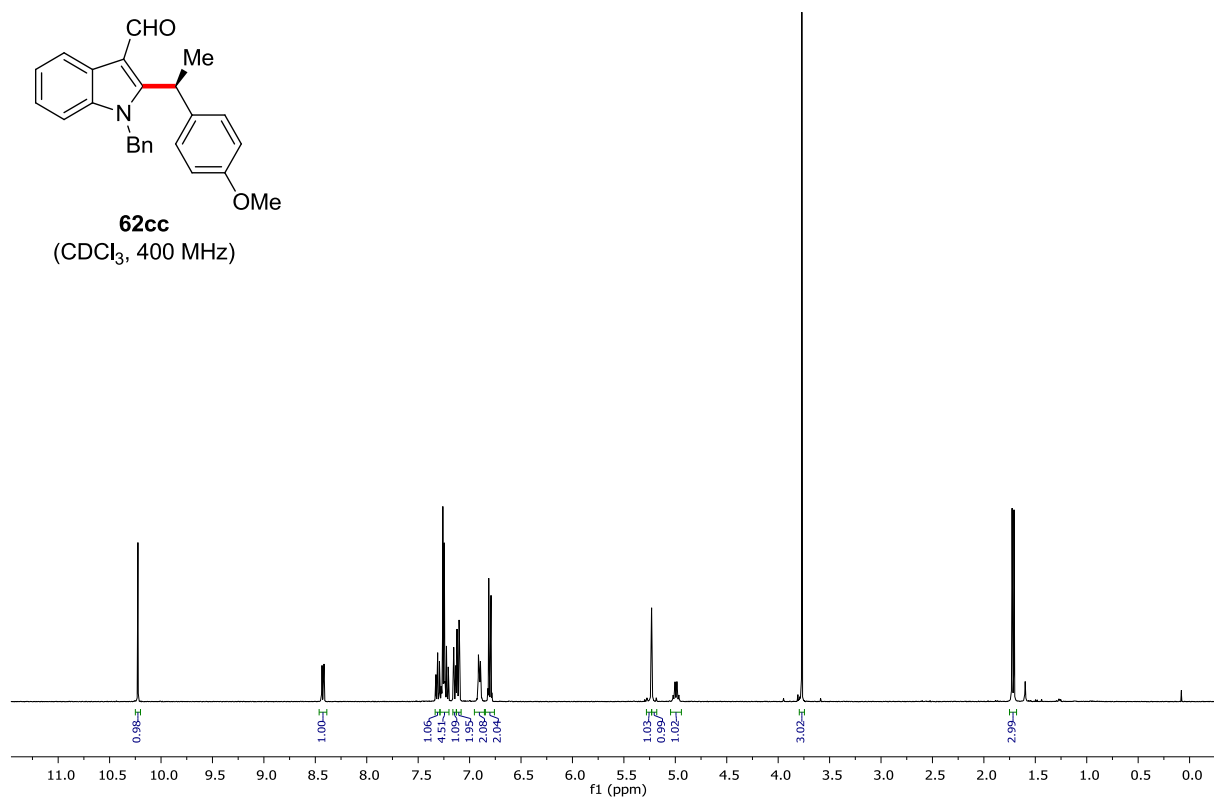
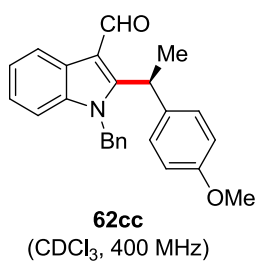
218
(CDCl₃, 100 MHz)



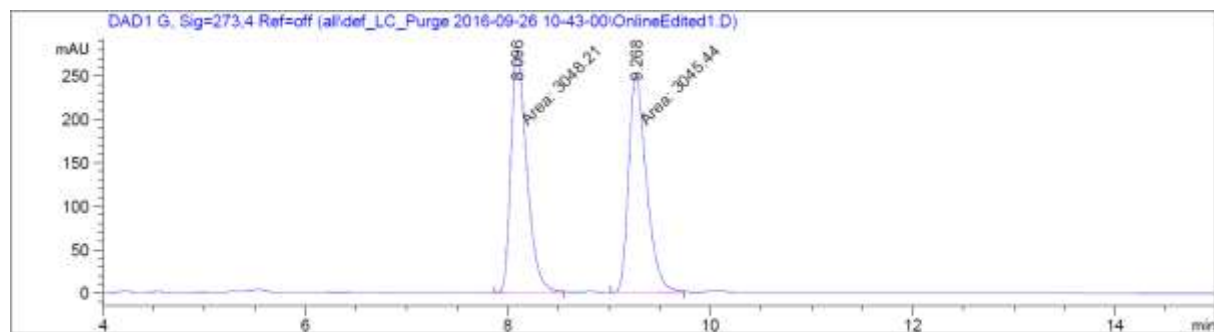


218
(CDCl₃, 162 MHz)

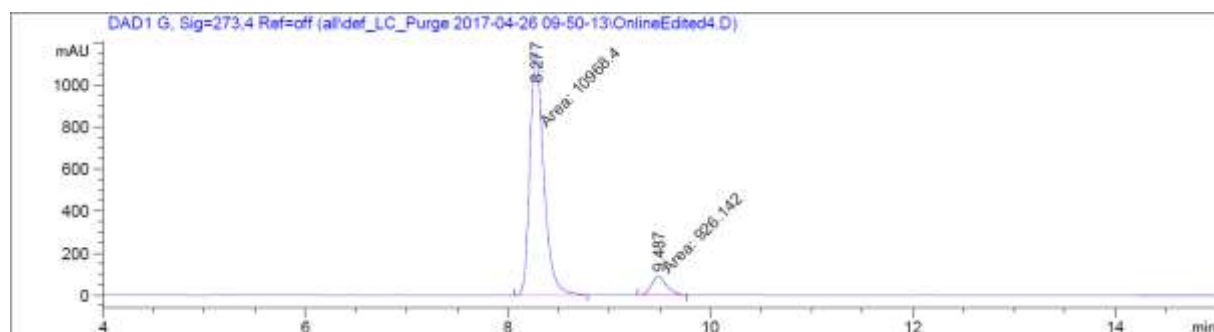




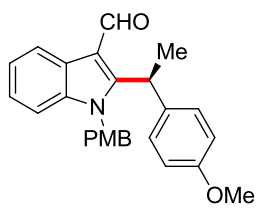
Chiral HPLC of **62cc**:



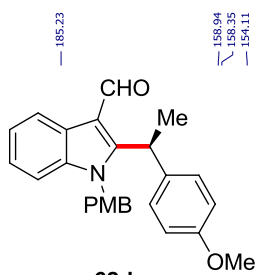
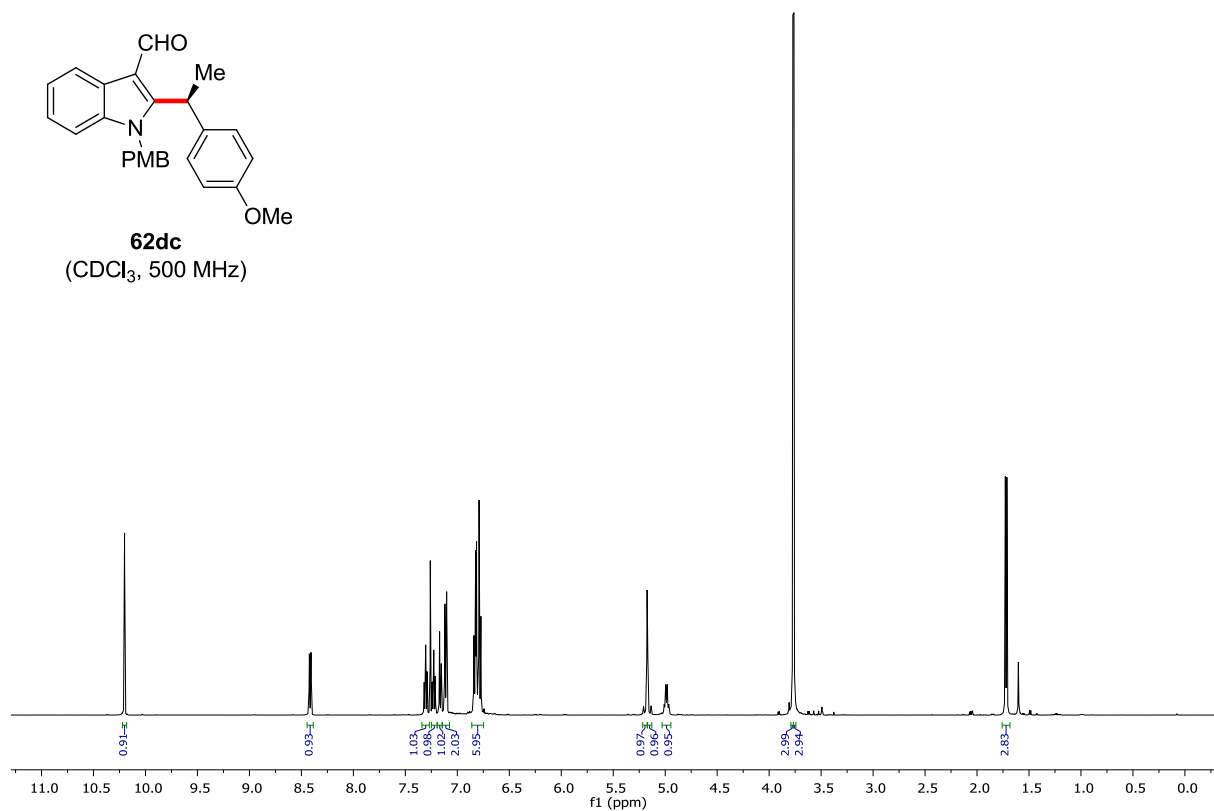
| Peak # | RetTime [min] | Type | Width [min] | Area [mAU*s] | Height [mAU] | Area % |
|--------|---------------|------|-------------|--------------|--------------|---------|
| 1 | 8.096 | MF | 0.1832 | 3048.21387 | 277.37827 | 50.0227 |
| 2 | 9.268 | MF | 0.2032 | 3045.44165 | 249.76355 | 49.9773 |



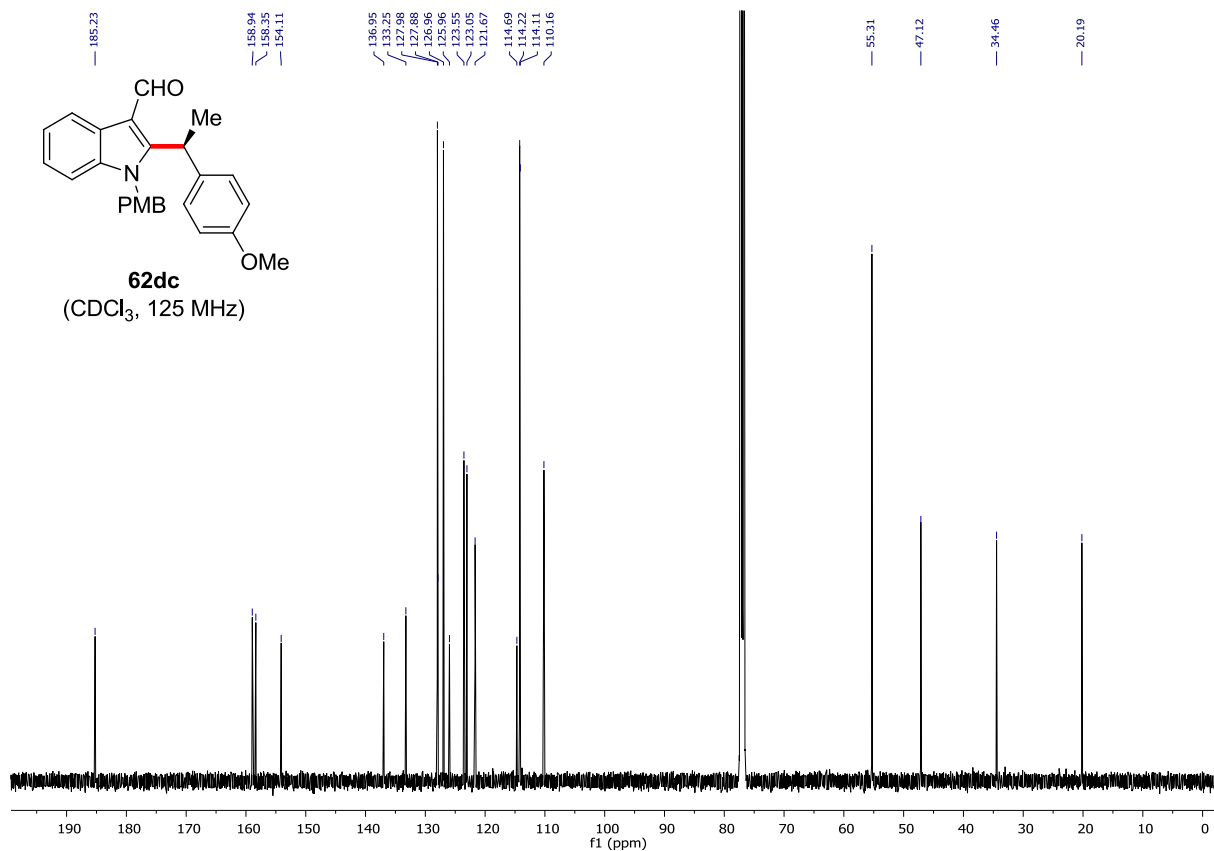
| Peak # | RetTime [min] | Type | Width [min] | Area [mAU*s] | Height [mAU] | Area % |
|--------|---------------|------|-------------|--------------|--------------|---------|
| 1 | 8.277 | MF | 0.1593 | 1.09684e4 | 1147.33240 | 92.2137 |
| 2 | 9.487 | MF | 0.1755 | 926.14203 | 87.97771 | 7.7863 |



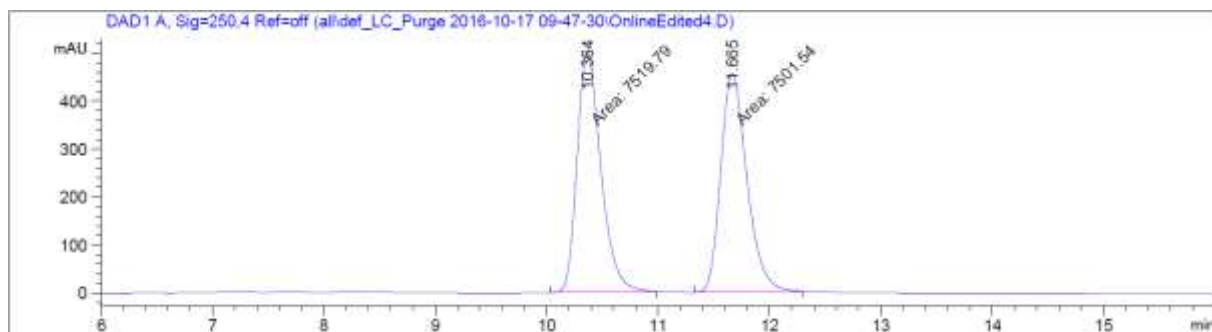
62dc
(CDCl₃, 500 MHz)



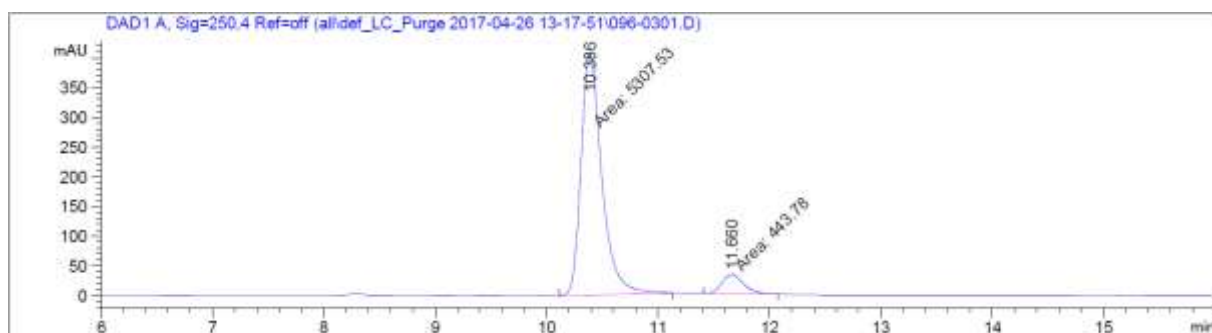
62dc
(CDCl₃, 125 MHz)



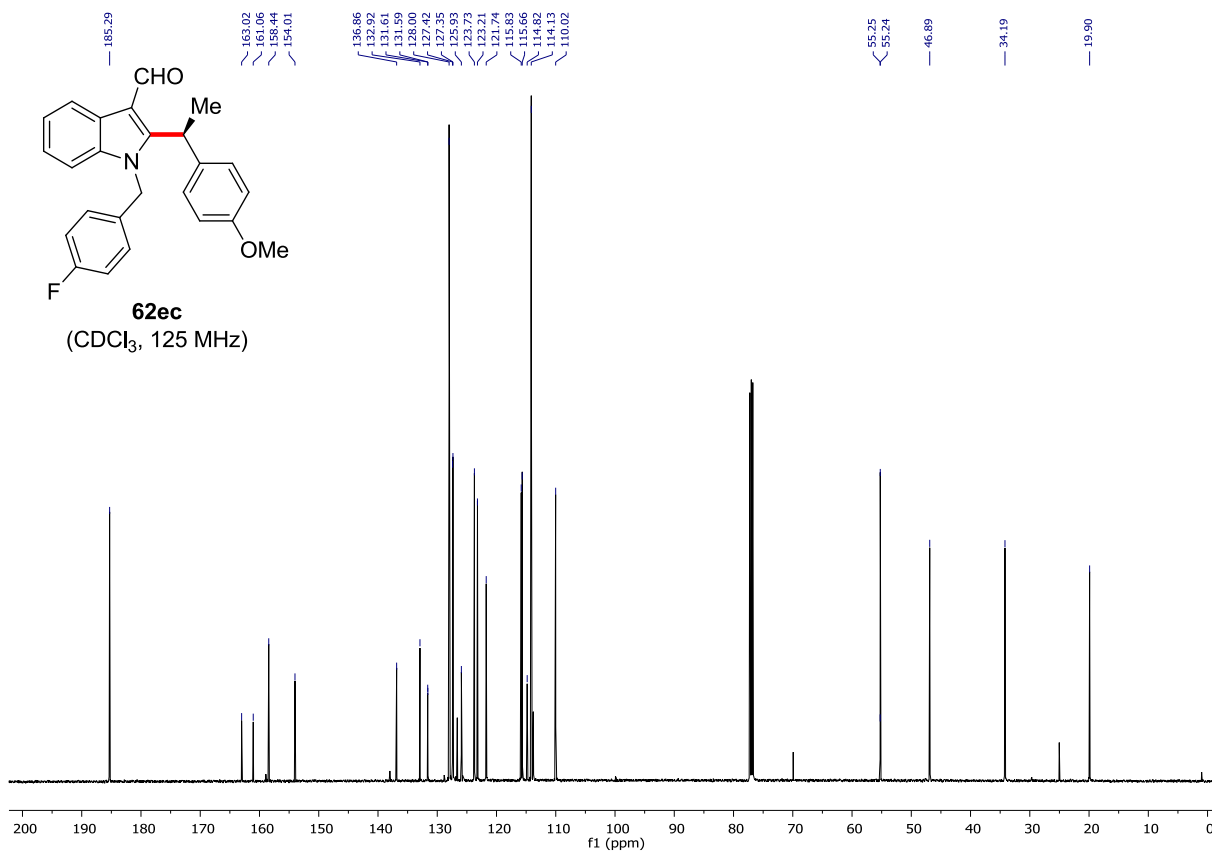
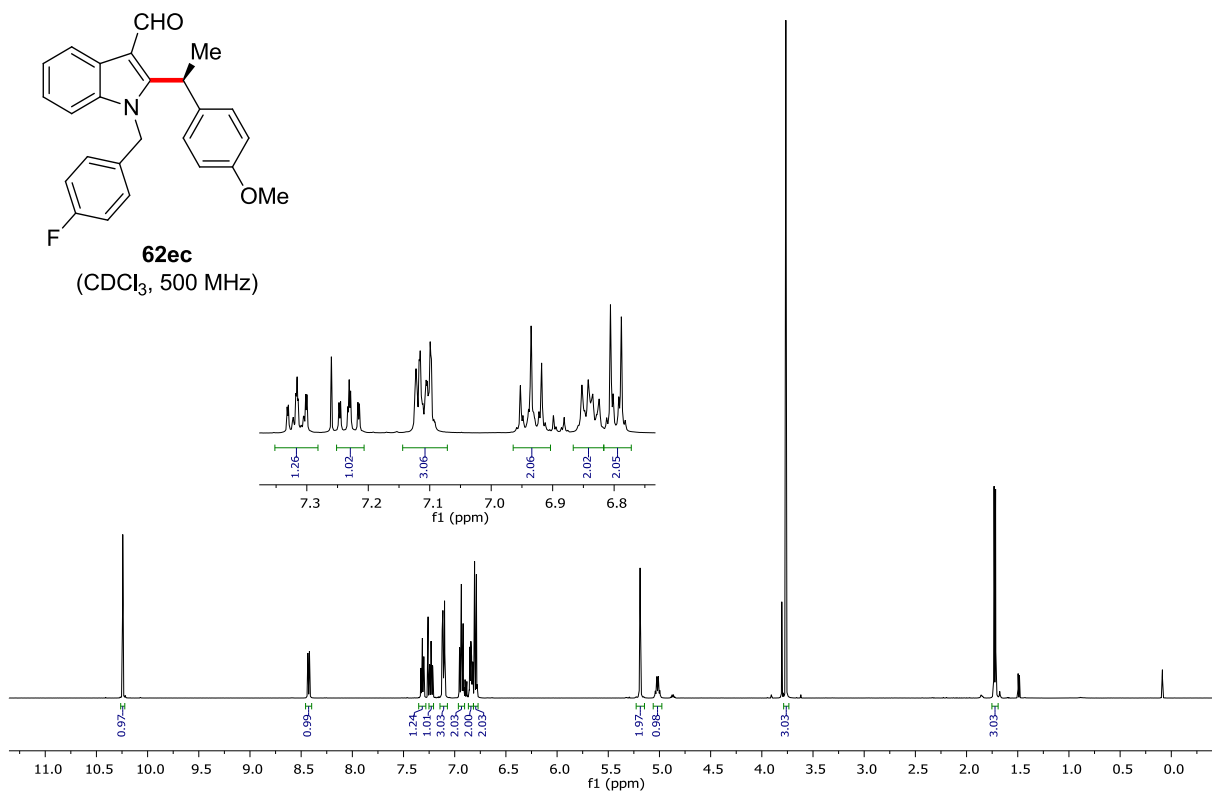
Chiral HPLC of **62dc**:

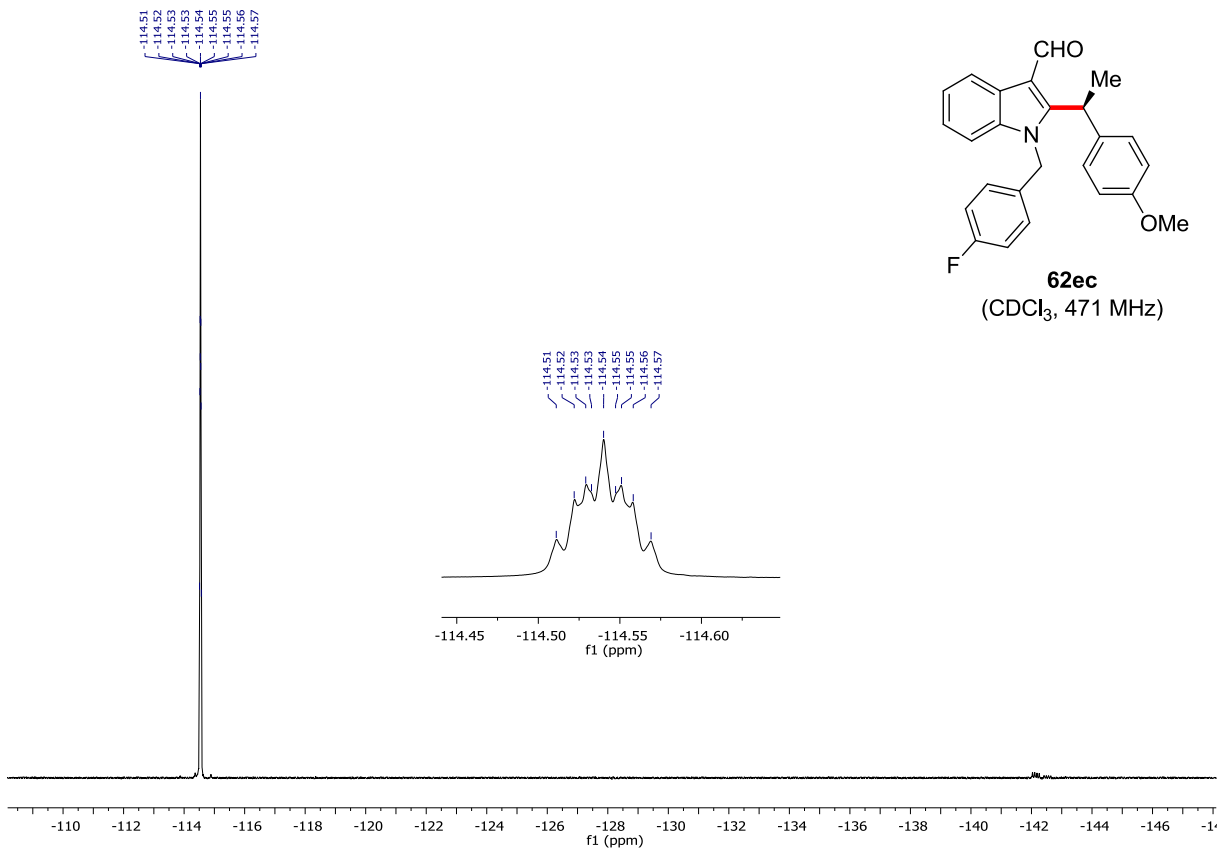


| Peak # | RetTime [min] | Type | Width [min] | Area [mAU*s] | Height [mAU] | Area % |
|--------|---------------|------|-------------|--------------|--------------|---------|
| 1 | 10.364 | MF | 0.2493 | 7519.79150 | 502.68008 | 50.0608 |
| 2 | 11.665 | MF | 0.2736 | 7501.53809 | 456.90005 | 49.9392 |

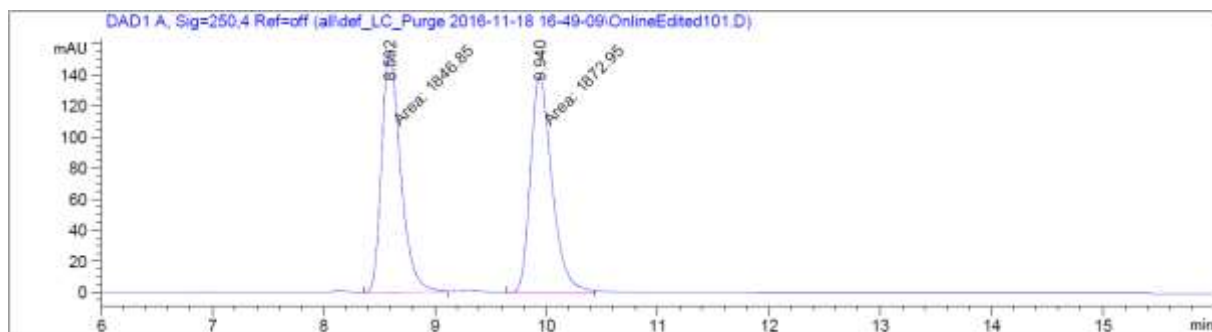


| Peak # | RetTime [min] | Type | Width [min] | Area [mAU*s] | Height [mAU] | Area % |
|--------|---------------|------|-------------|--------------|--------------|---------|
| 1 | 10.386 | MM | 0.2175 | 5307.53320 | 406.78348 | 92.2839 |
| 2 | 11.660 | MF | 0.2270 | 443.77972 | 32.59005 | 7.7161 |

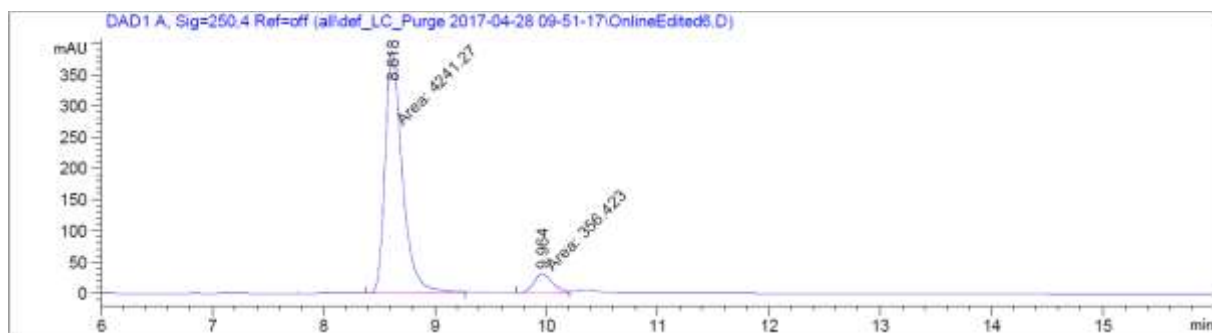




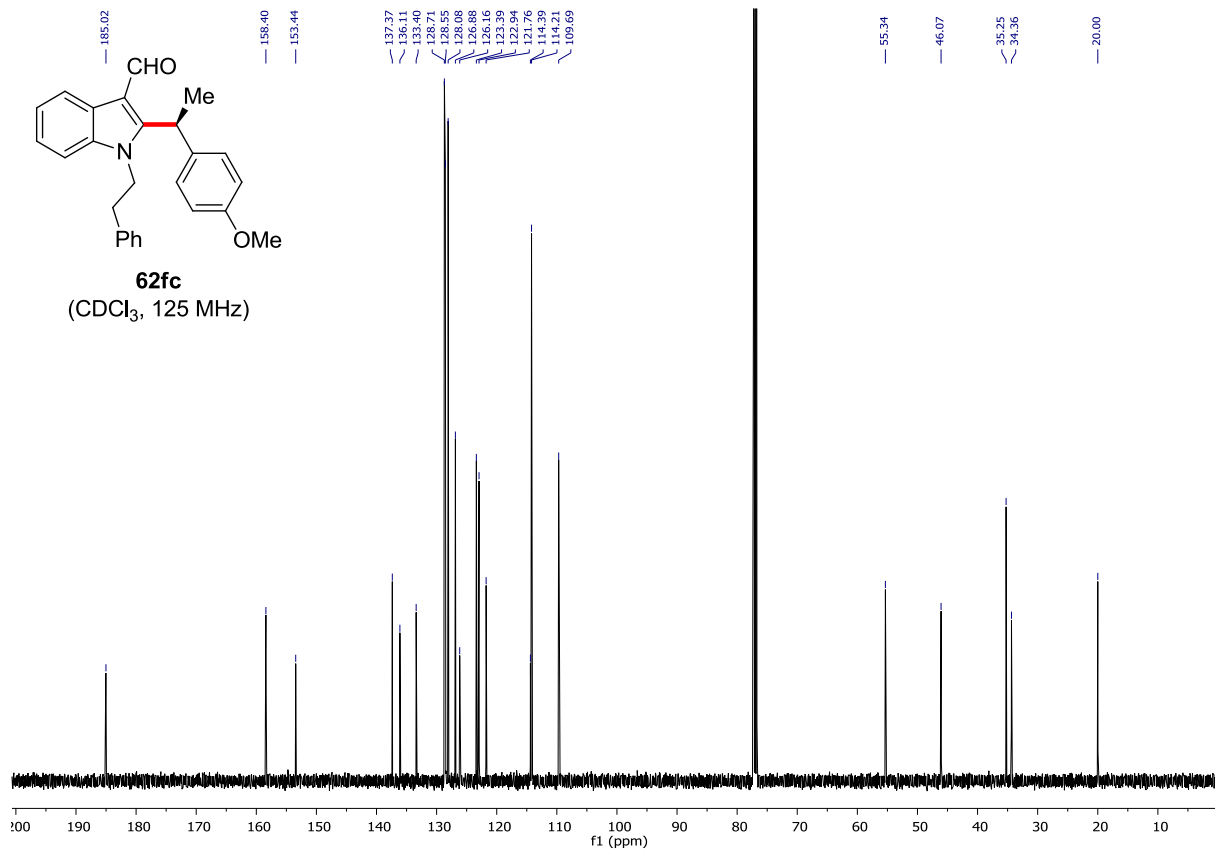
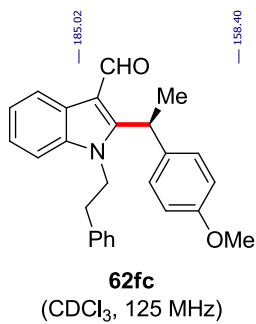
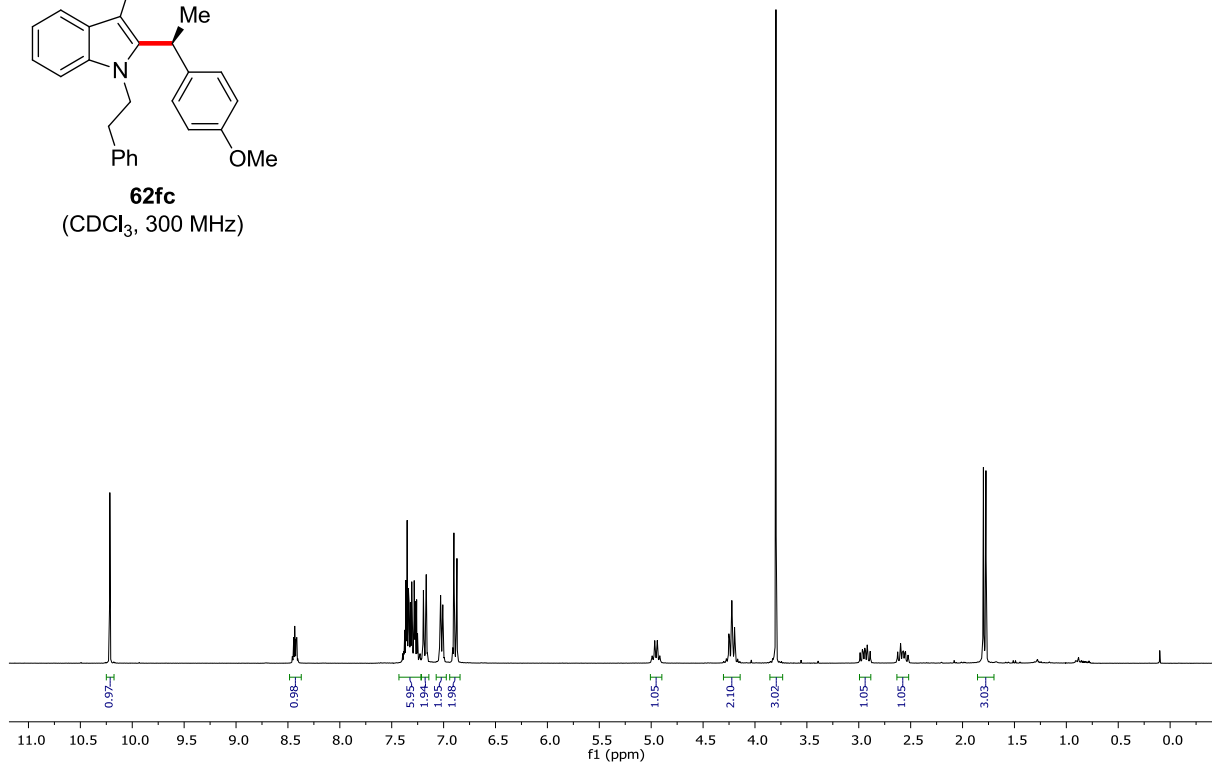
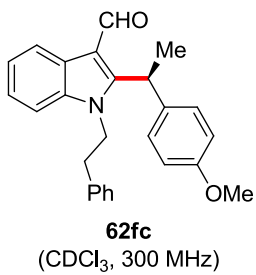
Chiral HPLC of **62ec**:



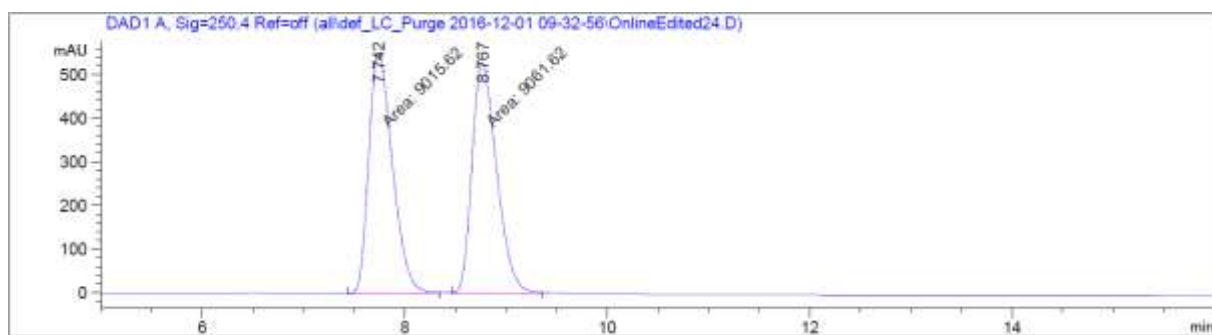
| Peak # | RetTime [min] | Type | Width [min] | Area [mAU*s] | Height [mAU] | Area % |
|--------|---------------|------|-------------|--------------|--------------|---------|
| 1 | 8.592 | MF | 0.1984 | 1846.85034 | 155.15952 | 49.6492 |
| 2 | 9.940 | MF | 0.2242 | 1872.94897 | 139.22650 | 50.3508 |



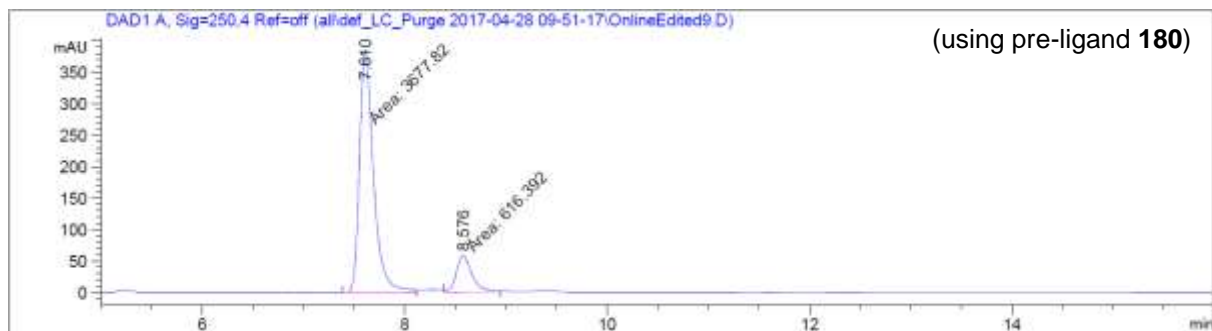
| Peak # | RetTime [min] | Type | Width [min] | Area [mAU*s] | Height [mAU] | Area % |
|--------|---------------|------|-------------|--------------|--------------|---------|
| 1 | 8.618 | MF | 0.1826 | 4241.26611 | 387.20792 | 92.2478 |
| 2 | 9.964 | MF | 0.1966 | 356.42282 | 30.21237 | 7.7522 |



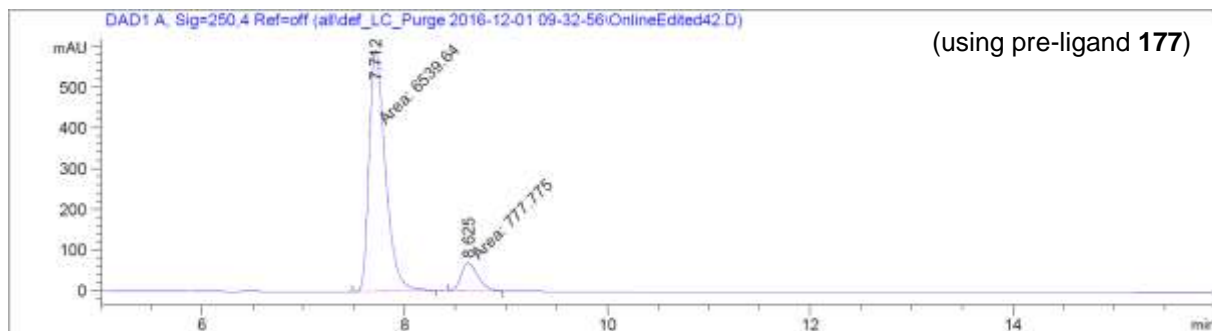
Chiral HPLC of **62fc**:



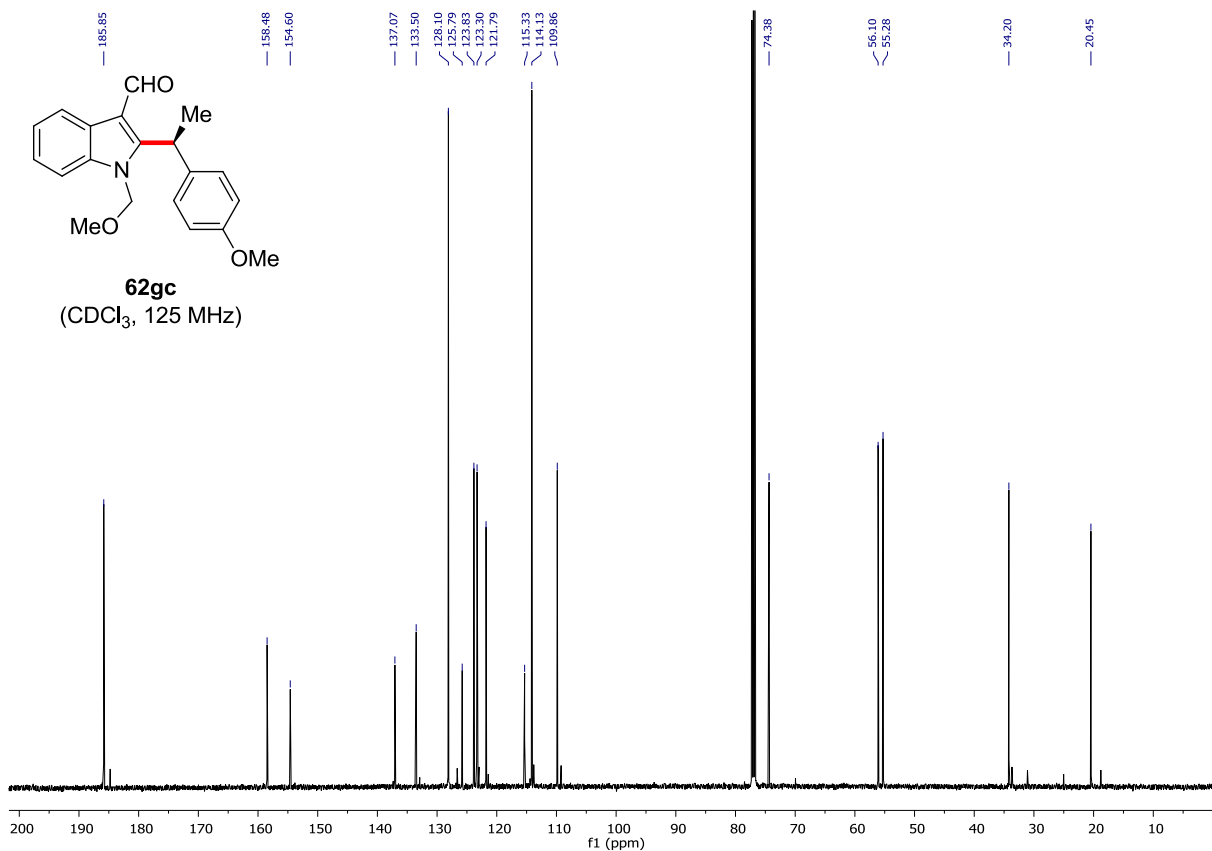
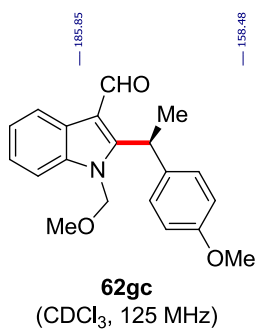
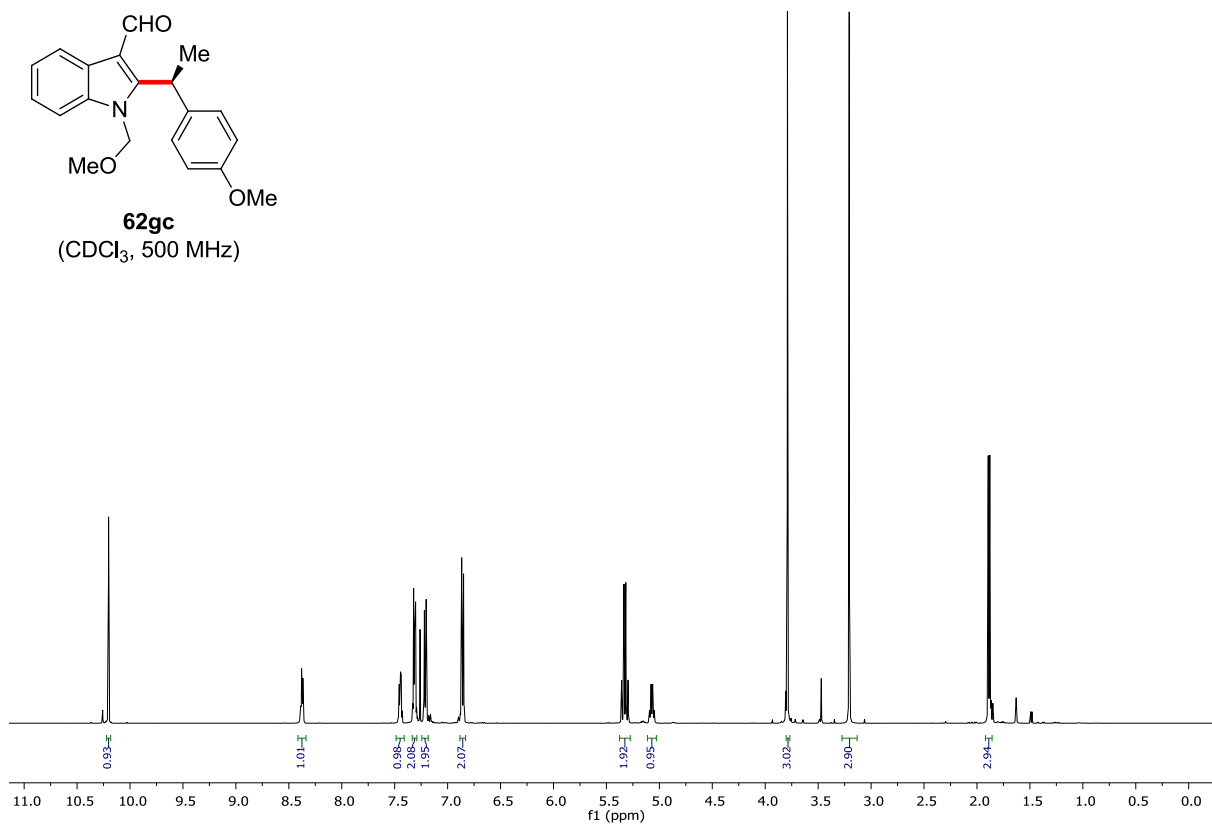
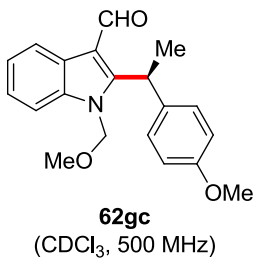
| Peak # | RetTime [min] | Type | Width [min] | Area [mAU*s] | Height [mAU] | Area % |
|--------|---------------|------|-------------|--------------|--------------|---------|
| 1 | 7.742 | MF | 0.2730 | 9015.62012 | 550.33301 | 49.8728 |
| 2 | 8.767 | MF | 0.2855 | 9061.61719 | 529.02570 | 50.1272 |



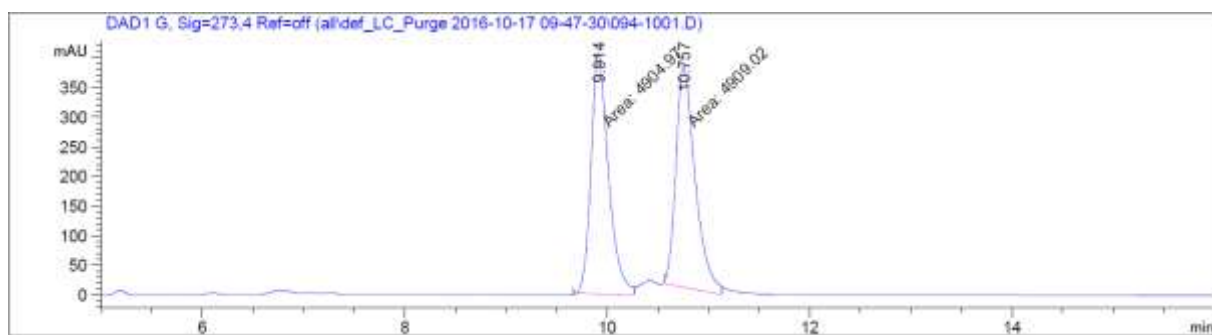
| Peak # | RetTime [min] | Type | Width [min] | Area [mAU*s] | Height [mAU] | Area % |
|--------|---------------|------|-------------|--------------|--------------|---------|
| 1 | 7.610 | MF | 0.1596 | 3677.81714 | 384.15280 | 85.6460 |
| 2 | 8.576 | MF | 0.1777 | 616.39221 | 57.80042 | 14.3540 |



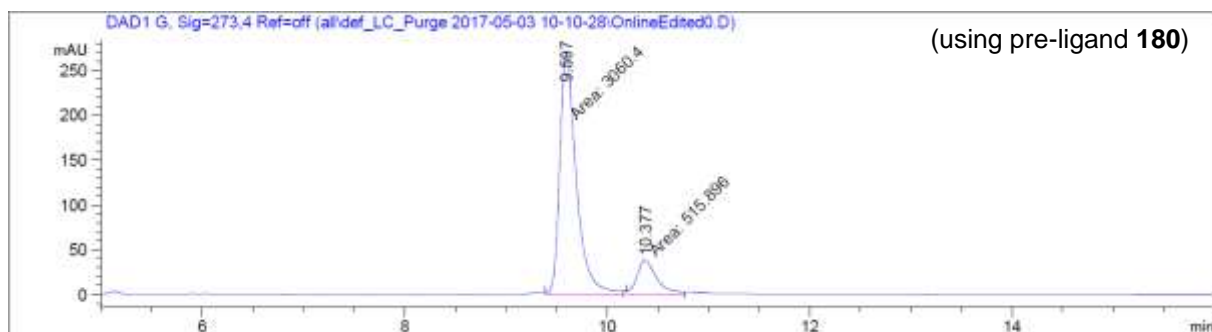
| Peak # | RetTime [min] | Type | Width [min] | Area [mAU*s] | Height [mAU] | Area % |
|--------|---------------|------|-------------|--------------|--------------|---------|
| 1 | 7.712 | MF | 0.1842 | 6539.64160 | 591.66425 | 89.3709 |
| 2 | 8.625 | MF | 0.1906 | 777.77527 | 68.00621 | 10.6291 |



Chiral HPLC of **62gc**:

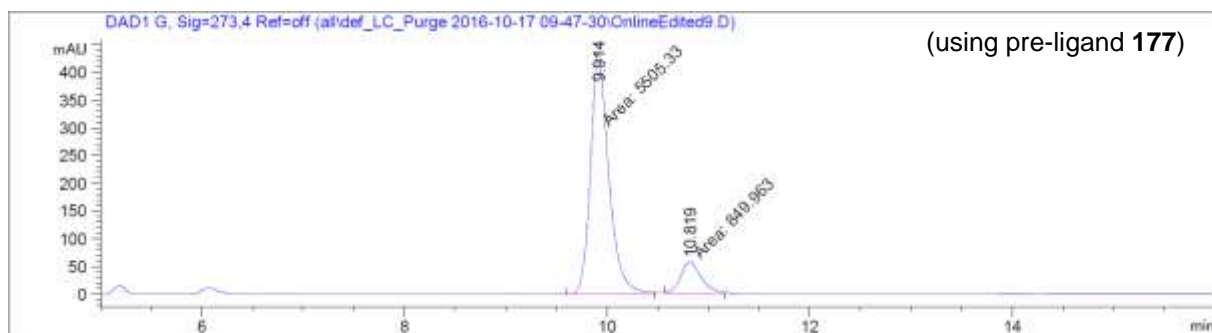


| Peak # | RetTime [min] | Type | Width [min] | Area [mAU*s] | Height [mAU] | Area % |
|--------|---------------|------|-------------|--------------|--------------|---------|
| 1 | 9.914 | MM | 0.2015 | 4904.97314 | 405.71075 | 49.9794 |
| 2 | 10.757 | MF | 0.2197 | 4909.02051 | 372.32123 | 50.0206 |



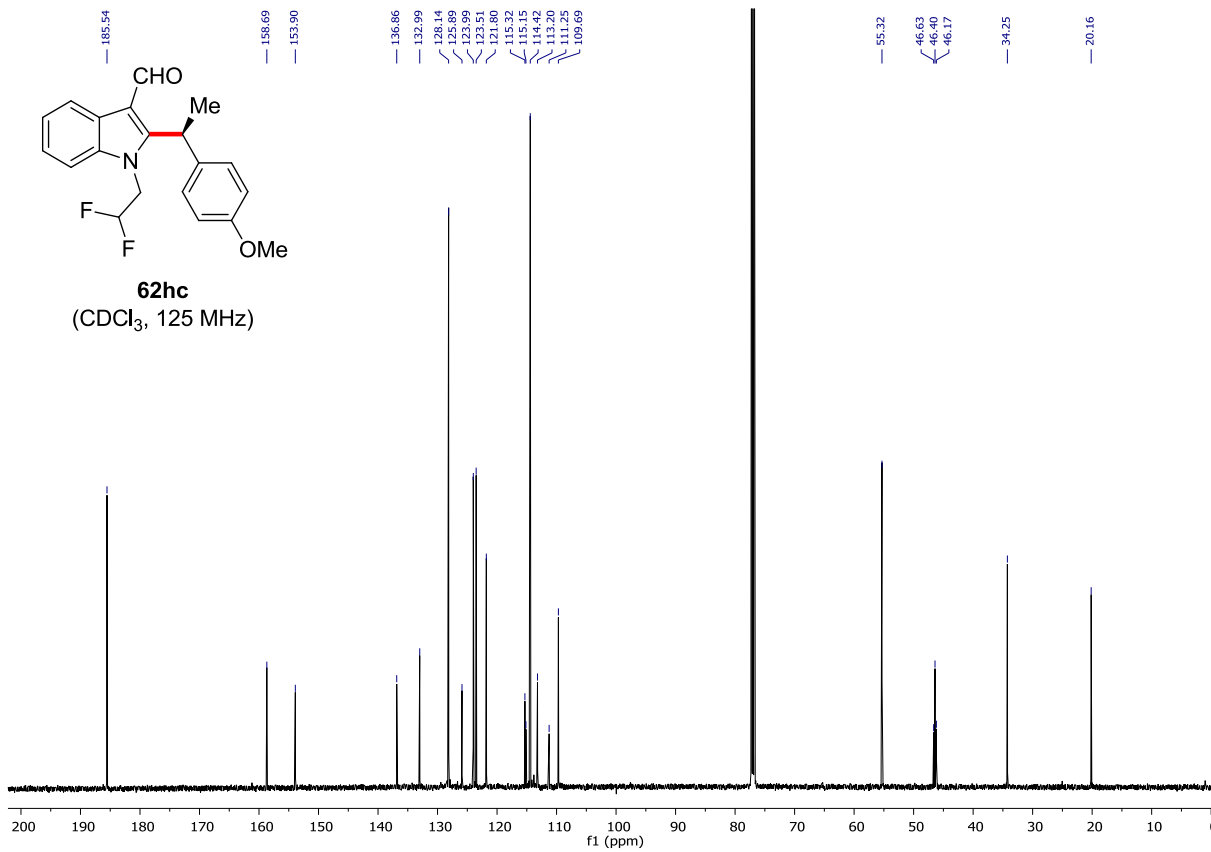
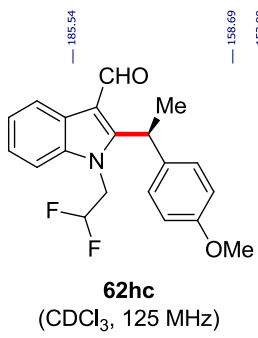
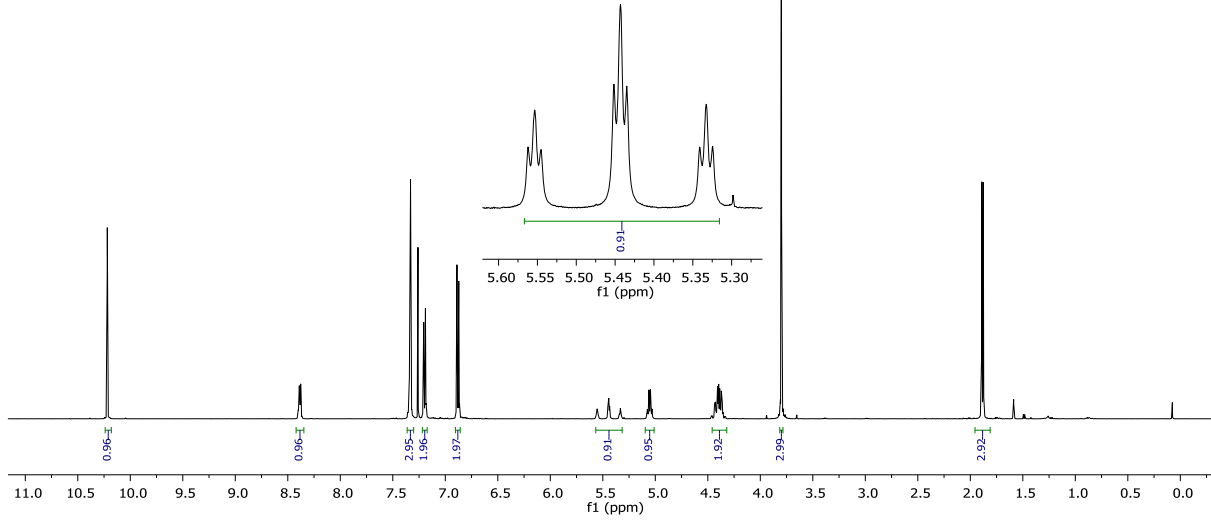
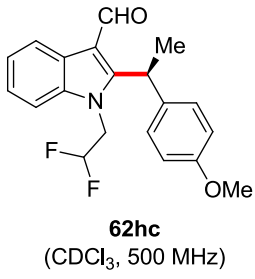
(using pre-ligand **180**)

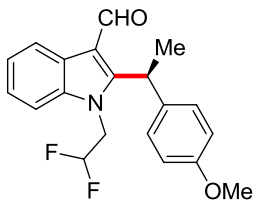
| Peak # | RetTime [min] | Type | Width [min] | Area [mAU*s] | Height [mAU] | Area % |
|--------|---------------|------|-------------|--------------|--------------|---------|
| 1 | 9.597 | MF | 0.1894 | 3060.40356 | 269.36618 | 85.5746 |
| 2 | 10.377 | MF | 0.2272 | 515.89612 | 37.84306 | 14.4254 |



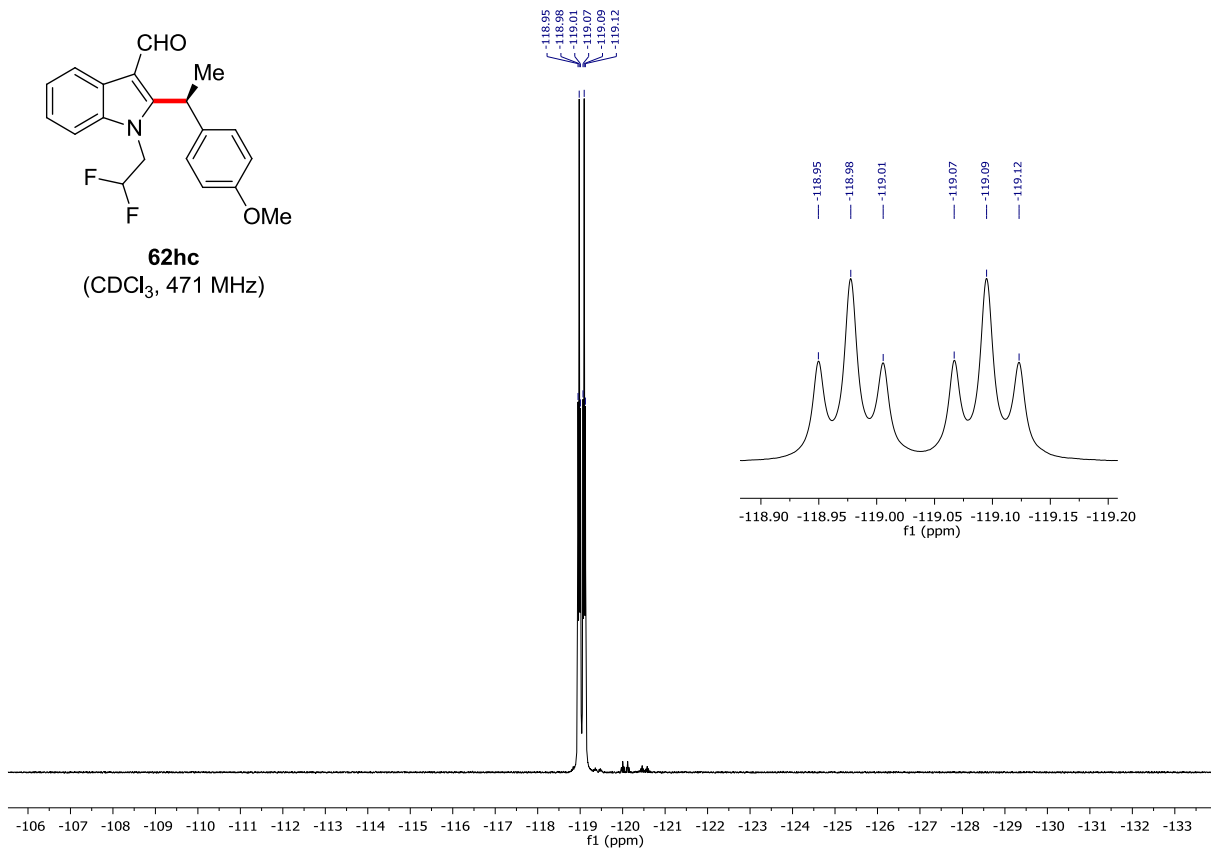
(using pre-ligand **177**)

| Peak # | RetTime [min] | Type | Width [min] | Area [mAU*s] | Height [mAU] | Area % |
|--------|---------------|------|-------------|--------------|--------------|---------|
| 1 | 9.914 | FM | 0.2106 | 5505.33203 | 435.65057 | 86.6259 |
| 2 | 10.819 | FM | 0.2443 | 849.96313 | 57.99336 | 13.3741 |

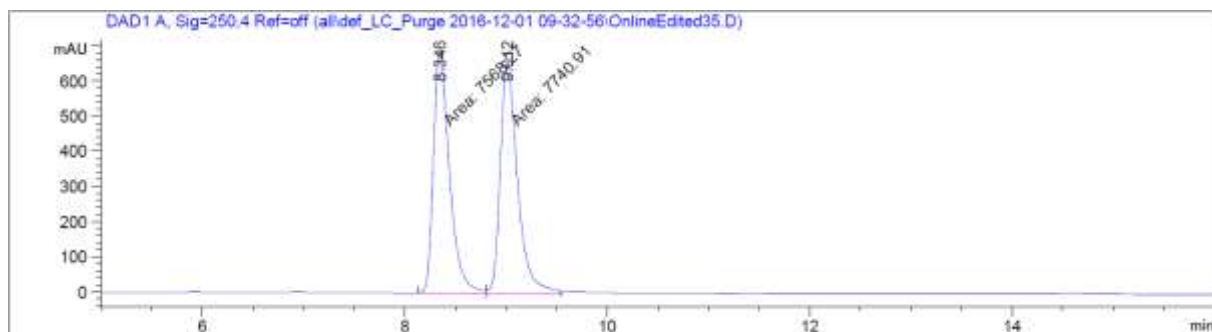




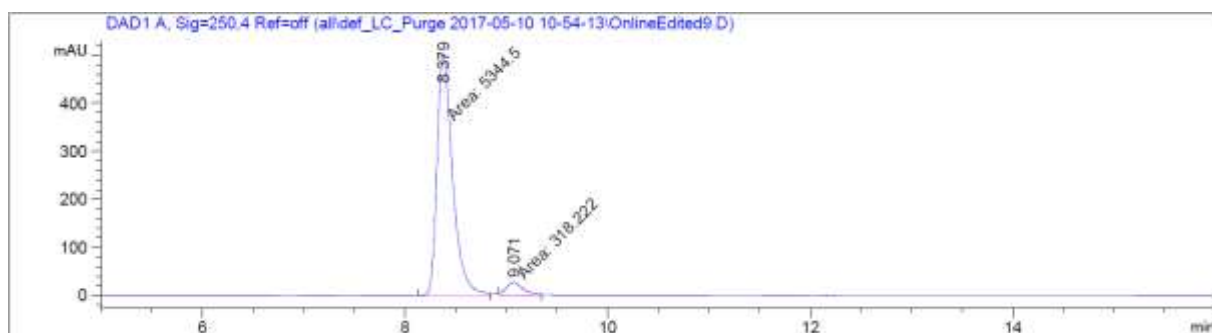
62hc
(CDCl₃, 471 MHz)



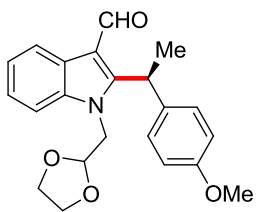
Chiral HPLC of **62hc**:



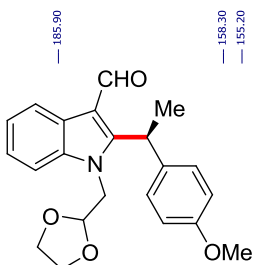
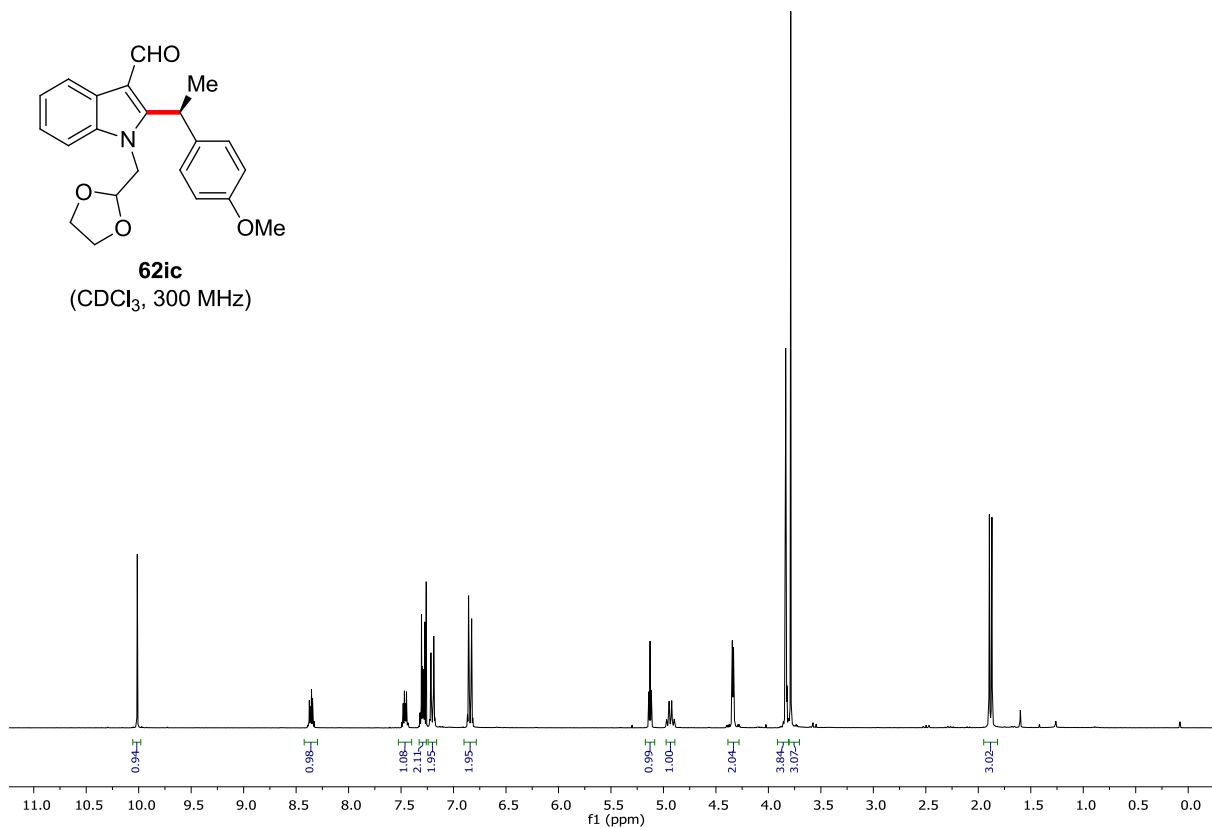
| Peak # | RetTime [min] | Type | Width [min] | Area [mAU*s] | Height [mAU] | Area % |
|--------|---------------|------|-------------|--------------|--------------|---------|
| 1 | 8.346 | FM | 0.1841 | 7568.26904 | 685.08722 | 49.4362 |
| 2 | 9.012 | MF | 0.1970 | 7740.90967 | 654.90601 | 50.5638 |



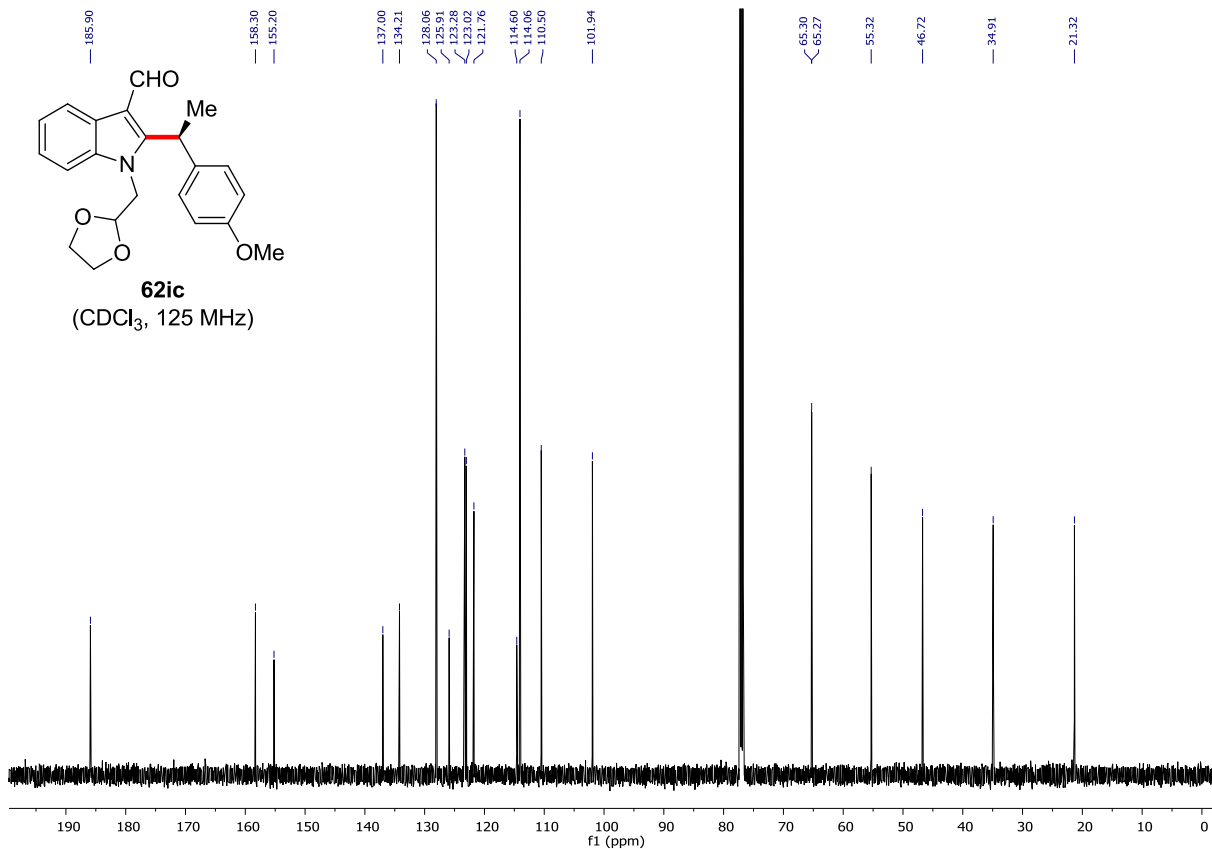
| Peak # | RetTime [min] | Type | Width [min] | Area [mAU*s] | Height [mAU] | Area % |
|--------|---------------|------|-------------|--------------|--------------|---------|
| 1 | 8.379 | MF | 0.1767 | 5344.49512 | 504.21869 | 94.3804 |
| 2 | 9.071 | MF | 0.1970 | 318.22235 | 26.91614 | 5.6196 |



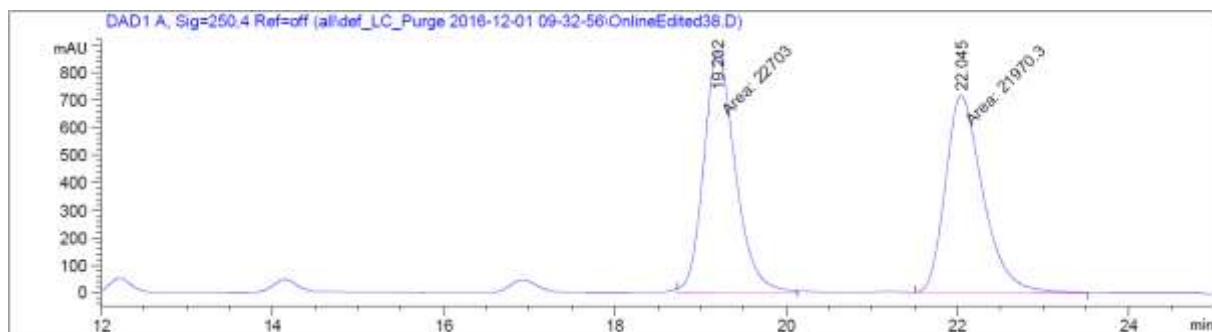
62ic
(CDCl₃, 300 MHz)



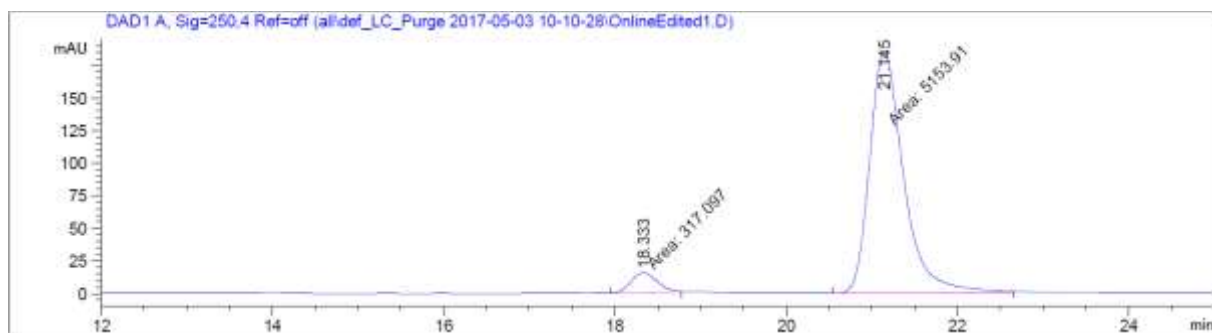
62ic
(CDCl₃, 125 MHz)



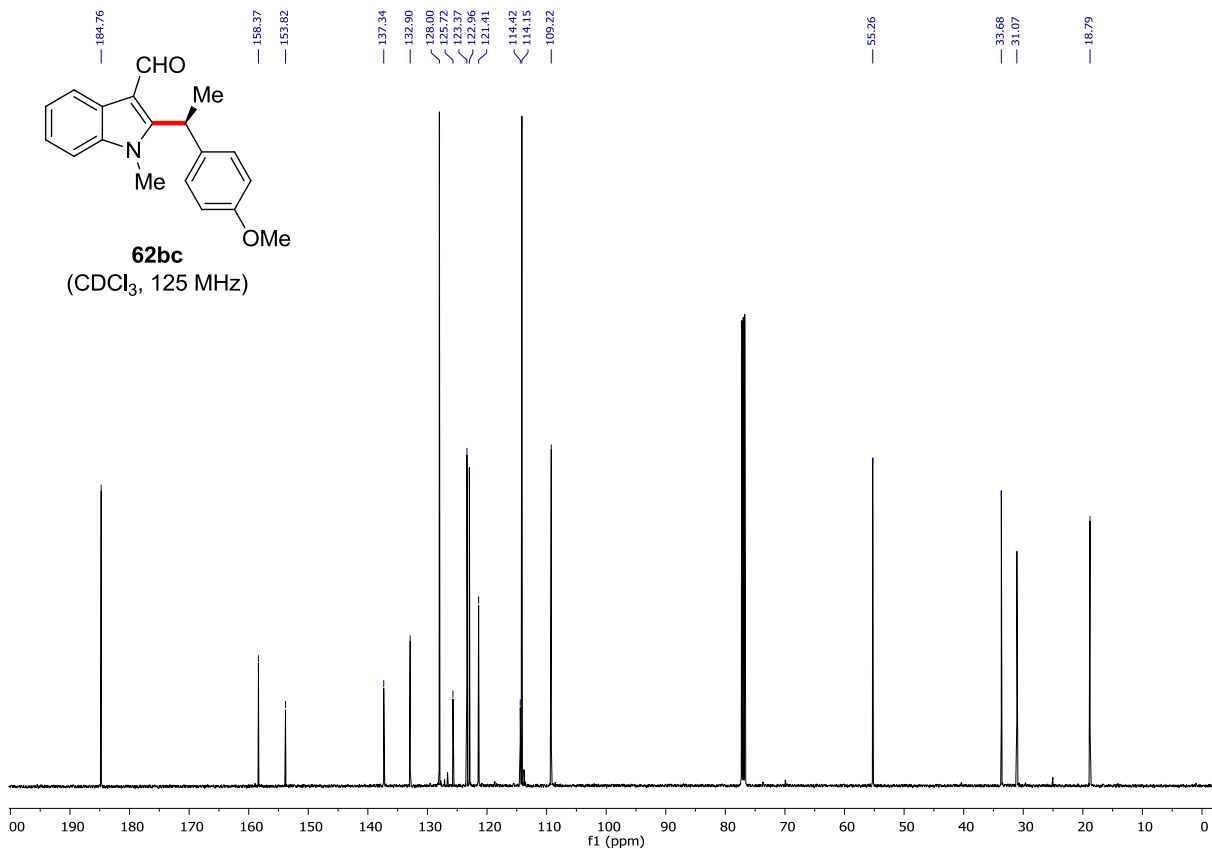
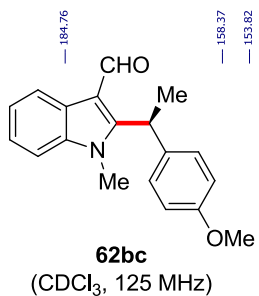
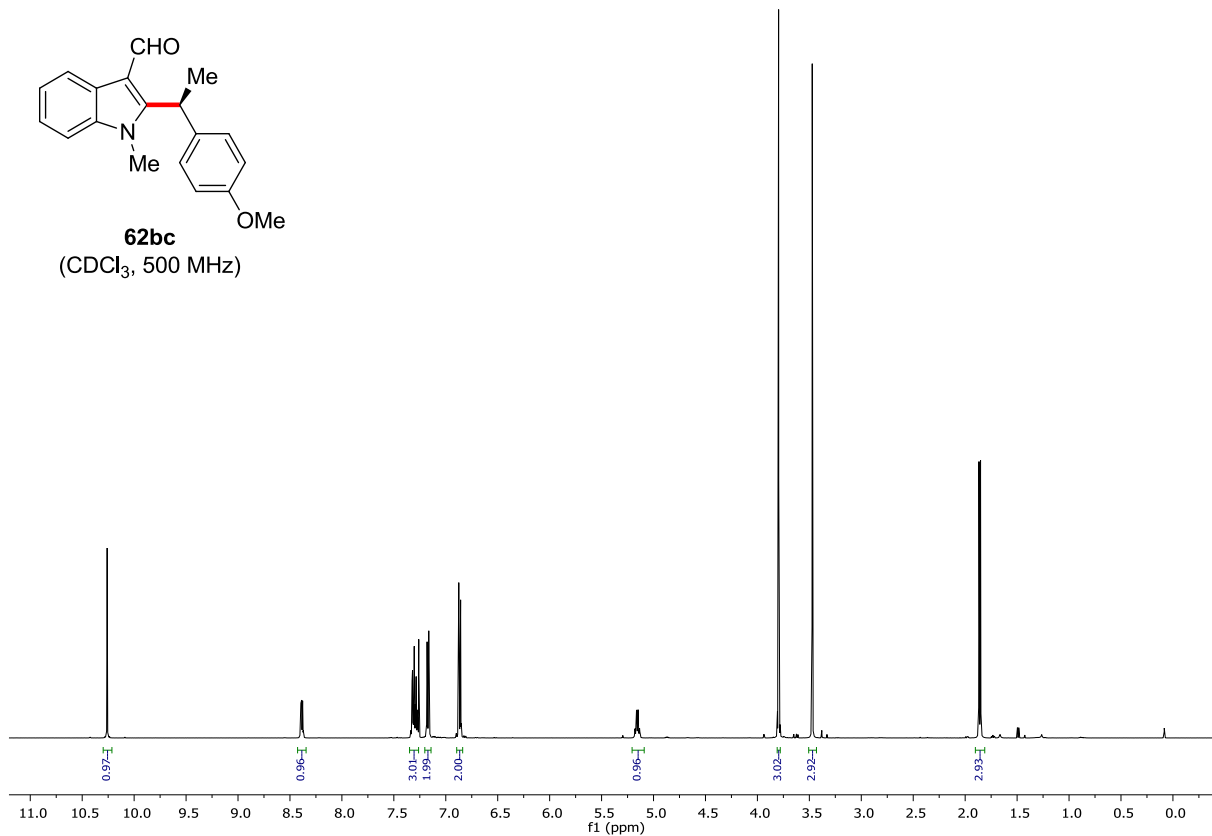
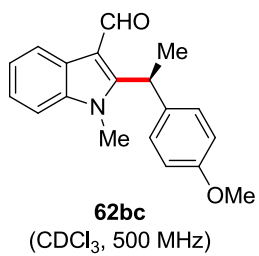
Chiral HPLC of **62ic**:



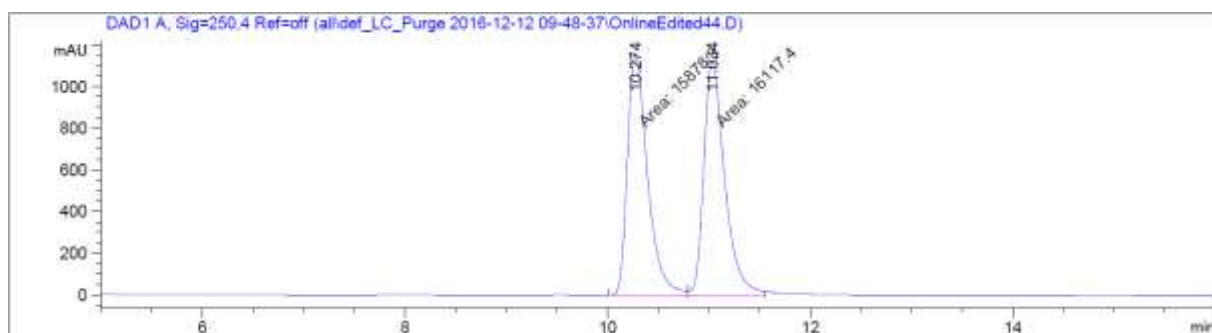
| Peak # | RetTime [min] | Type | Width [min] | Area [mAU*s] | Height [mAU] | Area % |
|--------|---------------|------|-------------|--------------|--------------|---------|
| 1 | 19.202 | FM | 0.4310 | 2.27030e4 | 877.93793 | 50.8200 |
| 2 | 22.045 | MF | 0.5104 | 2.19703e4 | 717.47906 | 49.1800 |



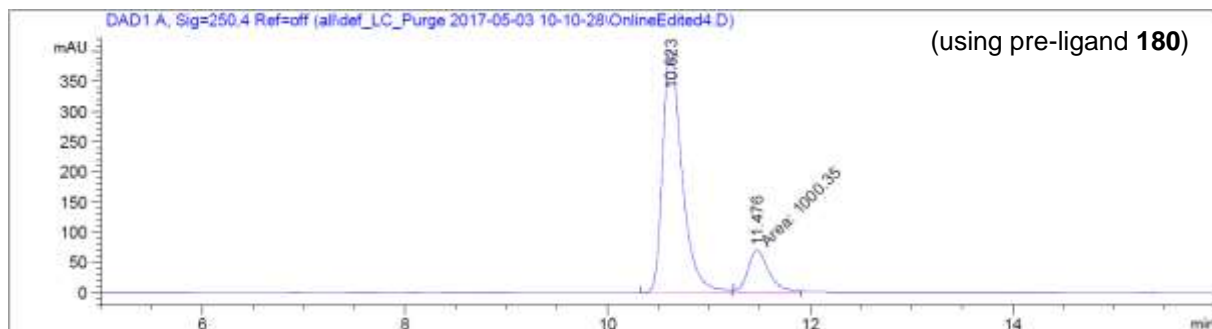
| Peak # | RetTime [min] | Type | Width [min] | Area [mAU*s] | Height [mAU] | Area % |
|--------|---------------|------|-------------|--------------|--------------|---------|
| 1 | 18.333 | MF | 0.3509 | 317.09686 | 15.05949 | 5.7959 |
| 2 | 21.145 | MF | 0.4633 | 5153.91260 | 185.39102 | 94.2041 |



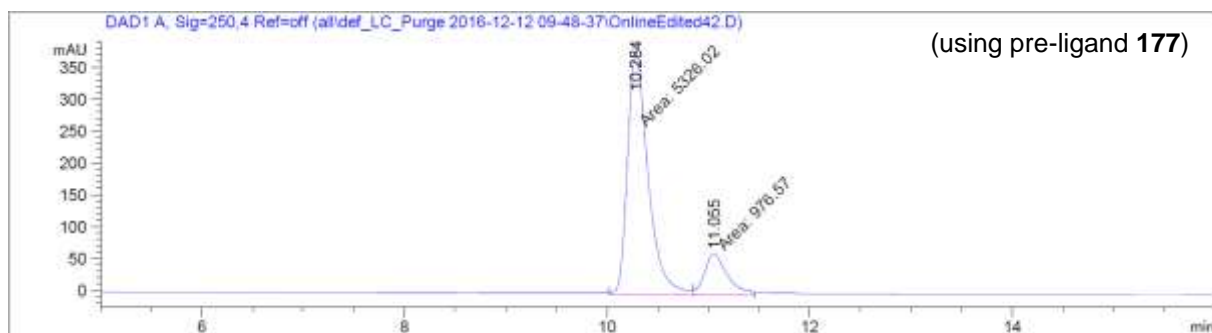
Chiral HPLC of **62bc**:



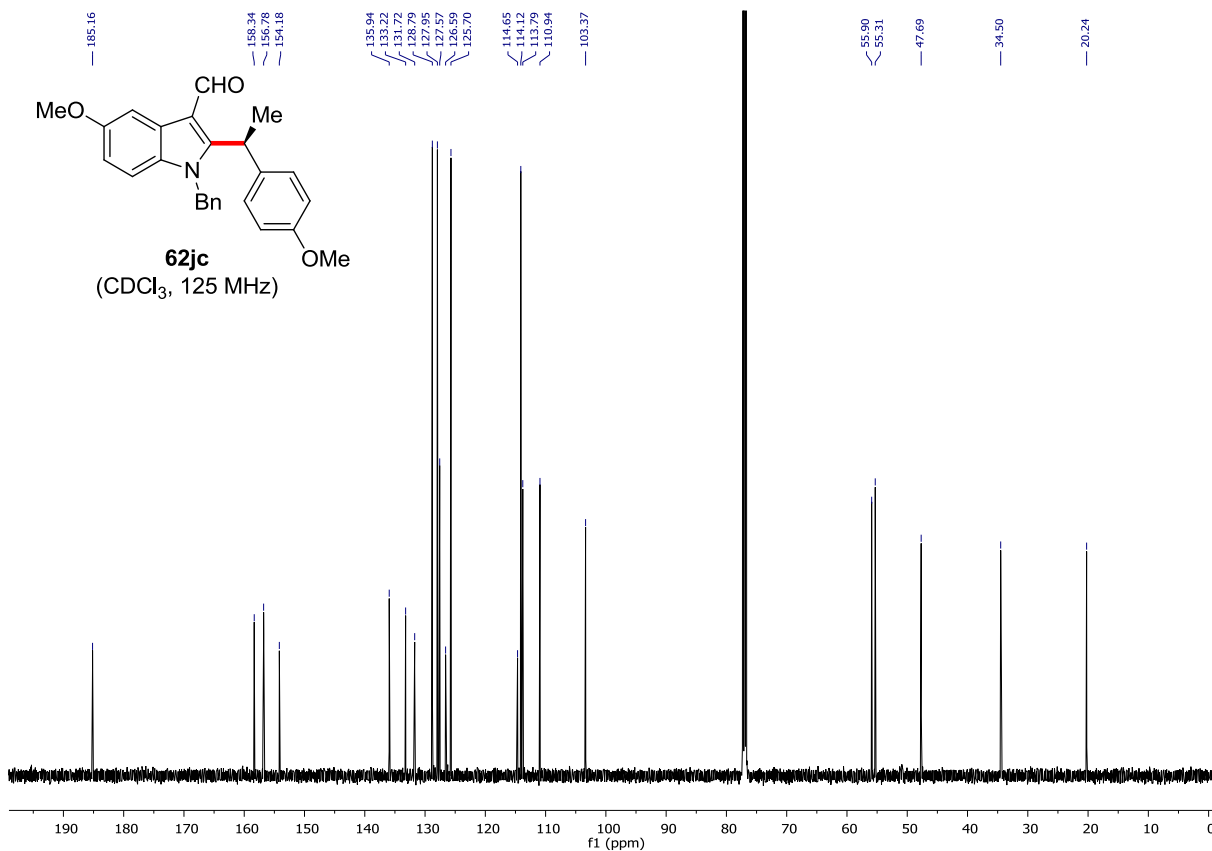
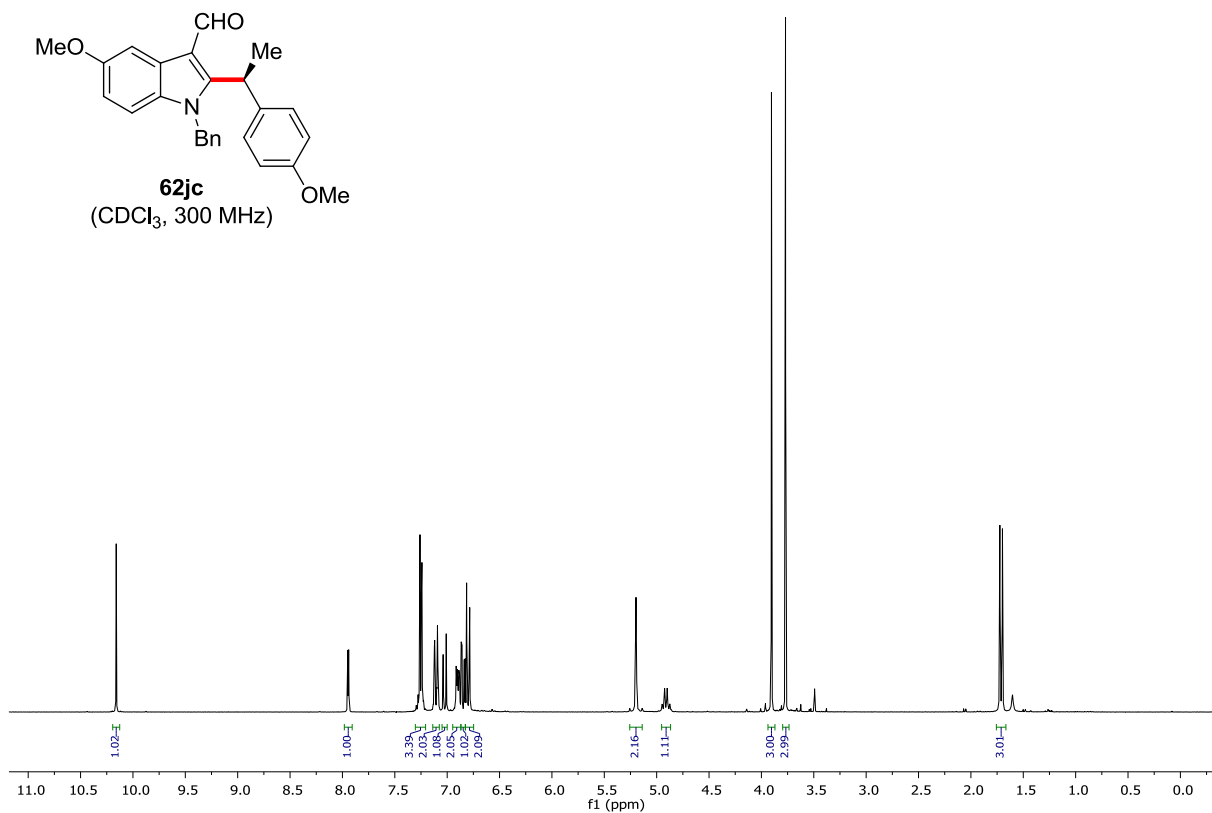
| Peak # | RetTime [min] | Type | Width [min] | Area [mAU*s] | Height [mAU] | Area % |
|--------|---------------|------|-------------|--------------|--------------|---------|
| 1 | 10.274 | FM | 0.2286 | 1.58783e4 | 1157.68665 | 49.6263 |
| 2 | 11.034 | MF | 0.2401 | 1.61174e4 | 1118.64575 | 50.3737 |



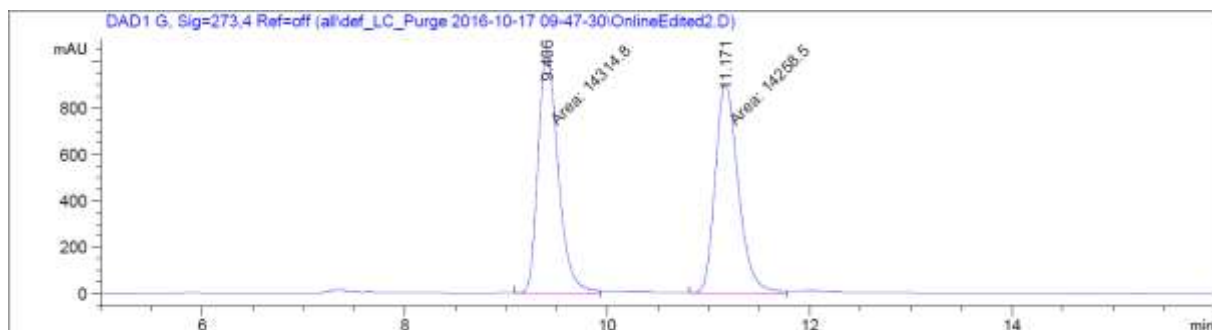
| Peak # | RetTime [min] | Type | Width [min] | Area [mAU*s] | Height [mAU] | Area % |
|--------|---------------|------|-------------|--------------|--------------|---------|
| 1 | 10.623 | BV | 0.1999 | 5330.50635 | 401.44138 | 84.1988 |
| 2 | 11.476 | MF | 0.2405 | 1000.35297 | 69.33299 | 15.8012 |



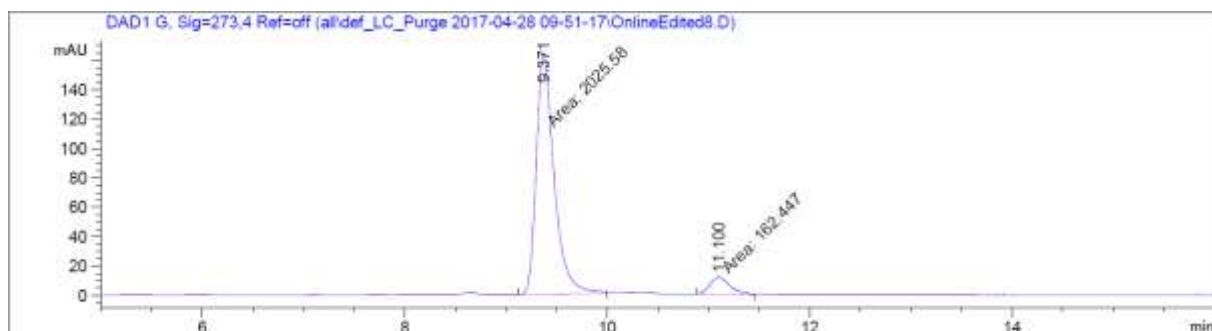
| Peak # | RetTime [min] | Type | Width [min] | Area [mAU*s] | Height [mAU] | Area % |
|--------|---------------|------|-------------|--------------|--------------|---------|
| 1 | 10.284 | MM | 0.2340 | 5326.01611 | 379.29617 | 84.5052 |
| 2 | 11.055 | MM | 0.2579 | 976.57019 | 63.11302 | 15.4948 |



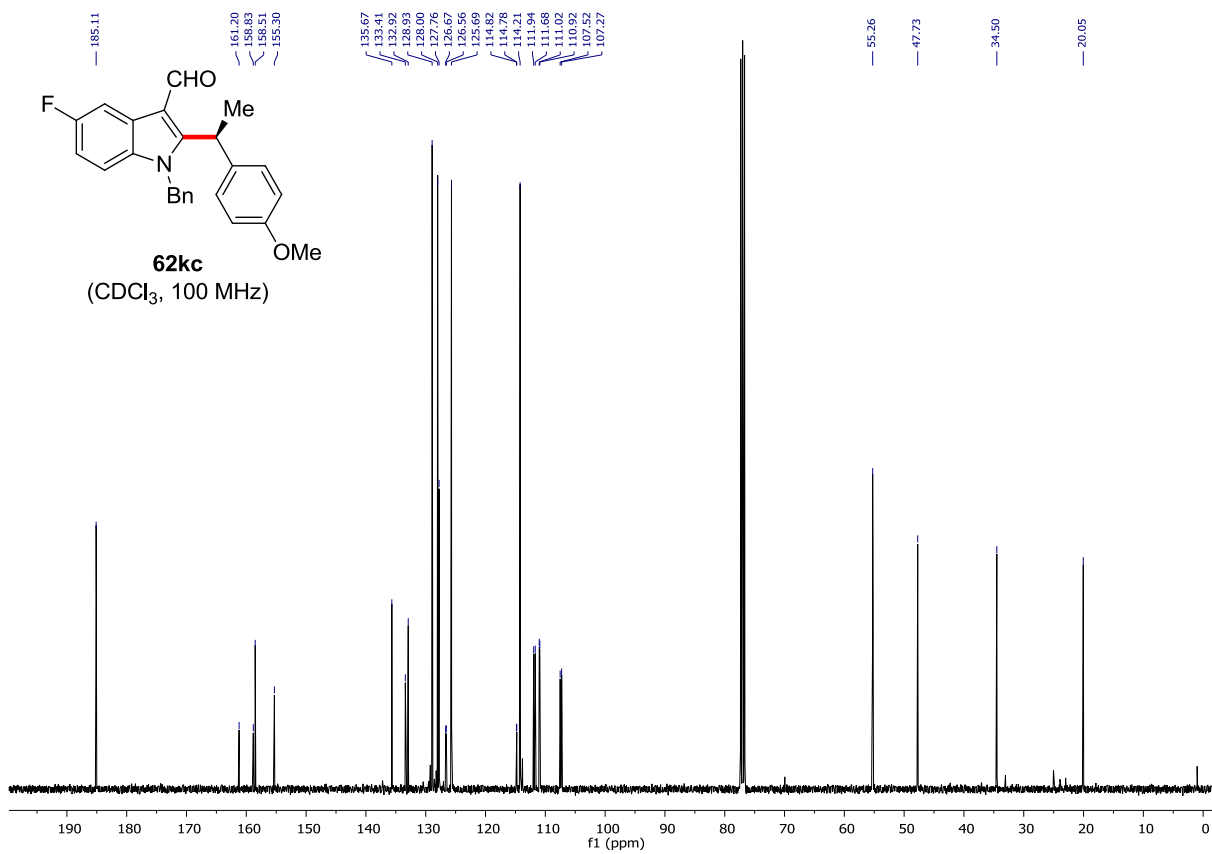
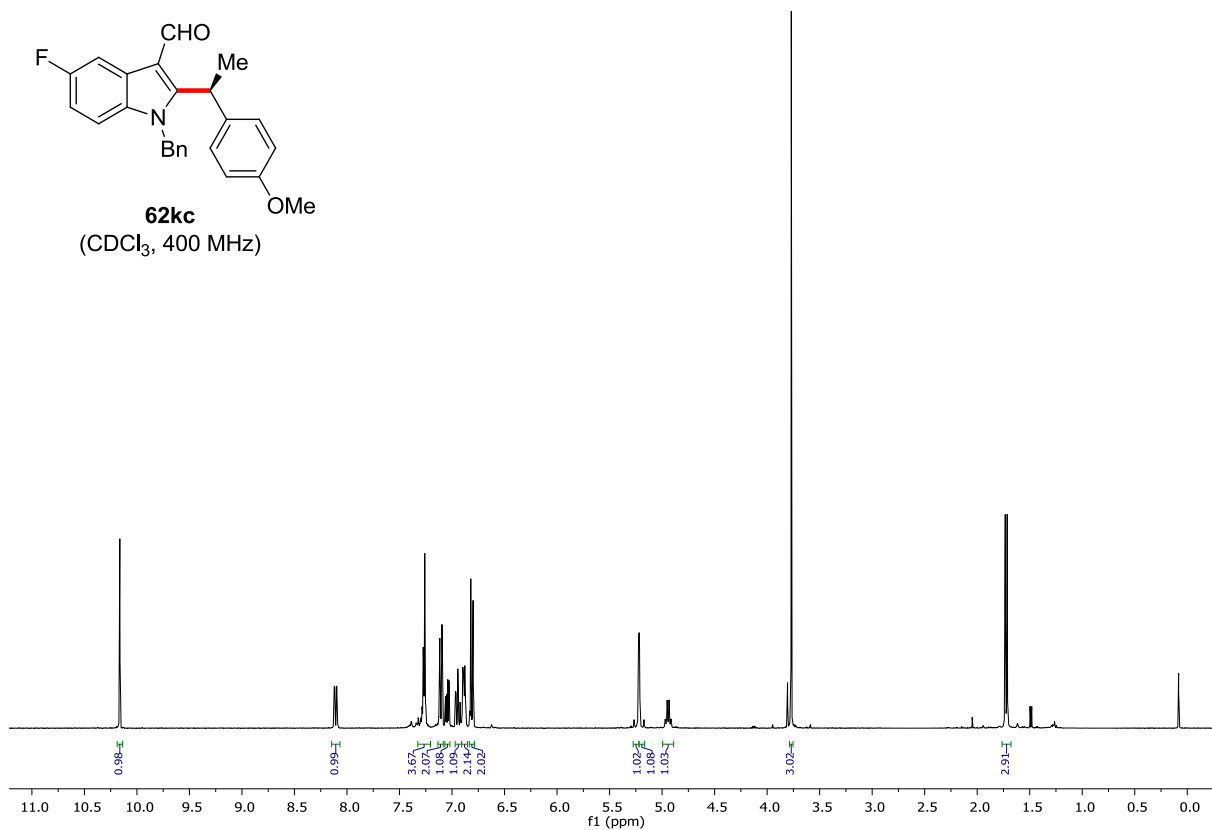
Chiral HPLC of **62jc**:

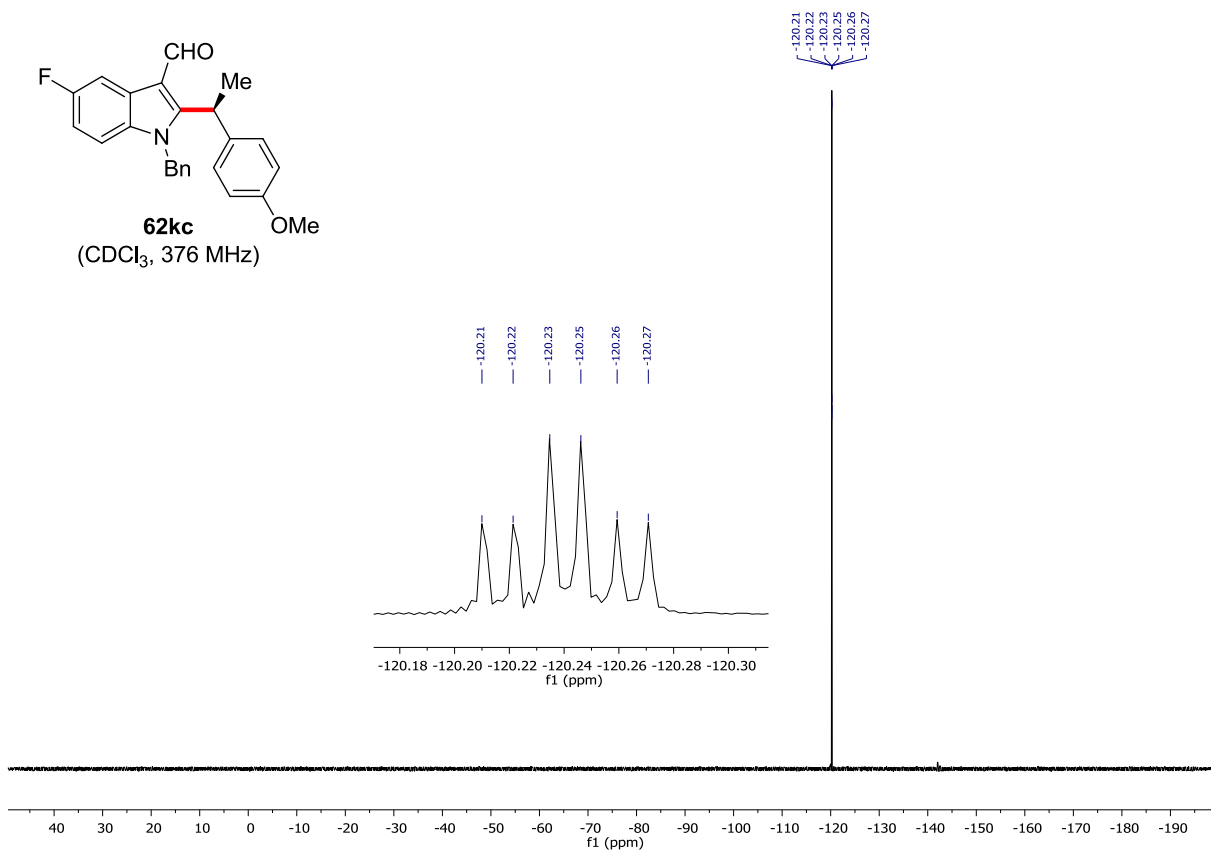


| Peak # | RetTime [min] | Type | Width [min] | Area [mAU*s] | Height [mAU] | Area % |
|--------|---------------|------|-------------|--------------|--------------|---------|
| 1 | 9.406 | MF | 0.2290 | 1.43148e4 | 1041.96765 | 50.0986 |
| 2 | 11.171 | MF | 0.2643 | 1.42585e4 | 899.23065 | 49.9014 |

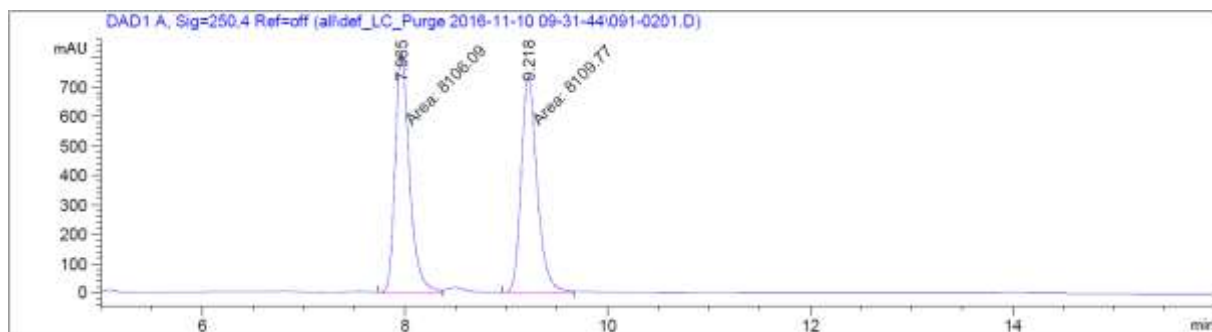


| Peak # | RetTime [min] | Type | Width [min] | Area [mAU*s] | Height [mAU] | Area % |
|--------|---------------|------|-------------|--------------|--------------|---------|
| 1 | 9.371 | MF | 0.2053 | 2025.58179 | 164.41907 | 92.5757 |
| 2 | 11.100 | MF | 0.2303 | 162.44678 | 11.75738 | 7.4243 |

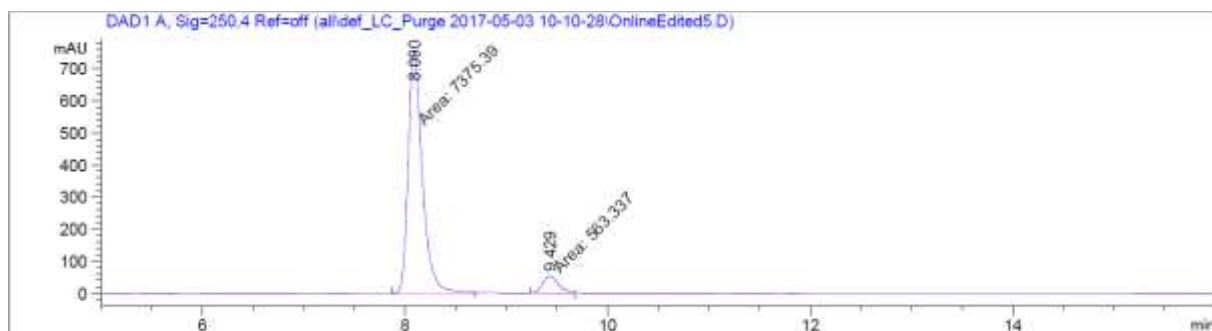




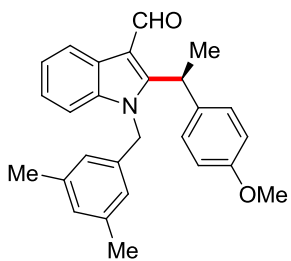
Chiral HPLC of **62kc**:



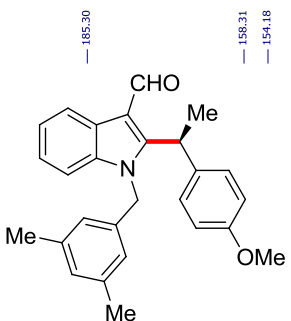
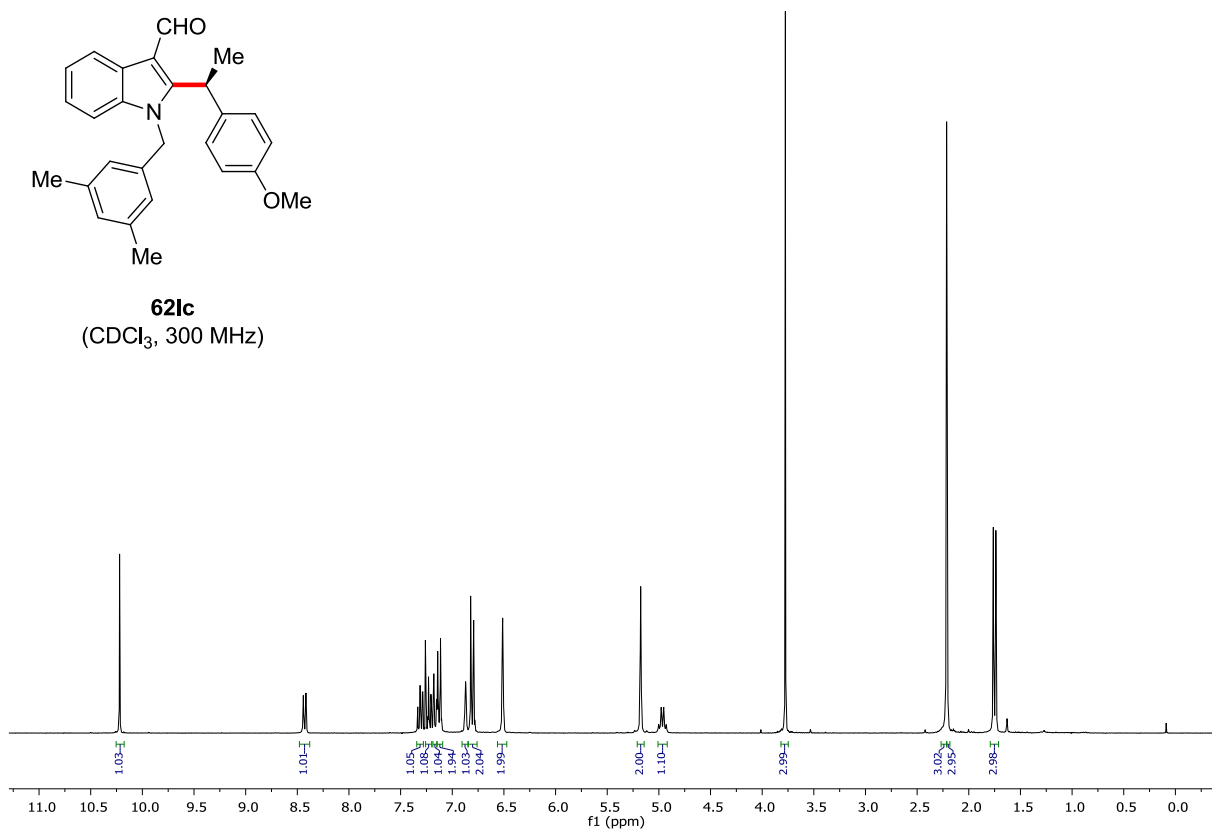
| Peak # | RetTime [min] | Type | Width [min] | Area [mAU*s] | Height [mAU] | Area % |
|--------|---------------|------|-------------|--------------|--------------|---------|
| 1 | 7.965 | MF | 0.1648 | 8106.08838 | 819.71826 | 49.9887 |
| 2 | 9.218 | MF | 0.1843 | 8109.76904 | 733.40509 | 50.0113 |



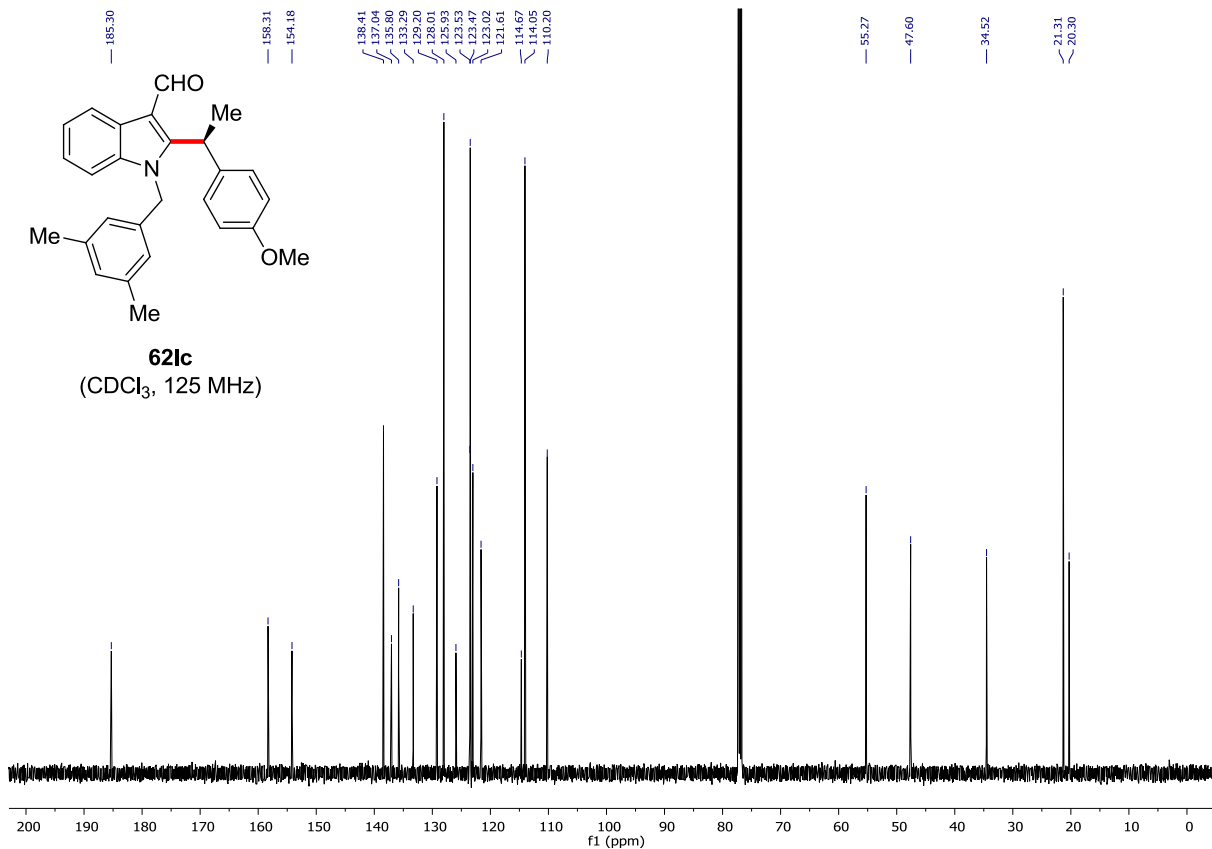
| Peak # | RetTime [min] | Type | Width [min] | Area [mAU*s] | Height [mAU] | Area % |
|--------|---------------|------|-------------|--------------|--------------|---------|
| 1 | 8.090 | MF | 0.1632 | 7375.38525 | 753.17700 | 92.9039 |
| 2 | 9.429 | MF | 0.1793 | 563.33740 | 52.35432 | 7.0961 |



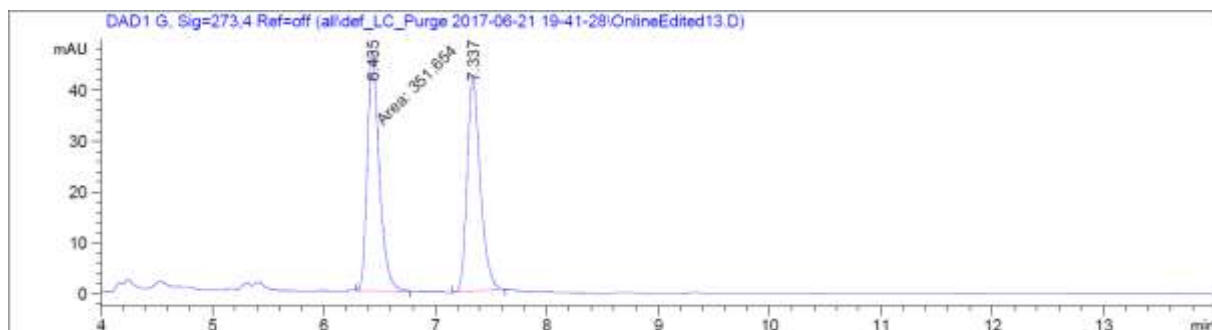
62Ic
(CDCl₃, 300 MHz)



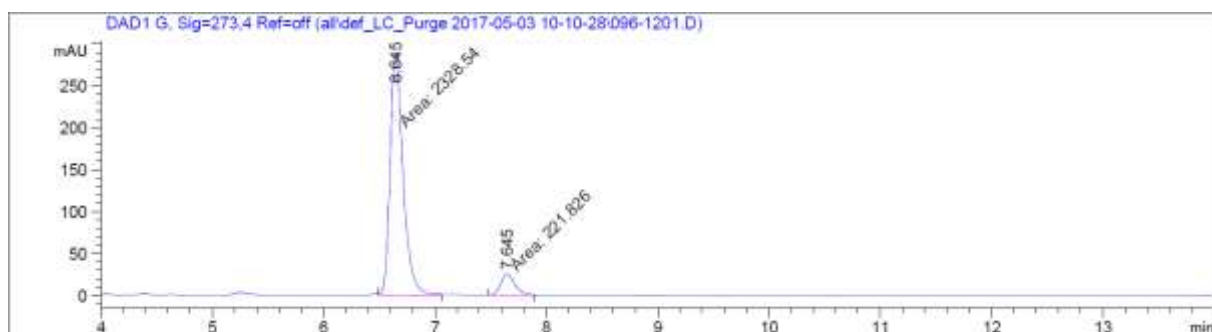
62Ic
(CDCl₃, 125 MHz)



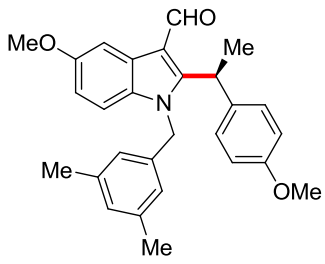
Chiral HPLC of **621c**:



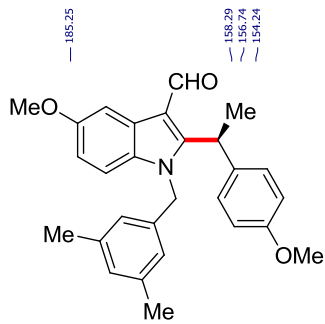
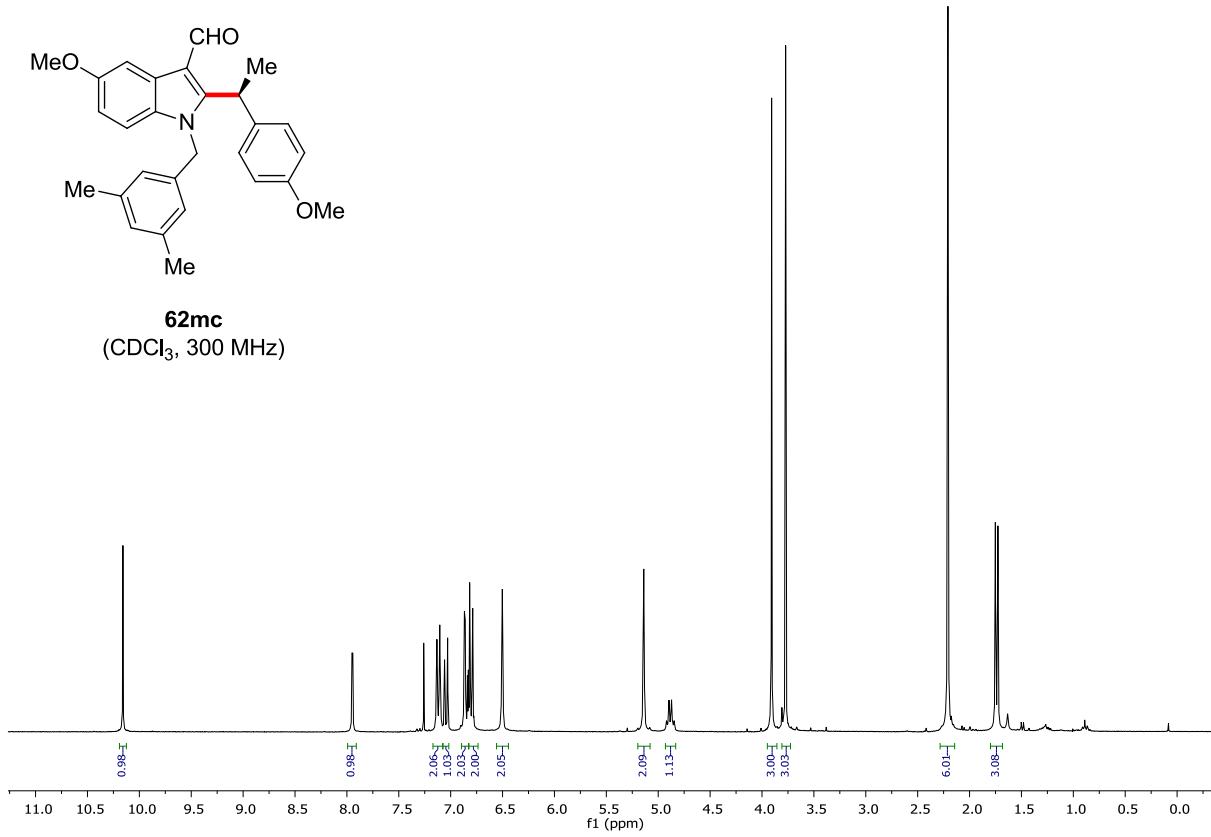
| Peak # | RetTime [min] | Type | Width [min] | Area [mAU*s] | Height [mAU] | Area % |
|--------|---------------|------|-------------|--------------|--------------|---------|
| 1 | 6.435 | MF | 0.1244 | 351.65396 | 47.11286 | 50.4522 |
| 2 | 7.337 | BB | 0.1248 | 345.35004 | 42.05161 | 49.5478 |



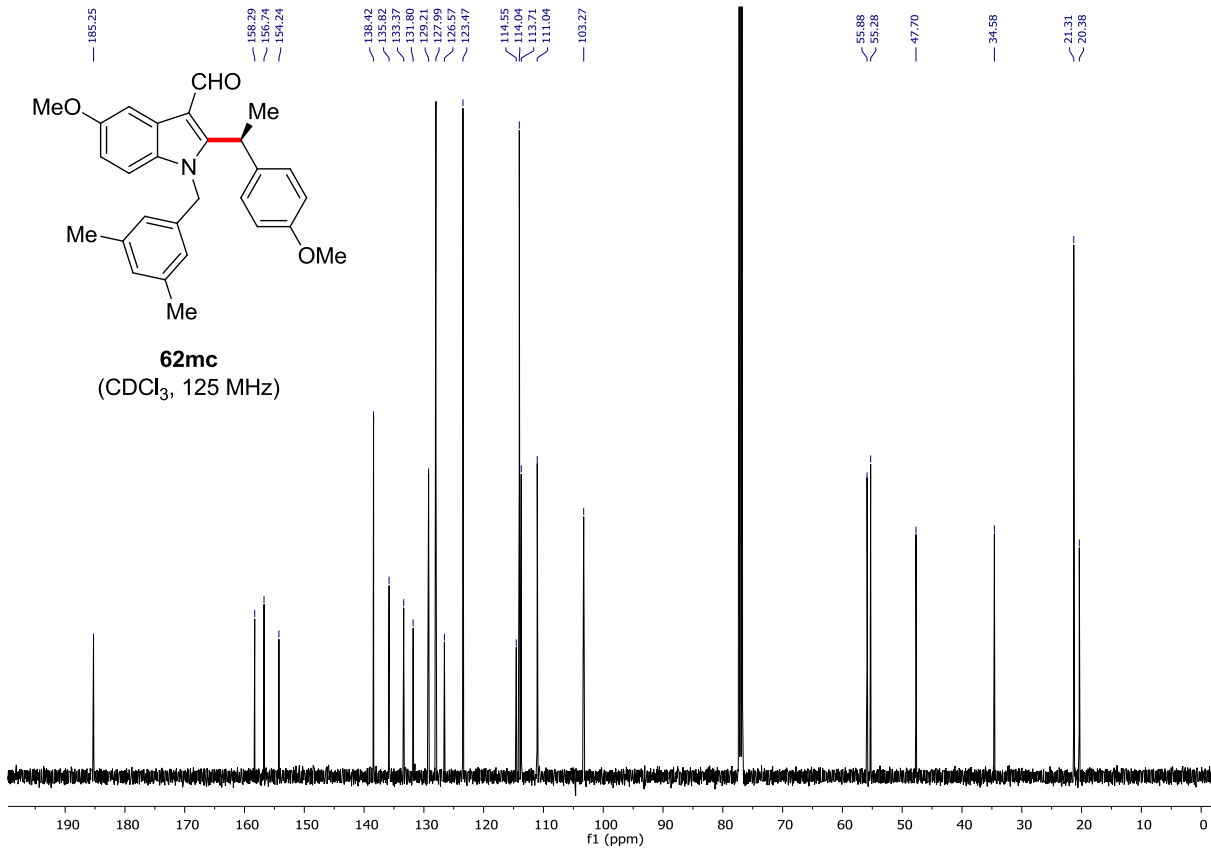
| Peak # | RetTime [min] | Type | Width [min] | Area [mAU*s] | Height [mAU] | Area % |
|--------|---------------|------|-------------|--------------|--------------|---------|
| 1 | 6.645 | FM | 0.1347 | 2328.54443 | 288.21570 | 91.3022 |
| 2 | 7.645 | FM | 0.1485 | 221.82639 | 24.88868 | 8.6978 |



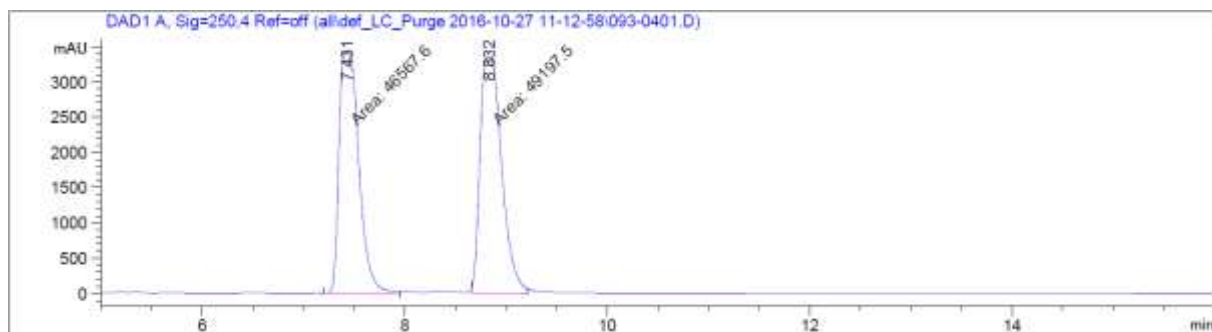
62mc
(CDCl₃, 300 MHz)



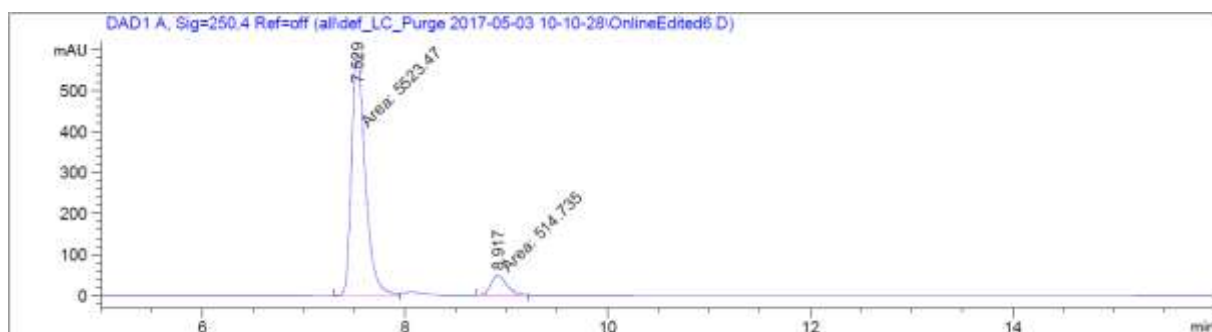
62mc
(CDCl₃, 125 MHz)



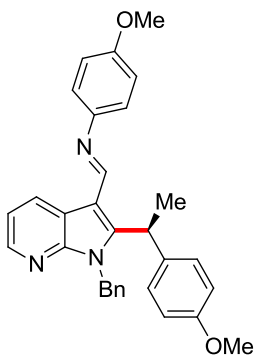
Chiral HPLC of **62mc**:



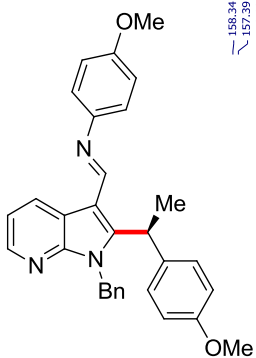
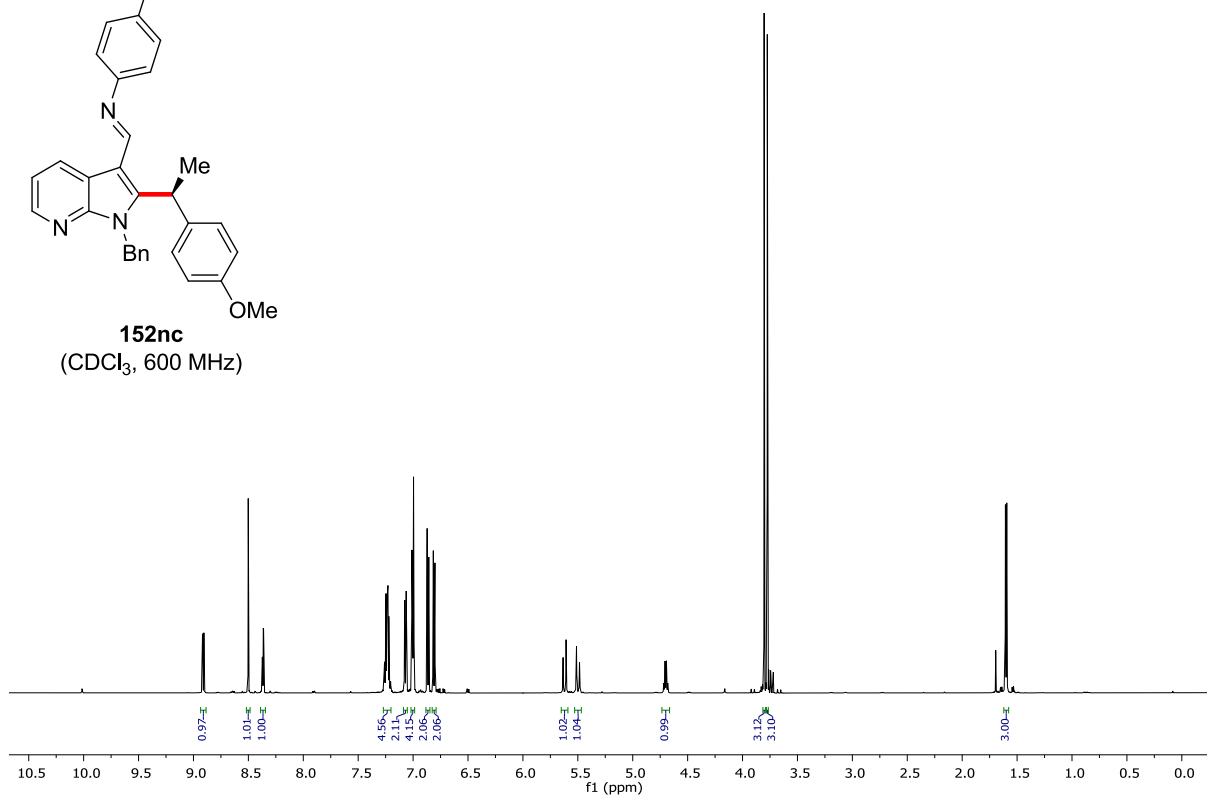
| Peak # | RetTime [min] | Type | Width [min] | Area [mAU*s] | Height [mAU] | Area % |
|--------|---------------|------|-------------|--------------|--------------|---------|
| 1 | 7.431 | MF | 0.2269 | 4.65676e4 | 3421.28369 | 48.6269 |
| 2 | 8.832 | MF | 0.2449 | 4.91975e4 | 3347.54712 | 51.3731 |



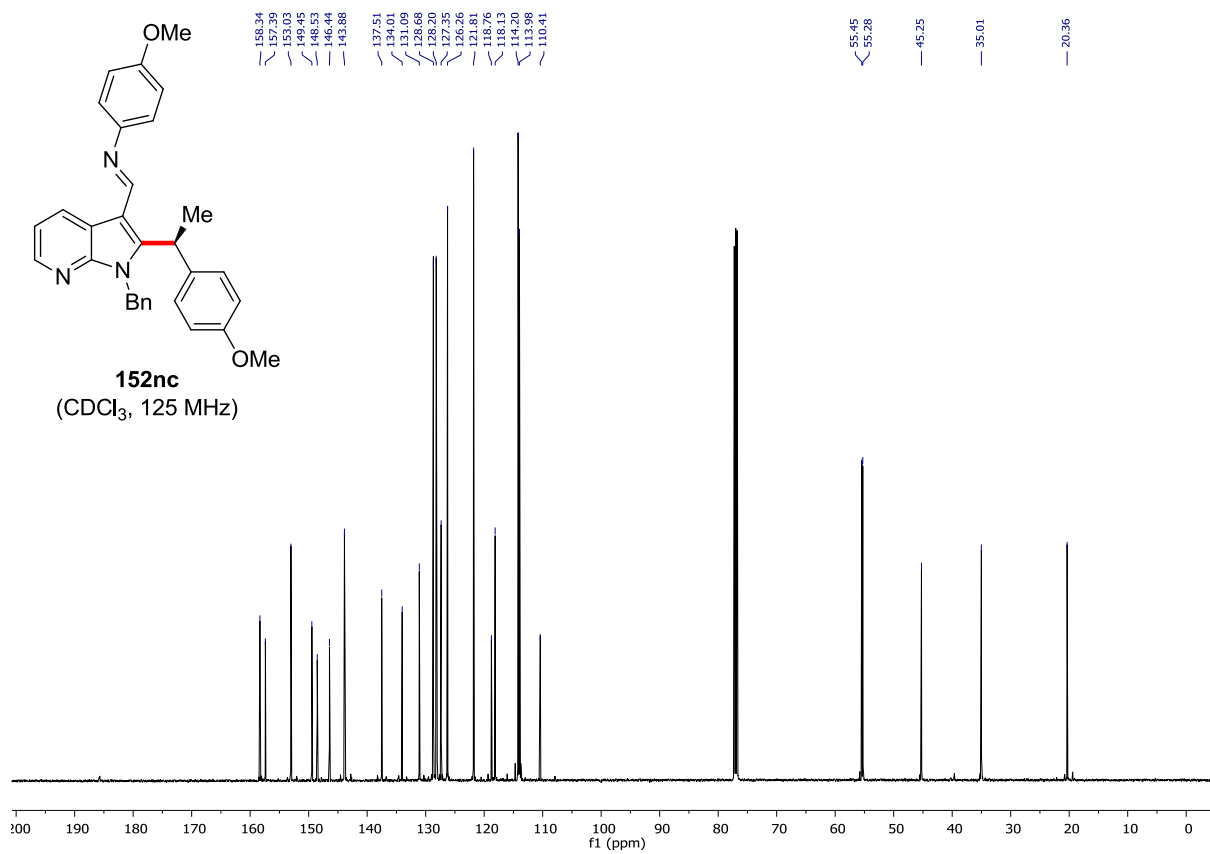
| Peak # | RetTime [min] | Type | Width [min] | Area [mAU*s] | Height [mAU] | Area % |
|--------|---------------|------|-------------|--------------|--------------|---------|
| 1 | 7.529 | MF | 0.1561 | 5523.46729 | 589.69330 | 91.4754 |
| 2 | 8.917 | MF | 0.1773 | 514.73529 | 48.38813 | 8.5246 |



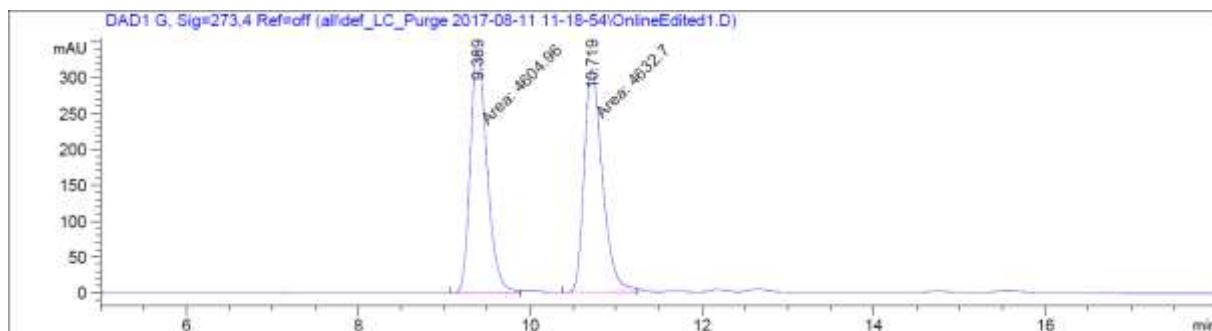
152nc
(CDCl₃, 600 MHz)



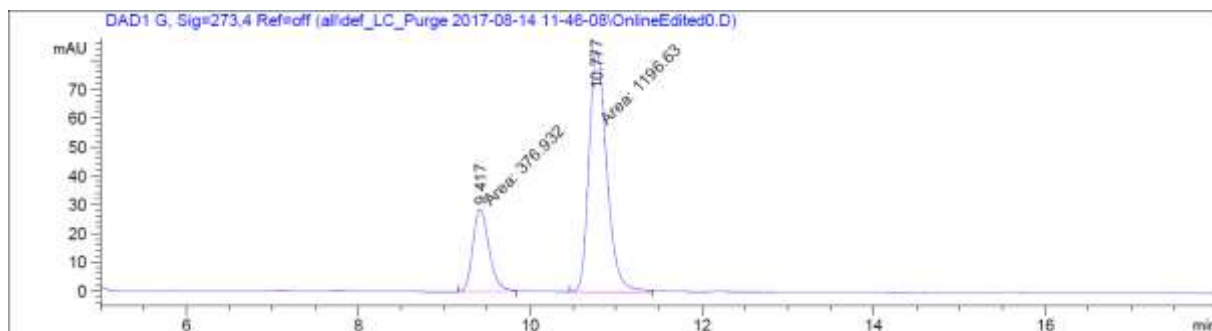
152nc
(CDCl₃, 125 MHz)



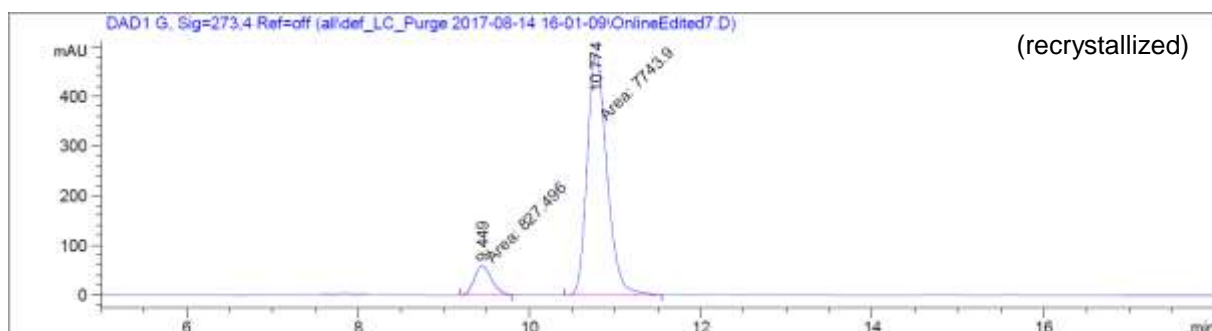
Chiral HPLC of 152nc:



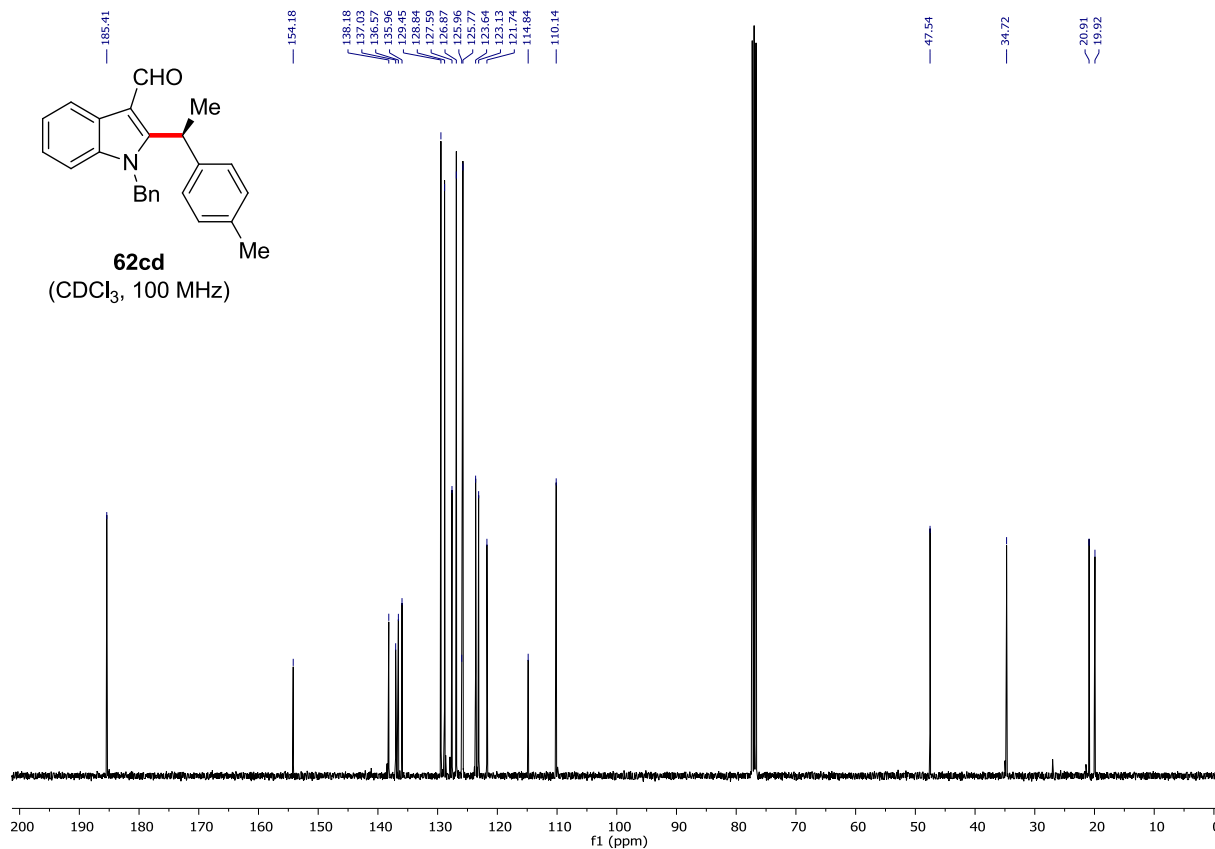
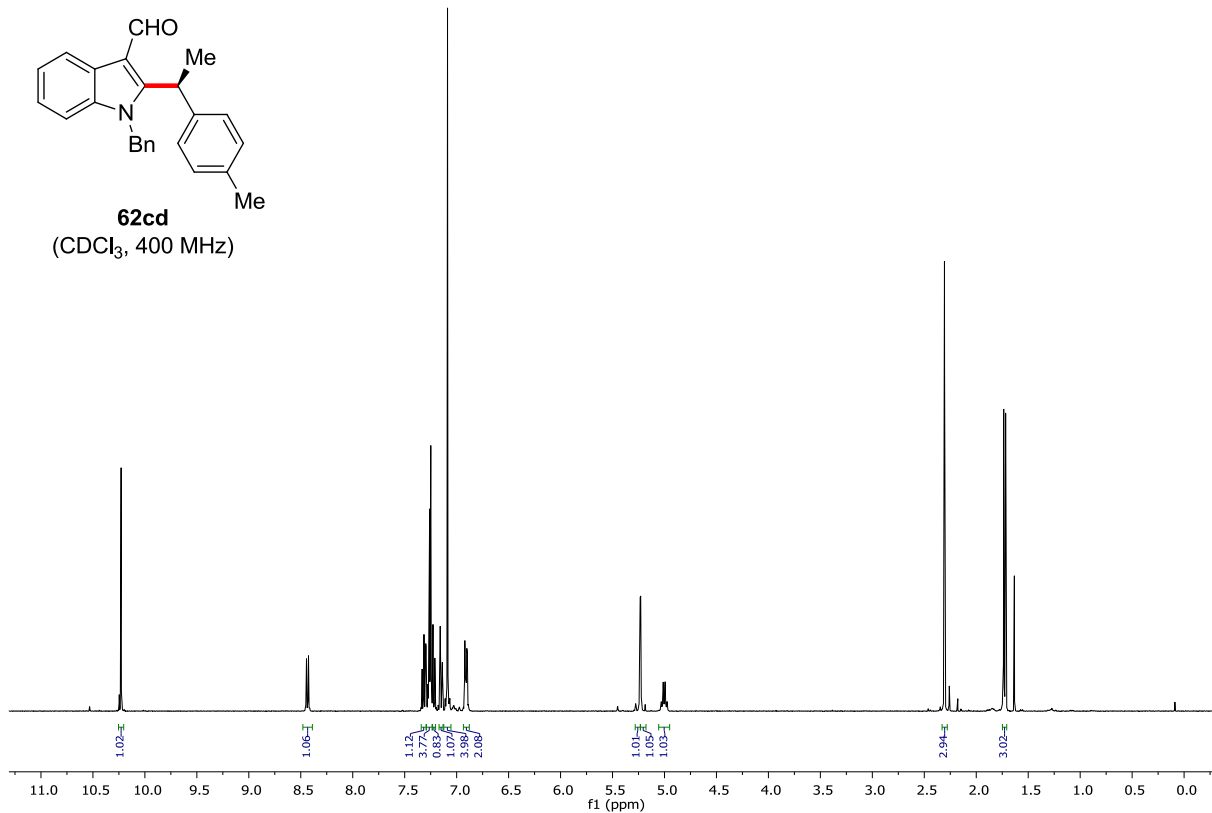
| Peak # | RetTime [min] | Type | Width [min] | Area [mAU*s] | Height [mAU] | Area % |
|--------|---------------|------|-------------|--------------|--------------|---------|
| 1 | 9.389 | MF | 0.2273 | 4604.95752 | 337.67624 | 49.8499 |
| 2 | 10.719 | MF | 0.2477 | 4632.69775 | 311.73004 | 50.1501 |



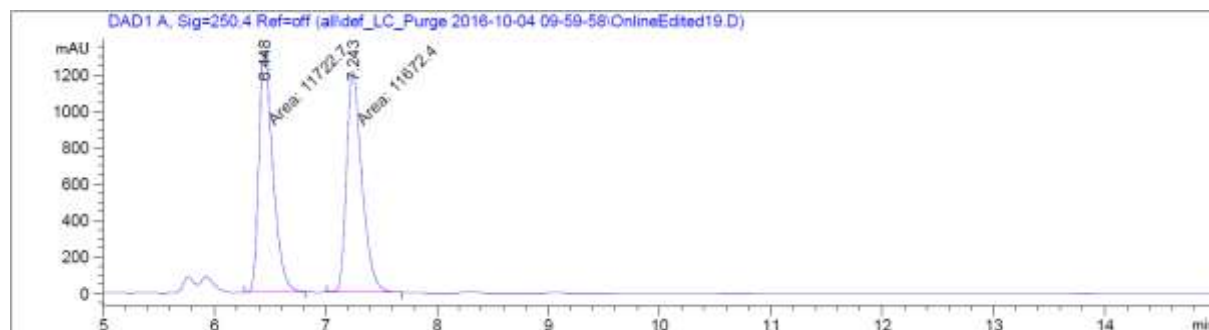
| Peak # | RetTime [min] | Type | Width [min] | Area [mAU*s] | Height [mAU] | Area % |
|--------|---------------|------|-------------|--------------|--------------|---------|
| 1 | 9.417 | FM | 0.2200 | 376.93225 | 28.56135 | 23.9540 |
| 2 | 10.777 | MF | 0.2384 | 1196.63416 | 83.66377 | 76.0460 |



| Peak # | RetTime [min] | Type | Width [min] | Area [mAU*s] | Height [mAU] | Area % |
|--------|---------------|------|-------------|--------------|--------------|---------|
| 1 | 9.449 | FM | 0.2332 | 827.49622 | 59.12883 | 9.6542 |
| 2 | 10.774 | MF | 0.2651 | 7743.89893 | 486.90933 | 90.3458 |



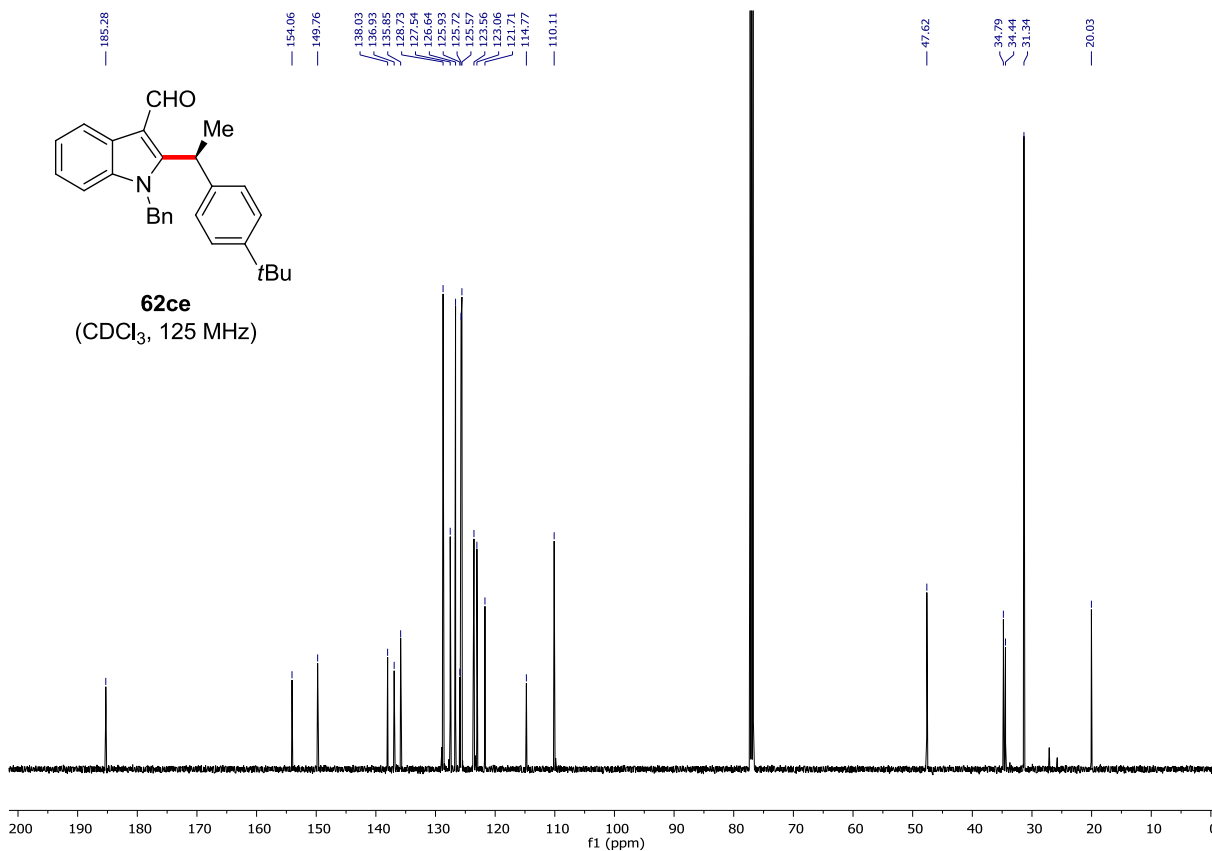
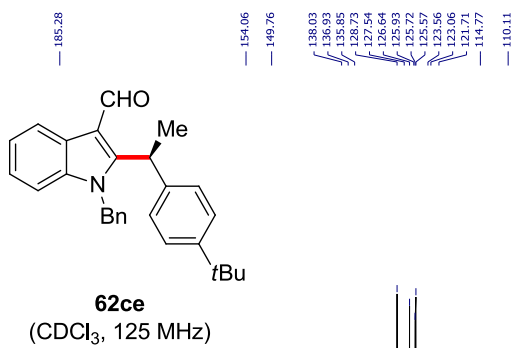
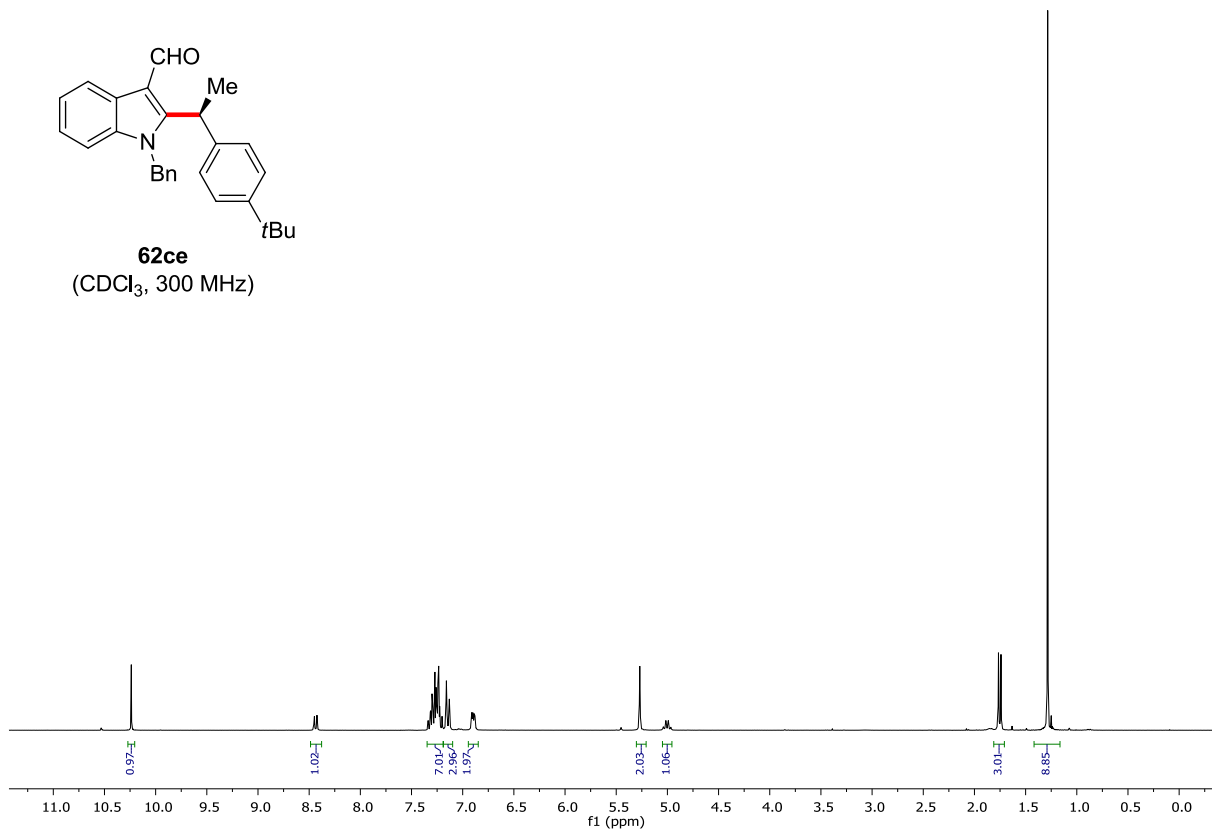
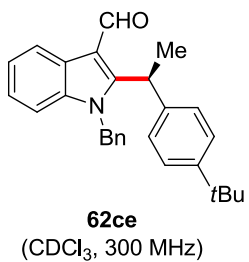
Chiral HPLC of **62cd**:



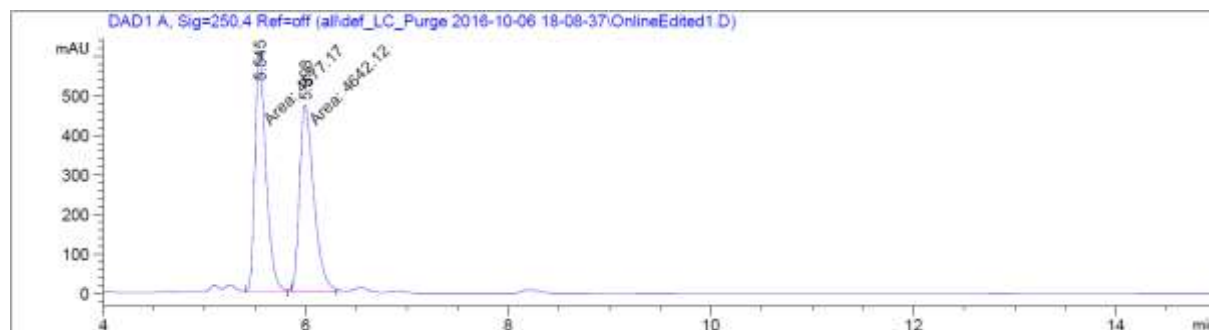
| Peak # | RetTime [min] | Type | Width [min] | Area [mAU*s] | Height [mAU] | Area % |
|--------|---------------|------|-------------|--------------|--------------|---------|
| 1 | 6.448 | MF | 0.1477 | 1.17227e4 | 1323.23694 | 50.1076 |
| 2 | 7.243 | MF | 0.1603 | 1.16724e4 | 1213.51294 | 49.8924 |



| Peak # | RetTime [min] | Type | Width [min] | Area [mAU*s] | Height [mAU] | Area % |
|--------|---------------|------|-------------|--------------|--------------|---------|
| 1 | 6.457 | MF | 0.1410 | 3460.54150 | 408.92322 | 89.7253 |
| 2 | 7.219 | MF | 0.1509 | 396.27701 | 43.75473 | 10.2747 |



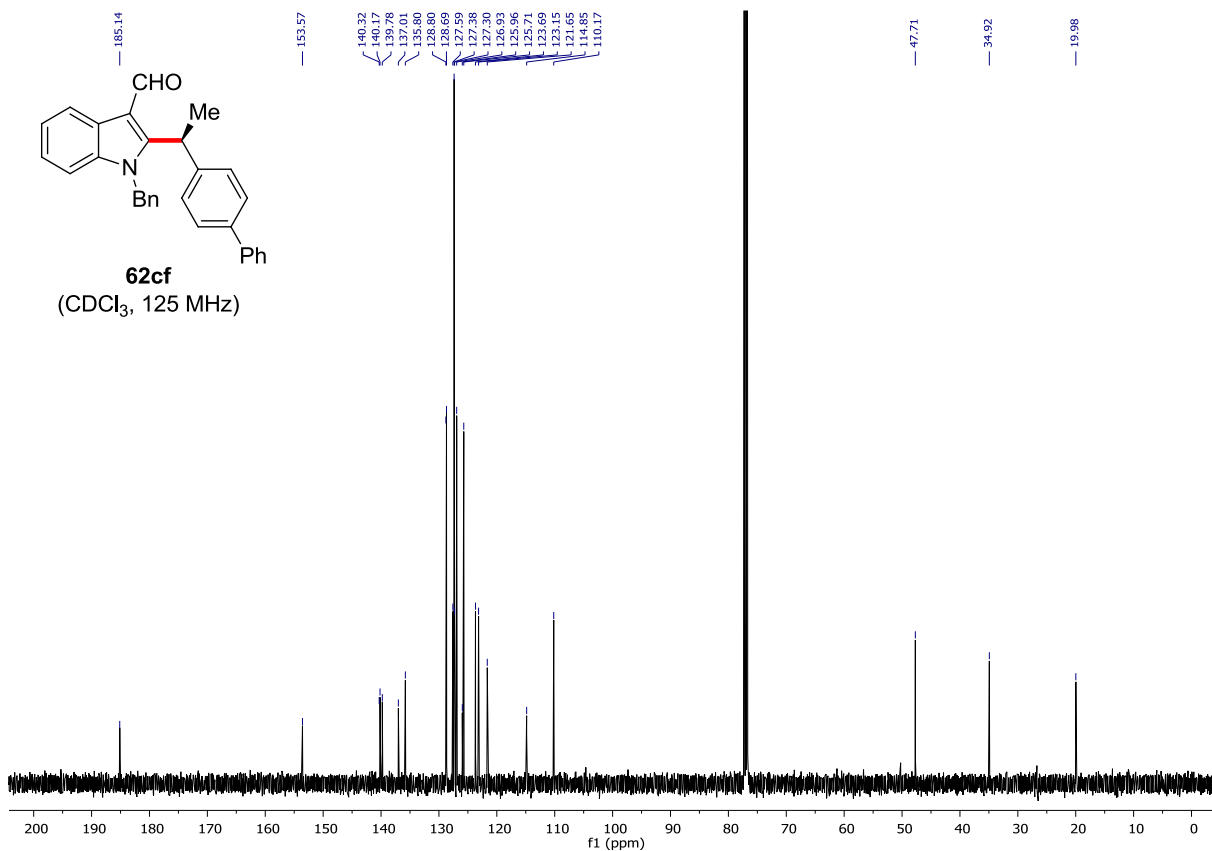
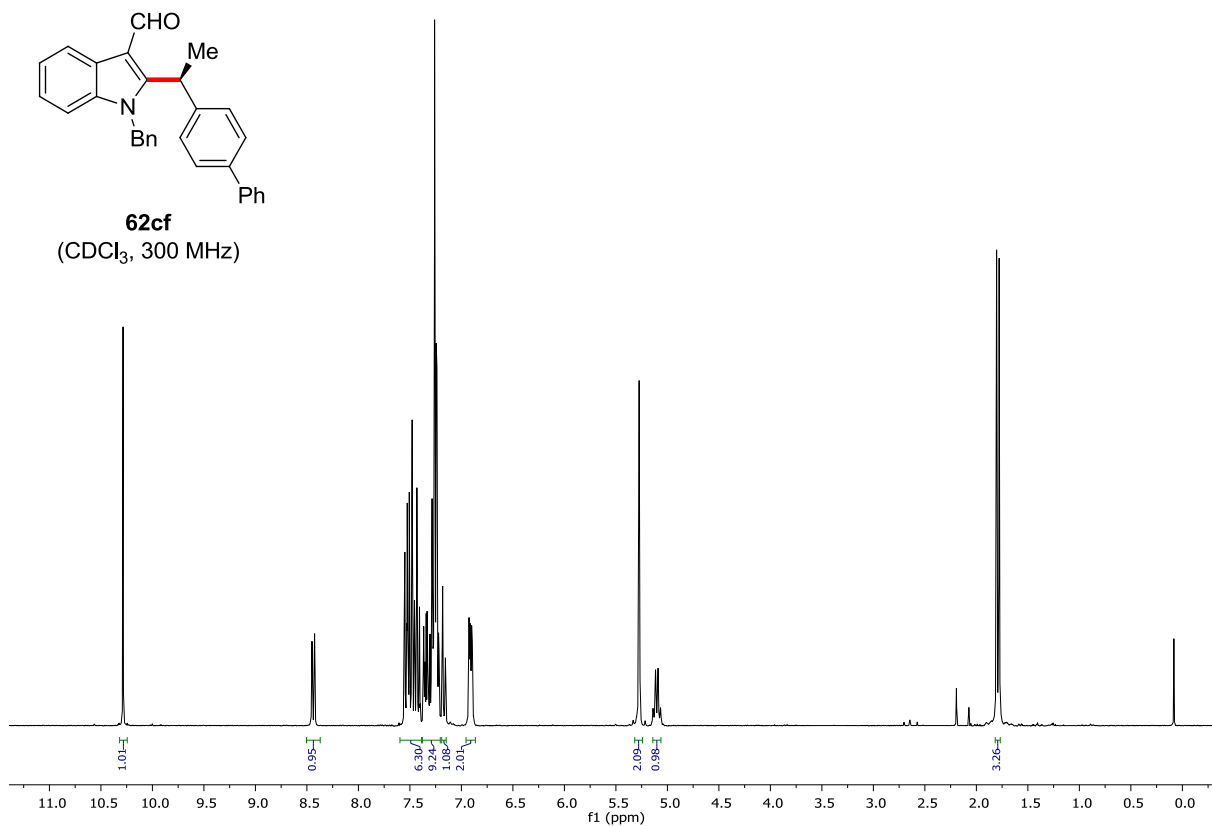
Chiral HPLC of **62ce**:



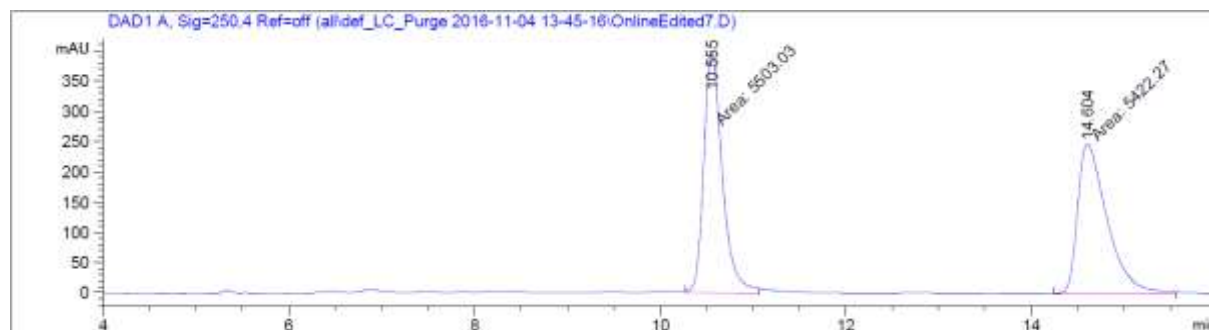
| Peak # | RetTime [min] | Type | Width [min] | Area [mAU*s] | Height [mAU] | Area % |
|--------|---------------|------|-------------|--------------|--------------|---------|
| 1 | 5.545 | MF | 0.1256 | 4577.17188 | 607.19360 | 49.6478 |
| 2 | 5.998 | MF | 0.1638 | 4642.11914 | 472.45178 | 50.3522 |



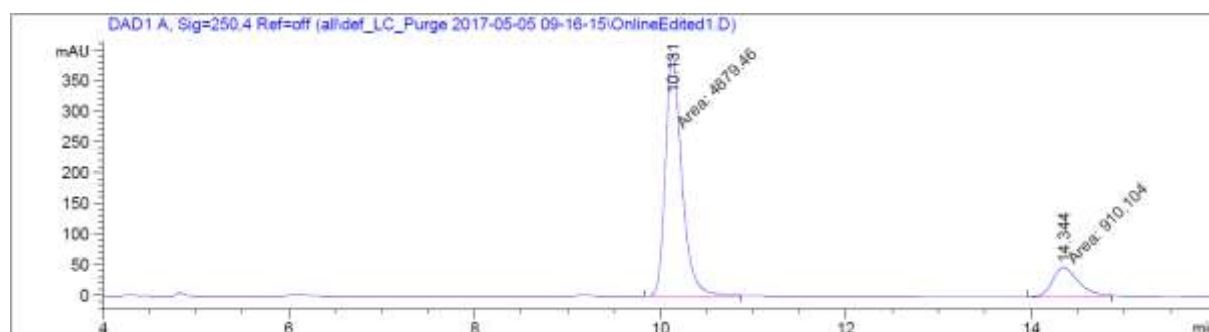
| Peak # | RetTime [min] | Type | Width [min] | Area [mAU*s] | Height [mAU] | Area % |
|--------|---------------|------|-------------|--------------|--------------|---------|
| 1 | 5.618 | MF | 0.1067 | 862.62433 | 134.74306 | 13.7674 |
| 2 | 6.070 | MF | 0.1463 | 5403.07227 | 615.59003 | 86.2326 |



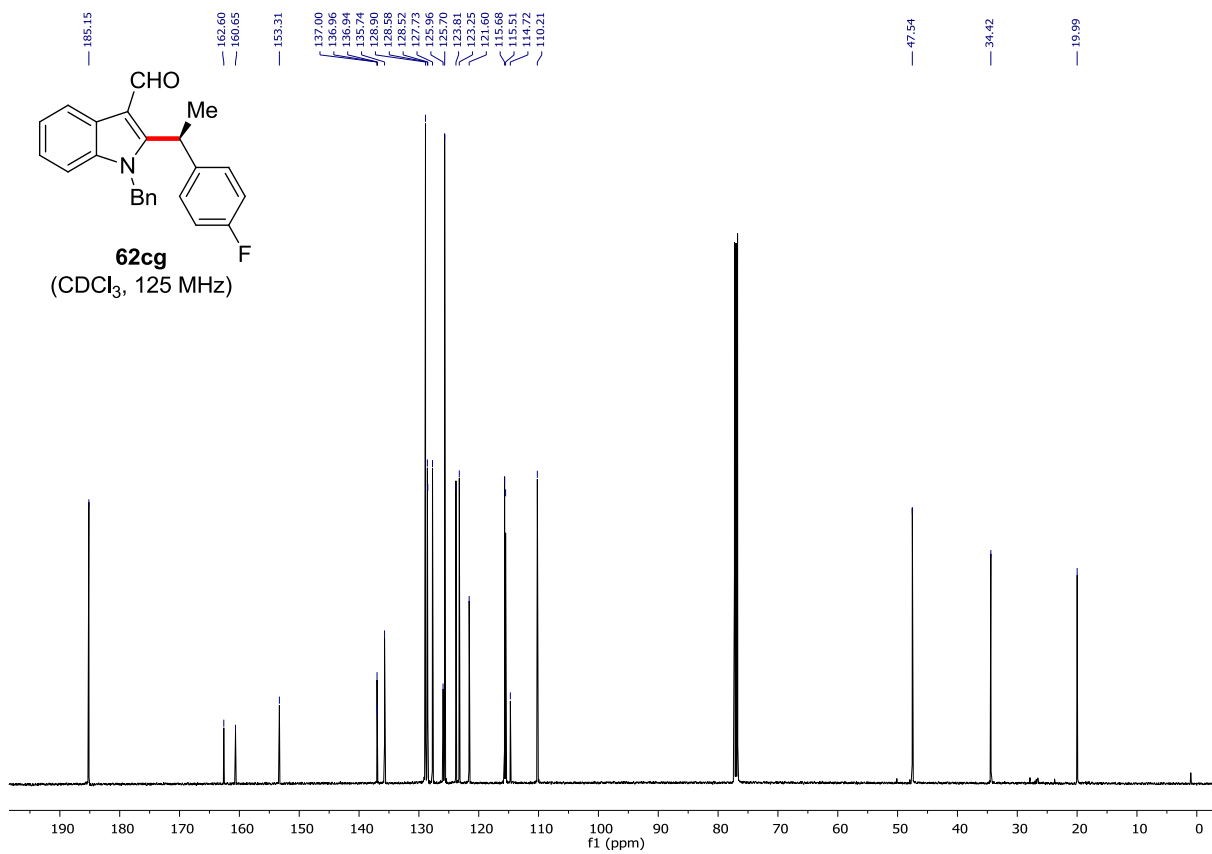
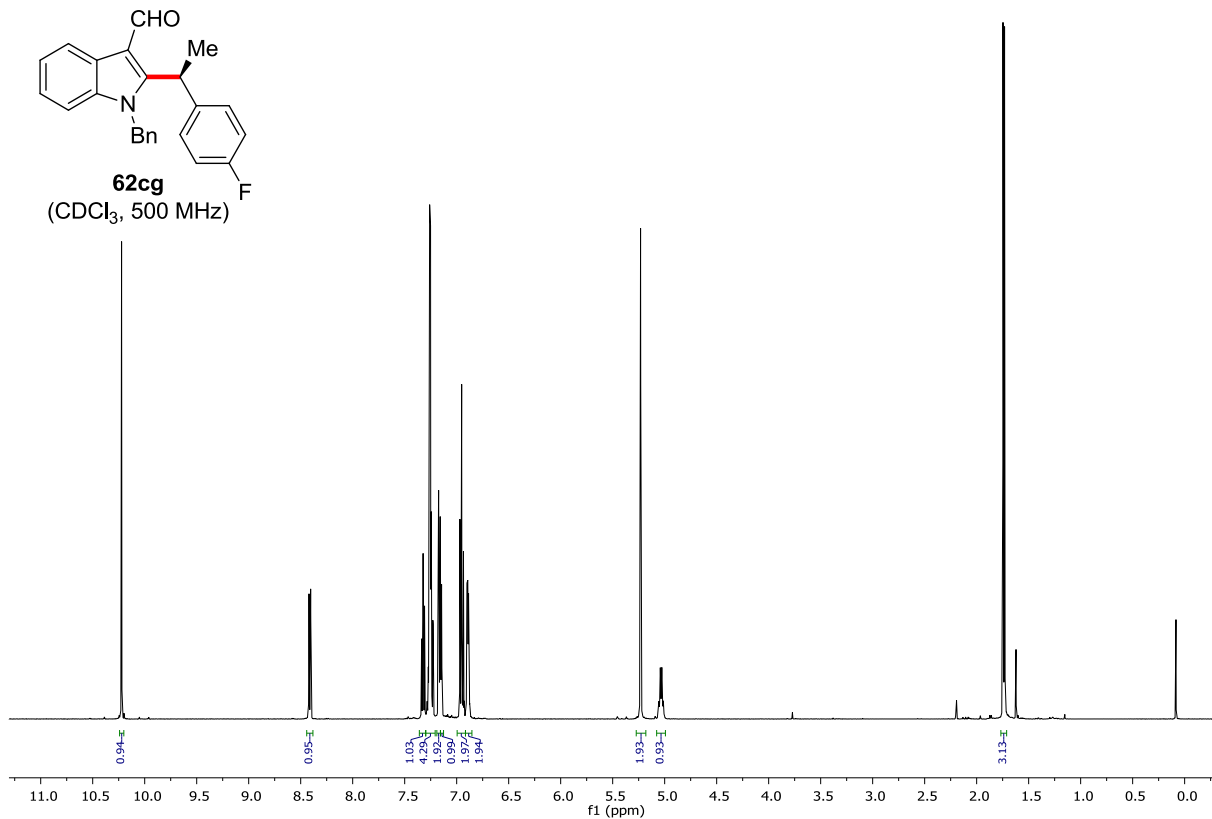
Chiral HPLC of **62cf**:

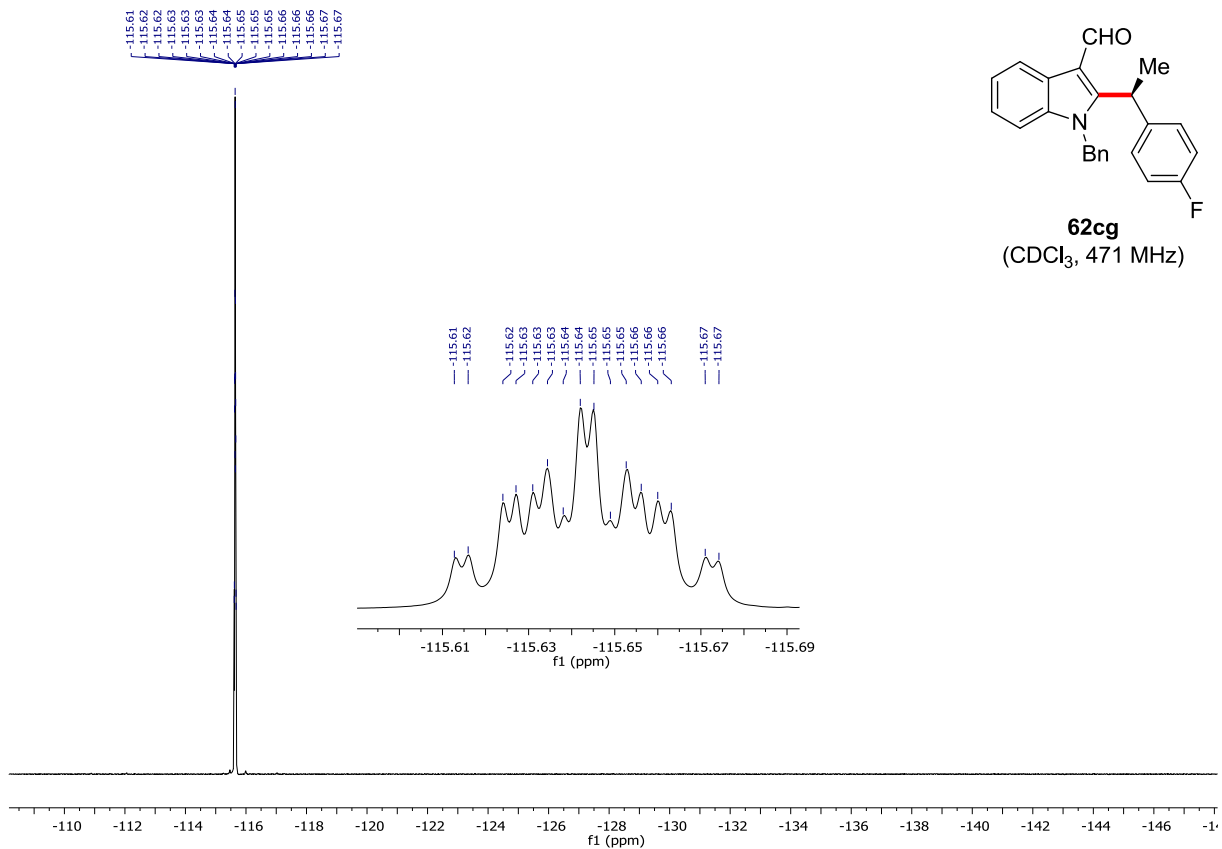


| Peak # | RetTime [min] | Type | Width [min] | Area [mAU*s] | Height [mAU] | Area % |
|--------|---------------|------|-------------|--------------|--------------|---------|
| 1 | 10.555 | MF | 0.2302 | 5503.02832 | 398.36981 | 50.3696 |
| 2 | 14.604 | MF | 0.3664 | 5422.27148 | 246.64539 | 49.6304 |

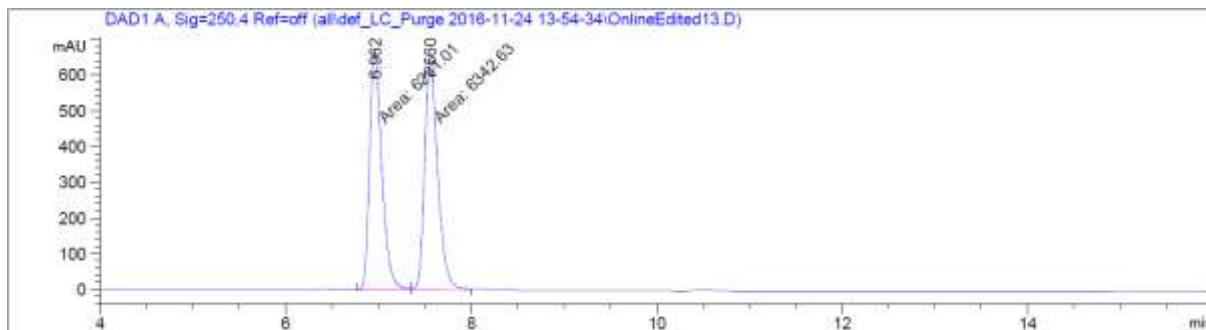


| Peak # | RetTime [min] | Type | Width [min] | Area [mAU*s] | Height [mAU] | Area % |
|--------|---------------|------|-------------|--------------|--------------|---------|
| 1 | 10.131 | MF | 0.2070 | 4879.46289 | 392.84244 | 84.2803 |
| 2 | 14.344 | MF | 0.3210 | 910.10425 | 47.25518 | 15.7197 |

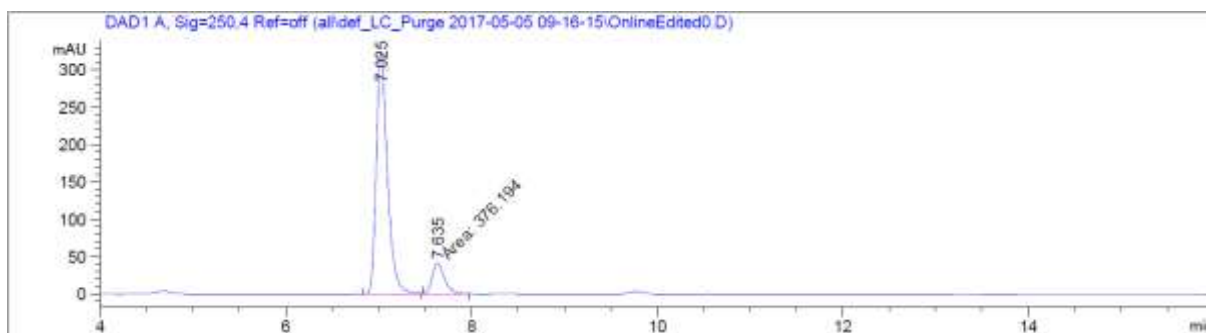




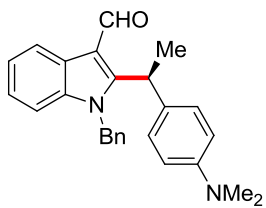
Chiral HPLC of **62cg**:



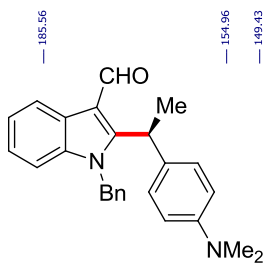
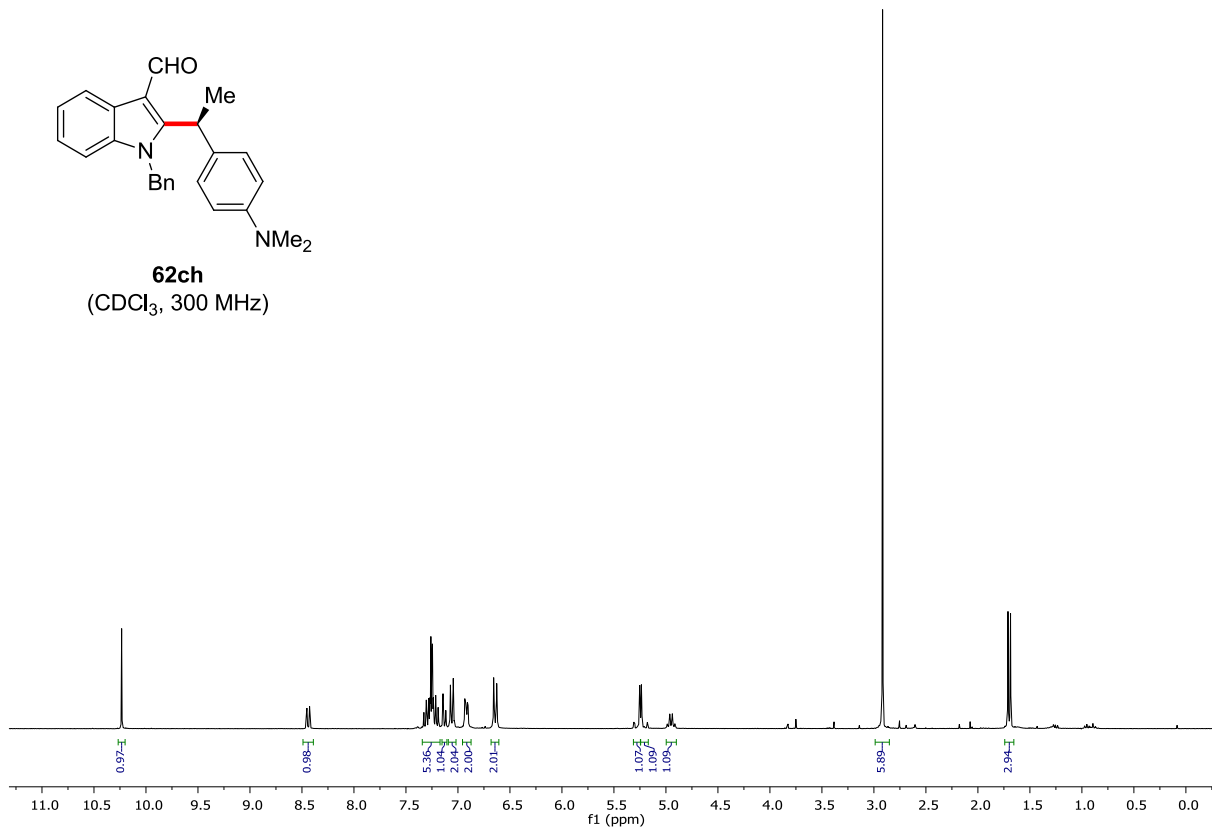
| Peak # | RetTime [min] | Type | Width [min] | Area [mAU*s] | Height [mAU] | Area % |
|--------|---------------|------|-------------|--------------|--------------|---------|
| 1 | 6.962 | FM | 0.1540 | 6231.00537 | 674.31134 | 49.5561 |
| 2 | 7.560 | MF | 0.1642 | 6342.62695 | 643.89337 | 50.4439 |



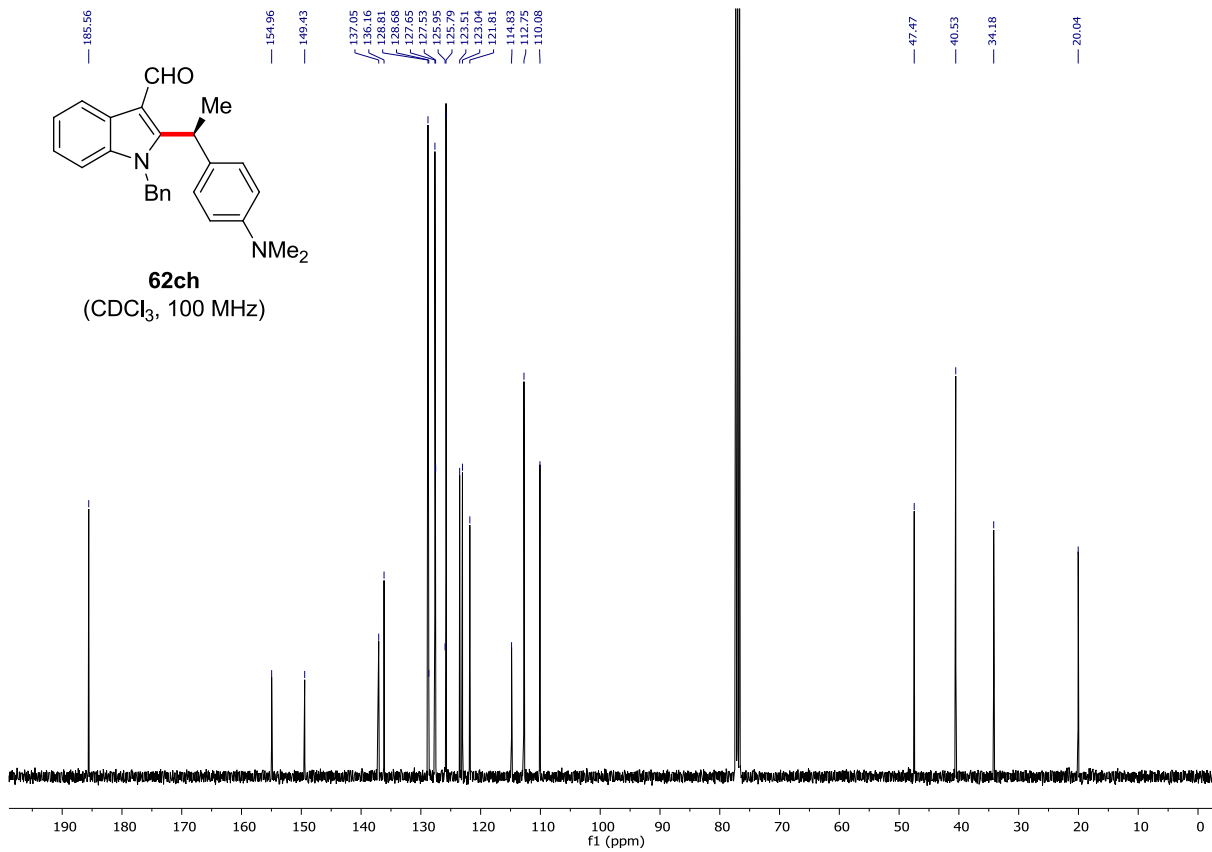
| Peak # | RetTime [min] | Type | Width [min] | Area [mAU*s] | Height [mAU] | Area % |
|--------|---------------|------|-------------|--------------|--------------|---------|
| 1 | 7.025 | BV | 0.1266 | 2705.27051 | 323.26282 | 87.7917 |
| 2 | 7.635 | MF | 0.1509 | 376.19437 | 41.54929 | 12.2083 |



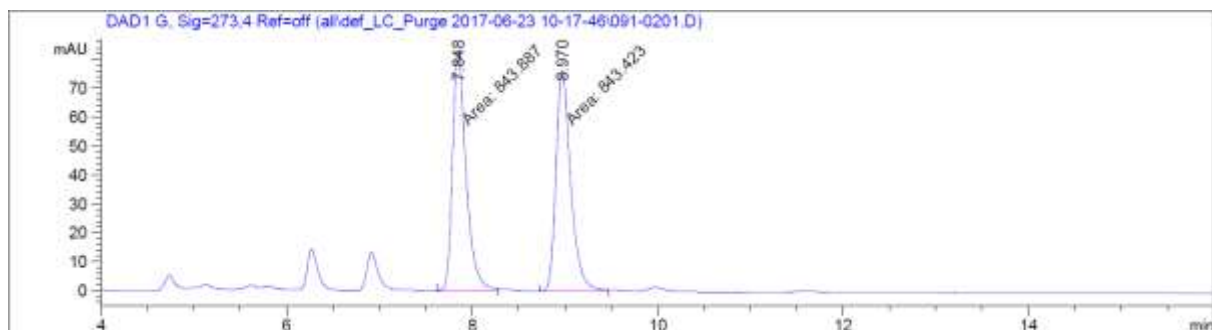
62ch
(CDCl₃, 300 MHz)



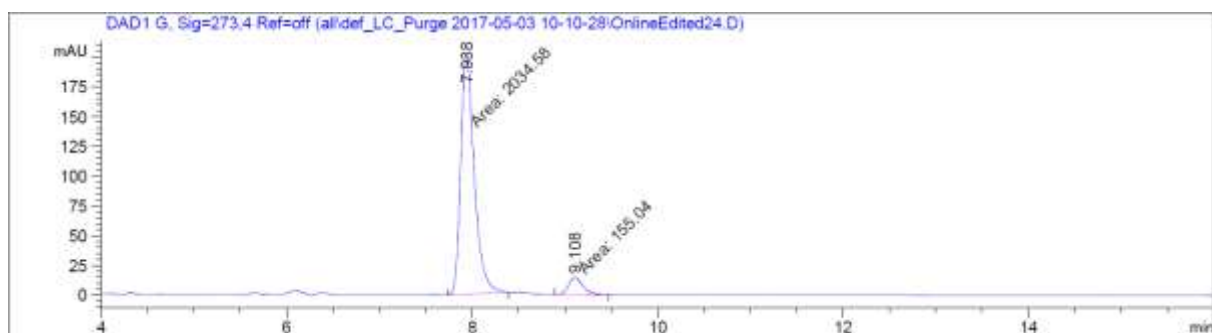
62ch
(CDCl₃, 100 MHz)



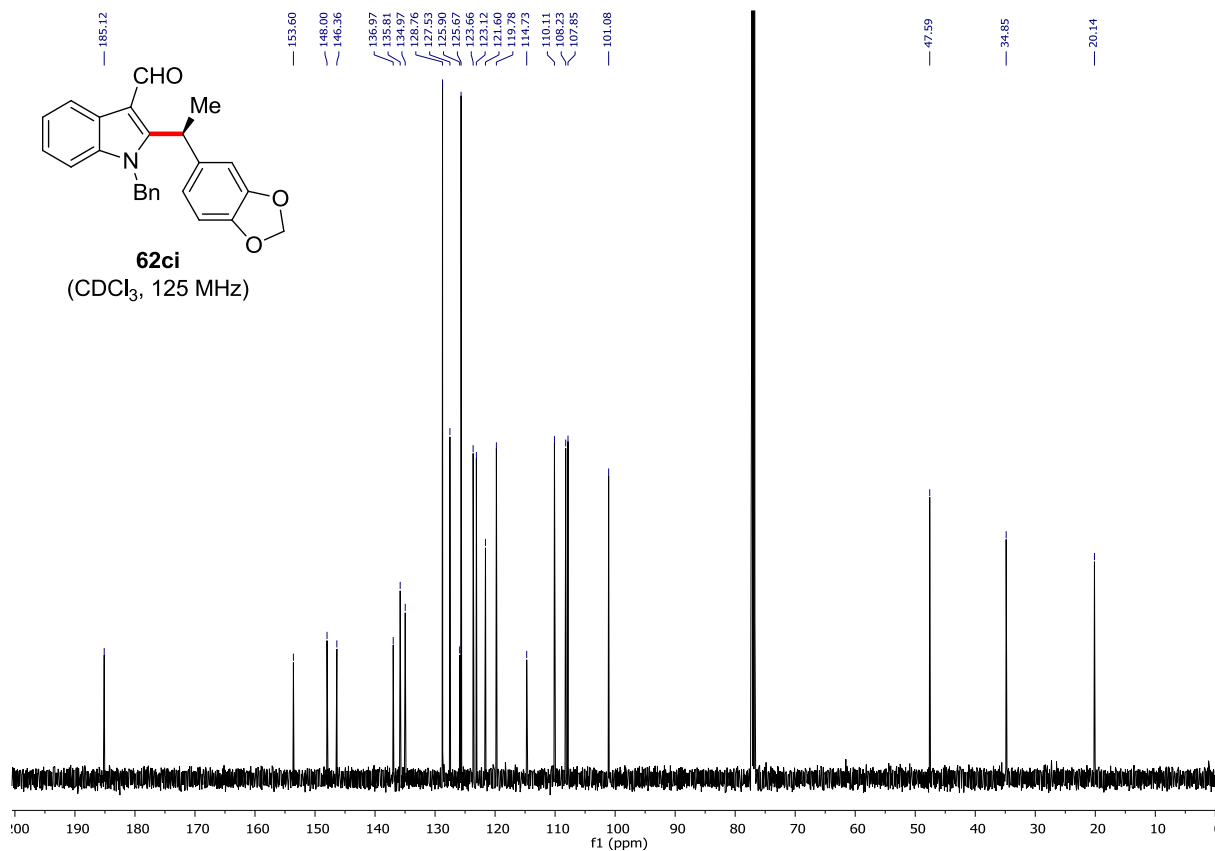
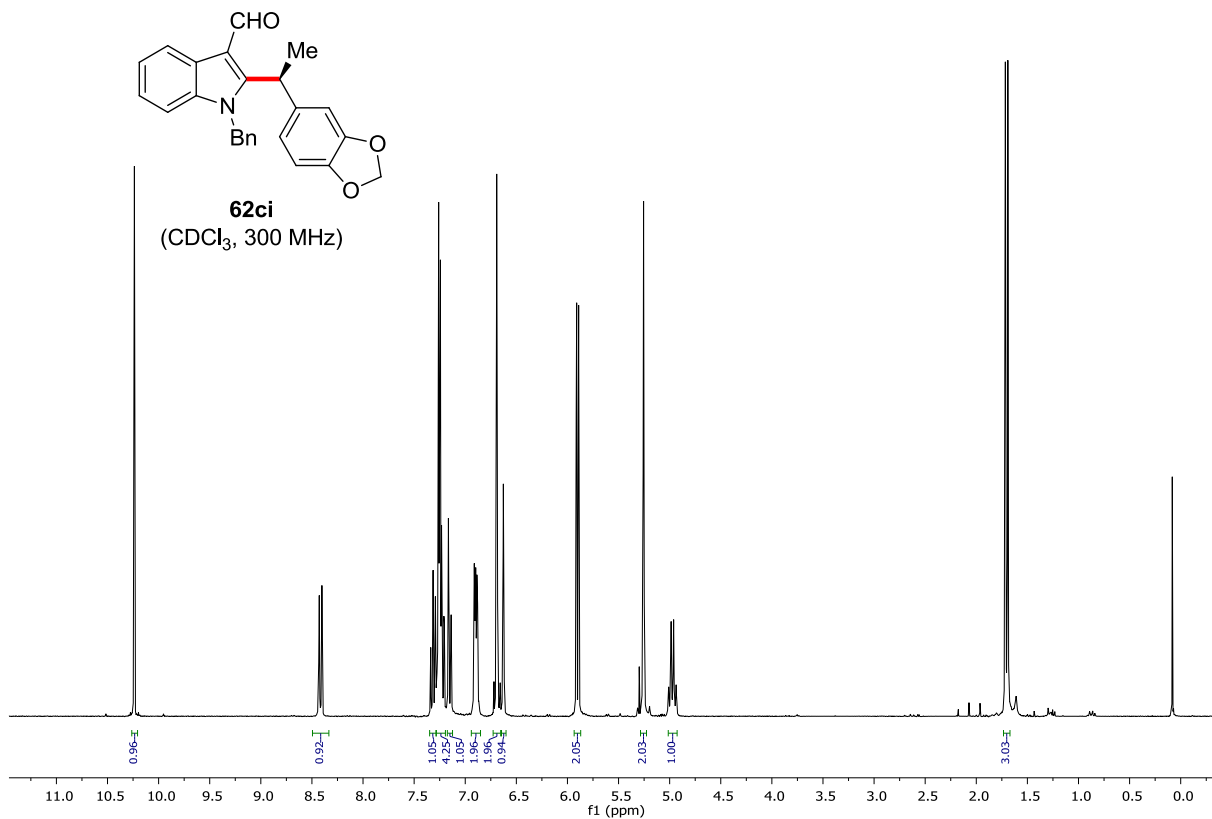
Chiral HPLC of **62ch**:



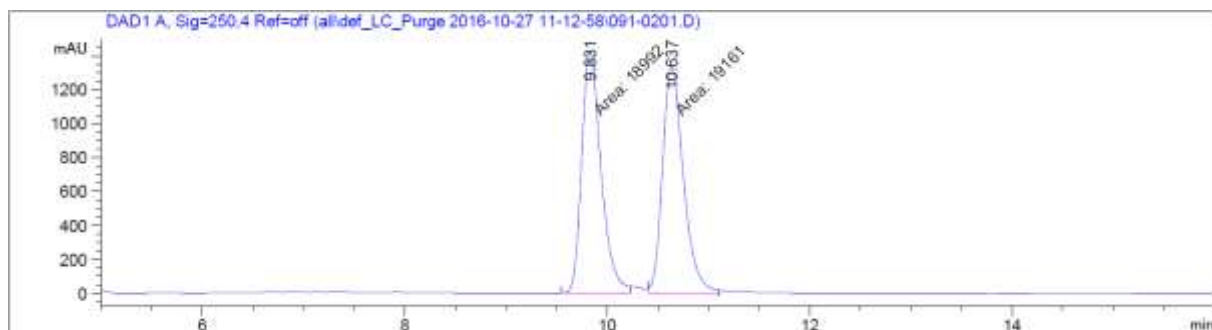
| Peak # | RetTime [min] | Type | Width [min] | Area [mAU*s] | Height [mAU] | Area % |
|--------|---------------|------|-------------|--------------|--------------|---------|
| 1 | 7.848 | MF | 0.1697 | 843.88696 | 82.85995 | 50.0137 |
| 2 | 8.970 | FM | 0.1836 | 843.42346 | 76.57423 | 49.9863 |



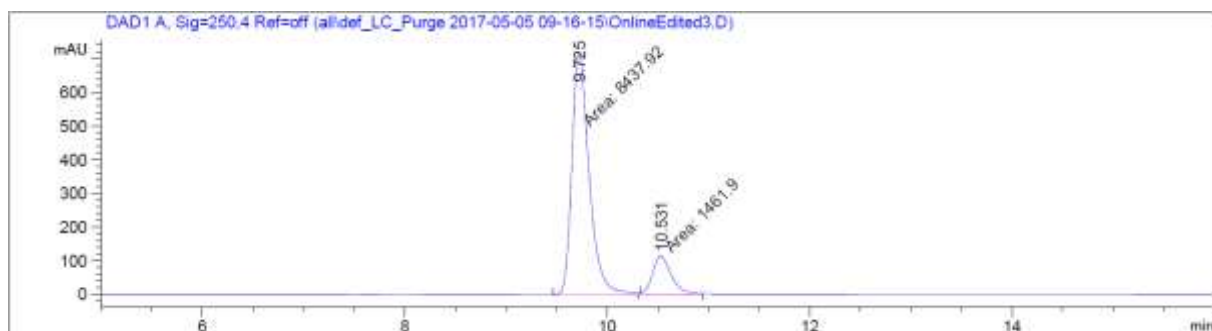
| Peak # | RetTime [min] | Type | Width [min] | Area [mAU*s] | Height [mAU] | Area % |
|--------|---------------|------|-------------|--------------|--------------|---------|
| 1 | 7.938 | MF | 0.1678 | 2034.57642 | 202.13528 | 92.9193 |
| 2 | 9.108 | MF | 0.1813 | 155.03995 | 14.25028 | 7.0807 |



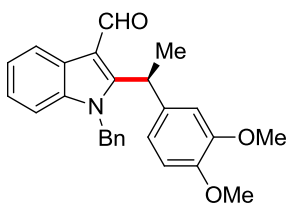
Chiral HPLC of **62ci**:



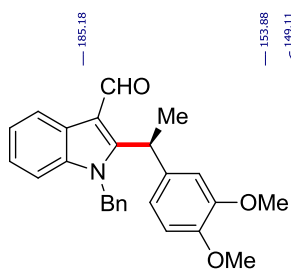
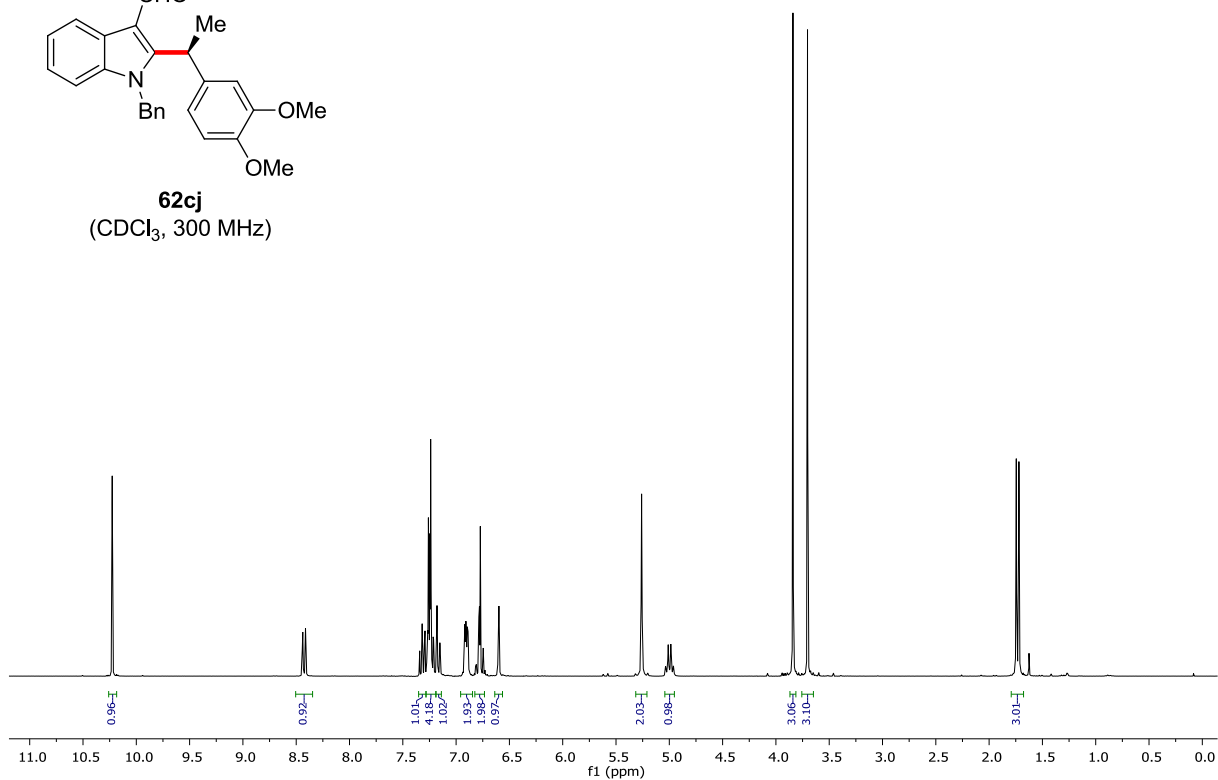
| Peak # | RetTime [min] | Type | Width [min] | Area [mAU*s] | Height [mAU] | Area % |
|--------|---------------|------|-------------|--------------|--------------|---------|
| 1 | 9.831 | MF | 0.2224 | 1.89920e4 | 1423.01062 | 49.7786 |
| 2 | 10.637 | MF | 0.2385 | 1.91610e4 | 1338.90820 | 50.2214 |



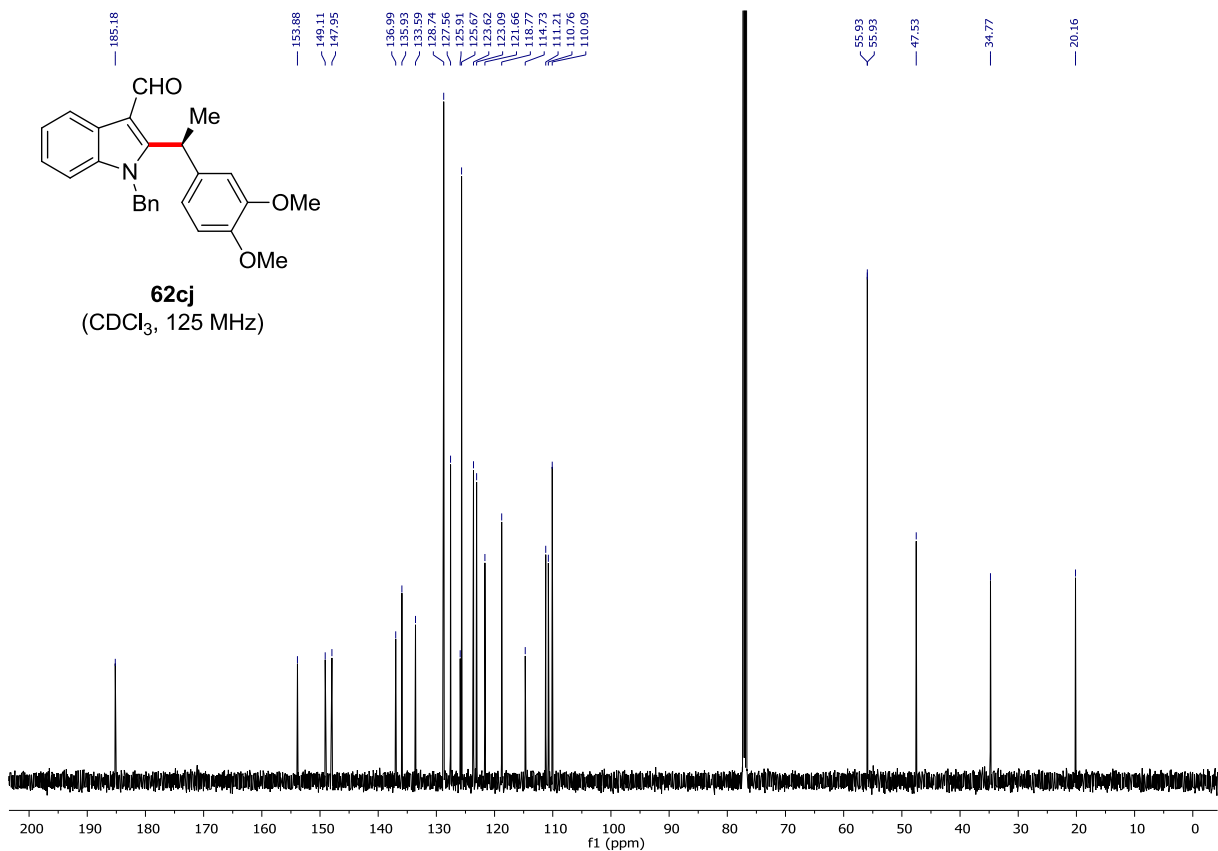
| Peak # | RetTime [min] | Type | Width [min] | Area [mAU*s] | Height [mAU] | Area % |
|--------|---------------|------|-------------|--------------|--------------|---------|
| 1 | 9.725 | FM | 0.1959 | 8437.92480 | 717.70392 | 85.2331 |
| 2 | 10.531 | FM | 0.2143 | 1461.89539 | 113.67721 | 14.7669 |



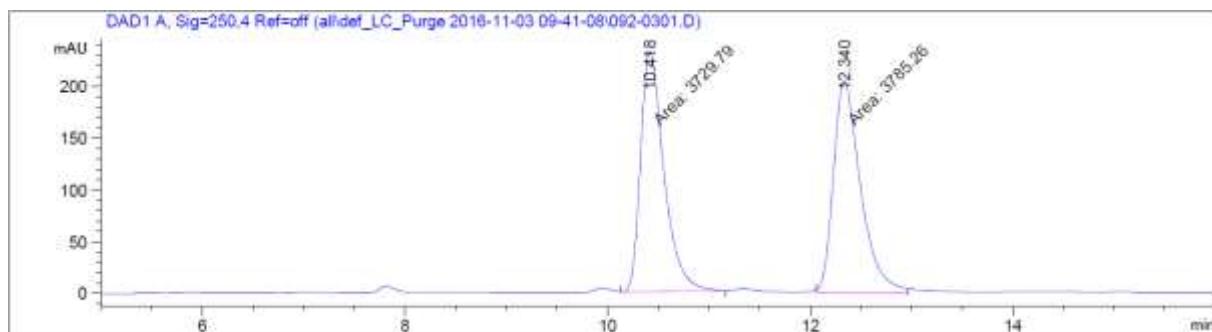
62cj
(CDCl₃, 300 MHz)



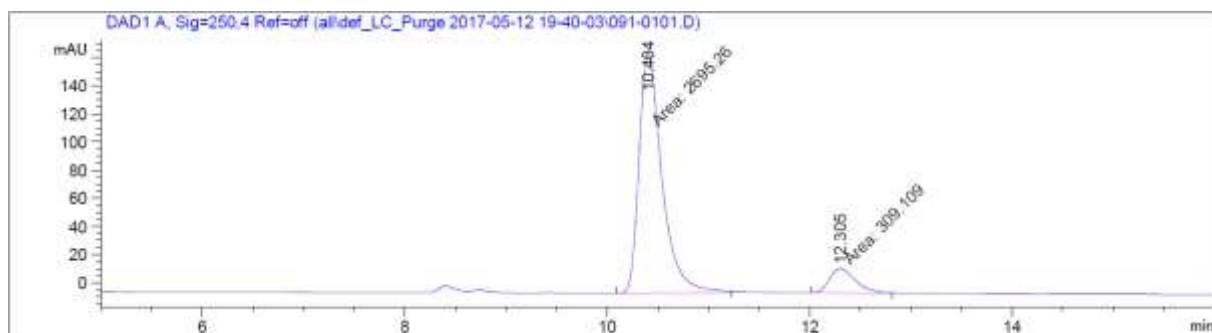
62cj
(CDCl₃, 125 MHz)



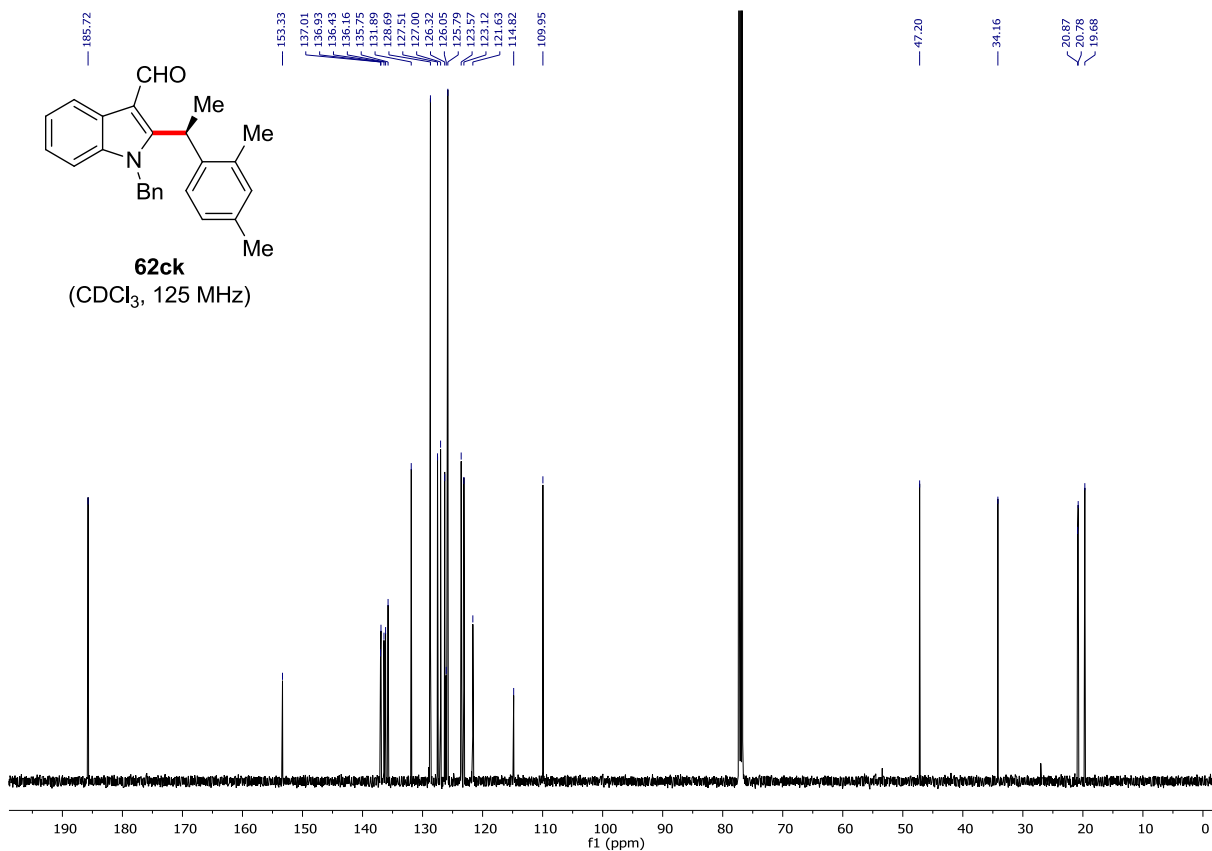
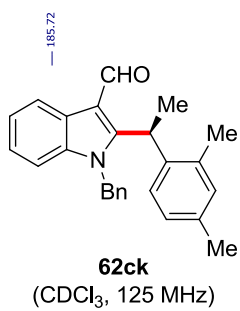
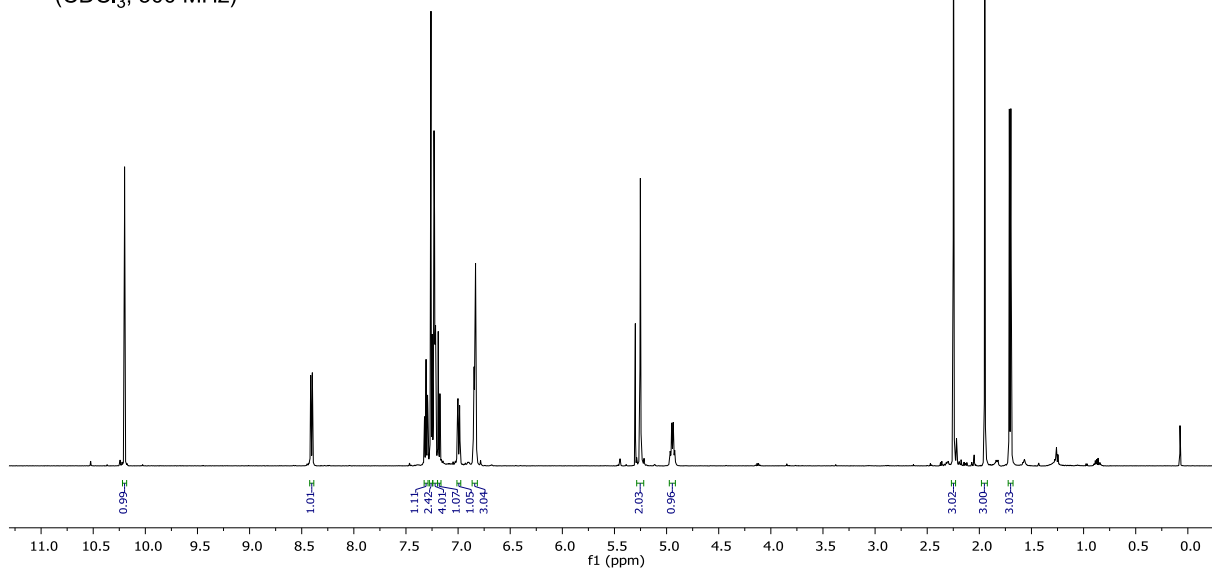
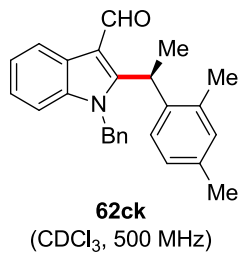
Chiral HPLC of **62cj**:



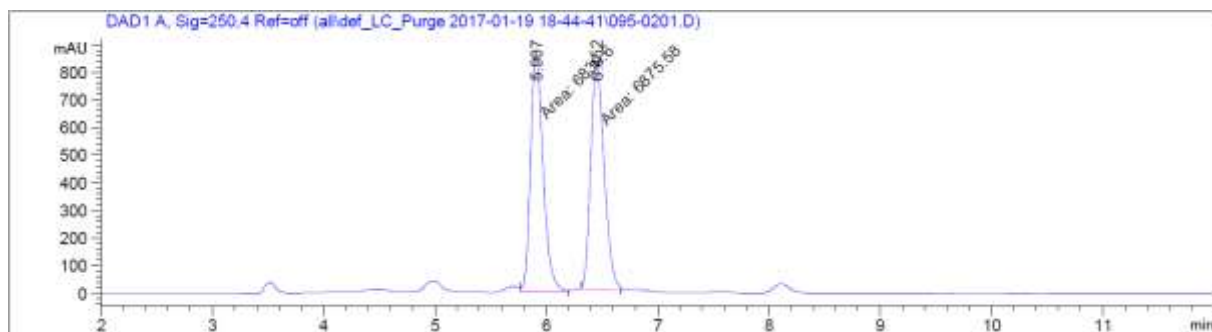
| Peak # | RetTime [min] | Type | Width [min] | Area [mAU*s] | Height [mAU] | Area % |
|--------|---------------|------|-------------|--------------|--------------|---------|
| 1 | 10.418 | FM | 0.2677 | 3729.79053 | 232.19543 | 49.6309 |
| 2 | 12.340 | MF | 0.3094 | 3785.26196 | 203.90834 | 50.3691 |



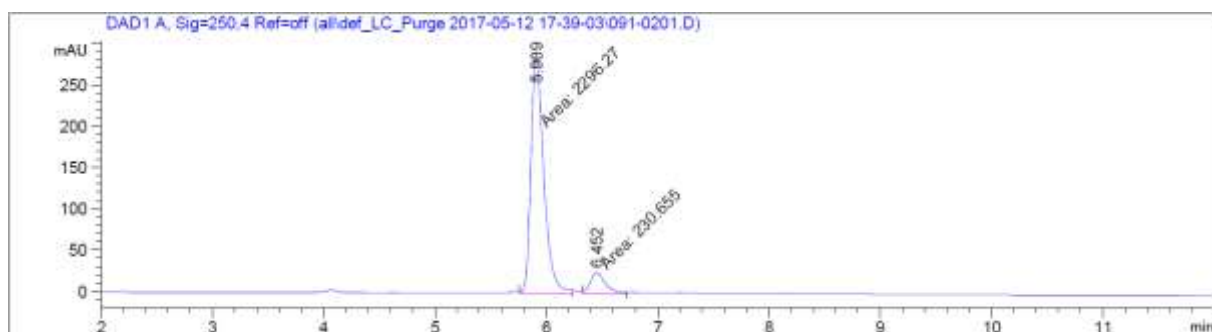
| Peak # | RetTime [min] | Type | Width [min] | Area [mAU*s] | Height [mAU] | Area % |
|--------|---------------|------|-------------|--------------|--------------|---------|
| 1 | 10.404 | MF | 0.2628 | 2695.26465 | 170.96188 | 89.7114 |
| 2 | 12.305 | MF | 0.2958 | 309.10907 | 17.41437 | 10.2886 |



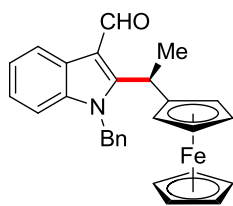
Chiral HPLC of **62ck**:



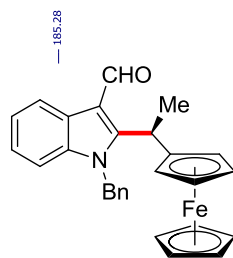
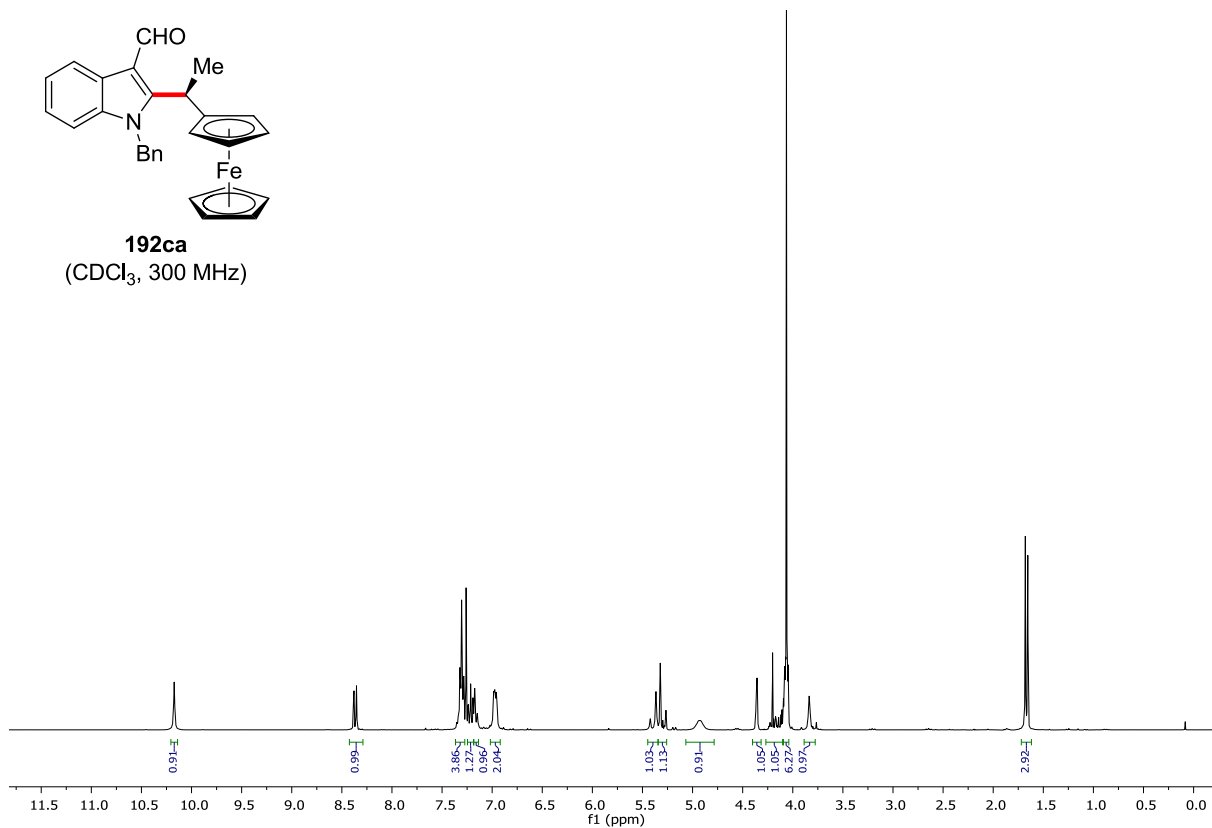
| Peak # | RetTime [min] | Type | Width [min] | Area [mAU*s] | Height [mAU] | Area % |
|--------|---------------|------|-------------|--------------|--------------|---------|
| 1 | 5.907 | FM | 0.1306 | 6830.60254 | 872.02826 | 49.8359 |
| 2 | 6.452 | MF | 0.1415 | 6875.58203 | 809.75299 | 50.1641 |



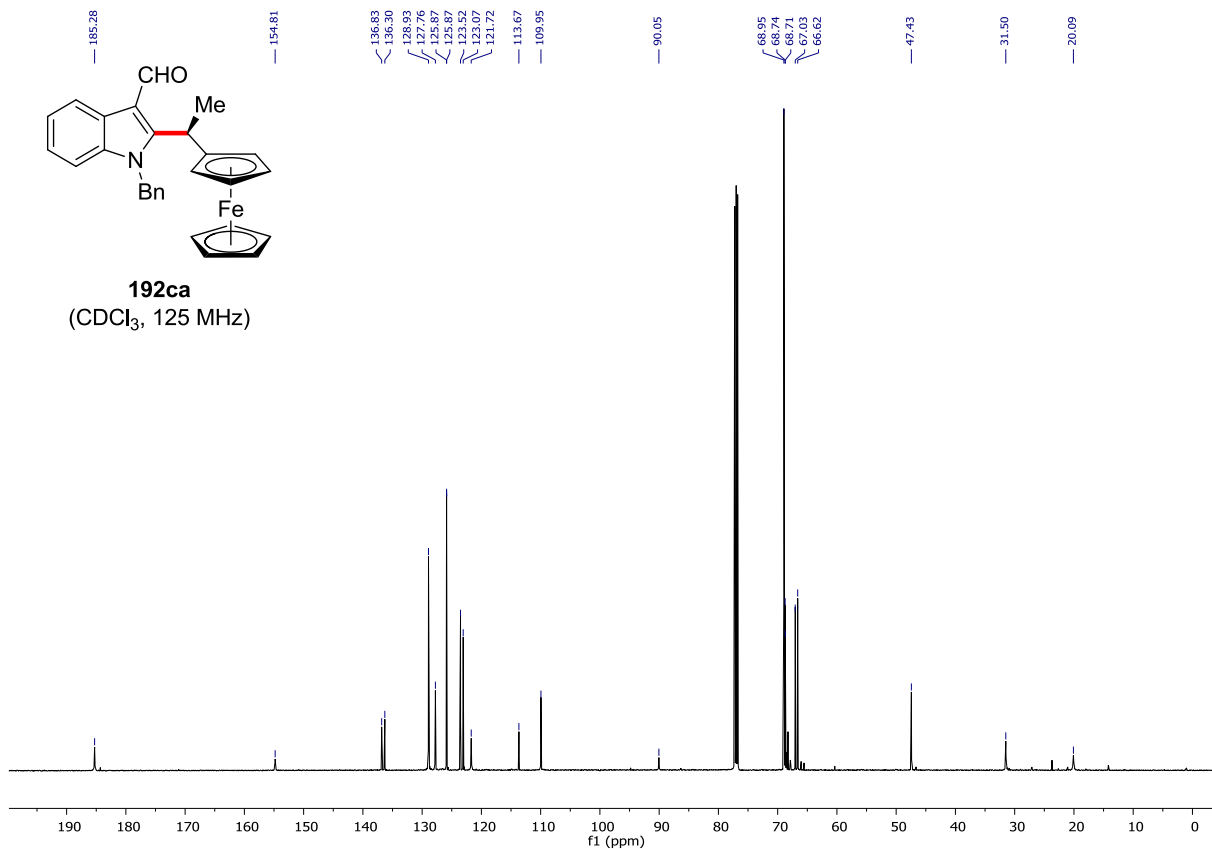
| Peak # | RetTime [min] | Type | Width [min] | Area [mAU*s] | Height [mAU] | Area % |
|--------|---------------|------|-------------|--------------|--------------|---------|
| 1 | 5.909 | MF | 0.1317 | 2296.26514 | 290.48779 | 90.8721 |
| 2 | 6.452 | MF | 0.1543 | 230.65512 | 24.92182 | 9.1279 |



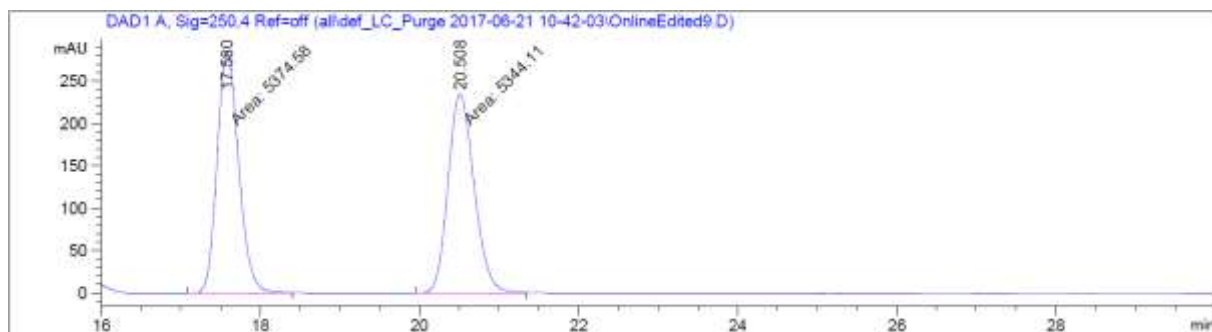
192ca
(CDCl₃, 300 MHz)



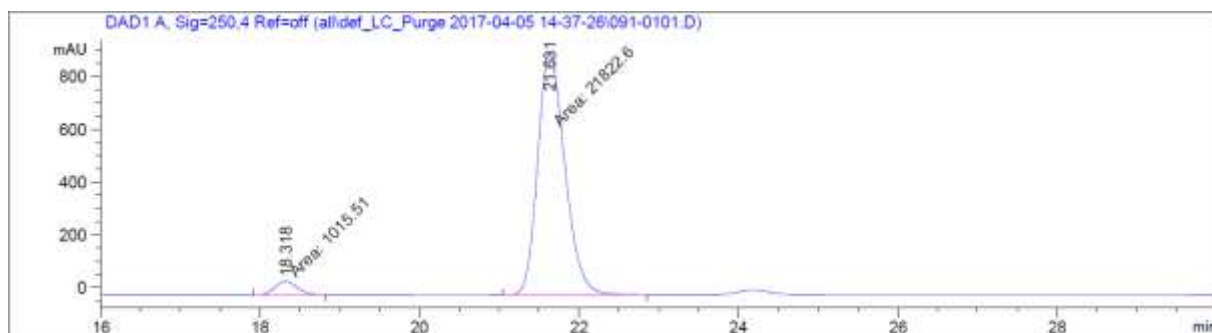
192ca
(CDCl₃, 125 MHz)



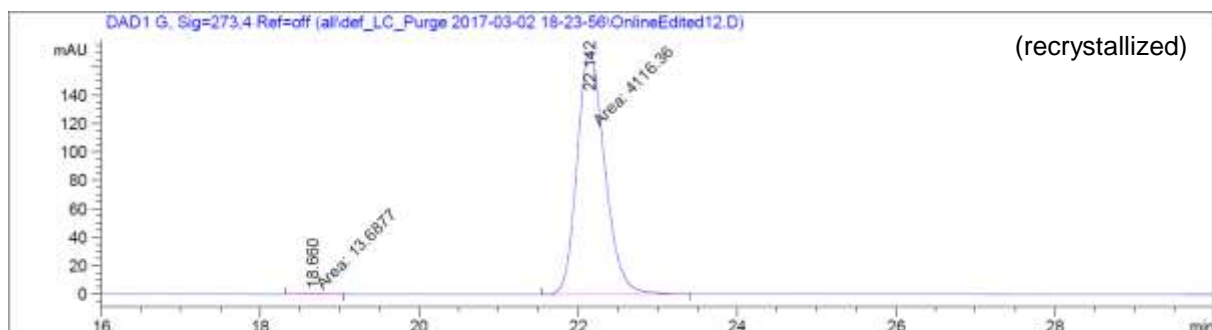
Chiral HPLC of 192ca:



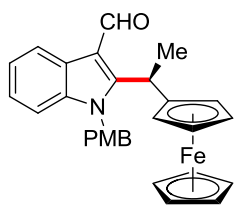
| Peak # | RetTime [min] | Type | Width [min] | Area [mAU*s] | Height [mAU] | Area % |
|--------|---------------|------|-------------|--------------|--------------|---------|
| 1 | 17.580 | MF | 0.3146 | 5374.57715 | 284.73135 | 50.1421 |
| 2 | 20.508 | MF | 0.3801 | 5344.11230 | 234.30211 | 49.8579 |



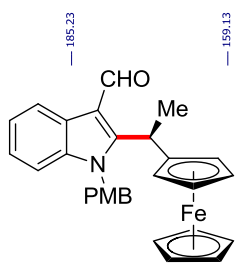
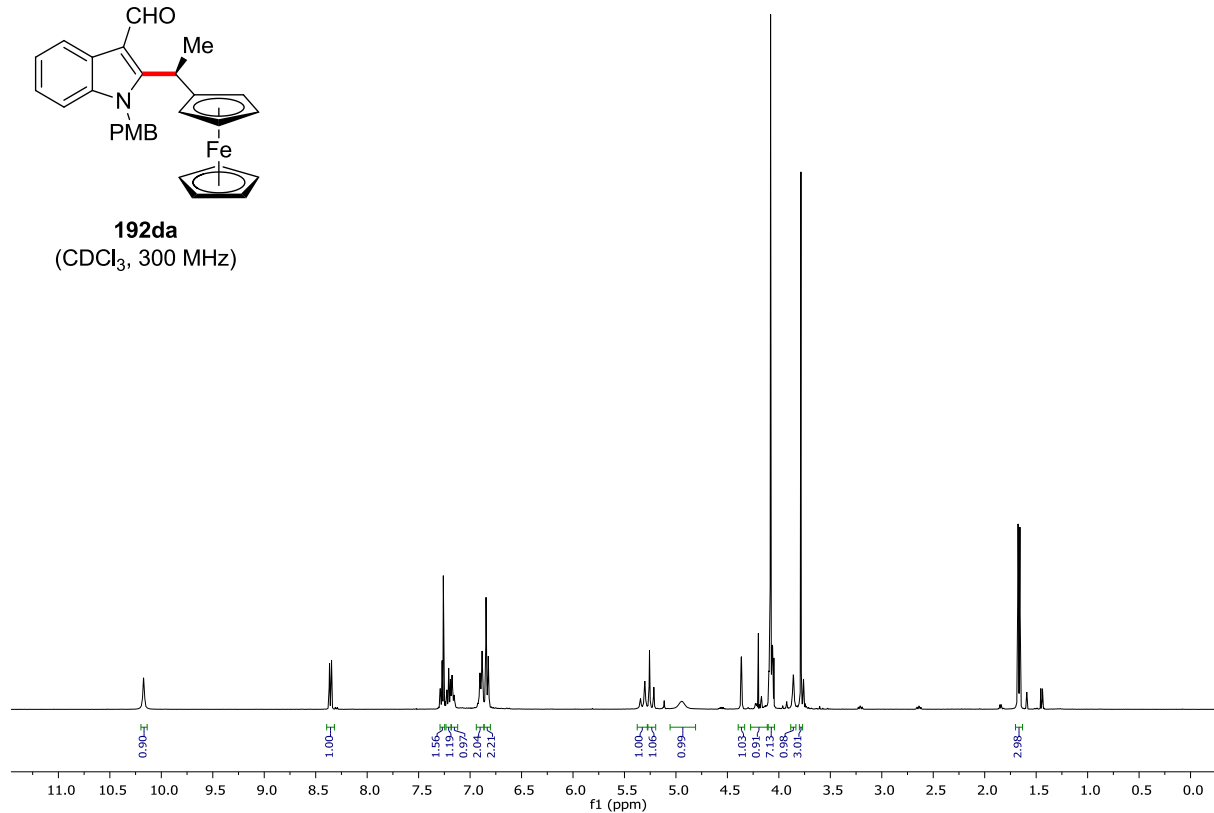
| Peak # | RetTime [min] | Type | Width [min] | Area [mAU*s] | Height [mAU] | Area % |
|--------|---------------|------|-------------|--------------|--------------|---------|
| 1 | 18.318 | MF | 0.3281 | 1015.51050 | 51.57914 | 4.4466 |
| 2 | 21.631 | FM | 0.3961 | 2.18226e4 | 918.25098 | 95.5534 |



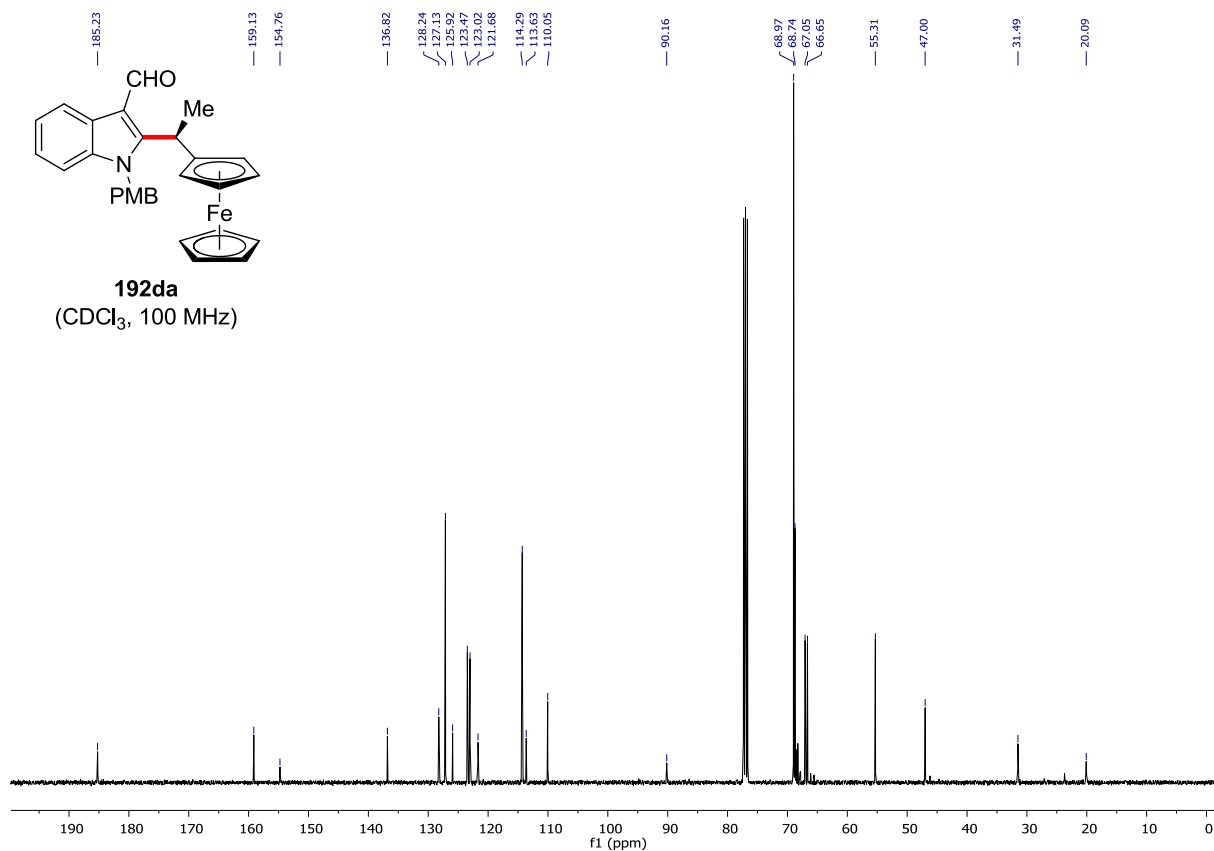
| Peak # | RetTime [min] | Type | Width [min] | Area [mAU*s] | Height [mAU] | Area % |
|--------|---------------|------|-------------|--------------|--------------|---------|
| 1 | 18.660 | MM | 0.3244 | 13.68770 | 7.03235e-1 | 0.3314 |
| 2 | 22.142 | MF | 0.4037 | 4116.36084 | 169.94774 | 99.6686 |



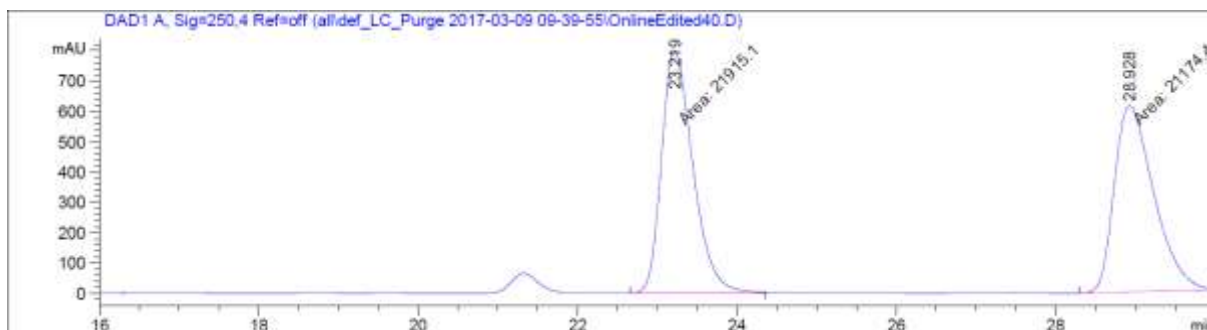
192da
(CDCl₃, 300 MHz)



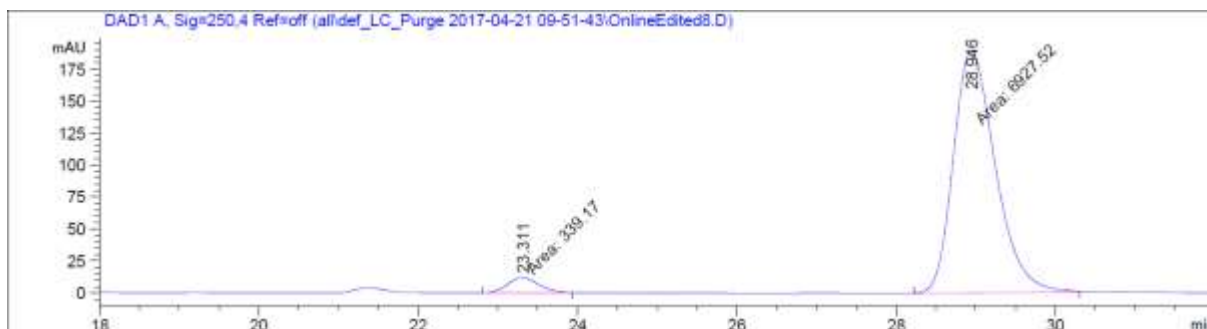
192da
(CDCl₃, 100 MHz)



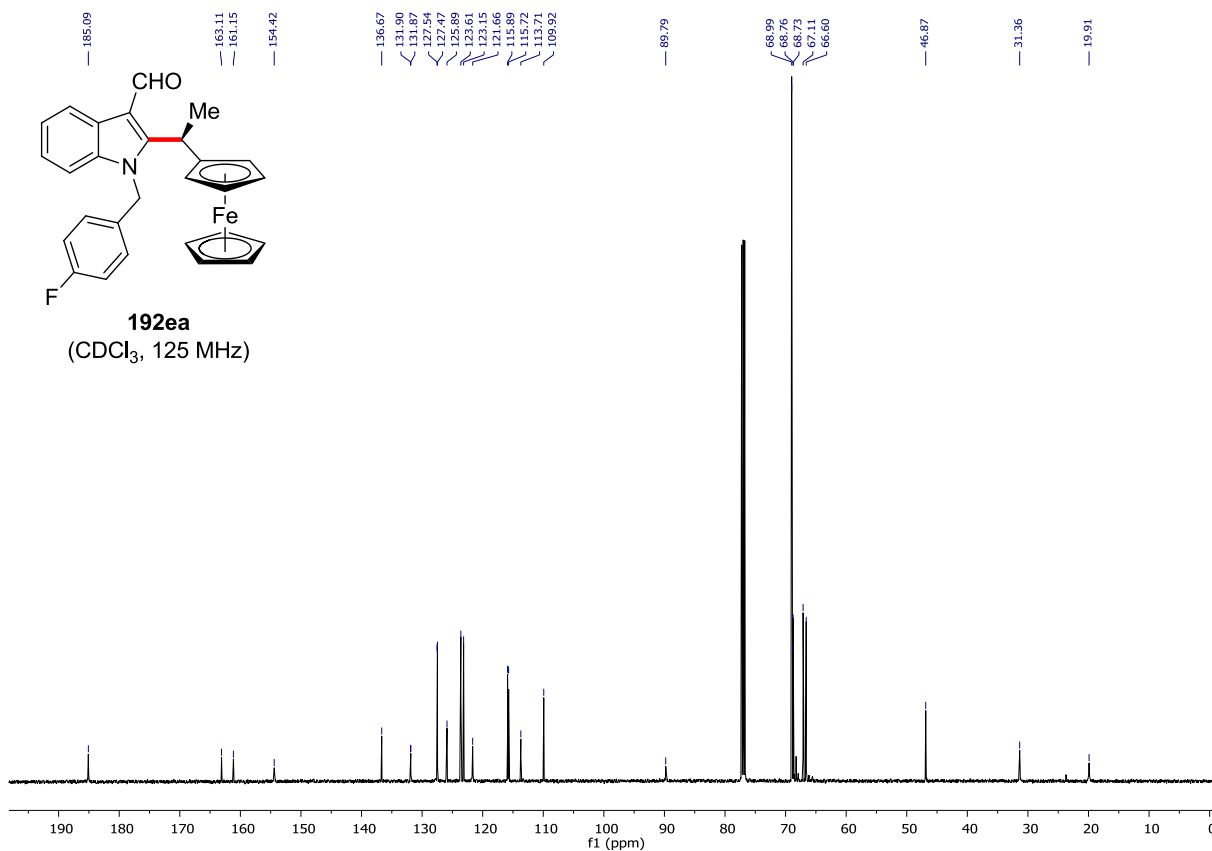
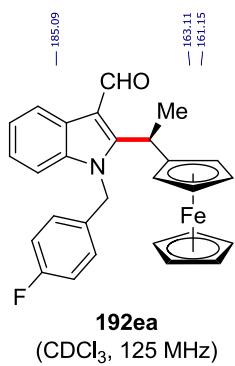
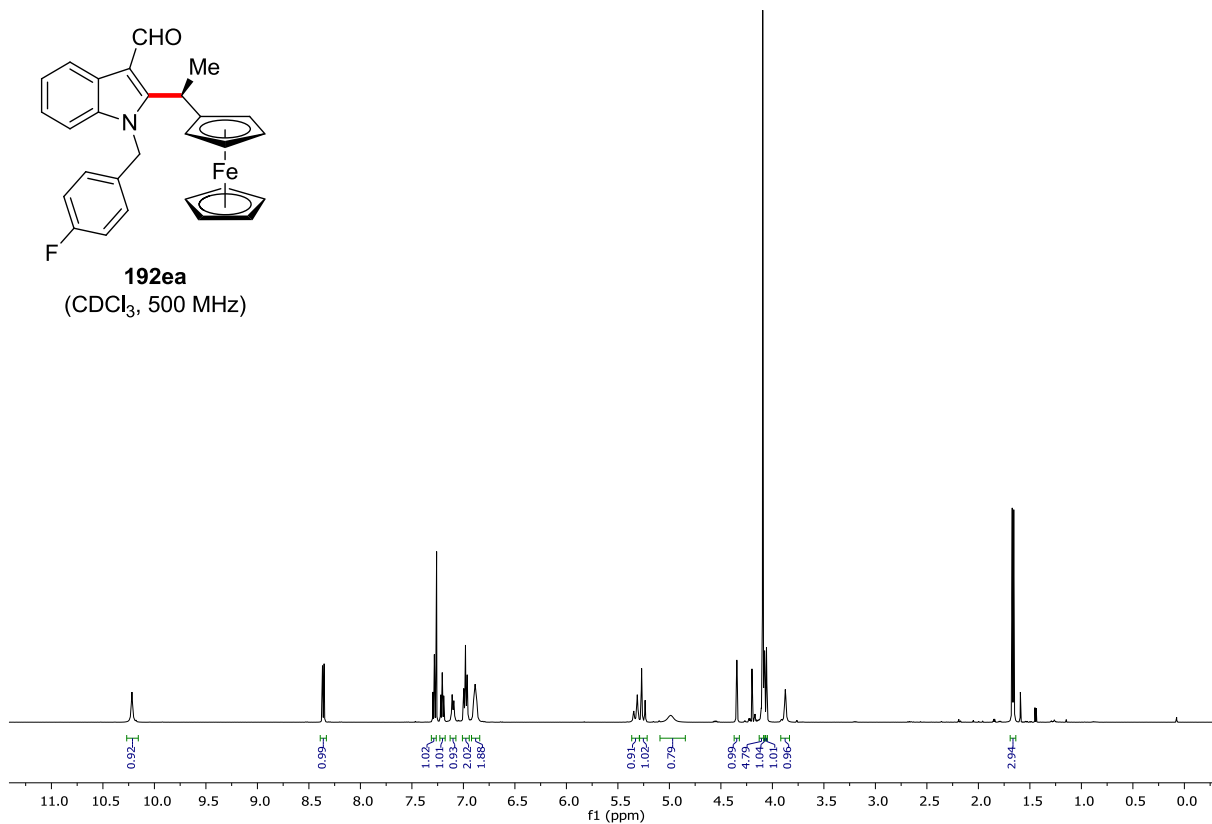
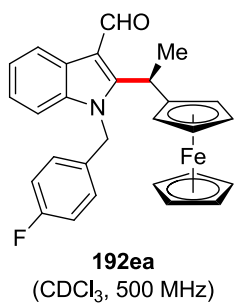
Chiral HPLC of **192da**:

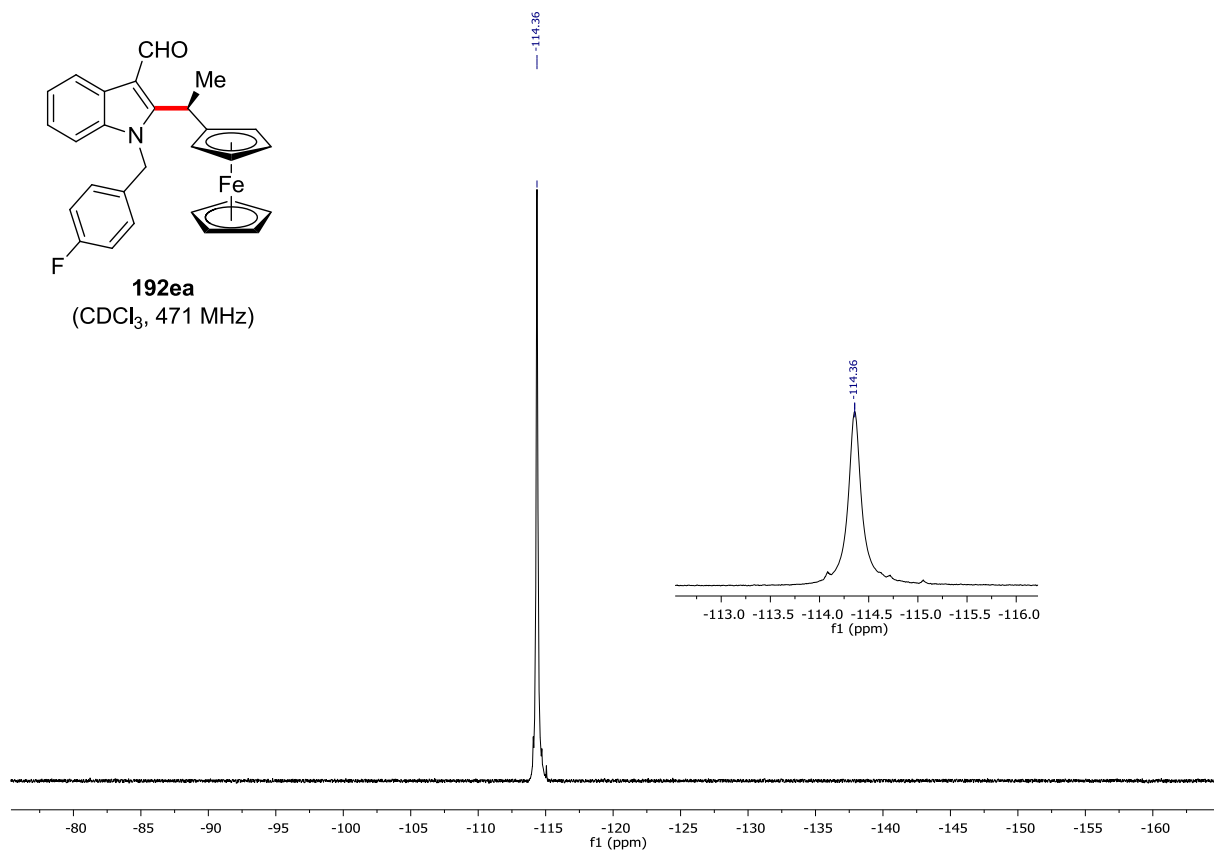
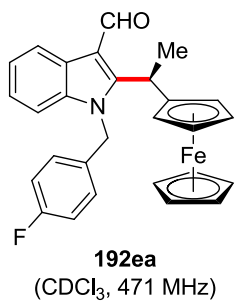


| Peak # | RetTime [min] | Type | Width [min] | Area [mAU*s] | Height [mAU] | Area % |
|--------|---------------|------|-------------|--------------|--------------|---------|
| 1 | 23.219 | MF | 0.4580 | 2.19151e4 | 797.41278 | 50.8595 |
| 2 | 28.928 | FM | 0.5751 | 2.11744e4 | 613.61267 | 49.1405 |

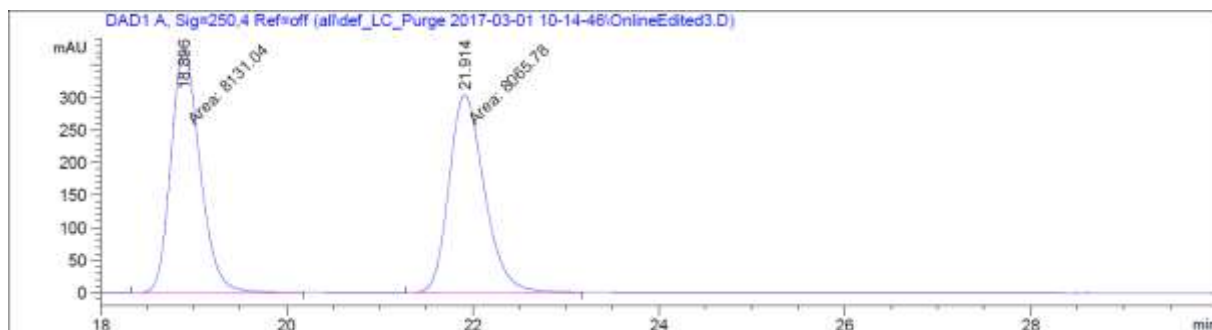


| Peak # | RetTime [min] | Type | Width [min] | Area [mAU*s] | Height [mAU] | Area % |
|--------|---------------|------|-------------|--------------|--------------|---------|
| 1 | 23.311 | MF | 0.4678 | 339.16953 | 12.08331 | 4.6675 |
| 2 | 28.946 | MF | 0.6109 | 6927.52148 | 188.98744 | 95.3325 |

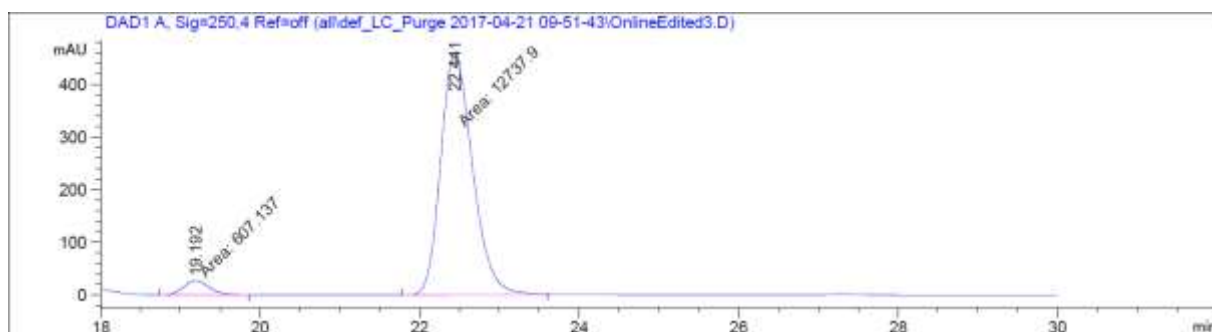




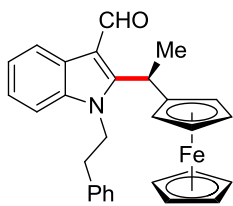
Chiral HPLC of **192ea**:



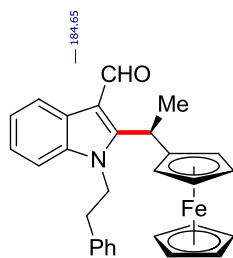
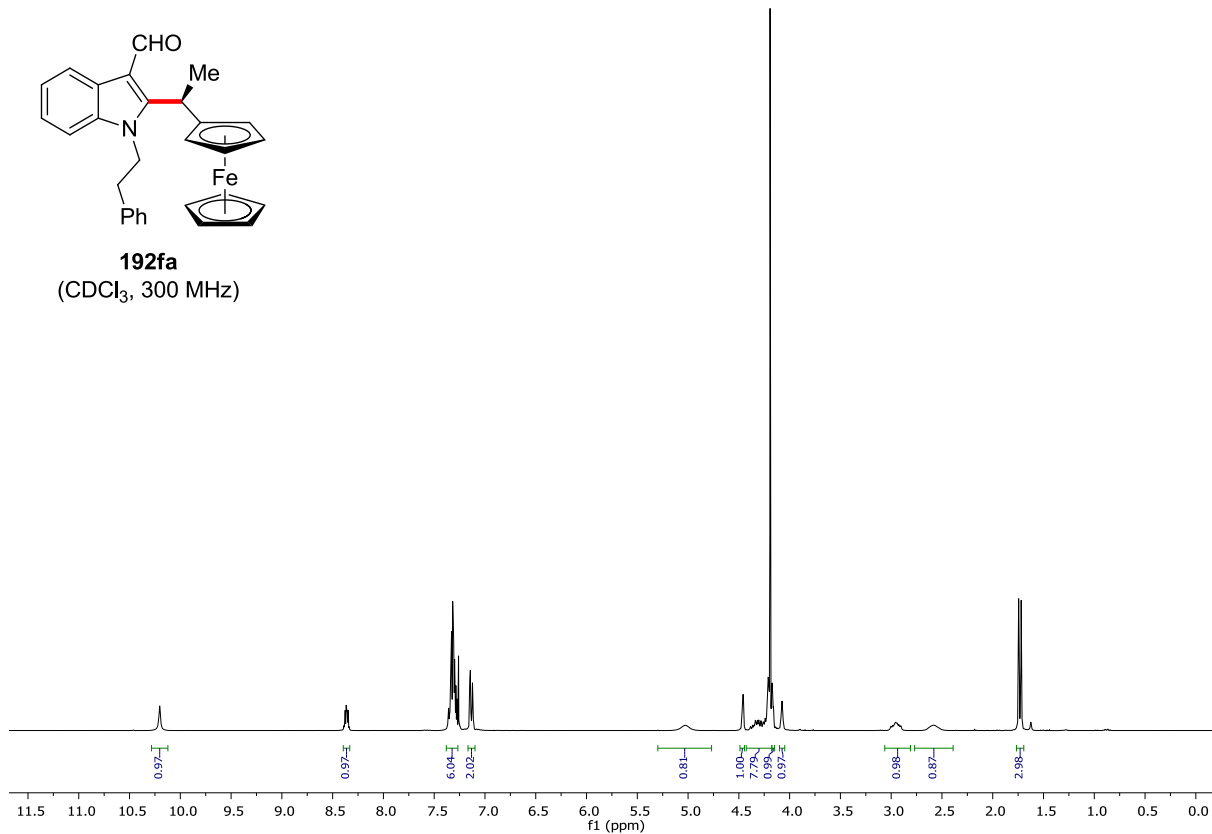
| Peak # | RetTime [min] | Type | Width [min] | Area [mAU*s] | Height [mAU] | Area % |
|--------|---------------|------|-------------|--------------|--------------|---------|
| 1 | 18.896 | MF | 0.3643 | 8131.04492 | 372.02515 | 50.2015 |
| 2 | 21.914 | MF | 0.4424 | 8065.77539 | 303.83292 | 49.7985 |



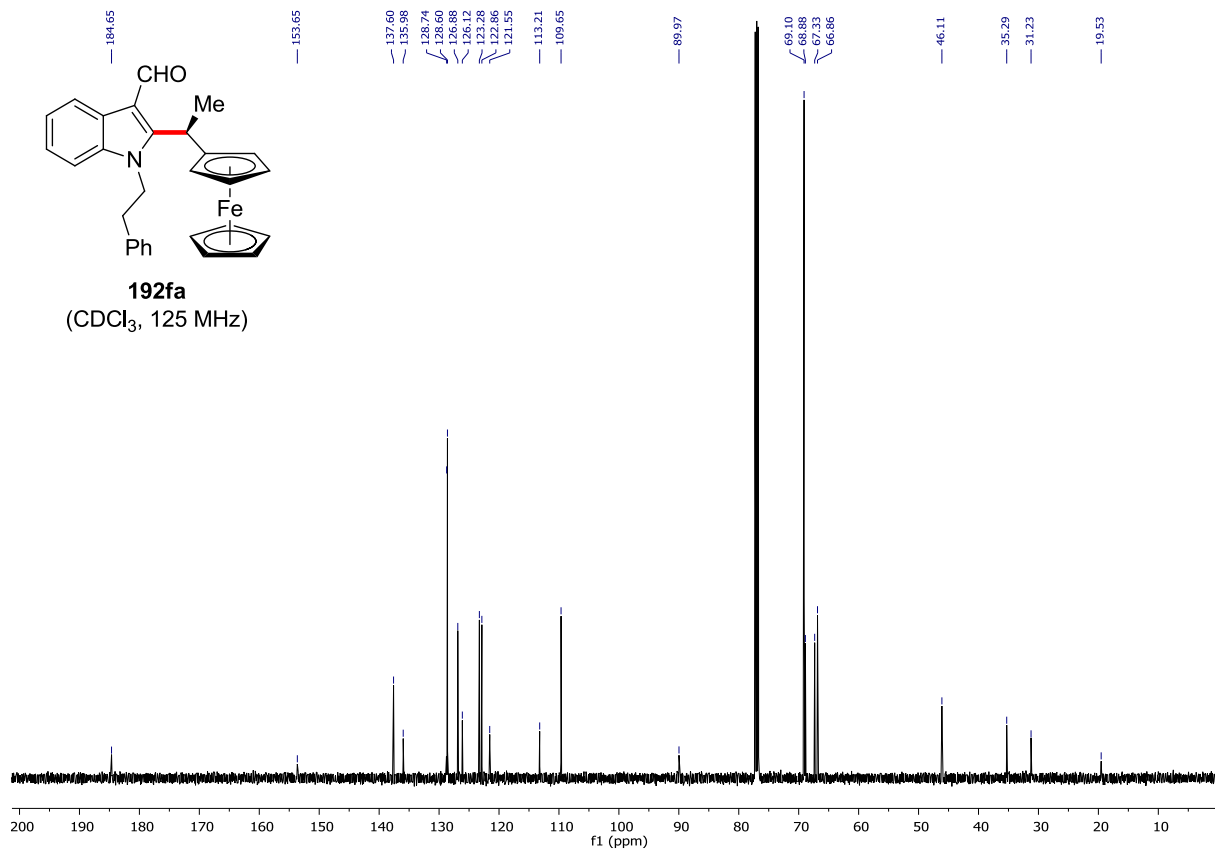
| Peak # | RetTime [min] | Type | Width [min] | Area [mAU*s] | Height [mAU] | Area % |
|--------|---------------|------|-------------|--------------|--------------|---------|
| 1 | 19.192 | MF | 0.3766 | 607.13715 | 26.86999 | 4.5496 |
| 2 | 22.441 | MF | 0.4618 | 1.27379e4 | 459.72525 | 95.4504 |



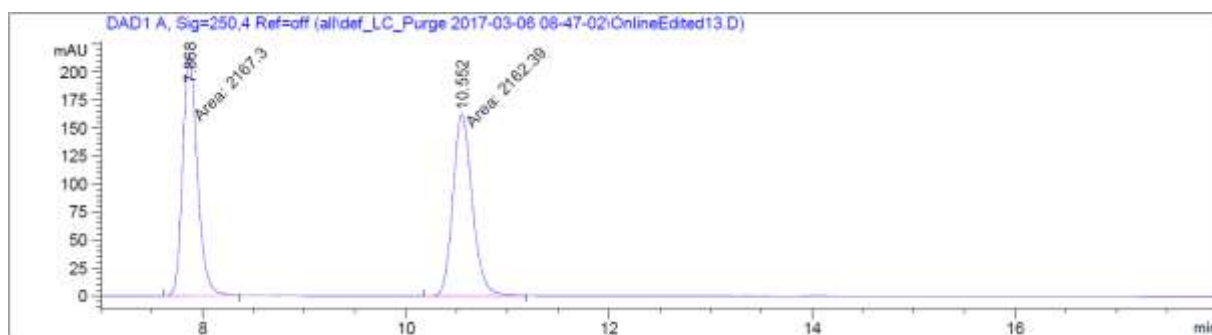
192fa
(CDCl₃, 300 MHz)



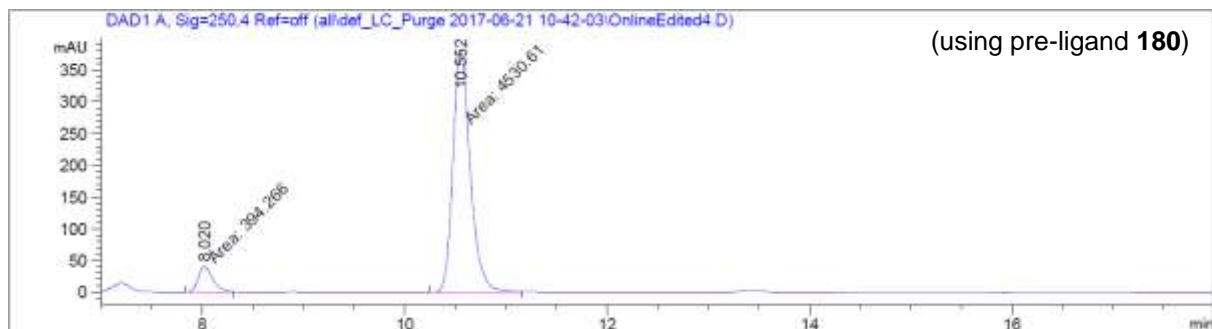
192fa
(CDCl₃, 125 MHz)



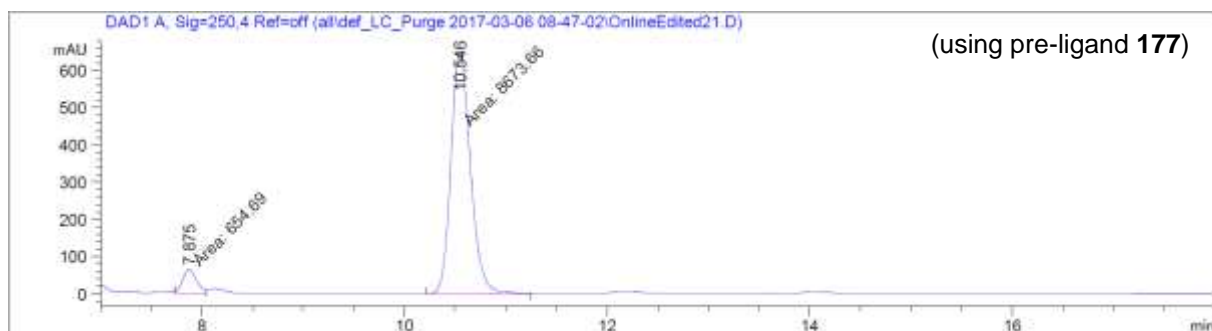
Chiral HPLC of **192fa**:



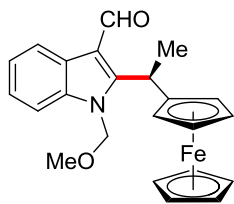
| Peak # | RetTime [min] | Type | Width [min] | Area [mAU*s] | Height [mAU] | Area % |
|--------|---------------|------|-------------|--------------|--------------|---------|
| 1 | 7.868 | MF | 0.1673 | 2167.29688 | 215.86284 | 50.0566 |
| 2 | 10.552 | MF | 0.2223 | 2162.39429 | 162.14938 | 49.9434 |



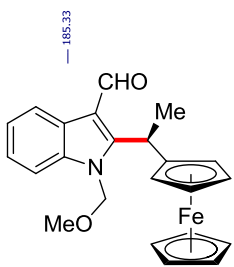
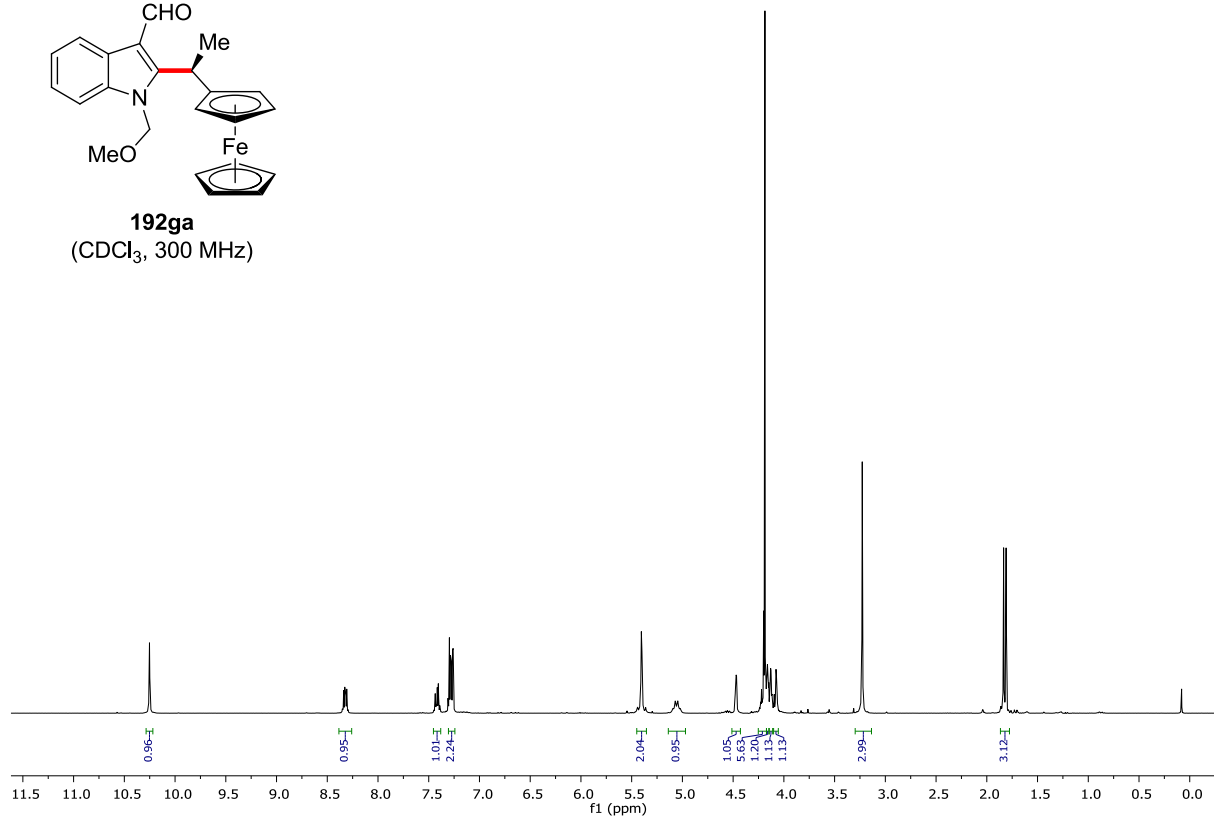
| Peak # | RetTime [min] | Type | Width [min] | Area [mAU*s] | Height [mAU] | Area % |
|--------|---------------|------|-------------|--------------|--------------|---------|
| 1 | 8.020 | MF | 0.1646 | 394.26550 | 39.91424 | 8.0056 |
| 2 | 10.552 | MF | 0.1982 | 4530.60693 | 381.06073 | 91.9944 |



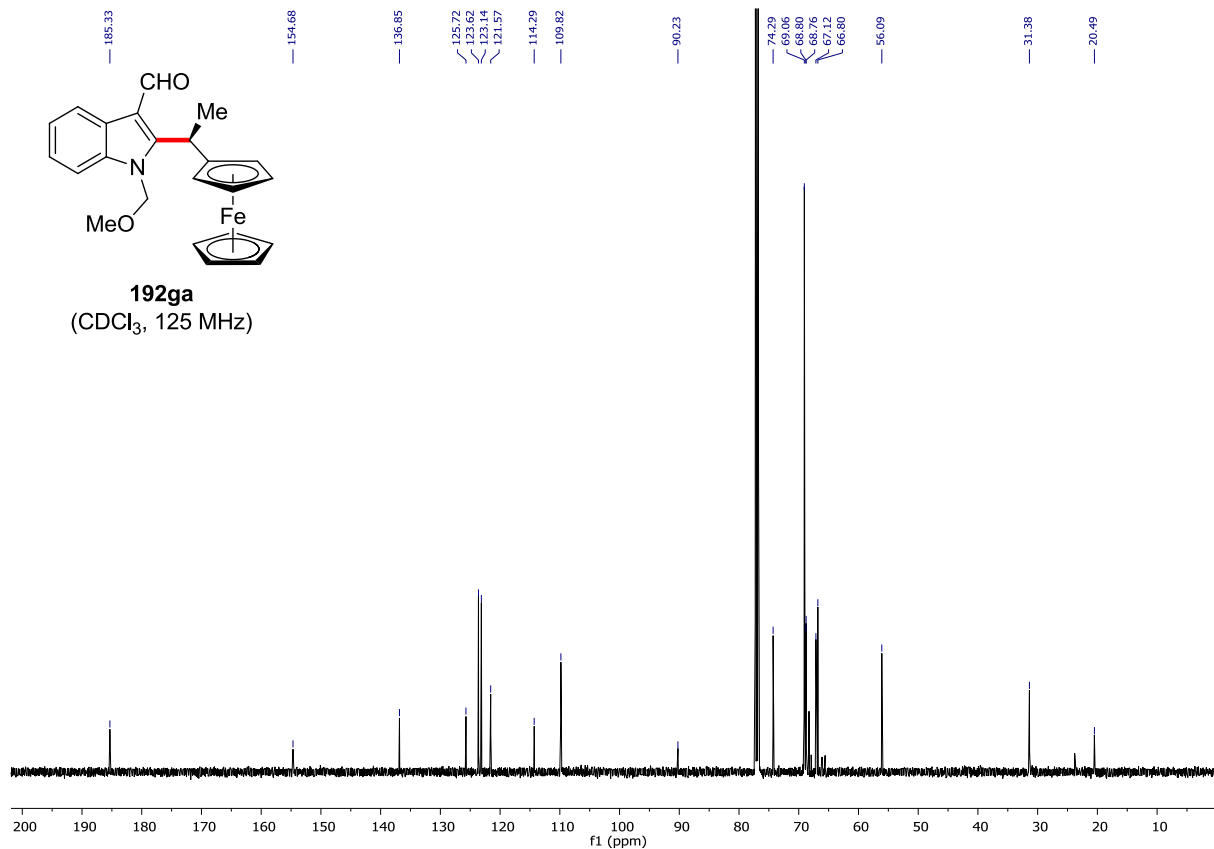
| Peak # | RetTime [min] | Type | Width [min] | Area [mAU*s] | Height [mAU] | Area % |
|--------|---------------|------|-------------|--------------|--------------|---------|
| 1 | 7.875 | MF | 0.1667 | 654.68970 | 65.43720 | 7.0183 |
| 2 | 10.546 | FM | 0.2229 | 8673.66016 | 648.41223 | 92.9817 |



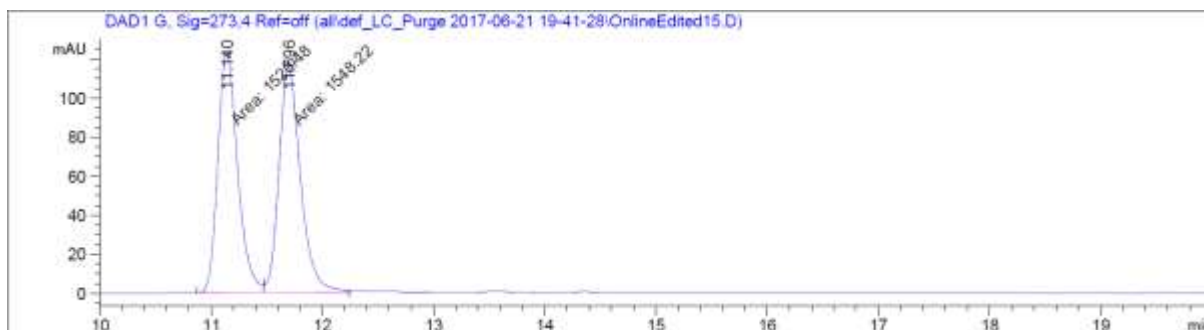
192ga
(CDCl₃, 300 MHz)



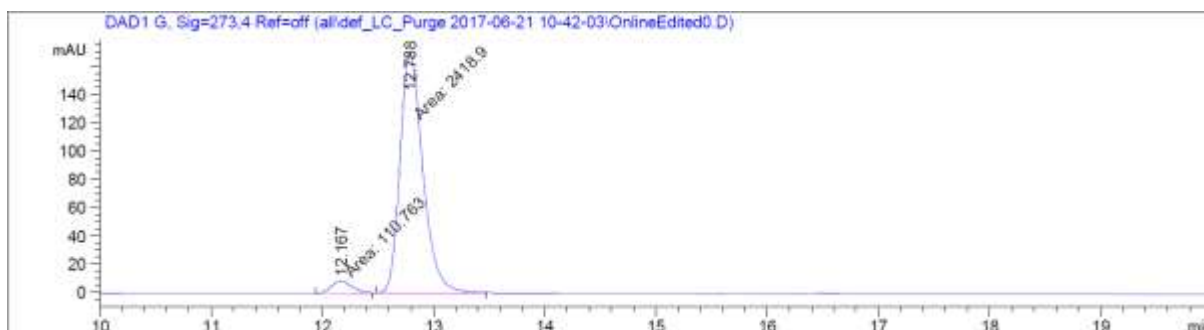
192ga
(CDCl₃, 125 MHz)



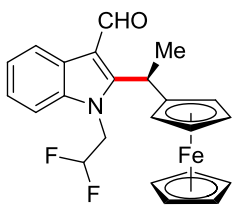
Chiral HPLC of **192ga**:



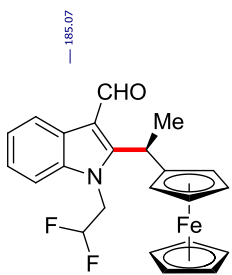
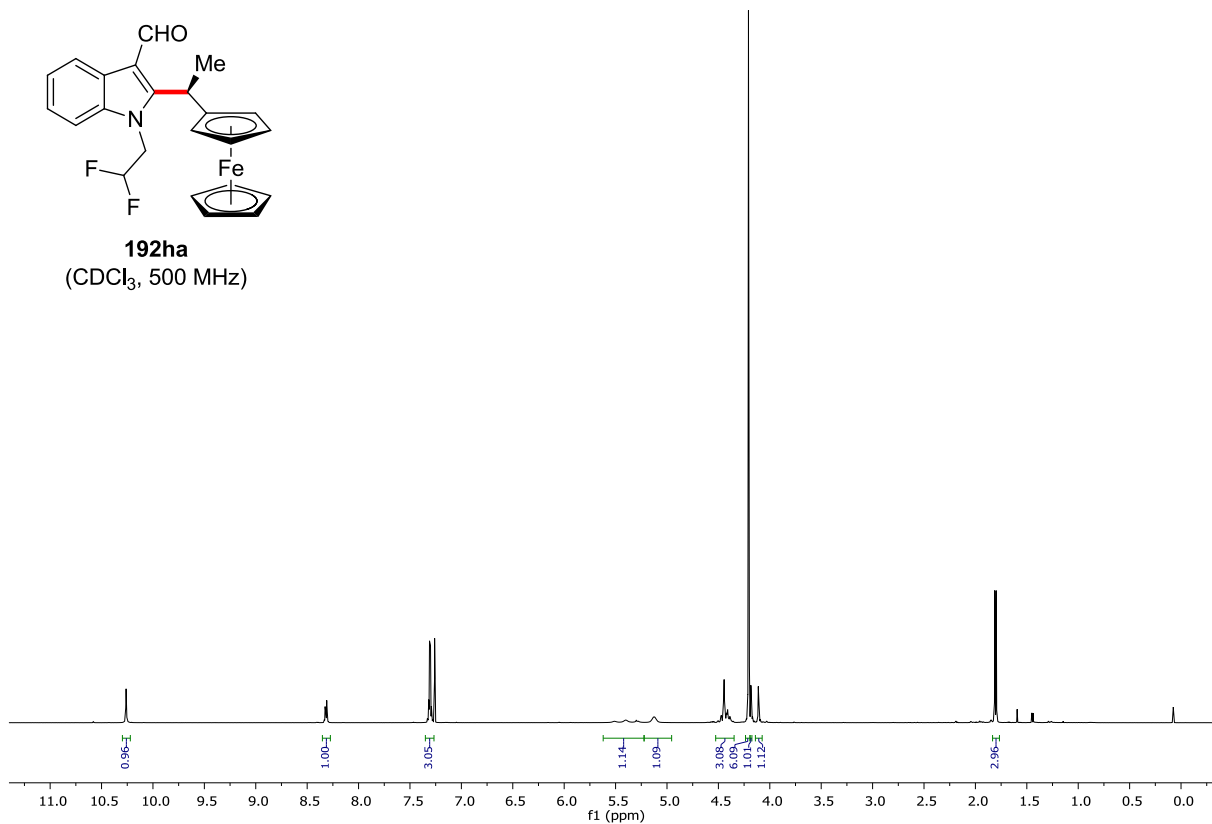
| Peak # | RetTime [min] | Type | Width [min] | Area [mAU*s] | Height [mAU] | Area % |
|--------|---------------|------|-------------|--------------|--------------|---------|
| 1 | 11.140 | FM | 0.2053 | 1520.48035 | 123.44520 | 49.5479 |
| 2 | 11.696 | MF | 0.2239 | 1548.22461 | 115.26640 | 50.4521 |



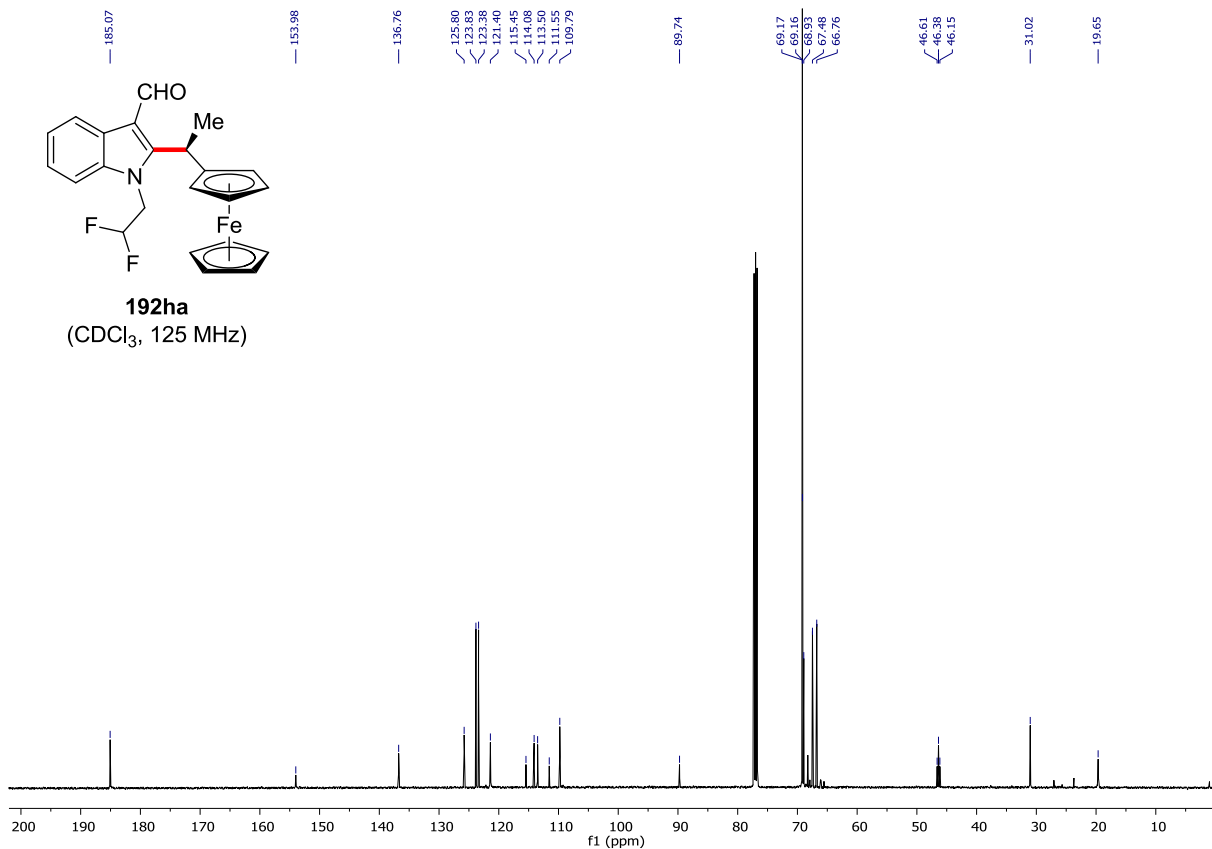
| Peak # | RetTime [min] | Type | Width [min] | Area [mAU*s] | Height [mAU] | Area % |
|--------|---------------|------|-------------|--------------|--------------|---------|
| 1 | 12.167 | FM | 0.2126 | 110.76287 | 8.68283 | 4.3786 |
| 2 | 12.788 | MF | 0.2373 | 2418.90063 | 169.87854 | 95.6214 |

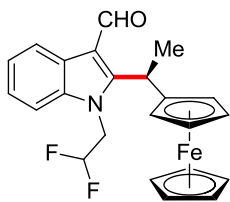


192ha
(CDCl₃, 500 MHz)

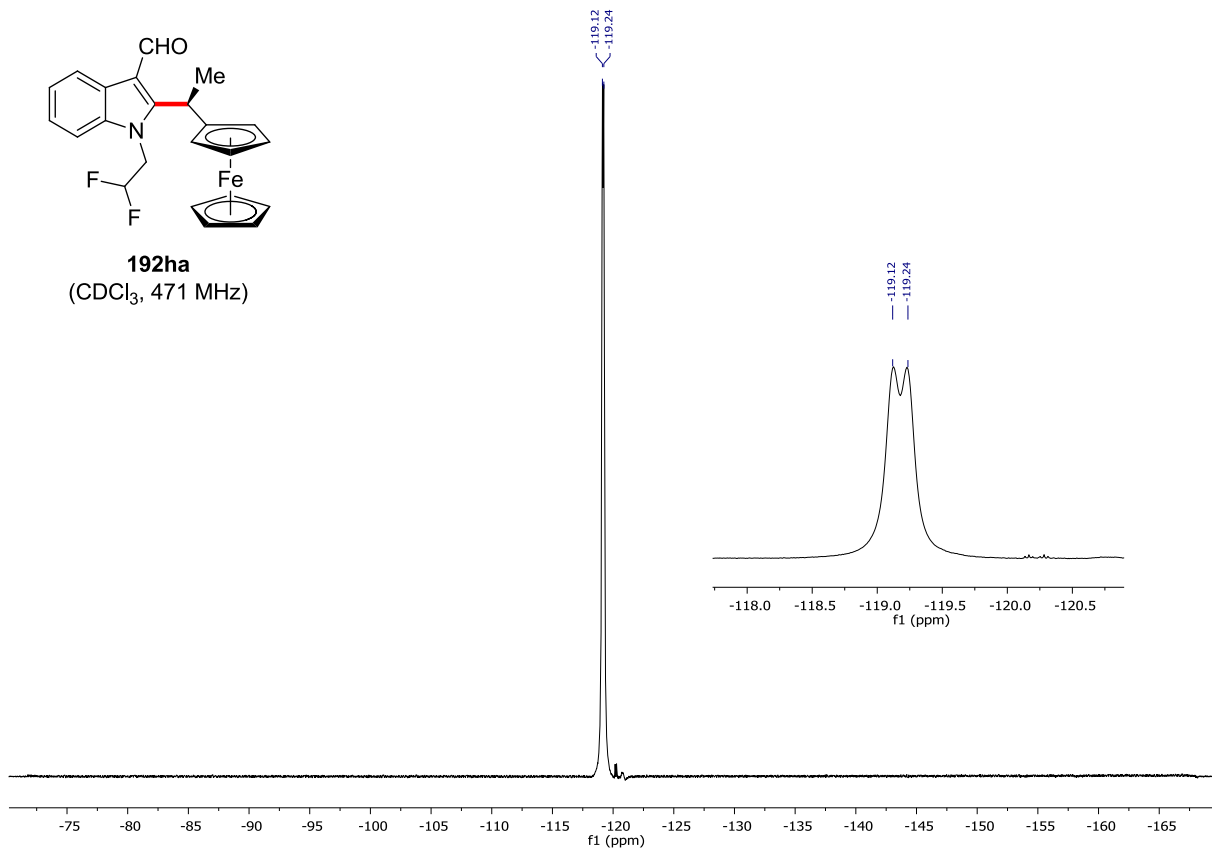


192ha
(CDCl₃, 125 MHz)

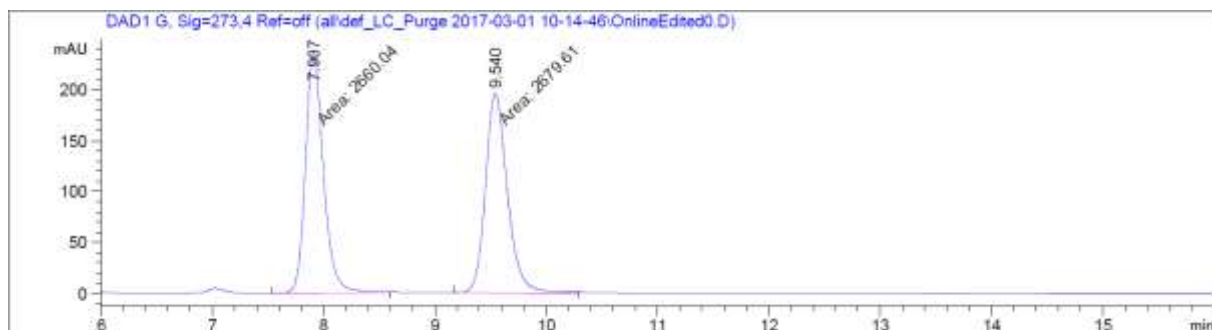




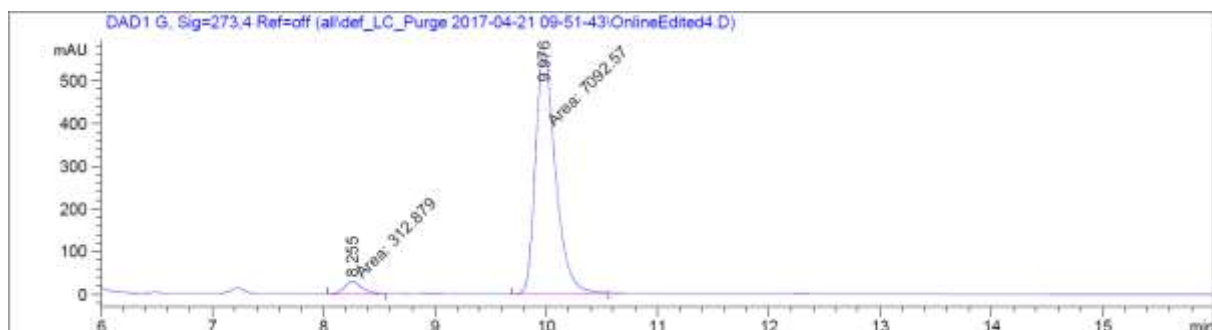
192ha
(CDCl₃, 471 MHz)



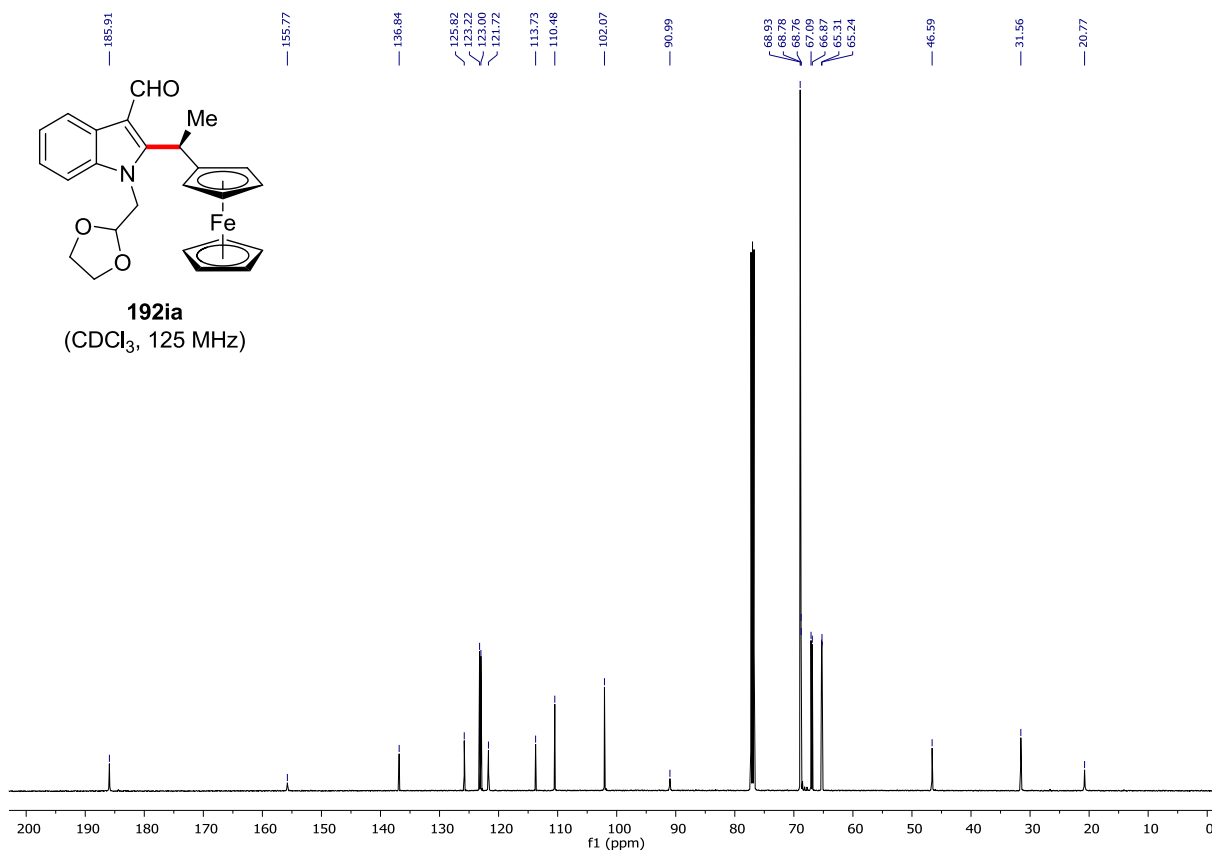
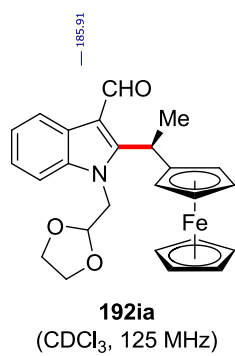
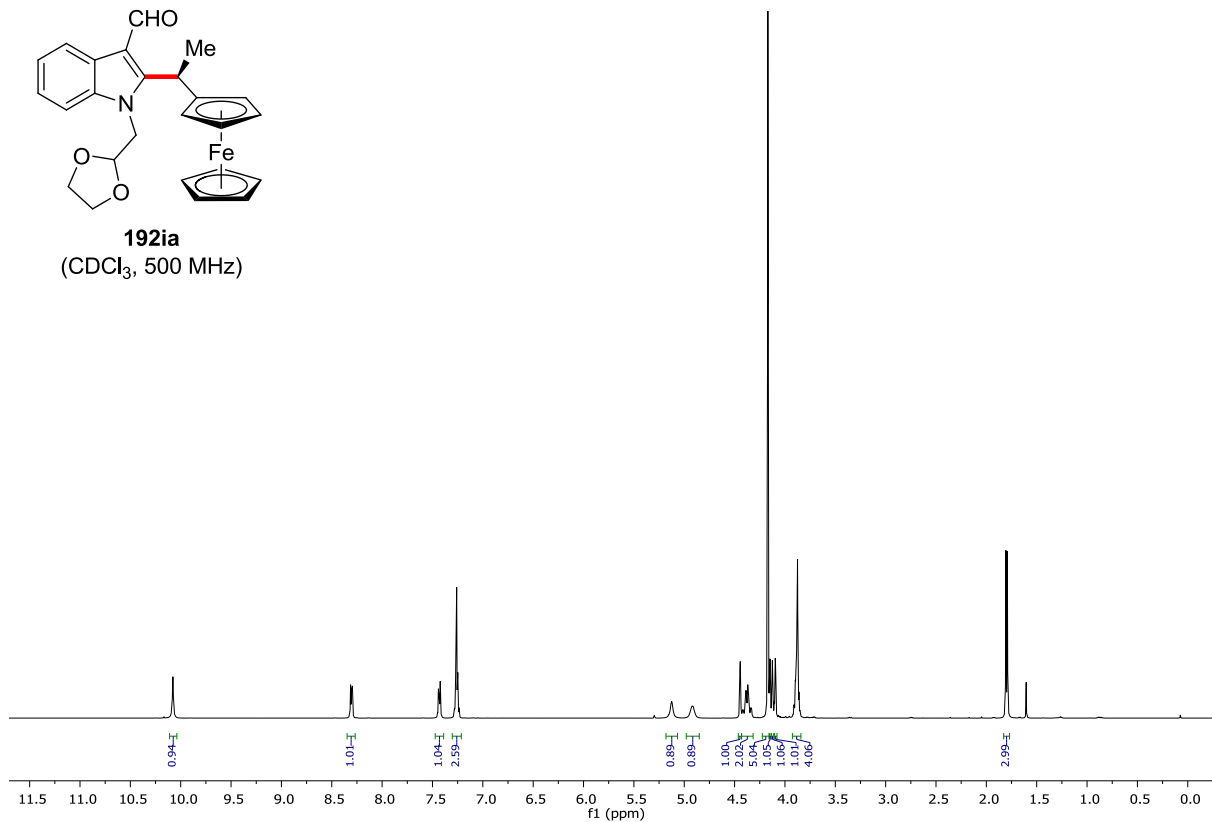
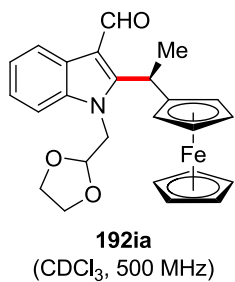
Chiral HPLC of **192ha**:



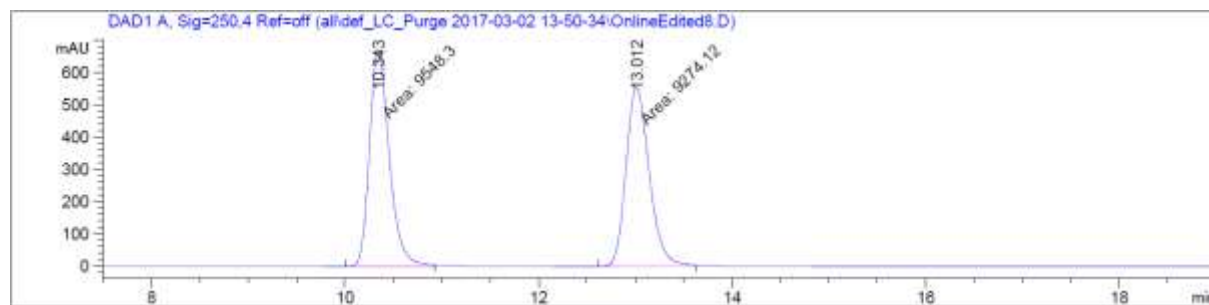
| Peak # | RetTime [min] | Type | Width [min] | Area [mAU*s] | Height [mAU] | Area % |
|--------|---------------|------|-------------|--------------|--------------|---------|
| 1 | 7.907 | MF | 0.1872 | 2660.03979 | 236.80971 | 49.8168 |
| 2 | 9.540 | MF | 0.2278 | 2679.60938 | 196.05734 | 50.1832 |



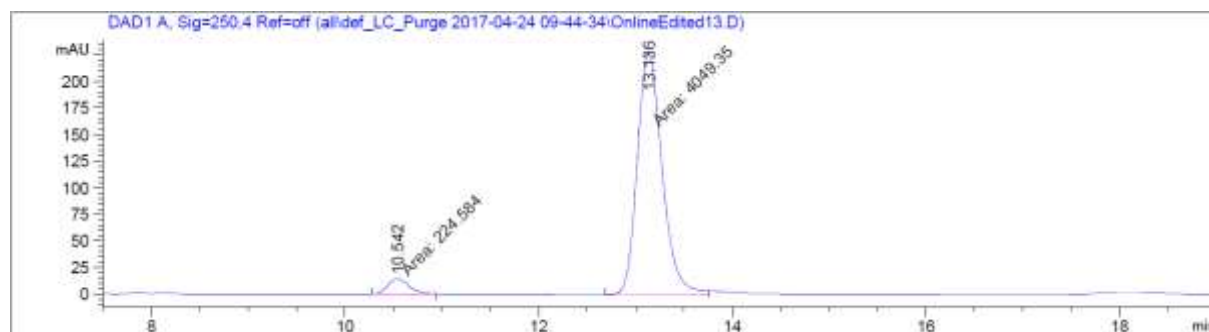
| Peak # | RetTime [min] | Type | Width [min] | Area [mAU*s] | Height [mAU] | Area % |
|--------|---------------|------|-------------|--------------|--------------|---------|
| 1 | 8.255 | FM | 0.1830 | 312.87869 | 28.49584 | 4.2250 |
| 2 | 9.976 | FM | 0.2093 | 7092.56982 | 564.91663 | 95.7750 |



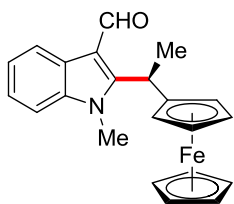
Chiral HPLC of **192ia**:



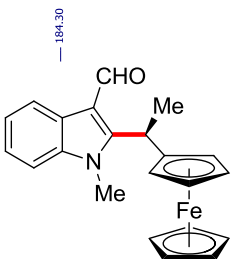
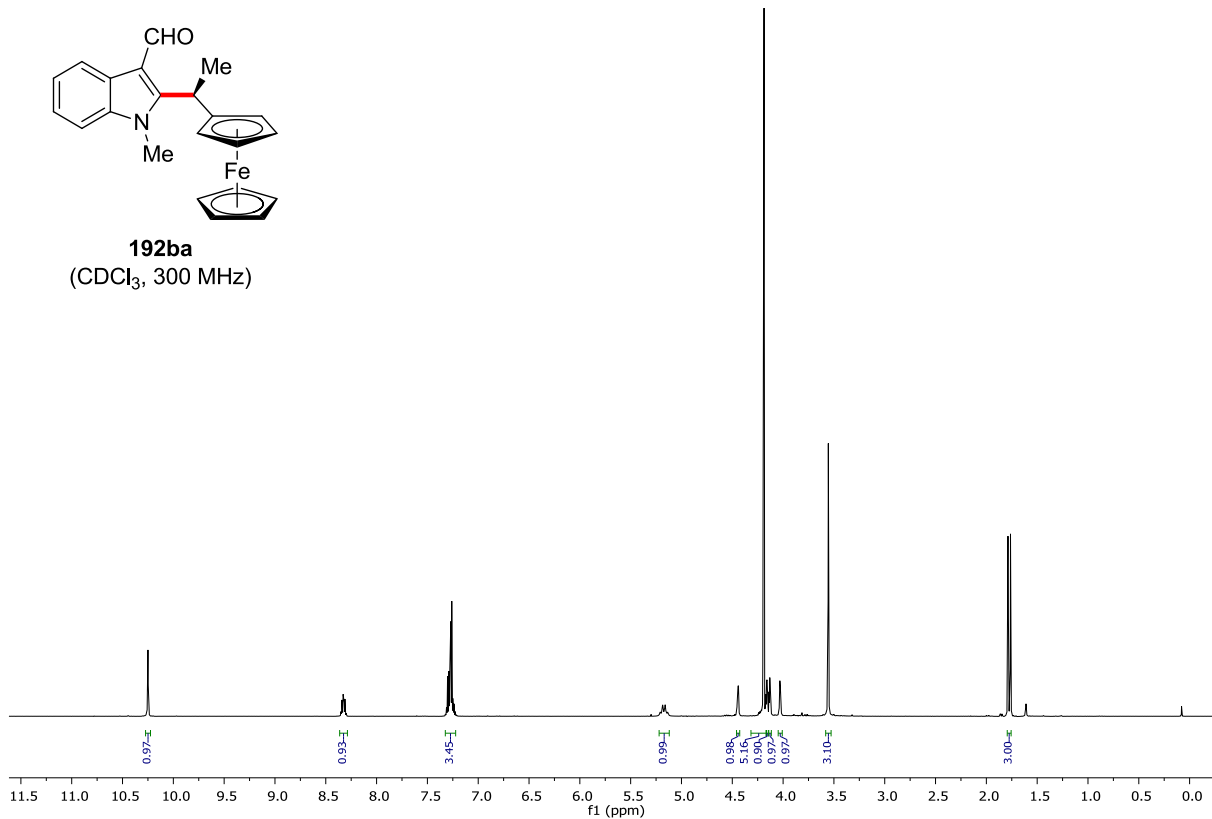
| Peak # | RetTime [min] | Type | Width [min] | Area [mAU*s] | Height [mAU] | Area % |
|--------|---------------|------|-------------|--------------|--------------|---------|
| 1 | 10.343 | MF | 0.2373 | 9548.29785 | 670.53973 | 50.7283 |
| 2 | 13.012 | MF | 0.2786 | 9274.12305 | 554.77954 | 49.2717 |



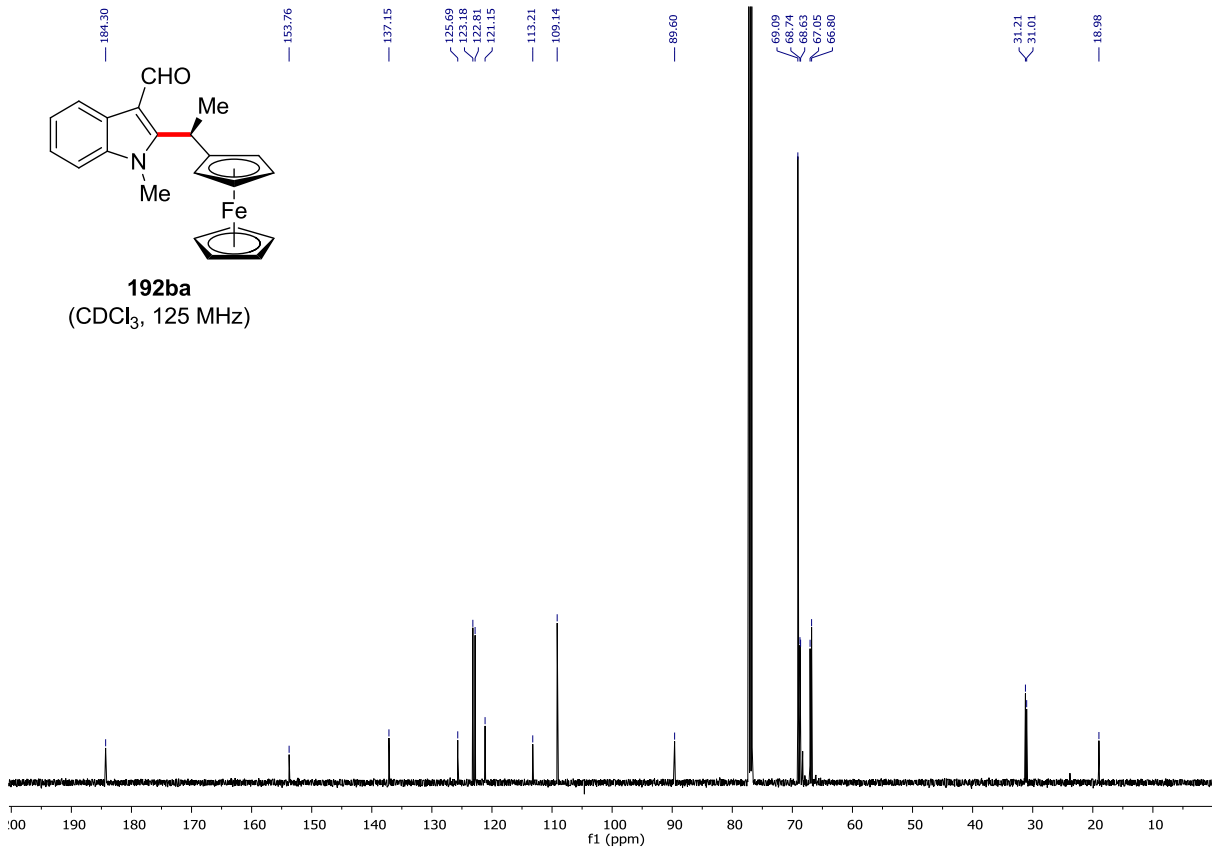
| Peak # | RetTime [min] | Type | Width [min] | Area [mAU*s] | Height [mAU] | Area % |
|--------|---------------|------|-------------|--------------|--------------|---------|
| 1 | 10.542 | MF | 0.2566 | 224.58365 | 14.58731 | 5.2547 |
| 2 | 13.136 | MF | 0.2973 | 4049.35449 | 227.03674 | 94.7453 |



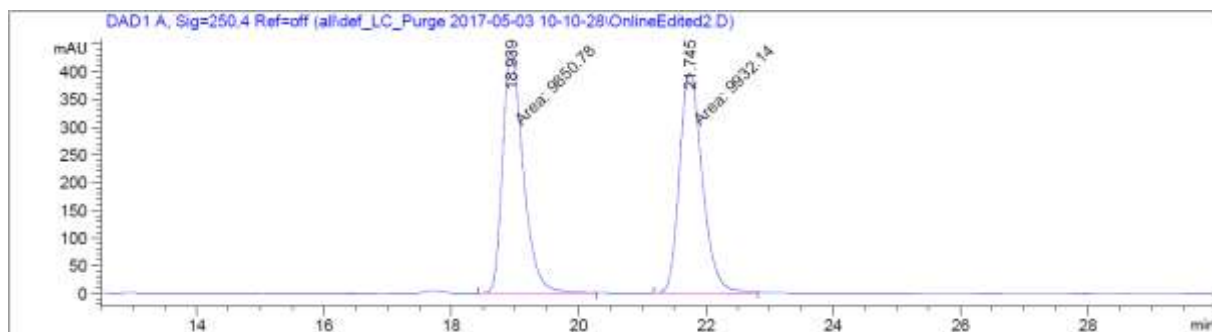
192ba
(CDCl₃, 300 MHz)



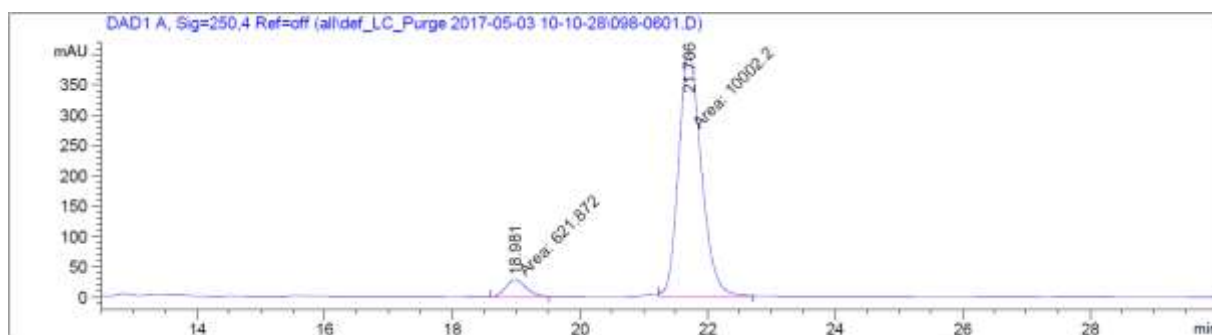
192ba
(CDCl₃, 125 MHz)



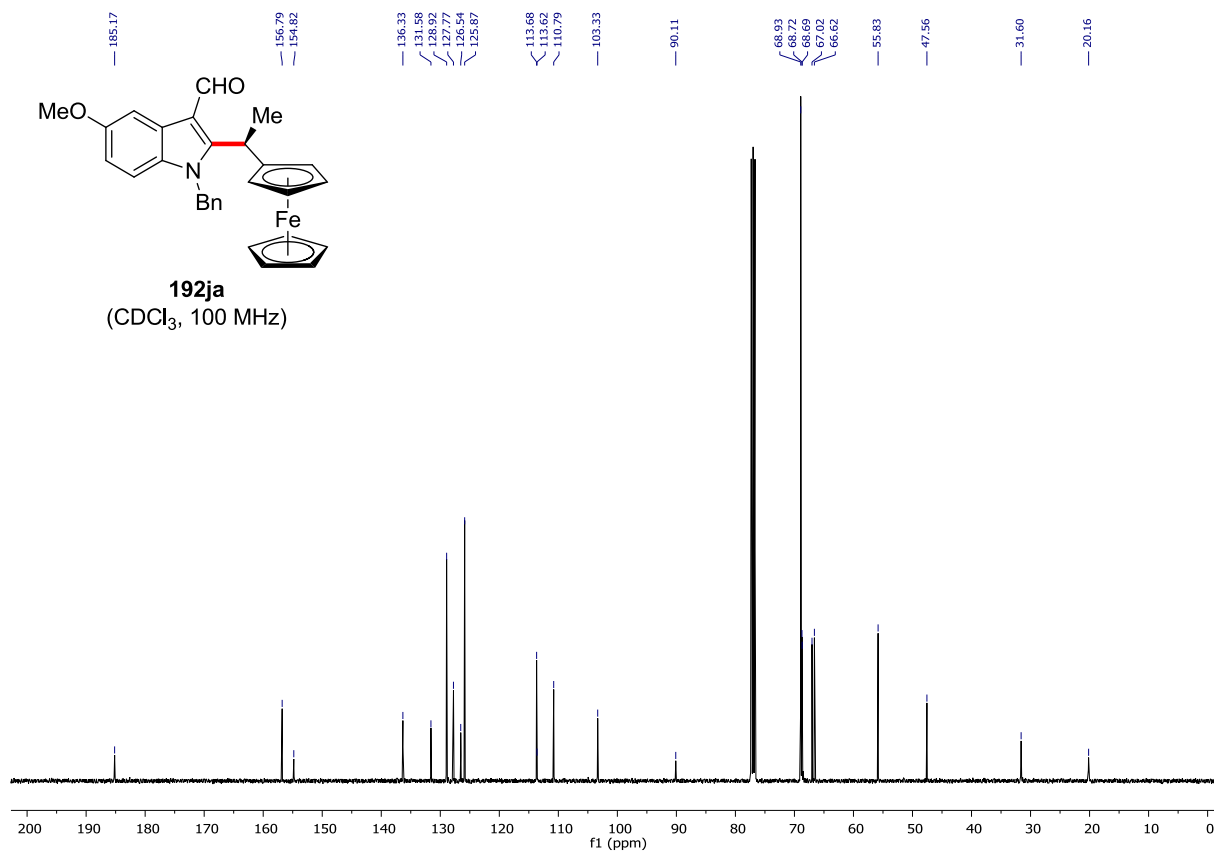
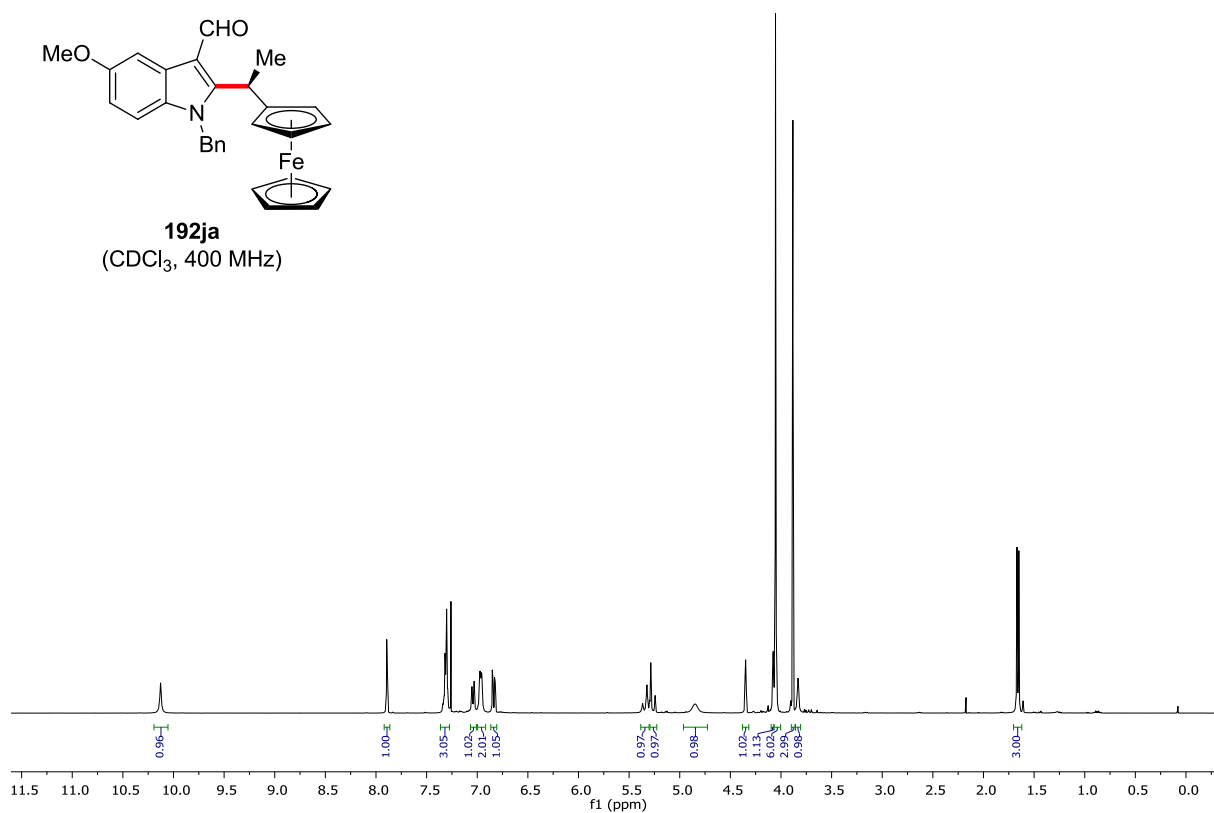
Chiral HPLC of **192ba**:



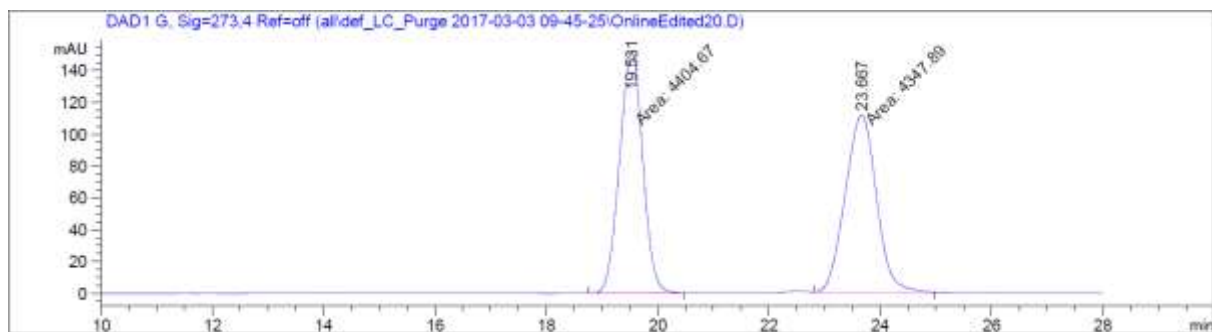
| Peak # | RetTime [min] | Type | Width [min] | Area [mAU*s] | Height [mAU] | Area % |
|--------|---------------|------|-------------|--------------|--------------|---------|
| 1 | 18.939 | MF | 0.3768 | 9850.78125 | 435.72021 | 49.7944 |
| 2 | 21.745 | MF | 0.4166 | 9932.14355 | 397.32584 | 50.2056 |



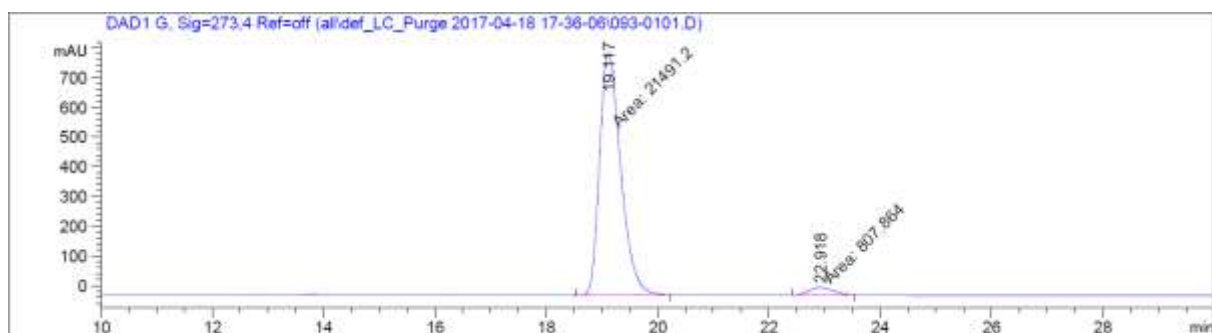
| Peak # | RetTime [min] | Type | Width [min] | Area [mAU*s] | Height [mAU] | Area % |
|--------|---------------|------|-------------|--------------|--------------|---------|
| 1 | 18.981 | MF | 0.3652 | 621.87238 | 28.38209 | 5.8534 |
| 2 | 21.706 | MF | 0.4168 | 1.00022e4 | 399.98477 | 94.1466 |



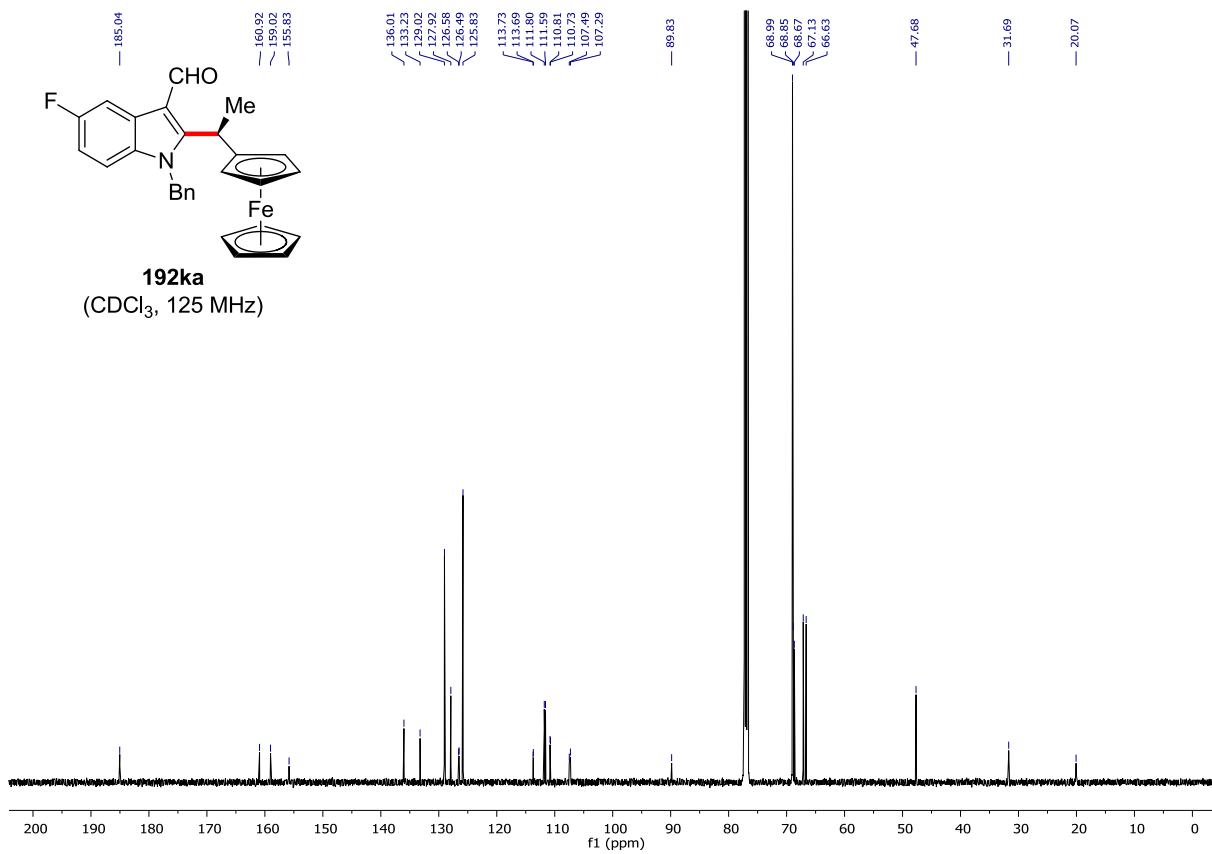
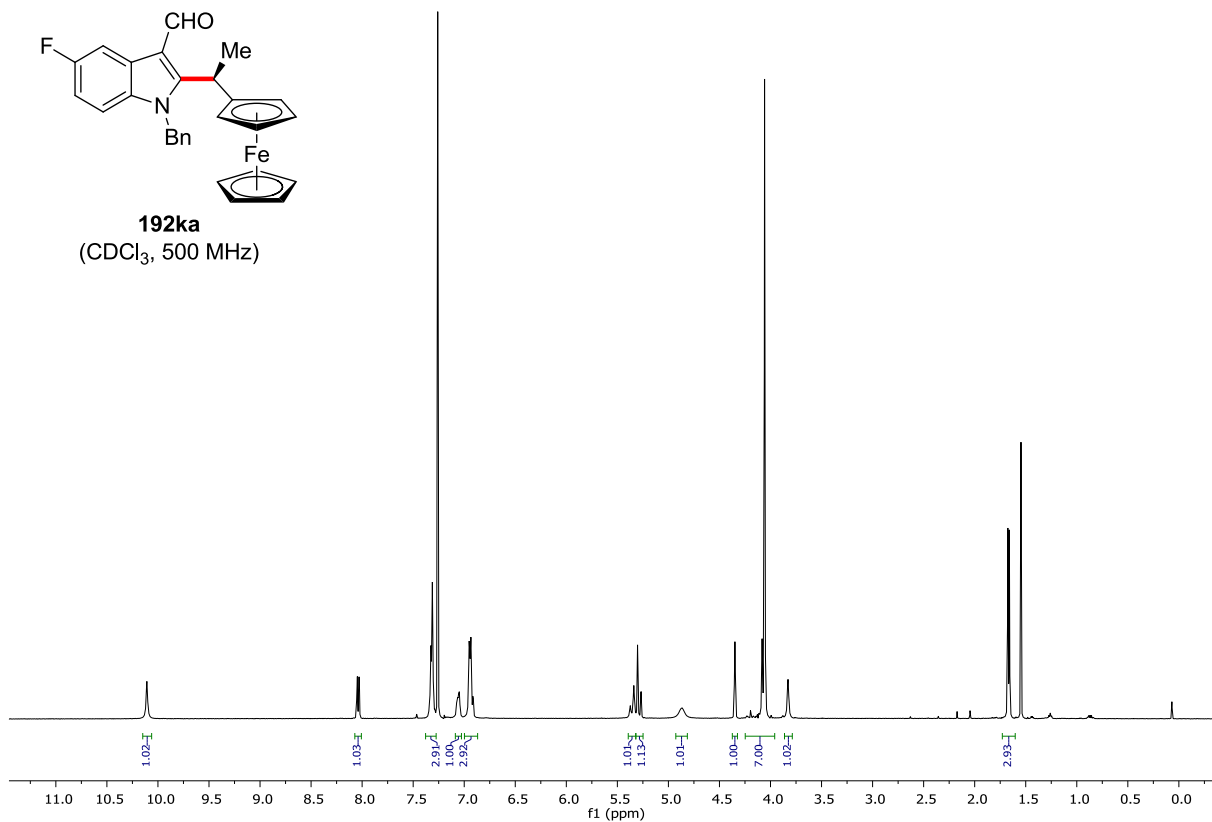
Chiral HPLC of **192ja**:

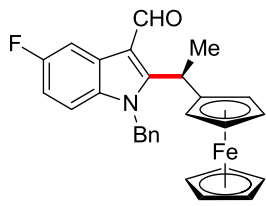


| Peak # | RetTime [min] | Type | Width [min] | Area [mAU*s] | Height [mAU] | Area % |
|--------|---------------|------|-------------|--------------|--------------|---------|
| 1 | 19.531 | MF | 0.4842 | 4404.67285 | 151.59796 | 50.3244 |
| 2 | 23.667 | MF | 0.6506 | 4347.89404 | 111.37720 | 49.6756 |

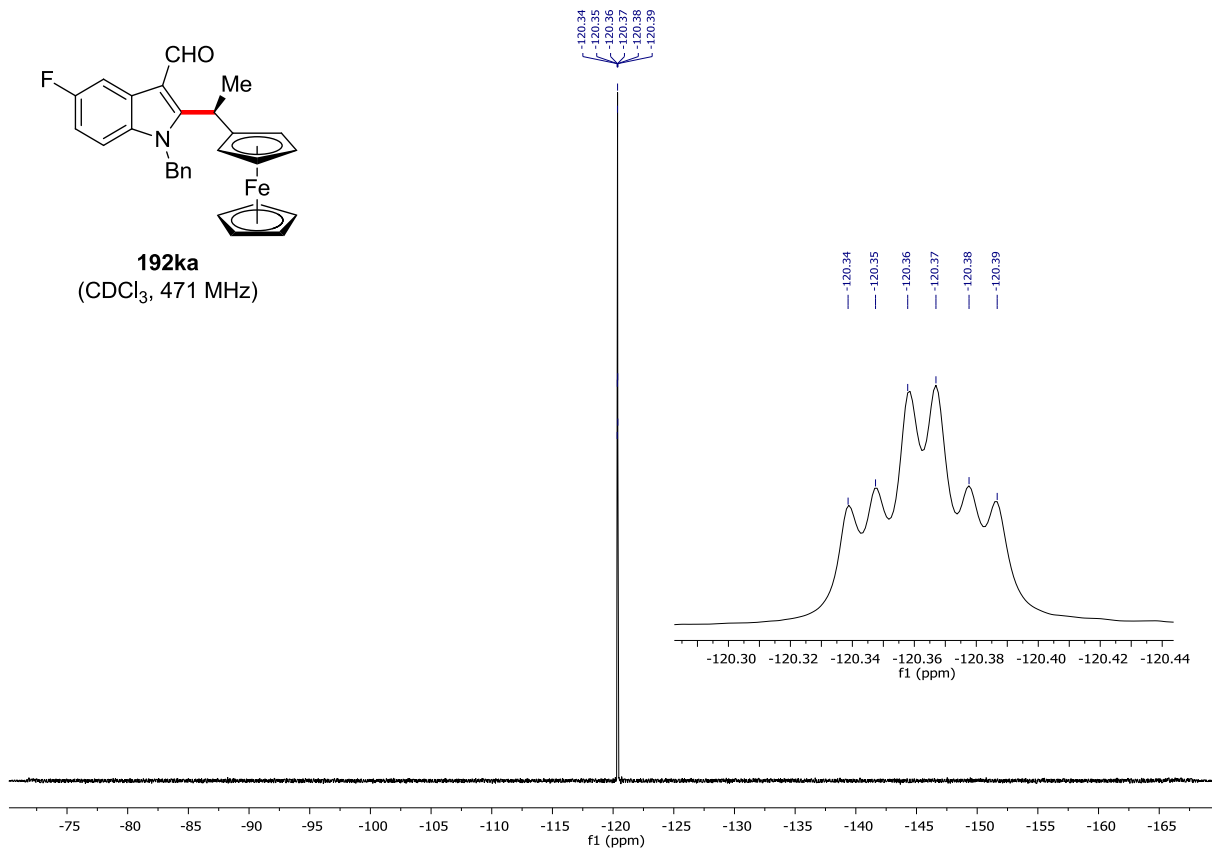


| Peak # | RetTime [min] | Type | Width [min] | Area [mAU*s] | Height [mAU] | Area % |
|--------|---------------|------|-------------|--------------|--------------|---------|
| 1 | 19.117 | MF | 0.4411 | 2.14912e4 | 812.02863 | 96.3771 |
| 2 | 22.918 | MF | 0.5198 | 807.86353 | 25.90467 | 3.6229 |

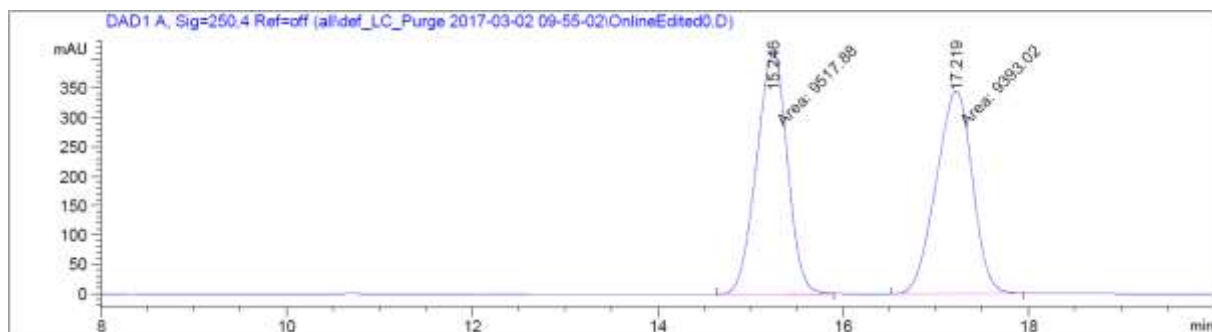




192ka
(CDCl₃, 471 MHz)



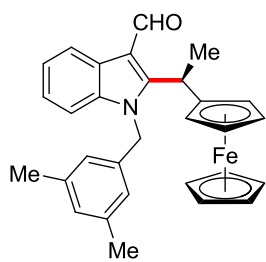
Chiral HPLC of **192ka**:



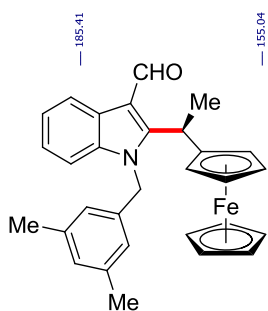
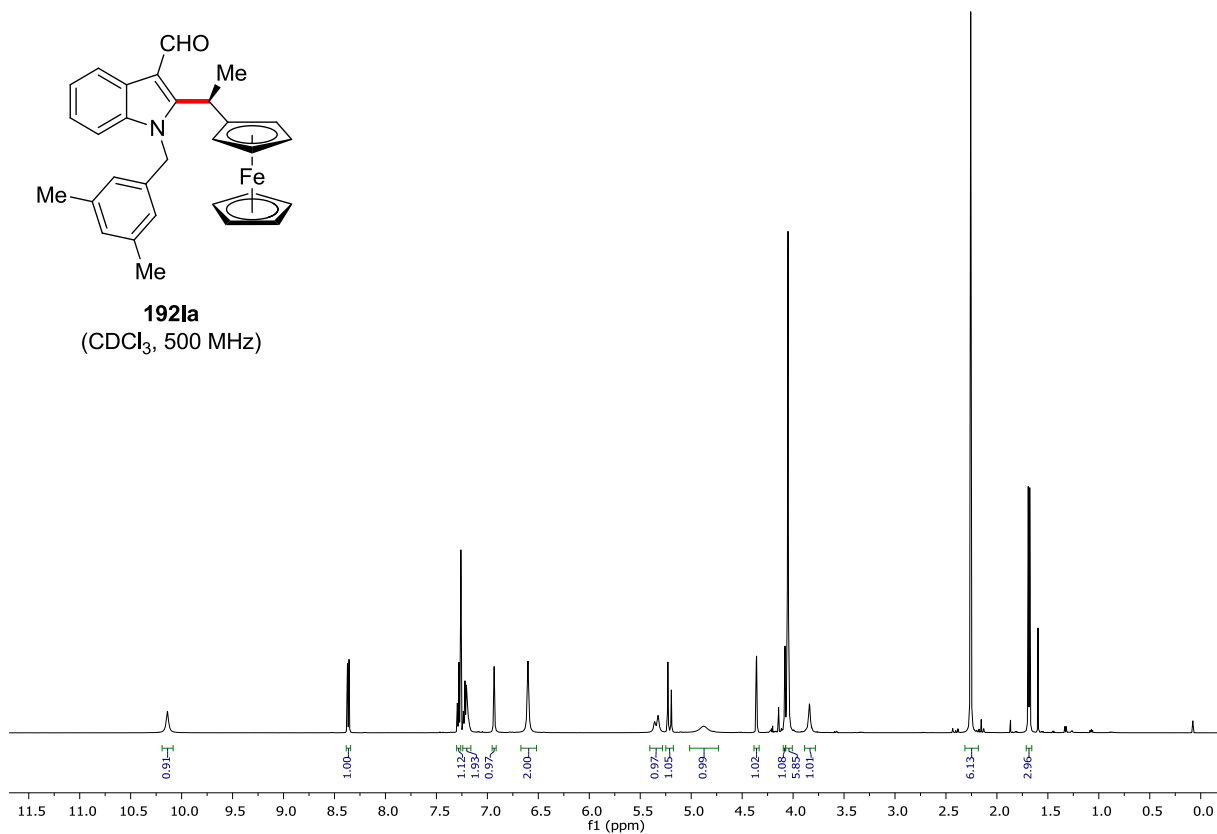
| Peak # | RetTime [min] | Type | Width [min] | Area [mAU*s] | Height [mAU] | Area % |
|--------|---------------|------|-------------|--------------|--------------|---------|
| 1 | 15.246 | MF | 0.3847 | 9517.87500 | 412.32162 | 50.3301 |
| 2 | 17.219 | MF | 0.4532 | 9393.02051 | 345.46524 | 49.6699 |



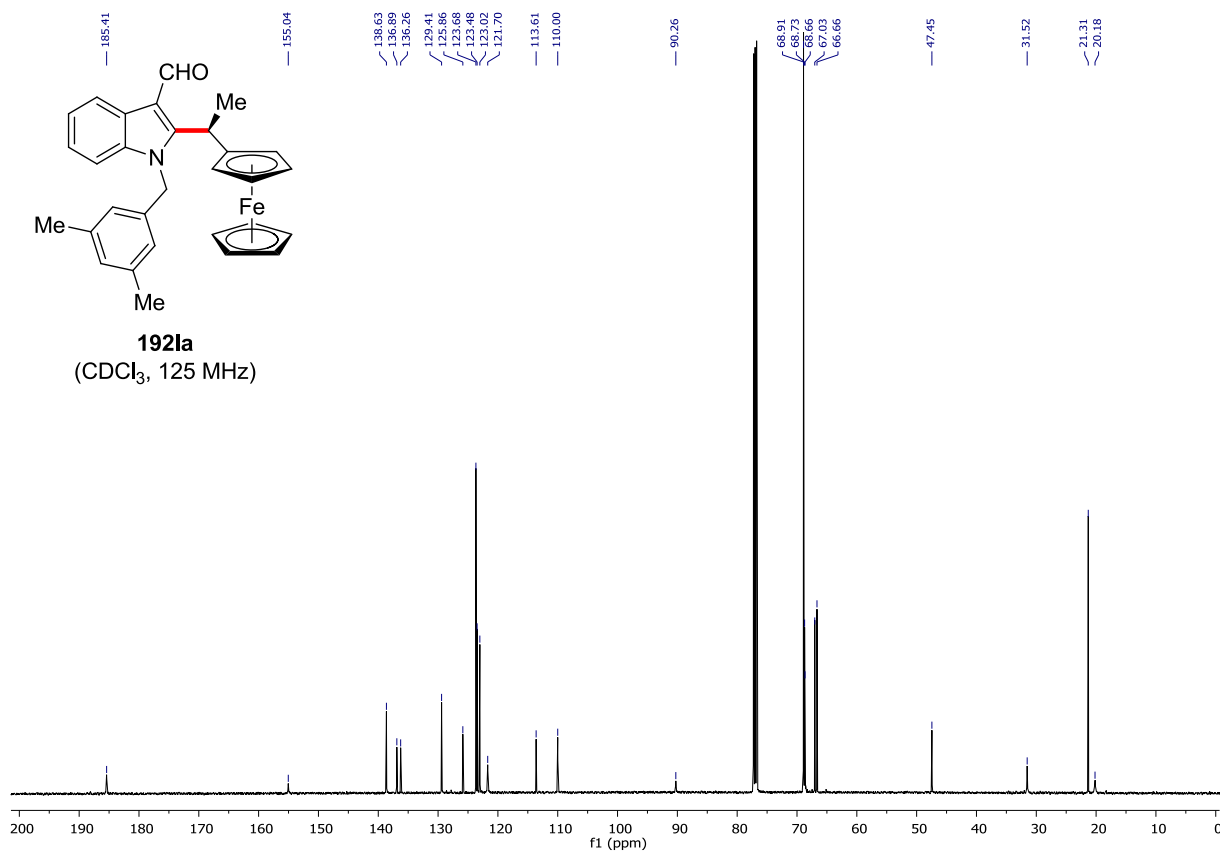
| Peak # | RetTime [min] | Type | Width [min] | Area [mAU*s] | Height [mAU] | Area % |
|--------|---------------|------|-------------|--------------|--------------|---------|
| 1 | 15.659 | MM | 0.3193 | 6876.88623 | 358.93790 | 95.1582 |
| 2 | 17.528 | MM | 0.3526 | 349.90988 | 16.54176 | 4.8418 |



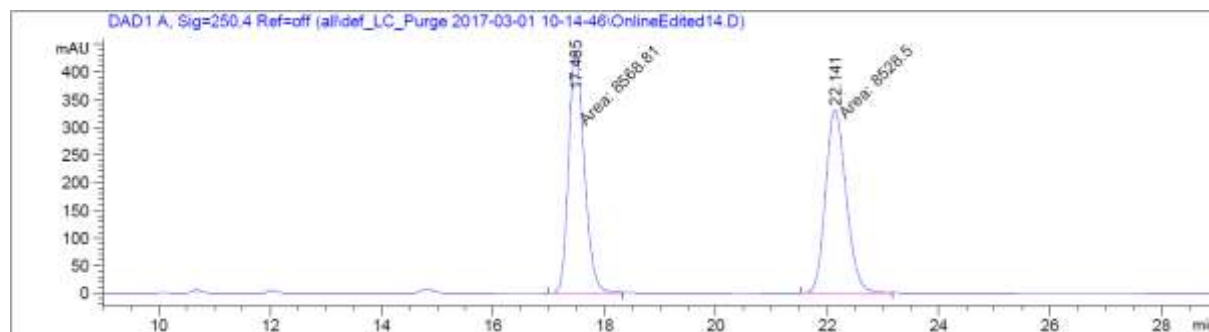
192la
(CDCl₃, 500 MHz)



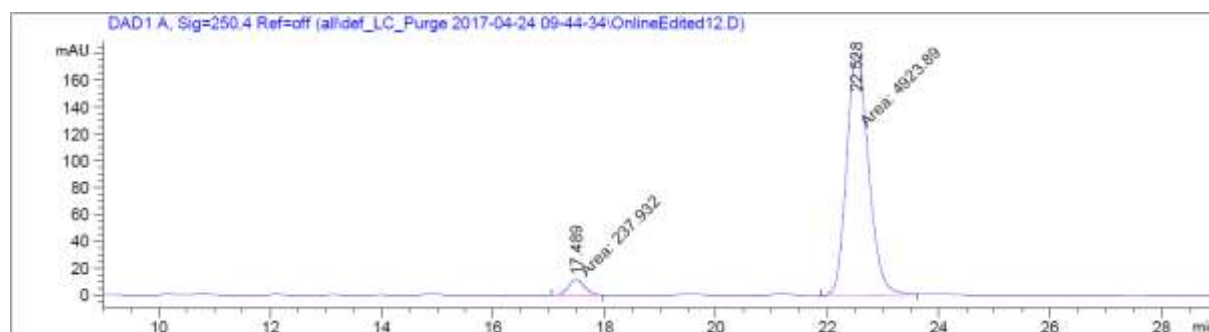
192la
(CDCl₃, 125 MHz)



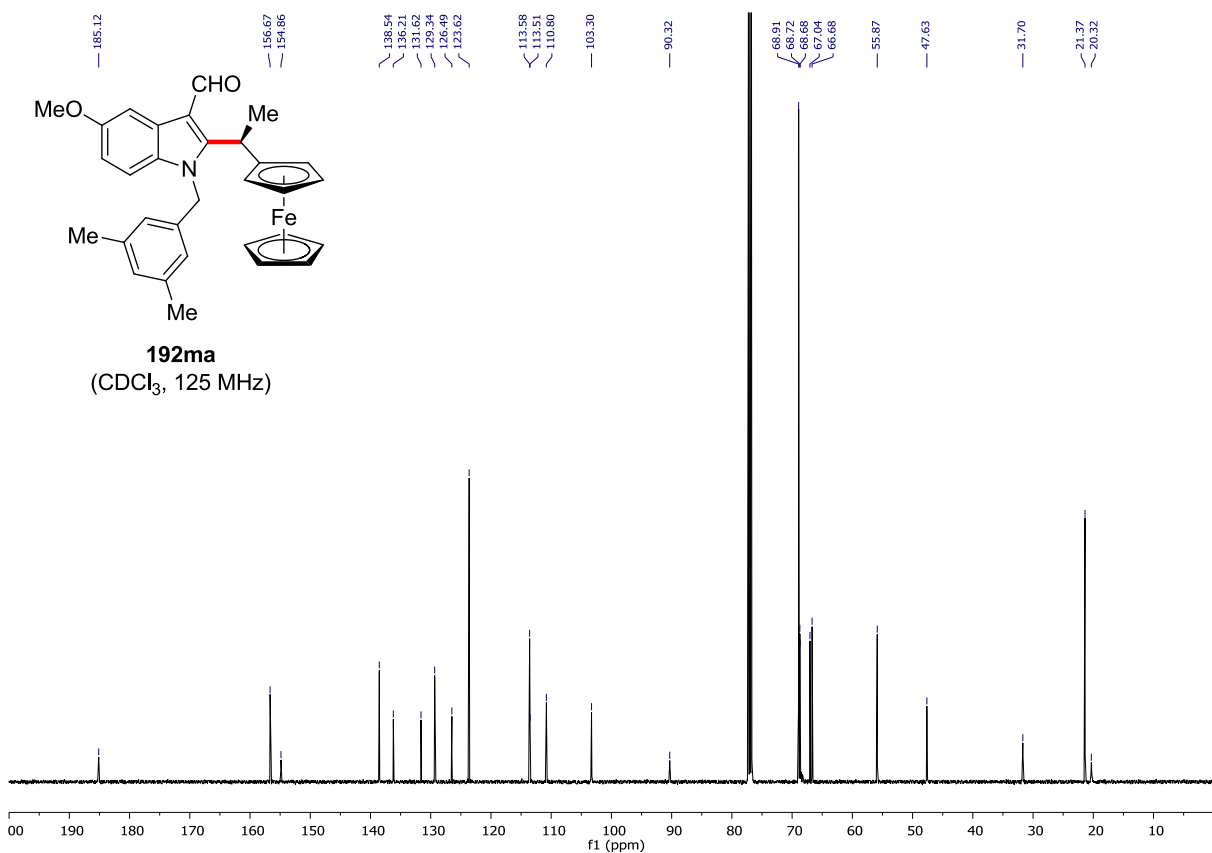
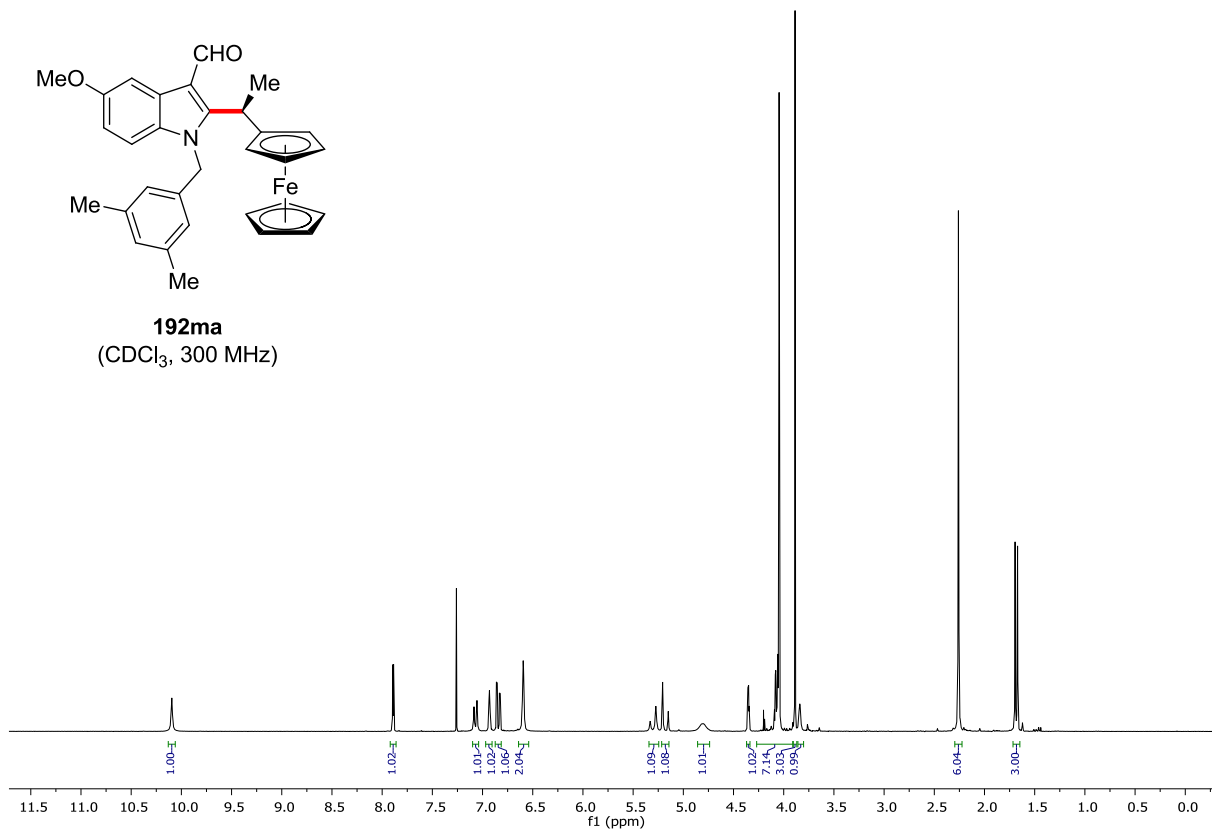
Chiral HPLC of **192Ia**:



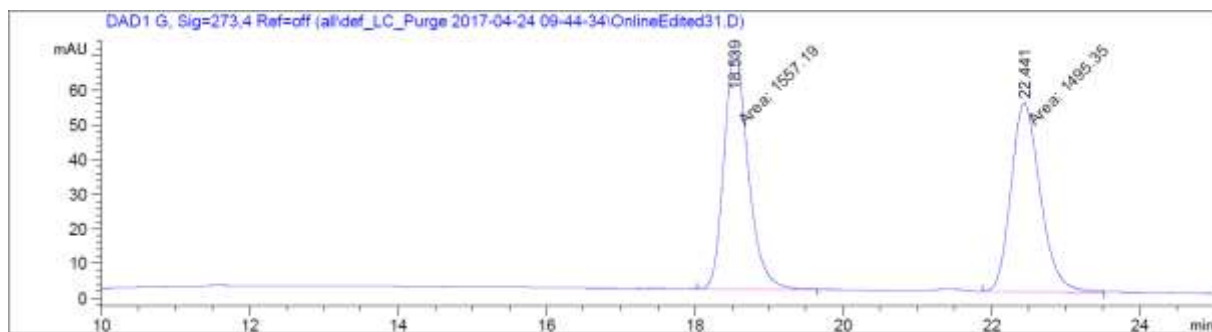
| Peak # | RetTime [min] | Type | Width [min] | Area [mAU*s] | Height [mAU] | Area % |
|--------|---------------|------|-------------|--------------|--------------|---------|
| 1 | 17.485 | FM | 0.3271 | 8568.80957 | 436.64896 | 50.1179 |
| 2 | 22.141 | MF | 0.4299 | 8528.50195 | 330.61792 | 49.8821 |



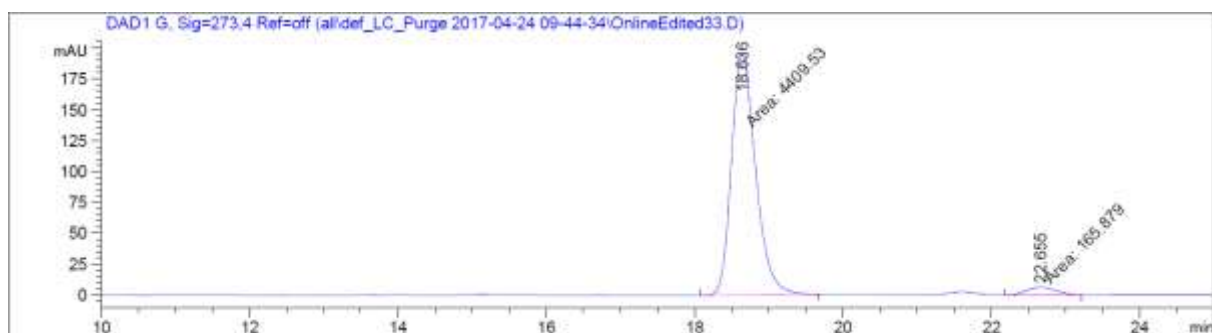
| Peak # | RetTime [min] | Type | Width [min] | Area [mAU*s] | Height [mAU] | Area % |
|--------|---------------|------|-------------|--------------|--------------|---------|
| 1 | 17.489 | MF | 0.3421 | 237.93228 | 11.59064 | 4.6095 |
| 2 | 22.528 | MF | 0.4565 | 4923.88916 | 179.77870 | 95.3905 |



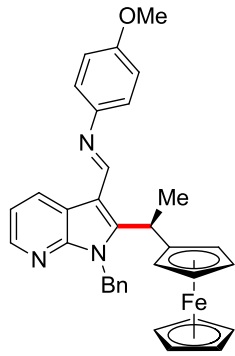
Chiral HPLC of **192ma**:



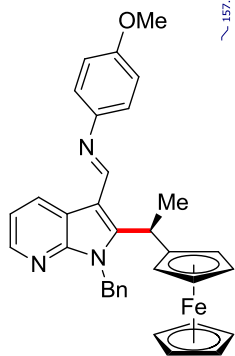
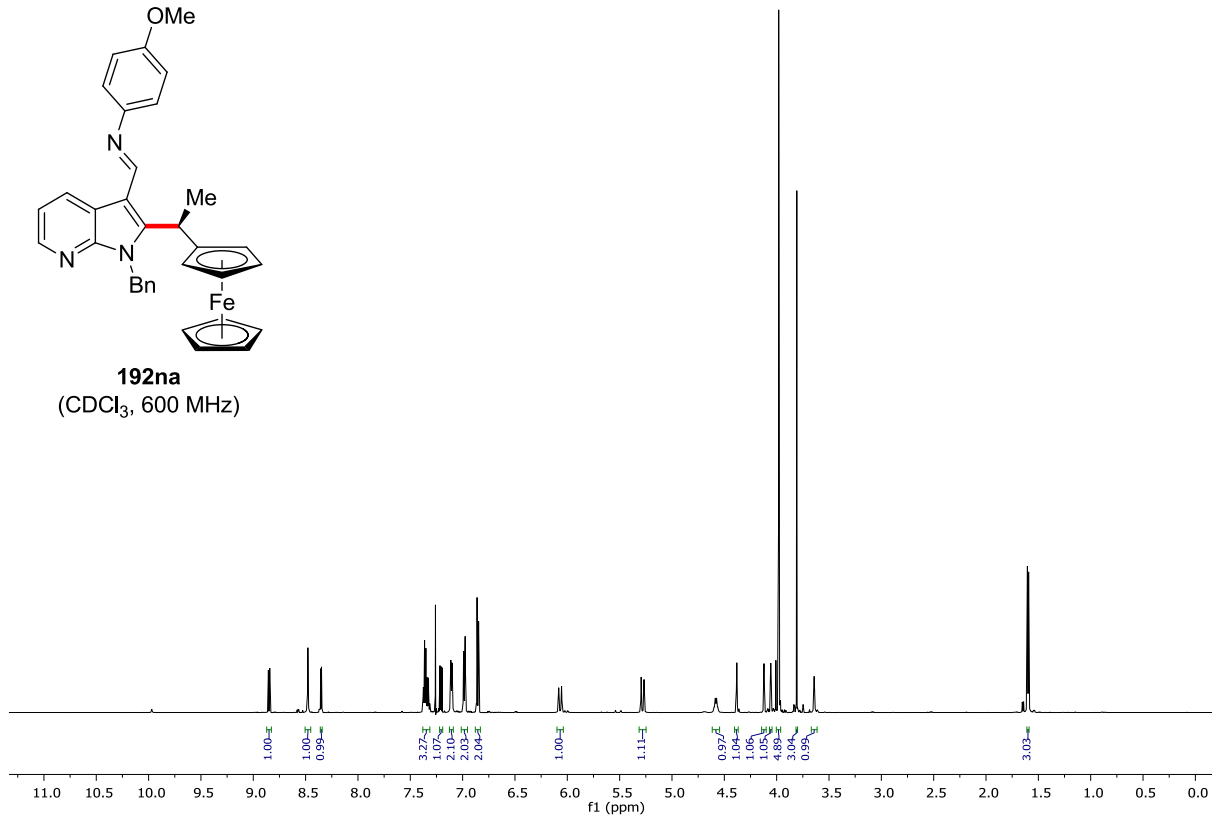
| Peak # | RetTime [min] | Type | Width [min] | Area [mAU*s] | Height [mAU] | Area % |
|--------|---------------|------|-------------|--------------|--------------|---------|
| 1 | 18.539 | MF | 0.3784 | 1557.18994 | 68.59011 | 51.0128 |
| 2 | 22.441 | MF | 0.4577 | 1495.35474 | 54.44636 | 48.9872 |



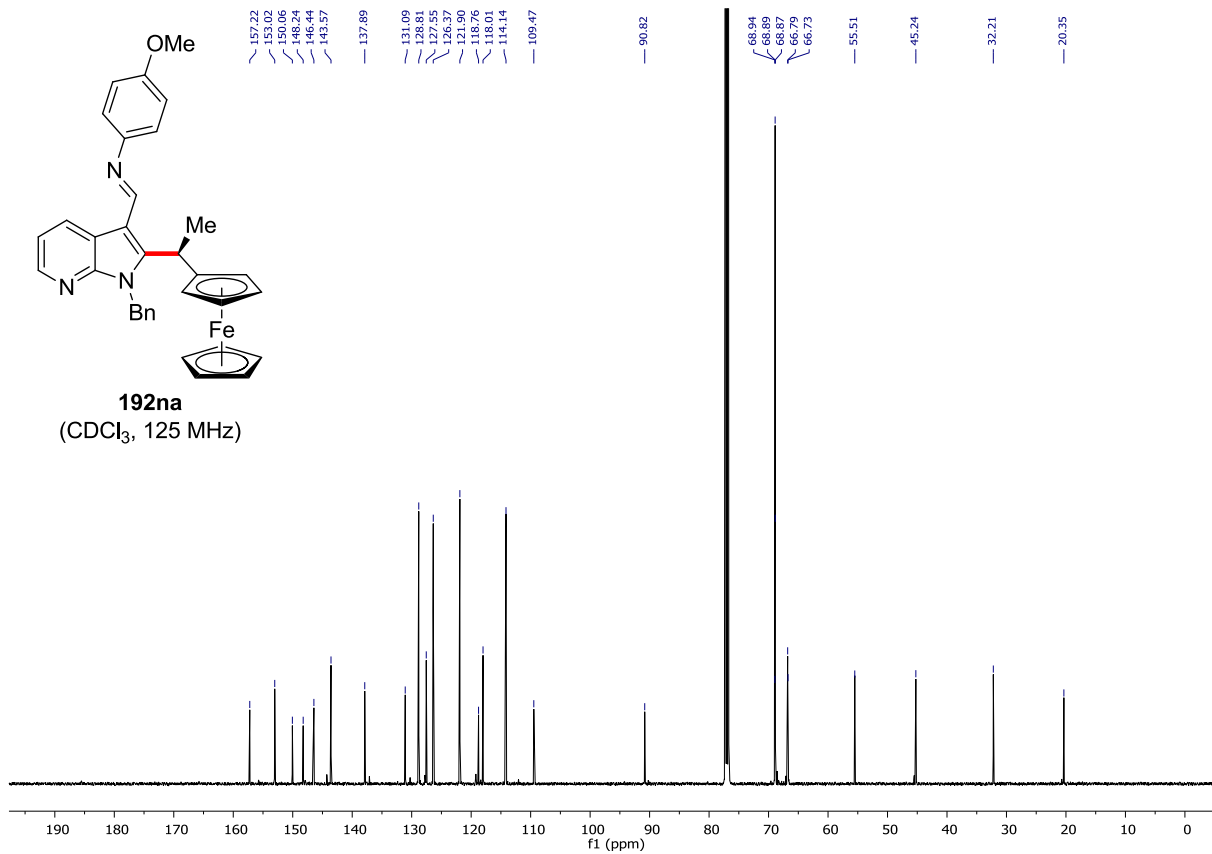
| Peak # | RetTime [min] | Type | Width [min] | Area [mAU*s] | Height [mAU] | Area % |
|--------|---------------|------|-------------|--------------|--------------|---------|
| 1 | 18.636 | MF | 0.3765 | 4409.53174 | 195.18329 | 96.3746 |
| 2 | 22.655 | MF | 0.4477 | 165.87866 | 6.17539 | 3.6254 |



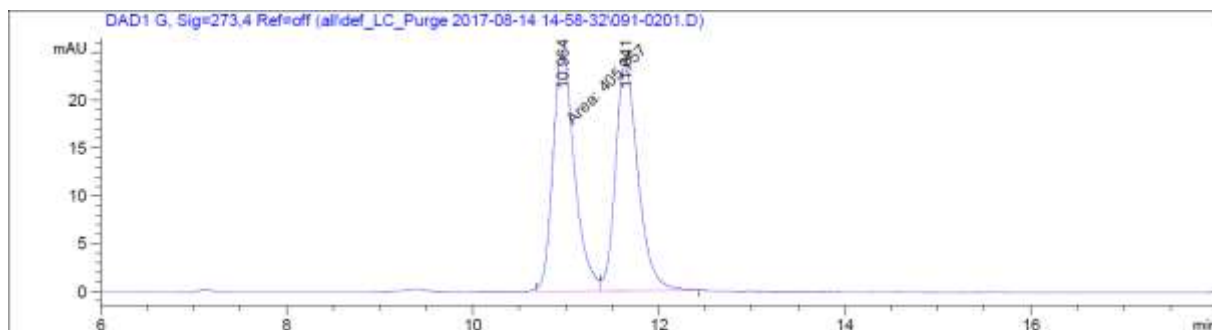
192na
(CDCl₃, 600 MHz)



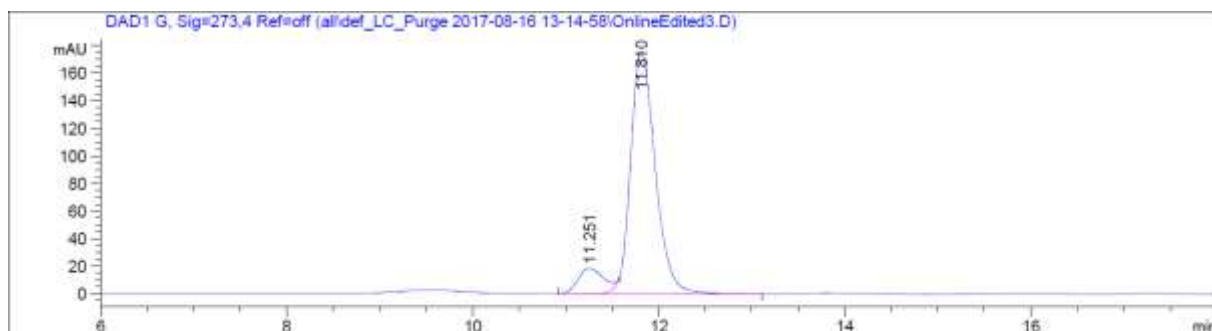
192na
(CDCl₃, 125 MHz)



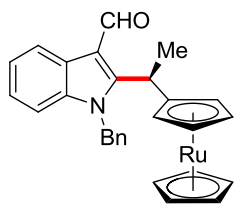
Chiral HPLC of **192na**:



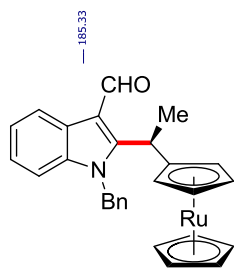
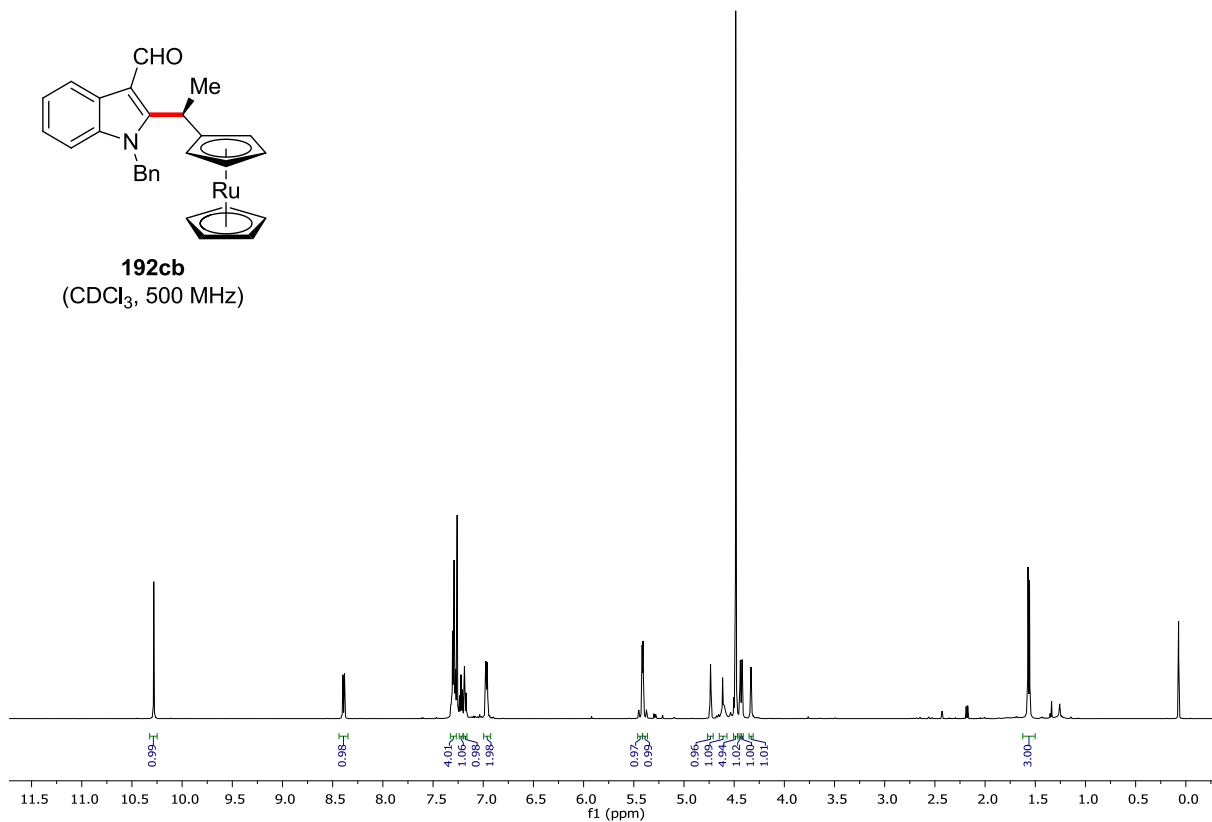
| Peak # | RetTime [min] | Type | Width [min] | Area [mAU*s] | Height [mAU] | Area % |
|--------|---------------|------|-------------|--------------|--------------|---------|
| 1 | 10.964 | FM | 0.2688 | 405.75687 | 25.15462 | 50.4067 |
| 2 | 11.641 | VB | 0.2583 | 399.20981 | 23.72052 | 49.5933 |



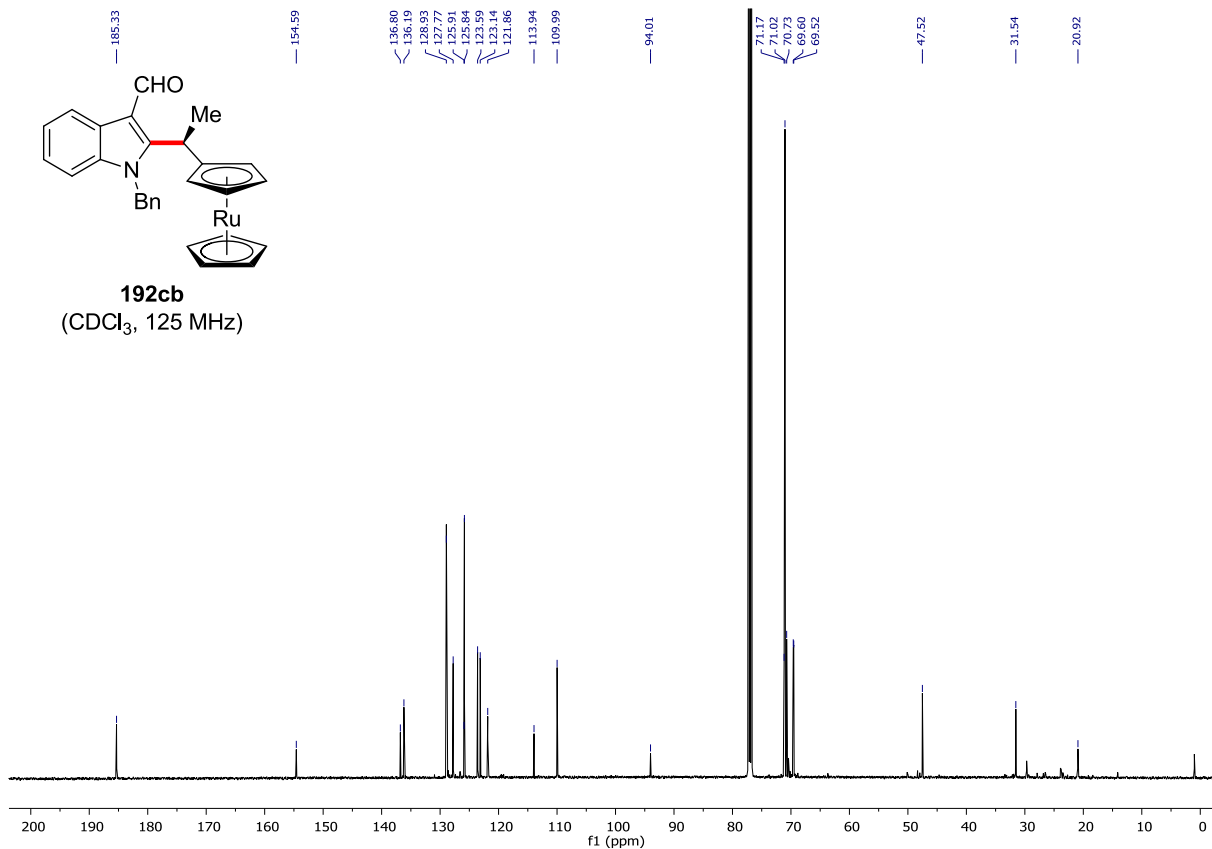
| Peak # | RetTime [min] | Type | Width [min] | Area [mAU*s] | Height [mAU] | Area % |
|--------|---------------|------|-------------|--------------|--------------|---------|
| 1 | 11.251 | BV E | 0.2841 | 347.67453 | 18.34724 | 9.7095 |
| 2 | 11.810 | VB R | 0.2841 | 3233.10596 | 175.34357 | 90.2905 |



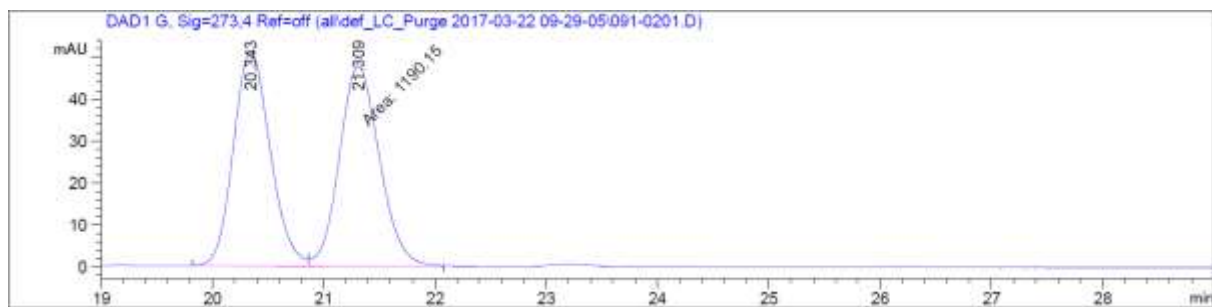
192cb
(CDCl₃, 500 MHz)



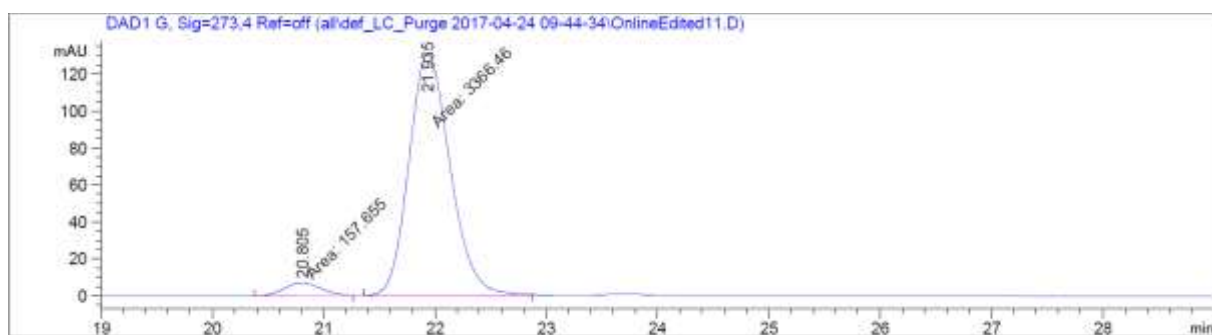
192cb
(CDCl₃, 125 MHz)



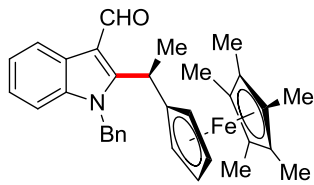
Chiral HPLC of **192cb**:



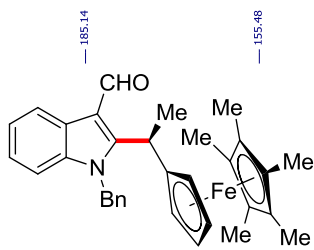
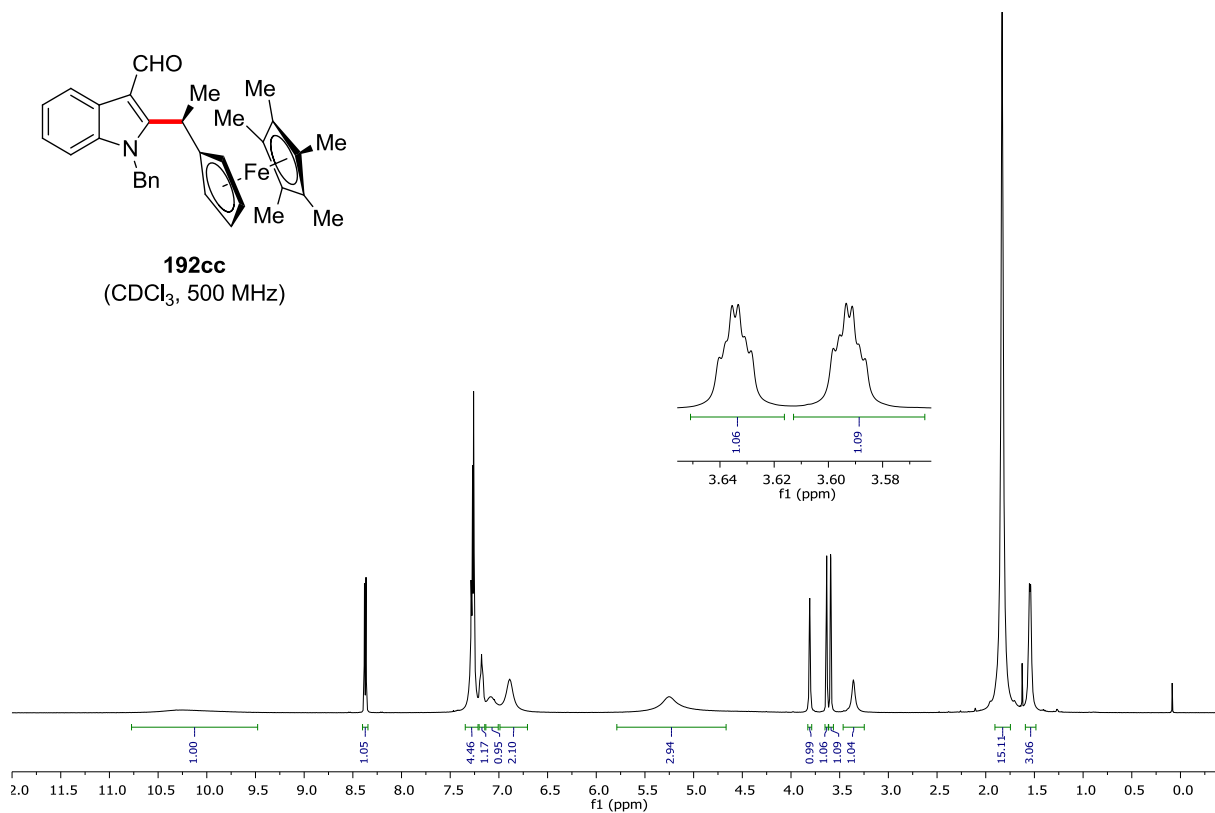
| Peak # | RetTime [min] | Type | Width [min] | Area [mAU*s] | Height [mAU] | Area % |
|--------|---------------|------|-------------|--------------|--------------|---------|
| 1 | 20.343 | BV | 0.3521 | 1170.22974 | 51.11890 | 49.5780 |
| 2 | 21.309 | MF | 0.4170 | 1190.15332 | 47.57173 | 50.4220 |



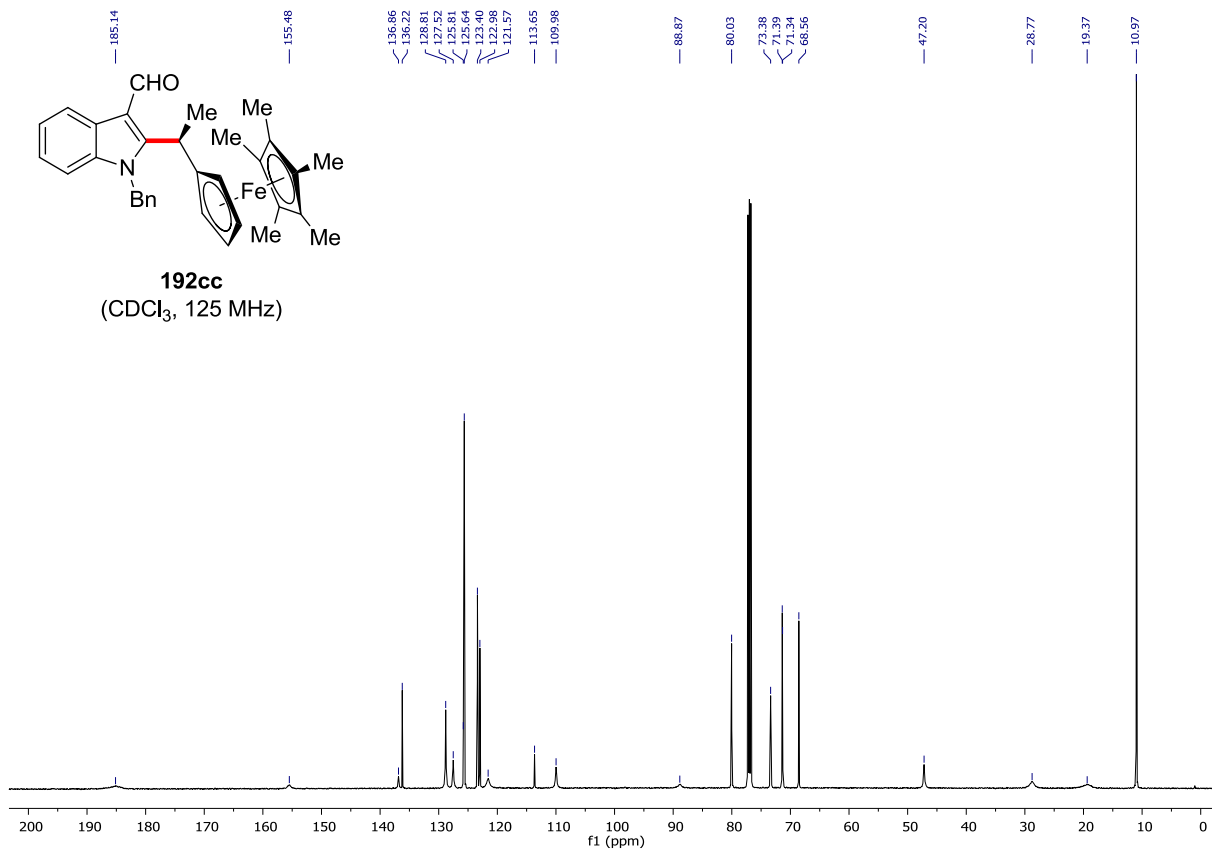
| Peak # | RetTime [min] | Type | Width [min] | Area [mAU*s] | Height [mAU] | Area % |
|--------|---------------|------|-------------|--------------|--------------|---------|
| 1 | 20.805 | FM | 0.3778 | 157.65451 | 6.95554 | 4.4736 |
| 2 | 21.935 | MF | 0.4289 | 3366.45825 | 130.80820 | 95.5264 |



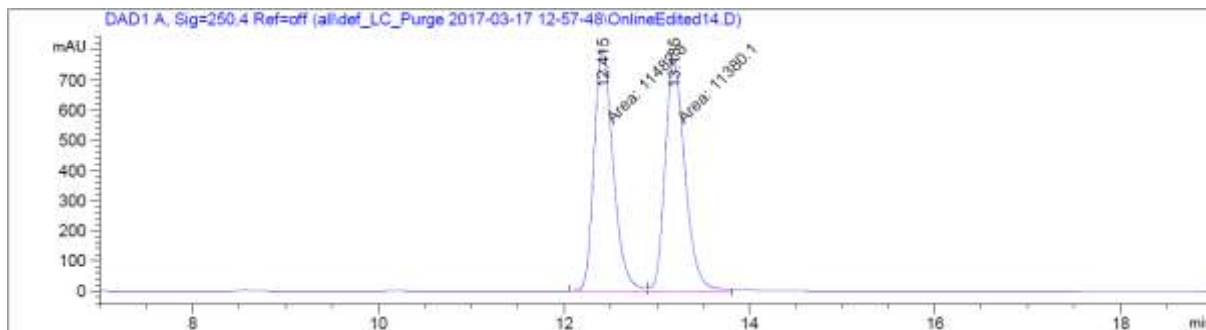
192cc
(CDCl₃, 500 MHz)



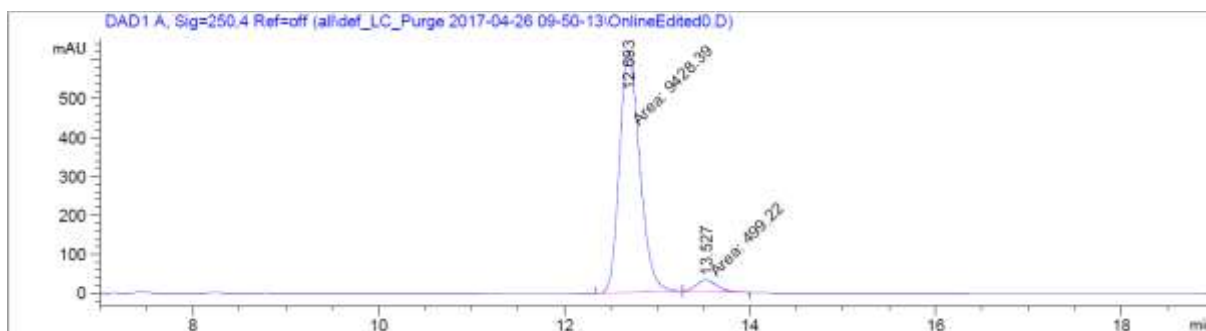
192cc
(CDCl₃, 125 MHz)



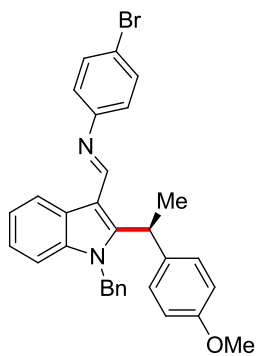
Chiral HPLC of 192cc:



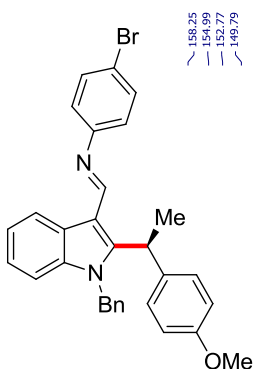
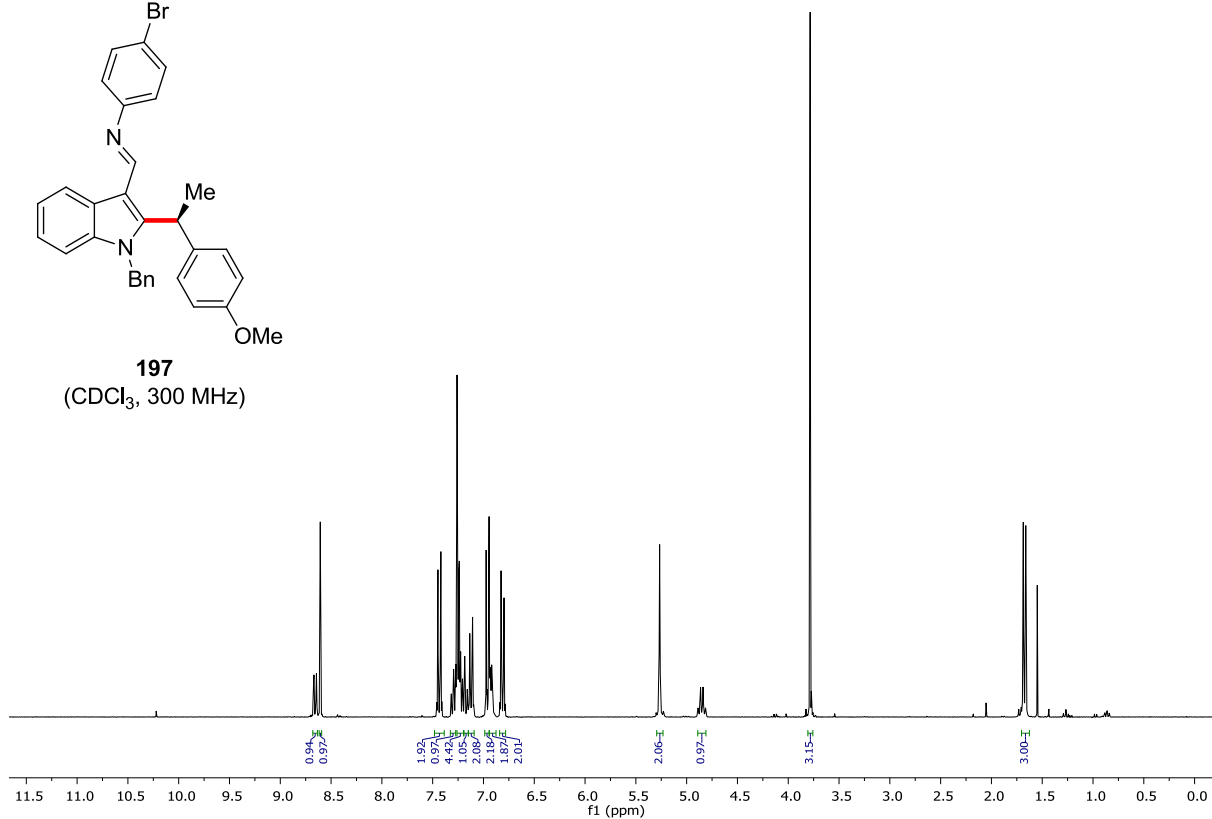
| Peak # | RetTime [min] | Type | Width [min] | Area [mAU*s] | Height [mAU] | Area % |
|--------|---------------|------|-------------|--------------|--------------|---------|
| 1 | 12.415 | FM | 0.2390 | 1.14822e4 | 800.56268 | 50.2234 |
| 2 | 13.185 | MF | 0.2514 | 1.13801e4 | 754.30182 | 49.7766 |



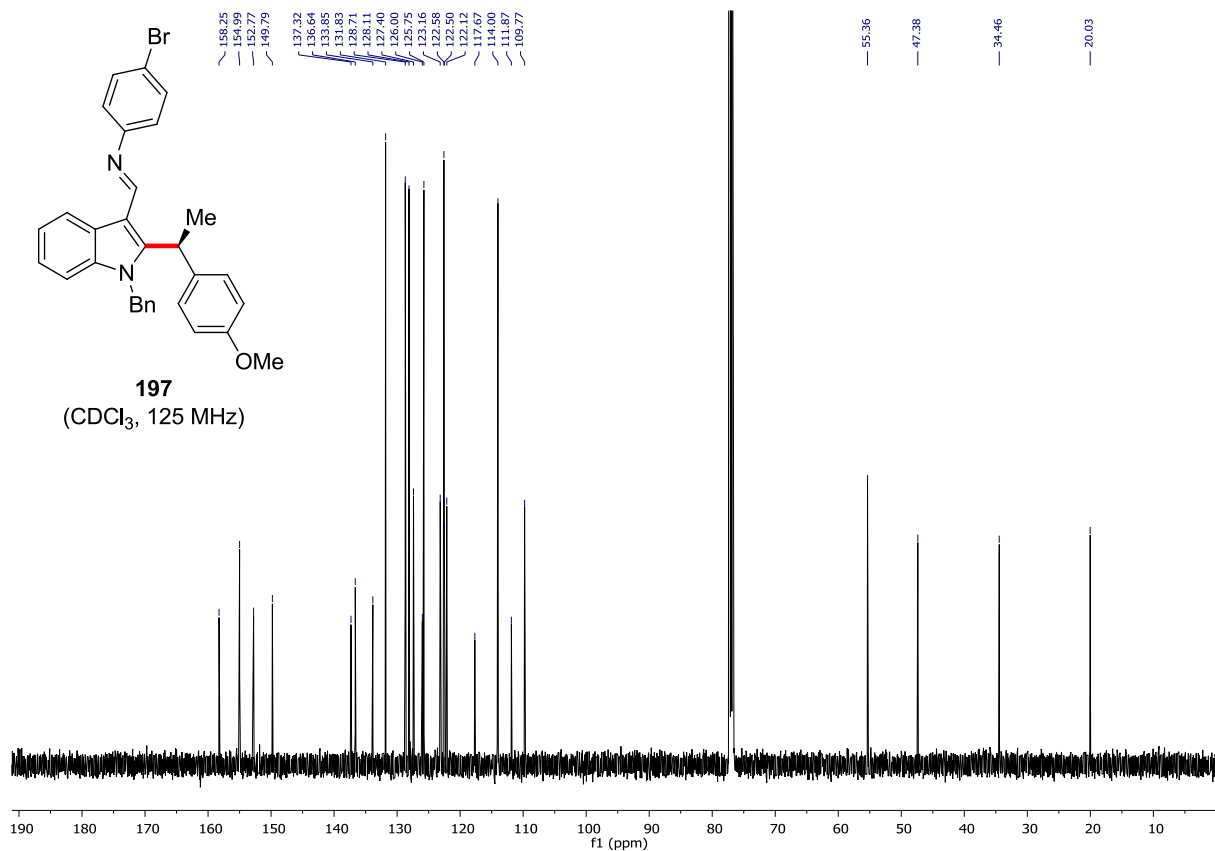
| Peak # | RetTime [min] | Type | Width [min] | Area [mAU*s] | Height [mAU] | Area % |
|--------|---------------|------|-------------|--------------|--------------|---------|
| 1 | 12.693 | MM | 0.2536 | 9428.38965 | 619.52576 | 94.9714 |
| 2 | 13.527 | MM | 0.2694 | 499.22003 | 30.88190 | 5.0286 |



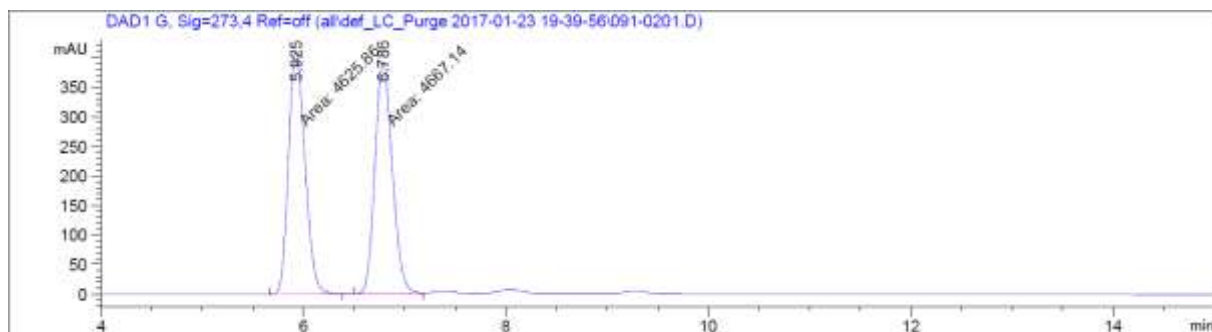
197
(CDCl₃, 300 MHz)



197
(CDCl₃, 125 MHz)



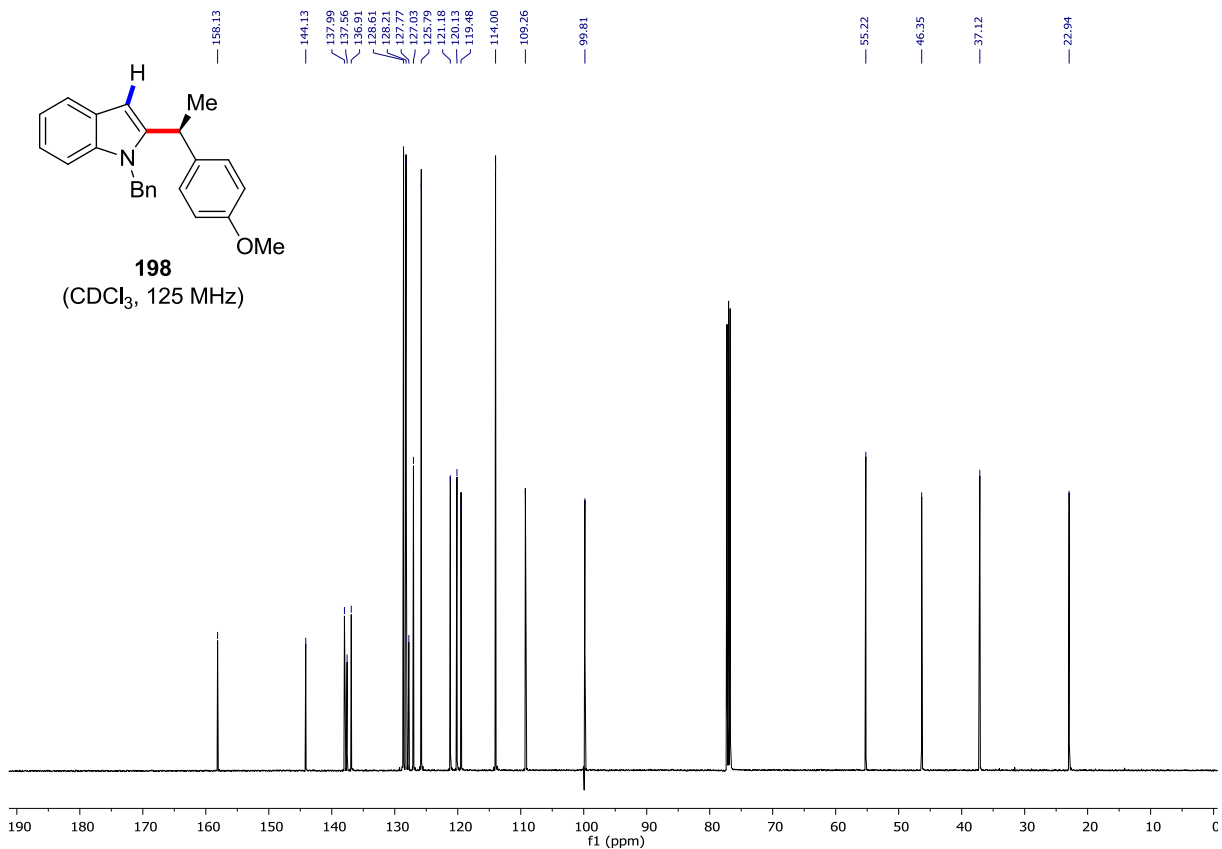
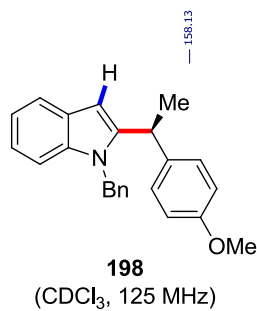
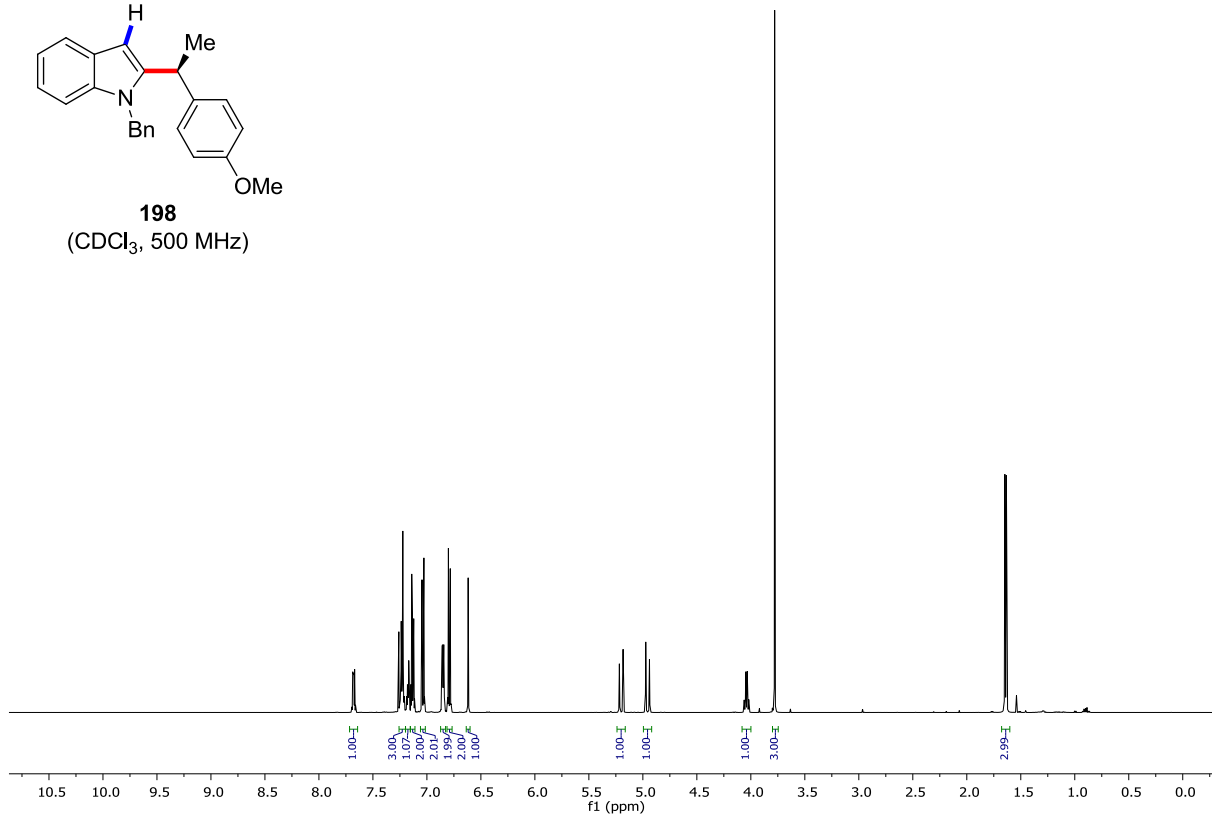
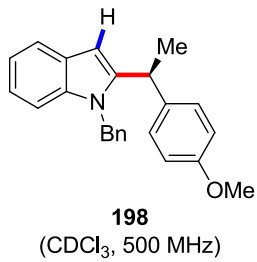
Chiral HPLC of **197**:



| Peak # | RetTime [min] | Type | Width [min] | Area [mAU*s] | Height [mAU] | Area % |
|--------|---------------|------|-------------|--------------|--------------|---------|
| 1 | 5.925 | MF | 0.1886 | 4625.85840 | 408.87909 | 49.7779 |
| 2 | 6.786 | FM | 0.1984 | 4667.13867 | 392.11099 | 50.2221 |



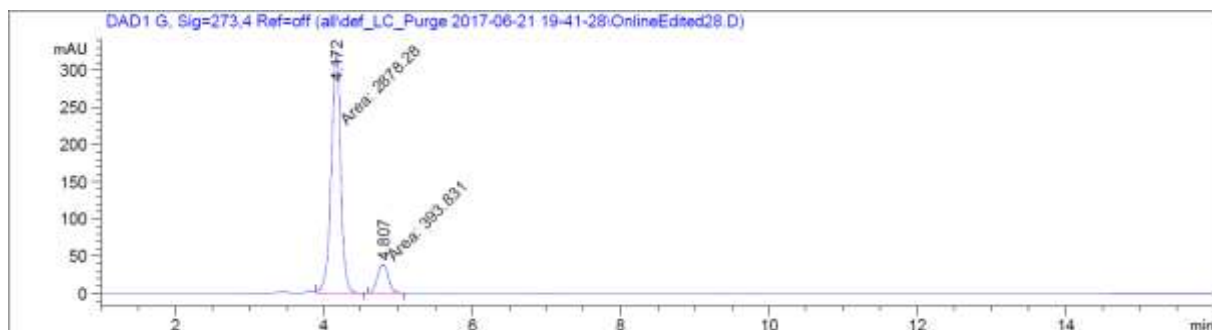
| Peak # | RetTime [min] | Type | Width [min] | Area [mAU*s] | Height [mAU] | Area % |
|--------|---------------|------|-------------|--------------|--------------|---------|
| 1 | 5.924 | MF | 0.1949 | 1.07301e4 | 917.63928 | 99.5297 |
| 2 | 6.703 | FM | 0.3075 | 50.70160 | 2.74827 | 0.4703 |



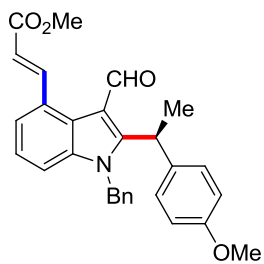
Chiral HPLC of **198**:



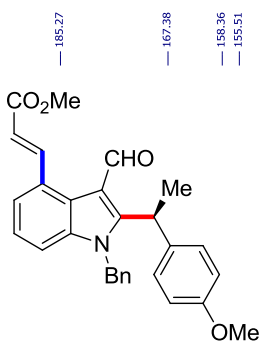
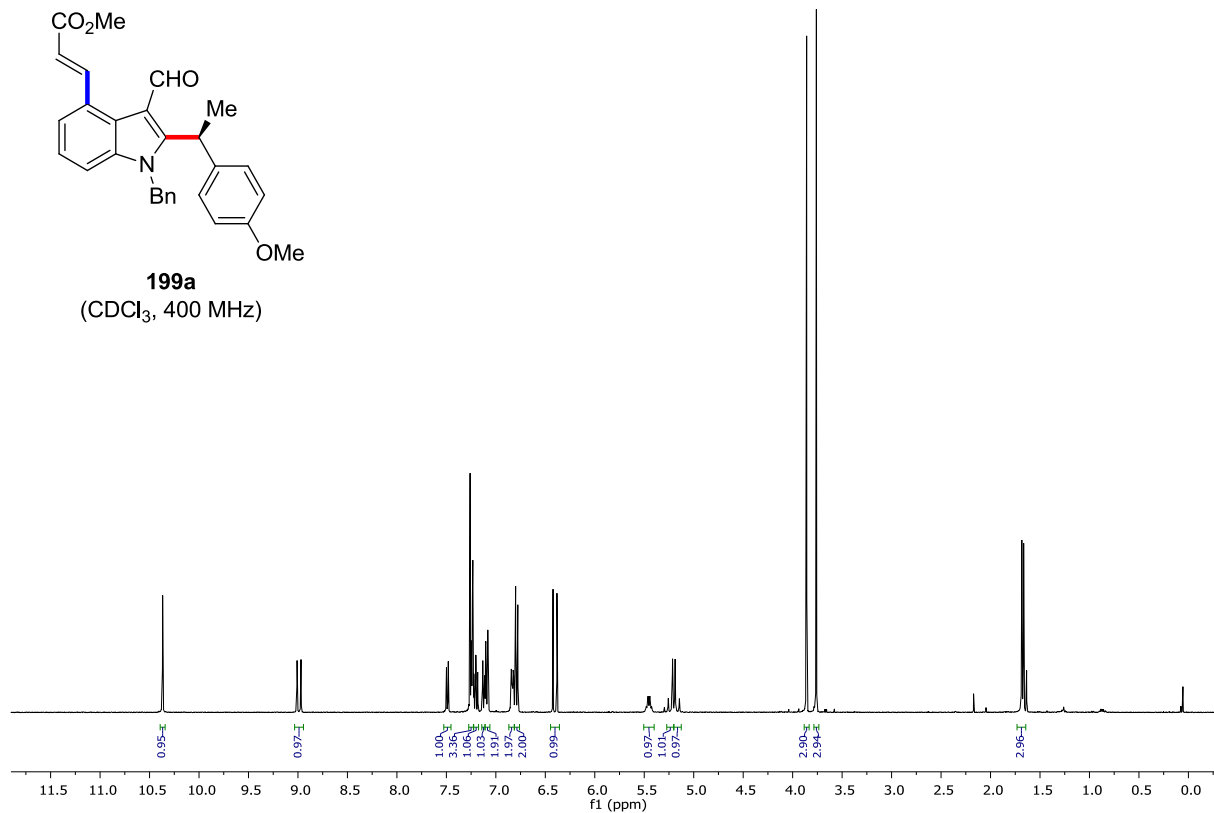
| Peak # | RetTime [min] | Type | Width [min] | Area [mAU*s] | Height [mAU] | Area % |
|--------|---------------|------|-------------|--------------|--------------|---------|
| 1 | 4.213 | MF | 0.0926 | 1333.80566 | 240.05545 | 50.9043 |
| 2 | 4.855 | BV | 0.0866 | 1286.41394 | 225.25159 | 49.0957 |



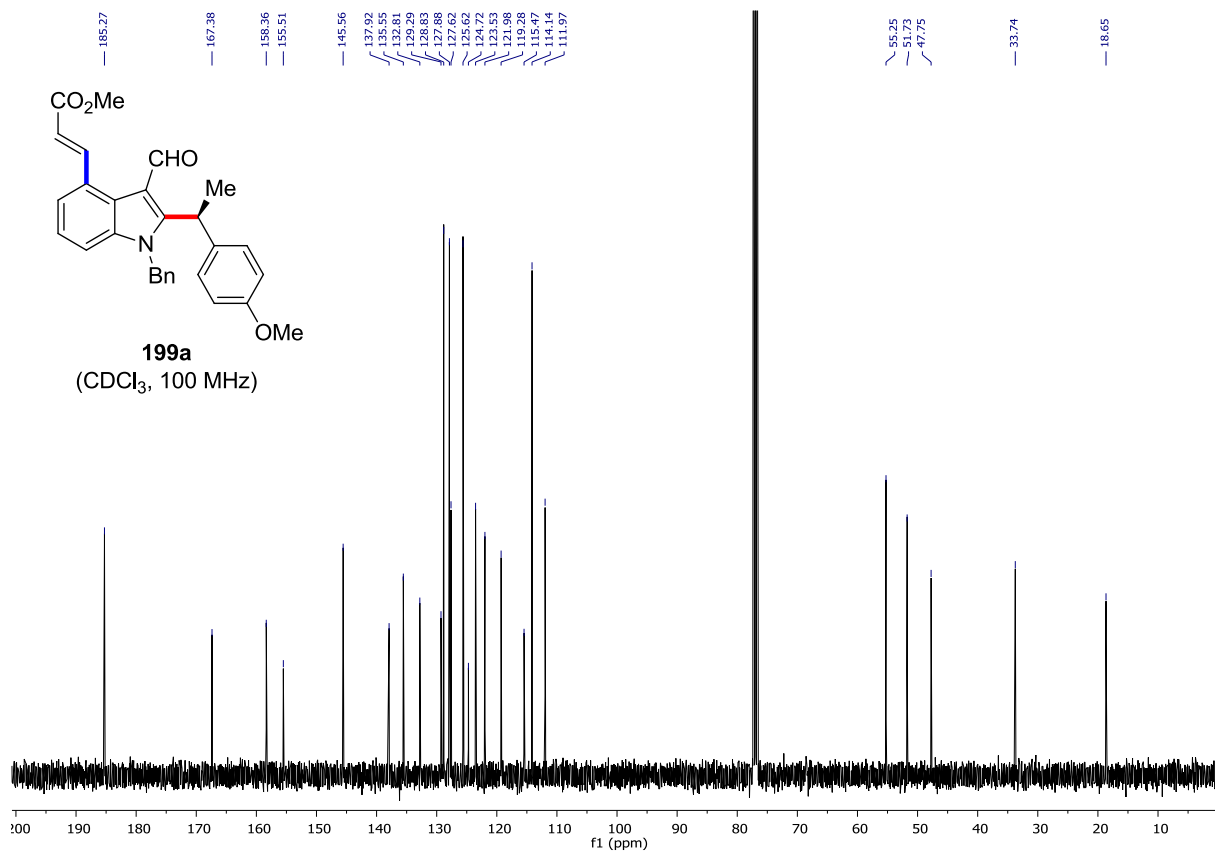
| Peak # | RetTime [min] | Type | Width [min] | Area [mAU*s] | Height [mAU] | Area % |
|--------|---------------|------|-------------|--------------|--------------|---------|
| 1 | 4.172 | MF | 0.1477 | 2878.27686 | 324.73309 | 87.9640 |
| 2 | 4.807 | FM | 0.1716 | 393.83102 | 38.24700 | 12.0360 |



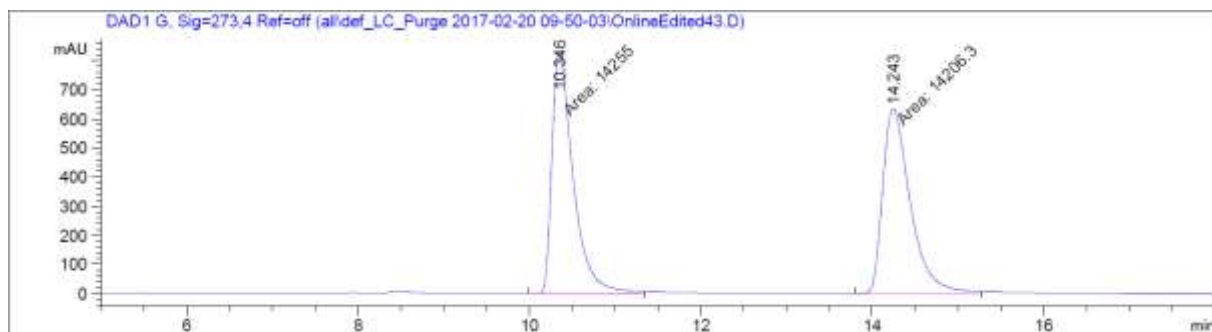
199a
(CDCl₃, 400 MHz)



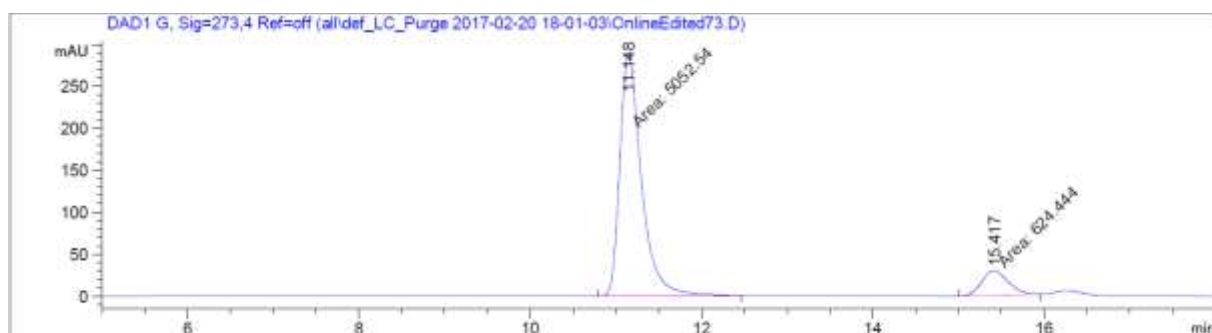
199a
(CDCl₃, 100 MHz)



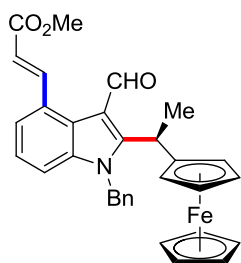
Chiral HPLC of **199a**:



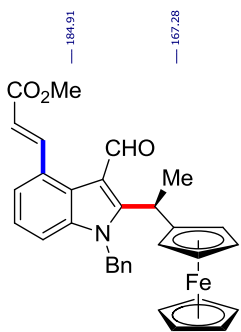
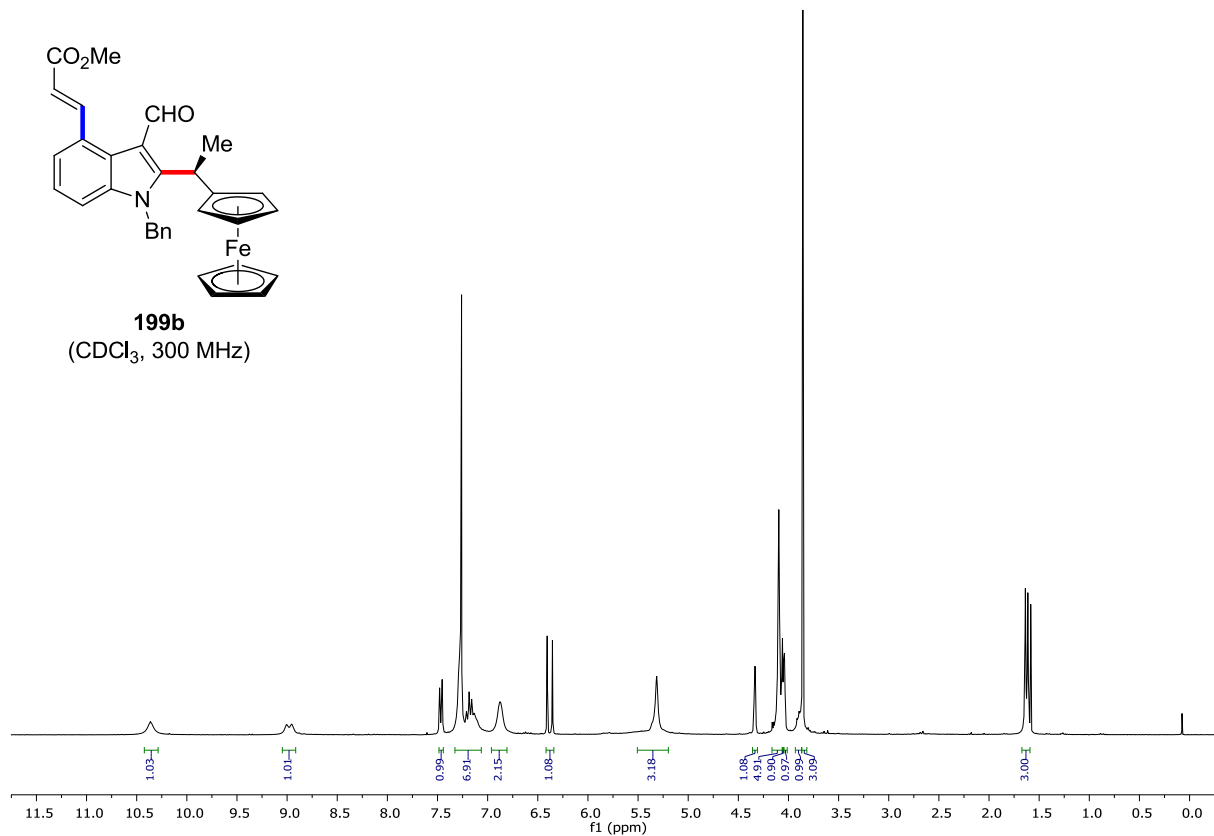
| Peak # | RetTime [min] | Type | Width [min] | Area [mAU*s] | Height [mAU] | Area % |
|--------|---------------|------|-------------|--------------|--------------|---------|
| 1 | 10.346 | MF | 0.2863 | 1.42550e4 | 829.86505 | 50.0855 |
| 2 | 14.243 | MF | 0.3736 | 1.42063e4 | 633.79132 | 49.9145 |



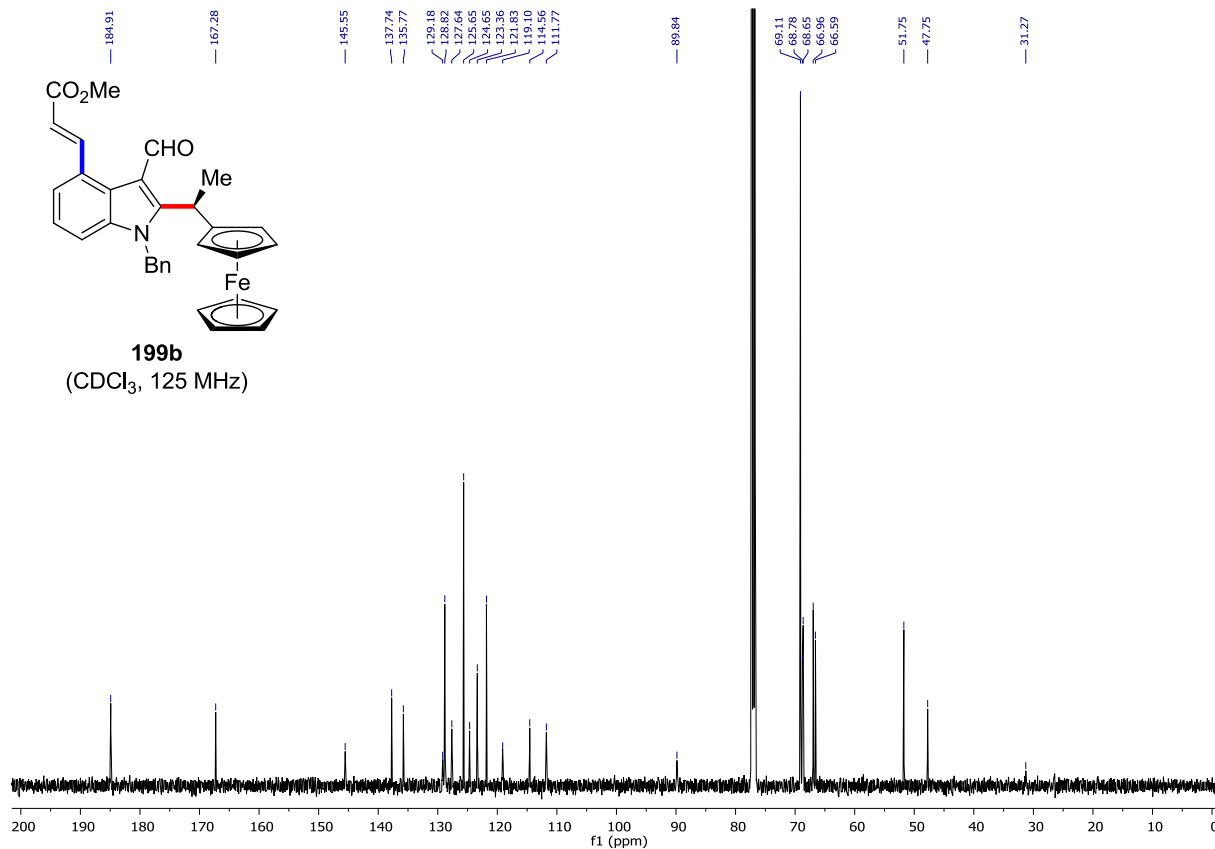
| Peak # | RetTime [min] | Type | Width [min] | Area [mAU*s] | Height [mAU] | Area % |
|--------|---------------|------|-------------|--------------|--------------|---------|
| 1 | 11.148 | MF | 0.2920 | 5052.54150 | 288.42307 | 89.0004 |
| 2 | 15.417 | FM | 0.3581 | 624.44385 | 29.06262 | 10.9996 |



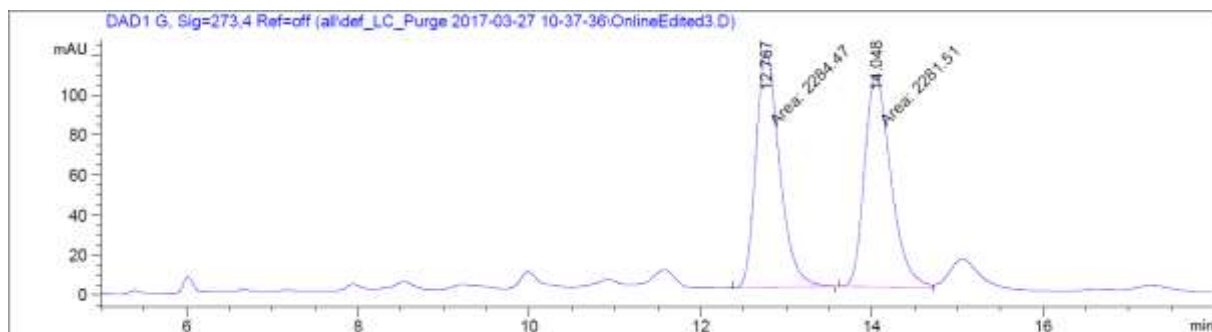
199b
(CDCl₃, 300 MHz)



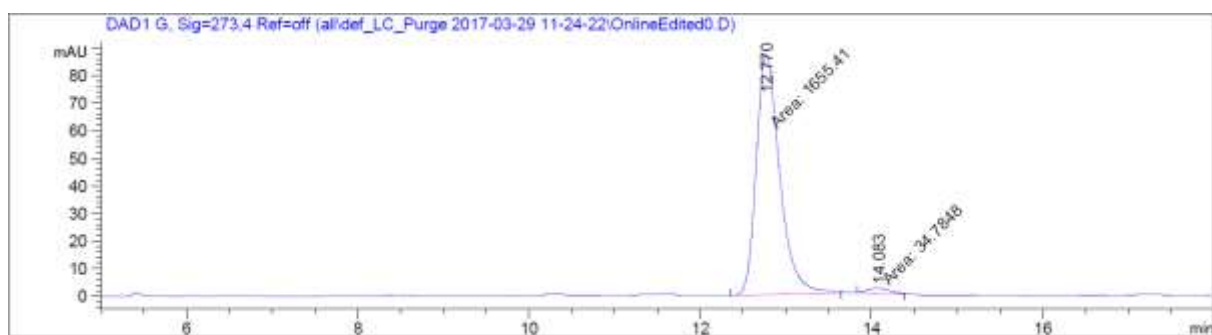
199b
(CDCl₃, 125 MHz)



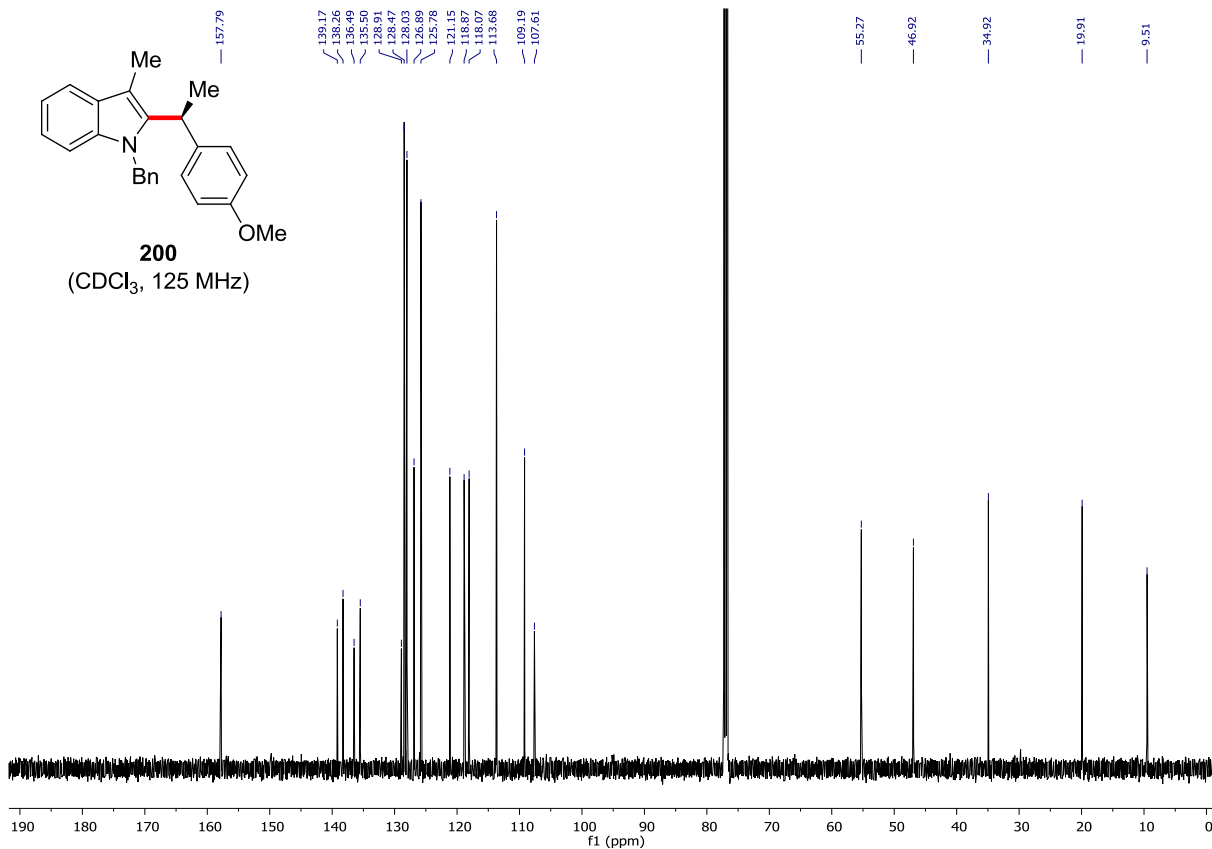
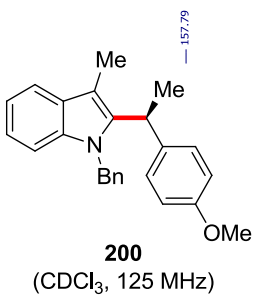
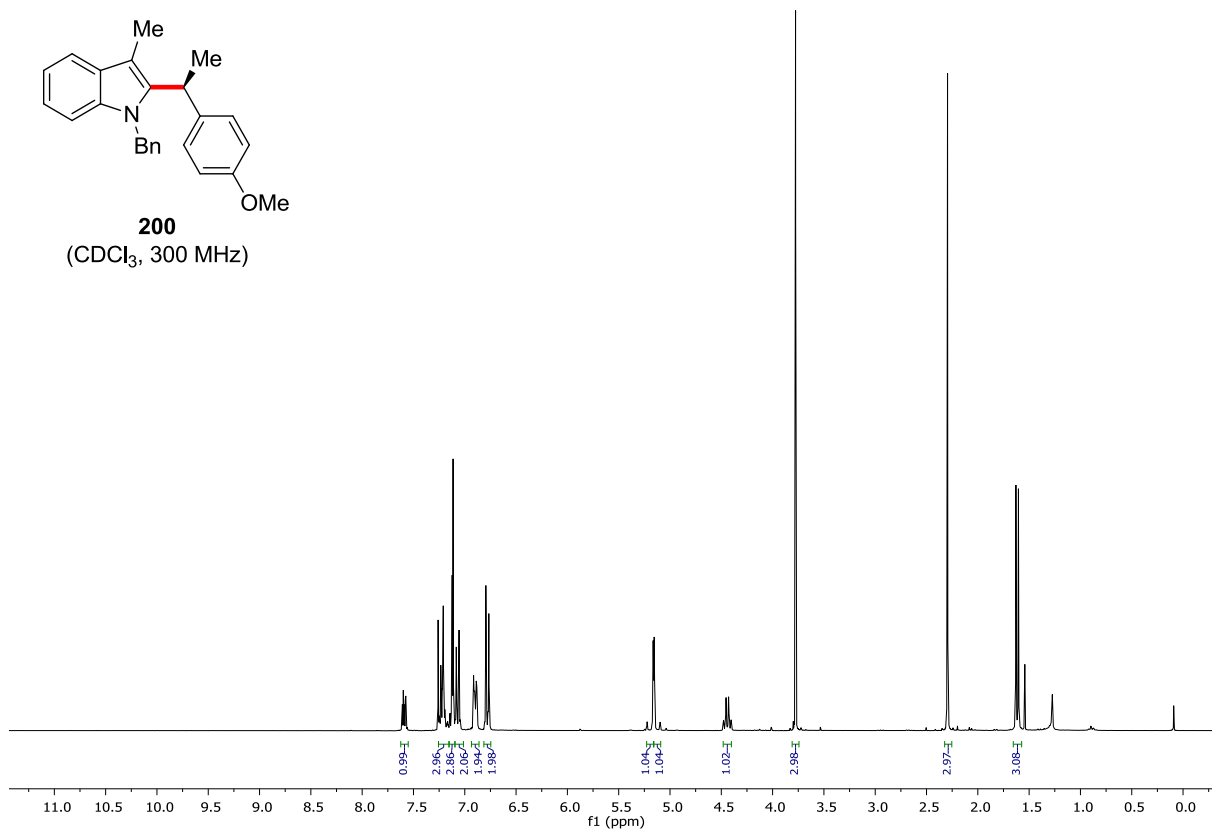
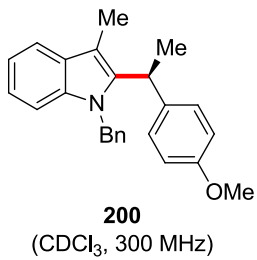
Chiral HPLC of **199b**:



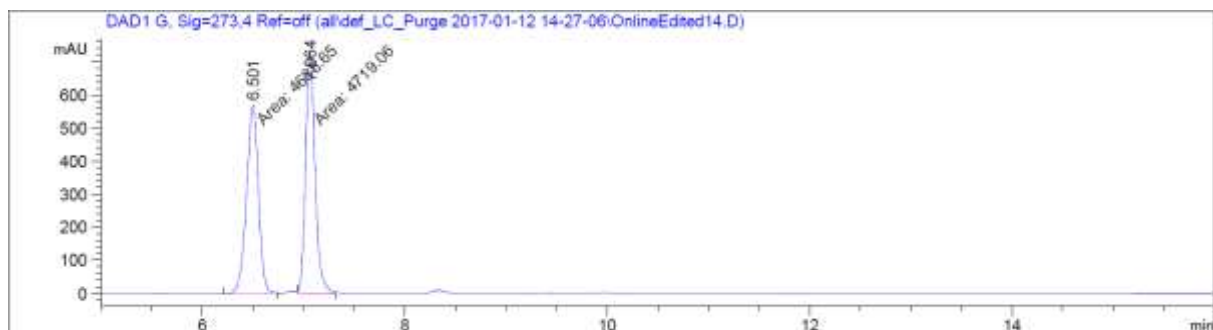
| Peak # | RetTime [min] | Type | Width [min] | Area [mAU*s] | Height [mAU] | Area % |
|--------|---------------|------|-------------|--------------|--------------|---------|
| 1 | 12.767 | MF | 0.3232 | 2284.47192 | 117.79989 | 50.0325 |
| 2 | 14.048 | MF | 0.3577 | 2281.50684 | 106.29260 | 49.9675 |



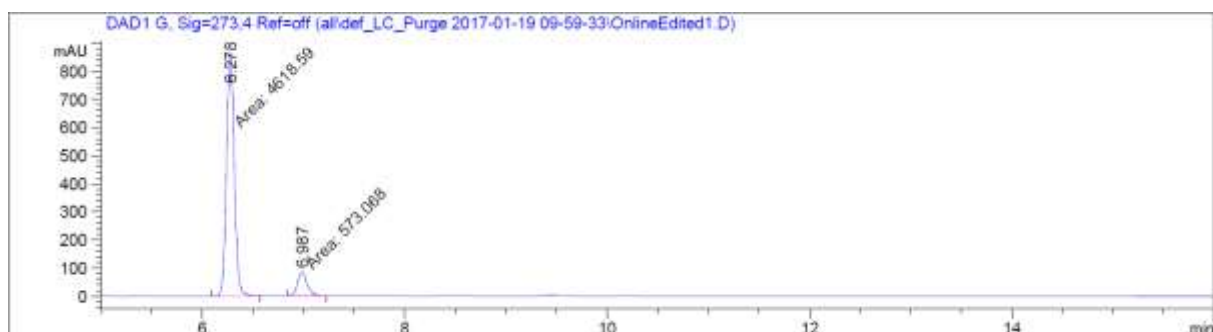
| Peak # | RetTime [min] | Type | Width [min] | Area [mAU*s] | Height [mAU] | Area % |
|--------|---------------|------|-------------|--------------|--------------|---------|
| 1 | 12.770 | MF | 0.3170 | 1655.41162 | 87.02285 | 97.9420 |
| 2 | 14.083 | FM | 0.3072 | 34.78480 | 1.88717 | 2.0580 |



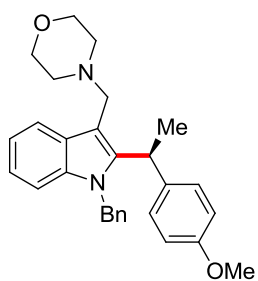
Chiral HPLC of **200**:



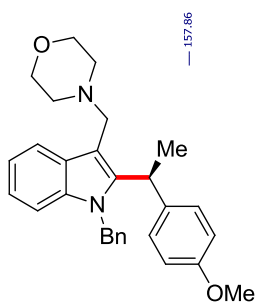
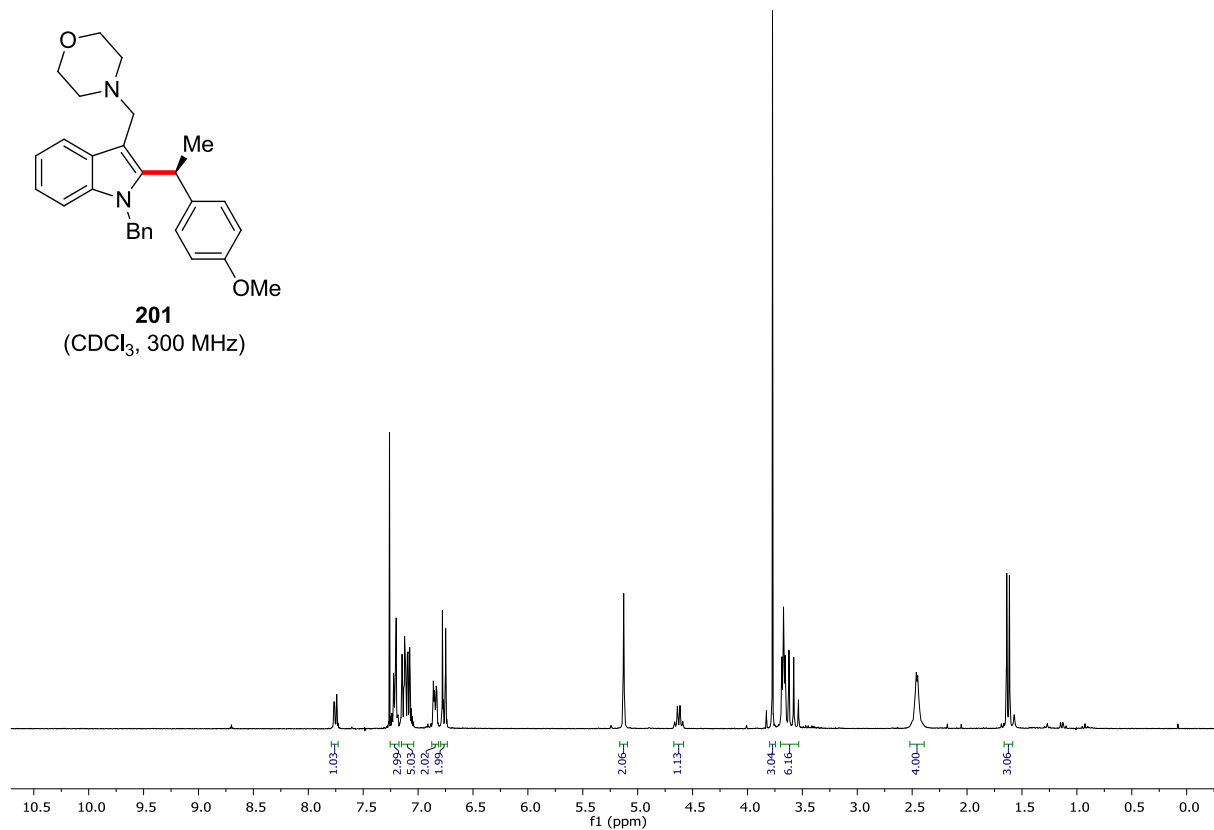
| Peak # | RetTime [min] | Type | Width [min] | Area [mAU*s] | Height [mAU] | Area % |
|--------|---------------|------|-------------|--------------|--------------|---------|
| 1 | 6.501 | MF | 0.1360 | 4638.64697 | 568.64288 | 49.5704 |
| 2 | 7.064 | MF | 0.1076 | 4719.05615 | 731.11206 | 50.4296 |



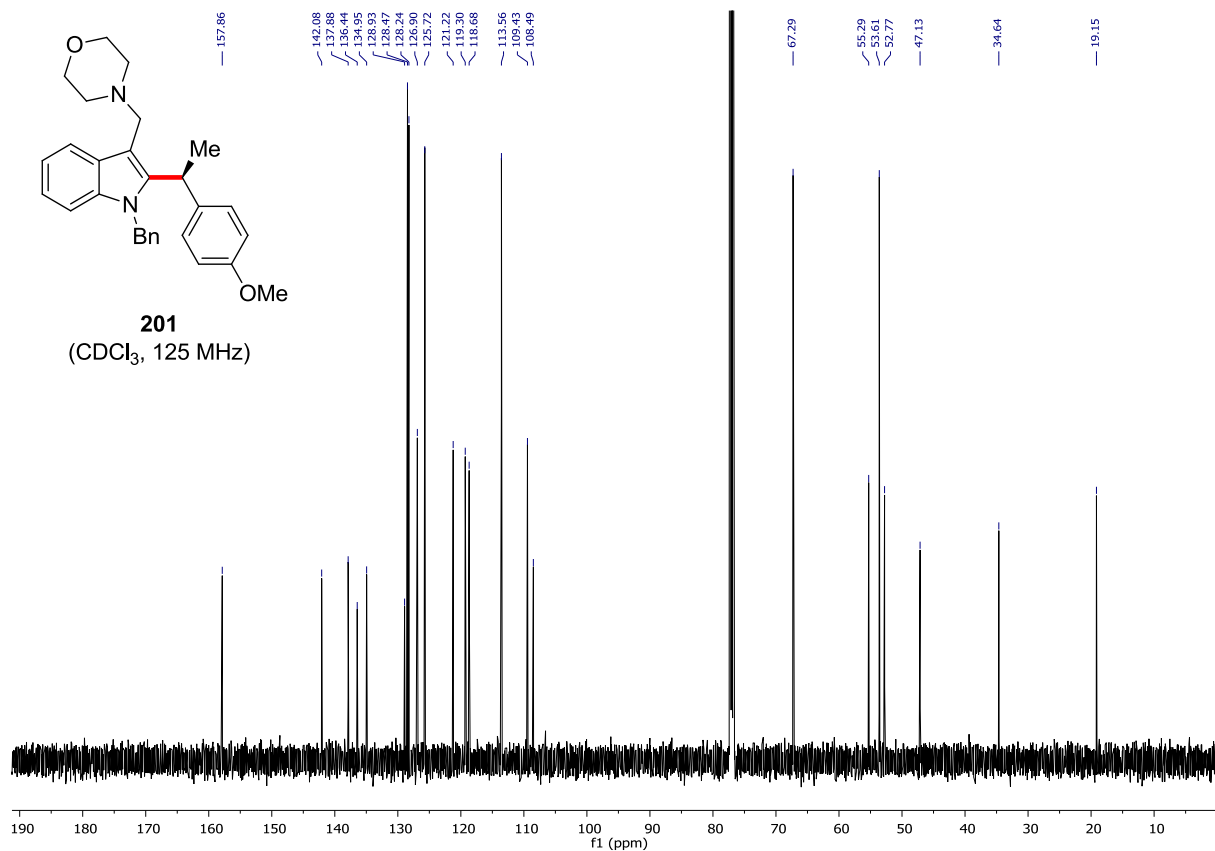
| Peak # | RetTime [min] | Type | Width [min] | Area [mAU*s] | Height [mAU] | Area % |
|--------|---------------|------|-------------|--------------|--------------|---------|
| 1 | 6.278 | FM | 0.0891 | 4618.59326 | 864.14508 | 88.9618 |
| 2 | 6.987 | MF | 0.1128 | 573.06763 | 84.66462 | 11.0382 |



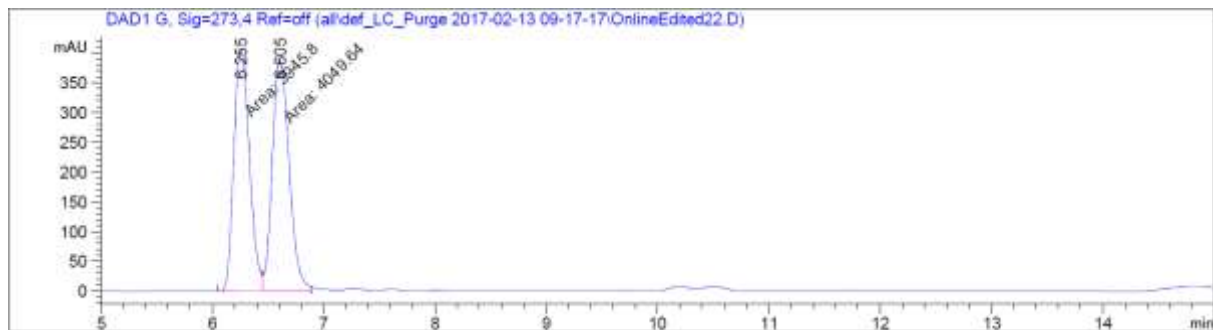
201
(CDCl₃, 300 MHz)



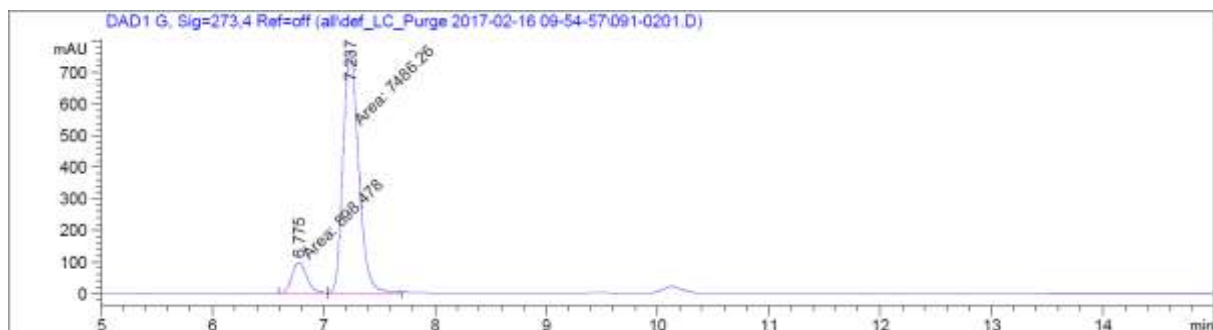
201
(CDCl₃, 125 MHz)



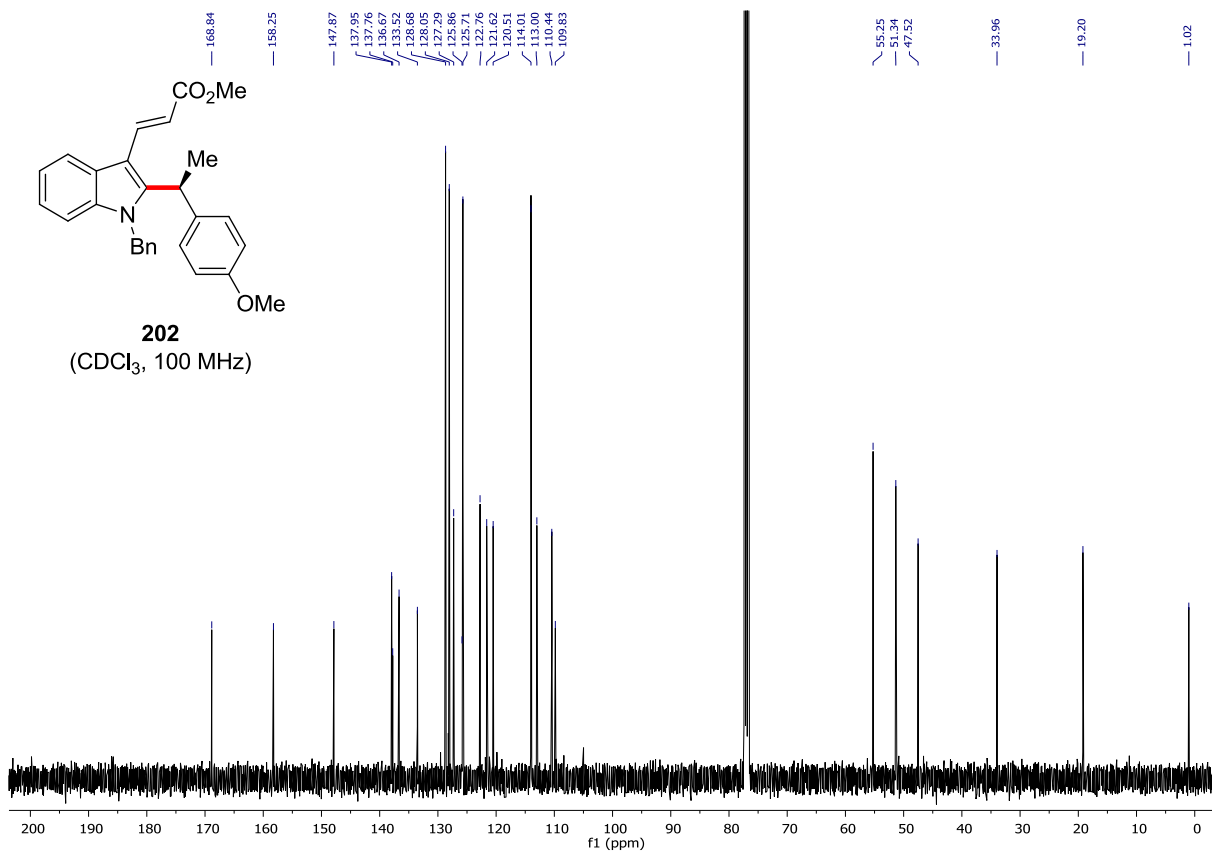
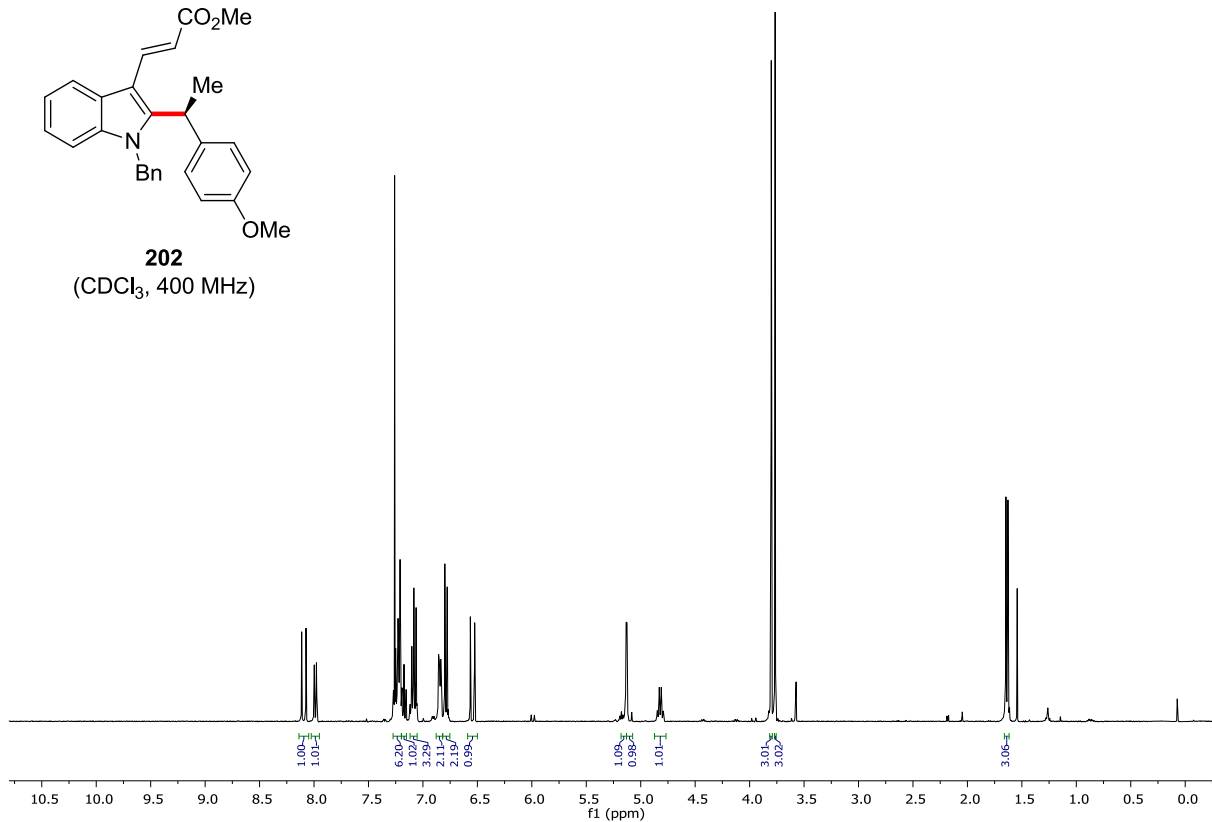
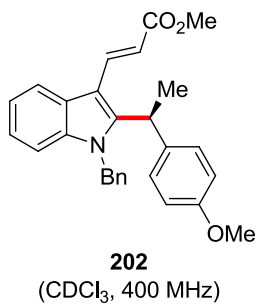
Chiral HPLC of **201**:



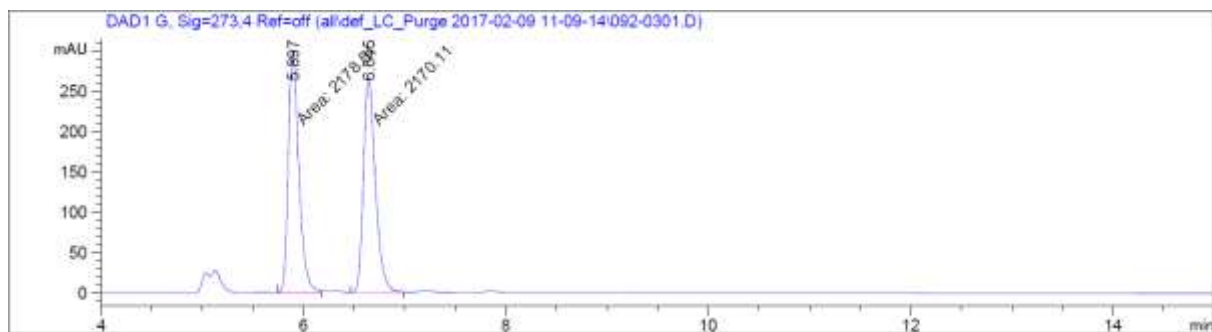
| Peak # | RetTime [min] | Type | Width [min] | Area [mAU*s] | Height [mAU] | Area % |
|--------|---------------|------|-------------|--------------|--------------|---------|
| 1 | 6.255 | FM | 0.1622 | 3945.80225 | 405.49960 | 49.3507 |
| 2 | 6.605 | MF | 0.1748 | 4049.63843 | 386.08386 | 50.6493 |



| Peak # | RetTime [min] | Type | Width [min] | Area [mAU*s] | Height [mAU] | Area % |
|--------|---------------|------|-------------|--------------|--------------|---------|
| 1 | 6.775 | FM | 0.1537 | 898.47784 | 97.43313 | 10.7156 |
| 2 | 7.237 | MF | 0.1630 | 7486.25684 | 765.39685 | 89.2844 |



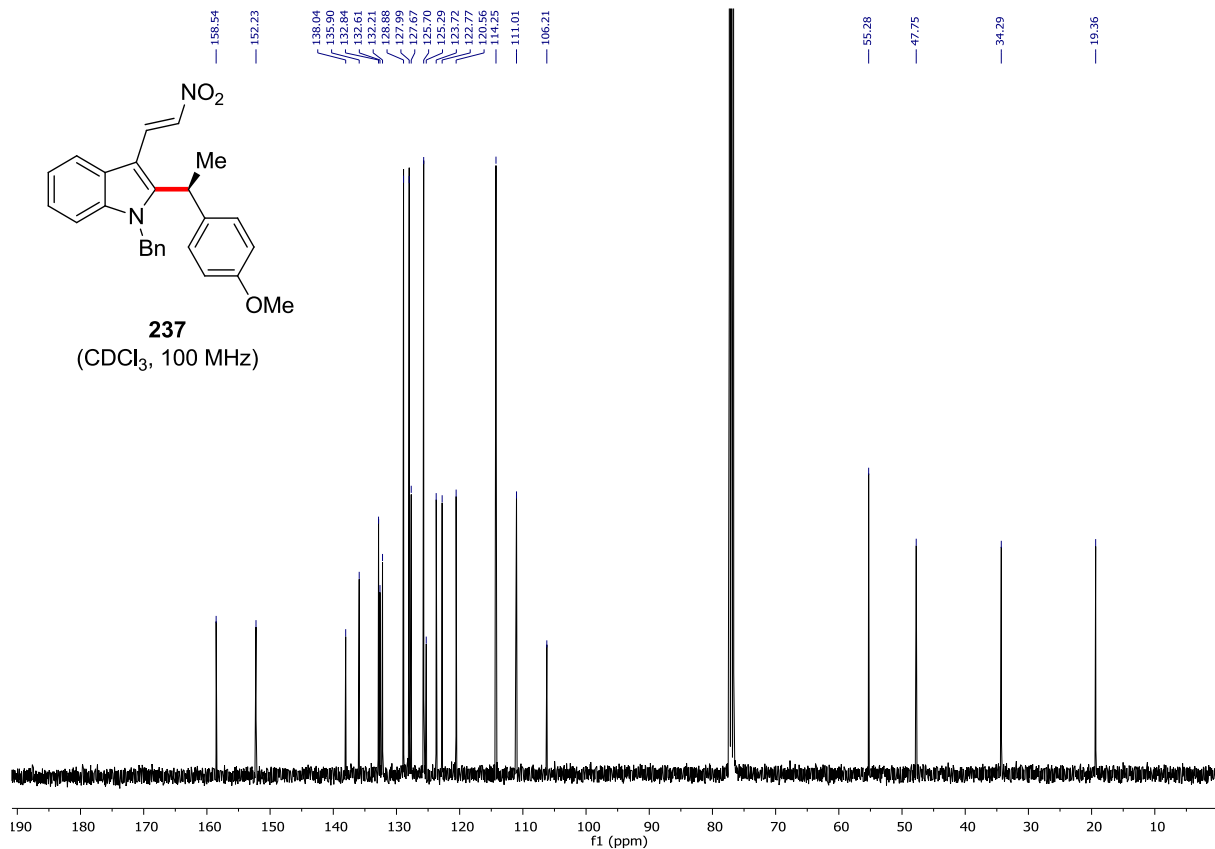
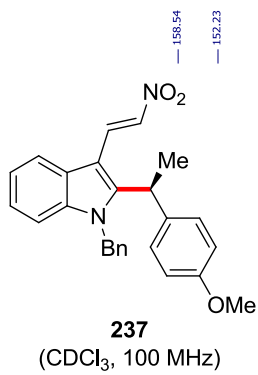
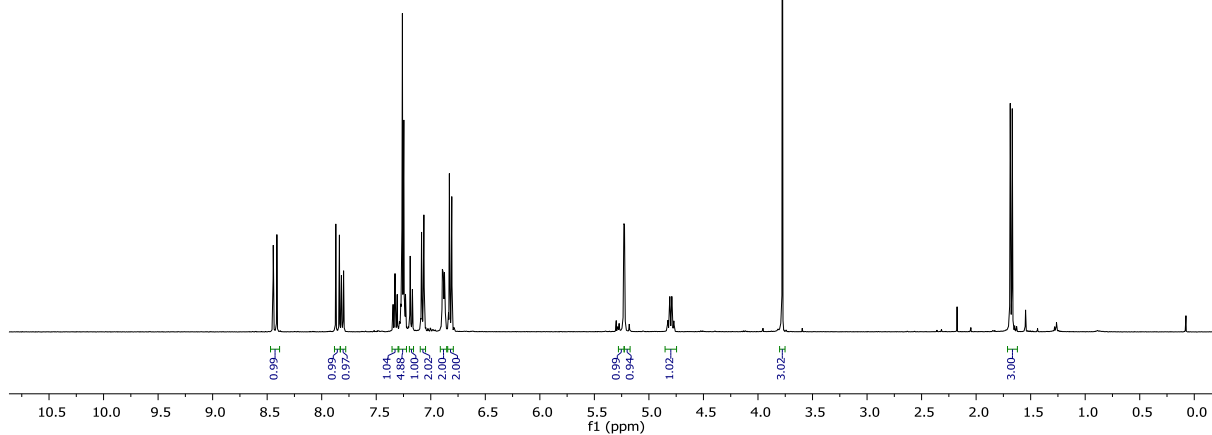
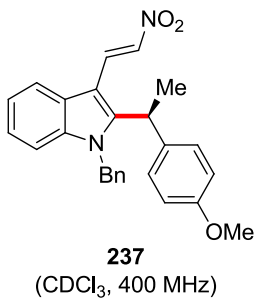
Chiral HPLC of **202**:



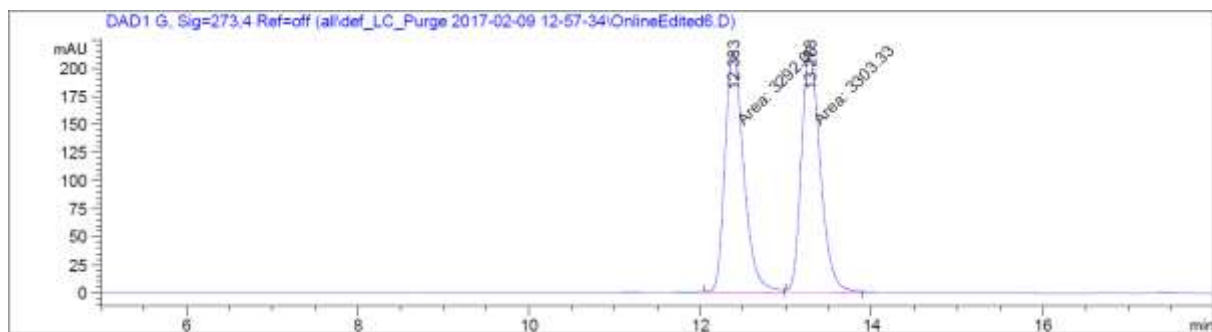
| Peak # | RetTime [min] | Type | Width [min] | Area [mAU*s] | Height [mAU] | Area % |
|--------|---------------|------|-------------|--------------|--------------|---------|
| 1 | 5.897 | FM | 0.1217 | 2178.50513 | 298.43298 | 50.0966 |
| 2 | 6.645 | MF | 0.1359 | 2170.10645 | 266.11761 | 49.9034 |



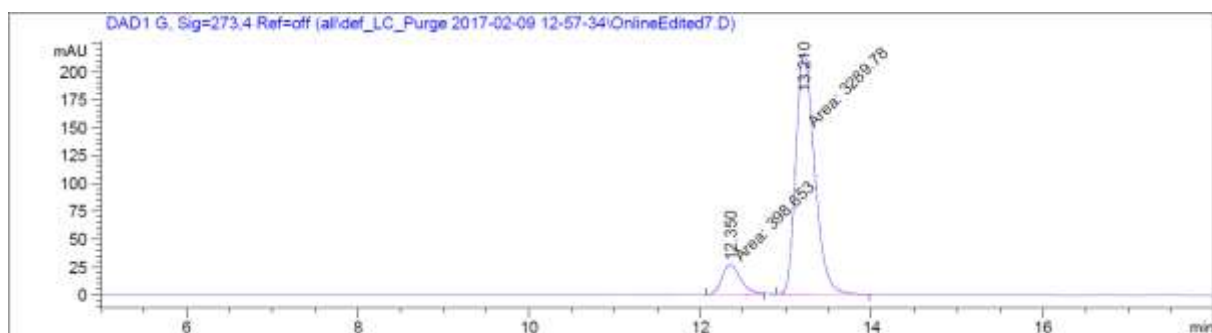
| Peak # | RetTime [min] | Type | Width [min] | Area [mAU*s] | Height [mAU] | Area % |
|--------|---------------|------|-------------|--------------|--------------|---------|
| 1 | 5.893 | MF | 0.1201 | 7587.96875 | 1052.84753 | 87.7853 |
| 2 | 6.643 | MF | 0.1376 | 1055.81055 | 127.91945 | 12.2147 |



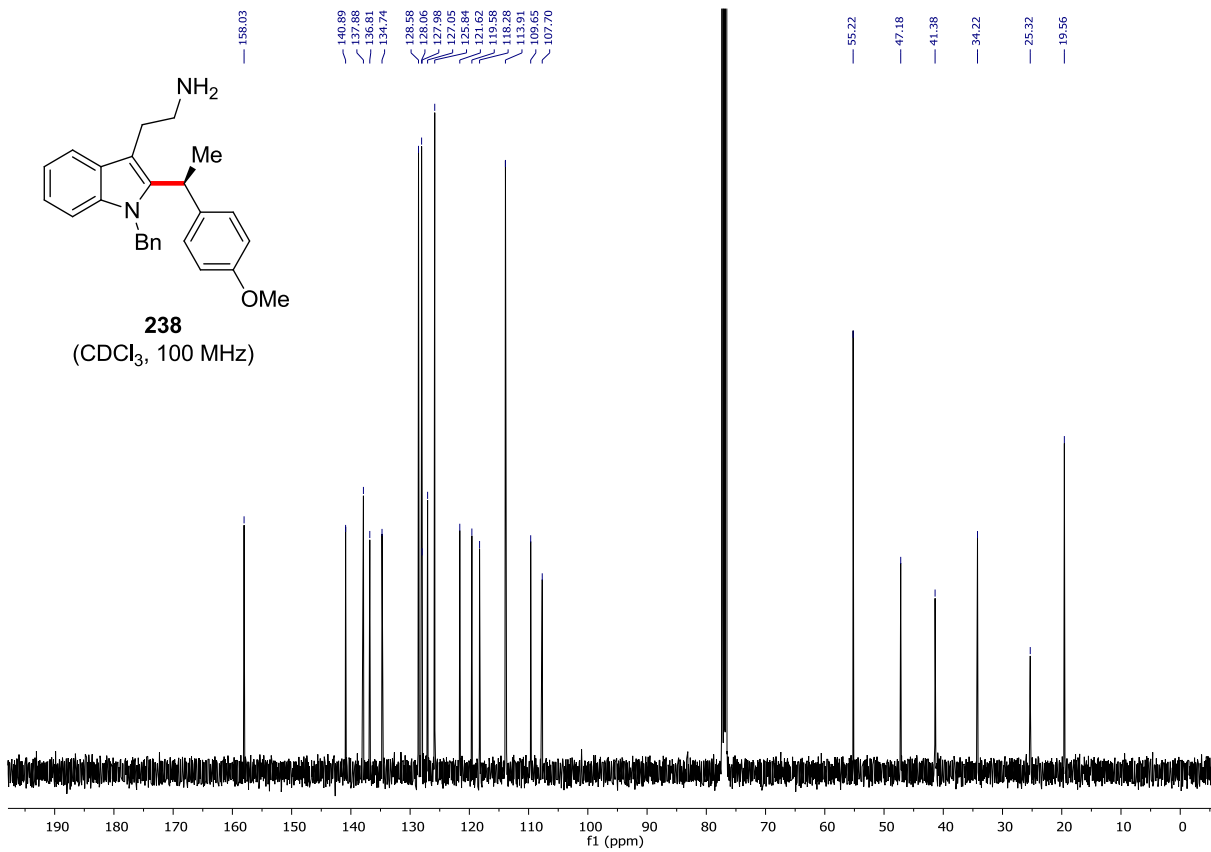
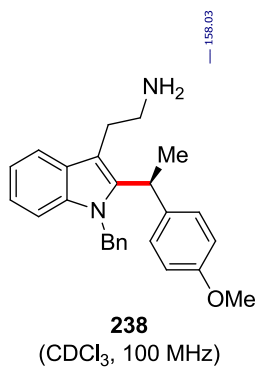
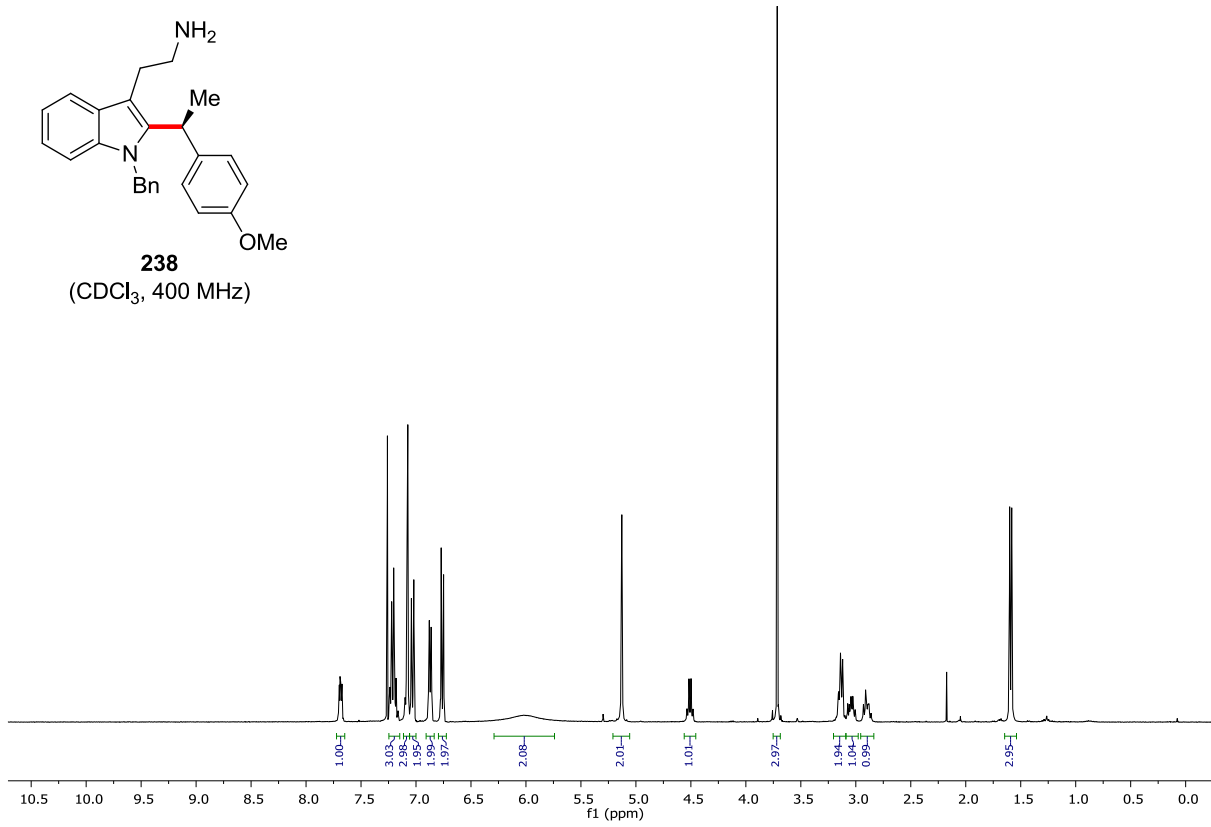
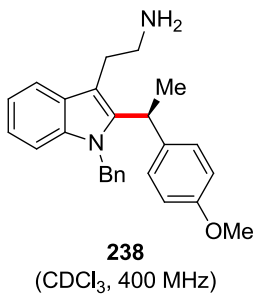
Chiral HPLC of **237**:

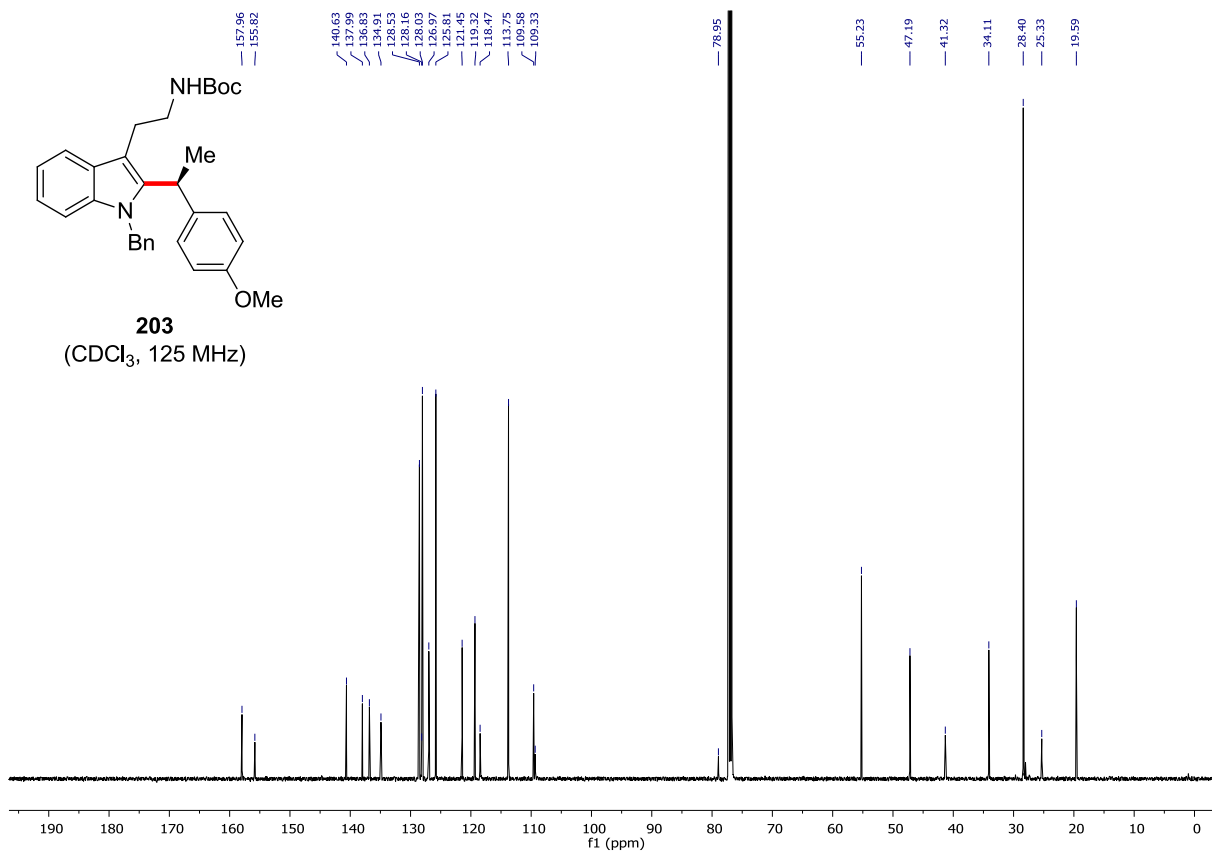
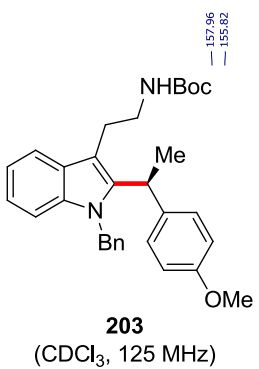
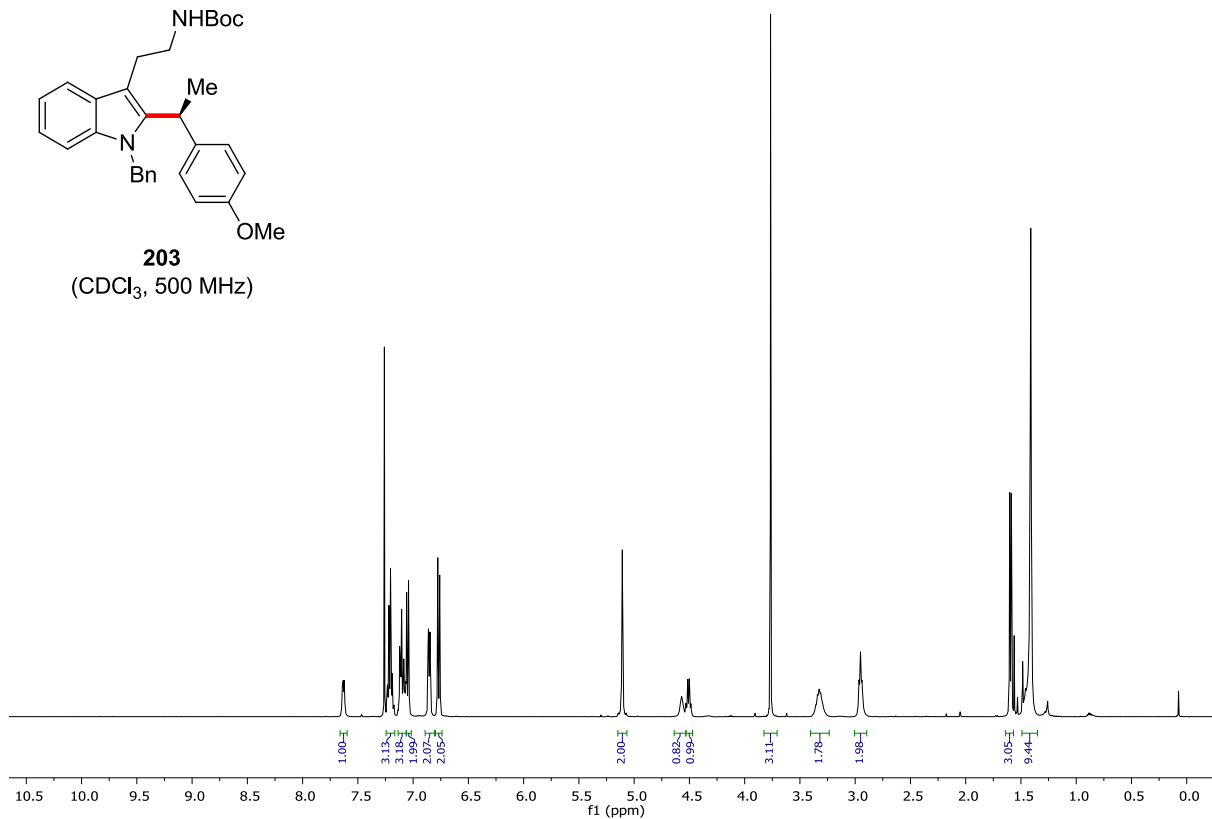
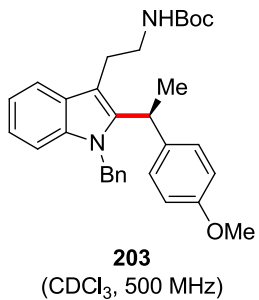


| Peak # | RetTime [min] | Type | Width [min] | Area [mAU*s] | Height [mAU] | Area % |
|--------|---------------|------|-------------|--------------|--------------|---------|
| 1 | 12.383 | FM | 0.2555 | 3292.05835 | 214.74976 | 49.9146 |
| 2 | 13.278 | MF | 0.2597 | 3303.32764 | 212.03716 | 50.0854 |

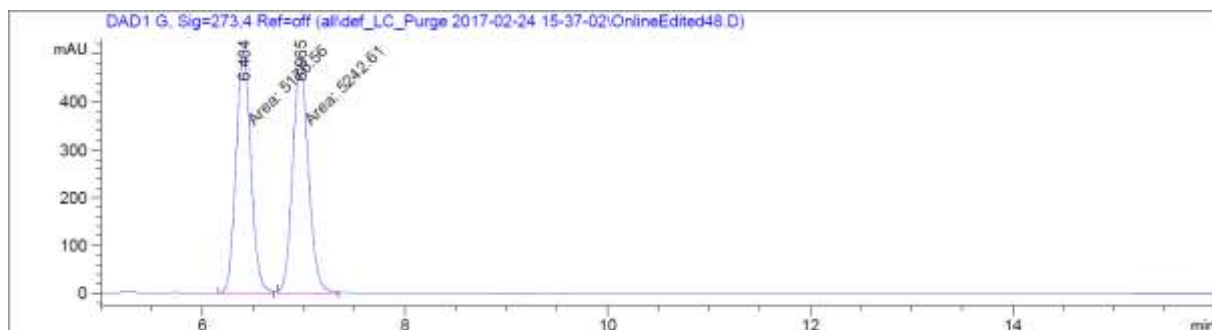


| Peak # | RetTime [min] | Type | Width [min] | Area [mAU*s] | Height [mAU] | Area % |
|--------|---------------|------|-------------|--------------|--------------|---------|
| 1 | 12.350 | MF | 0.2521 | 398.65347 | 26.35814 | 10.8082 |
| 2 | 13.210 | MF | 0.2542 | 3289.77954 | 215.67398 | 89.1918 |

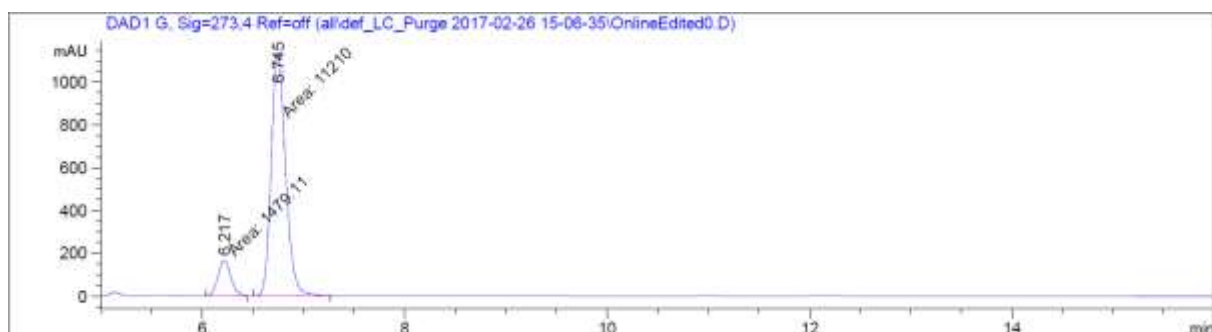




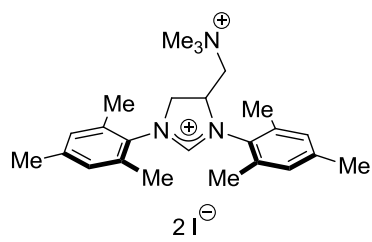
Chiral HPLC of **203**:



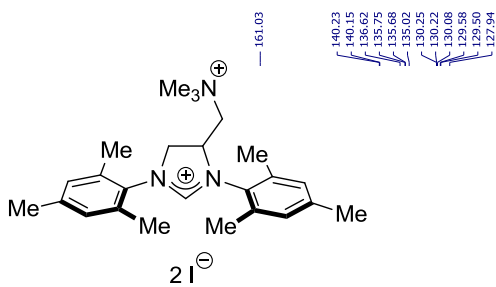
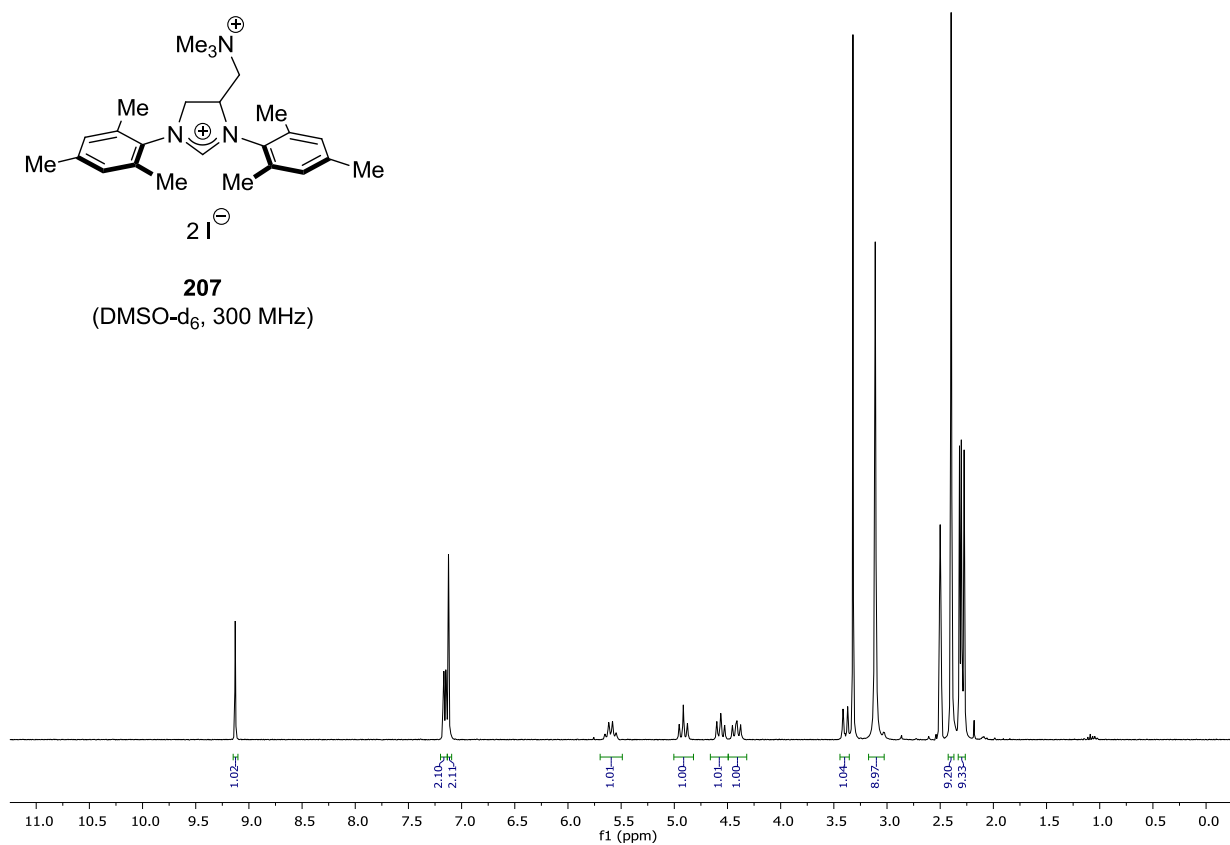
| Peak # | RetTime [min] | Type | Width [min] | Area [mAU*s] | Height [mAU] | Area % |
|--------|---------------|------|-------------|--------------|--------------|---------|
| 1 | 6.404 | FM | 0.1708 | 5176.56348 | 505.21802 | 49.6831 |
| 2 | 6.965 | FM | 0.1826 | 5242.60889 | 478.59128 | 50.3169 |



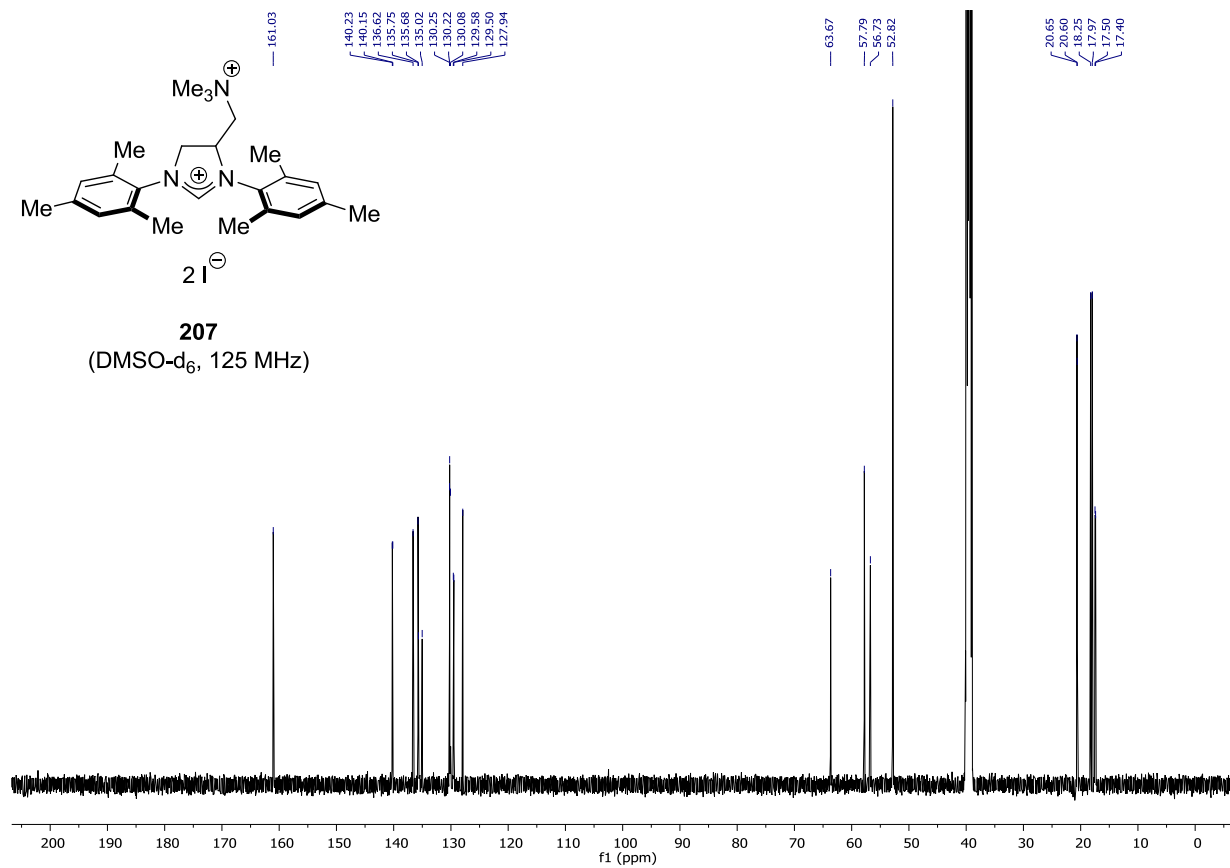
| Peak # | RetTime [min] | Type | Width [min] | Area [mAU*s] | Height [mAU] | Area % |
|--------|---------------|------|-------------|--------------|--------------|---------|
| 1 | 6.217 | MF | 0.1468 | 1479.11108 | 167.92061 | 11.6565 |
| 2 | 6.745 | MF | 0.1651 | 1.12100e4 | 1131.36987 | 88.3435 |

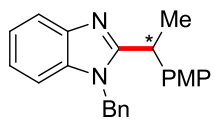


207
(DMSO- d_6 , 300 MHz)

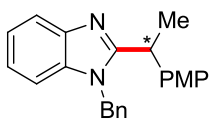
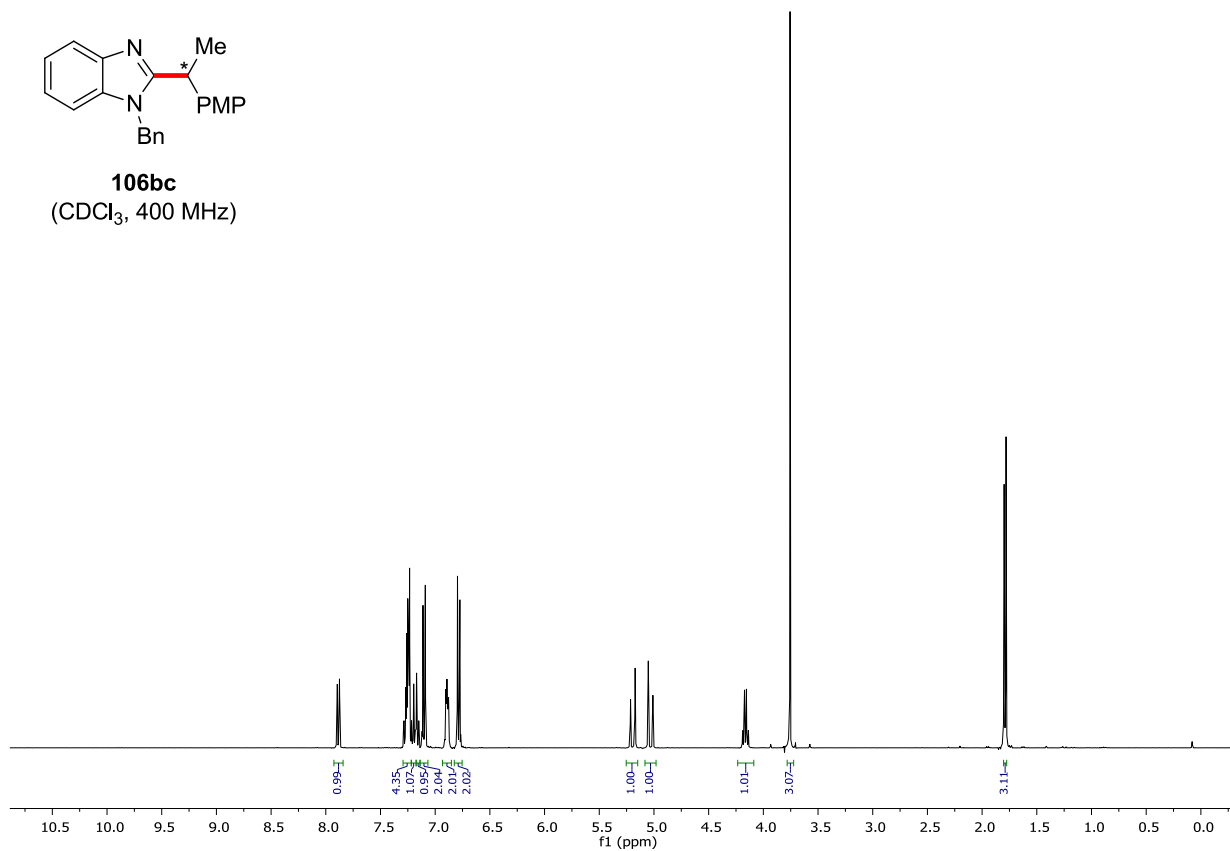


207
(DMSO- d_6 , 125 MHz)

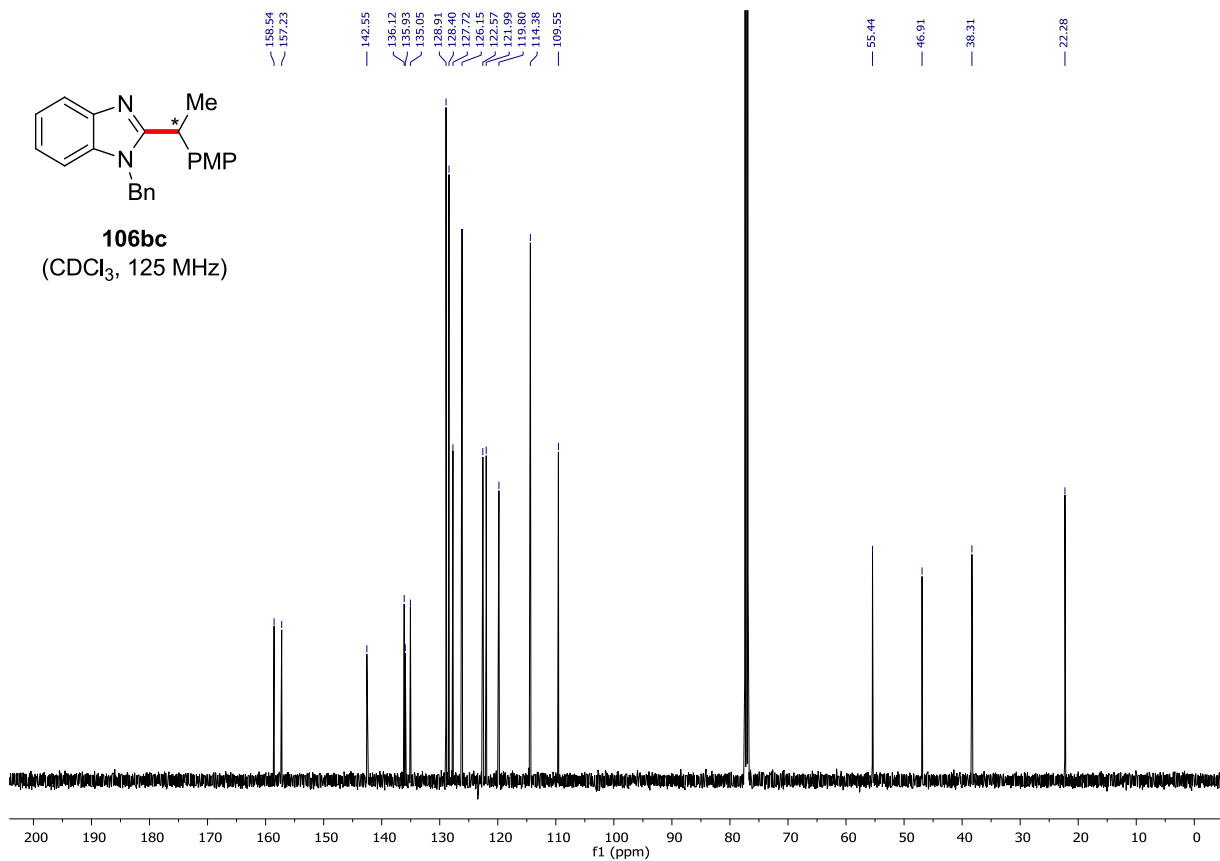




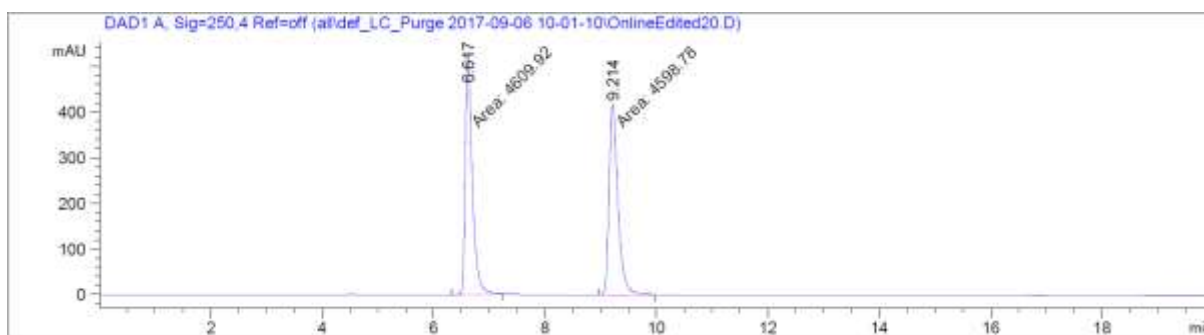
106bc
(CDCl₃, 400 MHz)



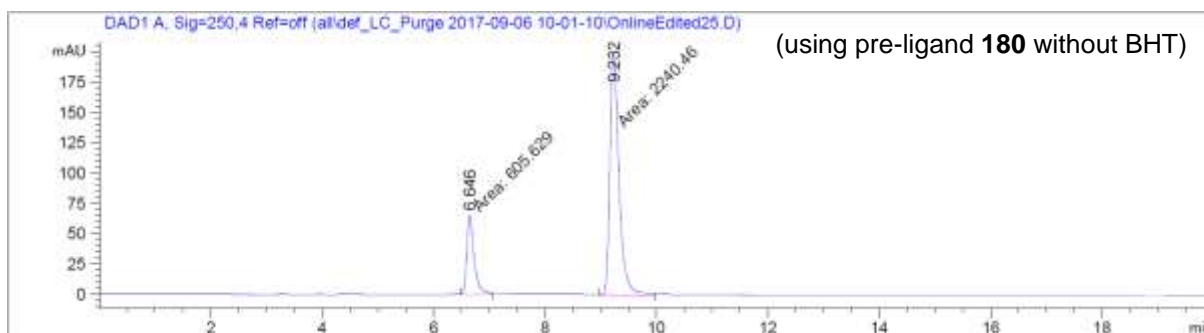
106bc
(CDCl₃, 125 MHz)



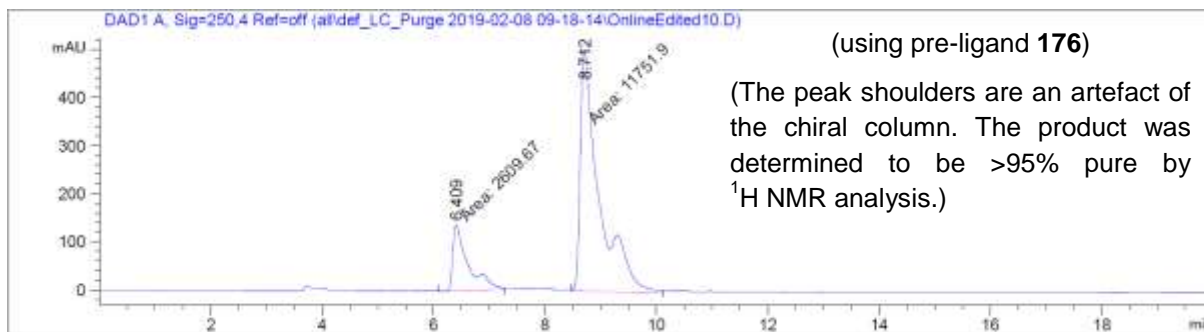
Chiral HPLC of **106bc**:



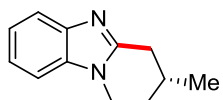
| Peak # | RetTime [min] | Type | Width [min] | Area [mAU*s] | Height [mAU] | Area % |
|--------|---------------|------|-------------|--------------|--------------|---------|
| 1 | 6.617 | MF | 0.1456 | 4609.91553 | 527.56226 | 50.0605 |
| 2 | 9.214 | MF | 0.1845 | 4598.77588 | 415.38992 | 49.9395 |



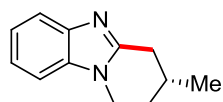
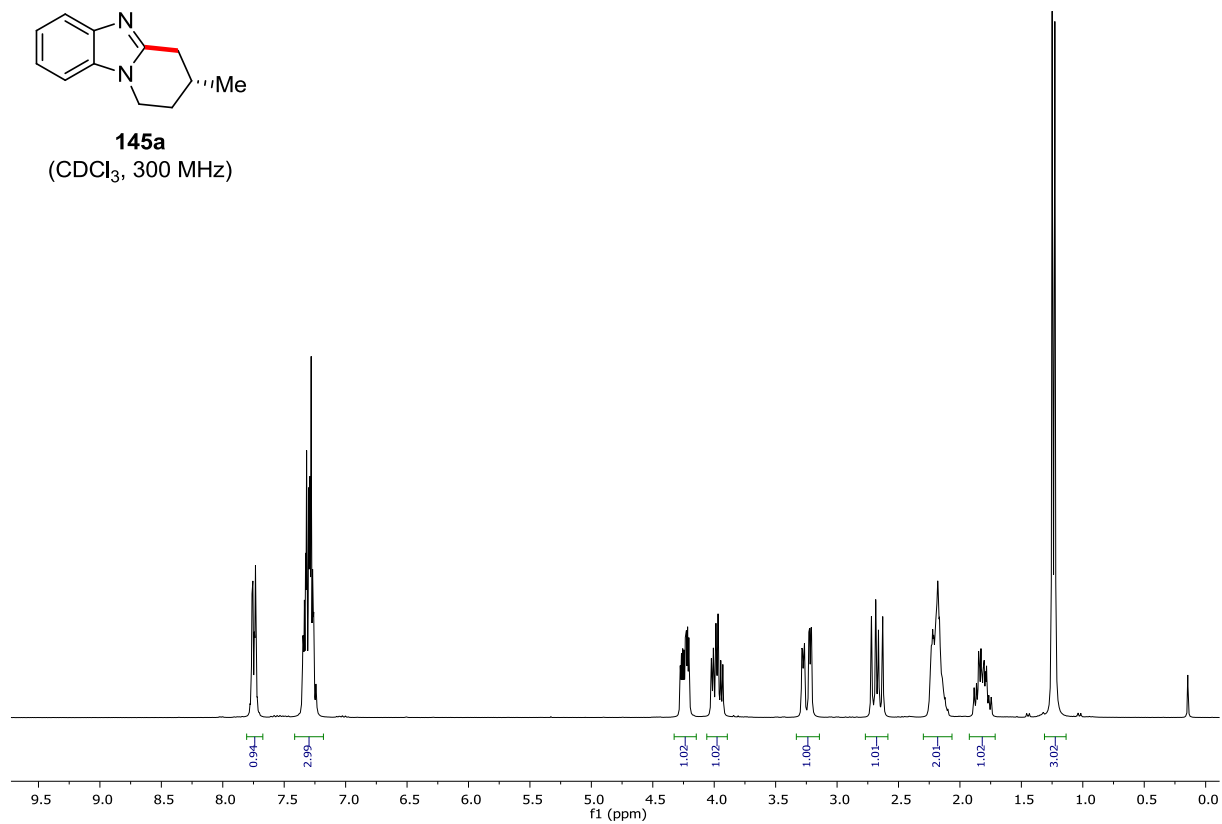
| Peak # | RetTime [min] | Type | Width [min] | Area [mAU*s] | Height [mAU] | Area % |
|--------|---------------|------|-------------|--------------|--------------|---------|
| 1 | 6.646 | MF | 0.1548 | 605.62933 | 65.19952 | 21.2793 |
| 2 | 9.232 | MF | 0.1878 | 2240.46460 | 198.84378 | 78.7207 |



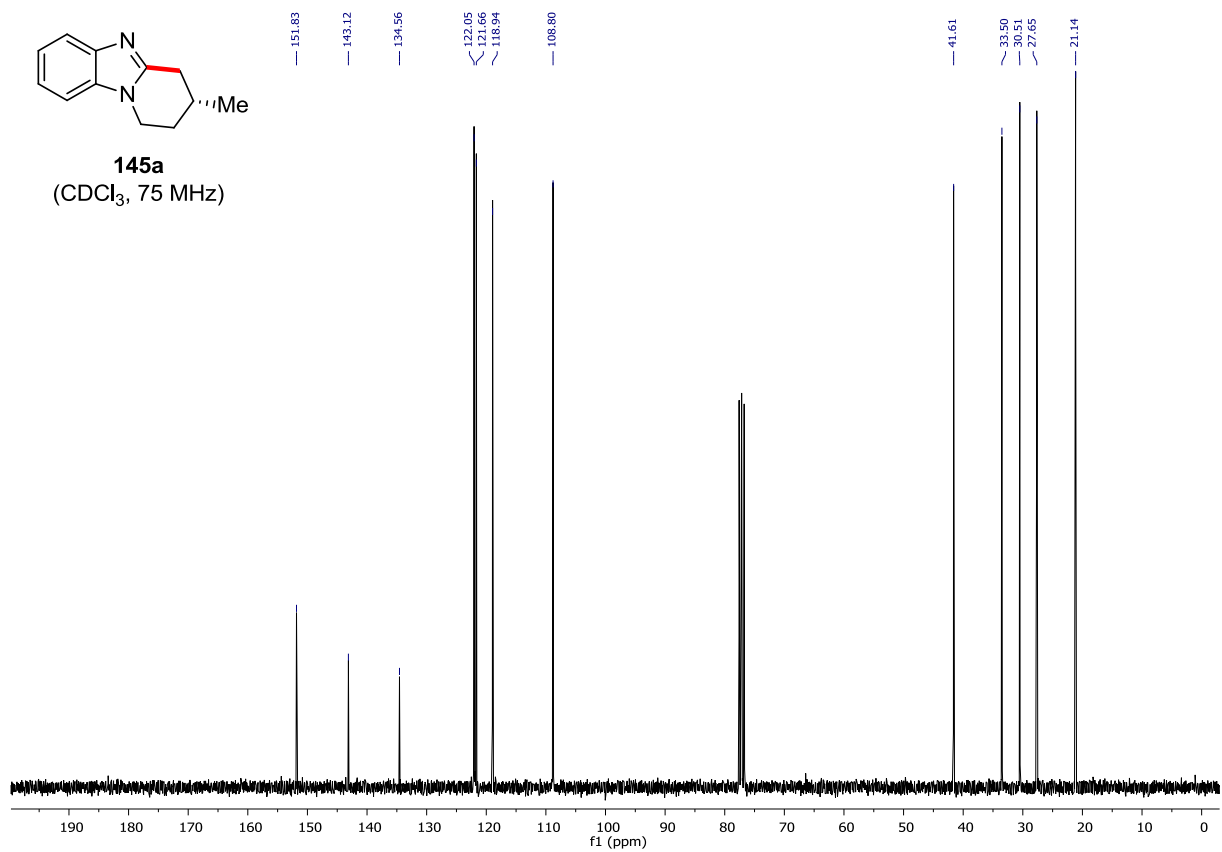
| Peak # | RetTime [min] | Type | Width [min] | Area [mAU*s] | Height [mAU] | Area % |
|--------|---------------|------|-------------|--------------|--------------|---------|
| 1 | 6.409 | MM | 0.3164 | 2609.67163 | 137.46823 | 18.1712 |
| 2 | 8.712 | MF | 0.3911 | 1.17519e4 | 500.74280 | 81.8288 |



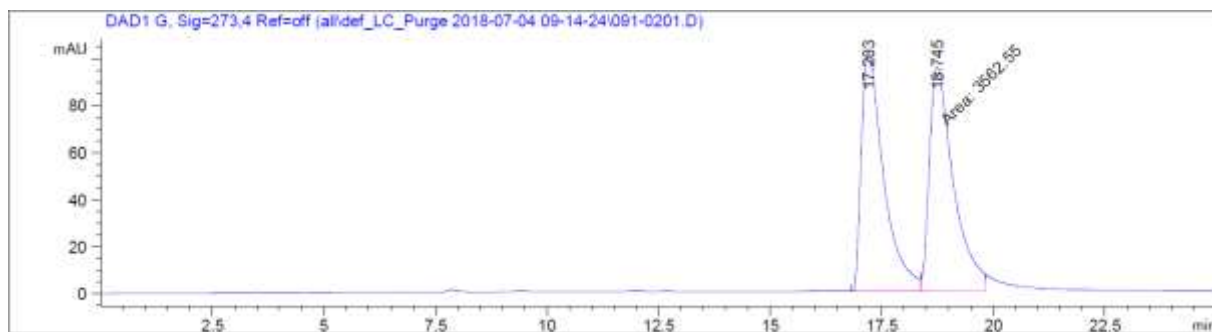
145a
(CDCl₃, 300 MHz)



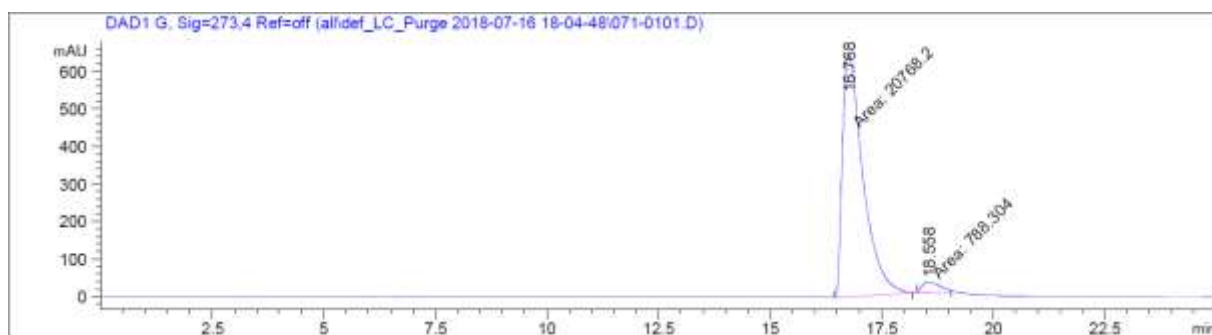
145a
(CDCl₃, 75 MHz)



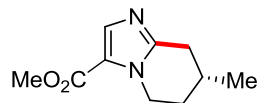
Chiral HPLC of **145a**:



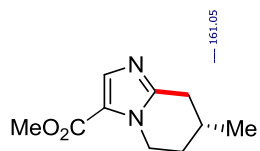
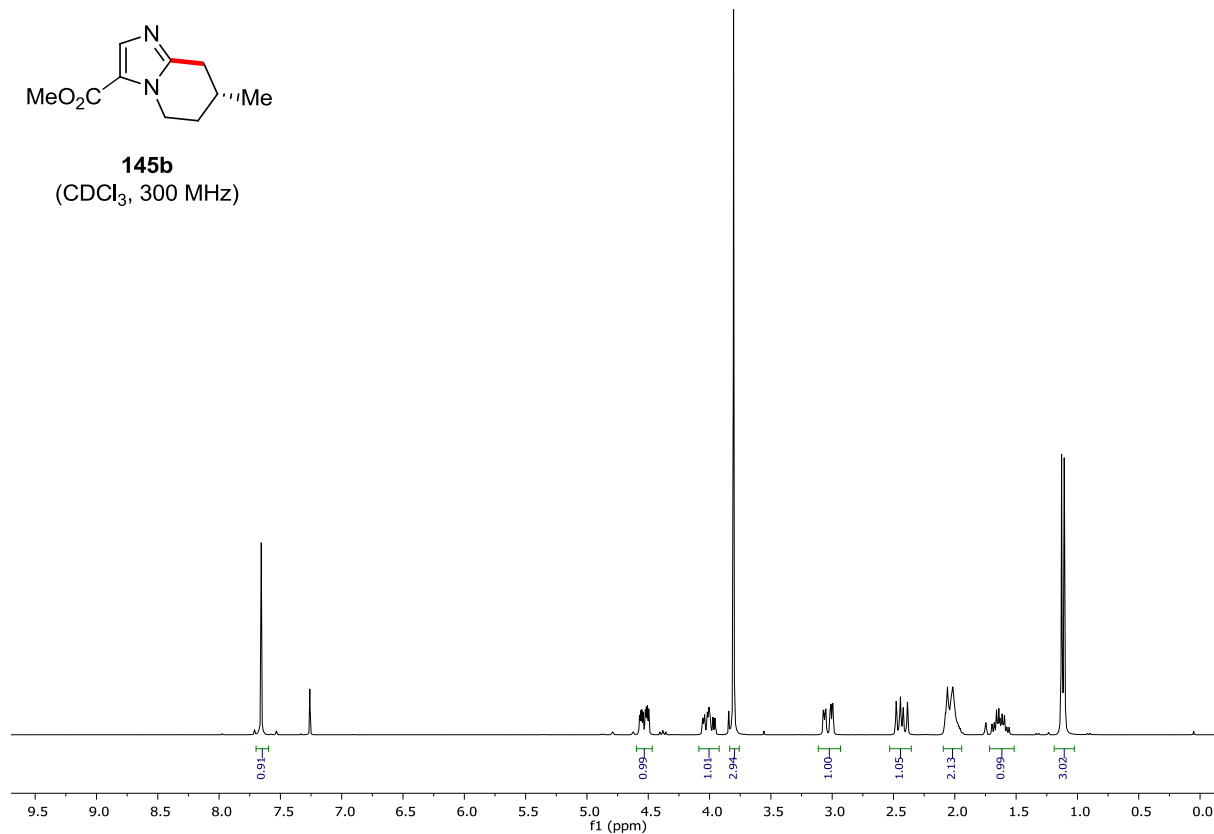
| Peak # | RetTime [min] | Type | Width [min] | Area [mAU*s] | Height [mAU] | Area % |
|--------|---------------|------|-------------|--------------|--------------|---------|
| 1 | 17.203 | BV | 0.5119 | 3516.55786 | 101.82705 | 49.6752 |
| 2 | 18.745 | MF | 0.6232 | 3562.54932 | 95.27898 | 50.3248 |



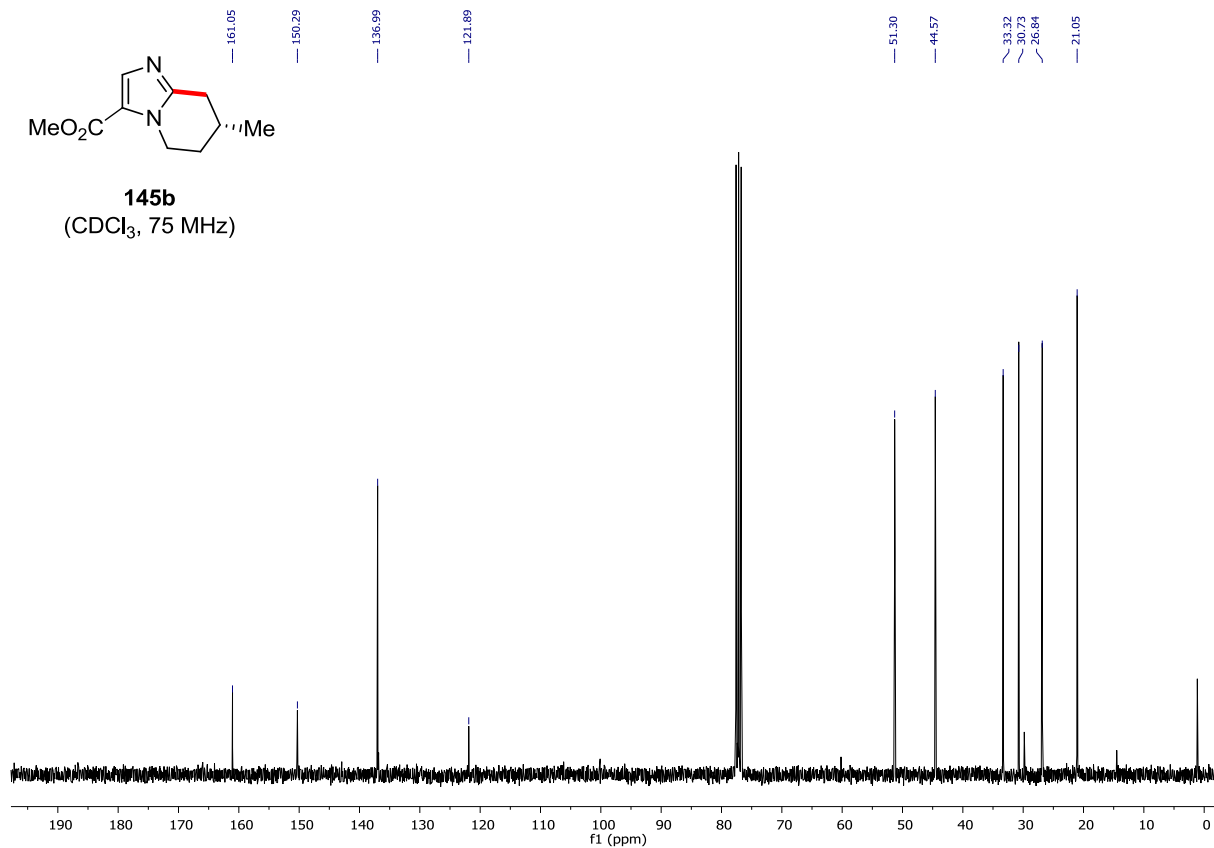
| Peak # | RetTime [min] | Type | Width [min] | Area [mAU*s] | Height [mAU] | Area % |
|--------|---------------|------|-------------|--------------|--------------|---------|
| 1 | 16.768 | MM | 0.5343 | 2.07682e4 | 647.85571 | 96.3431 |
| 2 | 18.558 | FM | 0.4771 | 788.30365 | 27.53768 | 3.6569 |



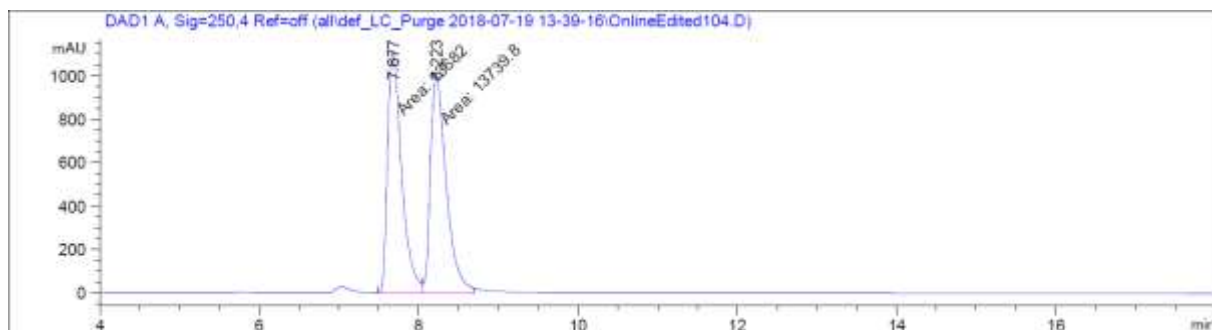
145b
(CDCl₃, 300 MHz)



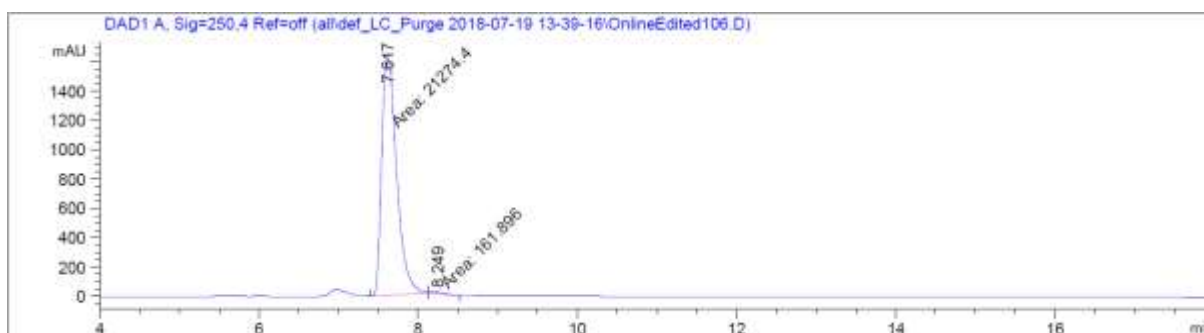
145b
(CDCl₃, 75 MHz)



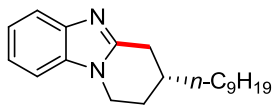
Chiral HPLC of **145b**:



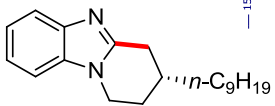
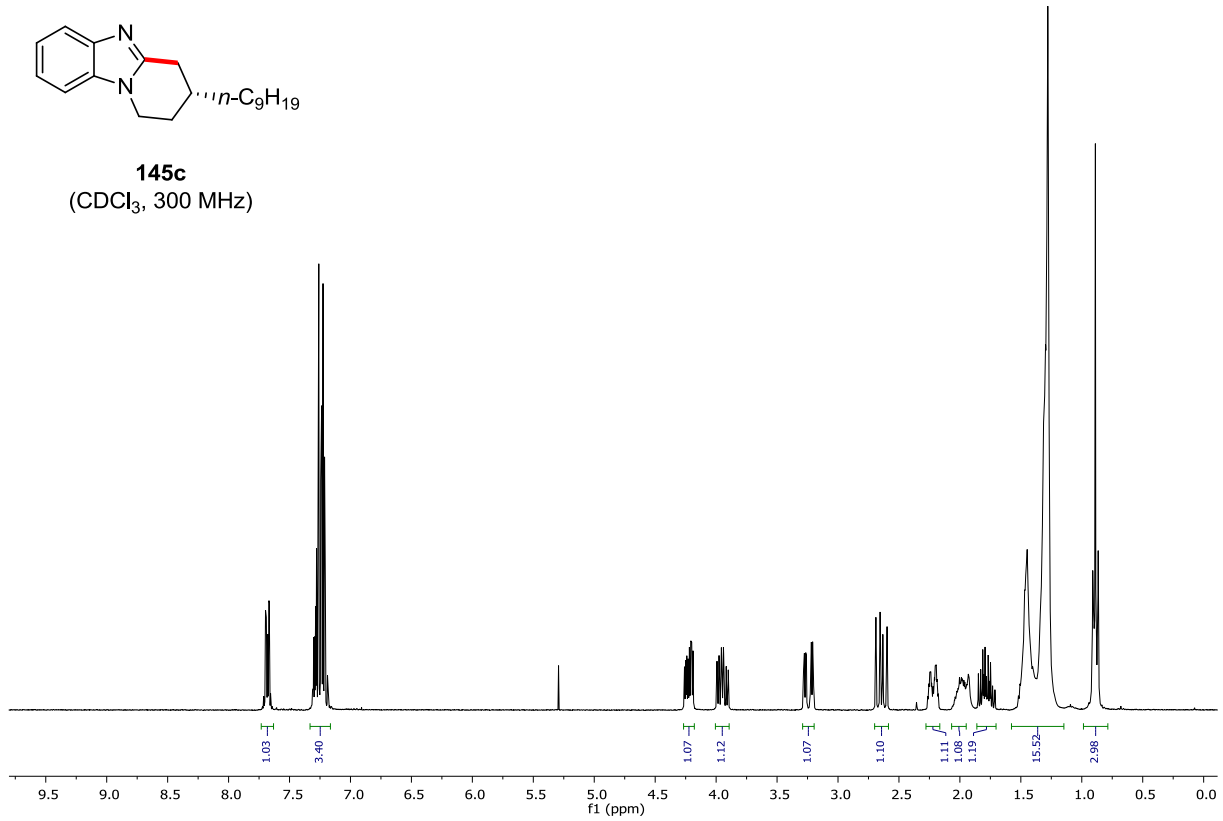
| Peak # | RetTime [min] | Type | Width [min] | Area [mAU*s] | Height [mAU] | Area % |
|--------|---------------|------|-------------|--------------|--------------|---------|
| 1 | 7.677 | FM | 0.2051 | 1.36820e4 | 1111.54712 | 49.8945 |
| 2 | 8.223 | MF | 0.2318 | 1.37398e4 | 988.07825 | 50.1055 |



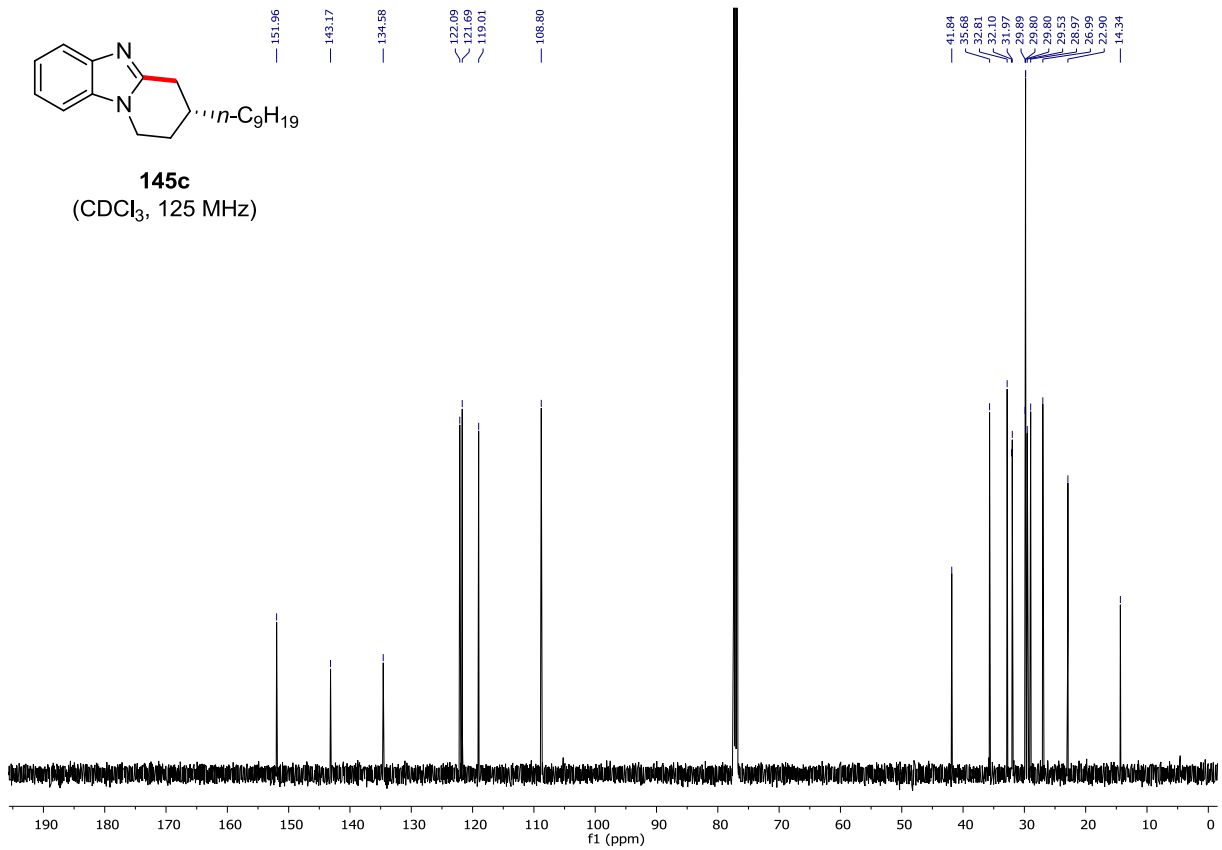
| Peak # | RetTime [min] | Type | Width [min] | Area [mAU*s] | Height [mAU] | Area % |
|--------|---------------|------|-------------|--------------|--------------|---------|
| 1 | 7.617 | MM | 0.2155 | 2.12744e4 | 1644.99255 | 99.2448 |
| 2 | 8.249 | MM | 0.2293 | 161.89574 | 11.76511 | 0.7552 |



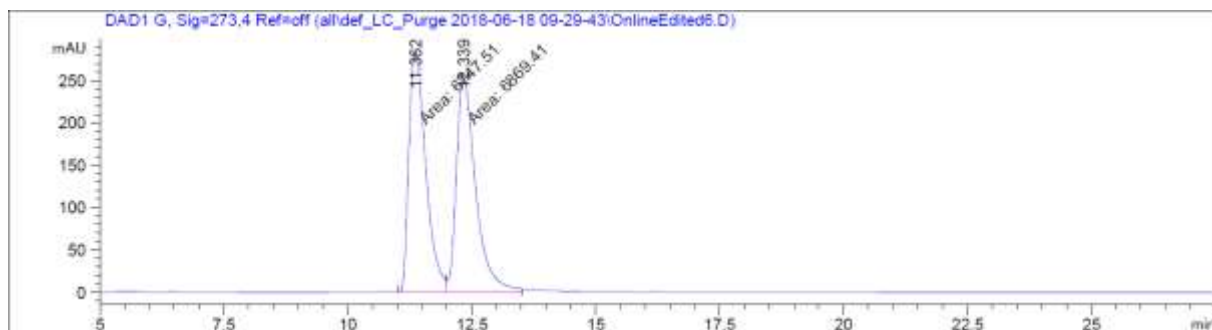
145c
(CDCl₃, 300 MHz)



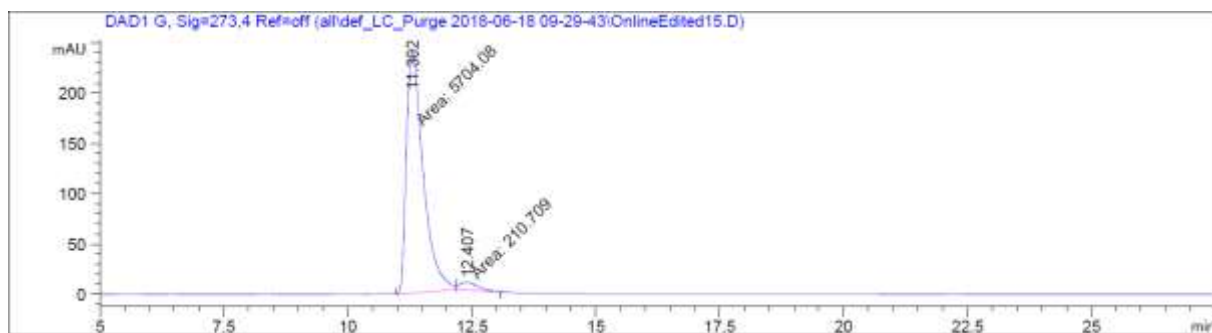
145c
(CDCl₃, 125 MHz)



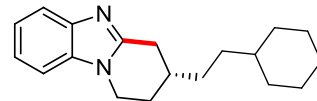
Chiral HPLC of **145c**:



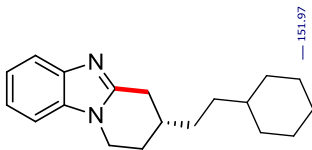
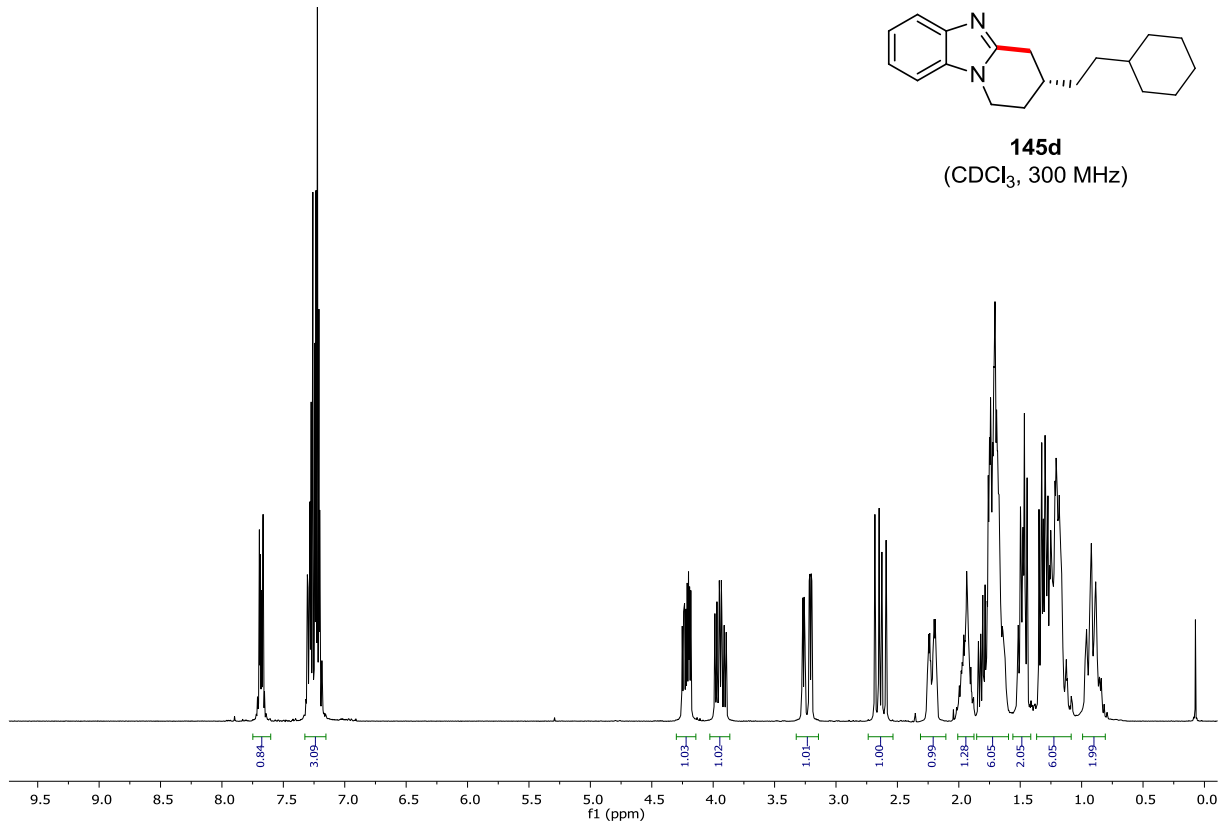
| Peak # | RetTime [min] | Type | Width [min] | Area [mAU*s] | Height [mAU] | Area % |
|--------|---------------|------|-------------|--------------|--------------|---------|
| 1 | 11.362 | FM | 0.3946 | 6747.50879 | 284.98068 | 49.5524 |
| 2 | 12.339 | MF | 0.4518 | 6869.40723 | 253.43456 | 50.4476 |



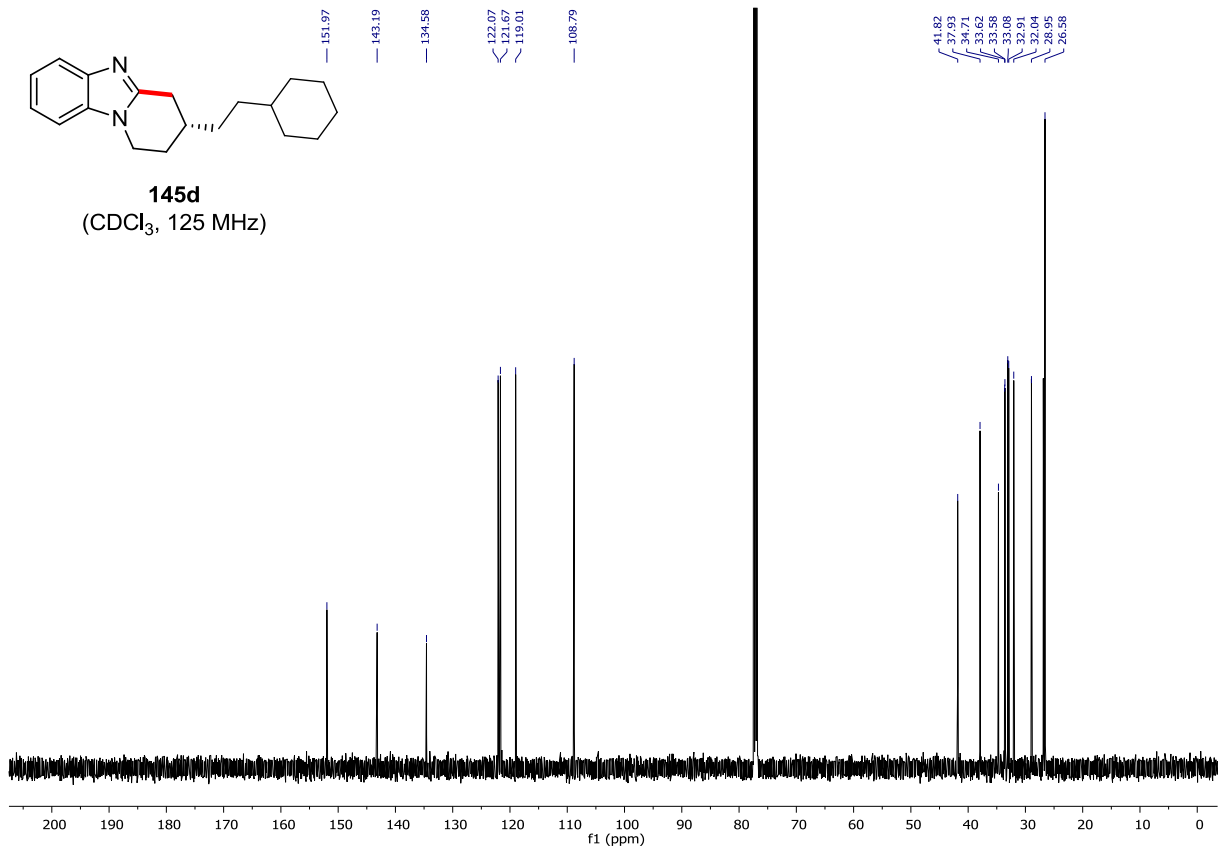
| Peak # | RetTime [min] | Type | Width [min] | Area [mAU*s] | Height [mAU] | Area % |
|--------|---------------|------|-------------|--------------|--------------|---------|
| 1 | 11.302 | MM | 0.3960 | 5704.08252 | 240.09137 | 96.4376 |
| 2 | 12.407 | MM | 0.4385 | 210.70900 | 8.00797 | 3.5624 |



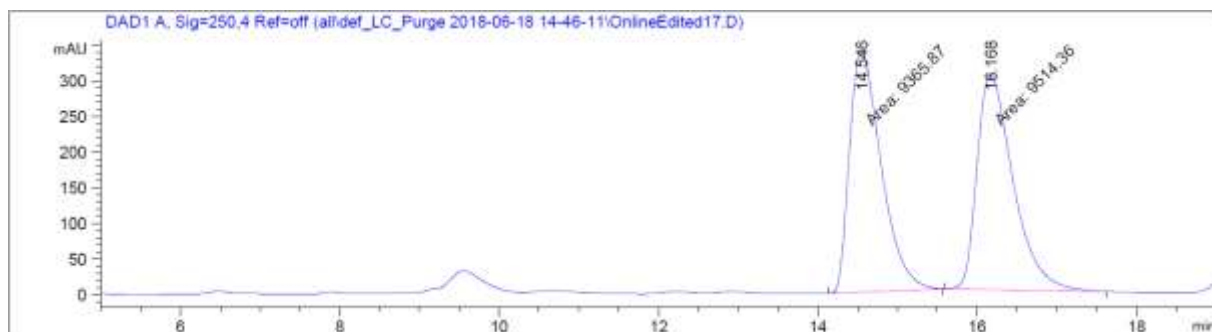
145d
(CDCl₃, 300 MHz)



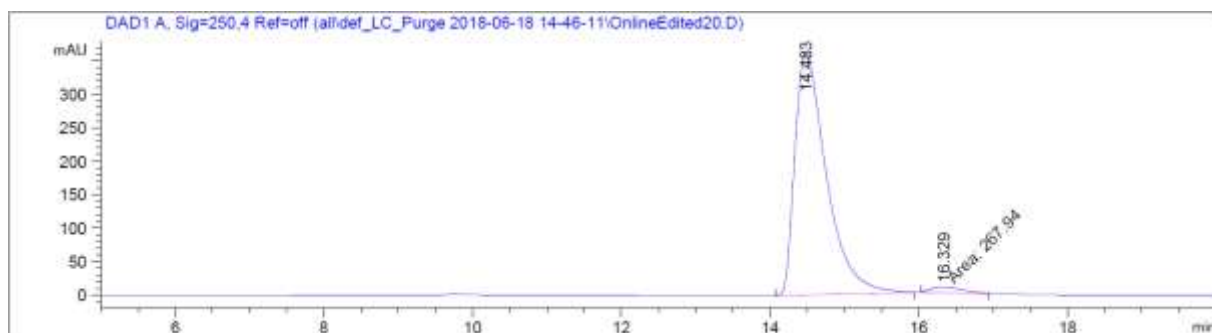
145d
(CDCl₃, 125 MHz)



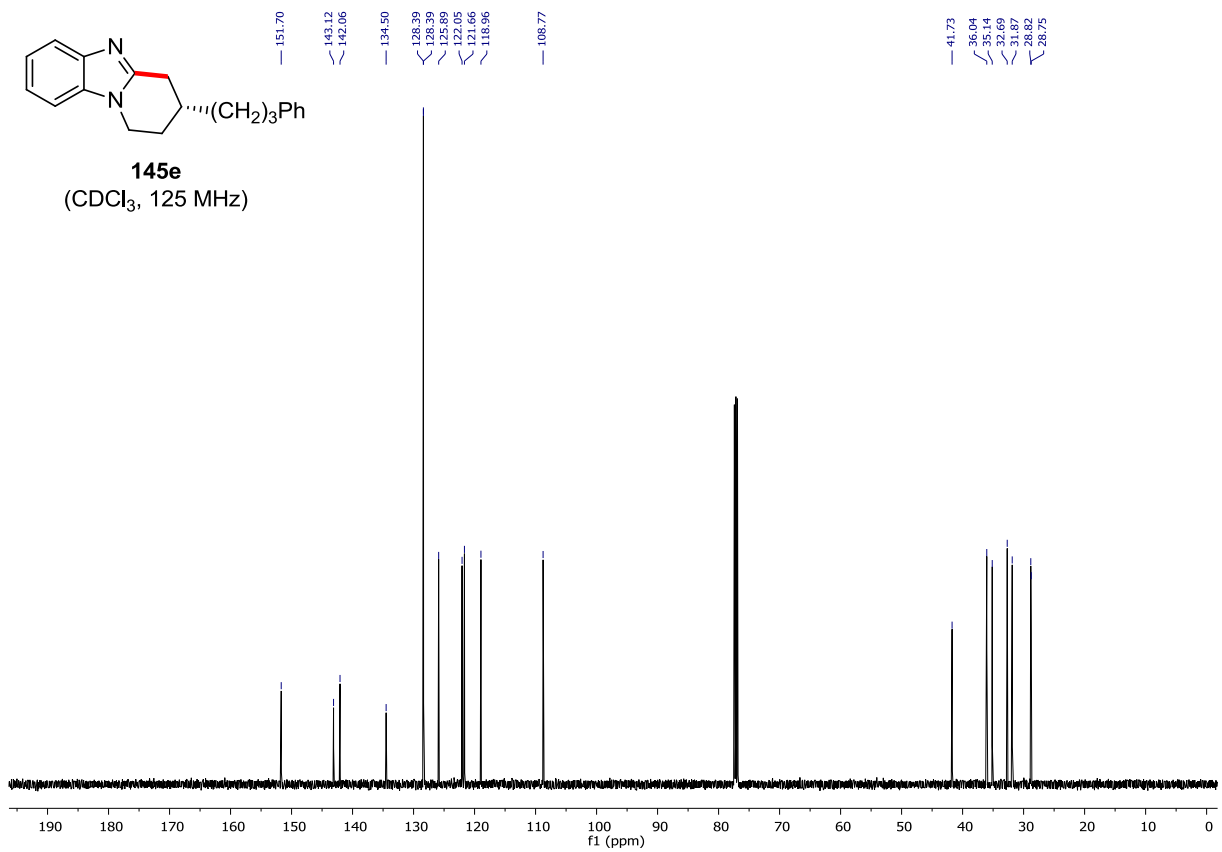
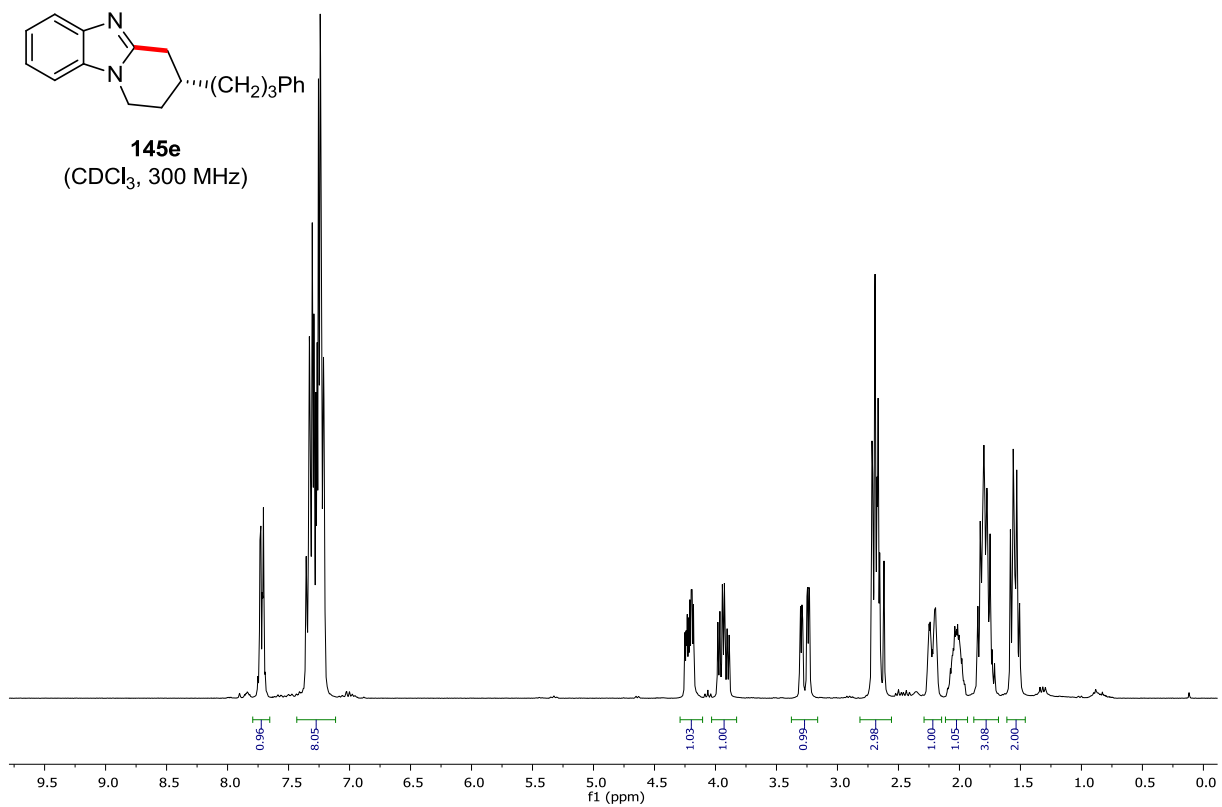
Chiral HPLC of **145d**:



| Peak # | RetTime [min] | Type | Width [min] | Area [mAU*s] | Height [mAU] | Area % |
|--------|---------------|------|-------------|--------------|--------------|---------|
| 1 | 14.546 | MF | 0.4636 | 9365.87012 | 336.72678 | 49.6068 |
| 2 | 16.168 | MF | 0.5251 | 9514.36230 | 301.95865 | 50.3932 |



| Peak # | RetTime [min] | Type | Width [min] | Area [mAU*s] | Height [mAU] | Area % |
|--------|---------------|------|-------------|--------------|--------------|---------|
| 1 | 14.483 | BB | 0.4462 | 1.06011e4 | 360.34625 | 97.5348 |
| 2 | 16.329 | MF | 0.5013 | 267.93982 | 8.90831 | 2.4652 |



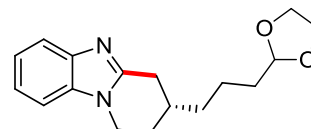
Chiral HPLC of **145e**:



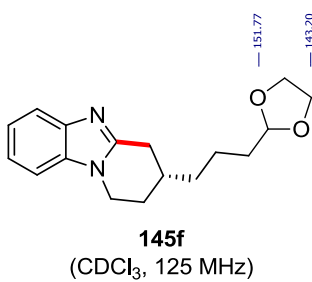
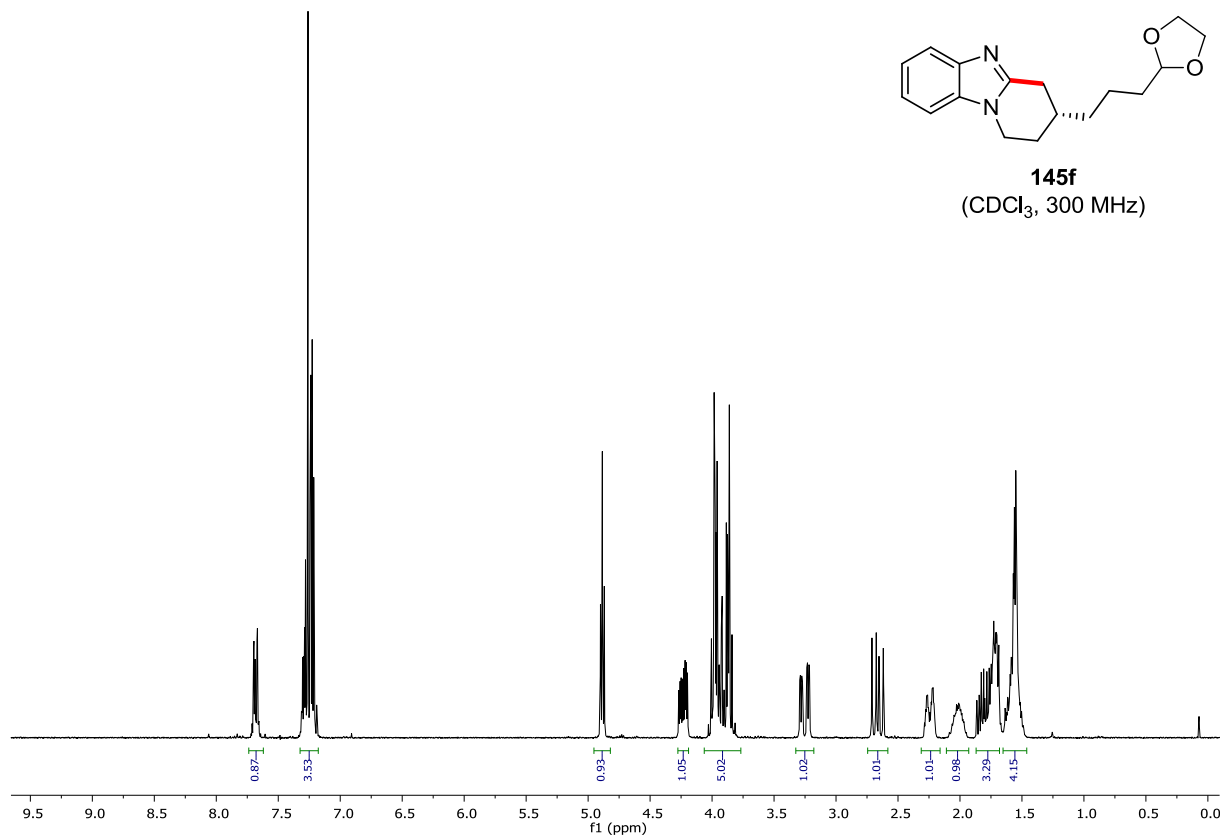
| Peak # | RetTime [min] | Type | Width [min] | Area [mAU*s] | Height [mAU] | Area % |
|--------|---------------|------|-------------|--------------|--------------|---------|
| 1 | 20.699 | MF | 0.6448 | 2.37519e4 | 613.93451 | 50.1536 |
| 2 | 24.956 | MF | 0.7807 | 2.36064e4 | 503.98380 | 49.8464 |



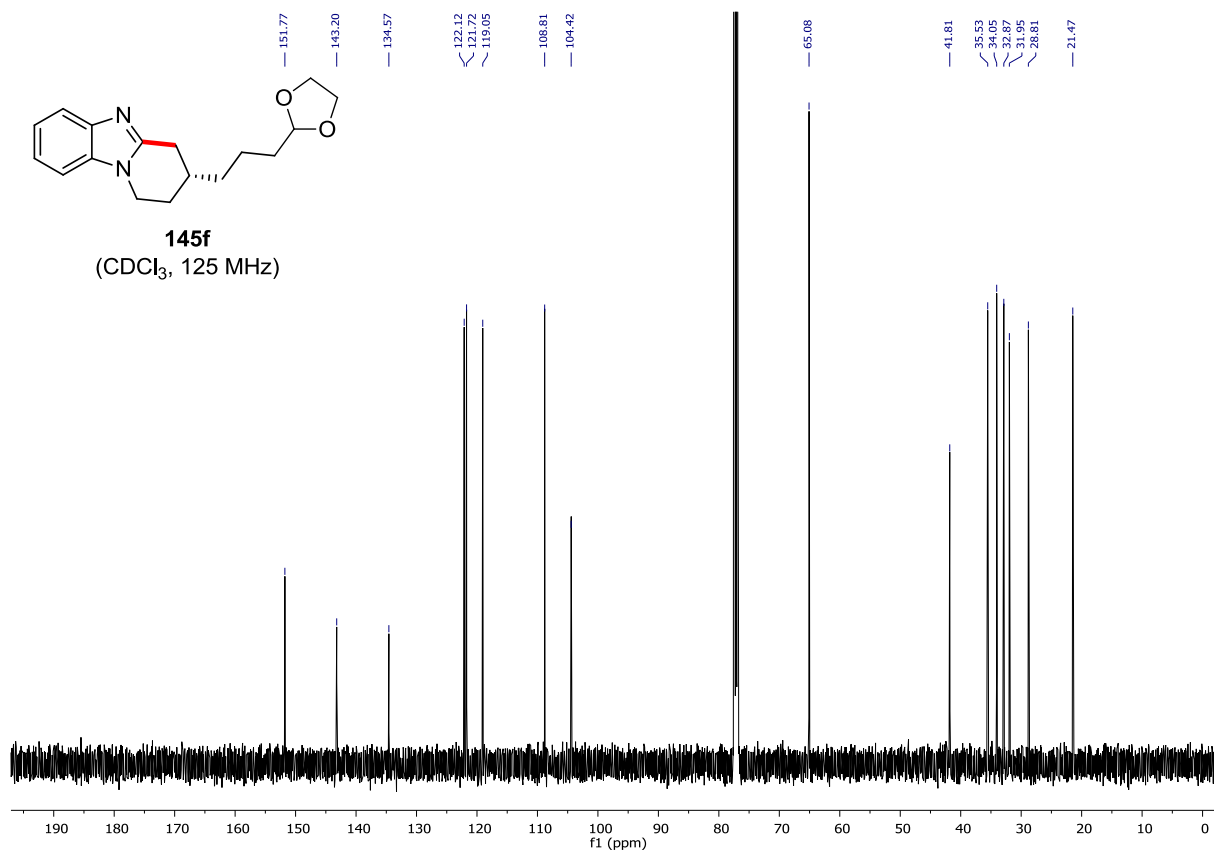
| Peak # | RetTime [min] | Type | Width [min] | Area [mAU*s] | Height [mAU] | Area % |
|--------|---------------|------|-------------|--------------|--------------|---------|
| 1 | 20.558 | MF | 0.7887 | 9.70282e4 | 2050.28638 | 96.8836 |
| 2 | 25.498 | MF | 0.8157 | 3121.02002 | 63.76646 | 3.1164 |



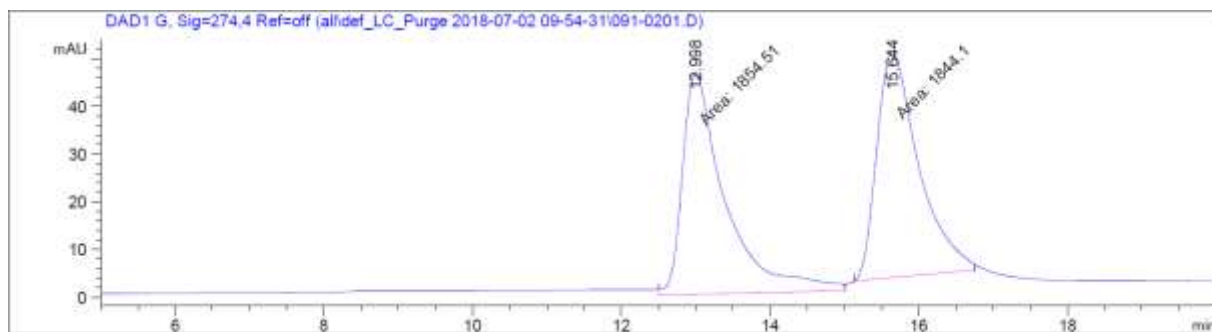
145f
(CDCl₃, 300 MHz)



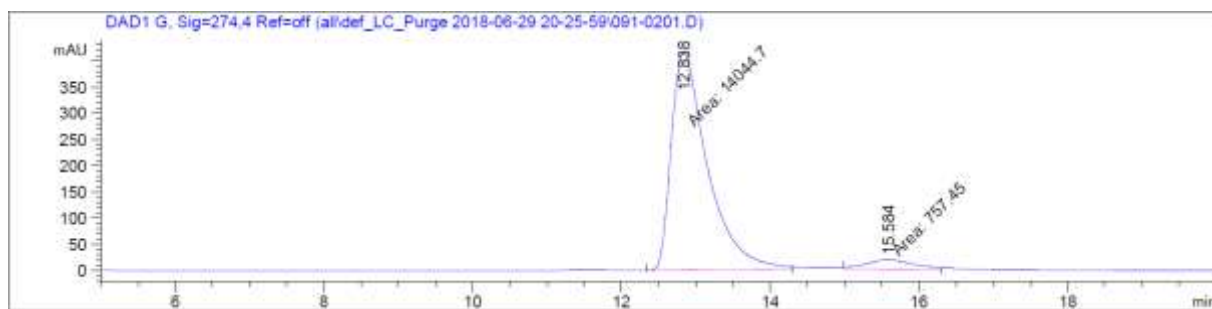
145f
(CDCl₃, 125 MHz)



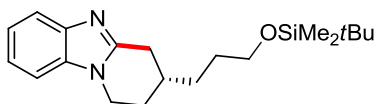
Chiral HPLC of **145f**:



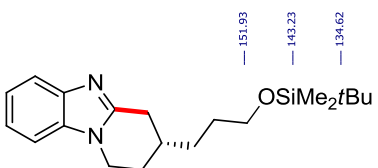
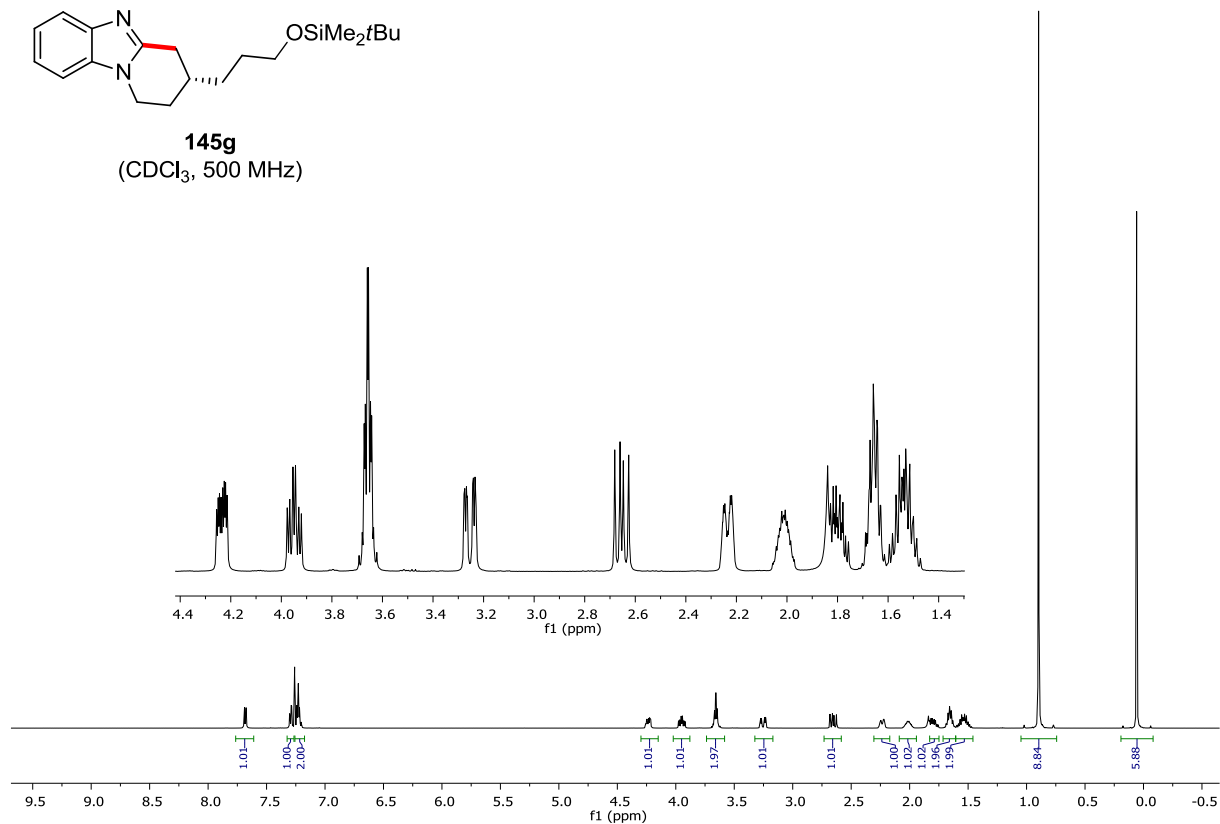
| Peak # | RetTime [min] | Type | Width [min] | Area [mAU*s] | Height [mAU] | Area % |
|--------|---------------|------|-------------|--------------|--------------|---------|
| 1 | 12.998 | MM | 0.6651 | 1854.51062 | 46.47122 | 50.1407 |
| 2 | 15.644 | MM | 0.6495 | 1844.10376 | 47.31788 | 49.8593 |



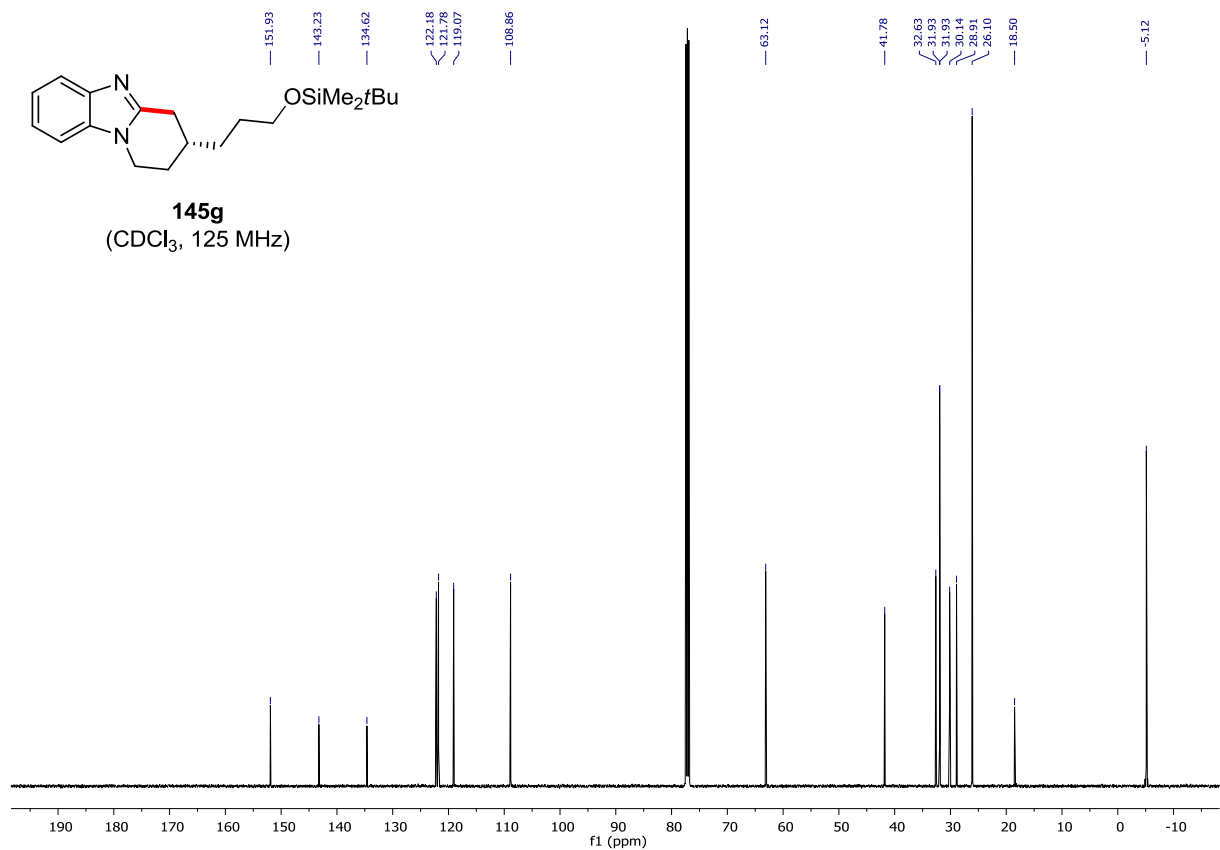
| Peak # | RetTime [min] | Type | Width [min] | Area [mAU*s] | Height [mAU] | Area % |
|--------|---------------|------|-------------|--------------|--------------|---------|
| 1 | 12.838 | MF | 0.5616 | 1.40447e4 | 416.79770 | 94.8828 |
| 2 | 15.584 | MF | 0.7181 | 757.44995 | 17.57906 | 5.1172 |



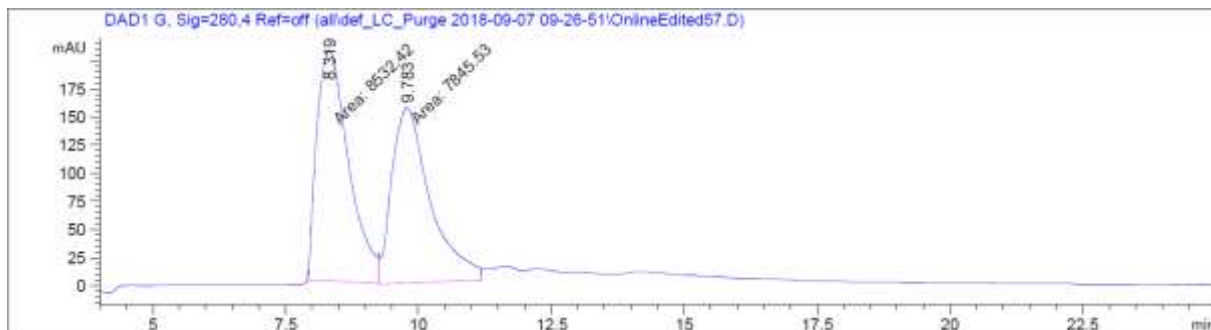
145g
(CDCl₃, 500 MHz)



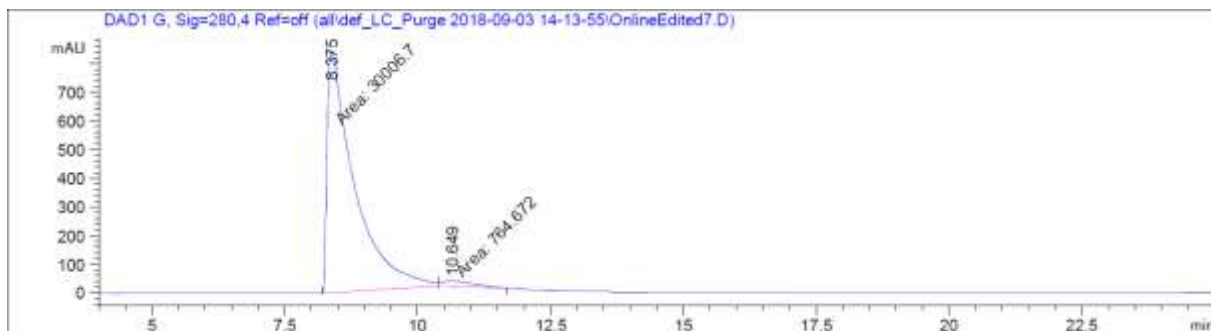
145g
(CDCl₃, 125 MHz)



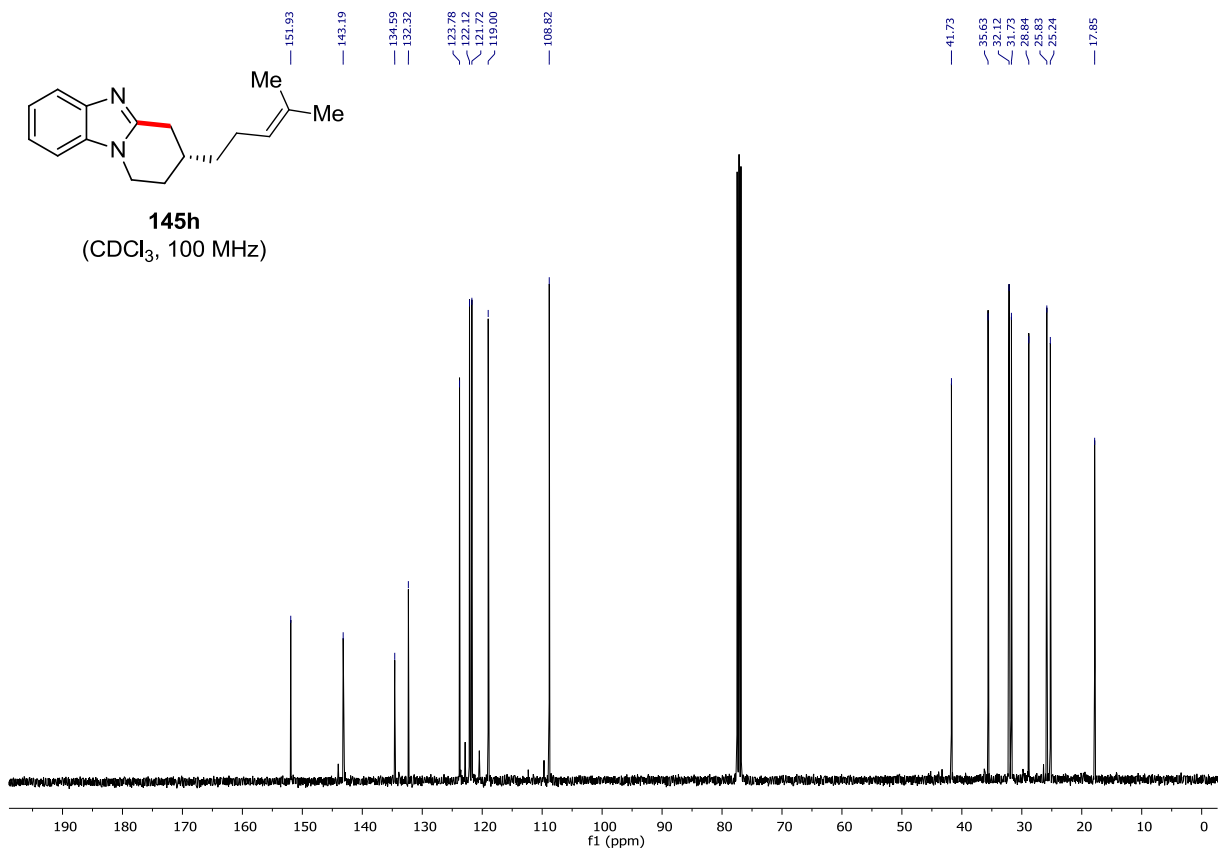
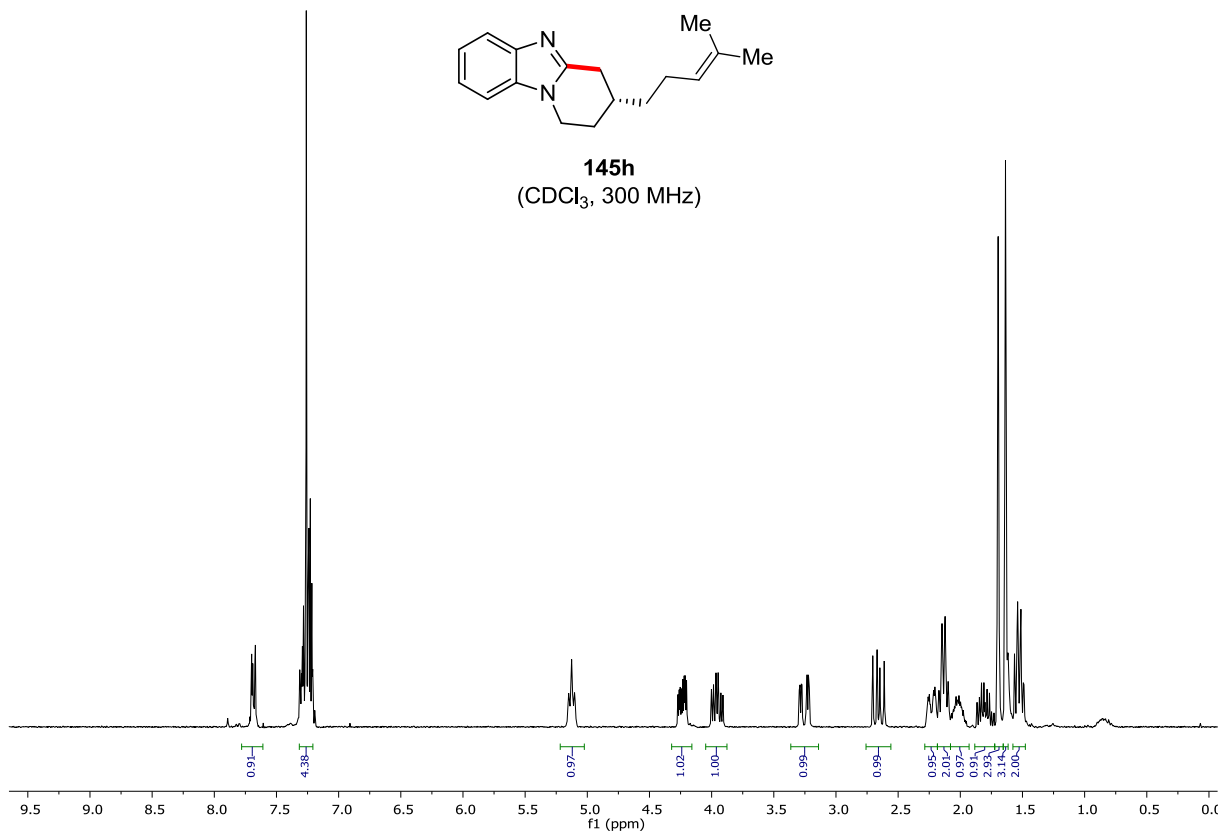
Chiral HPLC of **145g**:



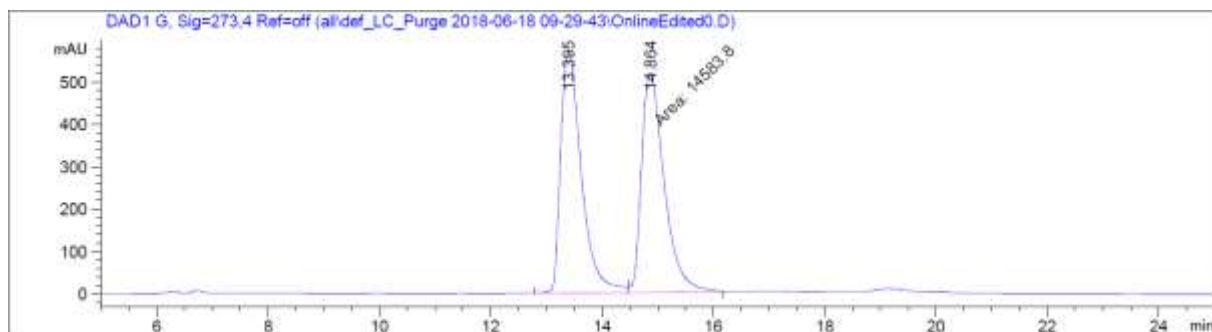
| Peak # | RetTime [min] | Type | Width [min] | Area [mAU*s] | Height [mAU] | Area % |
|--------|---------------|------|-------------|--------------|--------------|---------|
| 1 | 8.319 | MM | 0.6940 | 8532.42090 | 204.91148 | 52.0970 |
| 2 | 9.783 | MM | 0.8401 | 7845.52588 | 155.65579 | 47.9030 |



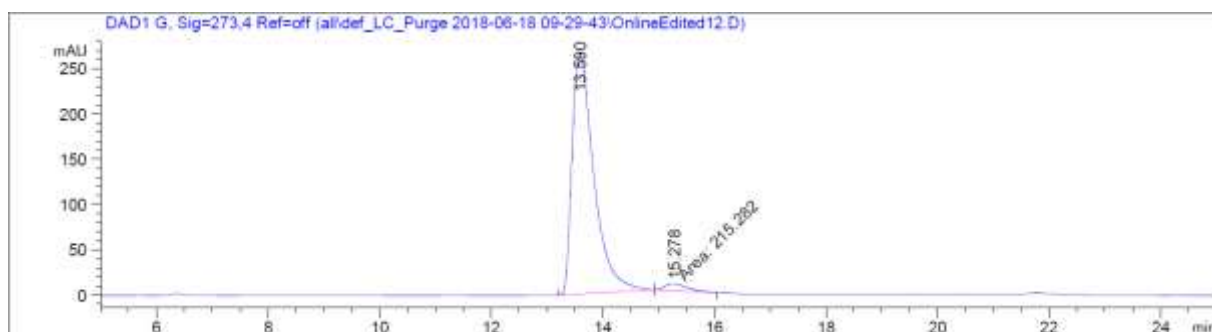
| Peak # | RetTime [min] | Type | Width [min] | Area [mAU*s] | Height [mAU] | Area % |
|--------|---------------|------|-------------|--------------|--------------|---------|
| 1 | 8.375 | MM | 0.5922 | 3.00067e4 | 844.53638 | 97.5150 |
| 2 | 10.649 | MM | 0.7022 | 764.67218 | 18.14847 | 2.4850 |



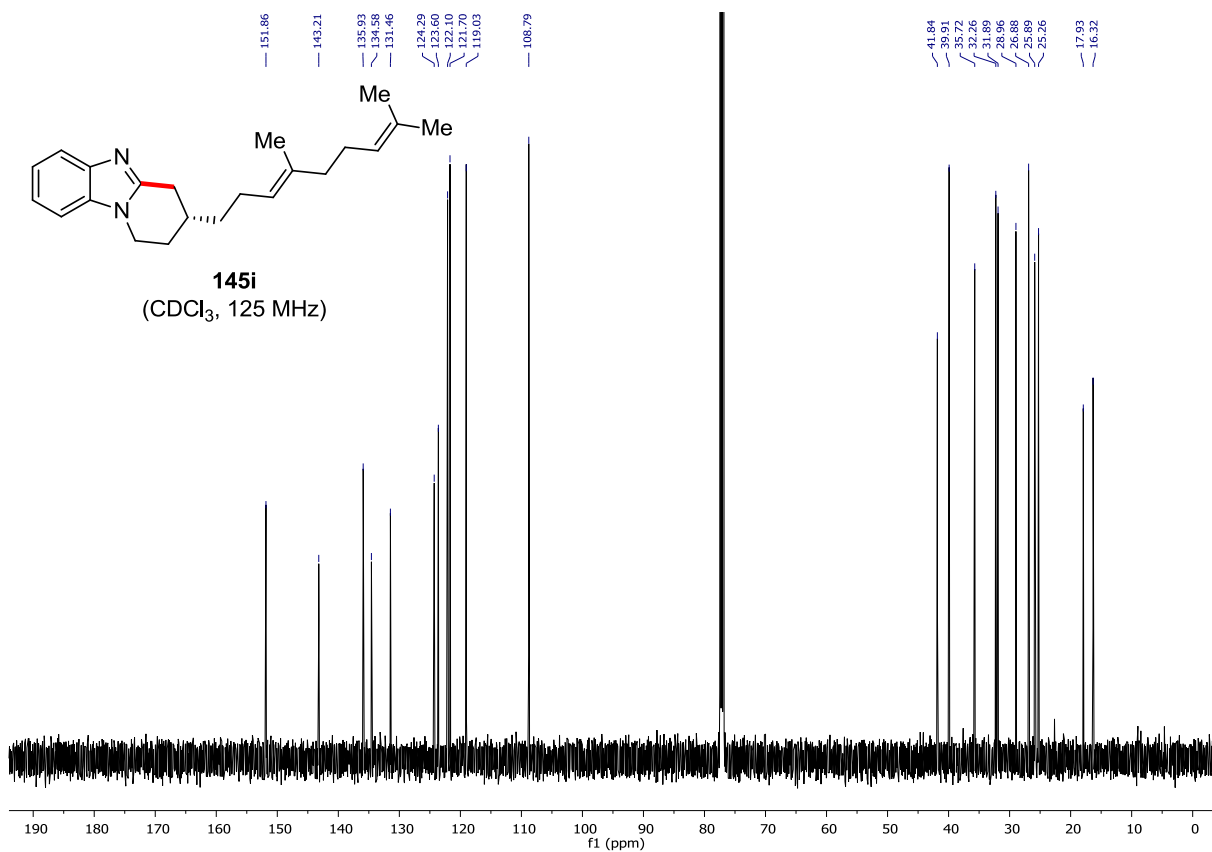
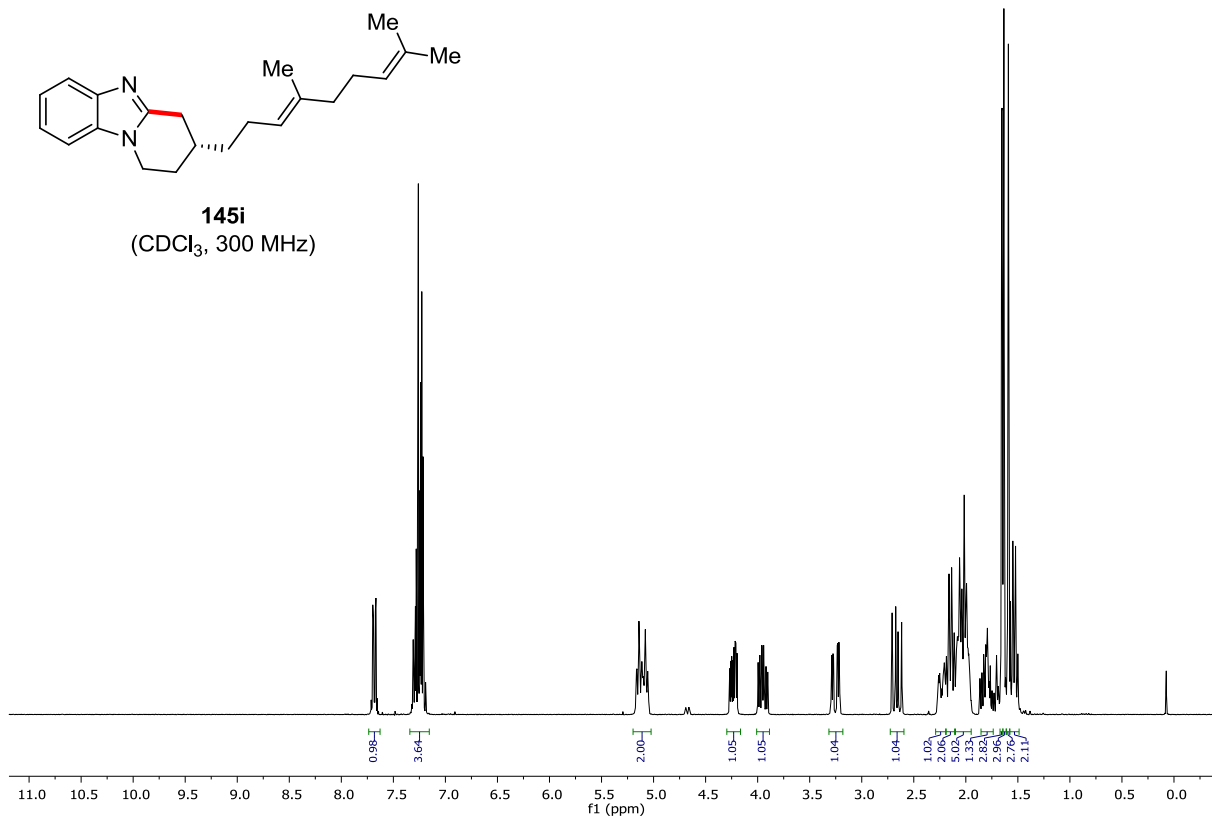
Chiral HPLC of **145h**:



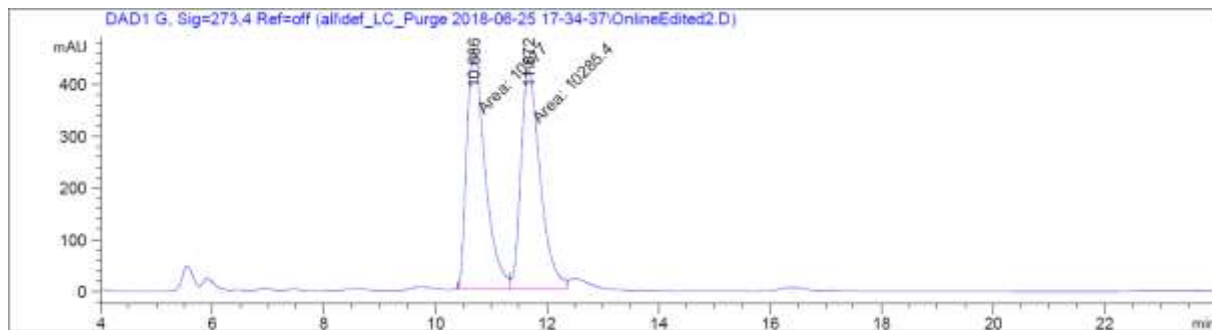
| Peak # | RetTime [min] | Type | Width [min] | Area [mAU*s] | Height [mAU] | Area % |
|--------|---------------|------|-------------|--------------|--------------|---------|
| 1 | 13.395 | BV | 0.3993 | 1.46962e4 | 567.08203 | 50.1919 |
| 2 | 14.864 | MF | 0.4696 | 1.45838e4 | 517.64801 | 49.8081 |



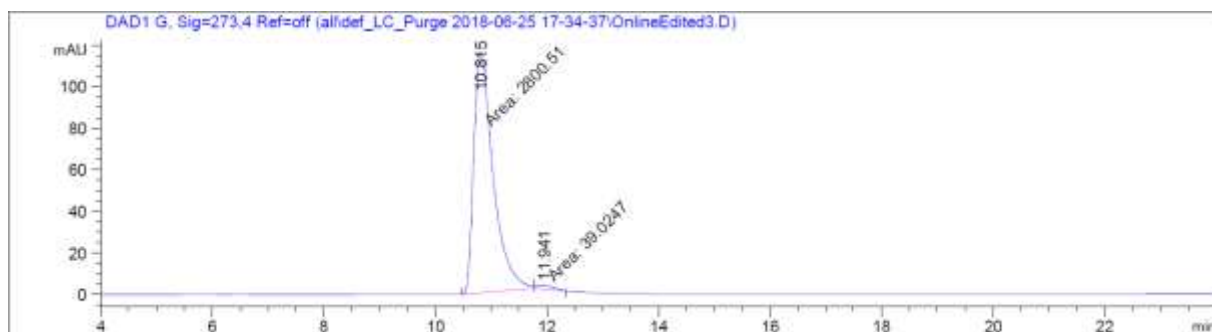
| Peak # | RetTime [min] | Type | Width [min] | Area [mAU*s] | Height [mAU] | Area % |
|--------|---------------|------|-------------|--------------|--------------|---------|
| 1 | 13.590 | BB | 0.4134 | 7197.62549 | 265.38815 | 97.0958 |
| 2 | 15.278 | MF | 0.4844 | 215.28246 | 7.40739 | 2.9042 |



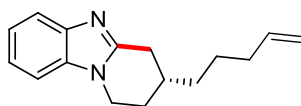
Chiral HPLC of **145i**:



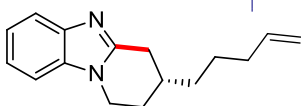
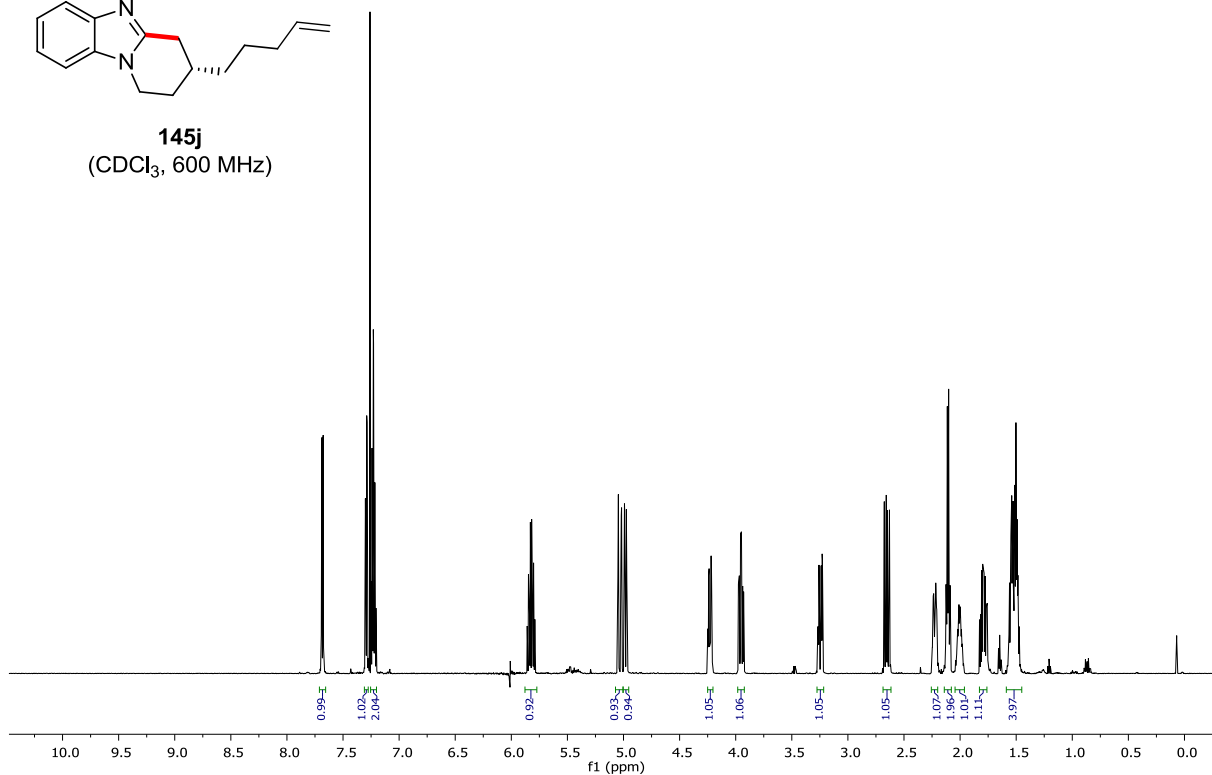
| Peak # | RetTime [min] | Type | Width [min] | Area [mAU*s] | Height [mAU] | Area % |
|--------|---------------|------|-------------|--------------|--------------|---------|
| 1 | 10.686 | FM | 0.3810 | 1.05770e4 | 462.74683 | 50.6989 |
| 2 | 11.672 | MF | 0.4039 | 1.02854e4 | 424.42429 | 49.3011 |



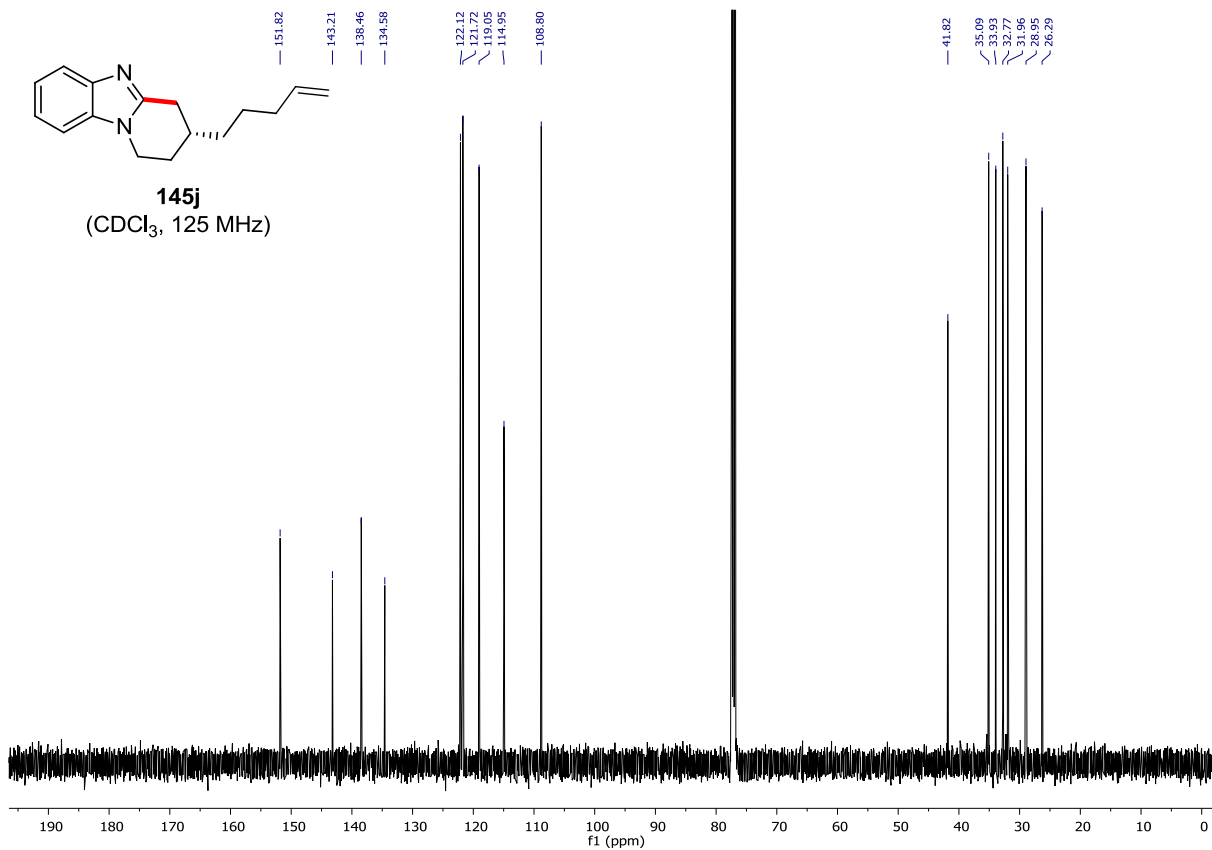
| Peak # | RetTime [min] | Type | Width [min] | Area [mAU*s] | Height [mAU] | Area % |
|--------|---------------|------|-------------|--------------|--------------|---------|
| 1 | 10.815 | MM | 0.4033 | 2800.51294 | 115.73122 | 98.6257 |
| 2 | 11.841 | MM | 0.3747 | 39.02470 | 1.73580 | 1.3743 |



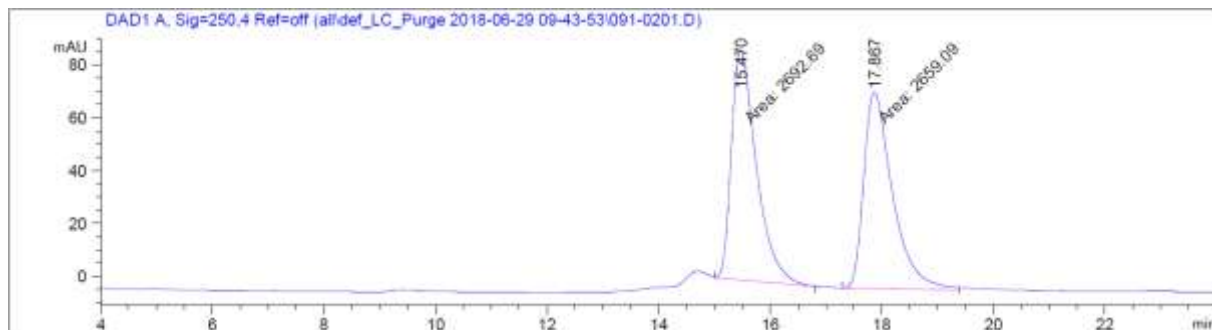
145j
(CDCl₃, 600 MHz)



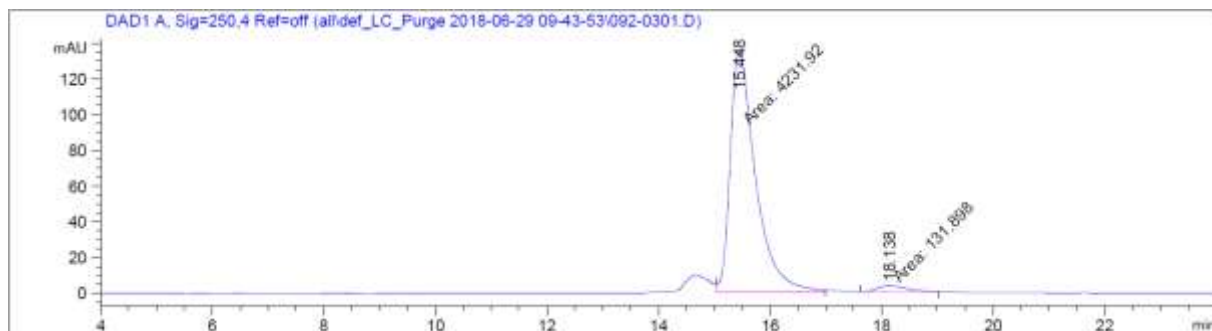
145j
(CDCl₃, 125 MHz)



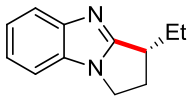
Chiral HPLC of **145j**:



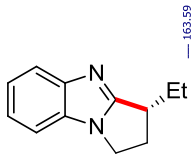
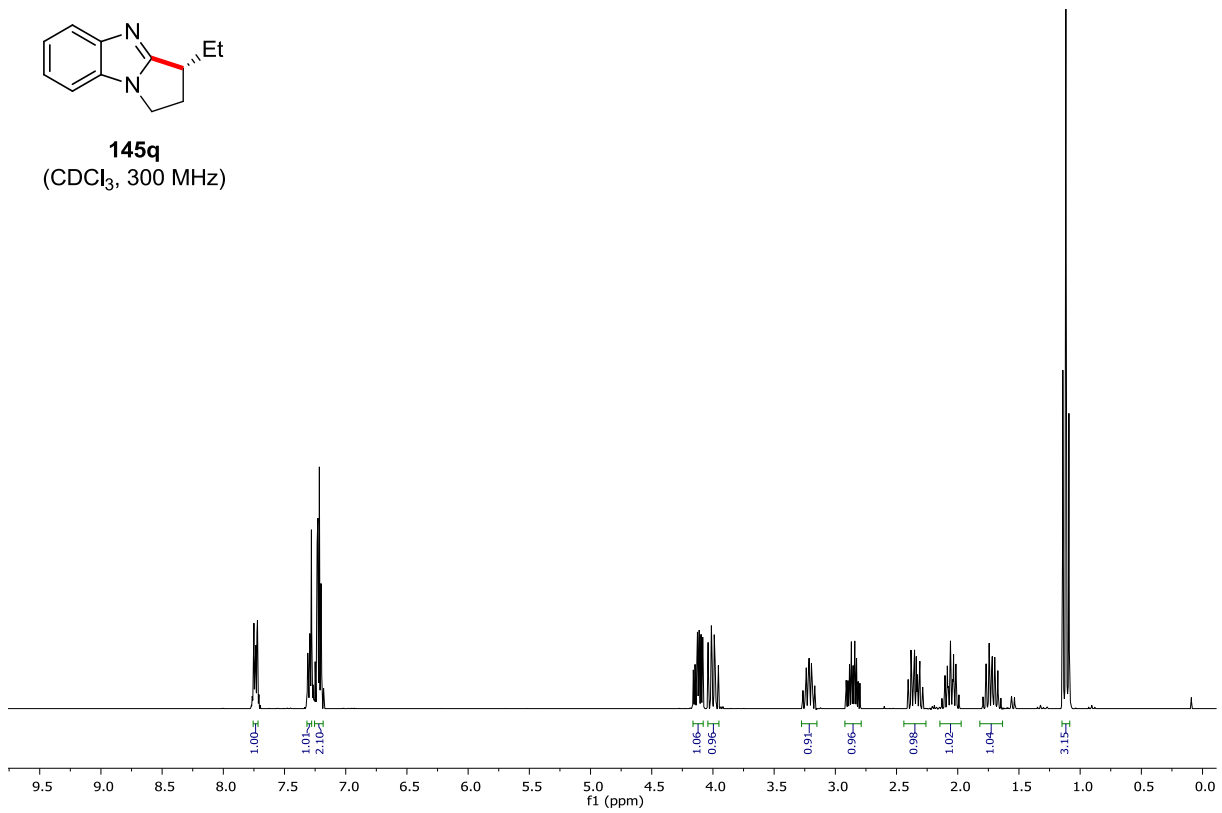
| Peak # | RetTime [min] | Type | Width [min] | Area [mAU*s] | Height [mAU] | Area % |
|--------|---------------|------|-------------|--------------|--------------|---------|
| 1 | 15.470 | MF | 0.5164 | 2692.69043 | 86.91150 | 50.3139 |
| 2 | 17.867 | MF | 0.5967 | 2659.09375 | 74.27447 | 49.6861 |



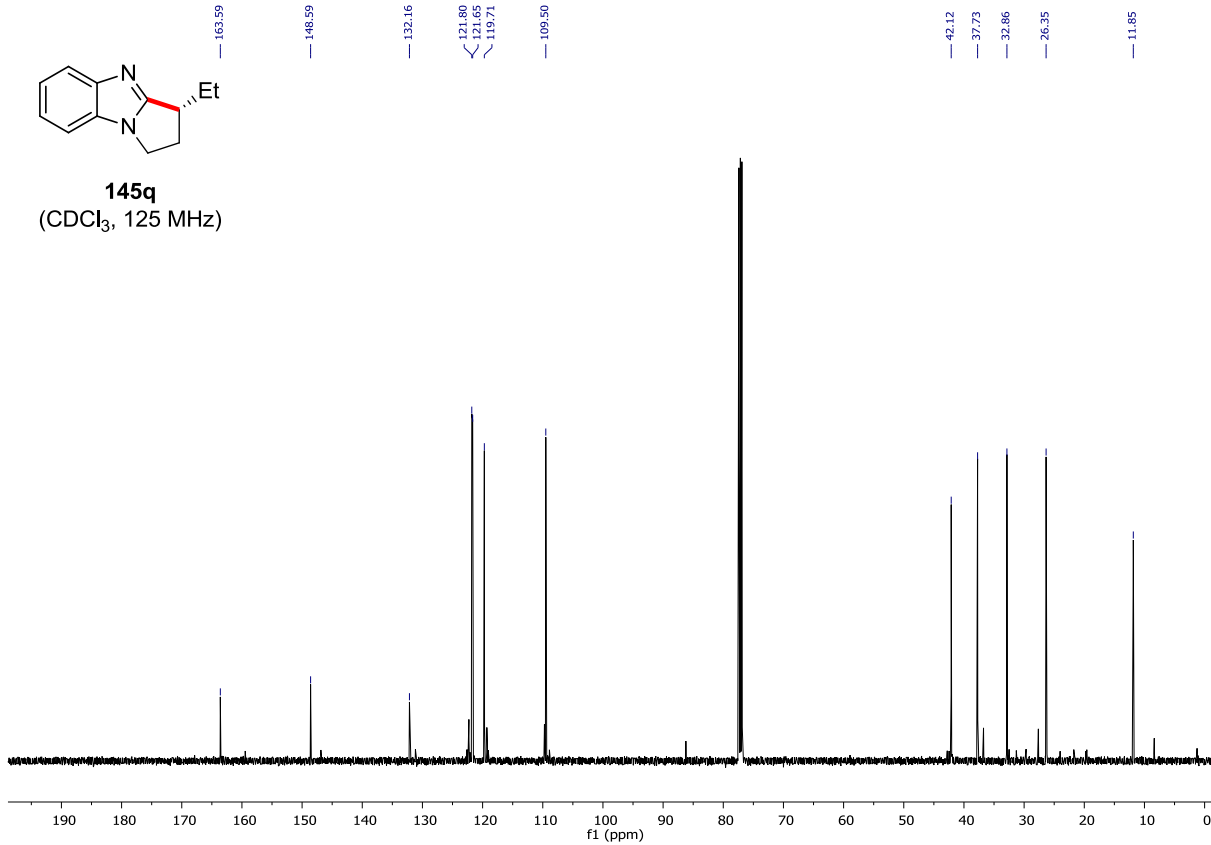
| Peak # | RetTime [min] | Type | Width [min] | Area [mAU*s] | Height [mAU] | Area % |
|--------|---------------|------|-------------|--------------|--------------|---------|
| 1 | 15.448 | MF | 0.5242 | 4231.92188 | 134.55379 | 96.9775 |
| 2 | 18.138 | MF | 0.6590 | 131.89804 | 3.33588 | 3.0225 |



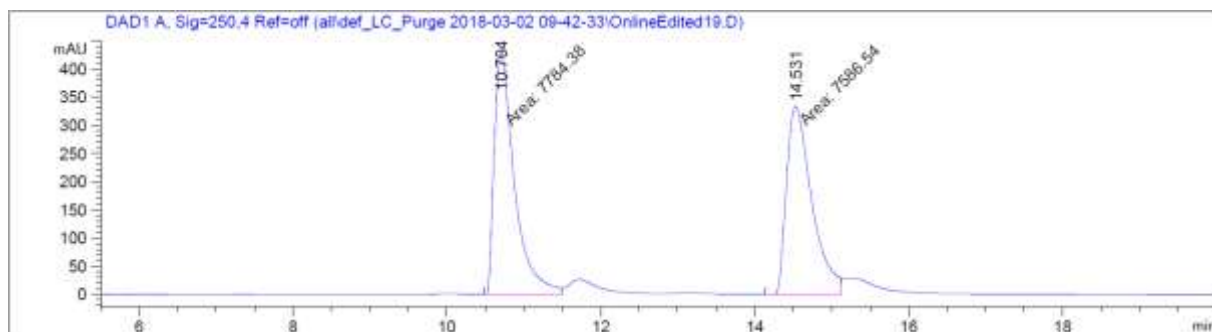
145q
(CDCl₃, 300 MHz)



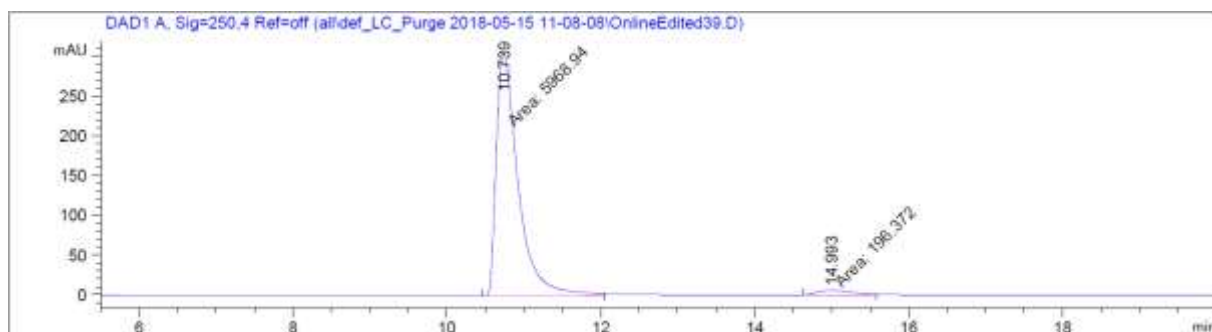
145q
(CDCl₃, 125 MHz)



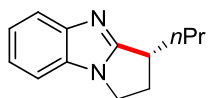
Chiral HPLC of **145q**:



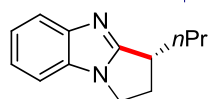
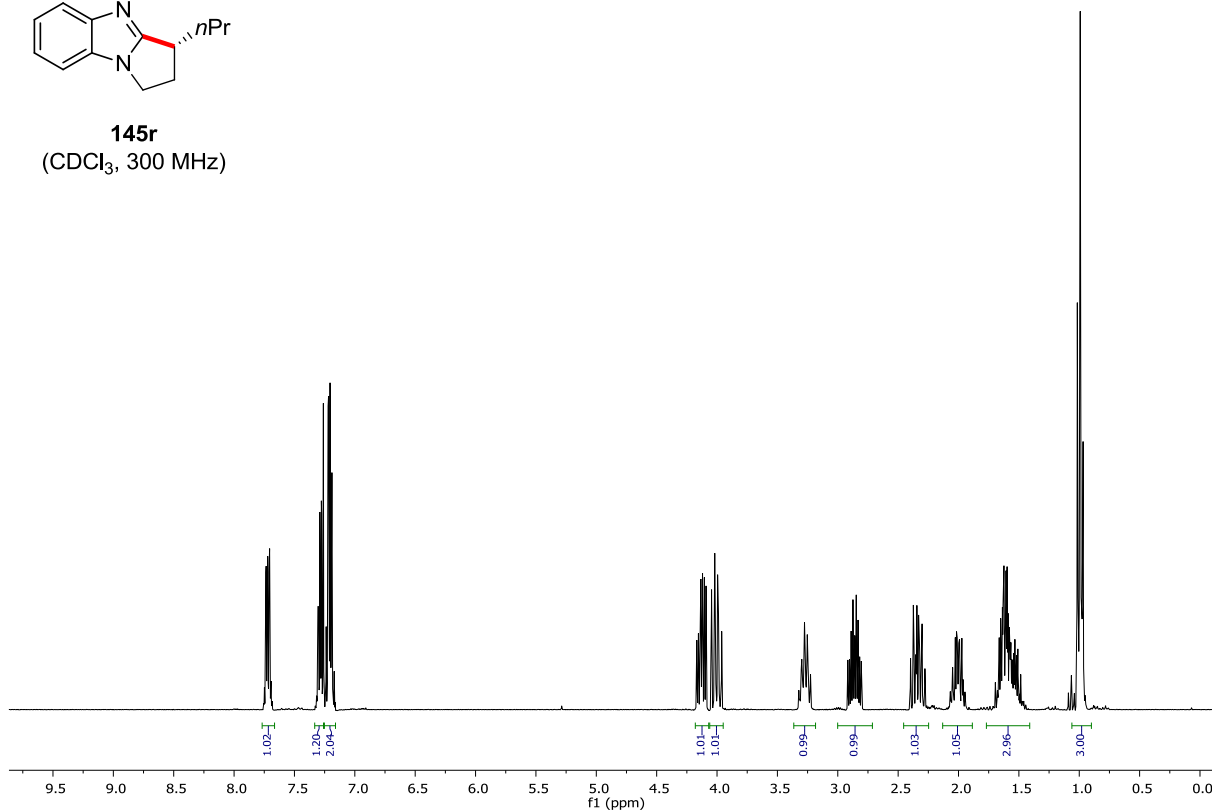
| Peak # | RetTime [min] | Type | Width [min] | Area [mAU*s] | Height [mAU] | Area % |
|--------|---------------|------|-------------|--------------|--------------|---------|
| 1 | 10.704 | MF | 0.3022 | 7784.37988 | 429.28778 | 50.6435 |
| 2 | 14.531 | MF | 0.3789 | 7586.54443 | 333.66656 | 49.3565 |



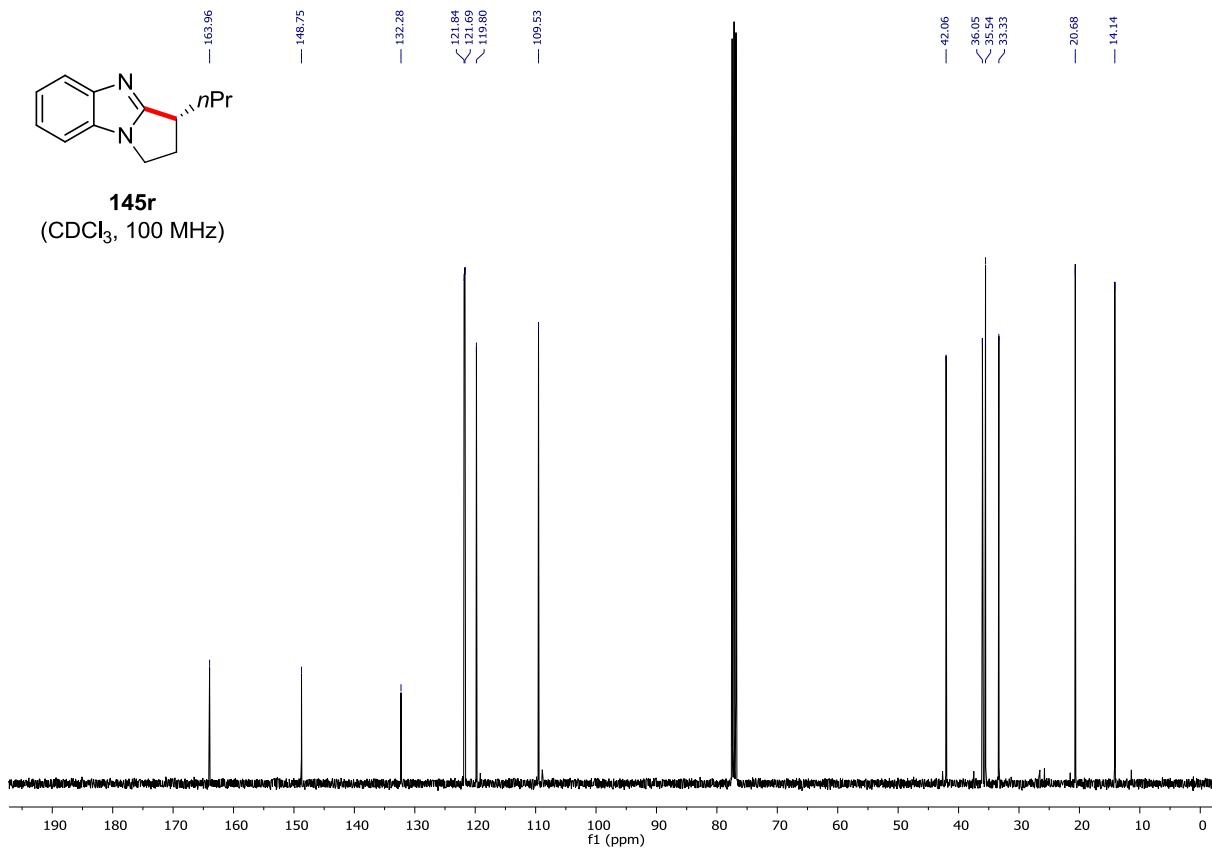
| Peak # | RetTime [min] | Type | Width [min] | Area [mAU*s] | Height [mAU] | Area % |
|--------|---------------|------|-------------|--------------|--------------|---------|
| 1 | 10.739 | MF | 0.3264 | 5968.94092 | 304.77304 | 96.8149 |
| 2 | 14.993 | MF | 0.5492 | 196.37163 | 5.95983 | 3.1851 |



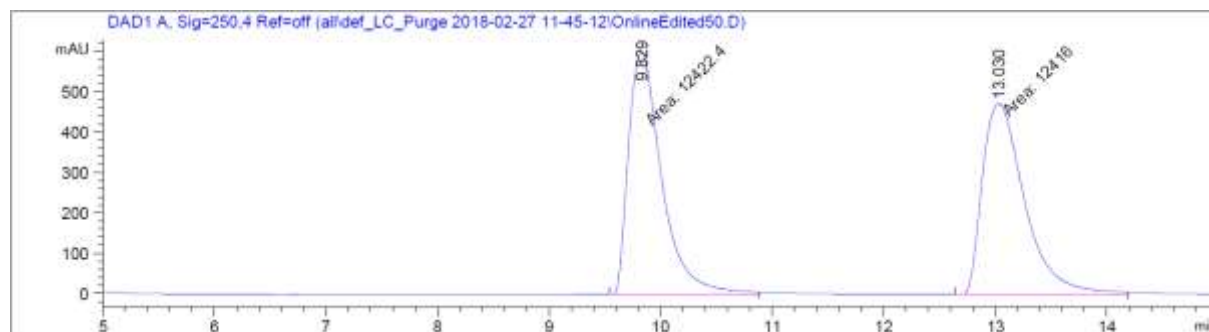
145r
(CDCl₃, 300 MHz)



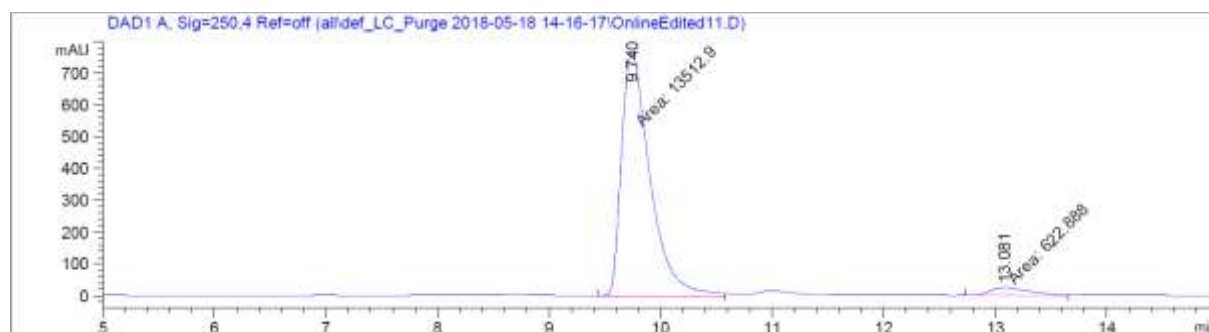
145r
(CDCl₃, 100 MHz)



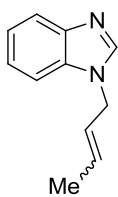
Chiral HPLC of **145r**:



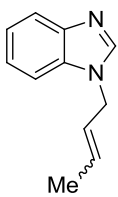
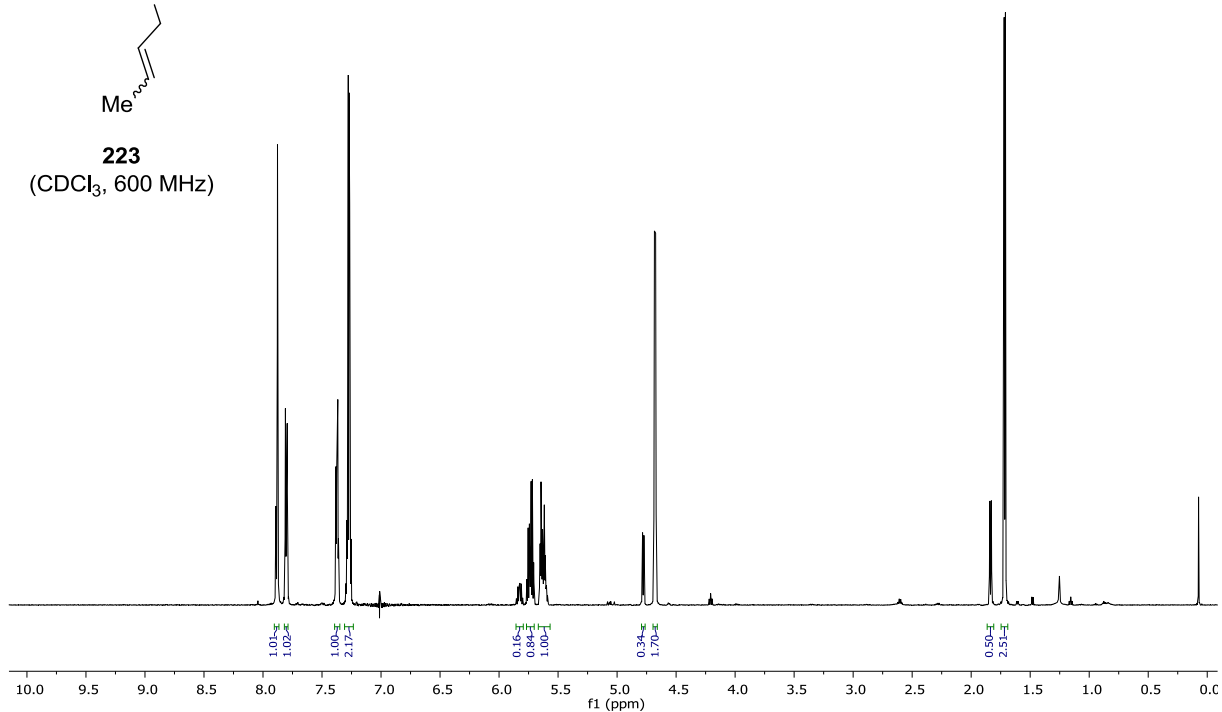
| Peak # | RetTime [min] | Type | Width [min] | Area [mAU*s] | Height [mAU] | Area % |
|--------|---------------|------|-------------|--------------|--------------|---------|
| 1 | 9.829 | MF | 0.3453 | 1.24224e4 | 599.66241 | 50.0130 |
| 2 | 13.030 | MF | 0.4388 | 1.24160e4 | 471.57504 | 49.9870 |



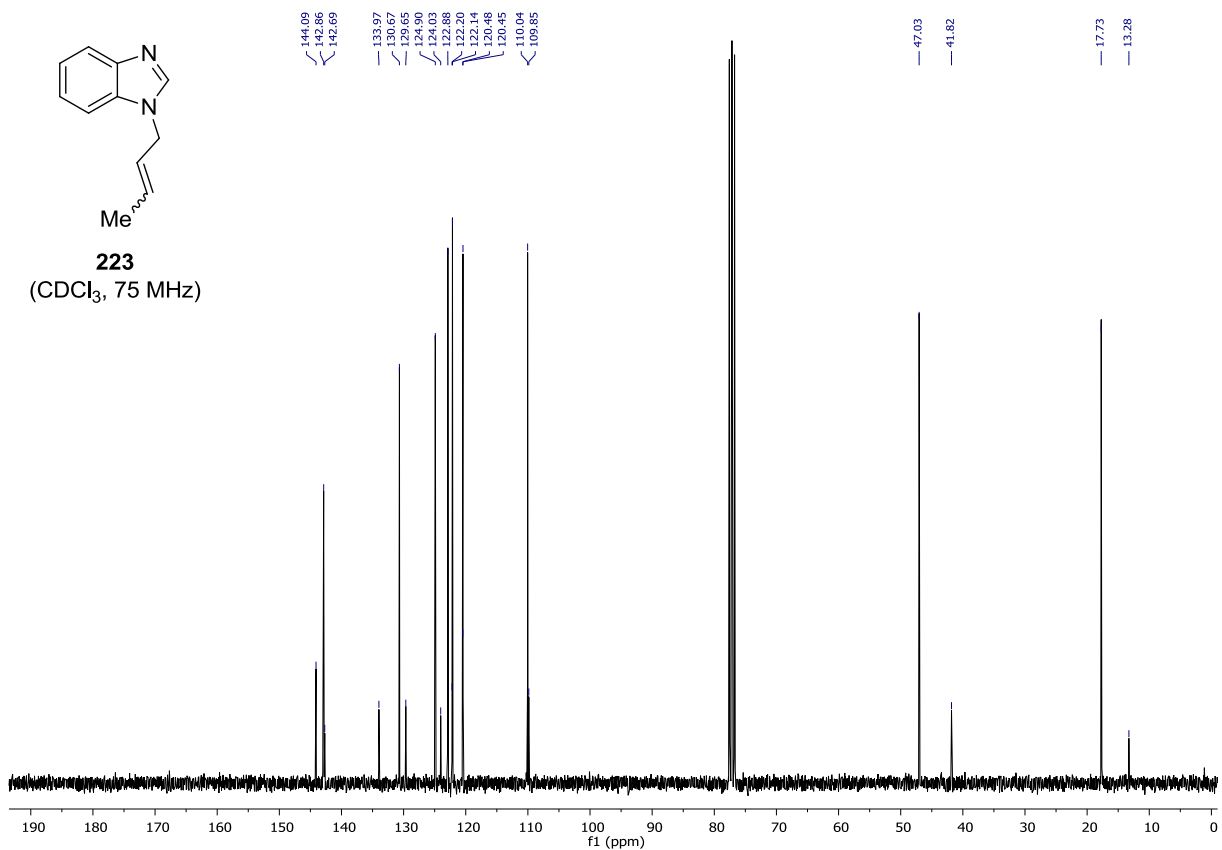
| Peak # | RetTime [min] | Type | Width [min] | Area [mAU*s] | Height [mAU] | Area % |
|--------|---------------|------|-------------|--------------|--------------|---------|
| 1 | 9.740 | MF | 0.2952 | 1.35129e4 | 762.80017 | 95.5936 |
| 2 | 13.081 | MF | 0.4197 | 622.88818 | 24.73671 | 4.4064 |

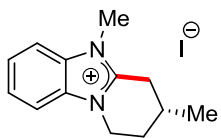


223
(CDCl₃, 600 MHz)

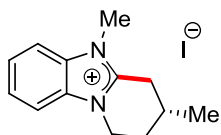
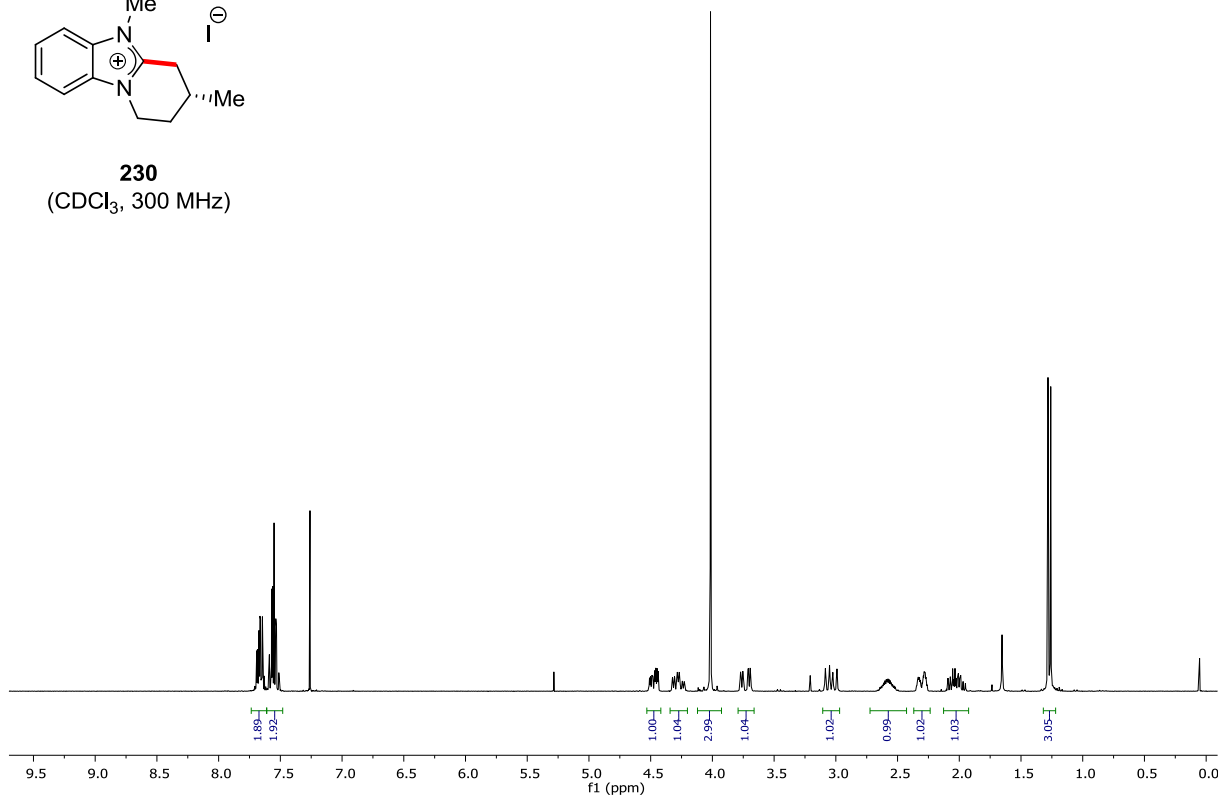


223
(CDCl₃, 75 MHz)

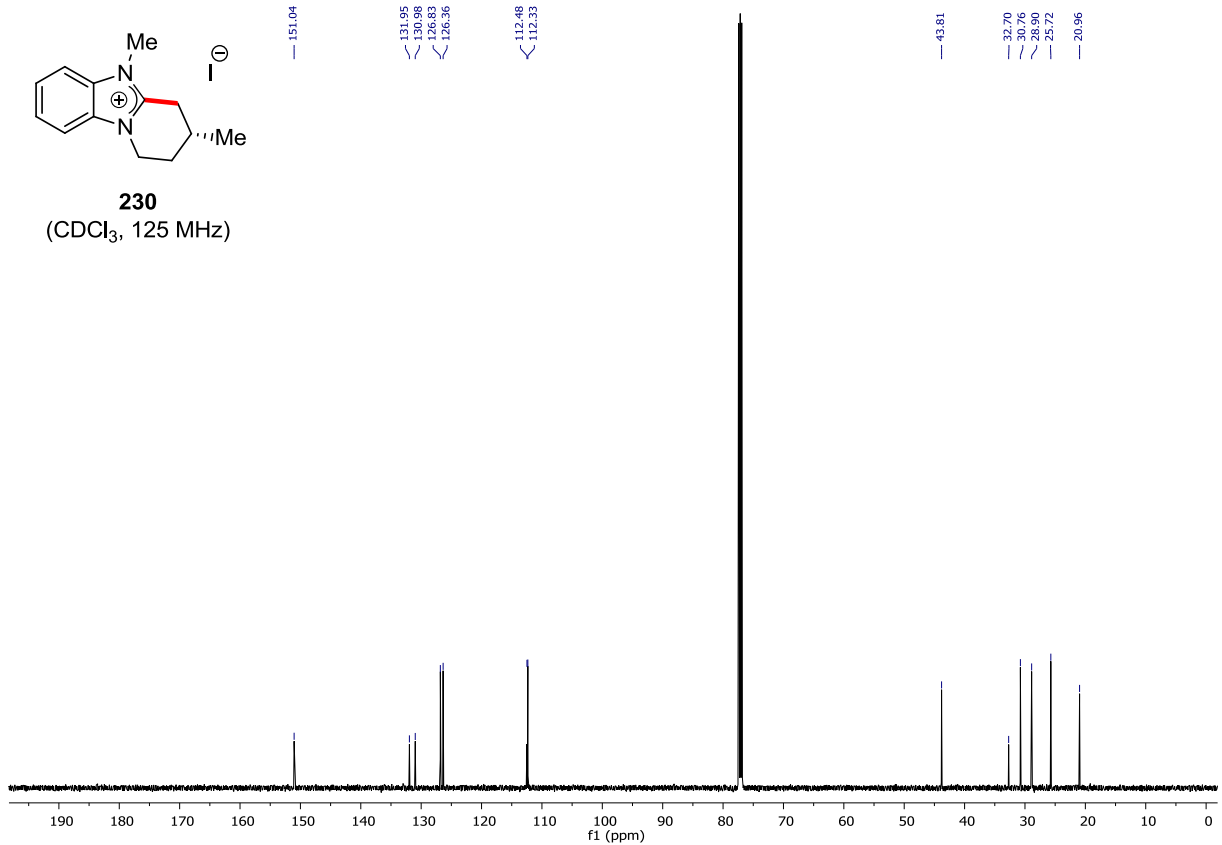


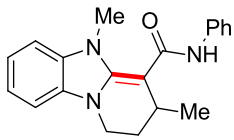


230
(CDCl₃, 300 MHz)

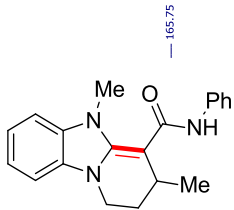
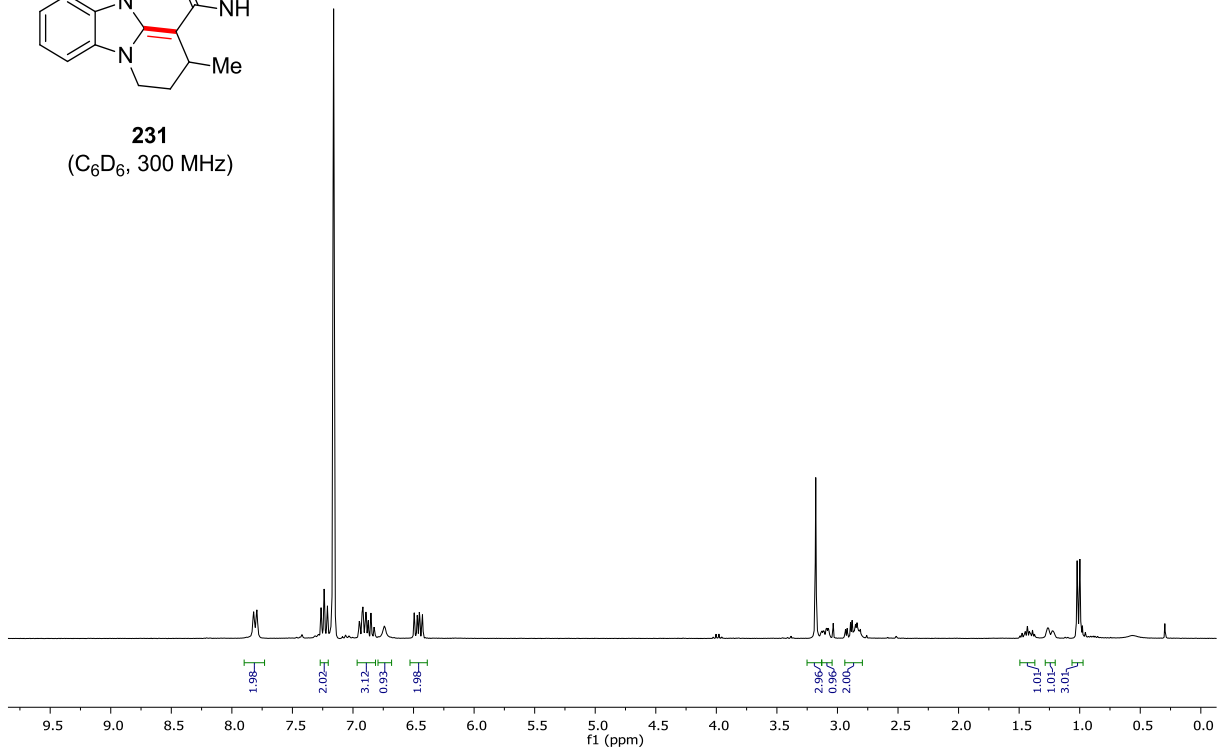


230
(CDCl₃, 125 MHz)

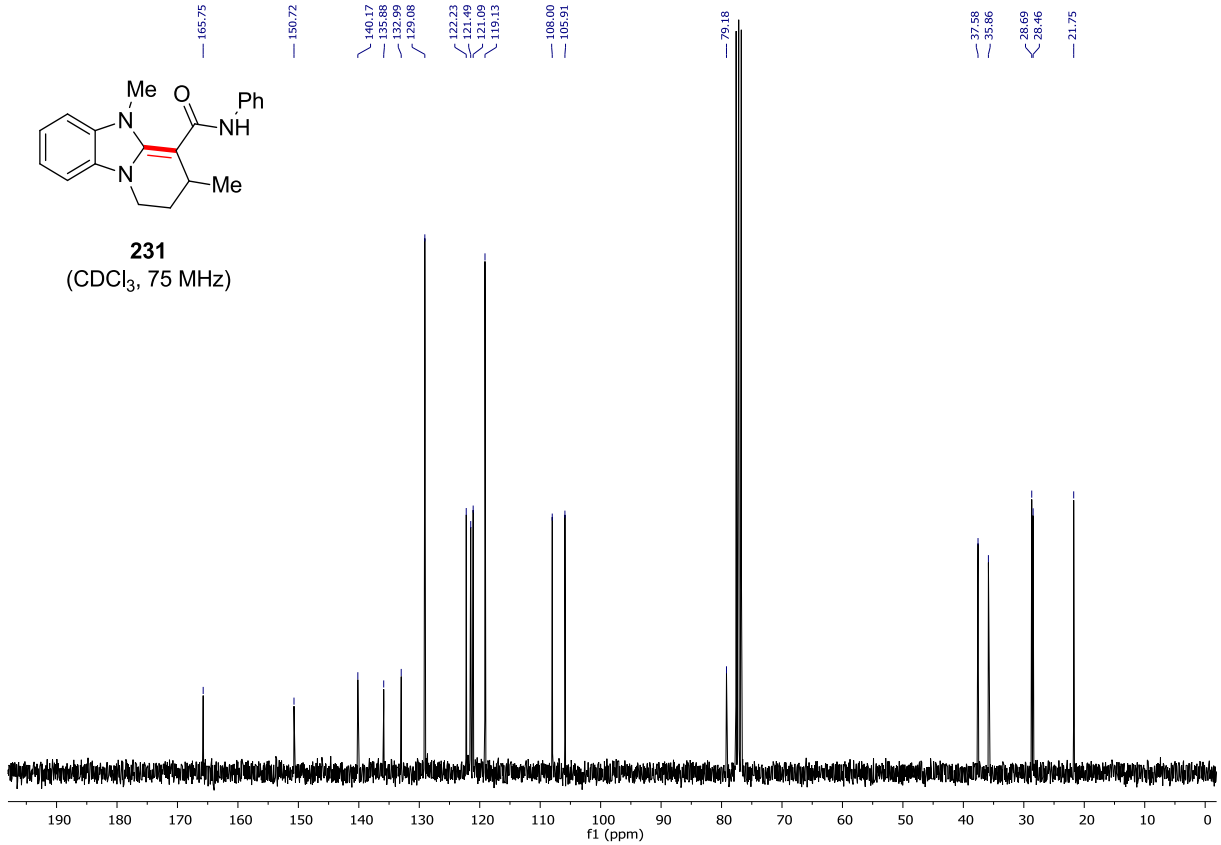




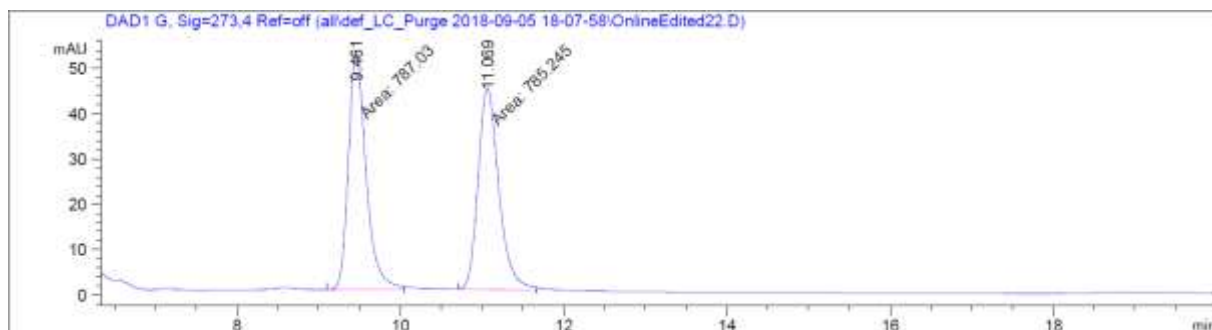
231
(C₆D₆, 300 MHz)



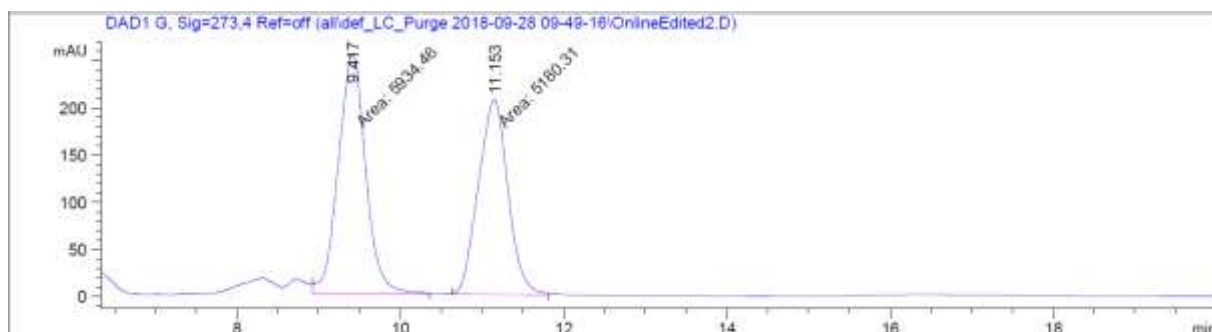
231
(CDCl₃, 75 MHz)



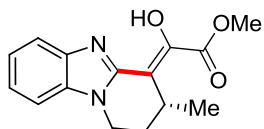
Chiral HPLC of **231**:



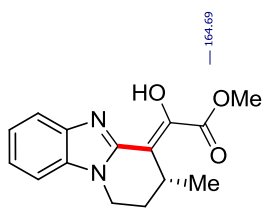
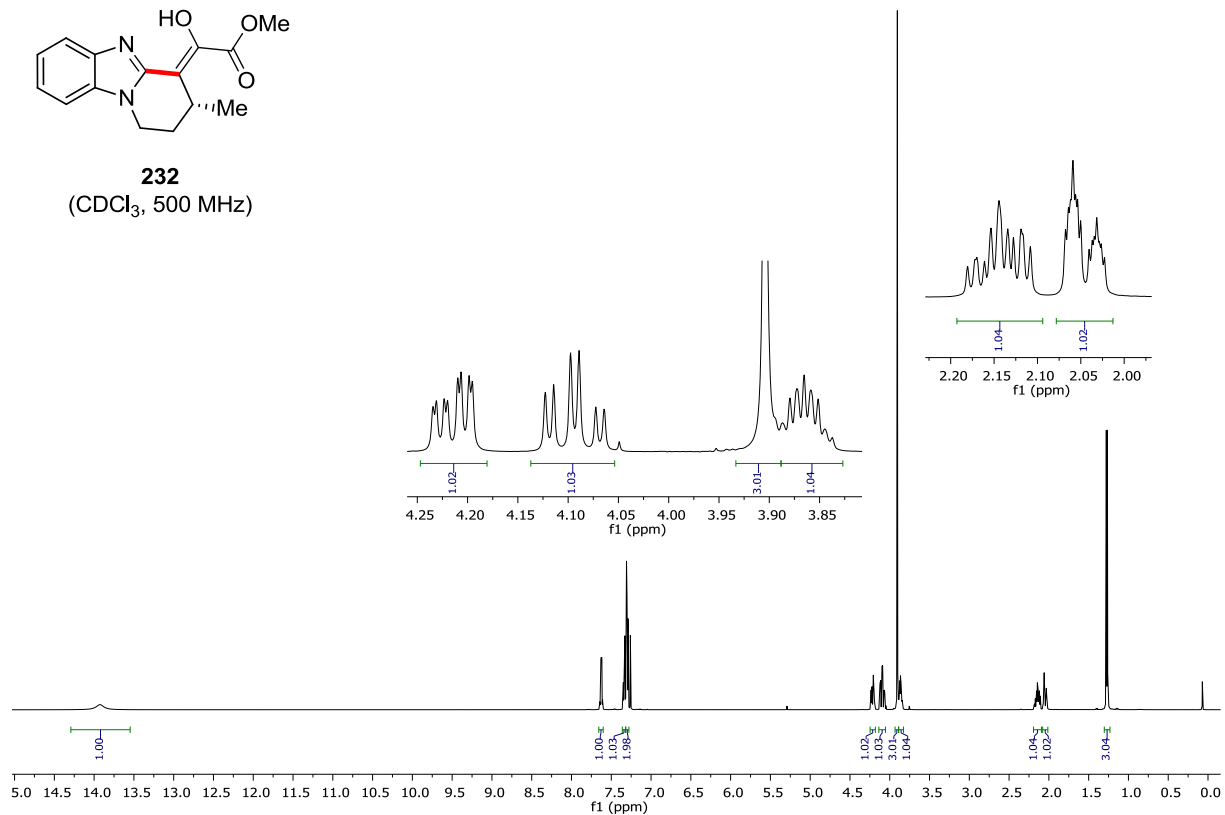
| Peak # | RetTime [min] | Type | Width [min] | Area [mAU*s] | Height [mAU] | Area % |
|--------|---------------|------|-------------|--------------|--------------|---------|
| 1 | 9.461 | MF | 0.2495 | 787.02972 | 52.56332 | 50.0568 |
| 2 | 11.069 | MF | 0.2942 | 785.24451 | 44.48877 | 49.9432 |



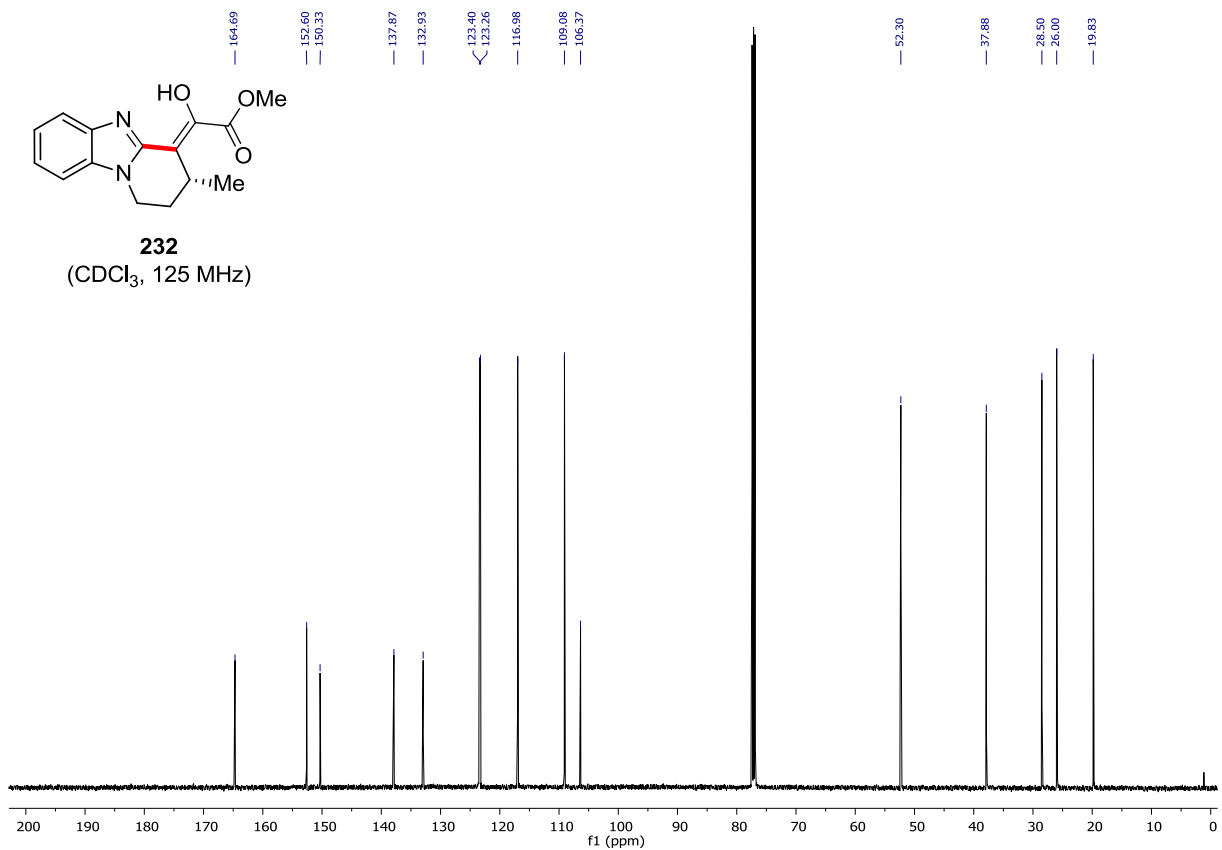
| Peak # | RetTime [min] | Type | Width [min] | Area [mAU*s] | Height [mAU] | Area % |
|--------|---------------|------|-------------|--------------|--------------|---------|
| 1 | 9.417 | MF | 0.3885 | 5934.45898 | 254.55949 | 53.3926 |
| 2 | 11.153 | MF | 0.4184 | 5180.30957 | 206.35019 | 46.6074 |



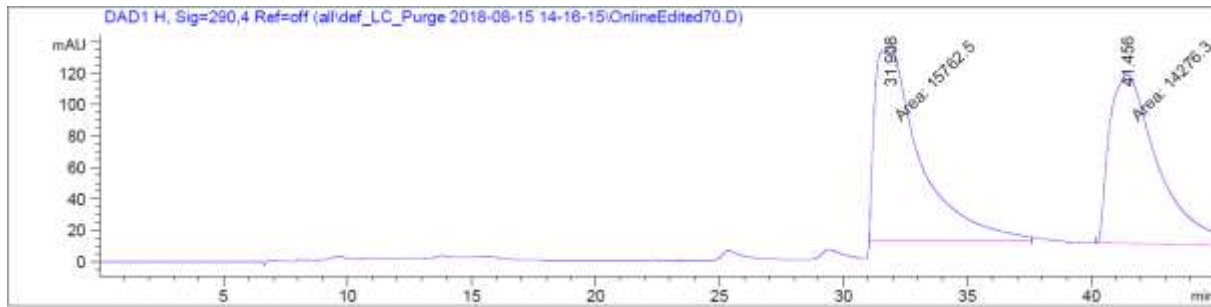
232
(CDCl₃, 500 MHz)



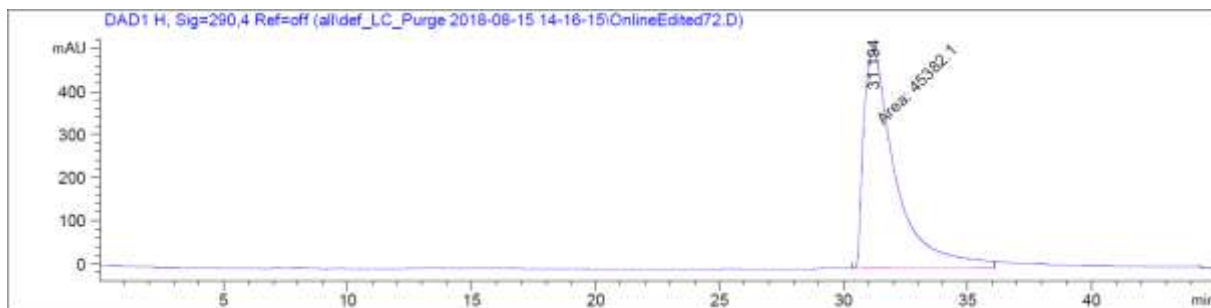
232
(CDCl₃, 125 MHz)



Chiral HPLC of **232**:



| Peak # | RetTime [min] | Type | Width [min] | Area [mAU*s] | Height [mAU] | Area % |
|--------|---------------|------|-------------|--------------|--------------|---------|
| 1 | 31.908 | MM | 2.1226 | 1.57625e4 | 123.76486 | 52.4738 |
| 2 | 41.456 | MM | 2.2140 | 1.42763e4 | 107.46957 | 47.5262 |



| Peak # | RetTime [min] | Type | Width [min] | Area [mAU*s] | Height [mAU] | Area % |
|--------|---------------|------|-------------|--------------|--------------|----------|
| 1 | 31.194 | MF | 1.4936 | 4.53821e4 | 506.41312 | 100.0000 |